J. FERNANDO AREVALO
EDITOR

Retinal Angiography and Optical Coherence Tomography

Springer

Retinal Angiography and Optical Coherence Tomography

Retinal Angiography and Optical Coherence Tomography

Edited by

J. Fernando Arevalo, MD, FACS
Professor and Chairman, Retina and Vitreous Service, Clinica Oftalmológica Centro Caracas,
The Arevalo-Coutinho Foundation for Research in Ophthalmology, Caracas, Venezuela

Springer

Editor
J. Fernando Arevalo, MD, FACS
Professor and Chairman, Retina and Vitreous Service, Clinica Oftalmológica Centro Caracas,
The Arevalo-Coutinho Foundation for Research in Ophthalmology, Caracas, Venezuela

ISBN: 978-0-387-68986-9 e-ISBN: 978-0-387-68987-6
DOI: 10.1007/978-0-387-68987-6

Library of Congress Control Number: 2008936992

Printed on acid-free paper

9 8 7 6 5 4 3 2 1

springer.com

To my parents:
Who gave me a wonderful life, and all the support and opportunities

To my wife, Oly:
Who has taught me how to be a better human being, who has beared with me for so many years, and has shared the good and the bad

To my son, Fernando Andrés:
Who has taught me how much my parents loved me, and for all the happiness he has brought to us

Preface

After more than 40 years since the introduction of fluorescein angiography (FA), more than 20 years after the introduction of indocyanine green angiography (ICGA), and more than 10 years since the introduction of optical coherence tomography (OCT), it is time for a comprehensive presentation of the current technical and clinical aspects of these diagnostic methods, which is contained in this book. Recent technologic developments in digital video imaging have allowed ICGA and FA better resolution and offer new opportunities to investigate the dynamics of the normal choroid circulation and correlate them with the retinal counterpart in a variety of choroidal abnormalities and retinal diseases. In addition, since the invention of OCT, this technology has emerged to become a widely used tool that has already revolutionized the diagnosis and therapy of eye disease. Optical coherence tomography has already produced wide changes in the way the eye is examined and in the way patients are treated. It is only natural to combine the topics of retinal angiography and OCT for the diagnosis and follow-up of eye diseases.

This book includes contributions from an internationally renowned group of experts from the United States, Spain, Mexico, Costa Rica, Italy, and Venezuela, and has been divided into three parts. Part I, Fluorescein and Indocyanine Green Angiography, includes nine chapters on retinal photography and angiography via film and digital imaging techniques, fluorescein, and ICGA, and discusses general aspects and interpretation; angiography of macular diseases, retinal vascular diseases, inflammatory diseases, optic nerve diseases, and retinal and choroidal tumors; and retinal angiography in pharmacologic retinal toxicity. Part II, Optical Coherence Tomography, includes 12 chapters on how OCT works; the basic principles of OCT; OCT in macular diseases, diabetic retinopathy, and age-related macular degeneration; the role of OCT imaging in the evaluation of ocular photodynamic therapy and antiangiogenic therapy; OCT in tractional maculopathies, ocular inflammatory diseases, glaucoma, optic nerve diseases, and intraocular tumors; and limitations in the evaluation of OCT images. Part III, Ophthalmic Imaging, Spectral Domain, and New Technologies, includes six chapters on ophthalmic fundus imaging, ultrawide-angle fluorescein angiography, fundus autofluorescence, ultrahigh-resolution OCT, high-speed Fourier domain OCT, and spectral OCT/scanning laser ophthalmoscope (SLO).

The impetus to edit this book has come from my students and my colleagues. In addition, I have felt the need for a book on a combination of topics that I have been working on for a long time, including courses at the American Academy of Ophthalmology. I call this book a hybrid of angiography and optical coherence tomography. I think, as a retina specialist, that this combination will be very appealing to my colleagues and students throughout the ophthalmic community. Furthermore, ICGA (an important topic in the angiography part of this book) has been the topic of very few books. The book is intended for retina and vitreous specialists, retina and vitreous fellows, ophthalmology residents, and comprehensive ophthalmologists.

The principal objective of this text is to present current information on retinal and choroidal angiography as well as OCT imaging interpretation from leading experts in the field. We hope their knowledge and experience will assist ophthalmologists and retina specialists approach a level of knowledge about angiography and OCT to benefit the patients in their clinical practice.

J. Fernando Arevalo, MD, FACS

Foreword

The field of ophthalmic fundus angiography is not new. Many articles and textbooks have been written on the subject. The field of optical coherence tomography, on the other hand, is still very much in its infancy. To bring these two critically important imaging techniques together in one comprehensive textbook was a monumental task. J. Fernando Arevalo set out to write a textbook whose principal objective was "to present current information on retinal and choroidal angiography as well as OCT imaging interpretation." This outstanding vitreoretinal specialist has clearly achieved his goal in the publication of this superbly organized and comprehensive text.

The techniques of fluorescein angiography and indocyanine green angiography are well known to all of us. The nuances of these techniques, however, require constant study and refinement. We are continually learning new things about the many disease states we study and treat on a day-to-day basis from our understanding of FA and ICG. Further clarification is always needed and always appreciated by those interested in these important areas of study. In the first section of this textbook the authors take us through a complete educational voyage of these imaging techniques. They begin with the very basics of both FA and ICG in very clear and eloquently written chapters. Choroidal, retinal vascular, and optic disc conditions are described and beautifully illustrated for the readers. For the novice this proves to be invaluable, while for the more advanced reader, the information is concise and serves as a wonderful resource for future reference.

The second section of the book deals with the new and exciting field of optical coherence tomography. The authors take this new field of imaging and, in a wonderfully orchestrated sequence of topics and chapters, develop and discuss OCT from the most basic principles needed to understand how OCT works to how it is applied to different disease states. Again, choroidal, retinal, and optic disc diseases are comprehensively discussed. Understanding that a picture is worth a thousand words and that images help the reader understand the concepts being described in the written text, the chapters contain a generous number of illustrations.

Finally, this textbook's last section deals with ophthalmic imaging, spectral domain, and new technologies, which to me is another way of saying computer processed imaging. If it were not for computers and their ability to process data, we would still be using film based FAs and ICGs. The authors delve into the difficult topic of fundus imaging and provide us today with a foundation for understanding ophthalmic imaging in the future.

Fernando Arevalo has assembled an excellent list of contributors who represent the "Who's Who" in their areas of expertise. With such a list of authors we have no reason to expect anything but the most current information in each of the chapters presented in this textbook. We are not disappointed in the result of their endeavors. We are pleased that Fernando and his coauthors have achieved their goal of producing a comprehensive text that brings together FA, ICG, and OCT in a single textbook that brings to us the most current knowledge on the topics discussed.

We have come a long way since the first photographic image of the retinal fundus. The authors of this book are distinguished authorities in their fields of interest, and have been given an opportunity to discuss and illustrate current topics of extreme importance in our care of patients and our understanding of the diseases that affect them. We are the beneficiaries of their experience and their willingness to share their knowledge and expertise with us. This textbook will be an important part of any library.

Alexander J. Brucker, M.D.
Professor of Ophthalmology
Scheie Eye Institute
University of Pennsylvania
Editor-in-Chief
RETINA, The Journal of
Retinal and Vitreous Diseases

Contents

Contributors

Santiago Abengoechea, MD
Vitreoretinal Surgery Service, Centro de Oftalmología Barraquer, Barcelona, Spain

Lourdes Arellanes-Garcia, MD
Uveitis and Intraocular Inflammation Service, Asociación para la Prevención de la Ceguera, Mexico City, Mexico

J. Fernando Arevalo, MD, FACS
Retina and Vitreous Service, Clinica Oftalmológica Centro Caracas, Arevalo-Coutinho Foundation for Research in Ophthalmology, Caracas, Venezuela

Caroline R. Baumal, MD
Tufts University School of Medicine, Vitreoretinal Service, New England Eye Center, Boston, Massachusetts

Raquel Benavides, MD
Department of Ophthalmology, Hospital Mexico, San Jose, Costa Rica

Royce W.S. Chen, BA
Tufts University School of Medicine, Vitreoretinal Service, New England Eye Center, Boston, Massachusetts

Antonio P. Ciardella, MD
Director of Ophthalmology, Denver Health Medical Center, Associate Professor of Ophthalmology, University of Colorado Health Science Center, Denver, Colorado

Thomas M. Clark, BSc, CRA
Department of Ophthalmology, Shiley Eye Center, Ophthalmic Photography and Electronic Imaging Department, University of California, San Diego, San Diego, California

Janet L. Davis, MD
Uveitis and Intraocular Inflammation Service, Bascom Palmer Eye Institute, University of Miami Miller School of Medicine, Miami, Florida

María F. de la Paz, MD
Centro de Oftalmología Barraquer, Barcelona, Spain

Jay S. Duker, MD
Tufts University School of Medicine, Vitreoretinal Service, New England Eye Center, Boston, Massachusetts

Chiara M. Eandi, MD, PhD
Eye Clinic University of Torino, Torino, Italy

Javier Elizalde, MD
Vitreoretinal Surgery Service, Centro de Oftalmología Barraquer, Barcelona, Spain

Carlos F. Fernandez, MD
Retina and Vitreous Service, Clinica Oftalmológica Centro Caracas, Arevalo-Coutinho Foundation for Research in Ophthalmology, Caracas, Venezuela

Yale L. Fisher, MD
LuEsther T. Mertz Retinal Research Center, Manhattan Eye, Ear and Throat Hospital, Department of Ophthalmology, New York, New York

Robert W. Flower, DSC
LuEsther T. Mertz Retinal Research Center, Manhattan Eye, Ear and Throat Hospital, Department of Ophthalmology, New York, New York, USA

Jans Fromow-Guerra, MD
Retina and Vitreous Service, Asociación para la Prevención de la Ceguera, Mexico City, Mexico

Dario Fuenmayor-Rivera, MD
Instituto de Oftalmologia y Otorrinolaringologia, Caracas, Venezuela

James G. Fujimoto, PhD
Research Laboratory of Electronics and Department of Electrical Engineering and Computer Science, Massachusetts Institute of Technology, Cambridge, Massachusetts

Anne Fung, MD
Pacific Eye Associates, California Pacific Medical Center, San Francisco, California

Patricia M.T. Garcia, MD
Advanced Retinal Imaging Laboratory, New York Eye and Ear Infirmary, New York, New York, Department of Ophthalmology, New York Medical College, Valhalla, New York

Reinaldo A. Garcia, MD
Retina and Vitreous Service, Clinica Oftalmológica Centro Caracas, Arevalo-Coutinho Foundation for Research in Ophthalmology, Caracas, Venezuela

Rafael A. Garcia-Amaris, MD
Retina and Vitreous Service, Clinica Oftalmológica Centro Caracas, Arevalo-Coutinho Foundation for Research in Ophthalmology, Caracas, Venezuela

Aura Giral, MD
Instituto de Oftalmologia y Otorrinolaringologia, Caracas, Venezuela

Nicole E. Gross, MD
LuEsther T. Mertz Retinal Research Center, Department of Ophthalmology, Manhattan Eye, Ear and Throat Hospital, New York, New York

Noga Harizman, MD
New York Eye and Ear Infirmary, New York, New York

Thomas R. Hedges III, MD
Tufts University School of Medicine, Neuro-Ophthalmology Service, New England Eye Center, Boston, Massachusetts

Bernard R. Hurley, MD
Retina Service, Wills Eye Hospital, Thomas Jefferson University, Philadelphia, Pennsylvania

Emely Z. Karam, MD
Neuro-Ophthalmology Service, Unidad Oftalmologica de Caracas, Associacion Venezolana para el Avance de la Oftalmologia, Caracas, Venezuela

Rubin W. Kim, MD
Tufts University School of Medicine, Vitreoretinal Service, New England Eye Center, Boston, Massachusetts

Christina M. Klais, MD
LuEsther T. Mertz Retinal Research Center, Department of Ophthalmology, Manhattan Eye, Ear and Throat Hospital, New York, New York

Daniel Krivoy, MD
New York Medical College, New York, New York, University of California at Los Angeles, Los Angeles, California

Jeffrey Liebmann, MD
New York Eye and Ear Infirmary, New York University, New York, New York

Nikolas London, MD
Pacific Eye Associates, California Pacific Medical Center, San Francisco, California

Miguel A. Materin, MD
Ocular Oncology Service, Wills Eye Hospital, Thomas Jefferson University, Philadelphia, Pennsylvania

Aristides J. Mendoza, MD
Retina and Vitreous Service, Clinica Oftalmológica Centro Caracas, Arevalo-Coutinho Foundation for Research in Ophthalmology, Caracas, Venezuela

Carlos E. Mendoza, MD
Tufts University School of Medicine, Neuro-Ophthalmology Service, New England Eye Center, Boston, Massachusetts

William F. Mieler, MD
Professor and Chairman, Department of Ophthalmology & Visual Science, University of Chicago, Chicago, Illinois

Michael D. Ober, MD
LuEsther T. Mertz Retinal Research Center, Department of Ophthalmology, Manhattan Eye, Ear and Throat Hospital, New York, New York

Scott C.N. Oliver, MD
Department of Ophthalmology, Jules Stein Eye Institute, University of California Los Angeles, Los Angeles, California

Lelia Adelina Paunescu, PhD
Tufts University School of Medicine, Vitreoretinal Service, New England Eye Center, Boston, Massachusetts

Andrea Porras, MD
Department of Ophthalmology, Hospital Mexico, San Jose, Costa Rica

Carl D. Regillo, MD
Retina Service, Wills Eye Hospital, Thomas Jefferson University, Philadelphia, Pennsylvania

Richard B. Rosen, MD, FACS, FASRS, CRA
Director of Ophthalmic Research, New York Eye and Ear Infirmary, New York, New York, Department of Clinical Ophthalmology, New York Medical College, Valhalla, New York, Department of Applied Optics, University of Kent, Canterbury, United Kingdom

Philip Rosenfeld, MD
Retina Service, Bascom Palmer Eye Institute, University of Miami Miller School of Medicine, Miami, Florida

Juan G. Sanchez, MD
Retina and Vitreous Service, Clinica Oftalmológica Centro Caracas, Arevalo-Coutinho Foundation for Research in Ophthalmology, Caracas, Venezuela

Stephen G. Schwartz, MD
Bascom Palmer Eye Institute, University of Miami Miller School of Medicine, Naples, Florida

Steven D. Schwartz, MD
Retina Service, Department of Ophthalmology, Jules Stein Eye Institute, University of California Los Angeles, Los Angeles, California

Carol L. Shields, MD
Ocular Oncology Service, Wills Eye Hospital, Thomas Jefferson University, Philadelphia, Pennsylvania

Jerry A. Shields, MD
Ocular Oncology Service, Wills Eye Hospital, Thomas Jefferson University, Philadelphia, Pennsylvania

Jason S. Slakter, MD
LuEsther T. Mertz Retinal Research Center, Manhattan Eye, Ear and Throat Hospital, Department of Ophthalmology, New York, New York

Richard F. Spaide, MD
LuEsther T. Mertz Retinal Research Center, Manhattan Eye, Ear and Throat Hospital, Department of Ophthalmology, New York, New York

Celso Tello, MD
New York Medical College, New York, New York

Anil Vedula, MD
Bascom Palmer Eye Institute, University of Miami Miller School of Medicine, Miami, Florida

Lihteh Wu, MD
Retina Service, Instituto de Cirugia Ocular, San Jose, Costa Rica

Lawrence A. Yannuzzi, MD
Department of Ophthalmology, Columbia University School of Medicine, Surgeon Director, Manhattan Eye, Ear, and Throat Hospital, Vitreous Retina Macula Consultants of New York, New York, New York

David G. Zeballos, MD
Retina and Vitreous Service, Clinica Oftalmológica Centro Caracas, Arevalo-Coutinho Foundation for Research in Ophthalmology, Caracas, Venezuela

Part I
Fluorescein and Indocyanine Green Angiography

1
Retinal Photography and Angiography via Film and Digital Imaging Techniques

Thomas M. Clark

In ophthalmic photography little else is as true as the phrase, "One picture is worth a thousand words." Ophthalmic photography has held a place of importance in ophthalmology since its beginning in 1886 when Jackman and Webster[1] produced the first published human fundus photographs. These images were able to show a visible optic nerve, but little vessel detail due to a large central light reflex artifact from the cornea. Prior to this time clinicians would rely solely on notes and hand-drawn illustrations to depict the changing condition of their patients' eyes. These visual notes and descriptions were very useful, but took time and were only as good as the artistic skills of the physician creating them.

As ophthalmic knowledge grew, artists were employed to illustrate, in great detail, every aspect of human ocular anatomy as well as many physiologic and pathologic changes. This laborious method worked well for texts used in teaching about the eye, but did little to aid the physician in treating his patients on a daily basis. What was needed was a quick and more detailed method of illustrating the eye. Though Jackman and Webster's initial images did little to aid in accurately illustrating the ocular fundus, they demonstrated that it could be done.

In 1899, a physician by the name of Frederick Dimmer demonstrated high-quality in vivo human fundus images.[2] Later, in 1907, Dimmer[3] published his images and described the technique and apparatus necessary to accomplish them. In 1921, Dimmer[4] published an ophthalmic textbook utilizing this revolutionary new method of illustrating in vivo the human ocular fundus. In 1927, Dimmer's[5] images were finally published in the first photographically illustrated ophthalmic atlas, and the discipline of fundus photography truly was born.

Along with this new ability to image the eye came a new set of problems of how to get clear, sharp pictures. This chapter addresses these problems in today's terms, and provides a clear, step-by-step method of conducting a successful photo session and producing good fundus images, whether they be color fundus or angiographic. This chapter is intended for physicians and office staff who have little or no experience taking ophthalmic pictures.

Chapter Organization

We begin by looking at patient management issues that are common to most types of imaging devices. We cover common color fundus protocols, the angiographic dyes used, some descriptive terminology, the circulatory characteristics and phases of angiography, and several angiographic protocols.

The imaging devices covered in this chapter are divided into two basic groups. The first group is based on conventional camera systems that use an eyepiece to view and focus the live ocular fundus and film or video to record the images. The second group utilizes a video screen to view and focus the live ocular fundus and a video/frame capture system to record the images, typically into a computer. In this chapter, for the sake of clarity, the terms *camera* and *imaging device* are used interchangeably.

Next, we delve into the operational differences of these systems and look at aspects of image quality, such as image clarity and how to achieve it, and artifacts and how to avoid them. We follow this with a look at the methods necessary for producing hardcopy images for a physician's review, and finally we address methods and procedures of maintaining photographic images and image data files. With the chapter organized in this manner, readers can go to those areas that apply to their particular situation.

Common Areas

Determine Diagnosis

The first question that must be asked is, Why are these images to be taken? Are they for documentation of the patient's current condition, or are they needed to answer diagnostic questions as well? It is important to have a clear idea of why the clinician wants the photographs so that the appropriate camera can be used. Often the best way to answer these questions is to use a photographic request form filled out by the referring physician. It should include the patient's name and basic

information, diagnosis, the reason for the photographs, and a basic diagram of the eye on which the referring physician can mark the area of interest. It is also a good idea to design the form so that the patient's name and basic information can be photographed on the first frame if a film camera is being used. This allows for easy identification of patients when more than one patient is photographed on the same roll of film.

Figure 1.1 is an example of a photographic request form for a patient with diabetes, which could indicate that the first images to be taken should be color fundus images to document the current condition of the patient's eye. However, the referring physician may have also sent the patient for photos to determine the extent of neovascularization or whether there is macular edema, which could indicate that the clinician is primarily concerned with the right eye. In this case color photographs and a fluorescein angiogram are called for, and a fundus camera or imaging device equipped with the proper filters to perform angiography is the camera of choice. A close review of Figure 1.1 shows how all of these questions can be answered with one simple form.

Patient Management

It is necessary to ensure that the patient's eye is properly dilated, as adequate dilation is imperative to get clear images. For most fundus cameras, a pupil dilated to 6 mm is typically adequate, but a rule of thumb is that the larger the dilation, the better the picture quality, particularly if the peripheral fundus is to be imaged. At times this may not be possible due to previous surgery or acute glaucoma. Also it is not advisable to dilate the eye in the presence of an iris clip intraocular lens (IOL). In this instance a nonmydriatic camera could be used, although this camera is primarily used for color photography and is not suited for an angiographic procedure. If angiography is required, a scanning laser ophthalmoscope (SLO), such as the Heidelberg retinal angiograph (HRA)[6] can be used to effectively image poorly dilated patients. This system produces monochromatic images suited for angiography and monochromatic fundus photography, but full-color fundus photography is not possible. In this chapter it is assumed that the patient can safely be dilated.

A common course of dilation for an adult is to use 1% tropicamide (Mydriacyl) and 2.5% to 10% phenylephrine (Neo-Synephrine). A useful protocol is one drop of each solution in each eye at time 0:00. If after 10 minutes adequate dilation has not been achieved, a second set of drops could be placed in the eyes. At times a third set of drops may be necessary, particularly in a very dark-eyed patient, in the presence of an ocular inflammatory disease, in an individual on glaucoma medication, or after cataract surgery. Often a physician can perform a fundus exam on a minimally dilated patient; however, it is best to re-drop the patient until a suitable dilation is achieved, provided that there are no contraindications to doing so.

While the patient is dilating, it is a good time to prepare the camera by cleaning and setting it to a neutral state. Fundus cameras when possible should adapt to the patient's height rather than the patient adapting to the camera. To accomplish this, the camera table and lens should be set for the median height position and all other settings be placed at their zero or neutral position prior to the patient's sitting down. If the camera is left in an extreme position from the previous patient, an inexperience photographer can waste valuable time trying to adapt the patient to an inappropriately positioned camera.

The chin rest and table should then be cleaned and disinfected. It is also necessary to ensure that the camera lens is clean and free of debris such as dust, smudges from noses or fingers, and teardrops. Figure 1.2 is an example of a lens prior to cleaning that was contaminated by a sneeze, and the resulting image of an incomplete attempt at cleaning the lens. Check with the camera manufacturer for the recommended solutions and techniques for cleaning the lenses of the camera or imaging device. As a suggestion, manufacturers of today's liquid-crystal display (LCD) monitors have started recommending a two-part optical quality cleaning system consisting of one pad lightly moistened with a cleaner and a second dry pad that is used to buff the screen. These cleaning pads also work well with many of today's fundus camera lens. It is imperative to first blow off any debris that may have accumulated on the lens, to avoid scratching it, and not to touch the part of the pad used on the lens surface. Powder-free examination gloves can help prevent the transfer of skin oils to these pads. Remember to always check the cleanliness of the lens prior to photography with the lens set in the anterior position and a light blank card in front of the lens. This is also an opportune time to set the eyepiece, which is discussed in greater detail later in the chapter.

Once the camera has been prepared and before the patient is fully dilated, it is a good idea to explain to the patient what procedures are going to be done. In the example mentioned above, the patient should be informed that color photographs will be taken of the eyes. It should be explained that there will be several bright flashes, but that it is perfectly safe with no lasting effect. The patient should be instructed to keep his or her eyes wide open, to ensure a clear picture. If the patient is to have an angiogram, as is our example, the procedure should be explained and the possible complications discussed. Do not assume that someone else has asked the proper questions to determine if there are contraindications to having the angiographic procedure, such as pregnancy or known allergies to the dyes. In the case of an allergic reaction the physician may determine that the procedure can continue with premedication. Often, 25 to 50 mg of diphenhydramine hydrochloride (Benadryl)[7] is used for a mild allergic reaction or 5 to 10 mg of prochlorperazine/maleate (Compazine)[8] is used if severe nausea has been experienced during a previous procedure. In either case it is the responsibility of the attending physician to make the determination.

Once the procedures have been explained, the patient should be asked if he or she has any questions, and the questions should be answered to the patient's satisfaction. Often an

Do not write in this space

Ophthalmic Photography, Fluorescein & ICG Angiography Request Form

Patient name: **Jonathan Brown**

Clinic number: **0123456** Date of Request: **11/30/2003**

Photo I.D. number: **12345 H** Requesting Physician: **Dr. Smith**

Clinic where photographs are to be stored: Hospital (Campus) Teach File

Indications: **Diabetic** VA OD: VA OS: FA Inj. Attemps

Diagnosis: **NVE/DME** Photog. Comments

Fundus Photographs:

(Color Photographs:) Stereo Disc 20 degree (30-35 degree) 55-60 degree

(**Fluorescein** Angiography) Film / (Digital) > (**OD**) **/ OS < ICG** Angiography

OCT OD / OS

7 Fields
O U

Circle Areas of Interest

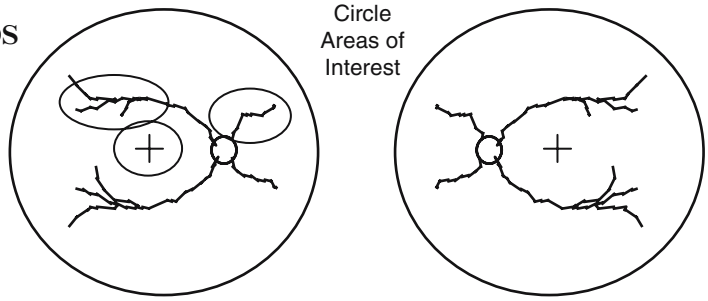

- ☐ 190.6 Malignant Mel.
- ☐ 362.16 Ret. Neov. NOS
- ☐ 362.41 Atypical CSR
- ☐ 362.42 SerDetach of RPE
- ☐ 362.43 Heme Det of RPE
- ☐ 362.52 Exudative
- ☐ 362.81 Retinal Hemorrhage
- ☐ 363.15 AMPPE
- ☐ 363.20 ChorioRet / Post. Uveitis / Serpig. ChorioRet.

Area of Interest:

Slit Lamp Photography:

Tissue of interest: Lids Conjunctiva Iris Orbit
Angle Epithelium Stroma Endothelium

Indicate Areas of Interest

External Photographs: Film / Digital **Protocol > Thyroid / Dermatochalasis / Ptosis**

Magnification: OD only OS only 2 Eyes OU - open / closed / below Full Face Side

tc 9/16/03

FIG. 1.1. A photo request form for a diabetic patient in which all pertinent information is communicated from the physician to the photographer.

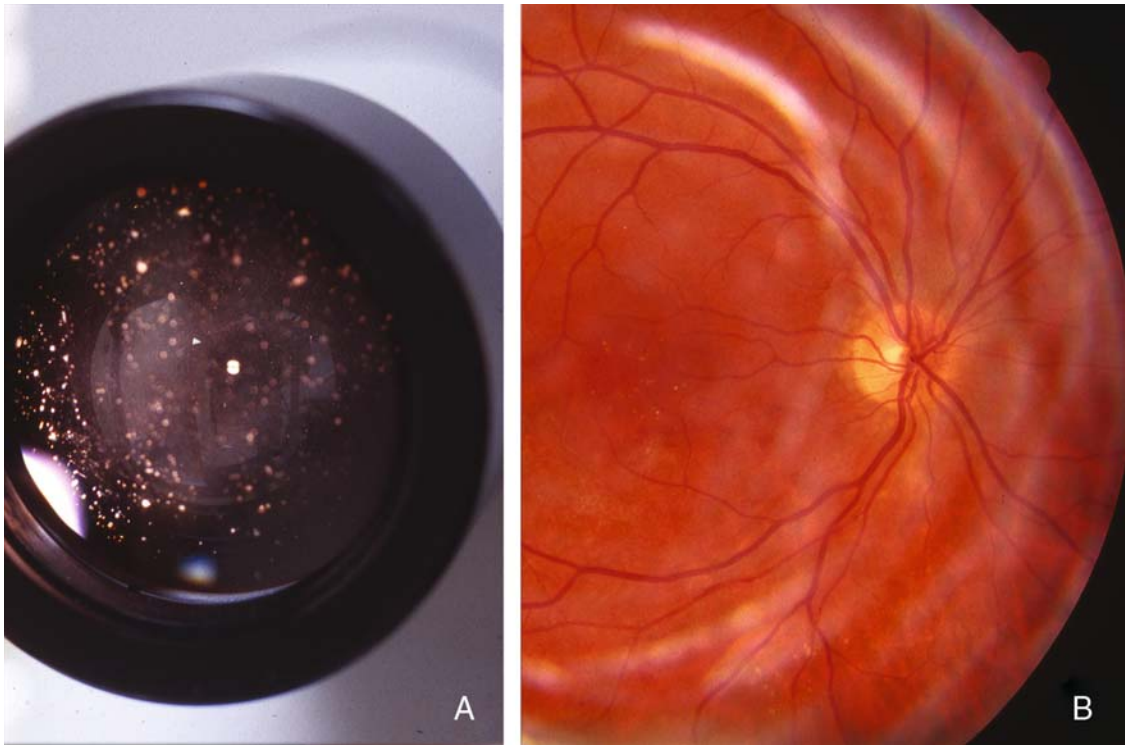

FIG. 1.2. (A) The front objective lens contaminated by the sneeze of a patient. (B) A partially cleaned lens that has been fogged by the photographer's breath to determine if the lens is in fact clean enough for photography. This lens would require additional attention.

informed consent form is filled out, and the patient's signature is required along with that of a witness. Even after this has been done, it is still good practice to explain the procedure to the patient as it is happening, all the while giving the patient positive reinforcement, thus making the patient a member of the imaging team and making the patient partly responsible for the quality of the pictures by maintaining a clear optical pathway free of eyelashes and blinks.

It is important that the patient be comfortable while sitting at the fundus camera. All imaging systems have their strengths and weaknesses in the area of ergonomics for the patient and the photographer, and a usable compromise must be found. An adjustable-height cushioned chair with back support is recommended for both the patient and the photographer. Particular attention should be paid to the patient's posture so that he or she is sitting up as straight as possible and not leaning too far forward. Photographic procedures can last anywhere from 5 to 30 minutes or longer, and it is important that the patient be comfortable and not unnecessarily fatigued in order to elicit full cooperation. This subject of posture applies to the photographer as well as it may be only one of many procedures performed in a single day. Posture and fatigue can be one of the greatest challenges for the photographer. Figure 1.3 shows a patient who is hunched over a bit too much and perhaps with a chin adjustment a little too low, while the photographer appears to be stretching up to fit the camera. If a lengthy procedure was to be performed, both the patient and the photographer would most likely become fatigued after only a short while.

The patient's height determines the position of the camera system. For a tall patient the seat is in a lower position, the headrest in a higher position, and the chin rest adjusted so that the patient's eye is at the level of the camera lens. The objective here is to keep the patient's back straight and allow for a comfortable working position for the photographer. For a short patient the seat is in a higher position, the headrest in a lower position, and the chin rest adjusted so that the patient's eyes are level with the camera lens, again keeping the patient's back straight. Unfortunately, some patients are harder to accommodate due to a large stomach or chest. Most camera-based systems also have a pivot point that extends toward the patient. This is a necessary design feature to maintain proper optical alignment as the camera is pivoted side to side. This pivot point can be seen in Figure 1.3, marked by a black knob just in front of the patient's right hand. In the case of a patient with a large chest, it may be necessary to drop the camera down a bit lower than normal so that the patient can lean forward onto the chin rest and headrest. Be sensitive to the added strain placed on the patient in this extended position.

If a child is to be photographed, often it is necessary to have him sit on a booster seat or have him kneel. An infant can be placed on an adjustable-height table and positioned horizontally at the proper level for photography. In either case a parent's gentle hand can help keep the child's head in position.

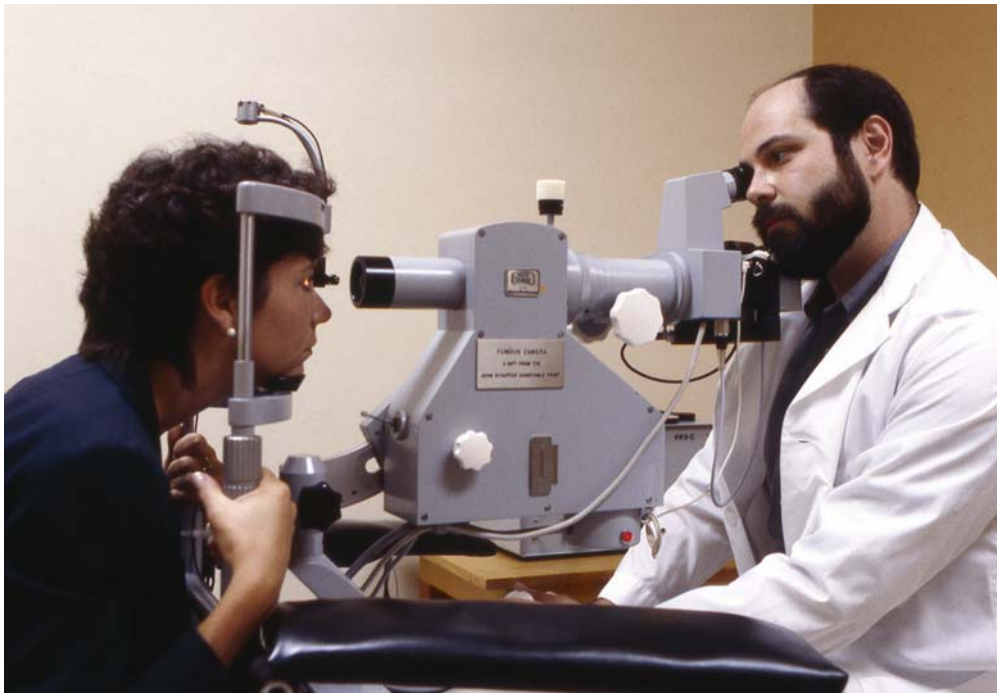

FIG. 1.3. An improperly positioned patient and photographer. The patient is bent over too far with her neck completely extended, which promotes fatigue. The photographer appears to be stretching up to the eyepiece with fully extended arms, which will quickly produce fatigue in the upper back and neck.

Proper head orientation is a critical element of getting good images, particularly over extended time periods. It is very important to ensure the head is in a proper upright position and not tilted or turned to either side. This misalignment can add to the difficulties for the photographer when switching from eye to eye and for the physician when trying to view the resulting stereo images. This difficulty is amplified if sequential images are being compared over a time period of several years. The issue of stereo photography is addressed later in this chapter.

It is very important to communicate with patients during the photography procedure. Let them know if they are doing what is needed. Let them know if they are looking in the proper direction or in an incorrect direction. Consider them an active member of the imaging team. By providing them with positive reinforcement and encouragement, they will be more cooperative and less apprehensive.

Just as the procedure was fully explained prior to starting the photography, is also necessary to remind patients of what to expect once the procedure is completed and they have left the office. If patients have had a fluorescein angiogram and there were no complications, they should be reminded that their skin might be slightly yellow for several hours and that their urine will be a bright yellow for up to 2 days. They should be assured that this yellow coloring is perfectly normal and nothing to worry about. Discuss the color issue in terms patients are familiar with, such as, “The fluorescein is simply a very concentrated yellow dye much like food coloring. ”

If there were complications during the procedure, it is important to discuss them with patients. If an extravasation has occurred, patients should be informed that if their arm and particularly the injection site becomes hot, red, and tender, they should seek medical attention. It should be explained that there is a possibility of the skin blistering and sloughing off at the injection site, but that this is a rare occurrence. The most common form of treatment for pain is the immediate application of an ice pack to minimize the discomfort. Once the stinging goes away, a warm compress can be applied to the injection site to help the body dissipate the dye. Several other serious complications should be discussed, but it should be made clear that they are relatively rare and should be treated by a doctor or other medically trained personnel. These other complications are discussed later (see Common Angiographic Dyes).

Common Color Protocols

Three common photographic protocols are used to image the ocular fundus in color. Most imaging devices have a normal field of view of approximately 30 degrees, with some cameras offering fields of view of as much as 60 degrees or as little as 10 degrees. The human eye, which is a sphere of 360 degrees, has approximately 150 to 180 degrees that can be readily photographed with very good dilation. In order to properly cover pathology that extends up to and a little beyond the main arcades, it is useful to employ a standard photographic protocol to ensure that all areas of importance are covered. The three protocols that are discussed here are based on specifications developed in

the middle and late 1970s and early 1980s by the Fundus Photography Reading Center (FPRC) at the University of Wisconsin, in Madison.[9] They can be reviewed with other protocols and tutorials at the following Web site: http://eyephoto.ophth.wisc.edu/.

Two- and Modified Three-Field Protocol

Several photographic protocols have been developed for use in studies over the years to illustrate problems of macular degeneration and diabetic retinopathy and edema. One such stereo macular protocol specifies two field definitions in which one set of stereo images is centered on the fovea and another set is centered on the optic nerve, whereas a more recent three-field stereo protocol requires that the macula be visible in each of three views across the posterior pole. Figure 1.4 shows an example of the modified three-standard-field protocol with the landmarks and meridians that both protocols use.[9]

Stereo Imaging

Since humans use binocular vision to gather three-dimensional details of their world, most protocols rely on a technique of stereo imaging in which the camera is moved slightly from one side of the pupil to the other side in order to get a pair of images from slightly different points of view. When done properly, the left stereo image can have a slightly darker left side and the right stereo image can have a slightly darker right side. This is due to the blockage of light from the pupil in that area. If these images are viewed in the proper orientation, a three-dimensional stereo view can be appreciated, which can aid in the determination of a diagnosis. If imaging the posterior pole, a simple side-to-side movement works well (Fig. 1.5A). However, when imaging the peripheral superior and inferior arcades, a diagonal side-to-side and front-to-back movement may be necessary to accommodate the change in the depth of focus (Fig. 1.5B). Due to space limitations, a discussion of the principles of stereo fundus photography has been greatly condensed. Saine and Tyler[10] devote the third chapter in their excellent book, *Ophthalmic Photography*, second edition, to this subject.

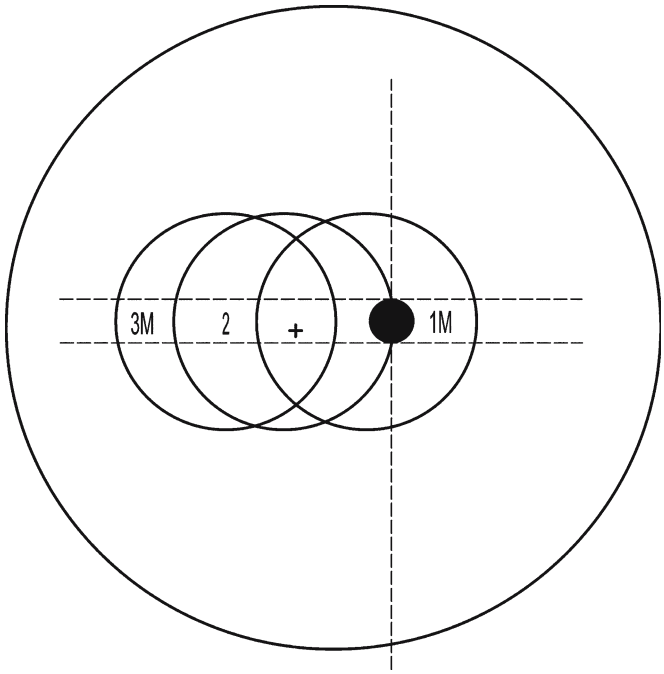

FIG. 1.4. The modified three-standard-field protocol developed by the Fundus Photography Reading Center (Madison, WI), for the use in studies of macular degeneration.

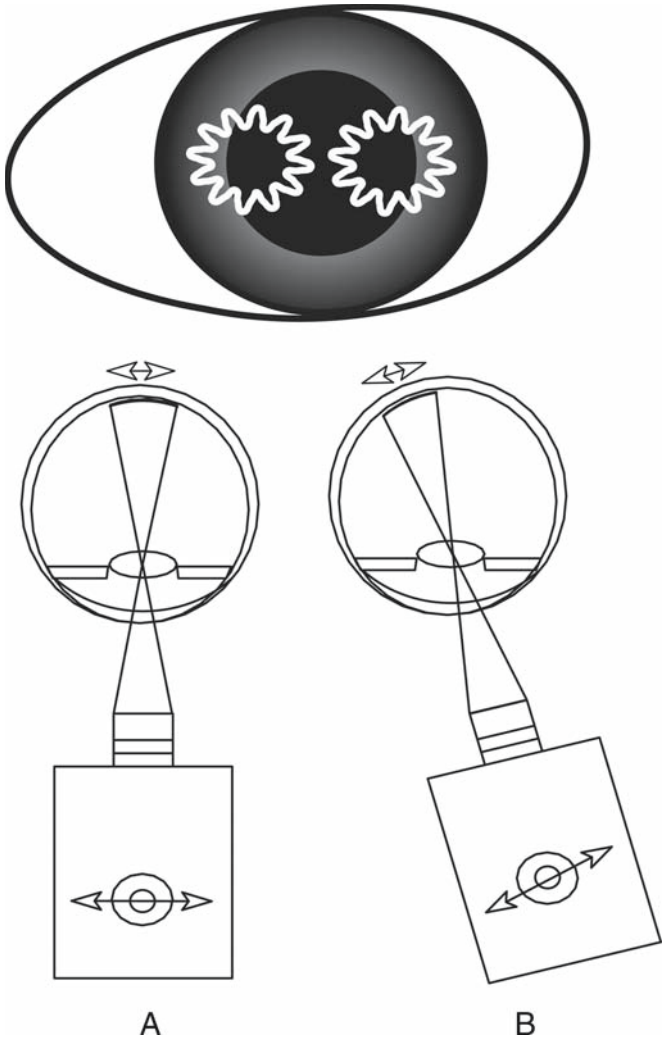

FIG. 1.5. (A) Just one of several possible techniques used to produce a stereo pair. (B) A modification of the straight side-to-side technique used to accommodate the increased depth of focus and curvature of the orbit. It should be noted that some cameras have means to correct for this curvature.

Modified Seven-Standard-Field Color Fundus Photography Protocol

If the diagnosis is proliferative diabetic retinopathy (PDR), a seven-field protocol should be used. This enables good coverage of the posterior pole and the superior and inferior arcades. Figure 1.6 shows the placement of these fields, and it can be appreciated that when using a 30- to 40-degree camera, the area of coverage could extend to 90 degrees diagonally side to side. Note that the alignment of the fields (one, two, and three) on the central horizontal meridian can cover about 60 degrees, and the fields on either side of the meridian running vertically through the optic nerve and tangent to the top and bottom of the optic nerve in the superior and inferior arcades account for approximately an additional 45 degrees, or about 100 degrees on a predominantly horizontal diagonal line. This protocol is a modified seven-field ETDRS protocol of the 1980s and is derived from the landmark Early Treatment Diabetic Retinopathy Study.[9]

Nine-Standard-Field Protocol for Fundus Photography

Another very good protocol for peripheral diseases is the cytomegalovirus retinitis (CMVR)/AIDS nine-standard-field protocol for fundus photography,[9] useful for AIDS retinopathy, peripheral retinitis (PVR), and uveitis diseases. This protocol relies on wide-angle cameras such as the Canon 60-degree camera (Canon USA), or at least the 50-degree setting on one of the other manufactured cameras. The goal is to achieve maximum coverage of the peripheral fields, which may be of greatest importance. Peripheral CMV retinitis, acute retinal necrosis with peripheral nonperfusion, lattice degeneration, peripheral vessel leakage, retinitis pigmentosa, and scleral buckles for retinal detachments are best illustrated with this nine-field protocol. Similar to the seven-field protocol, three fields of view are taken on the horizontal meridian, but are spaced to maximize coverage. In addition, three fields of view are taken of both the superior and inferior arcades, which are designed to include superior and inferior to the fovea, and four other views generally center on each of the vortex veins. Figure 1.7 illustrates this protocol.[9]

Other Protocols

In addition to the three previously described protocols there are also protocols for melanomas and branch vein occlusions that concentrate on overlapping fields in the involved quadrants of the eye. Many of these protocols have been defined by the FPRC over the years and are in wide use throughout the world. Several more protocol descriptions for macula degeneration, ocular hypertension, and many related study sites can be found at the Fundus Photography Reading Center Web site: http://eyephoto.ophth.wisc.edu/.[9]

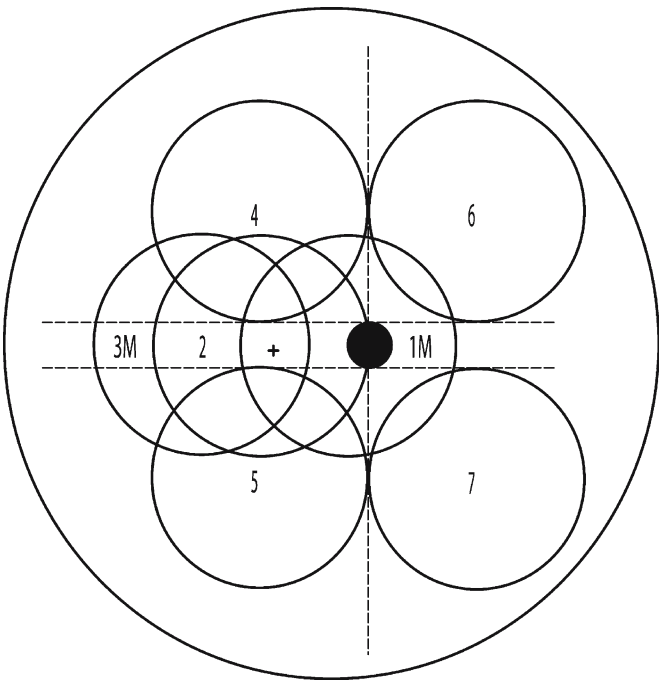

FIG. 1.6. The modified seven-standard-field color fundus photography protocol developed by the Fundus Photography Reading Center (Madison, WI), for to use in diabetic studies.

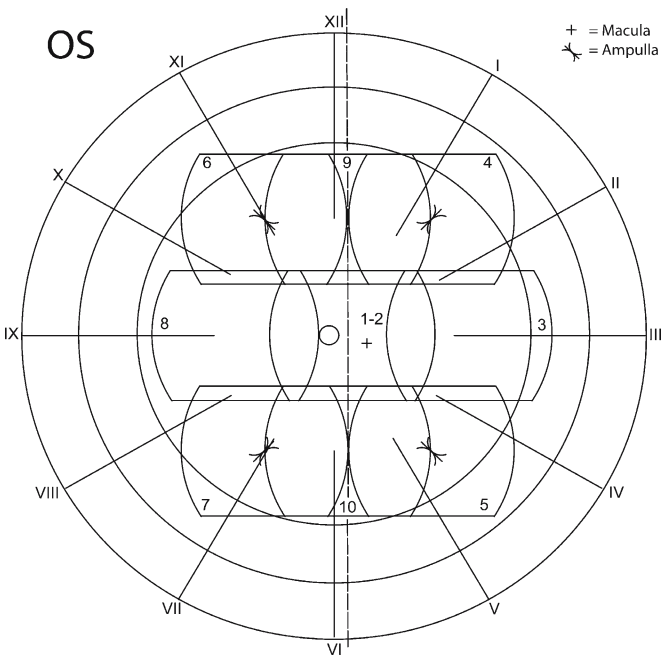

FIG. 1.7. The nine-standard-field protocol for fundus photography, developed by the Fundus Photography Reading Center (Madison, WI). This protocol is useful when photographing a patient with cytomegalovirus (CMV) peripheral retinitis, uveitis, or peripheral retinitis (PVR).

Common Angiographic Dyes

Two angiographic dyes are currently used in ophthalmic photography. This section presents a brief description of their characteristics, concentrations, and possible adverse reactions; discusses how to prepare them for use; and presents some descriptive terms commonly used when discussing the appearance of the dye during angiography. This section also discusses the six phases of fluorescein sodium angiography (FSA) and indocyanine green angiography (ICGA).

Fluorescein sodium (FS) is used to image the retinal vasculature of the eye. It is a man-made molecule synthesized from the petroleum derivatives phthalic anhydride and resorcinol.[11,12] Even in small quantities, fluorescein sodium is a highly fluorescent dye which has a maximum absorbance of blue-green light and fluorescent excitation in the wavelengths between 485 and 500 nm. The maximum fluorescent emission of this molecule is in the yellow-green 520- to 530-nm range.[13] A dosage of 500 mg in either a 2 mL (25%) or 5 mL (10%) solution with a pH of 8.5 is normal for an adult of average build. This dosage is based on the weight of the individual and can be aliquoted down for small adults or children. When the dye is injected into the bloodstream, 80% of the dye molecules are bound to the blood proteins, allowing the remaining 20% to fluoresce when exposed to the appropriate wavelength of light. These free fluorescein dye molecules are small and easily leak from the fenestrated vessels of the choroid, but the fluorescence is blocked by the tight junctions of the retinal pigment epithelium (RPE). The retinal vasculature, on the other hand, contains vessels with tight junctures and does not allow the dye to easily leak, resulting in well-defined arteries, veins, and capillaries. Fluorescein sodium is metabolized by the kidneys, is excreted through the urine, and clears the system within 24 to 48 hours. Often, a faint yellow blush can be seen in the patient's skin for several hours following angiography. It is important to inform patients of these possible color side effects and to assure them that it is perfectly normal and will pass. Due to the presence of dye in the blood, it is advised that the patient schedule blood work that may be influenced by this dye marker prior to or 2 days after angiography. A word of caution should be given to nursing mothers, as the dye is excreted in breast milk.[14]

Angiography is an invasive procedure in which complications and adverse reactions to the dye are infrequent, but range from mild to severe. Mild reactions include transient nausea and vomiting and do not require medical treatment. Extravasation, on the other hand, can start as a mild complication that is typically managed with a cold compress followed by a warm compress after the pain subsides. Depending on the volume of dye, extravasation can be a very painful complication due to the high pH of the dye. A subcutaneous granuloma as well as toxic neuritis can also develop. Extravasations can become a serious complication if skin sloughing or local necrosis occurs. In these instances medical intervention is necessary. Depending on the care taken to find a viable vein, the skill level of the clinician injecting the dye, and the patient management experience of the photographer, these problems should be infrequent and effect only about 3% to 10% of patients.

More severe reactions are rare, affecting only about 1% of patients, and they require medical attention. These reactions include pruritus (itching), urticaria, (hives), laryngeal edema (swelling of the larynx), bronchospasm (difficulty breathing), syncope (passing out) and anaphylaxis (allergic reaction requiring medicine).

By far the rarest (0.02%) and most severe reactions are myocardial infarction and cardiac arrest (heart attack and heart stoppage). Due to their severity, it is necessary that a physician be available during the angiography procedure and that a proper emergency reaction kit be available to manage these situations.

Indocyanine green (ICG) is the second type of dye used in ophthalmic angiography. It is a tricarbocyanine dye used to image primarily the choroidal vasculature of the eye. This synthetic dye was first produced in the 1950s by Eastman Kodak for the manufacturer of infrared photographic materials. It was one of several dyes offered to Dr. Irwin Fox of the Mayo Clinic after he successfully treated a patient who was an officer at Eastman Kodak.[15,16] The ICG dye is a relatively large and complex molecule that fluoresces about 1/25th as well as FS and cannot be easily imaged on standard film systems. Electronic imaging is necessary in order to amplify the weak fluorescence given off by the dye. ICG has a maximum absorbance of infrared light in the 800- to 810-nm range and peak fluorescent emission at 835 nm. When injected, 98% of the ICG dye is absorbed by the plasma proteins. Therefore, it does not pass easily from the choriocapillaris or the retinal vessels, which allows for good delineation of the choroidal vessels, in marked contrast to the fluorescein sodium dye. In the United States, ICG comes packaged in a vial as a 25-mg freeze-dried crystal with a pH of 6.0. It is designed to be rehydrated with a buffered sterile saline solution provided by the manufacturer, with a 5.5 to 6.5 pH. Once reconstituted, the dye is very unstable and must be used within a 10-hour time window.[17] Typical dosages can vary from 8.5 to 50 mg depending on the procedure to be performed and the imaging equipment to be used.

An example of a variation of the manufacturer's designed usage is performing a combined FS/ICG angiogram using an SLO, in which the freeze-dried crystal is mixed with FS dye instead of the provided saline solution. This is done so that a true simultaneous FS and ICG angiogram can be performed.[18] Another reason to deviate from the recommended mixture of dye when using a SLO is the inherent purity of the excitation light source. When imaging ICG dye with a conventional camera system, the excitation wavelength is just one of a broad spectrum of wavelengths given off by the xenon flash tube resulting in large amounts of nonessential extraneous light entering the eye. The SLO, on the other hand, emits a single tuned wavelength of light to excite the dye molecules, allowing for a lower overall quantity of photons to enter the eye. The single wavelength of light can also be increased to a level that allows for a lower dosage of ICG to be used, while

giving equivalent results to flash systems with less overall intensity and discomfort. We will look at other dosages used with various imaging devices later in this chapter.

The ICG dye differs from fluorescein sodium in a number of other ways. In addition to the fluorescent properties mentioned above, ICG dye is not metabolized after injection, but is filtered out by the liver and excreted in the bile. Discoloration of the skin is also absent, but stools may be discolored from 48 to 72 hours after injection. Extravasation is not as traumatic as fluorescein sodium, because the pH is closer to that of the surrounding tissues and the incidence of skin sloughing, localized necrosis, and subcutaneous granuloma is greatly reduced.

Adverse reactions are also less prevalent with angiograms using only ICG dye. The incidence of nausea and vomiting are reduced to about 0.5%, and the incidence of moderate adverse reactions such as urticaria and syncope are on the order of 0.2%. During manufacture, sodium iodide is added to make ICG soluble in water and safe for human use. Although many people believe that sodium iodide is a major component of ICG, it is in fact less than 5.0% by volume. Even at this level caution is recommended for those patients who are at risk of allergic reaction based on prior allergic reactions to shellfish or a previous reaction to an iodide material. ICG angiography is sometimes delayed with diabetic individuals using Glucophage until an appropriate schedule of delay and reintroduction can be set up.[17] As is true with fluorescein sodium, trained personnel should be on hand, as should an emergency kit in order to manage problem situations.

Dye Preparation and Injection

It is convenient to have a standard setup for use with the angiographic dyes (Fig. 1.8). This kit should consist of syringes and straight needles, butterfly needles, a three- or four-way stopcock, alcohol wipes, gauze pads, bandages, a tourniquet, and perhaps some sterile saline for a flush. Table 1.1 lists the minimum basic angiography kit.

A word of caution should be mentioned if ICG dye is to be used. The use of heparin as an anticoagulant, to keep the line open for an extended period of time, should be avoided. High concentrations of metabolized sodium bisulfite greatly reduces the peak absorption of ICG dye and negatively effect its fluorescent properties.[17] Sodium bisulfite is also used as a preservative in many canned food products, in commercial wines, as well as in drug products, so this too may be a possible concern.

Fluorescein Sodium Only

If only fluorescein sodium is to be injected, a syringe with a straight filtering needle is used to extract the liquid dye from the ampule or vial. A straight filtering needle is replaced with a 23- or 25-gauge scalp vein needle. This setup, along with a tourniquet, gauze pad, alcohol pad, and Band-Aid, should be placed within easy reach of the clinician doing the injection. If a saline flush is to be used after the dye injection, it should be placed on one port of a stopcock with the dye placed on another port and the scalp vein needle on the appropriate third port.

The imaging device is prepared with the correct red-free filter, and red-free images are taken, after which this filter is removed and replaced with the fluorescein Exciter and Barrier filters. A red-free image is a high contrast Back & White image taken through the camera's green filter, illuminating the eye with only green light, thereby suppressing the red wavelength of light returning from the eye from reaching the film or sensor in the camera. This is a good time to again briefly review the procedure with the patient. After an appropriate vein has been identified and breached, blood is drawn

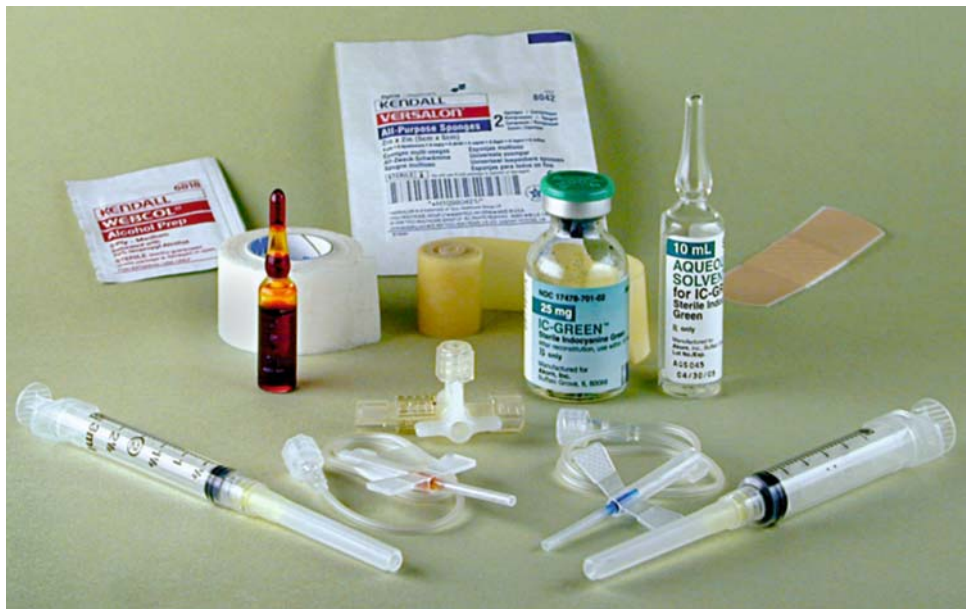

FIG. 1.8. An example of a standard injection setup consisting of different sizes of syringes, butterfly needles, a stopcock, dyes, alcohol pads, Band-Aids, gauze pad, tape, and a tourniquet. A complete list can be found in Table 1.1.

Table 1.1. Basic fluorescein and indocyanine green angiographic injection supplies.

Dyes	Fluorescein sodium 500 mg—2 mL (25%) and 5 mL (10%)
	Indocyanine green 25 mg with 10 mL buffered saline
Drugs	Benadryl 25-mg tablets for pre- and postallergy medication
	Compazine 5-mg tablets for premedication for nausea
Syringes	5-cc syringe with 20-g × 1.5-inch filtering needle
	3-cc syringe with 20-g × 1.5-inch filtering needle
	1-cc tuberculin syringe with 20-g × 1.5-inch filtering needle
Needles	20-g × 1.5-inch filtering needle
	21-g butterfly infusion set with 10-inch tubing
	23-g butterfly infusion set with 10-inch tubing
	25-g butterfly infusion set with 10-inch tubing
Stopcock	Three-port for single dye injection with a saline flush
	Four-port for double dye injection with a saline flush
Miscellaneous	Alcohol prep to clean the injection site
	Band-Aid for after the injection
	Cotton gauze sponge 2 × 2 inches to help control bleeding
	Emesis basin or double-lined trash can for nausea
	Gloves to protect the injector
	Ice pack to manage pain if extravasation occurs
	Sharps needle receptacle for contaminated needle disposal
	Tape 1-inch paper to hold down infusion set
	Tourniquet for getting veins to stand out
	Warm compress to help dissipate extravasated dye

into the tubing to ensure that the vein is patent. When the clinician, the photographer, and the patient are ready and conditions permit, the dye is injected at a rate of about 1 cc per second, after which the saline flush can follow. Valuable injection time information can be obtained if the camera timer is started at the beginning of the injection and an image is immediately taken, followed by another image taken at the end of the injection of the dye. If the injector uses keywords such as "starting" and "finished," these critical time points can be recorded without much difficulty. As the photographer continues with the predetermined angiographic protocol, the clinician removes and discards the needles, ensures that the patient is okay, and, once the bleeding has stopped, places a protective Band-Aid over the injection site. The use of a saline flush is determined by the individual institution, but is not mandatory.

Indocyanine Green Angiogram

If only ICG is to be injected, a syringe with a straight filtering needle is used to extract a predetermined amount of balanced saline, typically 2 to 5 cc, from the provided ampule. This is injected into the vial containing the ICG crystals and is gently rocked back and forth until all of the dye is dissolved. The liquid ICG dye is then drawn back into the syringe and the straight filtering needle is replaced with a 23- or 25-gauge scalp vein needle. This setup, along with a tourniquet, gauze pad, alcohol pad, and Band-Aid, is placed within easy reach of the clinician doing the injection. If a saline flush is to be used after the injection, the syringe is placed on one port of a stopcock, the dye placed on another port, and the scalp vein needle placed on an appropriate third port. The imaging device is prepared with the appropriate filters and the coordination of the injection and establishing photographs are similar as previously described for fluorescein angiography. As the photographer proceeds with the predetermined protocol the injector attends to the needs of the patient.

Sequential Fluorescein Sodium and Indocyanine Green Angiogram

Combined sequential FS and ICG angiography is performed as described above by using a four-way stopcock and deft coordination. With the imaging device set up for ICG, the injection of ICG dye starts and the establishing images, up to the early midphase images, are taken. The camera is changed to the fluorescein angiography (FA) settings, the stopcock is turned to the FS port, and the injection and photos proceed as previously described for FS only, up to the midphase photos. The camera is switched back to the ICG setup and late midphase images are taken at about 5 to 7 minutes. The camera is once again set for FA, and late-phase images are taken in the 7- to 10-minute range. The study concludes at about 15 minutes with the late-phase ICG images. An in-depth discussion of the various phases of angiography is presented later in this chapter.

Simultaneous Fluorescein Sodium and Indocyanine Green Angiogram

True simultaneous FS and ICG angiograms can be performed with a Heidelberg SLO. A syringe with a straight filtering needle is used to extract the fluorescein sodium dye from its ampule and is injected into the vial of crystallized ICG dye. The solution is gently rocked back and forth until the crystals are completely dissolved. A gentle rocking motion greatly reduces frothing of the mixed dye solution. The mixed solution is then drawn back into the syringe and the straight needle is replaced by a scalp vein needle. This setup can be used with or without a saline flush using a stopcock as previously described. The Heidelberg SLO has the ability to simultaneously project two colors of excitation light into the eye while recording the fluorescence of the two dyes with separate sensors. This arrangement gives the clinician the unique ability to appreciate both the choroidal and retinal vasculature together.[18]

Indocyanine Green Feeder Vessel

High-speed video ICG angiography is used to identify feeder vessels in the presence of occult neovascularization. The Heidelberg SLO has the ability to record individual images of the ICG choroidal transit phase at 12 frames per second (fps). Several paradigms have been devised to utilize this unique feature, and we will look at two basic methods that are currently in general use.

The first method uses a small bolus of dye injected into the arm immediately followed by a flush of the provided saline. The dye is prepared by mixing approximately 1.7 cc of the provided balanced saline with the 25-mg vial of ICG crystals. Approximately 0.8 cc of 12-mg ICG solution is drawn into two 1-cc tuberculin syringes and 8.0 cc of the balanced saline is drawn into a third 10-cc syringe. A stopcock is fitted with a scalp vein needle, and one of the tuberculin syringes contains the dye and the third syringe contains balanced saline.

The SLO is configured to record ICG fluorescence at a rate of 12 fps, with a 2-second-frame buffer. The operator initiates recording as soon as the dye is seen entering the eye and the SLO saves images 2 seconds before the operator starts the acquisition process. The syringe with 0.8 cc of dye is injected into the arm followed by a 4-cc saline flush. This small concentration of dye rapidly transits the eye and leaves low background fluorescence. Approximately 20 seconds of dye transit can be recorded each time, depending on the resolution selected and the available random access memory RAM memory installed. With pulsed doses of dye, middle and late angiographic images are usually of poorer quality, and do not add much information for identifying feeder vessels, but can provide important late-phase information.

The second method uses 5.0 cc of a 12-mg solution of ICG dye. A scalp vein needle is placed directly on the syringe and the saline flush is not used. With the SLO configured at 12 fps and a 2-second buffer, the bolus of dye is recorded as it enters the eye. All of the angiographic injection techniques covered above are presented as general guidelines and will vary slightly between institutions, based on local laws and the preference of the referring physician.

Descriptive Terms in Angiography

This section presents four descriptive terms used to discuss the appearance of angiographic images and some common angiographic protocols. The terms are *hypofluorescence, hyperfluorescence, pseudofluorescence*, and *autofluorescence*, the last two being special types of hyperfluorescence. The next section discusses the hemodynamic appearance of dye associated with the six phases of ocular angiography.

Hypofluorescence is the relative decrease of normal fluorescence of dye within the eye resulting from blockage or filling defects. An example of blockage could be due to hemorrhages or exudates. Preretinal hemorrhages (PRHs) block fluorescence both from the retinal and choroidal vasculature, whereas subretinal hemorrhages (SRHs) block the fluorescence origination from the choroid. Filling defects can be from branch vein occlusions, ischemic nonperfused areas, or capillary dropout (CDO). Figure 1.9 demonstrates both PRH and SRH in a diabetic patient, as well as CDO and nonperfusion in the periphery.

True hyperfluorescence is a relative increase of the normal fluorescence of dye within the eye due to pooling, staining, transmission defects, and leakage.

An example of pooling is central serous retinopathy (CSR), which can be seen in Figure 1.10A. Dye starts to fill the serous detachment in the early phase and progressively expands throughout the rest of the angiogram. Figure 1.10B is an example of a pigmented epithelial detachment (PED), in which the dye collects in the detached space under the pigmented epithelium evident in the mid- to late phases of the angiogram. A third example of pooling is the petaloid

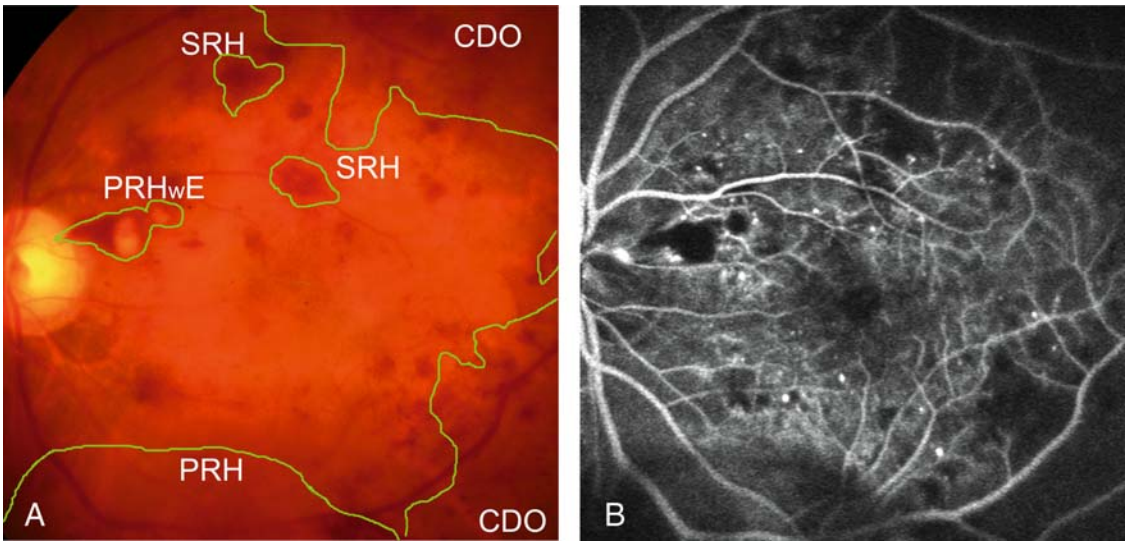

FIG. 1.9. (A) Two areas of preretinal hemorrhage (PRH). The first lies just above the retina and temporal to the disc and completely blocks fluorescence from the underlying vessels (seen in B). The second PRH is seen in the six to seven o'clock position, and is floating in the vitreous and partially blocks the fluorescence from below. Two areas of subretinal hemorrhage (SRH) demonstrate blockage of choroid fluorescence with retinal vessels visibly overlying the area of hypofluorescence (seen in B). (B) Capillary dropout can clearly be seen in the superior and inferior temporal areas of the angiogram as large areas of nonperfusion.

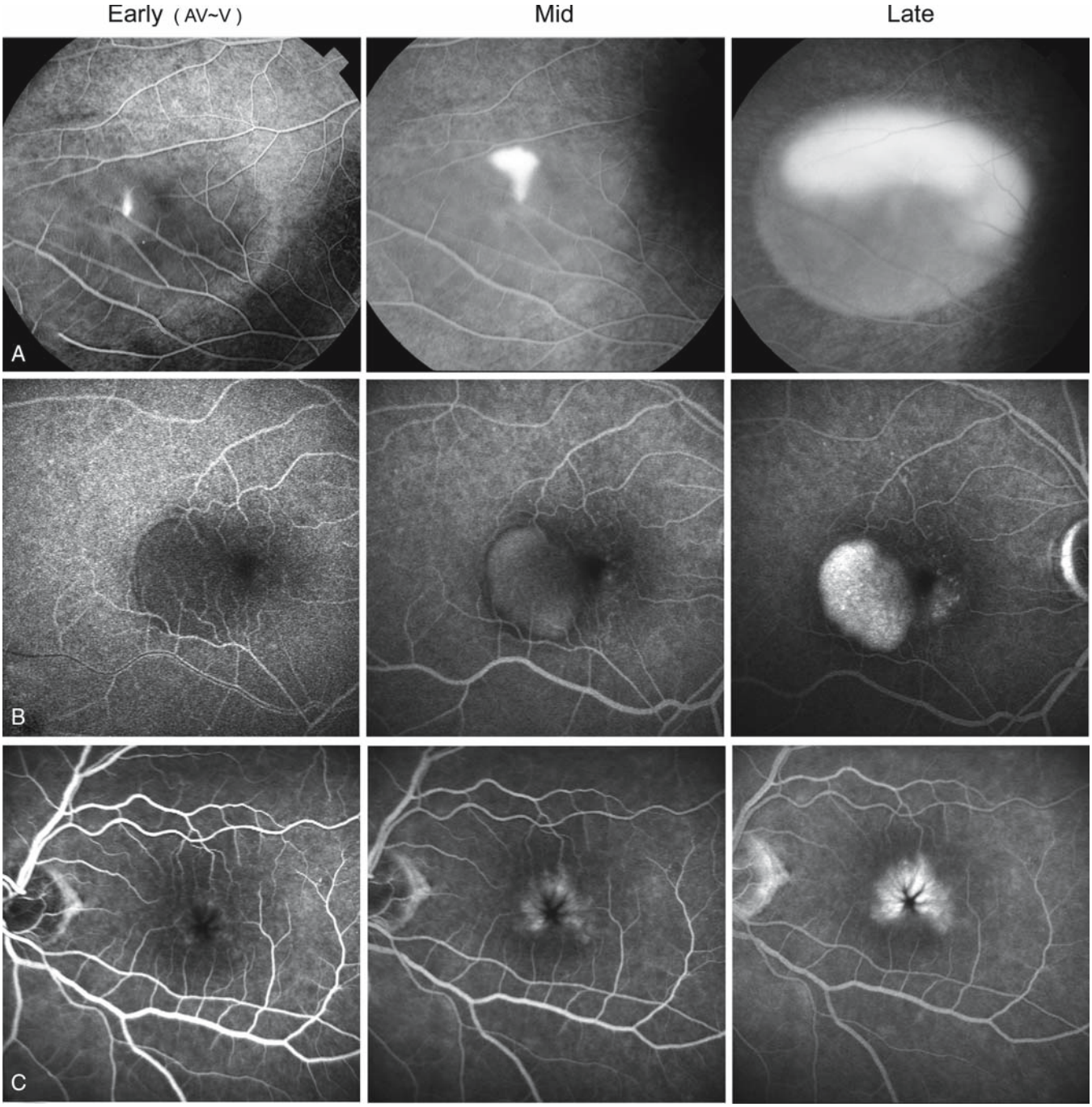

FIG. 1.10. (A) A central serous retinopathy (CSR) detachment and the enlarging pool of dye as time progresses. (B) A pigmented epithelial detachment (PED) filling with dye over time becoming more hyperfluorescent. (C) A typical petaloid appearance of CME as the cystic spaces surrounding the macula fill with dye.

appearance of cystoid macular edema (CME), in which the dye collects in cystic spaces caused by inflammation within the macula and surrounding the fovea (Fig. 1.10C). This type of hyperfluorescence is evident in the mid- to late phases of the angiogram.

Staining, the second cause of hyperfluorescence, is a result of dye leaking into surrounding ocular tissues. The diffusion of dye from diabetic macular edema or fenestrated vascular anomalies can result in perivascular staining. Drusen, the lamina cribrosa, and the rim of the optic nerve can also demonstrate a relative hyperfluorescence staining, though clinically this is considered normal (Fig. 1.11).

A third type of hyperfluorescence is from the transmission of light originating in the choriocapillaris through a break in the layer of RPE. This is called a window defect, as it enables the clinician to see the choroidal space through a nonpigmented

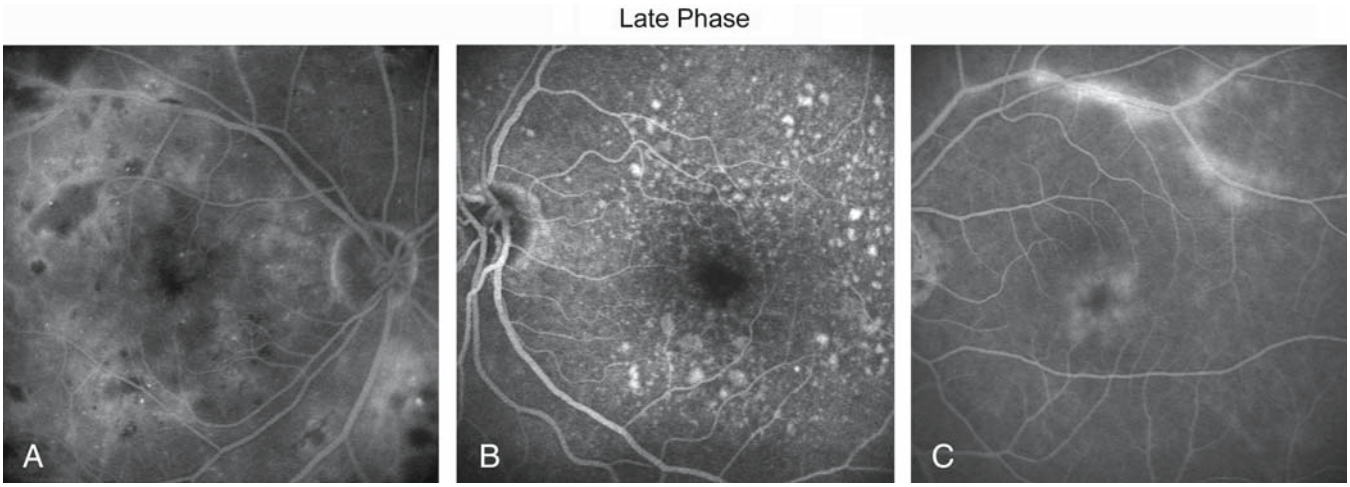

FIG. 1.11. Three late-phase angiographic images. (A) Background staining from diabetic retinopathy and of the optic nerve. (B) Staining of drusen and apparent hyperfluorescence of exudates. (C) Perivascular superotemporal staining due to weakened vascular tissue; notice the presence of cystoid macular edema.

region of the RPE. Geographic atrophy is a prime example of this type of defect in which the RPE has degenerated, providing a clear view of the choroidal vessels. Figure 1.12 demonstrates the six phases of a fluorescein angiogram in which choroidal vessels can clearly be seen in the arterial phase. The six phases of angiography are reviewed below. Note that the large diffuse area of hyperfluorescence in the posterior pole is from staining of the sclera.

The last true type of hyperfluorescence to be discussed is from dye leakage. Figure 1.13 is an example of subretinal neovascularization (SRNV). In this case, dye is used to delineate new vessel growth inside the eye, particularly in the posterior pole, from which blood or serous fluid has leaked.

Pseudofluorescence is a special type of apparent hyperfluorescence. Figure 1.14A shows examples of poorly matched exciter and barrier filters and filter sets worn out over time. Figure 1.14B demonstrates a ghost image in which light passes through a set of filters to the film or sensor forming an image, even though dye is not present in the eye.

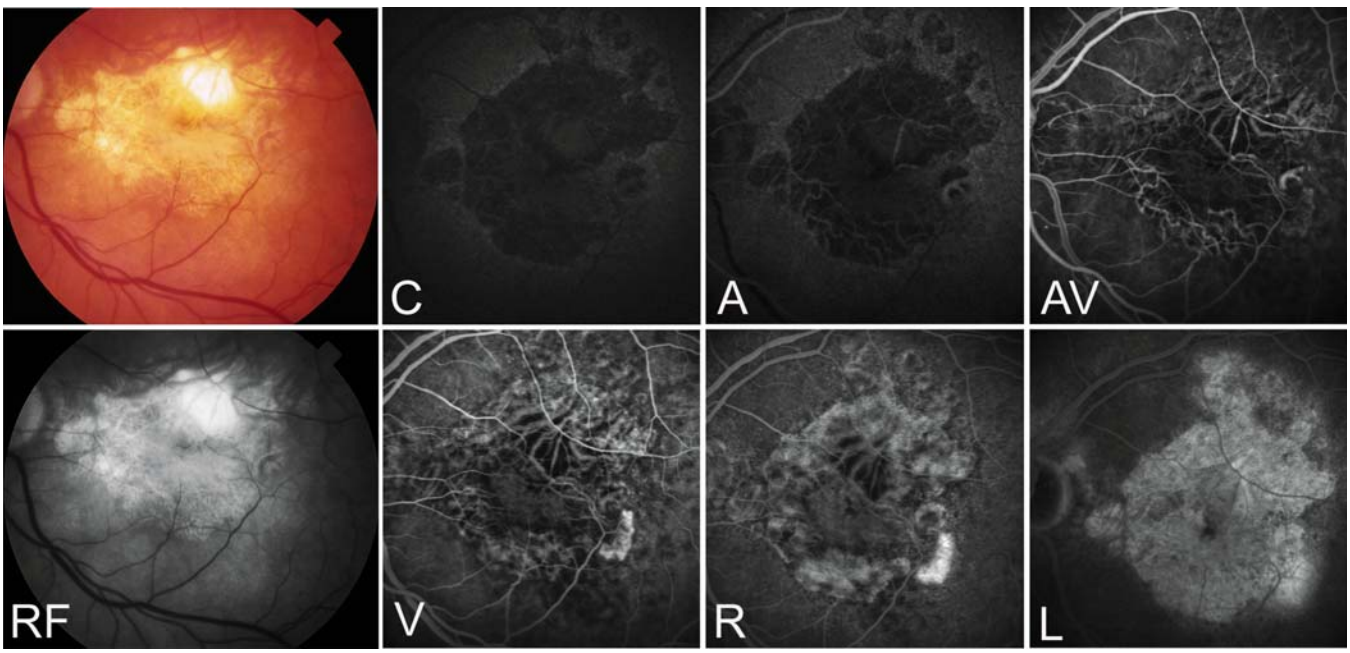

FIG. 1.12. Geographic atrophy and the six phases of fluorescein angiography. A light blush of dye can be seen in the choroidal (C) phase. Choroidal vessels can clearly be seen in the arterial (A) phase. A small area of neovascularization can be seen starting to develop in the arteriovenous (AV) phase. The area of neovascularization is well defined in the venous (V) phase. Staining of the sclera is evident in the recirculation (R) phase as is leakage of dye from the neovascular membrane. The late (L) phase demonstrates diffuse staining of the posterior whole and a slightly more hyperfluorescent staining of the tissue surrounding the neovascular membrane. RF, red-free photograph.

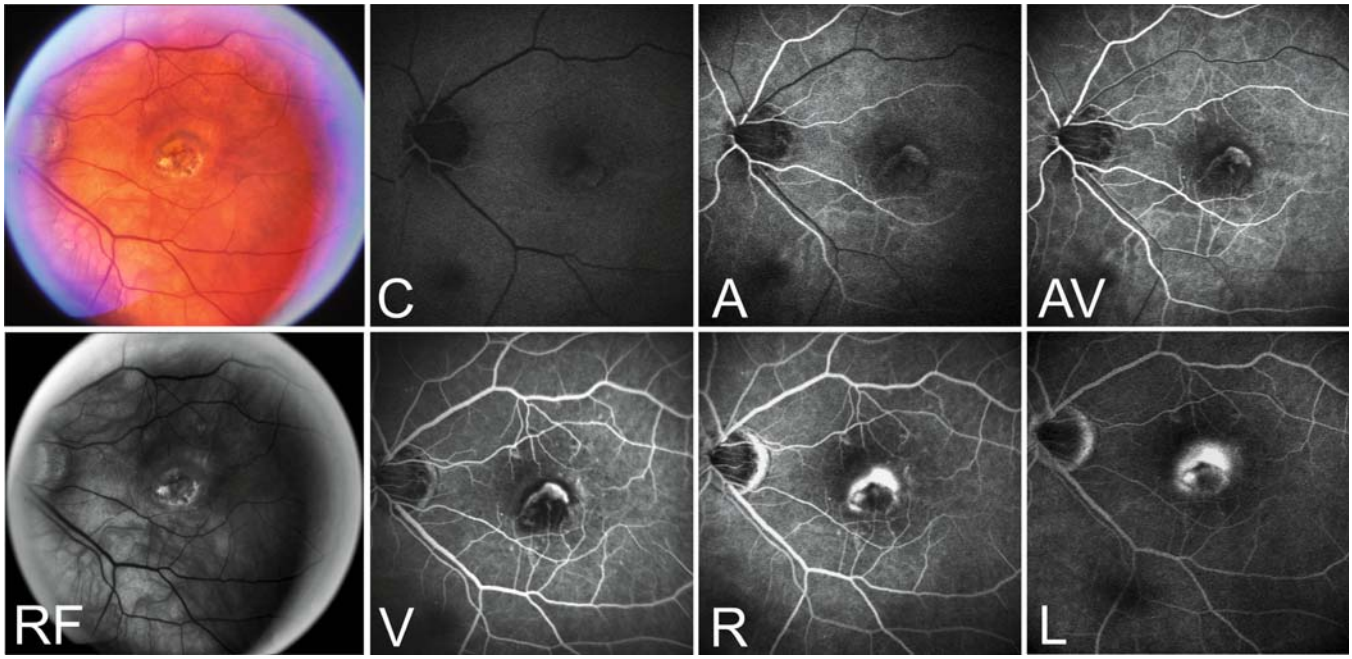

Fig. 1.13. A juxtafoveal subretinal neovascularization (SRNV) membrane. The borders of the membrane can be seen as early as the arterial (A) phase. The intensity of dye continues to grow through the arteriovenous (AV) and venous (V) phases. Dye is clearly seen leaking from the membrane in the recirculation (R) phase and continues to spread until the borders are obscured in the late (L) phase. C, choroidal phase; RF, red-free photograph.

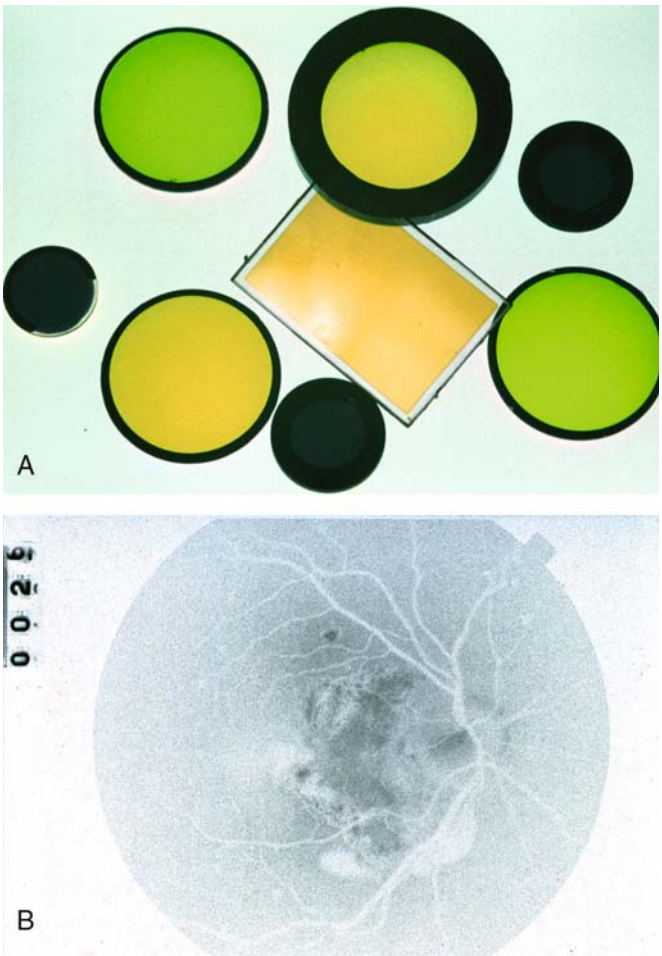

Fig. 1.14. (A) A collection of poorly matched and worn out exciter and barrier filters. (B) Apparent fluorescence from the retina. In fact, it is either the result of the exciter filter passing a broader wavelength of light that cannot be completely blocked by the barrier filter, or the barrier filter cannot block all of the excitation light.

Autofluorescence is the final type of apparent hyperfluorescence and can be attributed to the unique characteristics of structures within the eye. Fluorescence can be seen in patients presenting with true optic nerve head (ONH) drusen. Fluorescence emanates from ONH drusen when exposed to light from the exciter filter, even in the absence of dye (Fig. 1.15).

Six Phases of Fluorescein Sodium Angiography

The six phases of FSA, in order of appearance, are the choroidal (C), arterial (A), arteriovenous (AV), venous (V), recirculation (R), and late (L). The timing of the first four phases varies, depending on the patient's vascular makeup, the sensitivity of the imaging device being used, and the injection technique employed. It is the preference of the referring physician that determines the timing of the mid- and late-phase images.

In FSA the choroidal phase typically appears 8 to 20 seconds after start of the dye injection and is the earliest indication of dye entering the eye. It is marked by a patchy blush of hyperfluorescence in the background of the retina and the cilioretinal artery present in about 15% of the population begins to fill (Fig. 1.16).

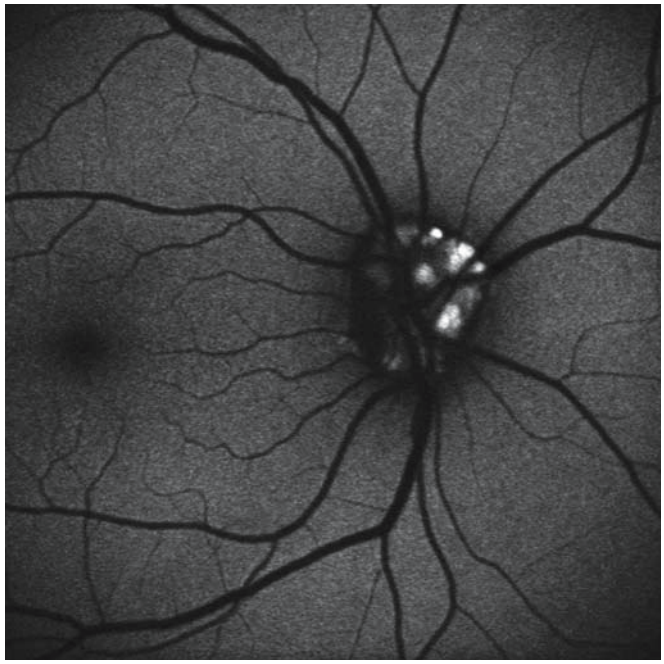

FIG. 1.15. A patient with optic nerve head drusen that normally fluoresce when exposed to light of about 485 nm. Optic nerve head (ONH) drusen emit light at a wavelength of approximately 525 nm.

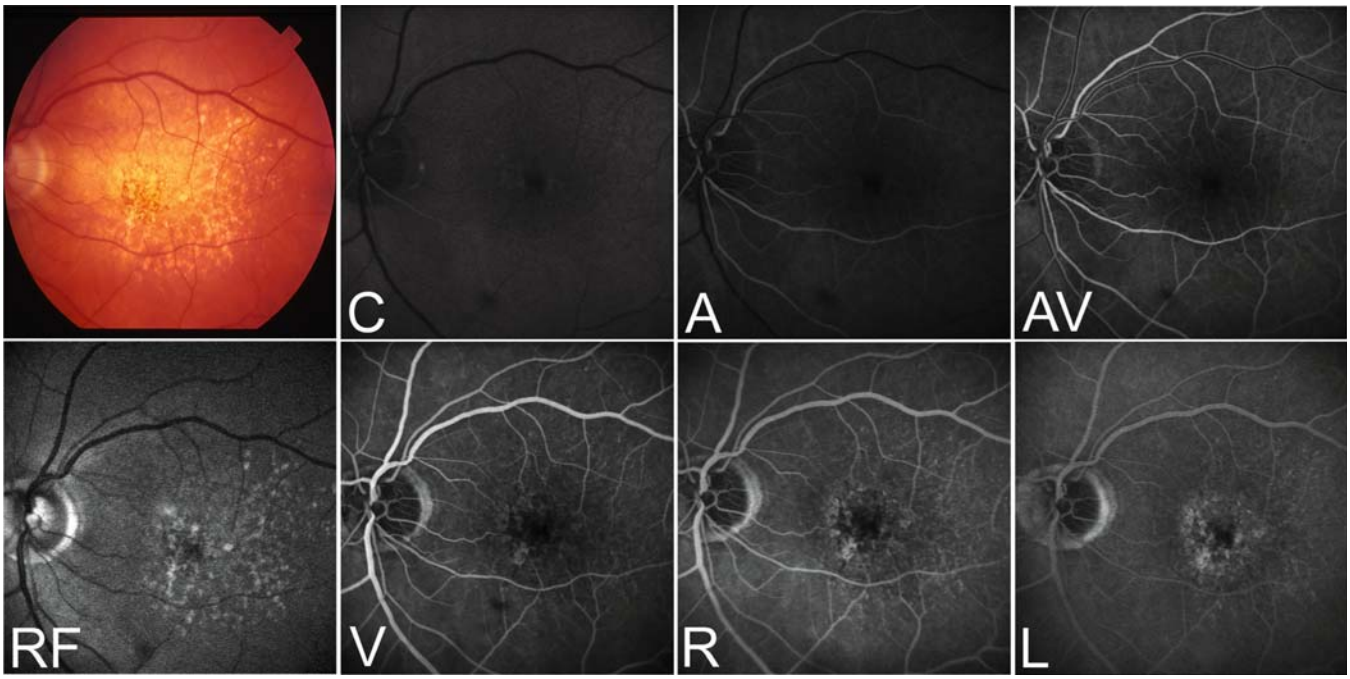

FIG. 1.16. The six phases of fluorescein sodium angiography (FSA) begin with a color and red-free (RF) photograph of a patient with macular degeneration. The choroidal (C) phase demonstrates a light blush of fluorescence from the choroid followed immediately by the arterial (A) phase, in which dye begins to fill the arterioles. In the arteriovenous (AV) phase the hemodynamics of the dye passing from the arteries through the capillary interface with the veins and is marked by laminar flow in the veins. In the venous (V) phase a greater fluorescent concentration of dye in the veins than in the arteries. The recirculation (R) phase shows a marked decrease in overall vascular fluorescence and a greater amount of abnormal fluorescent detail in the retina. The late (L) phase image shows even less background fluorescence with a greater degree of staining of drusen in the posterior pole and of the optic nerve head.

The arterial phase follows the choroidal phase by 1 to 2 seconds. Figure 1.16 demonstrates the arterial phases in which dye appears entering only in the retinal arterioles and an increase in background fluorescence. It is very short lived, lasting only a couple of seconds.

The arteriovenous phase occurs about 12 to 15 seconds after the dye first appears in the eye. A characteristic laminar flow is seen in the veins as dye passes from the arteries through the capillary interface and slowly begins to fill the veins while background fluorescence continues to increase.

The venous phase usually occurs around 25 seconds after the dye first shows up in the eye, and it lasts for several minutes. The veins are fully perfused with the concentration of dye being greater in the veins than in the arteries. In the middle to later part of this phase the veins appear slightly more hyperfluorescence than the arteries.

The recirculation phase, or what is sometimes called the midphase, begins about 2.5 minutes after the end of injection and is usually documented at the 3- to 5-minute postinjection mark. Both the arteries and veins are of equal brightness and a marked decrease of overall fluorescence can be appreciated. Dye leakage and pooling starts to be evident in the midphase.

The late phase is the sixth and final phase. Photographs are typically taken from 7 to 10 minutes after injection. The concentration of background dye is low and appears somewhat flat in contrast. The remaining hyperfluorescence is from staining, leakage, and pooling. As stated earlier, all times are approximations, as each person's circulatory makeup varies as do the techniques used and times preferred by the referring physician.

Phases of Indocyanine Green Angiography

Indocyanine green angiography, as described earlier, is used to image the choroid. It demonstrates similar phases to FS in the retinal vasculature, but does not always appear at the same time as FS. For example, when using a SLO device, the choroidal and arterial phases are essentially one and the same since the retinal pigment epithelium does not block the fluorescence of ICG. The initial choroidal flush of dye followed by retinal arterial filling is on the order of 1 to 1.5 seconds (Fig. 1.17).

The arterial and arteriovenous phases can be appreciated in both the choroidal and retinal circulation at high speed, though it can be very difficult to distinguish the difference partly due to the visibility of the choroidal and retinal vasculature in the same

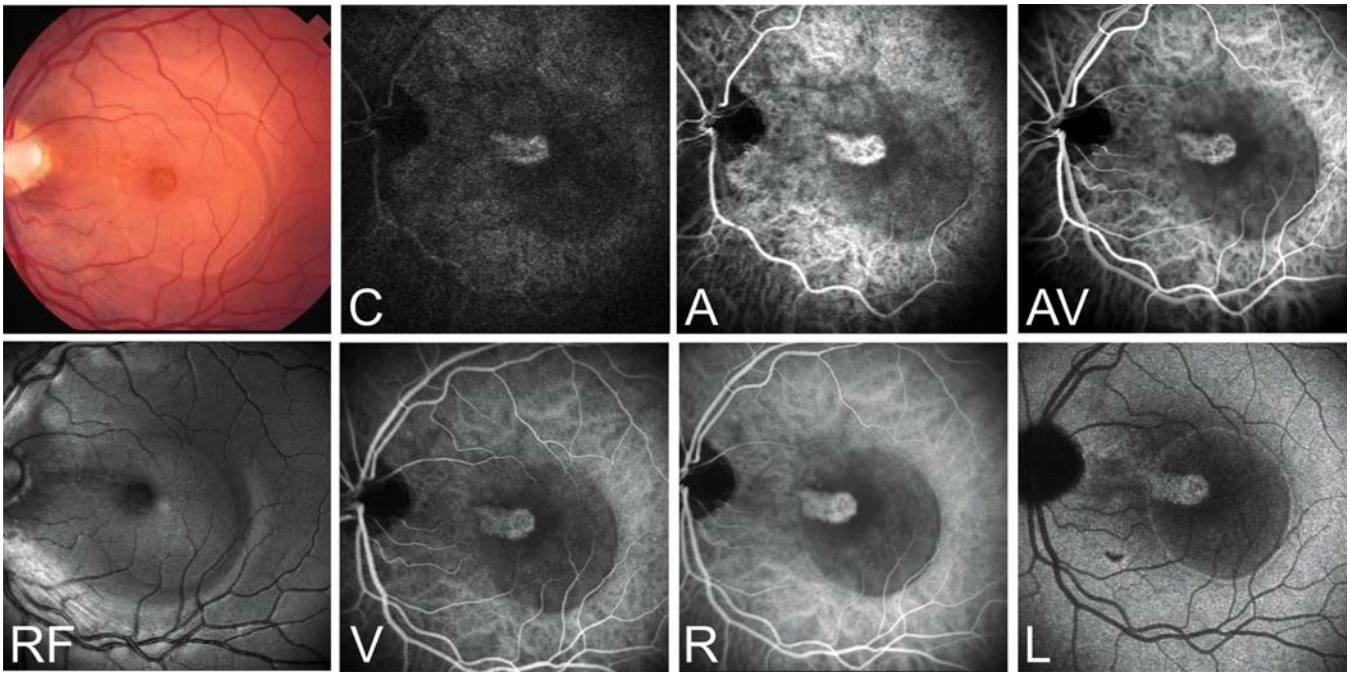

Fig. 1.17. The six phases of indocyanine green angiography (ICGA) starting with a color and red-free (RF) photograph of a patient with atypical central serous retinopathy. The choroidal (C) phase demonstrates a brighter blush of dye from the choroid in ICGA than for fluorescein sodium (FS), because the retinal pigment epithelium (RPE) layer does not act as a barrier for ICG dye. Individual choroidal vessels are well delineated in the arterial (A) and arteriovenous (AV) phases, which show that the ability to distinguish between arteries and veins in the choroid is harder than for the retina. This difficulty is due to the increased number of vessels visible and the torturous nature of the choroidal vasculature. The venous (V) phase shows a marked decrease in overall fluorescence; the sensory retinal detachment remains hypofluorescent as does the optic nerve. The recirculation (R) phase demonstrates a more diffuse staining of the choroid. In the late (L) phase, individual choroidal vessels are no longer visible, the detachment is well visualized, all fluorescence is absent from the retinal vasculature, and the optic nerve head remains hypofluorescent.

image and the tortuous nature of the choroidal vasculature. The ability to differentiate between these vascular networks and their interconnections is the basis of high-speed feeder vessel angiography. If using high-speed SLO, the choroidal arteries can be seen to fill the eye 0.25 second before the choroidal veins in about 1.5 seconds before the retinal vasculature fills.

The venous phase is closely related in time to the FS venous phase and is practically indistinguishable in time.

Due to the size of the molecules and their ability to bind to the blood proteins, the recirculation phase and the late phase occur much later for ICG than for FS. As an example, a recirculation-phase ICG would occur approximately the same time as a late-phase FS, with the late-phase ICG being imaged anywhere from 10 to 45 minutes after injection. This variability in late-phase times for ICG is based on the pathology to be imaged, the imaging equipment used, and the preferences of the referring physician.

Common Angiographic Protocols

With a basic understanding of descriptive terminology and an idea of the different phases of angiography, Tables 1.2 and 1.3 can be used to plan and anticipate a variety of angiographic procedures. It is recommended to look at these tables and review the above-cited figures to appreciate the relationship between time and angiographic phases. A word of caution is in order: The times presented in these tables are approximations and can only be used as a guide. Actual times depend on the individual patient and the requesting physician's preferences.

Similarities and Differences of Imaging Devices

Since Canon Inc.[19] first introduced in the late 1970s its nonmydriatic fundus camera using an infrared viewing system, photographers have had to change their kinesiologic view of the eye. They have had to develop new techniques of focusing, capturing, and even thinking about the physiology of the ocular fundus. For convenience, we can think of fundus cameras and imaging systems as falling into one of two basic classifications of direct or indirect viewing. In direct viewing systems, the photographer looks at and focuses the live fundus image via a beam-splitter and ocular placed in the optical pathway. In an indirect system the live ocular image falls on a charge-coupled device (CCD), or photomultiplier tube (PMT), and is displayed on a video monitor, which is used for viewing and focusing the eye. In the direct system the photographer and patient typically sit face to face, whereas in the indirect system the photographer may not even face the patient.

Most of the devices in these two basic systems are similar in their ability to adjust the camera head in relationship to the patient's eye. This three-dimensional alignment is typically accomplished by the use of hand-controlled joysticks or adjustment knobs in addition to some method of tilting and swinging the camera head up and down and from side to side. An exception to this is handheld imaging devices, in which the photographer aligns the imaging head simply by moving his hand in the desired direction. The act of aligning the imaging head is the first step in achieving good rough focus. All systems also include some method of adjusting the image for fine focus.

In the following subsections, some issues pertain to only one of the basic systems while others pertain to both. It is not practical to give specific operating instructions for each available system manufactured; therefore, it is necessary for readers to review and understand the specifics covered by their particular camera manufacturer's operations manual. In the following subsections we look at the direct viewing system and at methods necessary to take good color and angiographic images.

Direct or Indirect Viewing

Direct viewing systems include conventional cameras that use film and those that have been converted to or build from the ground up to capture a video image. These systems rely on viewing and focusing a live fundus image through the camera's eyepiece. In this subsection we examine the method of setting the eyepiece, look at issues relevant to positioning all cameras for rough and fine focus, and discuss methods of handling these imaging devices to avoid artifacts and ensure successful usable images.

Setting the Eyepiece

In conventional camera-based systems, images are recorded onto film, a CCD, or a PMT, with the images of the latter two eventually stored on a computer hard drive. As discussed earlier, the cameras should first be cleaned and set to a zero or a neutral state, prior to the patient's arrival. Once this has been done, the eyepiece must then be set. To have the brightest image available for focusing, camera-based systems use an aerial image to view the fundus rather than focusing on an image falling onto a ground glass. This is true whether using a camera that employs a separate eyepiece to focus or a conventional 35-mm single lens reflex camera. In order for this technique to work properly, the camera viewing systems must be set parfocal to the film or sensor plane. This means the image that the photographer sees in the eyepiece must be in focus at the same time as the image falling on the film or CCD. This is accomplished as follows.

There are discrete lines, called reticule lines, etched on an inside surface of the eyepiece. They must be brought into sharp focus for the photographer's eye. This is accomplished by first rotating the eyepiece to the full plus (+) diopter setting. These settings can be seen on the outside barrel of the eyepiece (Fig. 1.18). The camera lens is then focused at infinity and a blank 18% gray card is held in front of the lens. The light is adjusted

Table 1.2. Approximate time sequence of angiographic procedures.

						Angiographic phases					
Figure	Procedure	Diagnosis	Field of view	Preinjection pictures	Injection begin/end	Choroidal	Arterial	Arterio/venous	Venous	Mid or recirculation	Late
Fig. 1.10a–c, 1.11a–c, 1.12	Fluorescein Angiogram only	Classic SRNV	PP	RF	0–4 seconds	8–10 seconds	10–12 seconds	12–22 seconds	23–90 seconds	90 seconds to 5 minutes	10 minutes
Fig. 1.13, Fig. 1.16	Fluorescein Angiogram only	PDR/BRVO	PP > Quadrants > PP	RF	0–4 seconds	8–10 seconds	10–12 seconds	12–22 seconds	Sweep periphery 23–90 seconds	90 seconds to 5 minutes	10 minutes
Fig. 1.17	ICG only	Occult SRNV	PP	RF/AFL/IR	0–4 seconds	7–9 seconds	9–10 seconds	12–22 seconds	23–90 seconds	3–5 minutes	12–60 minutes
Fig. 1.10, 1.11, 1.12, 1.13, 1.16, 1.17	FA/ICG—sequential	Occult SRNV	PP	IR/RF/AFL	ICG 0–4 seconds FS starts at end of ICG A/V	7–9 seconds 8–10 seconds	9–10 seconds 10–12 seconds	12–22 seconds 12–22 seconds	23–90 seconds 23–90 seconds	3–5 minutes 3–5 minutes	12–60 minutes 8–10 minutes
Figs. 1.10, 1.11, 1.12, 1.13, 1.16, 1.17	FA/ICG—simultaneously SLO	Occult SRNV	PP	RF/AFL/IR	FS 0–4 seconds ICG 0–4 seconds	FS not taken ICG 7–9 seconds	FS not taken ICG 9–10 seconds	12–22 seconds 12–22 seconds	23–90 seconds 23–90 seconds	3–5 minutes 3–5 minutes	8–10 minutes 12–15 minutes
	ICG feeder vessel SLO	Occult CNV	PP	RF/AFL/IR	0–4 seconds	0–4 seconds	4–12 seconds	12–22 seconds	23–90 seconds	3–5 minutes	8–15 minutes
Fig. 1.10b & c,1.11a & c	Oral FA SLO	CME/DME	PP	RF/AFL/IR	0–10 seconds	NA	NA	NA	2–5 minutes	Every 5 minutes	15–20 minutes
Fig. 1.10b & c, 1.11c	Oral FA flash system	CME	PP	RF	0–10 seconds	NA	NA	NA	10–15 minutes	Every 5 minutes	30–45 minutes
	Iris FA	Preop muscle surgery	Iris and pupil	RF	0–4 seconds	NA	6–10 seconds	10–12 seconds	15–90 seconds	3–5 minutes	5–10 minutes

AFL, autofluorescence; BRVO, branch retinal vein occlusion; CME, cystoid macular edema; DME, diabetic macular edema; FA, fluorescein angiogram; ICG, indocyanine green; IR, infrared; PDR, proliferative diabetic retinopathy; PP, posterior poll; RF, red free; SLO, scanning laser ophthalmoscope; SRNV, subretinal neovascularization.

TABLE 1.3. Approximate dye transit times.

	Sec 0	4	6	7	8	10	12	15	20	30	40	50	Min 1	2	3	4	5	7.5	10	15	30	45	Hr 1
FA	B	E	–	–	C	A	AV	AV	AV	V	V	V	V	V–R	R	R	R	R–L	L				
ICG	B	E	–	C	C–A	A–AV	AV	AV	V	V	V	V	V	V	V	R	R	R	R–L	L	L	L	L
ICG feeder vessel	B	E	C–A	C–A	C–A	A–V	A–V	High-speed angiographic movie															
Oral FA HRA	B	E	–	–	–	–	–	–	–	–	–	–	–	–	–	–	–	V–R	V–R	V–R			
Oral FA camera	B	E	–	–	–	–	–	–	–	–	–	–	–	–	–	–	–	–	–	V–R	V–R	V–R	V–R

FA, fluorescein angiography; HRA, Heidelberg retinal angiograph; ICG, indocyanine green; B, begin injection; E, end injection; C, choroidal; A, arterial; AV, arteriovenous; V, venous; R, recirculation; L, late.

to the same level as is used during imaging. This should be bright enough that the lines are visible, but not so bright that it makes the card look light gray. Next, while looking through the eyepiece at the reticule lines, the barrel is slowly rotated toward the minus (–), diopter setting, just until the reticule lines are in sharp focus. It is important not to turn the eyepiece back and forth to achieve focus, as this would allow for the eye to accommodate, possibly resulting in an incorrect setting. This procedure should be repeated several times, making note of the results in order to determine the photographer's proper eyepiece setting for that session. This procedure should also be repeated throughout the day as the photographers' settings can change as their eye becomes fatigued. Fatiguing can be a particular problem in younger photographers. Figure 1.18 is an illustration of the proper eyepiece settings and appearance of the reticule in an individual with a –3 diopter correction for the viewing eye. The advantage of using the second classification of indirect devices in which a monitor is used for focus can be easily appreciated. The initial and subsequent eyepiece adjustments throughout the day, eye fatigue, and individual prescriptions are not as important in achieving good focus.

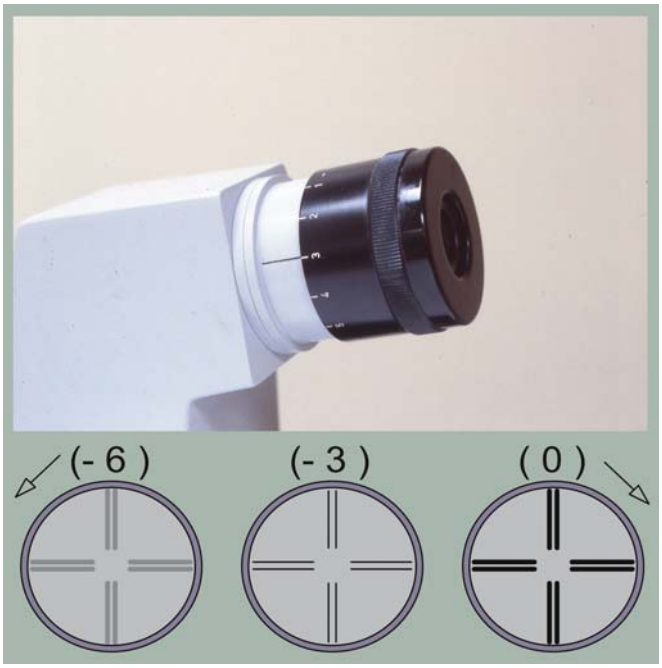

FIG. 1.18. The appearance of the reticule lines with a properly focused eyepiece for a photographer with a –3 diopter correction. If a white card and bright light are used to view the reticule lines, improper settings may be achieved due to the increased depth of field caused by a constricted pupil.

The next step is to select the proper film or CCD/PMT sensor settings to record the required images. Color photographs are the first images to be taken of a patient, so an appropriate color slide film in the International Standards Organization (ISO) 100 range should be loaded into the camera back. It is important to check that there are no filters inserted into the optical path of the camera, unless performing special monochromatic fundus photography. If a video/digital capture system is being used, it too should be checked for filters, and enough storage space should be made available to acquire the necessary images. Each system is different and the camera's manual should be the primary source for determining these settings.

Patient posture and head positioning are similar for all imaging systems, direct or indirect, whether they are conventional film-based cameras, nonmydriatic fundus cameras, or angiographic SLO devices. It must be remembered that the camera system should be adjusted to accommodate the patient's height and to ensure that unnecessary fatigue is avoided for both the patient and the photographer. Particular attention should be given to properly positioning the patient at the camera so that whenever possible a straight, upright spine is maintained throughout the procedure. Proper head position is also important in reducing fatigue and promoting good focus. Proper head position is also the first step to provide a clear optical pathway and to achieve good rough focus.

With the camera lens set parallel to the ground and prior to looking at the patient with the imaging device, the patient's head position must be properly set. Ideally, the chin rest should be adjusted in conjunction with the table height to maintain the patient's proper posture. The camera's front objective lens height should be adjusted so that it is perpendicular to the patient's pupil while maintaining alignment of both the patient and the camera lens. If the patient's head is tilted to one side, lateral movement between the left and right eye will require an additional adjustment of the camera head height. If the patient's

head is turned more to one side or the patient's forehead does not touch the headrest, the camera will need to be constantly readjusted for proper working distance. Also, if the patient's chin is too far back on the chin rest, the upper eyebrow may interfere with a clear optical pathway and make it difficult to retract the patient's eyelids if it is necessary to do so.

Once the head position is correct and while the photographer is still looking slightly from the side, the patient is instructed to look straight ahead. A fixation device should be provided so that patients can lock their gaze on one spot. A fixation device can be either an external light or internal one; however, if it is a physical internal device, remember to remove it from the field of view before taking an image. Once fixation has been achieved and the eye is looking in the proper direction, the camera can be moved toward the patient's eye until a sharp image of the viewing bulb's filament can be seen on the center of the patient's cornea (Fig. 1.19A). If the photographer were to look inside the eyepiece at this time, an image of the fundus would be seen. This technique is very useful when using direct imaging devices that rely on visible light such as a conventional camera system. However, if using an indirect imaging device that relies on invisible illumination such as nonmydriatic or SLO systems, the proper method of achieving initial rough focus is to adjust the device so the optical axis of the camera is parallel to the ground, then pull the camera head back while adjusting its height until the pupil of the eye can be seen and centered in the field of view. At this point the camera head is moved forward, maintaining centration until the fundus is seen filling the monitor.

Attention can now be turned to proper image saturation and the elimination of artifacts. While the photographer looks through the eyepiece or at a monitor, the joystick is slowly moved forward and backward to the point of greatest image saturation. Slight side-to-side and elevation adjustments are made to eliminate crescent artifacts (Fig. 1.19B). We discuss the elimination of artifacts in greater detail later in this chapter.

Once rough focus, good saturation, and the elimination of artifacts have been achieved, the task of critical or fine focus can begin. When using conventional direct viewing camera systems that use reticule lines in the eyepiece, the method of achieving proper focus is to adjust for critical focus in the area of greatest interest while maintaining visualization of sharp reticule lines. This task is not easy and requires constant practice (Fig. 1.19C). Some cameras have internal focusing devices that can assist in achieving focus. In addition to these considerations, the area of greatest interest and

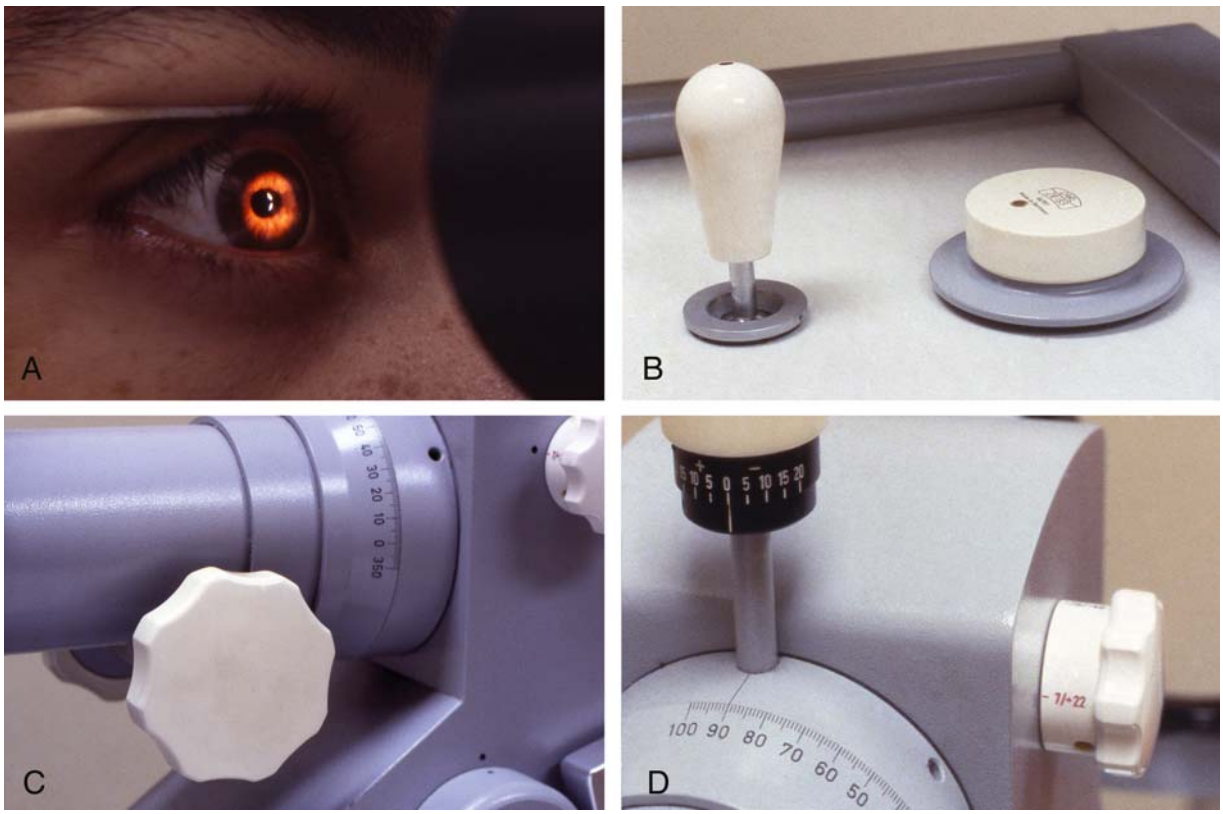

Fig. 1.19. (A) A properly aligned conventional film camera. The viewing bulb filament is focused on the cornea and centered on the pupil. At times it is necessary to hold the patient's eyelashes to provide a clear optical pathway. (B) The controls are used for adjusting alignment of the eye and to ensure a clear saturated image. (C) Once proper alignment and saturation of image has been achieved, fine critical focus can be adjusted. (D) At times the image can be further improved by the use of astigmatic correction controls.

the plane of critical focus vary greatly depending on the type of images to be taken, the pathology to be imaged, and the type of device to be used. When taking color photographs to document proliferative diabetic retinopathy, this plane of critical focus could either be at the level of the retina vessels overlying the macula or perhaps on a sea-fan vessel structure growing into the vitreous space.

If using an indirect viewing system that requires focusing on a computer monitor, the task is greatly simplified by focusing on the area of greatest interest, which produces the best possible image. It should also be noted that when imaging the choroid with ICG, the proper plane of focus is below the retina, thereby producing images in which the retinal vessels are slightly out of focus. Referring back to the example of ICG phases in Figure 1.17, it can be seen that the choroidal vessels are in focus and that the retinal vessels are slightly out of focus. Also by its very nature, a confocal SLO has only one plane in critical focus at any point in time.[20]

Sometimes these are the only steps that can be taken to achieve critical focus. However, if the imaging system is equipped with astigmatic compensation devices, they can be used to correct for deficiencies in the patient's natural visual system or for an ill-fitted IOL. At times when imaging the peripheral retina, astigmatic corrections can provide sharper images. The best guidance for using these devices is to get the best focus possible with them set to zero and then adjust them through their range to see if the image improves (Fig. 1.19D).

The elimination of image artifacts is the last area of image quality over which the photographer can exercise some control. Prevention of dark areas due to blocked images, proper image saturation, light crescents, and eyelashes are the photographer's responsibility. The patient's head position, the placement of the illumination filament on the cornea, and rough focus techniques are the first steps necessary for positioning the camera to avoid these problems. It has been said that if a photographer is able to create an artifact, then he has learned the skills necessary to prevent an artifact. The ability to achieve proper saturation and the skills to create and eliminate crescent artifacts are very useful tools in producing good stereo images. Figure 1.20 is an example of a photographer's exercise in creating a ring-around artifact montage. This exercise can be reproduced on all imaging systems and should be practiced whenever a new device is to be used.

The first in the series of exposures needed to produce the ring-around montage is the creation of a single well-focused, nicely saturated image, with good field definition (Fig. 1.20A). This is the look of an image a photographer is typically always trying to achieve.

Next, an unsaturated washed out image with bright fuzzy crescents is created by moving the camera head too close to the patient's eye (Fig. 1.20B).

The third image in this series is created by moving the camera too far away from the eye (Fig. 1.20C). The view is desaturated, and a blue-gray ring surrounds the image. This imaging

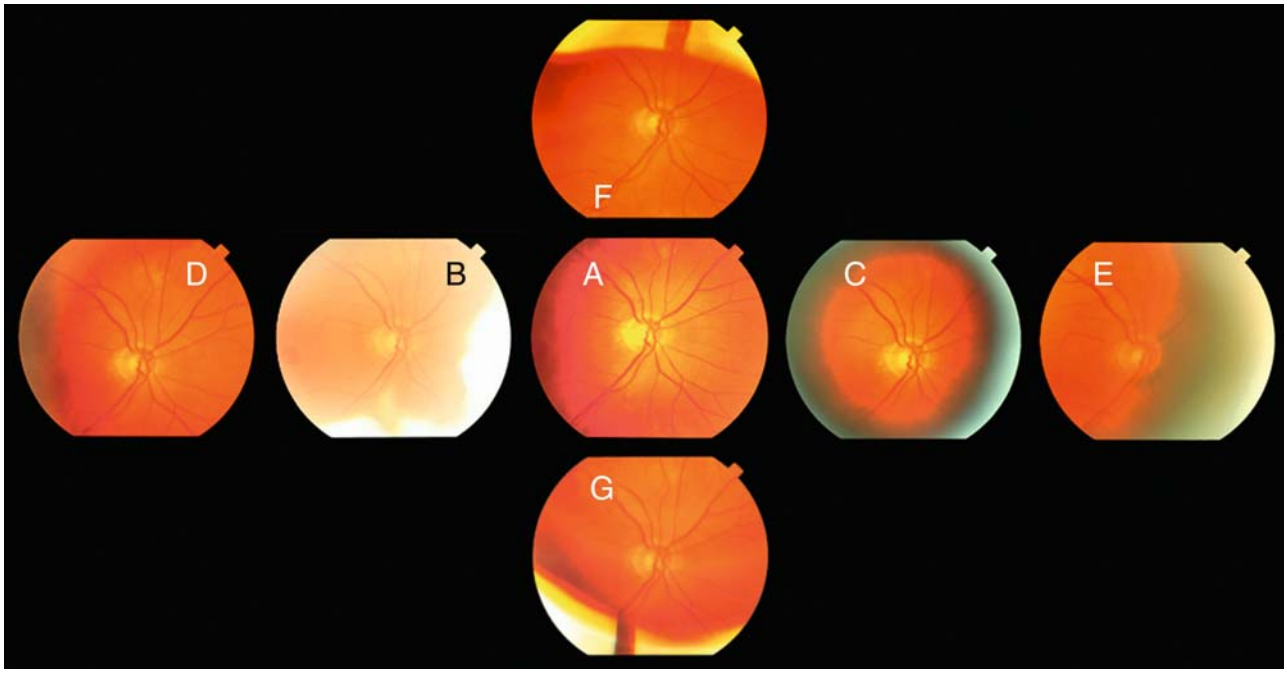

Fig. 1.20. An example of a photographic exercise in which artifacts are created in a ring around montage. (A) A well-focused and properly saturated image. (B) A camera position to close to the patient's eye, resulting in a washed-out image. (C) A camera position too far away from the patient's eye, and in fact the edge of the pupil can be seen. (D–G) Proper saturation of the image; however, a crescent is formed when the lens position is too high, too low, or too far to either side

technique is sometimes useful if the pathology extends anteriorly, such as in the case of a large peripheral melanoma.

The remaining four images (Fig. 1.20D–G) are created by starting with a properly positioned camera and a well-saturated image. From this point the camera is manipulated up and down and from side to side until a light crescent is created. The crescent can be created in each of the clock hour positions. Good stereo image pairs are created by starting in the position of Figure 1.20D,E. The first image of the stereo pair is taken once the camera is moved back toward the center and the crescent just disappears. The second of the pair is made by moving the camera in the opposite direction, backing off until the crescent is eliminated. The resulting stereo images demonstrate slightly darker edges on either the right or left side due to some of the light being blocked by the pupil.

Finally, after the patient is properly positioned, the camera controls have been mastered, the patient's eye and camera have been adjusted for the proper field of view, and a critical focus has been achieved, the image can be taken.

Operational Specifics

We have looked at areas of patient management and image acquisition. We conclude this chapter by looking at some operational specifics associated with the various imaging systems. These include the production of various types of hardcopy with which the clinician evaluates the patient's condition and maps out the treatment strategies. We briefly touch on ethical and privacy issues and various data management issues involved in making these documentary and diagnostic images.

To begin, the classic conventional camera systems utilizing film are still around but are becoming less available due to the speed, convenience, advances of image quality, and the decreased cost of the necessary hardware for digital imaging. As of this writing, film camera systems are still in the majority, but their numbers are decreasing. In addition to increased costs, decreased availability, and total elimination of certain photosensitive materials, it is difficult to justify a custom in-house photo laboratory. Added to these difficulties, it is getting harder to find commercial labs that process and print black- and -white materials. On the positive side, E-6 slide film is still used, and processing labs can still easily be found.

Digital imaging systems, on the other hand, can produce immediate results. For the cost of a few hundred dollars, an inkjet printer can be attached to a digital system and full-color fundus photographs or high-quality black- and -white angiography can be produced in a matter of minutes. In addition, the images can be enhanced with relative ease if the acquisition conditions are less than ideal. An example of this might be a patient with poor dilation or cataracts, or an individual in whom the dye was extravasated, resulting in images that are dark or low in contrast. These images can be computer enhanced so that usable diagnostic information can still be derived. The ease of enhancement, unfortunately, also allows for the unethical manipulation of images, though this can be said for conventional black- and -white printing too. When all things are considered, it becomes clear why, when classic film systems break down and economics permit, they are being replaced with the newer electronic systems.

However, that is not to say that the newer digital imaging systems are not without their own set of problems. By far the major reason for not upgrading to an electronic system is the cost. A camera conversion starts at around $40,000, and is out of the reach of many physicians. In addition, there is an inherent turnover and obsolescence of hardware. Several manufacturers of film systems have 20- and 30-year-old cameras still in use today, but it is rare to find an electronic system in its original configuration for more than 5 to 7 years. The driving force behind this change is the development of newer, better, and faster computer operating systems, along with acquisition hardware and storage devices. It is possible to find electronic systems that have progressed from optical storage to magnetic storage and back to optical, all the while increasing capacity and speed.

The area of data management, which includes production, manipulation, storage, and retrieval of data, is also an area in which changes in hardware can make management and retrieval of older records more difficult. With conventional film systems, slides and negatives are stored in the same record and can be taken conveniently from room to room. If the patient is seen again, the newer images are simply added to the record. Initially it takes time to process the film and prints, but when it is done, all of the images are available. On the other hand, electronic imaging systems require acquisition stations and typically at least one or more review stations, although these review stations could be in the next room or in the next city.

Patient privacy and security issues are also presenting a more challenging problem in these new networked systems. Hackers, viruses, and data thieves must constantly be guarded against, and attacks can be a constant source of problems.

Usually, necessary upgrades in the acquisition system require associated upgrades in all of the review stations of hardware or software. Proper storage of current and archive data is also subject to market change. As mentioned earlier, it is not uncommon for storage media and hardware to change or be eliminated over time. This change affects both the day-to-day backups and long-term archiving of patient data.

Data Storage

In any electronic imaging system, whether it is based on a conventional camera or a newer scanning laser system, data must be protected from loss. Systems that acquire images utilizing CCDs temporarily keep the data stored in RAM, which is not permanent and subject to loss if a power failure occurs. When the photographic protocol permits, or when the RAM is full, the data must be transferred to the computer hard drive.

At this point the data would not be lost if a power failure occurred—only if the hard drive were to crash. Unfortunately, other problems can result in the loss of data, such as a fire, so it is important to have the data backed up in a redundant form such as another hard drive or on some other storage medium. It is the need to have these data available in the future that makes archiving data necessary. Older records need to be transferred to new, currently used media systems and by the very nature of the industry change, this task is ongoing.[20]

Conclusion

We have looked at areas of patient management, both color and angiographic protocols, and the associated dyes used. We have discussed some terms commonly used to describe angiographic fluorescence, the various phases of angiography, common reasons for angiographic procedures, and the associated time sequences used to execute them. We have covered specific techniques necessary to achieve properly exposed and focused diagnostic images. Lastly, we have looked at some areas that make the systems different and the necessary considerations of data management.

A great deal of information has been touched on in this chapter that readers can put to immediate use. I hope that this chapter has raised additional questions for readers and that they will take it upon themselves to look at some of the fine reference materials listed below and continue their search for knowledge and skills in the field of ophthalmic photography.

References

1. Jackman WT, Webster JD. On the photographing the retina of the living human eye. Philadel Photogr 1886;23:275.
2. Bedell AJ. Stereoscopic fundus photography. JAMA 1935; 105:1502.
3. Dimmer F. Ueber die Photographie des Augrnhintergrundes. Wiesbaden, Germany: Bergmann, 1907.
4. Dimmer F. Der Augenspiegal und die Ophthalmoskopische Diagnostik. Leipzig, Germany: F. Deuticke, 1921.
5. Dimmer F, Pillat A. Atlas photograpischer Bilder des Menschlichen Augenhintergrundes. Leipzig, Germany: F. Deuticke, 1927.
6. Heidelberg retinal angiograph (HRA). Heidelberg Engineering GmbH, Gerhart-Hauptmann—Str. 30, 69221 Dossenheim, Germany. Available at www.HeidelbergEngineering.de.
7. Benadryl, Diphenhydramine Hydrochloride, Warner-Lambert Consumer Healthcare, Morris Plains, NJ 07950.
8. Compazine, Prochlorperazine Maleate, Mylan Pharmaceuticals, Morgantown, WV 26505.
9. Fundus Photography Reading Center, Department of Ophthalmology and Visual Sciences, University of Wisconsin—Madison, 406 Science Drive, Park West One, Suite 400, Madison, WI 53711. Available at http://www.eyephoto.ophth.wisc.edu/.
10. Martin T, Saine P. Stereo fundus photography: principles and techniques, stereo perception. In: Saine P, Tyler M, eds. Ophthalmic Photography, Retinal Photography, Angiography, and Electronic Imaging, 2nd ed., Woburn, MA: Butterworth-Heinemann, 2002:97–136.
11. Jacobs J. Fluorescein sodium—what is it? J Ophthalmic Photogr 1992;14:62.
12. The Ophthalmic Photographers' Society, Inc. Fundamentals of fluorescein angiography, angiography-ophthalmic photography. Available at http://www.opsweb.org/Op-Photo/Angio/FA/FA2.htm.
13. Morris P. Fluorescein sodium and indocyanine green: uses and side effects. In: Saine P, Tyler M, eds. Ophthalmic Photography, Retinal Photography, Angiography, and Electronic Imaging, 2nd ed., Woburn, MA: Butterworth-Heinemann, 2002:143–144.
14. Mattern J, Mayer P. [Excretion of fluorescein into breast milk [letter]. Am J Ophthalmol 1990;109:598.
15. Flower RW. Evolution of indocyanine green dye choroidal angiography. Opt Eng 1995;34(3):727–736.
16. Morris P. Fluorescein Sodium and Indocyanine green: uses and side effects. In: Saine P, Tyler M, eds. Ophthalmic Photography, Retinal Photography, Angiography, and Electronic Imaging, 2nd ed., Woburn, MA: Butterworth-Heinemann, 2002:159–16.
17. IC-Green. Buffalo Grove, IL: Akorn, Inc. 6-DCGN-01,1–6.
18. Freeman WR, Bartsch DU, Muller AJ, Banker AS, Weinreb RN. Simultaneous indocyanine green and fluorescein angiography using a confocal scanning laser ophthalmoscope. Arch Ophthalmol 1988;116:415–463.
19. Canon USA, Inc., One Canon Plaza, Lake Success, NY 11042. Available at http:www.usa.canon.com.
20. Clark T, Tyler M. Electronic imaging of the fundus: principles and techniques, scanning laser ophthalmoscopes. In: Saine P, Tyler M, eds. Ophthalmic Photography, Retinal Photography, Angiography, and Electronic Imaging, 2nd ed., Woburn, MA: Butterworth-Heinemann, 2002:306–321.

2
Fluorescein Angiography: General Principles and Interpretation

Bernard R. Hurley and Carl D. Regillo

Historical Perspectives

Since its first use as a diagnostic tool in the 1960s, fluorescein angiography has become an invaluable and increasingly sophisticated tool for studying, understanding, documenting, and treating ocular disease. The unique optical properties of the eye make the ocular fundus the only location in the human body where direct noninvasive monitoring of vascular flow is possible.[1] During fluorescein angiography, a rapid sequence of serial photographs is taken after the administration of intravenous fluorescein to visualize and document choroidal and retinal blood flow. Beyond blood flow, fluorescein angiography provides information about the integrity of the blood—retinal barrier, the fine details of the retinal pigment epithelium (RPE), and a glimpse of associated systemic pathology.[2] These properties have made fluorescein angiography one of the most useful office-based diagnostic tools in ophthalmology for the last 30 years.[3] In fact, the advent of angiography can be considered to have ushered in a new era in the subspecialty of ophthalmology: vitreoretinal surgery.[4]

Fluorescein dye was first synthesized by Adolf von Baeryer[5] in 1871. He first demonstrated its usefulness to assess circulatory properties by showing that a solution of sodium fluorescein poured into the Danube River could be detected in the Rhine River 300 miles and 3 days later![6] This successfully demonstrated that fluorescein could be detected in very small quantities after extreme dilution using a simple blue light. Ten years later, the use of sodium fluorescein to assess the living circulation was reported by Paul Ehrlich,[7] who detected fluorescein in a rabbit eye following parenteral administration. Use of fluorescein was further advanced by Burke,[8] when it was used to study the optic nerve and chorioretinal inflammatory disorders.

Once fluorescein was demonstrated to be nontoxic to biologic tissues, its usage began to permeate through ophthalmology. Practical uses included detection of corneal abrasion and surface irregularities, as well as wound leaks following surgery. Intravascular human use was pioneered by MacLean and Maumenee[9] in the late 1950s. In their initial technique, after the injection of fluorescein, the patient was observed at the slit lamp under cobalt blue illumination, which facilitates visualization of the vascular anomaly under study; however, no permanent record could be generated. Subsequent technologic advances, specifically the advent of superior fundus imaging systems and the electric flash, permitted the photographic documentation of fluorescein flow through the fundus in the early 1960s.[10] Modernization of the process with the addition of built-in barrier camera filters, improved optics, high-resolution and digital cameras, as well as improved understanding of the biologic properties of fluorescein have resulted in its current position as a sophisticated and invaluable tool in ophthalmology.

Properties of Sodium Fluorescein

Initially fabricated from plant extract, the fluorescein now used in ophthalmology is a hydrocarbon salt of sodium with molecular formula C20H10O5Na2 (Fig. 2.1).[6] It has a molecular weight of 376.67 daltons (d) and is highly water soluble. In its natural state, it assumes an orange/red/brown crystalline powder. Like all luminescent chemicals, fluorescein has the ability to give off light after exposure to a specific wavelength (excitation wavelength). The dye is able to absorb the energy of the excitation wavelength and subsequently emit the absorbed energy as light of a lower frequency. This is known as the principle of fluorescence and is illustrated in Figure 2.2. For sodium fluorescein, the excitation wavelength is 465 to 490 nm and the fluorescence wavelength is between 520 and 530 nm depending on the suspension medium. In the human bloodstream at a pH of 7.4, this absorption wavelength is refined to blue light of 465 nm and the emission wavelength to yellow-green light of 525 nm.[11]

The second major property of fluorescein, after its luminescence, which makes it ideal for the study of the retinal vascular properties, is its molecular weight: 376.27 d. This weight is sufficiently large to prevent its escape from capillaries of the central nervous system, including the retina, which have tight

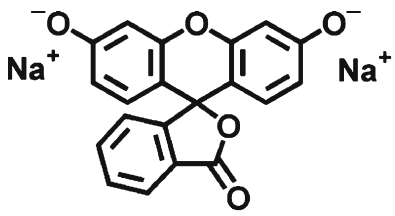

Fig. 2.1. Chemical structure of sodium fluorescein.

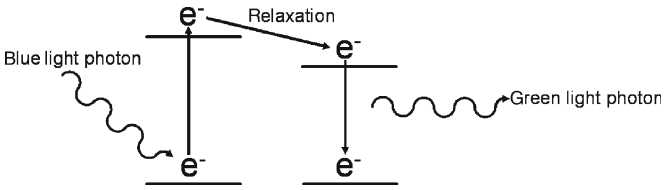

Fig. 2.2. The principle of fluorescence. Absorption of a photon of light excites an electron from its resting state to an excited state (left). This occurs for sodium fluorescein on exposure to a photon of blue light. After relaxation to a more stable state, the release of a photon of green light (right) occurs as the electron relaxes to its resting state.

junctions between endothelial cells (this constitutes the physiologic inner blood–retinal barrier). Similarly, fluorescein is too large to diffuse through the RPE (constituting the outer blood–retinal barrier) and the larger choroidal vessels. However, the fluorescein molecule is small enough to easily diffuse through the capillaries outside of the central nervous system, which gives rise to the light staining of skin and mucous membranes seen within 60 seconds of injection.[2] Most importantly, fluorescein is able to leak from components of the blood—retinal barrier, which are pathologically disrupted. This fact is the underlying principle allowing interpretation of hyperfluorescent lesions seen on the fluorescein angiogram.

In the bloodstream, 80% to 85% of fluorescein is bound to plasma proteins, chiefly albumin.[2,12] Bound fluorescein is less able to absorb and emit light and reduces the amount of dye visible during angiography. Fluorescein is eliminated through glomerular filtration in the kidney and metabolized by the liver. Excreted fluorescein dye in the urine will result in urine discoloration for up to 36 hours following administration.[13]

Technique

As in any procedure in medicine, fluorescein angiogram results are improved when time is taken to explain the technique to patients so that they understand what will happen during the test. This explanation will go far to alleviate patient fears and misconceptions and is an integral part of obtaining informed consent, which is required before the test may proceed.[14] Many patients are concerned that the dye is related to the iodinated dye used in many diagnostic radiology procedures, so patients should be informed that the fluorescein that will be injected into their veins is a "vegetable dye" and does not contain iodine.

The dye itself should be drawn up into a sterile 5-cc syringe from its sterile container. Two strengths of dye solutions are available and in common clinical use, a 10% and a 25% fluorescein solution. Typically, the clinician injects 5 mL of the 10% solution or 3 cc of the 25% solution, yielding a dose of approximately 10 mg/kg, although successful angiography can be performed with as little as one third of this dose with presumably fewer side effects. The 25% preparation may be better tolerated by the patient.[11]

Prior to dye injection, the clinician must ensure that the patient's pupil is sufficiently dilated to allow good-quality photos. This is best accomplished with pharmacologic agents instilled topically at least 30 minutes prior to the procedure.

As with any procedure involving venipuncture, universal precautions should be used; that is, the injector should wear gloves under the assumption that the patient may harbor an infectious condition. Injection may be successfully carried out with a 21- through 25-gauge butterfly catheter attached to the 5-cc syringe containing the fluorescein. Many sites are available for intravenous access including the dorsal hand veins, forearm veins, and the antecubital vein; however, as a rapid injection improves contrast and facilitates interpretation of the arm-to-retina time, the antecubital location is preferred.[6] Once the needle has been inserted into the vein, blood should be refluxed into the hub of the needle as a precaution against extravascular injection. The plunger is then quickly depressed to ensure rapid infusion of the dye. In rare incidences where venous access is impossible, one may administer the dye orally, mixed with orange juice. However, this method makes adequate documentation of the early phase of the angiogram impossible and reduces the contrast for all frames of the angiogram.

Obtaining high-quality photographs of the early frame of the angiogram requires that the patient be correctly positioned at the fundus camera prior to dye injection. This is facilitated by first obtaining the color and red-free photographs so that the patient is familiar with positioning and flash intensity prior to starting the active phase of the angiogram.

After dye injection, a series of film or digital photographs is quickly obtained. This allows for adequate documentation of the early filling and transient frames of the angiogram. The eye of primary interest should be identified for the photographer and should be positioned in the camera at the commencement of the angiogram. After approximately 45 seconds of photos are obtained from the first eye, the photographer switches to the other eye to record midframe images. Late-frame images are then recorded several minutes later from each eye.

The debate regarding the choice of digital versus film-based angiography continues to rage. Many practitioners believe that film-based angiography provides better resolution and superior stereoscopic images. However, the limitations with the use of film include the increased labor requirements of

processing the film, error or loss in processing, the space required for storage, and film degradation with time. Digital angiography affords the advantage of immediate access of images without requiring developing. In fact, results are so immediate that the photographer may adjust settings such as illumination, focus, and magnification while the angiogram is being performed to optimize the results. Digital images are easier to display, process, store, and recall on demand, even in several locations simultaneously.

Risks and Complications

The complications rate from fluorescein angiography is less than 5%, making it one of the safest invasive diagnostic procedures in modern medicine. Nonetheless, the test has certain common risks that must be discussed and certain dangerous side effects that physicians conducting fluorescein angiograms must be aware of and prepared to treat urgently.

The risks of angiography have been well described.[2,12,14,15] Mild reactions include nausea, emesis, pruritus, and vasovagal symptoms. The incidence of these minor reactions has been quoted to be as high as 15%[2] and as low as 0.6%.[6] Modern studies have quoted the rate of nausea, the most common side effect, as 0.8%. The emesis rate is reported to be 0.2%, and the rate of urticaria as 0.6%.[15] The majority of these effects are rapid in onset and resolution, normally less than 1.5 hours of duration,[2] although delays of up to 15 hours have been reported.

The patient must also be made aware of other nearly universal side effects of little significance. Fluorescein dye stains the skin and mucous membranes; consequently, patients may experience a yellow skin discoloration that may persist for several hours.[2] It is possible that this skin discoloration may be associated with increased photosensitivity, so that lightly pigmented individuals should be advised to avoid excessive sun exposure for a day or two following angiography. As the dye is eliminated by the kidneys, patients should also be advised that they will experience a transient discoloration of their urine. The presence of fluorescein in the urine may also give misleading results on urine sugar testing.[6]

As a safeguard against minor or even more serious complications, patients with a history of asthma, hay fever, or prior minor reaction to fluorescein may be premedicated with an antihistamine such as diphenhydramine. Some authors have even advocated a small test dose of 1/10 mL of fluorescein 1 or 2 minutes prior to injecting the entire dose in a patient in whom a severe adverse reaction may be possible.[6]

Extravasation of the dye is another possible minor adverse event during angiography. This is associated with immediate pain, which is usually self-limited with no long-term sequelae, although in rare instances it has resulted in necrosis of the tissues overlying the site of injection.[15] The sodium moieties conducted to the hydrocarbon backbone in the fluorescein molecule (Fig. 2.1) are responsible for the pain and burning sensation that results from interstitial extravasations.

During angiography, severe toxic responses are possible, and a plan of action must be readily available to deal with this possibility.[14] These severe reactions include anaphylactic reactions such as seizure, loss of consciousness, laryngeal edema, respiratory arrest, myocardial infarction, and death.[14] The chance of a reaction leading to death is extremely rare, less than 1 in 200,000.[16] Nonetheless, the possibility of such a reaction requires having certain emergency equipment available, such as oxygen, a stethoscope, a blood pressure cuff, an oral airway, intravenous needles, intravenous fluids, and drugs, including but not necessarily limited to epinephrine and an antihistamine.

The use of fluorescein angiogram during pregnancy has not been definitively studied, and although no deleterious effects of angiography have been linked to fluorescein dye use during pregnancy,[17] it is prudent to avoid its use unless absolutely necessary for diagnosis or treatment. There are no other known contraindications to angiography, although patients with neurologic or breathing difficulty may have difficulty remaining stationary behind the camera for sufficient periods of time.[2]

Interpretation

Phases of the Angiogram

Understanding the normal timing of dye propagation through the ocular fundus during angiography is essential for correct interpretation of the study. The angiogram may be subdivided into six phases, as summarized in Table 2.1. The timings quoted for these phases assume injection of dye into the antecubital vein. Dye is normally first visualized in the optic nerve and choroid within 10 to 15 seconds after injection. However, variation in timing may be influenced by factors such as the site of injection, rapidity of injection, dye concentration, the use of a tourniquet, the patient's age, and cardiovascular status.[12] Thus, normal timing can be highly variable.

The choroid normally fills in a lobular, patchy, and mottled fashion, reflecting the lobular nature of choroidal anatomy (Fig. 2.3). This pattern normally persists for 3 seconds after the initial appearance of dye in the choroid. By 5 seconds after dye is first visible in the choroid, there should be uniform filling with a diffuse and even background flush of fluorescence that will be seen throughout the remaining phases of the angiogram. The optic nerve will also appear fluorescent at

Table 2.1. The six phases of the fluorescein angiogram with normal transit times.

Phase	Timing
1. Choroidal filling	8 – 15 seconds after injection
2. Retinal arterial filling	1 – 2 seconds after choroidal filling
3. Venous lamellar filling	2 – 3 seconds after arterial filling
4. Full venous circulation	< 11 seconds after arterial filling
5. Recirculation	30 – 150 seconds after injection
6. Late phase	10 – 30 minutes after injection

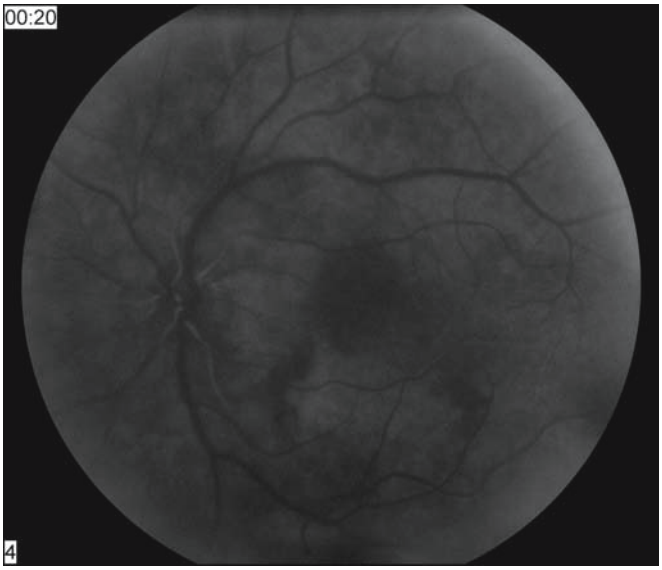

Fig. 2.3. The choroidal-filling phase of the angiogram demonstrating the normal lobular, patchy, and mottled filling pattern of the choroid.

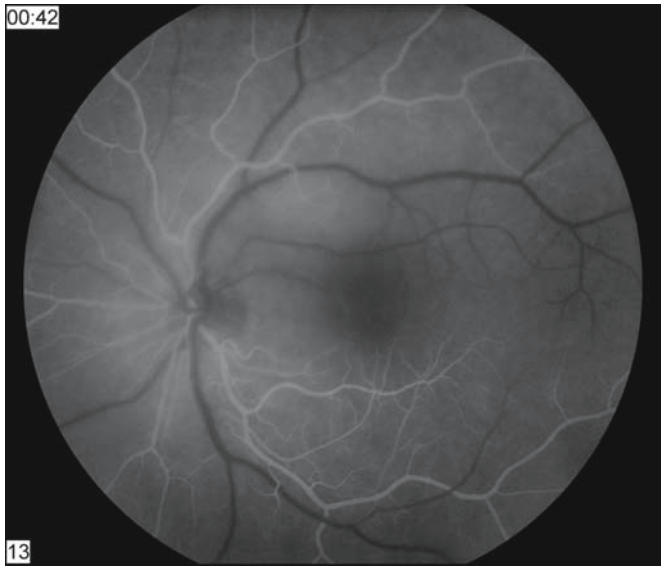

Fig. 2.5. Early arterial filling of the retina during the arterial phase of the angiogram. Arteries demonstrate good perfusion, being completely filled with fluorescein, while the veins remain dark, as no dye has yet entered the venous circulation.

this time, as it is supplied by the posterior ciliary arteries (arising from the choroidal circulation). Similarly, a cilio-retinal artery, present in about one third of individuals, will fill during the choroidal phase of the angiogram (Fig. 2.4).

Approximately 1 to 3 seconds after the initial appearance of dye in the choroidal circulation, filling of the central retinal artery and its superior and inferior branches will occur. Once the dye is present in the central retinal artery, complete arterial filling proceeds very rapidly (less than 1 second) and partial or lamellar arterial filling is difficult to capture in a normal individual (Fig. 2.5). The delay between the injection of dye into the antecubital vein and its first appearance in the retina is known as the arm-to-retina time and should be 11 ± 3 seconds for the normal adult.

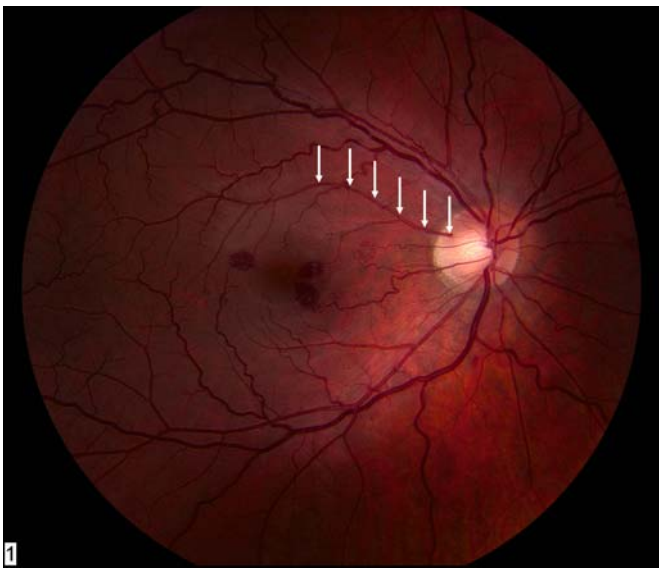

Fig. 2.4. A cilioretinal artery, which exhibits filling during the choroidal phase of the angiogram.

In contrast to the rapid arterial filling seen during angiography, venous filling is slow, and a laminar appearance of dye is seen normally in all individuals. This phase of the angiogram, the venous laminar filling phase, commences 2 to 3 seconds after complete arterial filling. The dynamics of fluid flow in a tube dictates that velocity of flow is greatest in the center of the lumen and slowest, due to frictional forces, at the wall of the tube. The forces generated by the faster flowing blood in the center of large venous channels keep the dye concentrated along the periphery of the retinal veins for several seconds (Fig. 2.6). This appearance is known as laminar venous filling. Complete venous filling should be seen within 11 seconds of fluorescein's first appearing in the retinal arterials. Cumulatively, the first four phases of the angiogram that have been described are known as the arterial-venous transient phase of the angiogram. The normal arterial-venous transient time, defined as the length of time between first appearance of dye in the retinal arteries to complete filling of the retinal veins should be 10 ± 2 seconds in the normal individual.

The recirculation phase begins about 30 seconds after injection of dye and lasts approximately 2 minutes. During this phase arteries and veins are now being filled for a second time. As the dye has now been circulated to the kidneys, where it is being rapidly removed from circulation, the concentration of dye seen in the normal fundus is steadily declining during this phase (Fig. 2.7). At this point, normal staining of the sclera and optic nerve are seen.

In the late phase of the angiogram (10 to 30 minutes following injection), choroidal and retinal fluorescence is nearly

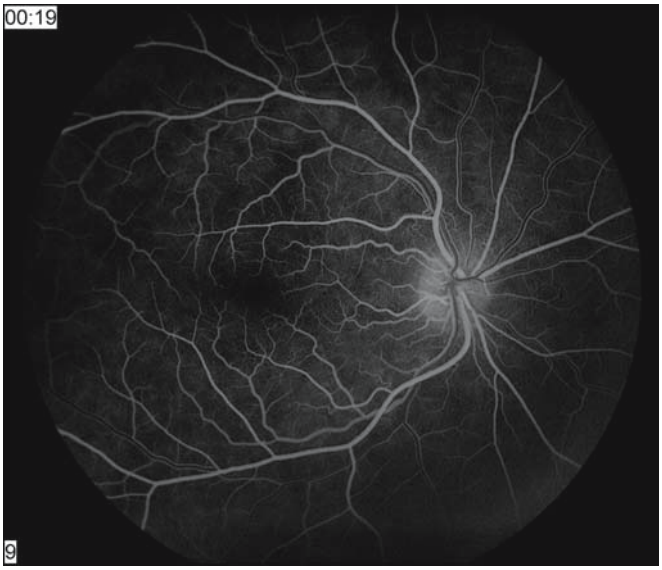

Fig. 2.6. The venous laminar-filling phase of the angiogram. Laminar filling is well demonstrated in the superior hemiretinal veins, with the primary inferior retinal vein demonstrating more complete filling.

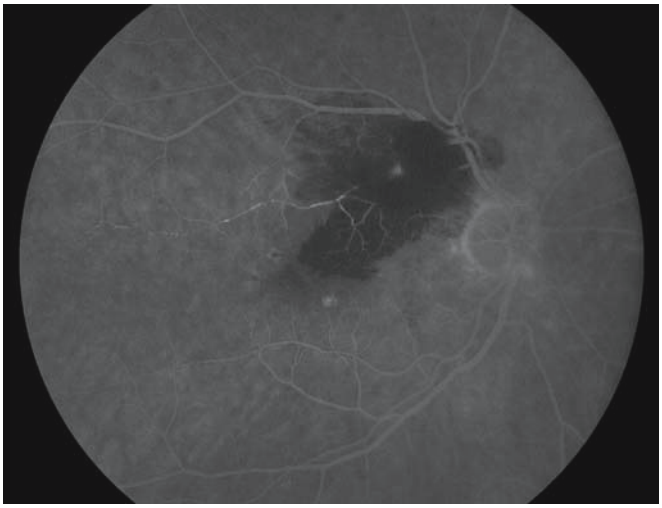

Fig. 2.7. The recirculation phase of the angiogram.

extinct. However, continued documentation of this phase of the angiogram is necessary to record vascular leakage secondary to inflammation or a vascular anomaly such as diabetes, central serous chorioretinopathy, or choroidal neovascular membrane.

Autofluorescence

Prior to the injection of dye, it is important to take several color and red-free photographs. The color photographs are important to enable comparison of angiographic findings with the clinical appearance and precisely localize pathology for subsequent treatment or accurate comparison with subsequent exams. Red-free photographs (images recorded prior to dye injection with the camera filters in place) are important, to avoid confusion arising from autofluorescence.

Many compounds occurring in nature exhibit a fluorescent spectrum similar to that of fluorescein dye. Some of these compounds that may be found within the eye include vitamin A, calcium salts, and lipofuscin pigment.[14] Clinically, the fluorescence that arises from structures containing these compounds is termed autofluorescence. Examples include optic nerve head drusen (Fig. 2.8) and astrocytic hamartomas (calcium salts), as well as the flecks associated with fundus flavimaculatus and Best's disease (lipofuscin pigment).

Other than autofluorescence, any abnormal fluorescein pattern may be characterized as either hyperfluorescent or hypofluorescent (Table 2.2).

Hypofluorescence

The etiology of hypofluorescence may be divided into vascular filling defects and blockage of fluorescence by an opaque medium within the eye, hiding underlying fluorescence (Table 2.2). Note that normal relative hypofluorescence is seen in the fovea where increased concentration of xanthophyll pigment blocks choroidal fluorescence (Fig. 2.9).

Common examples of blockage of underlying choroidal fluorescence include hemorrhagic lesions, lipofuscin deposition in fundus flavimaculatus and Best's disease, and hyperpigmentation lesions (Fig. 2.10). Common examples of hyperpigmented RPE lesions that block underlying choroidal fluorescence but preserve the visibility of overlying retinal vasculature include the macular hyperpigmentation in age-related macular degeneration (AMD), chorioretinal scars (i.e., the center of laser scars or cryo scars), and congenital hypertrophy of the retinal pigment epithelium (CHRPE).

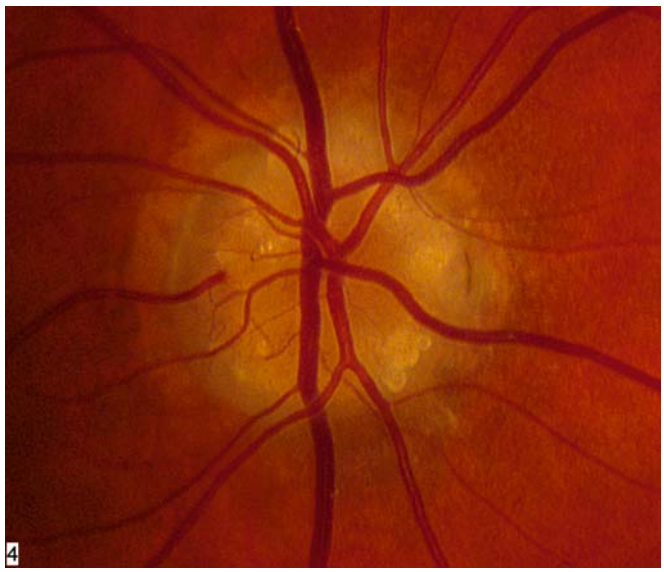

Fig. 2.8. The calcium salts of optic nerve head drusen often demonstrate autofluorescence.

TABLE 2.2. Pathologic patterns of fluorescence.

Pattern	Cause	Example	Appearance on angiogram
Hyper-fluorescence	Leakage	AMD (CNVM)	Hyperfluorescence increase with time (both intensity of dye and size of lesion)
		Neovascular tissue	
		CSCR	
	Staining	Scar	Amount of dye visible increases
		Scleral show	Size of lesion stays constant
	Pooling	Pigment epithelial defect	Dye accumulating in a fluid-filled space (well-defined border, elevation on clinical exam)
		Tumor	
	Window defect	Loss of RPE	Normal fluorescence of choroid accentuated (most apparent early, fades late)
		RPE tear	
		Drusen	
Hypo-fluorescence	Blockage	Blood	Fluorescence of dye blocked by opaque medium
		Pigment	
		Fibrous tissue	
	Nonper-fusion	Vascular occlusion	Vessels do not fill properly
		Coloboma	Absence of tissue/vessels

AMD, age-related macular degeneration; CNVM, choroidal neovascular membrane; CSCR, central serous chorioretinopathy; RPE, retinal pigment epithelium.

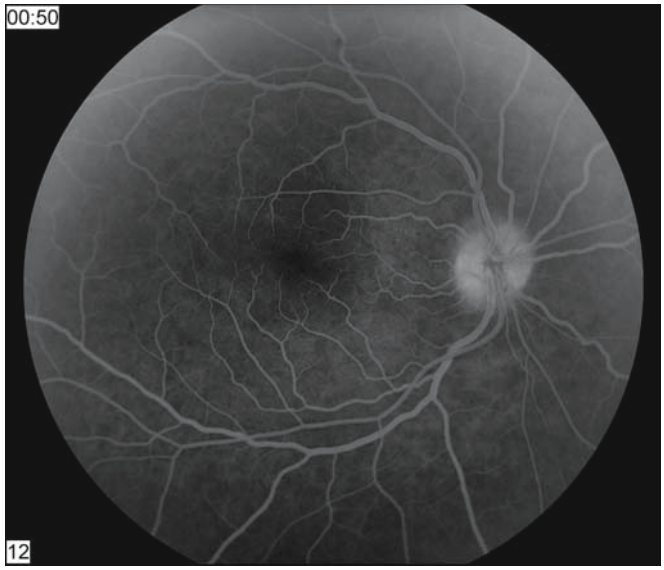

FIG. 2.9. Relative hypofluorescence of the macular area caused by increased concentration of xanthophyll pigment blocking underlying choroidal fluorescence.

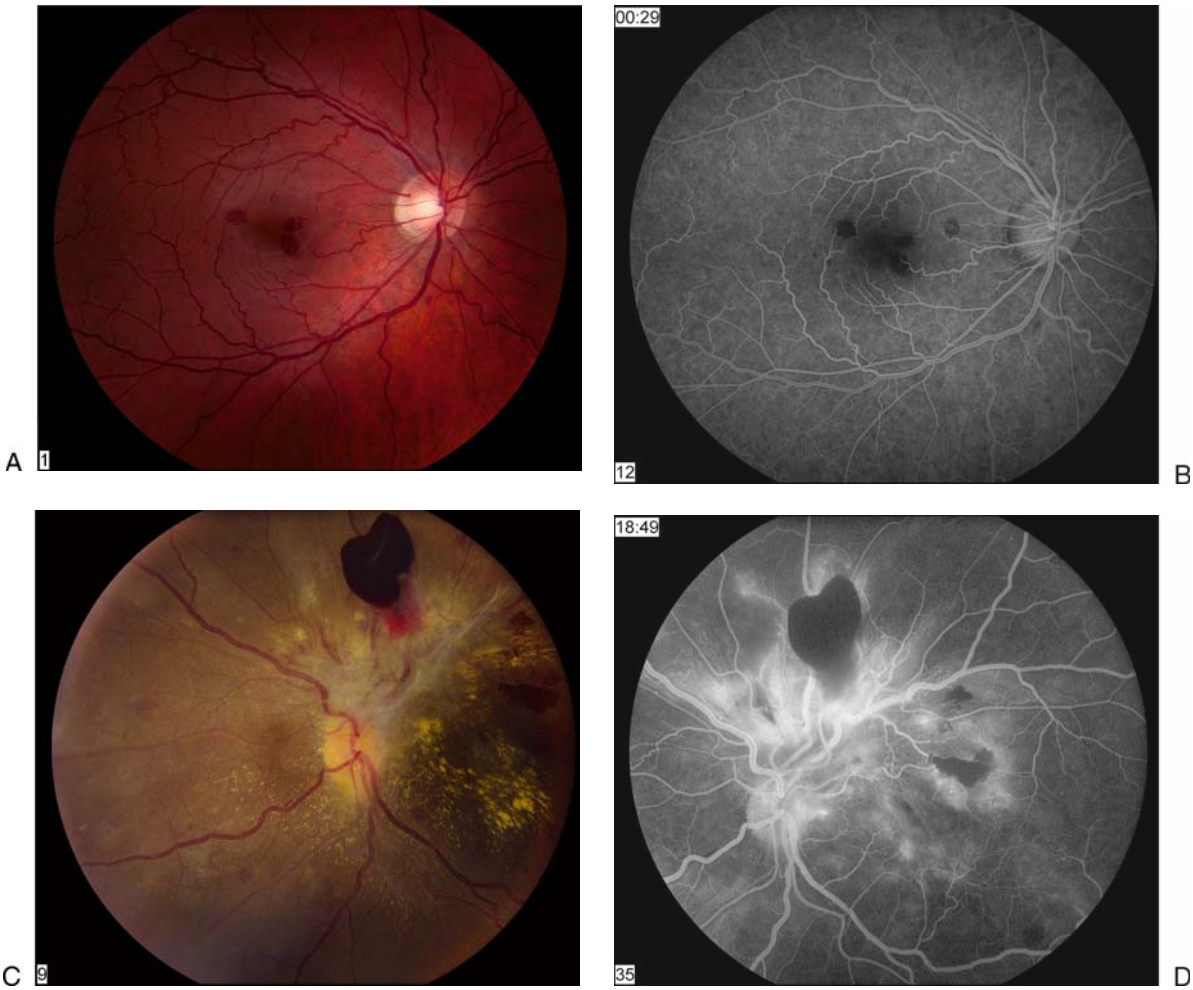

FIG. 2.10. Hypofluorescent lesions of various etiologies. (A,B) Subretinal blood, which allows visualization of the overlying retinal vessels. (C,D) Preretinal hemorrhage, which blocks all retinal vasculature. (E) Lipofuscin deposits of Best's disease. (F,G) Lipofuscin deposits present in fundus flavimaculatus. (H,I) Hyperpigmentation associated with pigment clumping in age-related macular degeneration (AMD).

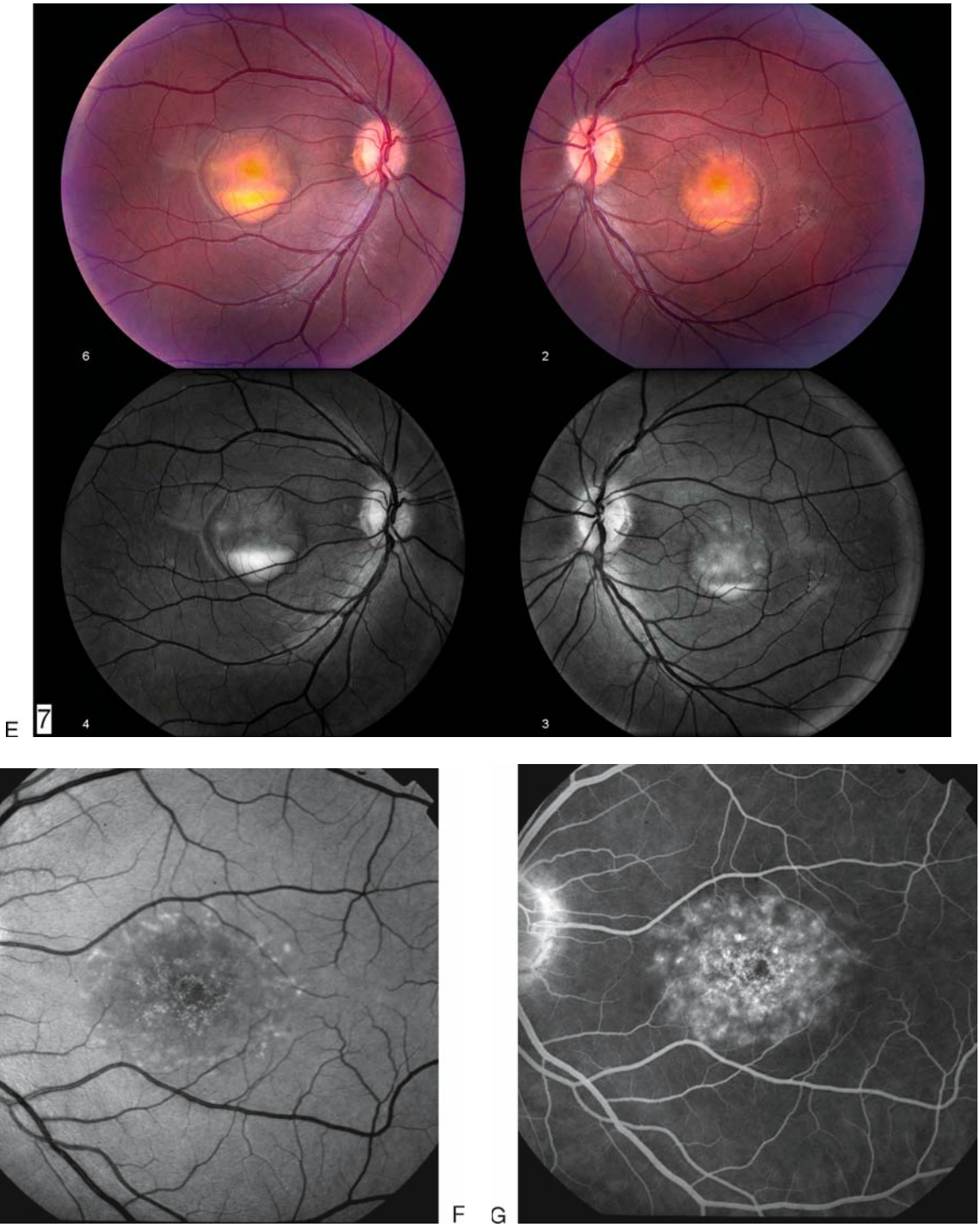

FIG. 2.10. (continued).

The visibility of fluorescein-filled retinal vessels within a blocking lesion helps to determine its depth. For example, a subretinal hemorrhage associated with an age-related choroidal neovascularization blocks choroidal fluorescence, but the overlying retinal vasculature is visible. Similarly, a deeper dot or blot hemorrhage, as seen in diabetes or the ocular ischemic syndrome, blocks capillary fluorescence but larger retinal vessels remain visible. Conversely, a flame-shaped hemorrhage located within the nerve fiber layer (innermost retina) blocks all fluorescence from the retinal vasculature and the choroid.

Vascular filling defects may occur at any level of retinal or choroidal circulation. Retinal arterial occlusion produces hypofluorescence of the retina and retinal vessels distal to the site of the occlusion (Fig. 2.11). This hypofluorescence may

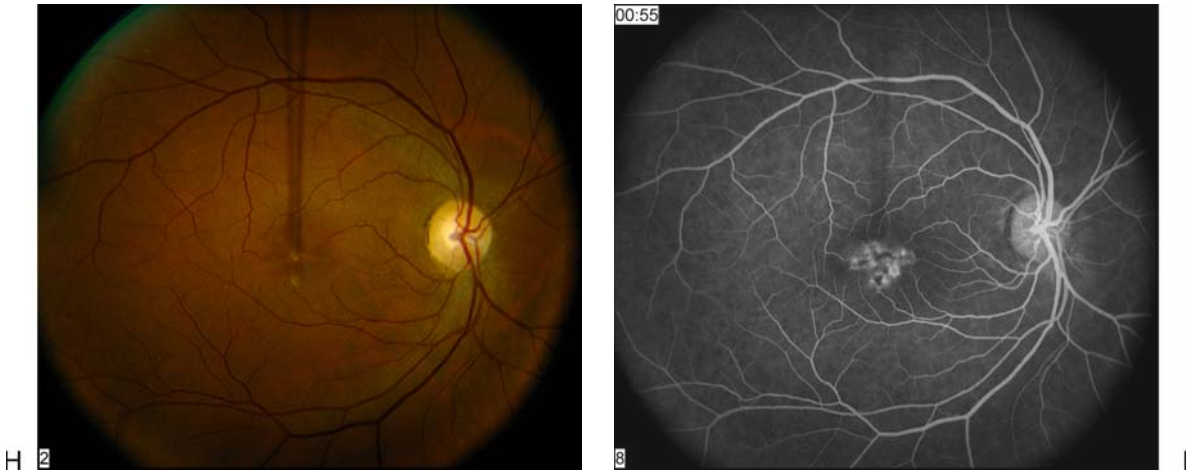

Fig. 2.10. (continued).

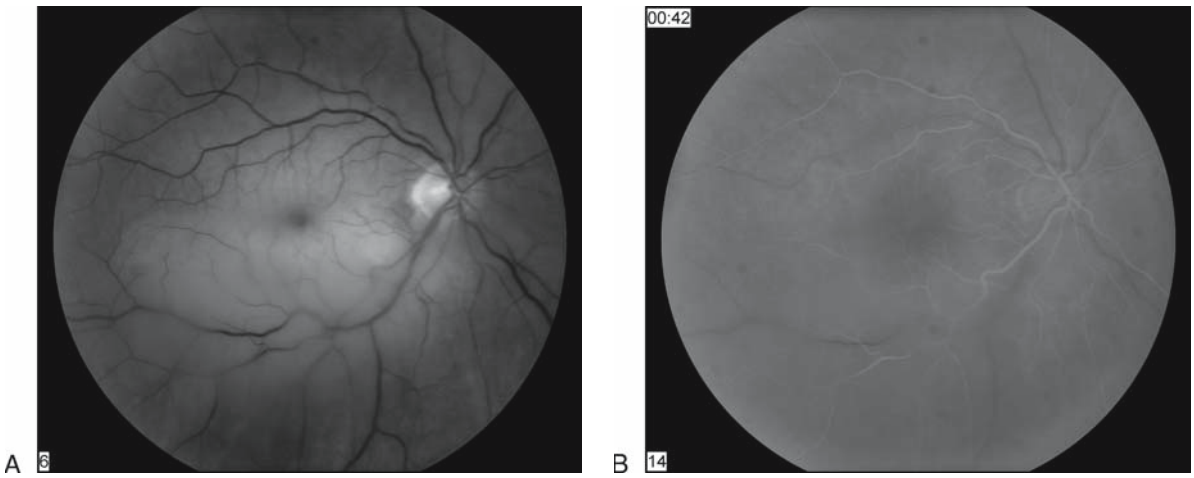

Fig. 2.11. (A,B) Hypofluorescence produced by retinal arterial occlusion.

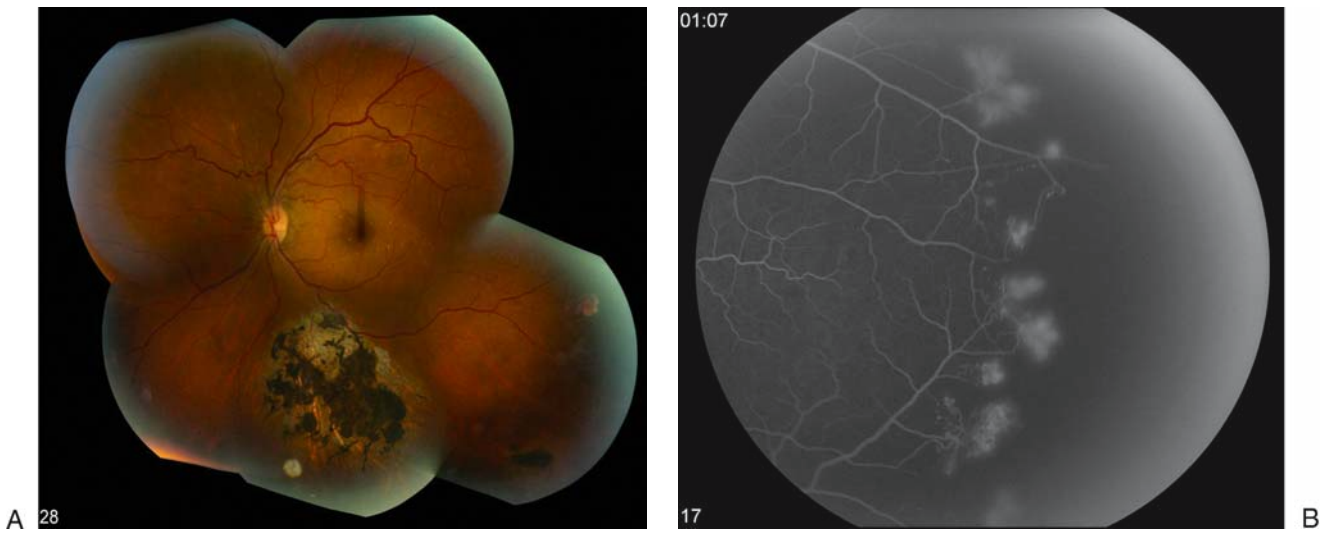

Fig. 2.12. " Pruning " of the retinal vasculature with hypofluorescence of the distal nonperfused retina in talc retinopathy (A,B) and sickle cell disease (C,D).

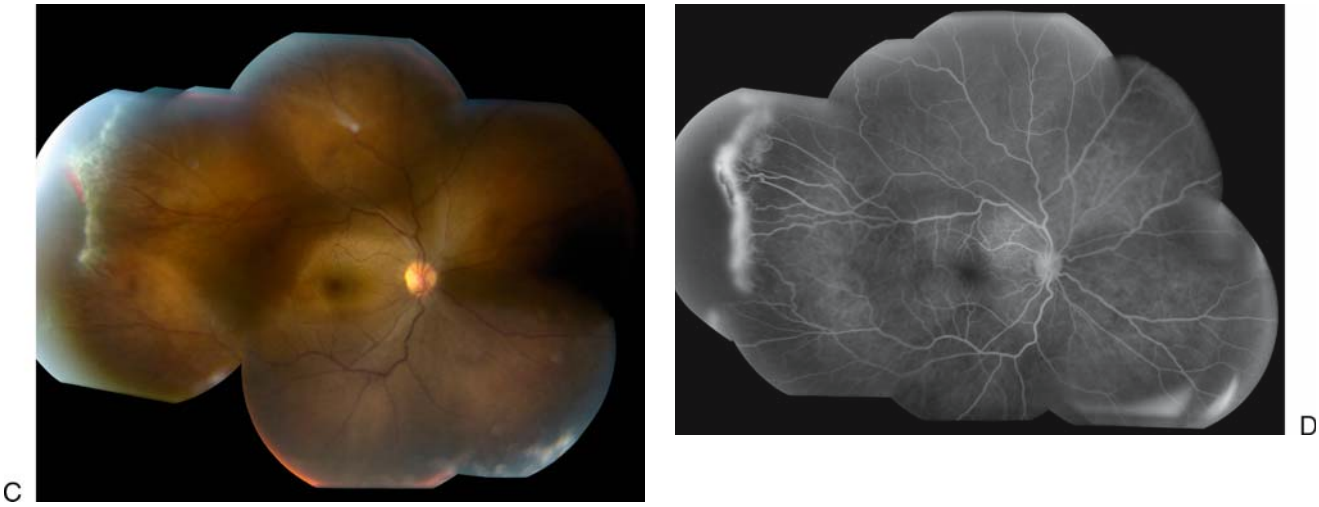

FIG. 2.12. (continued).

be accentuated by retinal edema that usually accompanies arterial nonperfusion and further blocks underlying choroidal fluorescence. Occlusion of small vessels, as seen in diabetes, radiation retinopathy, sickle cell disease, or talc retinopathy, reveals an abrupt end to the column of dye with a vessel. This is often accompanied by vascular remodeling at the border of the perfused and nonperfused retina (Fig. 2.12). Capillary nonperfusion, as seen in diabetes and retinal vein occlusion, results in relative hypofluorescence of the affected area compared with the adjacent retina (Fig. 2.13).

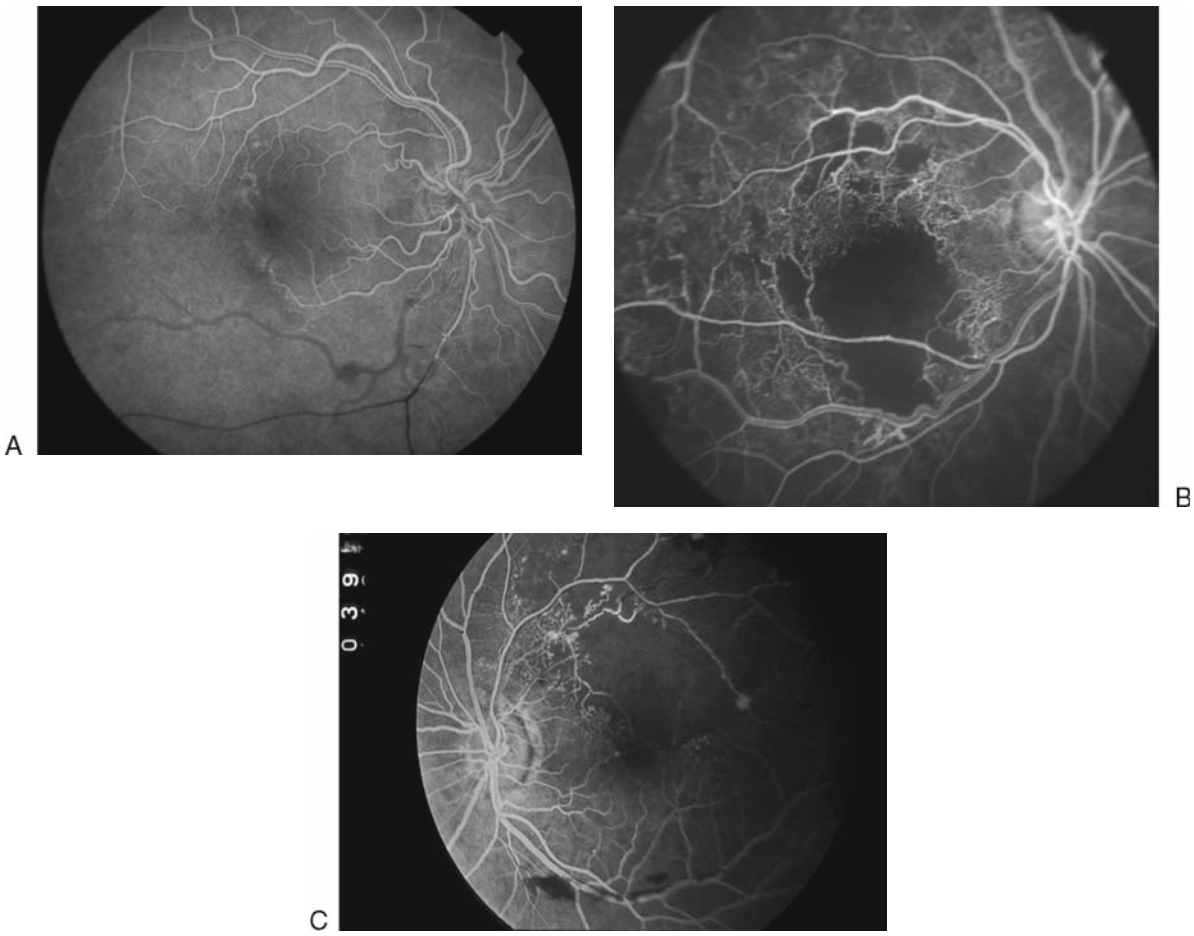

FIG. 2.13. Hypofluorescence results in capillary nonperfusion in retinal vein occlusion (A,B) and diabetic retinopathy (C).

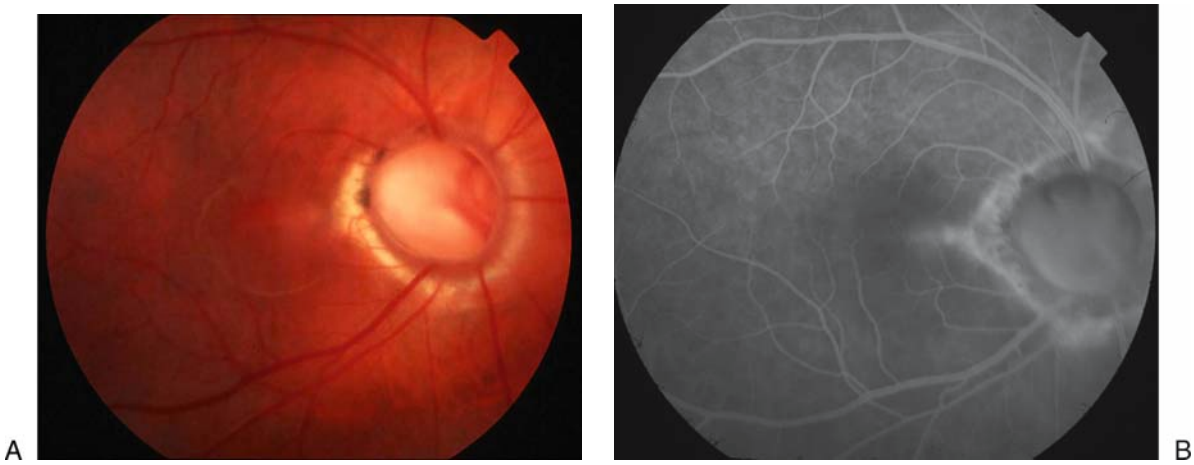

FIG. 2.14. (A–B) Optic nerve pit resulting in hypofluorescence of the optic nerve head.

Blockage of choroidal filling is less apparent in the angiogram because of the attenuation of the choroidal signal by the normal retinal pigment epithelium. Choroidal hypofluorescence may result from a variety of causes including malignant hypertension, toxemia of pregnancy, and vasculitis such as lupus. Giant cell arteritis may also present with delayed choroidal fluorescence and patchy choroidal nonperfusion. Areas of choroidal nonperfusion may be seen as wedge-shaped or diffuse zones of reduced choroidal flush in the later frames of the angiograms or subtle areas of hypofluorescence during the choroidal phase of the angiogram.

Optic nerve disease may be seen as a hypofluorescent lesion on the angiogram. Anterior ischemic optic neuropathy may give rise to sectoral hypofluorescence of the optic nerve. Optic nerve hypofluorescence may also be seen with optic nerve pits, optic nerve coloboma, and even glaucomatous cupping of the nerve head (Fig. 2.14).

Hyperfluorescence

There are four causes of hyperfluorescence: leakage, staining, pooling, and window defect. The first three causes imply excess dye accumulation. Window defect implies an area of reduced density or total absence of RPE. The resulting absence of the blocking effect of the RPE, which is normally exerted on the background fluorescence of the choroid, results in a localized and well-defined area of hyperfluorescence on the angiogram. As the window defect simply represents increased visibility of the choroidal fluorescence, it is most noted early in the angiogram and gradually fades in the later frames of the angiogram as dye exits the choroid. Examples of window defects include drusen, a rip or tear of the RPE, geographic atrophy of macular degeneration, chorioretinal scars, and macular holes (Fig. 2.15).

There are two large categories of retinal or choroidal pathology that may give rise to lesions that leak during angiography: inflammation and neovascularization. Inflammation, including vasculitis, implies the presence of increased vascular permeability, which allows normal vessels to become incompetent. Neovascularization implies the presence of new abnormal vascular tissue that is inherently leaky. In both cases, the hyperfluorescence that is seen expands in the late phase of the angiogram with respect to both the intensity and the size of the lesion. Leaking at the level of the choroid often implies the presence of choroidal neovascular membrane formation from a variety of causes including AMD, histoplasmosis, or myopic degeneration (Fig. 2.16). Examples of neovascularization at the level of the retina include the proliferative disease states of diabetes, sickle cell, and talc retinopathy (Fig. 2.17).

Leakage from normal vessels that have lost their ability to prevent the egress of dye occurs in a variety of conditions. Diabetic macular edema presents classically as leakage from microaneurysms (Fig. 2.18). In the Irvine-Gass syndrome (cystoid macular edema following cataract surgery), the leakage originates from incompetent perifoveal capillaries. The dye concentrates in the cystoid spaces of the outer plexiform layer of the retina giving the classic "petaloid" pattern of hyperfluorescence (Fig. 2.19). An identical pattern is seen in other forms of uveitis-induced cystoid macular edema. A final example of leakage occurs from the vascular incompetence that is seen with an arterial macroaneurysm (Fig. 2.20)

Pooling refers to the accumulation of dye within a fluid-filled space. Pooling lesions increase in intensity throughout the angiogram; however, in contrast to lesions that leak, the border of the lesions stay well defined, and elevation is seen on the clinical exam. Examples of lesions that exhibit pooling include pigment epithelial detachments seen in AMD, pooling within an intraocular tumor, and the subretinal pooling that is seen with central serous chorioretinopathy (Fig. 2.21).

The final cause of hyperfluorescence is staining. Staining defects result in an increased intensity of hyperfluorescence

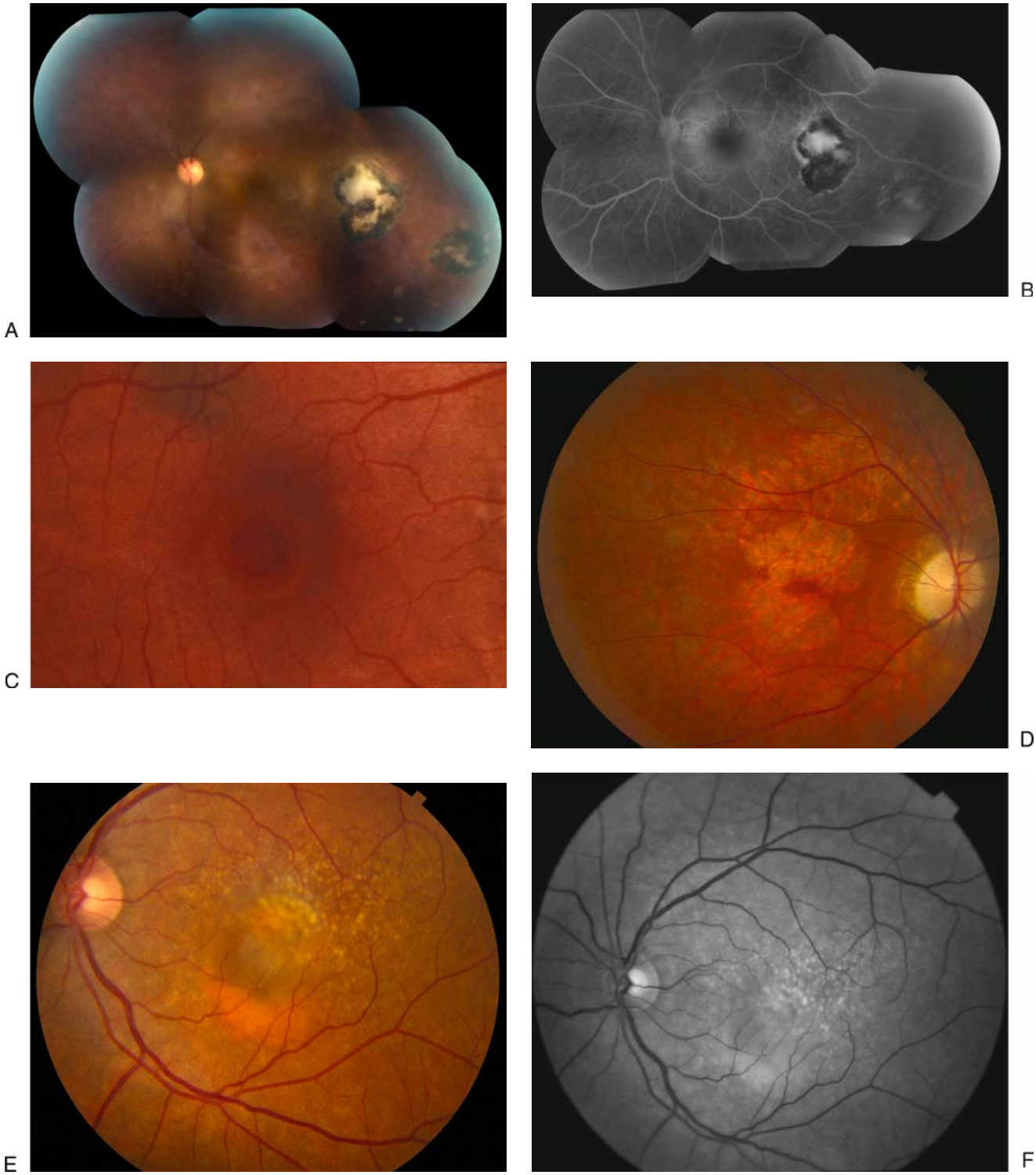

FIG. 2.15. Hyperfluorescent window defect as seen in chorioretinal scars (A,B), macular hole (C), geographic atrophy of macular degeneration (D), and drusen (E,F).

within a given lesion, but the size of the hyperfluorescent area remains constant, that is, there is no or minimal leakage of dye. Fluorescein dye is able to stain both healthy and abnormal ocular tissues. Examples of lesions that stain include disciform and other scars, regressed neovascular tissue, and visible areas of sclera as seen in peripapillary atrophy, myopic degeneration, and lesions such as gyrate atrophy (Fig. 2.22).

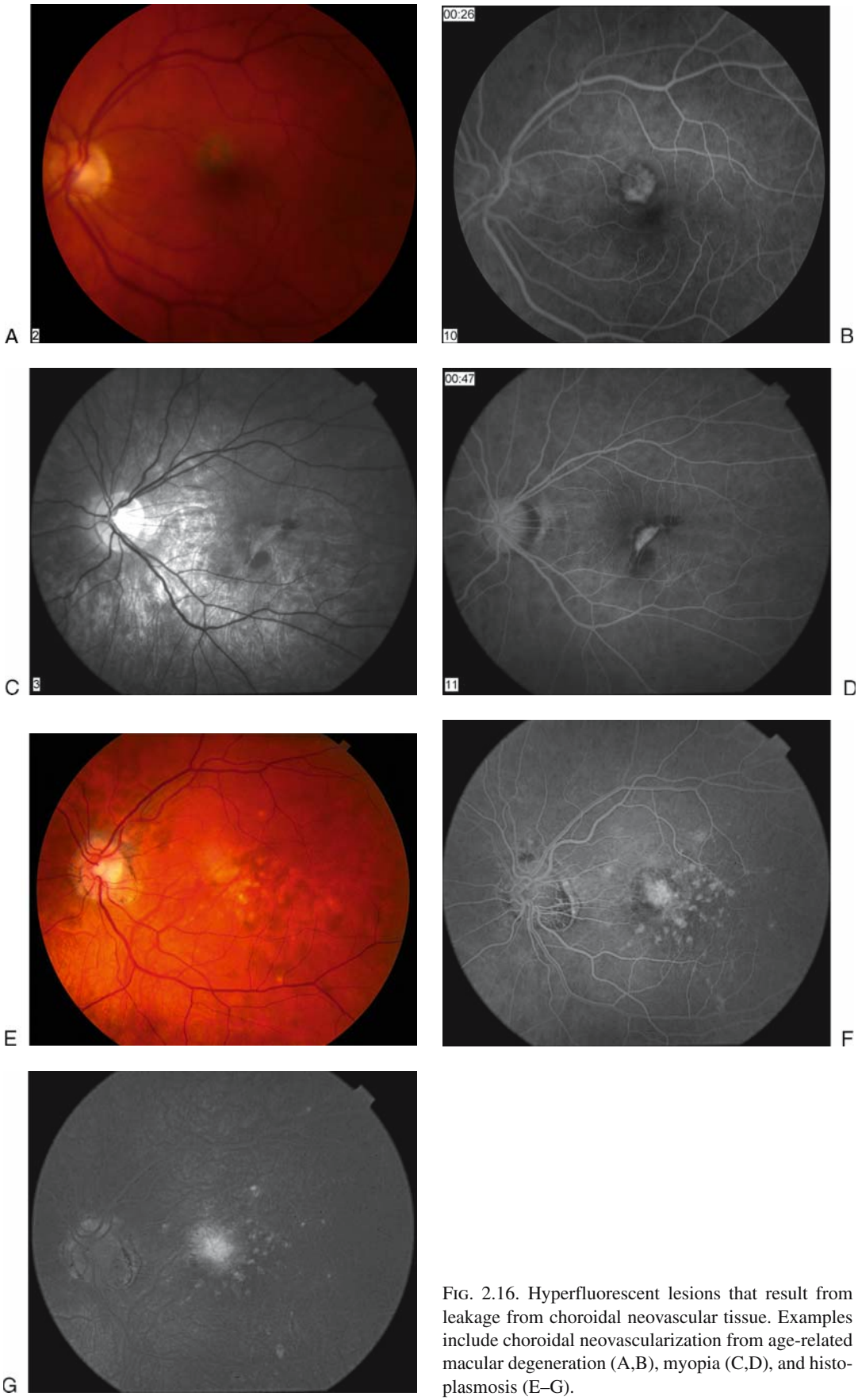

FIG. 2.16. Hyperfluorescent lesions that result from leakage from choroidal neovascular tissue. Examples include choroidal neovascularization from age-related macular degeneration (A,B), myopia (C,D), and histoplasmosis (E–G).

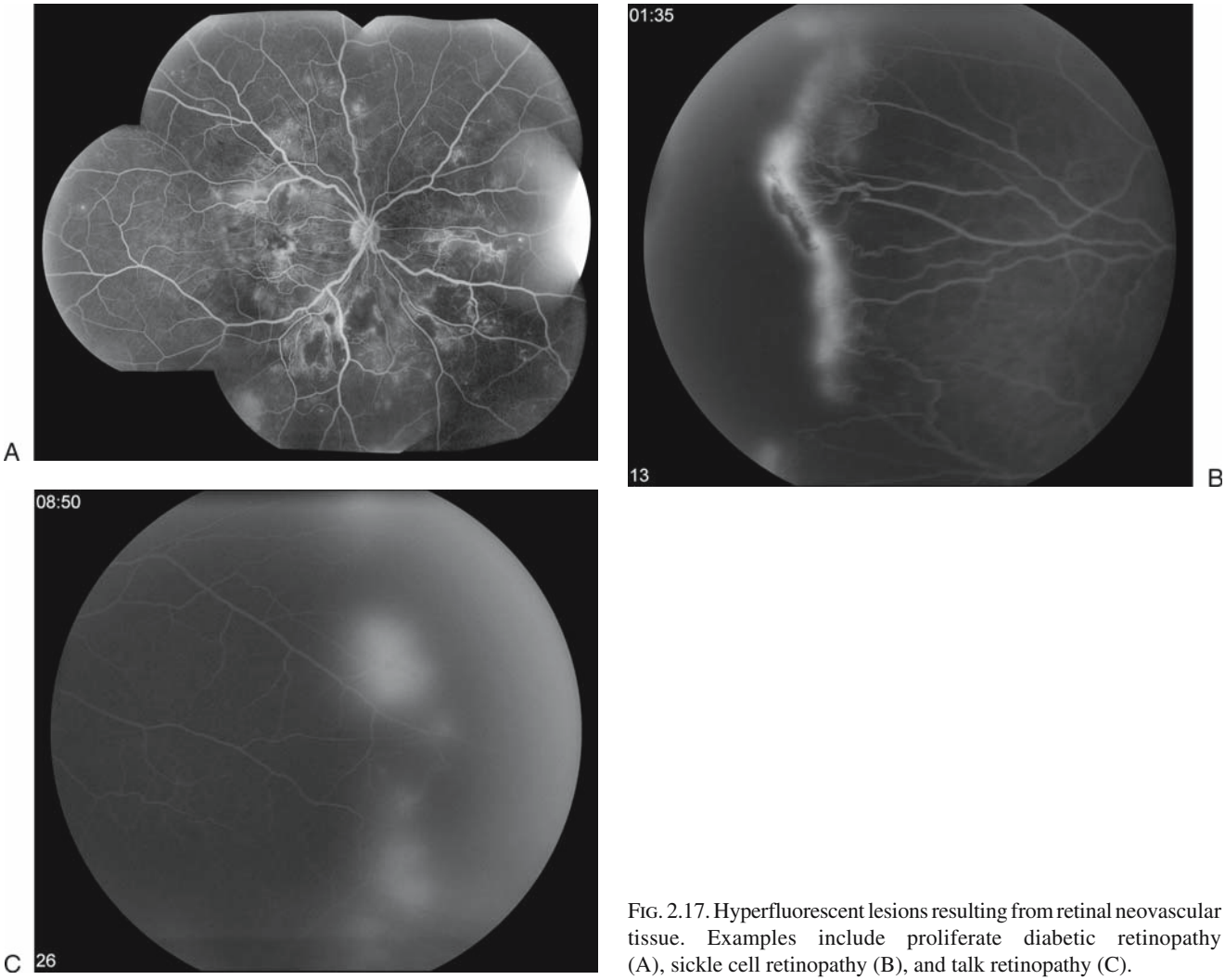

FIG. 2.17. Hyperfluorescent lesions resulting from retinal neovascular tissue. Examples include proliferate diabetic retinopathy (A), sickle cell retinopathy (B), and talk retinopathy (C).

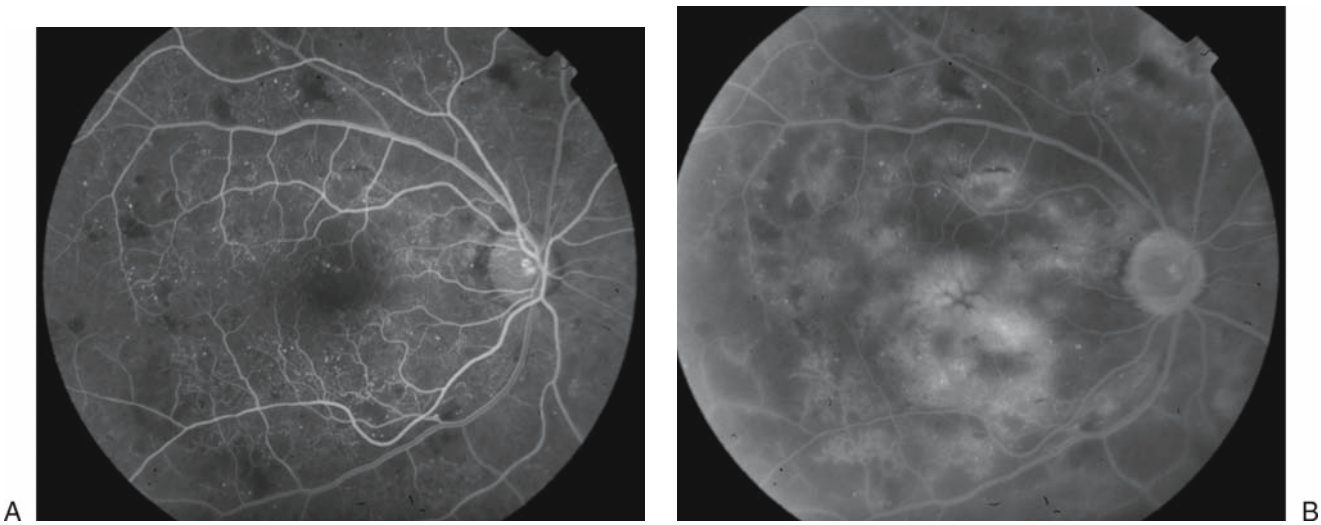

FIG. 2.18. (A,B) The hyperfluorescence of clinically significant diabetic macular edema results from leakage of dye from microaneurysms.

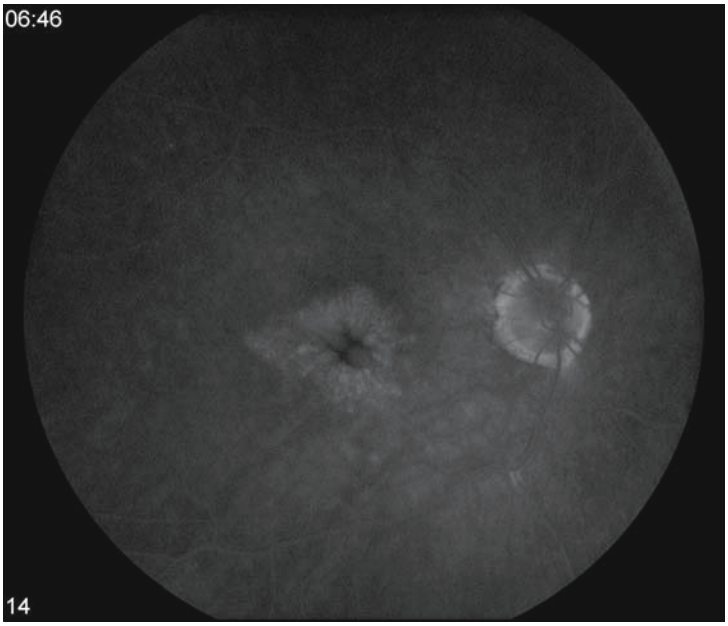

FIG. 2.19. The petaloid pattern of hyperfluorescence seen in this patient with cystoid macular edema following cataract extraction.

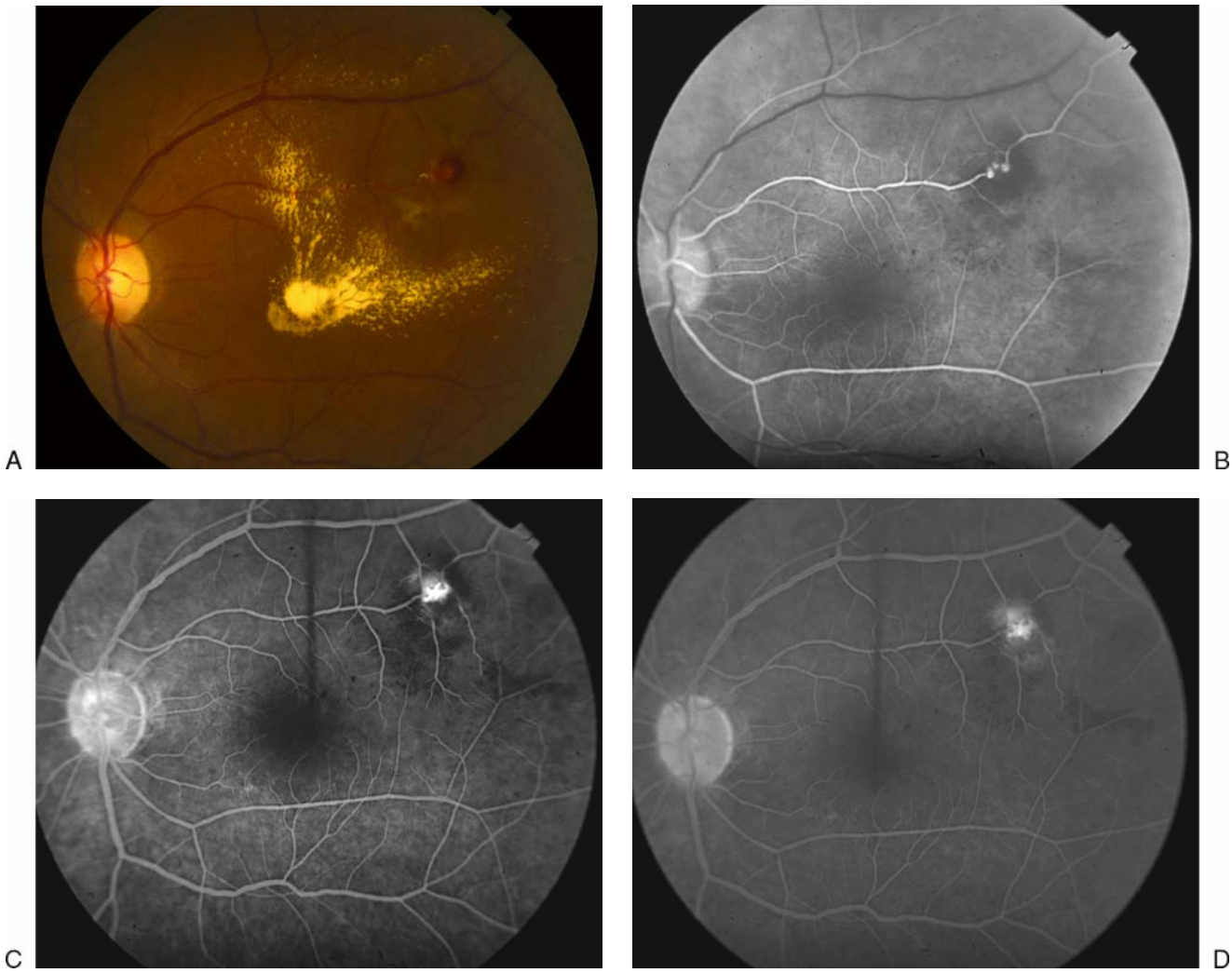

FIG. 2.20. (A–D) Leakage of dye from a macroaneurysm.

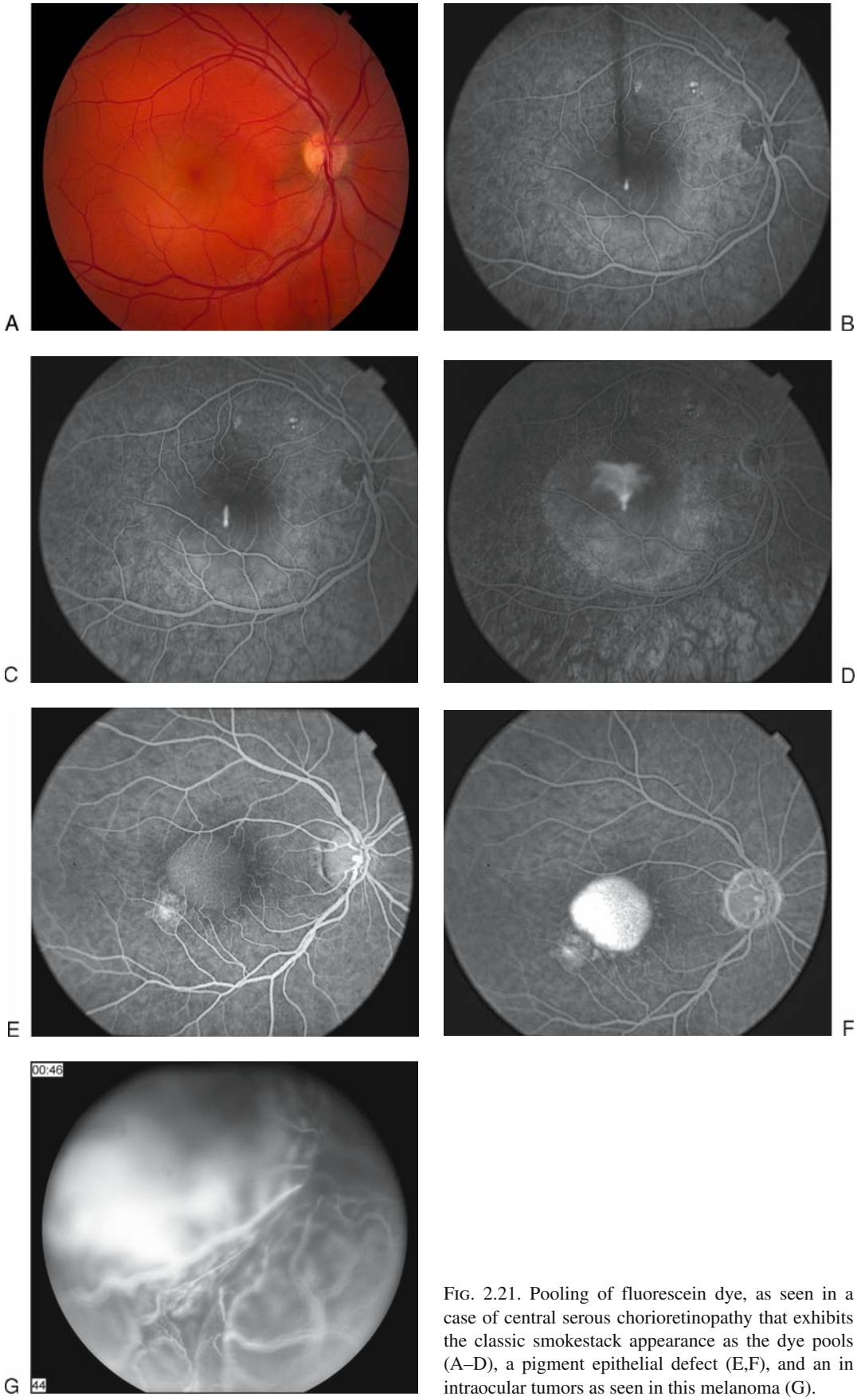

Fig. 2.21. Pooling of fluorescein dye, as seen in a case of central serous chorioretinopathy that exhibits the classic smokestack appearance as the dye pools (A–D), a pigment epithelial defect (E,F), and an in intraocular tumors as seen in this melanoma (G).

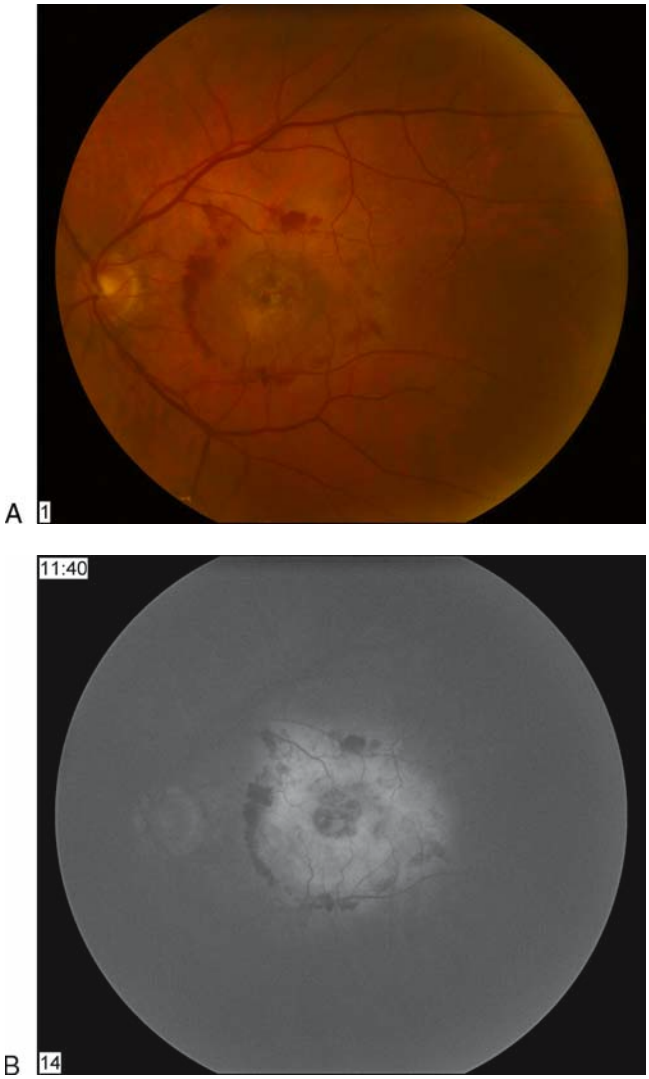

FIG. 2.22. (A,B) Hyperfluorescence that results from staining of a disciform scar seen in end-stage age-related macular degeneration.

Conclusion

Fluorescein angiography is a safe, effective, and routinely performed diagnostic test. It provides a wealth of information about the subtle details of the retinal and choroidal vasculature and provides a permanent record of the results. It also documents the integrity of the blood–retinal barrier and the RPE. Fluorescein angiography is useful to study, diagnose, plan treatment, and assess treatment response in a variety of ocular diseases, which make it one of the most useful diagnostic tools available within ophthalmology.

References

1. Rechtman E, Harris A, Kumar R, et al. An update on retinal circulation assessment technologies. Curr Eye Res 2003;27(6): 329–343.
2. Cavallerano AA. Ophthalmic fluorescein angiography. Optom Clin 1996;5(1):1–23.
3. Sinchai P. Office fluorescein angioscopy. Ann Ophthalmol 1977;9(2):177.
4. Yannuzzi LA, Ober MD, Slakter JS, et al. Ophthalmic fundus imaging: today and beyond. Am J Ophthalmol 2004;137(3): 511–524.
5. Von Baeryer A. Uber ein neue Klasse van farbstoffen. Der Deutschen Chem Ges 1871;4:555.
6. Anand R. Fluorescein angiography. Part 1. Technique and normal study. J Ophthalmic Nurs Technol 1989;8(2):48–52.
7. Ehrlich P. Uber provilirte fluoresceinzerscheinungen. Am Aug Dtsch Med Wochenschr 1882;8–21.
8. Burke A. Die klinische physiologische und pathologie bedeuting der fluorescein im auge nach darrerching von-uranin. Klin Monatsbl Augenheilkd 1910;48:445–454.
9. MacLean AL, Maumenee AE. Hemangioma of the choroid. Am J Ophthalmol 1959;57:171–176.
10. Novotny HR, Alvis DL. A method of photographing fluorescein in the human retina. Circulation 1961;24:72–77.
11. Brancato R, Trabucchi G. Fluorescein and indocyanine green angiography in vascular chorioretinal diseases. Semin Ophthalmol 1998;13(4):189–198.
12. Bloome MA. Fluorescein angiography: risks. Vision Res 1980;20(12):1083–1097.
13. Ciardella AP, Prall FR, Borodoker N, Cunningham ET Jr. Imaging techniques for posterior uveitis. Curr Opin Ophthalmol 2004;15(6):519–530.
14. Kelley JS. Fluorescein angiography: techniques and toxicity. Int Ophthalmol Clin 1977;17(2):25–33.
15. Jennings BJ, Mathews DE. Adverse reactions during retinal fluorescein angiography. J Am Optom Assoc 1994;65(7): 465–471.
16. Yannuzzi LA, Rohrer KT, Tindel LJ, et al. Fluorescein angiography complication survey. Ophthalmology 1986;93(5): 611–617.
17. Halperin LS, Olk J, Soubrane G, Coscas G. Safety of fluorescein angiography during pregnancy. Am J Ophthalmol 1990;109: 563–566.

3
Indocyanine Green Angiography: General Aspects and Interpretation

Christina M. Klais, Michael D. Ober, and Lawrence A. Yannuzzi

More than three decades ago, indocyanine green angiography (ICGA) was introduced into ophthalmology. The relatively poor fluorescence efficiency of the indocyanine green (ICG) molecule and its limited ability to produce high-resolution images on infrared film initially restricted its angiographic application; however, ICG has subsequently been found to have several advantages over sodium fluorescein, especially in imaging choroidal vasculature. The emergence of high-resolution infrared digital imaging systems, specifically designed for ICGA and a growing awareness of choroidal vascular lesions has led to a resurgence of interest in ICGA.[1] The applications of ICGA continue to grow in number; the full extent of its capabilities is not yet known.

History

Initially used in the photographic industry, ICG was introduced into medicine in 1957. Its first application in medicine was in measuring cardiac output. In 1969, the first attempts at using ICGA were performed by Kogure and Choromokos[2] studying cerebral circulation in a dog. In 1971, Hochheimer[3] modified the system for ICGA by changing the color film that had been used previously to black-and-white infrared film. In 1972, Flower and Hochheimer[4] performed the first intravenous ICGA to image the human choroid. In the following years, Flower [5] and coworkers began a series of studies on primates and human to evaluate the potential utility of ICGA in the investigation of the normal and pathologic eye. They refined the procedure with recommendations for the concentration of the dye and method of injection. Flower also modified the transmission and emission filters to improve the resolution of the choroidal vessels. Flower et al. eventually found that infrared film lacked the sensitivity to adequately capture low-intensity ICG fluorescence, which limited the clinical utility of ICGA.

The resolution of ICGA was improved in the mid-1980s by Hayashi and coworkers,[6] who developed improved filter combinations with sufficient sensitivity for near-infrared wavelength. They were instrumental in the transition from film to videotape by introducing videoangiography. Although the sensitivity of the video camera system was a vast improvement, its inability to study individual images and the potential light toxicity using a 300-watt halogen bulb restricted the duration and quality of the technique.

In 1989, Destro and Puliafito [7] performed ICGA with a system very similar to that described by Hayashi. Imaging was improved by better filter combinations, but images were still stored and later analyzed using videotape recording. In the same year, the use of scanning laser ophthalmoscope for ICG videoangiography was introduced by Scheider and Schroedel. [8] In 1992, the use of a 1024 × 1024 line digital imaging system was introduced to produce high-resolution ICGA.[1] Images were digitized, displayed on a high-resolution monitor, and stored on an optical disc, but the system lacked flash synchronization with the video camera. Finally, Yannuzzi and coworkers [9] described a 1024-line resolution system that was synthesized with the appropriate flash synchronization and image storage capability, permitting high-resolution, long-duration ICGA.

Chemical Properties

Indocyanine green is a sterile, water-soluble tricarbocyanine dye with the empirical formula C43H47N2NaO6S2 and molecular weight of 775 daltons. Chemically it is an anhydro-3,3,3′,3′-tetramethyl-1-1′-di-(4-sulfobutyl)-4,5,4′,5-dibenzo-indotricyanine hydroxide sodium salt with both lipophilic and hydrophilic characteristics.

Indocyanine green is the product of a complex, synthetic process. Sodium iodine is incorporated to create an ICG lyophilisate that can be dissolved in water. Once dissolved, ICG tends to precipitate at high concentration or when mixed in physiologic saline. It is supplied with a solvent consisting of sterile water at pH 5.5 to 6.5. The aqueous ICG dye solution can decay at a rate of approximately 10% in 10 hours and should be used within this time. The final product contains no more than 5% sodium iodine.

Optical Properties

Indocyanine green absorbs light in the near-infrared range of 790 to 805 nm. The emission spectrum ranges from 770 to 880 nm, peaking at 835 nm. Both absorption and emission spectra are shifted toward shorter wavelength when ICG is in an aqueous solution while the overall intensity of the fluorescence is diminished. Fluorescein angiography (FA) does not provide detailed information about the choroidal circulation. The physical characteristics of ICG allow for visualization of the dye through overlying melanin and xanthophyll. Retinal pigment epithelium (RPE) and choroid absorb 59% to 75% of blue-green light (500 nm) used in FA, but only 21% to 38% of near-infrared light (800 nm) used in ICGA. The activity of ICG in the near-infrared light also allows visualization through serosanguineous fluid, shallow hemorrhage, pigment, and lipid exudates (Fig. 3.1). Enhanced imaging of conditions such as choroidal neovascularization (CNV) and pigment epithelial detachment (PED) is the result (Fig. 3.2).

Pharmacokinetics

In vivo, ICG is 98% protein bound. It has both lipophilic and hydrophilic properties. Although it was previously thought to bind primarily to serum albumin, 80% of ICG molecules actually bind to globulins, such as A1-lipoprotein. Therefore, less dye escapes from the fenestrated choroidal vasculature, allowing enhanced imaging of choroidal vessels and choroidal lesions. This is in sharp contrast to fluorescein, which is

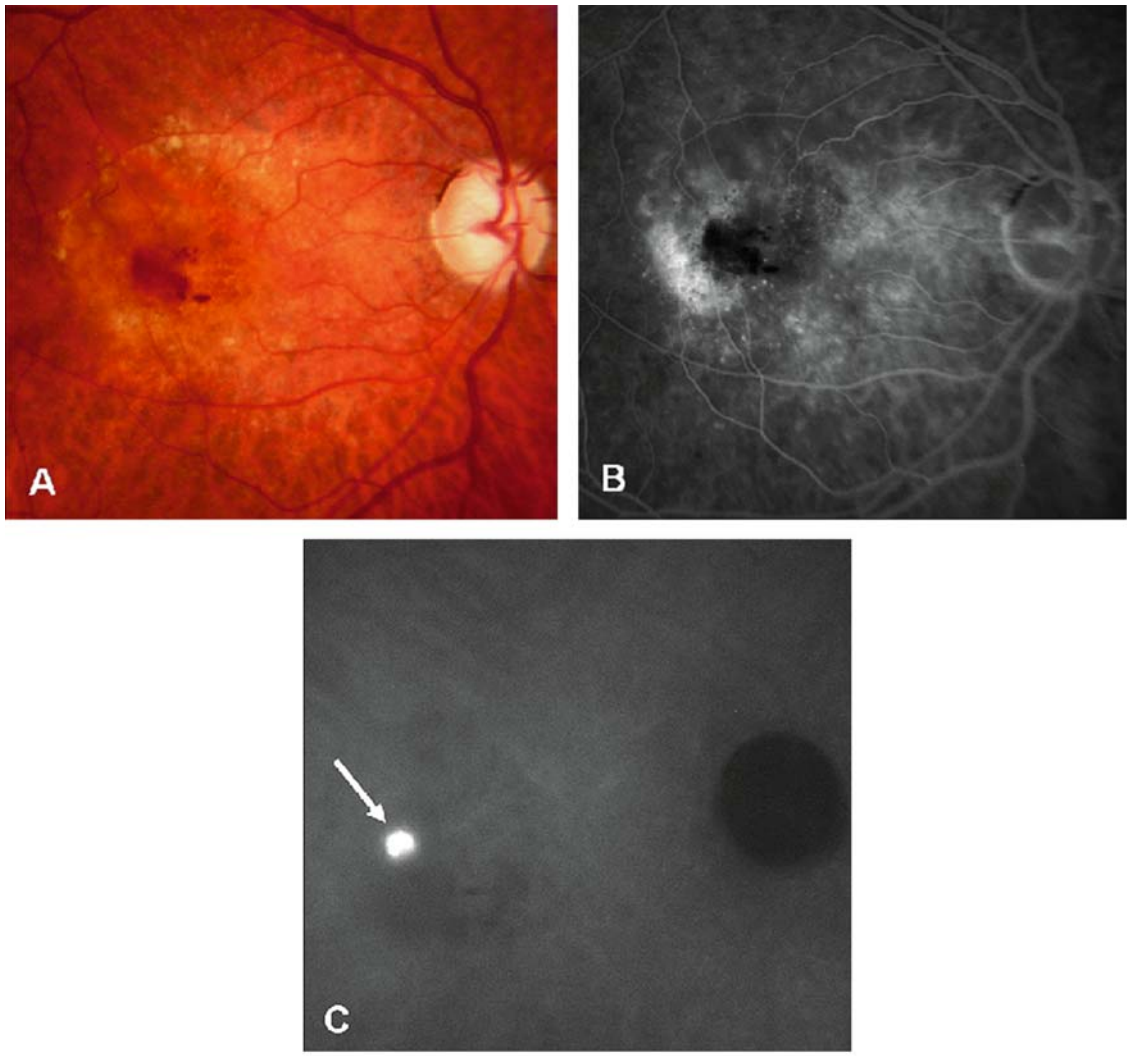

Fig. 3.1.(A) Clinical photograph demonstrates subretinal and intraretinal hemorrhages as well as detachment of the retinal pigment epithelium and the neurosensory retina in a patient with neovascular age-related macular degeneration. (B) Late-phase fluorescein angiogram reveals blocked fluorescence from the hemorrhages and indistinct leakage. (C) A late-phase indocyanine green (ICG) angiogram demonstrates a well-defined hyperfluorescence or so-called focal hot spot (arrow), representing a retinal angiomatous proliferation. This lesion is well visualized through the area of hemorrhage because of good penetration of the infrared light used in ICG angiography.

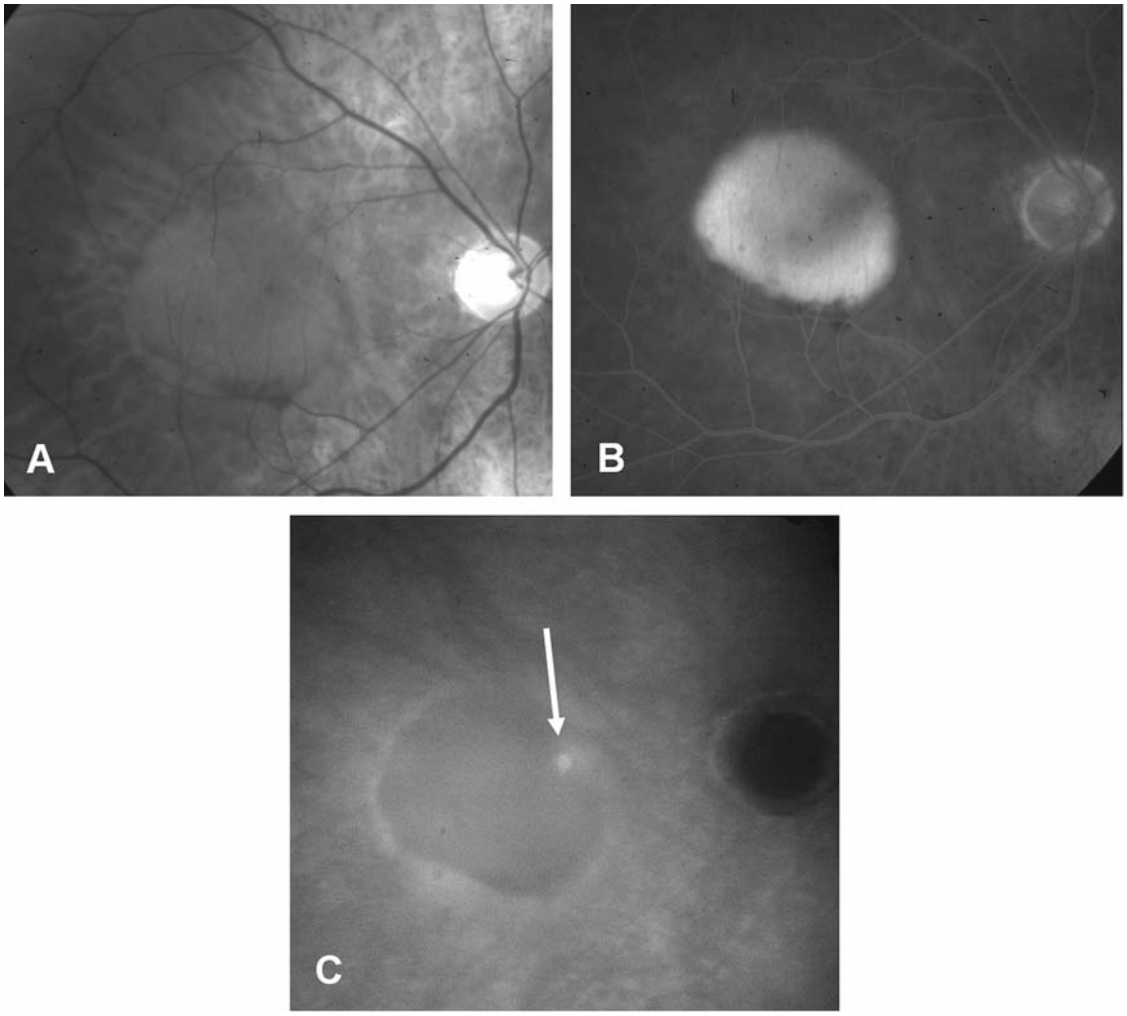

FIG. 3.2.(A) The red-free photograph of a patient with neovascular age-related macular degeneration shows a large pigment epithelial detachment (PED) in the central macula. (B) Late-phase fluorescein angiogram demonstrates hyperfluorescence of the serous PED. No focal area of choroidal neovascularization can be identified. (C) Late-phase indocyanine green (ICG) angiogram reveals a focal spot of hyperfluorescence (arrow), representing an area of localized choroidal neovascularization. The ICG molecule, which is 98% protein bound, does not leak from the neovascular membrane, and the PED remains relatively hypofluorescent throughout the study.

a relatively small molecule that remains mostly unbound from protein and extravasates rapidly from the choriocapillaris and fluoresces in the extravascular space, thus preventing delineation of choroidal anatomy.

It was thought that the protein-binding capacity of ICG limited the travel within the choroidal vessel walls. However, it has been demonstrated that ICG dye diffuses through the choroidal stroma during angiography, accumulating within the retinal pigment epithelium cells. It diffuses slowly, staining the choroid within 12 minutes after injection.

The ICG dye is excreted by the liver. It is taken up by hepatic parenchymal cells and secreted into the bile without metabolic alteration or entering enterohepatic circulation. In healthy individuals, the rate of ICG disappearance from the vascular compartment is 18% to 24% per minute with a half-life of 2 to 4 minutes; after 20 minutes, no more than 4% of the initial concentration of the dye should remain in the serum. As a result of strong binding to plasma proteins, ICG is not detected in kidney, lungs, and cerebrospinal fluid, nor does it cross the placenta.

Toxicity

Indocyanine green is a relatively safe dye; adverse reactions are rare, and less common than with sodium fluorescein. Mild reactions such as nausea, vomiting, and pruritus occur in 0.15% of patients. There have been isolated reports of vasovagal-type reactions, hypotensive shock, and anaphylactic shock. The dose of ICG does not appear to correlate with the

presence or severity of adverse reactions. Unlike sodium fluorescein, where extravasation of dye may lead to local tissue reaction and even necrosis of the overlying skin, ICG extravasation is well tolerated and resolves without complications.

Sterile ICG contains small amounts of iodine and therefore should be used with caution in patients with iodine allergy. It should also be avoided in uremic patients and in those with liver disease where delayed ICG clearance has been described. Indocyanine green has not been shown to be harmful to pregnant women or their fetus; however, it is classified as pregnancy category C due to lack of adequate studies. Therefore, there still exists reason for concern.

Injection Technique

Indocyanine green should be dissolved in aqueous solvent supplied by the manufacturer and be used within 10 hours after preparation. The standard dosage is 25 mg of ICG dissolved in 5 mL of solvent. In patients with poorly dilated pupils or heavily pigmented fundus, the dose of ICG may be increased to 50 mg. For wide-angle angiography, the dosage is increased to 75 mg. Rapid intravenous injection is essential, and the injection may be immediately followed by a 5-mL saline flush.

Digital Imaging System

An excitation filter placed over the light source allows only the passage of near-infrared light. This light is absorbed by the ICG molecules in the eye, which in turn emit slightly lower energy light. A barrier filter is used to capture only this light emitted from ICG into the camera by blocking wavelengths shorter than 825 nm.

Image acquisition can by produced by standard fundus camera, video camera, or scanning laser ophthalmoscope. The coupling of digital imaging system with an ICG camera enables production of high-resolution (1024-line) images necessary for ICGA.

Digital imaging systems contain electronic still and video cameras with special antireflective coatings as well as appropriate excitatory and barrier filters. A video camera is attached to the camera viewfinder and it is connected to a video monitor. The photographer selects the image and activates a trigger that sends the image to the video adapter. The charge-coupled device (CCD) camera captures the images and transmits these digitized (1024 × 1024-line resolution) images to a video board within a computer-processing unit. Flash synchronization allows high-resolution image capture, and images are displayed on a high-resolution video monitor.

Photographic Technique

For the purpose of obtaining an ICG study, the imaging protocol typically begins with color, red-free, and green-free fundus photographs. Indocyanine green angiography can be performed before or after FA. Images are initially taken 8 to 10 seconds after injection of the dye. This permits image capture in the early phase of choroidal filling. If the photographer waits until the dye is first noted on the alignment and focus monitor, the early phase of the study is often missed by the time the image capture is achieved. Images are obtained in a rapid, sequential manner at approximately 1-second intervals until retinal and choroidal circulations are at maximum brightness. The quality of the image exposure is continuously displayed on a high-resolution monitor, and modifications made to the image by adjusting the flash illumination control or gain setting. Initially, the gain must be set high in order to provide good illumination of the early choroidal filling phase, but reduction must be made immediately to compensate for the rapid influx of dye during the early retinal and larger choroidal filling phase.

After the images are obtained at the point of maximal brightness, they are further captured at 1-minute intervals until 5 minutes into the study. Thereafter, images are obtained at 3- to 5-minute intervals for a total duration of 30 to 50 minutes. Typically, ICG images are captured until all of the dye has exited to the retinal circulation and the optic nerve appears dark in contrast to the generalized gray background of the choroidal region. During the course of the study, the gradual decrease in the concentration of ICG dye in the retinal and choroidal circulation requires a corresponding increase in the intensity of the flash illumination.

When the angiogram is complete, the photographer reviews the images. Poorly focused, poorly aligned, or redundant information is deleted. Permanent storage is accomplished by downloading to a DVD, CD-ROM, or local server. The stored, unenhanced images can then be manipulated with the available software for enhanced analysis. Images can be "warped", a technique in which tracing of an image from the ICG study is overlaid onto the clinical or red-free photograph or fluorescein angiographic image to permit accurate localization of pathology.

New Techniques

Recent advances in the technology associated with ICGA include wide-angle,[10] digital subtraction,[11] and high-speed angiography. [8]

Wide-angle ICGA is achieved with the use of a wide-angle contact lens. Because the lens produces an image lying about 1 cm in front of the lens, the fundus camera is set on "A" or " + " in order to focus on the image plane of the contact lens. This system allows instantaneous imaging of a large fundus area up to 160 degrees of field (Fig. 3.3).[10]

Digital subtraction ICGA uses software to eliminate static fluorescence in sequentially acquired images and demonstrates the progression of the dye front within the choroidal circulation (Fig. 3.4). Pseudocolor imaging of the choroid allows differentiation and identification of choroidal arteries and veins. This technique allows imaging of occult choroidal neovascularization with greater detail and in a shorter period of time than with conventional ICGA.[11]

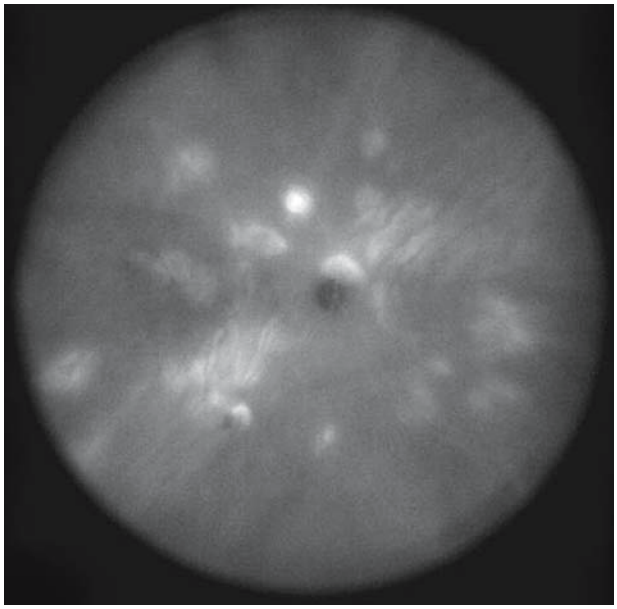

FIG. 3.3. The wide-angle indocyanine green (ICG) angiogram of a patient with central serous chorioretinopathy (CSCR) illustrates multifocal zones of choroidal hyperpermeability, which represent areas of presumed "occult" PED extending far beyond the posterior pole.

A fundamental problem for any kind of fundus imaging is reflection from interfaces of the ocular media. To obtain high-quality fundus images, these reflections must be eliminated. This is achieved by confocal scanning laser ophthalmoscopy, which separates the illuminating and the imaging beam in the eye, and can be used for high-speed ICGA. The scanning laser ophthalmoscope (SLO) can acquire FA images using an argon laser (488 nm), ICG images using an infrared diode laser (795 nm), simultaneous FA and ICGA, autofluorescence images, normal fundus reflectance images with green light (514 nm), and images of the nerve fiber layer with infrared light (830 nm). Barrier filters at 500 and 810 nm are added to provide a greater efficiency of fluorescent light detection. Single images can be acquired, as well as image sequences with a frame rate up to 30 images per second. Images are digitized in real time with a resolution of 256 × 256 or 512 × 512 pixels. The scanning laser system is able to record the filling phase with great temporal resolution but with a slight loss of spatial resolution.

Recently, three-dimensional confocal angiography has been reported.[12] This system allows for the potential to achieve reliable quantitative and qualitative analysis of defects, exudation, and proliferative vascular lesion.

Interpretation of Indocyanine Green Angiography

Age-Related Macular Degeneration

Definitions

The terminology used to describe the angiographic manifestations of age-related macular degeneration (AMD) corresponds, with certain exceptions described below, to definitions previously reported by the Macular Photocoagulation Study Group (MPS).[13] Most relevant to the interpretation of ICGA in AMD are the definitions of serous PED, vascularized PED (V-PED), classic CNV, and occult CNV.

Serous Pigment Epithelial Detachment

Serous PED is an ovoid or circular detachment of the retinal pigment epithelium (RPE). Indocyanine green angiography reveals a variable, minimal blockage of normal choroidal vessels, more evident in the midphase of the angiogram. In comparison to FA a serous PED is dark (hypofluorescent) on the ICG study. This difference is caused by the fact that the ICG molecules are larger and almost completely bound to plasma proteins, and are prevented from free passage of the ICG dye throughout the fenestrated choriocapillaris in the sub-RPE space.

Choroidal Neovascularization

Choroidal neovascularization (CNV) is defined as a choroidal capillary proliferation through a break in the outer aspect of Bruch's membrane under the RPE and the neurosensory retina. Choroidal neovascularization is divided into classic and occult based on the FA appearance.

Classic Choroidal Neovascularization. Classic CNV represents an area of bright hyperfluorescence that is usually not delineated as well as in an FA study.

Occult Choroidal Neovascularization. Occult CNV is characterized as either fibrovascular PED consisting of irregular elevation of the RPE, or late leakage of undetermined source. There are two main types of occult CNV that are recognized by the ICGA.

Without Serous Pigment Epithelial Detachment. The first type of occult CNV is caused by sub-RPE CNV that is not associated with a PED. The ICG angiogram reveals early vascular hyperfluorescence and late staining of the abnormal vessels. The image with distinct margins is considered to be a well-defined CNV on the ICGA.

With Serous Pigment Epithelial Detachment. The second type of occult CNV is associated with a serous PED of at least one disc diameter in size. Combined CNV and serous PED are called a vascularized PED (V-PED). This lesion is the result of sub-RPE neovascularization associated with a serous detachment of the RPE. Indocyanine green angiography reveals early vascular hyperfluorescence and late staining of the CNV. Indocyanine green is more helpful than FA in differentiating between a serous PED and a V-PED. It also permits better identification of the vascularized and serous component of V-PEDs. The serous component of a PED is hypofluorescent and the vascularized component is hyperfluorescent.

Occult CNV is also subdivided into two further types, one with a solitary area of well-defined focal neovascularization (hot spot) and the other with a larger, delineated area of neovascularization (plaque).

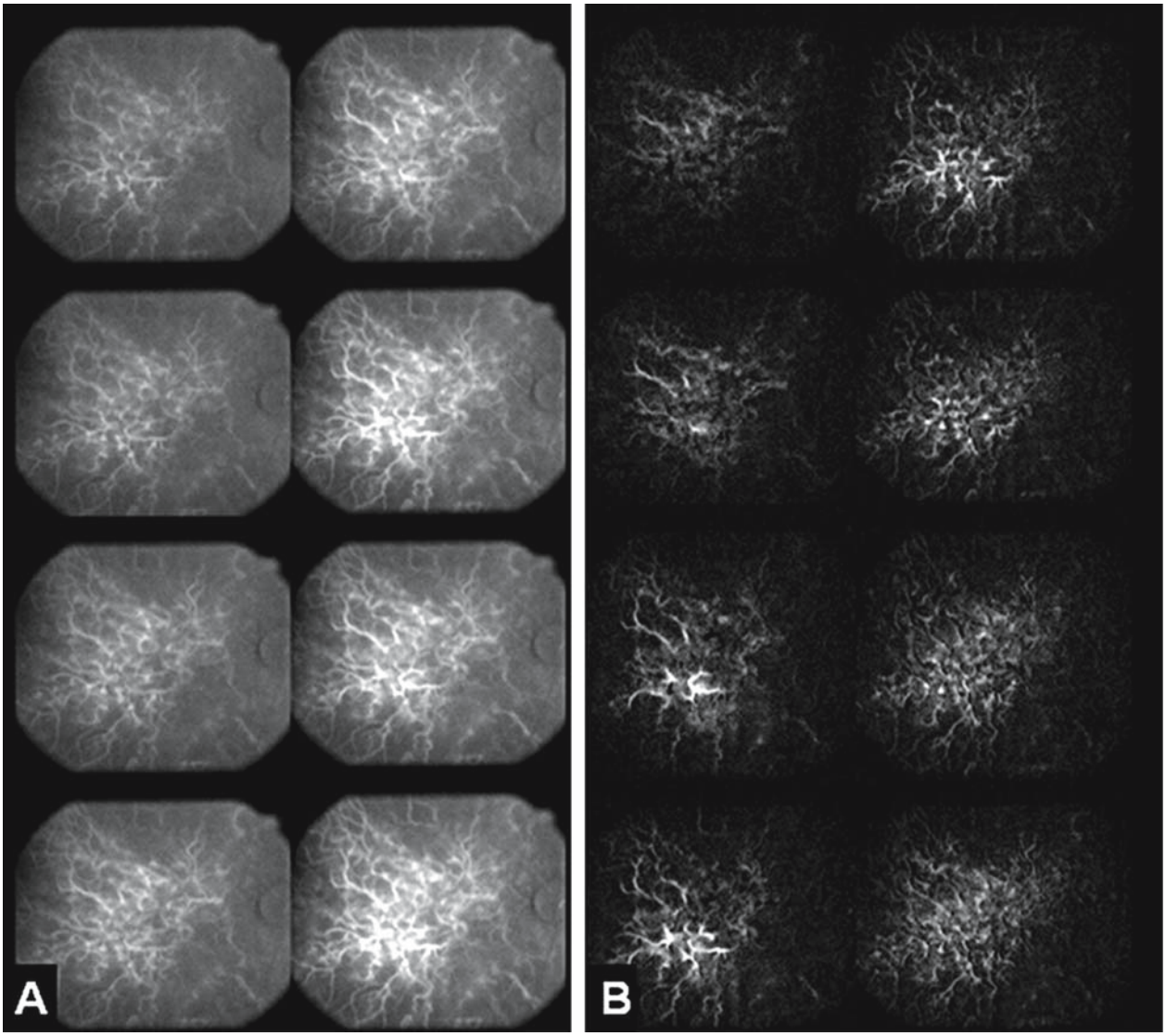

FIG. 3.4. Sequential subtraction of ICG angiogram images from the eye of a normal young male, acquired at 30 images per second (IPS) using fundus camera optics. (A) The two columns of images (read from top to bottom) are the original angiogram. (B) The two columns are the resultant subtracted images; the first image resulted from subtracting the first angiographic image from the second, the second image resulted from subtracting the second angiographic image from the third, etc. (Courtesy of Robert Flower).

Hot Spot (Focal Choroidal Neovascularization). Focal CNV or a "hot spot" is an area of occult CNV that is well delineated and no more than one disc diameter in size on ICGA. In addition, a hot spot represents an area of actively proliferating and more highly permeable areas of neovascularization (active occult CNV). Retinal angiomatous proliferation (RAP), focal occult CNV (Fig. 3.5), and polypoidal-type CNV may represent subgroups of hot spots.

Plaque. A plaque is an area of occult CNV larger than one disc diameter in size. A plaque is often formed by late-staining vessels that are more likely to be quiescent areas of neovascularization that are not associated with appreciable leakage (inactive occult CNV). Plaques of occult CNV seem to grow slowly in dimension with time. Both well-defined and ill-defined plaques are recognized on ICG study. A well-defined plaque has distinct borders throughout the study, allowing the assessment of the full extent of the lesion (Fig. 3.6). An ill-defined plaque has indistinct margins or may be the one in which any part of the neovascularization is blocked by the blood.

Imaging of Choroidal Neovascularization. Patz and associates[14] were the first to study CNV in AMD through ICGA. They could resolve only two of 25 CNVs with their early model. Bischoff and Flower [15] studied 100 ICG angiograms of patients with AMD. They found "delayed and/or irregular choroidal filling" in some patients. The significance of this finding is unclear, however, because these authors did not include an age-matched control group. Tortuous choroidal vessels and marked dilation of macular choroidal arteries, often with loop formation, were also observed.

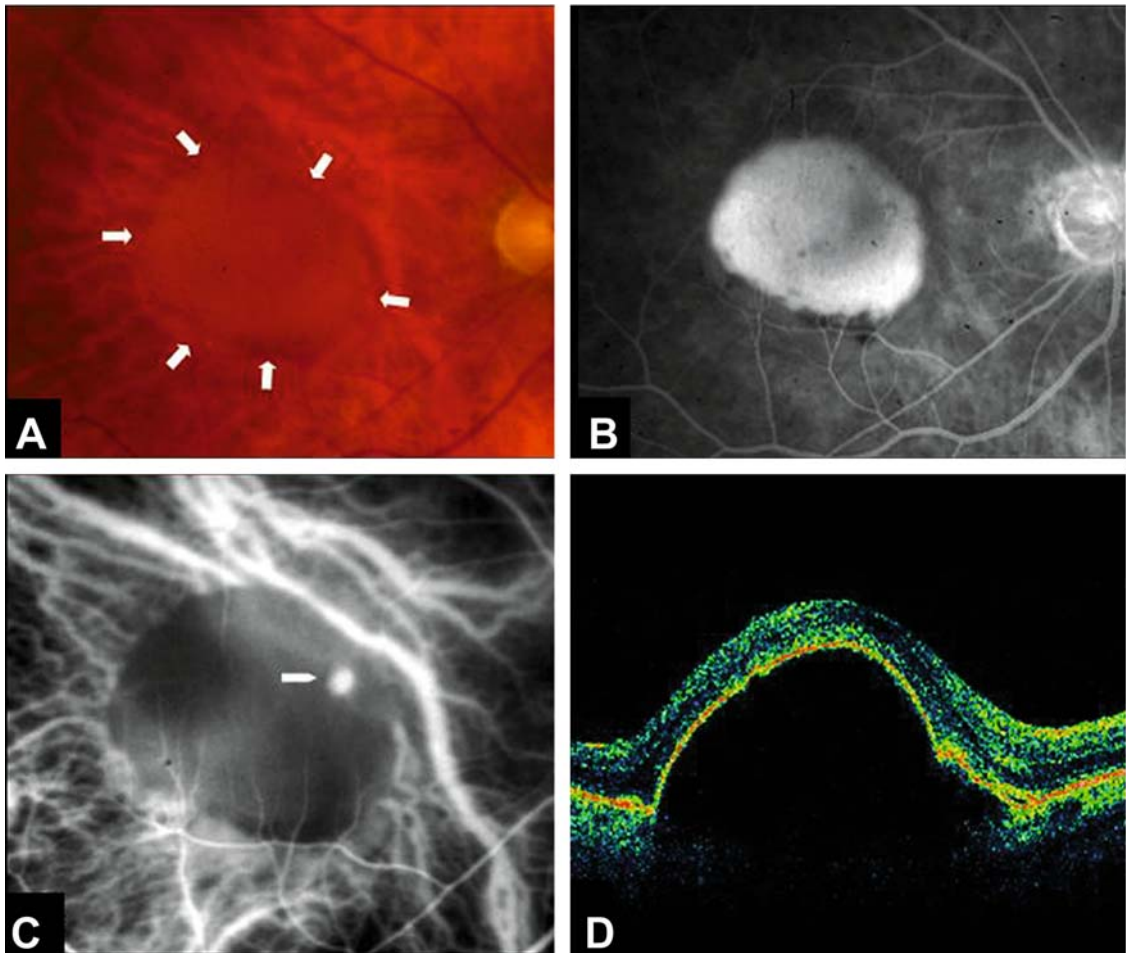

FIG. 3.5. (A) Clinical photograph showing a large PED (white arrows) in a patient with focal occult choroidal neovascularization (CNV). (B) Late-phase fluorescein angiogram illustrating late staining of the PED. (C) Midphase indocyanine green (ICG) angiogram showing a focal area of abnormal hyperfluorescence (hot spot). (D) The optical coherence tomography (OCT) scan confirms a large PED.

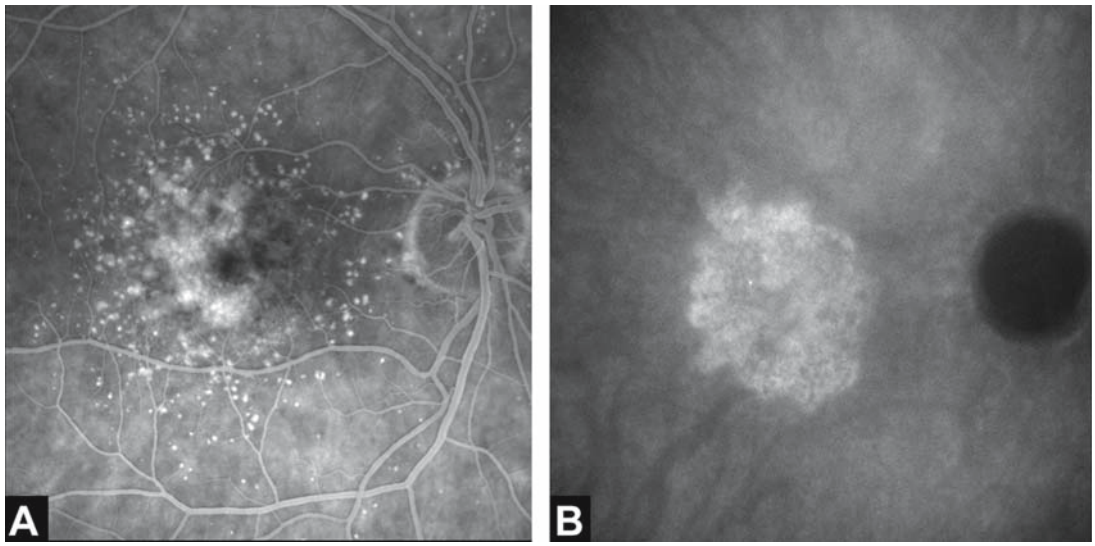

FIG. 3.6. (A) Fluorescein angiography reveals occult choroidal neovascularization. (B) Late-phase ICG angiogram shows a well-defined plaque.

Hayashi and associates[6] found that ICG videoangiography was useful in the detection of CNV. Indocyanine green angiography was able to confirm the FA appearance of CNV in patients with well-defined CNV. It revealed a well-defined neovascularization in 27 eyes with occult CNV by FA. In a subgroup of patients with poorly defined occult CNV, the ICG angiogram, but not the FA, imaged a well-defined CNV in nine of 12 (75%) cases. Indocyanine green videoangiography of the other three eyes revealed suspicious areas of neovascularization. These investigators were also the first to show that leakage of ICG from CNV was slow compared to the rapid leakage seen with sodium fluorescein. While the results of these investigators concerning ICG angiographic imaging of occult CNV were promising, the 512-line video monitor and analog tape of their ICG system limited the spatial resolution they could obtain.

Destro and Puliafito[7] reported that ICG videoangiography was particularly useful in studying occult CNV with overlying hemorrhage and recurrent CNV. It has been demonstrated that ICGA is useful in imaging occult CNV and that this technique might allow photocoagulation of otherwise untreatable lesions. Yannuzzi and associates[9] have shown that ICGA is extremely useful in converting occult CNV into a well-defined pattern of CNV. In their study, 39% of 129 patients with occult CNV were converted to a well-defined CNV based on the information added by ICGA. These authors reported that ICGA was especially useful in identifying occult CNV in patients with serous PED or with recurrent CNV.

Guyer and coauthors[16] reported their results on the ICGA study of 1000 consecutive eyes with occult CNV diagnosed by FA. They recognized focal spots in 29%, plaques in 61% (27% well-defined plaques and 34% poorly defined plaques), and combination lesions in 8% (3% marginal spots, 4% overlying spots and 1% remote spots). A follow-up study of patients with newly diagnosed unilateral occult CNV secondary to AMD showed that the patients tended to develop the same morphologic type of CNV in the fellow eye.

The above studies demonstrate that ICGA is an important adjunctive study to FA in the detection of CNV. While FA may image well-defined CNV better than ICGA in some cases, ICG videoangiography can enable treatment of about 30% of occult CNV lesions by the detection of well-defined CNV eligible for ICG-guided laser treatment. Thus, the best imaging strategy to detect the CNV is to perform both FA and ICGA.

Polypoidal Choroidal Vasculopathy

Polypoidal choroidal vasculopathy (PCV) is a primary abnormality of the choroidal circulation characterized by an inner choroidal vascular network of vessels ending in an aneurysmal bulge or outward projection, visible clinically as a reddish-orange, spheroid, polyp-like structure. The disorder is associated with multiple, recurrent, serosanguineous detachments of the RPE and neurosensory retina secondary to leakage and bleeding from the peculiar choroidal vascular abnormality. Indocyanine green angiography has been used to detect and characterize the PCV abnormality with enhanced sensitivity and specificity (Fig. 3.7). The early phase of ICGA shows a distinct network of vessels within the choroid. In patients with juxtapapillary involvement, the vascular channels extend in a radial, arching pattern and are interconnected with the smaller spanning branches that become more evident and more numerous at the edge of the PCV lesion. Larger choroidal vessels of the PCV network begin to fill before retinal vessels. The area within and surrounding the network is relatively hypofluorescent as compared to the uninvolved choroid (Fig. 3.8). The vessels of the network appear to fill at a slower rate than retinal vessels. Shortly after the network can be identified on the ICG angiogram, small hyperfluorescent “polyps” become visible within the choroid. These polypoidal structures

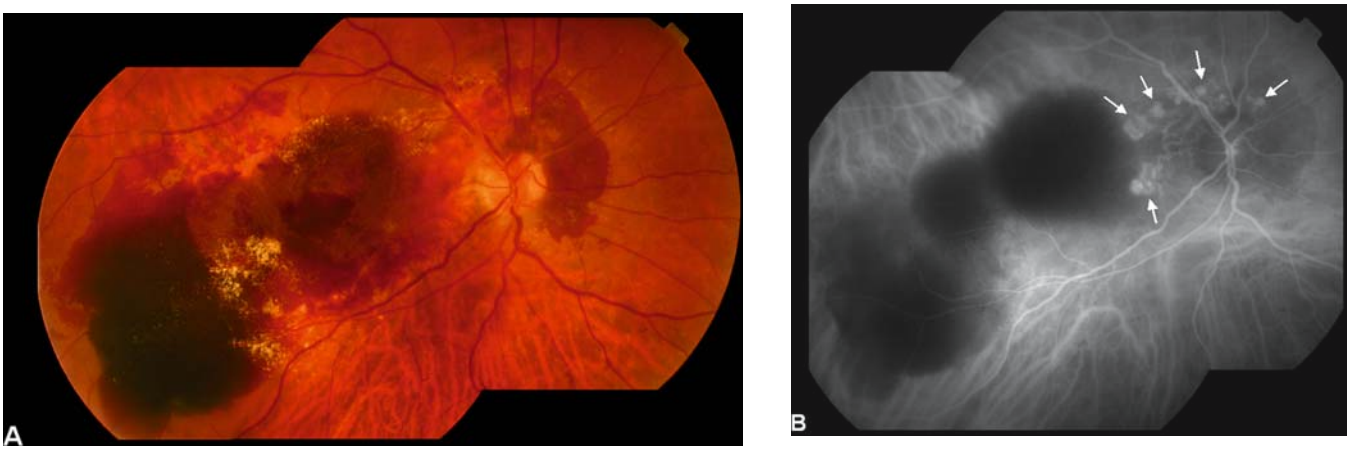

Fig. 3.7. Sudden deterioration of vision in the right eye of a 66-year-old Caucasian man. (A) Color composite photograph shows large subretinal and intraretinal hemorrhages at the posterior pole and surrounding the optic nerve. There are areas with dense lipid exudation. (B) Midphase ICG angiogram illustrates a large hyperfluorescent area. In the peripapillary area, there is a net of subretinal inner choroidal vessels that terminate in polypoidal lesions (white arrows).

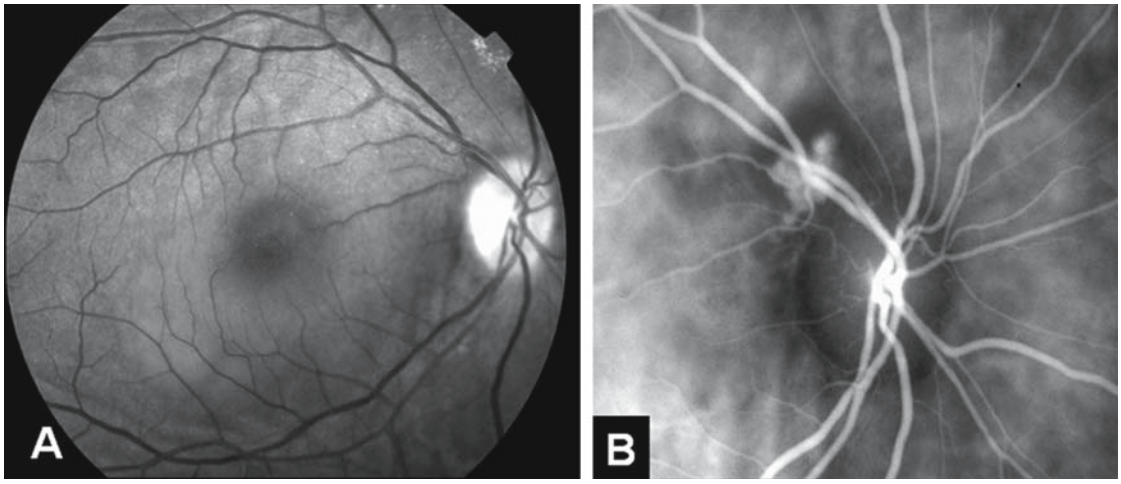

Fig. 3.8. (A) Red-free photograph of a 62-year-old woman's eye illustrating a neurosensory retinal detachment in the central macula. (B) An ICG angiogram reveals the presence of a polypoidal choroidal vascular abnormality in the superior temporal juxtapapillary region.

correspond to the reddish, orange choroidal excrescence seen clinically. They appear to leak slowly as the surrounding hypofluorescent area becomes increasingly hyperfluorescent. In the later phase of the angiogram there is uniform disappearance of dye ("washout") from the bulging polypoidal lesions. The late characteristic ICG staining of occult CNV is not seen in the PCV. Polypoidal lesions may be localized in the macular area without any peripapillary component, and it may be formed by a network of small branching vessels ending in polypoidal dilation difficult to image without ICGA.

Indocyanine green angiography has led to early discovery of polyps in the peripapillary, macular, and extramacular areas. With the identification of these choroidal polyps, new therapeutic possibilities are being explored, including the use of thermal laser treatment as well as photodynamic therapy.

Retinal Angiomatous Proliferation

Retinal angiomatous proliferation (RAP) is a distinct subgroup of neovascular AMD. Angiomatous proliferation within the retina is the first manifestation of the neovascularized process. Dilated retinal vessels, pre-, intra-, and subretinal hemorrhages, and exudates evolve surrounding the angiomatous proliferation as the process extends into the deep retina and subretinal space. One or more dilated compensatory retinal vessels perfuse and drain the neovascularization, sometimes forming a retinal –retinal anastomosis. Fluorescein angiography in these patients usually reveals indistinct staining simulating occult-CNV. Indocyanine green angiography is useful to make an accurate diagnosis in most cases. It reveals a focal area of intense hyperfluorescence corresponding to the neovascularization (hot spot) and some late extension of the leakage within the retina from the intraretinal neovascularization (Fig. 3.9). As the intraretinal neovascularization progresses toward the subretinal space and the RPE, the CNV becomes part of the neovascular complex. At this stage there is often clinical and angiographic evidence of a V-PED. Indocyanine green angiography is better for imaging the presence of a V-PED because the serous component of the PED remains dark during the study and the vascular component appears as a hot spot (Fig. 3.10). At this stage, ICGA may sometimes be able to image a direct communication between the retinal and the choroidal component of the neovascularization to form a retinal–choroidal anastomosis (RCA).

Indocyanine Green–Guided Laser Treatment of Choroidal Neovascularization in Age-Related Macular Degeneration

Patients potentially eligible for thermal laser photocoagulation therapy guided by ICGA are those with clinical and fluorescein angiographic evidence of occult CNV. Of the two types of occult CNV that can be identified by ICG study, hot spots and plaques, we recommend direct laser photocoagulation of only the hot spots. In fact, the hot spots represent areas of actively leaking neovascularization that can be obliterated by laser photocoagulation in an attempt to eliminate the associated serosanguineous complications, and to stabilize or improve the vision. On the other hand, the plaques seem to represent a thin layer of neovascularization that is not actively leaking and that may not require laser photocoagulation. This approach has practical considerations. In the case of a lesion combining a hot spot and a plaque and in which the hot spot is at the margin of the plaque (it may extend under the fovea), laser photocoagulation can be applied to the extrafoveal hot spot to spare the foveal area. But we have had poor success with the direct laser treatment of hot spots overlying plaques and confluent treatment of the entire plaque.

Two subtypes of hot spots are RCA and polypoidal-type CNV. When RCA is present, the success of laser

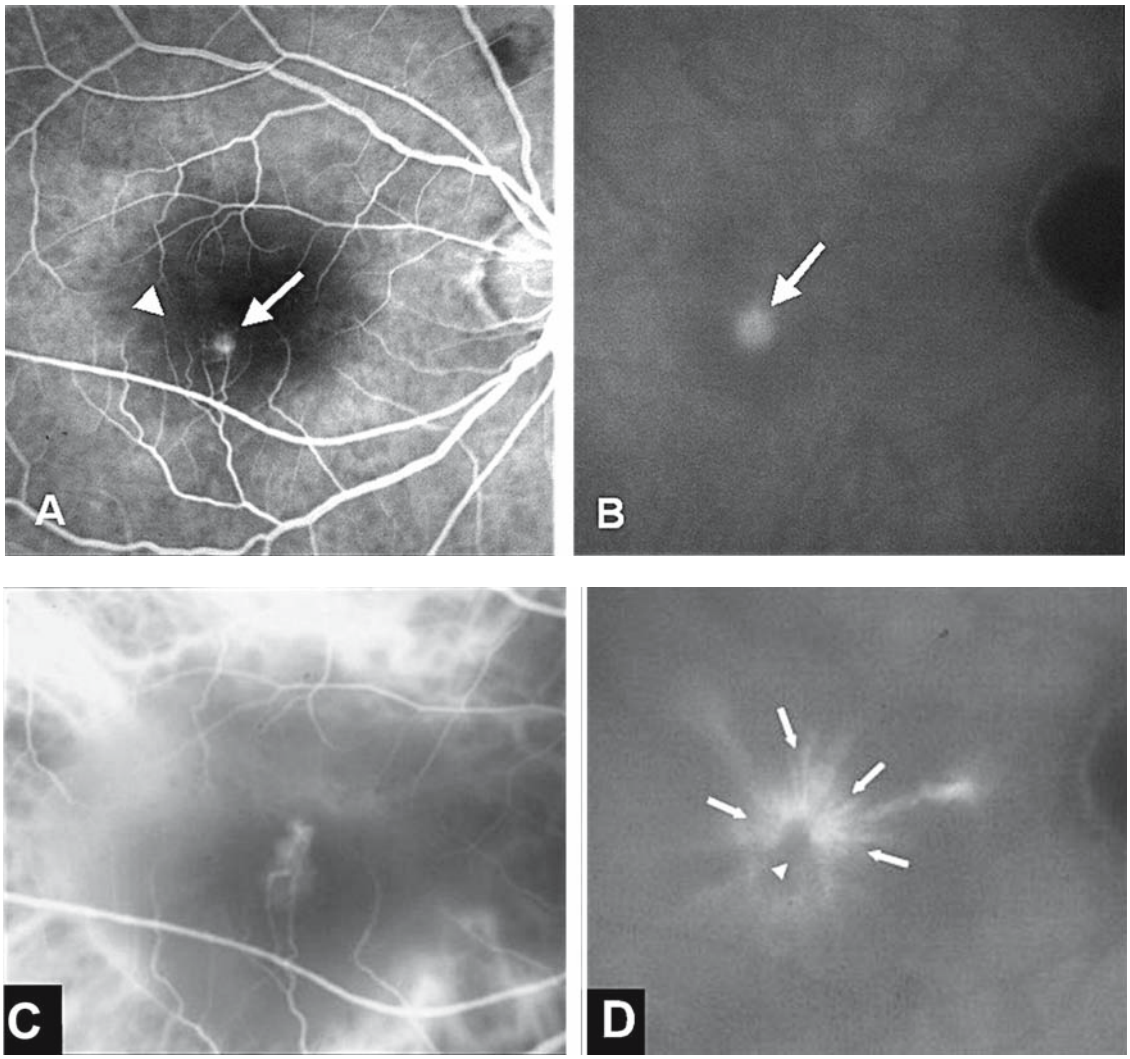

FIG. 3.9. (A) Fluorescein angiogram of a 73-year-old patient's eye reveals retinal angiomatous proliferation (RAP) stage I (arrow). Note the telangiectasia surrounding this area (arrowhead). (B) An ICG angiogram showing a focal area of intense hyperfluorescence (arrow) or so-called hot spot. (C) The ICG angiogram 1 year later illustrates a retinal–retinal anastomosis and subretinal neovascularization. (D) The late-phase ICG angiogram shows intraretinal leakage (arrows) surrounding the fading angiomatous proliferation (arrowhead).

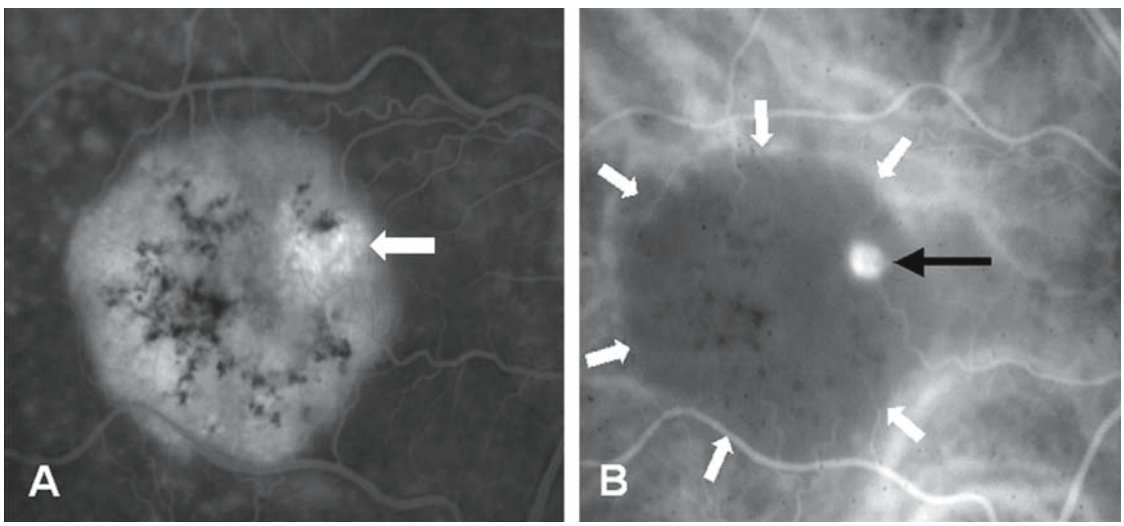

FIG. 3.10. (A) The fluorescein angiogram of a patient with RAP stage II reveals late staining of a PED. There is an increase in the intensity of fluorescence in the area of the RAP lesion (arrow). (B) The ICG angiogram shows hypofluorescence in the area of the PED (white arrows) and a "hot spot" corresponding to the RAP (black arrow).

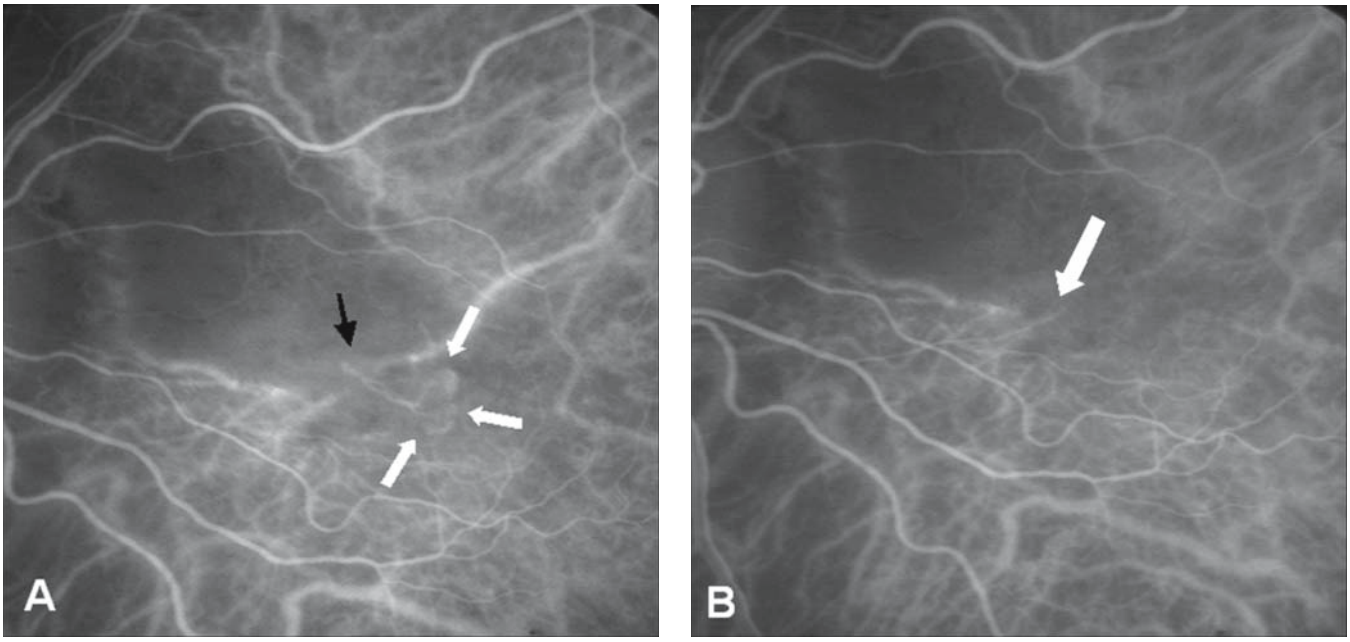

FIG. 3.11. (A) High-speed angiography of a patient with choroidal neovascularization (white arrows) demonstrates clearly the perfusing and draining feeder vessels (black arrow). (B) After focal thermal laser treatment of the feeder vessels, an ICG angiogram reveals closure of these vessels (arrow).

photocoagulation is negatively influenced by the presence of an associated serous PED.

Slakter and coauthors[17] performed ICG-guided laser photocoagulation in 79 eyes with occult CNV. Occult CNV was successfully eliminated in a majority of the cases. Visual acuity was stabilized or improved in 66% of eyes with occult CNV associated with neurosensory retinal elevations, and in 43% of eyes with occult CNV associated with PED. They demonstrated that in some cases ICGA imaging can successfully guide laser photocoagulation of occult CNV.

The high recurrence rate after laser photocoagulation of occult CNV, particularly when a V-PED is present, may be explained by the peculiar anatomy of the CNV in such cases.

Freund et al.[18] reported that approximately only 13% of patients with CNV secondary to AMD have a classic or well-defined extrafoveal choroidal neovascularization by FA that is eligible for laser treatment. With a recurrence rate of approximately 50% following fluorescein angiographic-guided laser photocoagulation for classic CNV, only approximately 6.5% of patients benefit from treatment. The remaining 87% of patients have occult CNV by fluorescein imaging. About 30% of these eyes have a potentially treatable focal spot by ICGA. Therefore, about one fourth of all eyes with exudative maculopathy may be treated by ICG-guided laser photocoagulation. With a success rate of 35%, this means that an additional 9% of patients can be successfully treated using ICG-guided laser photocoagulation. However, there are still 84.5% of patients who continue to be untreatable or are unsuccessfully treated by thermal laser photocoagulation of CNV.

Staurenghi et al.[19] considered a series of 15 patients with subfoveal CNV in whom feeder vessels (FVs) could be clearly detected by means of dynamic ICGA but not necessarily by FA (Fig. 3.11). Based on the indications of their pilot study, the authors studied a second series of 16 patients with FVs smaller than 85 μm. The FV was treated using the argon green laser, and ICGA was performed immediately after treatment. If an FV remained patent, it was immediately re-treated and the follow-up schedule was started again. The follow-up time ranged from 23 to 34 months for the pilot study, and from 4 to 12 months for the second series. In the pilot study, CNV was obliterated after the first treatment in only one patient; five patients needed more than one treatment and obliteration failed in nine patients (40% success rate). The success rate in the second series of 16 patients was higher (75%). The authors concluded that dynamic ICGA may detect smaller FVs. It enables controlling the laser effect and initiating immediate re-treatment in the case of incomplete FV closure and should be considered mandatory for this type of treatment. Clinical trials to evaluate the role of ICG-guided feeder vessel therapy are ongoing.

Central Serous Chorioretinopathy

The application of ICGA to the study of central serous chorioretinopathy (CSCR) has expanded our knowledge of the disease. The common findings in patients with CSCR are multifocal areas of hyperfluorescence in the early and middle phases of the study, which tend to fade in the late phases (Fig. 3.12). Typically, these areas of hyperfluorescence are

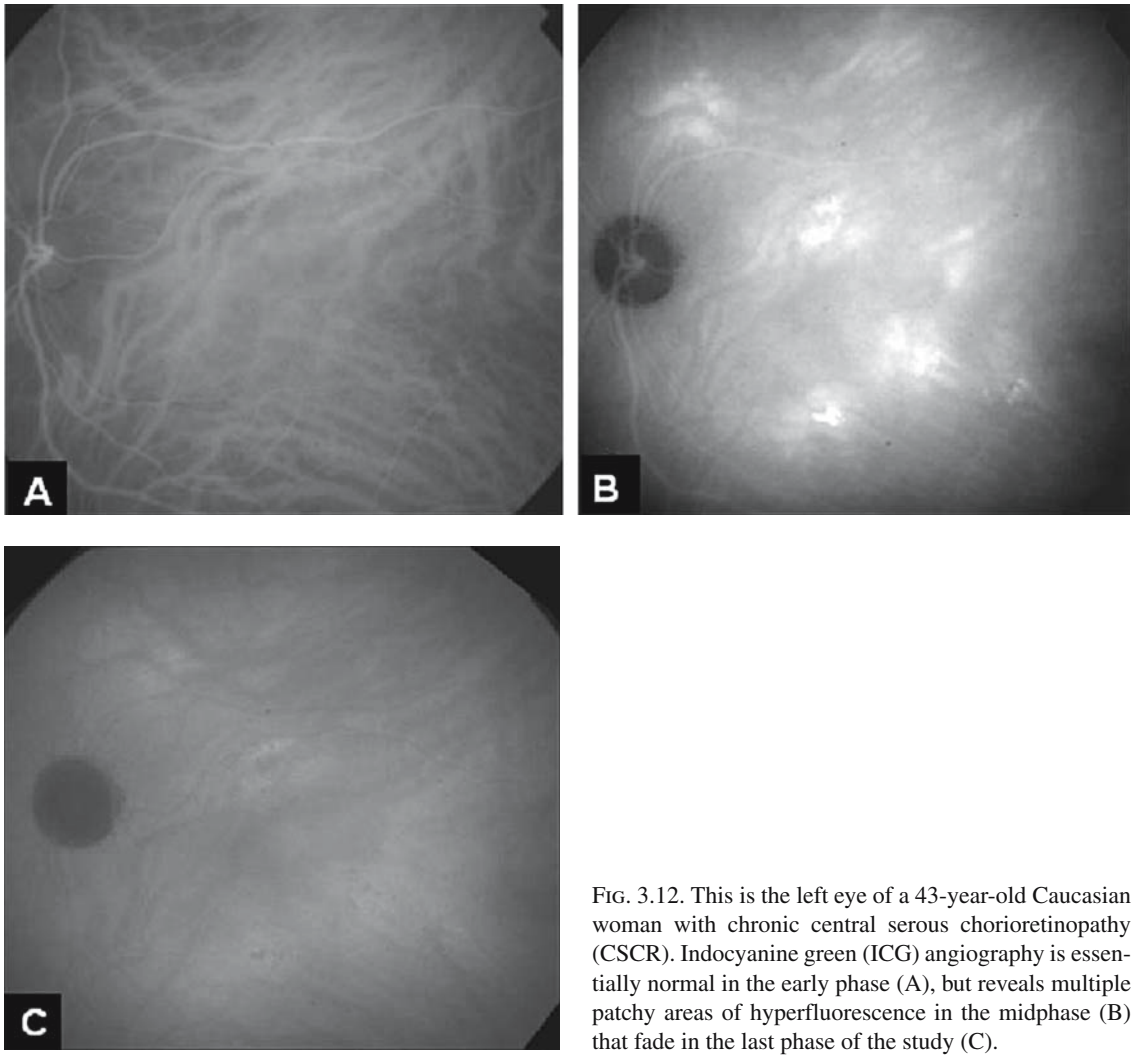

FIG. 3.12. This is the left eye of a 43-year-old Caucasian woman with chronic central serous chorioretinopathy (CSCR). Indocyanine green (ICG) angiography is essentially normal in the early phase (A), but reveals multiple patchy areas of hyperfluorescence in the midphase (B) that fade in the last phase of the study (C).

found not only in corresponding areas of leakage as seen on FA, but also with areas of the fundus that appear clinically and angiographically normal, as well as in the normal fellow eyes. The areas of early hyperfluorescence are believed to represent diffuse choroidal hyperpermeability.

Intraocular Tumors

Indocyanine green angiography is an important tool in the diagnostic and evaluation of intraocular tumors (see Chapter 8). Pigmented choroidal melanomas block ICG fluorescence because the near-infrared light is absorbed by melanin. The choroidal and tumor vasculature cannot be visualized through dense tumor pigmentation. Indocyanine green angiography can distinguish pigmented choroidal melanomas from non-pigmented tumors, such as hemangiomas and osteomas. In our experience, ICGA cannot distinguish melanomas from other pigmented lesions such as nevi or metastatic cutaneous melanoma. When a pigmented choroidal melanoma thickens or otherwise develops prominent intrinsic vasculature, ICGA shows an increase in fluorescence in the late phase.

Marked progressive hyperfluorescence is observed during ICGA of choroidal hemangiomas due to the vascularity of the lesion. A speckled pattern with stellate borders is observed. In early stages of the ICG study, a network of small-caliber vessels is seen. These vessels completely obscure the choroidal pattern. The technique is also useful in evaluating vascular lesions with overlying hemorrhage. Indocyanine green, unlike FA, may enable visualization of the tumor through an overlying hemorrhage.

Choroidal metastatic lesions show different pattern on ICGA depending on vascularity, pigmentation, and primary location of the lesion. In the early study phase, choroidal metastasis shows diffuse, homogeneous hypofluorescence. The normal perfusing choroidal pattern can often been visualized underneath. Breast metastasis shows moderate blockage on ICG videoangiography, while metastatic thyroid carcinoma and metastatic bronchial carcinoid tumors show hyperfluorescence.

Metastatic skin melanoma shows marked blockage on ICG videoangiography and thus appears indistinguishable from primary choroidal melanoma.

The early ICG phase in choroidal osteomas reveals characteristic small vessels that often leak too quickly to be detected by FA. Variable hypofluorescence is observed in the bony areas. These lesions may show midphase to late-phase ICG hyperfluorescence.

Varices of the vortex veins occasionally can be confused with choroidal tumors. Although the diagnosis usually can be made clinically, ICGA in these cases shows marked dilation of the vortex veins.

Chorioretinal Inflammatory Diseases

Serpiginous choroidopathy is a rare, progressive condition that appears to affect primarily the inner choroidal and RPE layers with secondary retinal involvement, beginning at the optic nerve and advancing centrifugally. The ICG videoangiography typically shows two patterns according also to the stage of the disease. In the acute phase, ICGA is characterized by generalized hypofluorescence through all phases of the study. In the subacute stage of the disease, mid- and large-sized choroidal vessels are visualized within the lesions. Persistent delay or nonperfusion of the choriocapillaris and smaller choroidal vessels is noted, giving the area a generalized hypofluorescent appearance but with less distinct margins and a more heterogeneous appearance (Fig. 3.13). This pattern is more typically seen after resolution of acute inflammatory changes and associated edema. In the late phase of the study, lesions present with sharp, well-demarcated borders. This is due to a combination of choroidal perfusion abnormalities as demonstrated on SLO and blockage by inflammatory exudative material, or edema of the RPE and outer retina. In the healed stages, deeper choroidal vessels become better visualized due to the associated development of RPE and choriocapillaris atrophy.

Acute multifocal placoid pigment epitheliopathy (AMPPE) is a syndrome of young adults characterized by the development of multifocal, yellow-white, flat, placoid lesions of the RPE in the posterior pole and midperipheral fundus. The lesions are hypofluorescent by ICGA in both the early and late phase of the study (Fig. 3.14). The ICG choroidal hypofluorescence in AMPPE may be due to a partial choroidal vascular occlusion secondary to occlusive vasculitis. The ICG study of healed lesions also demonstrates early hypofluorescence and more clearly delineates late choroidal hypofluorescence.

Multiple evanescent white dot syndrome (MEWDS) typically presents with unilateral acute loss of vision in healthy young women. It is a clinical condition of unknown cause, but it is thought to affect primarily the RPE-photoreceptor complex. With ICG, a pattern of hypofluorescent spots throughout the posterior pole and peripheral retina is seen (Fig. 3.15). These hypofluorescent spots appear approximately 10 minutes after dye injection in the mid-ICG phase and persist throughout the remainder of the study. These spots appear larger than the white dots seen clinically, varying in diameter from less

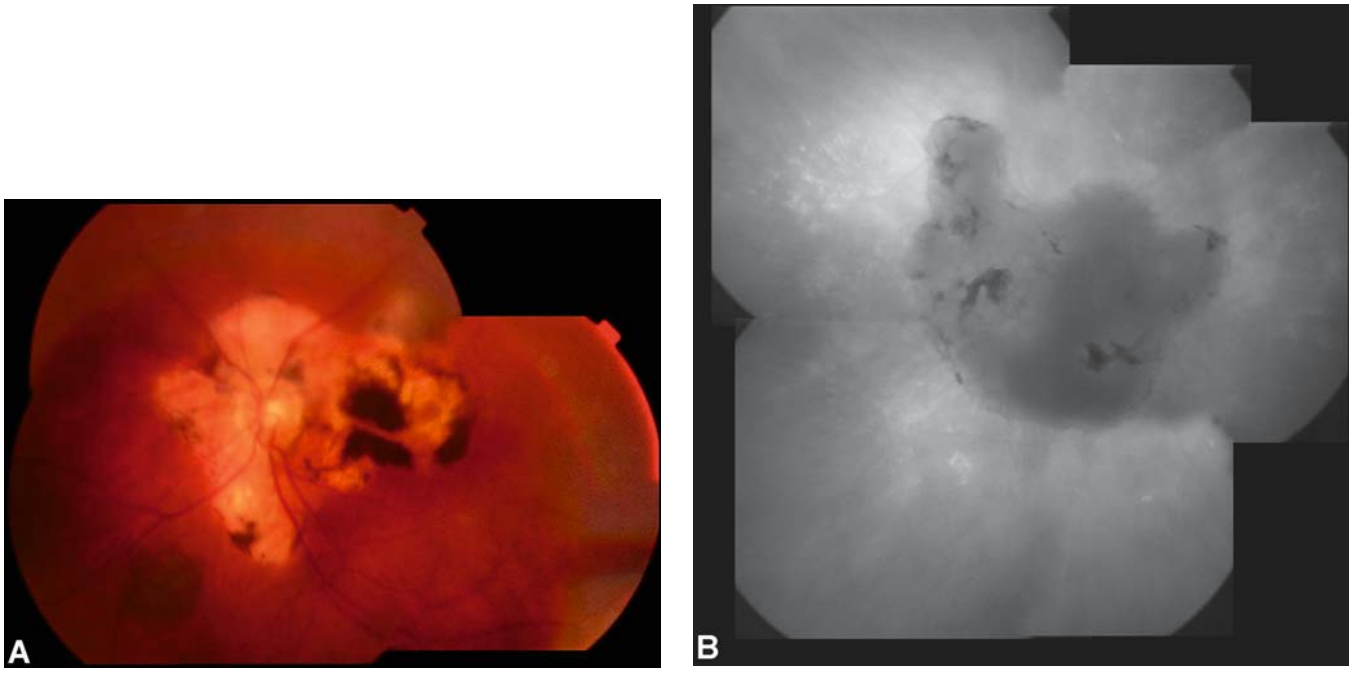

FIG. 3.13. (A) This is composite color photograph of an eye of a patient with serpiginous choroidopathy. (B) The composite of the indocyanine green (ICG) angiogram reveals a large area of hypofluorescence typical for the acute phase of the disease. The dark pigmented areas represent healed regions.

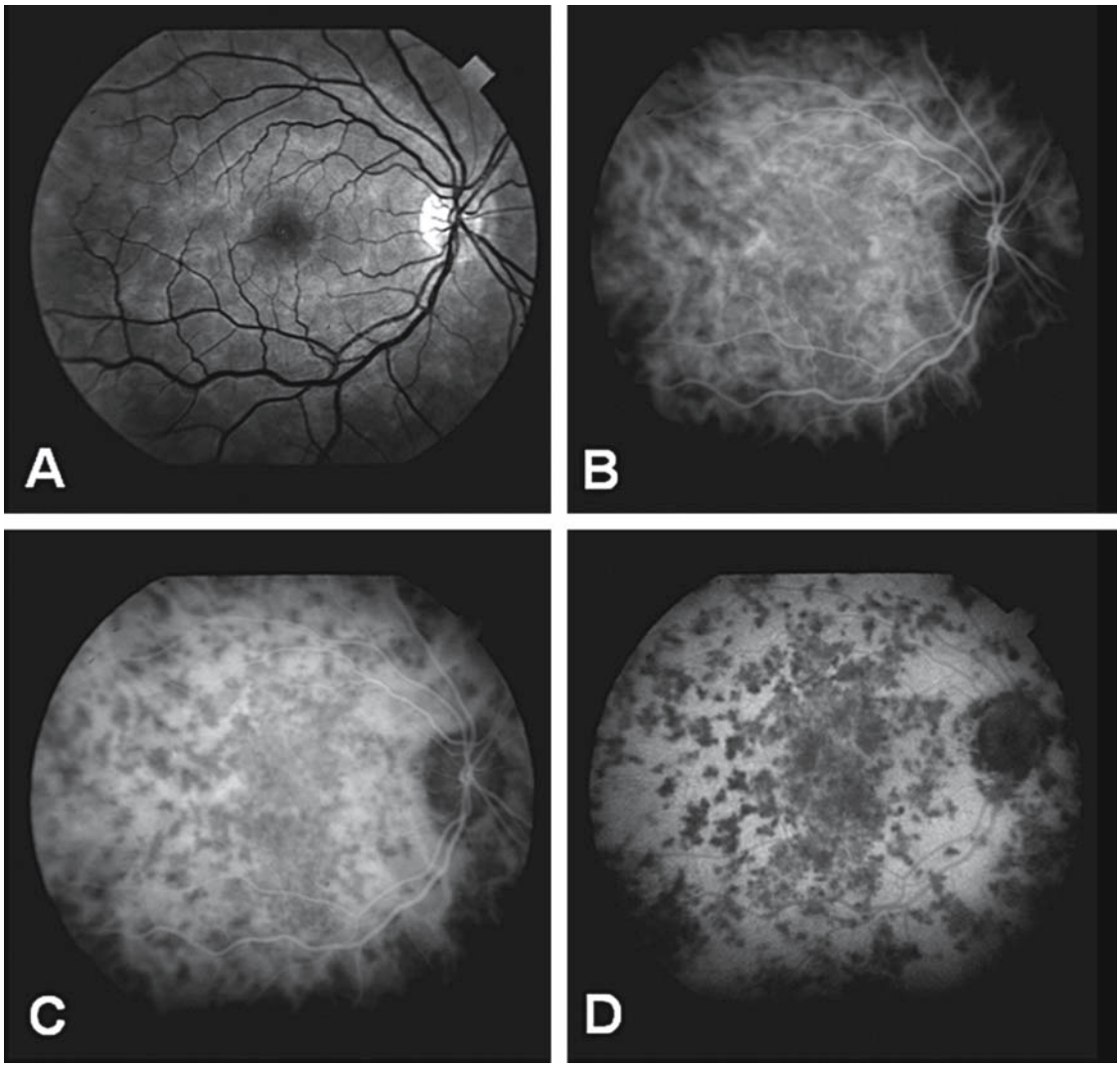

FIG. 3.14. (A) Red-free photograph of an eye of a patient with acute multifocal placoid pigment epitheliopathy (AMPPE), which shows multiple white, flat, placoid lesions. The lesions are hypofluorescent by ICGA in the early (B), middle (C), and late (D) phases of the study.

than 50 μm to about 500 μm. Many more lesions can easily be identified with ICGA than with fundus examination or fluorescence angiography. A ring of hypofluorescence surrounding the optic disc is seen in some cases. In these patients a blind spot enlargement on visual field examination is always present. During the convalescent phase, the return of visual function and normalization of the clinical examination does not correlate completely with resolution of the hypofluorescent spots seen on ICGA. These findings suggest that MEWDS may result in persistent abnormalities in choroidal circulation even after clinical symptoms disappear.

Bird-shot retinochoroidopathy is an uncommon, but potentially serious inflammatory disorder that involves both the choroid and retina. No relation to any systemic disease has been observed, while a strong association with the human leukocyte antigen (HLA) A29 class I suggests a genetic predisposition. Indocyanine green angiography reveals multiple hypofluorescent lesions resembling "holes" in the fluorescence of the choriocapillaris (Fig. 3.16). These lesions correspond to the clinical creamy lesions. The distribution of the patches follows the larger choroidal vessels. Howe et al.[20] found that ICGA detects bird-shot lesions more rapidly than FA and may be of benefit in assessing disease activity.

Multifocal choroiditis (MFC) is an idiopathic choroidal inflammatory disorder with varied presentation and clinical course. Clinical features include "punched out" chorioretinal spots, peripapillary atrophy, peripheral chorioretinal curvilinear lesions, and neovascularized macular degeneration or disciform scar. The MFC lesions block fluorescence on ICGA (Fig. 3.17). Hyperfluorescent foci that do not correlate with lesions seen clinically or by FA can also be observed. These hyperfluorescent areas may represent subclinical foci of choroiditis. Slakter et al.[21] reported on ICGA findings in a series of 14 patients with MFC. Four-

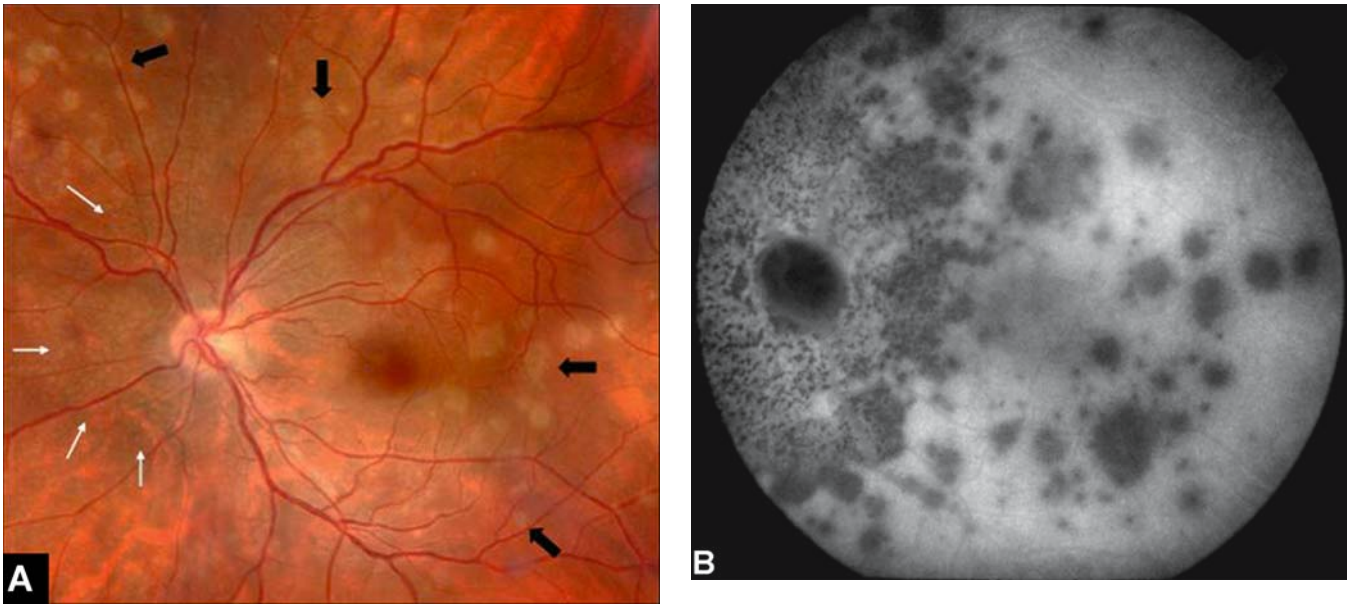

FIG. 3.15. This is an eye of a 29-year-old woman with unilateral visual disturbance caused by multiple evanescent white dot syndrome (MEWDS). (A) The clinical photograph shows multiple round, white to yellow-white spots (black arrows) distributed over the posterior fundus. In the peripapillary region, there are multiple small yellow dots (white arrows). (B) The midphase ICG reveals multiple large and small hypofluorescent spots in the posterior pole. Note the ring of hypofluorescence surrounding the optic disc.

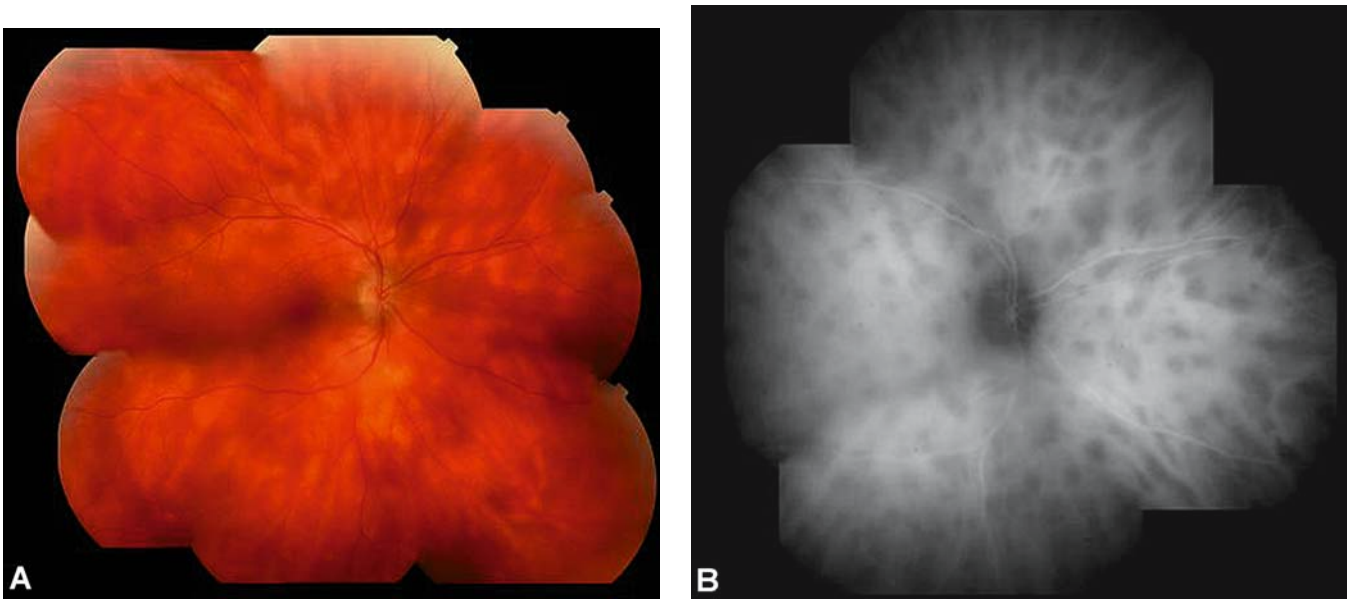

FIG. 3.16. This is an eye of a 46-year-old Caucasian woman with newly diagnosed birdshot retinochoroidopathy. (A) Clinical photograph composite reveals multiple creamy round lesions. (B) Midphase ICG illustrates multiple hypofluorescent lesions resembling "holes" in the fluorescence of the choriocapillaris.

teen (50%) of the 28 eyes were found to have large hypofluorescent spots in the posterior pole that did not correspond to clinically or fluorescein angiographically detectable lesions. In seven eyes exhibiting enlargement of the blind spot on visual field testing, ICGA showed confluent hypofluorescence surrounding the optic nerve. The ICG angiogram was useful in evaluating the natural course in two patients with MFC, as well as in evaluating the response to oral prednisolone treatment in four others. The ICGA performed in these patients showed changes correlating with the

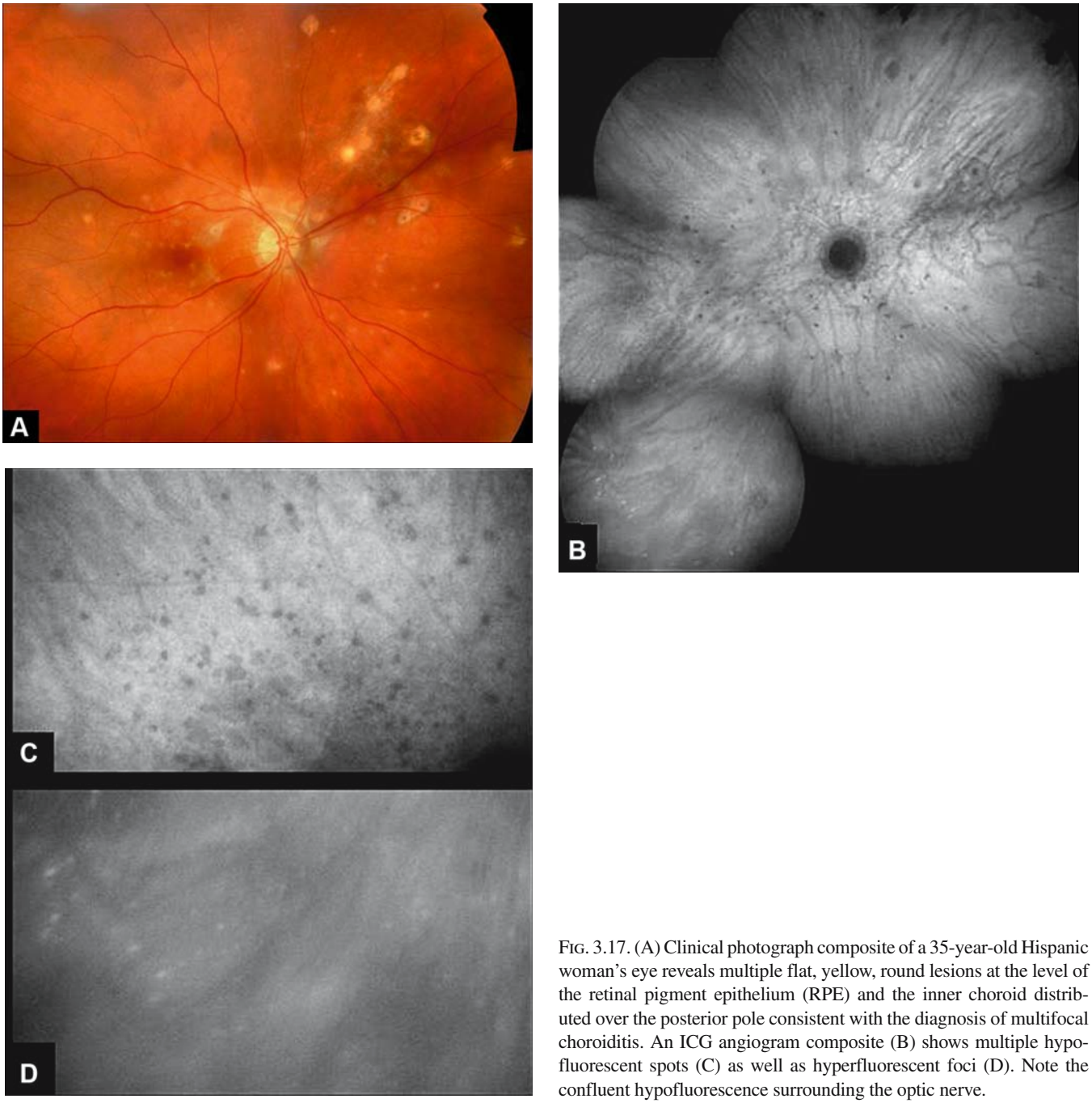

FIG. 3.17. (A) Clinical photograph composite of a 35-year-old Hispanic woman's eye reveals multiple flat, yellow, round lesions at the level of the retinal pigment epithelium (RPE) and the inner choroid distributed over the posterior pole consistent with the diagnosis of multifocal choroiditis. An ICG angiogram composite (B) shows multiple hypofluorescent spots (C) as well as hyperfluorescent foci (D). Note the confluent hypofluorescence surrounding the optic nerve.

clinical course. After administration of oral prednisolone, the patients were noted to have decreased symptoms and less vitreitis on clinical examination. Indocyanine green angiography showed a reduction in the size and number of the hypofluorescent spots in three patients, with complete resolution of these angiographic lesions in the fourth patient. Indocyanine green angiography was also helpful to differentiate MFC from presumed ocular histoplasmosis syndrome, which has similar clinical appearance. Patients with MFC clearly have hypofluorescent spots in the posterior pole during periods of relative activity, whereas patients with presumed ocular histoplasmosis syndrome may exhibit focal areas of hyperfluorescence.

Conclusion

Indocyanine green angiography is a highly specialized technique for imaging choroidal vasculature. It has several advantages over FA including lower toxicity, high protein

binding affinity, and infrared fluorescence for better penetration through pigment, serosanguineous fluid, and blood. The clinical applications of ICGA continue to expand as more experience is gained with current imaging techniques. Further advances in ICGA are likely to result from the newer high-speed imaging systems.

References

1. Guyer DR, Puliafito CP, Mones JM, et al. Digital indocyanine green angiography in chorioretinal disorders. Ophthalmology 1992;99:287–291.
2. Kogure K, Choromokos E. Infrared absorption angiography. J Appl Physiol 1969;26:154–157.
3. Hochheimer BF. Angiography of the retina with indocyanine green. Arch Ophthalmol 1971;86:564–565.
4. Flower RW, Hochheimer BF. Letter to the editor: clinical infrared absorption angiography of the choroid. Am J Ophthalmol 1972;73:458–459.
5. Flower RW. Infrared absorption angiography of the choroid and some observations on the effects of high intraocular pressures. Am J Ophthalmol 1972;74:600–614.
6. Hayashi K, Hasegawa Y, Tokoro T. Indocyanine green angiography of central serous chorioretinopathy. Int Ophthalmol 1986;9:37–41.
7. Destro M, Puliafito CA. Indocyanine green videoangiography of choroidal neovascularization. Ophthalmology 1989;96: 846–853.
8. Scheider A, Schroedel C. High resolution indocyanine green angiography with scanning laser ophthalmolscope. Am J Ophthalmol 1989;108:458–459.
9. Yannuzzi LA, Slakter JS, Sorenson JA, et al. Digital indocyanine green videoangiography and choroidal neovascularization. Retina 1992;12:191–223.
10. Spaide RF, Orlock DA, Herman-Delamazure B, et al. Wide-angle indocyanine green angiography. Retina 1998;18:44–49.
11. Spaide RF, Orlock DA, Yannuzzi LA, et al. Digital subtraction indocyanine angiography of occult choroidal neovascularization. Ophthalmology 1998;105:680–688.
12. Teschner S, Noack J, Birngruber R, Schmidt-Erfurth U. Characterization of leakage activity in exudative chorioretinal disease with three-dimensional confocal angiography. Ophthalmology 2003;110:687–697.
13. Macular Photocoagulation Study Group. Occult choroidal neovascularization. Influence on visual outcome in patients with age-related macular degeneration. Arch Ophthalmol 1996;114:400–412.
14. Patz A, Flower RW, Klein ML, Orth DH, Fleishman JA, MacLeod D. Clinical applications of indocyanine green angiography. Doc Ophthalmol Proc Series 1976;9:245–251.
15. Bischoff PR, Flower RW. Ten years experience with choroidal angiography using indocyanine green dye: a new routine examination or an epilogue? Doc Ophthalmol 1985;60:235–291.
16. Guyer DR, Yannuzzi LA, Slakter JS, et al. Classification of choroidal neovascularization by digital indocyanine green videoangiography. Ophthalmology 1996;103:2054–2060.
17. Slakter, JS, Yannuzzi, LA, Sorenson, JA, et al. A pilot study of indocyanine green videoangiography-guided laser photocoagulation of occult choroidal neovascularization in age-related macular degeneration. Arch Ophthalmol 1994;112:465–472.
18. Freund KB, Yannuzzi LA, Sorenson JA, et al. Age-related macular degeneration and choroidal neovascularization. Am J Ophthalmol 1993;115:786–791.
19. Staurenghi G, Orzalesi N, La Capria A, Aschero M. Laser treatment of feeder vessels in subfoveal choroidal neovascular membranes: a revisitation using dynamic indocyanine green angiography. Ophthalmology 1998;105:2297–2305.
20. Howe LJ, Stanford MR, Graham EM, Marshall J. Choroidal abnormalities in birdshot chorioretinopathy: an indocyanine green angiography study. Eye 1997;11:554–559.
21. Slakter JS, Giovannini A, Yannuzzi LA, et al. Indocyanine green angiography of multifocal choroiditis. Ophthalmology 1997;104:1813–1819.

4
Angiography of Macular Diseases

Lihteh Wu, Raquel Benavides, Andrea Porras, Rafael A. Garcia-Amaris, and J. Fernando Arevalo

The optical properties of the eye make the ocular fundus the only location in the human body where direct noninvasive monitoring of vascular flow is possible. During fluorescein angiography (FA) and indocyanine green videoangiography (ICGV), a rapid sequence of serial photographs taken after the intravenous administration of fluorescein or indocyanine green (ICG) is used to visualize and document choroidal and retinal blood flow. Other than blood flow, FA and ICG-V provide information about the integrity of the blood–retinal barriers and the fine details of the retinal pigment epithelium (RPE), and provide a glimpse of associated systemic pathology. Although both technologies reveal important and different aspects of retinal and choroidal diseases, some phases of various diseases are best seen with FA and other aspects are best revealed with ICGV.

This chapter reviews several macular pathologies of the retina, including age-related macular degeneration (AMD), retinal angiomatous proliferation (RAP), idiopathic polypoidal choroidal vasculopathy (IPCV), myopia, presumed ocular histoplasmosis syndrome (POHS), idiopathic choroidal neovascularization (CNV), choroidal rupture, chorioretinal folds, central serous chorioretinopathy (CSCR), optic disc pits, macular holes, epiretinal membranes (ERM), postoperative cystoid macular edema, Best's disease, Stargardt's disease, pattern dystrophies of the retinal pigment epithelium, and X-linked retinoschisis (XLRS).

Age-Related Macular Degeneration

Age-related macular degeneration (AMD) was first recognized by Otto Haab in 1885.[1] He described patients who were older than 50 years of age who lost vision secondary to atrophic and pigmentary macular changes. In 1905, Oeller was the first to use the term *disciform macular degeneration*.[2] In 1926, Junius and Kuhnt applied the term to the advanced exudative macular lesions seen in elderly patients.[2] However, it was not until 1967 that Gass[2] made the unifying observation that drusen, senile macular degeneration, and senile disciform macular degeneration represented different clinical manifestations of the same disease.

Epidemiology

Age-related macular degeneration is the most common cause of visual disability in patients older than 50 years of age in the developed world.[3] Age is the single most important risk factor identified. Of all the other risk factors, cigarette smoking stands out, as most studies have shown a strong association between it and AMD.[3] Epidemiologic data have not been consistent regarding the relationship of other risk factors such as light exposure, cataract and cataract surgery, hypertension, serum lipids, and leukocyte count to AMD.[3] Several twin studies have strongly suggested that a genetic predisposition for AMD exists.[3]

Pathophysiology

The underlying cause of AMD remains unclear. There is some evidence that AMD represents a chronic inflammatory state where macrophage dysfunction plays a role in the initial stages.[4] Proteins associated with complement activation and immune complexes accumulate between the basement membrane of the RPE and Bruch's membrane prior to drusen formation.[5] In addition, as we age RPE cells shed cellular debris into the extracellular space. This extracellular material accumulates between the basement membrane of the RPE and Bruch's membrane, and gives rise to the deposits that we call drusen (Fig. 4.1).[5] Recently, polymorphisms in the complement factor H gene have been associated with an increased risk of developing AMD, implicating the innate immune system in the pathogenesis of AMD.[6,7]

Why some eyes with drusen develop CNV whereas other eyes with drusen develop geographic atrophy (GA) remains unclear. Friedman[8] has hypothesized that with AMD the resistance of the choroidal circulation is increased. If this resistance is higher than the cerebrovascular resistance, then decreased choroidal perfusion results in RPE atrophy. If the choroidal

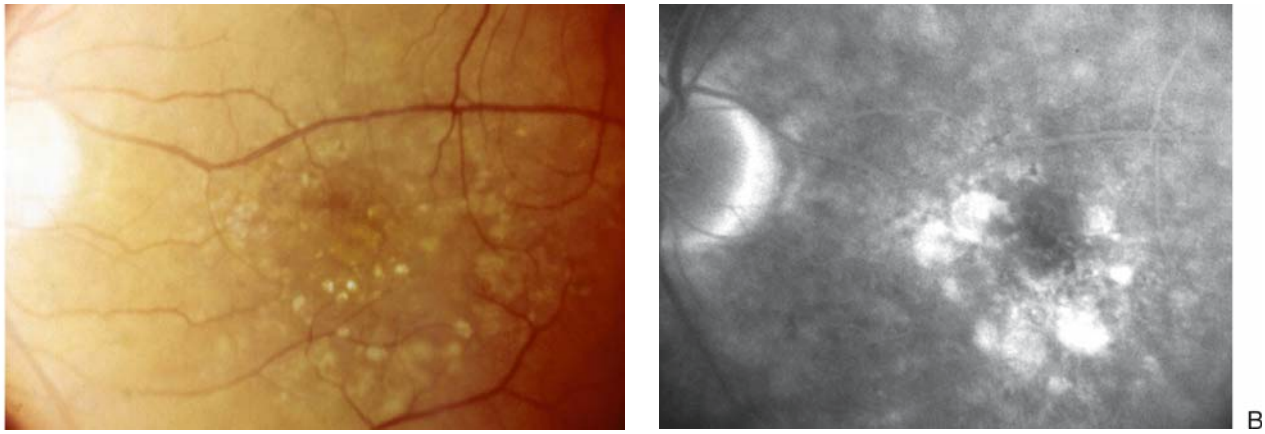

FIG. 4.1. A 67-year-old woman on routine examination was noted to have a visual acuity of 20/25. (A) Clinical photograph 2 years later shows disappearance of some of the drusen. In the areas where the drusen have faded, nongeographic atrophy of the retinal pigment epithelium (RPE) has appeared. The visual acuity has decreased to 20/40. (B) Late phase of the angiogram 2 years later demonstrating the large areas of hyperfluorescent nongeographic atrophy of the RPE.

resistance is lower than cerebrovascular resistance, the resulting elevated choriocapillaris pressure gives rise to a pigment epithelial detachment (PED) or CNV.

Drusen may provoke local tissue hypoxia with upregulation of vascular endothelial growth factor (VEGF) by blocking the diffusion of oxygen and nutrients from the choriocapillaris to the RPE and outer retina.[9] Alternatively, inflammatory cells may secrete VEGF.[10] VEGF has been temporally and spatially correlated with the development of CNV. Several researchers have induced CNV formation in animal models by overexpressing VEGF.[11] Once secreted, VEGF binds to its receptors in endothelial cells, activating several signal transduction pathways that end with the formation of a network of new vessels.[12]

Clinical Findings

Early Age-Related Macular Degeneration

Drusen are considered to be the clinical hallmark of the disease (Fig. 4.1A).[5] Their morphologic variation is considerable. Thus a distinction must be made between the several subtypes of drusen. Hard drusen are small, round, flat yellowish-white deposits. They usually measure less than 63 μm in diameter.[13,14] Soft drusen are larger than 63 μm in diameter. They can have indistinct fuzzy borders or distinct definite borders. Coalescence of several soft drusen may occur. Soft drusen represent a detachment of the RPE. Unlike hard drusen, soft drusen are a definite risk factor for the development of CNV or GA.[15,16]

Late Age-Related Macular Degeneration

Geographic atrophy of the RPE represents the end stage of nonexudative AMD. Initially, focal atrophy arises in the parafoveal areas as drusen fade or alternatively in areas of RPE pigmentary alterations (Fig. 4.1).[17,18] Clinically it is seen as a sharply defined oval area centered on the fovea where a change of color with respect to the surrounding retina is noted. The underlying choroidal vessels are more easily seen (Fig. 4.2). This area of atrophy represents loss of the RPE, choriocapillaris, and photoreceptors.

In addition, GA may result as pigment epithelial detachments decompensate and flatten out.[19] Even though GA spares the fovea until late in the course of the disease, patients complain of their diminished ability to read and their decreased ability to recognize faces early on. This is secondary to the parafoveal scotoma, reduced contrast sensitivity, and abnormal dark adaptation.[20] Up to 50% of eyes with GA and good visual acuity at baseline end up losing three or more lines of vision after 2 years of follow-up; by 4 years, 27% of eyes have a vision of 20/200 or worse.[21]

Several clinical variants of exudative AMD have been described: serous pigment epithelial detachment (S-PED), choroidal polypoidal vasculopathy, RAP, CNV and thick submacular hemorrhages.

It appears that with increasing age, in some eyes the composition of Bruch's membrane changes, impairing its hydraulic conductivity.[22,23] The normal flow of fluid from the vitreous cavity to the choroid is impaired causing an S-PED (Fig. 4.3). S-PED is seen as a round or oval yellowish-orange detachment of the RPE.

Choroidal neovascularization is usually diagnosed by angiographic criteria. However subretinal hemorrhages, lipid exudation, and subretinal fluid are clinical findings that suggest the presence of CNV (Fig. 4.4). Depending on the fluorescein angiographic findings, CNV may be subdivided into classic CNV and occult CNV.

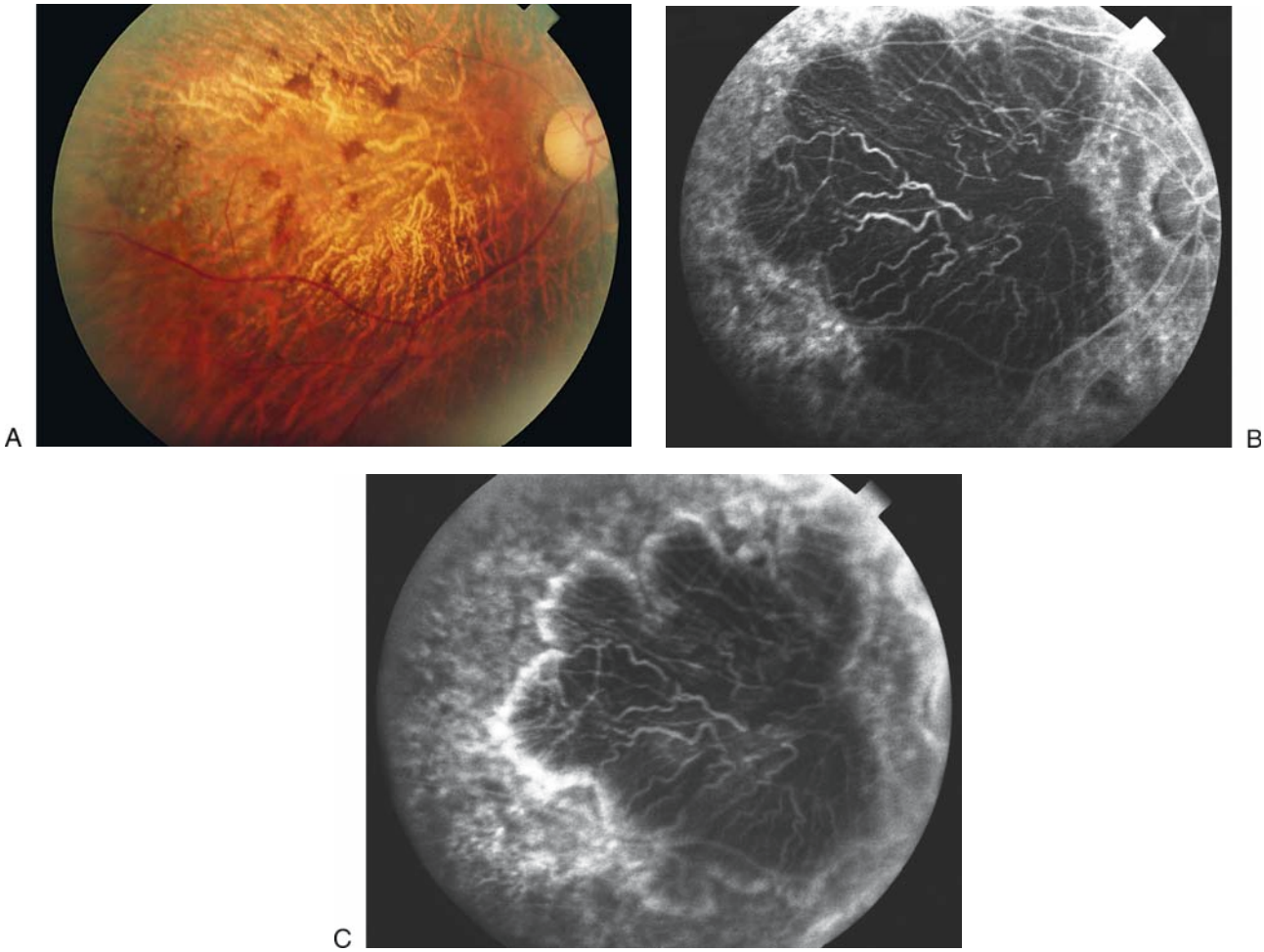

Fig. 4.2. A 65-year-old woman complains of a gradual and progressive loss of vision in her right eye over the past few years. She has a visual acuity of 3/200 and is noted to have geographic atrophy of the RPE. (A) Clinical photograph. Notice a sharply defined oval area centered on the fovea where a change of color with respect to the surrounding retina is noted. The underlying choroidal vessels are more easily seen. (B) Midphase fluorescein angiography (FA) frame shows a hypofluorescent lesion secondary to RPE and choriocapillaris loss. The large choroidal vessels are easily seen within the lesion. (C) Late-phase FA frame shows staining of the borders of the lesion.

The presence of five or more drusen, one large druse, focal hyperpigmentation of the RPE, and systemic hypertension have all been identified by the Macular Photocoagulation Study (MPS) as risk factors that puts the fellow eye of an eye affected with CNV at an increased risk of developing CNV. The 5-year incidence has been estimated to vary from 7% if no risk factors are present to 87% if all four risk factors are present.[24]

A disciform scar represents the end-stage lesion of the exudative process (Fig. 4.5). The lesion is mostly composed of subretinal fibrosis, but varying degrees of subretinal fluid, intraretinal or subretinal hemorrhages, macular edema, and lipid exudation may be present.

Classification

Traditionally AMD has been classified as dry or atrophic and wet or exudative. Drusen, hypopigmentation, and hyperpigmentation of the RPE, nongeographic atrophy, and GA of the RPE represent different manifestations of nonexudative AMD. Choroidal neovascularization, hemorrhagic or serous PED, polypoidal choroidal vasculopathy, RAP, chorioretinal anastomosis, and vitreous hemorrhage are clinical manifestations of the exudative process.

In 1995, Bird and colleagues[25] proposed a new international classification. According to this scheme, AMD is classified into an early stage and a late stage. Early AMD, also referred to as age-related maculopathy, includes eyes with soft drusen measuring at least 63 μm or eyes with hyperpigmentation or hypopigmentation of the RPE. Late AMD includes eyes with GA and eyes with neovascular manifestations of the disease.

Fluorescein Angiography

Angiographic assessment of hard drusen is characterized by early hyperfluorescence that corresponds to the drusen

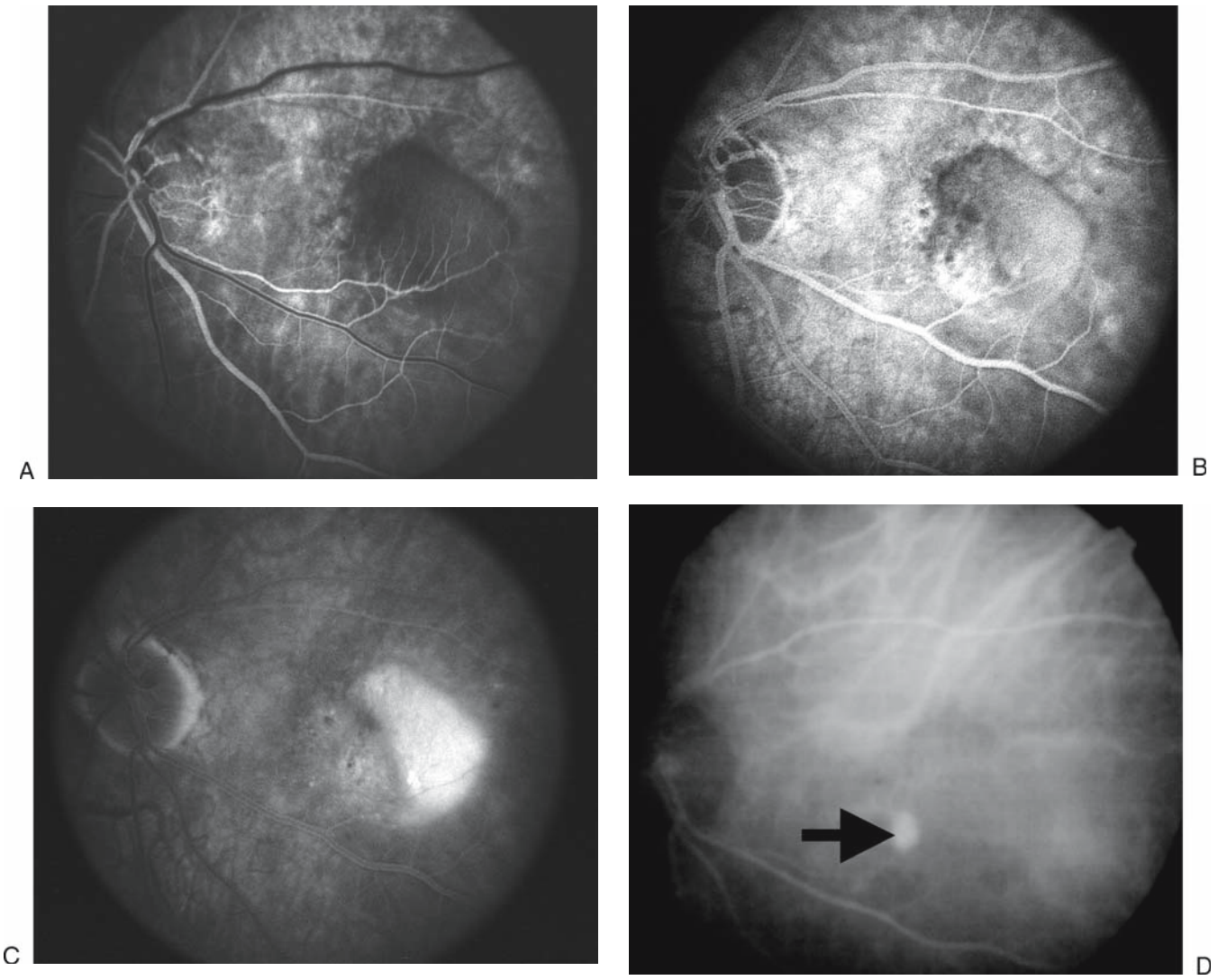

FIG. 4.3. Patient with a serous pigment epithelial detachment (S-PED) and choroidal neovascularization (CNV). (A) Early phase of the angiogram shows slow and irregular filling of the PED. (B) Midphase of the angiogram shows an oval-shaped, irregularly filled PED. (C) Late phase of the angiogram shows staining of the PED. (D) Static indocyanine green (ICG) shows a hot spot (arrow).

and the thinned overlying RPE. As the study progresses, this hyperfluorescence fades away. If the overlying RPE has not undergone atrophy, then the drusen might not hyperfluoresce. In general, angiography detects a greater number of hard drusen than clinical examination. Soft drusen are characterized by early hyperfluorescence, late staining or fading, but no leakage (Fig. 4.1B). Focal hyperpigmentation of the RPE blocks the normal background choroidal fluorescence. This blocked fluorescence must be differentiated from blood or fibrovascular proliferation through clinical correlation. Nongeographic atrophy is imaged as mottled hyperfluorescence that fades with the study. These areas correspond to the areas of RPE atrophy interspersed with areas of normal background fluorescence corresponding to areas of normal RPE.

Due to the loss of the choriocapillaries in GA of the RPE, these lesions appear as mildly hyperfluorescent or hypofluorescent. Sharp borders define the areas of GA and normal RPE. During the transit phase, the large choroidal vessels are easily seen within the lesion. In the late stages, staining of the choroidal and scleral layers lead to diffuse mild staining of the lesion (Fig. 4.2B,C).

Fluorescein angiography (FA) is an essential tool in managing and diagnosing CNV. The goal of any imaging technique is to identify CNV if it is present and to define its size and borders so that treatment can be undertaken in a precise manner. With FA, CNV may be definite (classic), presumed (occult), or a mixture of both (Figs. 4.6, 4.7, 4.8, and 4.9). A lesion that hyperfluoresces in the early choroidal phase of the angiogram, maintains well-demarcated borders, and

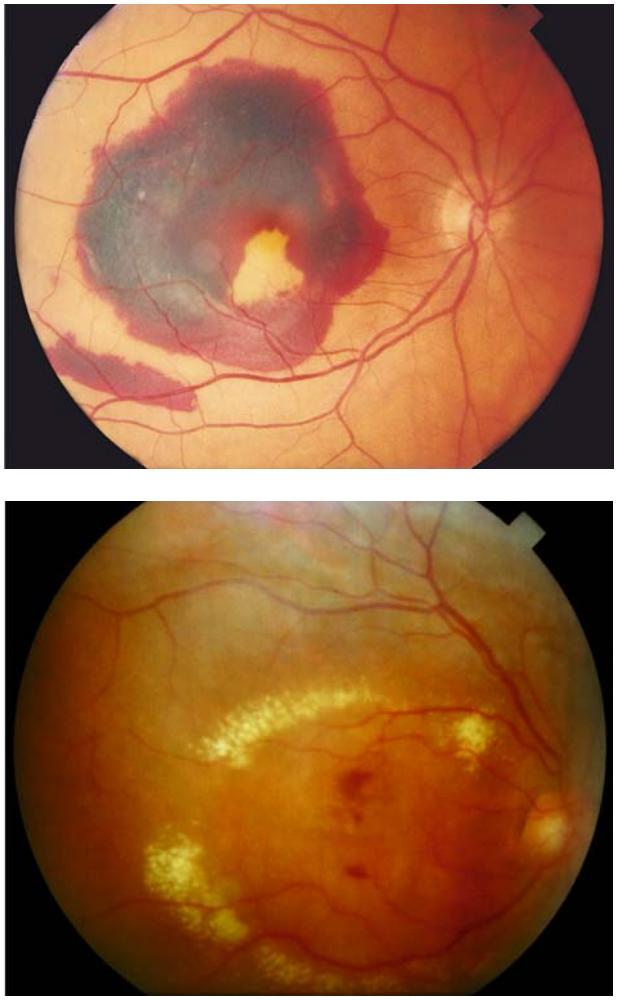

FIG. 4.4. Clinical clues to suspect CNV: (A) Subretinal hemorrhage. (B) Lipid exudation.

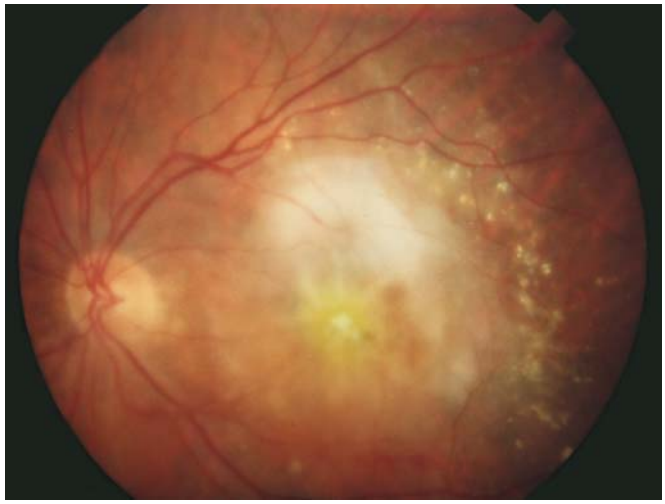

FIG. 4.5. A disciform scar represents the end-stage lesion of the exudative process.

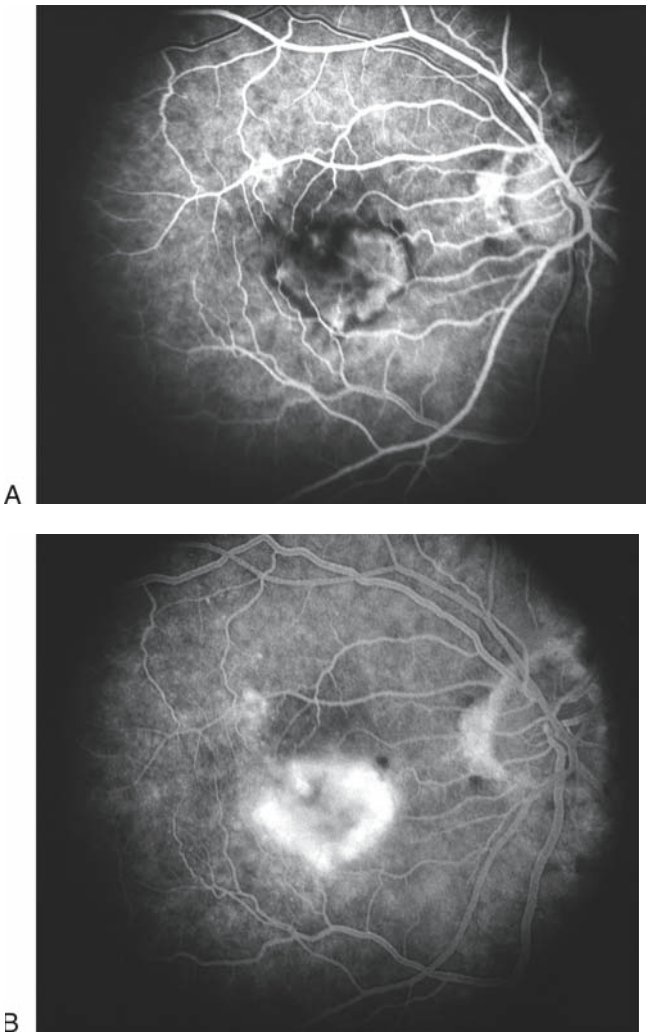

FIG. 4.6. Subfoveal classic CNV. (A) Early phase of the angiogram. (B) Late phase of the angiogram.

leaks late, obscuring its borders, is classic CNV.[26] A lesion whose borders cannot be determined by FA is occult CNV. The lesion may be well demarcated or poorly demarcated. Fibrovascular pigment epithelial detachment (FV-PED) and late leakage of undetermined source (LLUS) represent patterns of occult CNV.[26] An FV-PED is a lesion that is solid irregularly elevated and manifests stippled hyperfluorescence 1 to 2 minutes following dye injection (Fig. 4.8). In the late phases there is persistent staining or leakage into the overlying neurosensory retinal detachment. Late leakage of undetermined source is seen as an irregular, indistinct, late, sub-RPE leakage.[26]

An S-PED shows a lesion that has an intense early hyperfluorescence with persistent staining in the late phases that obscures any hyperfluorescence secondary to CNV (Fig. 4.3).[27] There are certain features in the fluorescein angiogram that suggest that the S-PED also harbors CNV. A slow irregular filling of the PED is suspicious for CNV. Irregularly shaped

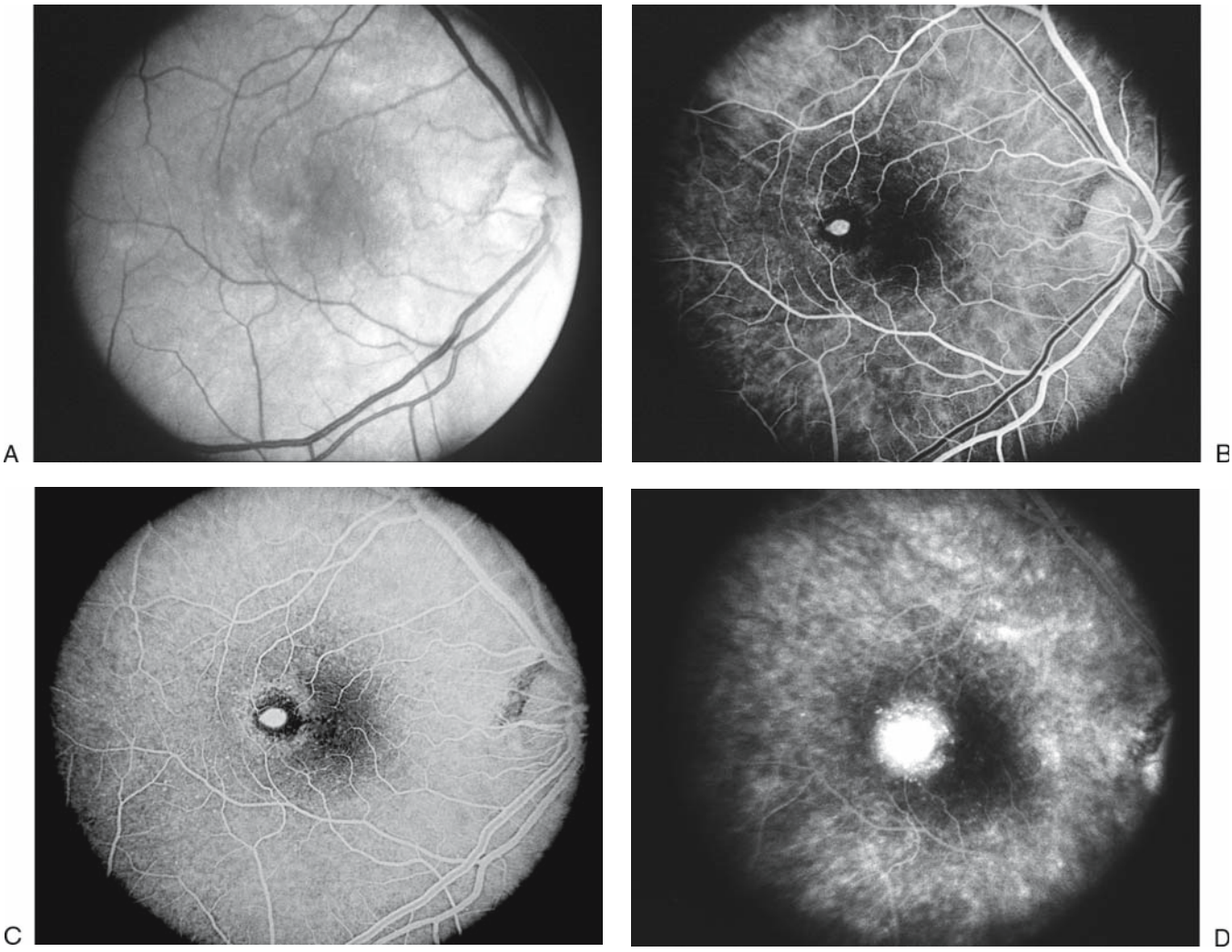

FIG. 4.7. Juxtafoveal CNV with both classic and occult components. There is a well-defined area of early choroidal hyperfluorescence with late leakage. An elevated area of blocked fluorescence with an encircling area of irregularly elevated RPE has stippled hyperfluorescence that persists into the late phase is present. (A) Red-free photograph. (B) Early phase of the angiogram. (C) Midphase of the angiogram. (D) Late phase of the angiogram.

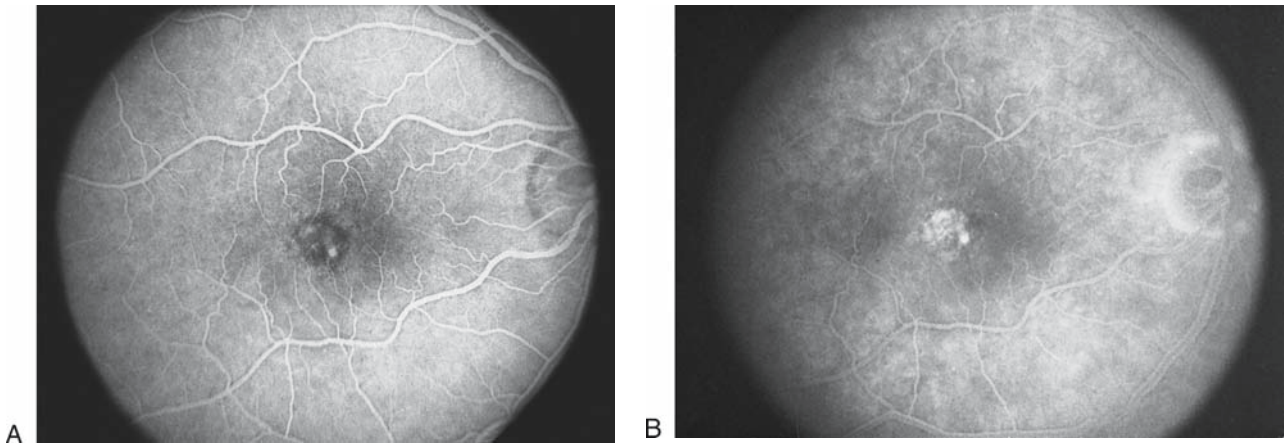

FIG. 4.8. Standard photographs used in the Macular Photocoagulation Study (MPS) to grade fibrovascular pigment epithelial detachment (FV-PED). (A) Early phase of the angiogram. (B) Late phase of the angiogram.

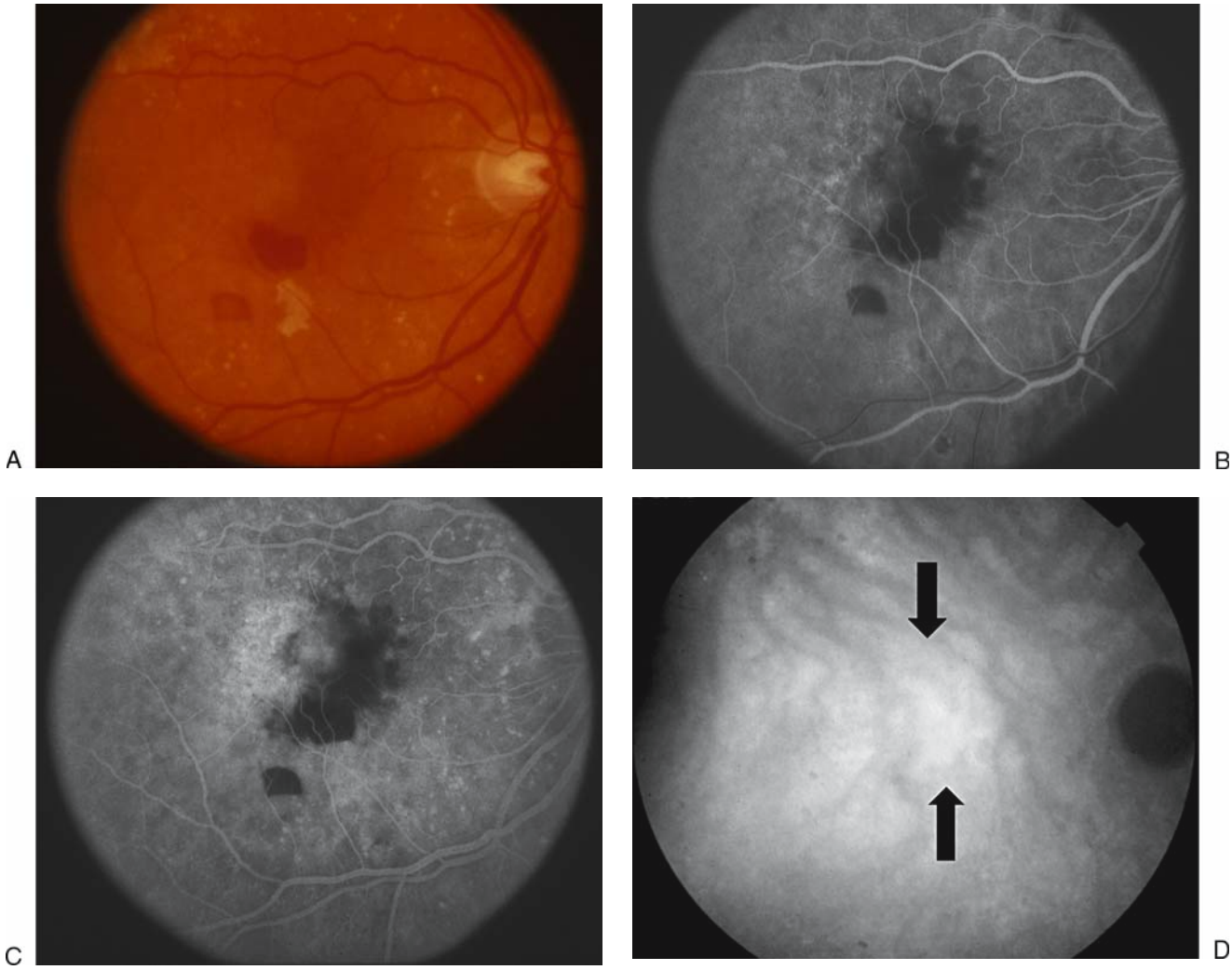

Fig. 4.9. Occult choroidal neovascularization. (A) Clinical photograph. (B) Early phase of the angiogram. (C) Midphase of the angiogram. (D) Late ICG shows an ill-defined hyperfluorescent subfoveal plaque (between arrows).

PEDs with a notch or doughnut shape are also suspected of having a CNV.[27]

Indocyanine Green Angiography

Indocyanine green is a water-soluble tricarbocyanine dye that contains 5% sodium iodide. After intravenous injection ICG is tightly bound to the plasma proteins (98%). Therefore, less dye escapes from the choroidal circulation, allowing better definition of the choroidal vasculature (Fig. 4.10). Indocyanine green has a peak absorption and fluorescence in the near-infrared range. This allows visualization of choroidal pathology through overlying serosanguineous fluid, pigment, or a thin layer of hemorrhage, which usually blocks visualization during fluorescein angiography. Indocyanine green angiography has been mainly used to better define CNV that was occult in the fluorescein study (Fig. 4.11).[28] Three types of ICG patterns that are assumed to represent CNV may be imaged. A hot spot is a well-defined focal hyperfluorescent area that is less than one disc area in size. Hot spots usually fluoresce early (Fig. 4.3D). A plaque refers to a hyperfluorescent lesion that is larger than one disc area in size. It usually does not fluoresce early and its intensity diminishes late (Fig. 4.9). Finally, some eyes harbor a combination of plaques and hot spots. In these eyes, the hot spots may be at the edge of the plaque, may overlie the plaque, or may be far from the plaque.

High-speed or dynamic ICG angiography (ICGA) uses a scanning laser ophthalmoscope that takes up to 32 frames per second.[29] These images are recorded like a movie and one can actually see flow in and out of vessels. The main use of

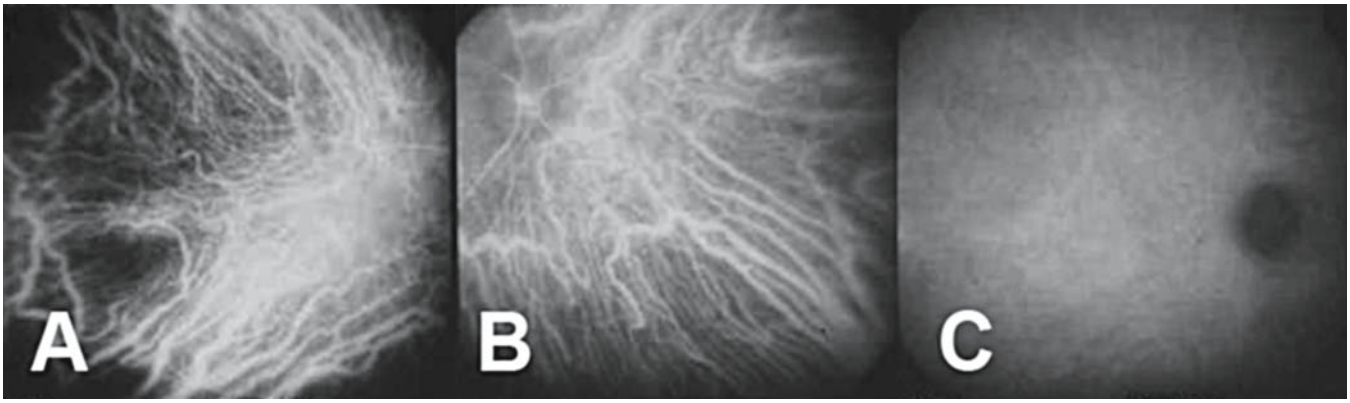

FIG. 4.10. Early, middle, and late phases of indocyanine green angiography. (A) The early phase permits image capture in the early phase of choroidal filling. During this phase, both the choroidal and retinal vessels are well visualized. (B) Middle phase demonstrates fading of choroidal fluorescence, and any abnormality that retains dye starts to appear as relatively hyperfluorescent. (C) The late phase begins approximately 18 minutes after the injection. Choroidal vessels appear as hypofluorescence channels, retinal vessels are not visible, and the optic nerve head appears dark.

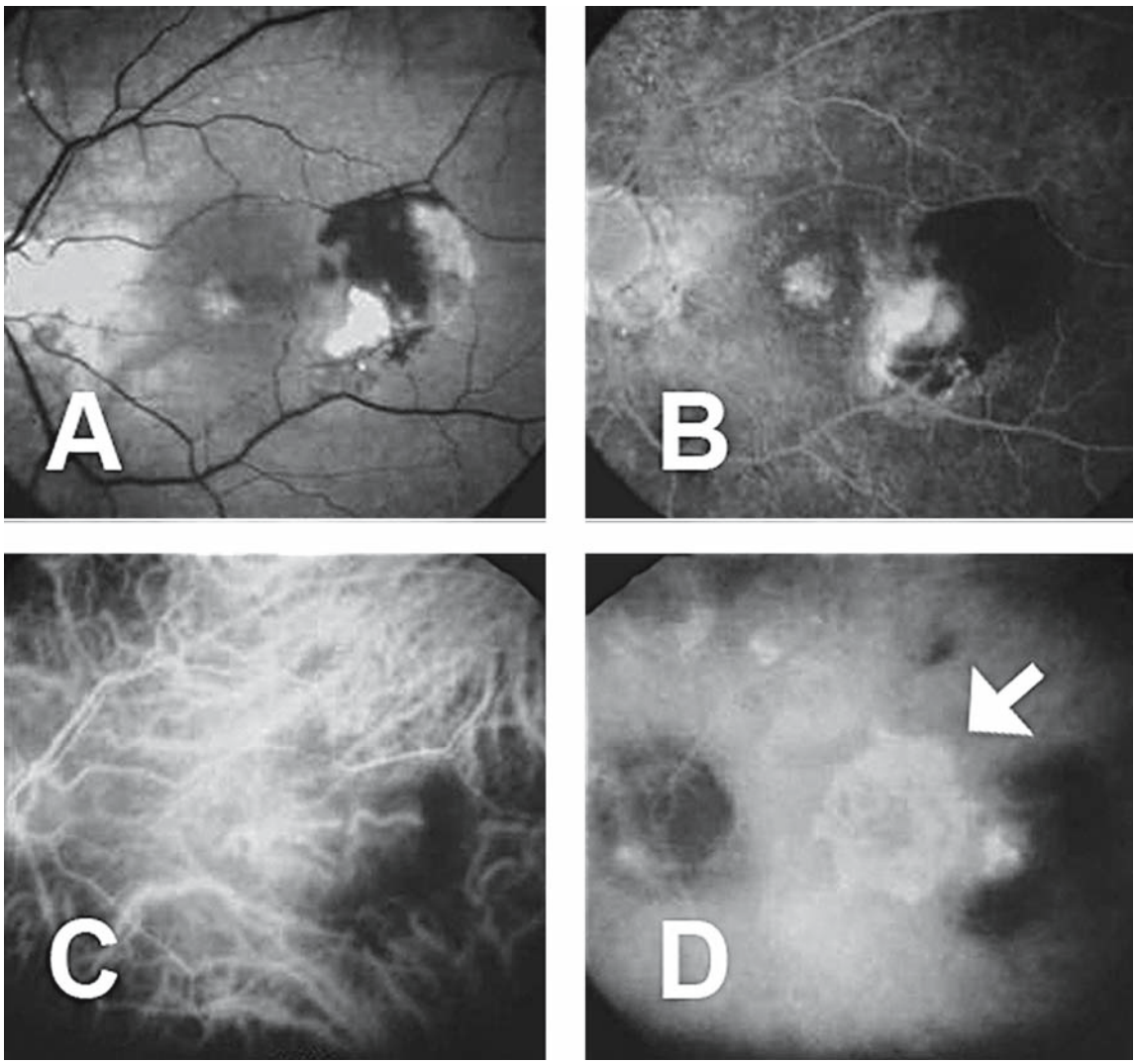

FIG. 4.11. Occult choroidal neovascularization. (A) Clinical photograph demonstrates subretinal and intraretinal hemorrhages, as well as detachment of the retinal pigment epithelium, and the neurosensory retina in a patient with neovascular age-related macular degeneration. (B) Late-phase fluorescein angiogram reveals blocked fluorescence from the hemorrhages and indistinct leakage. (C,D) Early- and late-phase indocyanine green angiograms (ICGA) demonstrate a well-defined hyperfluorescence or so-called plaque representing a choroidal neovascularization (arrow). This lesion is well visualized through the area of hemorrhage because of good penetration of the infrared light used in ICGA.

dynamic ICG is in the identification of CNV feeder vessels that are located in Sattler's layer of the choroid.[30,31]

Optical Coherence Tomography

Unlike fluorescein angiography, optical coherence tomography (OCT) images (Fig. 4.12) correlate very well with the anatomic histologic picture. The different clinical manifestations of both nonexudative and exudative AMD have distinct findings in OCT.[32]

Choroidal neovascularization causes thickening and fragmentation of the highly reflective RPE-choriocapillaris band. If the CNV is well defined, it is seen as a fusiform thickening of the RPE-choriocapillaris band. In contrast, poorly defined CNV is imaged as a diffuse area of choroidal hyperreflectivity that blends into the normal contour of the normal RPE band. A normal boundary cannot be defined.

Treatment

The Age-Related Eye Disease Study (AREDS) has shown that antioxidants (vitamin C, vitamin E, and beta-carotene) coupled with zinc supplementation at pharmacologic doses delays the progression of intermediate AMD to advanced AMD by up to 25%. The study has recommended this supplementation only in eyes with soft drusen or eyes where the fellow eye has advanced AMD.[33]

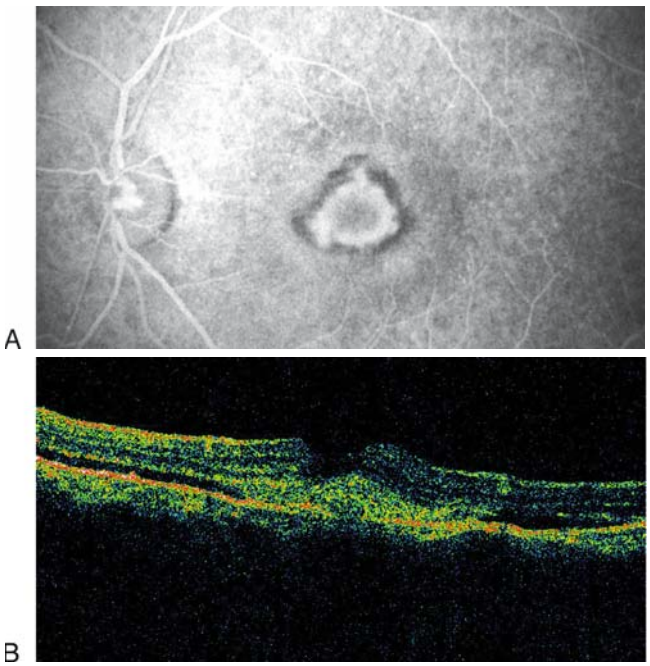

Fig. 4.12. Optical coherence tomography (OCT) image of exudative age-related macular degeneration (AMD). (A) Fluorescein angiography (FA) shows a classic subfoveal choroidal neovascularization (CNV). (B) Optical coherence tomography of the above subfoveal CNV revealing thickening of the choriocapillaris–RPE band with adjacent detachment of the neurosensory retina.

Laser to Drusen

Gass[18] first noted that drusen were reabsorbed following macular photocoagulation. However, prospective randomized trials have recommended against prophylactic laser treatment of drusen.[34]

Rheopheresis

Several epidemiologic studies have associated serum levels of high molecular weight plasma components such as cholesterol, fibrinogen, α2-macroglobulin, von Willebrand factor, and plasma viscosity with AMD. Rheopheresis consists of removal of these components from the patient's blood. Small pilot studies have shown encouraging results in patients with soft drusen, but these results need to be confirmed in larger studies.[35]

Macular Translocation

The outcome of several eyes with GA and recent visual loss that have undergone macular translocation have been reported. The short-term visual results appear promising. However, it is noteworthy that in one eye, an area of GA developed in the new translocated fovea 12 months after the surgical procedure.[36,37]

Exudative Age-Related Macular Degeneration

Laser Photocoagulation

According to its location relative to the center of the fovea, CNV has been classified as extrafoveal, juxtafoveal, or subfoveal.[38–42] Extrafoveal CNV is located at least 200 μm from the center of the fovea. The edge of juxtafoveal CNV is located from 1 to 199 μm from the center of the fovea. Subfoveal CNV is located under the fovea.

The MPS proved the efficacy of laser photocoagulation in the treatment of CNV secondary to AMD.[38–40] The goal of the treatment is to completely obliterate CNV with suprathreshold confluent laser burns (Fig. 4.13).[26] It is noteworthy that 55% of patients with exudative AMD had a recurrent or persistent CNV after laser photocoagulation.[43] In most cases, photocoagulation of these recurrent CNV is indicated. Thus 2 weeks following laser photocoagulation, a patient should be examined and have a fluorescein angiogram. Special attention should be paid to the borders, especially the foveal border, of the laser treatment zone to detect any persistence of CNV. Clinical examination cannot replace FA during the first 18 months after laser treatment, because most persistent and recurrent leakage occurs during this period.[44]

Photodynamic Therapy

Photodynamic therapy (PDT) represents a technique that uses light-activated drugs and nonthermal light to achieve selective destruction of CNV with supposedly minimal effects on the surrounding retina (Fig. 4.14).[45] Despite all the initial excitement, PDT provides marginal benefit. Most eyes continue losing vision, although at a slower rate, and only 15% of eyes manifest some visual improvement.

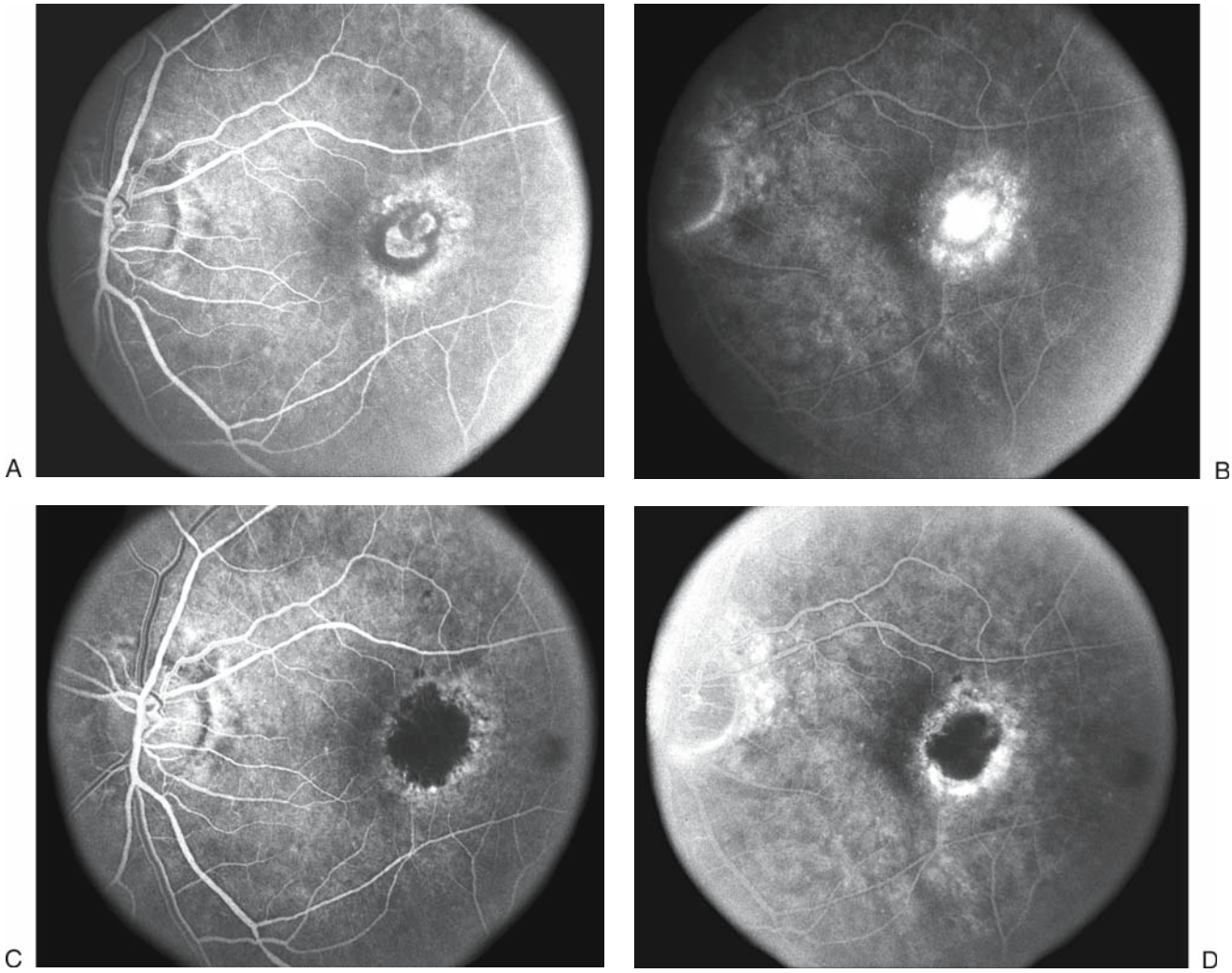

FIG. 4.13. Laser treatment of CNV according to the MPS protocol. (A) Early phase of the angiogram shows early hyperfluorescence. (B) Late phase of the angiogram shows leakage. (C) Two-week follow-up early phase angiogram after laser thermal ablation. (D) Two-week follow-up late-phase angiogram.

Transpupillary Thermotherapy

Transpupillary thermotherapy (TTT) refers to a low retinal irradiance, large spot size, long pulse infrared 810-nm diode laser protocol used to irradiate the CNV lesion. This hyperthermic reaction leads to thrombosis of the CNV.[46] A randomized clinical trial showed that TTT was no better than sham when treating eyes with subfoveal occult CNV.[47]

Feeder Vessel

With the advent of the scanning laser ophthalmoscope, dynamic ICGA can be performed, which allows easy imaging of the CNV feeder vessels that are located in Sattler's layer.[30] Once they are identified, they can be treated with the diode laser in an extrafoveal location. Small series have shown the efficacy and feasibility of this technique.[29,48–50]

Radiation Therapy

Radiation therapy has known antiangiogenic properties. However, some trials do not support radiation therapy as a treatment alternative in eyes with CNV secondary to AMD.[51,52]

Antiangiogenic Agents

As mentioned previously, VEGF plays an important role in the pathogenesis of CNV. Targeting VEGF allows a two hit strategy: antiangiogenesis and antipermeability (Fig. 4.15). Pegaptanib sodium is an aptamer against VEGF165, the isoform identified with pathologic angiogenesis, which has been shown to reduce visual loss when compared to sham. However, only a small number of eyes have an improvement of vision.[53] Ranibizumab is a recombinant humanized monoclonal antibody fragment against all isoforms of VEGF. Visual

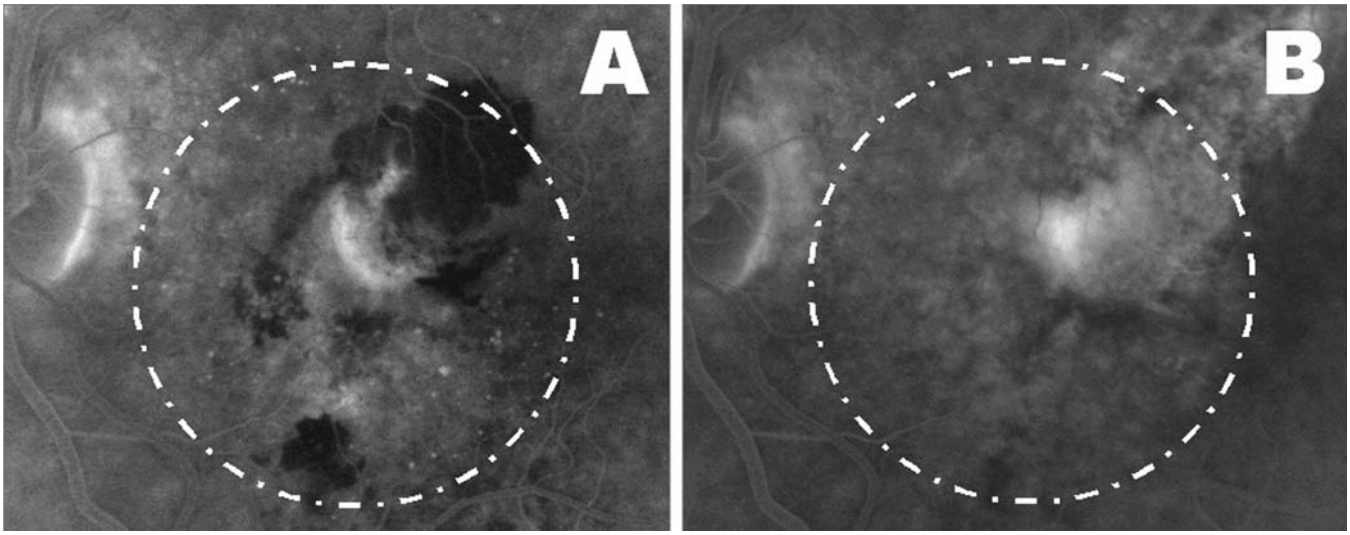

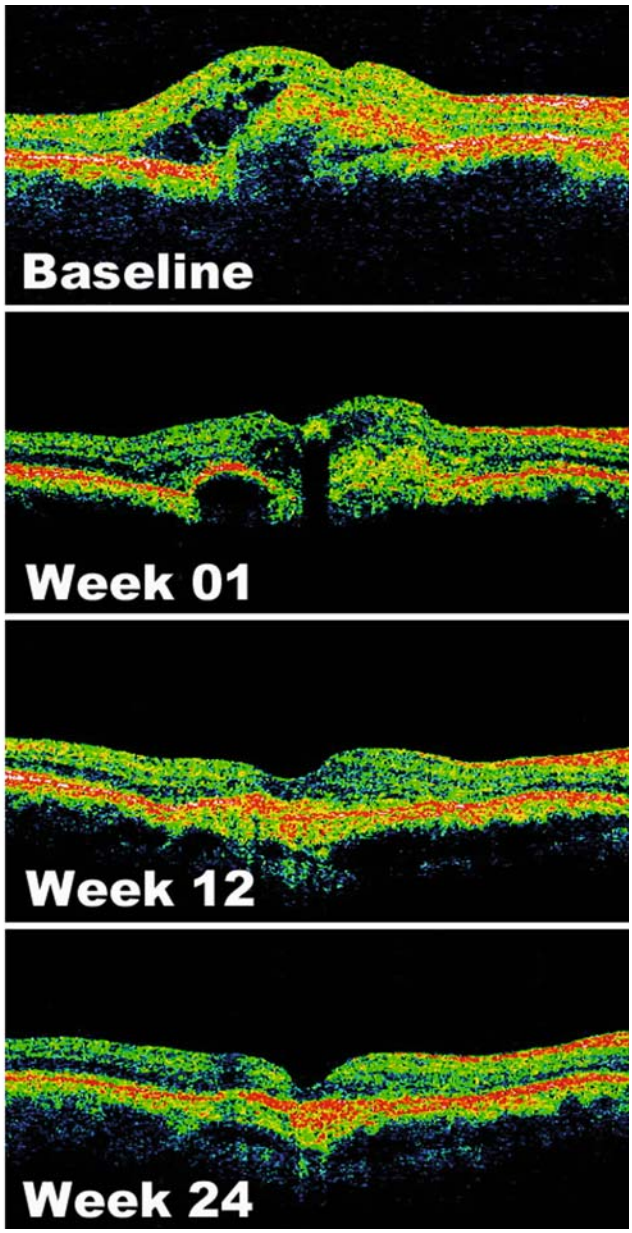

C

FIG. 4.14. Fluorescein angiography evaluation in a 69-year-old patient with age-related macular degeneration (AMD) complicated by an ill-defined neovascular lesion with subfoveal involvement who was submitted to photodynamic therapy (PDT). (A) Fluorescein blockage from subretinal and sub-RPE hemorrhage as well as some areas of stippled hyperfluorescence was seen at baseline (best corrected visual acuity [BCVA] = $20/800^{+1}$). (B) Twenty-four weeks after treatment, fluorescein staining of the quiescent neovascular lesion and no leakage from previous CNV was observed (BCVA = $20/160^{+2}$). Note that no clear angiographic damage was evidenced in the presumably normal choroidal and retinal tissues involved in the large (4.5-mm spot) treatment area (dashed circular line). (C) Optical coherence tomography evaluation of the same patient. Rapid resolution of the exudative manifestations was disclosed by horizontal 6-mm scans as early as 1 week after PDT. Considerable restoration of the macular architecture was seen in the subsequent follow-up visits 12 and 24 weeks after treatment. (Courtesy of Rogério Costa, MD.)

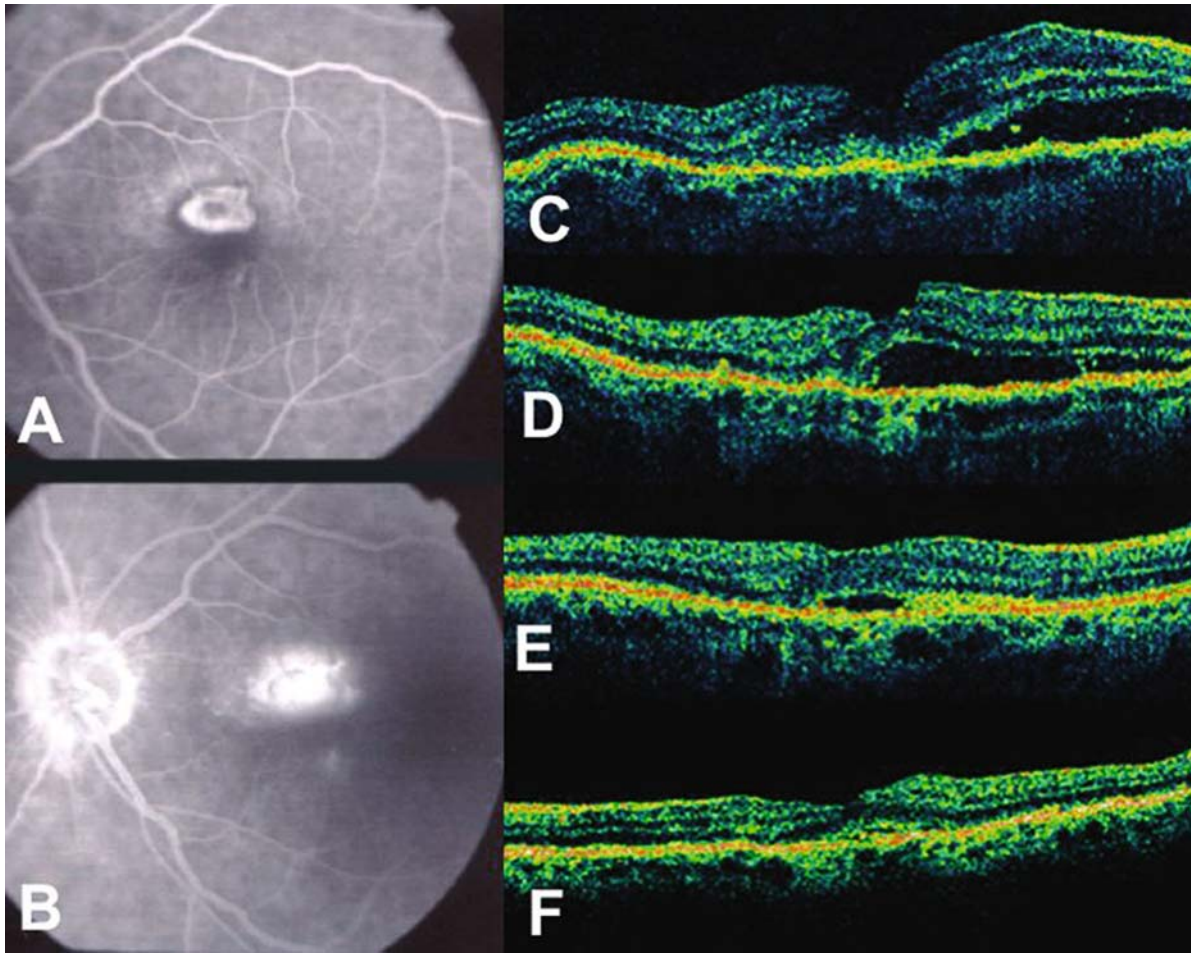

Fig. 4.15. (A,B) Early and late fluorescein angiogram of a patient with age-related macular degeneration and juxtafoveal choroidal neovascularization. (C–F) Improvement of visual acuity and optical coherence tomography findings at baseline (C), at 1 week (D; from 20/400 to 20/60), at 2 weeks (E; 20/40), and at 6 weeks (F; 20/40) after intravitreal bevacizumab.

stability or improvement was reported in 95% of cases, and visual improvement of three or more lines in 40% of cases 12 months after treatment.[54,55] However, in most parts of the world, both pegaptanib sodium and ranibizumab are not readily available, or are too expensive. A human recombinant monoclonal immunoglobulin G (IgG) antibody that binds and inhibits all VEGF isoforms, bevacizumab is readily available. It has been approved by the United States Food and Drug Administration as an adjuvant agent in the treatment of metastatic colorectal carcinoma. Several studies have shown its efficacy in the treatment of CNV.[56,57]

Gene Therapy

Animal studies have shown the feasibility of transducing choroidal endothelial cells with vectors coding for antiangiogenic molecules and then transplanting these cells into eyes with CNV. A phase 1 trial where patients receive an intravitreal injection of an adenoviral gene transfer vector encoding the complementary DNA (cDNA) of the human *PEDF* gene has been initiated.[58]

Submacular Surgery

In 1991, Thomas and Kaplan[59] described their surgical technique that allowed extraction of CNV through a small retinotomy. The goal is to remove CNV but to leave the underlying RPE and choriocapillaris intact. A large prospective clinical trial has shown that submacular surgery in eyes with CNV secondary to AMD generally do not have a good visual outcome.[60]

Macular Translocation

Given that in AMD, the subfoveal CNV damages the RPE and Bruch's membrane, some investigators proposed moving the

fovea to a new location where the RPE and Bruch's membrane was healthy. This surgery is technically feasible but there is a steep learning curve.[61]

Retinal Angiomatous Proliferation

Oeller in 1904 described an anastomosis between the retinal and choroidal circulations in an eye with an end-stage disciform scar secondary to AMD.[62] In 1988, Caskey and Folk[63] described intraretinal neovascularization as the culprit in the recurrence of CNV following laser photocoagulation. Since the 1990s several authors have described chorioretinal anastomosis in eyes with S-PED and AMD.[64]

Pathogenesis

Retinal angiomatous proliferation is a poorly understood condition. It is currently unclear as to what is the source of the neovascularization. Two different hypotheses have been proposed. Gass and coworkers[62] have proposed that occult CNV gives rise to a chorioretinal anastomosis. In contrast, Yannuzzi and colleagues[64] have suggested that the RAP lesion grows spontaneously within the retina toward the choroid and the retinal surface. They have referred to this initial stage as intraretinal neovascularization. Their stage 2 describes retinal–retinal anastomosis with formation of a subretinal neovascular net and S-PED formation. When stage 3 is diagnosed, CNV has formed. Interestingly, OCT has shown RAP lesions without any communication with the choroidal circulation, giving credence to Yannuzzi's hypothesis.[65]

Clinical Findings

Superficial retinal hemorrhages in eyes with drusen is an early sign of occult CNV and RAP (Fig. 4.16A).[62] Intraretinal hemorrhages or PEDs adjacent to dilated and tortuous telangiectatic retinal vessels that dive toward the RPE strongly suggest the presence of RAP.[64] The presence of macular edema is also suggestive of a RAP lesion.[64] Once an eye is diagnosed with RAP, the fellow eye is at high risk of also developing RAP.

Fluorescein Angiography

On occasion, FA can delineate an intraretinal lesion that is connected to the retinal circulation. In these cases there is early capillary perfusion and intense late staining. However, for the most part one sees angiographic findings characteristic of occult CNV.[62,64] Pinpoint hyperfluorescence, staining, and blockage from the retinal hemorrhages are present (Fig. 4.16B,C). When associated with a PED, these angiomatous lesions appeared in the center of the PED. The angiomatous lesion hyperfluoresces as it fills from the retinal circulation, and at late phases there was indistinct staining or leakage

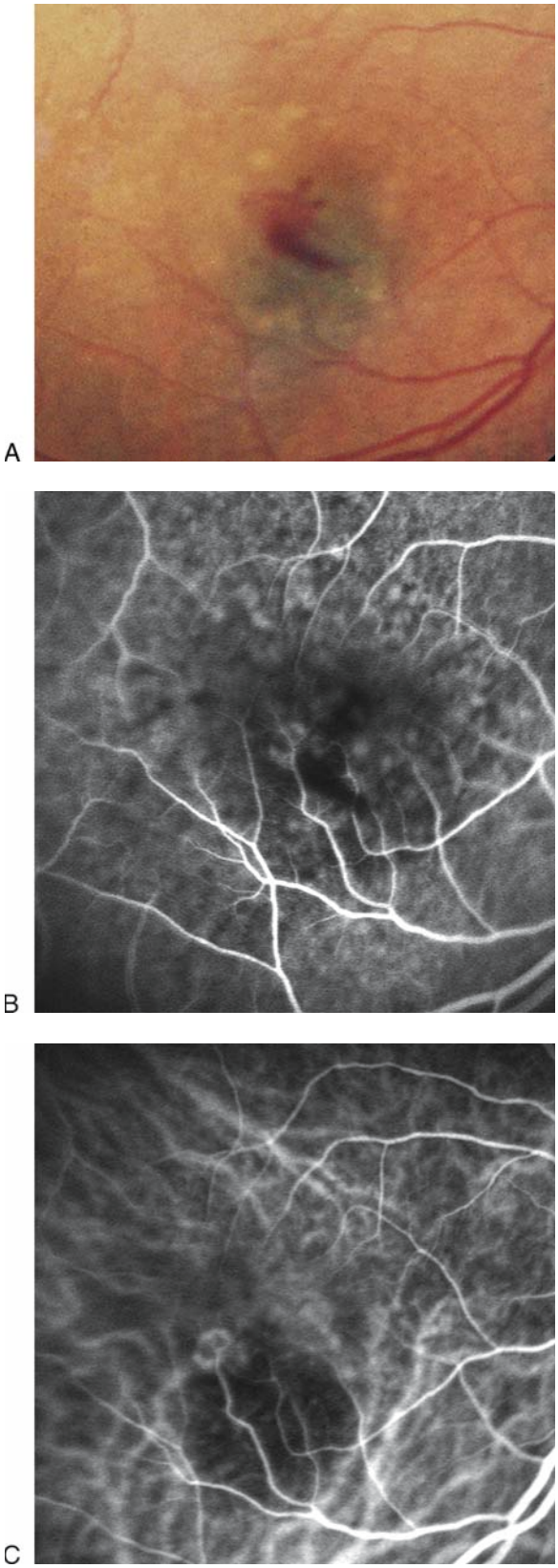

Fig. 4.16. Retinal angiomatous proliferation (RAP). (A) Clinical photograph shows an intraretinal hemorrhage and some drusen. (B) Early fluorescein angiogram frame shows pinpoint hyperfluorescence corresponding to the drusen. (C) Frame from high-speed indocyanine green angiography clearly shows a tuft of intraretinal neovascularization.

suggestive of occult CNV. The PED itself fills slowly and there is incomplete staining of the sub-RPE fluid.

Therefore, an S-PED that is associated with occult CNV with a hot spot near the retinal surface without an area of pigment epithelial atrophy is a RAP lesion until proven otherwise.[62,64]

Indocyanine Green Angiography Findings

Dynamic ICGA is the imaging method of choice (Fig. 4.16C). It clearly demonstrates the filling, emptying, and direction of flow of these angiomatous lesions.[66] With static ICG, abnormal late staining in the middle to late phases measuring less than one disc area in size are seen (hot spots). The retinal vessels can often be seen entering these hot spots.[62,67]

Optical Coherence Tomography

The intraretinal vascular complexes are imaged as focal hyperreflective areas in the neuroretinal layers that are close to the inner surface of the RPE. Very often, adjacent to these layers one finds areas of very low or no reflectivity, signifying intraretinal edema.[65]

Treatment

It has recently been suggested that treatment should be tailored according to the stage of the disease (L. Yannuzzi, personal communication). Focal photocoagulation appears to have good results in the early Yannuzzi stage 1 disease. Once Yannuzzi stage 2 disease is diagnosed, therapy with a pharmacologic agent such as intravitreal triamcinolone, anecortave acetate, or anti-VEGF therapy, in combination with either PDT or focal laser photocoagulation, is recommended. Laser photocoagulation, PDT, or TTT is usually unsuccessful in eradicating this condition if performed in the later stages of the disease.[62,68,69] Surgical ablation has been described in a small case series.[70]

Idiopathic Polypoidal Choroidal Vasculopathy

In the mid-1980s, a hemorrhagic maculopathy secondary to multiple recurrent serosanguineous RPE detachments was described in black women. The etiology was poorly understood, so it was called the posterior uveal bleeding syndrome or the syndrome of multiple recurrent serosanguineous detachments of the RPE. Yannuzzi's group[71] coined the term IPCV after the clinical findings that they reported.

Clinical Findings

Even though IPCV is seen across all ethnic groups, Asians and African Americans appear to be at a higher risk of developing IPCV.[71]

Idiopathic polypoidal choroidal vasculopathy is a disorder that affects primarily the choroidal vasculature. The characteristic lesion is an inner choroidal vascular network that ends as aneurysmal dilatations that is clinically seen as a reddish orange subretinal nodule. These nodular lesions were initially thought to occur more often in the peripapillary area, but more recently they have also been detected in the central macula or midperiphery (Fig. 4.17). These lesions may leak and bleed, causing multiple recurrent serosanguineous detachments of the RPE. Despite the subretinal bleeding, few eyes end up with a disciform scar. Most of these eyes do not have any drusen in the macular area.[71]

Fluorescein Angiography

Very often the fluorescein angiogram shows angiographic patterns consistent with occult CNV. Only rarely does it reveal dilated vascular channels with smaller vascular interconnections. Occasionally, early mottled hyperfluorescence that persists into the late phases, corresponding to the orange subretinal polypoidal lesions, may also be seen (Fig. 4.17B,C).[71]

Indocyanine Green Angiography

Indocyanine green angiography is superior to fluorescein angiography in delineating the choroidal lesions of IPCV and remains the diagnostic procedure of choice. Typically, branching vascular networks in the inner choroid with polypoidal dilatations at the terminal ends will be seen. The hyperfluorescent polypoidal dilatations appear to be adjacent to the hypofluorescent serosanguineous pigment epithelial detachment.[71]

Optical Coherence Tomography

The orange red subretinal polypoidal lesions are imaged by OCT as anteriorly protruding structures that have been described as dome-shaped elevations of the highly reflective RPE band with little reflective space under it.[72–74] Often a low reflective fluid-filled space adjacent to these polypoidal lesions, indicating the presence of a serous neuroretinal detachment, is seen. A serous detachment of the RPE also presents as an anterior protrusion, but the anterior wall is thinner and its contents are less reflective. Choroidal shadowing is more marked under polypoidal lesions than serous RPE detachments.[71]

Treatment

Even though the condition may resolve spontaneously, treatment is recommended for symptomatic cases. However, the best treatment modality is yet to be defined. Focal laser photocoagulation of feeder vessels identified by high-speed ICGA has been reported. Surgical drainage of thick submacular hemorrhage has been suggested. Photodynamic therapy with

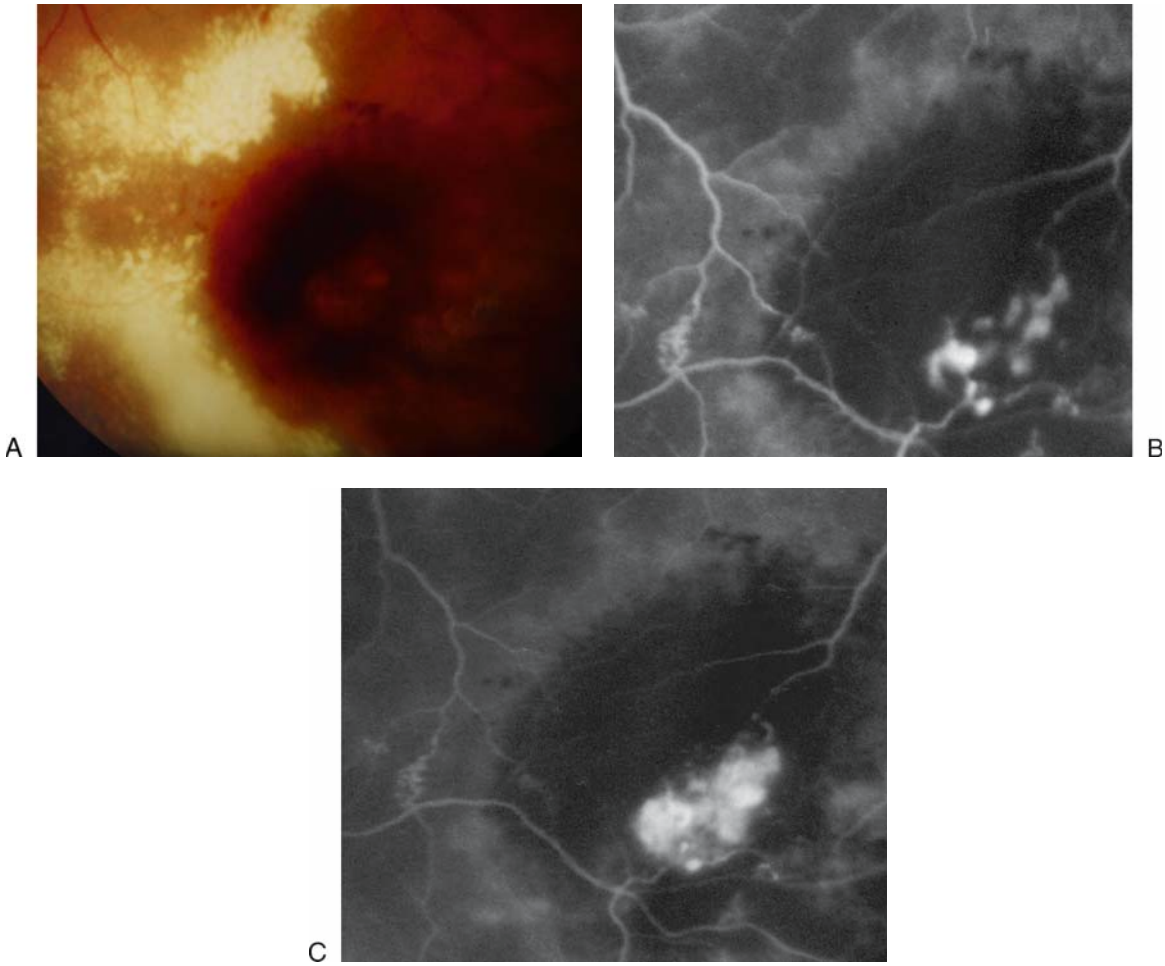

Fig. 4.17. A 75-year-old man was diagnosed with idiopathic polypoidal choroidal vasculopathy (IPCV). (A) Clinical photograph shows a hemorrhagic PED with extensive lipid exudation. (B) Mid-FA frame shows multiple lobular hyperfluorescent dilatations. (C) Late FA frame shows leakage from the aneurysmal dilatations.

verteporfin for exudative maculopathy secondary to IPCV has been reported to be beneficial.[71]

Myopia

Pathologic or degenerative myopia is a major cause of legal blindness in many developed countries. It is defined as an eye with a refractive error greater than −6.0 diopters or an axial length greater than 26 mm.[75] These eyes are characterized by an excessive and progressive elongation of the globe, which results in a variety of fundus changes with varying degrees of visual deterioration. The mechanisms that underlie these changes are poorly understood at this time.

Clinical Findings

The myopic optic disc is usually small and tilted. The nasal edge is elevated while the temporal side is flat. Progressive enlargement and thinning of the globe causes retraction of the juxtapapillary temporal RPE. This gives rise to a hypopigmented temporal crescent (Fig. 4.18). Many pathologic myopic eyes demonstrate a posterior staphyloma. This is an ectasia that involves the sclera, choroid, and RPE, especially in the posterior pole of the eye.

The choroid, choriocapillaris, and RPE may become markedly thinned and atrophied. The larger choroidal vessels may be seen through the transparent retina. This fundus appearance has been described as a tigroid or tessellated fundus. Bruch's membrane becomes calcified, which makes it brittle and thicker. Rapid loss of vision may be due to a rupture of Bruch's membrane and a consequent subretinal hemorrhage. These breaks in Bruch's membrane appear as single or multiple straight lines and are called lacquer cracks.[76]

Subretinal hemorrhages may be due to CNV or to lacquer cracks. When they are associated with lacquer cracks, reabsorption without visual sequelae is the norm. On average it takes 6 to 7 weeks for reabsorption to occur.[77] Choroidal

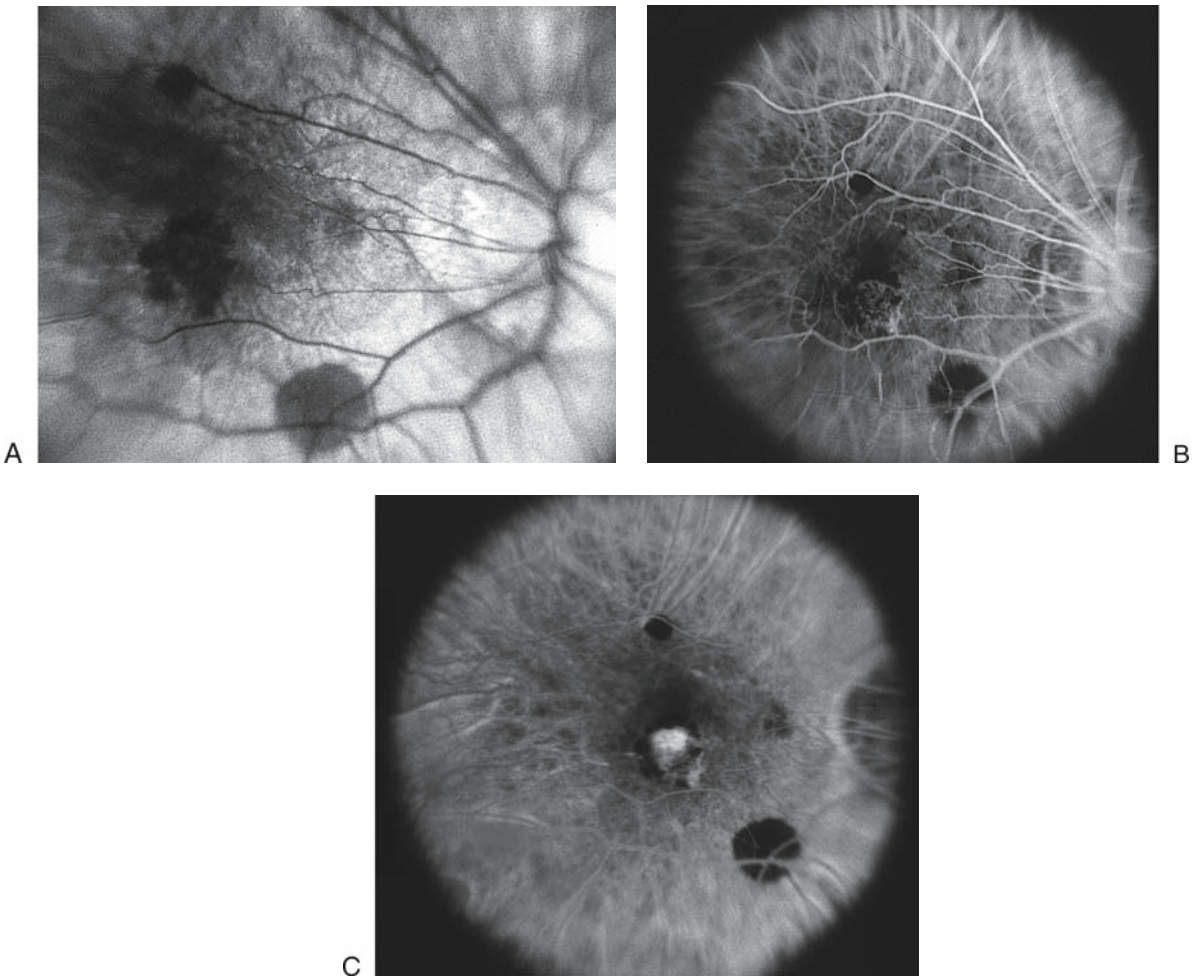

Fig. 4.18. A 31-year-old woman with high myopia developed metamorphopsia in her right eye 2 weeks prior to presentation. Her visual acuity was 20/50. (A) Red-free photo of her right eye shows a temporal crescent and a hemorrhage in the inferior central macula with adjacent pigment but without subretinal fluid. There are also deep hemorrhages along the proximal portions of the temporal arcades. (B) Early FA frame reveals well-defined CNV within the central macula. (C) Late FA frame reveals minimal leakage from the CNV.

neovascularization has been reported to occur in up to 10% of patients with high myopia.[78] Subretinal neovascularization is nearly always accompanied by metamorphopsia and a decrease in visual acuity (Fig. 4.18). The natural history of CNV in myopia is highly variable but generally poor. The CNV tends to regress, becoming flat while chorioretinal atrophy develops around it. In about 60% of the cases, the lesions lie in the juxtafoveolar area. The entire neovascular lesion may be surrounded by a pigmented ring.[79] Fuchs spots are the circular, pigmented, and slightly raised submacular lesions that represent involuting CNV.

Fluorescein Angiography

Atrophy of the choriocapillaries and the RPE produces pronounced hyperfluorescence with clear margins in the affected areas. There may be a few pigment clumps and an occasional branching choroidal vessel that may be crossed by a normal retinal vessel. In the late phase, the sclera stains slowly and progressively. The periphery of the atrophic zones is highlighted by a hyperfluorescent margin stemming from the adjacent choriocapillaris. An irregular hyperfluorescence outlines the course of the lacquer cracks, which stain slightly during the late phase but maintain their shape. There is no leakage of dye. The capillary network of the retina is always poorly visible. It is rather difficult to determine the location of the foveal avascular zone exactly, especially as the contrast of the xanthophyll pigment is not pronounced. Myopic CNV causes minimal hyperfluorescence and dye leakage (Fig. 4.18), which may be confused with the hyperfluorescence of a lacquer crack. There is early filling of the subretinal new-formed blood vessels during the arterial phase. This changes only a little during the intermediate phases of the angiogram. Only rarely is the vascular net within the lesion seen. In the late phases, the dye diffusion remains moderate. The diffusion becomes pronounced

at the surface extension of the lesion, which is small, but has blurred and irregular margins.

Indocyanine Green Angiography

Indocyanine green angiography enables imaging of the retrobulbar vessels, which are not noted in normal individuals. These vessels start to appear during the filling of the choroidal veins. Indocyanine green angiography demonstrates a widespread attenuation of the entire choroidal vasculature. The choroidal arteries are less numerous and are of a smaller caliber. The choroidal flush, which represents filling of the choriocapillaris, may be absent. Chorioretinal atrophy is seen as dark hypofluorescent patches in a uniform gray choroidal background. The CNV membranes fill during the choroidal phase. They can appear as hyperfluorescent lesions or lesions with a fluorescence similar to the background choroidal fluorescence but surrounded by a hypofluorescent rim. Indocyanine green angiography enables a more precise evaluation of lacquer cracks, which appear more numerous than the ones identified by FA. Lacquer cracks appear as dark hypofluorescent streaks and can be differentiated from the hyperfluorescent choroidal neovascular membranes.[80] More recently dynamic and sequential static ICGA have been used to identify feeder vessels of the CNV.[29,48,81]

Optical Coherence Tomography

Optical coherence tomography has been able to image myopic CNV at different stages. During active CNV a highly reflective dome-like elevation above the RPE is seen. Little or no subretinal fluid was detected. In the scar stage, a highly reflective surface with attenuation of the underlying tissue is seen. In the atrophic stage, no elevation was seen and the chorioretinal atrophy surrounding the regressed CNV was highly reflective.[82]

Treatment

Intravitreal anti-VEGF (bevacizumab) seems to be safe and efficacious in eyes with CNV secondary to pathologic myopia. Studies of laser and PDT for treatment of extrafoveal and juxtafoveal CNV secondary to myopic degeneration have been reported. However, these treatments have been not effective.[83]

Surgery

The options are CNVM removal, limited macular translocation, and macular translocation with 360-degree retinotomy.[84–86]

Presumed Ocular Histoplasmosis Syndrome

Presumed ocular histoplasmosis syndrome (POHS) is a distinct clinical entity believed to be secondary to exposure to *Histoplasma capsulatum*, although this fungus rarely has been isolated or cultured from an eye with the typically associated clinical findings.[87]

Pathophysiology

The initial infection occurs when spores of *H. capsulatum* are inhaled. Patients are usually asymptomatic or develop influenza-like symptoms. Hematogenous spread to the eye may occur. A focal granulomatous choroiditis, characterized as discrete, round, yellowish choroidal lesions, develops. With time, the lesions resolve, leaving the typical "punched-out" atrophic scars that disrupt Bruch's membrane. Reexposure to the histoplasmin antigen may account for the enlargement of old scars, the emergence of new scars, and the development of CNV.[88]

Clinical Findings

Presumed ocular histoplasmosis syndrome is characterized by peripheral atrophic chorioretinal scars, peripapillary scarring, maculopathy, and the absence of intraocular inflammation.[88] Visual loss in POHS is secondary to the development of CNV in the macular area (Fig. 4.19).

According to the MPS, a 2% per year risk of developing CNV in the fellow eye exists.[89] The risk depends on whether the fellow eye has peripapillary scarring (4% risk) or a macular atrophic spot (20% to 24% risk).[89]

Treatment

Laser Photocoagulation

The MPS demonstrated that laser photocoagulation is indicated in the treatment of extrafoveal and juxtafoveal CNV secondary to POHS (Fig. 4.20). The MPS has also recommended laser treatment of peripapillary CNV.[90] After 5 years of follow-up, the MPS reported that 26% and 33% of patients had recurrent or persistent CNV following laser photocoagulation to extrafoveal or juxtafoveal CNV, respectively.[40,91] In most cases, photocoagulation of recurrent CNV is indicated.[40,91]

Photodynamic Therapy

A small uncontrolled series has reported on the benefits of PDT with verteporfin.[92]

Corticosteroids

Even though scientific evidence is lacking, corticosteroids have been used in cases where subfoveal CNV is present.[93,94]

Submacular Surgery

Group H of the Submacular Surgery Trials evaluated the effect of surgical extraction of the CNV in eyes with POHS compared to observation. In general, there was no benefit to surgical intervention

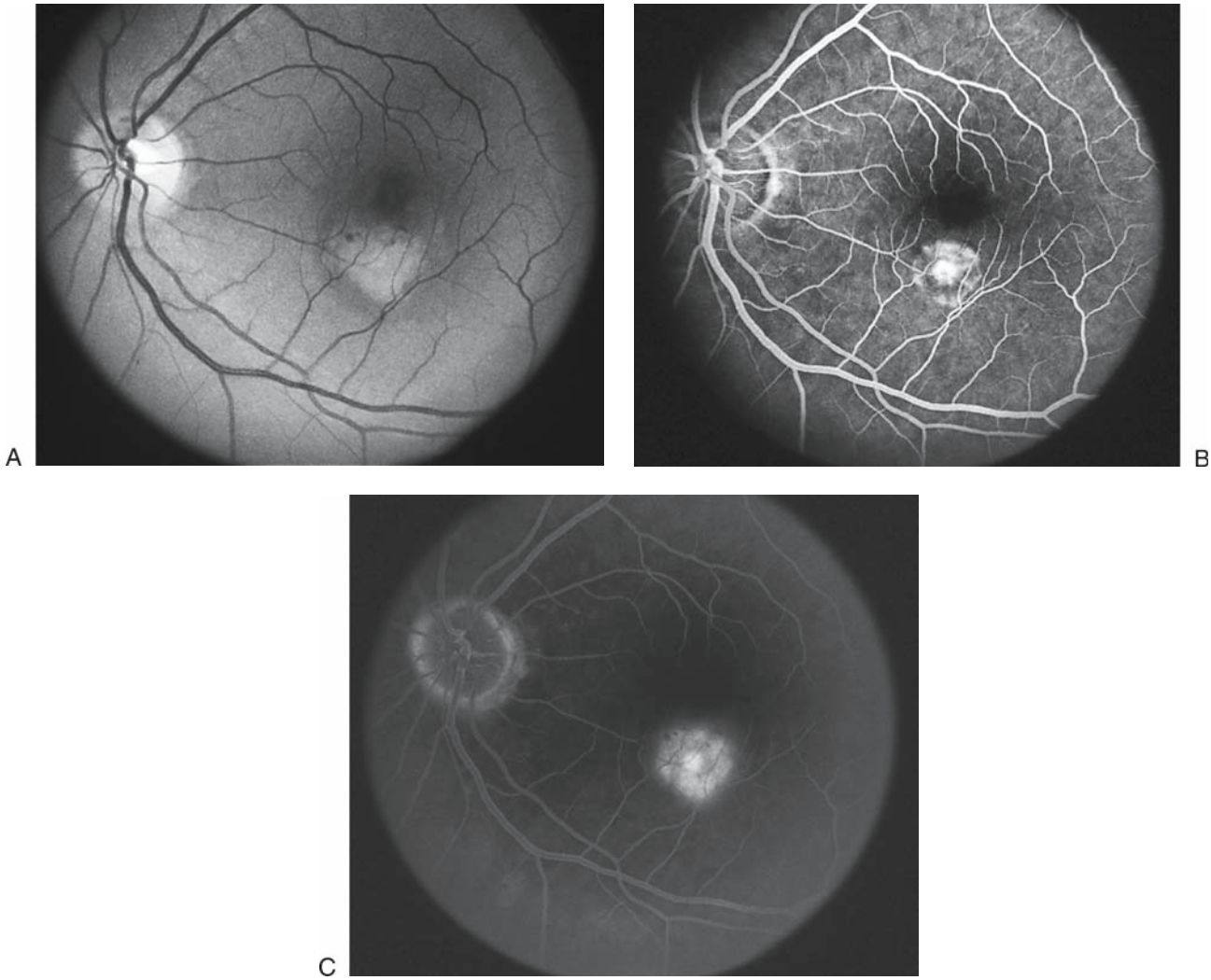

Fig. 4.19. A 35-year-old woman presented with a sudden decrease in vision in her left eye. The visual acuity was 20/60. (A) Red-free photo demonstrating detachment of the neurosensory retina along the inferior border of the fovea. (B) Early FA frame demonstrating a well-defined extrafoveal CNV. (C) Late FA frame shows leakage from the extrafoveal CNV.

unless a visual acuity of 20/100 or worse was found preoperatively. Recurrence of CNV following excision is observed in up to 44% of cases.[95]

Idiopathic Choroidal Neovascularization

Choroidal neovascularization is a major cause of visual loss. This disorder describes the growth of new blood vessels that originate from the choroid through a break in Bruch's membrane into the subretinal pigment epithelium (sub-RPE) or subretinal space. The mechanisms that regulate CNV formation are poorly understood. Virtually any pathologic process that involves the RPE and damages Bruch's membrane may lead to CNV. Idiopathic CNV is a diagnosis of exclusion, and all other ocular diseases associated with CNV formation must have been excluded before the diagnosis of idiopathic CNV can be entertained.[96]

Clinical Findings

Idiopathic CNV usually occurs in young people. As in other types of CNV, patients complain of blurred vision, metamorphopsia, or a scotoma. Clinically idiopathic CNV is characterized by subretinal fluid, lipid exudation, or subretinal hemorrhage. The CNV in idiopathic cases typically grows into the subretinal space. The natural history of idiopathic CNV appears to be much better than that in AMD. In fact many cases of idiopathic CNV involute spontaneously.[97]

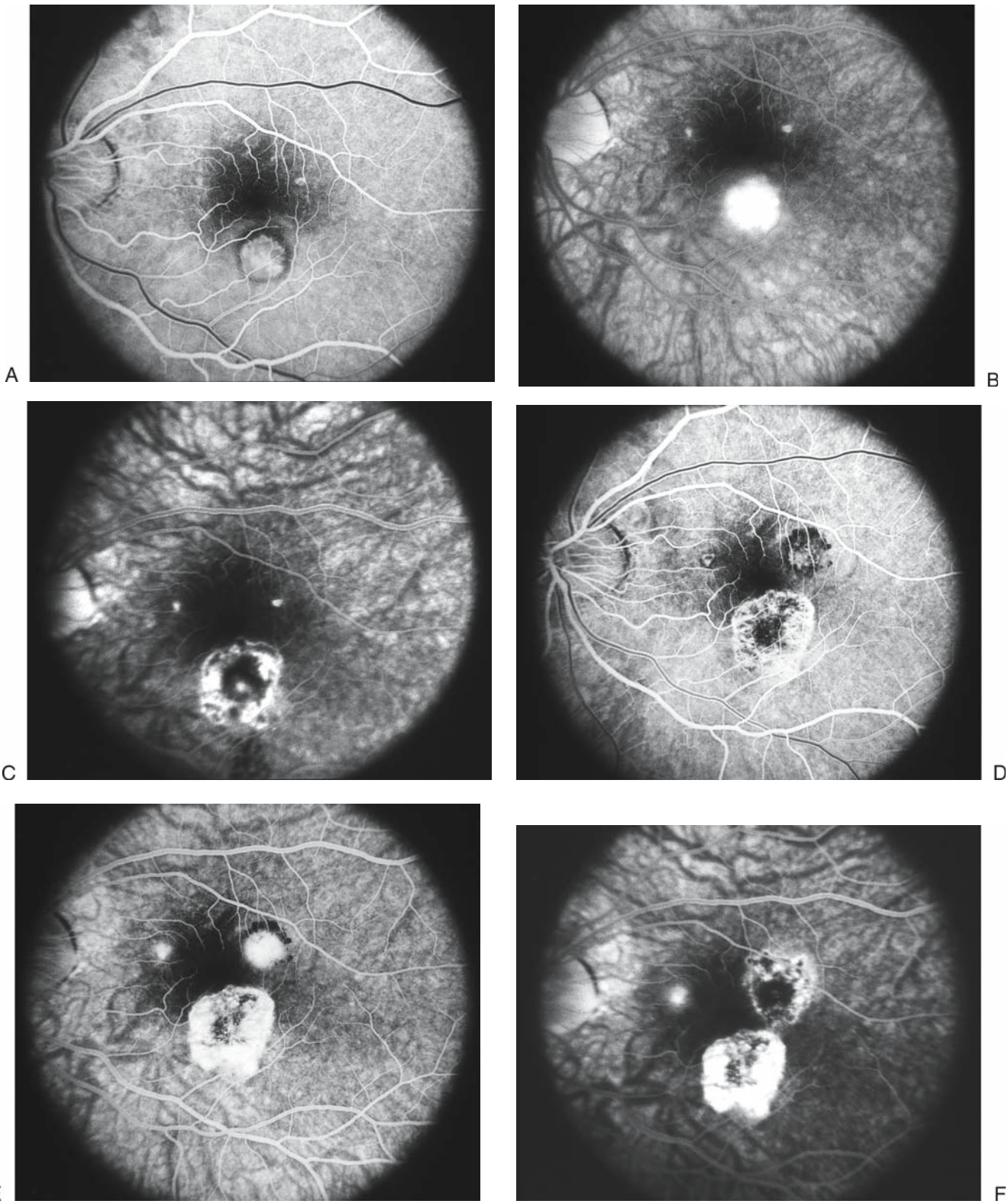

FIG. 4.20. A 42-year-old woman noticed distortion superior to fixation in her left eye on July 22, 1992. On examination her visual acuity in her left eye was 20/40. She was diagnosed with extrafoveal CNV secondary to presumed ocular histoplasmosis syndrome (POHS). (A) Early FA frame shows a well-defined area of early hyperfluorescence. (B) Late FA frame shows leakage from the lesion. Notice two small areas of hyperfluorescence nasal and temporal to the fovea consistent with atrophic histoplasmosis spots. (C) Late FA frame on July 29, 1992, after krypton laser photocoagulation shows staining of the scar but without any evidence of leakage. The two small areas of late hyperfluorescence are still present. (D) On December 9, 1992, the patient complained of new distortion below fixation in her left eye. Early FA frame on December 9, 1992, shows early hyperfluorescence superotemporal to the fovea. (E) Late FA frame on December 9, 1992, shows leakage from the well-defined extrafoveal CNV. There is some blocked fluorescence from the hemorrhage. There is some questionable late leakage from the atrophic histoplasmosis spot nasal to the fovea. (F) Late FA frame on December 21, 1992, shows staining of the two chorioretinal scars but no leakage. The histoplasmosis spot nasal to the fovea is suspicious for CNV. (G) Late FA frame on December 29, 1992, shows definite leakage consistent with CNV from the histoplasmosis spot nasal to the fovea.

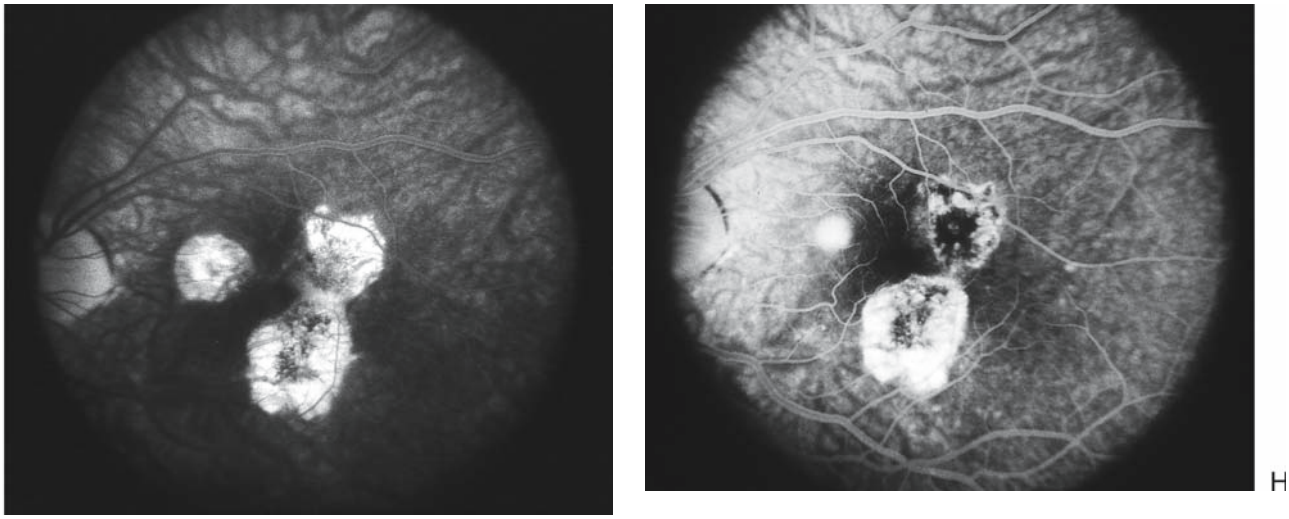

FIG. 4.20. (continued) (H) Late FA frame on March 3, 1993, shows one discrete chorioretinal scar nasal to the fovea secondary to krypton laser photocoagulation with no evidence of recurrence. The two other chorioretinal scars appear to have expanded toward each other. The visual acuity at this point was 3/200.

Fluorescein Angiography

As in other types of CNV, idiopathic CNV is characterized by lacy hyperfluorescence in the early phases with late leakage.

Indocyanine Green Angiography

Several authors have reported the presence of a hypofluorescent rim that surrounds the hyperfluorescent CNV. They suggest that this hypofluorescent rim is caused by reactive RPE cells that block the underlying ICG fluorescence. Thus the rim is more prominent in regressing and involuting CNV. Some investigators have used ICGA to identify the ingrowth site of CNV.[98]

Optical Coherence Tomography

Typically, active CNV causes a disruption in the highly reflective RPE choriocapillaris layer. It gives rise to a highly reflective multilayered nodular structure in the subretinal space. As the CNV undergoes regression, a layer of highly reflective RPE cells surrounds the CNV. This is seen as a dome-shaped highly reflective layer that corresponds to the RPE covering a moderately high reflective area that corresponds to CNV.[99]

Treatment

Laser Photocoagulation

The MPS reported that at 5 years following laser photocoagulation of extrafoveal idiopathic CNV, the relative risk of losing six or more lines was 2.3 when comparing untreated versus laser-treated eyes. Recurrent CNV was seen in 34% of eyes. In general, the results of laser photocoagulation for idiopathic CNV fall in between those seen with AMD and POHS.[38,40]

Photodynamic Therapy

Small case series have suggested a visual benefit of PDT with verteporfin for idiopathic CNV.[100]

Submacular Surgery

The Submacular Surgery Trials recently reported the lack of benefit of surgery in eyes with subfoveal idiopathic CNV unless the baseline visual acuity was worse than 20/100. Choroidal neovascularization recurrence was seen in 35% of operated eyes compared to 49% of observed eyes. However, 4% of operated eyes developed a retinal detachment.[95]

Choroidal Rupture

Blunt ocular trauma is the most common type of eye injury. Approximately 5% to 10% of these patients develop choroidal ruptures, which are breaks in the choroid, Bruch's membrane, and RPE. They may be secondary to indirect or direct trauma. These direct ruptures tend to be located more anteriorly at the site of impact and parallel to the ora, whereas those secondary to indirect trauma occur posteriorly. Indirect choroidal ruptures are almost four times as common as direct ruptures.[101] Eyes with angioid streaks appear to be more vulnerable and develop choroidal ruptures with any minor trauma.

Pathophysiology

Following blunt trauma, the ocular globe undergoes mechanical compression and then sudden hyperextension. Because of its tensile strength, the sclera can resist this insult; the retina also is protected because of its elasticity. Bruch's membrane

does not have enough elasticity or tensile strength, so it breaks.[101] Hemorrhage in conjunction with retinal edema may obscure the choroidal rupture during the acute phases. During the healing phase, choroidal CNV occurs.[101]

Clinical Findings

In the acute stage, patients complain of a paracentral or central scotoma and decreased vision. Retinal edema often accompanies choroidal ruptures. A hemorrhagic or serous detachment of the macula may also be seen.[102] If subretinal hemorrhage is present, it may obscure the ophthalmoscopic diagnosis of the choroidal rupture. Once the hemorrhage clears, the typical white curvilinear crescent-shaped streak concentric to the optic nerve may be seen (Fig. 4.21). If the rupture does not involve the fovea, good vision is expected. Vision loss also depends on the location and presence of CNV. The length of the rupture and distance of the rupture to the center of the fovea may be risk factors for the development of CNV. Regularly scheduled examinations with fluorescein angiograms, as circumstances dictate, are recommended during the first year since most CNV develops in this time frame. Nevertheless, CNV has also been reported to occur decades later.[102]

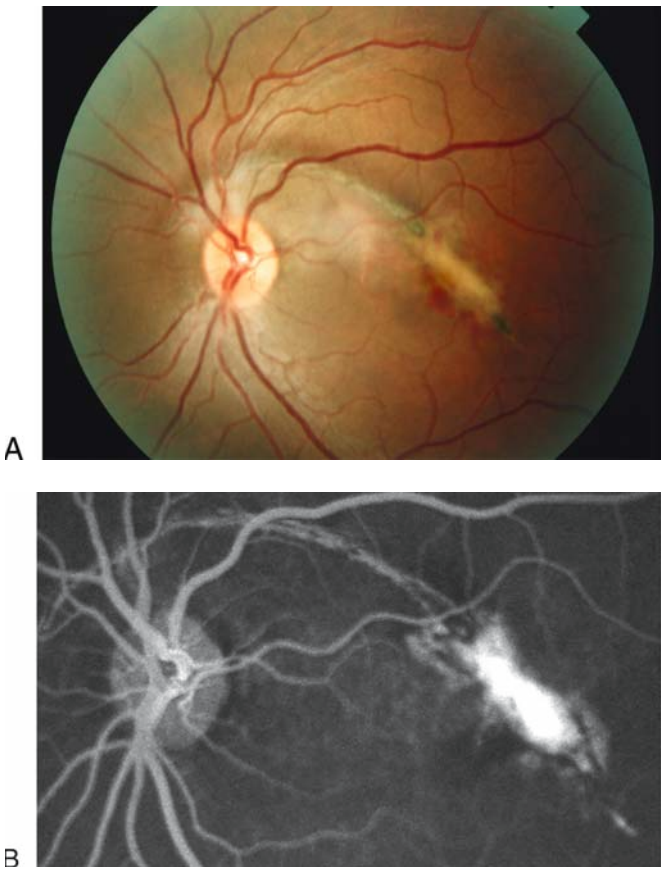

Fig. 4.21. A 23-year-old woman was struck in her left eye with a cigarette lighter. She was diagnosed with a choroidal rupture. (A) Clinical photograph shows the typical white curvilinear crescent-shaped streak concentric to the optic nerve. There is also some residual submacular hemorrhage. (B) Late FA frame shows staining of the macular scar.

Fluorescein and Indocyanine Green Angiography

Early fluorescein hypofluorescence due to disruption of the choriocapillaris is seen. During the later stages, hyperfluorescence occurs as fluorescence from the adjacent healthy choriocapillaris stains the tissue (Fig. 4.21). The choroidal rupture is depicted as a hyperfluorescent crescent-shaped lesion concentric to the optic nerve. If CNV is present, early hyperfluorescence followed by late leakage is present in the angiogram. If hemorrhages are associated, they may cause blockage of the fluorescein fluorescence. Indocyanine green angiography may be useful if subretinal blood blocks or hides CNV detection by a fluorescein angiogram.

Treatment

Conservative treatment is recommended for most choroidal ruptures. During the healing phase of virtually all choroidal ruptures, CNV is present. However, most CNV involutes spontaneously. In 15% to 30% of patients, CNV may recur and lead to a hemorrhagic or serous macular detachment with concomitant visual loss. If CNV is extrafoveal, it may be treated successfully with laser photocoagulation.[102] If CNV is subfoveal or juxtafoveal, pars plana vitrectomy with membrane extraction should be considered.[103] Photodynamic therapy with verteporfin has also been reported to be useful.[104]

Chorioretinal Folds

Chorioretinal folds were first described in 1884 by Nettleship[105] in a patient with papilledema secondary to a space-occupying lesion. Since then, it has been recognized that any condition that shrinks or thickens the sclera reduces the inner scleral surface, resulting in chorioretinal folds.[106,107] The most common ocular conditions associated with chorioretinal folds include hypermetropia, macular disciform scars, uveitis, choroidal nevi, choroidal tumors, papilledema, and posterior scleritis.[106,108,109] Chorioretinal folds can also occur postoperatively from alterations such as hypotony,[107] choroidal edema and hematomas,[110] or scleral buckles,[106,111] or iatrogenically from the use of the diode endolaser.[112] Orbital causes include orbital tumors, pseudotumor cerebri, chronic sinusitis, and Graves orbitopathy.[106,107] However, choroidal folds are most commonly idiopathic in nature.

Clinical Findings

If the chorioretinal folds are acutely acquired, patients usually complain of distortion. The folds appear as alternating bright

peaks and dark troughs or valleys predominantly involving the posterior pole (Fig. 4.22). The folds are approximately parallel and tend to vary in length and width, rarely extending beyond the equator. The folds usually broaden with time, becoming smoother and whiter in appearance.[107]

Fluorescein Angiography

The peaks or the crests of the folds represent areas where the overlying RPE is stretched thinner. In contrast, the RPE in the troughs is compressed.[113] During the early filling phase, the peaks hyperfluoresce because the stretched and thinned RPE allows better transmission of the background choroidal fluorescence whereas the troughs remain dark secondary to blockage of the background choroidal fluorescence (Fig. 4.22B). The contrast becomes more marked during the subsequent arterial and venous phases and creates a striking picture of alternating bright and dark lines. There is no leakage of fluorescein.[107,111] Often more folds are demonstrated with FA than with ophthalmoscopy. Chorioretinal folds do not remain visible longer than the retinal and choroidal vessels.

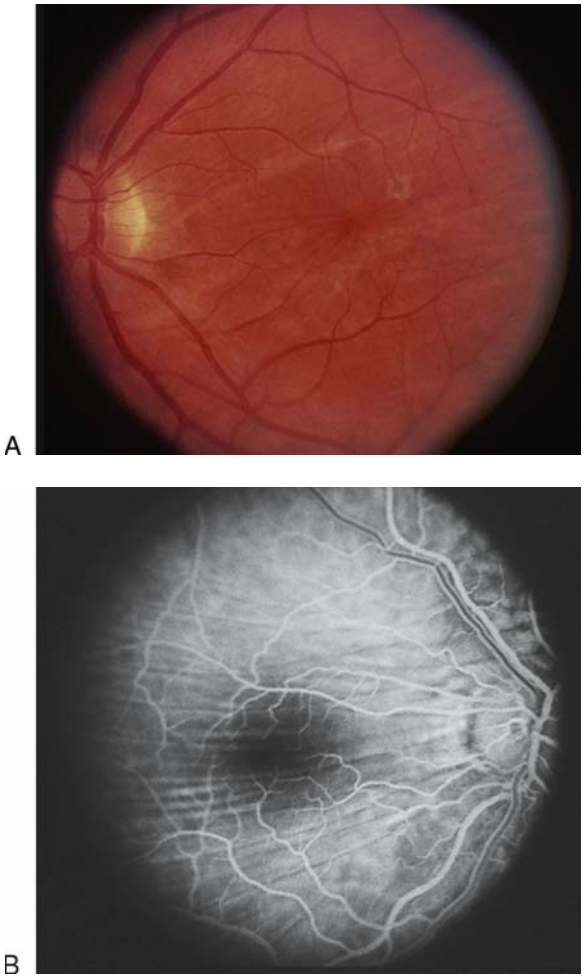

Fig. 4.22. Chorioretinal folds. (A) Clinical photograph shows chorioretinal folds as alternating bright peaks and dark troughs. (B) Fluorescein angiography on another patient highlights the crests and folds of the chorioretinal folds. The peaks hyperfluoresce because the stretched and thinned RPE allows better transmission of the background choroidal fluorescence, whereas the troughs remain dark secondary to blockage of the background choroidal fluorescence.

Indocyanine Green Angiography

Indocyanine green angiography demonstrates two different patterns that are thought to arise from the differences in depth of the troughs of the chorioretinal folds and the ability of the incident light of the fluorescein angiogram versus the indocyanine green angiogram to illuminate these areas. The first is characterized by ICG hyperfluorescent lines that are less numerous and wider than those seen in FA. The second pattern consists of the same number of lines but wider ICG hyperfluorescent lines compared to FA.

Treatment

Although chorioretinal folds are usually idiopathic, this is a diagnosis of exclusion and can be made only after a complete ocular and systemic evaluation. Management should be tailored toward treating the underlying cause.

Central Serous Chorioretinopathy

Central serous chorioretinopathy was first described by von Graefe in 1866 as a recurrent serous macular detachment and was called “idiopathic detachment of the macula.” In 1955 the term *central serous retinopathy* was applied by Bennett. In 1959, Maumenee, using fluorescein angioscopy, correctly identified a leaking site at the RPE as responsible for the macular detachment. In 1967 Gass provided the clinical and angiographic features of the condition.[114] Because the disease appears to involve both the choroid and the retina, the terminology more frequently used today is central serous chorioretinopathy (CSCR).

Pathogenesis

Central serous chorioretinopathy remains a poorly understood entity. Some authors believe that the RPE is dysfunctional.[114] According to this theory, for an unknown reason, some RPE cells start to pump ions into the subretinal space. Fluid follows this ionic gradient and leads to the accumulation of fluid in the sub-RPE and subretinal spaces. The findings of ICGA have given rise to a choroidal dysfunction theory.[115,116] According to this theory hyperpermeability of the choroidal vasculature is responsible for CSCR. This hyperpermeability causes an increased fluid leakage, which leads to serous detachment of the RPE. The accumulating fluid increases the hydrostatic pressure, which leads to fluid seeping into the subretinal space.

Clinical Findings

Central serous chorioretinopathy typically affects young and middle-aged males with type A personality who have had a preceding stressful event.[114] Additional risk factors include pregnancy,[114] use of corticosteroids,[117] and hypertension.[114] Patients complain of metamorphopsia, a positive scotoma, and micropsia. Visual acuity is often only moderately decreased and may be improved with the addition of a small hyperopic correction. The patient may be asymptomatic.

Acutely, serous fluid may accumulate in the subretinal space, in the sub-RPE space, or in both spaces at the posterior pole, causing a circumscribed round-to-oval area of macular detachment that varies from a small elevation at the fovea to a large detachment that may appear bullous (Fig. 4.23). One or more discrete round-to-oval, well-demarcated areas of detached RPE may be observed. A grayish white lesion may be seen at the site of leakage. This lesion seems to be a fibrinous exudate that accumulates in the subretinal space. In most cases CSCR resolves within a few months, and visual acuity returns to 20/25 or better. However, complaints of metamorphopsia, micropsia, color vision changes, or darkening of the central visual field and small pigment epithelial alterations often remain. Anywhere from 30% to 50% of patients have one or more recurrences.[114]

Approximately 5% of patients may have a poor visual outcome, usually caused by the chronic form of the disease. The chronic form of the disease is characterized by persistent subretinal fluid lasting more than 6 months. The RPE becomes atrophic and decompensates. These atrophic RPE areas are characterized by multiple teardrop, flask-shaped, and long-necked tracts that extend inferiorly from the macular area past the equator (Fig. 4.24). In addition, the retina may develop secondary changes such as pigment migration, cystoid macular edema, CNV, subretinal lipid deposition, choriocapillaris atrophy, capillary nonperfusion, and capillary dilation.

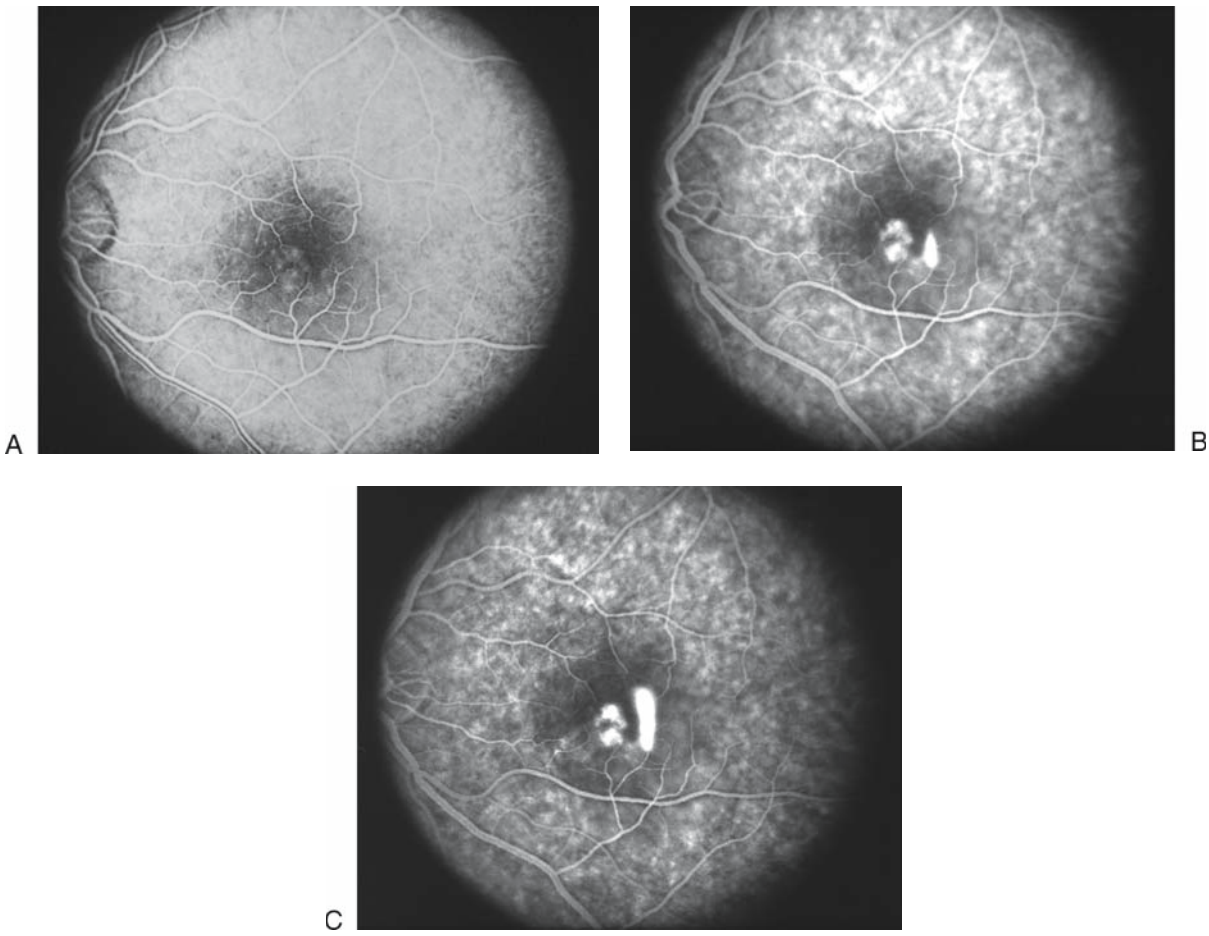

Fig. 4.23. Central serous chorioretinopathy. (A) Early FA frame shows pinpoint hyperfluorescent lesions in the foveal region. (B) Mid-FA frame shows some coalescence of the pinpoint lesions and the vertical rise of the dye. (C) Late FA frame shows a couple of ink blot lesions with a smokestack rising vertically.

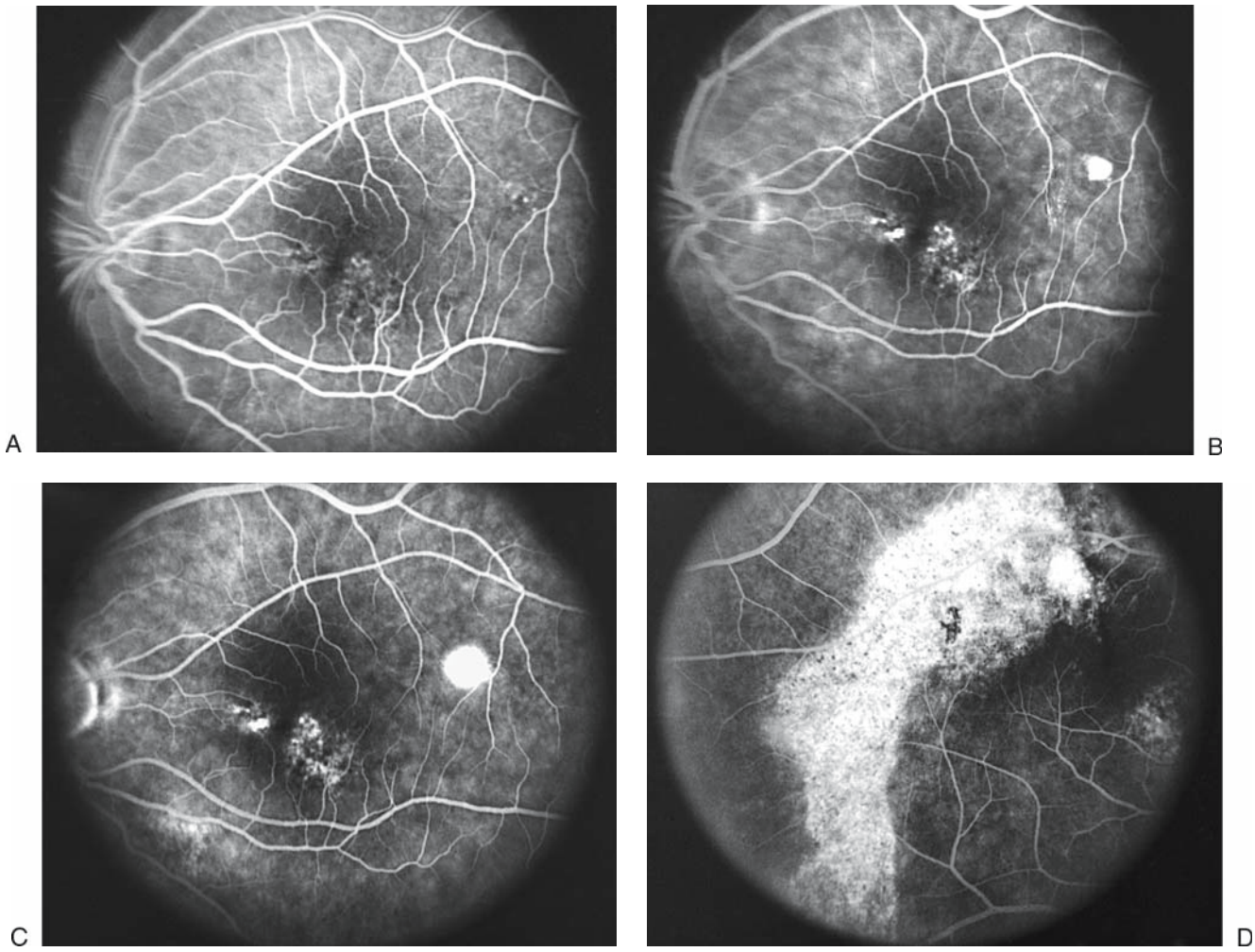

Fig. 4.24. Central serous chorioretinopathy. (A) Early FA frame shows some hyperfluorescence in the inferior parafoveal area. (B) Mid-FA frame shows leakage site as an inkblot in the superotemporal quadrant. The hyperfluorescent points in the inferior parafoveal location remain the same. (C) Late phase of the FA shows more intense hyperfluorescence in the superotemporal location. (D) Late FA frame shows a long-necked track extending inferiorly.

Fluorescein Angiography

Acutely one or several sites of leakage are seen at the level of the RPE. In 10% of cases, a smokestack leak is seen (Fig. 4.23).[118] This is characterized by the appearance of a small hyperfluorescent spot during the early phases of the study. During the late phases the dye passes into the subretinal space and ascends vertically from the point of leakage until it reaches the upper border of the detachment. The dye then spreads laterally until the entire area of detachment is filled. More commonly, the leakage site is seen as an inkblot that increases in size as the study progresses (Fig. 4.23).[117] Window defects in areas uninvolved by subretinal fluid may also be seen.

Indocyanine Green Angiography

Indocyanine green angiography reveals multifocal areas of choroidal hyperpermeability in the early and middle phases of the study (Fig. 4.25). Late phases show silhouetting of the larger choroidal vessels.[116,119] The areas of choroidal hyperpermeability do not always correlate with active leaks detected by FA. In addition, clinically and fluorescein angiographically silent serous pigment epithelial detachments may be detected. These are imaged as round lesions that hyperfluoresce early and hypofluoresce late surrounded by a rim of hyperfluorescence.

Optical Coherence Tomography

Optical coherence tomography images the neurosensory detachment as an area of hyporeflectivity between the neurosensory retina and the highly reflective RPE and choriocapillaris band (Fig. 4.26). This hyporeflectivity is caused by the attenuation of the subretinal fluid. The height of the detachment can be measured in an accurate manner. A pigment epithelial detachment is seen as a focal elevation of this reflective band with underlying hyporeflectivity. Optical coherence

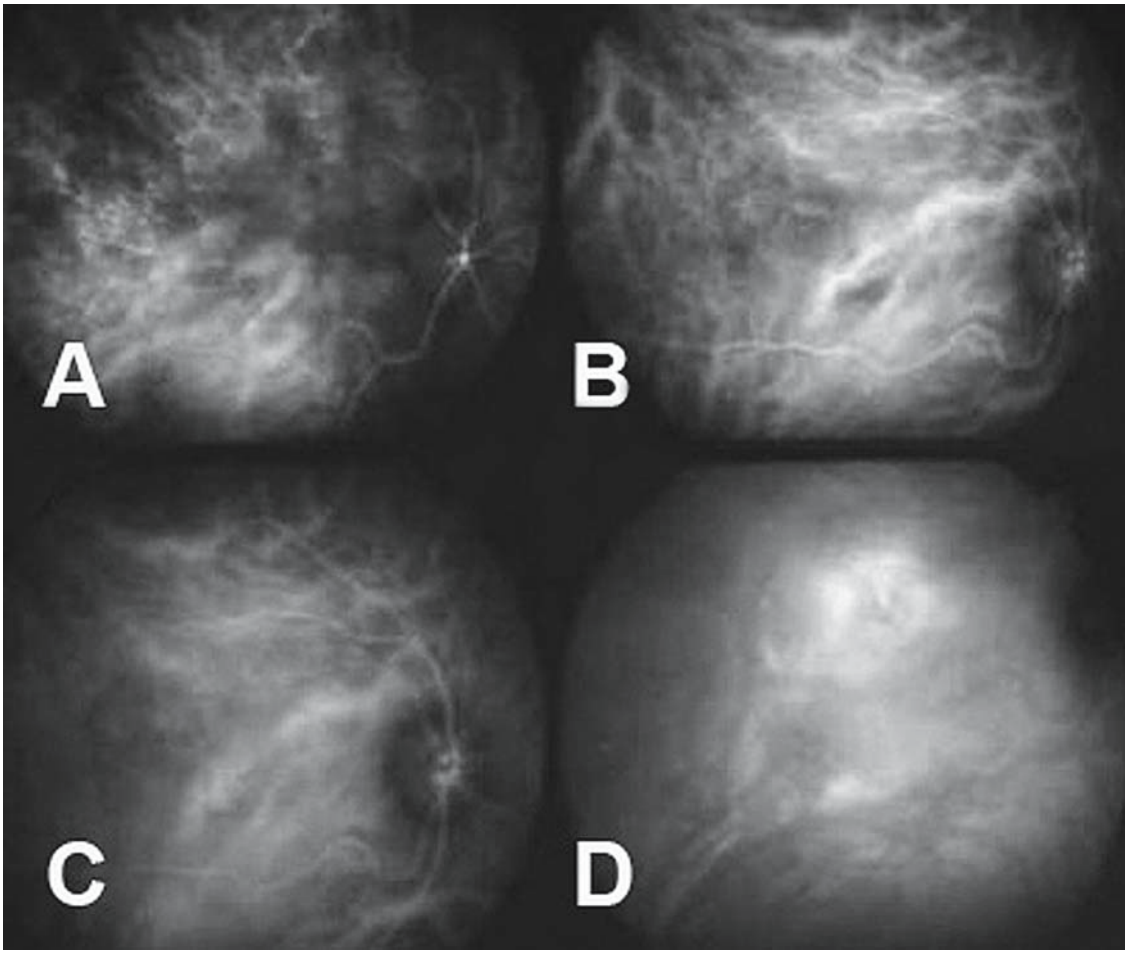

FIG. 4.25. Central serous chorioretinopathy (CSCR) in the right eye. (A) Indocyanine green angiography is essentially normal in the early phase. (B,C) Midphase reveals multiple patchy areas of hyperfluorescence. (D) Late phase reveals the typical hyperpermeability seen in CSCR.

tomography is also able to detect detachments that were not clinically evident.

Treatment

Medical treatment has not been shown to shorten the course of the macular detachment or lead to a better long-term prognosis. Treatment of the psychogenic components of the disorder has been advocated but not proven to be beneficial. Beta-blockers and acetazolamide have not been shown to be beneficial. Patients using corticosteroids are encouraged to discontinue them.[117]

The use of laser photocoagulation has been controversial.[120,121] However, since the overall visual prognosis is good without therapy, and there is a potential risk for iatrogenic CNV, photocoagulation is recommended only in special circumstances. These special cases include patients with occupational needs for binocular vision, persistent serous fluid for more than 6 months, and eyes with chronic pigment epithelial changes.

Chronic CSCR characterized by a decompensated RPE remains a therapeutic challenge. Laser photocoagulation and PDT have been tried but with limited success.[122,123]

Optic Disc Pits

The first optic disc pits were described by Wiethe in 1882. He observed gray excavations in both optic nerve heads of a 62-year-old patient. Since then several authors reported on the lack of gender predilection and a bilaterality of 10% to 15% of cases. Seventy percent of the pits are located on the temporal side.[124]

Pathogenesis

It appears that the failure of the embryonic fissure to close completely at its superior end is responsible for optic disc pits. More controversial is the source of the subretinal fluid responsible for the serous macular detachments. Some believe that

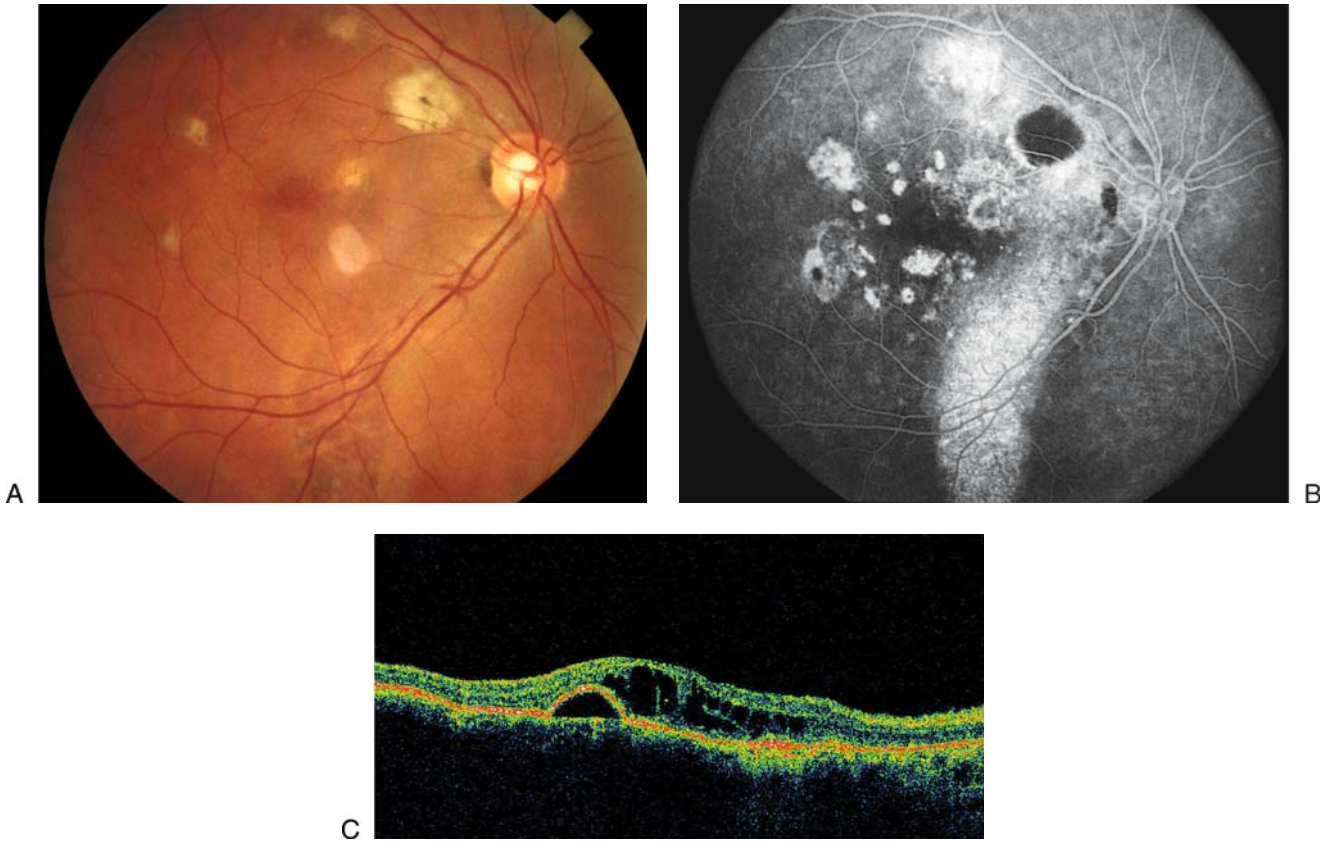

Fig. 4.26. Chronic central serous chorioretinopathy. (A) Clinical photograph shows no obvious detachment of the RPE. There is a subtle change in the color of the RPE in a track that runs inferiorly from the inferior temporal arcade. There are some chorioretinal scars secondary to previous laser treatment. (B) Late FA frame shows a hypofluorescent lesion consistent with the previous laser treatment. There is area of hyperfluorescence that tracks inferiorly in the area of RPE decompensation. In addition there are several areas of window defects in the posterior pole. (C) Optical coherence tomography shows a dome-shaped elevation of the highly reflective RPE layer. Underlying the dome is an area of hyporeflectiveness characteristic of fluid accumulation. Adjacent to it there are irregular hyporeflective intraretinal areas consistent with cystoid macular edema.

the cerebrospinal fluid from the subarachnoid space enters the optic pit. Others believe that the fluid comes from the vitreous and enters the subretinal space through the pit. Regardless of the source of the submacular fluid, it appears that the fluid enters the macular area through the optic pit and creates a macular schisis.[124]

Clinical Findings

Unless the optic pit is complicated by a serous macular detachment, patients may remain asymptomatic. Most pits are gray in color but may be yellow to black. A gray membrane may cover the pit in many cases. Up to 50% of optic pits are complicated by serous detachments of the macula (Figs. 4.27 and 4.28). The serous retinal detachment may resolve spontaneously. However, untreated macular detachments have a bad visual outcome. Long-term macular changes following serous macular detachments include macular holes, RPE mottling, and cystoid changes.[124]

Fluorescein Angiography

Early hypofluorescence of the pit with late staining of the optic disc pit is observed. In the late phases of the study, dye pools into the serous detachment and concentrates at its borders, making a hyperfluorescent border around the macular detachment (Fig. 4.29).[124]

Indocyanine Green Angiography

Indocyanine green angiography reveals complete hypofluorescence of the optic disc pit. During the middle phases of the angiogram, a hyperfluorescent rim delineating the extent of the macular detachment can be seen.

Optical Coherence Tomography

The optic pit is imaged as an area of no reflectivity. In eyes with a serous detachment of the macula, immediately adjacent

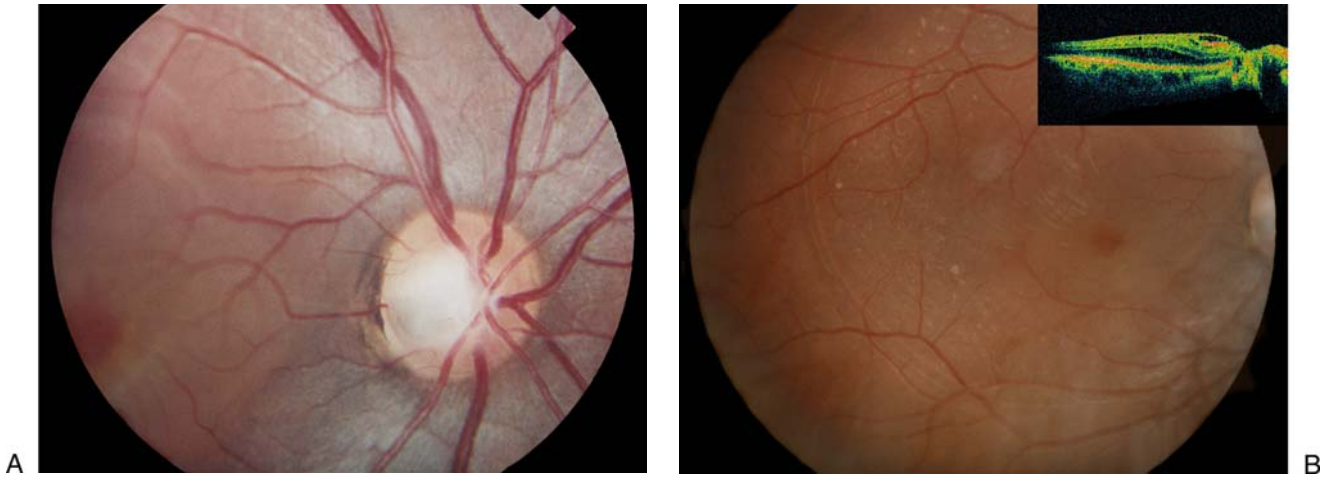

Fig. 4.27. A 16-year-old boy noticed decreased vision in his right eye. His visual acuity was 20/200. (A) Optic pit in the inferior border of the nerve. (B) Notice the extent of the macular detachment and OCT (insert), demonstrating serous detachment of the macula. Immediately adjacent to the pit, on its temporal side, resides an intraretinal cavity with no reflectivity that splits the retina.

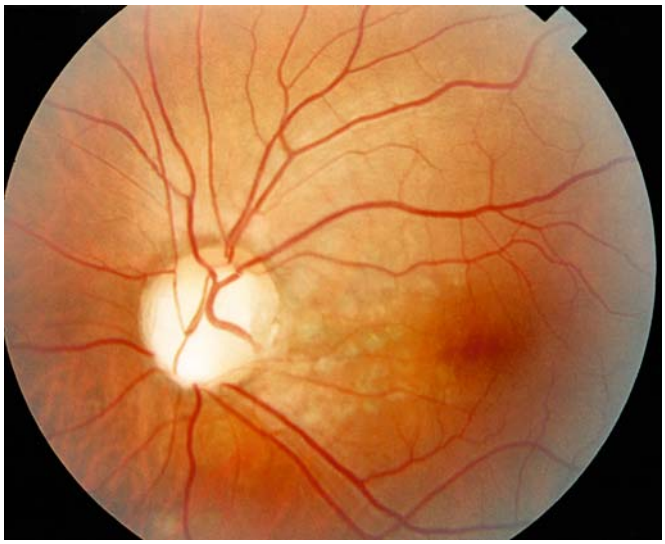

Fig. 4.28. A 35-year-old man was noted on routine examination to have an optic disc pit of his left eye. Clinical photograph shows a gray optic pit in the temporal aspect of the optic nerve after vitrectomy combined with laser photocoagulation and intraocular gas tamponade to treat macular detachment.

to the pit, on its temporal side, resides an intraretinal cavity with no reflectivity that splits the retina (insert on Fig. 4.27).[125]

Treatment

Systemic steroids and optic nerve sheath decompressions have not been proven to be effective. Laser photocoagulation is effective in flattening the serous detachment of the macula. Vitrectomy combined with laser photocoagulation and intraocular gas tamponade appears to be the treatment of choice (Fig. 4.28).[124]

Macular Holes

Macular holes are full-thickness retinal breaks located in the macular area. They were first described by Knapp in 1869.[126] Macular holes may arise from long-standing macular edema, trauma, or inflammation.[126] However, most macular holes are idiopathic in nature.

Pathogenesis

Perifoveal vitreous separation combined with strong vitreofoveolar adhesions leads to an increase in both tangential and anteroposterior vitreoretinal traction that initiates the formation of macular holes. An intrafoveal pseudocyst forms and may extend across the entire foveal thickness. If the pseudocyst spans the whole foveal thickness and becomes unroofed, a full-thickness macular hole results.[126]

Clinical Findings

Gass has proposed a classification system based on his biomicroscopic findings.[126] Stage 1 describes impending macular holes. In this stage, patients complain of metamorphopsia and mild loss of visual acuity. The cortical vitreous over the foveal area shrinks and causes foveolar detachment. The normal foveal reflex is diminished or lost. A yellow spot (stage 1A) or small ring (stage 1B) is seen. In stage 1B the center may appear red and have radiating striae. No definite hole is seen in stage 1. Approximately 60% of stage 1 holes undergo spontaneous resolution.

Stage 2 refers to a full-thickness hole that may be in the center of the yellow ring or eccentric at the margin of the ring (Fig. 4.30). Most stage 2 holes progress in a matter of weeks to a stage 3 hole. Stage 3 holes are full-thickness retinal defects that manifest vitreofoveal separation. Yellow deposits at the

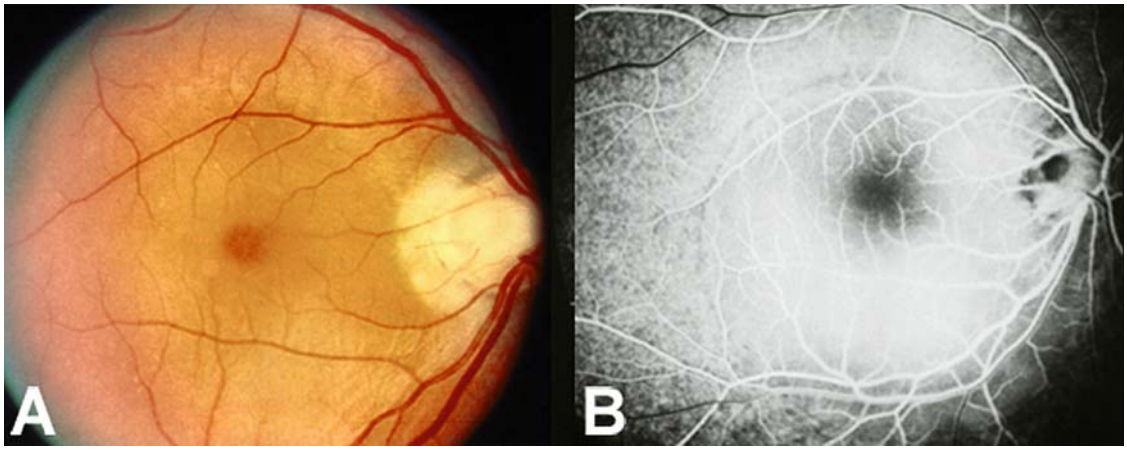

Fig. 4.29. (A) Color fundus photograph of a patient with subretinal fluid and temporal optic disc pit. (B) Fluorescein angiography (FA) showed early hypofluorescence in the area of the optic disc pit. In the early FA phase, the appearance of fluorescein dye in the area of the macular elevation is evident. The posterior pole hyperfluorescence, which is more intense in the papillomacular bundle region adjacent to the optic disc, does not have the typical appearance of choroidal transmission fluorescence.

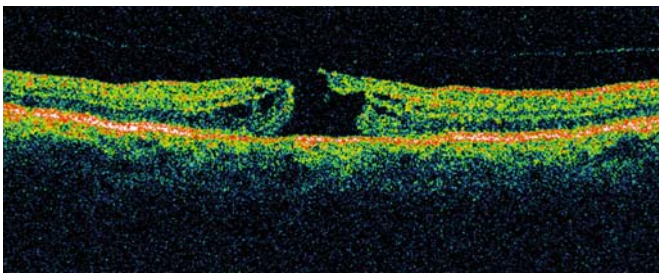

Fig. 4.30. Optical coherence tomography of a stage 2 macular hole. Notice the eccentric opening and the traction exerted by the vitreous. (Courtesy of Zlatko Piskulich, MD.)

base of the hole may be seen (Fig. 4.31). A vitreous opacity or pseudo-operculum may lie in front of the hole (Fig. 4.32). A neurosensory retinal detachment surrounds the defect. Stage 4 holes have the same findings as stage 3 but in addition have a posterior vitreous detachment (PVD), which is evidenced by a Weiss ring (Fig. 4.33).

Fluorescein Angiography

In impending macular holes, the FA is usually normal but may show a small window defect centered in the fovea (Fig. 4.34). Stage 2 holes show a round window defect with a more intense fluorescence than stage 1. Stage 3 and 4 holes show early hyperfluorescence at the base of the hole that fades with time (Fig. 4.31). A ground-glass appearance is seen in the area of the cuff of subretinal fluid.[126] Fluorescein angiography is not too helpful in differentiating macular holes from

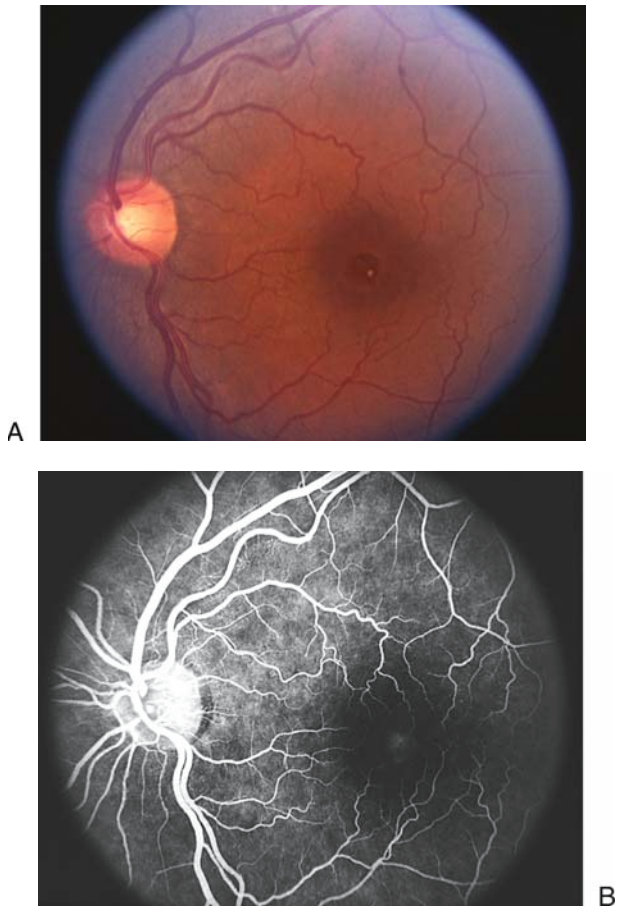

Fig. 4.31. Stage 3 macular hole. (A) Clinical photograph shows a full-thickness macular hole. Notice the yellow deposits at the base of the hole. (B) Mid-FA frame shows some faint hyperfluorescence at the base of the macular hole.

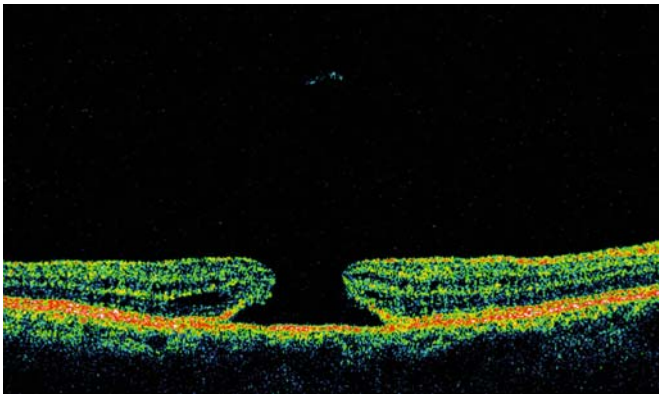

FIG. 4.32. Optical coherence tomography of a full-thickness macular hole. Notice the pseudo-operculum lying in front of the retinal defect. The margins of the retinal defect are thickened and hyporeflective.

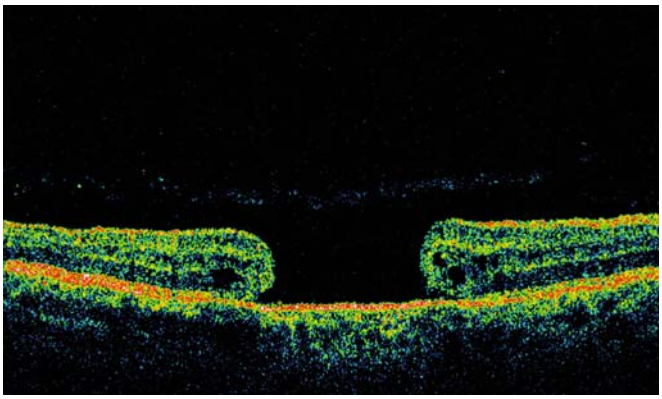

FIG. 4.33. Optical coherence tomography of a stage 4 macular hole. Notice that the vitreous is no longer attached to the macular area.

pseudoholes. Both conditions can present with hyperfluorescent window defects.

Optical Coherence Tomography

In a stage 1 macular hole, the normal foveal contour is lost. A hyporeflective area lies within the fovea indicating a foveal pseudocyst. A stage 2 macular hole is seen as a discontinuity of the retinal surface with an area completely devoid of retinal tissue (Fig. 4.30). A stage 3 hole demonstrates an area of complete loss of retinal tissue whose margins are thickened and hyporeflective, which correspond to the cuff of subretinal fluid. The posterior hyaloid is seen to be still attached to the retina (Fig. 4.32). A stage 4 hole has the same OCT findings as a stage 3 with the exception that the posterior hyaloid is completely separated from the retina (Fig. 4.33).

Optical coherence tomography reliably differentiates macular holes from lamellar holes, pseudoholes, and macular cysts. In addition, OCT can accurately measure the size of the macular hole.

Treatment

For more than 100 years, macular holes were deemed inoperable. In 1991, Kelly and Wendel proposed vitrectomy as a means of correcting this condition.[126] Since then, macular hole surgery has been refined and perfected. Most surgeons today report anatomic success rates of 90% or higher.[126]

Epiretinal Membranes

Membranes on the macular surface were first described by Iwanoff in 1865. These can be idiopathic or secondary to

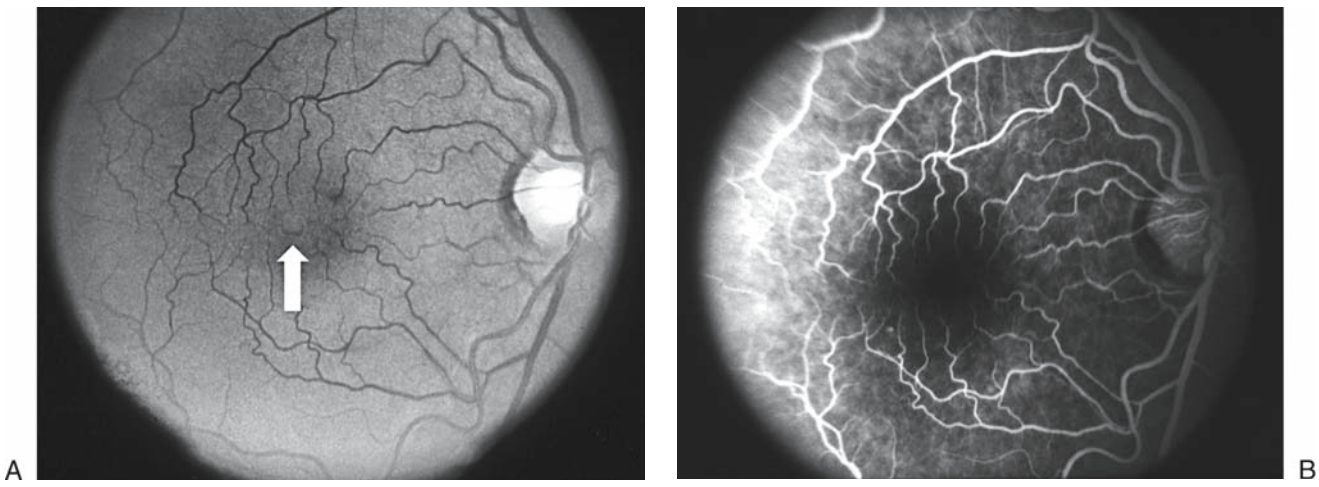

FIG. 4.34. A 60-year-old woman noticed some metamorphopsia of her right eye. Her visual acuity was 20/25 in that eye. She was diagnosed with a stage 1B macular hole. (A) Red-free photograph shows loss of the normal foveal reflex and a foveal yellow ring (arrow). (B) There is no hyperfluorescence in the foveal region as seen in the mid-FA frame.

retinal vascular diseases, ocular inflammatory conditions, intraocular surgeries, intraocular tumors, trauma, and macular holes. Epiretinal membranes (ERMs) are hypocellular collagen structures that in the literature have also been called macular puckers, cellophane maculopathy, surface wrinkling retinopathy, epiretinal membranes, preretinal membranes, premacular fibroplasia, and premacular fibrosis.[127]

Pathogenesis

The idiopathic type has been shown to be due to glial proliferation through a defect in the internal limiting membrane, which is usually created by a PVD. Other cellular components include fibroblasts, macrophages, and pigmented epithelioid cells. These cells have the ability to generate a contractile force that exerts traction on the underlying macula.[127]

Symptoms

The chances of developing an ERM increase with age. It has been reported that 2% of patients older than 50 years have ERMs compared to 20% in patients older than 70 years. Approximately 20% to 30% of ERMs are bilateral. A fair number of patients are asymptomatic and have a very fine cellophane-like ERM discovered on routine examination. Close to 67% of patients with idiopathic ERMs have a visual acuity of 20/30 or better. Only <5% of eyes with ERMs have a visual acuity of 20/200 or worse. In these patients a relatively rapid loss of vision, micropsia, metamorphopsia, or monocular diplopia occurs over a period of several weeks. The symptoms usually stabilize at a visual level at or near that noted on initial presentation.[127]

Signs

The clinical findings vary according to the degree of severity of the membrane. Asymptomatic patients have an irregular foveal light reflex with a subtle, transparent, cellophane-like membrane. With increasing severity, the membrane loses its transparency and becomes more opaque. The traction exerted by the membrane will also increase. This is evidenced by distortion of the retinal architecture between the arcades. Retinal striae appear and the macular surface becomes wrinkled. Retinal vascular distortion, tortuosity, and straightening of the vessels become evident. When the ERMs become chronic, the retinal capillaries may become dilated. This leads to microaneurysmal formation, small punctate hemorrhages, and macular edema (Fig. 4.35). If the membrane is centered away from the fovea, dragging will cause foveal ectopia that simulates a macular hole, hence the name *pseudohole*.[128,129]

Fluorescein Angiography

Fluorescein angiography is a useful adjunct in the management of ERMs. It delineates more clearly the distorted retinal architecture but adds little to the diagnosis of the condition (Fig. 4.35). Its main role is in differentiating ERMs from other conditions such as CNV, macular ischemia, and cystoid macular edema (CME).[129] Macular edema secondary to ERMs occurs as a result of retinal vascular leakage from the traction exerted on the retinal vessels. Angiographically this is seen as progressive, asymmetric, and irregular macular hyperfluorescence. This hyperfluorescence corresponds to the location of the ERM. This pattern of hyperfluorescence helps distinguish macular edema secondary to ERMs from the typical petaloid hyperfluorescence of CME. Pseudoholes often show early hyperfluorescence that fades in the area of the hole. This may result in misdiagnosis

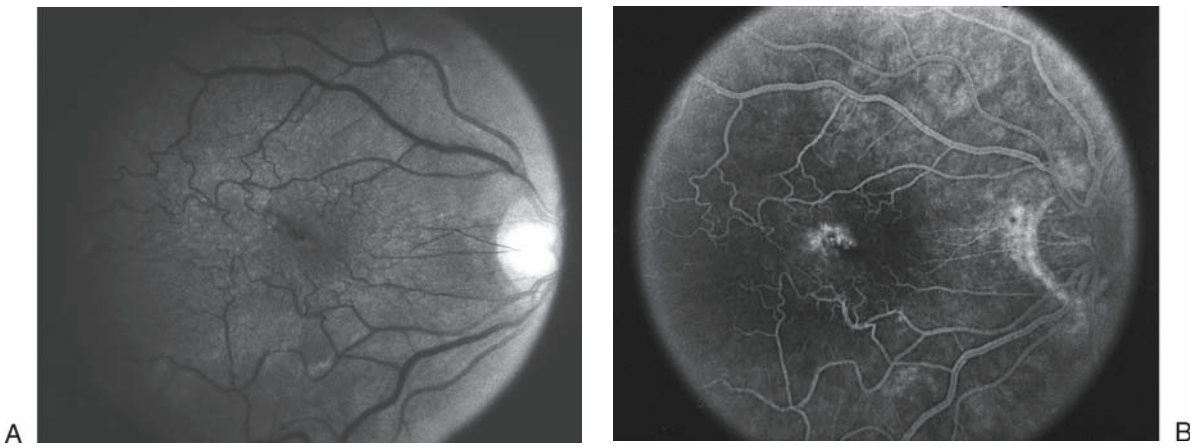

Fig. 4.35. A 65-year-old man complained of metamorphopsia and decreased vision in his right eye. His visual acuity was 20/100. He was diagnosed with an epiretinal membrane. (A) Red-free photograph shows wrinkling of the macular surface, retinal vascular distortion, tortuosity, and straightening of the vessels. In addition there are microaneurysms and hemorrhage. (B) Late FA frame shows the vascular tortuosity and fluorescein leakage signifying macular edema.

of the macular pseudohole as a full-thickness macular hole.[127] Optical coherence tomography is better suited to differentiating a pseudohole from a full-thickness macular hole.

Optical Coherence Tomography

On OCT scanning, ERMs appear as a highly reflective tissue adherent to or anterior to the retinal surface (Fig. 4.36). This higher reflectivity distinguishes them from the posterior hyaloid which exhibits low reflectivity. In approximately 7% of cases, OCT is unable to image the ERM.[130,131]

Treatment

Most ERMs are asymptomatic and nonprogressive. However, a few can cause visual loss. Treatment consists of peeling the ERM from the macular surface using pars plana vitrectomy techniques. Recurrence of epimacular proliferation occurs in up to 5% of cases.[127]

Postoperative Cystoid Macular Edema

In 1953 Irvine[132] noticed that eyes that underwent intracapsular cataract extraction and had vitreous strands adherent to the surgical wound suffered from a decrease in visual acuity. In 1966, Gass and Norton, based on the fluorescein angiographic findings, reported that this entity consisted of CME and papilledema. Subsequently this syndrome was named the Irvine-Gass syndrome. Postoperative CME has also been reported to occur following scleral buckling procedures,[133,134] penetrating keratoplasty,[135] glaucoma filtering procedures,[136,137] and neodymium:yttrium-aluminum-garnet (Nd:YAG) laser posterior capsulotomy.[138–140]

Clinical Findings

Postoperative CME is a manifestation of reaction to local trauma or insult. It can result in a temporary or, rarely, a permanent reduction in visual acuity. Up to 20% following uncomplicated extracapsular cataract extraction (ECCE) and phacoemulsification have angiographic findings of CME. Vision is generally not affected, and the condition is mild, innocuous, and self-limiting, subsiding spontaneously in a few days unless complications (rupture of the posterior capsule and vitreous loss, and vitreous incarceration in the surgical wound) arise during cataract extraction.

Clinically significant postoperative CME, which has an incidence of about 1.5% in uncomplicated ECCE, often presents with subtle symptoms. Most commonly the symptoms appear within the first 6 months, although they may be delayed for several years. Chronic CME develops later, even years after surgery, and typically persists for more than 6 months despite treatment.

Slit-lamp biomicroscopy reveals a loss of the foveal reflex. Macular thickening with cystoid concentric spaces arranged in a petaloid pattern around the fovea may be seen with the help of a fundus contact lens. Papilledema with peripapillary hemorrhages may appear.[132,141]

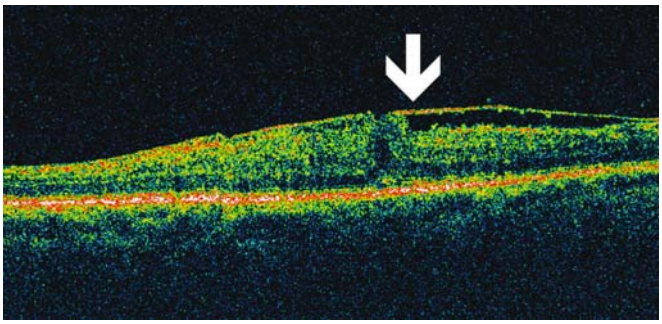

Fig. 4.36. An 82-year-old man was noted to have a visual acuity of 20/200 in is left eye. An epiretinal membrane was diagnosed. Optical coherence tomography demonstrated foveal thickness and traction exerted by the highly reflective epiretinal membrane (arrow).

Pathogenesis

The surgical trauma or insult, even in uncomplicated cases, results in the release of chemical mediators such as prostaglandins. These prostaglandins disrupt the inner blood–retinal barrier, which results in increased perifoveal and peripapillary capillary permeability.

In certain eyes mechanical stress plays a role. Vitreous incarceration in the surgical wound causes chronic vitreoretinal traction that results in chronic irritation. A badly designed or poorly positioned intraocular lens will be in contact with the uveal structures and cause chronic uveal irritation. Uveal irritation results in prostaglandin release.

Fluorescein Angiography

Early on, the perifoveal capillaries are seen as telangiectatic and start to leak fluorescein in the form of pinpoint spots. As the study progresses, the cystic spaces become filled with fluorescein dye. These hyperfluorescent spaces coalesce to form the classical stellate, petaloid perifoveal configuration. Late staining or leakage of the disc may be seen (Figs. 4.37 and 4.38).[142]

Ocular Coherence Tomography

Typically eyes with CME are shown by OCT to have an increased foveal thickness with areas of decreased intraretinal reflectivity consistent with intraretinal fluid (Fig. 4.38).

Treatment

The treatment of CME remains controversial but generally starts with conservative observation in isolated angiographic

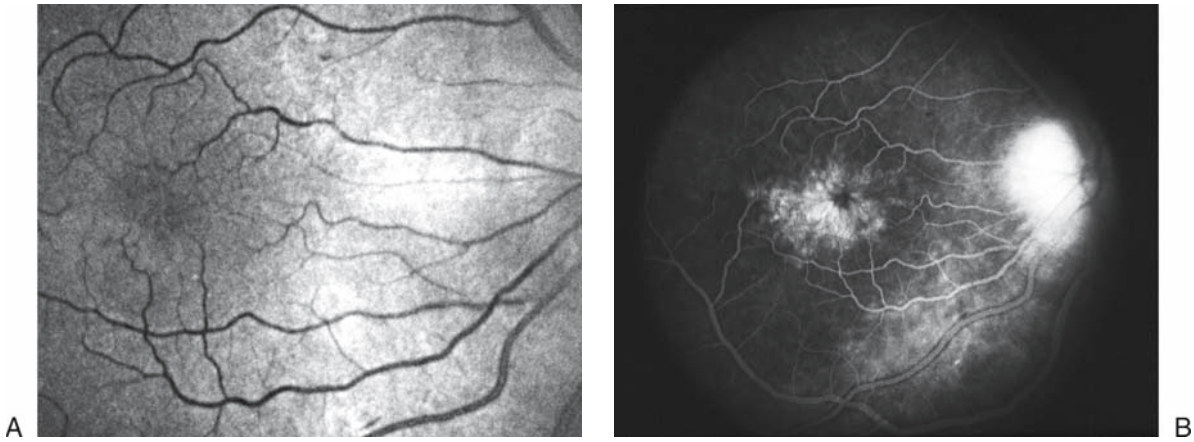

Fig. 4.37. A 65-year-old woman underwent uncomplicated phacoemulsification with a foldable intraocular lens. Her vision improved to 20/20, but 2 months later she noted decreased vision to 20/40. She was diagnosed with cystoid macular edema. (A) Red-free photograph shows some subtle changes in the foveal region. (B) Late FA frame shows leakage in a petaloid fashion. Notice the hyperfluorescence of the optic nerve.

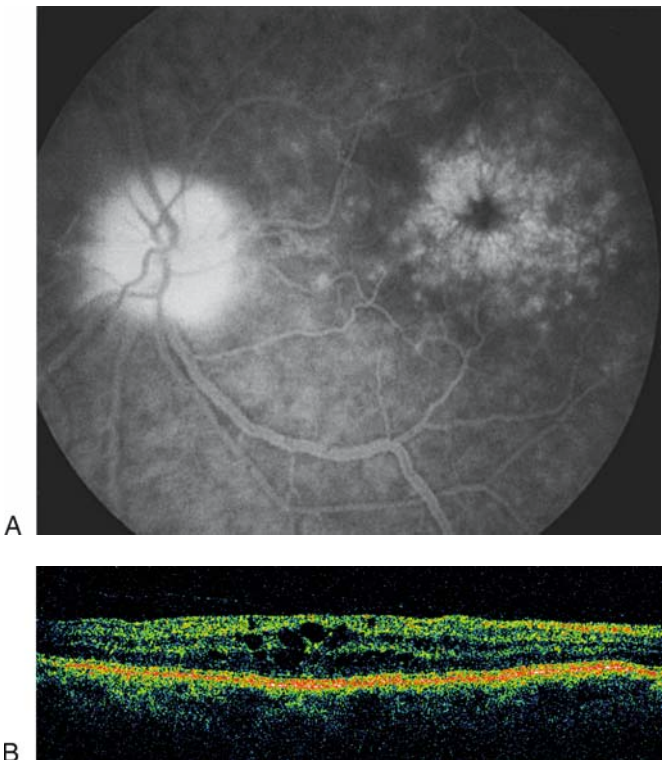

Fig. 4.38. A 62-year-old man was diagnosed with cystoid macular edema (CME) following uncomplicated phacoemulsification of his left eye. (A) Late FA frame shows CME. (B) Optical coherence tomography shows loss of the normal macular architecture and cystoid spaces within the retina. These are imaged as hyporeflective areas.

cases and progresses through topical nonsteroidal antiinflammatory drugs (NSAIDs); topical, periocular, intravitreal, or systemic steroids[143]; oral and topical carbonic anhydrase inhibitors[143,144]; laser surgery[141,145–150]; hyperbaric therapy; and surgical intervention in refractory cases.

Best's Disease

In 1883, Adams[151] published the first description of a patient with symmetric, yellow lesions in each fovea, which, in retrospect, was a patient with Best vitelliform macular dystrophy. In 1905, Best[152] described the first familial cases of this hereditary condition.

Inheritance

Best's disease has an autosomal dominant pattern of inheritance with variable penetrance. The disease-causing gene was first mapped to chromosome 11q13, and this gene, *VMD2*, encodes for a protein named bestrophin.[153] The evaluation is complete if patients are examined with electro-oculogram (EOG), but not if the examination is limited to ophthalmoscopy.

Clinical Findings

The visual prognosis in Best's disease tends to be good, with most patients retaining 20/40 visual acuity or better in at least one eye into the seventh decade of life.[154] Patients with Best's disease also complain of metamorphopsia and lacunar scotomas that make reading difficult. Dark adaptation is usually normal in patients with Best's disease. Contrast sensitivity is impaired at the high spatial frequencies and color discrimination is mildly diminished.

Ophthalmoscopic Findings

Best's disease can be subdivided into different stages based on the clinical appearance of the macula.[155] Patients with stage 0 have a normal-appearing macula but an abnormal EOG. Those with stage I show a disturbance of the macular RPE with window defects on fluorescein angiography.

Patients with stage II have the typical vitelliform or egg-yolk lesions 0.5 to 2 disc diameters in size; these lesions are usually bilateral and symmetric, but on rare occasions may be unilateral (Fig. 4.39). Those with stage IIa show a disruption of the vitelliform cyst or "scrambled-egg" phase, with pigment around or within the lesion becoming more prominent with time. Patients with stage III have a pseudohypopyon, in which yellow material forms a fluid level in the vitelliform cyst. Patients with stage IVa show atrophy of the macular pigment epithelium, those with stage IVb show macular scarring, and those with stage IVc show neovascularization. This staging system does not imply a sequential evolution from one stage to the next, and patients do not necessarily progress through each of the stages. In some patients, vitelliform lesions never develop; in others, these lesions develop in previously normal-appearing fundi.

Pathogenesis

Lipofuscin-like material accumulation has been found in some pigment epithelial cells in the fovea of patients with Best's disease. This material appears to be derived from degenerating pigment epithelial cells and contains also intact lipofuscin granules. Foveal photoreceptor loss occurs above the lesion and in the midperipheral sites where the subretinal space contains collections of outer segment debris and phagocytic cells. Best's disease appears to be a generalized disorder of the RPE that secondarily affects focal areas of the retina.[156]

Diagnostic Testing

All patients with Best vitelliform macular dystrophy, regardless of age or stage of disease, have abnormal EOG results, and the light-peak to dark-trough ratio of the EOG is abnormally low in such patients. Abnormal findings on an EOG are apparent, even in the absence of a clinically discernible retinal lesion. The electroretinogram is normal.

Angiography

The fluorescein angiographic findings are dependent on the type of fundus lesion present. The classic yellow vitelliform lesions block choroidal fluorescence in the early phases of the fluorescein angiogram. During the late phases, the vitelliform lesions usually remain hypofluorescent; however, they may exhibit variable degrees of hyperfluorescence. In those areas where the vitelliform material has begun to resolve and has left areas of RPE depigmentation and atrophy, FA reveals hyperfluorescent window defects (Fig. 4.40). In some areas, both the RPE and smaller choroidal vessels have disappeared, enabling the larger choroidal vessels to become more visible. Choroidal neovascularization shows early hyperfluorescence, followed by late, fuzzy hyperfluorescence. Disciform scars stain with dye in the late phases of the angiogram.

Treatment

There is no treatment for most of the lesions associated with Best's disease. In eyes that develop extrafoveal CNV, laser photocoagulation treatment could be beneficial. Photodynamic therapy with verteporfin has been used with good results in some cases.[157] Genetic counseling should be offered to patients with Best's disease.

Stargardt's Disease

The essential features of Stargardt's macular dystrophy were first described by Karl Stargardt[158] in 1909. Mutations in the adenosine triphosphate (ATP)-binding cassette transporter

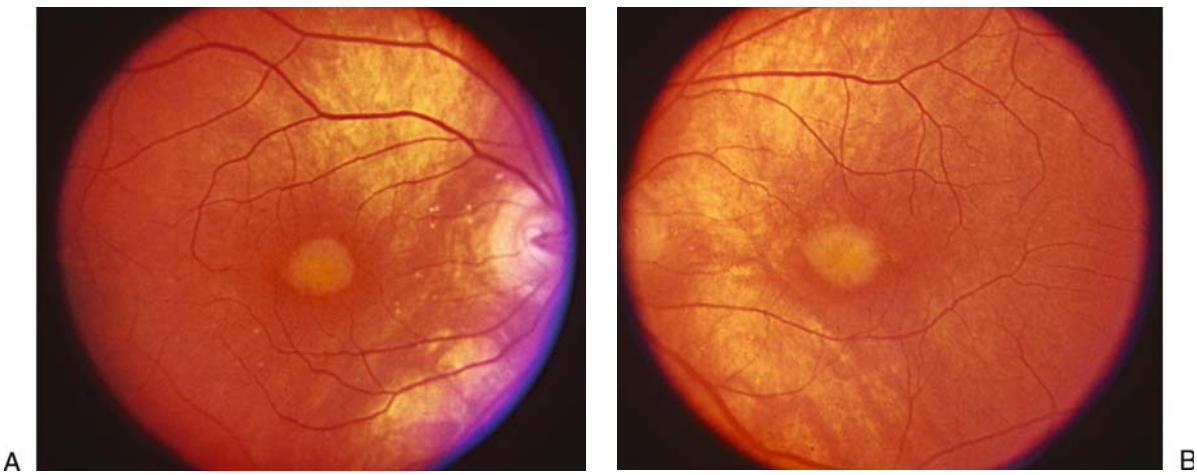

FIG. 4.39. A 19-year-old man with stage 2 Best's disease. (A) Clinical photograph of the right eye shows the typical egg yolk lesion. (B) Clinical photograph of the left eye shows the typical egg yolk lesion.

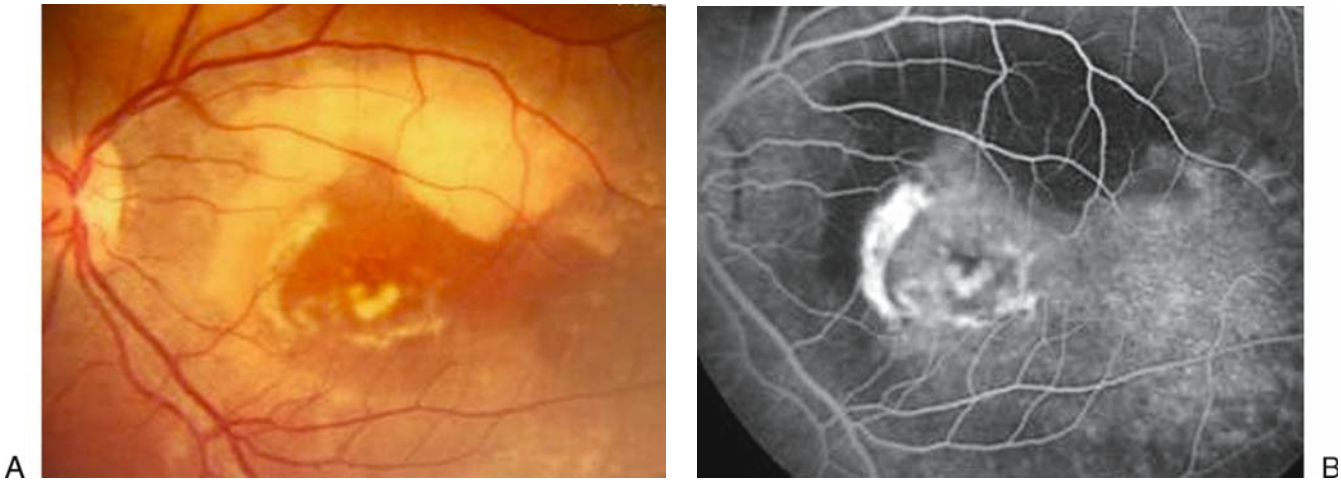

Figure 4.40. (A) Disruptive vitelliform lesions. (B) The yellow lesions block choroidal fluorescence in the early phases of the fluorescein angiogram. During the late phases, the vitelliform lesions usually remain hypofluorescent; however, they may exhibit variable degrees of hyperfluorescence. In those areas where the vitelliform material has begun to resolve and has left areas of RPE depigmentation and atrophy, FA reveals hyperfluorescent window defects. (Courtesy of Wael El Haig, MD.)

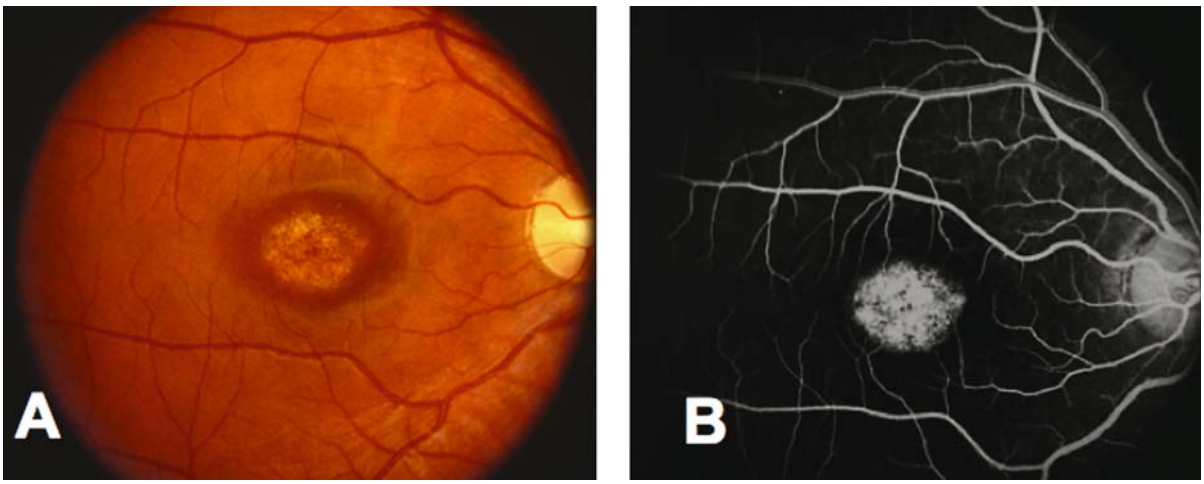

Fig. 4.41. A 22-year-old boy was diagnosed with Stargardt's disease. (A) Clinical photo shows macular atrophy. (B) An FA frame shows window defects in the macular area. Notice the "silent choroid" sign. The normal background choroidal hyperfluorescence is missing.

and *ABCR* gene *(ABCA4)* are responsible for Stargardt's macular dystrophy.[159] This aberrant *ABCR* gene leads to a massive intracellular accumulation of a lipofuscin-like material within the RPE because the metabolites of retinol cannot be transported out of the rod photoreceptors outer segments. It is generally inherited as an autosomal recessive condition; however, some autosomal dominant pedigrees have been reported.[160,161]

Clinical Findings

The onset of symptoms generally occurs in the first or second decade of life.[162] Patients complain of a gradual loss of vision after having had normal vision in childhood. Rarely patients may describe dyschromatopsia and photosensitivity. Nyctalopia and peripheral field loss are seldom noted. Early in the course of the disease, visual acuity may be worse than one might expect based on the normal-appearing fundus. Most patients have abnormalities of dark adaptation, and color vision is highly variable. Only rarely is central vision maintained.[163]

The central macula demonstrates loss of the foveolar reflex and symmetric atrophic RPE changes. Atrophy often is manifested by a beaten bronze appearance, granularity, mottling, or frank RPE destruction (Fig. 4.41). Macular atrophy is typically accompanied by adjacent surrounding flecks

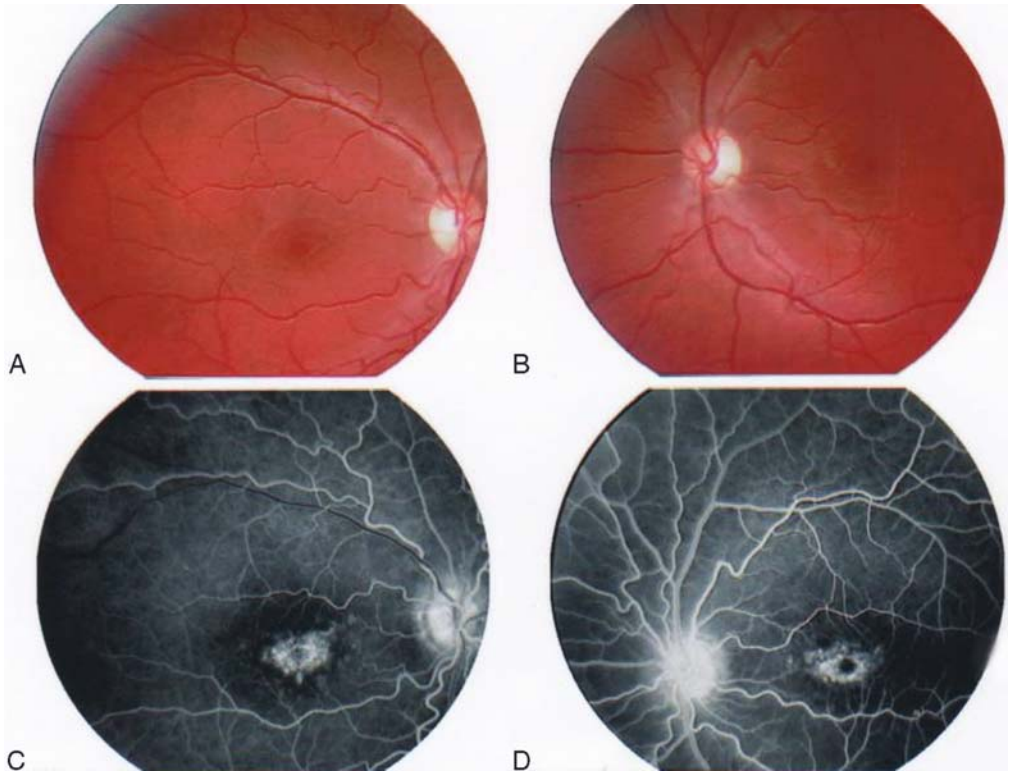

FIG. 4.42. A 20-year-old boy was diagnosed with Stargardt's disease. (A,B) Clinical photograph shows macular atrophy. (C,D) An FA frame shows window defects in the macular area and multiple specks around the fovea.

(Fig. 4.42). Disappearance of a fleck is associated with RPE and choriocapillaris atrophy. Development of subretinal neovascularization is rare. Stargardt's disease may manifest as macular degeneration without flecks, macular degeneration with perifoveal flecks, macular degeneration with diffuse flecks, and diffuse flecks without macular degeneration.

Fluorescein Angiography

Fluorescein angiography is extremely valuable in establishing a diagnosis. Initially, the funduscopic appearance is quite normal. An early pathognomonic sign is the presence of the dark choroid effect, which is present in approximately 85% of patients with Stargardt's disease (Fig. 4.41).[164] The normal choriocapillaris fluorescence is blocked by the lipofuscin engorged RPE.[165] This enhances the retinal vascularity against the dark choroid. As the disease progresses, the RPE and choriocapillaris become atrophic allowing the underlying fluorescence to be seen.[165,166] Flecks initially appear hypofluorescent on angiography because of transmission blockage. The progressive resorption of flecks, associated with RPE damage, leads to increasing hyperfluorescence secondary to window defects (Fig. 4.42). Occasionally, a bull's-eye pattern can be seen in the macula (Figs. 4.41 and 4.42). Fluorescein leakage never occurs.

Indocyanine Green Angiography

In eyes that exhibit the dark choroid effect in FA, the choroidal vasculature is imaged without a problem with ICGA.[167] Varying degrees of macular choroidal vessel nonperfusion in the early transit ICGA phases are seen.[167] There is late central uniform hypofluorescence of the macular area. This is probably secondary to masking from lipofuscin accumulation in the macular RPE.[167] Depending on the size and density of the flecks, varying degrees of reticular hypofluorescent lesions were seen at varying times of the angiogram.[167] Hypofluorescence occurs earlier, with large, dense flecks. Smaller flecks and subclinical flecks cause hypofluorescence progressively later as the background choroidal ICG dye clears. Peripapillary crescents of hypofluorescence that were not identified in FA or clinical examination appear in ICGA.[167]

Treatment

There is no known treatment for this condition.

Pattern Dystrophies of the Retinal Pigment Epithelium

The pattern dystrophies of the RPE were first described by Gass[168] in 1974. He has also subdivided them into several subgroups: adult foveomacular or pseudovitelliform, butterfly shaped, reticular, and coarse pigment mottling (fundus pulverulentus). They are inherited in an autosomal dominant fashion. Recently a mutation in the *RDS/peripherin* gene has been associated with pedigrees of both adult foveomacular dystrophy and butterfly-shaped dystrophy.[169,170]

Clinical Findings

The most common symptom is decreased vision, although some may also complain of metamorphopsia, photopsias, and scotomas.[171] These symptoms are associated with macular pigmentary deposition occurring during midlife. The deposits are of a variety of patterns and may be yellow, orange, or gray.

Adult foveomacular dystrophy is characterized by an oval-shaped yellow subretinal lesion with a central pigmented spot. With time the yellow lesion may acquire a gray or orange color (Fig. 4.43). Longer follow-up may result in fading of the yellow lesion, leaving an oval area of atrophic depigmented RPE. Some of these eyes may also develop CNV, but in general the visual prognosis is much better than AMD.[172,173] On occasion, the pigment assumes a symmetric triradiate pattern in the macular center. The RPE adjacent to the macular pigment is depigmented. These eyes have been classified as having a butterfly-shaped pigment dystrophy.[174–176] Eyes where the yellow pigment is organized like a network of chicken wire or a fishnet are known to have a reticular dystrophy.[177–179] Other eyes may manifest a central macular coarse point-like mottling of the RPE. These eyes are classified as having fundus pulverulentus.[180,181]

Fluorescein Angiography

The typical finding in adult foveomacular dystrophy is a small irregular ring of hyperfluorescence surrounding a central nonfluorescent spot.[168,171,172]

Indocyanine Green Angiography

The ICGA findings in adult foveomacular dystrophy are characterized by a foveal nonfluorescent spot that is seen throughout the study (Fig. 4.43). This spot becomes surrounded by a hyperfluorescent area within minutes of starting the study.[182,183]

Optical Coherence Tomography

Eyes with adult foveomacular dystrophy are characterized by a hyperreflective structure that focally elevates the neurosensory retina. This hyperreflective structure corresponds to the vitelliform lesion. However, its exact location with respect to the RPE remains unknown. Some have reported the lesion to be above, at the level of, or below the RPE.[183–188]

Treatment

Eyes with pattern dystrophies of the RPE that are complicated by CNV have been treated with PDT. If the CNV is classic, the visual acuity may be stabilized by PDT with verteporfin. If the CNV is occult, a bad visual outcome has been reported.[189] Currently there is no known treatment for this condition.

X-Linked Retinoschisis

X-linked retinoschisis (XLRS) was first described by Haas in 1898. Jager coined the term *retinoschisis* in 1953. Several other terms have been used in the literature to describe this inherited condition including *congenital cystic retinal detachment, vitreous veils,* and *congenital vascular vitreous veils in the vitreous*.[190]

Pathophysiology

X-linked retinoschisis is characterized by splitting of the retina at the level of the nerve fiber layer. The gene responsible for this condition has been identified as *XLRS1* and maps to the Xp22 band in the distal end of the X chromosome. The protein product of this gene is retinoschisin, which is expressed in photoreceptor and bipolar cells. Retinoschisin plays a role in cellular adhesion and cell-cell interactions and its deficiency or abnormality in patients with XLRS explains the clinical findings.[190]

Clinical Findings

X-linked retinoschisis is an important cause of childhood vision loss. The most common clinical finding seen in almost all patients is bilateral foveal schisis. This is characterized by radiating stellate folds that contain microcystic schisis cavities (Fig. 4.44). With time the schisis cavities coalesce and flatten out. Retinal pigment epithelium atrophy and pigment clumping may develop. Vitreous veils are commonly seen. They arise from the inner wall of the peripheral schisis cavity as it separates itself from the inner wall holes. Peripheral schisis is seen in 50% of patients. It usually occurs in the inferotemporal quadrant. Retinal detachments have been reported to complicate the course in up to 22% of eyes. Vitreous hemorrhage has been noted to occur in up to 40% of eyes.[190]

Fluorescein Angiography

Fluorescein angiography helps differentiate the maculopathy of XLRS from CME. No leakage or staining of the macula

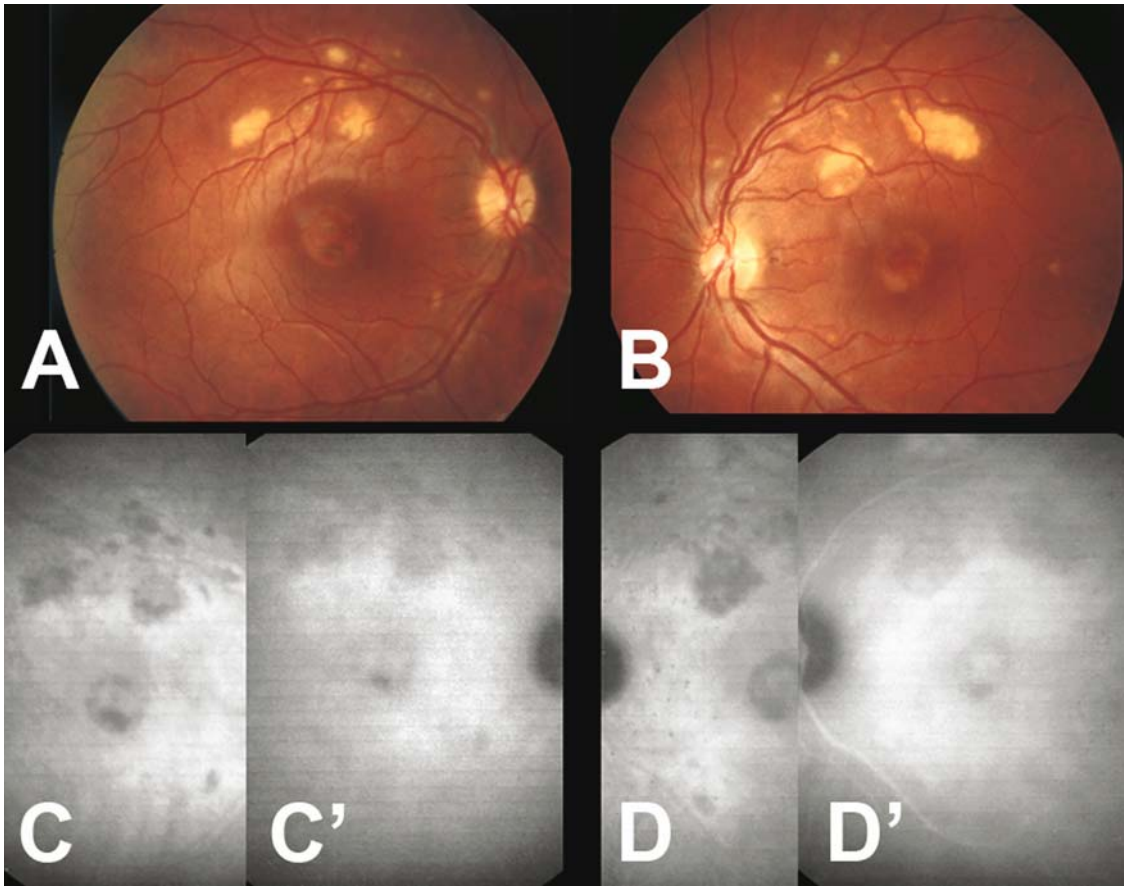

Fig. 4.43. Adult-onset foveomacular vitelliform dystrophy. (A,B) Color photograph of both eyes demonstrate an oval-shaped yellow subretinal lesion with a central pigmented spot. With time the yellow lesion may acquire a gray or orange color. (C,D) The indocyanine green (ICG) findings in adult-onset foveomacular vitelliform dystrophy are characterized by a foveal nonfluorescent spot that is seen throughout the study. This spot becomes surrounded by a hyperfluorescent area within minutes of starting the study.

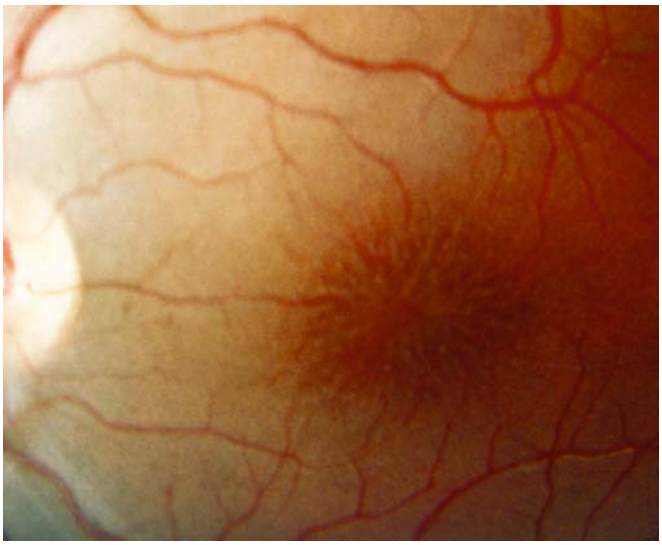

Fig. 4.44. A 19-year-old man with X-linked retinoschisis. Clinical photo of the left eye. Notice the characteristic radiating stellate folds that contain microcystic schisis cavities in the foveal region.

occurs in XLRS. Window defects may be seen in areas of RPE atrophy. Peripheral areas of capillary nonperfusion have also been reported.[190]

Optical Coherence Tomography

The best use of OCT is to differentiate retinal detachment from retinoschisis. Retinoschisis is imaged as a splitting of the neurosensory retina. In retinal detachments, there is a complete separation of full-thickness neurosensory retina from the RPE. In the foveal area, OCT images the splitting of the retina and the cystic structures within it (Fig. 4.45).[190]

Treatment

Treatment of the schisis cavity is not indicated in the majority of cases. Scatter laser photocoagulation and surgical maneuvers to flatten the schisis cavity may result in retinal detachment. Most eyes with a vitreous hemorrhage may be managed conservatively unless the hemorrhage is particularly dense or

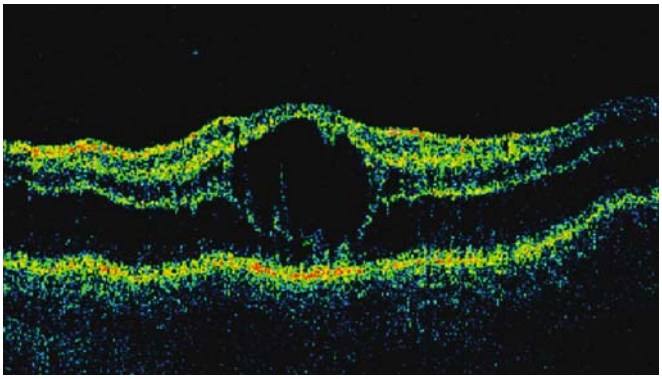

FIG. 4.45. Optical coherence tomography through the fovea of a 17-year-old boy with X-linked retinoschisis. Notice both foveal and lamellar schisis. (Courtesy of Kimberly Drenser, MD, and Michael Trese, MD.)

covers the macula. Vitreoretinal surgery is often successful in stabilizing the visual function in these eyes.[190]

Conclusion

Indocyanine green angiography is a highly specialized technique for imaging choroidal vasculature. Fluorescein angiography is highly specialized in the identification of morphologic and dynamic changes of the retinal circulation and RPE. Although, retinal fluorescein and ICG-V have many physical and chemical differences, both technologies complement each other in the evaluation of a variety of retinal diseases revealing important and different aspects of retinal or choroidal diseases. Additionally, some stages of various diseases are best seen with FA while other aspects are best revealed with ICG-V.

Fluorescein angiography and ICG-V have both become very important tools in the evaluation and diagnosis of macular retinal diseases.

References

1. Sarks SH, Sarks JP. Age-related maculopathy: nonneovascular age-related macular degeneration and the evolution of geographic atrophy. In: Schachat AP ed. Retina, vol 2, 3rd ed. St Louis: Mosby, 2001.
2. Gass JD. Pathogenesis of disciform detachment of the neuroepithelium. Am J Ophthalmol 1967;63(suppl 3):1–139.
3. Seddon JM, Chen CA. The epidemiology of age-related macular degeneration. Int Ophthalmol Clin 2004;44(4):17–39.
4. Ambati J, Anand A, Fernandez S, et al. An animal model of age-related macular degeneration in senescent Ccl-2– or Ccr-2–deficient mice. Nat Med 2003;9(11):1390–1397.
5. Abdelsalam A, Del Priore L, Zarbin MA. Drusen in age-related macular degeneration: pathogenesis, natural course, and laser photocoagulation-induced regression. Surv Ophthalmol 1999;44(1):1–29.
6. Klein RJ, Zeiss C, Chew EY, et al. Complement factor H polymorphism in age-related macular degeneration. Science 2005;308(5720):385–389.
7. Donoso LA, Kim D, Frost A, et al. The role of inflammation in the pathogenesis of age-related macular degeneration. Surv Ophthalmol 2006;51(2):137–152.
8. Friedman E. A hemodynamic model of the pathogenesis of age-related macular degeneration. Am J Ophthalmol 1997;124(5): 677–682.
9. Starita C, Hussain AA, Patmore A, Marshall J. Localization of the site of major resistance to fluid transport in Bruch's membrane. Invest Ophthalmol Vis Sci 1997;38(3):762–767.
10. Grossniklaus HE, Ling JX, Wallace TM, et al. Macrophage and retinal pigment epithelium expression of angiogenic cytokines in choroidal neovascularization. Mol Vis 2002;8:119–126.
11. Baffi J, Byrnes G, Chan CC, Csaky KG. Choroidal neovascularization in the rat induced by adenovirus mediated expression of vascular endothelial growth factor. Invest Ophthalmol Vis Sci 2000;41(11):3582–3589.
12. Campochiaro PA, Soloway P, Ryan SJ, Miller JW. The pathogenesis of choroidal neovascularization in patients with age-related macular degeneration. Mol Vis 1999;5:34.
13. Bressler NM, Bressler SB, West SK, et al. The grading and prevalence of macular degeneration in Chesapeake Bay watermen. Arch Ophthalmol 1989;107(6):847–852.
14. Klein R, Klein BE, Linton KL. Prevalence of age-related maculopathy. The Beaver Dam Eye Study. Ophthalmology 1992;99(6):933–943.
15. Bressler NM, Bressler SB, Seddon JM, et al. Drusen characteristics in patients with exudative versus non-exudative age-related macular degeneration. Retina 1988;8(2):109–114.
16. Gregor Z, Bird AC, Chisholm IH. Senile disciform macular degeneration in the second eye. Br J Ophthalmol 1977;61(2):141–147.
17. Sarks JP, Sarks SH, Killingsworth MC. Evolution of geographic atrophy of the retinal pigment epithelium. Eye 1988;2(pt 5):552–577.
18. Gass JD. Drusen and disciform macular detachment and degeneration. Arch Ophthalmol 1973;90(3):206–217.
19. Casswell AG, Kohen D, Bird AC. Retinal pigment epithelial detachments in the elderly: classification and outcome. Br J Ophthalmol 1985;69(6):397–403.
20. Sunness JS, Rubin GS, Applegate CA, et al. Visual function abnormalities and prognosis in eyes with age-related geographic atrophy of the macula and good visual acuity. Ophthalmology 1997;104(10):1677–1691.
21. Sunness JS. The natural history of geographic atrophy, the advanced atrophic form of age-related macular degeneration. Mol Vis 1999;5:25.
22. Fisher RF. The influence of age on some ocular basement membranes. Eye 1987;1(pt 2):184–189.
23. Moore DJ, Hussain AA, Marshall J. Age-related variation in the hydraulic conductivity of Bruch's membrane. Invest Ophthalmol Vis Sci 1995;36(7):1290–1297.
24. Garcia-Arumi J, Corcostegui B, Cavero L, Sararols L. The role of vitreoretinal surgery in the treatment of posttraumatic macular hole. Retina 1997;17(5):372–377.
25. Bird AC, Bressler NM, Bressler SB, et al. An international classification and grading system for age-related maculopathy and age-related macular degeneration. The International ARM Epidemiological Study Group. Surv Ophthalmol 1995;39(5):367–374.

26. Subfoveal neovascular lesions in age-related macular degeneration. Guidelines for evaluation and treatment in the macular photocoagulation study. Macular Photocoagulation Study Group. Arch Ophthalmol 1991;109(9):1242–1257 .
27. Gass JD. Serous retinal pigment epithelial detachment with a notch. A sign of occult choroidal neovascularization. Retina 1984;4(4):205–220.
28. Yannuzzi LA, Slakter JS, Sorenson JA, et al. Digital indocyanine green videoangiography and choroidal neovascularization. Retina 1992;12(3):191–223.
29. Staurenghi G, Orzalesi N, La Capria A, Aschero M. Laser treatment of feeder vessels in subfoveal choroidal neovascular membranes: a revisitation using dynamic indocyanine green angiography. Ophthalmology 1998;105(12):2297–2305.
30. Flower RW. Optimizing treatment of choroidal neovascularization feeder vessels associated with age-related macular degeneration. Am J Ophthalmol 2002;134(2):228–239.
31. Flower RW. Experimental studies of indocyanine green dye-enhanced photocoagulation of choroidal neovascularization feeder vessels. Am J Ophthalmol 2000;129(4):501–512.
32. Hee MR, Baumal CR, Puliafito CA, et al. Optical coherence tomography of age-related macular degeneration and choroidal neovascularization. Ophthalmology 1996;103(8):1260–1270.
33. Rohrschneider K, Bultmann S, Kruse FE, Volcker HE. Functional changes measured with SLO in idiopathic macular holes and in macular changes secondary to premacular fibrosis. Function in macular holes. Int Ophthalmol 2001;24(4):177–184.
34. Friberg TR, Musch DC, Lim JI, et al. Prophylactic treatment of age-related macular degeneration report number 1: 810–nanometer laser to eyes with drusen. Unilaterally eligible patients. Ophthalmology 2006;113(4):622 e1.
35. Pulido JS. Multicenter prospective, randomized, double-masked, placebo-controlled study of Rheopheresis to treat nonexudative age-related macular degeneration: interim analysis. Trans Am Ophthalmol Soc 2002;100:85–106; discussion 7.
36. Eckardt C, Eckardt U. Macular translocation in nonexudative age-related macular degeneration. Retina 2002;22(6):786–794.
37. Benner JD, Sunness JS, Ziegler MD, Soltanian J. Limited macular translocation for atrophic maculopathy. Arch Ophthalmol 2002;120(5):586–591.
38. Argon laser photocoagulation for neovascular maculopathy. Five-year results from randomized clinical trials. Macular Photocoagulation Study Group. Arch Ophthalmol 1991;109(8): 1109–1114.
39. Laser photocoagulation of subfoveal neovascular lesions of age-related macular degeneration. Updated findings from two clinical trials. Macular Photocoagulation Study Group. Arch Ophthalmol 1993;111(9):1200–1209.
40. Laser photocoagulation for juxtafoveal choroidal neovascularization. Five-year results from randomized clinical trials. Macular Photocoagulation Study Group. Arch Ophthalmol 1994;112(4):500–509.
41. Krypton laser photocoagulation for neovascular lesions of age-related macular degeneration. Results of a randomized clinical trial. Macular Photocoagulation Study Group. Arch Ophthalmol 1990;108(6):816–824.
42. Laser photocoagulation of subfoveal neovascular lesions in age-related macular degeneration. Results of a randomized clinical trial. Macular Photocoagulation Study Group. Arch Ophthalmol 1991;109(9):1220–1231.
43. Persistent and recurrent neovascularization after krypton laser photocoagulation for neovascular lesions of age-related macular degeneration. Macular Photocoagulation Study Group. Arch Ophthalmol 1990;108(6):825–831.
44. Persistent and recurrent neovascularization after laser photocoagulation for subfoveal choroidal neovascularization of age-related macular degeneration. Macular Photocoagulation Study Group. Arch Ophthalmol 1994;112(4):489–499.
45. Wu L, Murphy RP. Photodynamic therapy: a new approach to the treatment of choroidal neovascularization secondary to age-related macular degeneration. Curr Opin Ophthalmol 1999;10(3):217–220.
46. Lanzetta P, Michieletto P, Pirracchio A, Bandello F. Early vascular changes induced by transpupillary thermotherapy of choroidal neovascularization. Ophthalmology 2002;109(6):1098–1104.
47. Reichel E, Musch D, Blodi B, et al. Results From the TTT4CNV Clinical Trial. Invest Ophthalmol Vis Sci 2005;46:E-Abstract 2311.
48. Shiraga F, Ojima Y, Matsuo T, et al. Feeder vessel photocoagulation of subfoveal choroidal neovascularization secondary to age-related macular degeneration. Ophthalmology 1998;105(4):662–669.
49. Desatnik H, Treister G, Alhalel A, et al. ICGA-guided laser photocoagulation of feeder vessels of choroidal neovascular membranes in age-related macular degeneration. Indocyanine green angiography. Retina 2000;20(2):143–150.
50. Coscas F, Stanescu D, Coscas G, Soubrane G. [Feeder vessel treatment of choroidal neovascularization in age-related macular degeneration]. J Fr Ophthalmol 2003;26(6):602–608.
51. Hart PM, Chakravarthy U, Mackenzie G, et al. Visual outcomes in the subfoveal radiotherapy study: a randomized controlled trial of teletherapy for age-related macular degeneration. Arch Ophthalmol 2002;120(8):1029–1038.
52. Spaide RF, Guyer DR, McCormick B, et al. External beam radiation therapy for choroidal neovascularization. Ophthalmology 1998;105(1):24–30.
53. Gragoudas ES, Adamis AP, Cunningham ET Jr, et al. Pegaptanib for neovascular age-related macular degeneration. N Engl J Med 2004;351(27):2805–2816.
54. Rosenfeld PJ, Brown DM, Heier JS, et al. Ranibizumab for neovascular age-related macular degeneration. N Engl J Med 2006;355(14):1419–1431.
55. Brown DM, Kaiser PK, Michels M, et al. Ranibizumab versus verteporfin for neovascular age-related macular degeneration. N Engl J Med 2006;355(14):1432–1444.
56. Avery RL, Pieramici DJ, Rabena MD, et al. Intravitreal bevacizumab (Avastin) for neovascular age-related macular degeneration. Ophthalmology 2006;113(3):363–372 e5.
57. Bashshur ZF, Bazarbachi A, Schakal A, et al. Intravitreal bevacizumab for the management of choroidal neovascularization in age-related macular degeneration. Am J Ophthalmol 2006;142(1):1–9.
58. Rasmussen H, Chu KW, Campochiaro P, et al. Clinical protocol. An open-label, phase I, single administration, dose-escalation study of ADGVPEDF.11D (ADPEDF) in neovascular age-related macular degeneration (AMD). Hum Gene Ther 2001;12(16):2029–2032.
59. Thomas MA, Kaplan HJ. Surgical removal of subfoveal neovascularization in the presumed ocular histoplasmosis syndrome. Am J Ophthalmol 1991;111(1):1–7.
60. Hawkins BS, Bressler NM, Miskala PH, et al. Surgery for subfoveal choroidal neovascularization in age-related macular

degeneration: ophthalmic findings: SST report no. 11. Ophthalmology 2004;111(11):1967–1980.
61. Lai JC, Lapolice DJ, Stinnett SS, et al. Visual outcomes following macular translocation with 360–degree peripheral retinectomy. Arch Ophthalmol 2002;120(10):1317–1324.
62. Gass JD, Agarwal A, Lavina AM, Tawansy KA. Focal inner retinal hemorrhages in patients with drusen: an early sign of occult choroidal neovascularization and chorioretinal anastomosis. Retina 2003;23(6):741–751.
63. Caskey PJ, Folk JC. Retinal revascularization following laser photocoagulation treatment for choroidal neovascular membranes. Arch Ophthalmol 1988;106(11):1528–1532.
64. Yannuzzi LA, Negrao S, Iida T, et al. Retinal angiomatous proliferation in age-related macular degeneration. Retina 2001;21(5):416–434.
65. Brancato R, Introini U, Pierro L, et al. Optical coherence tomography (OCT) in retinal angiomatous proliferation (RAP). Eur J Ophthalmol 2002;12(6):467–472.
66. Axer-Siegel R, Bourla D, Priel E, et al. Angiographic and flow patterns of retinal choroidal anastomoses in age-related macular degeneration with occult choroidal neovascularization. Ophthalmology 2002;109(9):1726–1736.
67. Fernandes LH, Freund KB, Yannuzzi LA, et al. The nature of focal areas of hyperfluorescence or hot spots imaged with indocyanine green angiography. Retina 2002;22(5):557–568.
68. Kuhn D, Meunier I, Soubrane G, Coscas G. Imaging of chorioretinal anastomoses in vascularized retinal pigment epithelium detachments. Arch Ophthalmol 1995;113(11):1392–1398.
69. Hartnett ME, Weiter JJ, Garsd A, Jalkh AE. Classification of retinal pigment epithelial detachments associated with drusen. Graefes Arch Clin Exp Ophthalmol 1992;230(1):11–19.
70. Borrillo JL, Sivalingam A, Martidis A, Federman JL. Surgical ablation of retinal angiomatous proliferation. Arch Ophthalmol 2003;121(4):558–561.
71. Ciardella AP, Donsoff IM, Huang SJ, Costa DL, Yannuzzi LA. Polypoidal choroidal vasculopathy. Surv Ophthalmol 2004;49(1):25–37.
72. Iijima H, Iida T, Imai M, et al. Optical coherence tomography of orange-red subretinal lesions in eyes with idiopathic polypoidal choroidal vasculopathy. Am J Ophthalmol 2000;129(1):21–26.
73. Giovannini A, Amato GP, D'Altobrando E, Giuliani M. Optical coherence tomography (OCT) in idiopathic polypoidal choroidal vasculopathy (IPCV). Doc Ophthalmol 1999;97(3–4):367–371.
74. Otsuji T, Takahashi K, Fukushima I, Uyama M. Optical coherence tomographic findings of idiopathic polypoidal choroidal vasculopathy. Ophthalmic Surg Lasers 2000;31(3):210–214.
75. Curtin BJ. Physiologic vs pathologic myopia: genetics vs environment. Ophthalmology 1979;86(5):681–691.
76. Ohno-Matsui K, Ito M, Tokoro T. Subretinal bleeding without choroidal neovascularization in pathologic myopia. A sign of new lacquer crack formation. Retina 1996;16(3):196–202.
77. Avila MP, Weiter JJ, Jalkh AE, et al. Natural history of choroidal neovascularization in degenerative myopia. Ophthalmology 1984;91(12):1573–1581.
78. Hotchkiss ML, Fine SL. Pathologic myopia and choroidal neovascularization. Am J Ophthalmol 1981;91(2):177–183.
79. Miller DG, Singerman LJ. Natural history of choroidal neovascularization in high myopia. Curr Opin Ophthalmol 2001;12(3):222–224.
80. Quaranta M, Arnold J, Coscas G, et al. Indocyanine green angiographic features of pathologic myopia. Am J Ophthalmol 1996;122(5):663–671.
81. Costa RA, Calucci D, Teixeira LF, et al. Selective occlusion of subfoveal choroidal neovascularization in pathologic myopia using a new technique of ingrowth site treatment. Am J Ophthalmol 2003;135(6):857–866.
82. Baba T, Ohno-Matsui K, Yoshida T, et al. Optical coherence tomography of choroidal neovascularization in high myopia. Acta Ophthalmol Scand 2002;80(1):82–87.
83. Ruiz-Moreno JM, Montero JA. Long-term visual acuity after argon green laser photocoagulation of juxtafoveal choroidal neovascularization in highly myopic eyes. Eur J Ophthalmol 2002;12(2):117–122.
84. Tano Y. Pathologic myopia: where are we now? Am J Ophthalmol 2002;134(5):645–660.
85. Hamelin N, Glacet-Bernard A, Brindeau C, et al. Surgical treatment of subfoveal neovascularization in myopia: macular translocation vs surgical removal. Am J Ophthalmol 2002;133(4):530–536.
86. Bottoni F, Perego E, Airaghi P, et al. Surgical removal of subfoveal choroidal neovascular membranes in high myopia. Graefes Arch Clin Exp Ophthalmol 1999;237(7):573–582.
87. Khalil MK. Histopathology of presumed ocular histoplasmosis. Am J Ophthalmol 1982;94(3):369–376.
88. Gass JDM. Presumed Ocular Histoplasmosis Syndrome (POHS). In: Stereoscopic Atlas of Macular Diseases: Diagnosis and Treatment, vol 1. St. Louis: Mosby, 1997 .
89. Five-year follow-up of fellow eyes of individuals with ocular histoplasmosis and unilateral extrafoveal or juxtafoveal choroidal neovascularization. Macular Photocoagulation Study Group. Arch Ophthalmol 1996;114(6):677–688.
90. Laser photocoagulation for neovascular lesions nasal to the fovea. Results from clinical trials for lesions secondary to ocular histoplasmosis or idiopathic causes. Macular Photocoagulation Study Group. Arch Ophthalmol 1995;113(1):56–61.
91. Lisch W. Follow-up study of X-linked retinoschisis. Graefes Arch Clin Exp Ophthalmol 1991;229(5):497.
92. Saperstein DA, Rosenfeld PJ, Bressler NM, et al. Photodynamic therapy of subfoveal choroidal neovascularization with verteporfin in the ocular histoplasmosis syndrome: one-year results of an uncontrolled, prospective case series. Ophthalmology 2002;109(8):1499–1505.
93. Martidis A, Miller DG, Ciulla TA, et al. Corticosteroids as an antiangiogenic agent for histoplasmosis-related subfoveal choroidal neovascularization. J Ocul Pharmacol Ther 1999;15(5):425–428.
94. Schlaegel TF Jr. Corticosteroids in the treatment of ocular histoplasmosis. Int Ophthalmol Clin 1983;23(2):111–123.
95. Hawkins BS, Bressler NM, Bressler SB, et al. Surgical removal vs observation for subfoveal choroidal neovascularization, either associated with the ocular histoplasmosis syndrome or idiopathic: I. Ophthalmic findings from a randomized clinical trial: Submacular Surgery Trials (SST) Group H Trial: SST Report No. 9. Arch Ophthalmol 2004;122(11):1597–1611.
96. Argon laser photocoagulation for idiopathic neovascularization. Results of a randomized clinical trial. Arch Ophthalmol 1983;101(9):1358–1361.
97. Ho AC, Yannuzzi LA, Pisicano K, DeRosa J. The natural history of idiopathic subfoveal choroidal neovascularization. Ophthalmology 1995;102(5):782–789.
98. Shiraga F, Shiragami C, Matsuo T, et al. Identification of ingrowth site of idiopathic subfoveal choroidal neovascularization by indocyanine green angiography. Ophthalmology 2000;107(3):600–607.

99. Fukuchi T, Takahashi K, Ida H, et al. Staging of idiopathic choroidal neovascularization by optical coherence tomography. Graefes Arch Clin Exp Ophthalmol 2001;239(6):424–429.
100. Chan WM, Lam DS, Wong TH, et al. Photodynamic therapy with verteporfin for subfoveal idiopathic choroidal neovascularization: one-year results from a prospective case series. Ophthalmology 2003;110(12):2395–2402.
101. Aguilar JP, Green WR. Choroidal rupture. A histopathologic study of 47 cases. Retina 1984;4(4):269–275.
102. Fuller B, Gitter KA. Traumatic choroidal rupture with late serous detachment of macula. Report of successful argon laser treatment. Arch Ophthalmol 1973;89(4):354–355.
103. Gross JG, King LP, de Juan E Jr, Powers T. Subfoveal neovascular membrane removal in patients with traumatic choroidal rupture. Ophthalmology 1996;103(4):579–585.
104. Conrath J, Forzano O, Ridings B. Photodynamic therapy for subfoveal CNV complicating traumatic choroidal rupture. Eye 2004;18:946–947.
105. Nettleship E. Peculiar lines in the choroid in a case of postpaillitic atrophy. Trans Ophthalmol Soc U K 1883–1884;4:167–168.
106. Cangemi FE, Trempe CL, Walsh JB. Choroidal folds. Am J Ophthalmol 1978;86(3):380–387.
107. Newell FW. Choroidal folds. The seventh Harry Searls Gradle Memorial lecture. Am J Ophthalmol 1973;75(6):930–942.
108. Haruyama M, Yuzawa M, Kawamura A, et al. Indocyanine green angiographic findings of chorioretinal folds. Jpn J Ophthalmol 2001;45(3):293–300.
109. Singh G. Choroidal folds in posterior scleritis. Arch Ophthalmol 1989;107(2):168–169.
110. Augsburger JJ, Coats TD, Lauritzen K. Localized suprachoroidal hematomas. Ophthalmoscopic features, fluorescein angiography, and clinical course. Arch Ophthalmol 1990;108(7):968–972.
111. Norton EWD. A characteristic angiographic pattern in choroidal folds. Proc R Soc Med 1969;62:119–128.
112. Discin J, Maguire AM, Margherio RR. Choroidal folds induced with diode endolaser. Arch Ophthalmol 1992;110(6):754.
113. Gass JDM. Chorioretinal folds. In: Stereoscopic Atlas of Macular Diseases: Diagnosis and Treatment, vol 1, 4th ed. St. Louis: Mosby, 1997 .
114. Hussain D, Gass JD. Idiopathic central serous chorioretinopathy. Indian J Ophthalmol 1998;46(3):131–137.
115. Spaide RF, Hall L, Haas A, et al. Indocyanine green videoangiography of older patients with central serous chorioretinopathy. Retina 1996;16(3):203–213.
116. Guyer DR, Yannuzzi LA, Slakter JS, et al. Digital indocyanine green videoangiography of central serous chorioretinopathy. Arch Ophthalmol 1994;112(8):1057–1062.
117. Bouzas EA, Karadimas P, Pournaras CJ. Central serous chorioretinopathy and glucocorticoids. Surv Ophthalmol 2002;47(5):431–448.
118. Shimizu K, Tobari I. Central serous retinopathy dynamics of subretinal fluid. Mod Probl Ophthalmol 1971;9:152–157.
119. Prunte C, Flammer J. Choroidal capillary and venous congestion in central serous chorioretinopathy. Am J Ophthalmol 1996;121(1):26–34.
120. Gilbert CM, Owens SL, Smith PD, Fine SL. Long-term follow-up of central serous chorioretinopathy. Br J Ophthalmol 1984;68(11):815–820.
121. Ficker L, Vafidis G, While A, Leaver P. Long-term follow-up of a prospective trial of argon laser photocoagulation in the treatment of central serous retinopathy. Br J Ophthalmol 1988;72(11):829–834.
122. Jalkh AE, Jabbour N, Avila MP, et al. Retinal pigment epithelium decompensation. II. Laser treatment. Ophthalmology 1984;91(12):1549–1553.
123. Yannuzzi LA, Shakin JL, Fisher YL, Altomonte MA. Peripheral retinal detachments and retinal pigment epithelial atrophic tracts secondary to central serous pigment epitheliopathy. Ophthalmology 1984;91(12):1554–1572.
124. Poulson AV, Snead DR, Jacobs PM, et al. Intraocular surgery for optic nerve disorders. Eye 2004;18(11):1056–1065.
125. Krivoy D, Gentile R, Liebmann JM, et al. Imaging congenital optic disc pits and associated maculopathy using optical coherence tomography. Arch Ophthalmol 1996;114(2):165–170.
126. Ho AC, Guyer DR, Fine SL. Macular hole. Surv Ophthalmol 1998;42(5):393–416.
127. Pournaras CJ, Donati G, Brazitikos PD, et al. Macular epiretinal membranes. Semin Ophthalmol 2000;15(2):100–107.
128. Fish RH, Anand R, Izbrand DJ. Macular pseudoholes. Clinical features and accuracy of diagnosis. Ophthalmology 1992;99(11):1665–1670.
129. Klein BR, Hiner CJ, Glaser BM, et al. Fundus photographic and fluorescein angiographic characteristics of pseudoholes of the macula in eyes with epiretinal membranes. Ophthalmology 1995;102(5):768–774.
130. Wilkins JR, Puliafito CA, Hee MR, et al. Characterization of epiretinal membranes using optical coherence tomography. Ophthalmology 1996;103(12):2142–2151.
131. Azzolini C, Patelli F, Codenotti M, et al. Optical coherence tomography in idiopathic epiretinal macular membrane surgery. Eur J Ophthalmol 1999;9(3):206–211.
132. Irvine SR. A newly defined vitreous syndrome following cataract surgery. Am J Ophthalmol 1953;36:599–619.
133. Lobes LA, Jr., Grand MG. Incidence of cystoid macular edema following scleral buckling procedure. Arch Ophthalmol 1980;98(7):1230–1232.
134. Meredith TA, Reeser FH, Topping TM, Aaberg TM. Cystoid macular edema after retinal detachment surgery. Ophthalmology 1980;87(11):1090–1095.
135. Kramer SG. Penetrating keratoplasty combined with extracapsular cataract extraction. Am J Ophthalmol 1985;100(1):129–133.
136. Melamed S, Neumann D, Blumenthal M. Trabeculectomy with anterior vitrectomy in aphakic and pseudophakic glaucoma. Int Ophthalmol 1991;15(3):157–162.
137. Lotufo DG. Postoperative complications and visual loss following Molteno implantation. Ophthalmic Surg 1991;22(11):650–656.
138. Steinert RF, Puliafito CA, Kumar SR, et al. Cystoid macular edema, retinal detachment, and glaucoma after Nd:YAG laser posterior capsulotomy. Am J Ophthalmol 1991;112(4):373–380.
139. Johnson SH, Kratz RP, Olson PF. Clinical experience with the Nd:YAG laser. J Am Intraocul Implant Soc 1984;10(4):452–460.
140. Bukelman A, Abrahami S, Oliver M, Pollack A. Cystoid macular oedema following neodymium:YAG laser capsulotomy a prospective study. Eye 1992;6(Pt 1):35–38.
141. Fung WE. Vitrectomy for chronic aphakic cystoid macular edema. Results of a national, collaborative, prospective, randomized investigation. Ophthalmology 1985;92(8):1102–1111.

142. Gass JD, Norton EW. Cystoid macular edema and papilledema following cataract extraction. A fluorescein fundoscopic and angiographic study. Arch Ophthalmol 1966;76(5):646–661.
143. Wolfensberger TJ, Herbort CP. Treatment of cystoid macular edema with non-steroidal anti-inflammatory drugs and corticosteroids. Doc Ophthalmol 1999;97(3–4):381–386.
144. Wolfensberger TJ. The role of carbonic anhydrase inhibitors in the management of macular edema. Doc Ophthalmol 1999;97(3–4):387–397.
145. Tchah H, Rosenberg M, Larson RS, Lindstrom RL. Neodymium: YAG laser vitreolysis for treatment and prophylaxis of cystoid macular oedema. Aust N Z J Ophthalmol 1989;17(2):179–183.
146. Alpar JJ. The role of 1% sodium hyaluronate in treating vitreous incarceration with the neodymium:YAG laser in patients with corneal decompensation. J Cataract Refract Surg 1986;12(5):502–506.
147. Alpar JJ. Experiences with the neodymium: YAG laser: interruption of anterior hyaloid membrane of the vitreous and cystoid macular edema. Ophthalmic Surg 1986;17(3):157–165.
148. Fung WE. The national, prospective, randomized vitrectomy study for chronic aphakic cystoid macular edema. Progress report and comparison between the control and nonrandomized groups. Surv Ophthalmol 1984;28(suppl):569–575.
149. Fung WE. Anterior vitrectomy for chronic aphakic cystoid macular edema. Ophthalmology 1980;87(3):189–193.
150. Fung WE. Surgical therapy for chronic aphakic cystoid macular edema. Ophthalmology 1982;89(8):898–901.
151. Adams JE. Case showing peculiar changes in the macula. Trans Ophthalmol Soc U K 1883;3:113–114.
152. Best F. Ueber eine hereditäire Maculaaffecktion. Ztschr F Augenh 1905;13:199–212.
153. Seddon JM, Sharma S, Chong S, et al. Phenotype and genotype correlations in two best families. Ophthalmology 2003;110(9):1724–1731.
154. Fishman GA, Baca W, Alexander KR, et al. Visual acuity in patients with best vitelliform macular dystrophy. Ophthalmology 1993;100(11):1665–1670.
155. Mohler CW, Fine SL. Long-term evaluation of patients with Best's vitelliform dystrophy. Ophthalmology 1981;88(7): 688–692.
156. O'Gorman S, Flaherty WA, Fishman GA, Berson EL. Histopathologic findings in Best's vitelliform macular dystrophy. Arch Ophthalmol 1988;106(9):1261–1268.
157. Andrade RE, Farah ME, Costa RA. Photodynamic therapy with verteporfin for subfoveal choroidal neovascularization in best disease. Am J Ophthalmol 2003;136(6):1179–1181.
158. Stargardt K. Über amiliare, progressive degeneration in der makulagegend des auges. Graefes Arch Ophthalmol 1909;71:534–550.
159. Souied EH, Ducroq D, Gerber S, et al. Age-related macular degeneration in grandparents of patients with Stargardt disease: genetic study. Am J Ophthalmol 1999;128(2):173–178.
160. Donoso LA, Edwards AO, Frost A, et al. Autosomal dominant Stargardt-like macular dystrophy. Surv Ophthalmol 2001;46(2):149–163.
161. Molday LL, Rabin AR, Molday RS. ABCR expression in foveal cone photoreceptors and its role in Stargardt macular dystrophy. Nat Genet 2000;25(3):257–258.
162. Weleber RG. Stargardt's macular dystrophy. Arch Ophthalmol 1994;112(6):752–754.
163. Armstrong JD, Meyer D, Xu S, Elfervig JL. Long-term follow-up of Stargardt's disease and fundus flavimaculatus. Ophthalmology 1998;105(3):448–457; discussion 57–58.
164. Fishman GA, Farber M, Patel BS, Derlacki DJ. Visual acuity loss in patients with Stargardt's macular dystrophy. Ophthalmology 1987;94(7):809–814.
165. Eagle RC Jr, Lucier AC, Bernardino VB Jr, Yanoff M. Retinal pigment epithelial abnormalities in fundus flavimaculatus: a light and electron microscopic study. Ophthalmology 1980;87(12):1189–1200.
166. Birnbach CD, Jarvelainen M, Possin DE, Milam AH. Histopathology and immunocytochemistry of the neurosensory retina in fundus flavimaculatus. Ophthalmology 1994;101(7):1211–1219.
167. Wroblewski JJ, Gitter KA, Cohen G, Schomaker K. Indocyanine green angiography in Stargardt's flavimaculatus. Am J Ophthalmol 1995;120(2):208–218.
168. Gass JD. A clinicopathologic study of a peculiar foveomacular dystrophy. Trans Am Ophthalmol Soc 1974;72:139–156.
169. Yang Z, Lin W, Moshfeghi DM, et al. A novel mutation in the RDS/peripherin gene causes adult-onset foveomacular dystrophy. Am J Ophthalmol 2003;135(2):213–218.
170. Zhang K, Garibaldi DC, Li Y, et al. Butterfly-shaped pattern dystrophy: a genetic, clinical, and histopathological report. Arch Ophthalmol 2002;120(4):485–490.
171. Lim JI, Enger C, Fine SL. Foveomacular dystrophy. Am J Ophthalmol 1994;117(1):1–6.
172. Vine AK, Schatz H. Adult-onset foveomacular pigment epithelial dystrophy. Am J Ophthalmol 1980;89(5):680–691.
173. Brecher R, Bird AC. Adult vitelliform macular dystrophy. Eye 1990;4(pt 1):210–215.
174. Deutman AF, van Blommestein JD, Henkes HE, et al. Butterfly-shaped pigment dystrophy of the fovea. Arch Ophthalmol 1970;83(5): 558–569.
175. Gutman I, Walsh JB, Henkind P. Vitelliform macular dystrophy and butterfly-shaped epithelial dystrophy: a continuum? Br J Ophthalmol 1982;66(3):170–173.
176. Mejia JR, Gieser RG. Sporadic butterfly macular dystrophy. Ann Ophthalmol 1981;13(11):1253–1254.
177. Deutman AF, Rumke AM. Reticular dystrophy of the retinal pigment epithelium. Dystrophia reticularis laminae pigmentosa retinae of H. Sjogren. Arch Ophthalmol 1969;82(1):4–9.
178. Chopdar A. Reticular dystrophy of retina. Br J Ophthalmol 1976;60(5):342–344.
179. Fishman GA, Woolf MB, Goldberg MF, Busse B. Reticular tapeto-retinal dystrophy. As a possible late stage of Sjogren's reticular dystrophy. Br J Ophthalmol 1976;60(1):35–40.
180. Marmor MF, Byers B. Pattern dystrophy of the pigment epithelium. Am J Ophthalmol 1977;84(1):32–44.
181. O'Donnell FE, Schatz H, Reid P, Green WR. Autosomal dominant dystrophy of the retinal pigment epithelium. Arch Ophthalmol 1979;97(4):680–683.
182. Battaglia Parodi M, Iustulin D, Russo D, Ravalico G. Adult-onset foveomacular vitelliform dystrophy and indocyanine green videoangiography. Graefes Arch Clin Exp Ophthalmol 1996;234(3):208–211.

183. Pierro L, Tremolada G, Introini U, et al. Optical coherence tomography findings in adult-onset foveomacular vitelliform dystrophy. Am J Ophthalmol 2002;134(5):675–680.
184. Sanfilippo P, Troutbeck R, Vandeleur K, Lenton L. Optical coherence tomography of adult-onset fovemacular vitelliform dystrophy. Clin Experiment Ophthalmol 2004;32(1):114–118.
185. Benhamou N, Messas-Kaplan A, Cohen Y, et al. Adult-onset foveomacular vitelliform dystrophy with OCT 3. Am J Ophthalmol 2004;138(2):294–296.
186. Cruz-Villegas V, Villate N, Knighton RW, et al. Optical coherence tomographic findings in acute exudative polymorphous vitelliform maculopathy. Am J Ophthalmol 2003;136(4):760–763.
187. Ghazi NG. Adult-onset foveomacular vitelliform dystrophy: a study by optical coherence tomography. Am J Ophthalmol 2003;136(5):962–964; author reply 4.
188. Hayami M, Decock C, Brabant P, et al. Optical coherence tomography of adult-onset vitelliform dystrophy. Bull Soc Belge Ophtalmol 2003(289):53–61.
189. Battaglia Parodi M, Da Pozzo S, Ravalico G. Photodynamic therapy for choroidal neovascularization associated with pattern dystrophy. Retina 2003;23(2):171–176.
190. Tantri A, Vrabec TR, Cu-Unjieng A, et al. X-linked retinoschisis: a clinical and molecular genetic review. Surv Ophthalmol 2004;49(2):214–230.

5
Angiography of Retinal Vascular Diseases

Lihteh Wu, Andrea Porras, Raquel Benavides, David G. Zeballos,
and J. Fernando Arevalo

The optical properties of the eye make the ocular fundus the only location in the human body where direct noninvasive monitoring of vascular flow is possible. During fluorescein angiography (FA) and indocyanine green videoangiography (ICGV), a rapid sequence of serial photographs taken after the intravenous administration of fluorescein or indocyanine green (ICG) is used to visualize and document choroidal and retinal blood flow. Other than blood flow, FA and ICGV provide information about the integrity of the blood–retinal barriers and the fine details of the retinal pigment epithelium (RPE), and provide a glimpse of associated systemic pathology. Although both technologies reveal important and different aspects of retinal and choroidal diseases, some phases of various diseases are best seen with FA and other aspects are best revealed with ICGV.

This chapter reviews several vascular pathologies of the retina including diabetic retinopathy (DR), retinal vascular occlusions, retinal arterial macroaneurysms, radiation retinopathy, ocular ischemic syndrome, hypertensive retinopathy, Coats' disease, parafoveal telangiectasia, sickle cell retinopathy, and Eales' disease.

Diabetic Retinopathy

Currently we are facing a worldwide epidemic of diabetes mellitus (DM). In the year 2000, more than 176 million people throughout the world suffered from DM. The World Health Organization has estimated that by the year 2030 there will be 370 million people affected with DM in the world, and every one of them will be at risk of developing retinopathy. The degree and duration of hyperglycemia, as well as hypertension and hyperlipidemia are risk factors that increase the severity and development of diabetic retinopathy (DR).[1–4]

The first report of DR, specifically diabetic macular edema (DME), appeared in 1856.[5,6] Prior to the advent of panretinal photocoagulation, proliferative diabetic retinopathy (PDR) was the main culprit of diabetic blindness. Since the development of laser photocoagulation, DME has become the most common cause of visual loss in diabetic patients in the developed world. It is estimated that in the United States alone there are 500,000 patients with DME, with 95,000 new cases every year.[7–9]

Pathogenesis

Hyperglycemia, by a poorly understood mechanism, causes leukostasis, which leads to endothelial dysfunction and progressive retinal ischemia.[10] In fact, DR is the prototype for the ischemic retinopathies where ongoing retinal ischemia causes upregulation of vascular endothelial growth factor (VEGF).[11] Diabetic macular edema is characterized by the accumulation of intraretinal fluid, which is modulated by the balance between oncotic and hydrostatic pressures as described by Starling's law.[12] Vascular endothelial growth factor, also known as vascular permeability factor (VPF), plays a central role in the pathogenesis of DME.[13–15] Disruption of the blood–retinal barrier, which results in an increase of vascular permeability, is caused by VEGF. As the intraocular levels of VEGF increase, its angiogenic properties promote retinal neovascularization and its sequelae.[14]

Classification

Although the modified Airlie House Classification used in the Early Treatment of Diabetic Retinopathy Study (ETDRS) is considered to be the gold standard classification scheme for DR, most ophthalmologists and even retinal specialists shun its use in their daily clinical work. It is an excellent tool in the research setting but its clinical applicability is limited due to its complexity.

At the 2002 joint meeting of the American Academy of Ophthalmology and the Pan-American Association of Ophthalmology, a new classification was unveiled: the International Clinical Diabetic Retinopathy Disease Severity Scale,

which is based on the findings of the Wisconsin Epidemiologic Study of Diabetic Retinopathy and the ETDRS. It consists of five levels: no DR, mild nonproliferative diabetic retinopathy (NPDR), moderate NPDR, severe NPDR, and PDR. In addition, the presence or absence of macular edema should be noted. If edema is present, then one should note if the edema involves the center (severe DME), threatens the center (moderate DME), or is far from the center (mild DME) (Fig. 5.1).[16]

Mild NPDR consists solely of microaneurysms. The findings in moderate NPDR fall in between mild and severe NPDR. The diagnosis of severe NPDR is based on the 4:2:1 rule of the ETDRS. One can easily diagnose severe NPDR by mentally dividing the fundus into four quadrants centered on the optic nerve and examining the four midperipheral quadrants with slit-lamp biomicroscopy. If hemorrhages of at least the magnitude of standard photograph Figure 5.2A are present in all four quadrants, then by definition severe NPDR is present. If two quadrants or more have venous beading of the same magnitude or greater than standard photograph Figure 5.2B, then by definition severe NPDR is present. If one or more quadrant has intraretinal microvascular abnormalities (IRMAs) of the same magnitude or greater than standard photograph Figure 5.2C, then by definition severe NPDR is present (Fig. 5.2).

Clinical Findings

Diabetic retinopathy represents a spectrum of disease that can be broadly divided into a nonproliferative stage and a proliferative stage. The first clinical sign of NPDR is the appearance of microaneurysms. With increasing severity, intraretinal hemorrhages start to appear. These hemorrhages may be flame shaped or round dot blots. If the retinal ischemia persists, cotton-wool spots, venous beading, tortuosity of the retinal veins, and IRMAs will develop.

As the degree of ischemia increases, PDR develops (Figs. 5.3 and 5.4). It is characterized by all the prior in addition to neovascular and fibrovascular proliferation. It may appear at the disc (neovascularization of the disc [NVD]) or at the junction of perfused and nonperfused retina (neovascularization elsewhere [NVE]). Partial posterior vitreous detachment caused tangential and anteroposterior traction that leads to vitreous hemorrhage, rhegmatogenous, and tractional retinal detachment.

Diabetic macular edema may be present at any stage of DR and may be focal or diffuse. In the focal type, usually there are microaneurysms surrounded by a ring of hard exudates (Fig. 5.5). In the diffuse type, usually there are no hard exudates or microaneurysms. In a small number of eyes, one may observe a glistening, taut, and thickened posterior hyaloid that exerts vitreomacular traction.[17]

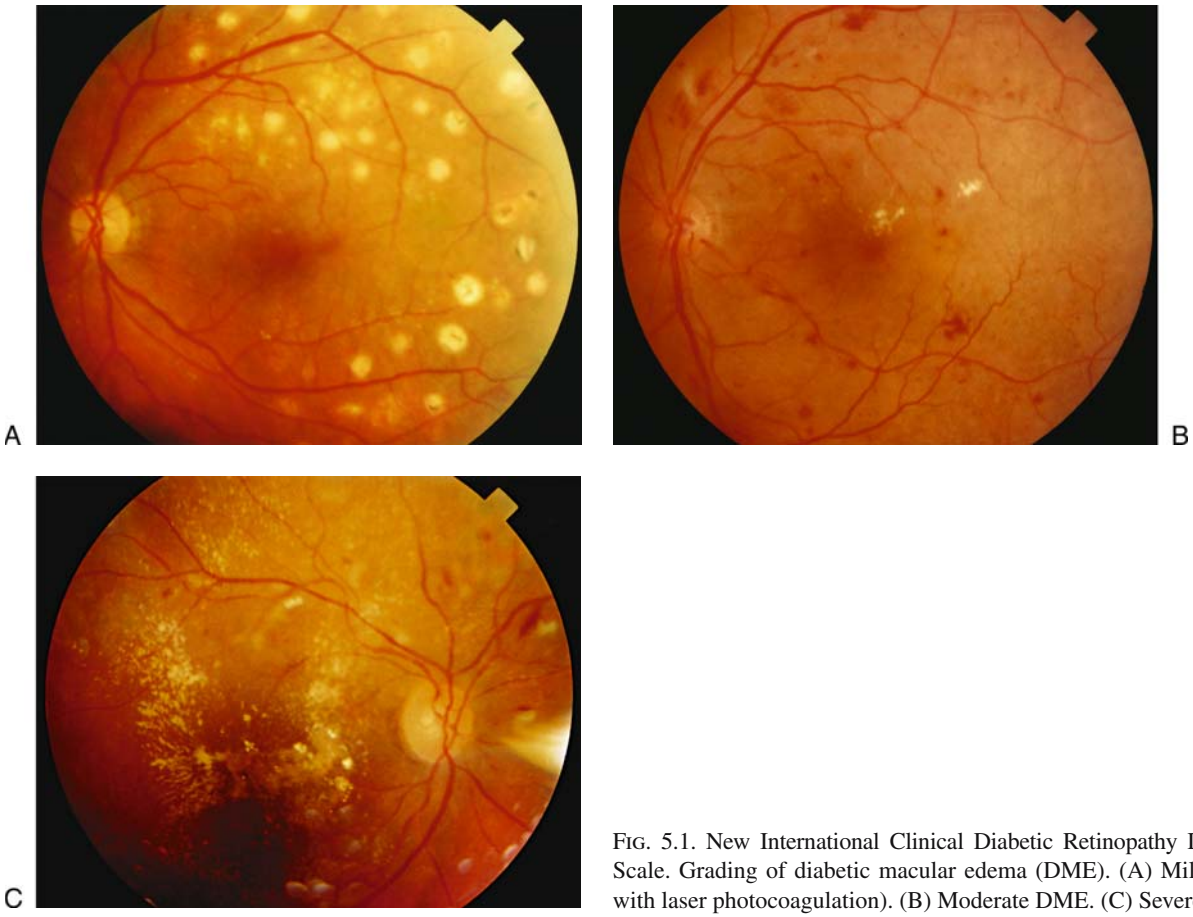

Fig. 5.1. New International Clinical Diabetic Retinopathy Disease Severity Scale. Grading of diabetic macular edema (DME). (A) Mild DME (treated with laser photocoagulation). (B) Moderate DME. (C) Severe DME.

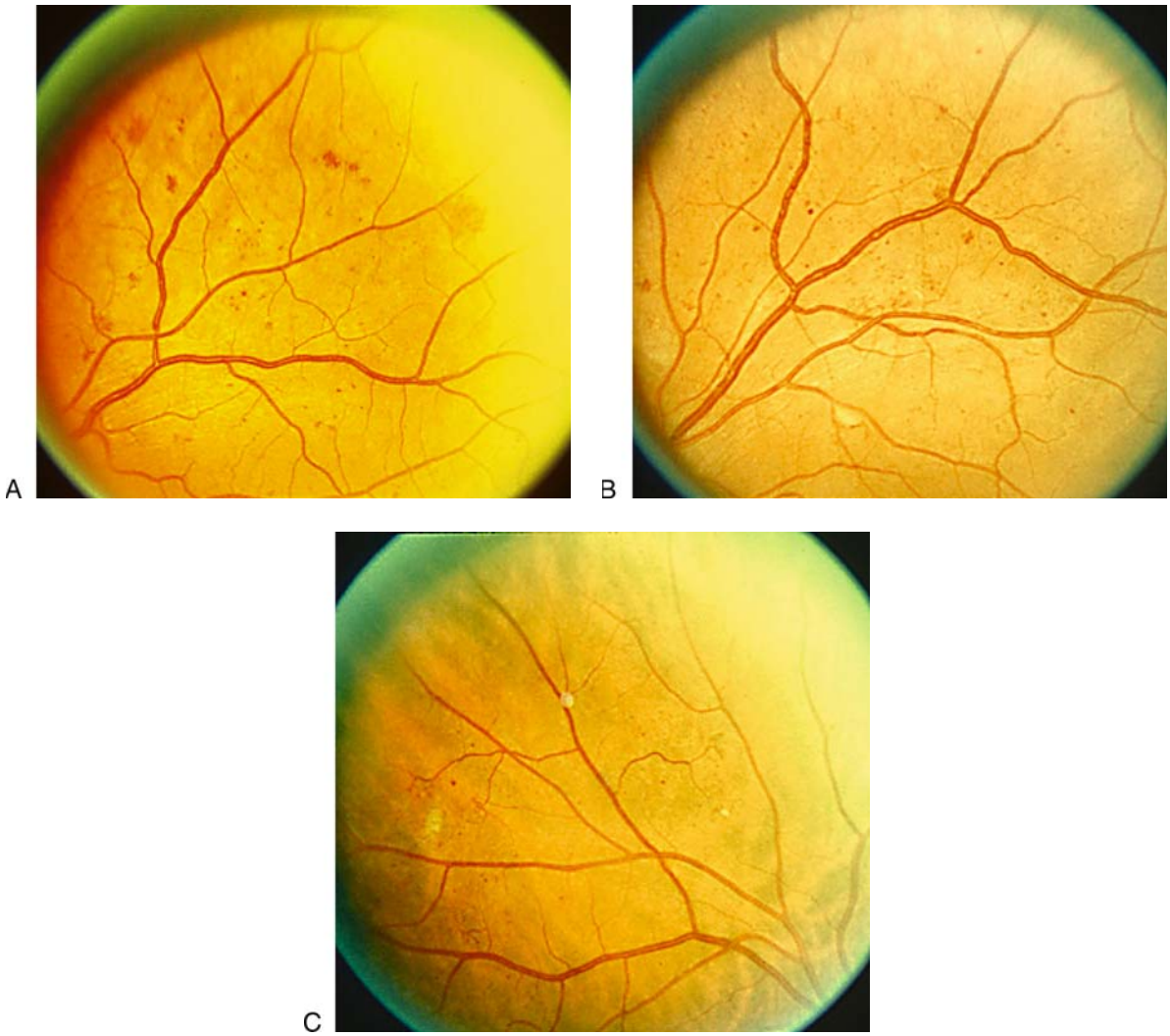

FIG. 5.2. Clinical determination of severe nonproliferative diabetic retinopathy (NPDR). (A) If hemorrhages of at least the magnitude of this standard photograph are present in all four quadrants, then by definition severe NPDR is present. (B) If two quadrants or more have venous beading of the same magnitude or greater than this standard photograph, then by definition severe NPDR is present. (C) If one or more quadrant has intraretinal microvascular abnormality (IRMA) of the same magnitude or greater than this standard photograph, then by definition severe NPDR is present. (Reprinted with permission from the Fundus Photograph Reading Center, Department of Ophthalmology and Visual Sciences, University of Wisconsin, Madison, WI.)

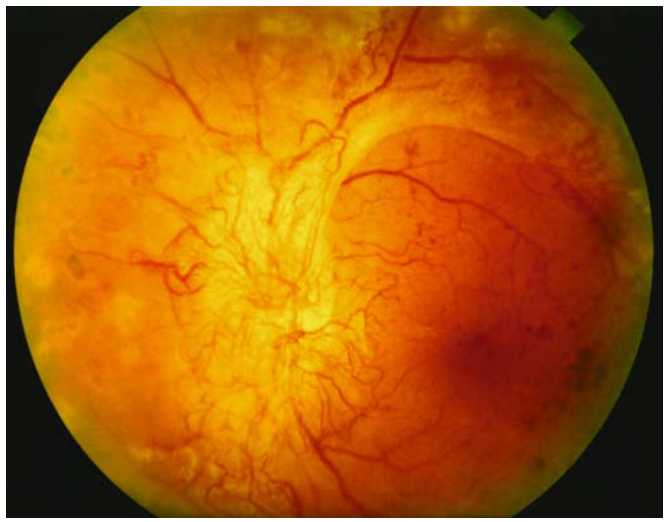

FIG. 5.3. Proliferative diabetic retinopathy. Neovascularization of the disc (NVD).

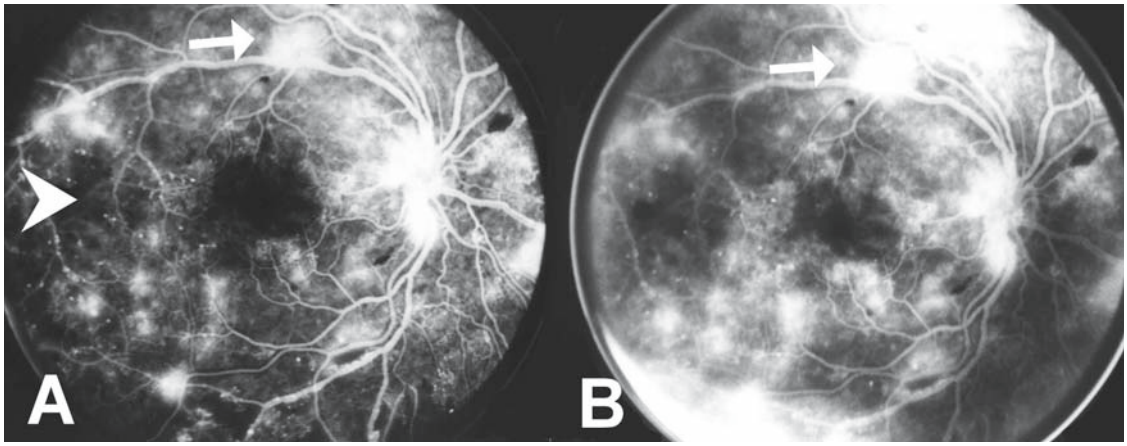

Fig. 5.4. Fluorescein angiography (FA) in proliferative diabetic retinopathy demonstrating neovascularization elsewhere (NVE). (A) Microaneurysms appear as pinpoint hyperfluorescent lesions, and capillary nonperfusion is seen as hypofluorescent zones (arrowhead). (B) Fluorescein angiography shows the sequence of leakage from a patch of neovascularization superior to the optic disc (arrows in A and B).

Fluorescein Angiography

Microaneurysms appear as pinpoint hyperfluorescent lesions that fade in the later phases of the angiogram. The hypofluorescence of dot and blot hemorrhages distinguishes them from the hyperfluorescent microaneurysms. Areas of capillary nonperfusion are seen as homogeneous dark patches.

Neovascularization usually occurs at the border of perfused and nonperfused retina. Prior to the appearance of frank neovascularization, IRMA develops. The angiographic appearance of IRMA is of collateral vessels that do not leak. On the other hand, neovascularization is characterized by hyperfluorescent leaking areas that increase in size and intensity as the study progresses (Figs. 5.4 and 5.6).

The earliest change in diabetics is an increased vascular permeability, which is seen as late hyperfluorescence emanating from the retinal vessels (Fig. 5.7). If the macula is not clinically edematous, this hyperfluorescence should not be interpreted as macular edema.

Optical Coherence Tomography

Optical coherence tomography (OCT) has come to revolutionize the management of macular diseases because it can objectively measure retinal thickness, which correlates better with visual acuity rather than fluorescein leakage.[18] Normal foveal thickness as measured by OCT has been reported to be 152 ± 21 μm.[19] Diabetic macular edema is imaged as a zone of low reflectivity in the outer retinal layers. The low reflectivity is due to the accumulation of intraretinal fluid.

Treatment

Laser Photocoagulation

The ETDRS showed that panretinal photocoagulation reduces the risk of severe visual loss in eyes with high-risk characteristics

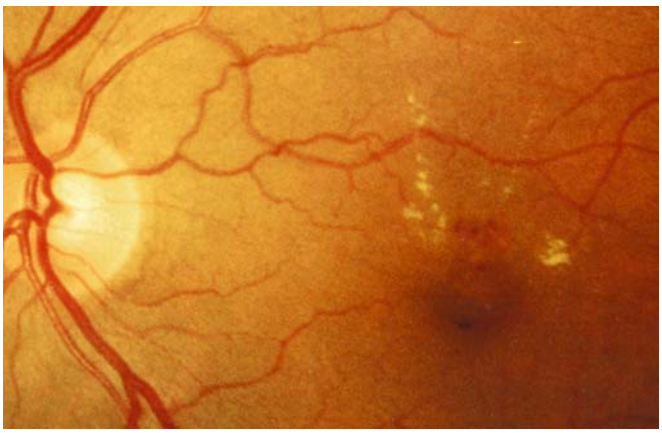

Fig. 5.5. Diabetic macular edema (DME). Focal DME threatening the fovea in an eye with mild NPDR. Notice the hard exudates and the microaneurysms.

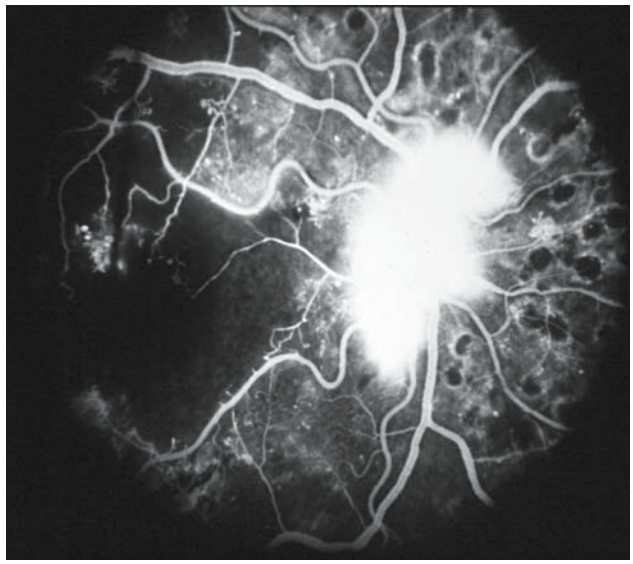

Fig. 5.6. Fluorescein leakage from neovascularization. Late-phase fluorescein angiogram shows leakage from a patch of NVE superior to the optic disc.

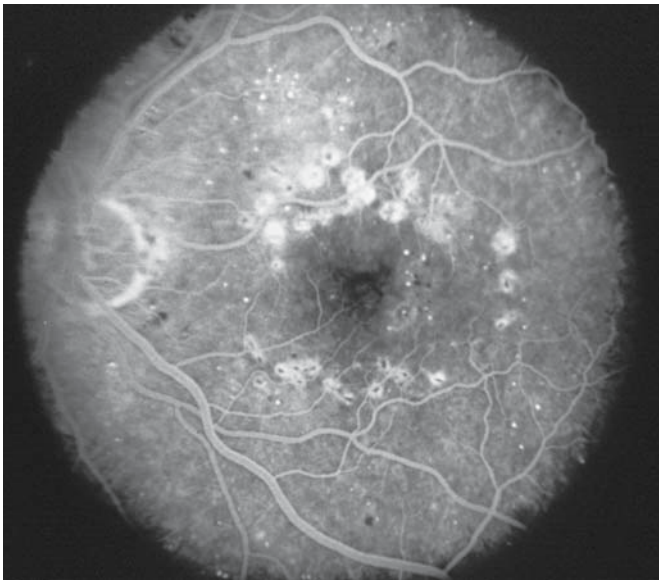

FIG. 5.7. Diabetic macular edema. FA frame shows laser scars in a circular pattern around the fovea.

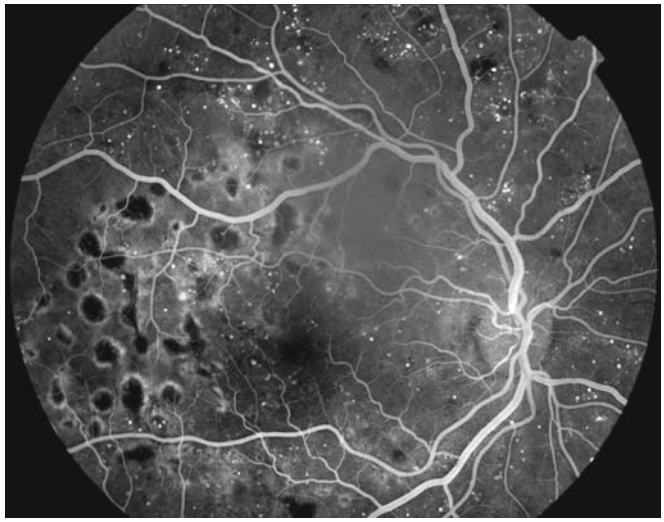

FIG. 5.9. Expansion of the chorioretinal scars with time. Three years prior to this photograph, the patient underwent focal photocoagulation for DME. Notice how some of the laser scars (original laser spot size 75 μm) have expanded and coalesced.

by 50% (Fig. 5.8).[20] The ETDRS has defined cotton-spot macular edema (CSME) as retinal thickening within 500 μm of the foveal center; hard exudates within 500 μm of the foveal center, if they are associated with adjacent retinal thickening; and retinal thickening of at least one disc area in size, with part of this thickening being within one disc area of the foveal center, and should be considered for focal or grid macular photocoagulation. In eyes with severe NPDR, similar results were seen.

Macular photocoagulation is a very safe procedure. Without a doubt, inadvertent foveal photocoagulation is a disaster. To avoid this complication, it is recommended that any eye with DME with distortion of the macular anatomy should be treated in two or more sessions. Iatrogenic breaks of Bruch's membrane secondary to small spot sizes have caused choroidal neovascular membranes. Thermal ablation has been tried with limited success.[21,22] The use of photodynamic therapy with verteporfin and submacular surgery have been described.[23,24] It has been reported that laser scar expansion occurs with time (Fig. 5.9). Thus laser scars can coalesce and lead to paracentral scotomas. Subretinal fibrosis is a fairly uncommon complication in DME. Although it has been reported that subretinal fibrosis is associated with the intensity of the burn and small spot sizes, the ETDRS has shown that the severity of hard exudates is the most common risk factor.[25]

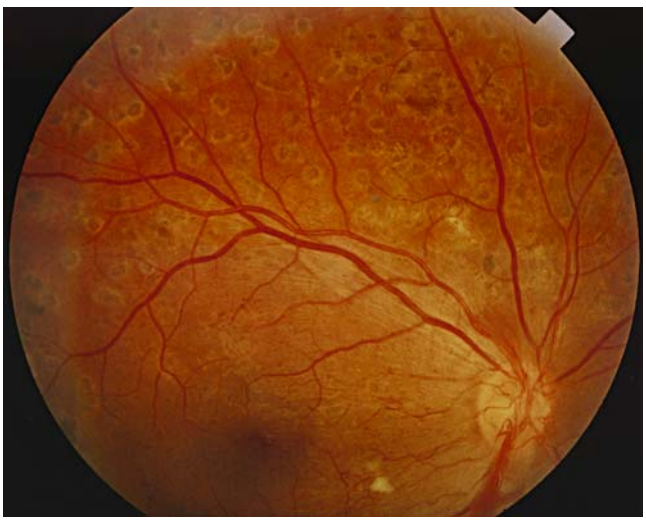

FIG. 5.8. Panphotocoagulation in an eye with neovascularization of the disc (NVD). Notice the chorioretinal scars outside the arcades.

Corticosteroids

Recently it has been shown that triamcinolone through its antipermeability properties secondary to its anti-VEGF effects strengthens the blood–retinal barrier and prevents its disruption.[26] Intravitreal injection of 4 to 25 mg of triamcinolone has been described in the literature. The most common dose is 4 mg since it is easy to aliquot and inject 0.1 cc from the commercially available 40-mg/mL vial.[27,28] Optical coherence tomography has documented reduction in macular thickness and normalization of the macular anatomy following an intravitreal injection of triamcinolone (Fig. 5.10). Many eyes show an improvement in visual acuity. Complications include the progression of nuclear sclerosis, increase of intraocular pressure,[29] retinal detachments, sterile endophthalmitis,[30] and infective endophthalmitis.[31]

Anti–Vascular Endothelial Growth Factor Agents

Since VEGF plays a major role in the pathogenesis of DME, anti-VEGF treatments have been proposed as an alternative treatment. The short-term functional and anatomic results

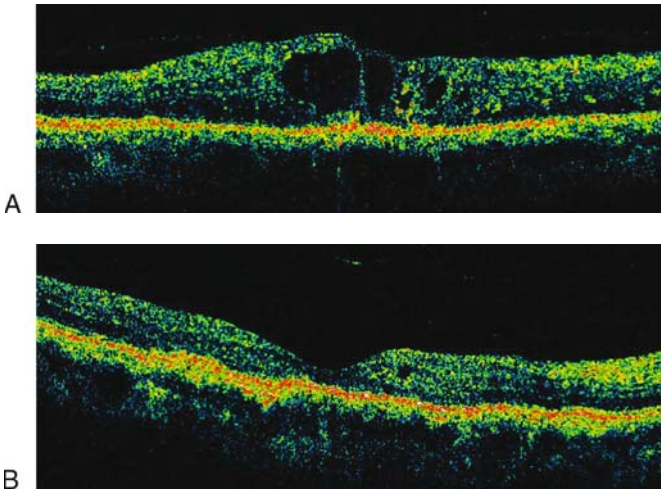

Fig. 5.10. Intravitreal triamcinolone. (A) Eye with DME refractory to laser treatment injected with 4 mg of intravitreal triamcinolone. (B) Optical coherence tomography (OCT) of the same eye 3 weeks following triamcinolone injection.

following an intravitreal injection of bevacizumab are very promising (Fig. 5.11).[32]

Vitrectomy

The development and refinement of vitreous surgery has also been shown to be beneficial in the treatment of eyes with advanced proliferative disease. The indications of vitrectomy in DR include nonclearing vitreous hemorrhage, tractional retinal detachment, combined tractional and rhegmatogenous retinal detachment, severe fibrovascular proliferation, and DME.[33] Optical coherence tomography has documented a subset of eyes with DME secondary to vitreomacular traction and foveal serous detachment. Vitrectomy in these eyes improves visual acuity significantly. Others have reported visual success in eyes with DME without any macular tractional component.[34]

Other Treatments

Several large prospective randomized clinical trials have shown that visual loss from DR can be avoided by macular photocoagulation, scatter photocoagulation, or vitreous surgery.[35] However, despite the findings and recommendations of these major clinical trials over the past few decades, diabetic retinopathy, especially DME remains an important cause of visual loss.

Central Retinal Vein Occlusion

Much confusion exists in the literature because central retinal vein occlusion (CRVO) and branch retinal vein occlusion (BRVO) often are clumped and studied together. But the natural history and complication rate for each entity is quite different. The treatments and their results vary from one condition to the other.

The first description of a CRVO was reported by Liebreich in 1854, but it was not until 1877 that von Michel correctly identified thrombosis as the cause of this condition. Histopathologic studies have shown thrombosis of the central retinal vein at the level of the lamina cribrosa.[36]

A survey from the Wilmer Eye Institute found that retinal vein occlusions (branch and central) were the second most common retinal vascular disorders after diabetic retinopathy. Epidemiologic studies have identified cardiovascular disease, diabetes mellitus, age over 55 years, and hypertension as important associations with CRVO.[37,38]

Clinical Findings

The most common symptom is a sudden loss of central vision. Some patients may complain of transient obscurations of vision that last from a few seconds to minutes. Patients with neovascular glaucoma (NVG) complain of ocular pain and redness.

Acutely, CRVOs are characterized by some degree of dilation and tortuosity of the retinal veins. Intraretinal hemorrhages are seen in all four quadrants. The severity of these hemorrhages varies from a few scattered superficial hemorrhages to extensive full retinal thickness hemorrhages with breakthrough into the vitreous cavity. Patches of cotton-wool spots may be seen. The optic nerve is usually swollen (Fig. 5.12). Vitreous hemorrhage is occasionally seen.

In the chronic stages, the hemorrhages may have disappeared. Optic nerve head collaterals and macular edema may be the only residual ophthalmoscopic evidence that a prior CRVO had occurred.

One of the two major complications resulting from CRVO is macular edema (Fig. 5.13). Macular edema results from diffuse capillary leakage. Chronic macular edema may lead to epiretinal membrane formation, cystoid degeneration, and pigmentary degeneration.

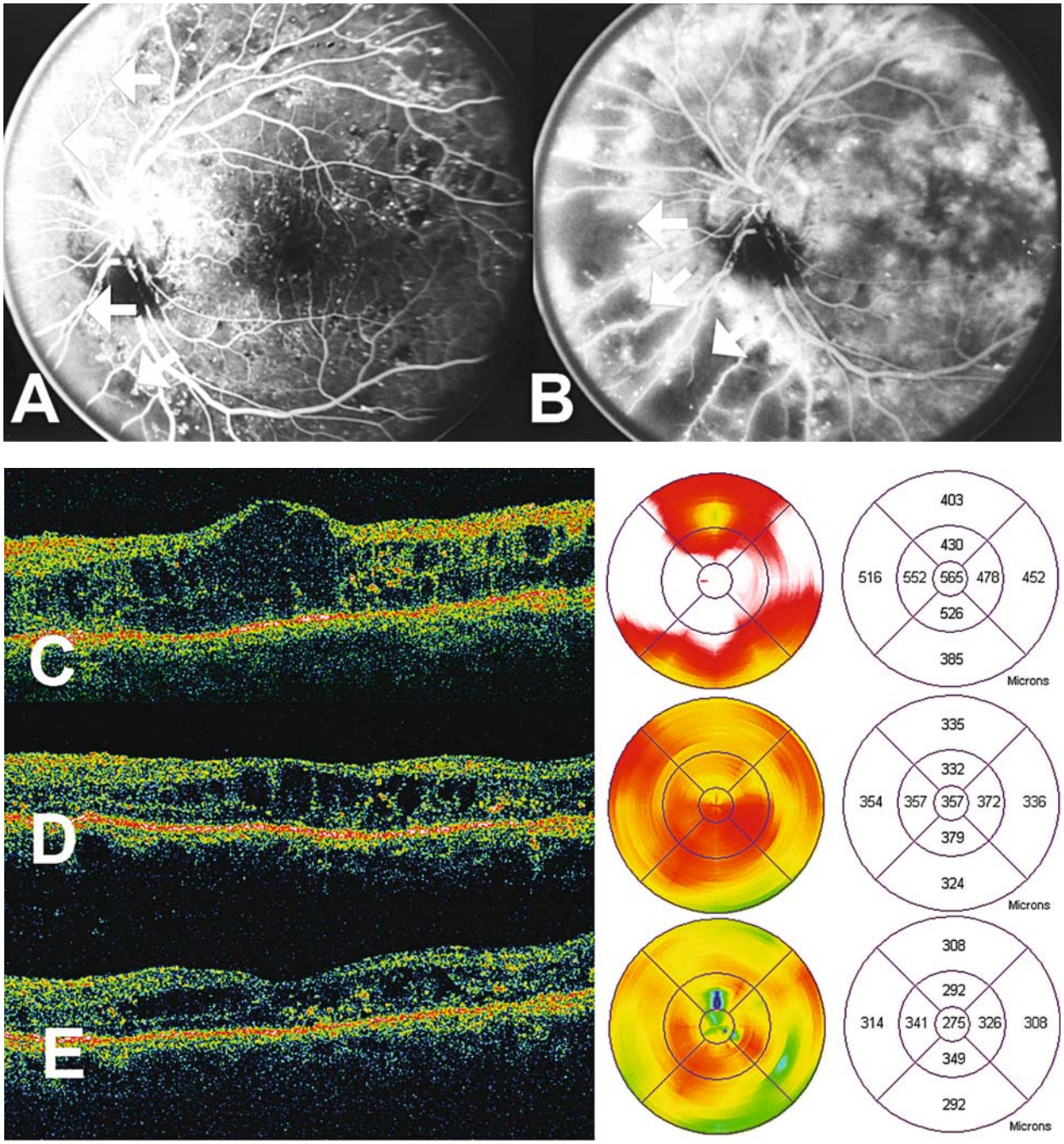

FIG. 5.11. A 78-year-old woman with a history of diabetic retinopathy complained of decreased vision in her left eye. Her visual acuity in this eye was 20/200. Retinal examination showed dot and blot hemorrhages throughout the posterior pole in addition to increased retinal thickness. (A) Early-phase fluorescein angiogram (FA) revealed presence of perifoveal dots of hyperfluorescence consistent with microaneurysms. In addition, nasal nonperfusion is demonstrated (arrows). (B) Late-phase FA showed leakage consistent with macular edema. In addition, nasal nonperfusion is again demonstrated (arrows). (C) A horizontal optical coherence tomography (OCT) scan obtained through the fovea revealed loss of the normal foveal contour, diffuse macular thickening, and areas of low intraretinal reflectivity consistent with intraretinal cysts and fluid accumulation. The retinal map analysis revealed a foveal thickness of 565 μm. The patient underwent an intravitreal injection of bevacizumab at a dose of 2.5 mg in this eye. (D) One week after the injection, an OCT scan showed that the foveal thickness had decreased to 357 μm. (E) One month after the injection the cystic spaces had resolved almost completely and her visual acuity (VA) improved to 20/80. The foveal thickness had decreased to 275 μm.

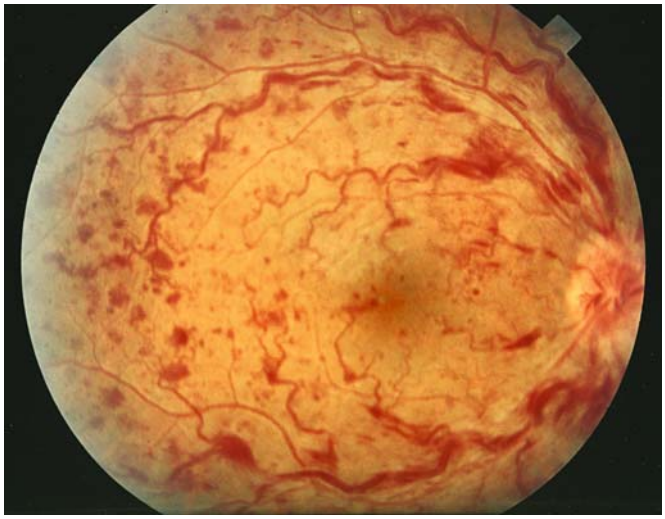

FIG. 5.12. Acute central retinal vein occlusion (CRVO). Notice the venous dilatation, tortuosity, swollen optic nerve, and the scattered intraretinal hemorrhages in all four quadrants.

The other major complication is intraocular neovascularization. It occurs more commonly in the anterior segment. It results from the secretion of angiogenic factors such as VEGF from areas of nonperfused retina.[39] Depending on the degree of capillary nonperfusion, CRVOs have often been classified in the literature as being perfused or nonperfused, incomplete or complete, and nonischemic or ischemic.

In the Central Vein Occlusion Study (CVOS), eyes were arbitrarily classified as nonperfused if the fluorescein angiogram revealed more than 10 disc areas of capillary nonperfusion. This differentiation is important because up to one third of nonperfused eyes in the CVOS developed anterior segment neovascularization. The greatest risk of developing neovascularization occurs in the first 7 months.[40] It is noteworthy that 15% of eyes initially classified as perfused became nonperfused after 4 months of follow-up. An additional 19% progressed to nonperfusion after 3 years of follow-up. The CVOS has recommended a monthly visit for the first 8 months where undilated slit-lamp examination of the pupillary border and gonioscopy are performed to detect early neovascularization in the anterior segment.

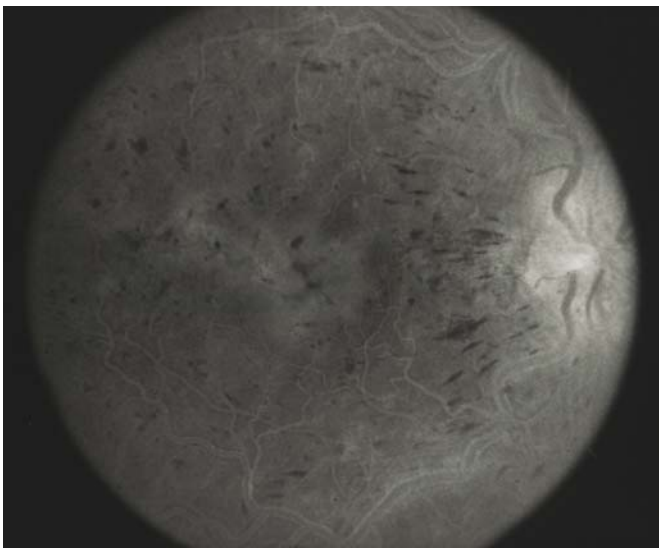

FIG. 5.13. A 66-year-old woman complains of decreased vision in the right eye for the past 6 weeks. Macular edema secondary to CRVO is the cause of her loss in vision. Late-phase fluorescein angiogram shows macular edema and staining of the retinal veins.

Fluorescein Angiography

The angiographic findings depend in great part on the ophthalmoscopic findings at the time of the FA. In all eyes there is a delay in the filling of the retinal circulation, with relatively normal choroidal filling. Blockage of the underlying retinal circulation and choroidal circulation may occur if extensive intraretinal hemorrhages are present. Invariably there is some degree of capillary nonperfusion. Fluorescein angiography is a useful ancillary test to help determine the perfusion characteristics of the eye (Fig. 5.14). Retinal capillary nonperfusion is an important precursor of intraocular neovascularization. It may range from minimal to extensive and serves as the basis of the classification of CRVO into perfused or nonperfused types. There is also some leakage from the optic nerve head secondary to disc edema.

Treatment

Laser Photocoagulation

The CVOS demonstrated that grid laser treatment was of no visual benefit in the treatment of macular edema despite the elimination of macular edema in those eyes that were treated. It also showed that the best strategy in nonperfused eyes was to delay panretinal photocoagulation until two clock hours of iris neovascularization or any angle neovascularization was observed.[41] Panretinal photocoagulation is effective in controlling anterior segment neovascularization (Fig. 5.15).

Chorioretinal Anastomosis

In an attempt to restore venous outflow, McAllister and Constable[42,43] have pioneered the creation of a chorioretinal anastomosis in order to bypass the occlusion in eyes with perfused CRVO. To successfully create a chorioretinal anastomosis, Bruch's membrane and the adjacent retinal vein must be ruptured with the argon and yttrium-aluminum-garnet (YAG) laser. Successful rupture of the vein is seen in about a third of cases treated with the argon laser. In those cases where the vein has not ruptured with the argon laser, a YAG laser is used to rupture the vein. Using the above sequential technique, a chorioretinal anastomosis can be created in 67% of cases.[44] Complications arising from this treatment include distal vein closure, fibrovascular proliferation, and vitreous hemorrhage.[45]

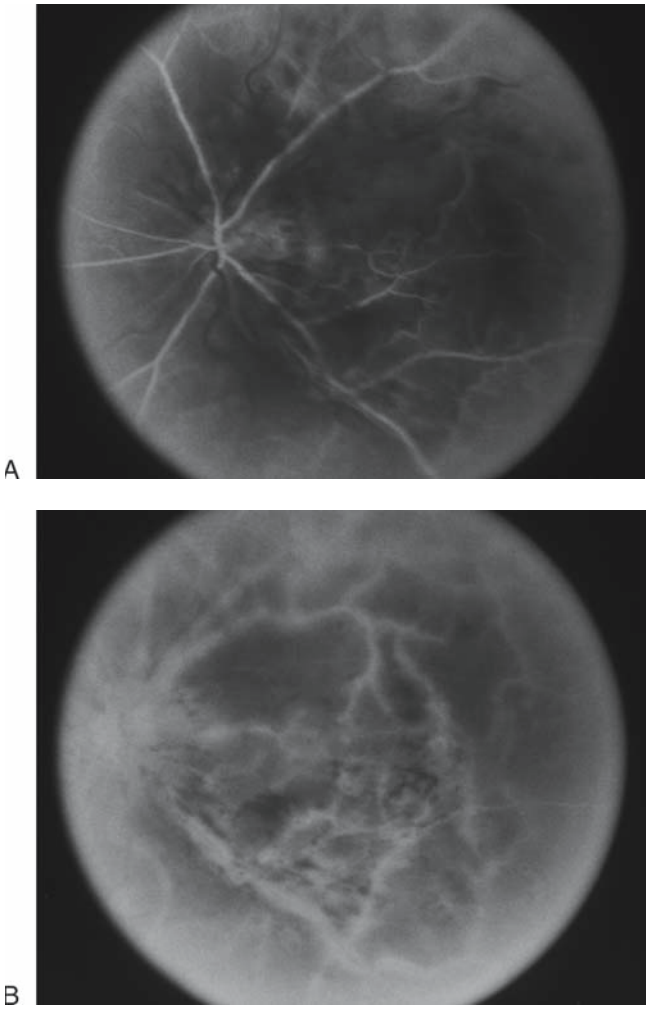

FIG. 5.14. A 76-year-old man complains of decreased vision in his left eye for a month. The visual acuity is 1/200. (A) Early-phase fluorescein angiogram shows delayed filling of the retinal veins. (B) Late-phase fluorescein angiogram shows perivenular leakage and severe capillary nonperfusion.

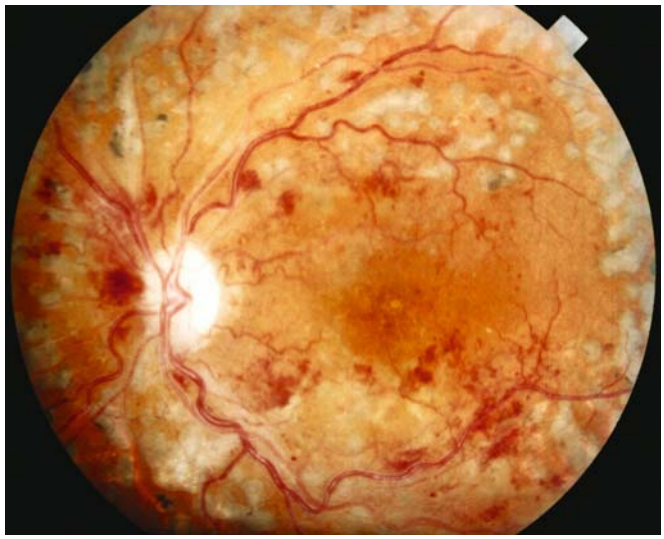

FIG. 5.15. A 55-year-old woman was diagnosed with neovascular glaucoma secondary to a CRVO of her left eye. She underwent prompt panretinal photocoagulation.

Intravitreal Triamcinolone

The combined effects of vascular damage and the secretion of VEGF lead to the formation of macular edema. Corticosteroids have been shown to downregulate VEGF expression and strengthen the blood–retinal barrier. [26] In patients with macular edema secondary to CRVO who have been injected with intravitreal triamcinolone, an increase in visual acuity with a concomitant reduction in macular thickness as measured by OCT has been reported (Fig. 5.16).[46]

Radial Optic Neurotomy

Some investigators have proposed that a CRVO results from a compartment syndrome at the level of the optic nerve. [47,48] They hypothesize that by decompressing the optic nerve, resolution of the CRVO may occur. More recently radial optic neurotomy (RON), which is an internal approach through a pars plana vitrectomy followed by a radial cut into the substance of the optic nerve, has been advocated to relieve this compartment syndrome. Some researchers think that perhaps a radial optic neurotomy works by creating a chorioretinal anastomosis rather than through decompression of a compartment syndrome.[49] RON may improve visual acuity (VA) in some eyes with CRVO but complications are common (Fig. 5.17). A large controlled prospective clinical trial is necessary to determine its role in the management of CRVO.

Thrombolytic Therapy

In an attempt to lyse the venous clot at the lamina cribrosa, systemic thrombolytic therapy with tissue plasminogen activator (t-PA) was used and found to be effective in a pilot study. Unfortunately, the complications from such treatment included a fatal stroke. In order to avoid such systemic complications, some investigators have injected t-PA intravitreally. [50]

FIG. 5.16. A 42-year-old woman with 20/100 vision in her right eye for 2 weeks (same patient as Fig. 5.12). Three months post–intravitreal injection of 4 mg of triamcinolone, macular edema and retinal hemorrhages have resolved. Vision has returned to 20/20.

Others have pursued cannulation of the retinal venous system followed by an injection of t-PA.[51]

Branch Retinal Vein Occlusion

Etiology

Anatomic, hypertensive, atherosclerotic, inflammatory, or thrombophilic conditions may lead to retinal endothelial vascular damage with subsequent intravascular thrombus formation. Inflammatory conditions that have been associated with a BRVO include sarcoidosis,[52] Lyme disease, and serpiginous choroiditis.[53] Thrombophilic conditions such as protein S deficiency, protein C deficiency, resistance to activated protein C (factor V Leiden), antithrombin III deficiency,[54] antiphospholipid antibody syndrome,[55] lupus erythematosus, and gammopathies have also been associated with BRVO.

Eyes with arteriovenous crossings appear to be at risk of developing BRVO.[56,57] In these eyes, the thick-walled artery is anterior to the thin-walled vein in most cases. In the presence of systemic vascular disease, the risk of occlusion may be accentuated when arteriolar sclerosis results in an increased rigidity of the crossing artery, which causes compression of the underlying vein. Turbulent flow results, which in turn damages the vascular endothelium, creating a local environment favorable to intravascular thrombus formation.

Symptoms

Most patients present complaining of a sudden onset of painless loss of vision. Another common symptom is a paracentral scotoma. Rarely, if the BRVO is located in the nasal half, the patient is asymptomatic.

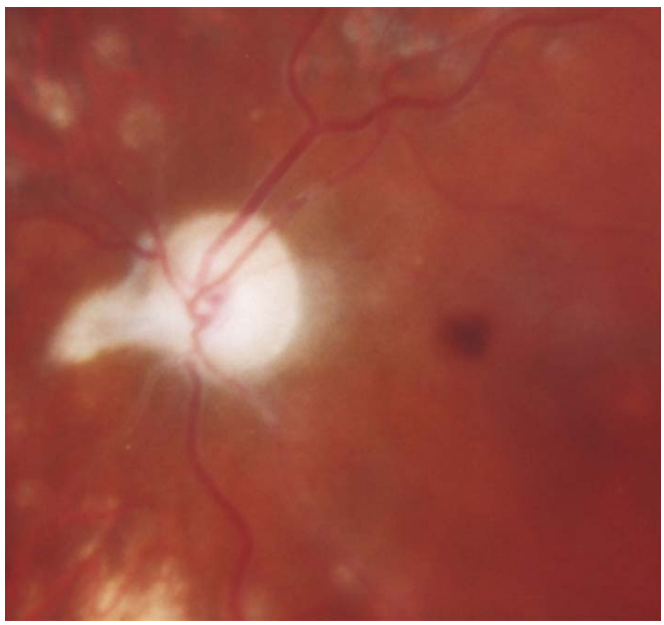

FIG. 5.17. Optic nerve atrophy 3 months after radial optic neurotomy for central retinal vein occlusion.

Clinical Findings

Leber first described the condition ophthalmoscopically in 1877.[37] Most occlusions occur in the superotemporal quadrant since most arteriovenous crossings occur in this location. During the acute phase, intraretinal hemorrhages (usually flame shaped), retinal edema, and cotton-wool spots are seen in the distribution of a retinal vessel (Fig. 5.18). Serous detachment of the macula may also be seen.[58] During the chronic stage, hemorrhages may be absent. Macular edema may be the only sign present. Telangiectatic vessels may extend across the horizontal raphe. The upstream side of the occlusion may become fibrotic. In certain eyes with large areas of nonperfusion, retinal neovascularization may be seen. Vitreous hemorrhage with tractional retinal detachments may ensue. Further traction may create retinal breaks, creating combined rhegmatogenous and tractional retinal detachments. Both NVG and NVD are rare events with BRVO.

Angiographic Findings: Fluorescein and Indocyanine Green

In the acute stage of a partial or complete venous occlusion the FA shows venous engorgement upstream of the crossing, resulting in ischemia, hemorrhage, and cotton-wool spot formation. If fluorescein angiography is performed when the intraretinal hemorrhages are still present, a hypofluorescent area corresponding to the blood will block both the retinal and choroidal circulations during the early phases. In the late phases, some leakage that results from the endothelial cell damage and the increased intracapillary pressure may be seen extending beyond the hemorrhages. Typical angiographic findings following clearing of the intraretinal hemorrhages include a prolonged retinal circulation time, perivenous staining in the obstructed area, evidence of capillary leakage, macular leakage consistent with cystoid macular edema (Fig. 5.19), areas of capillary nonperfusion, and in certain cases retinal neovascularization. These collaterals usually support enough flow to maintain some retinal function. It typically takes 6 to 24 months for the collaterals to mature and stabilize. Reduction of leakage and edema often results in an improvement in visual acuity, provided that no irreversible foveal damage has occurred.

Due to its fluorescence in the infrared, ICG penetrates blood much better than fluorescein. Even though ICG may be performed in the acute phase while the intraretinal hemorrhages are still present, [59] no one has been able to show that the information gathered from an ICGA is useful in the management of a BRVO.

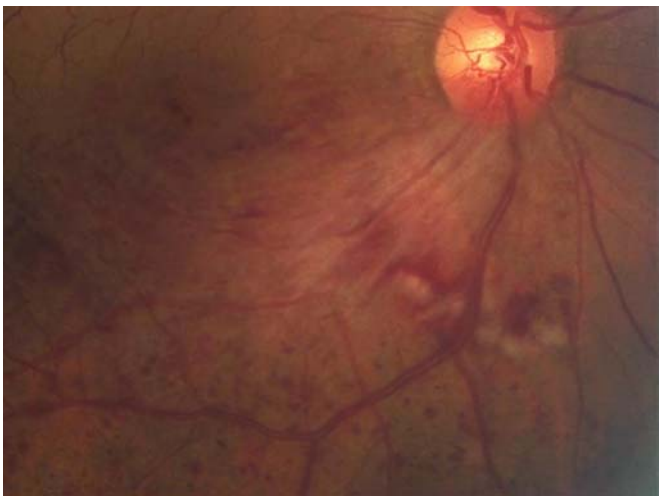

Fig. 5.18. A 55-year-old man with systemic hypertension noticed decreased vision in his right eye. He had a visual acuity of 20/400 and was diagnosed with an inferotemporal branch retinal vein occlusion (BRVO).

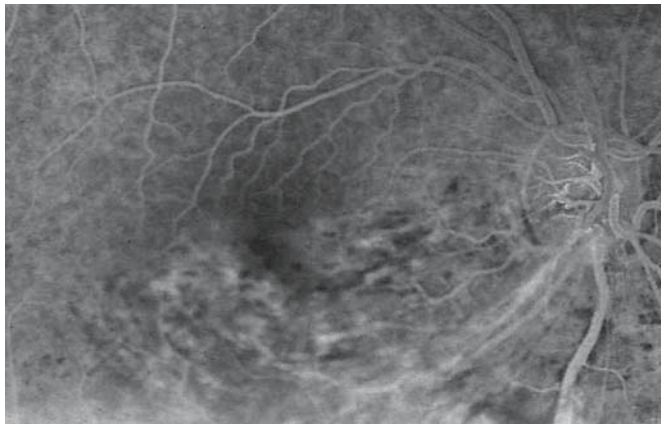

Fig. 5.19. Late-phase FA shows telangiectatic vessels and macular edema in the same patient as in Figure 5.18.

Optical Coherence Tomography

The benefits of studying macular thickness with regard to visual function as compared to fluorescein leakage has already been discussed and applies to BRVO as well.[60] Optical coherence tomography has been shown to be more sensitive than FA in demonstrating cystoid macular edema in eyes with BRVO. In addition, OCT documented the presence of serous retinal detachment and subretinal hemorrhage in eyes with BRVO where both ophthalmoscopy and FA failed to do so.[58]

Treatment

Medical treatment has not been shown to be effective in this condition nor in its complications. These complications include macular edema and the sequelae from retinal neovascularization (i.e., vitreous hemorrhage, tractional retinal detachment, epiretinal membrane formation, and NVG).[59]

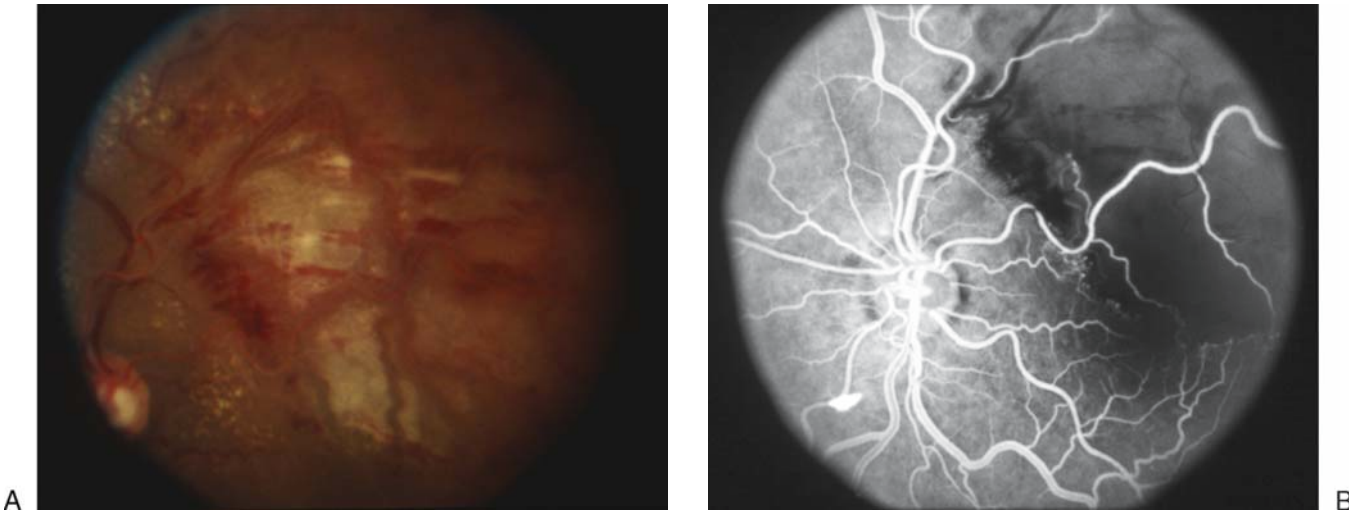

Fig. 5.20. A 60-year-old man with diabetes mellitus (DM) and systemic hypertension complained of decreased vision in his left eye for the past 3 months. He had developed a superotemporal BRVO and visual acuity was 5/200. (A) Color photograph shows involvement of the superotemporal quadrant with retinal edema, lipid exudation, and intraretinal hemorrhages. (B) Early frame of the FA shows large areas of capillary nonperfusion distal to the site of the occlusion.

Macular Grid Laser Photocoagulation

Macular grid laser photocoagulation has been shown to be effective in the treatment of macular edema in a prospective multicenter randomized clinical trial, the Branch Retinal Vein Occlusion Study (BVOS).[61] The current recommendation is to wait 3 months to see if spontaneous improvement in vision occurs. If no improvement is seen and the hemorrhages have mostly cleared from the macular area, an FA is obtained. Conversely, if macular ischemia is responsible for the loss of vision, laser photocoagulation should not be offered to the patient. If the FA shows leakage in the macular area that is responsible for the decrease in vision, a macular grid laser is recommended. After 3 years of follow-up care, 63% of laser-treated eyes improved two or more lines of vision compared to 36% of control eyes. But on average, eyes gained only 1.3 lines of visual acuity from baseline.[61] If the FA reveals macular nonperfusion, laser is not warranted and observation is recommended (Fig. 5.20).

Intravitreal Steroid Injection

Due to its potent antipermeability and antiinflammatory properties, intravitreal triamcinolone has recently been used to treat macular edema from different etiologies (Fig. 5.21).[62]

Scatter Photocoagulation

Neovascularization usually occurs at the border between the ischemic and nonischemic retina. Eyes with NVD are believed to have more extensive ischemia than those without NVD. According to the BVOS, approximately 40% of eyes with large areas of ischemia (more than five disc areas of nonperfusion) are at risk of developing neovascularization (Fig. 5.22).[63] Of the eyes that do develop neovascularization, 60% have a vitreous hemorrhage. The BVOS demonstrated that scatter photocoagulation reduces the prevalence of neovascularization by one half (from 40% to 20%). However, if one were to treat all eyes with nonperfusion, a large percentage of patients (60%) who would never develop neovascularization would be treated with scatter photocoagulation. Therefore, the recommendation is to wait until neovascularization actually develops before considering scatter photocoagulation.

Laser-Induced Chorioretinal Anastomosis

Bypass of the normal retinal venous drainage channels is attempted by creating a communication between the obstructed vessel and the choroid by literally blasting a hole through the RPE and choriocapillaris with a high-energy argon or YAG laser.[64] Complications from the procedure include tractional retinal detachment and vitreous hemorrhage.

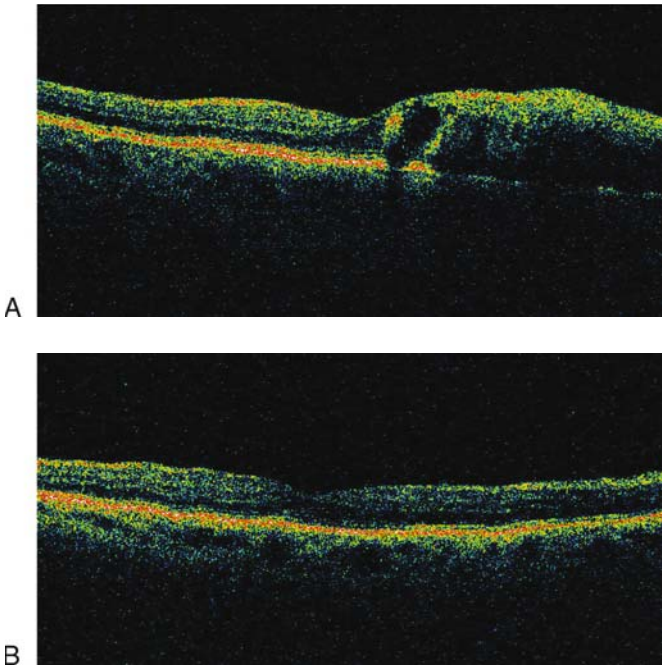

FIG. 5.21. A 55-year-old man with macular edema secondary to BRVO underwent intravitreal triamcinolone injection of 4 mg. (A) Preinjection OCT demonstrates macular edema. (B) Three weeks postinjection OCT shows normalization of the foveal anatomy.

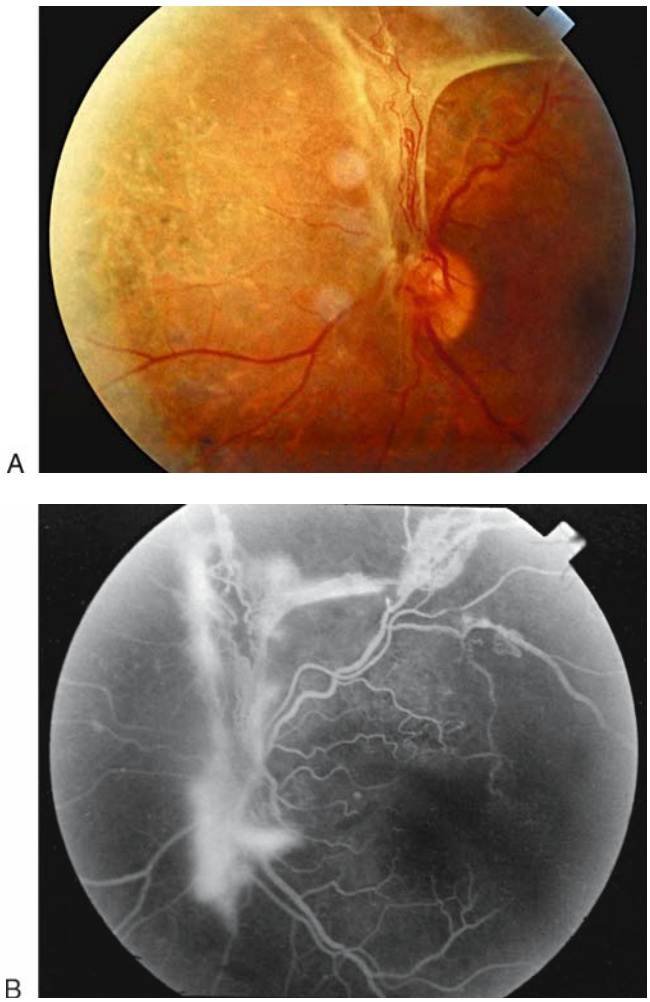

FIG. 5.22. A 65-year-old woman has visual acuity of 20/50 in her left eye. She was diagnosed with a superotemporal BRVO complicated by disc neovascularization and vitreous hemorrhage. She underwent prompt scatter photocoagulation. (A) Clinical photograph shows NVD and vitreoretinal traction. Notice the laser scars nasal to the disc. (B) Fluorescein angiogram shows leakage from the NVD.

Ocular Ischemic Syndrome

When the ipsilateral carotid artery has more than 90% stenosis,[65] the perfusion of the ipsilateral central retinal artery drops 50%. The ocular changes seen with this condition were initially described by Kearns and Hollenhorst[66] in 1963 with the name of venous stasis retinopathy.

Clinical Findings

The majority of patients complain of a gradual and progressive loss of vision. About 12% suffer a visual loss of sudden onset. Upon presentation 43% of eyes have a visual acuity between 20/20 and 20/50, while 37% have a visual acuity of counting fingers or worse. In up to 40% of cases, ocular pain is present.

Two thirds of eyes have rubeosis iridis at presentation. However, only about 50% of these eyes suffer from NVG. A cataract may develop as the disease progresses. The retinal arteries are narrow and the veins are dilated but do not show tortuosity. NVD is present in 35% of eyes, NVE in 8% of eyes, and vitreous hemorrhage occurs in 4% of eyes. A cherry red spot occurs in 12% of eyes.[65]

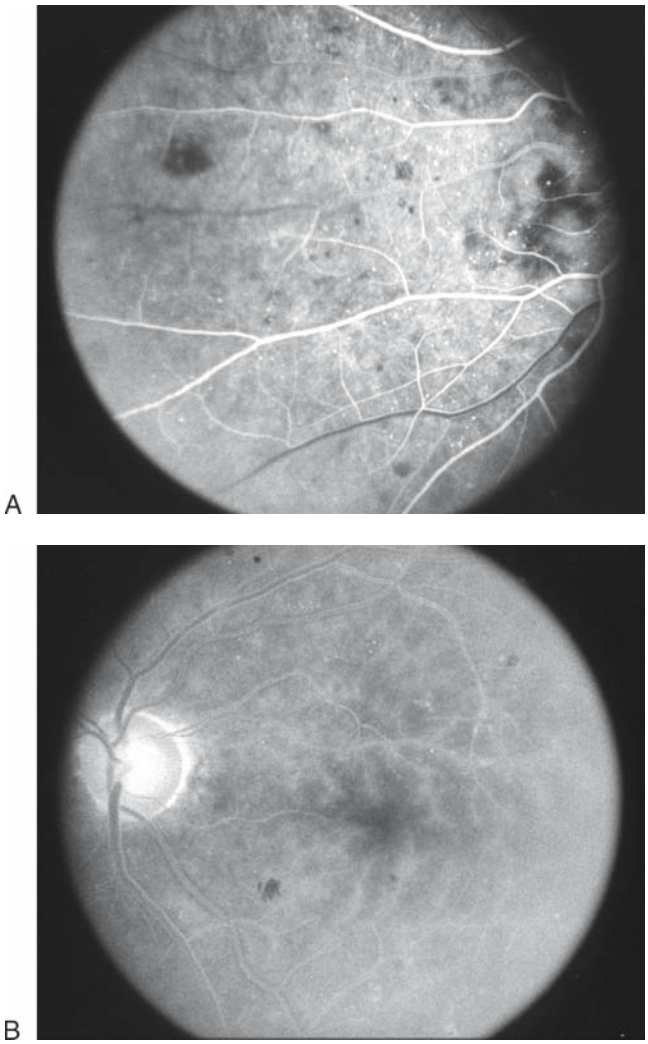

FIG. 5.23. A 61-year-old man with complete occlusion of the left common carotid artery noticed decreased vision for the past 2 weeks. His visual acuity was 20/100. (A) Midphase FA frame shows that the nasal retina also fills slowly. There are hypofluorescent areas consistent with intraretinal hemorrhages. (B) Late-phase FA frame shows the absence of macular edema. But there is staining of the vessels in the posterior pole.

Fluorescein Angiography

These eyes most often have a marked prolongation or patchy choroidal filling with delayed retinal arteriovenous transit time. Macular edema is seen in 17% of eyes. Other angiographic findings include retinal capillary nonperfusion, optic nerve head hyperfluorescence, intraretinal hemorrhages, and microaneurysmal hyperfluorescence (Fig. 5.23).

Treatment

Most eyes with rubeosis iridis end up with legal blindness after a year of follow-up. Carotid endarterectomy has been recommended in symptomatic patients with a high-grade stenosis (70% to 99%) and asymptomatic patients with a hemodynamically significant stenosis (≥60%).[67,68] Although the studies did not specifically address ocular ischemic syndrome, carotid endarterectomy should be considered in these eyes if the carotid stenosis is of high grade.

Scatter photocoagulation is indicated when rubeosis iridis or retinal neovascularization are present. However, only about 36% of eyes show regression of the neovascularization following laser treatment.

Retinal Arterial Obstruction

In 1859, von Graefe[69] described a patient with endocarditis and multiple systemic emboli who suffered an embolic central retinal artery obstruction. Based on the location of the obstruction, retinal artery obstructions can be classified as follows:

1. Central retinal artery obstruction (57% of cases)
2. Branch retinal artery obstruction (38% of cases)
3. Cilioretinal artery obstruction (5% of cases)
4. Combined central retinal artery and vein obstruction

Systemic Associations

Once a retinal artery obstruction is diagnosed, a complete systemic workup is necessary. Up to 90% of patients have an associated systemic condition.[70,71] In patients older than 30 years of age, carotid atherosclerosis and cardiac disease are the usual culprits. Carotid stenosis or ipsilateral plaque is seen in 45% of eyes with retinal artery obstruction. If the stenosis is 60% or greater, it is considered to be hemodynamically signifi-

cant. Almost 50% of patients with a retinal artery obstruction suffer from cardiac disease. Nevertheless, cardiac pathology is severe enough in only 10% of these people to warrant cardiac surgery or systemic anticoagulation.[72] Giant cell arteritis must be ruled out in patients older than 50 years of age.[73] The etiology of retinal arterial obstructions of patients younger than 30 years of age is somewhat different and includes conditions such as migraine, cardiac disease, trauma, hemoglobinopathies, optic nerve drusen, and prepapillary arterial loops (Fig. 5.24).

Clinical Presentation

Patients with central retinal artery obstruction complain of a painless loss of vision. The visual acuity ranges between counting fingers and light perception in 90% of eyes. An afferent pupillary defect is usually present. The funduscopic appearance may be completely normal if the obstruction is very recent. In the acute stage, the retina in the posterior pole loses its transparency and acquires a whitish appearance. A cherry red spot is present in the region of the foveola (Fig. 5.25). Segmentation of the blood column, also called "boxcarring," is seen in the retinal arterioles. In most cases the retina assumes its normal color over a period of 4 to 6 weeks, leaving a pale optic disc, narrowed retinal vessels, and visible absence of the nerve fiber layer in the region of the optic disc. Neovascularization of the disc has also been noted to occur, and develops in about 2% of eyes.[74] The incidence of rubeosis iridis is approximately 20%; it develops 4 to 5 weeks after the event. If rubeosis iridis is present at the time of the obstruction, the presence of a concomitant carotid artery obstruction should be considered. The incidence of neovascularization of the iris and subsequent NVG following acute central retinal artery occlusion (CRAO) is reported to be between 1% and 5%. Approximately 25% of eyes with an acute central retinal artery obstruction have a patent cilioretinal artery that supplies part or all of the papillomacular bundle (Fig. 5.26).[75] Emboli are visible within the arterial system in about 20% of eyes. The most common variant is the glistening yellow crystal cholesterol embolus that is called the Hollenhorst plaque. It is often seen at the bifurcation of the vessels. It most commonly arises from atherosclerotic plaques in the carotid arteries. Other types of emboli include fibrin-platelet thrombi and calcium emboli.

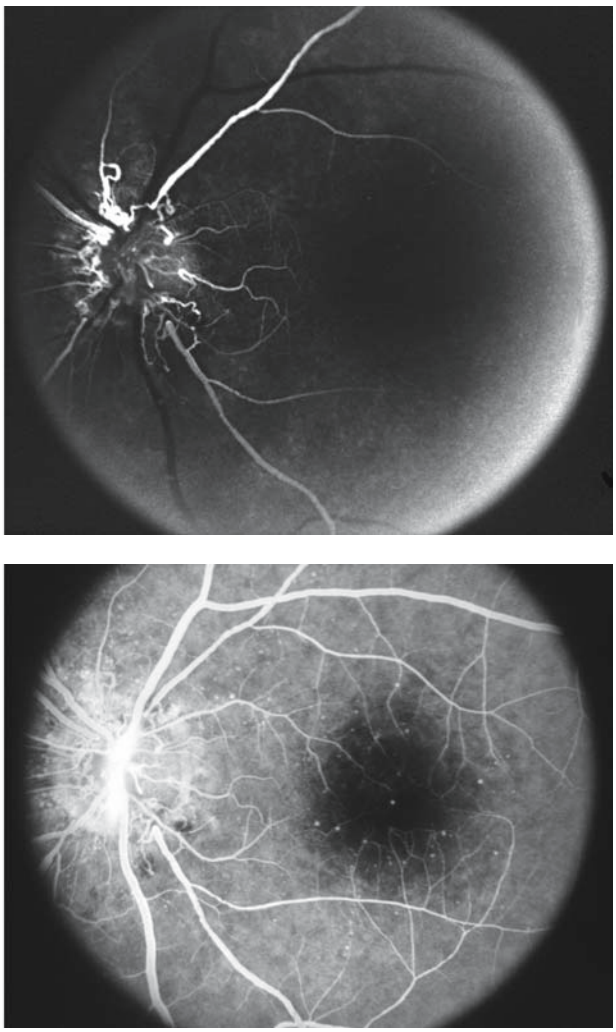

Fig. 5.24. A 56-year-old woman noted decreased vision in her left eye of 9 months, duration. Her current visual acuity was 20/200. (A) Early FA frame shows the dye circulating in the vascular loop, vessels in the disc, and the four branches of the central retinal artery. (B) Mid-FA frame demonstrating obliteration of the perifoveal capillary bed.

Patients with a branch retinal artery obstruction complain of a scotoma that is unilateral, painless, and sudden in onset. Over 90% of branch retinal artery obstructions involve the temporal retinal vessels (Fig. 5.27). Ophthalmoscopic findings include retinal whitening corresponding to the distribution of the affected retinal artery. The involved artery is narrowed and "boxcarring" may be seen. Artery-to-artery collateral vessels may develop in the retina and are pathognomonic for branch artery obstruction. Ocular neovascularization after a branch retinal artery obstruction is a rare event.[76] The visual prognosis in eyes with branch retinal artery obstruction is usually quite good, unless the fovea is completely surrounded by retinal edema and ischemia.

Cilioretinal arteries are clinically and angiographically present in 20% and 32% of eyes, respectively. Cilioretinal artery occlusion presents itself as retinal whitening along the course of the vessel. They may occur as isolated events, in combination with a central retinal vein occlusion or in conjunction with anterior ischemic optic neuropathy. The visual outcome is very good for eyes with isolated cilioretinal artery obstruction. Eyes with combined anterior ischemic optic neuropathy and cilioretinal artery obstruction have a poor visual outcome.

A combined central retinal artery obstruction and central retinal vein occlusion is a rare occurrence. Most patients complain of a sudden decrease of vision. Ophthalmoscopic examination reveals retinal whitening, a cherry red spot, dilated and tortuous veins, retinal hemorrhages, macular edema, and a swollen optic disc. Rubeosis and NVG eventually occur in 80% of these eyes.[77]

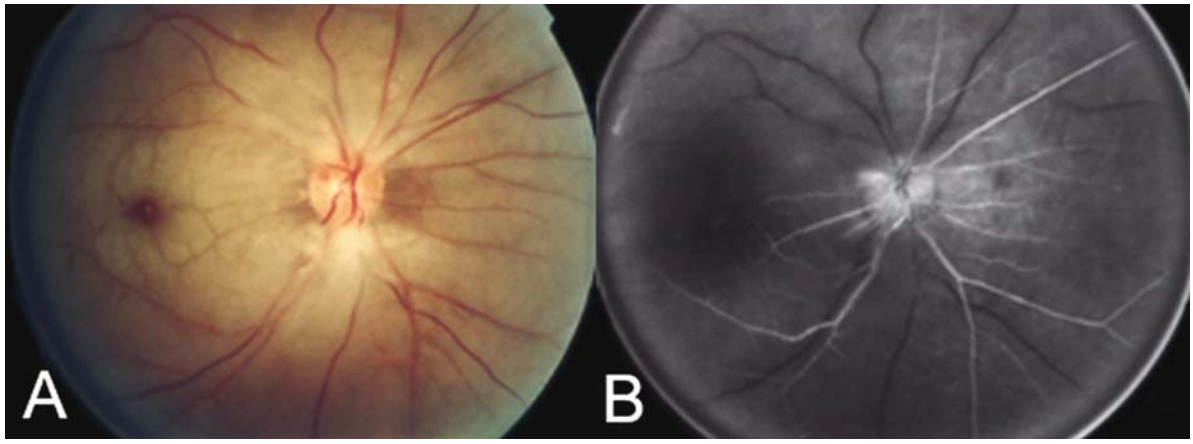

Fig. 5.25. Central retinal artery occlusion (CRAO) demonstrates a cherry red spot in the region of the foveola. (A) Color photograph. (B) Fluorescein angiogram.

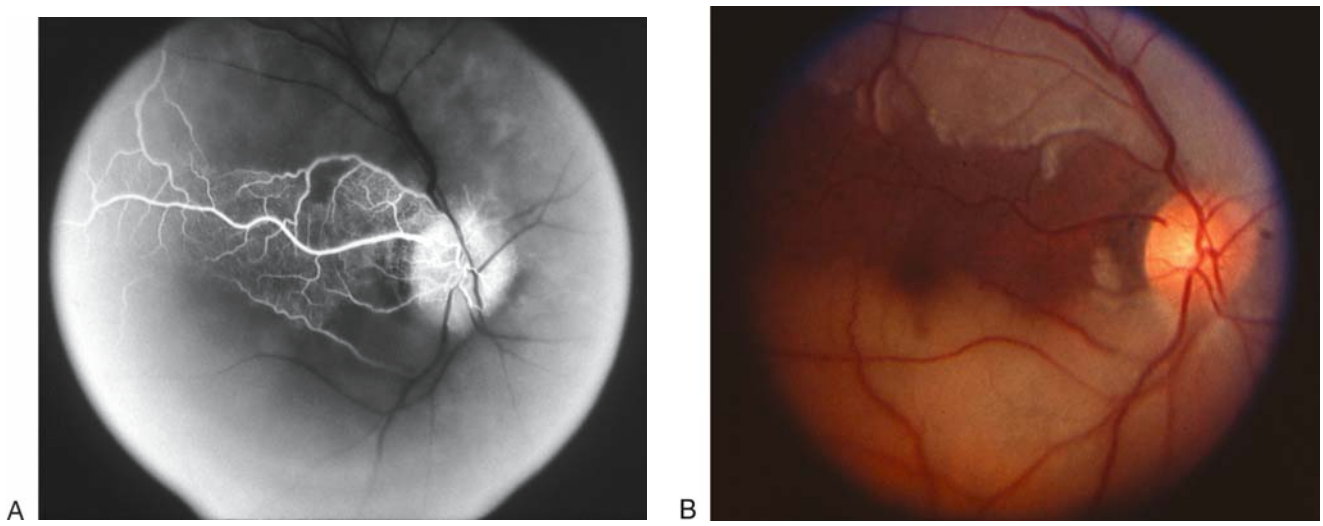

Fig. 5.26. A 58-year-old healthy woman developed sudden loss of vision in her right eye 2 days prior to presentation. Her vision was 5/200. (A) Clinical photograph shows whitening of the inner retina in the posterior pole sparing the inferocentral and nasal macula. No visible emboli are seen. (B) Early FA frame shows prompt filling of a cilioretinal artery with filling of the superior macular area.

Fluorescein Angiography

In central retinal artery obstructions the choroidal circulation fills normally. In a normal eye, the choroid fills 1 to 2 seconds prior to filling of the retinal arteries and is completely filled within 5 seconds of the appearance of the dye. When the central retinal artery is obstructed, a delay in retinal arterial filling or a delay in the retinal arteriovenous transit time is commonly seen. Irregular and sluggish filling of the retinal arteries is the hallmark of the disease (Fig. 5.25). Late staining of the optic disc is variable.

In eyes with a branch retinal artery obstruction, the fluorescein dye does not perfuse into the branch of the artery (Fig. 5.27). The involved sector of the retina has a ground-glass appearance due to tissue swelling from ischemia. The veins in the area of the retina fed by the blocked portion of the artery do not contain fluorescein, Sometimes a retrograde flow of dye into the branches of the artery or veins in the area of occlusion is seen. When the branch artery is only partially occluded, filling in the area will be delayed.

Eyes with a cilioretinal artery obstruction demonstrate poor filling of the obstructed vessel and retinal capillary nonperfusion in the area of distribution of the vessel. Eyes with a combined artery and vein obstruction have a delayed arterial filling phase, a prolonged arteriovenous transit time, severe retinal capillary nonperfusion, and a sudden termination of the midsized retinal vessels.

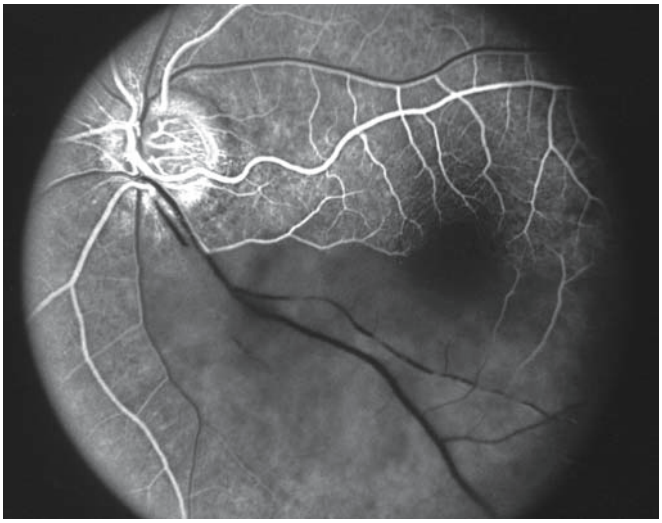

FIG. 5.27. A 72-year-old man complained of a sudden loss of vision in his left eye for 2 days. The visual acuity was 1/200 and a superior altitudinal defect was noted. Early FA frame shows lack of flow in the inferotemporal branch of the central retinal artery. There is marked capillary nonperfusion in the inferotemporal quadrant.

Treatment

Several treatment modalities including carbogen administration, anterior chamber paracentesis, and ocular massage have been described in the literature. More recently intraarterial fibrinolysis, YAG laser arteriotomy, and embolectomy has been reported.[78,79] However, none has been proven to be effective at all.

Hypertensive Retinopathy

Systemic hypertension is one of the most widespread diseases in the world today. It is a major public health challenge because of the morbidity and mortality that it causes. According to the Seventh Report of the Joint National Committee of Prevention, Detection, Evaluation, and Treatment of High Blood Pressure (JNC VII),[80] the classification of blood pressure (expressed in mm Hg) for adults aged 18 years or older is as follows:

1. Normal: systolic <120 mm Hg, diastolic <80 mm Hg
2. Prehypertension: systolic 120–139 mm Hg, diastolic 80–99 mm Hg
3. Stage 1: systolic 140–159 mm Hg or diastolic 90–99 mm Hg
4. Stage 2: systolic ≥160 mm Hg or diastolic ≥100 mm Hg

Sustained elevation of arterial blood pressure leads to vascular lesions in the heart, central nervous system, kidneys, and eyes.

Clinical Findings

Most patients are asymptomatic unless accelerated hypertension is present. Depending on the vascular bed affected, hypertension can give rise to retinopathy, choroidopathy, and optic neuropathy.

The hallmark of hypertensive retinopathy is diffuse arteriolar narrowing. Hypertension induces a progressive increase in the thickness of the arteriolar wall called arteriolosclerosis. Normally, the arteriolar wall is invisible during ophthalmoscopy, and one solely sees the red blood column of the arteriole. As the arteriolar wall becomes thicker and the lumen narrower, the arterioles manifest a reddish-brown color known as copper wiring. If the thickening continues, the column of blood can no longer be visualized in the arteriole. This gives rise to a whitish color or silver wiring. Usually the arteriole is anterior to the venule. With increasing arteriolosclerosis, compression of the underlying venule by the arteriole occurs. This is seen as a nick in the arteriovenous crossing.

If the blood pressure is very elevated, there is a breakdown of the inner blood–retinal barrier. Retinal hemorrhages, microaneurysms, cotton-wool spots, and lipid exudation may be seen. A macular star, papilledema, and shutdown of the retinal capillaries may occur if the elevation in blood pressure is very severe (Fig. 5.28).

Localized bullous detachments of the neurosensory retina and retinal pigment epithelium can occur secondary to this ischemia. The subretinal fluid is usually turbid because of the protein-rich exudate.[81] Focal chorioretinal atrophy known as Elschnig's spots may also be seen. Siegrist's streaks are linear hyperpigmentation lesions that overly the choroidal arteries.

Optic neuropathy is manifested as optic disc edema with retinal hemorrhages and capillary dilation (Fig. 5.29).

Fluorescein Angiography

Hypertensive choroidopathy is manifested as patchy nonperfusion of the choriocapillaris. Acutely, Elschnig's spots (Fig. 5.30)

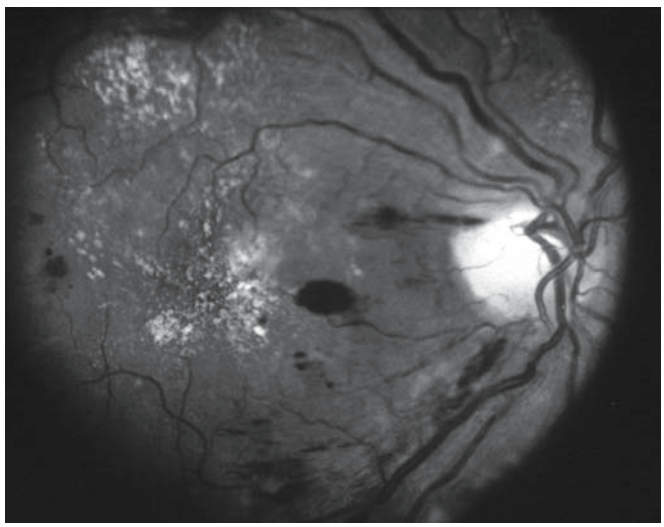

FIG. 5.28. Red-free photograph of the right eye of a 55-year-old man shows splinter hemorrhages on the disc, lipid deposition in the macula, and intraretinal hemorrhages.

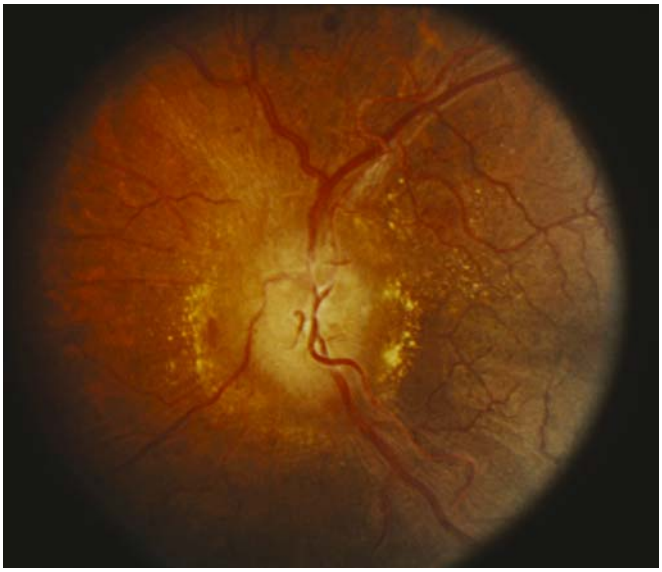

FIG. 5.29. A 45-year-old man complaining of headaches and blurry vision for 2 weeks was seen in the emergency room and diagnosed with acute systemic hypertension. He had a blood pressure of 200/120 mm Hg. Photo of the optic disc also shows edema and lipid exudation.

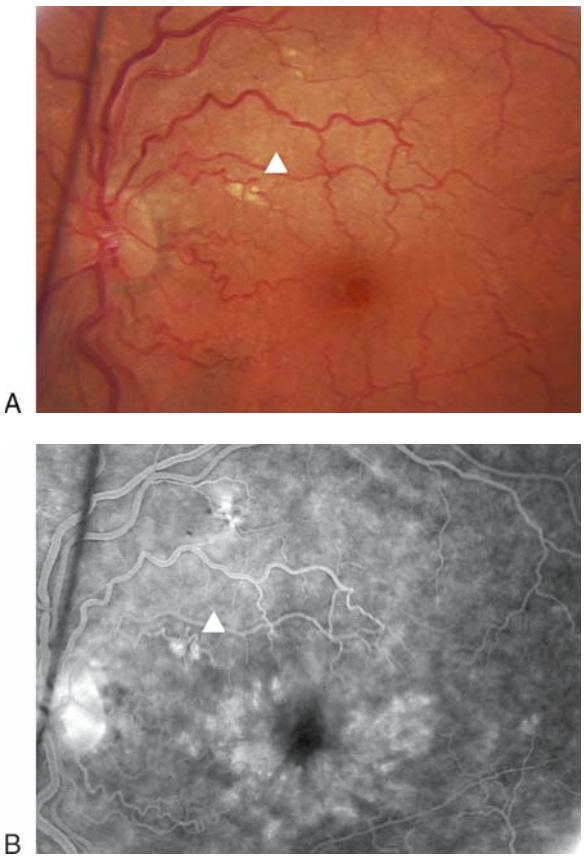

FIG. 5.30. Hypertensive choroidopathy is manifested as patchy nonperfusion of the choriocapillaris. Acutely, Elschnig's spots can be seen. (A) Elschnig's spots (arrowhead) in color photograph. (B) Elschnig's spots (arrowhead) in late-phase fluorescein angiogram on a patient with concomitant pseudophakic cystoid macular edema.

profusely leak fluorescein. Once they heal, Elschnig's spots no longer leak fluorescein. Instead window defects are seen.

Cotton wool spots give a ground-glass appearance to the involved retina. Staining of the vessel walls occur in areas of vascular damage. If hypertensive optic neuropathy is present, leakage or staining of the nerve may be seen.

Treatment

Patients with hypertensive retinopathy should be referred to an internist for appropriate treatment.

Retinal Arterial Macroaneurysms

In 1880 Loring described an asymptomatic 25-year-old man who had bulging of the inferotemporal retinal artery. In 1920 Fernandez associated retinal artery macroaneurysms with systemic hypertension. Finally in 1973, Robertson[82] defined retinal arterial macroaneurysm as a distinct clinical entity.

Clinical Findings

Retinal arterial macroaneurysms are more commonly seen in women in their 50s and 60s who suffer from hypertension and arteriosclerotic vascular changes. They are usually unilateral, but up to 10% may be bilateral. Retinal arterial macroaneurysms are usually single but may be multiple in up to 20% of cases (Fig. 5.31).[83]

The most common presenting symptom is an acute visual loss secondary to hemorrhage, exudation, or macular edema, although many may be asymptomatic and picked up on routine examination. The classic description is of a round or fusiform dilatation of the arterial wall of the retinal arterioles within the first three orders of arterial bifurcation. Close to 50% of eyes have an associated retinal hemorrhage that surrounds the macroaneurysms. This hemorrhage may be preretinal, intraretinal, or subretinal. If the hemorrhage occurs in all layers, it is called an hourglass hemorrhage. Breakthrough vitreous hemorrhage occurs in about 10% of cases.[84] Intraretinal lipid deposition manifested as hard exudates surrounding the macroaneurysms in a circinate ring or as a distal effect on the macula is commonly seen (Fig. 5.31). A detachment of the neurosensory retina may on occasion surrounds the macroaneurysm.

Fluorescein Angiography

The macroaneurysm typically fills uniformly in the early phase of the angiogram.[85] If the filling is delayed or incomplete, an involuted macroaneurysm may be present. The artery is usually narrowed just distal and proximal to the macroaneurysm. However, sometimes if a large and thick hemorrhage is present, fluorescein angiography may be unable to image the macroaneurysm because of the blockage caused by the hem-

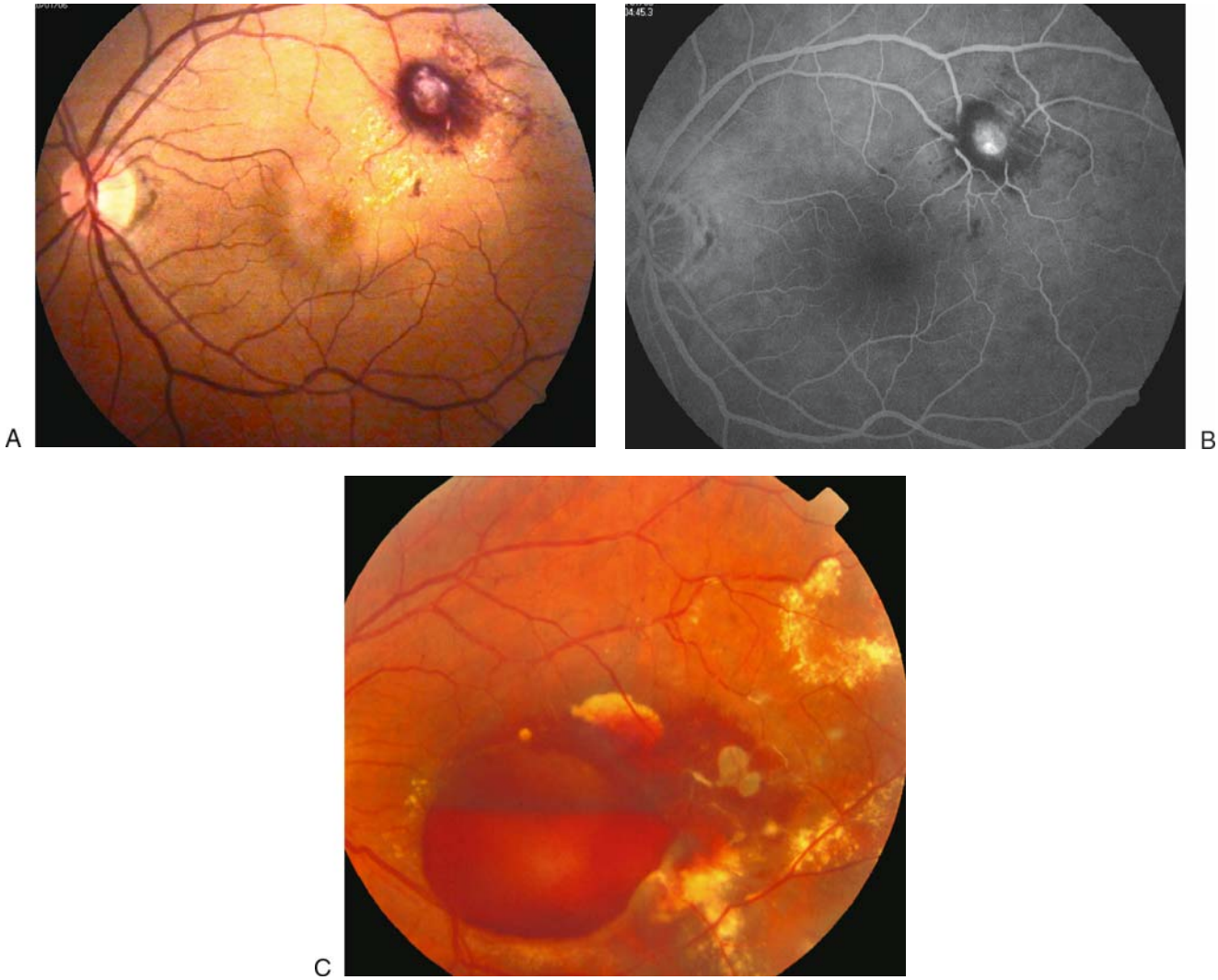

FIG. 5.31. Retinal arterial macroaneurysm along the superotemporal artery. (A) Color photograph demonstrates a retinal arterial macroaneurysm surrounded by hemorrhage and lipid exudation. (B) Late-phase FA frame shows hyperfluorescent arterial macroaneurysm. (C) Another ruptured arterial macroaneurysm with subhyaloidal hemorrhage and lipid exudation. (Courtesy of Dr. Juan Verdaguer.)

orrhage. Depending on the damage caused by the macroaneurysm to the vessel wall, the late phases may show little or no staining of the vessel wall or marked leakage (Fig. 5.31). Small areas of capillary nonperfusion or microaneurysms may surround the macroaneurysm.

Indocyanine Green Angiography

Indocyanine green angiography is useful in elucidating the diagnosis if preretinal, intraretinal, or subretinal blood is too dense to allow a clinical or fluorescein diagnosis.[86] Round focal hot spots adjacent to the retinal arterioles are indicative of an retinal arterial macroaneurysm.

Treatment

Some retina specialists feel that the visual outcome of retinal arterial macroaneurysms is very good because they can undergo spontaneous thrombosis, fibrosis, and involution. However, it must be kept in mind that even though most macroaneurysms involute, some do not. Preretinal hemorrhages may be complicated by epiretinal membrane formation (Fig. 5.31). Subretinal hemorrhages pose a different problem. Blood in the subretinal space is toxic to the photoreceptors. Pars plana vitrectomy with intraoperative fibrinolysis of these hemorrhages should be considered.[87]

Macular edema and its sequelae is the most common cause of poor vision following a retinal arterial macroaneurysm. Permanent structural damage to the macula may result from

the chronic lipid exudation. Laser photocoagulation may be directed toward the macroaneurysm itself or around it.[88]

Radiation Retinopathy

Radiation therapy has been used to treat tumors for many years. Radiation retinopathy was first recognized by Stallard[89] in 1933, who described retinal exudation and hemorrhages as a consequence of radon treatment for retinoblastoma.

Clinical Findings

Injury to the eye may result from direct radiation of intraocular tumors or when the ocular structures are within the treatment beam for extraocular tumors. If the eye receives a total radiation dose of 3000 rad or more; if the daily fractionation dose is in excess of 200 rad; if concurrent adjunctive chemotherapy or bone marrow transplantation is performed; and if simultaneous treatment with external beam radiotherapy and hyperbaric oxygen are given, a higher risk of developing retinopathy is reported. Systemic conditions that are associated with a higher risk of developing radiation retinopathy include diabetes mellitus, collagen vascular diseases, pregnancy, and hypertension.[90]

Symptoms range from metamorphopsia, blurred central vision, and scotomas, to abrupt complete loss of vision. It is uncommon for it to occur within 6 months of the ocular irradiation or more than 3 years after treatment.

Radiation retinopathy is a slowly progressive occlusive microangiopathy where the primary damage is at the level of the retinal capillary endothelium. The microvascular changes include microaneurysms, retinal telangiectasias, dot and blot intraretinal hemorrhages, cotton-wool spots, macular exudates, macular edema, perivascular sheathing, and intraretinal microvascular abnormalities (Figs. 5.32 and 5.33). The severity of the retinopathy is dependent on the extent of the resultant capillary nonperfusion and retinal ischemia. As the retinopathy progresses, extensive retinal vascular occlusion, NVD, NVE, and iris neovascularization occur. This may lead to vitreous hemorrhage, NVG, and traction retinal detachment.

Radiation retinopathy is commonly associated with optic neuropathy, which can present in either of two forms: anterior ischemic optic neuropathy or retrobulbar ischemic optic neuropathy. Both are due to vascular occlusion.

Fluorescein Angiography

The principal fluorescein angiographic finding is capillary nonperfusion. In addition, capillary leakage, microaneurysmal leakage, and neovascularization are commonly seen (Fig. 5.33).[91] Transmission hyperfluorescence corresponding to the areas of retinal pigment epithelial atrophy may be seen. Ophthalmoscopy may reveal hypopigmented patches, which appear as hypofluorescent area. When radiation optic neuropathy is present, ischemia of the optic nerve head with superficial areas of nonperfusion and leakage can be seen.

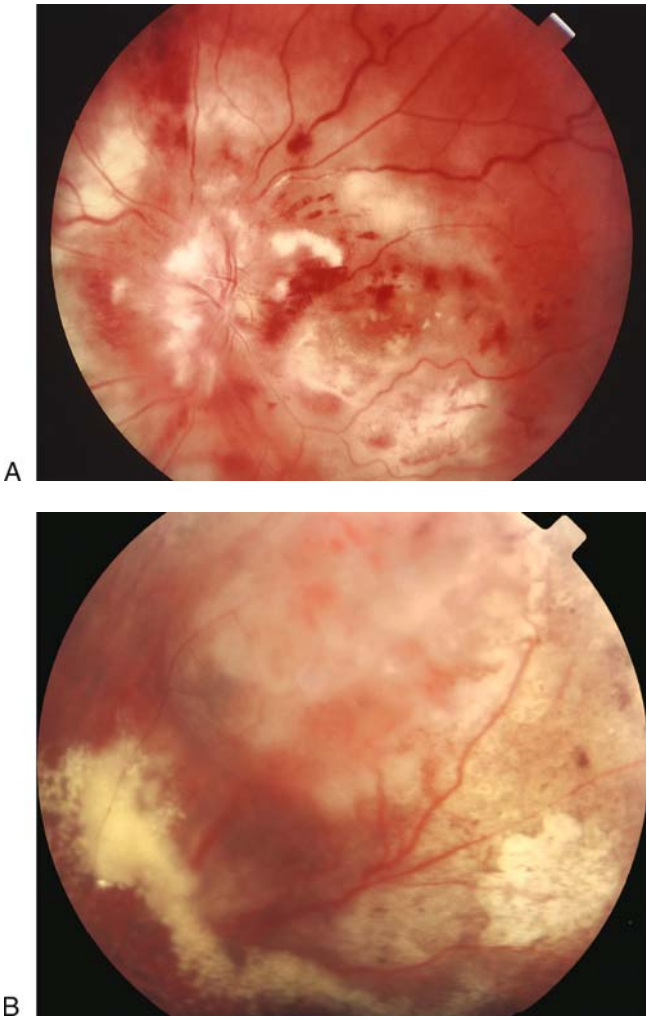

Fig. 5.32. Microvascular changes in radiation retinopathy include microaneurysms, retinal telangiectasias, dot and blot intraretinal hemorrhages, cotton-wool spots, macular exudates, macular edema, perivascular sheathing, and intraretinal microvascular abnormalities. (A) Radiation retinopathy and papillopathy after brachytherapy for retinoblastoma. (B) Radiation retinopathy and papillopathy after brachytherapy for choroidal melanoma. (Courtesy of Drs. Carol and Jerry Shields.)

Indocyanine Green Angiography

Indocyanine green angiography has demonstrated that ocular and periocular radiation treatment can also cause a radiation-induced choroidopathy.[92] This is characterized by widespread progressive vaso-occlusion of the choriocapillaries and small choroidal vessels. The ICG shows capillary dropout, and small discrete diffuse perfusion defects of the choriocapillaries in the midperipheral zones. Late ICG choroidal staining in the area where radiation retinopathy developed may be observed. Interestingly, many of the areas of choriocapillaris

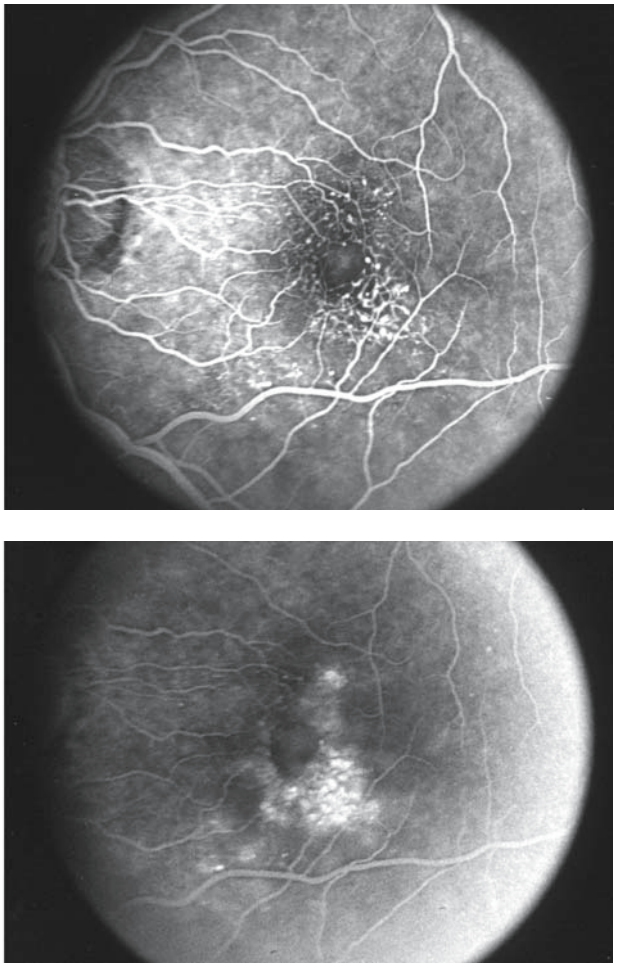

FIG. 5.33. A 49-year-old woman had a left-sided brain tumor removed. She subsequently underwent 20 sessions of radiation therapy. Three years later she complained of blurry vision in her left eye. (A) Early FA frame shows telangiectatic parafoveal capillaries. (B) Mid-FA frame delineating the parafoveal telangiectasia even better.

nonperfusion are distinct from those of retinal ischemia, indicating the widespread nature of the choroidal vascular insult. For the most part, the large choroidal vessels remain normal. At the border of nonperfused and perfused choroid, saccular dilatations and areas of choroidal neovascularization may appear. Choroidal veins can undergo remodeling through the formation of venovenous anastomoses.

Treatment

Focal and diffuse macular edema can be treated with focal or grid laser photocoagulation. Alternatively, one may consider the use of intravitreal triamcinolone. Repeated injections seem to be needed to maintain the initial effect.[93] Severe nonproliferative and proliferative radiation retinopathy should be treated with scatter retinal photocoagulation, which has been shown to be effective in decreasing and obliterating the proliferative new vessels.[94] Despite laser photocoagulation, some treated eyes may continue to lose vision, due to optic neuropathy and macular ischemia. Tractional retinal detachment, fibrovascular proliferation, and nonclearing vitreous hemorrhage may require standard pars plana vitrectomy techniques.[90]

Coats' Disease

In 1908, George Coats[95] described an idiopathic entity characterized by unilateral retinal vascular abnormalities with intraretinal and subretinal exudation. He further classified this entity into three groups. Group I had massive subretinal exudates but no visible retinal vascular abnormalities. Group II had massive subretinal exudates with retinal vascular abnormalities. Group III had massive exudates with arteriovenous malformations. von Hippel later characterized this group III as a distinct entity: angiomatosis retinae. In 1912 Theodor Leber described a similar condition characterized by retinal aneurysms, hemorrhages, and telangiectasia, but without the massive subretinal exudates. This condition was named Leber's multiple miliary aneurysm disease. However, in 1915, Leber himself recognized that his disease was the earlier stage of the same entity as the one described by Coats. Reese in 1956 confirmed this concept by describing an eye that had Leber's multiple miliary aneurysms that developed the classic picture of Coats' disease with time.

Clinical Findings

Coats' disease affects males more commonly than females in a 3:1 ratio. Up to 80% of cases are unilateral. There is no known racial or ethnic predilection.[96] A juvenile and an adult form of the disease are recognized. The juvenile cases usually present with leukocoria, strabismus, or loss of vision. About two thirds of these cases present before the age of 10. The adult form is virtually indistinguishable from the juvenile form, with the exception that the adult form has been associated with hypercholesterolemia and seldom presents with strabismus.

Several case reports have been reported in the literature where Coats' disease has been diagnosed in conjunction with other diseases such as retinitis pigmentosa, Senior-Loken syndrome, Turner's syndrome, and Hallermann-Streiff syndrome.

The underlying problem of Coats' disease is the peripheral retinal vascular abnormality, which causes the breakdown of the blood–retinal barrier. Affected retinal vessels may show sheathing, saccular aneurysmal dilatations, anomalous vascular communications, telangiectasia, and tortuosity. The majority of these abnormalities are located in the inferior and temporal quadrants between the equator and the ora serrata. Leakage of plasma constituents lead to the typical funduscopic findings of yellow intraretinal and subretinal exudates, which find their way to the macular area even if the vascular abnormalities are located in the retinal periphery (Fig. 5.34). The subretinal fluid accumulates inferiorly, causing a bullous retinal detachment.

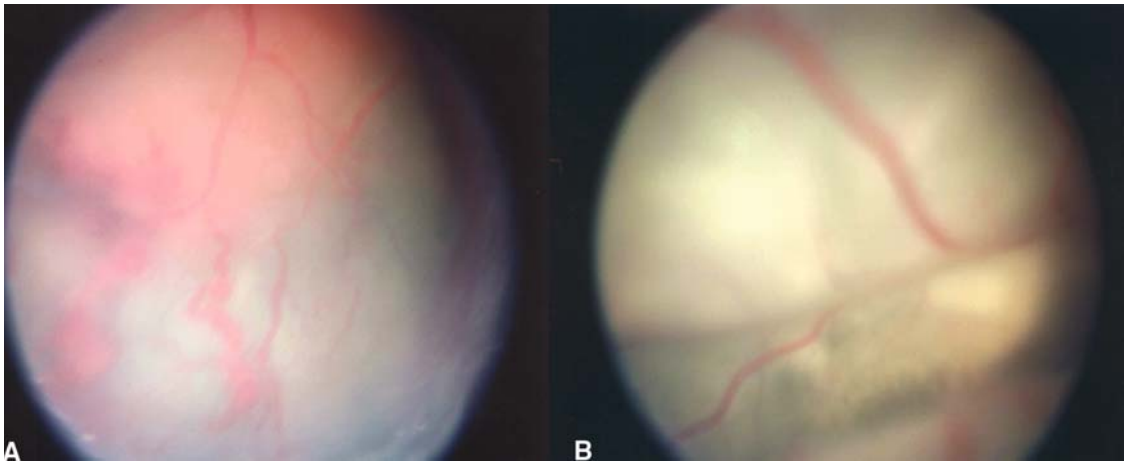

Fig. 5.34. (A,B) Affected retinal vessels show sheathing, saccular aneurysmal dilatations, anomalous vascular communications, telangiectasia, and tortuosity. Leakage of plasma constituents lead to the typical funduscopic findings of yellow intraretinal and subretinal exudates, which find their way to the macular area even if the vascular abnormalities are located in the retinal periphery. The subretinal fluid accumulates inferiorly causing a bullous retinal detachment.

Fibrovascular tissue formation and choroidal neovascularization may follow. Larger zones of capillary nonperfusion can be associated with neovascularization and vitreous hemorrhage.

Complications associated with long-standing retinal detachment include hemorrhagic retinal macrocysts, secondary vasoproliferative tumors, cataract, iridocyclitis, corneal edema, iris neovascularization, anterior chamber cholesterolosis, NVG, and phthisis bulbi.

Fluorescein Angiography

Fluorescein angiography is a useful adjunct in the diagnosis and management of Coats' disease. The angiogram shows early hyperfluorescence secondary to increased vasopermeability in the area of the affected vessels. If the lipid exudation is extensive, hypofluorescence may be seen. Areas of capillary dropout may be seen in the region of telangiectasia, but retinal neovascularization is rare. In the late phases, mild hyperfluorescence secondary to pooling of the dye in the subretinal fluid may be seen. Hyperfluorescence secondary to leakage from macular edema may also be seen.

Classification

Shields et al.[97] have proposed the following classification scheme:

Stage 1: Retinal telangiectasia only
Stage 2: Telangiectasia and exudation

A. Extrafoveal exudation
B. Foveal exudation

Stage 3: Exudative retinal detachment

A. Subtotal detachment

1. Extrafoveal
2. Foveal

B. Total retinal detachment

Stage 4: Total retinal detachment and glaucoma
Stage 5: Advanced end-stage disease

Treatment

The main goal of treatment is to avoid visual loss if possible. If the patient presents early on when there are only retinal vascular abnormalities and extrafoveal exudation or no exudation at all, the ophthalmologist is presented with an opportunity to prevent visual loss by aggressive scatter laser photocoagulation of the involved areas. Once foveal exudation develops, visual loss is common despite treatment. Cryotherapy is the preferred initial method when there are peripheral telangiectasias associated with extensive exudation or subtotal retinal detachment.

Eyes with extensive bullous retinal detachment may benefit from retinal reattachment surgical techniques such as scleral buckle, vitrectomy, and subretinal fluid drainage in combination with photocoagulation and cryotherapy.[98,99] Advanced cases with secondary glaucoma often require enucleation.

Parafoveal Telangiectasia

In 1956, Reese coined the term *retinal telangiectasia* to describe a developmental retinal vascular disorder characterized by retinal capillary ectasia. If the abnormalities are limited to the parafoveal area, then the condition is known as parafoveal or juxtafoveal telangiectasia. Gass has classified this entity into three major groups with the following subdivisions[100]:

1. Unilateral parafoveal telangiectasia

a. Congenital
b. Acquired

2. Bilateral acquired parafoveal telangiectasia
3. Bilateral idiopathic perifoveal telangiectasia and capillary obliteration

Clinical Findings

Patients in group 1 are males in their 40s with unilateral involvement of the perifoveal capillary network. The perifoveal area involved differs between groups 1A and 1B. The eyes in group 1A patients have the temporal area affected one to two disc diameters. Group 1B eyes have only one clock hour involved.

Patients in group 2 have no gender predilection and both eyes are involved. Other findings include right-angle draining venules, retinal pigment epithelial hyperplasia, macular edema, and exudation (Fig. 5.35). Chorioretinal anastomosis and retinal pigment epithelial plaques precede the development of choroidal neovascularization.[100]

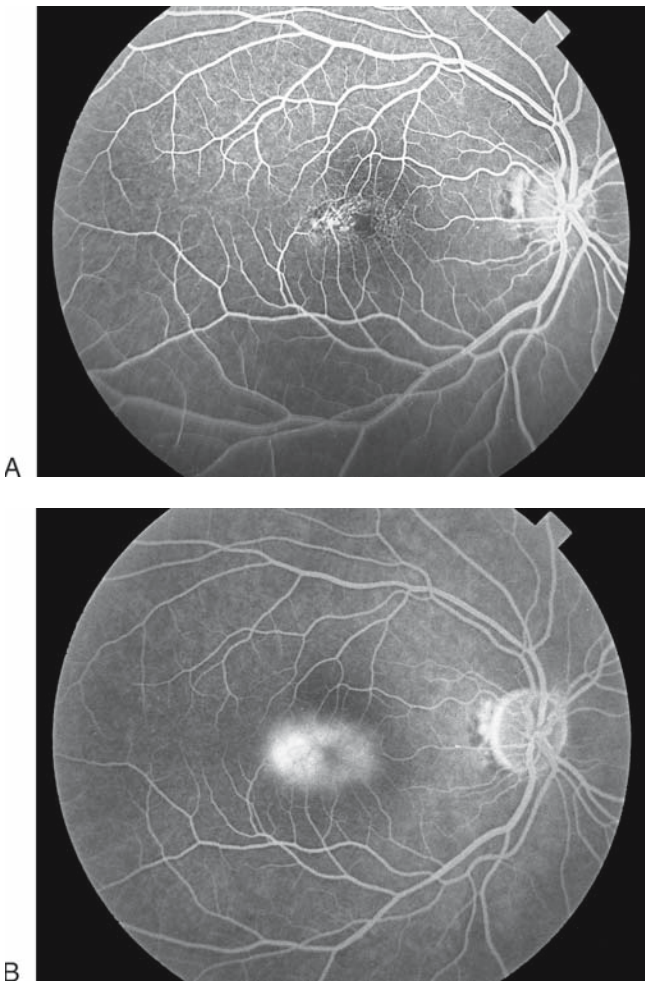

Fig. 5.35. A 42-year-old woman complained of a gradual loss of vision in right eye. Her visual acuity is 20/60 in both eyes. A diagnosis of idiopathic parafoveal telangiectasis was made. (A) Early FA frame of the right eye shows telangiectatic changes in the foveal capillary bed. (B) Late FA frame of the right eye also shows a ring of fluorescein leakage surrounding the fovea.

Pathogenesis

Histopathologic studies have demonstrated changes very similar to those of diabetic retinopathy in these eyes.[101] These abnormal capillaries are dilated and incompetent like the ones seen in diabetic retinopathy.

Fluorescein Angiography

During the arteriovenous phase, the abnormal capillaries are seen as dilations especially on the parafoveal temporal side. The abnormalities do not respect the horizontal raphe. If they do, a branch retinal vein occlusion should be strongly suspected. In the late phases leakage occurs secondary to macular edema (Fig. 5.35). Fluorescein angiography has documented that eyes with parafoveal telangiectasia have a small foveal avascular zone.[102]

Treatment

A small case series reported no benefit from laser photocoagulation. A poor outcome has been reported following submacular surgery in cases of choroidal neovascular membranes. These membranes appear to be very adherent to the neurosensory retina, making their extraction technically difficult and hazardous.[103] Photodynamic therapy with verteporfin has been reported to stop leakage from the choroidal neovascular membrane, but leakage from the telangiectasia persists. Intravitreal triamcinolone has been reported to be useful in a single case report.[104]

Sickle Cell Retinopathy

Sickle cell disease is a hemoglobinopathy where a point mutation causes a single amino acid substitution in the β-globin chain. This abnormal hemoglobin can occur in combination with normal hemoglobin A or abnormal hemoglobin S or C, leading to various hemoglobinopathies. This results in increased cell hemolysis, blood viscosity, and vaso-occlusion.

Clinical Findings

Most patients are usually asymptomatic. Retinopathy has been classified as nonproliferative or proliferative depending on the retinal findings.

The precapillary arterioles of the optic disc may undergo repetitive occlusive insults. Angioid streaks may also be seen radiating from the optic nerve.[105] In the posterior pole, an increased vascular tortuosity, arterial occlusion, and nonperfusion lead to an enlargement of the foveal avascular zone and microaneurysms. The macula may become thinned and atrophic, giving rise to a concavity in the area of thinning. This is called the macular depression sign.

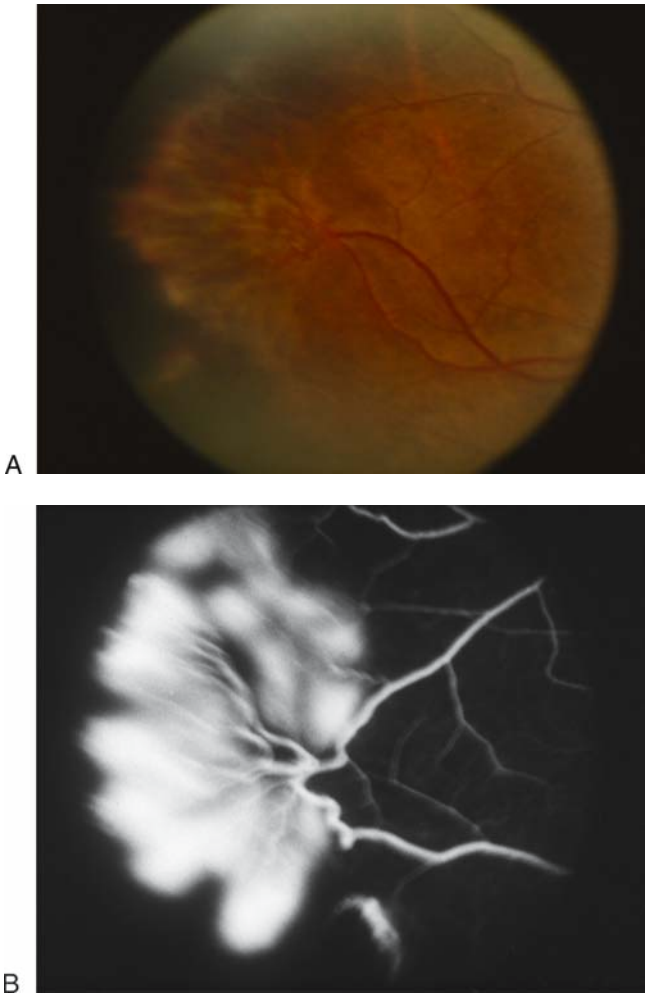

Fig. 5.36. Clinical findings in sickle cell retinopathy. (A) Retinal neovascularization in a sea-fan configuration. (B) The FA frame shows leakage from the sea fan.

In the midperiphery, repetitive episodes of occlusion and ischemia end up weakening the vascular walls. Preretinal or superficial retinal hemorrhages that are oval or round in shape with well-defined borders may occur. The hemorrhage is flat or elevated in a dome-like fashion. With time the red color of the hemorrhage turns into red-orange and then to salmon color. The blood may dissect anteriorly into the vitreous cavity or posteriorly into the subretinal space. These lesions are referred to as salmon patches.[106] Once the hemorrhage of the salmon patch is absorbed, thinning of the underlying retina occurs. A schisis cavity with multiple glistering yellow deposits may develop. These deposits consist of hemosiderin-laden macrophages. These lesions are called iridescent spots. If blood happens to dissect posteriorly, the RPE can undergo a migratory hyperplastic response to it. The result is a round or oval flat black lesion called a black sunburst.

The onset of clinically detectable proliferative sickle cell retinopathy may begin in the first decade of life, but more commonly occurs between 15 and 30 years of age. Proliferative sickle retinopathy is a peripheral retinal vascular disease.[107] The initial event is a peripheral arteriolar occlusion that Goldberg has classified as stage 1. The capillary bed and venules that drain the affected retina become nonperfused. Stage 2 describes the formation of peripheral arteriovenous anastomoses at the border of the perfused and nonperfused retina. Stage 3 is characterized by definite retinal neovascularization that assumes a sea-fan configuration. The sea fan arises from the venous side of the arteriovenous anastomoses and grows from perfused retina toward the peripheral nonperfused retina. Stage 4 refers to vitreous hemorrhage secondary to ongoing vitreoretinal traction. Finally, stage 5 describes tractional or rhegmatogenous retinal detachment.

Fluorescein Angiography

The hallmark of sickle cell retinopathy is the repetitive nature of the arterial occlusions in the different vascular beds. The angiographic findings demonstrate hypofluorescent areas and nonperfused vessels. The sea fans demonstrate fluorescein leakage (Fig. 5.36).

Treatment

Up to 60% of eyes with sea fans undergo autoinfarction. Therefore, not all eyes with a sea fan have to be treated. The goal of management is early treatment of lesions in stage 3. Feeder vessel photocoagulation has been shown to be effective in achieving infarction of 88% of eyes with peripheral neovascularization.[108] Scatter photocoagulation is also effective in reducing the risk of developing vitreous hemorrhage. Cryotherapy is reserved for those cases with media opacities.[109] Pars plana vitrectomy carries a high risk of intraoperative and postoperative complications, so it should be reserved for eyes with retinal detachment and nonclearing vitreous hemorrhage.

Eales' Disease

In 1880 Henry Eales[110] described in seven young patients, who had no evidence of primary retinal or systemic disease, recurrent vitreous hemorrhages associated with distended tortuous retinal veins and epistaxis. He thought that constipation and the ensuing elevated venous pressure caused this condition. Although the etiology of this condition is currently unknown, it has been linked to tuberculous infection. An immune mechanism has been postulated to play a role in the pathogenesis of retinal perivasculitis in patients with tuberculin hypersensitivity.[111] Once the vasculitis subsides, the retinal vascular walls begin to atrophy, remodel, and become ensheathed by glial tissue. This idiopathic peripheral obliterative vasculopathy produces retinal ischemia, neovascularization, and vitreous hemorrhage. Currently, Eales' disease remains a diagnosis of exclusion.

Clinical Findings

Eales' disease affects mostly healthy young Indian, Pakistani, and Afghan males, usually between 20 and 30 years of age. It is bilateral in up to 90% of patients.

The symptoms that most patients complain of are those secondary to vitreous hemorrhage including floaters, blurring of vision, and gross diminution of vision.

The first stage of the disease is the inflammatory stage. The patients present with a retinal perivasculitis affecting the peripheral retina. This is followed by the second stage, which is characterized by sclerosis of the retinal vessels, which leads to ischemia, The final stage is the proliferative stage where NVE, NVD, and recurrent vitreous hemorrhages with or without retinal detachment occur (Fig. 5.37). Peripheral NVE is reported in 36% to 84% of cases, and NVD in only 9%. Recurrent vitreous hemorrhage is the hallmark of the disease, which affects 37% of the patients. If the hemorrhage remains unresolved, it can lead to organization and retinal detachment.

Macular changes are seen in 18% of the eyes. The findings include macular edema, exudates, epiretinal membrane, subhyaloid hemorrhage, macular hole, and submacular fibrosis.[112]

Fluorescein Angiography

In cases of active retinal vasculitis, staining of vessels is seen during the early venous phase with extravasation in the late phase. In the healed stage only staining of the vessel wall occurs. Areas of capillary closure, engorged tortuous capillaries and venovenous shunts can be seen in the ischemic stage. Neovascularization is seen with a characteristic sea-fan pattern that hyperfluoresces intensely in the early arteriovenous phase, and leaks profusely in the late venous phase.

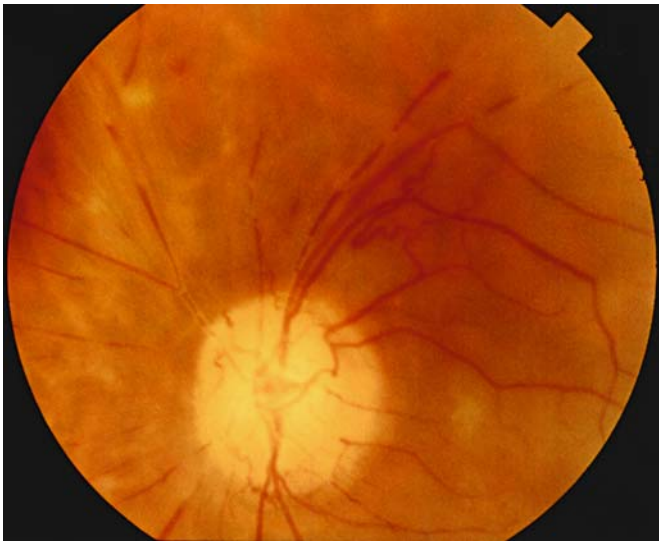

Fig. 5.37. Eales' disease. The patient complained of a sudden decrease in vision of her left eye. She had an afferent pupillary defect and rubeosis iridis. The left optic disc shows pallor, prominent shunt vessels, sheathing, and attenuation of the retinal vessels.

Treatment

The treatment of Eales' disease depends on the stage of the disease. During the acute inflammatory stage, oral steroids are the mainstay of treatment. Oral prednisolone on the order of 1 mg/kg of body weight is recommended. It is tapered to 10 mg per week over 6 to 8 weeks. In patients who do not respond to systemic steroids or have unacceptable side effects, immunosuppressive agents can be used. Patients with the regressed stage of perivasculitis are observed periodically every 6 months to 1 year. Patients with fresh vitreous hemorrhage are observed at intervals of 4 to 6 weeks, since most of these hemorrhages clear in 6 to 8 weeks. Scatter laser photocoagulation is performed in cases of capillary nonperfusion, NVE, or NVD.[113] Vitreoretinal surgery is required in cases of nonclearing vitreous hemorrhage, especially if retinal detachment is present. The results from such interventions are usually satisfactory.

Conclusion

Indocyanine green angiography is a highly specialized technique for imaging choroidal vasculature. Fluorescein angiography is highly specialized in the identification of morphologic and dynamic changes of the retinal circulation and RPE. Although retinal fluorescein and ICGV have many physical and chemical differences, the technologies complement each other in the evaluation of a variety of retinal diseases, revealing important and different aspects of retinal or choroidal diseases. Additionally, some stages of various diseases are best seen with FA while other aspects are best revealed with ICGV.

Fluorescein angiography and ICGV have both become very important tools in the evaluation and diagnosis of vascular retinal diseases.

References

1. Klein R. The epidemiology of diabetic retinopathy: findings from the Wisconsin Epidemiologic Study of Diabetic Retinopathy. Int Ophthalmol Clin 1987;27:230–238.
2. Klein R, Klein BE, Moss SE, Davis MD, DeMets DL. The Wisconsin Epidemiologic Study of Diabetic Retinopathy. IX. Four-year incidence and progression of diabetic retinopathy when age at diagnosis is less than 30 years. Arch Ophthalmol 1989;107:237–243.
3. The effect of intensive treatment of diabetes on the development and progression of long-term complications in insulin-dependent diabetes mellitus. The Diabetes Control and Complications Trial Research Group. N Engl J Med 1993;329:977–986.
4. Kohner EM, Aldington SJ, Stratton IM, et al. United Kingdom Prospective Diabetes Study, 30: diabetic retinopathy at diagnosis of non-insulin-dependent diabetes mellitus and associated risk factors. Arch Ophthalmol 1998;116:297–303.

5. Wolfensberger TJ. The historical discovery of macular edema. Doc Ophthalmol 1999;97:207–216.
6. Duke-Elder S, Dobree JH. Diseases of the retina. In: Duke-Elder S, ed. System of ophthalmology, vol X. St. Louis: CV Mosby, 1967:410.
7. Klein R, Klein BE, Moss SE, Davis MD, DeMets DL. The Wisconsin epidemiologic study of diabetic retinopathy. IV. Diabetic macular edema. Ophthalmology 1984;91:1464–1474.
8. Klein R, Klein BE, Moss SE, Cruickshanks KJ. The Wisconsin Epidemiologic Study of Diabetic Retinopathy: XVII. The 14-year incidence and progression of diabetic retinopathy and associated risk factors in type 1 diabetes. Ophthalmology 1998;105:1801–1815.
9. Klein R, Klein BE, Moss SE, Cruickshanks KJ. The Wisconsin Epidemiologic Study of Diabetic Retinopathy. XV. The long-term incidence of macular edema. Ophthalmology 1995;102:7–16.
10. Miyamoto K, Ogura Y. Pathogenetic potential of leukocytes in diabetic retinopathy. Semin Ophthalmol 1999;14:233–239.
11. Vinores SA, Youssri AI, Luna JD, et al. Upregulation of vascular endothelial growth factor in ischemic and non-ischemic human and experimental retinal disease. Histol Histopathol 1997;12:99–109.
12. Kristinsson JK, Gottfredsdottir MS, Stefansson E. Retinal vessel dilatation and elongation precedes diabetic macular oedema. Br J Ophthalmol 1997;81:274–278.
13. Aiello LP. The potential role of PKC beta in diabetic retinopathy and macular edema. Surv Ophthalmol 2002;47(suppl 2): S263–S269.
14. Aiello LP, Avery RL, Arrigg PG, et al. Vascular endothelial growth factor in ocular fluid of patients with diabetic retinopathy and other retinal disorders. N Engl J Med 1994;331:1480–1487.
15. Antonetti DA, Barber AJ, Khin S, Lieth E, Tarbell JM, Gardner TW. Vascular permeability in experimental diabetes is associated with reduced endothelial occluding content: vascular endothelial growth factor decreases occluding in retinal endothelial cells. Penn State Retina Research Group. Diabetes 1998;47:1953–1959.
16. Wilkinson CP, Ferris FL III, Klein RE, et al. Proposed international clinical diabetic retinopathy and diabetic macular edema disease severity scales. Ophthalmology 2003;110:1677–1682.
17. Lewis H. The role of vitrectomy in the treatment of diabetic macular edema. Am J Ophthalmol 2001;131:123–125.
18. Nussenblatt RB, Kaufman SC, Palestine AG, Davis MD, Ferris FL III. Macular thickening and visual acuity. Measurement in patients with cystoid macular edema. Ophthalmology 1987;94:1134–1139.
19. Hee MR, Puliafito CA, Wong C, et al. Quantitative assessment of macular edema with optical coherence tomography. Arch Ophthalmol 1995;113:1019–1029.
20. Photocoagulation treatment of proliferative diabetic retinopathy: the second report of diabetic retinopathy study findings. Ophthalmology 1978;85:82–106.
21. Berger AR, Boniuk I. Bilateral subretinal neovascularization after focal argon laser photocoagulation for diabetic macular edema. Am J Ophthalmol 1989;108:88–90.
22. Lewis H, Schachat AP, Haimann MH, et al. Choroidal neovascularization after laser photocoagulation for diabetic macular edema. Ophthalmology 1990;97:503–510; discussion 510–511.
23. Shah GK. Photodynamic therapy for choroidal neovascularization after thermal laser photocoagulation for diabetic macular edema. Am J Ophthalmol 2003;135:114–116.
24. Kychenthal A, Siebert A, Dorta P, Aylward B. Surgical removal of a laser-induced choroidal neovascular membrane. Retina 2001;21:69–71.
25. Fong DS, Segal PP, Myers F, Ferris FL, Hubbard LD, Davis MD. Subretinal fibrosis in diabetic macular edema. ETDRS report 23. Early Treatment Diabetic Retinopathy Study Research Group. Arch Ophthalmol 1997;115:873–877.
26. Nauck M, Karakiulakis G, Perruchoud AP, Papakonstantinou E, Roth M. Corticosteroids inhibit the expression of the vascular endothelial growth factor gene in human vascular smooth muscle cells. Eur J Pharmacol 1998;341:309–315.
27. Martidis A, Duker JS, Greenberg PB, et al. Intravitreal triamcinolone for refractory diabetic macular edema. Ophthalmology 2002;109:920–927.
28. Jonas JB, Kreissig I, Sofker A, Degenring RF. Intravitreal injection of triamcinolone for diffuse diabetic macular edema. Arch Ophthalmol 2003;121:57–61.
29. Jonas JB, Kreissig I, Degenring R. Intraocular pressure after intravitreal injection of triamcinolone acetonide. Br J Ophthalmol 2003;87:24–27.
30. Roth DB, Chieh J, Spirn MJ, Green SN, Yarian DL, Chaudhry NA. Noninfectious endophthalmitis associated with intravitreal triamcinolone injection. Arch Ophthalmol 2003;121:1279–1282.
31. Moshfeghi DM, Kaiser PK, Scott IU, et al. Acute endophthalmitis following intravitreal triamcinolone acetonide injection. Am J Ophthalmol 2003;136:791–796.
32. Arevalo JF, Fromow-Guerra J, Quiroz-Mercado H, et al. Primary intravitreal bevacizumab (Avastin) for diabetic macular edema: results from the Pan-American Collaborative Retina Study Group at 6-month follow-up. Ophthalmology 2007;114:743–750.
33. Early vitrectomy for severe vitreous hemorrhage in diabetic retinopathy. Two-year results of a randomized trial. Diabetic Retinopathy Vitrectomy Study report 2. The Diabetic Retinopathy Vitrectomy Study Research Group. Arch Ophthalmol 1985;103:1644–1652.
34. Tachi N, Ogino N. Vitrectomy for diffuse macular edema in cases of diabetic retinopathy. Am J Ophthalmol 1996;122:258–260.
35. Preliminary report on effects of photocoagulation therapy. The Diabetic Retinopathy Study Research Group. Am J Ophthalmol 1976;81:383–396.
36. Green WR, Chan CC, Hutchins GM, Terry JM. Central retinal vein occlusion: a prospective histopathologic study of 29 eyes in 28 cases. Trans Am Ophthalmol Soc 1981;79:371–422.
37. Orth DH, Patz A. Retinal branch vein occlusion. Surv Ophthalmol 1978;22:357–376.
38. Rath EZ, Frank RN, Shin DH, Kim C. Risk factors for retinal vein occlusions. A case-control study. Ophthalmology 1992;99:509–514.
39. Risk factors for central retinal vein occlusion. The Eye Disease Case-Control Study Group. Arch Ophthalmol 1996;114:545–554.
40. Pe'er J, Folberg R, Itin A, Gnessin H, Hemo I, Keshet E. Vascular endothelial growth factor upregulation in human central retinal vein occlusion. Ophthalmology 1998;105:412–416.
41. Hayreh SS, Rojas P, Podhajsky P, Montague P, Woolson RF. Ocular neovascularization with retinal vascular occlusion-III. Incidence of ocular neovascularization with retinal vein occlusion. Ophthalmology 1983;90:488–506.
42. McAllister IL, Constable IJ. Laser-induced chorioretinal venous anastomosis for treatment of nonischemic central retinal vein occlusion. Arch Ophthalmol 1995;113:456–462.

43. McAllister IL, Douglas JP, Constable IJ, Yu DY. Laser-induced chorioretinal venous anastomosis for nonischemic central retinal vein occlusion: evaluation of the complications and their risk factors. Am J Ophthalmol 1998;126:219–229.
44. McAllister IL, Vijayasekaran S, Yu DY, Constable IJ. Chorioretinal venous anastomoses: effect of different laser methods and energy in human eyes without vein occlusion. Graefes Arch Clin Exp Ophthalmol 1998;236:174–181.
45. Browning DJ, Rotberg MH. Vitreous hemorrhage complicating laser-induced chorioretinal anastomosis for central retinal vein occlusion. Am J Ophthalmol 1996;122:588–589.
46. Ip M, Kahana A, Altaweel M. Treatment of central retinal vein occlusion with triamcinolone acetonide: an optical coherence tomography study. Semin Ophthalmol 2003;18:67–73.
47. Arciniegas A. Treatment of the occlusion of the central retinal vein by section of the posterior ring. Ann Ophthalmol 1984;16:1081–1086.
48. Opremcak EM, Bruce RA, Lomeo MD, Ridenour CD, Letson AD, Rehmar AJ. Radial optic neurotomy for central retinal vein occlusion: a retrospective pilot study of 11 consecutive cases. Retina 2001;21:408–415.
49. Garciia-Arumii J, Boixadera A, Martinez-Castillo V, Castillo R, Dou A, Corcostegui B. Chorioretinal anastomosis after radial optic neurotomy for central retinal vein occlusion. Arch Ophthalmol 2003;121:1385–1391.
50. Elman MJ, Raden RZ, Carrigan A. Intravitreal injection of tissue plasminogen activator for central retinal vein occlusion. Trans Am Ophthalmol Soc 2001;99:219–221; discussion 222–223.
51. Bynoe LA, Weiss JN. Retinal endovascular surgery and intravitreal triamcinolone acetonide for central vein occlusion in young adults. Am J Ophthalmol 2003;135:382–384.
52. Kimmel AS, McCarthy MJ, Blodi CF, Folk JC. Branch retinal vein occlusion in sarcoidosis. Am J Ophthalmol 1989;107:561–562.
53. Friberg TR. Serpiginous choroiditis with branch vein occlusion and bilateral periphlebitis. Case report. Arch Ophthalmol 1988;106:585–586.
54. Tekeli O, Gursel E, Buyurgan H. Protein C, protein S and antithrombin III deficiencies in retinal vein occlusion. Acta Ophthalmol Scand 1999;77:628–630.
55. Glacet-Bernard A, Bayani N, Chretien P, Cochard C, Lelong F, Coscas G. Antiphospholipid antibodies in retinal vascular occlusions. A prospective study of 75 patients. Arch Ophthalmol 1994;112:790–795.
56. Staurenghi G, Lonati C, Aschero M, Orzalesi N. Arteriovenous crossing as a risk factor in branch retinal vein occlusion. Am J Ophthalmol 1994;117:211–213.
57. Weinberg D, Dodwell DG, Fern SA. Anatomy of arteriovenous crossings in branch retinal vein occlusion. Am J Ophthalmol 1990;109:298–302.
58. Spaide RF, Lee JK, Klancnik JK Jr, Gross NE. Optical coherence tomography of branch retinal vein occlusion. Retina 2003;23:343–347.
59. Harino S, Oshima Y, Tsujikawa K, Ogawa K, Grunwald JE. Indocyanine green and fluorescein hyperfluorescence at the site of occlusion in branch retinal vein occlusion. Graefes Arch Clin Exp Ophthalmol 2001;239:18–24.
60. Panozzo G, Gusson E, Parolini B, Mercanti A. Role of OCT in the diagnosis and follow up of diabetic macular edema. Semin Ophthalmol 2003;18:74–81.
61. Argon laser photocoagulation for macular edema in branch vein occlusion. The Branch Vein Occlusion Study Group. Am J Ophthalmol 1984;98:271–282.
62. Chen SD, Lochhead J, Patel CK, Frith P. Intravitreal triamcinolone acetonide for ischaemic macular oedema caused by branch retinal vein occlusion. Br J Ophthalmol 2004;88:154–155.
63. Argon laser scatter photocoagulation for prevention of neovascularization and vitreous hemorrhage in branch vein occlusion. A randomized clinical trial. Branch Vein Occlusion Study Group. Arch Ophthalmol 1986;104:34–41.
64. McAllister IL, Yu DY, Vijayasekaran S, Barry C, Constable I. Induced chorioretinal venous anastomosis in experimental retinal branch vein occlusion. Br J Ophthalmol 1992;76:615–620.
65. Brown GC, Magargal LE. The ocular ischemic syndrome. Clinical, fluorescein angiographic and carotid angiographic features. Int Ophthalmol 1988;11:239–251.
66. Kearns TP, Hollenhorst RW. Venous-stasis retinopathy of occlusive disease of the carotid artery. Mayo Clin Proc 1963;38:304–312.
67. MRC European Carotid Surgery Trial: interim results for symptomatic patients with severe (70–99%) or with mild (0–29%) carotid stenosis. European Carotid Surgery Trialists' Collaborative Group. Lancet 1991;337:1235–1243.
68. Beneficial effect of carotid endarterectomy in symptomatic patients with high-grade carotid stenosis. North American Symptomatic Carotid Endarterectomy Trial Collaborators. N Engl J Med 1991;325:445–453.
69. von Graefe A. Ueber Embolie der arteria centralis retinae als Urscahe plotzlicher Erblingdung. Arch fur Ophthalmol 1859;5:136–157.
70. Brown GC, Magargal LE. Central retinal artery obstruction and visual acuity. Ophthalmology 1982;89:14–19.
71. Wilson LA, Warlow CP, Russell RW. Cardiovascular disease in patients with retinal arterial occlusion. Lancet 1979;1:292–294.
72. Sharma S, Naqvi A, Sharma SM, Cruess AF, Brown GC. Transthoracic echocardiographic findings in patients with acute retinal arterial obstruction. A retrospective review. Retinal Emboli of Cardiac Origin Group. Arch Ophthalmol 1996;114:1189–1192.
73. Mohan K, Gupta A, Jain IS, Banerjee CK. Bilateral central retinal artery occlusion in occult temporal arteritis. J Clin Neuroophthalmol 1989;9:270–272.
74. Duker JS, Brown GC. Neovascularization of the optic disc associated with obstruction of the central retinal artery. Ophthalmology 1989;96:87–91.
75. Marmor MF, Jampol LM, Wohl L. Cilioretinal collateral circulation after occlusion of the central retinal artery. Br J Ophthalmol 1985;69:805–809.
76. Shah GK, Sharma S, Brown GC. Iris neovascularization following branch retinal artery occlusion. Can J Ophthalmol 1998;33:389–390.
77. Brown GC, Duker JS, Lehman R, Eagle RC Jr. Combined central retinal artery-central vein obstruction. Int Ophthalmol 1993;17:9–17.
78. Beatty S, Au Eong KG. Local intra-arterial fibrinolysis for acute occlusion of the central retinal artery: a meta-analysis of the published data. Br J Ophthalmol 2000;84:914–916.
79. Reynard M, Hanscom TA. Neodymium:yttrium-aluminum-garnet laser arteriotomy with embolectomy for central retinal artery occlusion. Am J Ophthalmol 2004;137:196–198.

80. Chobanian AV, Bakris GL, Black HR, et al. The Seventh Report of the Joint National Committee on Prevention, Detection, Evaluation, and Treatment of High Blood Pressure: the JNC 7 report. JAMA 2003;289:2560–2572.
81. de Venecia G, Jampol LM. The eye in accelerated hypertension. II. Localized serous detachments of the retina in patients. Arch Ophthalmol 1984;102:68–73.
82. Robertson DM. Macroaneurysms of the retinal arteries. Trans Am Acad Ophthalmol Otolaryngol 1973;77:OP55–O67.
83. Rabb MF, Gagliano DA, Teske MP. Retinal arterial macroaneurysms. Surv Ophthalmol 1988;33:73–96.
84. Nadel AJ, Gupta KK. Macroaneurysms of the retinal arteries. Arch Ophthalmol 1976;94:1092–1096.
85. Amalric P, Dauban F, Courtois M, Broqua JP. [Clinical symptoms and angiography of retinal artery macro-aneurysms]. Bull Soc Ophthalmol Fr 1979;79:109–111.
86. Townsend-Pico WA, Meyers SM, Lewis H. Indocyanine green angiography in the diagnosis of retinal arterial macroaneurysms associated with submacular and preretinal hemorrhages: a case series. Am J Ophthalmol 2000;129:33–37.
87. Lewis H. Intraoperative fibrinolysis of submacular hemorrhage with tissue plasminogen activator and surgical drainage. Am J Ophthalmol 1994;118:559–568.
88. Hudomel J, Imre G. Photocoagulation treatment of solitary aneurysm near the macula lutea. Report of a case. Acta Ophthalmol (Copenh) 1973;51:633–638.
89. Stallard HB. Radiant energy as (a) a pathogenic and (b) a therapeutic agent in ophthalmic disorders. Br J Ophthalmol Suppl 1933;6:1–126.
90. Kinyoun JL, Lawrence BS, Barlow WE. Proliferative radiation retinopathy. Arch Ophthalmol 1996;114:1097–1100.
91. Gass JD. A fluorescein angiographic study of macular dysfunction secondary to retinal vascular disease. VI. X-ray irradiation, carotid artery occlusion, collagen vascular disease, and vitreitis. Arch Ophthalmol 1968;80:606–617.
92. Amoaku WM, Lafaut B, Sallet G, De Laey JJ. Radiation choroidal vasculopathy: an indocyanine green angiography study. Eye 1995;9(pt 6):738–744.
93. Sutter FK, Gillies MC. Intravitreal triamcinolone for radiation-induced macular edema. Arch Ophthalmol 2003;121:1491–1493.
94. Thorne JE, Maguire AM. Good visual outcome following laser therapy for proliferative radiation retinopathy. Arch Ophthalmol 1999;117:125–126.
95. Coats G. Forms of retinal disease with massive exudation. R London Ophthalmol Hosp Rep 1908;17:440–459.
96. Egerer I, Tasman W, Tomer TT. Coats disease. Arch Ophthalmol 1974;92:109–112.
97. Shields JA, Shields CL, Honavar SG, Demirci H, Cater J. Classification and management of Coats disease: the 2000 Proctor Lecture. Am J Ophthalmol 2001;131:572–583.
98. Kranias G, Krebs TP. Advanced Coats' disease successfully managed with vitreo-retinal surgery. Eye 2002;16:500–501.
99. Kreusel KM, Krause L, Broskamp G, Jandeck C, Foerster MH. Pars plana vitrectomy and endocryocoagulation for paracentral Coats' disease. Retina 2001;21:270–271.
100. Engelbrecht NE, Aaberg TM Jr, Sung J, Lewis ML. Neovascular membranes associated with idiopathic juxtafoveolar telangiectasis. Arch Ophthalmol 2002;120:320–324.
101. Chew EY, Murphy RP, Newsome DA, Fine SL. Parafoveal telangiectasis and diabetic retinopathy. Arch Ophthalmol 1986;104:71–75.
102. Mansour AM, Schachat A. Foveal avascular zone in idiopathic juxtafoveolar telangiectasia. Ophthalmologica 1993;207:9–12.
103. Berger AS, McCuen BW II, Brown GC, Brownlow RL Jr. Surgical removal of subfoveal neovascularization in idiopathic juxtafoveolar retinal telangiectasis. Retina 1997;17:94–98.
104. Alldredge CD, Garretson BR. Intravitreal triamcinolone for the treatment of idiopathic juxtafoveal telangiectasis. Retina 2003;23:113–116.
105. Condon PI, Serjeant GR. Ocular findings in sickle cell thalassemia in Jamaica. Am J Ophthalmol 1972;74:1105–1109.
106. Gagliano DA, Goldberg MF. The evolution of salmon-patch hemorrhages in sickle cell retinopathy. Arch Ophthalmol 1989;107:1814–1815.
107. Goldberg MF. Classification and pathogenesis of proliferative sickle retinopathy. Am J Ophthalmol 1971;71:649–665.
108. Jacobson MS, Gagliano DA, Cohen SB, et al. A randomized clinical trial of feeder vessel photocoagulation of sickle cell retinopathy. A long-term follow-up. Ophthalmology 1991;98:581–585.
109. Lee CB, Woolf MB, Galinos SO, Goldbaum MH, Stevens TS, Goldberg MF. Cryotherapy of proliferative sickle retinopathy. Part I. Single freeze-thaw cycle. Ann Ophthalmol 1975;7:1299–1308.
110. Eales H. Cases of retinal hemorrhage associated with epistaxis and constipation. Birmingham Med Rev 1880;9:262.
111. Madhavan HN, Therese KL, Doraiswamy K. Further investigations on the association of Mycobacterium tuberculosis with Eales' disease. Indian J Ophthalmol 2002;50:35–39.
112. Biswas J, Sharma T, Gopal L, Madhavan HN, Sulochana KN, Ramakrishnan S. Eales disease—an update. Surv Ophthalmol 2002;47:197–214.
113. Atmaca LS, Gunduz K, Idil A. Photocoagulation in Eales disease. Ocul Immunol Inflamm 1993;1:49–54.

6
Angiography of Inflammatory Diseases in Immunocompetent and Immunocompromised Patients

J. Fernando Arevalo, Reinaldo A. Garcia, Lourdes Arellanes-Garcia, and Jans Fromow-Guerra

Retinal fluorescein angiography (FA) constitutes a valuable study in the diagnosis and follow-up of patients with inflammatory eye diseases.[1] Changes in fluorescence secondary to inflammation are divided into those that produce a hyperfluorescent image and those that produce hypofluorescence (Table 6.1).[2] Hyperfluorescence may be secondary to abnormal blood vessels, dye filtration or to a defect in the retinal pigment epithelium (RPE), allowing the choroidal circulation to become more apparent. Hypofluorescence is due to a block in fluorescence (i.e., pigment accumulation) or to a defect in vascular filling.[2]

Indocyanine green (ICG) is a dye that has several advantages over sodium fluorescein for visualization of choroidal vasculature. It is recognized that ICG provides better visualization of choroidal vessels. The dye absorbs (805 mm) and fluoresces (835 mm) in the near-infrared range,[3] and visualization of fluorescence is possible through hemorrhage, lipid, RPE, and xanthophyll. Indocyanine green is highly bound to protein and, therefore, leaks more slowly through the fenestrations of the choriocapillaris. Advances combining digital imaging systems with ICG fundus cameras have allowed high-resolution digital ICG videoangiography (ICGV). Several reports have demonstrated the usefulness of ICGV in the diagnosis of occult choroidal neovascularization (CNV) secondary to age-related macular degeneration,[4–7] other chorioretinal disorders, [8–13] and choroidal tumors.[14–16]

Indications for Fluorescein and Indocyanine Green Angiography in Inflammatory Diseases

Retinal fluorescein and ICG angiography (ICGA) in inflammatory diseases are especially important in three circumstances, as discussed in the following subsections.[17]

Identification of Macular Complications

Retinal fluorescein and ICGA identify macular complications of anterior or posterior uveitis, such as cystoid macular edema, retinal or choroidal ischemia, CNV, or epiretinal membranes. These complications appear in several other conditions and are not specific to the underlying condition that may be causing it.

Cystoid Macular Edema

With the formation of numerous cystoid spaces, fluid collects in the fovea and parafoveal areas of the sensory retina. The arteriovenous phase of the angiogram shows early leakage of dye in the parafoveal area. In the late arteriovenous phase a characteristic "petaloid" or flower-petal pattern appears on the angiogram in parafoveal area, and at the recirculation phase FA shows persistent pooling of dye in cystoid spaces.[18] Cystoid macular edema (CME) is one of the major causes of decreased vision in many types of intraocular disease and is a common complication in pars planitis (PP); it can be found in 63% of cases and is commonly associated with optic disc and capillaries hyperfluorescence ("fern pattern") (Fig. 6.1).[19] One of the most important characteristics of CME in pars planitis is that it becomes evident in the early and intermediate phases of FA, which differentiates it from the late-phase CME found in other disease processes (Fig. 6.2). Other intraocular inflammatory diseases that may be associated with CME are sarcoidosis, birdshot retinochoroidopathy, and any chronic iridocyclitis.[19] Behçet disease, Vogt-Koyanagi-Harada (VKH) syndrome, and multifocal choroiditis are uveitic syndromes associated with diffuse macular edema, an example of hyperfluorescence secondary to tissue staining.[20–22]

Macular, Retinal, and Choroidal Ischemia

In macular ischemia, closure of perifoveal vessels manifests as an enlarged irregular foveal avascular zone, best seen in the early venous phase of FA. Macular ischemia is predominantly seen in Adamantiades-Behçet disease, sarcoidosis, and idiopathic vasculitis.[17] In retinal ischemia, hypofluorescence may be secondary to a vascular filling defect or to a blocked fluorescence. Tissue destruction due to severe inflammation causes blood vessel disappearance and a vascular filling defect. Vascular occlusion affecting arteries and veins can be

Table 6.1. Fluorescein angiography patterns

	Filtration	Pooling Staining
Hyperfluorescence	Increased vessel permeability	
	Window defect which manifests choroidal hyperfluorescence	
Hypofluorescence	Blocked fluorescence	Preretinal Intraretinal Subretinal
	Vascular filling defect	

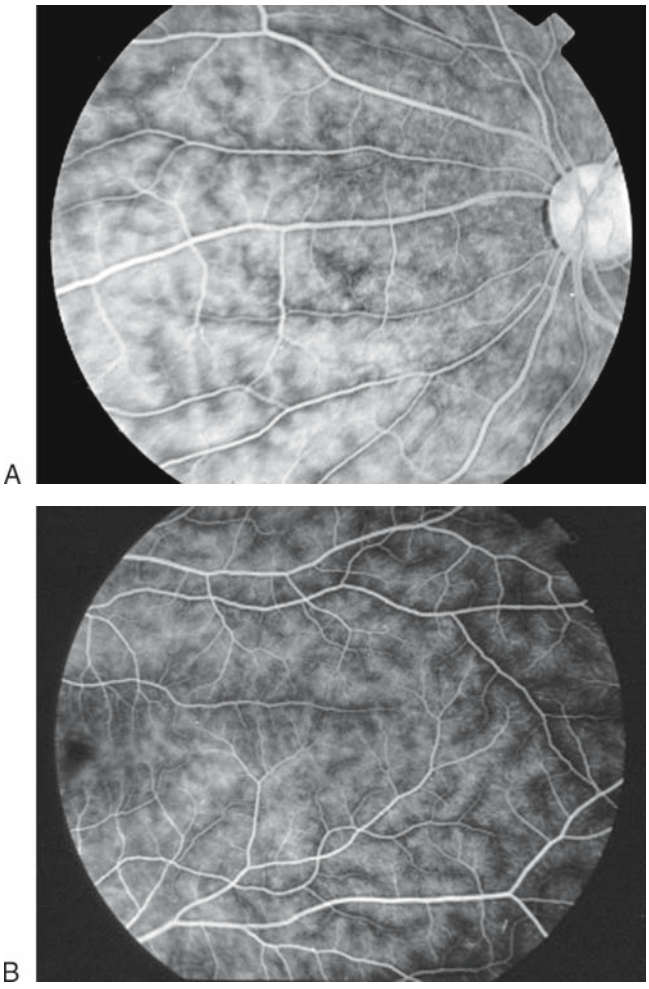

Fig. 6.1. (A,B) Capillaries hyperfluorescence. "Fern pattern" in a patient with pars planitis.

found in polyarteritis nodosa and acute retinal necrosis[23]; vein occlusion is predominantly seen in systemic lupus erythematosus (SLE) and in Eales' disease, which also compromises capillaries. In choroidal ischemia, occlusion of choroidal vessels is seen in Behçet disease, acute posterior multifocal placoid pigment epitheliopathy, VKH syndrome, and some collagenopathies (Fig. 6.3).[20,24]

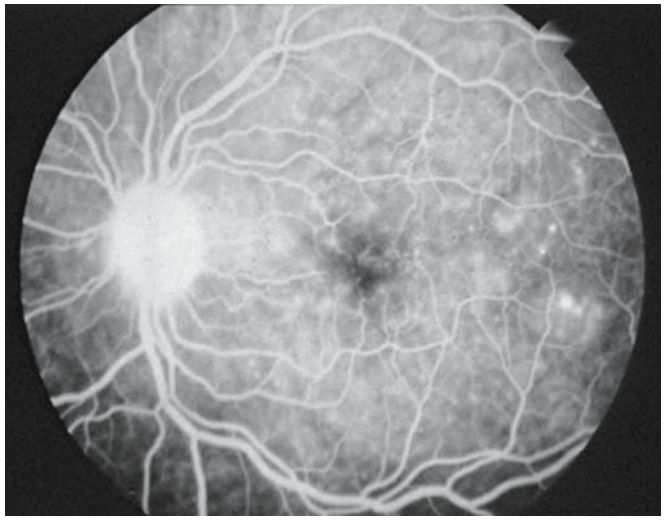

Fig. 6.2. Early-phase cystoid macular edema and papillary hyperfluorescence in a patient with pars planitis.

Many inflammatory diseases are thought to be associated with abnormalities in the choroidal blood flow. Unfortunately, the excitation and fluorescence of fluorescein dye are absorbed and scattered by the RPE. In addition, fluorescein dye rapidly leaks from the fenestrated vessels of the choriocapillaris, leading to a diffuse background choroidal fluorescence. The resulting diffuse fluorescence from the subpigment epithelial space prohibits evaluation of the choroidal blood flow with fluorescein. It is recognized that ICG provides better visualization of choroidal vessels in these cases.

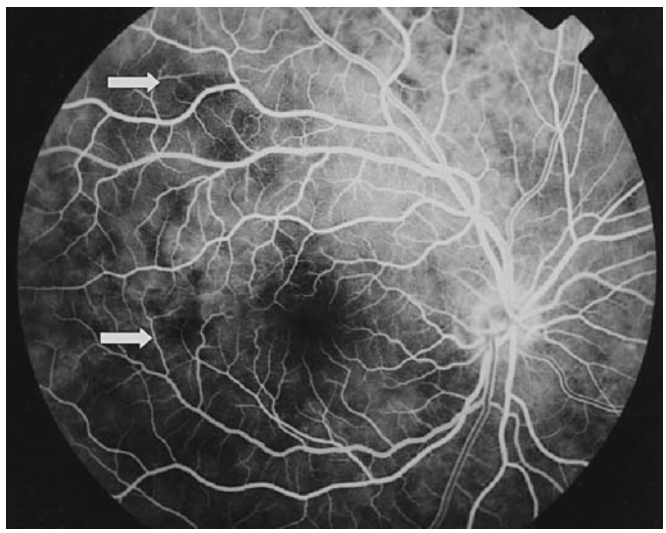

Fig. 6.3. Occlusion of choroidal vessels in a patient with Vogt-Koyanagi-Harada syndrome.

Choroidal Neovascularization

Choroidal new vessels that have broken through Bruch's membrane into the sub-RPE or subretinal space fill with dye early; they have a characteristic pattern of hyperfluorescence with fuzzy margins that expands through the transit into reperfusion. The accumulation of blood, fibrin, or pigment necessarily prevents the study of any underlying structures by FA. This limitation is avoided by indocyanine green.

Choroid

Subretinal neovascular membranes can be found in sarcoidosis, birdshot retinochoroidopathy, multifocal choroiditis, serpiginous choroiditis (SC), VKH syndrome, and presumed ocular histoplasmosis syndrome (POHS) (Fig. 6.4).

Neovascularization at the retina is a common finding in occlusive vasculitis such as Behçet disease, SLE, and Eales' disease (Fig. 6.5). Sometimes it can be found in ocular toxoplasmosis when the retinochoroidal scar causes vascular occlusion.[15,24] Inflammatory choroidal neovascular membranes differ from those associated with macular degeneration in that they are typically pigmented and not associated with drusen, pigment epithelial detachment (PED), or a large degree of hemorrhage.[17]

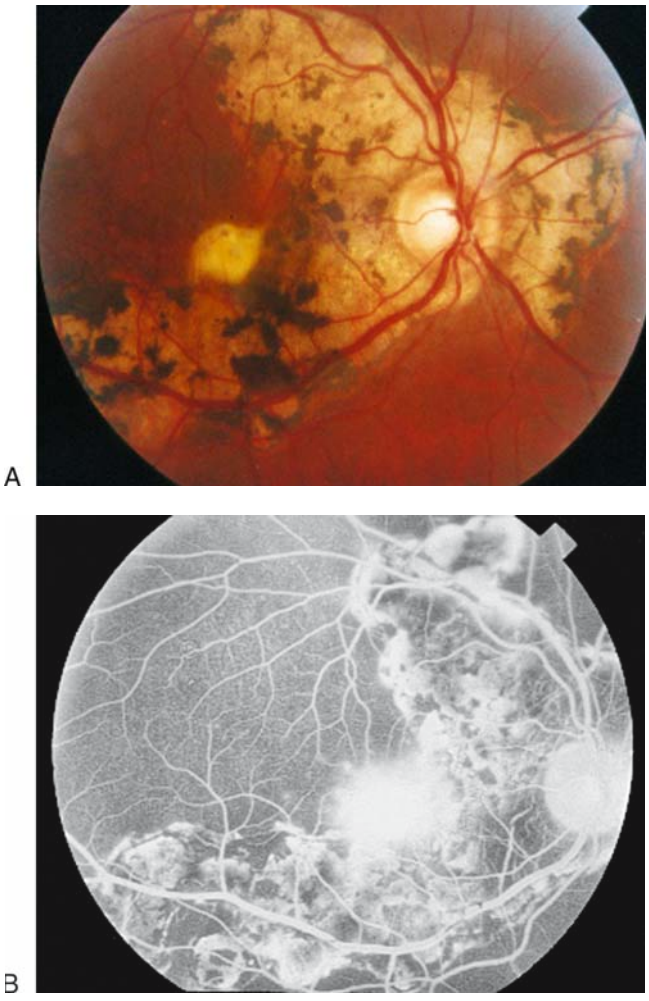

Fig. 6.4. (A,B) Clinical picture and angiography hyperfluorescence of a patient with serpiginous choroiditis showing choroidal neovascularization.

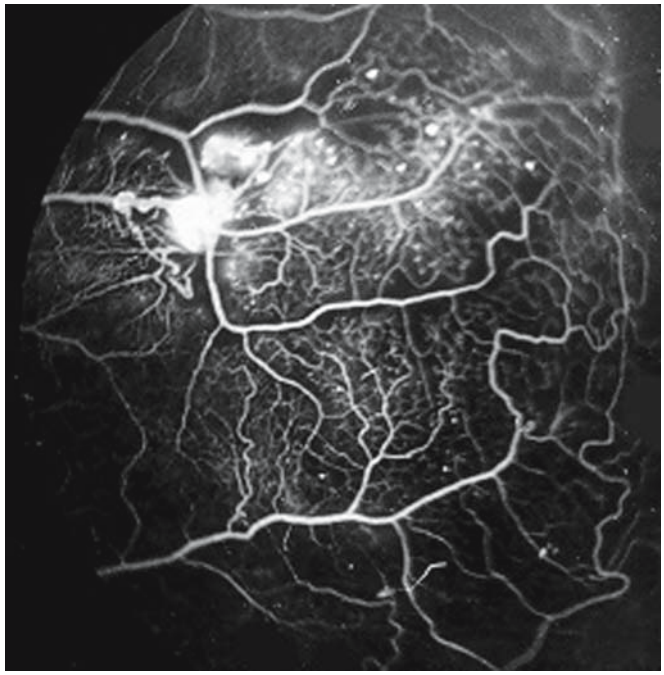

Fig. 6.5. Retinal neovascularization and closure of the capillary net in a patient with Eales' disease.

Epiretinal Membrane

Fluorescein angiography demonstrates the characteristic corkscrew appearance of retinal vessels in patients with contraction of internal limiting membrane by epiretinal membranes. The straightening of some retinal vessels is associated with the corkscrew-like twisting of others. The vessels appear to be pulled to a point near the fovea, and some of the affected vessels may leak fluorescein. Leakage is most common soon after the membrane contracts and in eyes more likely to progress, so FA can help in the timing of surgical intervention.[17]

Detection of Subtle Retinal Vasculopathy or Choroidopathy

Retinal fluorescein and ICGA detect subtle retinal vasculopathy or choroidopathy that may be more apparent on angiography than on clinical examination.

Retinal Vasculopathy

Ocular inflammation may increase the permeability of retinal vessels. In these cases FA shows staining of the vessels

walls, well before the inflammation can be seen clinically. This hyperfluorescence, called parietal hyperfluorescence (Fig. 6.6), can be seen in pars planitis, ocular toxoplasmosis, sarcoidosis, Behçet disease, cytomegalovirus (CMV) retinitis, and acute retinal necrosis, among others.[19–21,26,27] Vogt-Koyanagi-Harada syndrome is a typical example of filtration hyperfluorescence, with pooling of dye into the subretinal space, an angiographic sign of serous retinal detachment secondary to an inflammatory exudate rising from multiple foci of choroiditis (Fig. 6.7).[28]

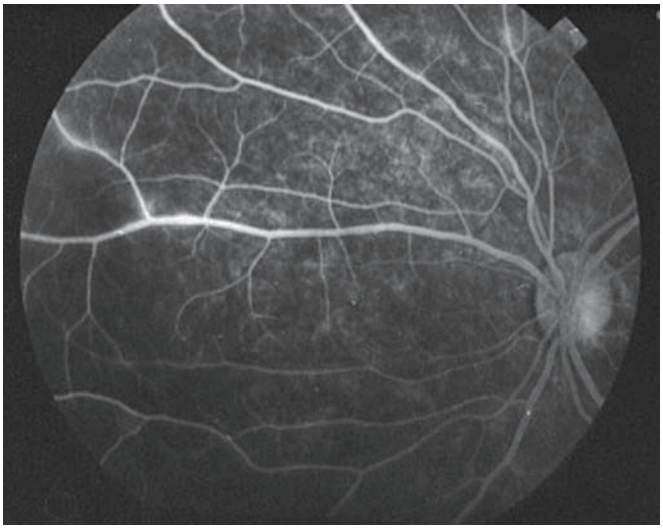

FIG. 6.6. Parietal hyperfluorescence secondary of vascular wall staining in a patient with pars planitis.

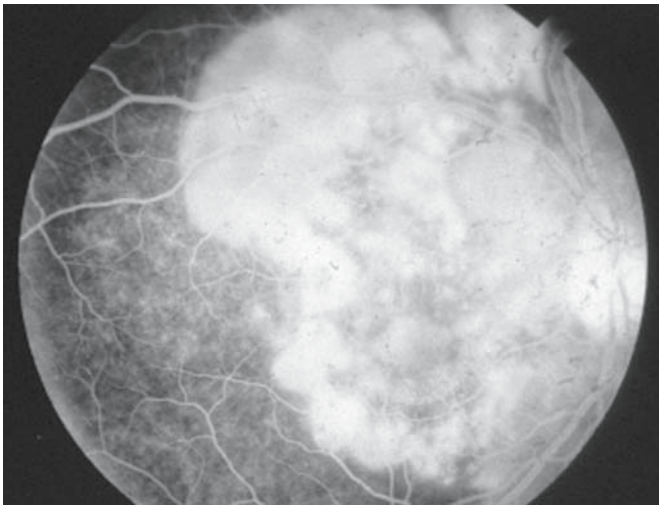

FIG. 6.7. Hyperfluorescence in a patient with pooling in the subretinal space secondary to an inflammatory exudate rising from multiple foci of choroiditis in a patient with Vogt-Koyanagi-Harada syndrome.

Choroidopathy

Atrophic spots due to fine defects of the RPE barrier that are often a sequela of inflammatory nodules look like sharply defined hyperfluorescent transmission defects during early dye transit with FA.[17] A window defect manifests as choroidal hyperfluorescence, and VKH syndrome, sympathetic ophthalmia, multiple evanescent white dot syndrome (MEWDS), presumed ocular histoplasmosis syndrome (POHS), and multifocal choroiditis are examples of hyperfluorescence secondary to an RPE defect.[23,29]

Diagnosis of Conditions with Stereotypic Findings on Fluorescein Angiography or Indocyanine Green Videoangiography

Noninfectious Diseases

White-Dot Chorioretinal Inflammatory Syndromes

White-dot chorioretinal inflammatory syndromes are a group of unrelated conditions that present with scattered white or yellow spots in the retina, with or without an associated posterior uveitis and sometimes preceding nonspecific flu-like systemic disease. Most of these diseases are recognized and categorized according to the specific anatomic and illustrative changes they induce in the fundal appearance. Although there is a superficial similarity in the fundus appearance of these conditions, they are different and their fluorescein and ICG angiograms are different.[30]

Multiple Evanescent White Dot Syndrome

Multiple evanescent white dot syndrome (MEWDS) is an acute, multifocal, usually unilateral retinopathy that is predominantly seen in young women with blurred central vision, bothersome photopsias, paracentral scotomas or enlargement of the blind spot, and headaches that usually resolve spontaneously over 2 months. The condition is manifest by small white dots (100 to 200 μm) seen at the level of the RPE or outer sensory retina. The white dots are mostly concentrated in the paramacular area, usually sparing the fovea itself, and are less prominent and numerous beyond the mayor vascular arcades. In addition, there is often a granular appearance to the macula, vitreal cells, retinal venous sheathing, blurring of the disc margins, and abnormalities shown on electroretinography during the acute phase.

Fluorescein Angiography. The white dots in the acute phase show early hyperfluorescence and late staining. Each lesion consists of a cluster of hyperfluorescent dots surrounding a relatively dark center in the arteriovenous stage of the angiogram. These lesions superficially resemble photocoagulation scars. Some window defects may be seen in the macula at the site of the irregular granularity. These lesions usually resolve in about 7 weeks on average, and vision returns to normal (Fig. 6.8).

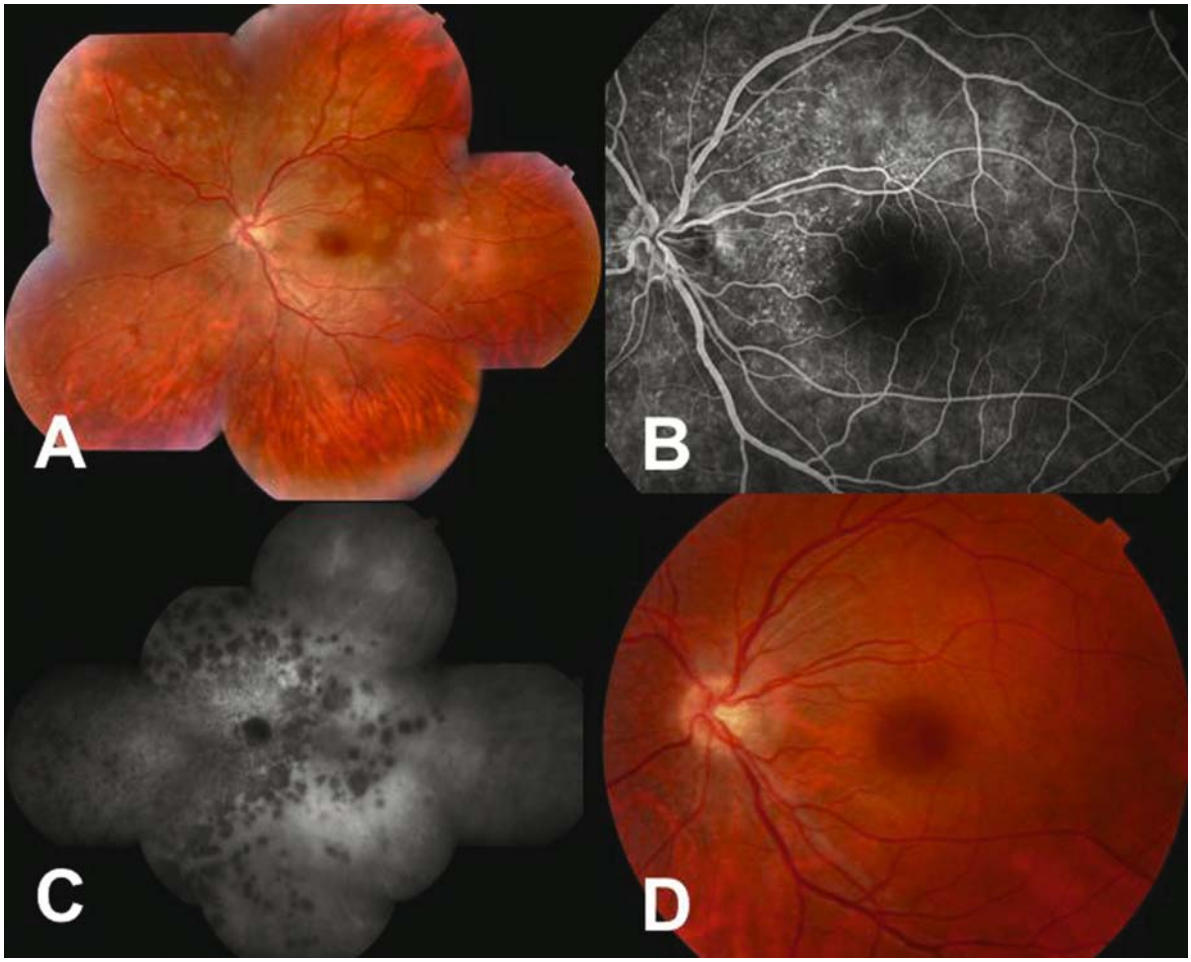

Fig. 6.8. A 25-year-old woman presented with photopsia, scotomas, and blurry vision in the left eye after a flu-like illness. Her vision was 20/20 OD, 20/60 OS. (A) Fundus examination revealed small and large spots scatted trough the fundus in the left eye. (B) Fluorescein angiography (FA) showed punctate hyperfluorescence. (C) Indocyanine green videoangiography (ICGV) demonstrated small and large hypofluorescent spots. A diagnosis of multiple evanescent white dot syndrome (MEWDS) was made. (D) One month later the spots in the fundus had disappeared and she had recovered her vision. (Courtesy of Antonio Ciardella, MD.)

Indocyanine Green Videoangiography. In the acute phase ICGV is characteristic, with numerous hypofluorescent spots throughout the posterior pole and periphery at about 10 minutes. These spots are larger than those seen on FA. In some patients, there is a ring of hypofluorescence around the optic nerve that seems to correlate with the presence of blind-spot enlargement (Fig. 6.8).

Acute Posterior Multifocal Placoid Pigment Epitheliopathy

Acute posterior multifocal placoid pigment epitheliopathy (APMPPE) can cause transient visual loss in young patients, is commonly bilateral (as opposed to MEWDS), and consists of focal, flat, gray-white lesions at the level of the RPE. The ocular lesions evolve fairly rapidly, changing from gray-white to partly depigmented. Typically, these lesions resolve spontaneously over weeks, with a delayed but reliable improvement in visual acuity to a subnormal level.

Fluorescein Angiography. The APMPPE lesions are considerably larger and block fluorescence early in the fluorescein angiogram, as opposed to early hyperfluorescence in MEWDS. More pigment disruption develops with APMPPE than with MEWDS. Therefore, the early phase FA of APMPPE shows irregular areas of blocked fluorescence characteristic of acute lesions. At the arteriovenous phase, acute lesions still block fluorescence and are well demarcated. Mid- and late-phase angiograms demonstrate diffuse even staining of the acute lesions. The lesions may involve the fovea; even with foveal involvement, the prognosis for a return of a good visual acuity is favorable. In the recovery phase of APMPPE, the lesions are primarily simple pigment epithelial window defects. These

lesions have the same map-like contours of acute lesions, with no leakage or staining (Fig. 6.9).

Indocyanine Green Videoangiography. Indocyanine green videoangiography demonstrates (especially in the late phases) the dark lesions that exactly correspond to the lesions that block fluorescence and stain late on the fluorescein angiogram. In healed APMPPE, more clearly delineated areas of hypofluorescence persist. Controversy exists about if there are blockage of fluorescence by inflammatory debris at the RPE cells or if there is transient occlusion of the choroidal arterioles. Because the hypofluorescence persist after the healed phase of the ICG and the patients usually recover good visual acuity, the more accepted theory is a partial choroidal vascular occlusion.[17]

Serpiginous Choroiditis

Serpiginous choroiditis (SC) is a bilateral recurrent inflammatory disease of unknown cause that affects the choroid and RPE. It typically occurs in white middle-aged persons. Acute lesions have a gray-white or yellow appearance that begins around the optic nerve or the posterior pole advancing centrifugally by recurrences (weeks to years) to the midperiphery in an irregular serpentine fashion, leading to scarring and choroidal atrophy, and may result in CNV in as many as 25% of patients.[31] Acute lesions last up to several months; however, over time, lesions become atrophic, with disappearance of the choriocapillaris and involvement of the underlying large choroidal vessels. New recurrent lesions most frequently occur adjacent to an area of choroidal and RPE atrophy, and

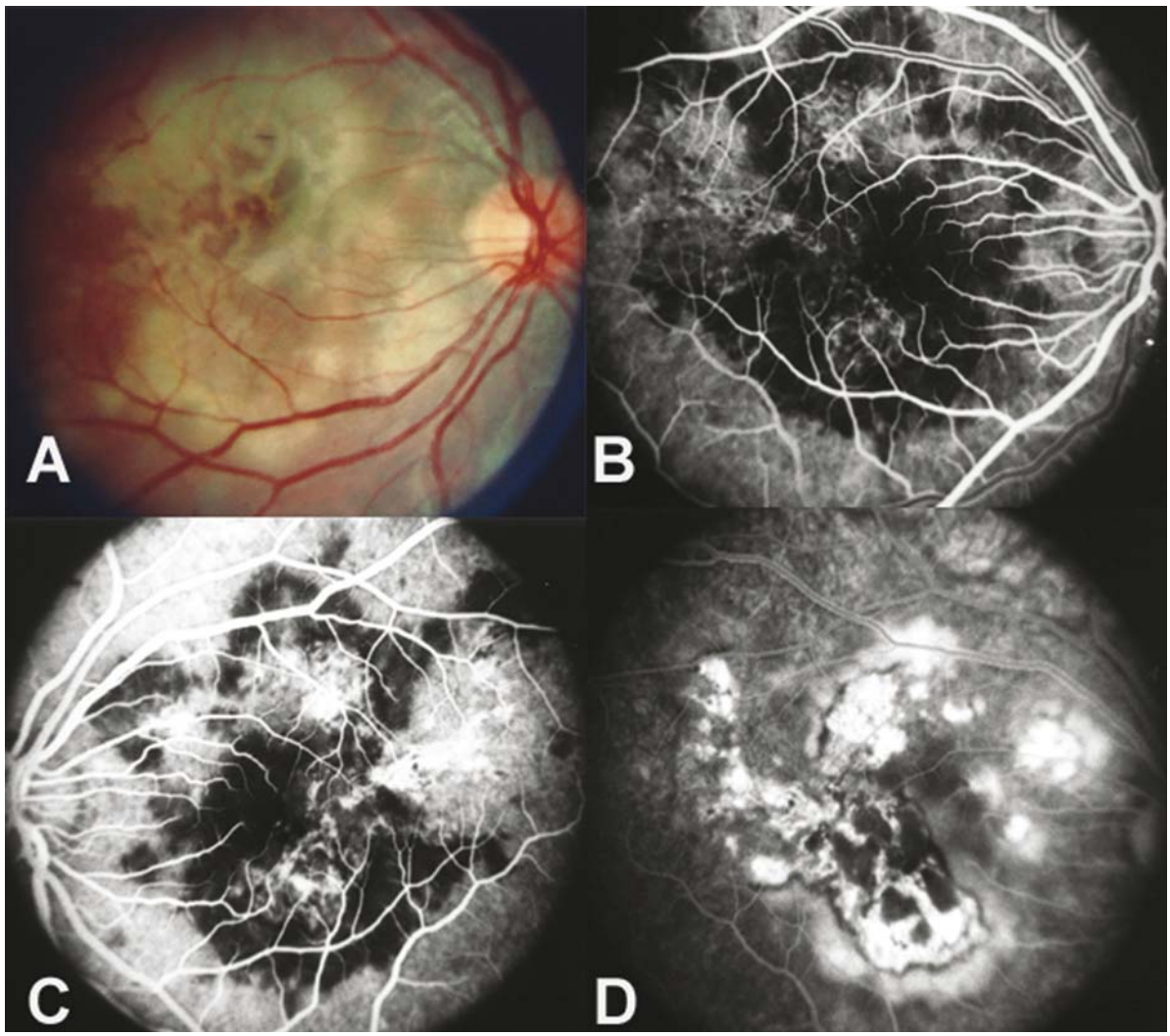

Fig. 6.9. (A) Early-phase FA in acute posterior multifocal placoid pigment epitheliopathy (APMPPE) shows irregular areas of blocked fluorescence characteristic of acute lesions. (B) At the arteriovenous phase, acute lesions still block fluorescence and are well demarcated. (C,D) Mid- and late-phase angiograms demonstrate diffuse even staining of the acute lesions.

inflammatory response in the anterior chamber or vitreous sometimes occurs.[32] Even in the absence of CNV, visual acuity is usually poor if the lesion extends into the fovea.

Fluorescein Angiography. Fluorescein angiography should show early blockage. As the angiogram proceeds, the active margins progressively become hyperfluorescent. This hyperfluorescence spreads toward the center of the lesion as it absorbs dye from the choriocapillaris. The early hypofluorescence may be due to blockage by swollen RPE cells, but usually represents the impaired choroidal vasculature (Figs. 6.10 and 6.11).[32] In the late phases of the angiogram, the margins stains with dye. During the inactive stage of the disease, the main portion of the lesion may show a mottled hyperfluorescence or a window defect type of fluorescence if the underlying choriocapillaris is still present. However, because in deep lesions the choriocapillaris is usually destroyed, in most patients the main part of the lesion is dark. Sometimes visualization of perfused deep choroidal vessels is facilitated by the loss of RPE and inner choroidal layers. Hyperfluorescent borders of the lesion are noted, which may represent dye leakage from intact adjacent choriocapillaris or staining of the scar tissue. [33] In the chronic stages, CNV may be present and cause late staining and leakage.[5(30)]

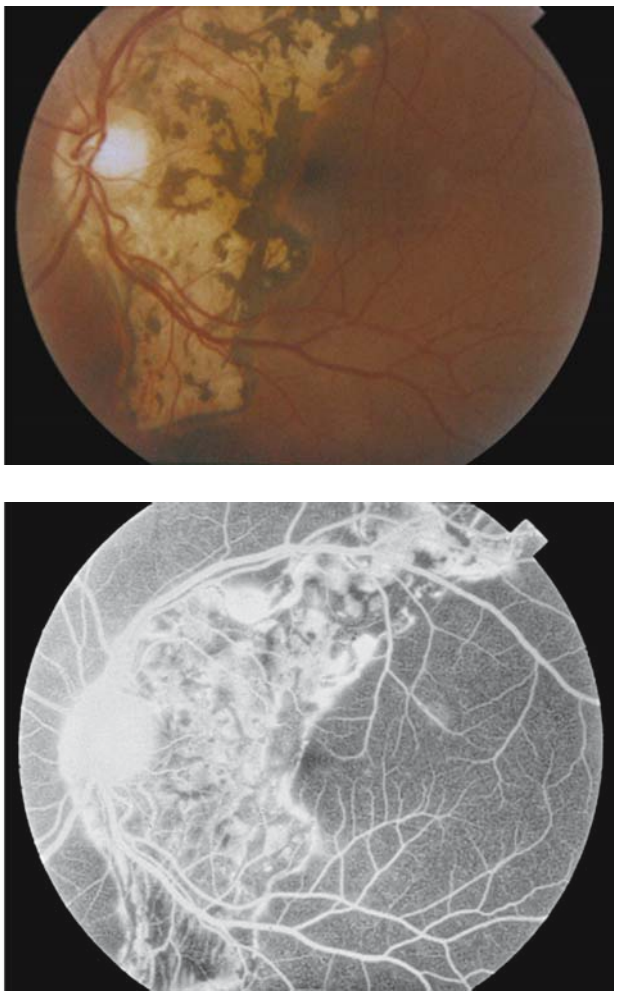

FIG. 6.10. Clinical photograph (A) and angiography (B) of a patient with serpiginous choroiditis showing pigment migration.

Indocyanine Green Videoangiography. Indocyanine green videoangiography may help to better describe the full extent of the disease because ICGV usually demonstrates many more lesions than are seen with fluorescein angiography. Therefore, ICGV can help to monitor disease progression. On ICGV, active lesions display marked hypofluorescence throughout the study. In the healed stage, with associated development of RPE and choriocapillaris atrophy, there may be delayed or absent choroidal filling in the early transit phase, but the patches of hypofluorescence resolve at least partially, and the deep choroidal vessels usually are better visualized with the associated loss of RPE and inner choroid.[17] When there is associated CNV, hyperfluorescence of the neovascular lesion is noted on the ICG study.

Birdshot Retinochoroidopathy

The characteristic spots of depigmentation, which are usually cream-colored at the level of RPE or deeper, are the most distinctive sign of birdshot retinochoroidopathy. The lesions radiate outward from the disc in a linear pattern that seems to follow the choroidal vessels. There is no noticeable thinning or atrophy of the retina and choroid at the site of these lesions. It is seen in middle-aged (40- to 60-year-old) healthy patients, is usually bilateral, and usually demonstrates significant vitreous reaction and retinal vascular leakage in an eye that appears externally quiet. Acute onset is not characteristic of birdshot retinochoroidopathy, and human leukocyte antigen (HLA) A29 is very frequently found to be positive in these patients. Retinal vascular abnormalities, such as hyperpermeability of capillaries with resultant cystoid macular edema, diffuse narrowing or retinal arterioles, perivascular hemorrhages in the nerve fiber layer, tortuosity of vessels, and optic disc swelling, are common findings in birdshot retinochoroidopathy. Although the precise etiology of the disease remains unknown, an immune-mediated process is strongly implicated.[34]

Fluorescein Angiography. There is usually an increase in the retinal circulation time, and the retinal vessels may leak fluorescein in the active stage. The angiographic characteristics of the spots depend on their stage in the disease. Early on, when there is choroidal infiltration with minimal RPE atrophy, the spots are hypofluorescent in the transit phase of the study and become mildly hyperfluorescent in the later phases as dye from the choriocapillaris stains the extrachoroidal vascular space (Fig. 6.12). This is consistent with a deep-seated inflammatory focus that gradually accumulates fluorescein. As RPE atrophy ensues, the spots may show early alteration of fluorescence or a hyperfluorescent window defect, followed by late staining, expected from choriocapillary atrophy or depigmentation of

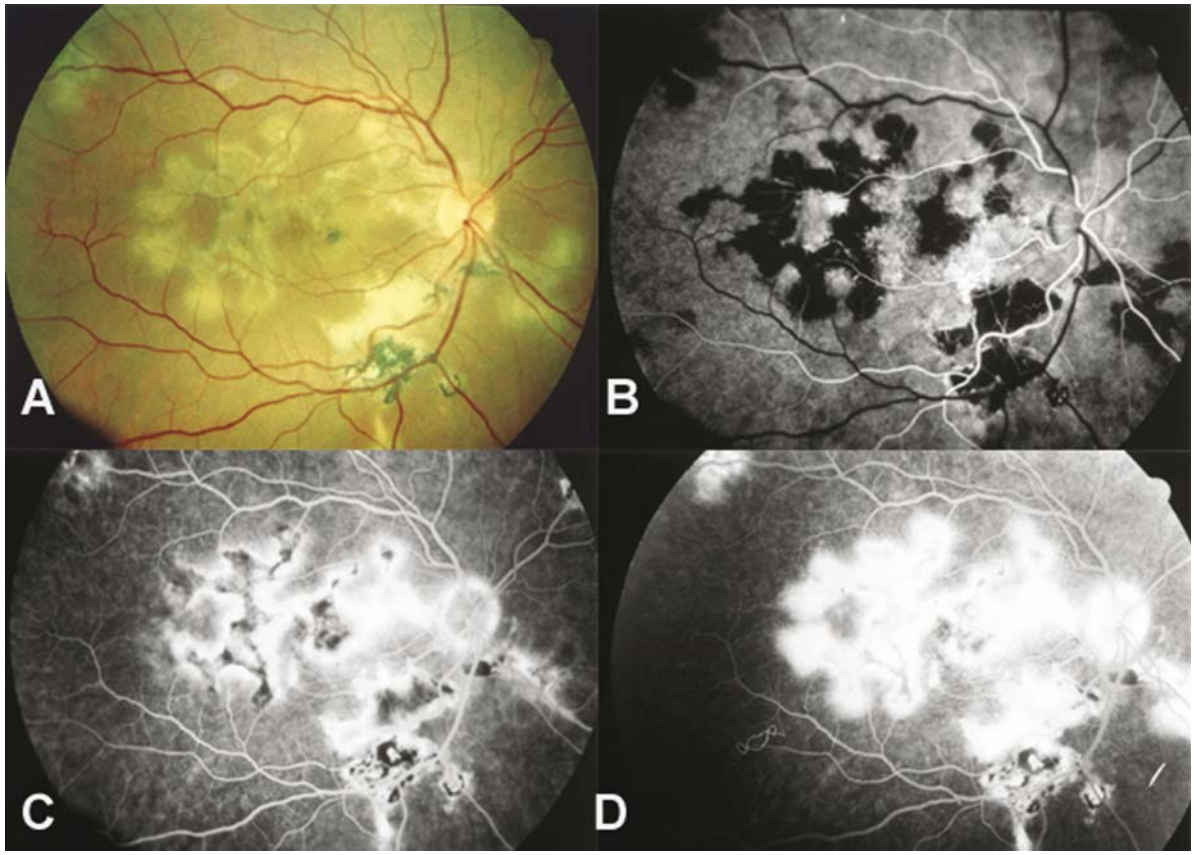

Fig. 6.11. Serpiginous choroiditis. (A) Color fundus photograph. (B) Fluorescein angiography shows early blockage. (C,D) As the angiogram proceeds, the active margins progressively become hyperfluorescent and spread toward the center of the lesion as it absorbs dye from the choriocapillaris.

the RPE, respectively. In many instances the lesions are more apparent by ophthalmoscopy than by angiography.

Indocyanine Green Videoangiography. There is a characteristic early pattern of scattered hypofluorescent (within 5 minutes of dye injection), well-delineated, round to oval spots often located between large choroidal vessels. The early appearance of the spots differentiate these lesions from the late spots seen with multifocal choroiditis. In contrast to the hyperfluorescent spots of FA, the hypofluorescent spots of ICGV exceed the number of depigmented lesions seen clinically, and they persist throughout the study and the convalescence phase of birdshot retinochoroidopathy, making it a useful diagnostic clue.[17,34] The focal loss of choroidal tissue may explain the persistence and expansion of hypofluorescent areas in long standing disease.[34]

Multifocal Choroiditis with Panuveitis

Cantrill and Folk[35] reported patients who presented with multifocal choroiditis with panuveitis (MCP) that progressed to subretinal fibrosis. Because MCP, punctate inner choroidopathy (PIC), and subretinal fibrosis are three conditions with similar clinical pictures and similar underlying causes, some authors prefer to classify them into the same group.[36]

Multifocal choroiditis with panuveitis is more common in females between 20 and 50 years of age. It is bilateral in the majority of affected patients. The several hundred yellow and sometimes gray lesions at the level of RPE and choriocapillaris, from 50 to 500 μm in diameter, can be seen in the peripapillary region, within the arcades, and in the midperiphery. They have a punched-out appearance with sharp margins. Inflammation is prominent, and the associated uveitis responds to corticosteroid treatment. Acute subretinal lesions may evolve into choroidal neovascularization or atrophy, and vision may be poor due to macular involvement.

Fluorescein Angiography. Very acute lesions hypofluoresce early in the FA and then gradually fill as the study progresses. Late in the angiogram the initially hypofluorescent lesions leak fluorescein. Atrophic punched-out scars behave as window defects with early hyperfluorescence that fades in the late phases of the study, typical of an RPE window defect.[36]

Indocyanine Green Videoangiography. Indocyanine green videoangiography tends to show more presumptive lesions

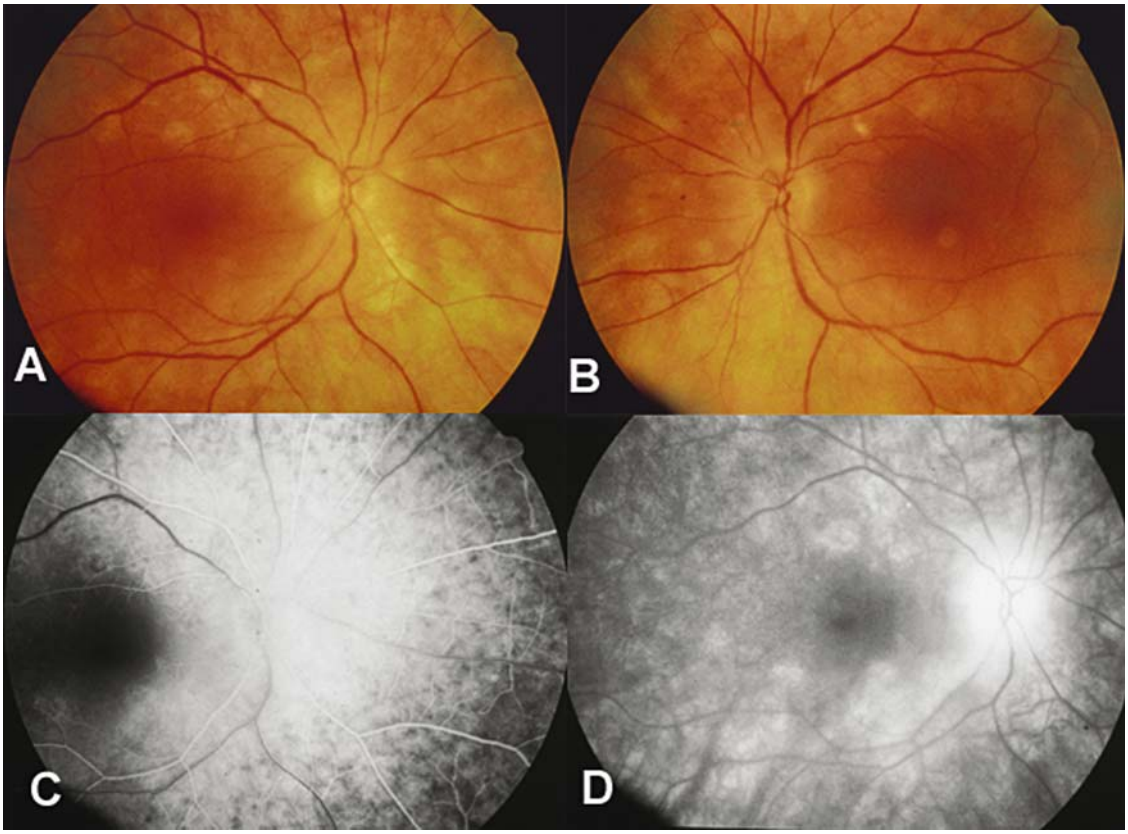

Fig. 6.12. Birdshot retinochoroidopathy. (A,B) Color fundus photograph of right and left eye, respectively. (C) Early FA: when there is choroidal infiltration with minimal retinal pigment epithelium (RPE) atrophy, the spots are hypofluorescent. (D) The lesions become mildly hyperfluorescent in the later phases of the study as dye from the choriocapillaris stains the extrachoroidal vascular space.

than are noted on a clinical examination or on FA. Because in some patients early ICGV fluorescence patterns can be normal, the appearance of these dark spots in the late phase of the angiogram suggests that they represent blocked fluorescence by focal accumulations of inflammatory cells or postinflammatory debris obscuring the underlying choroidal fluorescence.[37] The hypofluorescent spots observed on ICGV did seem to correlate with the degree of inflammation, and these hypofluorescent lesions did not typically correspond to lesions seen clinically or with FA (Fig. 6.13).[36,37]

Punctate Inner Choroidopathy

Punctate inner choroidopathy (PIC) seems to be a variant of multifocal choroiditis. It usually affects young myopic women. The ocular changes noted are essentially the same as those already described for MCP, except that there are no signs of ocular inflammation. Tiffin et al.[38] reported ICG hypofluorescence in subretinal lesions indicative of choroidal hypoperfusion, and some choroidal vessels had localized points of hyperfluorescence along vessel walls probably in relation to choroidal vasculitis. Both PIC and MCP are associated with risk of subretinal membranes.

Diffuse Subretinal Fibrosis

This condition is usually bilateral but asymmetric. It occurs in young women and is characterized by chronic inflammation in the vitreous with numerous small yellow lesions at the level of the deep retina/RPE/choriocapillaris that appear to be gliotic or fibrotic. The lesions typically clustered in the posterior pole and sometimes the midperipheral retina. Some patients had turbid subretinal or subretinal pigment epithelial fluid prior to massive subretinal scarring.

Fluorescein Angiography. In the active phase FA demonstrates early hypofluorescence followed by late leakage in areas of the lesions and turbid subretinal fluid. In the later phase, staining of the lesions without leakage can be noted.

Vogt-Koyanagi-Harada's Syndrome

Patients with VKH syndrome are usually heavily pigmented and may develop neurologic or cutaneous manifestations including headache, aseptic meningitis, paresthesias, dysacusia, tinnitus, poliosis, vitiligo, and alopecia. Ophthalmoscopy shows the presence of well-circumscribed yellowish subretinal (choroidal) white-creamy patches of dots (white dots), which

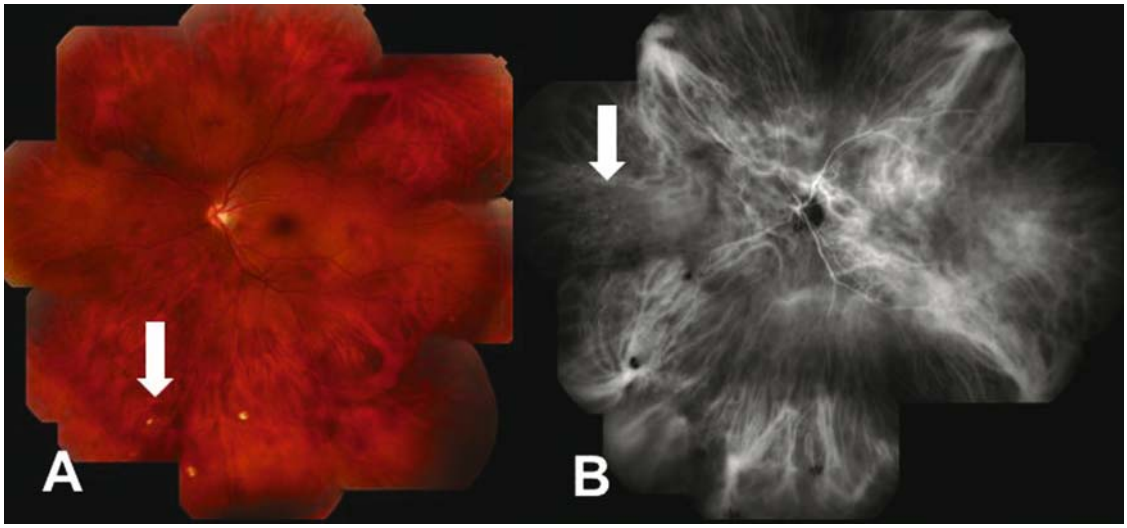

FIG. 6.13. Same patient as in Figure 6.8. (A) Three years later she developed a few chorioretinal scars inferiorly (arrow, multifocal choroiditis [MFC]-like picture), suggestive of some similarity between multiple evanescent white dot syndrome and MFC. (B) On indocyanine green videoangiography (ICGV) there were new small hyperfluorescent spots nasally (arrow). (Courtesy of Antonio Ciardella, MD.)

tend to increase in size and coalesce. They may be accompanied by serous retinal detachment in the periphery or the posterior pole or both. Hyperemia of the disc is often observed. At the nonactive phase of the disease, the posterior portion of the globe shows the "sunset-glow appearance" caused by RPE or choroid depigmentation.[39]

Fluorescein Angiography. During the acute stage of the disease, FA shows early irregular patchy fluorescence of the choroidal circulation, with possible blockage created by choroidal infiltrate. There are multiple pinpoint areas of leakage at the level of the RPE, giving a picture described as a "starry night. " Later, the localized hyperfluorescent spots increase in size, coalesce, and expand into the subretinal space in areas of serous detachment, leading to a large area of leakage. Generally the optic disc shows blurred fluorescent margins and late leakage. During the convalescent period or when the disease becomes chronic, diffuse pigmentary changes with markedly pigmented areas adjoining hypopigmented ones may be the hallmark of the fundal condition.

Indocyanine Green Videoangiography. Indocyanine green videoangiography demonstrates hypofluorescent dark dots of regular size in the early phase and up through the midphase, distributed mainly posteriorly, in excess of those seen clinically and on FA. The late phases of the ICGV vary with the disease activity. In the active stage, the hypofluorescent spots fade and are replaced by hyperfluorescence that does not always correlate with the area of detachment or choroidal nodules and may represent focal sites of active choroidal inflammation. In areas of serous retinal detachment there can be hypofluorescence inside and around the detachment. Freund and Yannuzzi[40] state, "It is possible that the highly protein-bound ICG molecule does not readily leak into the subpigment epithelial and subneurosensory space because the disruption of the outer blood–retinal barrier by the inflammatory process is sufficient to permit leakage of the smaller fluorescein molecule but not the ICG molecule or the ICG protein conjugate. " During the convalescent, chronic, or healed stages of the disease, hypofluorescent dark dots are seen at all phases of ICGV, but they are inapparent on fundus or FA evaluation (Fig. 6.14).[17]

Behçet's Disease

Behçet's disease is a chronic relapsing inflammatory disease. Its definition requires recurrent oral ulceration plus two of the following: recurrent genital ulceration, eye lesions (the most common are iridocyclitis and retinal vasculitis), skin lesions such as erythema nodosum and acneiform eruptions, or a positive pathergy test. The essential retinal finding is retinal vasculitis, which may involve both veins and arteries.

Fluorescein Angiography. Fluorescein angiography shows marked dilation and occlusion of the retinal capillaries. In the active stage of the disease, there is a diffuse fluorescein leakage from retinal capillaries. Leakage may persist even with resolution of inflammatory disease. Fluorescein angiography may show late vascular staining, large zones of capillary dropout, vascular tree rearrangement as collateral vascular formation, secondary retinal telangiectasia, and retinal neovascularization. The loss of a clearly defined capillary free zone is commonly seen.

Indocyanine Green Videoangiography. The importance of retinal vascular involvement and the severity disruption of the

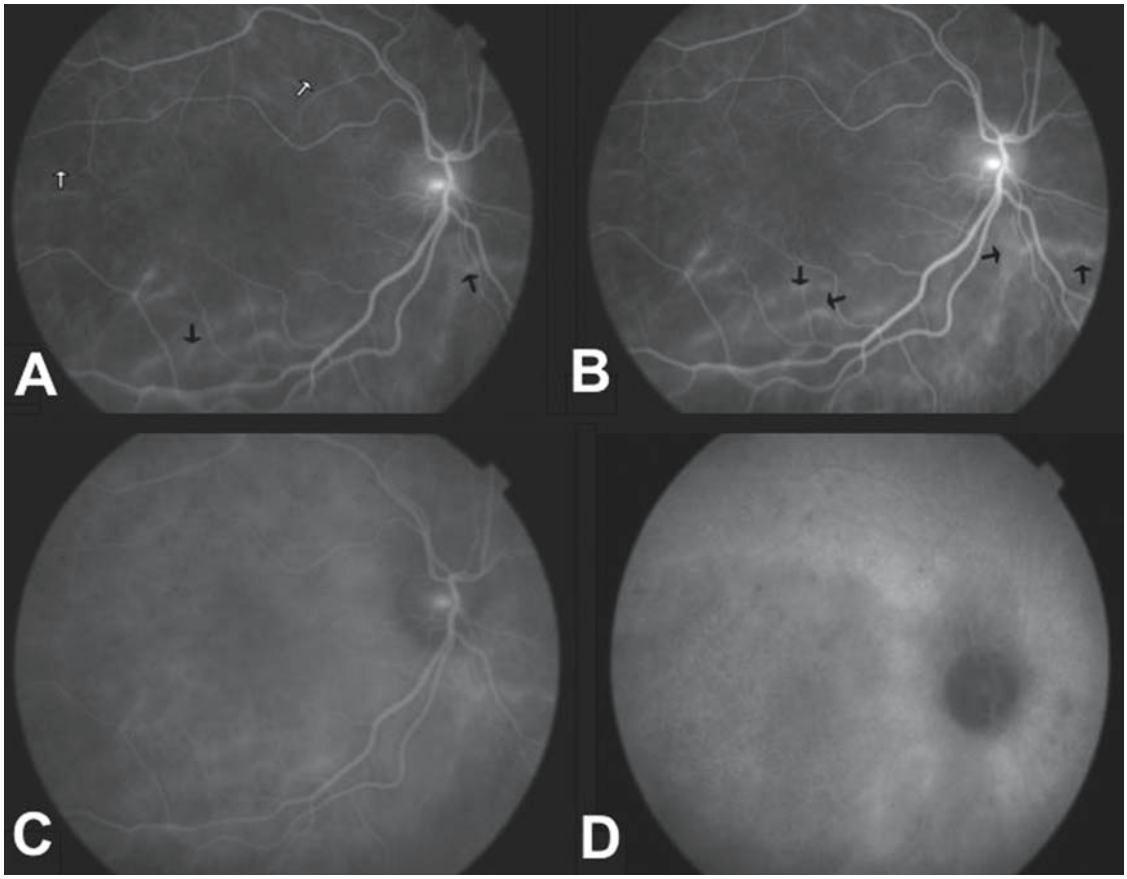

Fig. 6.14. Vogt-Koyanagi-Harada's disease. (A,B) Individual leaking choroidal vessels (black arrows) indicating inflammatory choroidal vasculopathy and patchy hypofluorescent areas (white arrows) were visible in the early phase ICGV in the acute disease. Note marked decrease in the number of large choroidal vessels in the early-phase ICGV in the acute disease. (C) Evenly sized hypofluorescent spots are observed in the intermediate-phase ICGV at the acute phase of the disease. (D) Some of the spots are persisting into the late phase. (Courtesy of Leyla Atmaca, MD.)

blood–retinal barrier is best show by FA. Indocyanine green videoangiography may show hyperfluorescent areas up to the late phase of the study that can be related to disease duration. Choroidal vascular involvement in the disease processes of Behçet's remains unclear; however, Bozzoni-Pantaleoni et al.[41] reported some ICGV findings undetectable with FA. They described three ICGV patterns. The most important and frequent pattern was poorly defined areas of choroidal hyperfluorescence in the posterior pole at the intermediate and late phases of the study. This pattern may be related to ICG diffusion by choriocapillaris or ICG leakage in large choroidal vessels. The second pattern consisted of multiple, well-defined hypofluorescent areas becoming isofluorescent in the late phase of the ICGV. The third pattern consisted of large poorly defined hypofluorescent areas in the early to late phases. Both the second and third patterns were located in the midperiphery and may represent partial- and whole-thickness, space-occupying choroidal inflammatory lesions, respectively (Fig. 6.15).

Infectious Diseases

Nonimmunocompromised Patients

Toxoplasmic Retinochoroiditis. Toxoplasmosis is a common cause of retinitis in immunocompetent individuals. Its incidence in AIDS patients seems to be relatively low, with 49 cases reported in the literature, 34 of which were reported in France where the incidence of toxoplasmosis in the nonimmunosuppressed population is very high.[42] Atypical forms of retinochoroiditis by toxoplasma include large destructive lesions, punctate inner retinal lesions, punctate outer retinal lesions, unilateral pigmentary retinopathy, neuroretinitis, and others. However, ocular toxoplasmosis most often starts in the superficial retina, and classically the ocular fundus shows a yellowish-white or gray exudate from 0.1 disc diameter to two retinal quadrants in extension, with ill-defined borders caused by surrounding retinal edema. Usually, marked vitreitis is present over the lesion, and when it is extensive it produces

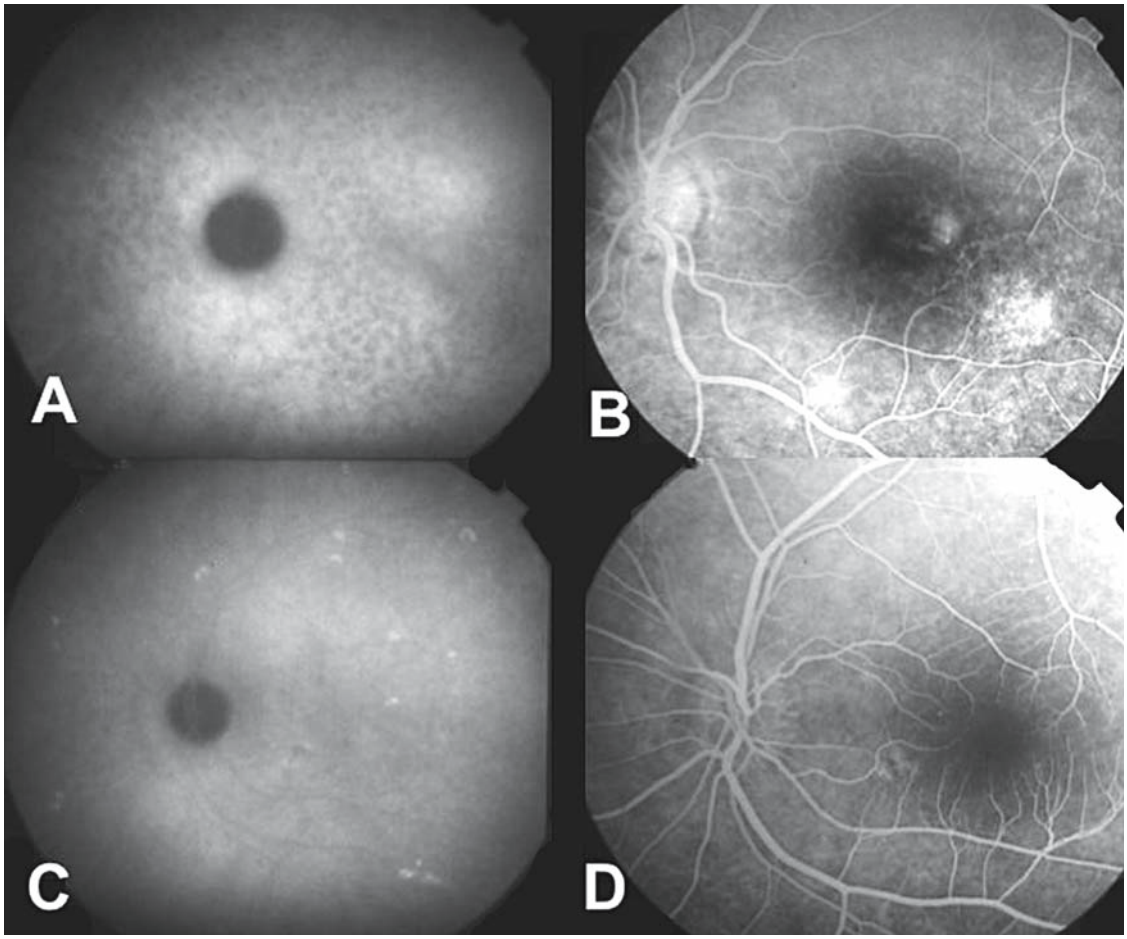

Fig. 6.15. Behçet's disease. (A) Hypofluorescent spots in the late phase of ICGV. (B) These spots cannot be seen on FA. Hyperfluorescence is shown due to pigment epithelial changes. (C) Hyperfluorescent spots in the late phase of ICGA. (D) These spots cannot be seen on FA. (Courtesy of Leyla Atmaca, MD.)

the classic appearance of a headlight in the fog. With time the lesion becomes atrophic with well-defined borders, central retinochoroidal atrophy, and peripheral RPE hyperplasia. In general, a large macular atrophic scar is due to congenital toxoplasmosis.

Fluorescein Angiography. Fluorescein angiography demonstrates central hypofluorescence because of blockage by the retinal inflammation in active disease. Leakage occurs later, expanding from the margins of the lesion. In retinochoroidal scars, irregular RPE hypertrophy and atrophy may result in blockage and window defect, respectively, leading to a mottled appearance of the lesion. In late phases of the study FA shows staining of the lesion margins (Fig. 6.16).

Indocyanine Green Videoangiography. Indocyanine green videoangiography characteristics have been reported in some cases of toxoplasmic retinochoroiditis. The ICGV study is useful for the early diagnosis of recurrent ocular toxoplasmosis because it can identify an area of reactivation not yet detectable by funduscopic exam or FA. Auer et al.[43] reported that the main focus of retinochoroiditis was hypofluorescent at all phases of the ICGV in 89% of cases, although in some patients hyperfluorescence is seen in early and late phases. In addition, they found multiple hypofluorescent satellite dark dots (SDDs) in 75% of cases.[43] In old lesions, ICGV is hypofluorescent throughout the exam.

Presumed Ocular Histoplasmosis Syndrome. If *Histoplasma capsulatum* plays a role in ocular histoplasmosis, the role still remains to be elucidated. The fungal organism has never been cultured or isolated from an eye with classic lesions of POHS. However, epidemiologic and skin testing evidence has been used to implicate this fungus as the etiologic agent of POHS. A triad of disseminated choroiditis (histo [histoplasmosis] spots), maculopathy (macular chorioretinal or disciform scar), and peripapillary chorioretinal degenerative changes (atrophic and pigmentary changes) constitutes the classic syndrome of

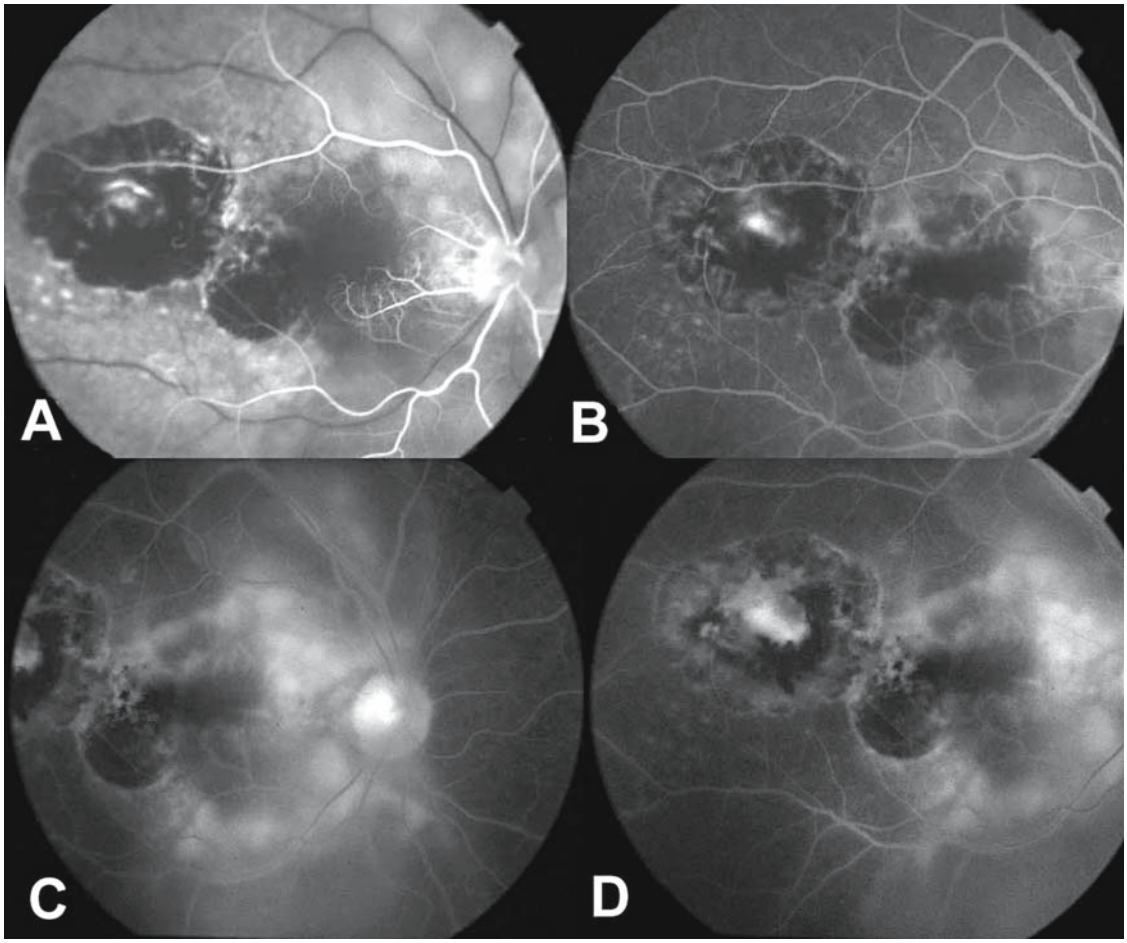

FIG. 6.16. (A) Arterial phase fluorescein angiogram (FA) demonstrates active toxoplasma chorioretinitis adjacent to a classic chorioretinal scar. (B) Arteriovenous-phase FA demonstrates the classic old pigmented lesion with hypofluorescence at the center and hyperfluorescence at the margins of the lesion. (C,D) Late-phase FA shows juxtapapillary multiple hyperfluorescent dots that correspond to new active lesions adjacent to the primary pigmented scar.

POHS. The diagnosis of POHS is essentially clinical; however, FA and ICGV usually show choroidal macular neovascularization characteristic of the syndrome (Fig. 6.17).

Immunocompromised Patients

Toxoplasmic Retinochoroiditis. Ocular toxoplasmosis in AIDS patients probably results from reactivation of latent infection in other parts of the body or acquired infection. Its low incidence may result in part from the extensive use in AIDS patients of prophylactic drugs for *Pneumocystis* pneumonia that may also prevent toxoplasmosis, and in part from the introduction of highly active antiretroviral therapy.

Fluorescein angiography does not add much information regarding diagnosis or management. In contrast, ICGV brings new information that could result in improved management of toxoplasmic retinochoroiditis and may give new insights into the pathophysiology of the disease. In one of our cases (Fig. 6.18), the described hypofluorescent SDDs on ICGV associated with toxoplasmic retinochoroiditis were not seen.[43] This finding may be related to limited choroidal inflammatory response in an AIDS patient not on highly active antiretroviral therapy (HAART). Satellite dark dots on ICGV in toxoplasmic retinochoroiditis cases tend to disappear with antitoxoplasmic therapy, and a purely inflammatory mechanism has been suggested. In addition, in our patient the choroidal hypofluorescence seen on ICGV under the focus of retinochoroiditis extended beyond the clinical and FA limits of the lesion.

Cytomegalovirus Retinitis. Cytomegalovirus (CMV) retinitis may affect AIDS patients with a $CD4^+$ lymphocyte count under 50 cell/μL.[44–46] It is characterized by a necrotizing retinitis with superficial hemorrhages and absent or mild intraocular inflammation (Fig. 6.19); this clinic characteristic was so important before the HAART era that in any patient with vitreous inflammation and necrotizing retinitis another diagnosis had to be considered. Until recently severe intraocular inflammation in this group of patients was rare, although there are some reports in the literature.[47,48] Serous macular exudates have been described in CMV retinitis in AIDS patients. Palestine and Frishberg[49]

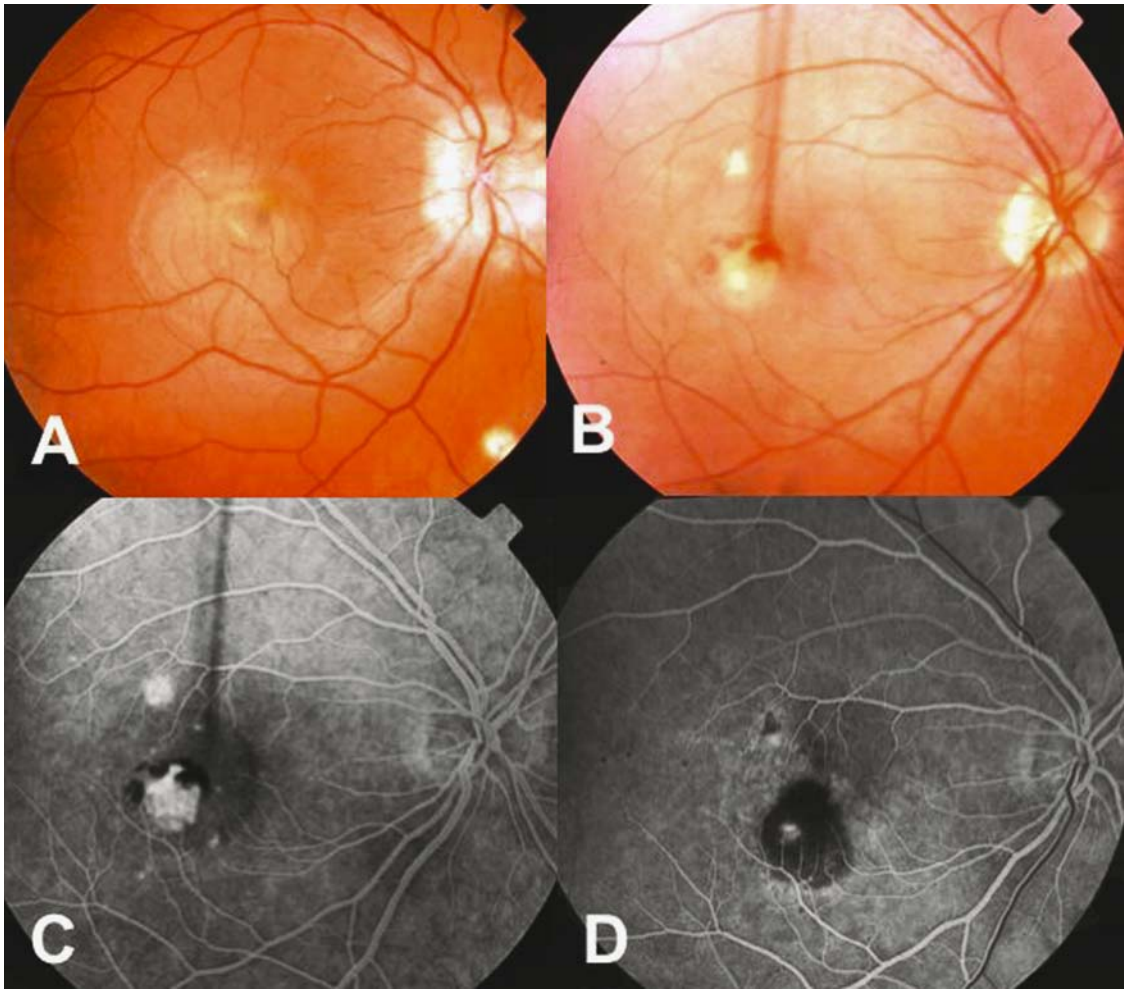

Fig. 6.17. (A) Disseminated choroiditis (histo spots), maculopathy, and peripapillary chorioretinal degenerative changes in a patient with the presumed ocular histoplasmosis syndrome. (B) Disseminated choroiditis (histo spots), maculopathy, and peripapillary chorioretinal degenerative changes in another patient with the presumed ocular histoplasmosis syndrome. (C) Fluorescein angiography of the patient in B revealed serosanguinous retinal detachment with faint pigment halo in right macula and choroidal neovascularization. (D) Fluorescein angiography of patient in B revealed hypofluorescence after photodynamic therapy with verteporfin. (Courtesy of Steve Bloom, MD.)

described an AIDS patient with macular edema, cotton-wool exudates, and other microvascular alterations. Weinberg and Moorthy[50] published a case report of a patient with AIDS and CME along with CMV retinitis. It has been suggested that the severe immunodeficiency of AIDS patients has a protective effect against the inflammatory complications induced by necrotizing retinitis.[51] In 1998, Karavellas et al.[48] described a case of immune recovery vitreitis related to inactive CMV retinitis (all patients had received HAART) (Fig. 6.20). Two types of clinical appearances may be seen. The first is a perivascular fluffy white lesion with many scattered hemorrhages. Another manifestation is a more granular-appearing lesion that has few associates hemorrhages and often has a central area of clearing, with atrophic retina and stippled retinal pigment epithelium.

Fluorescein Angiography. Fluorescein angiography may be of benefit if the diagnosis is uncertain. These techniques may be used to document progression of retinitis, and fluorescein leakage in areas of retinitis may be helpful in confirming the diagnosis.

Arevalo and Fuenmayor-Rivera[52] have published the results of a study comparing FA to ICGV in patients with CMV retinitis and HAART. The goal of the study was to determine if ICG angiography was useful in diagnosing choroidal inflammation associated with CMV. The mean $CD4^+$ lymphocyte cell count in these patients was 160 cell/μL. In the ICGV group all eyes (13 eyes, eight patients) showed a hypofluorescence pattern (much larger than the area of retinitis seen clinically), which was maintained throughout the study. Nine cases showed some degree of hyperfluorescence during the study. The earliest hyperfluorescence was identified at 26.4 seconds, while the maximum fluorescence was seen at 147.1 seconds (Fig. 6.21). Other findings with this diagnostic tool included an area of late hypofluorescent choroiditis in nine eyes (69.2%) and late hot spots in seven eyes (53.8%)

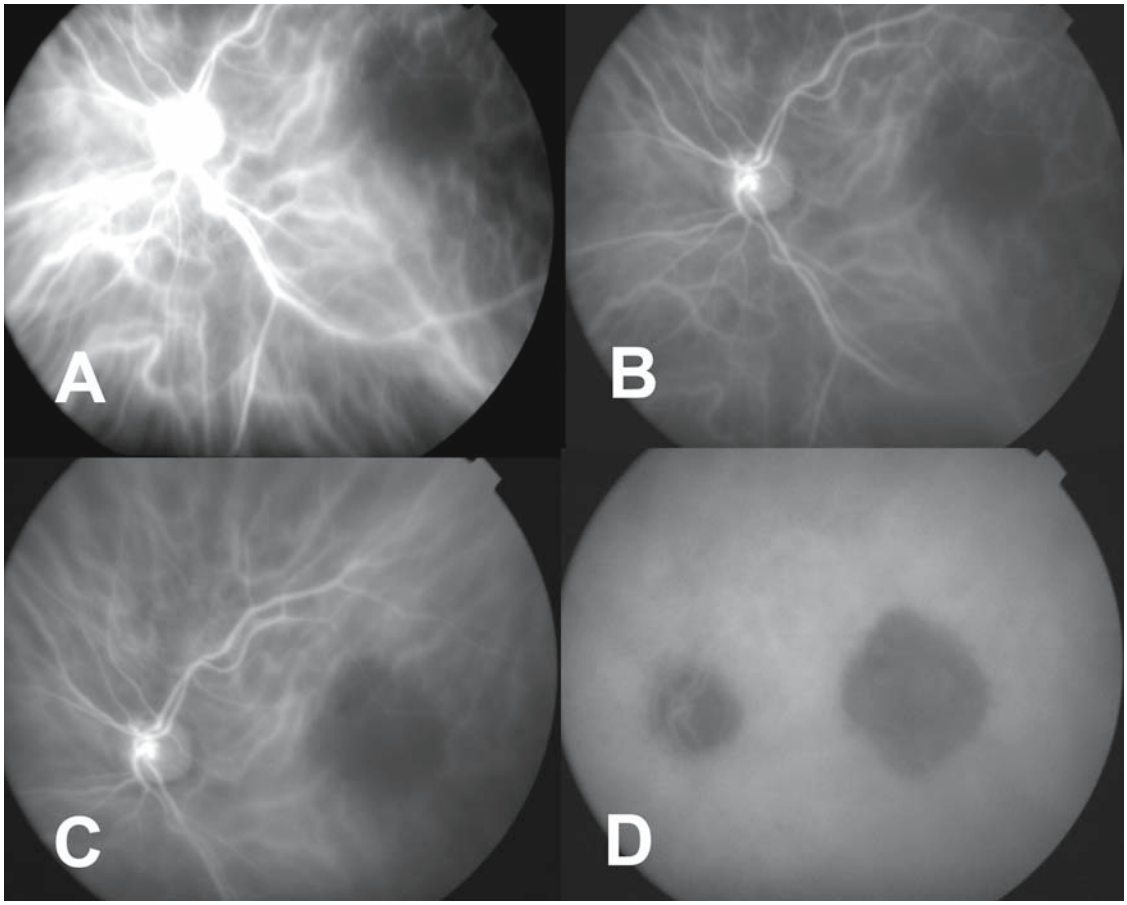

FIG. 6.18. Toxoplasmic chorioretinitis in an AIDS patient. An indocyanine green videoangiography confirmed the presence of a lesion that affected the choroid. This lesion masked fluorescence throughout the study (A–D), and remained hypofluorescent in the late frames (D). It was bigger than that seen on fundus examination and fluorescein angiography.

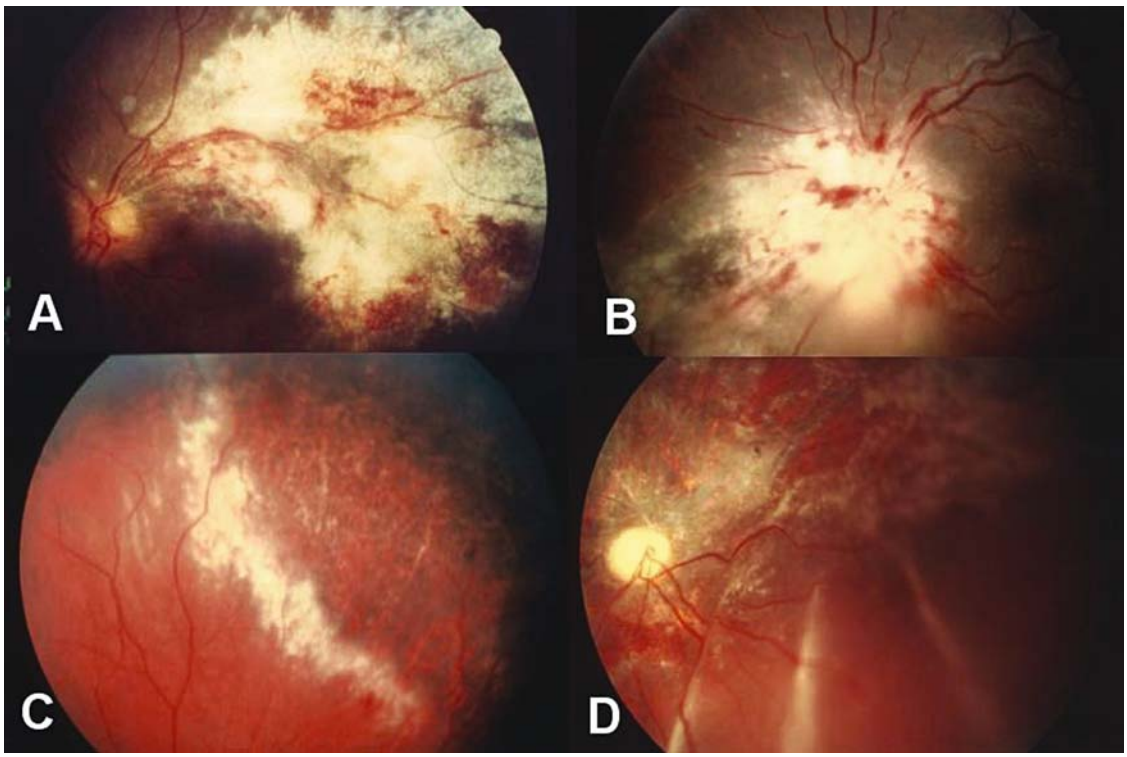

FIG. 6.19. Cytomegalovirus retinitis is characterized by a necrotizing retinitis with superficial hemorrhages and absent or mild intraocular inflammation. (Courtesy of William R. Freeman, MD.)

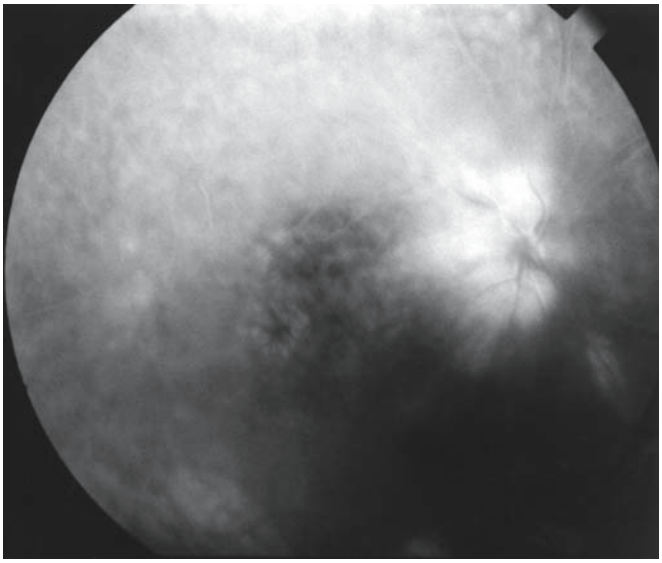

FIG. 6.20. Patient with immune recovery vitreitis, papillitis, and cystoid macular edema related to inactive cytomegalovirus retinitis.

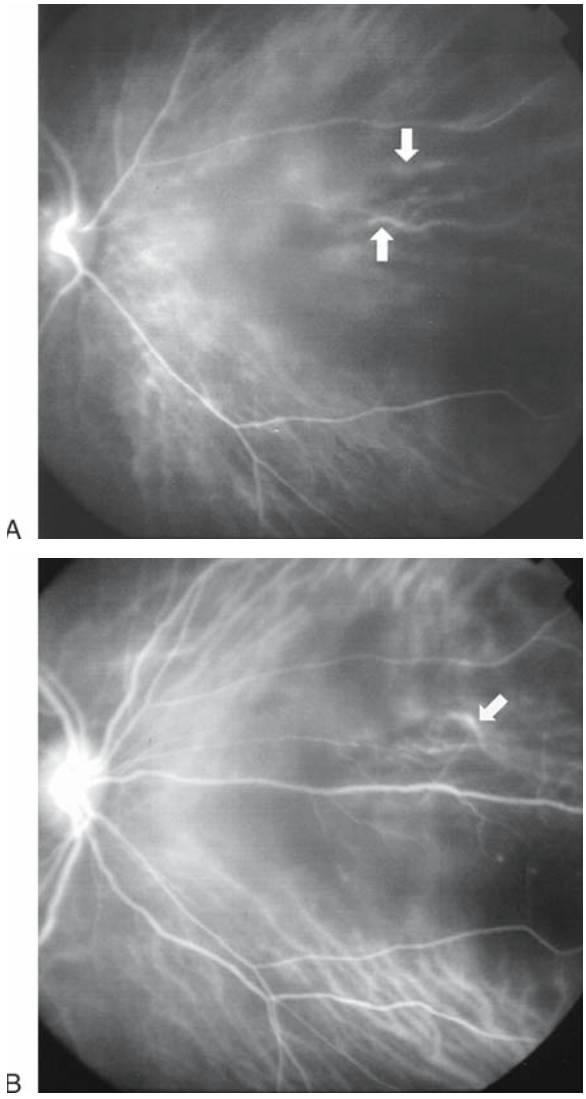

FIG. 6.21. Cytomegalovirus retinitis in an AIDS patient. (A) Early indocyanine green videoangiography (ICGV) frame shows the onset of fluorescence. (B) Maximum fluorescence on ICGV.

(Fig. 6.22). In one case a hyperfluorescent choroidal ring around the macular area was observed, which has not been previously described (Fig. 6.23). In the FA the beginning of fluorescence can be seen at 44.8 seconds (Fig. 6.24A) and maximum fluorescence can be seen at 209.5 seconds (Fig. 6.24B).

Also, hot spots were observed in later phases as well as nonperfusion areas (Fig. 6.25). As a whole, ICGV in cases of CMV retinitis has specific characteristics that distinguish it from FA. The test can be a valuable complementary, noninvasive study in the diagnosis of patients with CMV choroiditis, HAART, and a stronger inflammatory and immunologic response.

Cryptococcus neoformans Choroiditis. Cryptococcus neoformans is a saprophytic fungus that causes opportunistic infections in AIDS patients. Mainly systemic involvement presents as meningitis and is referred to the ophthalmologist as diplopia, internuclear ophthalmoplegia, nystagmus, cranial nerve palsies, optic atrophy, choroiditis, and papilledema.[53] *C. neoformans* is a rare cause of disease in the human host and can affect healthy individuals, although it is more common in immunocompromised patients. The clinical characteristics of choroiditis due to this microorganism are vitreous cells with localized choroidal lesions (Fig. 6.26). The most common intraocular manifestation (usually following meningitis) is chorioretinitis. The earliest sign is focal or multifocal choroiditis, in which yellowish to white, subretinal, slightly elevated lesions one fifth to one optic disc diameter in size are usually observed. The presence of the fungus in the choroid implies hematogenous spread of the infection and a poor prognosis for the patient. The fluoroangiographic characteristics of the disease have been described in very few reports of cryptococcal choroiditis (Fig. 6.27). We presented a few years ago, the first report on the attributes of ICG in an AIDS patient with choroidal cryptococcus (Fig. 6.28).[54]

Fluorescein angiography can show masked fluorescence of round lesions early during the study, with no significant leakage in the late stages of the angiogram, although some late hyperfluorescence may be seen around the optic disc. The retinal component on the FA usually is normal.

Arevalo et al.[54] reported on an AIDS patient with visual symptoms and a funduscopic aspect consistent with an alteration in the RPE or choroid based on the ICGV and FA. The diagnosis of cryptococcal choroiditis was established with a lumbar puncture done a week later in which data associated with cryptococcal meningitis was observed. The diagnosis of cryptococcal choroiditis was presumed after extensive lab

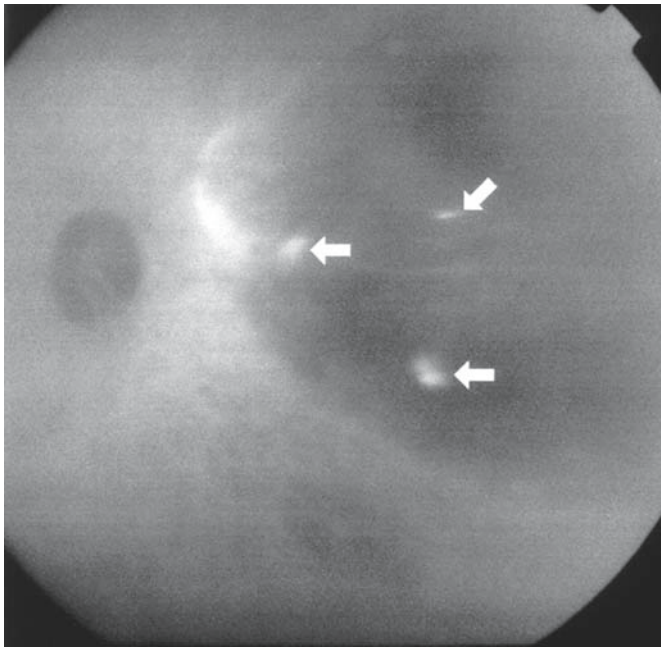

FIG. 6.22. Cytomegalovirus retinitis in an AIDS patient. Hot spots (arrows) are seen on late frames on indocyanine green videoangiography.

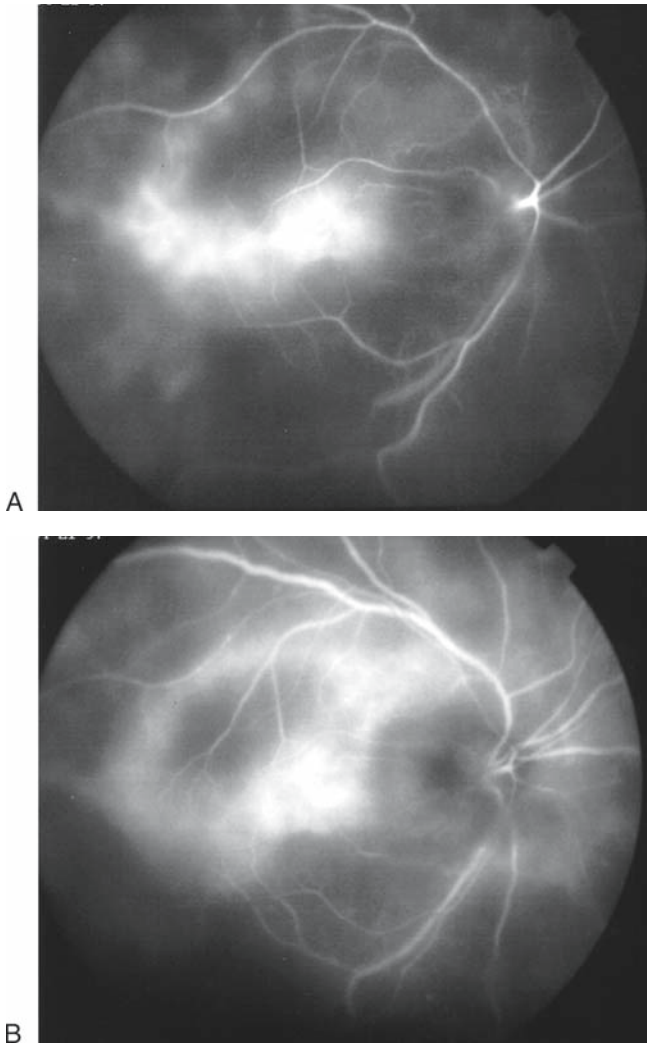

FIG. 6.23. Cytomegalovirus retinitis in an AIDS patient. A previously undescribed annular choroidal hyperfluorescence of another patient with CMV retinitis imaged with ICGV. (A) Early fluorescence. (B) Maximum fluorescence.

work and blood cultures proved that this patient had no evidence of any other hematogenous opportunistic infection. In addition, the visual symptoms and fundus lesions began to disappear with systemic treatment. Nonetheless, the patient died due to systemic complications 3 weeks later. In our case the multifocal pattern and irregularly shaped hypofluorescent spots on ICGV were seen also on fluorescein angiography. This finding may be related to a very active disease stage that may have involved the choriocapillaris. Hypofluorescent spots on ICGV were detected in greater number than would correspond to the yellowish areas seen in color and red-free photographs. Their distribution was most dense surrounding the optic nerve and the fovea. In addition, they had a tendency to be confluent, and this characteristic was better depicted with ICGV (Fig. 6.28, bottom) than with fluorescein angiography.

Choroidal infiltration, which prevented normal choroidal indocyanine green impregnation, most probably was the physiopathologic explanation for these persistent hypofluorescent dark spots. These ICGV features described in our case were nonspecific for the disease. Similar findings have been described in other inflammatory conditions involving the choroid, such as birdshot chorioretinopathy, VKH syndrome, sympathetic ophthalmia, posterior sarcoidosis, posterior tuberculosis, toxoplasmic retinochoroiditis, and acute posterior multifocal placoid pigment epitheliopathy

Conclusion

In patients with very lightly pigmented fundi, some lesions may not appear on fundus photographs and fluorescein angiography, and ICGV may be very helpful in confirming, detecting, and documenting the extent of retinochoroidal involvement. Sometimes ICGV can help us limit the differential diagnosis of a patient with inflammatory eye disease. Furthermore, FA and ICGV may provide information on the pathophysiology of some ocular inflammatory diseases, may be useful in monitoring the effect of therapeutic interventions, and may show disease recurrence before the development of the classic ocular fundus changes. The ophthalmologist plays a valuable role in the management of patients with AIDS since an important number of these

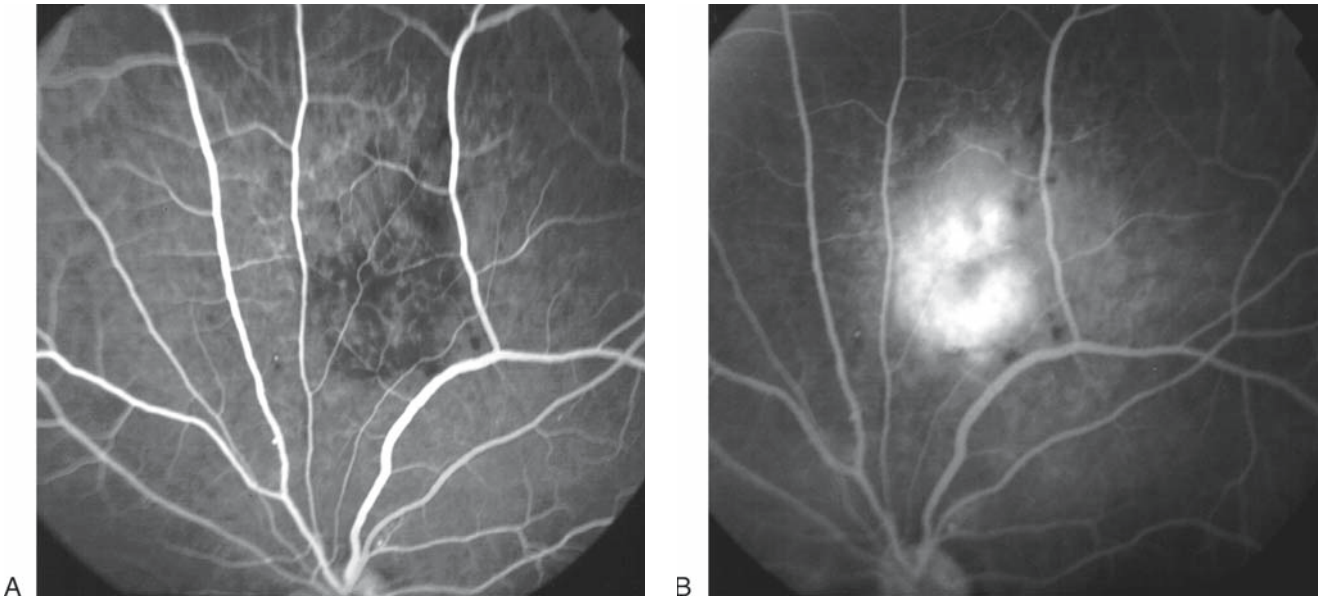

FIG. 6.24. Cytomegalovirus retinitis in an AIDS patient. (A) Intravenous fluorescein angiography (IVFA) frame showing the onset of fluorescence. (B) Maximum fluorescence during IVFA.

patients have ocular disease. Cytomegalovirus retinitis is the most common ocular opportunistic infection, although its incidence has decreased in the last few years due to the introduction of highly active antiretroviral therapy. The incidence of opportunistic infections that metastasize to the choroid is much lower and includes *C. neoformans*, *Mycobacterium avium,* and *Pneumocystis carinii*. The prognosis for these patients is very poor by this stage, and the diagnosis may elude the physician until choroidal involvement develops. It is, therefore, important for ophthalmologists to recognize the pattern of choroidal involvement produced by opportunistic infections in AIDS, as prompt treatment will prolong life.

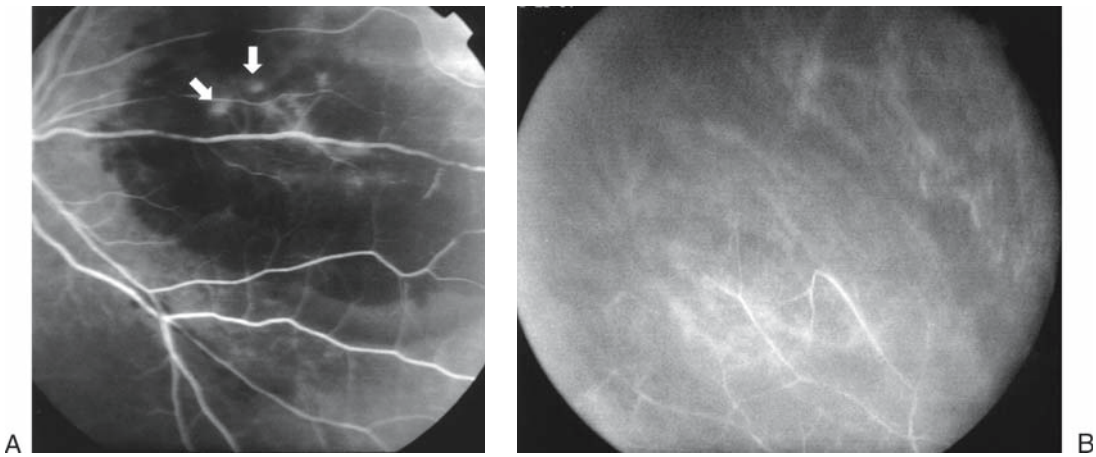

FIG. 6.25. Cytomegalovirus retinitis in an AIDS patient. (A) Hot spots (arrows) are seen on late frames on intravenous fluorescein angiography (IVFA). (B) Lack of perfusion seen on IVFA.

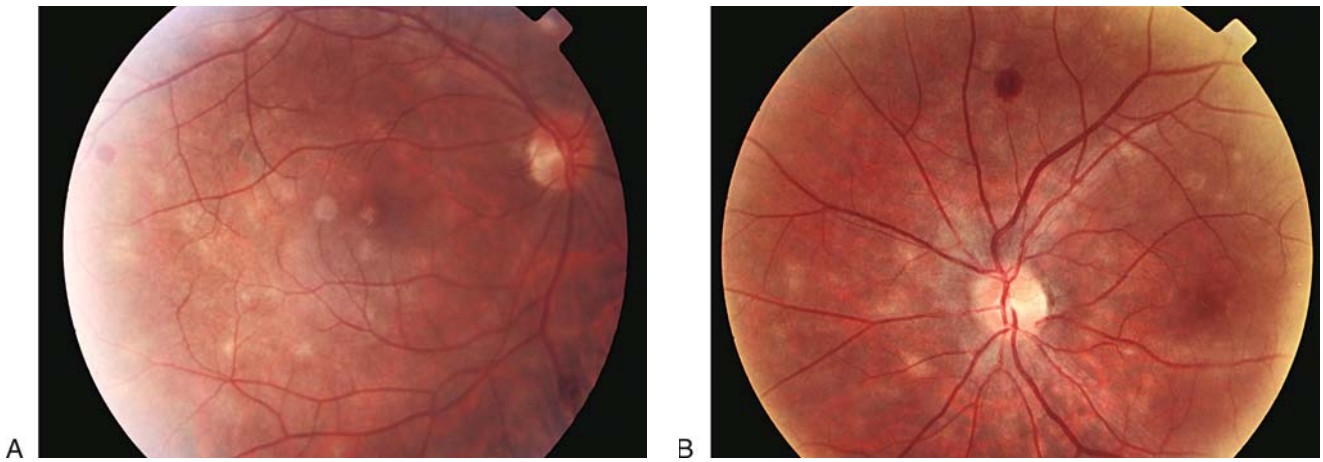

FIG. 6.26. Cryptococcal choroiditis in an AIDS patient. Fundus photographs of the right (A) and left (B) eyes revealed multiple deep 300- to 400-μm yellowish lesions that seem to be located beneath the retina at the level of the retinal pigment epithelium and choroid.

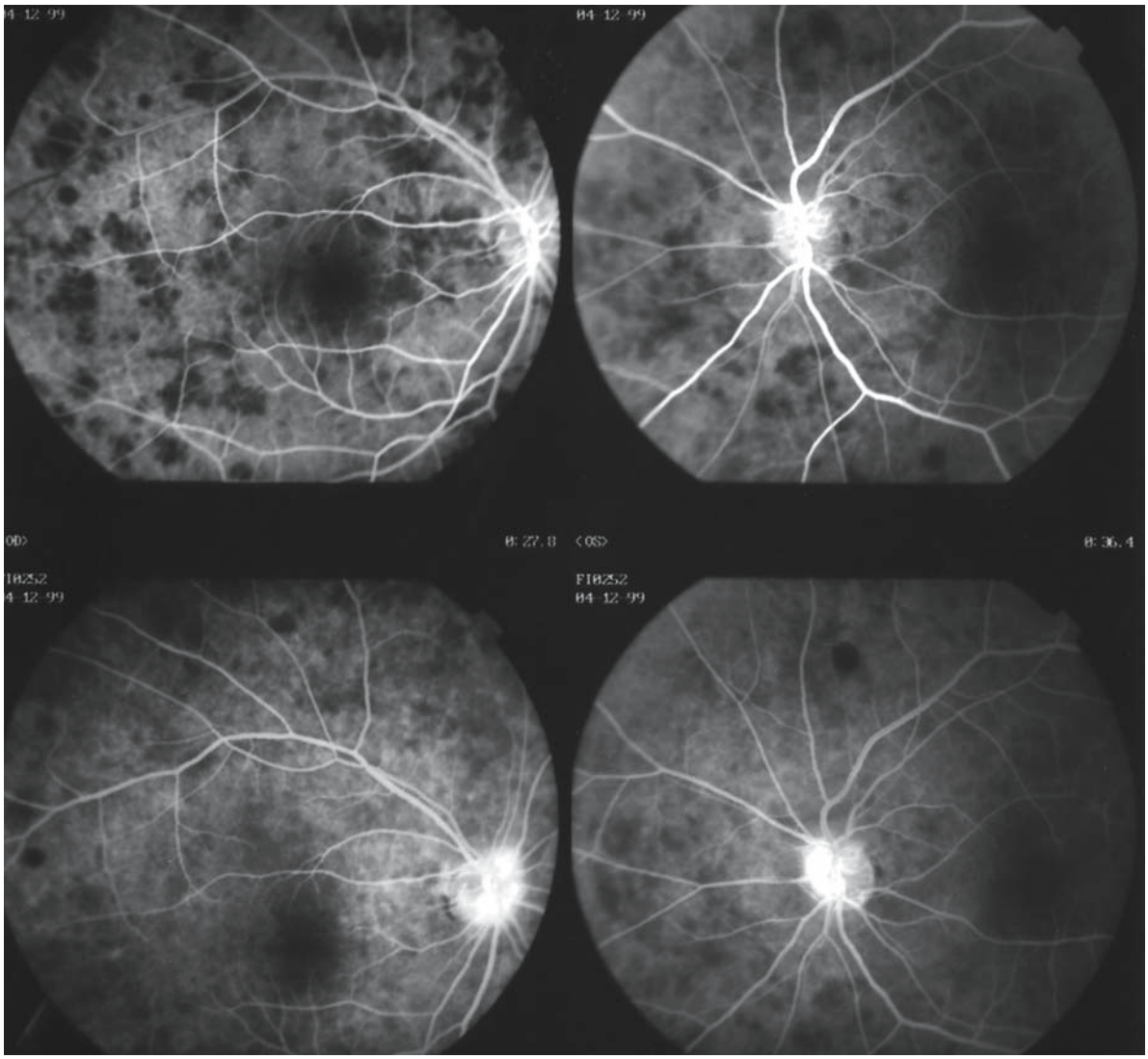

FIG. 6.27. Cryptococcal choroiditis in an AIDS patient. Fluorescein angiogram confirmed the presence of rounded lesions that were located underneath the neuroretina. These lesions masked fluorescence early during the study (top pictures). There was no significant leakage in the late stages of the angiogram, although some late hyperfluorescence may be seen on the nasal aspect of the optic disc in both eyes (bottom pictures).

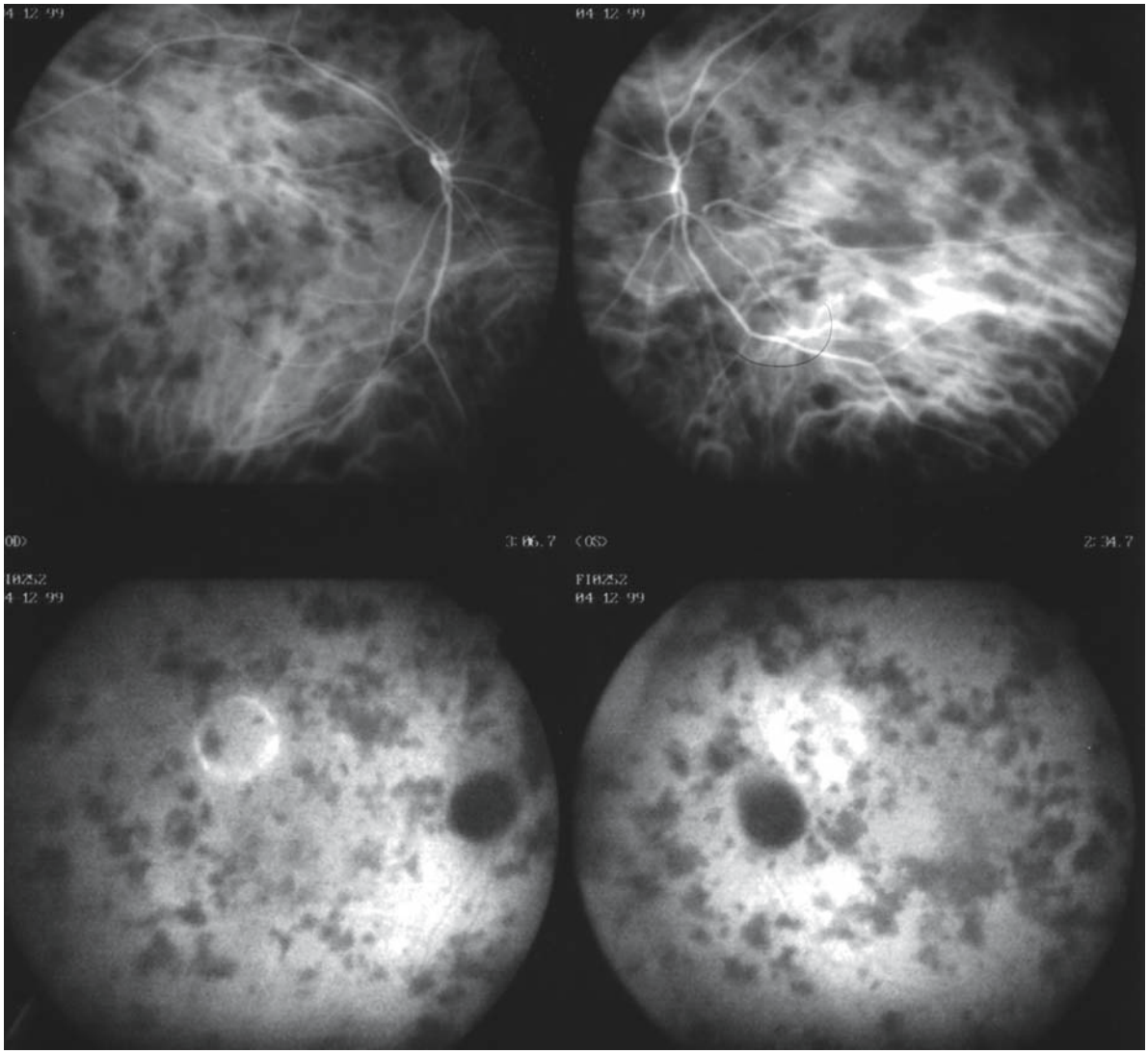

FIG. 6.28. Cryptococcal choroiditis in an AIDS patient. Indocyanine green videoangiography (ICGV) confirmed the presence of lesions that were at the level of the choroid. These lesions masked fluorescence throughout the study. Most of these hypofluorescent dark spots were already visible at the early phase of the ICGV, became more sharply delineated in the intermediate angiographic frames (top pictures), and remained hypofluorescent in the late frames (bottom pictures). The white circle in the bottom pictures is an artifact.

References

1. Nussenblatt RB, Whitcup SM, Palestine AG. Diagnostic testing. In: Uveitis. Fundamentals and Clinical Practice. St. Louis: Mosby, 1996:79–90.
2. Richard G. Evaluating a fluorescein angiogram. In: Richard G, ed. Fluorescein and ICG Angiography. Textbook and Atlas. New York: Thieme Verlag Medical Publishers, 1998:10–17.
3. Benson RC, Kues HA. Fluorescence properties of indocyanine green as related to angiography. Phys Med Biol 1978;23: 159–163.
4. Yannuzzi LA, Slakter JS, Sorenson JA, Guyer DR, Orlock DA. Digital indocyanine green videoangiography and choroidal neovascularization. Retina 1992;12:191–223.
5. Sorenson JA, Yannuzzi LA, Slakter JS, Guyer DR, Ho AC, Orlock DA. A pilot study of digital indocyanine green videoangiography for recurrent occult choroidal neovascularization in age-related macular degeneration. Arch Ophthalmol 1994;112:473–479.
6. Yannuzzi LA, Hope-Ross M, Slakter JS, et al. Analysis of vascularized pigment epithelial detachments using indocyanine green videoangiography. Retina 1994;14:99–113.
7. Guyer DR, Yannuzzi LA, Slakter JS, Sorenson JA, Hope-Ross M, Orlock DR. Digital indocyanine-green videoangiography of occult choroidal neovascularization. Ophthalmology 1994;101:1727–1737.
8. Guyer DR, Puliafito CA, Mones JM, Friedman E, Chang W, Verdooner SR. Digital indocyanine-green angiography in chorioretinal disorders. Ophthalmology 1992;99:287–291.

9. Dhaliwal RS, Maguire AM, Flower RW, Arribas NP. Acute posterior multifocal placoid pigment epitheliopathy: an indocyanine green angiographic study. Retina 1993;13:317–325.
10. Garcia-Saenz MC, Gili Manzanaro P, Banuelos Banuelos J, Villarejo Diaz-Maroto I, Arias Puente A. [Indocyanine green angiography in chorioretinal inflammatory diseases]. Arch Soc Esp Oftalmol 2003;78:675–683.
11. Guyer DR, Yannuzzi LA, Slakter JS, Sorenson JA, Ho A, Orlock D. Digital indocyanine green videoangiography of central serous chorioretinopathy. Arch Ophthalmol 1994;112:1057–1062.
12. Ie D, Glaser BM, Murphy RP, Gordon LW, Sjaarda RN, Thompson JT. Indocyanine green angiography in multiple evanescent white-dot syndrome. Am J Ophthalmol 1994;117:7–12.
13. Yuzawa M, Kawamura A, Matsui M. Indocyanine green video angiographic findings in acute posterior multifocal placoid pigment epitheliopathy. Acta Ophthalmol 1994;72:128–133.
14. Shields CL, Shields JA, De Potter P. Patterns of indocyanine green videoangiography of choroidal tumours. Br J Ophthalmol 1995;79:237–245.
15. Sallet G, Amoaku WMK, Lafaut BA, Brabant P, De Laey JJ. Indocyanine green angiography of choroidal tumors. Graefes Arch Clin Exp Ophthalmol 1995;233:677–689.
16. Arevalo JF, Shields CL, Shields JA, Hykin PG, De Potter P. Circumscribed choroidal hemangioma: characteristics features with indocyanine green video-angiography. Ophthalmology 2000;107:344–350.
17. Chan R, Tawansy KA, El-Helw Tamer, Foster CS, Carter BL. Diagnostic imaging studies for inflammatory systemic diseases with eye manifestations. In: Foster SF, Vitale AT, eds. Diagnosis and Treatment of Uveitis, 1st ed. Philadelphia: WB Saunders, 2002:104–139.
18. Whitcup SM. Diagnostic testing. In: Nussenblatt RB, Whitcup SM, eds. Uveitis. Fundamentals and Clinical Practice, 3rd ed. St. Louis: Mosby, 2004:76–87.
19. Arellanes L, Navarro P, Recillas C. Pars planitis in the Mexican Mestizo population: ocular findings, treatment and visual outcome. Ocular Immunol Inflamm 2003;11:53–60.
20. Listhaus AD, Freeman WR. Fluorescein angiography in patients with posterior uveitis. Int Ophthalmol Clin 1990;30:297–308.
21. Michelson JB, Chisari FJ. Behçet's disease. Surv Ophthalmol 1982;26:190–203.
22. Joondeph BC, Tessler HH. Multifocal choroiditis. Int Ophthalmolol Clin 1990;30:286–290.
23. Fisher JP. The acute retinal necrosis syndrome. Clinical manifestations. Ophthalmology 1982;89:1309–1316.
24. Richard G. Inflammatory diseases of the retina and choroid. In: Richard G, ed. Fluorescein and ICG Angiography. Textbook and Atlas. New York: Thieme Verlag Medical Publishers, 1998: 252–277.
25. Moorthy RS, Chong LP, Smith RE, Rao NA. Subretinal neovascular membranes in Vogt-Koyanagi-Harada syndrome. Am J Ophthalmol 1993;116:164–170.
26. Michelson JB. Cytomegalic virus inclusion disease. In: Michelson JB, ed. Color Atlas of Uveitis. St. Louis: Mosby, 1992:119–120.
27. Gormam BD, Nadel AJ, Coles RS. Acute retinal necrosis. Ophthalmology 1992,89:809–814.
28. Tsujikawa A, Yamashiro K, Yamamoto K, Nonaka A, Fujihara M, Kurimoto Y. Retinal cystoid spaces in acute Vogt-Koyanagi-Harada syndrome. Am J Ophthalmol 2005;139: 670–677.
29. Lewis H, Jampol LM. White dot syndromes. In: Pepose JS, Holland GN, Wilhelmus KR, eds. Ocular Infection and Immunity. St. Louis: Mosby Year Book, 1996:560–569.
30. Berkow JW, Flower RW, Orth DH, Kelley JS. Miscellaneous conditions. In: Berkow JW, Flower RW, Orth DH, Kelley JS, eds. Fluorescein and Indocyanine Angiography, Technique and Interpretation, 2nd ed. 155–175.
31. Akpek EK, Baltatzis S, Yang J, et al. Long-term immunosuppressive treatment of serpiginous choroiditis. Ocul Immunol Inflamm 2001;9:153–167.
32. Nussenblatt RB. Serpiginous choroidopathy. In: Nussenblatt RB, Whitcup SM, eds. Uveitis. Fundamentals and Clinical Practice, 3rd ed. St. Louis: Mosby, 2004:76–87.
33. Monés JM, Slakter JS. Serpiginous choroidopathy. In: Yannuzzi LA, Flower RW, Slakter JS, eds. Indocyanine Green Angiography, 1st ed. St. Louis: Mosby, 1997:247–252.
34. Chang B, Lumbroso L, Rabb MF, Yannuzzi LA. Birdshot chorioretinopathy. In: Yannuzzi LA, Flower RW, Slakter JS, eds. Indocyanine Green Angiography, 1st ed. St. Louis: Mosby, 1997:231–238.
35. Cantrill HL, Folk JC. Multifocal choroiditis associated with progressive subretinal fibrosis. Am J Ophthalmol 1986;101:170–180.
36. Folk JC, Gehrs KM. Multifocal choroiditis with panuveitis, diffuse subretinal fibrosis, and punctate inner choroidopathy. In: Schachat AP, Ryan SJ, eds. Retina, 3rd ed. St. Louis: Mosby, 2001:1709–1720.
37. Slakter JS, Giovannini A. Multifocal choroiditis and the presumed ocular histoplasmosis syndrome. In: Yannuzzi LA, Flower RW, Slakter JS, eds. Indocyanine Green Angiography, 1st ed. St. Louis: Mosby, 1997:271–278.
38. Tiffin PA, Maini R, Roxburgh ST, Ellingford A. Indocyanine green angiography in a case of punctate inner choroidopathy. Br J Ophthalmol 1996;80:90–91.
39. Nussenblatt RB. Vogt-Koyanagi-Harada syndrome. In: Nussenblatt RB, Whitcup SM, eds. Uveitis. Fundamentals and Clinical Practice, 3rd ed. St. Louis: Mosby, 2004:324–338.
40. Freund BK, Yannuzzi LA. Vogt-Koyanagi-Harada syndrome. In: Yannuzzi LA, Flower RW, Slakter JS, eds. Indocyanine Green Angiography, 1st ed. St. Louis: Mosby, 1997:259–269.
41. Bozzoni-Pantaleoni F, Gharbiya M, Pirraglia MP, Accorinti M, Pivetti-Pezzi P. Indocyanine green angiographic findings in Behcet disease. Retina 2001;21:230–236.
42. Cochereau-Massin I, LeHoang P, Lautier-Frau M, et al. Ocular toxoplasmosis in human immunodeficiency virus-infected patients. Am J Ophthalmol 1992;114:130–135.
43. Auer C, Bernasconi O, Herbort CP. Toxoplasmic retinochoroiditis: new insights provided by indocyanine green angiography. Am J Ophthalmol 1997;123:131–133.
44. Holland GN, Pepose JS, Pettit TH, et al. Acquired immune deficiency syndrome: ocular manifestations. Ophthalmology 1983;90:859–873.
45. Kuppermann BD, Petty JG, Richman DD, et al. Correlation between $CD4^+$ counts and prevalence of cytomegalovirus retinitis and human immunodeficiency virus-related noninfectious retinal vasculopathy in patients with acquired immunodeficiency syndrome. Am J Ophthalmol 1993;115:575–582.
46. Lowder CY, Butler CP, Dodds EM, Secic M, Recillas C, Gilbert C. $CD8^+$ lymphocytes and cytomegalovirus in patients with acquired immunodeficiency syndrome. Am J Ophthalmol 1995;120:283–290.

47. Gangan PA, Besen G, Munguia D, Freeman WR. Macular serous exudation in patients with acquired immunodeficiency syndrome and cytomegalovirus retinitis. Am J Ophthalmol 1994;118:212–219.
48. Karavellas MP, Lowder CY, Macdonald JC, Avila CP, Freeman WR. Immune recovery vitreitis associated with inactive cytomegalovirus retinitis: a new syndrome. Arch Ophthalmol 1998;116:169–175.
49. Palestine AG, Frishberg B. Macular edema in acquired immunodeficiency syndrome-related microvasculopathy. Am J Ophthalmol 1991;111:770–771.
50. Weinberg DV, Moorthy RS. Cystoid macular edema due to cytomegalovirus retinitis in a patient with acquired immune deficiency syndrome. Retina 1996;16:343–344.
51. Maguire AM, Nichols CW, Crooks GW. Visual loss in cytomegalovirus retinitis caused by cystoid macular edema in patients without the acquired immune deficiency syndrome. Ophthalmology 1996;103:601–605.
52. Arevalo JF, Fuenmayor-Rivera D. Cytomegalovirus (CMV)-related choroidopathy: indocyanine green video-angiography findings in AIDS patients with highly active antiretroviral therapy (HAART). Arch AAOO 2000;28:15–23.
53. Carney MD, Combs JL, Waschler W. Cryptococcal choroiditis. Retina 1990;10:27–32.
54. Arevalo JF, Fuenmayor-Rivera D, Giral AE, Murcia E. Indocyanine green videoangiography of multifocal *Cryptococcus neoformans* choroiditis in a patient with acquired immunodeficiency syndrome. Retina 2001;21:537–541.

7
Angiography of Optic Nerve Diseases

J. Fernando Arevalo, Reinaldo A. Garcia, Juan G. Sanchez, Lihteh Wu, Dario Fuenmayor-Rivera, and Aura Giral

The diagnosis of optic nerve disease is usually made by clinical history and ophthalmoscopic features. Fluorescein angiography (FA) and indocyanine green videoangiography (ICGV) findings are not pathognomonic for any optic nerve condition. However, there are some instances in which FA can be helpful in making a diagnosis. Furthermore, in some cases, FA may shed light on the pathophysiology of an unknown disease. Indocyanine green videoangiography may be useful in confirming the diagnosis of choroidal hemangioma, and defining occult choroidal neovascularization and chorioretinal inflammatory diseases. Generally speaking, ICGV is not very helpful in the evaluation and diagnosis of optic nerve diseases.

This chapter focuses on the fluorescein angiographic features of optic nerve diseases.

Blood Supply to the Anterior Optic Nerve

The anterior portion of the optic nerve may be divided into four lamellar regions, each with its own unique microvascular features: the superficial nerve fiber layer, the prelaminar region, the laminar region, and the retrolaminar region (Fig. 7.1).

The superficial nerve fiber layer is supplied principally from the arterioles in the adjacent retina. Most of these vessels are capillaries originating in the peripapillary nerve fiber layer. Emanating from the retinal arterioles at the disc are the radial papillary capillaries. These capillaries are rather straight and long, have few anastomoses, and lie in the superficial portion of the peripapillary nerve fiber layer. These vessels, as with all capillary beds within the optic nerve, are not fenestrated, and the tight junctions between their endothelial cells constitute the blood–ocular barrier. The temporal nerve fiber layer may have an additional arterial contribution from a cilioretinal artery when present. No direct choroidal contribution is observed in the superficial nerve fiber layer region.

In the prelaminar zone, the branches of the arterioles and capillaries form a diffuse network around and within the nerve bundles. The prelaminar capillaries anastomose freely with one another and arise primarily from the short posterior ciliary arteries and peripapillary choroid. Hayreh[1] believes that the central retinal artery does not supply the laminar and prelaminar zones. The anterior pial vessels do not seem to course directly into the prelaminar zone but probably anastomose with the deeper ramifications of the prelaminar capillary network.[2]

In the laminar zone a similar anastomotic net is formed by branches from the choroid and the short posterior ciliary arteries. As the laminar zone merges with the postlaminar zone, the choroidal supply decreases and is replaced by the pial vessels peripherally and branches of the central retinal artery axially.

The vascular pattern in the postlaminar area is like that of the remainder of the anterior aspect of the intraorbital optic nerve. The main blood supply to the intraorbital portion of the optic nerve is derived from the vessels of the pia mater. The pia of the intraorbital portion of the optic nerve derives its blood supply from the ophthalmic artery. Controversy exists about the blood supply of the axial anterior orbital portion of the optic nerve. At present, most investigators endorse the observations of Hayreh.[1] According to his findings, the axial vascular system of the nerve anterior to the entrance of the central retinal artery arises partly from this vessel, as there is no central artery of the optic nerve. The pial arterioles become capillaries as they pass through the pial septa into the axial portion of the nerve.[2]

The microvascular structure of the optic disc is continuous with the peripapillary retinal capillaries and with the optic nerve capillaries behind the eye. Ultrastructurally, all these vascular channels resemble those of the central nervous system. They are not fenestrated. They have tight junctions and abundant intramural pericytes. They do not leak fluorescein or other tracers despite the fact that many of them are derived from the posterior ciliary arteries, which also supply branches to the peripapillary choriocapillaris. In contrast, the choriocapillaris has a fenestrated endothelium and few pericytes, and it leaks fluorescein. A cuff of nonfenestrated capillaries lies within the choroid at the boundary of the peripapillary choroid and optic nerve head (ONH). Thus, although the vascular

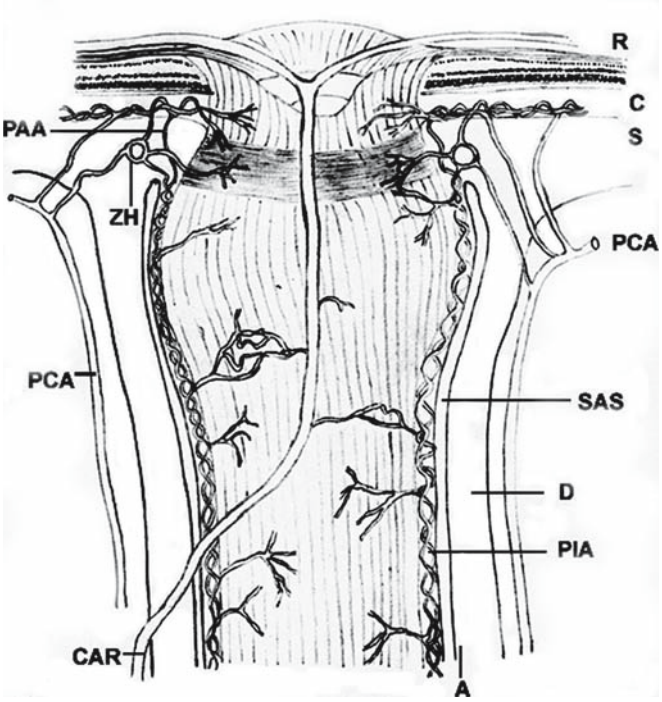

FIG. 7.1. Schematic representation of the blood supply of the optic nerve. R, retina; C, choroid; S, sclera; PCA, posterior ciliary artery; SAS, subarachnoid space; D, dura; A, arachnoid; CAR, central artery of the retina; ZH, Zinn-Haller ring; PAA, pial arteries anastomosis.

bed of the disc is mostly derived from the vessels supplying the choroid, its ultrastructure resembles more the retina–optic nerve vascular system.[3]

The blood from the prelaminar region of the optic nerve and its overlying nerve fiber layer drains mainly into the central retinal vein. Only a small proportion of this blood is drained into the choroidal circulation through small venous capillaries. These small channels represent potential bypass vessels that dilate when blood is directed away from a chronically constricted or occluded central retinal venous system into the choroidal veins, as occurs in optic nerve sheath meningiomas (ONSMs). These venous capillaries under normal conditions are ophthalmoscopically invisible since they are empty of blood. They are empty because the pressure in the retinal and choroidal veins is the same. When the central retinal vein is chronically compressed and venous pressure in the eye rises, blood is diverted through the lower pressure system, the retinochoroidal capillary system. As it fills, the capillaries become visible ophthalmoscopically. Some authors mistakenly call them opticociliary shunts, a misnomer because they are not true shunts (defined as a congenital artery that empties into a vein and that skips the capillary bed, sometimes part of the Wyburn-Mason syndrome), and they are not optic because they emanate from the retina. Most accurately they should be called retinovenous or ciliovenous collaterals.

Normal Papillary Fluorescein Angiogram

Figure 7.2 is an example of a normal papillary FA.

Preinjection

Given its whiteness, the optic disc is a tissue that intensely reflects light. Hence it can display pseudofluorescence. This is evident when a picture is taken under blue light prior to the administration of fluorescein.

Choroidal Phase

Initially a light diffuse fluorescence appears deep in the sectors corresponding to the areas where the choroid fluoresces. This fluorescence is due to the filling of the capillaries situated at the lamina cribrosa and behind it. These capillaries depend on the choroidal peripapillary vessels, which are branches of the short posterior ciliary arteries. Normally the nasal and temporal sectors of the choroid and the disc fluoresce first followed by the superior and inferior sectors, which acquire a diffuse fluorescence. If a cilioretinal artery is present, the temporal sector will begin to fluoresce. This artery can irrigate up to a third of the disc. One second later, fluorescence increases and it acquires a capillary shape due to filling of the prelaminar plexus or prepapillary racemose capillaries, made up of sinuous capillaries that irrigate all the disc area.

Arterial Phase

During this phase, fluorescence increases, given the presence of more fluorescein in the plexus mentioned before.

Arteriovenous Phase

In the early arteriovenous time, the fluorescence increases, taking advantage of the filling of a superficial capillary plexus (Fig. 7.2B). This plexus is made up of straight capillaries that come out of the disc in radial form, expanding up to a disc diameter. They are called radial epipapillary capillaries. These capillaries are of a venous nature and they act as drainage channels from the peripapillary region. They fluoresce as they get fluorescein from the retinal arterioles. In most cases, fluorescence initiates at the superior and inferior peripapillary regions followed by the nasal and temporary regions. In the venous phase, the disc fluorescence decreases due to a decreased amount of fluorescein in the disc capillaries. At the same time the fluorescence acquires an annular shape (Fig. 7.2C).

Late Phase

The disc has become fluorescent and it contrasts with the rest of the ocular fundus. The annular fluorescence decreases in intensity toward the center because the fluorescein filters from the borders of the choriocapillaris that surrounds the disc (Fig. 7.2D).

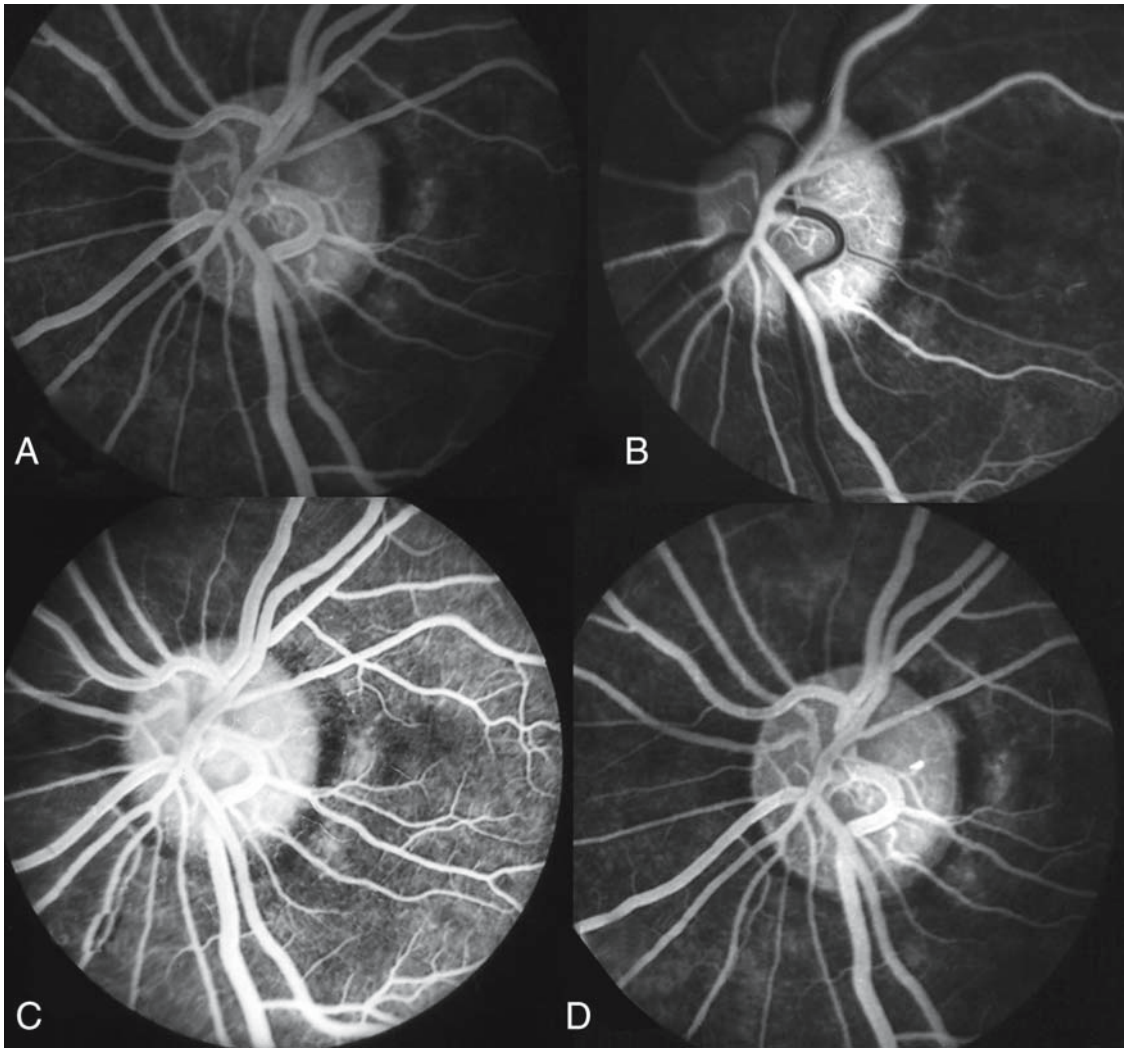

Fig. 7.2. Normal fluorescein angiogram of the optic disc. (A) Red-free photograph. (B) In the early arteriovenous phase, the fluorescence increases, taking advantage of the filling of the superficial capillary plexus. (C) In the venous phase, the disc fluorescence decreases due to the diminishing amount of fluorescein in the disc capillaries. (D) In the late phase, the disc has become fluorescent and it contrasts with the rest from the ocular fundus, which has become dark. This fluorescence, which began in an annular fashion, is of a decreasing intensity toward the center because fluorescein filters from the borders of the choriocapillaris that surrounds the optic disc.

Normal Papillary Indocyanine Green Videoangiography

Figure 7.3 is an example of a normal papillary ICGV. Indocyanine green videoangiography is not very helpful for the diagnosis of optic nerve diseases. During the first second, the choroidal arteries fill rapidly beneath the peripapillary area toward the periphery. Within the first 2 seconds, the posterior pole appears partially uniform with areas of delayed filling that are filled approximately 2 seconds after the dye first enters the eye. Most areas of the periphery become filled at this point. As the fluorescence from the choroidal arteries fade, between 2 and 5 seconds, the silhouette of the large choroidal veins may be easily seen. After 5 seconds, the choroidal fluorescence progressively diminishes. The optic nerve finally becomes dark after several minutes.

Abnormal Fluorescein Angiogram of the Optic Disc

Hypofluorescence

The first step in the diagnosis of optic nerve diseases based on FA is to recognize areas of abnormal fluorescence and

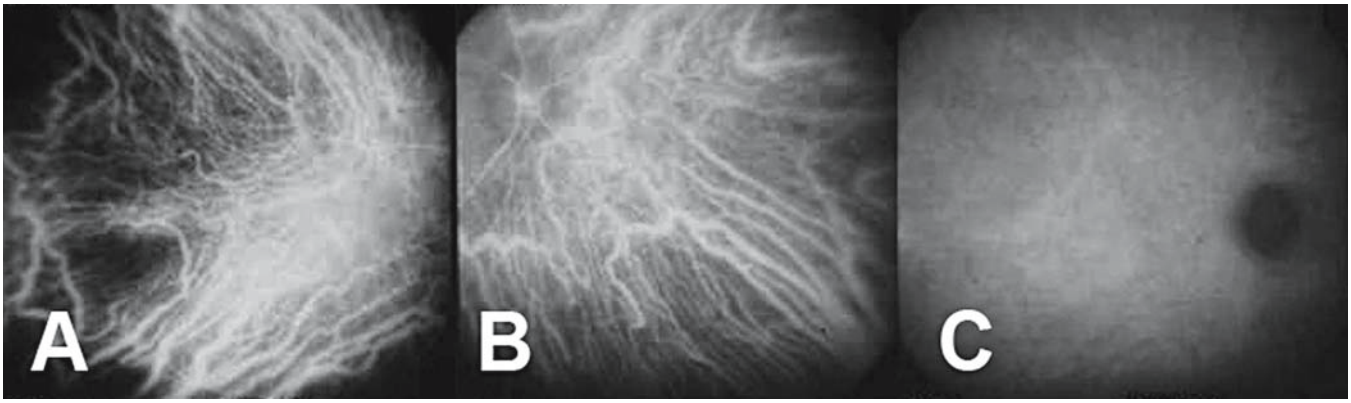

Fig. 7.3. Early, middle, and late phase indocyanine green videoangiography (ICGV). (A) The early phase permits image capture in the early phase of choroidal filling. During this phase, both the choroidal and retinal vessels are well visualized. (B) The middle phase demonstrates fading of choroidal fluorescence, and any abnormality that retains dye starts to appear as relatively hyperfluorescent. (C) The late phase begins approximately 18 minutes after the injection. Choroidal vessels appear as hypofluorescence channels, retinal vessels are not visible, and the optic nerve head appears dark.

determine if they are hypofluorescent or hyperfluorescent. Hypofluorescence refers to any abnormally dark area on the positive print of an angiogram. There are two possible causes of hypofluorescence: blocked fluorescence or a vascular filling defect.

Fluorescein is present but cannot be seen in blocked fluorescence. For example, blood in the vitreous or a layer of blood in front of the retina obscures the view of the underlying retinal, choroidal, or disc circulations. With vascular filling defects, fluorescein cannot be seen because it is not present. The key in differentiating blocked fluorescence from vascular filling defects is to correlate the hypofluorescence on the angiogram with the ophthalmoscopic findings. If there is a lesion that is ophthalmoscopically visible that corresponds in size, shape, and location to the hypofluorescence on the angiogram, then blocked fluorescence is present. If there is no corresponding ophthalmoscopic lesion, then it must be assumed that fluorescein has not perfused the vessels and that the hypofluorescence is caused by a vascular filling defect.

Vascular filling defects of the disc occur because the capillaries of the optic nerve head fail to fill. This failure can be caused by optic atrophy, vascular occlusion such as in cases of ischemic optic neuropathy, and congenital absence of disc tissue as in an optic pit or optic nerve head coloboma. Each one of these conditions is characterized by early hypofluorescence caused by nonfilling and late hyperfluorescence resulting from staining of the involved tissue.

Hypofluorescence by Congenital Absence of Disc Tissue

Congenital cavitary anomalies of the optic nerve that may be associated with serous detachments of the macula include optic disc pit, optic nerve coloboma, and morning glory disc anomaly. The origin of the fluid and precise pathogenesis of the macular detachment associated with cavitary optic disc anomalies remains unclear but probably they all share the same mechanism.

Congenital Pits of the Optic Nerve Head

Congenital pits of the optic nerve head are rare abnormalities that are attributed to imperfect closure of the embryogenic fissure. They occur in approximately 1 in 11,000 patients.[4] The pit may be bilateral, slit-like or oval in shape, and may vary from yellow to black in color. Typically, they are located in the temporal aspect of the optic disc, although they may occur elsewhere (Fig. 7.4).[5] Visual acuity is usually unaffected unless the pit is complicated by a serous macular retinal detachment, which develops in 25% to 75% of cases.[4,5] Considerable controversy exists regarding the pathogenesis and pathologic nature of the macular detachments associated with optic nerve pits. Given that an increase in vascular permeability is not demonstrable by FA, most authors agree that the submacular fluid originates from either the vitreous or cerebrospinal fluid (CSF).[6,7] Experimental evidence favors liquid vitreous as the fluid source. In collie dogs, India ink passes into the subretinal space when injected intrathecally.[8] However, in a single human subject, intrathecally administered fluorescein failed to be visualized in the subretinal space by fluoroscopy. [9] On the other hand, rare cases of subretinal migration of vitreous substitutes (gas and silicone oil) through anomalous disc excavations have been reported. Furthermore, intraoperative drainage of subretinal fluid through cavitary disc anomalies is possible.[8] Regardless of the presumed source, most authors previously assumed that macular detachments were a result of fluid entering directly into the subretinal space by way of a defect at the site of the pit.[6,7,9] In 1988, Lincoff et al.[10]

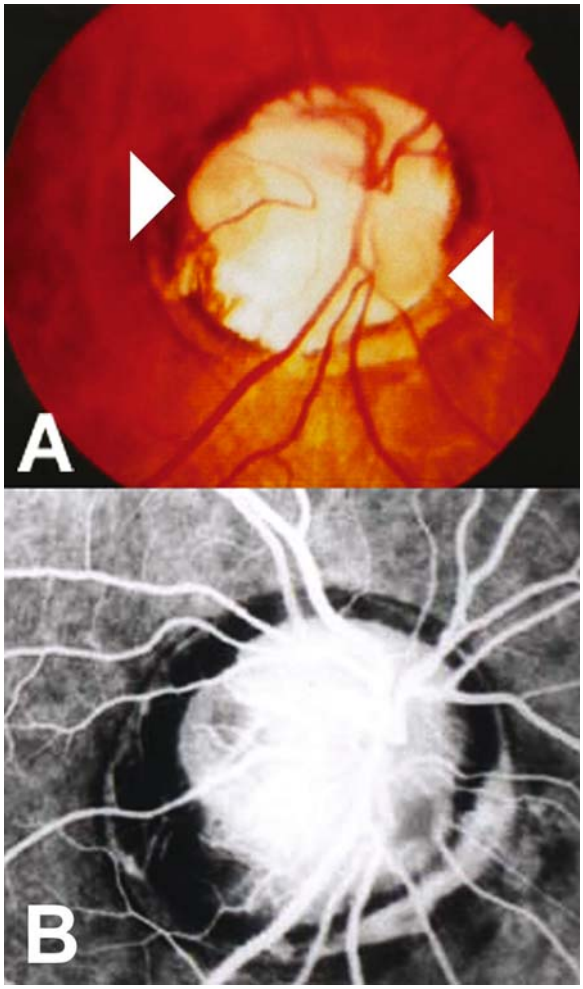

Fig. 7.4. (A) Color fundus photo showing two yellow-gray oval pits located in the temporal and nasal aspect of the optic disc (arrowheads). Notice a large excavation with a defect in the neural rim inferiorly. (B) Fluorescein angiography showing hypofluorescence through all the times of the angiogram in the area of the optic disc pits.

proposed that fluid typically enters the neurosensory retina directly from the pit, separating the inner retinal layers to produce a primary schisis-like macular elevation. In contrast to earlier theories, they hypothesized that macular detachments are a secondary phenomenon that start in the macula and may persist without communication with the pit due to the development of an outer lamellar macular hole. Several years later, optical coherence tomography (OCT) showed that the schisis-like separation precedes macular detachment and that it invariably communicates with the optic disc, even when the associated macular detachment does not.[8,11] Several authors have suggested that CSF from the perineural subarachnoid space may be responsible for the maculopathy complicating optic pits and related anomalies. Furthermore, communications between the subarachnoid space and subretinal space and between the subarachnoid space and vitreous cavity have been proven clinically. As Irvine et al.[12] suggested, the vitreous, subarachnoid, and subretinal spaces may all be variably interconnected since the herniated tissues composing the optic nerve anomaly remain porous in nature due to its incomplete differentiation. It follows that the subretinal fluid in a given case might be vitreous fluid, CSF, or a mixture of both fluids. This anatomic factor and the transmission of intracranial pressure fluctuations to the pit via the perineural subarachnoid space may be responsible in part for the pathogenesis of macular detachments associated with optic nerve pits.[8]

Fluorescein Angiographic Findings

Fluorescein angiography showed early hypofluorescence (Fig. 7.5) and late staining in the area of the optic disc pit. More precisely, at the midphases of the angiogram, the optic disc pit showed a slight staining of the pit margin, which gradually increased during the subsequent phases. At the late stages of the examination, lesser or greater hyperfluorescent

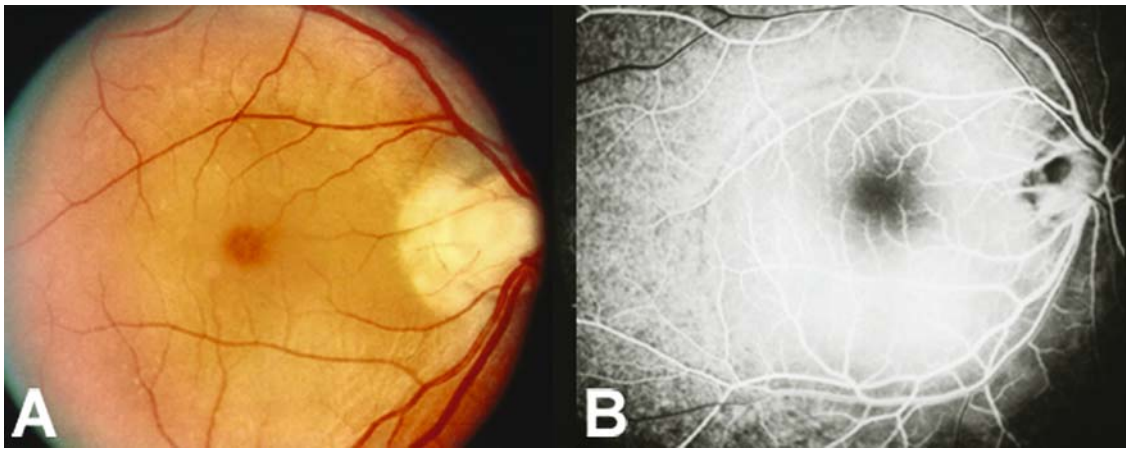

Fig. 7.5. (A) Color fundus photo of a patient with subretinal fluid and temporal optic disc pit. (B) Fluorescein angiography (FA) showed early hypofluorescence in the area of the optic disc pit. In the early FA phase, the appearance of fluorescein dye in the area of the macular elevation is evident. The posterior pole hyperfluorescence, which is more intense in the papillomacular bundle region adjacent to the optic disc, does not have the typical appearance of choroidal transmission fluorescence.

of the optic disc pit can be noted. Fluorescein angiography shows a well-delineated round or oval area of late hyperfluorescence corresponding to the area of macular elevation. In the early FA phases, the appearance of fluorescein dye in the area of the macular elevation is evident (Fig. 7.5). The dye increases in intensity during the late phases of the procedure. The hyperfluorescence, which is more intense in the papillomacular bundle region adjacent to the optic disc, does not have the typical appearance of choroidal transmission fluorescence. The hyperfluorescence is localized under the level of the retinal vasculature and seems to be caused by leakage of the dye into the schisis cavity and subretinal fluid. Theodossiadis et al.[13] hypothesized that the dye passes through the optic pit into the fluid of the schisis cavity first. Afterward it flows into the subretinal fluid through the existing outer layer lamellar macular hole. The well-delineated area of hyperfluorescence corresponds exactly with the macular elevation. The authors postulated that the halo of hyperfluorescence could be attributed to the more intense concentration of dye at the limits of the macular elevation. The intensity of the hyperfluorescence of the elevated macula, which varies in each individual case, could be related to the degree of fluid viscosity within the schisis cavity.

Optic Disc Coloboma and Morning Glory Syndrome

The morning glory syndrome is a congenital optic nerve anomaly that has received scant attention since it was first described by Handmann in 1929. There have been documented variations of the syndrome. The syndrome is usually unilateral, hereditary, and associated with other congenital anomalies. The majority of patients have a visual acuity between 20/200 and counting fingers in the affected eye, although cases with 20/20 vision and no light perception have been reported. The anomaly is usually limited to the eye, and the retrobulbar nerve and brain appear normal, as documented by ultrasound and computed tomography. However, the syndrome may be associated with basal encephalocele in patients with midline facial defects. Surprisingly, increasing fibrovascular tissue produces traction on the disc substance and vasculature, vitreous, macula, and peripapillary retina. These findings may place these patients within a spectrum of congenital optic nerve anomalies ranging from staphylomata to posterior persistent hyperplastic primary vitreous.[14] The morning glory anomaly usually presents itself as leukokoria in the first months or years of life. On funduscopic examination, a funnel-shaped excavation of the optic disc and peripapillary retina is seen. The disc is enlarged and has indistinct borders, which are surrounded by depigmented areas. A white, elevated, hyperplastic glial tissue occupies the central disc, obscuring the central retinal vessels. Abnormally narrow, straight vessels radiate from the disc margins

Fig. 7.6. On funduscopic view, the morning glory anomaly is characterized by an enlarged optic disc with indistinct border surrounded by depigmented areas, white, elevated, hyperplastic glial tissue that occupy the central disc and obscures the central retinal vessels, and abnormally narrow, straight vessels radiated from the disc margins.

(Fig. 7.6). There is an increased risk of non-rhegmatogenous serous retinal detachment in eyes with the morning glory syndrome.

Fluorescein Angiographic Findings

Fluorescein angiography shows hypofluorescence at the center of the disc, and numerous radial vessels are seen around this central hypofluorescent glial tissue. Peripapillary changes around the disc cause a mottled fluorescence. Exudative changes from accumulation of subarachnoid fluid or a small retinal break in the abnormal retina adjacent to the disc anomaly are responsible for the retinal detachment, which is present in one third of cases.

Persistence of Fetal Vasculature

The spectrum of persistence of fetal vasculature (posterior persistent hyperplastic primary vitreous) includes persistence of the hyaloid artery, Bergmeister's papilla, nonattachment of the retina, retinal folds, macular hypoplasia, and optic nerve head hypoplasia. In Bergmeister's papilla (Fig. 7.7), white intravitreal membranes can attach to the optic nerve, distorting its margins and obscuring its cup. Fluorescein angiography demonstrates hypofluorescence of the white intravitreal membranes. The membranes are associated with retinal folds in two thirds of cases and usually with tortuosity of peripapillary vessels.

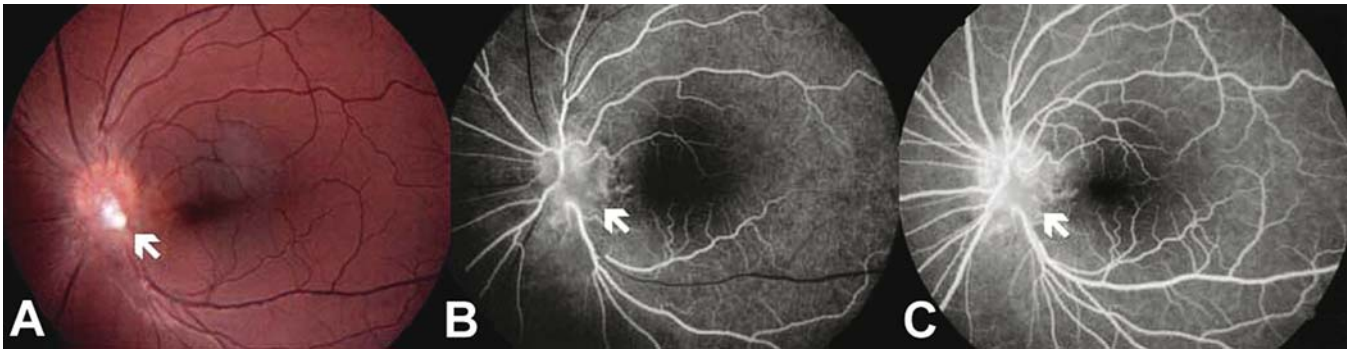

FIG. 7.7. (A) In Bergmeister's papilla, white intravitreal membranes can attach to the optic nerve (arrow), distorting its margins and obscuring its cup. (B) Early fluorescein angiogram (FA). (C) Late FA showing hypofluorescence of the white intravitreal membranes (white arrow in A–C).

Tilted Disc Syndrome

The association between tilted disc and optic pit has been described, as well as the relationship among optic pit, optic coloboma, and morning glory syndrome.[15] These conditions represent different degrees of dysplasia in the spectrum of optic nerve malformations related to faulty closure of the embryonic (fetal) fissure of the optic stalk and cup.[16]

Tilted disc syndrome is a relatively common congenital anomaly, occurring in 1% to 2% of the population. It is characterized by an inferonasal "tilting" of the disc, with the upper and temporal portion of the disc lying anterior to the inferonasal portion (Fig. 7.8). Associated findings typically include an obliquely directed long axis of the disc, an inferonasal crescent, a posterior staphyloma of the affected inferonasal region of the fundus, and situs inversus. Situs inversus is characterized by the emergence of the retinal vessels from the upper and temporal sides rather than from the nasal side.[17] The most important of these associations is myopic astigmatism, which happens to be most pronounced in the region of the staphyloma. Superotemporal or bitemporal visual field depression is another important associated finding.[17] Macular pigmentary changes have been reported in up to 11% of eyes with tilted disc syndrome,[18] but these are usually asymptomatic. Visual loss may be caused by choroidal neovascularization.[19]

In 1998, Cohen et al.[20] described a previously unreported complication of tilted disc syndrome: serous retinal detachment. It is caused by subretinal leakage that mimics chronic idiopathic central serous chorioretinopathy (ICSCR). In their cases, the site of leakage was at the edge of the staphyloma in an area of retinal pigment epithelium (RPE) changes. The staphyloma corresponds to an area of scleral ectasia but also to choriocapillaris rarefaction and RPE hypopigmentation. The leakage could be caused by anatomic factors. They hypothesized

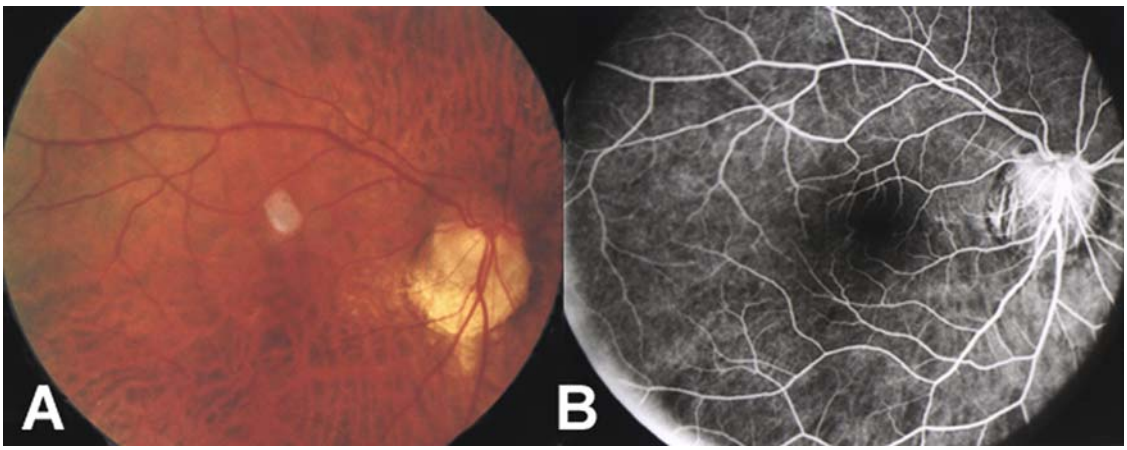

FIG. 7.8 (A) Color fundus photograph shows inferonasal "tilting" of the disc, with the upper and temporal portion of the disc lying anterior to the inferonasal portion associated with an inferior crescent, and posterior staphyloma of the affected inferior region of the fundus. (B) Fluorescein angiography shows the background choroidal fluorescence through the inferior crescent. The macula demonstrates normal hypofluorescence.

that the junctional area between the staphyloma and normal fundus corresponds to a region in which mechanical forces or hemodynamic changes, or both, facilitate the development of subretinal leakage. Although it is not possible to rule out a coincidental association of ICSC and tilted disc syndrome, the constant location of the leakage site in a particular anatomic area strongly suggests a specific pathogenesis, although it is unclear at this time. In 1999, Tosti[21] confirmed the presence of this association and added three cases to the initial report of five affected eyes. He suggested that anomalies at the junction between the altered disc margin and the peripapillary retina may play a role, similar to what happens in optic pit syndrome. However, we recently saw a 39-year-old woman with the site of leakage at the edge of the staphyloma in an area of diffuse atrophy of the RPE. Multiple OCT scans over the temporal margin of the optic disc in our case failed to demonstrate anomalies at the junction between the altered disc margin and the peripapillary retina (Fig. 7.9).

Leys and Cohen[22] reported the ophthalmoscopic and fluorescein angiographic features of this association. They demonstrated linear pigmentary changes at the border of the staphyloma with one or more leaking or staining sites. In several patients, the leaking sites changed at different visits, some having disappeared and new ones appearing. A long-standing or recent neurosensory detachment was identified. Retinal pigment epithelium changes caused by chronic retinal detachment or serous elevation with or without subretinal exudates were observed clinically and documented by FA. In eyes with chronic disease, they noted deep atrophy at the sites of subretinal leakage and large atrophic tracts due to chronic serous retinal detachment.

In our case (Fig. 7.9), the site of leakage was apparent at the edge of the staphyloma in an area of diffuse atrophy of the RPE. We concur with Cohen et al.[20] in believing that the staphyloma associated with the tilted disc syndrome represents the major cause of leakage. In addition, an ICGV performed 2 months before the development of the active leakage site enabled the observation of dilated choroidal vessels. The hyperfluorescent areas corresponded with choroidal hyperpermeability and was observed in the same area of the venous dilatation as was reported previously by Giovannini et al.[23] in ICSC. Although it may not be possible to rule out a coincidental association of ICSC and tilted disc syndrome or myopic staphyloma, maybe this particular anatomic alteration predisposes to increased venous pressure that causes venous choroidal congestion and increased choroidal permeability, thus giving rise to a picture indistinguishable from ICSC in these cases.

There are a few cases of subretinal neovascular membranes associated with tilted disc syndrome (Fig. 7.10). Stur[24] in 1988 fist reported a case with this association. The pathogenesis of subretinal neovascular membranes and tilted disc syndrome remains unclear. Prost and De Laey[25] suggest that a combination of factors that include associated RPE disturbances adjacent to both a break in Bruch's membrane and an abnormal choriocapillaris contribute to the pathogenesis of the subretinal membranes in this condition. In addition, the superotemporal elevation of a tilted optic disc could lead to mechanical disruption of peripapillary tissue, creating a pathway for the ingrowth of neovascular tissue analogous to peripapillary subretinal neovascular membranes described in association with optic nerve drusen.[19]

Peripapillary Atrophy

Peripapillary atrophy can be defined as an inner crescent area of chorioretinal atrophy where the sclera and choroidal vessels are visible. It is also characterized by an outer irregular area of hypopigmentation and hyperpigmentation located outside the scleral ring of Elschnig. It is seen not only in progressive glaucoma but also in patients with nonprogressive glaucoma, ocular hypertensives, and normal individuals. There may also be some alterations in parapapillary tissue when there is a progressive axial enlargement producing myopia. Jonas and coworkers[26,27] divided peripapillary atrophy into two zones: (1) a peripheral "alpha" zone with irregular hyperpigmentation and hypopigmentation, and (2) a central "beta" zone characterized by marked chorioretinal atrophy with visible large choroidal vessels and sclera. Both zones were significantly larger and more frequent in eyes with glaucoma than in normal subjects (Fig. 7.11).

The peripapillary blood flow is directed away from the optic disc margin toward the peripheral choroid. At the prelaminar and laminar levels of the optic nerve, the only vessels between the optic nerve and the peripapillary choroid are the small arterial and venous connections. There is a conspicuous absence of the capillary bed in this area. Since arteriolar blood flow is directed away from the peripapillary region, either toward the choroid or the central optic nerve, and the peripapillary region is likely a low-pressure system as compared to the rest of the choroid,[28] the area between the optic nerve head and the peripapillary choroid may act as a "watershed zone." This region may be susceptible to localized ischemia during periods of decreased arterial perfusion. If this concept is combined with the vertically oriented watershed zones, the peripapillary region certainly becomes a potential site for ischemic damage, especially at the superior and inferior temporal regions. During periods of decreased systemic blood pressure or increased intraocular pressure, localized hypoperfusion may occur in these regions.[29]

During clinical examinations, parapapillary atrophy may range from irregular pigmentation to severe loss of the RPE that results in visualizing bare sclera and the large choroidal vessels at the parapapillary area. Tezel et al.[30] observed that the severity of parapapillary atrophy may increase in ocular hypertensive eyes as assessed by the conversion of the alpha zone to the beta zone in some of their study eyes. These observations correlate with the histopathologic findings that the alpha zone of parapapillary atrophy represents pigmentary and structural changes of the RPE and the beta zone represents more

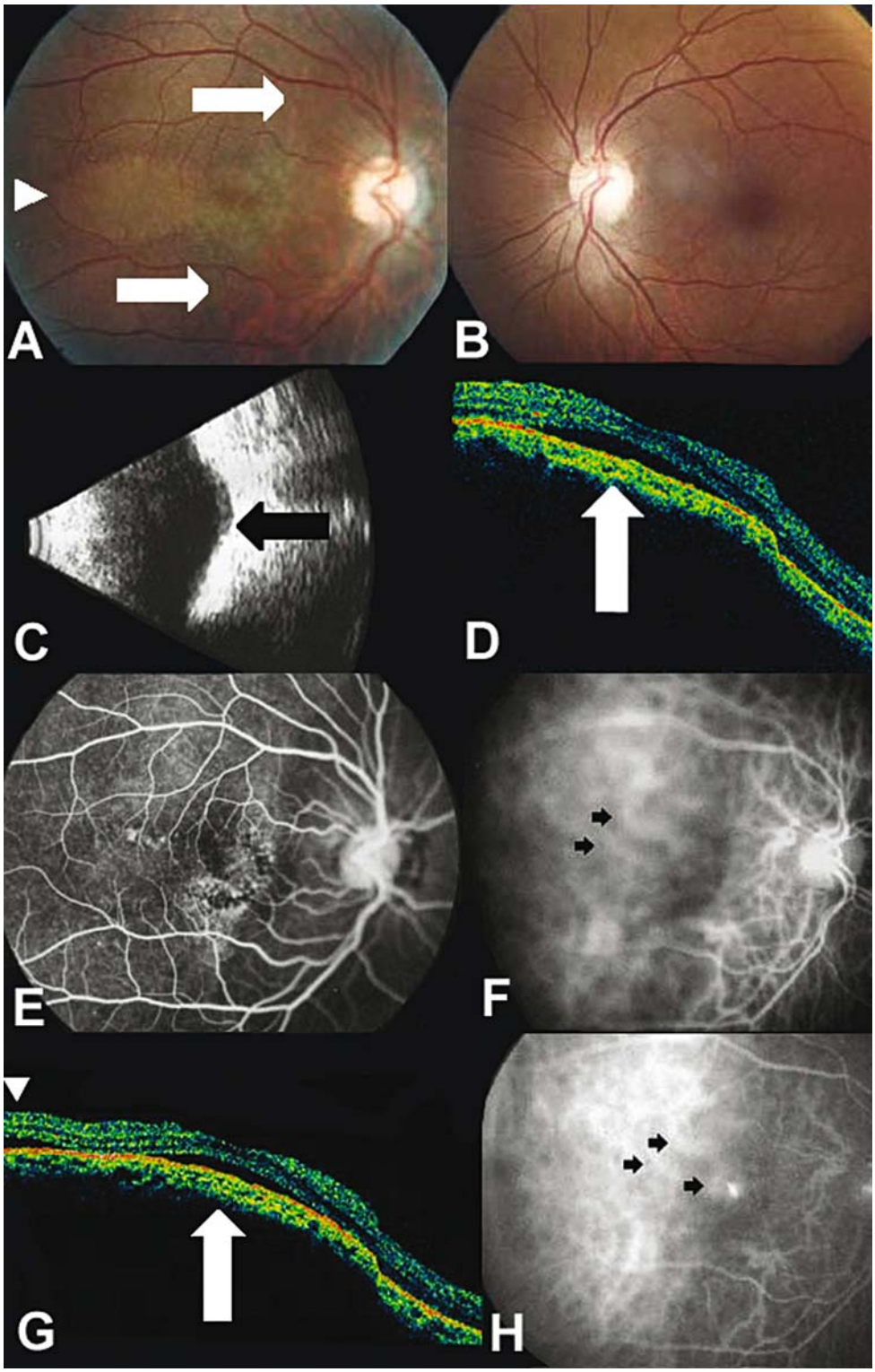

FIG. 7.9. Fundus examination revealed a posterior staphyloma in the right eye (RE) and no abnormalities in the left eye (LE). (A) In the RE there was a large staphyloma around the optic disc (arrows). There was an oval area of hypopigmentation temporal to the macular area (arrowhead), and several folds at the inner limiting membrane in a radial fashion. (C) As measured by B-scan ultrasonography, the staphyloma was 4 mm in depth (black arrow). (D) Optical coherence tomography (OCT) of the RE showed a shallow macular serous retinal detachment with diffuse retinal pigment epithelium (RPE) disturbance (white arrow) at the junction between the normal fundus and the posterior staphyloma. (E) Fluorescein angiography revealed multiple early focal hyperfluorescence spots in the macular area connected to the temporal border of the staphyloma. These hyperfluorescence spots did not change in size or shape during the late phases of the angiogram. (F) Digital indocyanine green videoangiography (ICGV) revealed discrete areas of dilatation of the choroidal vessels (black arrows). (G) After photodynamic therapy, a new site of subretinal fluid was depicted with OCT (arrowhead). In addition, reaccumulation of subretinal fluid was seen under the fovea (white arrow). (H) ICGV revealed increased hyperfluorescence, leakage from the RPE active site, and an increase in size and extent of the area of presumed choroidal hyperpermeability (black arrows).

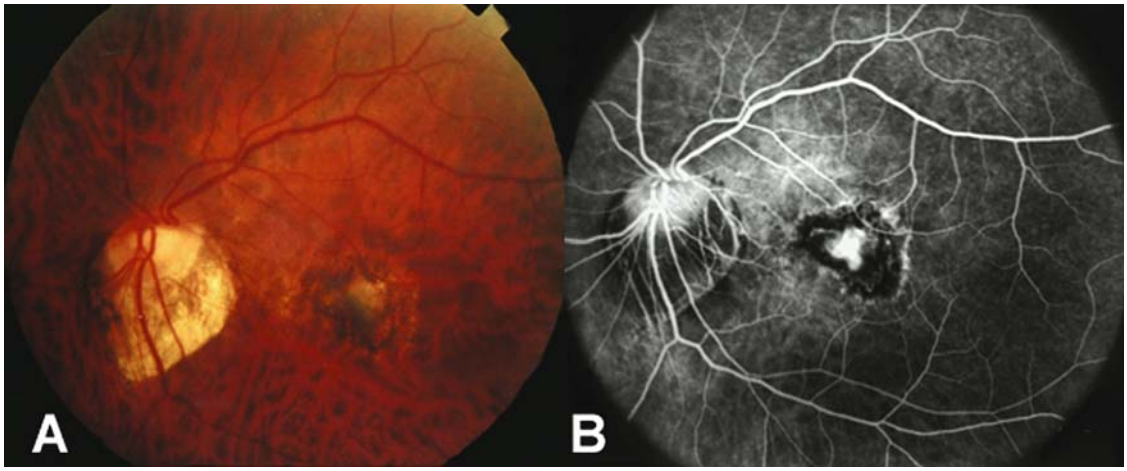

FIG. 7.10. (A) Color fundus photograph in a patient with choroidal neovascular membrane (CNV) associated with tilted disc syndrome. (B) Fluorescein angiography demonstrating late leakage from CNV.

advanced damage of the parapapillary tissues with a complete loss of RPE cells, adjacent photoreceptors, and choriocapillaris (Fig. 7.11). Tezel et al. found an important association between a larger baseline size of parapapillary atrophy, especially beta zone, and its subsequent progressive changes. Because healthy RPE modulates the structure and function of the choriocapillaris, its destruction causes choriocapillary atrophy. The larger area and extension of parapapillary atrophy may signify a greater susceptibility of the parapapillary tissues to injury.[29] In patients with ocular hypertension, progressive changes in parapapillary atrophy might occur before clinically noticeable optic disc or visual field defects. These changes have a 49% sensitivity and a 90% specificity. Alpha and beta zones have to be differentiated from the scleral crescent in highly myopic eyes and from the inferior scleral crescent in eyes with "tilted optic discs."[29]

Peripapillary crescents surrounding the optic disc are a hallmark of eyes with a highly myopic refractive error. In the early FA phase usually there is consistent hypofluorescence across the entire crescent. In the late phases, the crescent can be divided into a hyperfluorescent outer zone and a hypofluorescent inner zone. Differential fluorescence between the outer and inner myopic crescent occurs only in the late-phase FAs. The outer zone

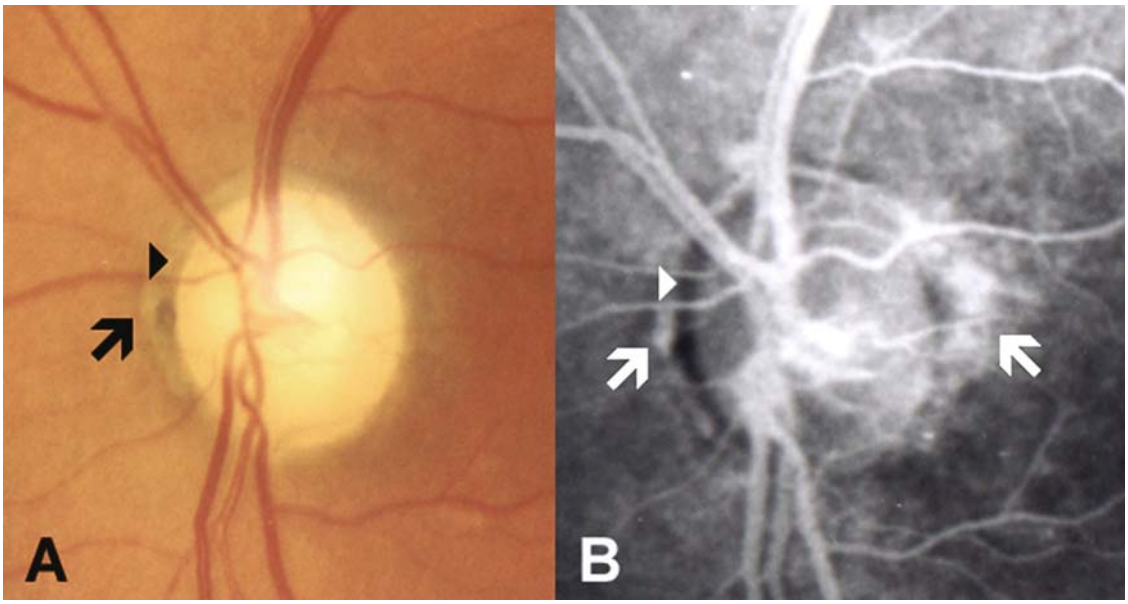

FIG. 7.11. (A) Color fundus photograph shows peripheral zone "alpha" with irregular hyperpigmentation and hypopigmentation (black arrow) and a central zone "beta" characterized by chorioretinal atrophy (black arrowhead). (B) Fluorescein angiogram (FA) shows zone alpha more clearly and demonstrates hyperfluorescence due to a window defect (white arrows), and zone beta remains consistently hypofluorescent by FA (white arrowhead). Zone beta represents more advanced damage of parapapillary tissues with a complete loss of retinal pigment epithelium cells combined with the loss of adjacent photoreceptors and choriocapillaris.

represents delayed choroidal filling. In contrast, the inner zone represents the complete loss of choroidal vessels.

Peripapillary atrophy in glaucoma is divided into a central beta zone and a peripheral alpha zone. According to Funaki et al.,[31] the alpha zone demonstrates hyperfluorescence secondary to a window defect. The beta zone remains consistently hypofluorescent by FA (Fig. 7.11). Comparison of these angiographic features indicates that the beta zone in glaucomatous eyes and the inner zone in highly myopic eyes had the same FA features. The outer zone of the myopic crescents was hypofluorescent in the early phase and became hyperfluorescent in the late phase in contrast with the consistent hyperfluorescence of the alpha zone in glaucomatous eyes. Based on their FA findings, Yasuzumi et al.[32] reported that the Zinn-Haller ring was dislocated at the border between the outer and inner zones. Dislocation of the ring might be caused by mechanical stretching around the optic disc, suggesting that the inner zone of the myopic crescent also develops as a result of mechanical stretching around the optic disc. During follow-up, 60 of their 88 study eyes (68.2%) had significant enlargement of the myopic crescent. Further analysis revealed that in most of these eyes only the outer zone enlarged significantly. The outer zone might represent choroidal circulatory disturbances, as well as mechanical stretching. These two factors contribute to crescent enlargement in highly myopic eyes.[32]

Choroidal occlusions are more clearly demonstrated on ICGV than retinal vascular defects, the opposite of what is observed with FA. Atrophy of the vascular bed occurs in a variety of conditions. During the late-phase ICGV, pathologic myopia with a posterior staphyloma usually shows peripapillary hypofluorescence caused by extensive choriocapillaris atrophy.

Nonarteritic Anterior Ischemic Optic Neuropathy

This common form of optic neuropathy typically occurs in adults between the ages of 50 and 70 years. It is usually an isolated event without associated arteritis, evidence of ocular inflammation, or laboratory evidence of a systemic arteritis. It most often occurs in healthy individuals but has been reported in association with systemic hypertension, diabetes mellitus, blood loss, recent intraocular surgery, and increased intraocular pressure. Nonarteritic anterior ischemic optic neuropathy (NAION) is usually manifested by an abrupt, painless, unilateral loss of central or peripheral vision. The peripheral visual loss most frequently involves the inferior visual field in the form of an altitudinal or arcuate defect (Fig. 7.12). Upper field defects are also commonly seen (Fig. 7.13). This loss is accompanied by a relative afferent pupillary defect and dyschromatopsia. In at least 40% of patients, the fellow eye may also develop NAION. Repeated episodes in the same eye are reported to be infrequent.

The optic nerve head characteristically undergoes sectorial swelling with initial hyperemia and superficial nerve fiber layer hemorrhage at the disc margin. Shortly thereafter the disc edema resolves and is followed by pallor in the involved sector.

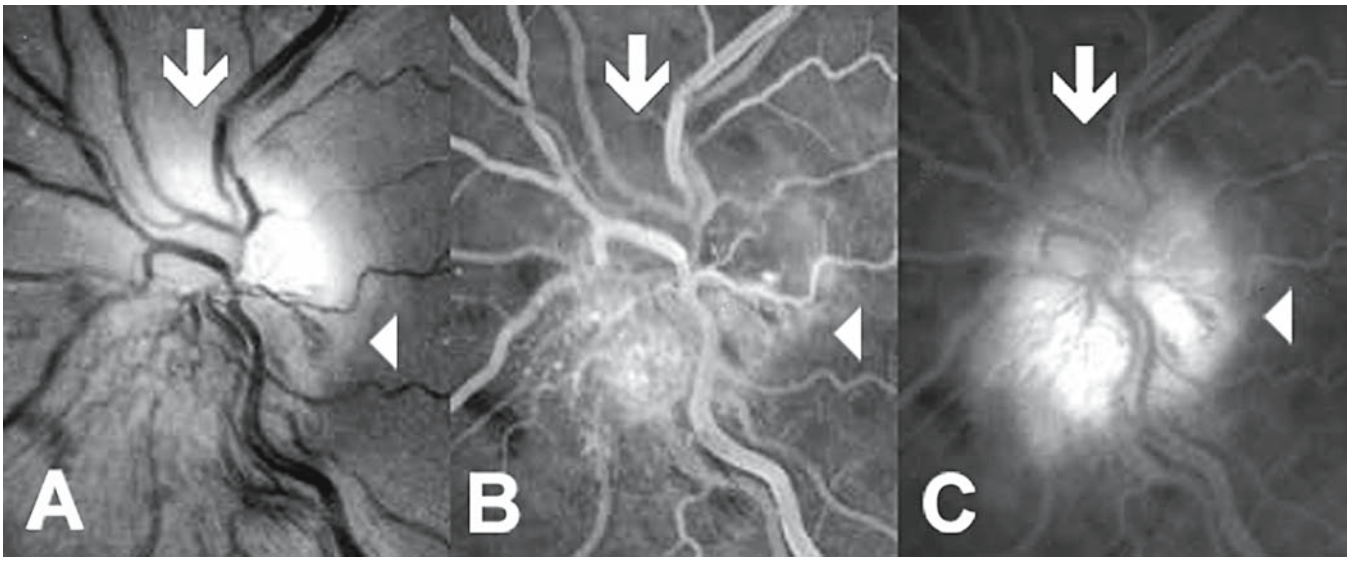

FIG. 7.12. (A) Red-free photograph of a 64-year-old woman with acute visual loss and an inferior altitudinal field defect. The photo demonstrates a superior pale hemidisc and an inferior optic disc edema with superficial hemorrhages. Early (B) and late (C) fluorescein angiogram shows superior hypofluorescence due to hemidisc ischemia of the optic disc (white arrow) and inferior hyperfluorescence due to leakage from the edematous disc encircling the ischemic area (white arrowhead).

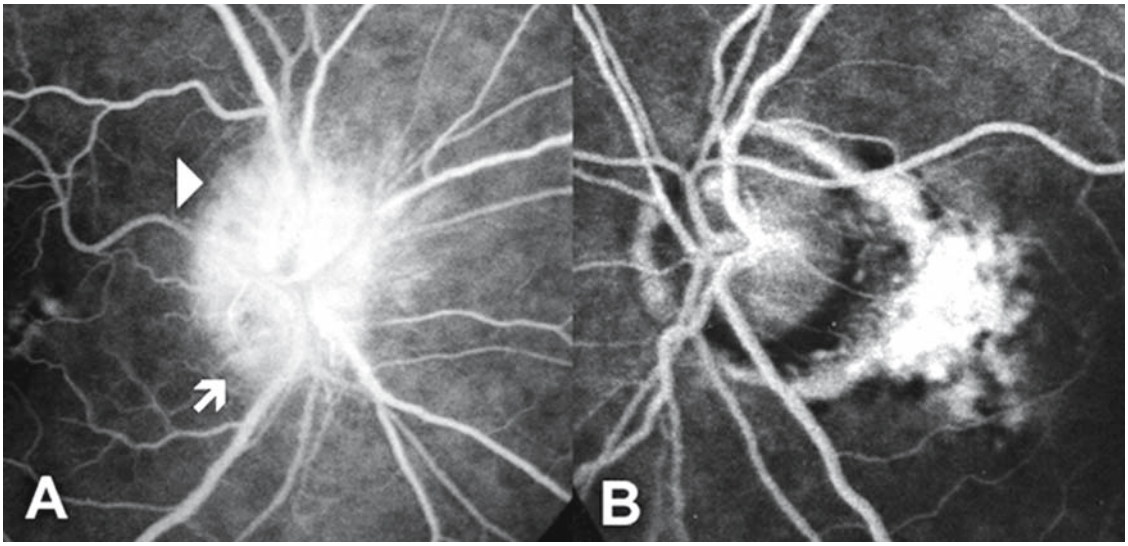

FIG. 7.13. (A) A 73-year-old woman with poor vision and a superior altitudinal field defect 2 months after cataract surgery in the right eye. Fluorescein angiography (FA) shows an inferior hypofluorescent area due to segmental ischemia of the optic disc and superior hyperfluorescence due to leakage from the edematous disc encircling the ischemic areas. (B) The small and "crowded" fellow optic disc shows inconspicuous or absent physiologic excavations and increased number of branches of the central retinal vessels within the disc. FA shows peripapillary hyperfluorescence due to a window defect. The difference between the disc that leaks (A) and the normal disc (B) is quite obvious on FA.

Patients with NAION often have optic discs that appear small and "crowded" ("disc at risk") with inconspicuous or absent physiologic excavations and increased numbers of branches of the central retinal vessels within the disc (Fig. 7.13B). The eyes tend to be more hypermetropic. The small size of the optic cup may indirectly reflect the small size of the scleral canal, which has been considered to be the anatomically determining element for the increased risk of NAION.

The pathogenesis of NAION is multifactorial and includes structural and blood flow abnormalities. Olver et al.[33] proposed that reduced perfusion pressure in the region of the paraoptic branches of the short posterior ciliary arteries results in optic disc hypoperfusion. In vivo, the posterior ciliary arteries behave physiologically as end arteries. The position and extent of the watershed zone in relation to the optic nerve head vary greatly, being located anywhere between the fovea and the nasal peripapillary choroid. It has been suggested that the disc is more vulnerable to ischemia when the watershed zone is located at the peripapillary choroid.[34]

There are three angiographic features that are well studied in NAION:

1. Peripapillary choroidal delay or choroidal dye filling delay: Early reports on angiography in NAION emphasized delayed filling of the disc and peripapillary choroid. However, recent angiographic studies have revealed a generalized choroidal filling delay only in arteritic disease. Patients with nonarteritic disease demonstrate only a focal delay (with filling times similar to those of controls).[35] Hayreh[36] described massive choroidal nonperfusion in patients with arteritic anterior ischemic optic neuropathy (AAION). He suggested that such choroidal abnormalities are extremely rare in NAION. Similarly, comparative analysis from ICGV and FA techniques did not show a statistically significant increase in the frequency of the peripapillary choroidal watershed zone filling delay in NAION.[37]
2. Leakage from the disc: FA can show hyperfluorescence due to diffuse or focal leakage from the disc. ICGV is unable to demonstrate optic disc leakage.
3. Disc filling defects: FA demonstrates hypofluorescent areas encircled by hyperfluorescence. The hypofluorescence is due to segmental optic disc ischemia. Hyperfluorescence occurs secondary to leakage from the edematous disc (Figs. 7.12 and 7.13).

Arteritic vs. Nonarteritic Anterior Ischemic Optic Neuropathy

Patients with giant-cell arteritis may also develop ischemic optic neuropathy as a consequence of acute occlusion of the posterior ciliary arteries. These patients are usually 60 years of age or older and may have systemic symptoms of cranial arteritis. The sedimentation rate is typically elevated. During the acute phase of the disease, the entire choroid supplied by the occluded posterior ciliary artery does not fill on FA during its early phases. By the late retinal venous phase the occluded choroid starts to fill in a retrograde fashion from the vortex veins.[37] The blood in the vortex vein has a very high concentration of

oxygen, which prevents the development of choroidal infarcts and parapapillary atrophy in most AAION eyes. Moreover, within a few days, the occluded choroid starts to establish a collateral circulation and the filling on FA normalizes.[38]

Very importantly, in AAION there is a total infarction of the involved part of the ONH caused by permanent thrombotic occlusion of the posterior ciliary arteries by giant cell arteritis. This results in massive loss of not only the axons but also the other tissues in the involved part of the ONH. Some time later fibrosis of the longitudinal septa in the retrolaminar region develops. Hayreh et al[39] reported angiographic and clinical findings of about 1000 patients with NAION. In contrast to the situation in AAION, none of the eyes developed an occlusion of the posterior ciliary arteries with the exception of an extremely rare case with embolic occlusion of the posterior ciliary artery. Instead, they only found evidence of a transient hypoperfusion or nonperfusion of the ONH during sleep caused by a fall of perfusion pressure in the ONH capillaries secondary to a nocturnal fall of blood pressure. This is indicated by the fact that angiography does not reveal any evidence of posterior ciliary artery occlusion. Furthermore, at least three quarters of the patients with NAION discover the visual loss on waking up from sleep. Finally, the visual loss in NAION is usually not as marked as in AAION. Thus the severity, duration, and extent of ischemia are far greater in one type of AION than in the other. Consequently, the extent and severity of ONH damages is entirely different in AAION and NAION. In this connection it should be noted that contrary to popular belief, neural ischemia is not an "all-or-none phenomenon" but there is an entire spectrum of ischemia varying from subclinical to most severe. The ischemia of the ONH is most severe in AAION and only transient in nature, and mild to moderate in NAION.[40]

Siatkowski et al.[35] found in eyes with AAION a delayed dye appearance in the retina with consecutive delayed laminar flow and venous filling. Valmaggia et al.[41] attempted to see the value of an ICGV in the management of patients with AAION and NAION by comparing ICGV with FA. They found that the angiographic temporal features such as choroidal dye appearance, retinal dye appearance, laminar flow, venous filling, or complete choroidal filling were not significantly different between the two types of angiography in both diseases. Therefore, ICGV does not provide any additional useful information with respect to FA when evaluating AAION and NAION.

Hyperfluorescence at the Optic Disc

Hyperfluorescence refers to any abnormally light area on the positive print of an angiogram, that is, an area showing fluorescence in excess of what would be expected on a normal angiogram. Hyperfluorescence at the optic disc depends in part on the relationship of its appearance to the timing of the fluorescein injection. Depending on the angiographic phase, it is termed autofluorescence or early or late hyperfluorescence.

Autofluorescence is the emission of fluorescent light from ocular structures in the absence of sodium fluorescein. Conditions that cause autofluorescence are optic nerve head drusen and astrocytic hamartoma. Indocyanine green videoangiography is not helpful in conditions such as optic nerve head drusen and optic disc edema, the opposite of what may be observed with some intraocular tumors. Details of ICGV features of intraocular tumors are discussed in Chapter 8.

Optic Nerve Head Drusen

Drusen of the optic disc may be easily diagnosed when glowing yellow hyaline bodies are visible on ophthalmoscopy. However, diagnostic difficulties may be encountered when drusen are buried deep within the nerve tissue in the optic nerve head. In these circumstances, they can resemble true optic disc swelling based on the ophthalmoscopic appearance alone. According to Kurz-Levin and Landau,[42] the most useful and sensitive diagnostic technique for the diagnosis of optic disc drusen is ultrasonography. After comparing B-scan echography, orbital computed tomography (CT) scan, and preinjection control photography for detection of autofluorescence, almost half of their cases were detected only by B-scan echography and by no other diagnostic method. Although CT scan also images calcium deposits, evaluation by this method missed a substantial number of cases of drusen of the optic nerve head. This is because the slice viewed in the region of the optic nerve head and bone windows is routinely 1.5 mm thick, which might not be small enough for detecting smaller drusen. Computed tomography has the advantage over ultrasonography of providing simultaneous images of the brain. For this reason authors differ as to which imaging method is preferable.

Alternatively, photographs taken with the filters normally used for FA in place, but without the injection of fluorescein dye, show that superficial disc drusen often demonstrate the phenomenon of autofluorescence.[42] This method is suitable for confirming visible drusen of the optic disc but not reliable in detecting drusen that are buried deep in the disc tissue. Preinjection control photography detected superficial drusen of the optic disc in over 96% of the eyes diagnosed. In contrast, only 27% of the eyes diagnosed with buried drusen were detected with this method. The overlying tissue might cause attenuation of the underlying autofluorescence that is emitted by the deeply situated optic nerve head drusen. Such attenuated autofluorescence might be too weak to be detected by preinjection control photography.[42] After intravenous fluorescein injection, drusen exhibit a nodular hyperfluorescence that corresponds to the location of the visible drusen.[41] The late phases may be characterized by some minimal blurring of the drusen that may either fade or maintain fluorescence (Fig. 7.14).[43] Unlike papilledema, there is no visible leakage along the major vessels. Venous anomalies (venous stasis, venous convolutions, and retinociliary venous communications) and staining of the peripapillary vein walls occasionally are seen in

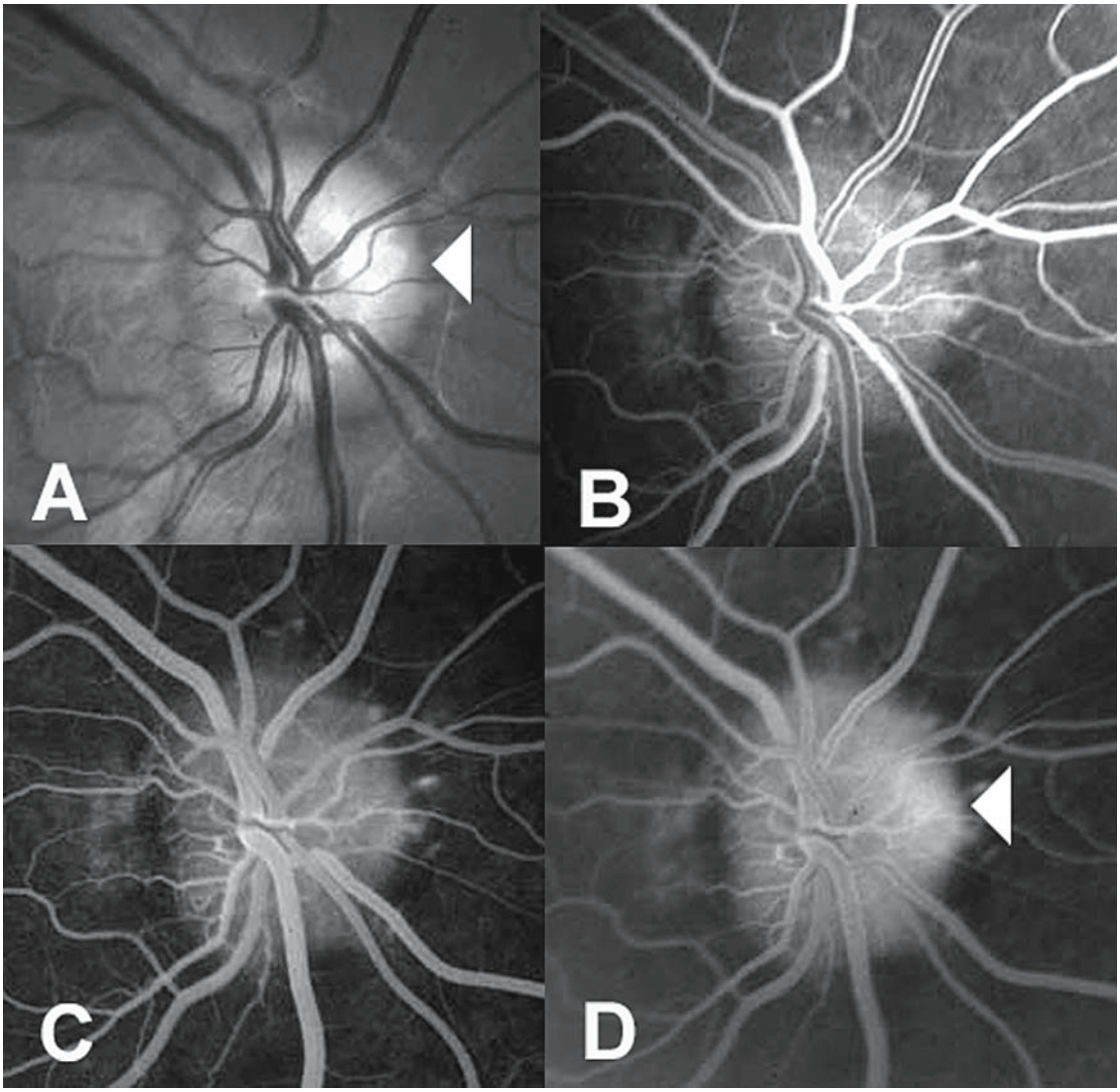

FIG. 7.14. (A) Red-free photography. Appearance of anomalously elevated optic disc is caused by buried (white arrowhead), nonvisible drusen. Note the anomalous branching pattern of some of the vessels. Early (B) and late (C) arteriovenous phase shows as a result of dye in the capillary net on the optic disc that drusen can no longer be differentiated from other tissue. (D) In late phases drusen retain some fluorescein dye and are brighter than in early prearterial phase (white arrowhead). Unlike papilledema, there is no visible leakage along the major vessels.

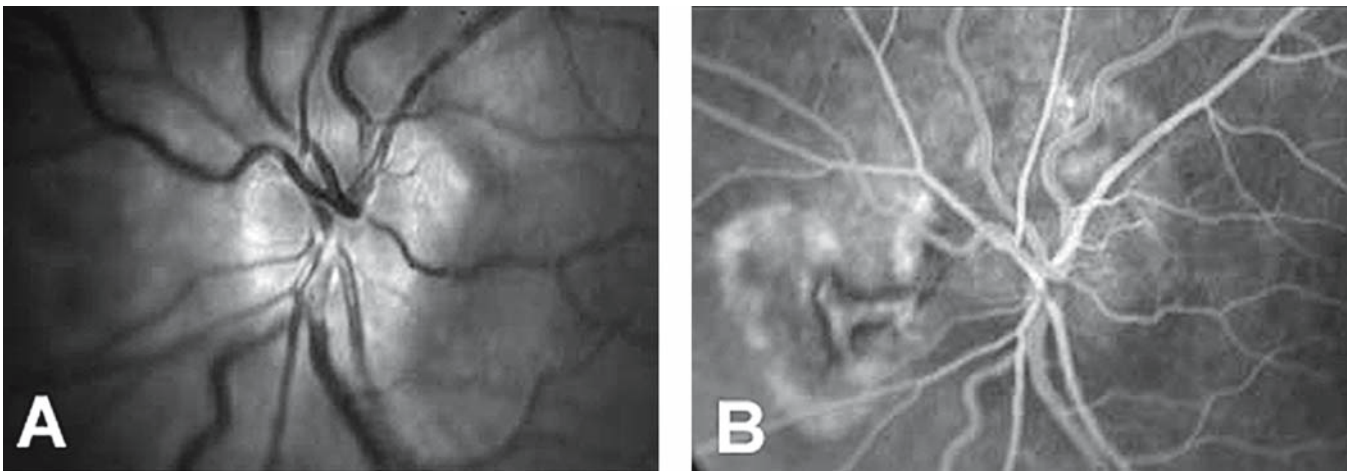

FIG. 7.15. (A) Red-free photography shows swollen left optic disc secondary to hyaline bodies in a 43-year-old patient. (B) Note the gray, type 2 subretinal neovascular membrane extending nasally from the left optic disc. Fluorescein angiography revealed evidence of perfusion and staining of the neovascular membrane.

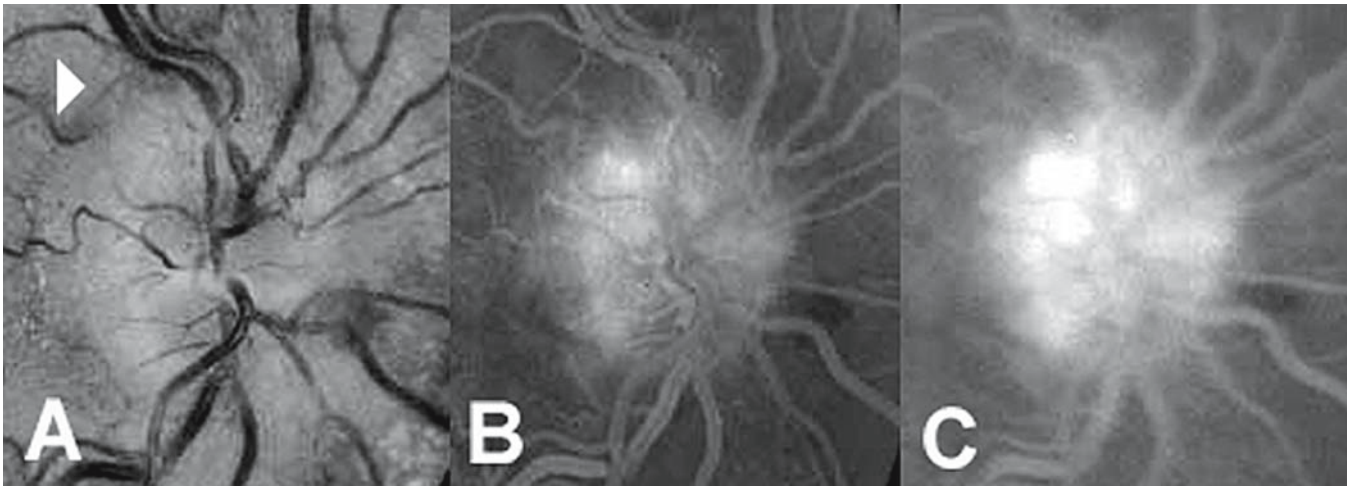

Fig. 7.16. (A) Red-free photography shows swollen optic disc with splinter hemorrhages, Paton lines (white arrowhead), tortuosity, and minimal dilatation of retinal veins secondary to papilledema. (B) Early fluorescein angiogram shows the dilated capillaries of the disc. (C) In late phase of the angiogram staining and fluorescein leakage are persistent.

eyes with optic disc drusen.[43] Finally, FA is helpful in identifying subretinal neovascularization associated with drusen (Fig. 7.15). We have not found this technique helpful in detecting drusen that were not visible biomicroscopically.

Papilledema and Optic Disc Edema

The difference between normal and abnormal leakage at the disc may be subtle. In both papilledema (Fig. 7.16) and optic disc edema (Fig. 7.17), the capillaries of the optic nerve are dilated and leak fluorescein. Because the fluorescein picture is not specific to these conditions, the diagnosis is made by the clinical history and ophthalmoscopic findings. The angiogram is similar in each case, demonstrating leakage associated with swelling of the optic nerve head. In the early phases of the angiogram, dilation of the capillaries on the optic nerve head may be seen. In the late phases of the angiogram, the dilated vessels leak, resulting in a fuzzy fluorescence of the disc margin.[44]

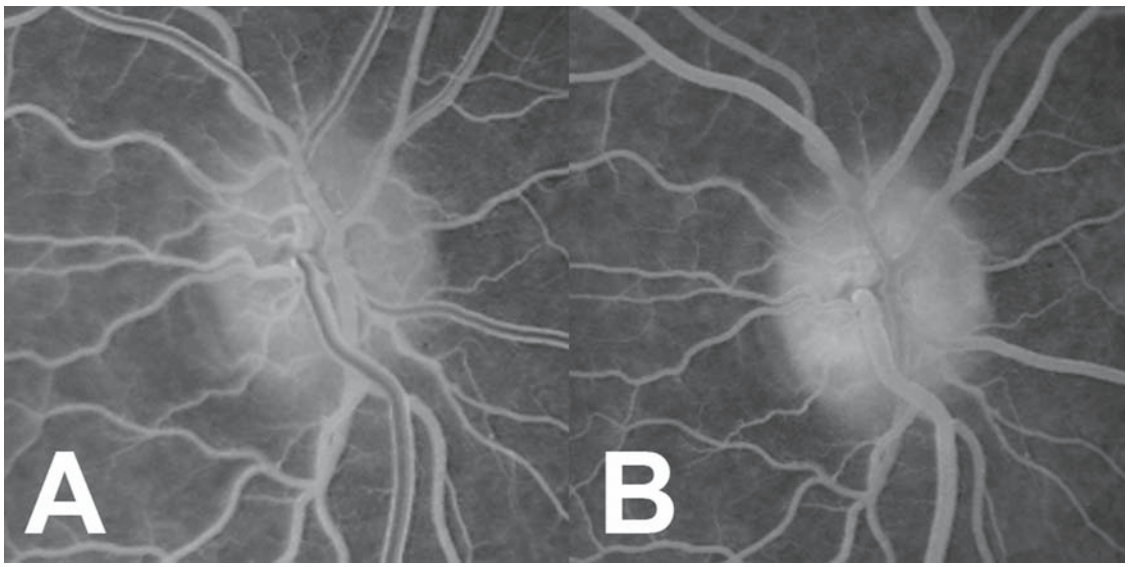

Fig. 7.17. (A) Early arteriovenous fluorescein angiography of papillitis in a 34-year-old woman with acute visual loss, pain, and central scotoma. (B) Late angiogram showing dilated vessels leaking, resulting in a fuzzy fluorescence of the disc margin. (Courtesy of Emely Karam, MD.)

Ocular Tumors

Melanocytoma of the Optic Nerve

Melanocytoma of the optic nerve commonly occurs in black patients. It is a variant of a melanocytic nevus (Fig. 7.18). The main clinical significance of a melanocytoma of the optic nerve lies in the differentiation from malignant melanoma. The melanocytoma may be confined to the disc itself or have contiguous involvement of the choroid or sensory retina. It may cause disc edema, vascular obstruction, and field loss. It should be recognized as a black lesion on the disc. In 75% of cases there is a fibrillated margin, reflecting involvement of the peripapillary nerve fiber layer of the retina.[45] Although melanocytomas tend to be circumscribed tumors, they can occasionally show small degrees of growth. Finally, malignant transformation of melanocytoma of the optic disc is very rare (Fig. 7.19).

Clinical features such as the deep black pigmentation, the fibrillated margin, the commonly occurrence in black patients, nonprogressive growth, and no visual loss can help in making the diagnosis of a melanocytoma. Fluorescein angiography can provide further information regarding the extent of the tumor. In most cases, FA of a melanocytoma of the optic nerve demonstrates hypofluorescence throughout the angiogram. This is presumably because of the deeply pigmented, densely packed cells, which have little vascularity. In the late phases the disc margin can stain (Fig. 7.18). In patients with associated optic disc edema, there is intense hyperfluorescence of the optic disc adjacent to the tumor.[45]

Peripapillary Choroidal Melanoma

In contrast to retinoblastoma, which has a marked tendency toward neural invasion, most uveal melanomas show little inclination to invade the optic nerve. They occur almost exclusively in whites. Even tumors that are adjacent to the optic disc tend to stop abruptly at the disc margin. Some peripapillary diffuse choroidal melanomas, however, show a marked tendency for optic nerve invasion.[46]

Peripapillary melanoma can occasionally simulate an optic neuritis on direct ophthalmoscopy. Shields et al.[47] reviewed the FA pattern of choroidal melanomas. Although fluorescein shows no pattern that is pathognomonic for choroidal melanoma, occasionally it can be helpful in differentiating a melanoma from certain pseudomelanomas (Figs. 7.20 and 7.21). A very small choroidal melanoma occasionally may show no appreciable abnormality with FA. This normal fluorescein pattern has been correlated with an intact RPE over a melanoma composed of rather tightly packed spindle cells.[48] A slightly larger melanoma that disrupts the RPE has rather typical angiographic features. In the arterial or early venous phase, there is mottled hyperfluorescence of the tumor. The areas of orange pigment are hypofluorescent at this time. In the venous phase, pinpoint foci of hyperfluorescence often become apparent on the surface of the tumor, particularly near its margins. There is progressive fluorescence of the lesion during the recirculation phase. In the late angiograms, the pinpoint foci of hyperfluorescence remain. The overlying orange pigment either remains hypofluorescent or shows slight hyperfluorescence.[48,49] There may be late staining of overlying or adjacent subretinal fluid.

A large dome-shaped melanoma demonstrates mottled hyperfluorescence in the early venous phase with late intense hyperfluorescence of the lesion. During the late arterial or early venous phase, a mushroom-shaped melanoma with prominent blood vessels in the dome of the tumor shows relative hyperfluorescence caused by the presence of fluorescein within their lumina. The simultaneous fluorescence of the retinal and choroidal vessels has been named the “double circulation” pattern, which is highly characteristic of many choroidal melanomas.[48,50] During the recirculation phase, the fluorescence of the large vessels begins to fade. Progressive mottled hyperfluorescence of the extravascular portions of the dome becomes apparent. In the

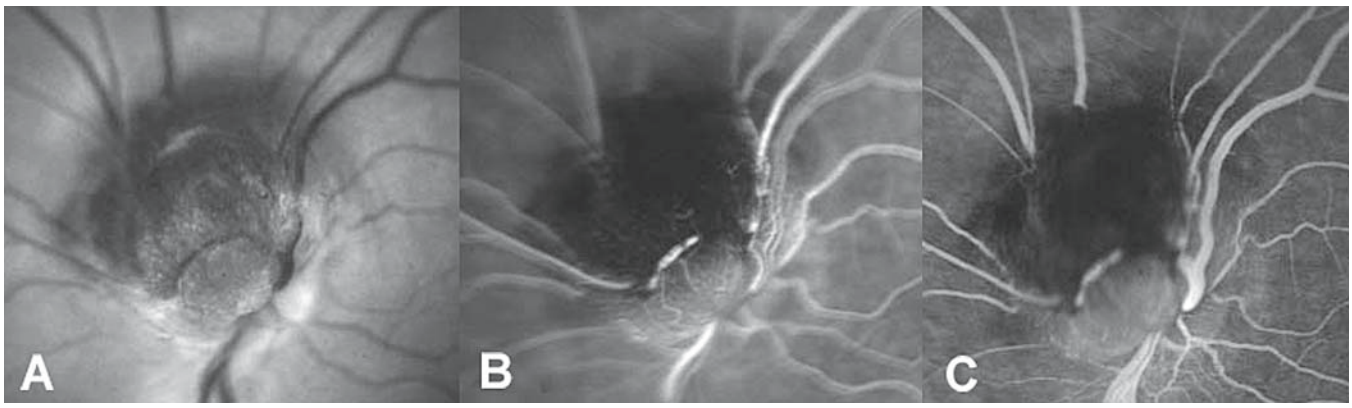

Fig. 7.18. (A) Large elevated melanocytoma covers most of the optic disc. (B) Fluorescein angiogram in the early venous phase shows marked hypofluorescence of lesion. (C) Late angiogram shows continued hypofluorescence.

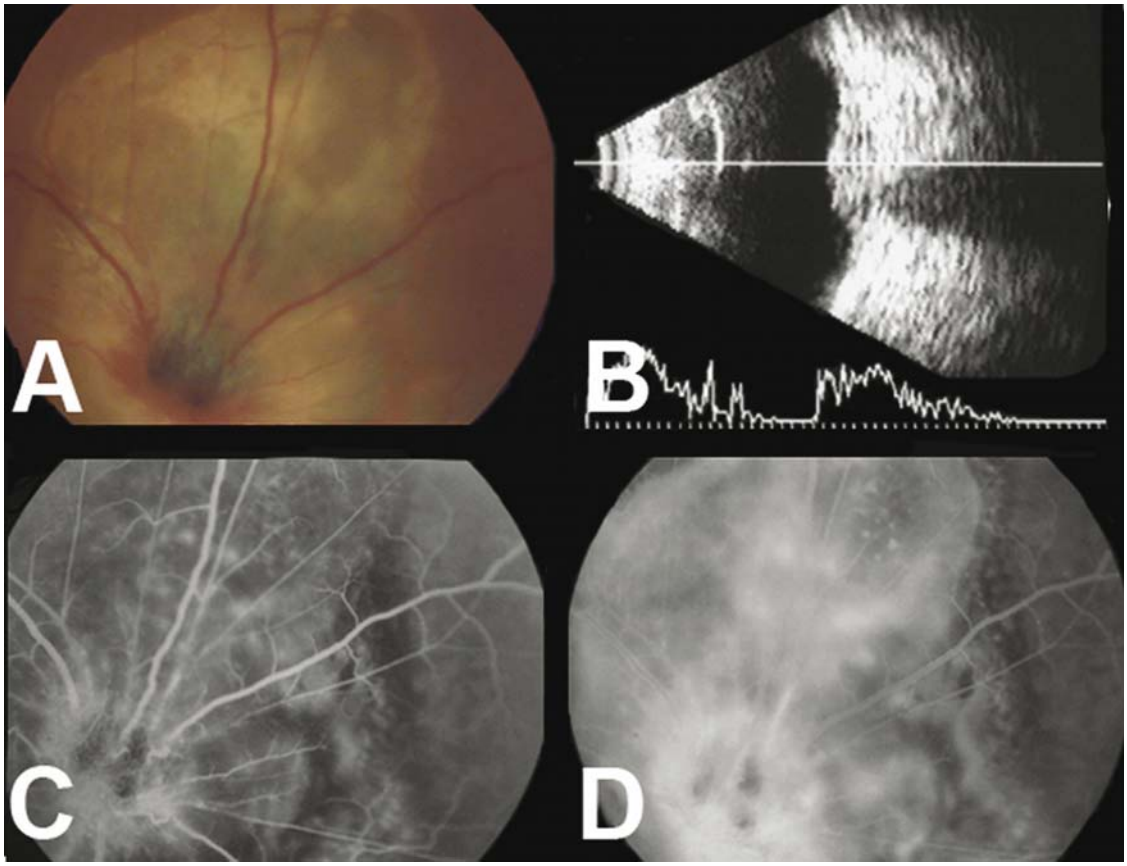

FIG. 7.19. Malignant transformation of melanocytoma. (A) Color fundus photograph shows darkly pigmented tumor overlying the optic disc with peritumor hemorrhage, peridisc and superior extension, and exudative subretinal fluid. (B) Axial B-scan echogram shows moderate elevated lesion overlying surface of optic nerve. Note A-scan shows regular internal structure and high reflectivity of lesion. (C) The arteriovenous phase shows hypofluorescence due to blockage of tumor pigment and pinpoint foci of hyperfluorescence apparent on the surface of the tumor superiorly. Note dilated capillaries over the disc. (D) In late frames of the angiogram, the pinpoint foci of hyperfluorescence remain, the overlying subretinal fluid shows slight hyperfluorescence, and prominent leakage can be seen into swollen disc around the tumor.

late stages, there is hypofluorescence of the large vessels and hyperfluorescence of the extravascular tissues, causing the large vessels to be silhouetted against the light background. Small areas of hyperfluorescence have been correlated with eventual sites of breaks through Bruch's membrane.[48,51]

Retinal Capillary Hemangioma

The peripheral retinal capillary hemangioma is usually so characteristic that the diagnosis can be suspected prior to performing ancillary studies. Fluorescein angiography is a very helpful ancillary study in confirming the diagnosis. In the arterial phase, the tumor fills rapidly by way of the feeding retinal artery and shows numerous fine capillaries within the tumor. In the venous phase, the lesion shows marked hyperfluorescence as the dye leaks from the capillaries. In the late phase, fluorescein leaks from the tumor into the overlying vitreous (see Chapter 8).[52]

Tumors on the optic disc may sometimes be more difficult to diagnose. Fluorescein angiography is useful in differentiating the lesion from papilledema and optic neuritis. The fine capillaries in the tumor fill rapidly in the arterial phase. The tumor becomes rapidly fluorescent in the venous phase and shows intense late hyperfluorescence with leakage into the overlying vitreous.[52]

Optic Nerve Sheath Meningioma and Optociliary Veins

The retinociliary veins may also be found with optic nerve tumors, particularly spheno-orbital meningiomas, optic nerve drusen, glaucoma, papilledema, after central retinal vein occlusion, and many others diseases. These optociliary vessels along with chronic visual loss and optic atrophy constitute the three elements of an optic nerve sheath meningioma

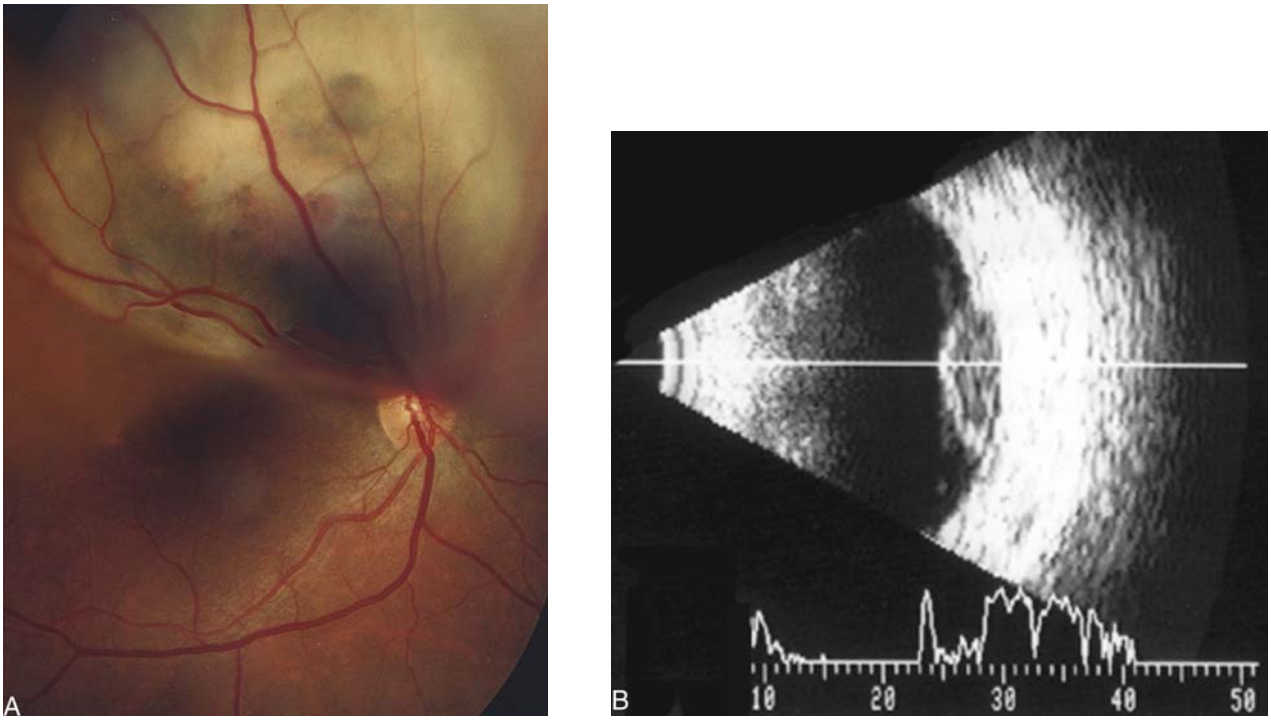

FIG. 7.20. (A) A 42-year-old woman with a nonpigmented choroidal melanoma superior to the optic disc erroneously interpreted as choroidal metastasis. Note the retinal pigment epithelial proliferation on the surface of the nonpigmented lesion. (B) B-scan ultrasonography of medium-sized choroidal melanoma in Figure 7.21 shows a dome-shaped tumor with regular internal structure. Note the A-scan high initial spike and the low to medium internal reflectivity in the tumor, which is characteristic of choroidal melanoma.

(ONSM), known as the Hoyt-Spencer triad. Optic nerve sheath meningioma is usually so characteristic that the diagnosis can be suspected prior to performing ancillary studies. If there is optic disc edema, the late venous FA shows a hyperfluorescent disc with superficial capillary dilation and collateral retinociliary veins at the margins of the optic disc (Fig. 7.22). In optic atrophy, failure of the capillaries of the optic nerve head to fill is seen. When present, FA allows visualization of retinociliary veins at the margins of the optic disc in the early venous phase of the angiogram in all cases. Muci-Mendoza et al.[53] studied eyes suffering from optociliary veins and ONSM with ICGV, which enabled a better delineation of the optociliary veins from the disc margin to the choroid. Interestingly, they found an inverse relationship between the degree of optic disc edema and the development and ease of visualization of the optociliary veins and their draining course through the choroidal circulation. They believe that sustained pressure around the optic nerve by the tumor progressively destroys axons, and as they grow scarcer the optic disc atrophies. At the same time, this compression obstructs the venous drainage through the central retinal vein, diverting blood toward the ciliary system, establishing an inverse relationship between the severity of the edema and the prominence of optociliary veins.[53]

Optic Disc Metastasis

Metastasis to the optic disc accounts for 5% of all intraocular metastases. It can occur as invasion from a juxtapapillary choroidal metastasis or as an isolated optic disc metastasis. Breast and lung cancers are the most common primary neoplasms that account for metastasis to the optic disc. The primary site is never determined in 20% of patients. The characteristic clinical features of optic disc metastasis should help differentiate it from other causes of swollen optic disc. In general, during the arterial phase the FA demonstrates relative hypofluorescence of the mass. A gradual hyperfluorescence begins in the late venous phase and turns into a moderate to intense fluorescence of the mass in the late angiogram with slight fluorescence of the overlying vitreous (Figs. 7.23 and 7.24).[54]

Optic Nerve Phacomas

Astrocytic hamartomas usually appear as sessile white lesions at the level of the retina or protruding above and overlying the optic disc (Fig. 7.25). They tend to occur as part of tuberous sclerosis or neurofibromatosis. They can develop yellow refractile calcifications that can be remembered as a fish-egg

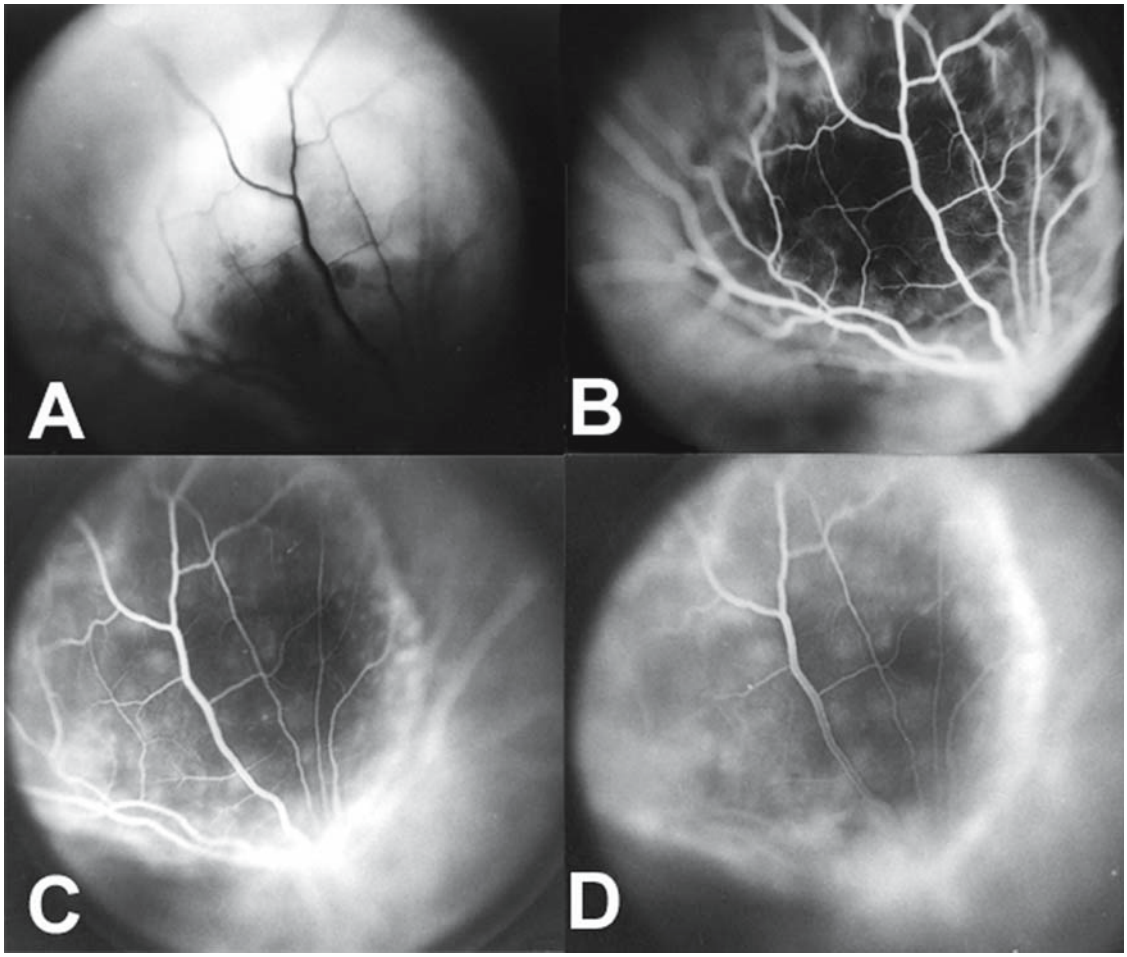

FIG. 7.21 (A) Red-free photography of a nonpigmented choroidal melanoma. (B) Early venous phase of fluorescein angiography (FA) shows hypofluorescence due to blockage of tumor pigment. (C) In the venous phase, pinpoint foci of hyperfluorescence often become apparent on the surface of the tumor, particularly near its margins. (D) In late-phase FA there is progressive fluorescence of the lesion, the pinpoint foci of hyperfluorescence remain, and the perilesional subretinal fluid shows slight hyperfluorescence.

appearance. During the arterial phase of the FA, little tortuous vessels can be seen on the relatively hypofluorescent tumor surface. In the venous phase, the blood vessels usually become more apparent over the tumor. These fine vessels tend to leak during the late venous phase and finally show diffuse homogeneous staining of the mass in the late frames.[55]

Conclusion

When it comes to diseases of the optic nerve, the clinician bases his correct diagnosis on the unique tools of clinical history and ophthalmoscopy. Fluorescein angiography and ICGV have been extremely valuable for expanding our knowledge of the anatomy and pathophysiology of some of these diseases.

Acknowledgments

The authors have no proprietary or financial interest in any products or techniques described in this article. This work is supported in part by the Arevalo-Coutinho Foundation for Research in Ophthalmology (FACO), Caracas, Venezuela.

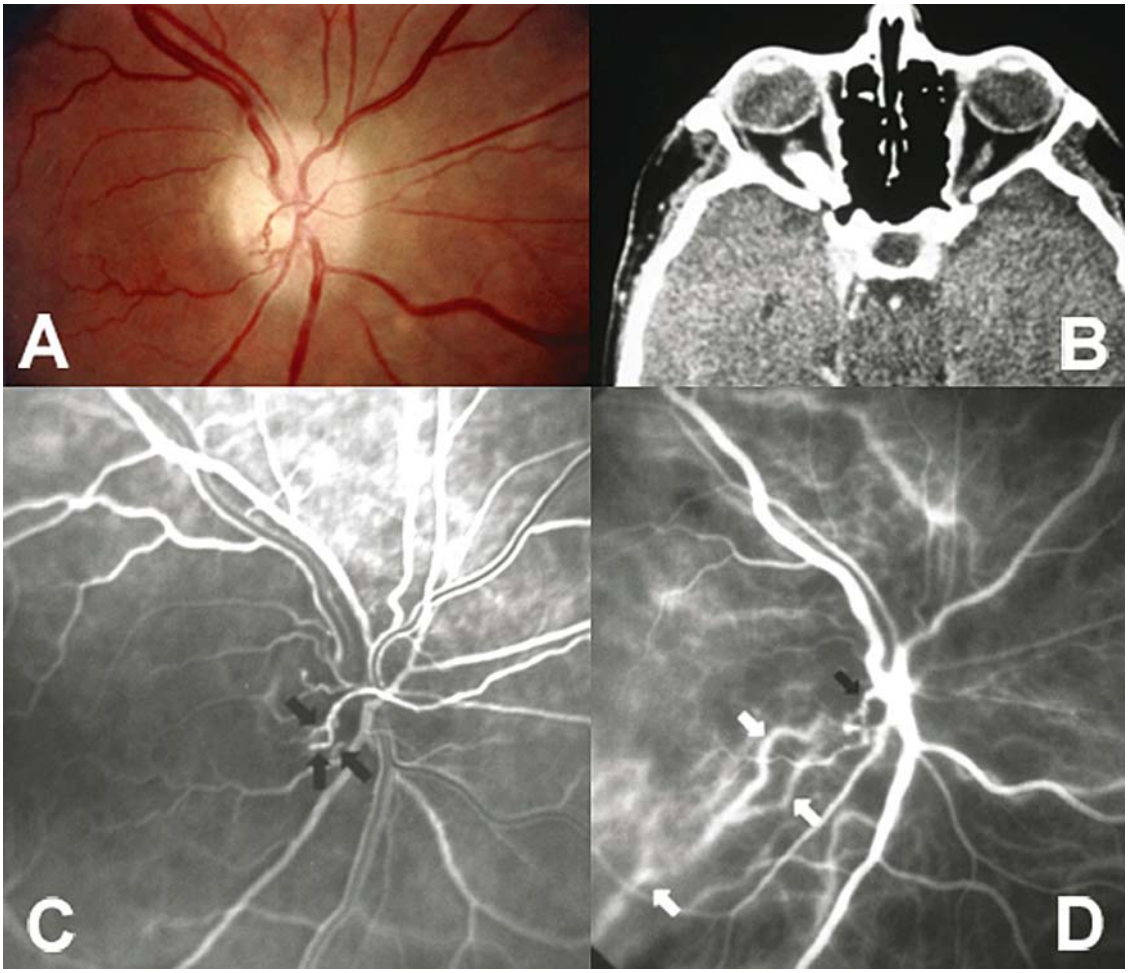

Fig. 7.22. (A) Color fundus photograph of right optic disc edema in atrophic phase shows arteriolar attenuation and moderate venous enlargement. Collateral optociliary veins are visible at the 6:30, 7, and 8 o'clock positions. (B) Axial computed tomographic scan shows enlarged, tortuous right optic nerve with discal calcification, normal caliber optic foramen, and pneumosinus dilatans of the ipsilateral posterior clinoid process. (C) Early venous phase fluorescein angiography of the same case shows filling of abnormal venous collaterals (arrows). (D) Indocyanine green videoangiography of the same case shows venous collaterals (black arrow) draining in the choroid (white arrows). (From Muci-Mendoza et al.,[53] with permission.)

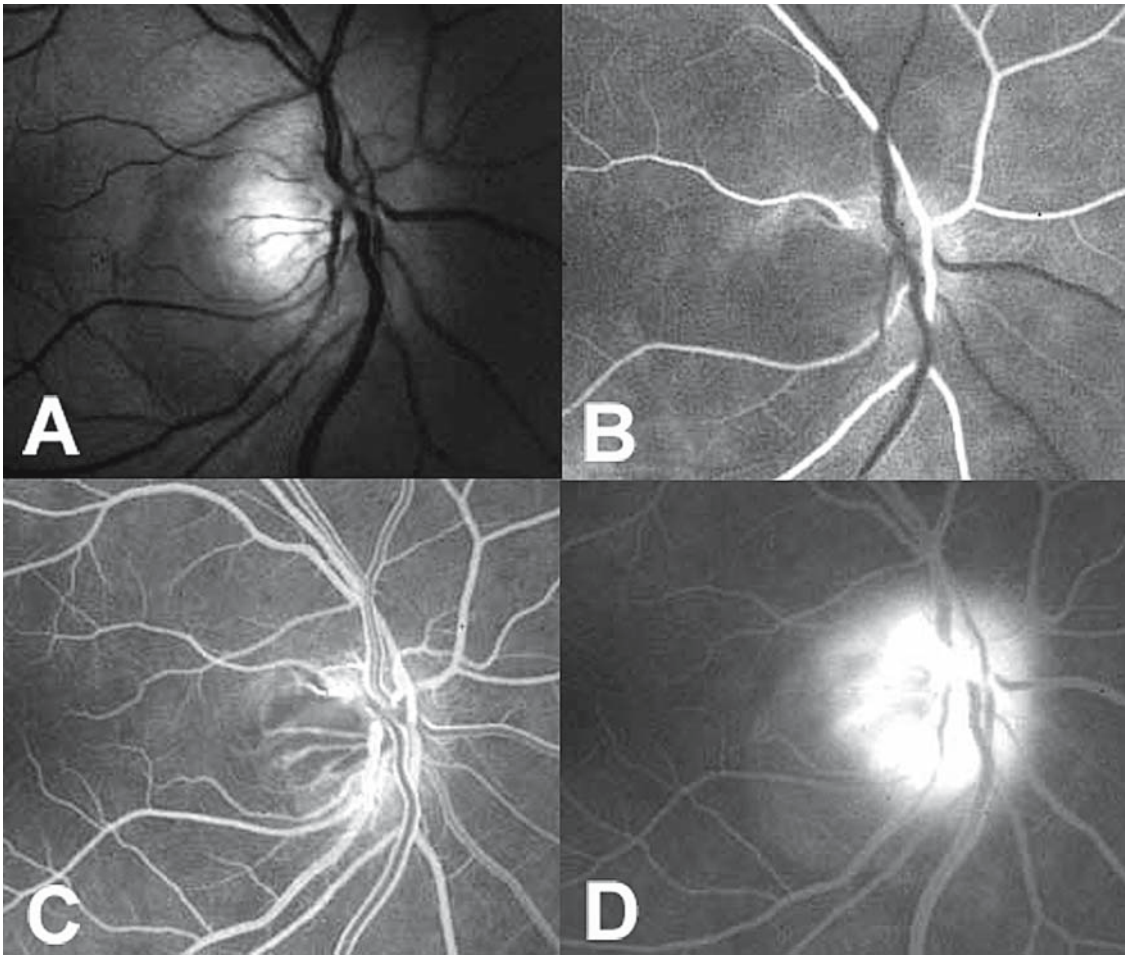

Fig. 7.23. (A) Red-free photography in a woman with breast cancer and optic disc metastasis. (B) Arterial phase fluorescein angiogram shows relative hypofluorescence of the mass. (C) Gradual hyperfluorescence beginning in the venous phase. (D) Moderate to intense fluorescence of the mass in late angiogram with slight fluorescence of the overlying vitreous.

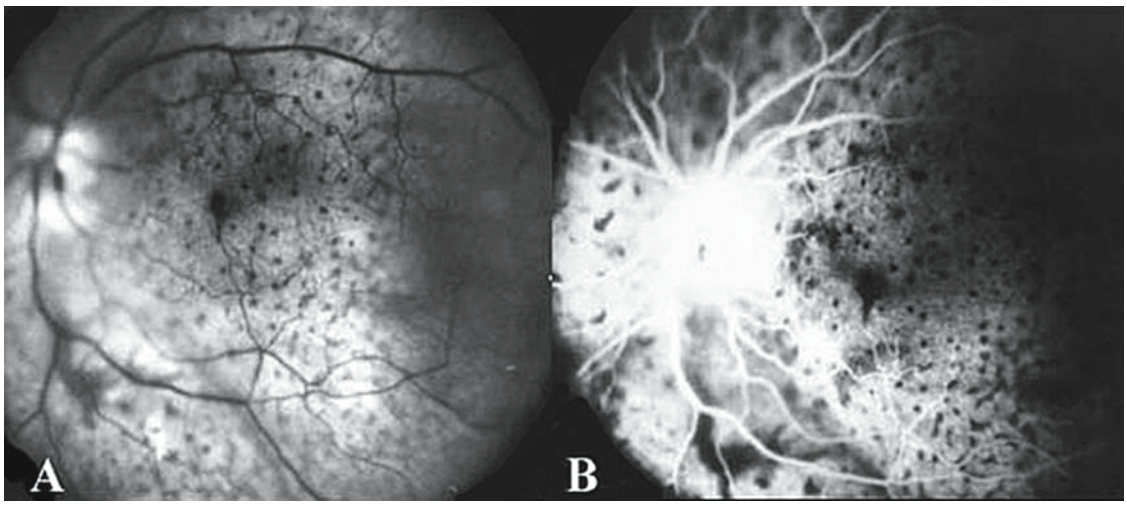

Fig. 7.24. A 63-year-old woman with a medical history significant for breast cancer 8 years earlier and evidence of liver metastasis 2 years ago received radiotherapy and six sessions of chemotherapy. The left ocular fundus showed a central dome-shaped creamy yellow choroidal tumor with clumps of brown pigment on the surface of the tumor, associated with a serous retinal detachment that involved the macula. (A) Red-free photograph. (B) Fluorescein angiography revealed early hyperfluorescence of the disc (hot disc) and hypofluorescence of the mass with the typical "leopard spots."

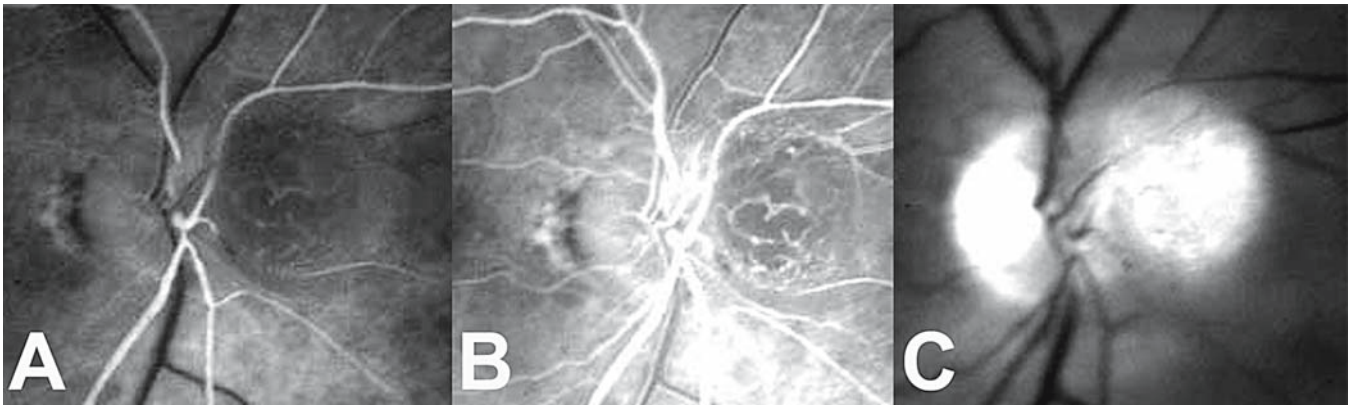

FIG. 7.25. (A) In the early arterial phase of fluorescein angiography, the tumor tends to be relatively hypofluorescent and usually little tortuous vessels can be seen on the tumor. (B) In the venous phase, the blood vessels usually become more apparent over the tumor. (C) These fine vessels tend to leak during the late venous phase, and finally show diffuse homogeneous staining of the mass in late frames.

References

1. Hayreh SS. Structure and blood supply of the optic nerve. In: Heilman K, Richardson T, eds. Glaucoma: Conceptions of a Disease. Philadelphia: WB Saunders, 1978:78–103.
2. Rao NA, Spencer WH. Optic nerve. In: Spencer WD, ed. Ophthalmic Pathology an Atlas and Textbook, vol 7, 1998 ed. Philadelphia: WB Saunders, 1996.
3. Cohen AI. Is there a potential defect in the blood-retinal barrier at the choroidal level of the optic nerve canal? Invest Ophthalmol 1973;12:513–519.
4. Kranenburg EW. Crater-like holes in the optic disc and central serous retinopathy. Arch Ophthalmol 1960;64:912–924.
5. Brodsky MC. Congenital optic disc anomalies. Surv Ophthalmol 1994;39:89–112; Erratum in Surv Ophthalmol 1995;40:172.
6. Gass JD. Serous detachment of the macula. Secondary to congenital pit of the optic nervehead. Am J Ophthalmol 1969;67:821–841.
7. Jack MK. Central serous retinopathy with optic pit treated with photocoagulation. Am J Ophthalmol 1969;67:519–521.
8. Johnson TM, Johnson MW. Pathogenic implications of subretinal gas migration through pits and atypical colobomas of the optic nerve. Arch Ophthalmol 2004;122:1793–1800.
9. Kalina RE, Conrad WC. Intrathecal fluorescein for serous macular detachment. Arch Ophthalmol 1976;94:1421.
10. Lincoff H, Lopez R, Kreissig I, Yannuzzi L, Cox M, Burton T. Retinoschisis associated with optic nerve pits. Arch Ophthalmol 1988;106:61–67.
11. Rutledge BK, Puliafito CA, Duker JS, Hee MR, Cox MS. Optical coherence tomography of macular lesions associated with optic nerve head pits. Ophthalmology 1996;103:1047–1053.
12. Irvine AR, Crawford JB, Sullivan JH. The pathogenesis of retinal detachment with morning glory disc and optic pit. Retina 1986;6:146–150.
13. Theodossiadis GP, Ladas ID, Panagiotidis DN, Kollia AC, Voudouri AN, Theodossiadis PG. Fluorescein and indocyanine green angiographic findings in congenital optic disc pit associated with macular detachment. Retina 1999;19:6–11.
14. Beyer WB, Quencer RM, Osher RH. Morning glory syndrome. A functional analysis including fluorescein angiography, ultrasonography, and computerized tomography. Ophthalmology 1982;89:1362–1367.
15. Slusher MM, Weaver RG Jr, Greven CM, Mundorf TK, Cashwell LF. The spectrum of cavitary optic disc anomalies in a family. Ophthalmology 1989;96:342–347.
16. Glaser JS. Topical diagnosis: prechiasmal visual pathways. In: Tasman W, ed; Jaeger EA, asst. ed. Duane's Ophthalmology. CD-ROM, vol 1. Philadelphia: Lippincott-Raven, 1998.
17. Apple DJ, Rabb MF, Walsh PM. Congenital anomalies of the optic disc. Surv Ophthalmol 1982;27:3–41.
18. Giuffre G. Chorioretinal degenerative changes in the tilted disc syndrome. Int Ophthalmol 1991;15:1–7; erratum in Int Ophthalmol 1991;145:285.
19. Khairallah M, Chatti T, Messaoud R, Ladjimi A, Chachia N. Peripapillary subretinal neovascularization associated with tilted disc syndrome. Retina 1996;16:449–451.
20. Cohen SY, Quentel G, Guiberteau B, Delahaye-Mazza C, Gaudric A. Macular serous retinal detachment caused by subretinal leakage in tilted disc syndrome. Ophthalmology 1998;105:1831–1834.
21. Tosti G. Serous macular detachment and tilted disc syndrome. Ophthalmology 1999;106:1453–1455.
22. Leys AM, Cohen SY. Subretinal leakage in myopic eyes with a posterior staphyloma or tilted disc syndrome. Retina 2002;22:659–665.
23. Giovannini A, Scassellati-Sforzolini B, D'Altobrando E, Mariotti C, Rutili T, Tittarelli R. Choroidal findings in the course of idiopathic serous pigment epithelium detachment detected by indocyanine green videoangiography. Retina 1997;17:286–293.
24. Stur M. Congenital tilted disc syndrome associated with parafoveal subretinal neovascularization. Am J Ophthalmol 1988;105:98–99.
25. Prost M, De Laey JJ. Choroidal neovascularization in tilted disc syndrome. Int Ophthalmol 1988;12:131–135.
26. Jonas JB, Naumann GO. Parapapillary chorioretinal atrophy in normal and glaucoma eyes. II. Correlations. Invest Ophthalmol Vis Sci 1989;30:919–926.
27. Jonas JB, Nguyen XN, Gusek GC, Naumann GO. Parapapillary chorioretinal atrophy in normal and glaucoma eyes. I. Morphometric data. Invest Ophthalmol Vis Sci 1989;30:908–918.
28. Hayreh SS. Microangioarchitecture of optic papilla. Jpn J Ophthalmol 1989;33:519–525.
29. Van Buskirk EM, Cioffi GA. Microvasculature of the optic disc and glaucoma. In: Bucci MG, ed. Glaucoma: Decision Making in Therapy, 1st ed. Milano: Springer-Verlag Italia, 1996:25–30.

30. Tezel G, Kolker AE, Wax MB, Kass MA, Gordon M, Siegmund KD. Parapapillary chorioretinal atrophy in patients with ocular hypertension. II. An evaluation of progressive changes. Arch Ophthalmol 1997;115:1509–1514.
31. Funaki S, Shirakashi M, Abe H. [Parapapillary chorioretinal atrophy and parapapillary avascular area in glaucoma.] Nippon Ganka Gakkai Zasshi 1997;101:598–604.
32. Yasuzumi K, Ohno-Matsui K, Yoshida T, et al. Peripapillary crescent enlargement in highly myopic eyes evaluated by fluorescein and indocyanine green angiography. Br J Ophthalmol 2003;87:1088–1090.
33. Olver JM, Spalton DJ, McCartney AC. Microvascular study of the retrolaminar optic nerve in man: the possible significance in anterior ischaemic optic neuropathy. Eye 1990;4:7–24.
34. Hayreh SS. Inter-individual variation in blood supply of the optic nerve head. Its importance in various ischemic disorders of the optic nerve head, and glaucoma, low-tension glaucoma and allied disorders. Doc Ophthalmol 1985;59:217–246.
35. Siatkowski RM, Gass JD, Glaser JS, Smith JL, Schatz NJ, Schiffman J. Fluorescein angiography in the diagnosis of giant cell arteritis. Am J Ophthalmol 1993;115:57–63.
36. Hayreh SS. Anterior ischaemic optic neuropathy. Differentiation of arteritic from non-arteritic type and its management. Eye 1990;4:25–41.
37. Oto S, Yilmaz G, Cakmakci S, Aydin P. Indocyanine green and fluorescein angiography in non-arteritic anterior ischemic optic neuropathy. Retina 2002;22:187–191.
38. Hayreh SS, Chopdar A. Occlusion of the posterior ciliary artery. V. Protective influence of simultaneous vortex vein occlusion. Arch Ophthalmol 1982;100:1481–1491.
39. Hayreh SS, Podhajsky P, Zimmerman MB. Role of nocturnal arterial hypotension in optic nerve head ischemic disorders. Ophthalmologica 1999;213:76–96.
40. Hayreh SS, Jonas JB. Optic disc morphology after arteritic anterior ischemic optic neuropathy. Ophthalmology 2001;108:1586–1594.
41. Valmaggia C, Speiser P, Bischoff P, Niederberger H. Indocyanine green versus fluorescein angiography in the differential diagnosis of arteritic and non-arteritic anterior ischemic optic neuropathy. Retina 1999;19:131–134.
42. Kurz-Levin MM, Landau K. A comparison of imaging techniques for diagnosing drusen of the optic nerve head. Arch Ophthalmol 1999;117:1045–1049.
43. Mustonen E, Nieminen H. Optic disc drusen a photographic study. I. Autofluorescence pictures and fluorescein angiography. Acta Ophthalmol 1982;60:849–858.
44. Johnson RN, Schatz H, McDonald R, Ai E. Fluorescein angiography: basic principles and interpretation. In: Ryan SJ, Schachat AP, eds. Retina (Medical Retina, Vol 2), 3rd ed. St. Louis: Mosby, 2001:875–942.
45. Shields J. Shields C. Melanocytoma. In: Intraocular Tumors: A Text and Atlas. Philadelphia: 1992:101–115 .
46. Shields J. Shields C. Posterior uveal melanoma: clinical and pathologic features. In: Intraocular Tumors: A Text and Atlas. Philadelphia: 1992:117–136.
47. Meyer D, Ge J, Blinder KJ, Sinard J, Xu S. Malignant transformation of an optic disc melanocytoma. Am J Ophthalmol 1999;127:710–714.
48. Shields J. Shields C. Diagnostic approaches to posterior uveal melanoma. In: Intraocular Tumors: A Text and Atlas. Philadelphia: 1992:117–136.
49. Shields JA, Rodrigues MM, Sarin LK, Tasman WS, Annesley WH Jr. Lipofuscin pigment over benign and malignant choroidal tumors. Trans Am Acad Ophthalmol Otolaryngol 1976;81:871–881.
50. Edwards WC, Layden WE, Macdonald R Jr. Fluorescein angiography of malignant melanoma of the choroid. Am J Ophthalmol 1969;68:797–808.
51. Leff SR, Augsburger JJ, Shields JA. Focal fluorescence of choroidal melanoma. Br J Ophthalmol 1986;70:104–106.
52. Shields J. Shields C. Diagnostic approaches to posterior uveal melanoma. In: Intraocular Tumors: A Text and Atlas. Philadelphia: 1992:393–420.
53. Muci-Mendoza R, Arevalo JF, Ramella M, et al. Optociliary veins in optic nerve sheath meningioma. Indocyanine green videoangiography findings. Ophthalmology 1999;106:311–318.
54. Shields JA, Shields CL, Singh AD. Metastatic neoplasms in the optic disc: the 1999 Bjerrum Lecture: part 2. Arch Ophthalmol 2000;118:217–224.
55. Shields J, Shields C. Glial tumors of the retina and the optic disc. In: Intraocular Tumors: A Text and Atlas. Philadelphia: 1992:421–435.

8
Angiography of Retinal and Choroidal Tumors

J. Fernando Arevalo, Carol L. Shields, Jerry A. Shields,
Miguel A. Materin, and Aristides J. Mendoza

The evaluation of intraocular tumors differs from almost all other oncologic evaluations because there is little reliance on tissue diagnosis. Definitive therapies such as enucleation and radiation are usually based on the results of ophthalmoscopy, and a limited number of ancillary studies without the aid of biopsy. Although biopsies can be performed on most intraocular tumors, the ocular morbidity associated with these procedures is usually not worth the added benefit of a tissue diagnosis.

Fluorescein angiography (FA) is a diagnostic procedure commonly employed in the evaluation of chorioretinal vascular abnormalities, especially relating to retinal neovascularization, choroidal neovascularization (CNV), noninfective vasculitis, age-related macular degeneration, and diabetic retinopathy. Fluorescein studies can provide the clinician with helpful information in the evaluation of a suspected intraocular tumor.[1–3] Fluorescein angiography has been used extensively in the evaluation of tumors of the choroid and retina during the past quarter of a century. Several excellent reviews on the subject of fluorescein angiography of intraocular tumors have been published,[4–7] and interested readers are referred to those sources for additional information on this subject. The role of FA in patients with an intraocular tumor is largely documentary in nature, but in certain cases it can be of differential diagnostic value. The essential clinical importance of FA in the evaluation of choroidal and retinal tumors appears to be its ability to reveal patterns inconsistent with the presumptive diagnosis rather than to elucidate pathognomonic features.[8]

The special properties of indocyanine green (ICG) dye and the advent of digital imaging techniques offer the promise of enhanced imaging of the choroid for more accurate and specific diagnoses and possibly for new insight into therapeutic strategies. In many conditions affecting the choroid, the expectations and hopes of investigators who use ICG angiography have yet to be proved on a scientific basis.[9,10] Indocyanine green-videoangiography (ICG-V) has been used to visualize several types of tumors, as discussed later. However, there is no correlation of the use of ICG-V with treatment decisions and clinical outcomes at this time.[11]

This chapter summarizes the role and importance of angiography in various tumors of the choroid and retina

Melanocytic Tumors of the Choroid

Choroidal Nevus

Choroidal nevus is a flat to slightly elevated, pigmented or amelanotic choroidal tumor with distinct or ill-defined borders. It is usually between 1.5 and 5 mm at the base and less than 2 mm in thickness. Visual field defects, overlying drusen, orange pigment, and subretinal fluid can occur. Choroidal neovascularization and retinal pigment epithelium (RPE) detachment are found less commonly. Pathologically a choroidal nevus is composed of low-grade spindle cells with variable amounts of pigmentation. One should take baseline fundus photographs and ultrasonogram for periodic observation, and to treat as an early melanoma if it grows.

Fluorescein angiography of nevi can demonstrate hypofluorescence induced either by the pigmentation of the nevus or by a local circulatory disturbance in the choroid. Hyperfluorescence can be related to prominent intrinsic vascularity, overlying retinal pigment epithelial defects and focal leaks, and late staining from overlying drusen.[12,13] Angiographic features vary depending on the degree of pigmentation. Deeply pigmented nevi are relatively hypofluorescent, while less pigmented ones tend to be hyperfluorescent. When the nevi encroaches on or replaces part of the choriocapillaris, the lesions may appear hypofluorescent. Thicker nevi with overlying drusen can show hyperfluorescence. Deep-setting nevi that spare choriocapillaris give relatively normal fluorescence. Fluorescein angiography appears to be of little diagnostic value in the evaluation of suspected choroidal nevi. Ophthalmoscopy is usually sufficient to allow one to decide with reasonable certainty whether a melanotic choroidal lesion is a choroidal nevus or an equivocal lesion that may be either a large nevus or a small choroidal melanoma.[14] Fluorescein

angiography rarely if ever helps significantly in clarifying this differential diagnosis.

In some choroidal nevi, RPE hyperfluorescent leak sites show up during the early frames of the study, and gradually increase in prominence and smudginess as the study continues.[15] In some cases, fluorescein will leak into an ophthalmoscopically evident localized blister of subretinal fluid.[15] Unfortunately, demonstration of such leak sites of subretinal fluid does not clarify whether a lesion is a choroidal melanoma or a benign nevus. Small melanotic choroidal lesions that have associated prominent clumps of orange pigment are generally regarded as more likely to be malignant melanomas than benign nevi.[16] However, observation of such orange pigment clumps does not reliably clarify the diagnosis. If one performs fluorescein angiography on a lesion with prominent orange pigment clumps,[5–7,16] the clumps appear intensely hypofluorescent (more so than the background choroidal lesion) throughout the study. This intense hypofluorescence of the orange pigment clumps appears to be due to blocking of choroidal fluorescence transmitted through the melanocytic choroidal lesion.

Occasional choroidal nevi and small melanomas have an associated overlying choroidal neovascular membrane.[17] Such lesions can usually be anticipated on the basis of ophthalmoscopically detectable hemorrhagic or exudative subretinal fluid. Fluorescein angiography[5,6,17] reveals a typical subretinal neovascular network that appears brightly in the early frames of the study and leaks progressively by the late frames. The principal role of fluorescein angiography in melanocytic choroidal lesions suspected of being prominent nevi versus small melanomas is usually documentary in nature.

Choroidal nevi may demonstrate various patterns with ICG-V. The pigmented nevus remains relatively diffusely hypofluorescent compared to the surrounding choroid on early, middle, and late angiograms. Minimal late staining may occur despite the lack of early fluorescence, but the staining is usually much less intense than normal surrounding choroid. A nonpigmented choroidal nevus is generally more hyperintense as intrinsic tumor vasculature becomes evident. Most amelanotic nevi are hyperfluorescent or isofluorescent in the early and middle frames. In the late frames there is often a soft, diffuse fluorescence of the nevus that may be hyperfluorescent, isofluorescent, or hypofluorescent when compared to the surrounding choroid. Despite the relative lack of pigment in an amelanotic choroidal nevus, it may appear hypofluorescent on ICG-V, perhaps because of compression of the choroidal vessels from the choroidal mass.[10]

Choroidal Malignant Melanoma

Choroidal malignant melanoma is the most common primary intraocular malignancy of adults. It has substantial local growth potential in addition to its well-known propensity to metastasize and thereby prove fatal to the host. Choroidal melanoma is clinically very variable, and can present as a nodular, mushroom-shaped, or diffuse mass with RPE alterations, and secondary non-rhegmatogenous retinal detachment.

The diagnosis is based largely on the clinical experience of the examiner, and modern diagnostic tests. Important elements of the examination consist of indirect ophthalmoscopy, fluorescein angiography, scleral transillumination, B-scan ultrasonography, and sequential diagnostic examinations. Using all these methods, the Collaborative Ocular Melanoma Study (COMS) reported a diagnostic accuracy rate of 99.7%.[18] The differential diagnosis includes choroidal nevus, extramacular disciform scar, RPE hypertrophy or hyperplasia, choroidal hemangioma, metastatic carcinoma, and lymphoma.[19]

Fluorescein angiography can provide evidence in support of the diagnosis of choroidal melanoma but rarely if ever is sufficient by itself to establish the diagnosis. Consequently, fluorescein angiography is of more importance in documentation than in diagnosis. In most cases fluorescein angiography findings can be described only as compatible or incompatible, but not diagnostic, for a choroidal melanoma.

Fluorescein angiography is only moderately helpful, with a 50% diagnostic accuracy rate. Some larger melanomas have an intrinsic tumor circulation, the fluorescein pattern is called double circulation because tumoral and retinal blood vessels fluoresce, demonstrating late staining of the lesion and multiple pinpoint leaks at the level of the RPE (Fig. 8.1). Several distinct fluorescein angiographic patterns can be associated with choroidal melanomas.[4–7] These distinct patterns depend on the cross-sectional growth pattern of the tumor, its pigmentation, and the presence or absence of retinal invasion.

Fluorescein angiography characteristically shows the tumor to be generally hypofluorescent throughout most of the study. If prominent clumps of orange lipofuscin pigment are present on the surface of the tumor, they appear intensely hypofluorescent throughout the entire study by virtue of blockage of the underlying choroidal and tumor vascular fluorescence. During the arterial phase frames of the study, several ill-defined large caliber deep intralesional blood vessels usually become identifiable against the hypofluorescent background. As the study continues, the large intralesional blood vessels leak progressively, so that the surface of the lesion commonly appears hyperfluorescent in the late frames (Fig. 8.1). Fluorescein can also appear in the overlying retina and RPE as tiny discrete pinpoint loci of intense hyperfluorescence. If there is associated serous retinal detachment, the fluorescein can also accumulate in the surrounding and overlying subretinal fluid by the late frames. The vascular pattern of the overlying retina commonly appears unremarkable in such cases.

In choroidal melanomas that are clinically relatively amelanotic in color, the early frames of the angiogram show less lesional hypofluorescence and more prominent intralesional blood vessels (Fig. 8.2). The remainder of the angiogram is similar to that seen in more typically pigmented melanomas. A substantial proportion of the melanomas erupt through the overlying Bruch's membrane to form an apical cap, giving the lesion a mushroom shape in cross section. In most cases, the apical cap tends to appear substantially less darkly pigmented than does the base of the tumor (although exceptions

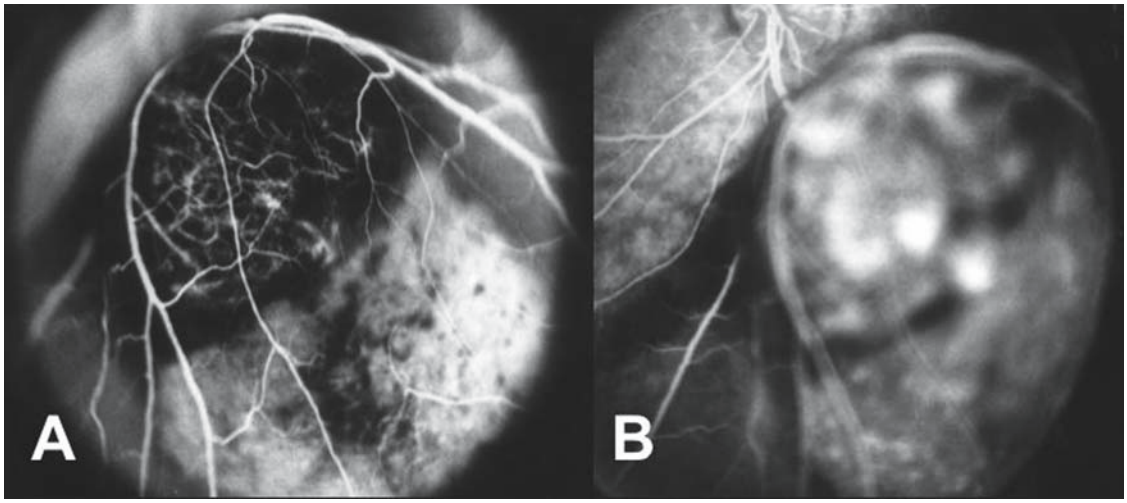

FIG. 8.1. Some larger melanomas have an intrinsic tumor circulation. The fluorescein pattern is called double circulation because tumoral and retinal blood vessels fluoresce, demonstrating late staining of the lesion and multiple pinpoint leaks at the level of the retinal pigment epithelium. (A) Early phase. (B) Late phase.

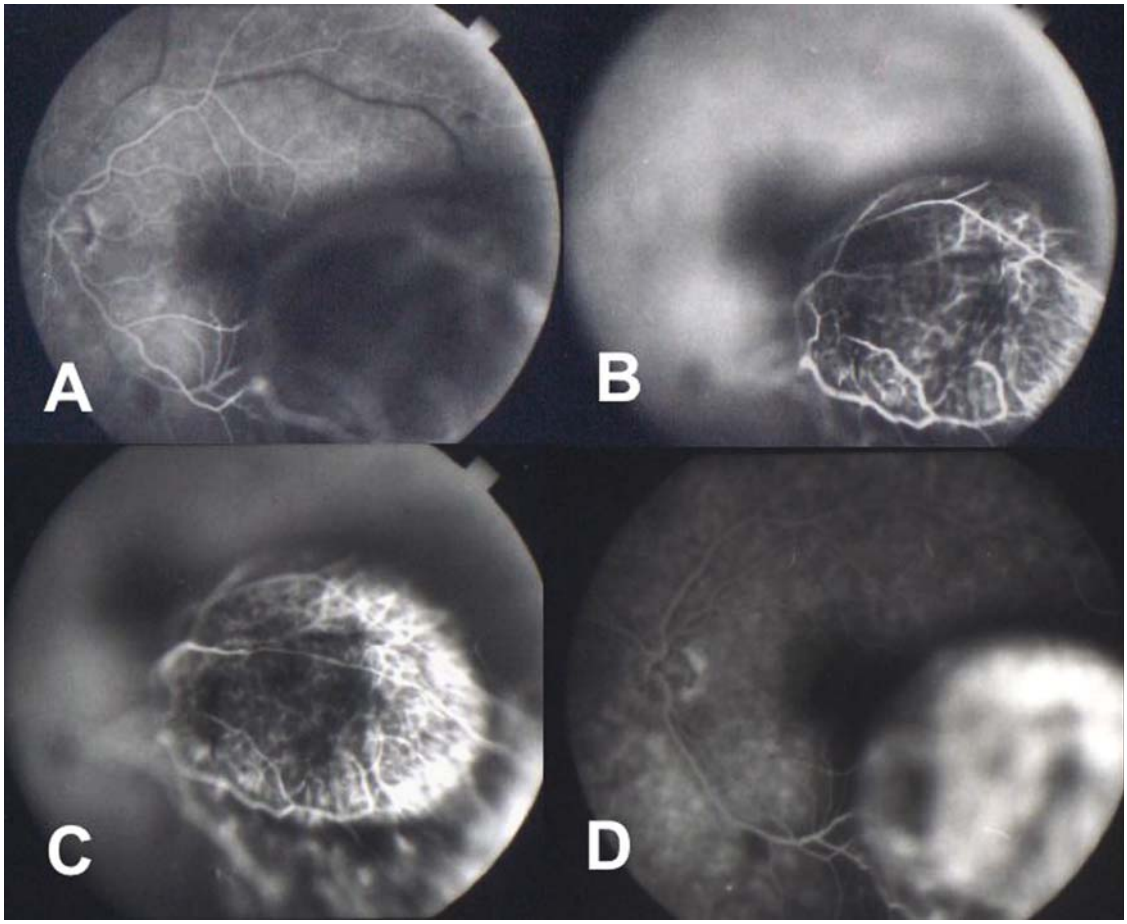

FIG. 8.2. In choroidal melanomas that are clinically relatively amelanotic in color, the early frames of the angiogram show less lesional hypofluorescence and more prominent intralesional blood vessels. In addition, a malignant choroidal melanoma that breaks through Bruch's membrane typically shows hypofluorescence of the entire lesion during the early frames (A,B), slow filling of the visible apical blood vessels of the lesion in the venous (C) and recirculation frames, and intense late staining in the late phase frames (D).

do occur). Many large-caliber intralesional blood vessels can often be observed ophthalmoscopically within the apical portion of the mass. These correspond with the tumor veins that are congested in response to the constricting effect of the intact portion of Bruch's membrane.[20] Fluorescein angiography in such cases[4–6,20–22] typically shows hypofluorescence of the entire lesion during the early frames, slow filling of the visible apical blood vessels of the lesion in the venous and recirculation frames, and intense late staining in the late-phase frames (Fig. 8.2). In addition, the overlying retina is often markedly thinned, and the retinal vasculature commonly shows broadening of the intercapillary spaces and even vascular obliteration in some cases.[21,22] Some choroidal melanomas develop darkly pigmented mats of retinal invasion on their surface. [4,5,22] These mats appear clinically as homogeneous dark brown velvety lesions obscuring the examiner's view of the large retinal vessels. Fluorescein angiography of such lesions shows the darkly pigmented mass to be completely nonfluorescent throughout the entire study. The retinal blood vessels at the margins of the lesion are often abnormal and leaky, as might be expected on the basis of the associated retinal invasion.

A number of choroidal tumors have been studied with ICG-V.[9,10] Pigmented choroidal melanomas block ICG fluorescence because of the absorption of the near-infrared light by the melanin-containing lesion. As a result, the choroidal and tumor vasculature cannot be visualized through the dense pigmentation (Fig. 8.3). In addition, ICG-V has failed to provide distinguishing features that might help to differentiate a melanoma from other pigmented lesions, such as nevi or pigmented metastatic lesions. Indocyanine green videoangiography in amelanotic melanomas reveals variable blockage, depending on the amount of pigmentation present in the lesion. Corkscrew vessels have been seen with ICG angiography (ICG-V), but not with FA, in some patients with amelanotic melanoma (Fig. 8.4).[9,10] The meaning of this vascular pattern currently is unclear, but it may eventually assist in the differentiation of these primary ocular tumors from metastatic lesions.

Recently, a large retrospective histopathologic study identified nine different microvascularization patterns (silent, normal, straight, parallel with and without cross-linking, arcs with and without branches, loops, and networks) in uveal melanoma and correlated the presence of these microvascularization patterns in histologic sections with data on death from metastatic disease after enucleation.[23,24] Two of these microvascularization patterns (networks, and parallel with cross-linking) showed a very strong correlation with metastatic disease. Two other microvascularization patterns (silent, and parallel without cross-linking) were correlated with a more favorable outcome for the patient.[24] The histologic assessment of microvascular patterns seems to have a strong prognostic value when performed with the proper technique, and inclusion of this feature in routine histologic examinations of uveal melanomas is therefore recommended.[25]

Microvascularization patterns can be imaged by ICG-V using a confocal scanning laser ophthalmoscope.[26] The identification of microvascularization patterns using confocal ICG-V is superior to FA using a conventional acquisition technique with a fundus camera.[26] It is well known that conventional FA using a fundus camera does not show a pathognomonic fluorescence pattern in choroidal melanomas[27,28] nor are microvascularization patterns consistently seen. Size and pigmentation of the tumor has considerable influence on the appearance of

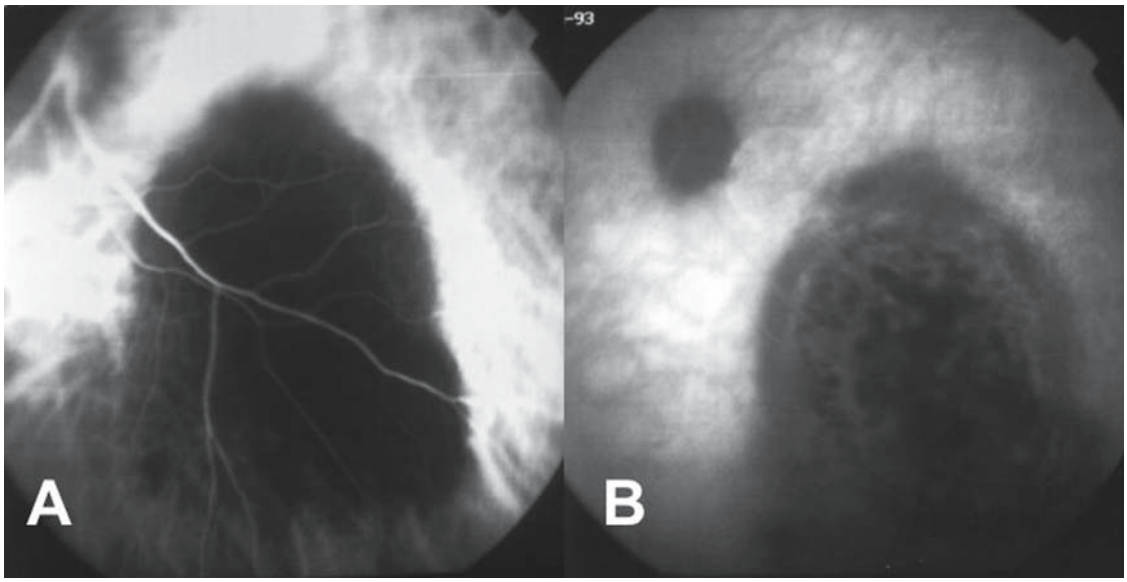

FIG. 8.3. Pigmented choroidal melanomas block indocyanine green (ICG) fluorescence because of the absorption of the near-infrared light by the melanin-containing lesion. As a result, the choroidal and tumor vasculature cannot be visualized through the dense pigmentation. (A) Early phase. (B) Late phase.

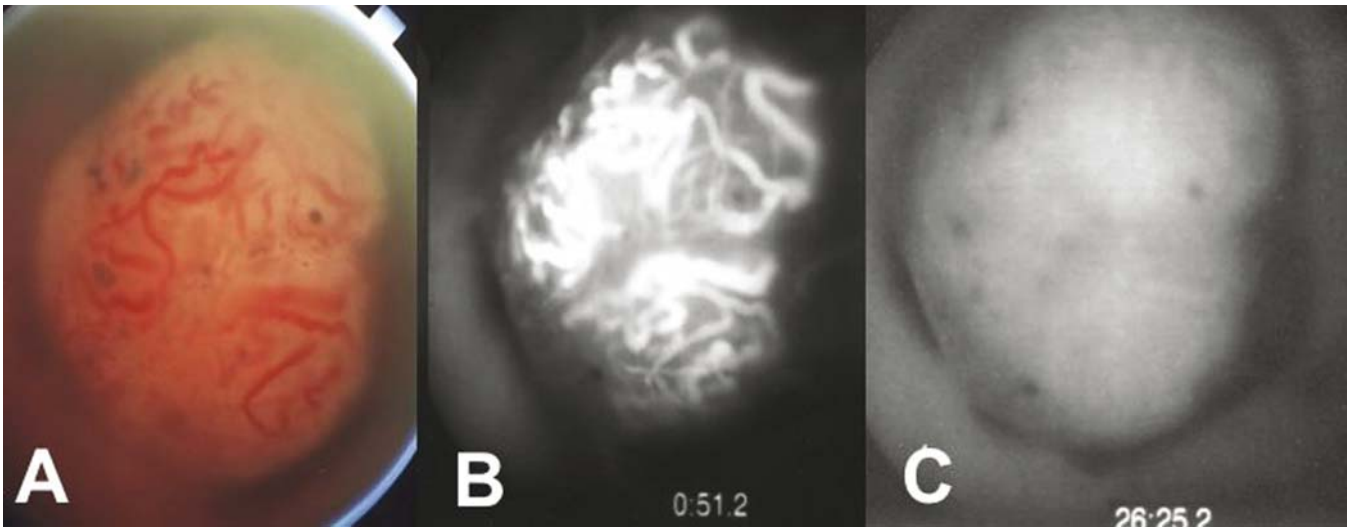

FIG. 8.4. Corkscrew vessels have been seen with ICG angiography, but not with fluorescein angiography, in some patients with amelanotic melanoma. (A) Color photograph. (B) Midphase indocyanine green videoangiography (ICG-V). (C) Late-phase ICG-V.

the fluorescein angiogram. The effect of the tumor on adjacent ocular structures, particularly the RPE, also contributes significantly to its FA appearance. If the overlying retinal pigment epithelium is completely intact, a fairly normal fluorescein angiogram may result. Overlying retinal vessels are usually clearly visible during all phases. However, the so-called double or tumor circulation (simultaneous visualization of retinal and choroidal circulation) is often difficult to recognize, and the absence of this finding does not indicate lack of extensive tumor vasculature.

Indocyanine green angiography penetrates the pigmented layers of the fundus more easily than the short-wavelength light used in FA.[29,30] Recently, simultaneous confocal ICG-V/FA has been demonstrated.[31,32] These sensitive digital image acquisition and processing techniques have considerably improved the horizontal image resolution of ICG-V to below 20 μm. The size of the reported histologic microvascularization patterns fall in this range,[24] and must therefore be imageable. Mueller et al.[33] have shown that the angiographic presence of complex microcirculation patterns (MCPs) by confocal ICG-V (Fig. 8.5) is associated with clinical evidence of lesion growth. The MCPs are visible more frequently with confocal ICG-V (94%) compared with FA (6%). Equally important, they showed that an absence of complex MCPs is associated with a stable lesion size, perhaps indicative of benign behavior. It has been suggested previously that a subset of melanomas exists that contains the same MCPs as nevi (lacking evidence of complex MCP) and that these nevus-like melanomas tend to follow a more indolent clinical course.[34]

Angiographic methods such as ICG-V and FA may be used to demonstrate the vascularization features of tumors.[35–37] Intratumoral vessels can be detected in addition to choroidal and retinal vessels. Chemical and physical differences between the two imaging techniques enable varying tumor visualization. While FA visualizes only superficial vessels with the RPE intact, the scanning laser method of ICG-V demonstrates deeper structures, since the RPE is not a barrier to ICG.[38] Indocyanine green videoangiography is superior to FA in demonstrating intraocular tumor vessels.[35–37] Intratumoral vessels are detected in 89% of all tumors by ICG-V but in only 33% by FA. Both ICG-V and FA demonstrate blockage of choroidal filling by the tumor in 100% of cases.

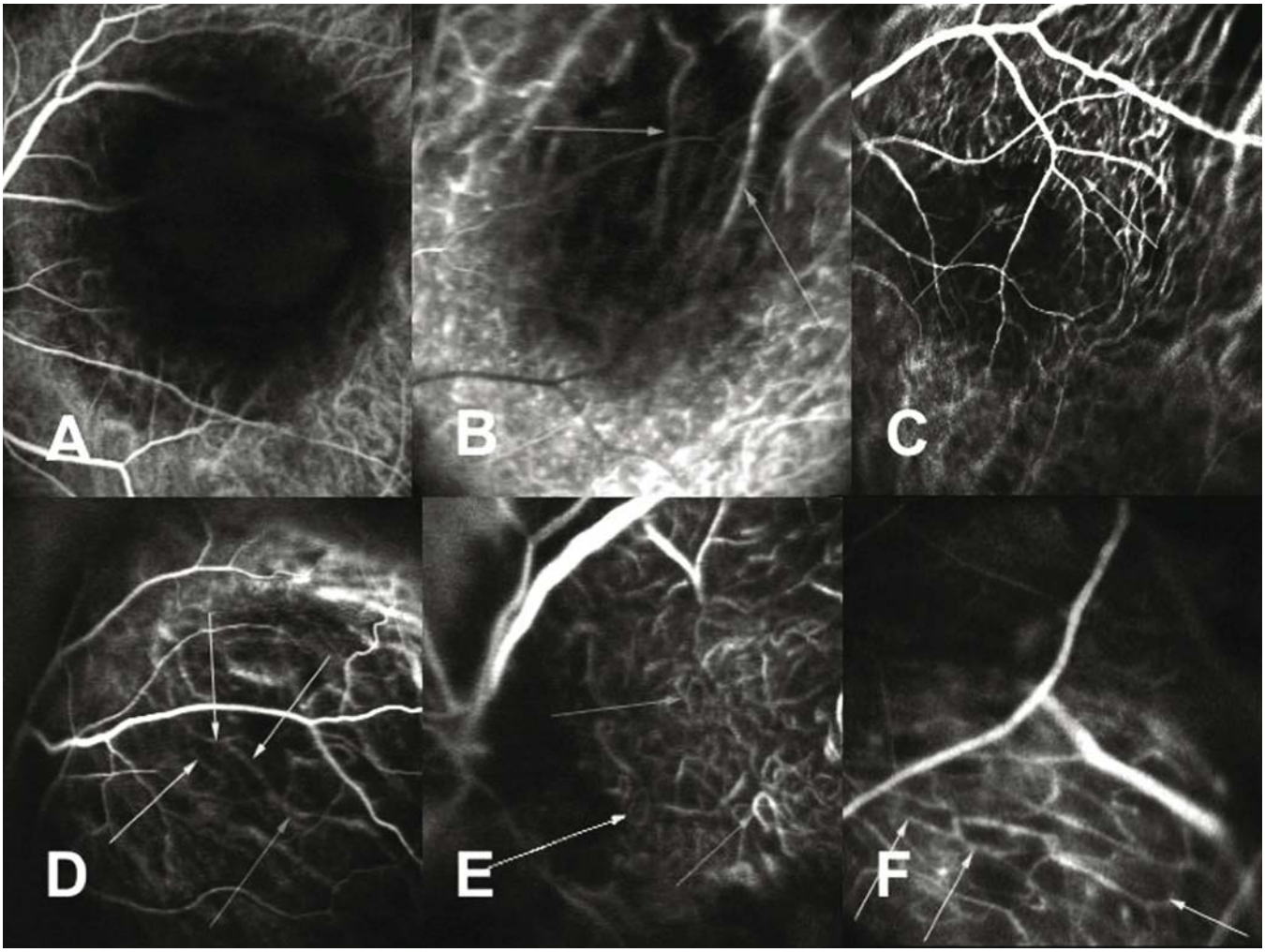

FIG. 8.5. Angiographic presence of complex microcirculation patterns (MCPs) by confocal indocyanine green angiography. (A) Silent. (B) Normal MCP (arrows). (C) Straight MCP (arrows). (D) Parallel with cross-linking MCP (arrows). (E) Arcs with branching MCP (arrows). (F) Network MCP (arrows). (Courtesy of Arthur Mueller, MD.)

Vascular Tumors of the Uvea

Circumscribed Choroidal Hemangioma

Choroidal hemangioma is a benign vascular tumor believed to be congenital in origin.[39–41] This tumor is classified into two types, circumscribed and diffuse, on the basis of the extent of choroidal involvement. Circumscribed choroidal hemangioma (CCH) is almost always unifocal and unilateral without systemic associations. Circumscribed choroidal hemangioma is a red-orange colored choroidal mass usually in the macular area. It produces symptoms similar to central serous chorioretinopathy. Its pathology shows cavernous vascular spaces lined by thin endothelial cells.[42]

Fluorescein angiography is probably of most diagnostic value in the assessment of circumscribed choroidal hemangiomas. [43,44] Fluorescein angiography showed early lacy mild hyperfluorescence in the prearterial or early arterial phase and diffuse intense late hyperfluorescence in all cases. A fluorescein angiogram of a typical CCH[43,44] shows prominent fluorescence of multiple large-caliber intralesional vessels prior to the earliest filling of the normal choroidal vasculature or retinal vessels. By the retinal arterial phase frames, the entire lesion is usually diffusely and intensely hyperfluorescent without identifiable distinct intralesional vessels. Fluorescein leaks through the characteristically degenerated overlying RPE into the subretinal space, and commonly stains the subretinal fluid and retina diffusely in the late phase frames (Fig. 8.6A–C).

Because most circumscribed choroidal hemangiomas are reliably diagnosed on the basis of ophthalmoscopic appearance alone, fluorescein angiography is again probably of more value in documentation and monitoring of response to therapy. The most frequent pattern is characterized by irregular linear hyperfluorescence of the large choroidal vessels within the tumor during the prearterial or the early

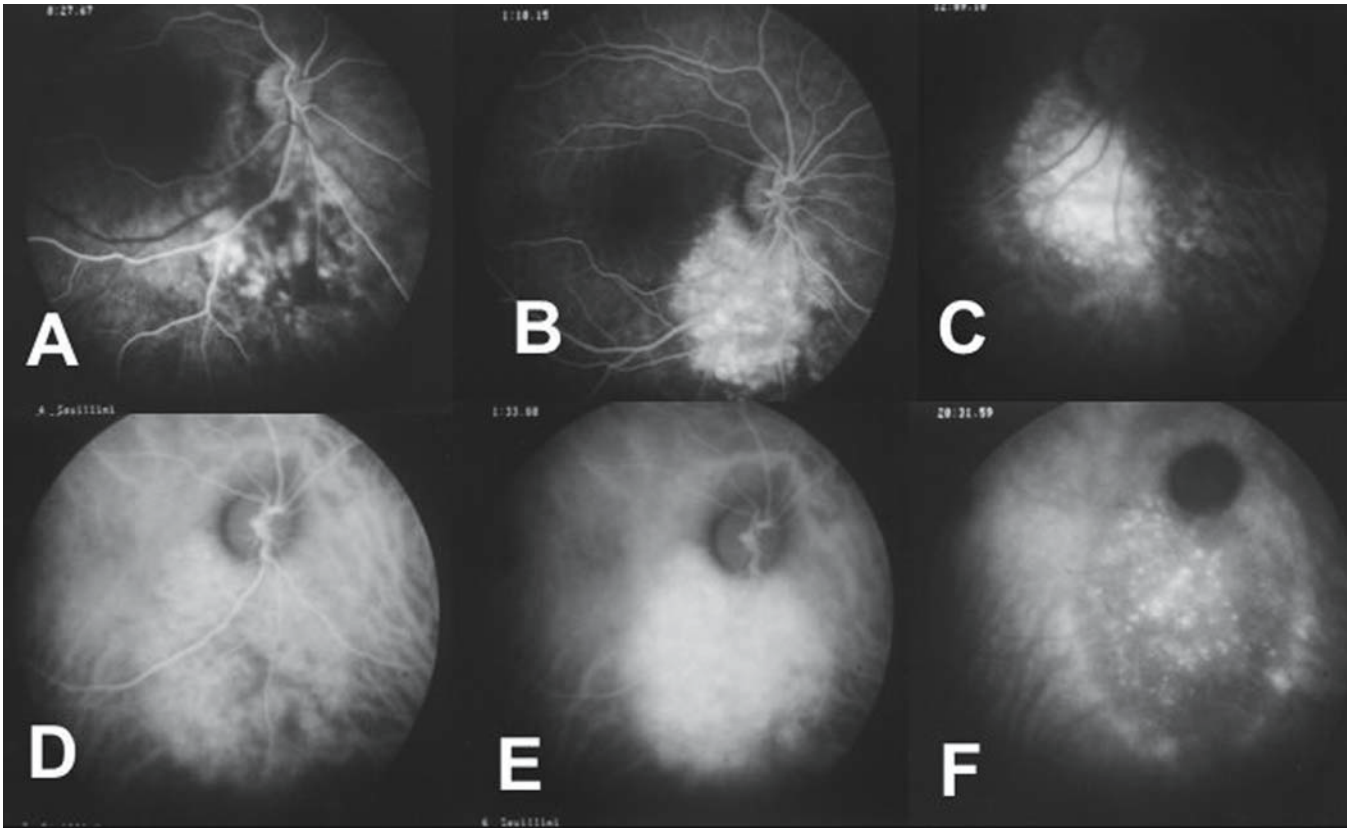

FIG. 8.6. (A–C) Fluorescein angiography in circumscribed choroidal hemangioma shows early lacy mild hyperfluorescence in the prearterial or early arterial phase (A) and diffuse intense late hyperfluorescence (B, C) in all cases. (D–F) Circumscribed choroidal hemangioma have specific characteristics on ICG-V that are not visualized with intravenous fluorescein angiography because of specific angiographic features including early hyperfluorescence (D), middle hyperfluorescence (E), followed by late hypofluorescence (washout of dye) and a hyperfluorescent rim (F).

arterial phases. In the arterial and venous phases, there is a progressive staining of the extravascular tissue within the tumor, often with pinpoint foci of hyperfluorescence over the tumor. The late phase reveals intraretinal hyperfluorescence secondary to leakage of fluorescein into the cystoid spaces within the retina (Fig. 8.6A–C).[41,45]

Circumscribed choroidal hemangioma have specific characteristics on ICG-V that are not visualized with intravenous FA[45] because of specific angiographic features including early hyperfluorescence followed by late hypofluorescence (washout of dye) and a hyperfluorescent rim (Fig. 8.6D–F). Indocyanine green videoangiography, therefore, may be a significant aid in diagnosing difficult cases and preferable to FA in detecting intrinsic vessels and feeder vessels of the tumor. [45] The blood supply to these tumors is provided directly by short posterior ciliary arteries or by ramifications of choroidal arteries. An adjacent compromised choroidal perfusion may be present.[46]

Indocyanine green angiography is critical for demonstrate the high-flow state of the choroidal hemangioma with rapid filling by 1 minute, often followed by a "washout" phenomenon (Fig. 8.7).[45,47] These features would not likely be found with choroidal melanoma or metastasis, in which filling on both FA and ICG-V is slower and less intense.[47]

Diffuse Choroidal Hemangioma

Choroidal hemangiomas may be circumscribed and solitary or diffuse. Diffuse choroidal hemangiomas are characteristically associated with Sturge-Weber syndrome and are typically unilateral and ipsilateral to other manifestations of the syndrome. Sturge-Weber syndrome is usually diagnosed on clinical grounds by the combination of typical symptoms and nevus flammeus. The cutaneous abnormality is commonly present in the distribution of the trigeminal nerve, usually ophthalmic, but is not essential for diagnosis.[48]

Sturge-Weber syndrome may also include facial vascular lesions, ipsilateral intracranial hemangiomas, anomalous conjunctival vessels, malformed anterior chamber angle, and glaucoma. Retinal and choroidal detachments have been reported.

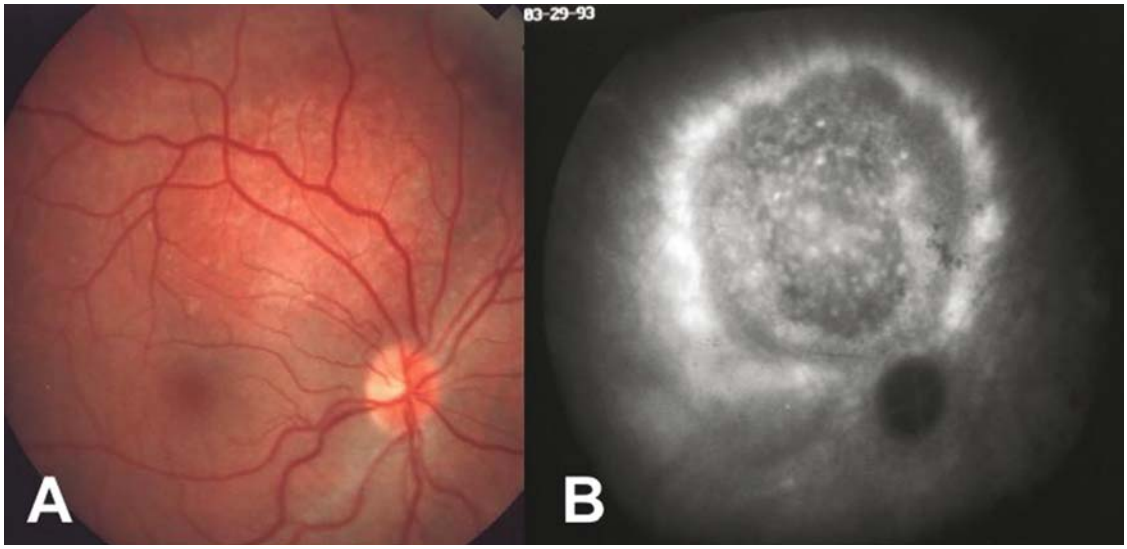

FIG. 8.7. (A) Color photograph of circumscribed choroidal hemangioma. (B) Indocyanine green angiography is critical to demonstrate the high-flow state of the choroidal hemangioma with rapid filling by 1 minute, often followed by a "washout" phenomenon.

Ocular hemangiomas involving the choroid are estimated to occur in approximately one third of cases, and these may be seen at funduscopy.[49–51] Visual symptoms are caused by cystoid degeneration of the fovea and exudative retinal detachment. The typical fundus lesions of Sturge-Weber syndrome are subtle, lack defined borders, and often cover more than one half of the fundus area. Ultrasonography, FA, and magnetic resonance imaging can be useful in confirming the diagnosis. Fluorescein angiography demonstrates a characteristic early diffuse speckled choroidal flush.[52] The characteristic angiographic findings in choroidal hemangiomas are (1) a pattern of fluorescence indicative of large vascular channels corresponding to the location of the tumor in the prearterial and arterial phase of angiography (Fig. 8.8A), (2) widespread and irregular areas of fluorescence secondary to diffuse leakage of dye from the surface of the tumor (Fig. 8.8B), and (3) a diffuse multiloculated pattern of fluorescein accumulation in the outer retina characteristic of polycystic degeneration and edema during the later stages of angiography (Fig. 8.8C).[6,53,54]

Few studies have been carried out with ICG-V in diffuse choroidal hemangiomas.[55] Wen and Wu[55] demonstrated with ICG-V that the vascular tissue in diffuse hemangioma filled rapidly with dye during the arterial phase of the choroidal angiogram; copious dye leakage appeared early and persisted into the late phase of angiography. The late "washout" phenomenon was not observed 30 minutes after dye injection. Sectors of reduced choroidal perfusion in the upper or lower half of the midperiphery were present.[55]

Choroidal Metastasis

Metastatic intraocular tumors are the most common intraocular malignancy. Most ocular metastases arise in the choroid. The most common primary tumor is breast cancer in women and lung cancer in men. Metastatic carcinomas to the choroid are usually readily diagnosed on the basis of ophthalmic examination coupled with investigation of the clinical history.[56,57] Fluorescein angiography appears to add little diagnostic information.

Choroidal metastasis appears as a creamy-yellow mass usually in the posterior choroid. It may produce extensive adjacent retinal detachment and may be multifocal or bilateral. Management is chemotherapy for systemic disease, and observation or radiation therapy for ocular tumors. Noninvasive ancillary tests such as FA and ICG-V can play an important role in the early diagnosis of choroidal metastasis by helping to distinguish it from true ocular inflammatory diseases, raising the level of suspicion, and leading to the prompt use of more invasive but definitive diagnostic procedures.

A few reports in the literature have described some of the FA findings for these patients. These findings have included hypofluorescent detachments of the RPE,[58,59] early and late hyperfluorescent subretinal lesions,[60,61] and perivasculitis by means of optic nerve staining.[61] On fluorescein angiography, the typical lesion appears relatively hypofluorescent in the early frames of the study, contains few if any intralesional vessels that appear during the arterial to venous phase frames of the study, and leaks diffusely in the late frames (Fig. 8.9).[5–7] Because of the damaging effects of the expanding choroidal tumor on the overlying RPE, there is commonly noted to be diffuse and multifocal hypofluorescence and hyperfluorescence at the RPE level overlying the lesion as indications of this damage (Fig. 8.10). In addition, pinpoint hyperfluorescent foci at the retinal pigment epithelial level, which are generally attributed to microcystic retinal pigment epithelial degeneration, commonly become apparent over the surface of the tumor by the late frames. Fluorescein typically leaks through the RPE to accumulate in the overlying and surrounding subretinal space by the late frames.

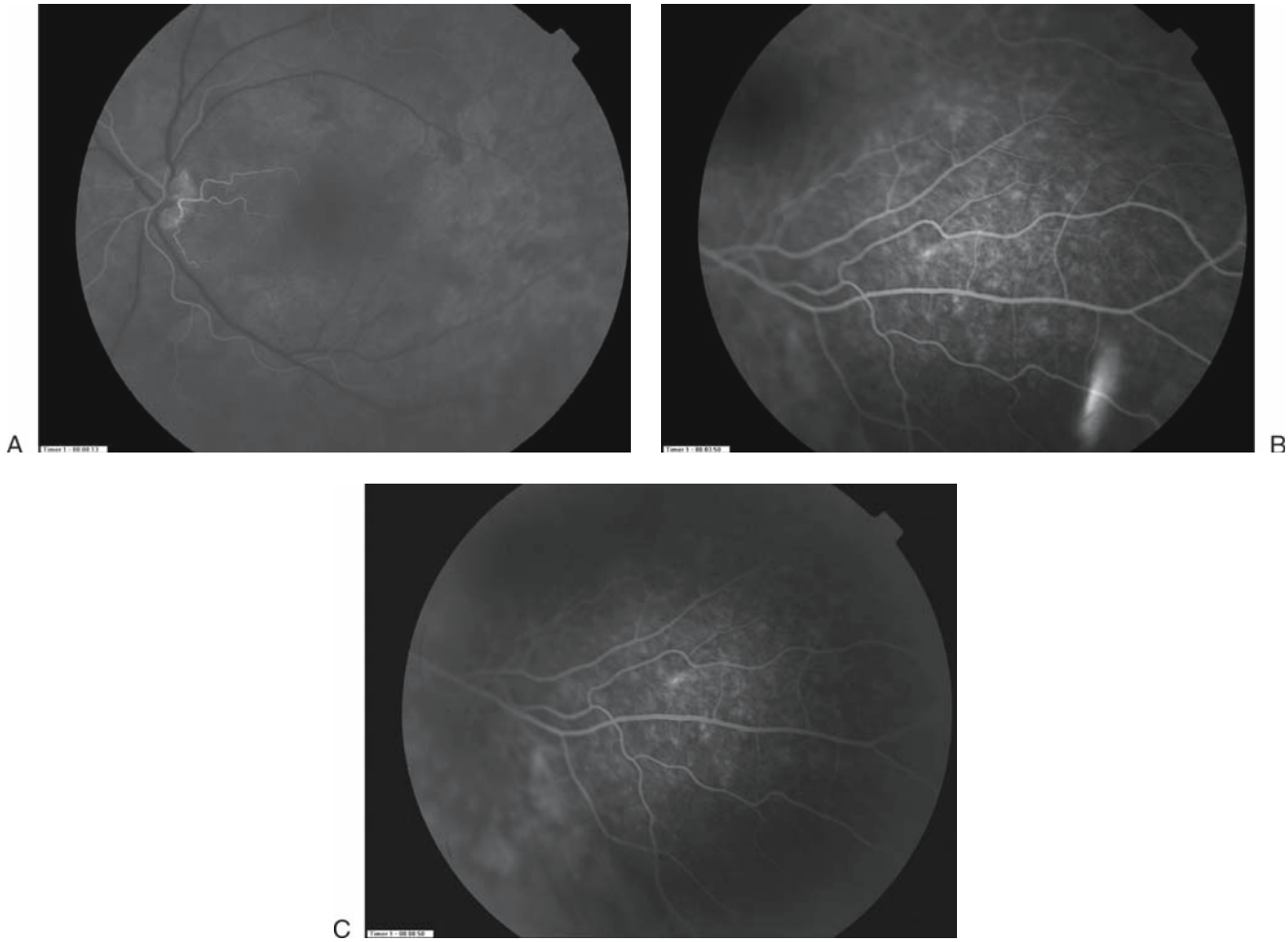

FIG. 8.8. The characteristic angiographic findings in diffuse choroidal hemangiomas. (A) A pattern of fluorescence indicative of large vascular channels corresponding to the location of the tumor in the prearterial and arterial phase of angiography. (B) Widespread and irregular areas of fluorescence secondary to diffuse leakage of dye from the surface of the tumor. (C) A diffuse multiloculated pattern of fluorescein accumulation in the outer retina characteristic of polycystic degeneration and edema during the later stages of angiography.

Fluorescein angiography is rarely useful as an aid in the differential diagnosis of metastatic choroidal tumors because it does not allow the definite differentiation of pseudometastatic lesions such as choroidal hemangiomas or melanomas. Angiography is more helpful in assessing the size of the lesion. Relatively flat areas of choroidal invasion are difficult to recognize clinically, but there is almost always some alteration in the overlying RPE, which is often highlighted on the angiogram.

The so-called double circulation pattern, thought to be characteristic of choroidal melanomas that have broken through Bruch's membrane, is a rare finding in metastatic tumors.[22]

Indocyanine green may be a useful adjunct in the differentiation of choroidal metastasis demonstrating maximal fluorescence at an average of 9 minutes. Choroidal metastasis shows diffuse homogeneous hypofluorescence in comparison with the surrounding normal choroid. The normal choroidal pattern can often be visualized underlying or within the metastasis as if the tumor were acting as a relative filter of the fluorescence of the underlying choroid. This filtering effect extends for the entire base of the metastasis and stops abruptly at the margin of the tumor. In the late frames (by 30 minutes), the choroidal vessels show subtle diffuse staining and leakage (Fig. 8.11).[62] Choroidal metastasis demonstrates on ICG-V a blockage of the background, and a patchy staining of the tumor surface. Intratumoral vessels could be detected using ICG-V in only 13% of cases. Some authors speculate that intrinsic vessels are not observed because of the relative thinness of the tumor. With thicker choroidal metastases one might possibly visualize intrinsic tumor vessels. Most of the metastases tend to show a patchy staining of the tumor surface.[63]

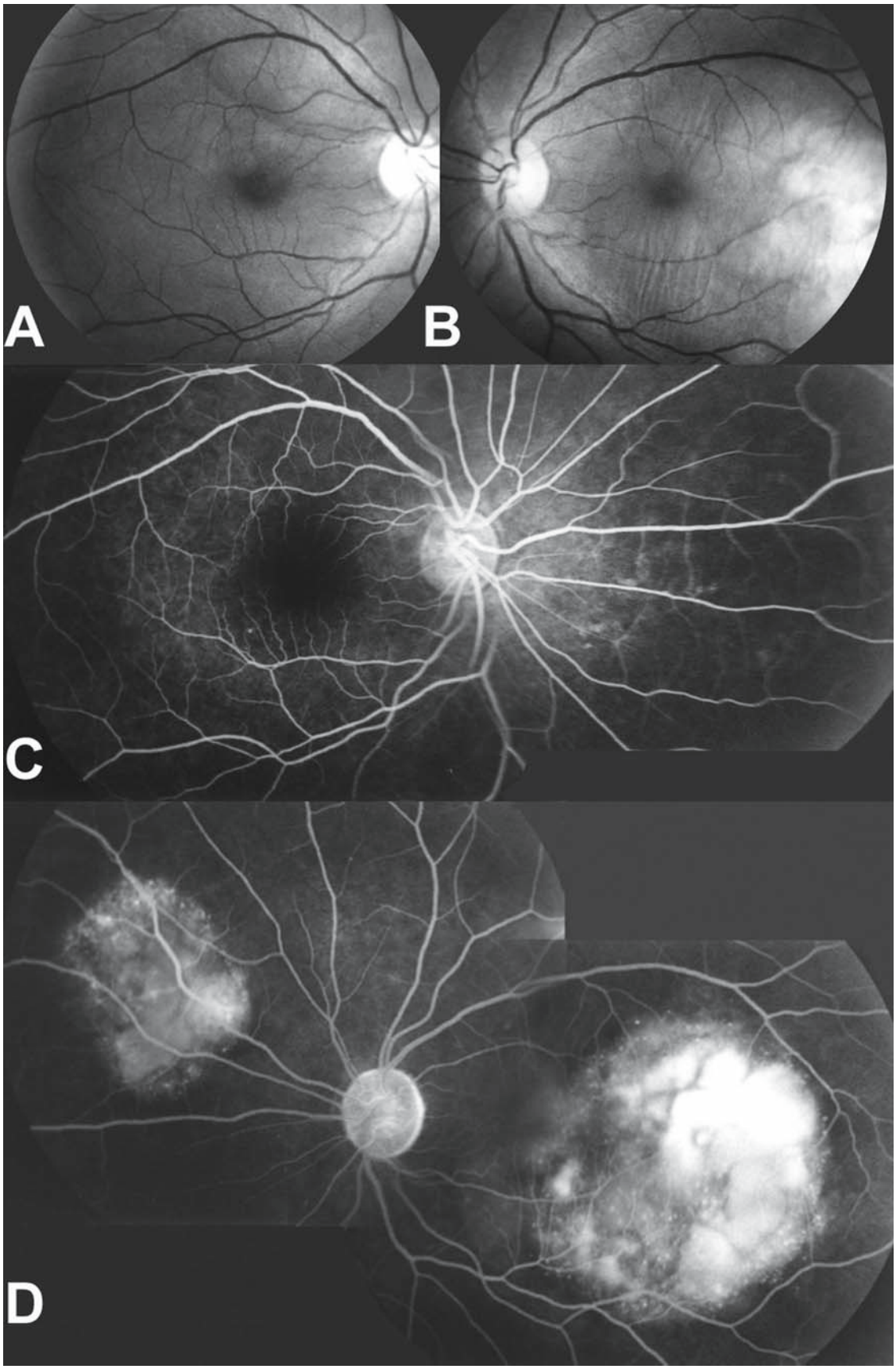

FIG. 8.9. (A,B) Red-free photographs of choroidal metastasis in both eyes. (C,D) On fluorescein angiography, the typical lesion of choroidal metastasis appears relatively hypofluorescent in the early frames of the study (C), contains few if any intralesional vessels that appear during the arterial to venous phase frames of the study, and leaks diffusely in the late frames (D).

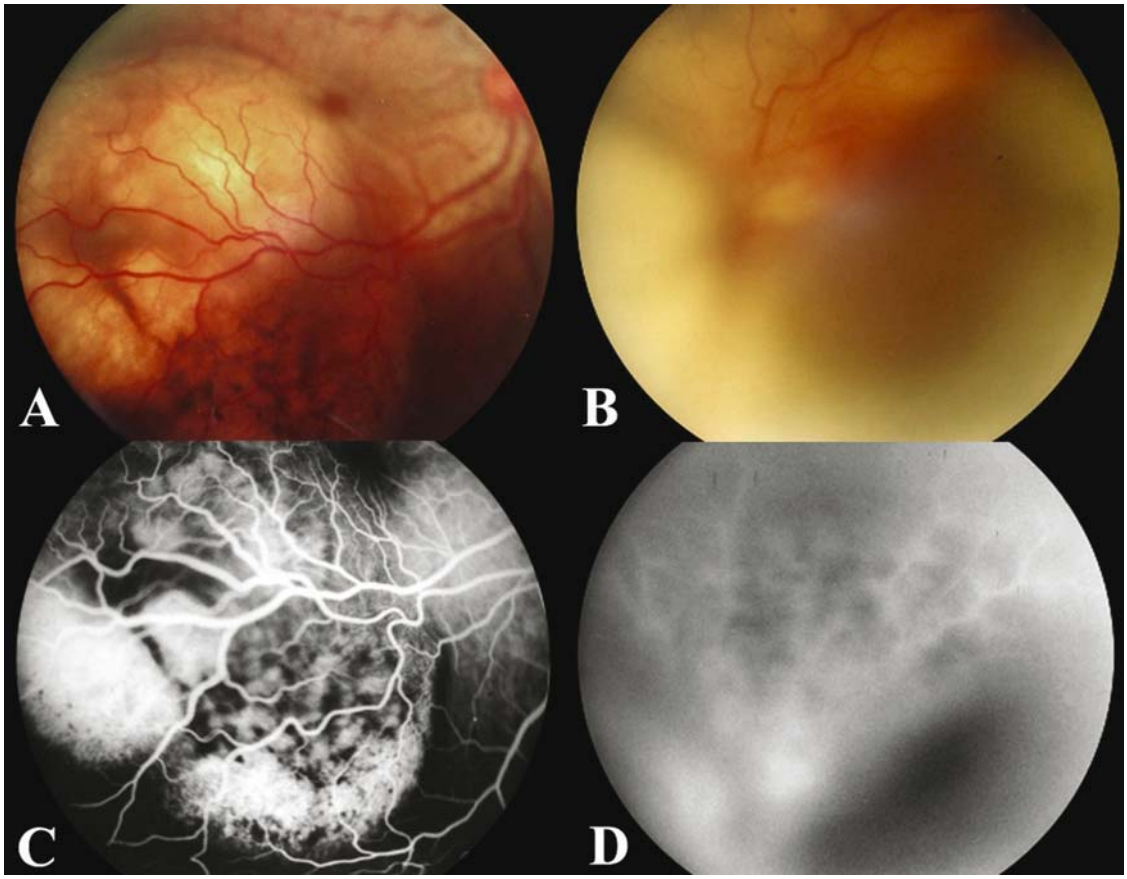

FIG. 8.10. (A,B) Color photographs of choroidal metastasis in both eyes. (C) Because of the damaging effects of the expanding choroidal tumor on the overlying retinal pigment epithelium (RPE), there is commonly noted to be diffuse and multifocal hypofluorescence and hyperfluorescence at the RPE level overlying the lesion as indications of this damage. (D) Fluorescein angiography (FA) of left eye with a choroidal metastasis and exudative retinal detachment. There is no apparent contribution of the tumor to FA.

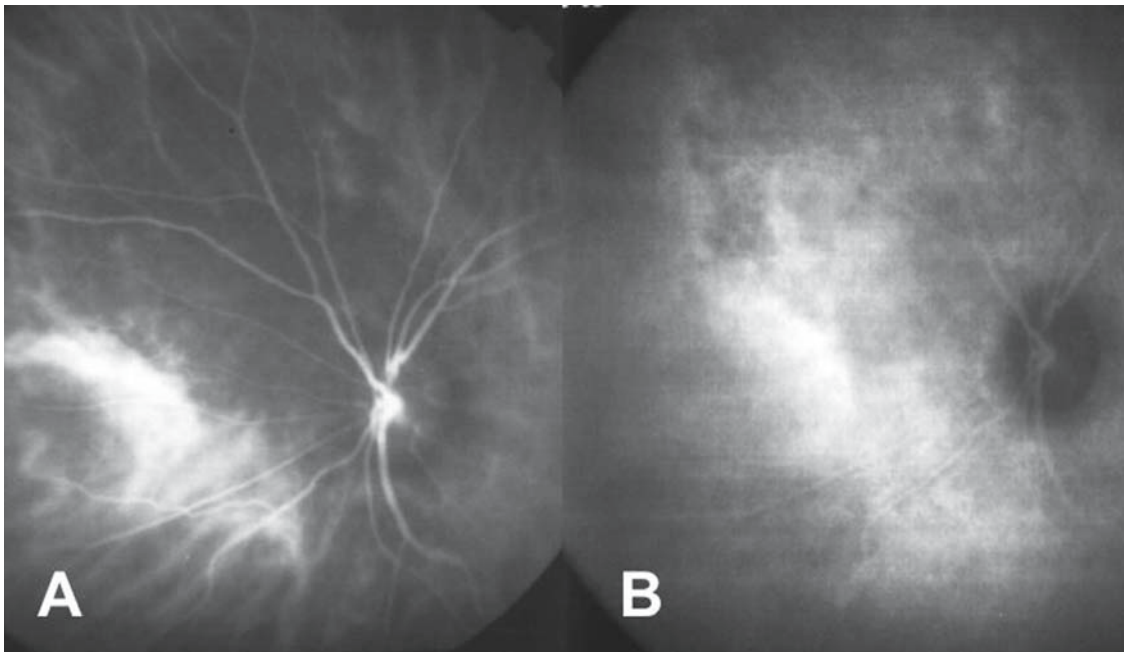

FIG. 8.11. (A) Choroidal metastasis shows diffuse homogeneous hypofluorescence in comparison to the surrounding normal choroid. The normal choroidal pattern can often be visualized underlying or within the metastasis as if the tumor were acting as a relative filter of the fluorescence of the underlying choroid. This filtering effect extends for the entire base of the metastasis and stops abruptly at the margin of the tumor. (B) In the late frames, the choroidal vessels show subtle diffuse staining and leakage.

Osseous Tumors of the Uvea

Choroidal Osteoma

Choroidal osteoma is a benign bony tumor, unilateral or bilateral, acquired, and slowly growing choroidal mass usually in the juxtapapillary location.[64,65] Choroidal osteoma is usually found in healthy young women between the second and the third decades of life.[65,66] The pathologic finding of choroidal osteoma is a plaque of mature bone involving full thickness of the choroid, usually sparing the RPE. The diagnosis of choroidal osteoma is made by demonstrating ossification in the lesion with ultrasonography or computed tomography (CT) scan. This benign tumor may show slight enlargement over several years and cause visual loss due to subfoveal osteoma, serous retinal detachment, and CNV.

Fluorescein angiography typically reveals early patchy hyperfluorescence and diffuse late staining (Fig. 8.12). The choroidal vascular tufts on the inner surface of the tumors may be seen to fill early, but they generally fade into the later phases of the study. Late-phase fluorescein angiograms enable assessment of the extension of the osteoma as it is variably hyperfluorescent due to tumor staining combined with a variable degree of overlying RPE changes.[67] More important than simple documentation of the lesion's appearance is the assessment of any possible associated choroidal neovascularization, which occasionally complicates choroidal osteoma.[65] Choroidal neovascularization usually manifests as a local area of lacy hyperfluorescence that demonstrates increasing leakage throughout the study (Fig. 8.13). When present, a choroidal neovascular membrane lesion appears as an abnormal subretinal neovascular network pattern beneath the RPE or sensory retina in the early frames of the study and as a smudgy hyperfluorescent lesion showing progressive increase in fluorescence and late staining with leakage in the late frames.

The early phase of ICG-V on choroidal osteoma shows hypofluorescence due to blockage, corresponding with the extent of the osteoma, but the borders may be difficult to demarcate. However, a pattern of small vessels during early ICG-V is characteristic of choroidal osteomas.[9,10] These tiny vessels are often unidentifiable on FA because of rapid leakage from the incompetent vascular endothelium. Indocyanine green videoangiography, in the late phases, demonstrates hyperfluorescent areas accompanied by several small hypofluorescent foci corresponding with very subtle ophthalmoscopically observed changes in the vicinity of the osteoma. There is also evidence of abnormal dilated and tortuous choroidal vessels that leaked dye, causing hyperfluorescence in the intermediate, and late phases. In the late phases of the ICG-V, hypofluorescence due to choriocapillaris loss and hyperfluorescence due to leakage from abnormal choroidal vessels are combined (Fig. 8.14).[68–70]

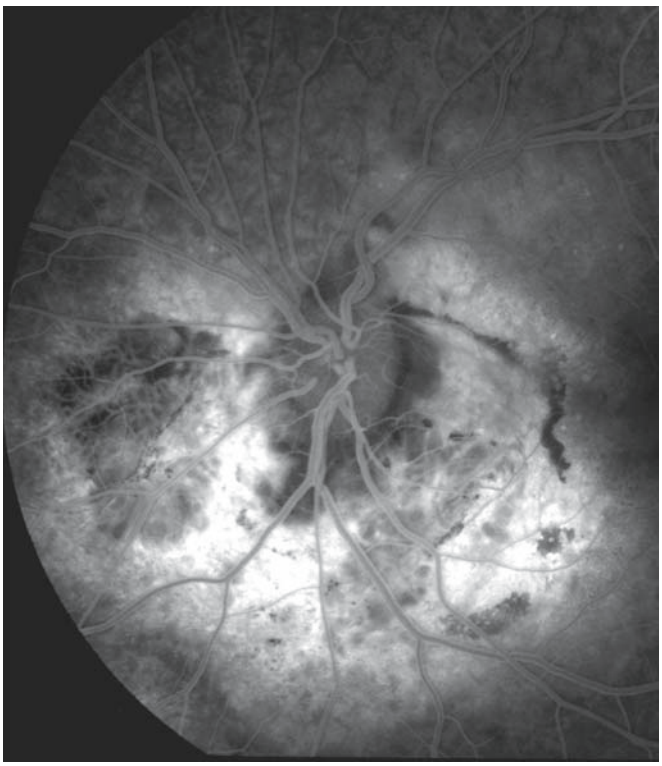

Fig. 8.12. Choroidal osteoma. Fluorescein angiography typically reveals early patchy hyperfluorescence and diffuse late staining.

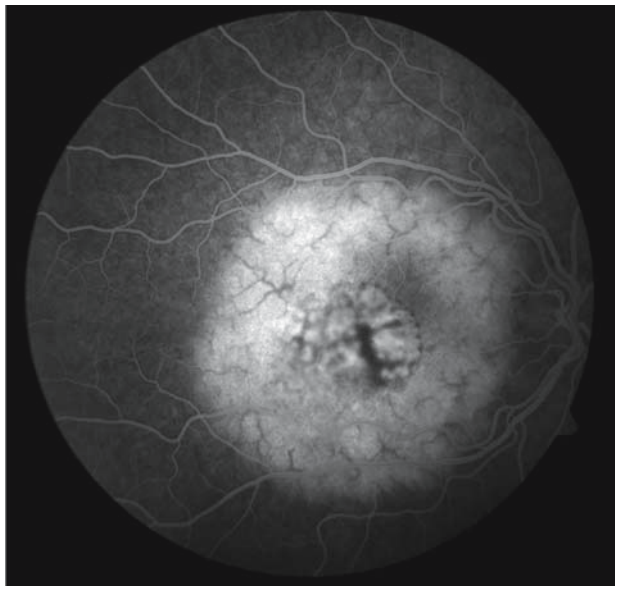

Fig. 8.13. Choroidal neovascularization in choroidal osteoma usually manifests as a local area of lacy hyperfluorescence that demonstrates increasing leakage throughout the study. When present, a choroidal neovascular membrane lesion appears as an abnormal subretinal neovascular network pattern beneath the retinal pigment epithelium or sensory retina in the early frames of the study and as a smudgy hyperfluorescent lesion showing a progressive increase in fluorescence and late staining with leakage in the late frames.

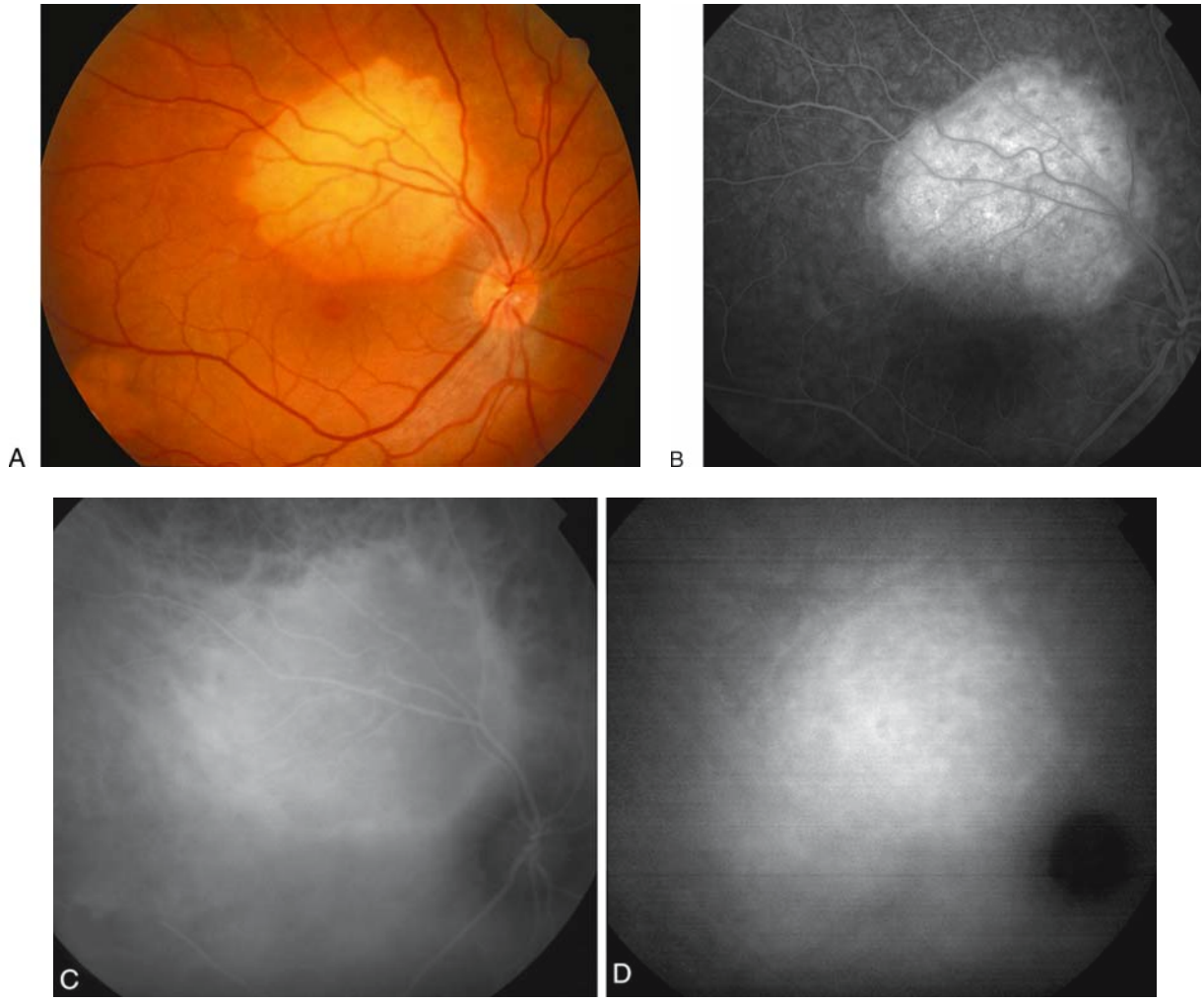

FIG. 8.14. (A) Color photograph of a choroidal osteoma along the superotemporal arcades and superior to the fovea. (B) Fluorescein angiography demonstrates hyperfluorescence throughout the study. (C) The early phase of indocyanine green videoangiography (ICG-V) demonstrates hypofluorescence due to blockage, corresponding with the extent of the osteoma but the borders may be difficult to demarcate. However, a pattern of small vessels during early ICG-V is characteristic of choroidal osteomas. (D) ICG-V, in the late phases, demonstrates hyperfluorescent areas accompanied by several small hypofluorescent foci corresponding with very subtle ophthalmoscopically observed changes in the vicinity of the osteoma. There is also evidence of abnormal dilated and tortuous choroidal vessels that leaked dye, causing hyperfluorescence in the intermediate and late phases. In the late phases of the ICG-V, hypofluorescence due to choriocapillaris loss and hyperfluorescence due to leakage from abnormal choroidal vessels are combined. (Courtesy of Patrick De Potter, MD.)

Vascular Tumors of the Retina

Capillary Hemangioma

Capillary hemangioma shows a reddish retinal mass with dilated feeding and draining retinal vessels. This tumor may produce exudative retinal detachment. Retinal capillary hemangiomas (RCHs) are angiomatous hamartomas of the retina. Typically, they are peripheral and endophytic[71,72] but can be exophytic and posterior, or reactive.[73] Retinal capillary hemangioma is a highly vascular, well-circumscribed, slowly growing neoplasm of particular interest to the ophthalmologist because of the frequent association with von Hippel–Lindau disease and its potential to threaten vision because of secondary effects on the retina. The diagnosis is primarily clinical but ancillary testing may be helpful. Standard fundus photography is the most useful to assist with follow-up to confirm growth, stability, or regression after treatment. If fluorescein angiography is performed on a typical retinal capillary hemangioma,[5–7,74] it shows rapid filling of the afferent artery, brisk filling of the entire retinal vascular lesion, and intense hyperfluorescence of the entire vascular lesion shortly thereafter, followed by rapid filling of the efferent vessel (Fig. 8.15). Retinal capillary hemangiomas characteristically leak fluorescein exuberantly into the overlying vitreous, so that the late-phase frames are often extremely hazy due to the diffuse vitreous fluorescence. Because many retinal capillary hemangiomas are also associated with exudative subretinal fluid, fluorescein commonly accumulates in

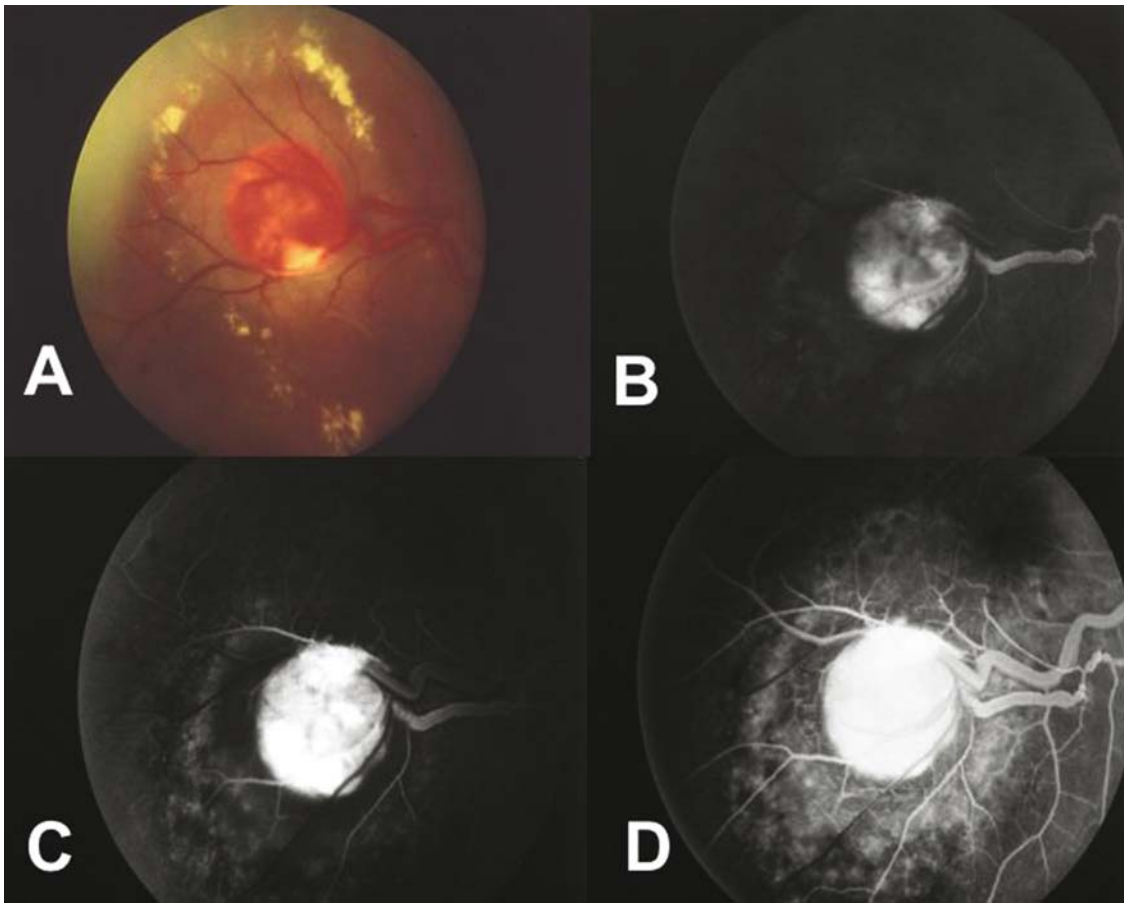

FIG. 8.15. Retinal capillary hemangioma (A) shows rapid filling of the afferent artery (B), brisk filling of the entire retinal vascular lesion (C), and intense hyperfluorescence of the entire vascular lesion shortly thereafter, followed by rapid filling of the efferent vessel (D).

the subretinal space by the late frames. Fluorescein traverses the tumor so rapidly that it is difficult for an angiogram to capture more than a fleeting frame of the arterial phase. Diffuse leakage of fluorescein is noted in the middle and late frames (Fig. 8.15C,D). Small peripheral lesions may be difficult to find clinically, but they light up on fluorescein angiography, allowing their identification.

Cavernous Hemangioma

Cavernous hemangioma of the retina (CHR) is a rare vascular tumor first described in 1934 by Niccol and Moore,[75] who termed this condition angiomatosis retinae. Gass[76] later recognized CHR as a distinct clinical entity. Cavernous hemangioma of the retina appears most commonly as a solitary vascular lesion of limited size (one or two disc diameters) in the midperipheral or peripheral retina, although occasionally the lesion can be found in the posterior pole or optic nerve head.[77] Cavernous hemangioma makes blue globular retinal lesion which may resemble a bunch of grapes. It does not produce exudate but can lead to vitreous hemorrhage. There is an association between CHR and cavernous hemangiomas involving the central nervous system (CNS). Typically, ophthalmoscopy reveals clusters of saccular aneurysms filled with dark venous blood. Superficial retinal hemorrhages are occasionally seen, but hard exudation has not been observed. In some cases, a gray-white preretinal membrane can partly obscure the surface of the tumor. Although the retinal vasculature elsewhere is usually normal, other associated vascular anomalies can occur.

Fluorescein angiography may show autofluorescence of the gray-white epiretinal membrane overlying the tumor. In early frames of the FA, the vascular channels within the CHR remain hypofluorescent. As the angiogram progresses, these vascular channels fill slowly with the dye. The aneurysms fill slowly and often incompletely up to 30 minutes after dye injection. In late frames, a blood–fluorescein interface is characteristically observed in the saccular dilations within the tumor. This phenomenon seems to be related to sedimentation of erythrocytes in the inferior aspect of the venous aneurysm, which appears hypofluorescent. The presence of plasma in the superior aspect of this vascular space, which stains with fluorescein, appears hyperfluorescent (Fig. 8.16). There is no extravascular leakage of dye in CHR.[78]

On ICG-V the tumor is seen with a mottled hypofluorescence and isofluorescence in the early frames (up to approximately 30 seconds) (Fig. 8.17). The isofluorescence is presumed to

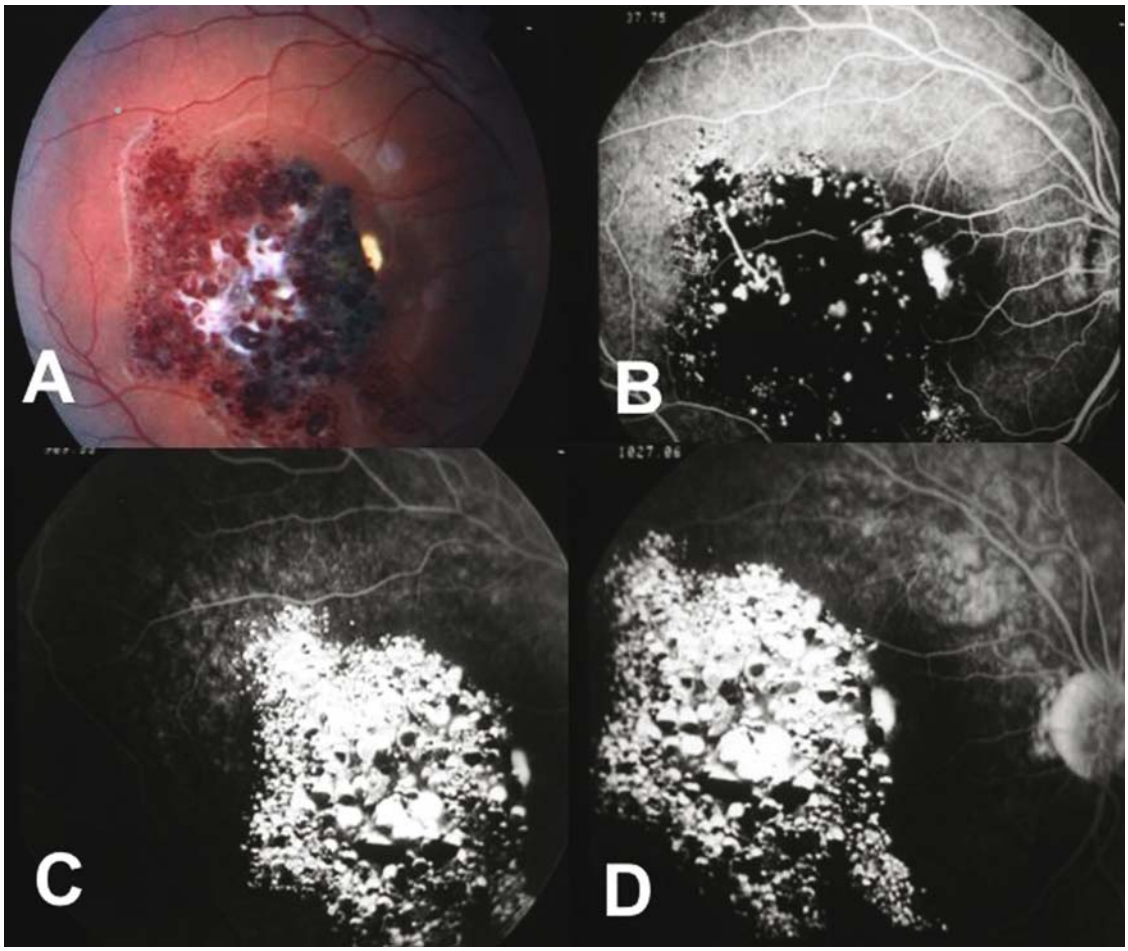

FIG. 8.16. (A) Color photograph of cavernous hemangioma. (B–D) Fluorescein angiography (FA) in the early frames, the vascular channels within the cavernous hemangioma of the retina (CHR) remain hypofluorescent. As the angiogram progresses, these vascular channels fill slowly with the dye. The aneurysms fill slowly and often incompletely up to 30 minutes after dye injection. In late frames, a blood–fluorescein interface is characteristically observed in the saccular dilations within the tumor.

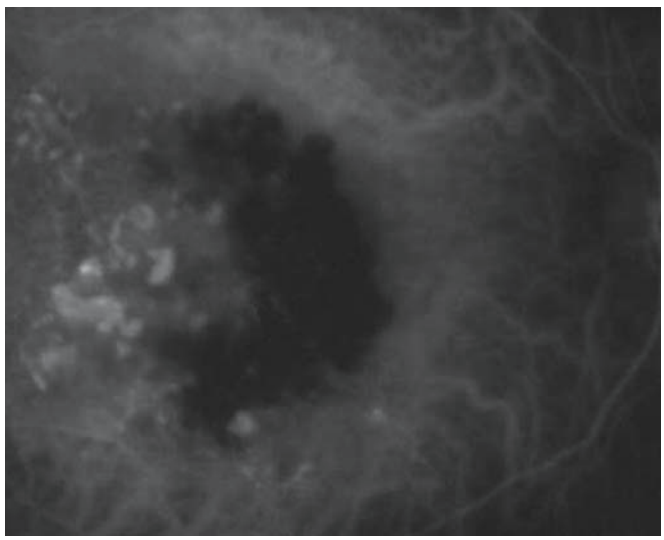

FIG. 8.17. Late-phase ICG-V of cavernous hemangioma demonstrates a faint filling of most of the vascular channels. Layering of ICG superiorly and blood inferiorly is seen in some channels.

be caused by early tumor filling, more likely from the retinal circulation than the choroidal circulation. The hypofluorescence is presumed to be a result of a vascular defect from the overlying nonfilling portion of the retinal tumor. By 1 minute after the injection of the dye the tumor vessels begin to show a silhouette of the vascular channels by entrapped dye. By 2 minutes after injection the injection of the dye there is dye–blood layering within many of the vascular channels similar to that seen with sodium fluorescein but much less intense.[10]

Vasoproliferative Tumor of the Retina

Vasoproliferative tumor of the retina (VPTR) is a reactionary glial cell proliferation with secondary vasoproliferation[79,80] sporadically seen in a patient after a retinal injury that is either iatrogenic (e.g., surgery) or due to disease (e.g., pars planitis, sickle-cell retinopathy, retinitis pigmentosa), but most often occurs idiopathically.[81–83] Commonly associated complications are intra- and subretinal exudation with or without secondary exudative retinal detachments, intra- and subretinal hemorrhages, vitreous cells, vitreous hemorrhages, and macular edema.[80,81]

Shields et al. [81] reclassified vasoproliferative retinal tumors as primary or secondary. Primary tumors according to their classification are characteristically unilateral, solitary lesions with normal feeder and draining vessels, occurring most commonly in the inferotemporal quadrant of the fundus. Secondary tumors have been associated with many ocular conditions including retinitis pigmentosa, retinopathy of prematurity, retinal detachment surgery, and Coats' disease. Such tumors tend to be smaller lesions and have associated areas of RPE proliferation.[79]

Fluorescein angiography demonstrates connections between retinal feeder vessels and a rich capillary network within the tumors (Fig. 8.18). The retinal feeder vessels are not or only mildly dilated. Leakage of dye from tumor vessels is seen during the arteriovenous passage and in the later frames of fluorescein angiography. Telangiectatic dilations of tumor vessels have been noted in most of the cases.[79]

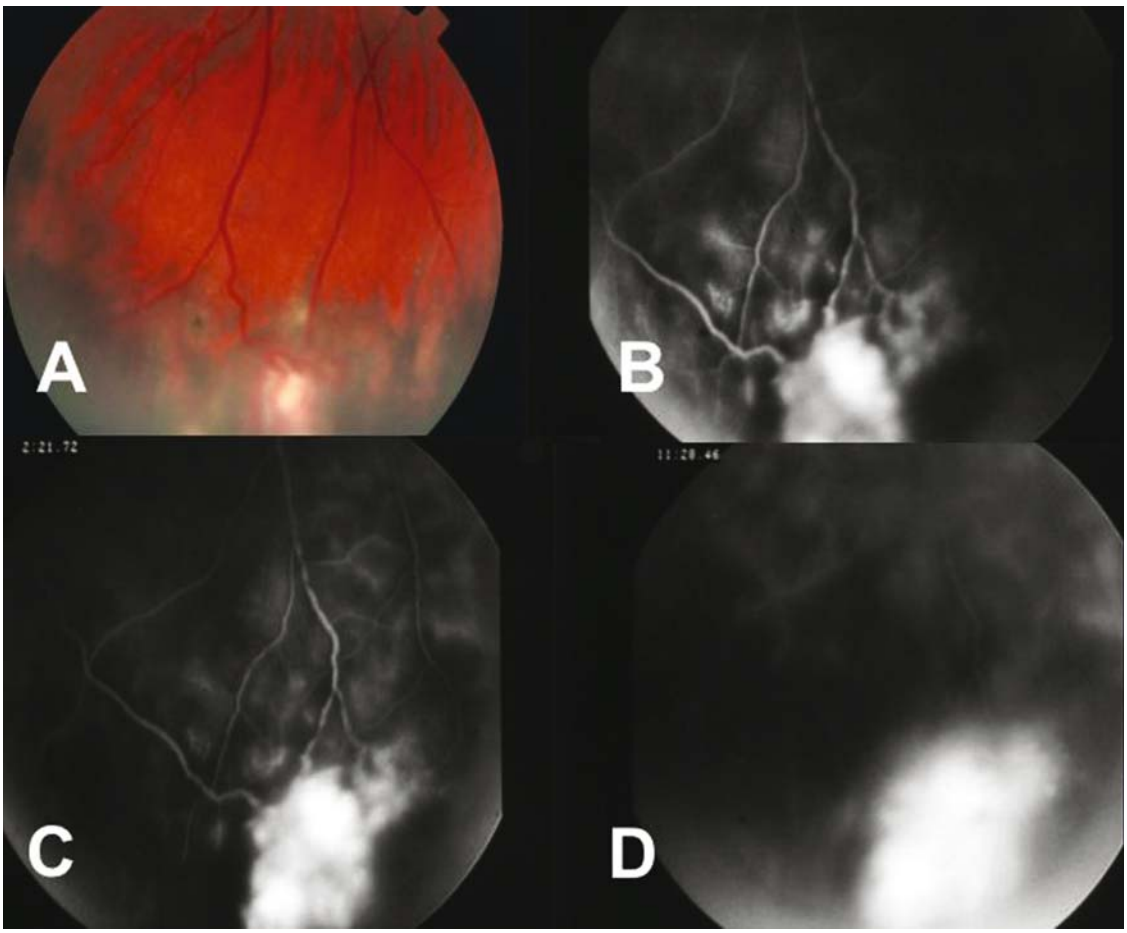

Fig. 8.18. (A) Color photograph of vasoproliferative tumor of the retina. (B–D) Fluorescein angiography presents connections between retinal feeder vessels and a rich capillary network within the tumors. The retinal feeder vessels are not or only mildly dilated. Leakage of dye from tumor vessels is seen during the arteriovenous passage and in the later frames of fluorescein angiography. Telangiectatic dilations of tumor vessels have been noted in most of the cases.

Intraocular Lymphoid Tumors

Primary Intraocular Lymphoma

Malignant lymphoma can be seen in the eye. Large cell lymphoma, formerly called histiocytic lymphoma or reticulum cell sarcoma, is the most common. The retinovitreal form is often associated with CNS involvement and can be proved by vitreous biopsy. The diagnosis should be considered in an older patient presenting with the signs of bilateral uveitis and vitreitis. The choroidal form is often associated with visceral lymphoma and may produce choroidal nodules or typical tumor detachments of the RPE.

Primary intraocular lymphoma (PIOL), previously referred to as reticulum cell sarcoma, is mostly a large B-cell, non-Hodgkin's lymphoma that arises from the eye, brain, spinal cord, and leptomeninges.[84] It is also known as non-Hodgkin's lymphoma of the CNS. Ocular involvement occurs in approximately 25% of patients with PIOL.[85] The most common ocular symptoms include blurred vision and floaters; redness and pain are rare. The disease is fatal, with a mean survival time of 20 months from the time of ocular diagnosis.[86]

The clinical presentation of PIOL is diverse. Although vitreitis is the most common finding, present in 66% of previously described patients, the prototypical cream-colored subretinal yellow infiltrates are often absent, reported in only 41% of cases.[87] Other possible clinical findings include phlebitis and anterior segment involvement with anterior chamber cells or keratic precipitates. Patients are often followed up for years with a diagnosis of intermediate or posterior uveitis before a definitive diagnosis of PIOL is made. Noninvasive ancillary tests such as FA can play an important role in the early diagnosis of PIOL by helping to distinguish it from true ocular inflammatory diseases, raising the level of suspicion, and leading to the prompt use of more invasive but definitive diagnostic procedures.

Few reports in the literature have described some of the FA findings for these patients. These findings have included hypofluorescent detachments of the RPE,[58,59] early and late hyperfluorescent subretinal lesions,[60,61] and perivasculitis by means of optic nerve staining.[61] Findings such as hyperfluorescent "white spots,"[61] retinal vasculitis with disc edema,[61] early blockage with late staining of lesions,[60] and hyperfluorescent areas consistent with window defects[88] have been described. In the literature, emphasis has been placed on the presence of hypofluorescent pigment epithelial detachments, which have been histopathologically confirmed to correspond to tumor infiltrates and are considered pathognomonic for this disease (Fig. 8.19).[58,59] It would be misleading to assume, however, that such a finding would be easily identified in most patients with PIOL. In a report of 44 cases of PIOL,[89] the most common FA findings were window defects (54.5%) and hypofluorescent round lesions (34%). Less common findings included vasculitis (13.63%), papilledema (3.7%), and cystoid macular edema (2.46%). Another study[90] showed a lower rate of perivascular staining (4%), a higher rate of optic nerve staining or leakage (41%), a higher rate of cystoid macular edema (21%), and a higher rate of normal results of FA (14%) in the presence of clinical findings.

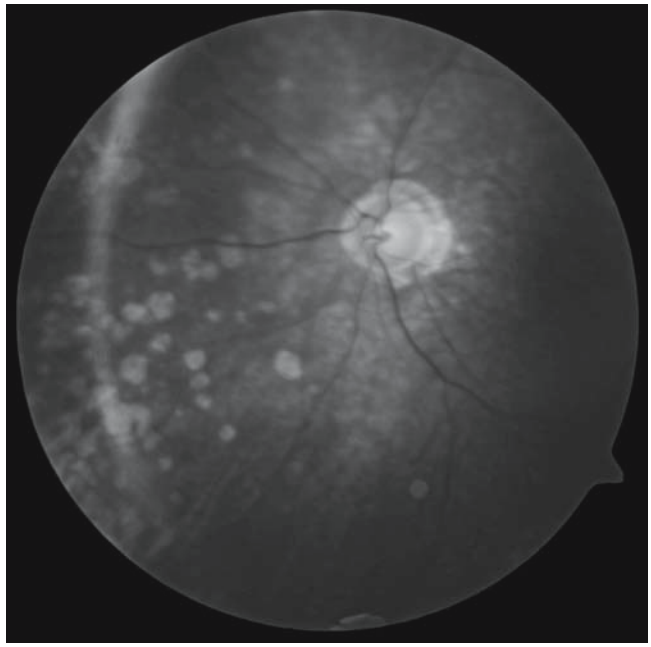

Fig. 8.19. Hypofluorescent pigment epithelial detachments on FA, which have been histopathologically confirmed to correspond to tumor infiltrates and are considered pathognomonic for primary intraocular lymphoma.

Conclusion

Retinal and choroidal angiography frequently provide helpful information in the evaluation of suspected intraocular tumors. Fluorescein angiography is a diagnostic technique used in the interpretation of ocular pathologic states. It allows the sequential visualization of blood flow simultaneously through retinal, choroidal, and iris tissues, and it gives diagnostic support to clinical impressions based on alterations in fluid dynamics resulting from ocular disease processes. The role of FA in patients with an intraocular tumors is largely documentary in nature, but in certain cases it can be of differential diagnostic value. The essential clinical importance of fluorescein angiography in the evaluation of choroidal and retinal tumors appears to be its ability to reveal patterns inconsistent with the presumptive diagnosis rather than to elucidate pathognomonic features. Because of the limitations of FA in imaging the choroidal circulation and associated pathology, investigators have searched for alternative dyes to improve choroidal angiography. The most promising has been ICG dye.

Indocyanine green has several advantages over sodium fluorescein for visualization of choroidal disease. It is recognized that ICG provides better visualization of choroidal

vessels. The dye absorbs and fluoresces in the near infrared range, and visualization of fluorescence is possible through hemorrhage, lipid, RPE, and xanthophylls pigment. Indocyanine green is highly bound to protein, and therefore leaks more slowly through the fenestrations of the choriocapillaris. Indocyanine green has been used to visualize several types of tumors as discussed in this chapter.

This chapter discussed diagnostic tests from the vantage point of the useful and appropriate role of angiography in retinal and choroidal tumors; specifically, how angiography functions in the diagnosis, prognosis, therapy, management, follow-up care, and pathogenesis of these different diseases.

The chapter demonstrated that ICG-V is superior to FA particularly in the assessment of choroidal hemangioma because of specific angiographic features including early hyperfluorescence followed by late hypofluorescence ("washout" of dye) and a hyperfluorescent rim. Indocyanine green videoangiography may therefore be a significant aid in diagnosing difficult cases and preferable to FA in differentiating benign from malignant conditions.

Acknowledgments. This work is supported in part by the Arevalo-Coutinho Foundation for Research in Ophthalmology, Caracas, Venezuela.

References

1. Federman JL. Fluorescein angiography. In: Duane TD, ed. Clinical Ophthalmology. New York: Harper & Row, 1976.
2. Federman JL, Shields JA, Tomer TL. Fluorescein angiography of intraocular tumors. In: Yannuzzi LA, Gitter KA, Schatz H, eds. The Macula. Baltimore: Williams & Wilkins, 1979.
3. Shields JA, McDonald PR. Improvements in the diagnosis of posterior uveal melanomas. Arch Ophthalmol 1974;91:259–264.
4. Snyder WB, Allen L, Frazier O. Fluorescence angiography of ocular tumors. Trans Am Acad Ophthalmol Otolaryngol 1967;71:820.
5. Gass JDM. Fluorescein angiography: an aid in the differential diagnosis of intraocular tumors. Int Ophthalmol Clin 1972;12:85.
6. Gass JDM. Differential Diagnosis of Intraocular Tumors: A Stereoscopic Presentation. St. Louis: CV Mosby, 1974.
7. Federman JL, Shields JA, Tomer TL. Intraocular tumors. In: Yannuzzi LA, Gitter KA, Schatz H, eds. The Macula: A Comprehensive Text and Atlas. Baltimore: Williams & Wilkins, 1979.
8. Augsburger JJ. Fluorescein Angiography of Retinal and Choroidal Tumors Duanes' Ophthalmology on CD-ROM. Philadelphia: Lippincott Williams & Wilkins, 2000.
9. Guyer DR, Yannuzzi LA, Krupsky S, et al. Digital indocyanine-green videoangiography of intraocular tumors. Semin Ophthalmol 1993;8:224–229.
10. Shields CL. Clinical evaluation of choroidal tumors. In: Yannuzzi LA, Flower DW, Slakter JS, eds. Indocyanine Green Angiography. St. Louis: CV Mosby, 1997.
11. Stanga PE, Lim JI, Hamilton P. Indocyanine green angiography in chorioretinal diseases: indications and interpretation. Ophthalmology 2003;110:15–24.
12. Oosterhuis J, von Winning C. Naevus of the choroid. Ophthalmologica 1979;178:156–165.
13. Smith L, Irvine A. Diagnostic significance of orange pigment accumulation over choroidal tumors. Mod Probl Ophthalmol 1974;12:536–543.
14. Augsburger JJ, Schroeder RP, Territo C, et al. Clinical parameters predictive of enlargement of melanocytic choroidal lesions. Br J Ophthalmol 1989;73:911.
15. Pro M, Shields JA, Tomer TL. Serous detachment of the macula associated with presumed choroidal nevi. Arch Ophthalmol 1978;96:1374.
16. Shields JA, Rodrigues MM, Satin LK, et al. Lipofuscin pigment over benign and malignant choroidal tumors. Trans Am Acad Ophthalmol Otolaryngol 1976;81:871.
17. Waltman DD, Gitter KA, Yannuzzi L, Schatz H. Choroidal neovascularization associated with choroidal nevi. Am J Ophthalmol 1978;85:704.
18. Albert DM. The ocular melanoma story LIII Edward Jackson memorial lecture: part II. Am J Ophthalmol 1997;123:729–741.
19. Shields JA, Augsburger JJ, Brown GC, Stephens RF. The differential diagnosis of posterior uveal melanoma. Ophthalmology 1980;87:518–522.
20. Wolter JR, Schut AL, Martonyi CL. Hemangioma-like clinical appearance of collar-button melanoma caused by the strangulation effect of Bruch's membrane. Am J Ophthalmol 1973;76:730.
21. Cantrill HL, Cameron JD, Ramsay RC, Knobloch WH. Retinal vascular changes in malignant melanoma of the choroid. Am J Ophthalmol 1984;97:411.
22. Augsburger JJ, Golden MI, Shields JA. Fluorescein angiography of choroidal malignant melanomas with retinal invasion. Retina 1984;4:232–241.
23. Folberg R, Rummelt V, Parys-Van Ginderdeuren R, et al. The prognostic value of tumor blood vessel morphology in primary uveal melanoma. Ophthalmology 1993;100:1389–1398.
24. Rummelt V, Folberg R, Rummelt C, et al. Microcirculation architecture of melanocytic nevi and malignant melanomas of the ciliary body and choroid. Ophthalmology 1994;101:718–727.
25. McLean I, Keefe K, Burnier M. Uveal melanoma. Comparison of the prognostic value of fibrovascular loops, mean of the ten largest nucleoli, cell type, and tumor size. Ophthalmology 1997;104:777–780.
26. Mueller AJ, Bartsch D-U, Goldbaum M, Bitner D, Weinreb R, Freeman W. Microcirculation pattern of choroidal melanomas using confocal indocyanine green angiography. Ophthalmology 1995;102:161.
27. Edwards W, Layden W, MacDonald R. Fluorescein angiography of malignant melanoma of the choroid. Am J Ophthalmol 1969;68:797–808.
28. Flindall R, Gass J. A histopathologic fluorescein angiographic correlative study of malignant melanomas of the choroid. Can J Ophthalmol 1971;6:258–267.
29. Flower R, Hochheimer B. Clinical infrared absorption angiography of the choroid. Am J Ophthalmol 1972;73:458–459.
30. Flower R, Hochheimer B. A clinical technique and apparatus for simultaneous angiography of the separate retina and choroidal circulations. Invest Ophthalmol 1973;12:248–261.
31. Freeman WR, Bartsch DU, Mueller AJ, Banker AS, Weinreb RN. Simultaneous indocyanine green and fluorescein angiography using a confocal scanning laser ophthalmoscope. Arch Ophthalmol 1998;116:455–463.
32. Holz FG, Bellmann C, Rohrschneider K, Burk RO, Volcker HE. Simultaneous confocal scanning laser fluorescein and indocyanine green angiography. Am J Ophthalmol 1998;125:227–236.

33. Mueller AJ, Freeman WR, Schaller UC, Kampik A, Folberg R. Complex microcirculation patterns detected by confocal indocyanine green angiography predict time to growth of small choroidal melanocytic tumors: MuSIC Report II. Ophthalmology 2002;109:2207–2214.
34. Albert DM, Niffenegger AS, Willson JKV. Treatment of metastatic uveal melanoma: review and recommendation. Surv Ophthalmol 1992;36:429–438.
35. Mueller AJ, Bartsch DU, Folberg R, et al. Imaging the microvasculature of choroidal melanomas with confocal indocyanine green scanning laser ophthalmoscopy. Arch Ophthalmol 1998;116:31–39.
36. Mueller AJ, Freeman WR, Folberg R, et al. Evaluation of microvascularisation pattern visibility in human choroidal melanomas: comparison of confocal fluorescein with indocyanine green angiography. Graefes Arch Clin Exp Ophthalmol 1999;237:448–456.
37. Sallet G, Amoaku WMK, Lafaut BA, Brabant P, De Laey JJ. Indocyanine green angiography of choroidal tumors. Graefes Arch Clin Exp Ophthalmol 1995;233:677–689.
38. Guyer DR, Orlock DA. Digital indocyanine green videoangiography and choroidal neovascularisation. Retina 1992;12:191–223.
39. Gass JDM. Stereoscopic Atlas of Macular Diseases. Diagnosis and Treatment, 4th ed. St. Louis: Mosby, 1997:208–213.
40. Shields JA, Shields CL. Atlas of Intraocular Tumors. Philadelphia: Lippincott Williams & Wilkins, 1999:170–179.
41. Shields JA, Shields CL. Intraocular Tumors: A Text and Atlas. Philadelphia: Saunders, 1992:239–260.
42. Witschel H, Font RL. Hemangioma of the choroid. A clinicopathologic study of 71 cases and a review of the literature. Surv Ophthalmol 1976;20:415–431.
43. Norton EWD, Gutman F. Fluorescein angiography and hemangiomas of the choroid. Arch Ophthalmol 1967;78:121–125.
44. Anand R, Augsburger JJ, Shields JA. Circumscribed choroidal hemangiomas. Arch Ophthalmol 1989;107:1338–1342.
45. Arevalo JF, Shields CL, Shields JA, et al. Circumscribed choroidal hemangioma: characteristic features with indocyanine green videoangiography. Ophthalmology 2000;107:344–350.
46. Piccolino FC, Borgia L, Zinicola E. Indocyanine green angiography of circumscribed choroidal hemangiomas. Retina 1996;16:19–28.
47. Shields CL, Shields CL, De Potter P. Patterns of indocyanine green videoangiography of choroidal tumours. Br J Ophthalmol 1995;79:237–245.
48. Roach ES. Diagnosis and management of neurocutaneous syndromes. Semin Neurol 1985;9:91–141.
49. Font RL, Ferry AP. The phakomatoses. Int Opthalmol Clin 1972;12:1–50.
50. Kallay O Jr, Boucquey D, Maes E, Brucher JM. Sturge-Weber syndrome: a propos of an anatomico-clinical case report with prepapillary glial proliferation. Bull Soc Belge Opthalmol 1992;243:17–22.
51. Alexander GL. Sturge-Weber syndrome. In: Vinken B, ed. Handbook of Clinical Neurology, Vol 14. Amsterdam: North Holland, 1972:223–240.
52. Bains HS, Cirino AC, Ticho BH, Jampol LM. Photodynamic therapy using verteporfin for a diffuse choroidal hemangioma in Sturge-Weber syndrome. Retina 2004;24:152–155.
53. Gass JDM. Photocoagulation of macular lesions. Trans Am Acad Ophthalmol Otolaryngol 1971;75:580–608.
54. Gass JDM. Stereoscopic Atlas of Macular Diseases: Diagnosis and Treatment, 2nd ed. St. Louis: CV Mosby, 1977:130–193.
55. Wen F, Wu D. Indocyanine green angiographic findings in diffuse choroidal hemangioma associated with Sturge-Weber syndrome. Graefes Arch Clin Exp Ophthalmol 2000;238:625–627.
56. Ferry AP, Font RL. Carcinoma metastatic to the eye and orbit. I. A clinicopathologic study of 227 cases. Arch Ophthalmol 1974;92:276.
57. Stephens RF, Shields JA. Diagnosis and management of cancer metastatic to the uvea: a study of 70 cases. Ophthalmology 1979;86:1336.
58. Gass JD, Sever RJ, Grizzard WS, et al. Multifocal pigment epithelial detachments by reticulum cell sarcoma. A characteristic funduscopic picture. Retina 1984;4:135–143.
59. Dean JM, Novak MA, Chan CC, Green WR. Tumor detachments of the retinal pigment epithelium in ocular/central nervous system lymphoma. Retina 1996;16:47–56.
60. Kirmani MH, Thomas EL, Rao NA, Laborde RP. Intraocular reticulum cell sarcoma: diagnosis by choroidal biopsy. Br J Ophthalmol 1987;71:748–752.
61. Ridley ME, McDonald HR, Sternberg P Jr, Blumenkranz MS, Zarbin MA, Schachat AP. Retinal manifestations of ocular lymphoma (reticulum cell sarcoma). Ophthalmology 1992;99:1153–1160.
62. Shields CL, Shields JA, De Potter P. Patterns of indocyanine green videoangiography of choroidal tumours. Br J Ophthalmol 1995;79:237–245.
63. Krause L, Bechrakis NE, Kreusel KM, Servetopoulou F, Heinrich S, Foerster MH. [Indocyanine green angiography in choroid metastases.] Ophthalmologe 2002;99:617–619.
64. Gass JDM, Guerry RK, Jack RL, Harris G. Choroidal osteoma. Arch Ophthalmol 1978;96:428–435.
65. Shields CL, Shields JA, Augsberger JJ. Choroidal osteoma. Surv Ophthalmol 1988;33:17–27.
66. Aylward GW, Chang TS, Pautler SE, Gass DM. A long-term follow-up of choroidal osteoma. Arch Ophthalmol 1998;116:1337–1341.
67. Lafaut BA, Mestdagh C, Kohno T, Gaudric A, De Laey JJ. Indocyanine green angiography in choroidal osteoma. Graefes Arch Clin Exp Ophthalmol 1997;235:330–337.
68. Lafaut BA, Mestdagh C, Kohno T, et al. Indocyanine green angiography in choroidal osteoma. Graefes Arch Clin Exp Ophthalmol 1997;235:330–337.
69. Yuzawa M, Kawamura A, Haruyama M, Matsui M. Indocyanine green video-angiographic findings in choroidal osteoma. Eur J Ophthalmol 1994;4:191–198.
70. Kadrmas EF, Weiter JJ. Choroidal osteoma. Int Ophthalmol Clin 1997;37:171–182.
71. Moore AT, Maher ER, Rosen P, et al. Ophthalmological screening for von Hippel–Lindau disease. Eye 1991;5:723–728.
72. Salazar FG, Lamiell JM. Early identification of retinal angiomas in a large kindred with von Hippel–Lindau disease. Am J Ophthalmol 1980;89:540–545.
73. Schindler RF, Sarin LK, MacDonald PR. Hemangiomas of the optic disc. Can J Ophthalmol 1975;10:305–318.
74. Augsburger JJ, Shields JA, Goldberg RE. Classification and management of hereditary retinal angiomas. Int Ophthalmol 1981; 4:93.
75. Niccol W, Moore RF. A case of angiomatosis retinae. Br J Ophthalmol 1934;18:454–457.
76. Gass JD. Cavernous hemangioma of the retina: a neuro-oculocutaneous syndrome. Am J Ophthalmol 1971;71:799–814.
77. Shields JA, Shields CL. Vascular tumors of the retina and optic disc. In: Shields JA, Shields CL, eds. Intraocular Tumors: A Text and Atlas. Philadelphia: WB Saunders, 1992.
78. Hewick S, Lois N, Olson JA. Circumferential peripheral retinal cavernous hemangioma. Arch Ophthalmol 2004;122:1557–1560.

79. Irvine F, O'Donnell N, Kemp E, Lee WR. Retinal vasoproliferative tumors: surgical management and histological findings. Arch Ophthalmol 2000;118:563–569.
80. Heimann H, Bornfeld N, Vij O, et al. Vasoproliferative tumors of the retina. Br J Ophthalmol 2000;84:1162–1169.
81. Shields CL, Shields JA, Barrett J, De Potter P. Vasoproliferative tumors of the ocular fundus. Classification and clinical manifestations in 103 patients. Arch Ophthalmol 1995;113:615–623.
82. Gottlieb F, Fammartino JJ, Stratford TP, Brockhurst RJ. Retinal angiomatous mass. A complication of retinal detachment surgery. Retina 1984;4:152–157.
83. Barbezetto IA, Smith RT. Vasoproliferative tumor of the retina treated with PDT. Retina 2003;23:565–567.
84. Whitcup SM, de Smet MD, Rubin BI, et al. Intraocular lymphoma. Clinical and histopathologic diagnosis. Ophthalmology 1993;100:1399–1406.
85. Hochberg FH, Miller DC. Primary central nervous system lymphoma. J Neurosurg 1988;68:835–853.
86. Freeman LN, Schachat AP, Knox DL, Michels RG, Green WR. Clinical features, laboratory investigations, and survival in ocular reticulum cell sarcoma. Ophthalmology 1987;94:1631–1639.
87. Velez G, de Smet MD, Whitcup SM, Robinson M, Nussenblatt RB, Chan CC. Iris involvement in primary intraocular lymphoma: report of two cases and review of the literature. Surv Ophthalmol 2000;44:518–526.
88. Kuming BS, Fritz VU, Bezwoda WR. Ocular reticulum cell sarcoma. A case report. S Afr Med J 1988;73:49–53.
89. Cassoux N, Merle-Beral H, Leblond V, et al. Ocular and central nervous system lymphoma: clinical features and diagnosis. Ocul Immunol Inflamm 2000;8:243–250.
90. Velez G, Chan CC, Csaky KG. Fluorescein angiographic findings in primary intraocular lymphoma. Retina 2002;22:37–43.

9
Angiography in Pharmacologic Retinal Toxicity

Stephen G. Schwartz and William F. Mieler

Retinal angiography, specifically fluorescein angiography (FA), is important for the diagnosis and follow-up of pharmacologic retinal toxicity. At this time, there does not appear to be a significant role for indocyanine green (ICG) videoangiography, and even the role of optical coherence tomography (OCT) for these conditions is very limited. Fluorescein angiography appears to be particularly helpful in early cases of possible toxicity where the clinical findings may be mild. Early diagnosis is beneficial, as prompt discontinuation of the offending agent may on occasion reduce the risk of permanent vision loss.

Toxicity with Diffuse Retinal Changes

Toxicity with Pigmentary Degeneration

Quinolines

Chloroquine (Aralen, Sanofi Winthrop Pharmaceuticals, New York, NY) and hydroxychloroquine (Plaquenil, Sanofi Winthrop Pharmaceuticals, New York, NY) are quinoline antimalarials. In the United States, they are primarily used in the management and treatment of various autoimmune diseases, especially rheumatoid arthritis and systemic lupus erythematosus (SLE).

Quinoline toxicity typically follows a well-described course, in which objective clinical changes precede subjective visual disturbance.[1–4] Although FA is not always necessary to make the diagnosis,[5] it remains quite useful for documentation purposes and for clinically borderline situations. In early cases, there is a loss of the foveal light reflex with no definite FA changes. This may progress to nonspecific macular pigmentary alterations, with associated transmission hyperfluorescence (window defects) on FA (Fig. 9.1). The classic bull's-eye lesion develops in fairly advanced cases (Figs. 9.2 and 9.3). In the end stage, a retinitis pigmentosa (RP)-type picture may develop, with diffuse pigmentary changes, vascular attenuation, and optic atrophy (Fig. 9.4). While retinal toxicity is more common with chloroquine, it does occasionally occur with hydroxychloroquine alone (Fig. 9.5).

Additional adjunctive tests include the Amsler grid,[6] automated perimetry,[7] and color vision testing,[8] though the role of these tests in the diagnosis and management of toxicity is limited. There is a yet to be fully defined role for electroretinography (ERG),[9] multifocal ERG (mfERG),[10] and OCT.[11]

Early retinopathy typically stabilizes or resolves upon discontinuation of the agent, although advanced cases oftentimes progress.[12] Because of the unusually long clearance time of these agents,[13] occasional patients develop toxicity years after discontinuation of the medication[13] (Fig. 9.6).

The American Academy of Ophthalmology (AAO) recommended guidelines for monitoring patients on hydroxychloroquine therapy.[14] Suggested at the initiation of quinoline therapy is a baseline ocular examination consisting of a dilated posterior segment examination, along with Amsler grid testing or automated perimetry.[15] Baseline fundus photography and FA are not routinely indicated, but may be useful in patients with preexisting macular pigmentary changes. Patients are classified as being at a higher risk of developing toxicity if they exceed 3 mg/kg/day of chloroquine or 6.5 mg/kg/day of hydroxychloroquine, have been on medication in excess of 5 years, have a high fat level body habitus, have renal or liver disease, or are older than 60 years of age. These patient's need to be monitored more closely; otherwise, patients can be followed as recommended by the AAOs Preferred Practice Pattern.[16] However, obese patients require additional monitoring because quinolines are stored to a greater degree in lean body tissues than in fat. When determining an individual patient's risk of toxicity, the dose should be calculated based on ideal weight rather than actual weight.[17] If signs of toxicity develop, the medication should be discontinued, as toxicity may progress even after the medication has been discontinued.

Quinine

The related compound quinine (Quinamm, Marion Merrell Dow, Inc., Kansas City, MO) is associated with a distinct toxicity. Quinine is prescribed for benign nocturnal muscle cramps, and may cause toxicity with acute overdose. The syndrome is characterized by headache, nausea, vomiting, tremor, hypotension,

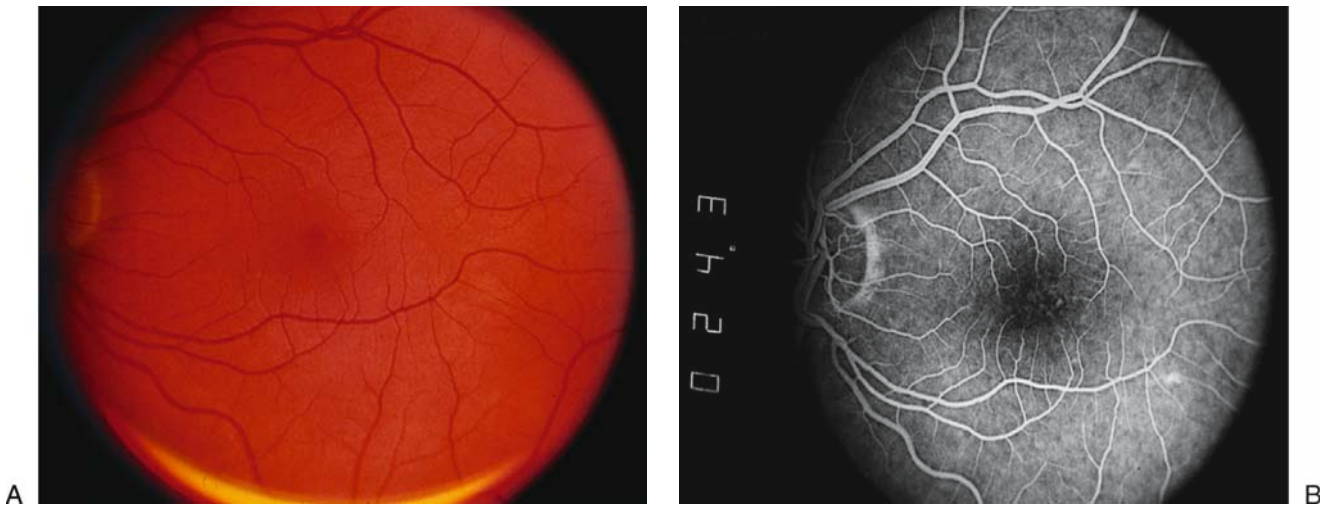

FIG. 9.1. (A) Color photograph of the left eye (OS) shows subtle retinal pigmentary changes along the temporal border of the macula in a patient on chloroquine. (B) Fluorescein angiography (FA) shows transmission defects corresponding to the areas of retinal pigment mottling.

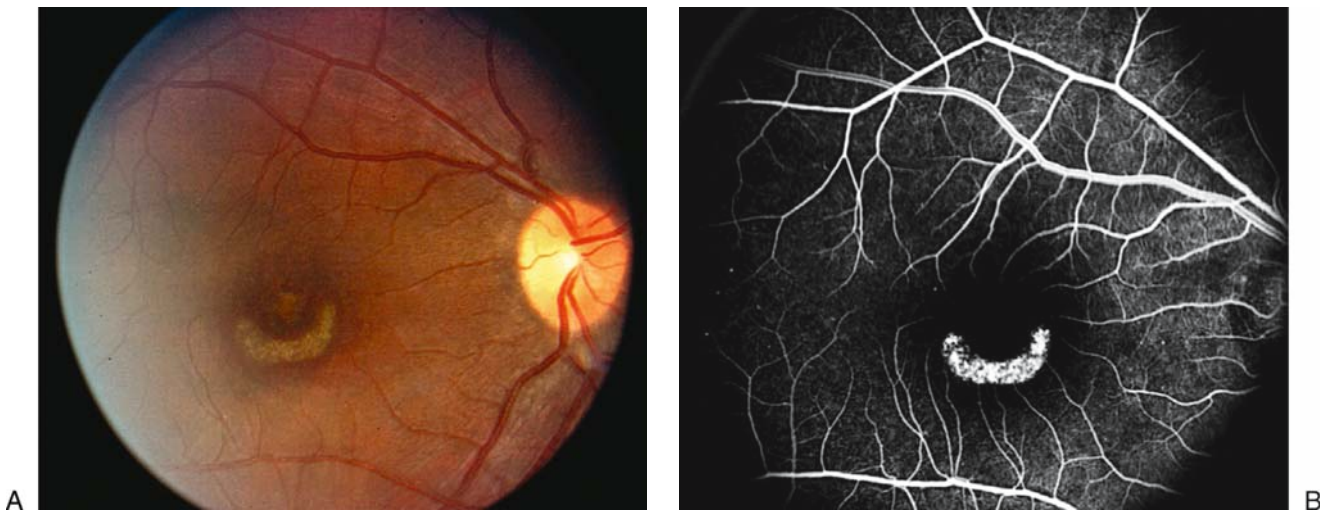

FIG. 9.2. (A) Color photograph of the right eye (OD) shows a partial (inferior) bull's-eye lesion in a patient on chloroquine. (B) Fluorescein angiography reveals a transmission defect corresponding to the area of retinal pigment atrophy.

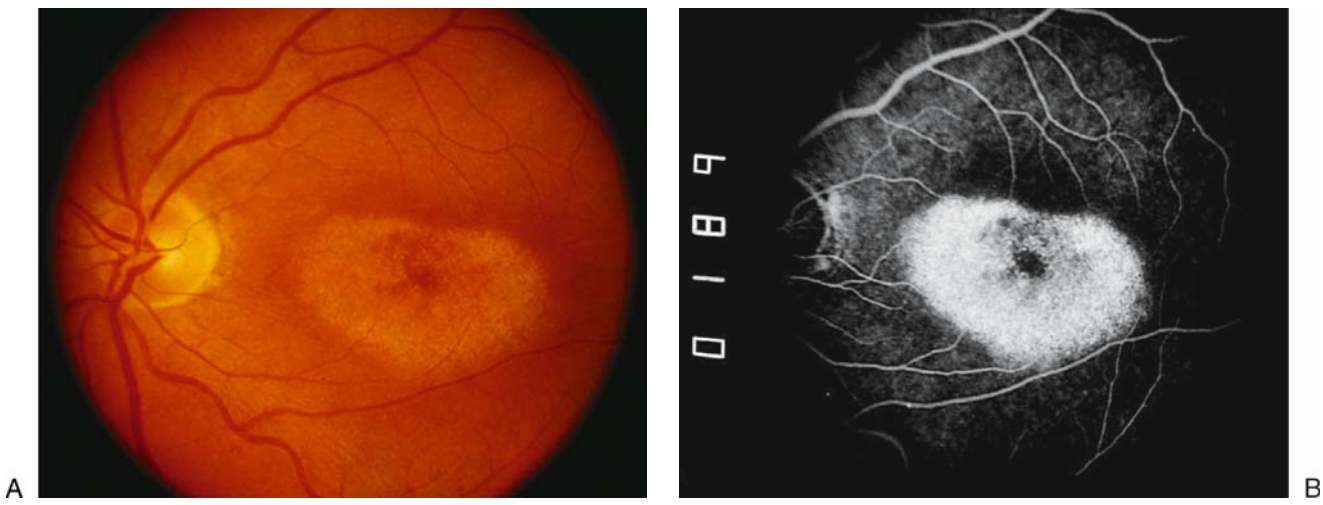

FIG. 9.3. (A) Color photograph OS documents a complete bull's-eye lesion in a patient on chloroquine, who had lost central vision. (B) Fluorescein angiography shows a transmission defect corresponding to the area of central retinal pigment atrophy.

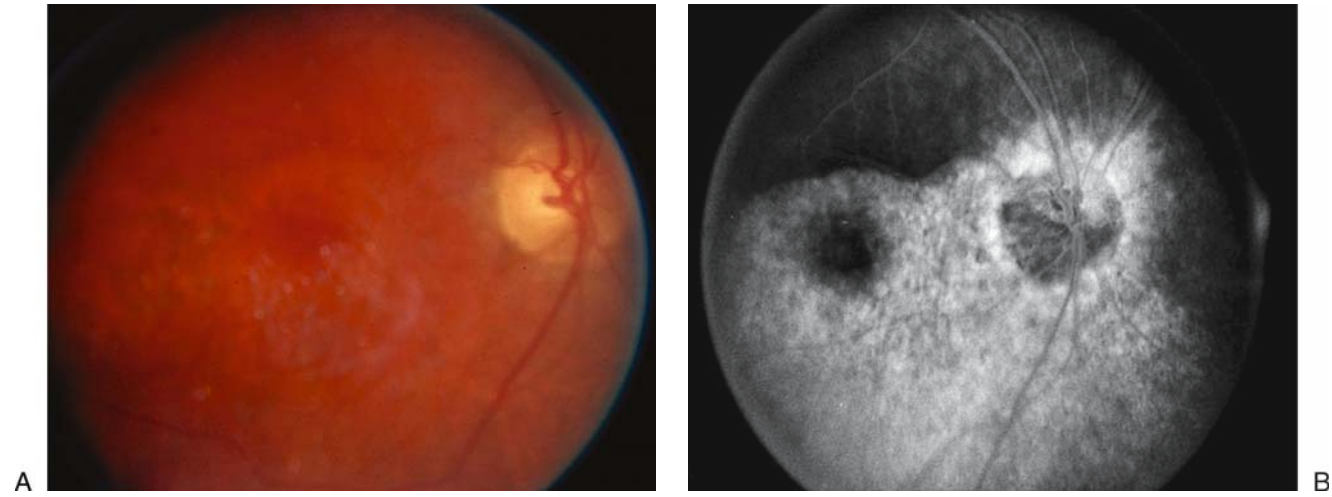

FIG. 9.4. (A) Color photograph OD shows extensive, diffuse retinal pigment atrophy, disc pallor, and vascular attenuation in a patient on long-standing chloroquine therapy. The area of pigment atrophy extends far beyond the area of the macula. (B) Fluorescein angiography documents the extensive transmission defect corresponding to the area of retinal pigment atrophy.

and loss of consciousness associated with profound vision loss, which may be irreversible.[18]

Acutely, there is mild retinal edema with mild venous dilation. Over several weeks, arteriolar attenuation and optic atrophy develop (Fig. 9.7). There may also be a mild degree of diffuse retinal pigment mottling. The FA may show minimal changes or may be normal.[19] More pronounced abnormalities may be documented on perimetry, ERG, mfERG, electro-oculography (EOG), dark adaptometry, and visual evoked potentials (VEPs).[20,21] Acutely, hemodialysis may be beneficial in the treatment of an overdose. Visual outcomes, however, are extremely variable.

Phenothiazines

The phenothiazines are antipsychotic agents whose use in the United States has declined over the years. Of the phenothiazines, the most toxic potential is found in the piperidines, particularly with thioridazine (Mellaril, Sandoz Pharmaceuticals, East Hanover, NJ).

Toxicity manifests as decreased vision, nyctalopia, and dyschromatopsia (red or brown).[22] Mild, nonspecific macular pigmentary changes are seen initially (Fig. 9.8), and may be followed by salt-and-pepper pigmentary loss (Fig. 9.9). This pattern of pigment loss may coalesce into broader zones of

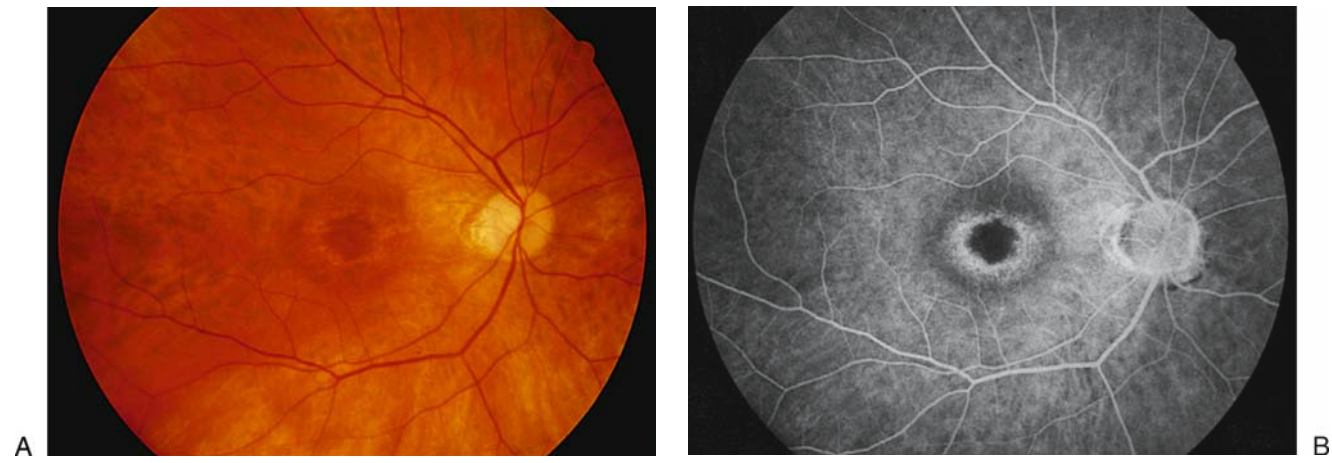

FIG. 9.5. (A) Color photograph OD of a patient on hydroxychloroquine for rheumatoid arthritis. The patient had never been on chloroquine. The patient was frail, weighing only 100 lb, and the dose of hydroxychloroquine exceeded the recommended daily dose. (B) Fluorescein angiography documents a transmission defect corresponding to the zone of retinal pigment atrophy seen on clinical examination.

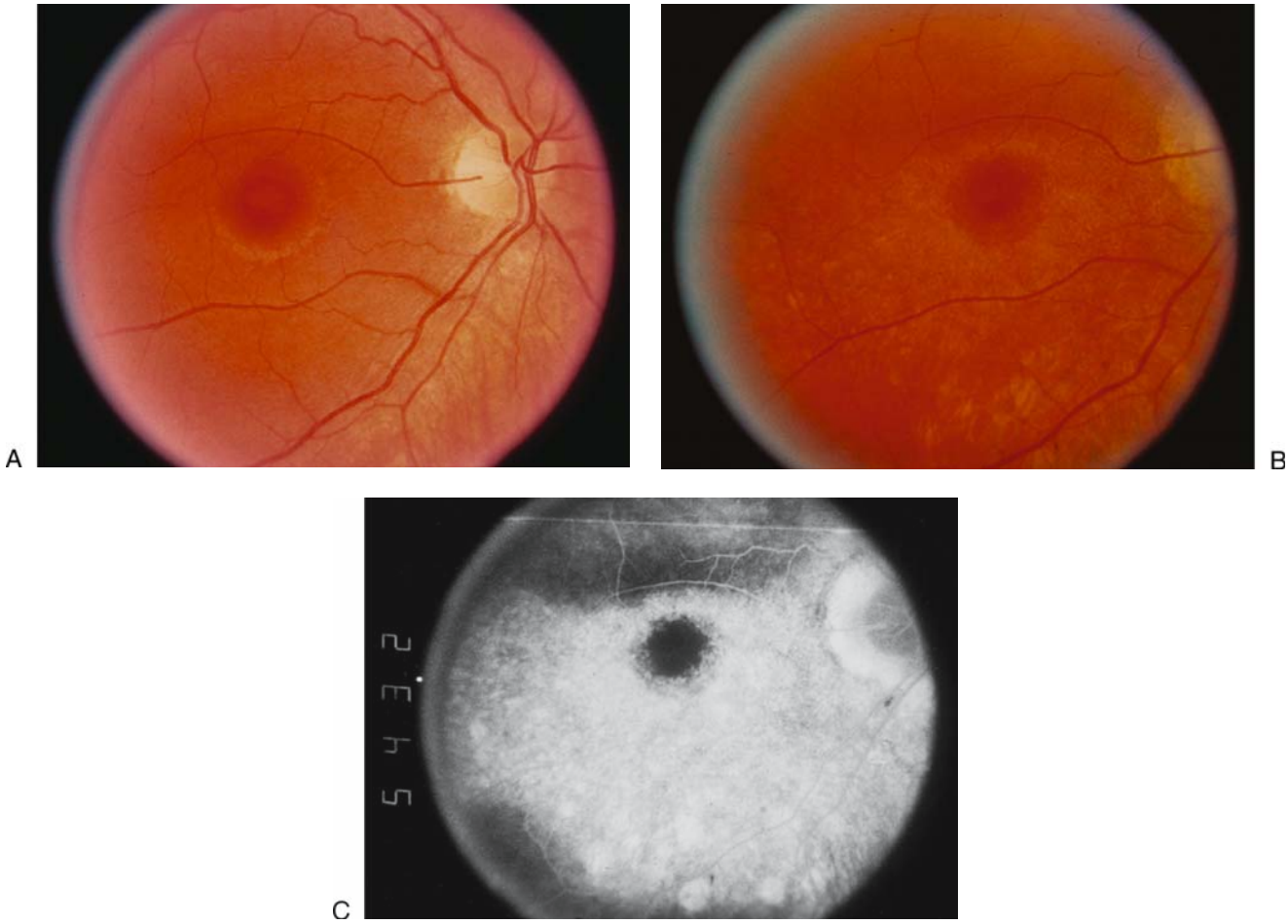

FIG. 9.6. (A) Color photograph OD showing a bull's-eye lesion in a patient on chloroquine. The medication was discontinued, and there was no further exposure to quinoline medications. (B) Two years later, the patient returned, describing loss of central vision. There had been progressive loss of retinal pigmentation extending far beyond the macular region. (C) Fluorescein angiography reveals a prominent transmission defect corresponding to the area of retinal pigment atrophy.

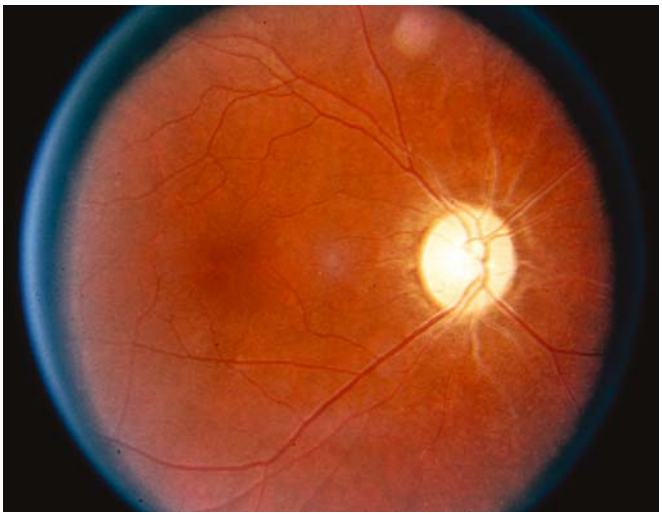

FIG. 9.7. Color photograph of a patient 2 months following quinine ingestion in an attempted suicide. Note the profound optic atrophy, along with the vascular attenuation and very slight retinal pigment mottling. Minimal vision returned, as the patient was left with light perception acuity.

FIG. 9.8. Color photograph OD shows mild retinal pigment clumping temporal to the macula in a patient on thioridazine.

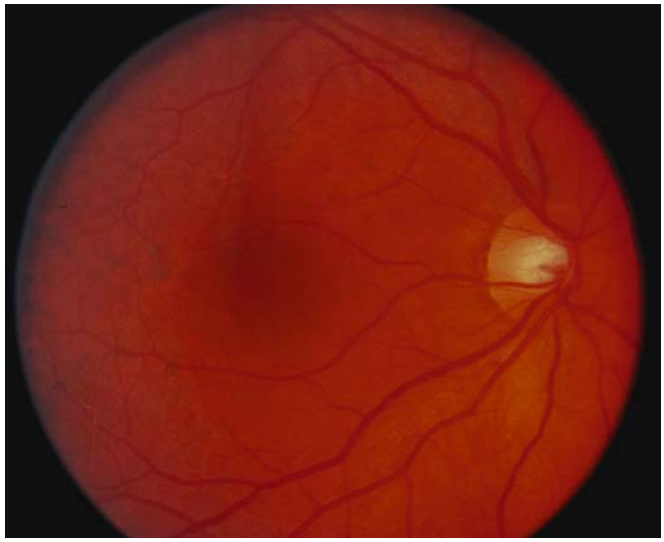

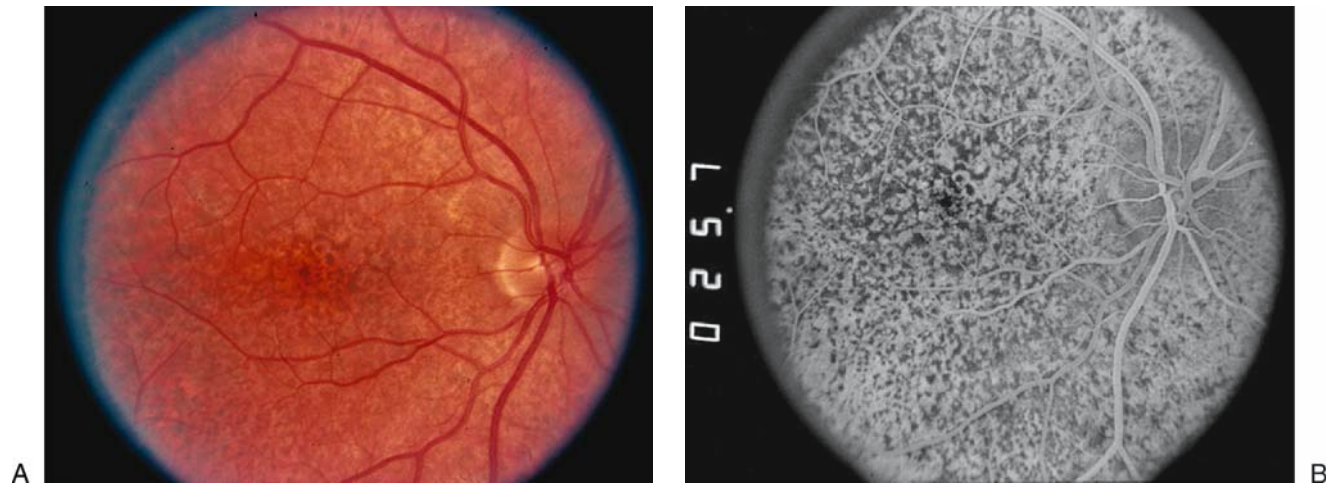

FIG. 9.9. (A) Color photograph OD reveals a salt-and-pepper pattern of pigmentary change in a patient on long-term thioridazine therapy. (B) Fluorescein angiography documents the very prominent pattern of transmission defects interspersed with areas of blocked fluorescence due to pigment clumping (salt-and-pepper pattern).

atrophy (Fig. 9.10) and eventually be followed by nummular areas of loss of the retinal pigment epithelium and choriocapillaris[23] (Fig. 9.11). In severe cases, generalized changes may occur, including vascular attenuation, optic atrophy, and diffuse pigmentary alterations, with virtually a complete loss of the choriocapillaris and retinal pigment epithelium[24] (Fig. 9.12). This end result may appear similar to the condition of choroideremia. The pigmentary disturbance is even more apparent with FA. Adjunctive tests include perimetry, ERG, dark adaptometry, and EOG,[25] although they are of limited value in establishing the diagnosis or in monitoring disease progression.

Discontinuation of the agent may allow for spontaneous improvement on rare occasion, though more commonly visual loss remains or even progresses. This is felt to be secondary to a continued decline in function of the previously damaged cells, rather than a prolonged effect of the medication.[26] Therefore, if a patient is found to have retinal pigmentary disturbance due to thioridazine, the medication should be discontinued.

Deferoxamine

Deferoxamine (desferrioxamine, Desferal, Novartis, East Hanover, NJ) is a chelator of iron and aluminum. The drug prevents toxicity from these elements in patients receiving repeated blood transfusions. Toxicity consists of decreased vision, nyctalopia, and visual field loss. The most common presenting sign is a gray discoloration of the macula, which progresses to diffuse pigmentary changes (Fig. 9.13). In some patients, however, FA abnormalities (early blocked fluorescence, late staining) may precede ophthalmoscopic findings.[27]

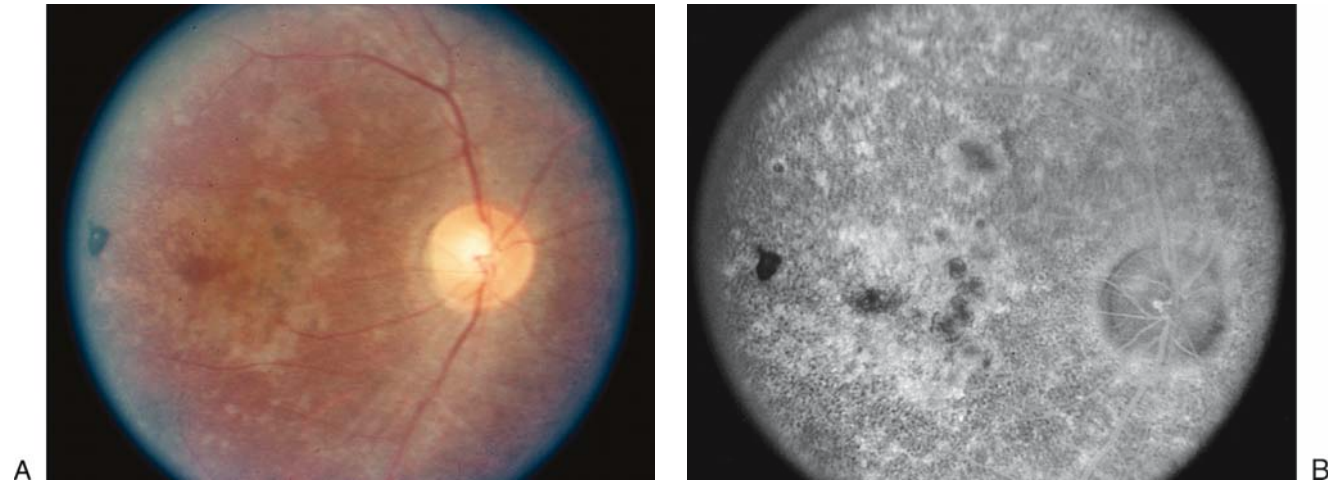

FIG. 9.10. (A) Color photograph OD from a patient on long-term thioridazine shows coalesced areas of retinal pigment atrophy, interspersed with areas of pigment clumping. (B) Fluorescein angiography reveals prominent transmission defects, along with areas of blocked fluorescence corresponding to the appearance of the retinal pigment epithelium.

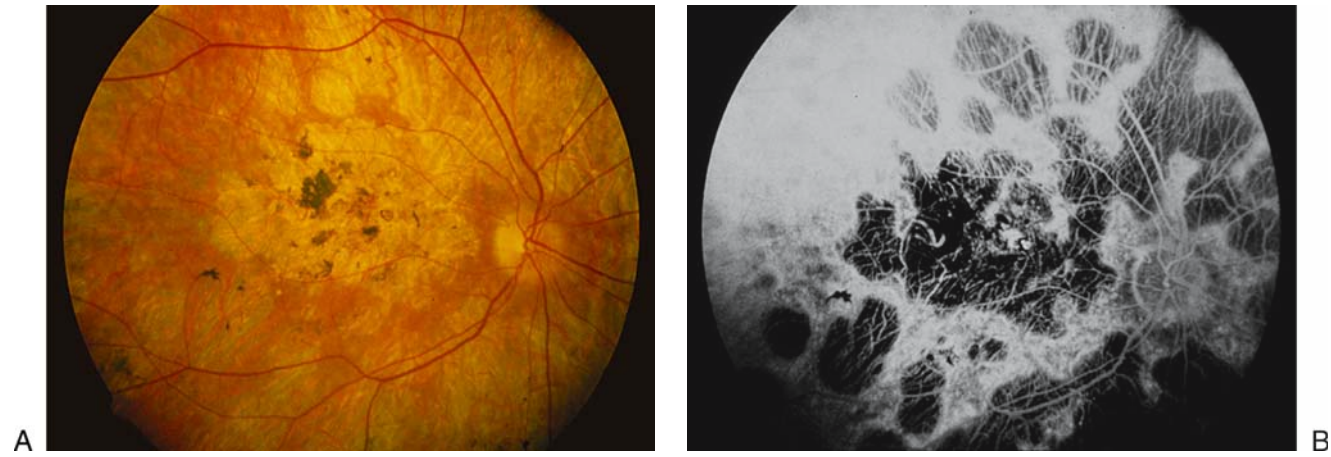

FIG. 9.11. (A) Color photograph OD reveals widespread loss of the retinal pigment in a nummular pattern. (B) Fluorescein angiography documents zones of absent fluorescence, indicative of loss of the underlying choriocapillaris in the areas where the retinal pigment epithelium was also absent.

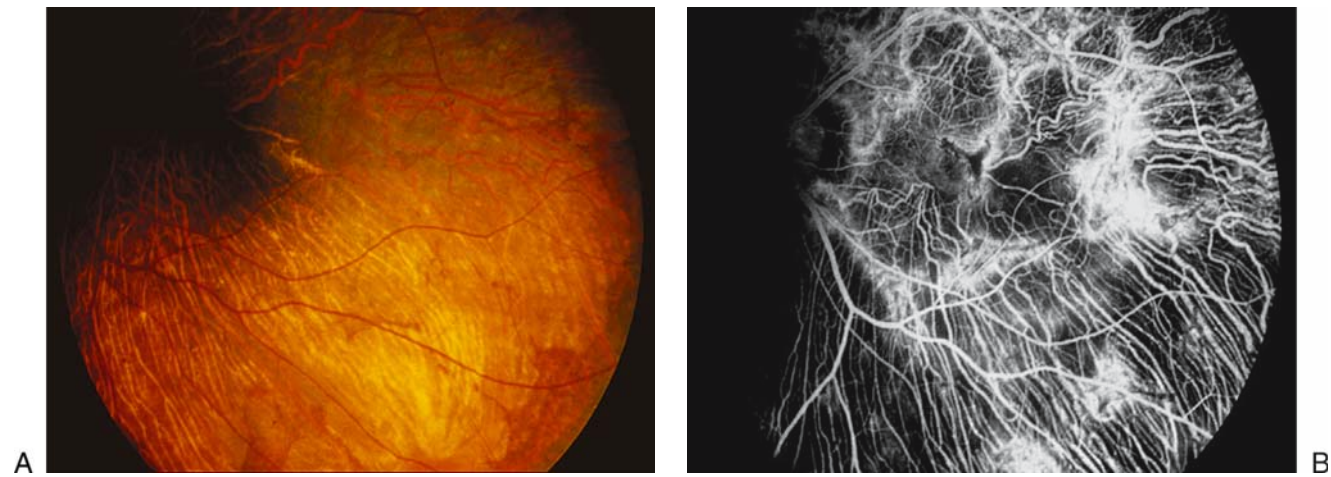

FIG. 9.12. (A) Color photograph OS shows complete loss of the retinal pigment, allowing visualization of the underlying choroidal vessels. (B) Fluorescein angiography documents loss of choriocapillaris. Large choroidal vessels are very readily seen.

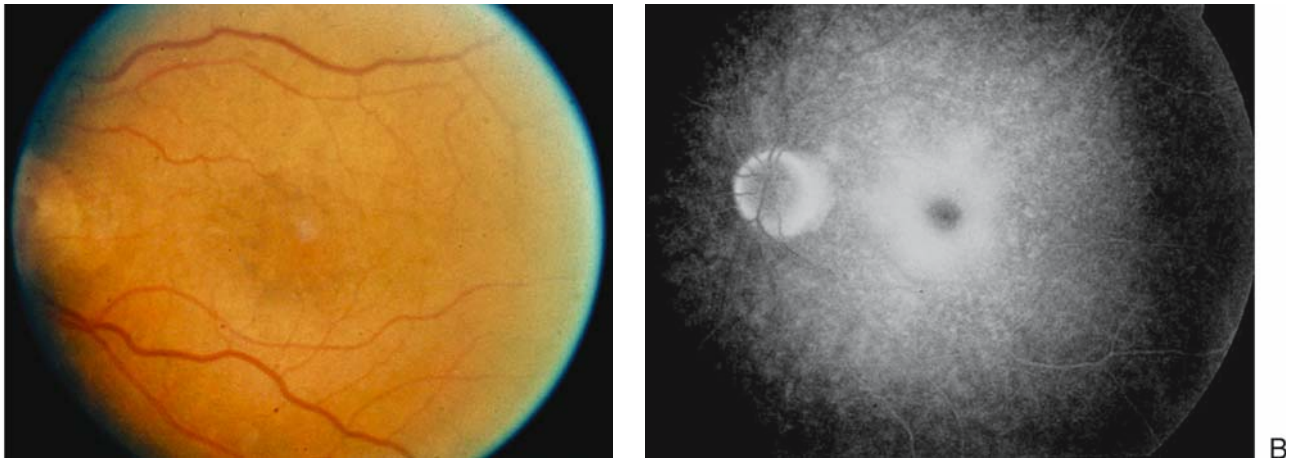

FIG. 9.13. (A) Color photograph OS shows macular pigment mottling in a patient being treated with deferoxamine. (B) Fluorescein angiography documents a transmission defect, along with mild macular leakage.

Abnormalities also may be noted with color vision testing, perimetry, ERG, EOG, and dark adaptometry.[28] Vision loss may persist despite discontinuation of the medication,[29] and toxicity may occur from a single dose.[30]

Toxicity with Crystalline Deposits

Tamoxifen

Tamoxifen (Nolvadex, AstraZeneca, Wilmington, DE), an estrogen antagonist, is primarily used in the management of metastatic breast adenocarcinoma. Toxicity in the form of retinal crystals may be asymptomatic, or may cause mild central visual impairment along with dyschromatopsia.[31] These latter two visual symptoms generally occur secondary to development of cystoid macular edema (CME).

White refractile deposits (crystals) are noted in the posterior pole generally in a circular pattern surrounding the macular region (Fig. 9.14), and may be associated with mild pigmentary changes. In advanced cases, CME may also develop. Fluorescein angiography or OCT are utilized to confirm the presence of CME, though the crystals are not seen on FA.

Asymptomatic patients with retinal crystals may be monitored. Most patients may be continued on the medication, as it is needed in the treatment of their metastatic breast adenocarcinoma. Patients with documented vision loss or CME, however, should discontinue the agent to limit or prevent permanent visual compromise.[32] It is estimated that approximately 2% to 3% of patients on the recommended therapeutic dose of tamoxifen develop retinal crystals.

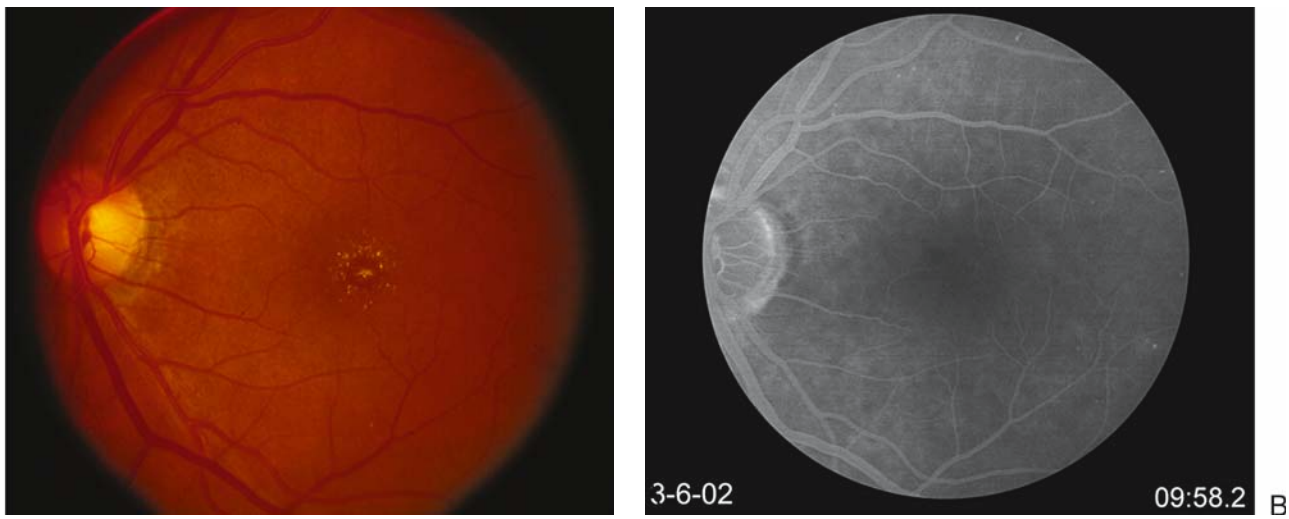

FIG. 9.14. (A) Color photograph shows a small ring of retinal crystals surrounding the macular region in a patient being treated with tamoxifen. The patient was visually asymptomatic. (B) Fluorescein angiography shows no macular abnormality. (Courtesy of Eric R. Holz, MD, Houston, TX.)

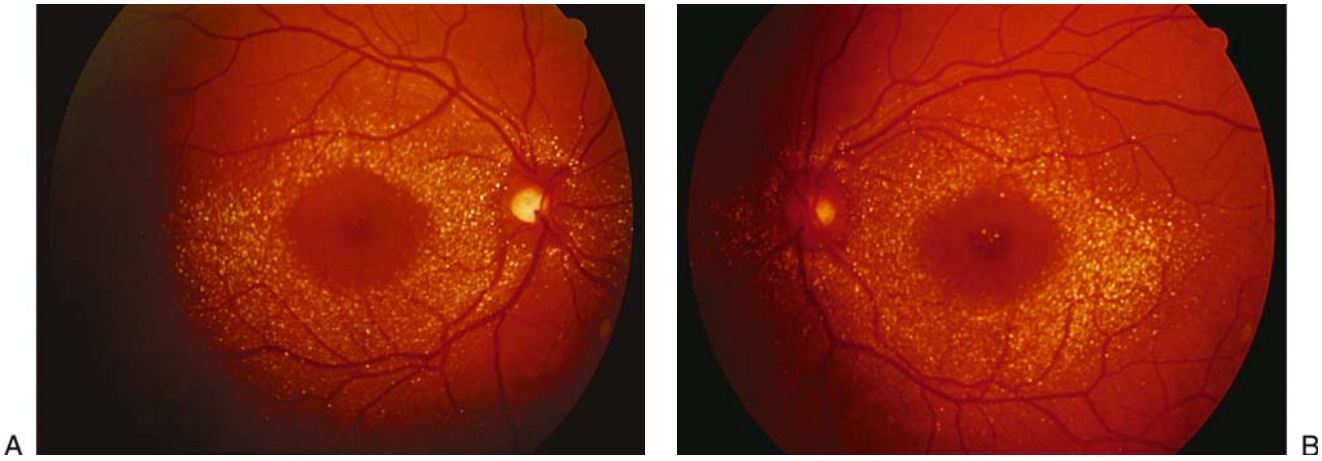

Fig. 9.15. Color photographs OD (A) and OS (B) from a patient who consumed canthaxanthine for sun-tanning purposes. The patient was visually asymptomatic with visual acuity of 20/20 in both eyes. The patient was encouraged to discontinue the medication. (Courtesy of Scott R. Sneed, MD, Traverse City, MI.)

Canthaxanthine

Canthaxanthine (Orobronze, Dewitte, Greenville, SC) is a carotenoid pigment prescribed for vitiligo and photosensitivity disorders. Ocular abnormalities are rarely seen when canthaxanthine is utilized in the treatment of these conditions. In some countries, the drug is marketed as an over-the-counter oral sun-tanning agent. Toxicity is characterized by an asymptomatic ring of yellow-orange crystals in the macular region[33] (Fig. 9.15). The FA is usually normal, but abnormalities may occur on perimetry, ERG, EOG, or dark adaptometry.[34]

When retinal crystals are seen on clinical examination, it is recommended that the patient discontinue the medication, as it is generally not being employed for a true medical indication. Upon discontinuation of the agent, the crystals generally resorb slowly, with corresponding improvement in electrophysiologic parameters.[35]

Methoxyflurane

The inhalational anesthetic methoxyflurane (Penthrane) is rarely used today in the United States, because of associated potential renal toxicity, which can lead to a form of secondary hyperoxaluria. This is mediated by deposition of calcium oxalate crystals in the renal tubules.[36] In a similar fashion, yellow-white punctate crystals may be found in the macular region or filling the retinal arterioles (Fig. 9.16). The deposits do not show hyperfluorescence on FA.[37,38]

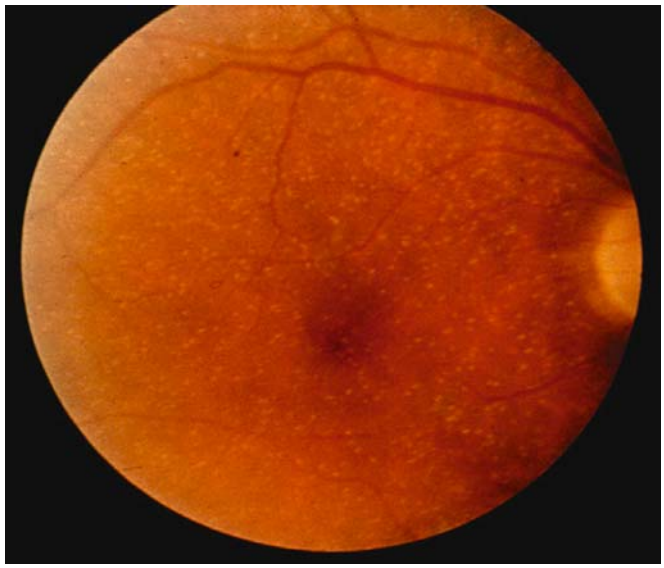

Fig. 9.16. Color photograph OD of a patient who underwent a prolonged surgical procedure in which methoxyflurane was used as one of the anesthetic agents. Renal failure ensued, and methoxyflurane-induced retinal crystals were seen dispersed throughout the posterior pole of both eyes.

Toxicity Without Fundus Changes

Cardiac Glycosides

Xanthopsia from foxglove (*Digitalis purpurea*) has been noted for almost 300 years.[39] Modern cardiac glycosides, including digoxin (Lanoxin, GlaxoSmithKline, Research Triangle Park, NC), are structurally similar and may cause the same toxicity. Visual acuity may be reduced, and color vision is usually diminished. Fundus examination, FA, and EOG are typically normal, although the ERG may show characteristic depressions during toxic episodes.[40]

Sildenafil

The widely used erectile dysfunction agent sildenafil (Viagra, Pfizer, New York, NY) is an inhibitor of phosphodiesterase 5 (PDE-5) in the penile corpora cavernosa, but demonstrates cross-activity with the PDE-6 in the photoreceptors.[41]

A single dose may cause transient and reversible dyschromatopsia,[42,43] though symptoms are generally dose-related. Typically, the funduscopic examination and FA are normal, but rare reported complications include retinal hemorrhages, retinal vascular occlusion,[44] nonarteritic anterior ischemic optic neuropathy,[45] acceleration of proliferative diabetic retinopathy,[46] and central serous chorioretinopathy.[47] Changes commensurate with the above noted diagnoses may be seen on FA or OCT.

More reproducible abnormalities, even in asymptomatic subjects, include transient depressions in ERG and mfERG.[48]

In most cases, sildenafil appears to cause no apparent long-term retinal damage,[49] although individuals with preexisting retinal disease may be at increased risk.[50]

Toxicity with Retinal Edema

Methanol

Methanol, while not prescribed for consumption, is occasionally accidentally ingested, or used in an attempt to commit suicide. Significant vision loss is typical, with development of acute retinal and optic disc edema (Fig. 9.17), leading to eventual optic atrophy, with corresponding FA changes.[51,52] The visual prognosis as well as prognosis for life correlates quite closely with the extent of systemic acidosis. Abnormalities of perimetry, ERG, and VEP may be noted.[53]

Toxicity with Retinal Necrosis

Corticosteroid Preparations

Although most preparations of corticosteroids are quite safe for intravitreal use,[54] the vehicles of some preparations may induce retinal necrosis with formation of retinal breaks and rhegmatogenous retinal detachment. Two particularly toxic compounds are betamethasone acetate/betamethasone sodium phosphate (Celestone Soluspan, Schering-Plough, Kenilworth, NJ) and methylprednisolone acetate (Depo-Medrol, Pfizer, New York, NY).[55,56]

Toxicity with Retinal Vascular Changes

Aminoglycosides

Aminoglycosides may cause ocular toxicity by almost any route of delivery,[57,58] though toxicity is most commonly seen when the medication is injected intravitreally for the treatment of endophthalmitis. Gentamicin appears more toxic than tobramycin or amikacin.[59] The medication is employed less commonly today, as most cases of endophthalmitis are treated with ceftazidime and vancomycin.

With gentamicin toxicity, severe vision loss is characteristic, with vascular changes including retinal edema, cotton-wool spots, intraretinal hemorrhages, arteriolar attenuation, and venous beading (Fig. 9.18). Fluorescein angiography is oftentimes quite striking, as it demonstrates profound macular capillary nonperfusion.[60] Late manifestations include widespread pigmentary retinopathy, optic atrophy, and anterior segment neovascularization.

Talc

Magnesium silicate (talc) is found as a vehicle in many oral medications. Talc may gain access to the systemic vascular

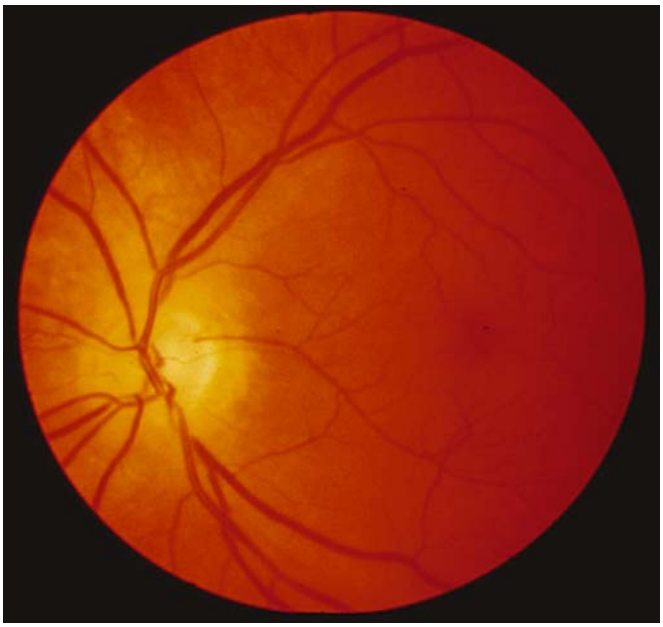

Fig. 9.17. Color photograph OS of a patient following accidental ingestion of methanol. Note the mild diffuse retinal edema. The patient recovered from the incident with vision of 20/60 in both eyes.

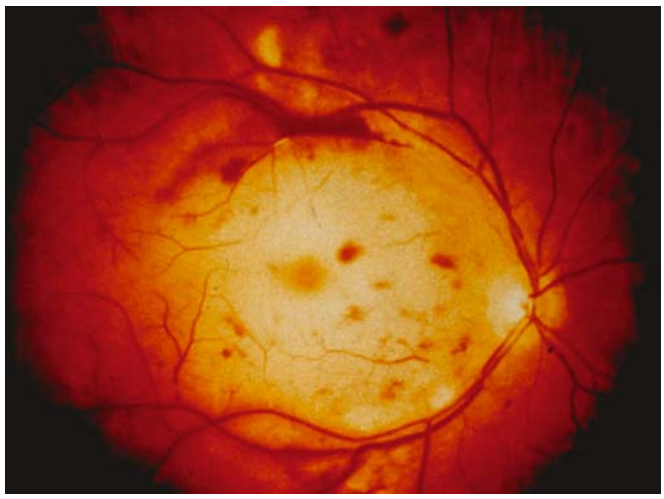

Fig. 9.18. Color photograph OD of a patient 1 day following treatment for endophthalmitis, which included an intravitreal injection of gentamicin 200 μg. The patient exhibited macular infarction, along with scattered retinal hemorrhages. Vision never recovered beyond hand motions.

system when individuals abuse these medications by dissolving them and injecting them intravenously. [61] Small talc particles clear the pulmonary capillary network and enter the arterial system. Chronic injection of talc may cause arteriovenous shunt formation, with access to the central retinal artery possible even for larger particles.[62]

Initially, talc emboli are asymptomatic,[63] but may lead to an ischemic retinopathy. Clinical examination and FA oftentimes demonstrate the intraarteriole talc particles (Fig. 9.19), along with capillary nonperfusion, microaneurysms, cotton-wool spots, and later with retinal neovascularization[64–66] (Fig. 9.20).

Oral Contraceptives

Oral contraceptive preparations are linked to systemic thromboembolic events, including retinal vascular occlusions, with corresponding FA abnormalities.[67–69] These complications were more common with older formulas of the contraceptives, which contained higher concentrations of synthetic agents,[70,71] and estrogen in particular. When vascular occlusive disease is seen today, it generally occurs in patients who are in the older age range for oral contraceptive usage, and there is generally a history of underlying systemic vascular disease.

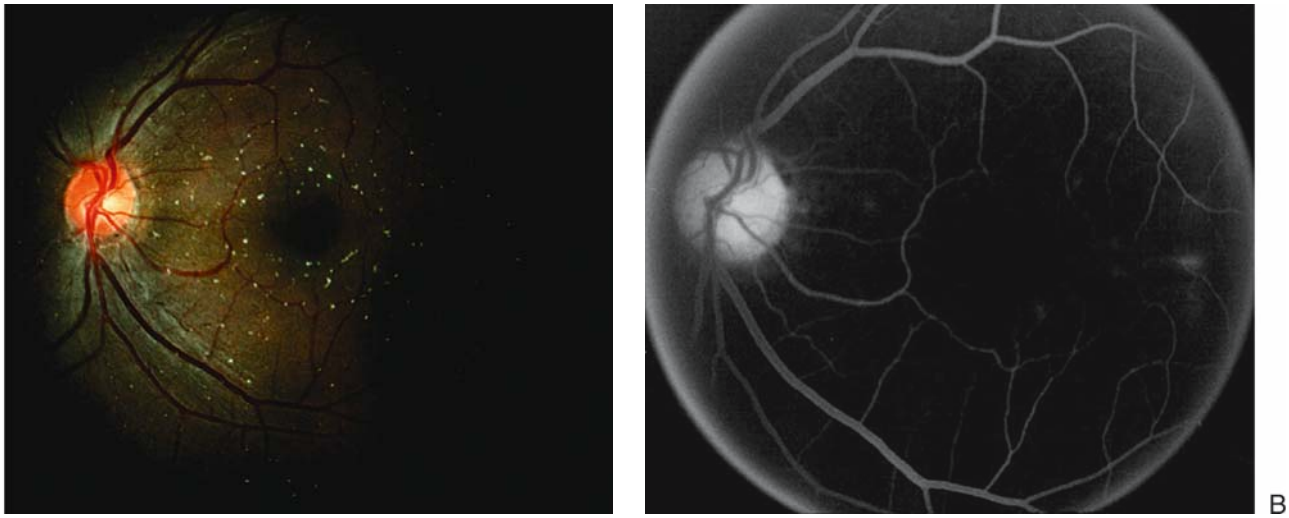

Fig. 9.19. (A) Color photograph OS of a patient who intravenously abused illicit drugs. Numerous talc particles are seen dispersed through the retinal arterioles. (B) The FA demonstrates significant retinal ischemia.

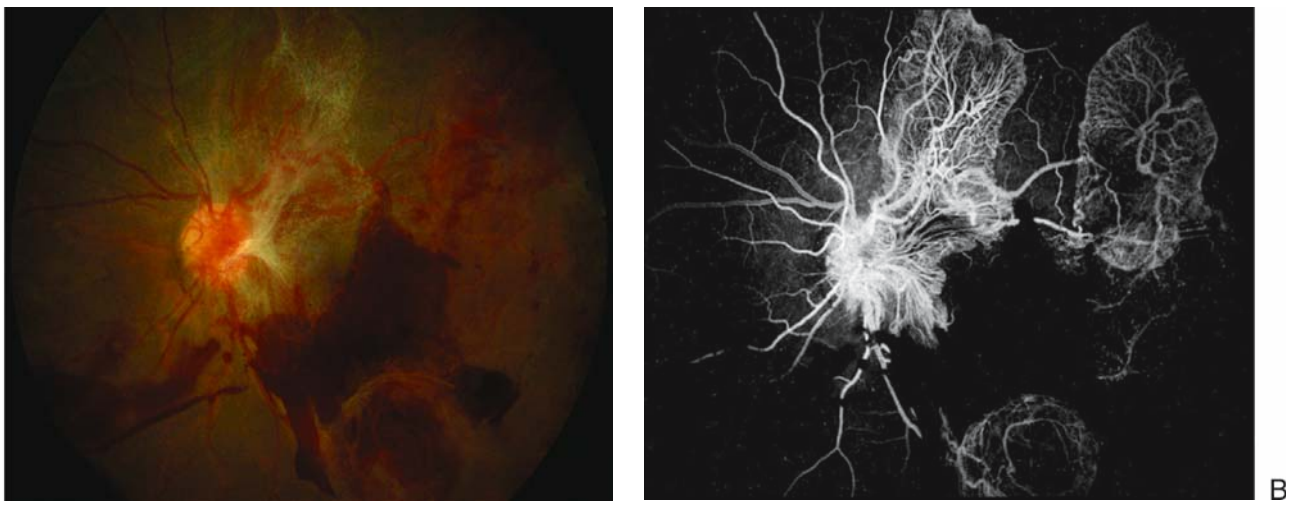

Fig. 9.20. (A) Color photograph OS of a patient with a long-standing history of intravenous drug abuse. Previous ocular examinations demonstrated arteriolar emboli from talc. The patient subsequently developed profound retinal ischemia with development of prominent neovascularization. (B) Fluorescein angiography documents the extensive whorl-like retinal neovascularization with distal retinal ischemia.

Interferon-Alpha

Interferon (IFN) alpha-2a (Roche Pharmaceuticals, Nutley, NY) and alpha-2b (Schering, Kenilworth, NJ) are antiviral agents used to treat chronic hepatitis and various malignancies.

In most patients, visual acuity is normal, with varying degrees of cotton-wool spots and intraretinal hemorrhages[72] (Fig. 9.21). Vision loss may occur secondary to retinal vascular occlusions[73] and cystoid macular edema,[74] with corresponding FA findings. Systemic vascular disease (e.g., diabetes mellitus) is a risk factor for retinal toxicity.[75]

Toxicity with Maculopathy

Toxicity with Cystoid Macular Edema (CME)

Epinephrine and Dipivefrin

The related compounds epinephrine (Epifrin, Allergan, Irvine, CA) and dipivefrin (Propine, Allergan, Irvine, CA) are no longer commonly used to treat glaucoma in the United States. They were previously associated with well-described cystoid macular edema, particularly in aphakic eyes.[76,77]

Latanoprost

Latanoprost (Xalatan, Pfizer, New York, NY) and other prostaglandin agents may cause reversible cystoid macular edema with or without iridocyclitis.[78,79] Risk factors include intraocular surgery, dipivefrin, epiretinal membrane, branch retinal vein occlusion, iridocyclitis, and diabetes mellitus.[80,81]

Toxicity with Other Maculopathies

Niacin

Niacin (nicotinic acid, vitamin B_3) is used to treat hyperlipidemia and hypertriglyceridemia. It causes an unusual toxicity that clinically resembles CME but lacks late fluorescein angiographic leakage.[82,83] Because of the lack of findings on FA, OCT may be particularly helpful to make the diagnosis and for documentation purposes.[84] This pseudo-CME is probably caused by intracellular fluid accumulation, as opposed to true edema, which is in the extracellular space.[85] Treatment is discontinuation of the medication, which generally allows for rapid resolution of the pseudo-CME, and restoration of visual function (Fig. 9.22).

Sympathomimetics

Intravenous sympathomimetics, including epinephrine, may cause a unique macular toxicity with loss of vision or paracentral scotoma formation, similar to acute macular neuroretinopathy, an idiopathic condition.[86] Concomitant elevation of the blood pressure is not necessary to cause this toxicity.[87] Reddish-brown wedge-shaped lesions develop in the outer retina, associated with faint hyperfluorescence on FA (Fig. 9.23). When exposure to the sympathomimetics is discontinued, the ocular findings generally resolve spontaneously.

Toxicity with Retinal Folds

Sulfanilamide-Like Medications

Several related medications (generally containing sulfa), may induce a syndrome including ciliary body swelling, choroidal effusion, and anterior displacement of the lens–iris diaphragm. Anterior segment complications include nonpupillary block angle closure, and posterior segment complications include induced-myopia and retinal folds (Fig. 9.24). The FA generally shows no vascular leakage, supporting the concept that the folds are most likely caused by mild vitreous traction on the macula during axial elongation of the eye. Drugs associated with this syndrome include sulfanilamide,[88] acetazolamide (Diamox, Lederle Pharmaceuticals, Inc., Pearl River, NJ),[89] metronidazole,[90] hydrochlorothiazide,[91] and topiramate (Topamax, Ortho-McNeil, Raritan, NJ).[92] When the offending medication is identified and discontinued, the retinal abnormalities generally return to normal.

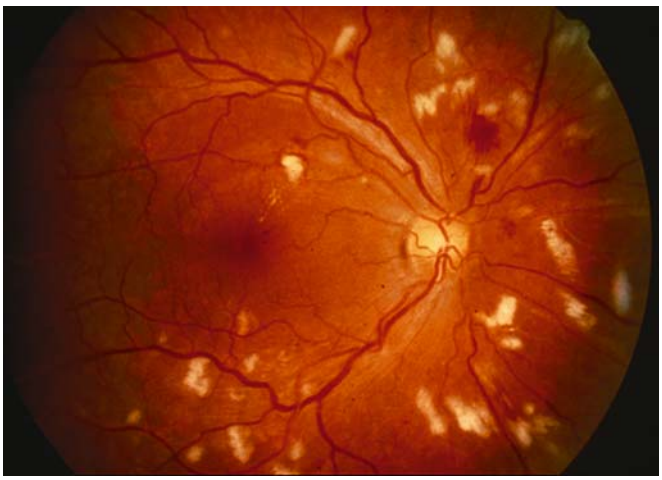

Fig. 9.21. Color photograph OD of a patient being treated with interferon for chronic hepatitis C. Multiple cotton-wool spots developed along with several intraretinal hemorrhages, though the cotton-wool spots gradually dissipated. The patient remained on the interferon therapy.

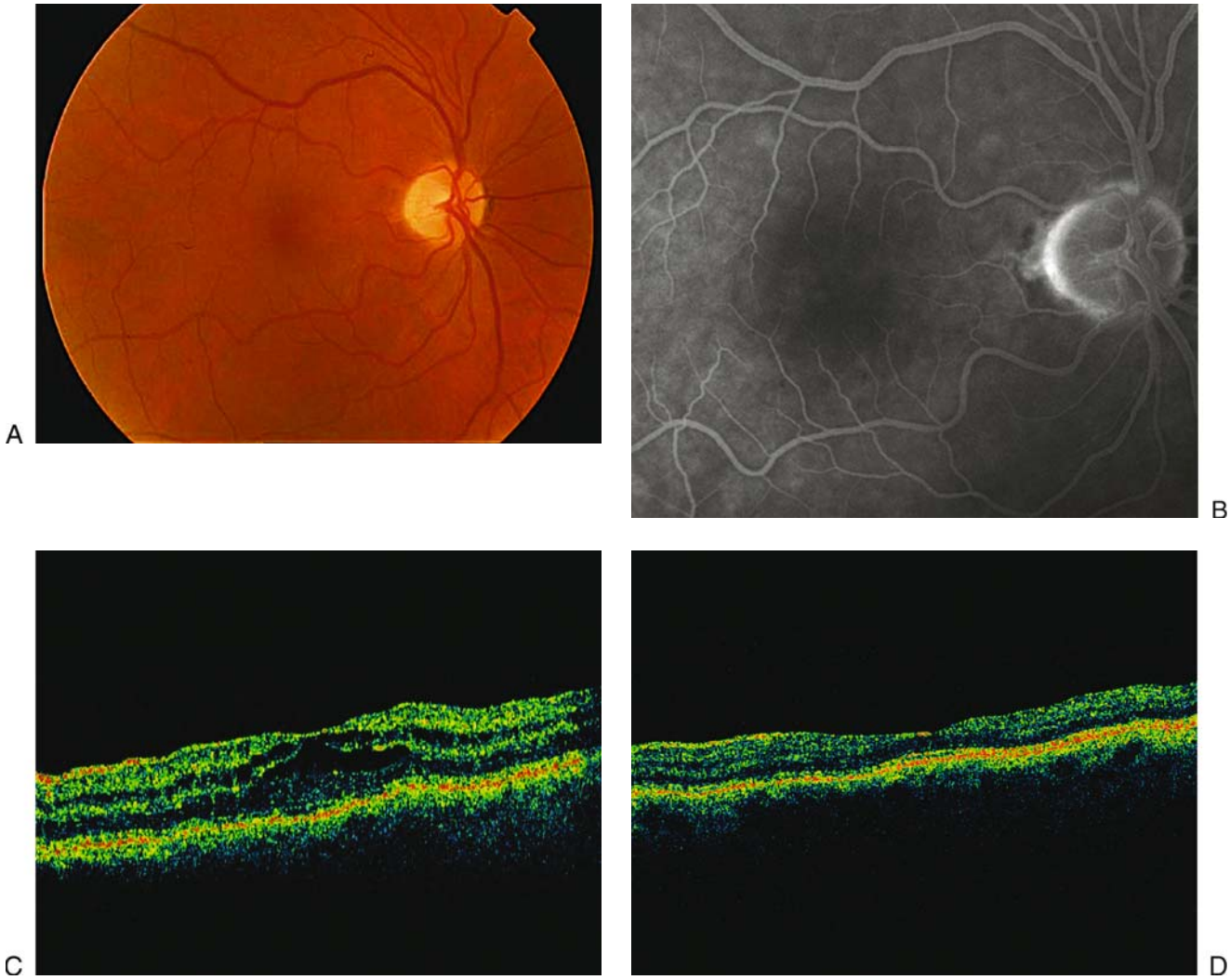

FIG. 9.22. (A) Color photograph OD of a patient taking systemic niacin. The visual acuity is 20/40 and there is blunting of the foveal reflex. (B) Fluorescein angiography shows no appreciable late leakage. (C) Optical coherence tomography (OCT) while on niacin demonstrates the presence of macular thickening. (D) Optical coherence tomography taken 2 weeks following cessation of the niacin therapy has returned to normal, and the vision recovered back to 20/20 as well. (Courtesy of Lawrence A. Yannuzzi, MD, New York, NY.)

Conclusion

In view of the thousands of medications on the market, pharmacologic retinal toxicity remains a limited yet important cause of visual morbidity. Retinal changes may occur when agents are employed at therapeutic dosages, or when the agent is abused. It is important to recognize patterns of toxicity, as there rarely are confirmatory diagnostic tests, short of pattern recognition on clinical examination. In select situations, the fluorescein angiogram is essential for the correct diagnosis, while in most cases it is mainly supportive of the diagnosis.

Acknowledgments. This work is partially supported by National Institutes of Health (NIH) center grant P30-EY014801, and by an unrestricted grant to the University of Miami from Research to Prevent Blindness, New York, NY.

FIG. 9.23. (A) Color photograph OS demonstrating reddish wedge-shaped lesions in the macular region compatible with sympathomimetic-induced macular neuroretinopathy. (B) Fluorescein angiography documents no appreciable late macular leakage.

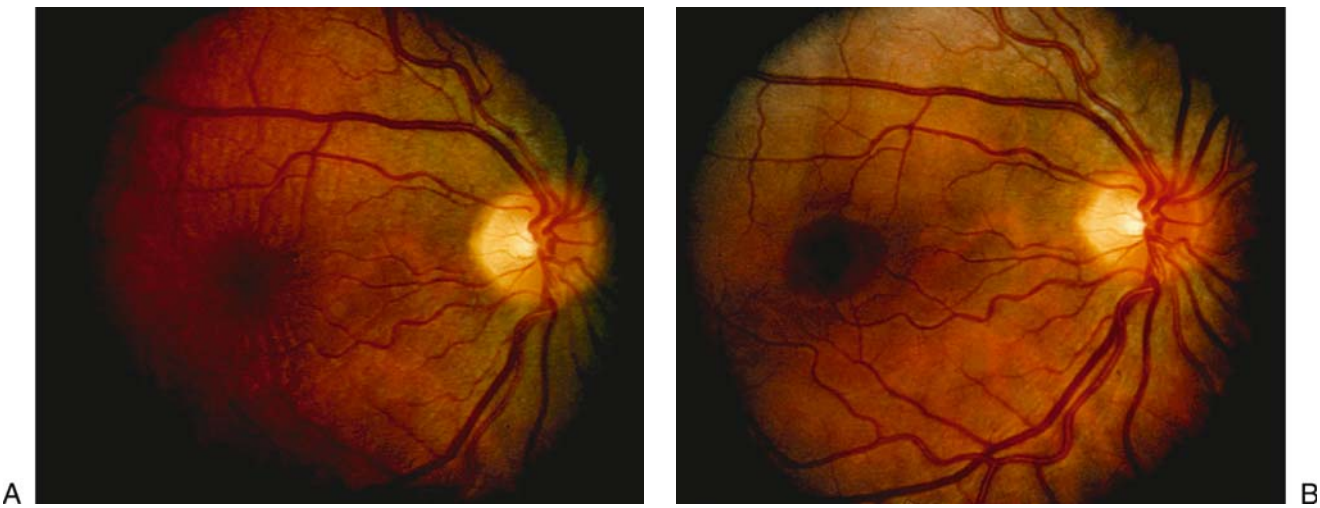

FIG. 9.24. (A) Color photograph OD documenting retinal folds in a patient recently started on topiramate. The patient actually presented with angle-closure glaucoma. (B) Color photograph OD taken 2 weeks after the topiramate was discontinued documents the spontaneous resolution of the retinal folds.

References

1. Cambiaggi A. Unusual ocular lesions in a case of systemic lupus erythematosus. Arch Ophthalmol 1957;57:451–453.
2. Hobbs HE, Sorsby A, Freedman A. Retinopathy following chloroquine therapy. Lancet 1959;2:478–480.
3. Henkind P, Rothfield NF. Ocular abnormalities in patients treated with synthetic antimalarial drugs. N Engl J Med 1963;269: 433–439.
4. Okun E, Gouras P, Berstein H, von Sallman L. Chloroquine retinopathy. Arch Ophthalmol 1963;69:59–71.
5. Cruess AF, Schachat AP, Nicholl J, Augsburger JJ. Chloroquine retinopathy: is fluorescein angiography necessary? Ophthalmology 1985;92:1127–1129.
6. Easterbrook M. The use of Amsler grids in early chloroquine retinopathy. Ophthalmology 1984;91:1368–1372.
7. Hart WM, Burde RM, Johnston GP, Drews RC. Static perimetry in chloroquine retinopathy: perifoveal patterns of visual field depression. Arch Ophthalmol 1984;102:377–380.
8. Vu BLL, Easterbrook M, Hovis JK. Detection of color vision defects in chloroquine retinopathy. Ophthalmology 1999;106: 1799–1804.

9. Tzekov RT, Serrato A, Marmor MF. ERG findings in patients using hydroxychloroquine. Doc Ophthalmol 2004;108:87–97.
10. Maturi RK, Yu M, Weleber RG. Multifocal electroretinographic evaluation of long-term hydroxychloroquine users. Arch Ophthalmol 2004;122:973–981.
11. Rodriguez-Padilla JA, Hedges TR 3rd, Monson B, et al. High-speed ultra-high resolution optical coherence tomography findings in hydroxychloroquine retinopathy. Arch Ophthalmol 2007; 125:775–780.
12. Brinkley JR, Dubois EL, Ryan SJ. Long-term course of chloroquine retinopathy after cessation of medication. Am J Ophthalmol 1979;88:1–11.
13. Rubin M, Bernstein HN, Zvaifler NJ. Studies on the pharmacology of chloroquine. Arch Ophthalmol 1963;70:80–87.
14. Ehrenfeld M, Nesher R, Merin S. Delayed-onset chloroquine retinopathy. Br J Ophthalmol 1986;70:281–283.
15. Marmor MF, Carr RE, Easterbrook M, Farjo AA, Mieler WF. Recommendations on screening for chloroquine and hydroxychloroquine retinopathy: a report by the American Academy of Ophthalmology. Ophthalmology 2002;109:1377–1382.
16. American Academy of Ophthalmology. Comprehensive Adult Medical Eye Evaluation, Preferred Practice Pattern. San Francisco: American Academy of Ophthalmology, 2000.
17. Easterbrook M. Current concepts in monitoring patents on antimalarials. Aust N Z J Ophthalmol 1998;26:101–103.
18. Brinton GS, Norton EWD, Zahn JR, Knighton RW. Ocular quinine toxicity. Am J Ophthalmol 1980;90:403–410.
19. Toxic maculopathy part II: a result of quinine usage as demonstrated by fluorescein angiography and electroretinography. Ann Ophthalmol 1975;7:1475–1481.
20. Bacon P, Spalton DJ, Smith SE. Blindness from quinine toxicity. Br J Ophthalmol 1988;72:219–224.
21. Verdon W. Clinical electrophysiology in quinine induced retinal toxicity. Optom Vis Sci 2008;85:17–26.
22. Weekley RD, Potts AM, Reboton J, May RH. Pigmentary retinopathy in patients receiving high doses of a new phenothiazine. Arch Ophthalmol 1960;64:65–76.
23. Meredith TA, Aaberg TM, Willerson D. Progressive chorioretinopathy after receiving thioridazine. Arch Ophthalmol 1978;96: 1172–1176.
24. Miller FS III, Bunt-Milam AH, Kalina RE. Clinical-ultrastructural study of thioridazine retinopathy. Ophthalmology 1982;89: 1478–1488.
25. Miyata M, Imai H, Ishikawa S, Nakajima S. Changes in human electroretinography associated with thioridazine administration. Ophthalmologica 1980;181:175–180.
26. Marmor MF. Is thioridazine retinopathy progressive? Relationship of pigmentary changes to visual function. Br J Ophthalmol 1990;74:739–742.
27. Haimovici R, D'Amico DJ, Gragoudas ES, Sokol S, for the Deferoxamine Retinopathy Study Group. The expanded clinical spectrum of deferoxamine retinopathy. Ophthalmol 2002;109;164–171.
28. Mehta AM, Engstrom RE, Kreiger AE. Deferoxmaine-associated retinopathy after subcutaneous injection. Am J Ophthalmol 1994;118:260–262.
29. Rodriguez AS, Oterino JAM, Fernandez MAF. Unusual toxicity of deferoxamine. Ann Pharmacol 1999;33:505–506.
30. Bene C, Manzler A, Bene D, Kranias G. Irreversible ocular toxicity from single "challenge" dose of deferoxamine. Clin Nephrol 1989;31:43–48.
31. Heier JS, Dragoo RA, Enzenauer RW, Waterhouse WJ. Screening for ocular toxicity in asymptomatic patients treated with tamoxifen. Am J Ophthalmol 1994;117:772–775.
32. Gorin MB, Day R, Constantino JP, et al. Long-term tamoxifen citrate use and potential ocular toxicity. Am J Ophthalmol 1998;125:493–501.
33. Cortin P, Corriveau LA, Rousseau AP, et al. [Maculopathy with golden particles]. Can J Ophthalmol 1982;17:103–106.
34. Boudreault G, Cortin P, Corriveau LA, et al. [Canthaxanthine retinopathy: 1. Clinical study in 51 consumers]. Can J Ophthalmol 1983;18:325–328.
35. Weber U, Goerz G, Baseler H, Michaelis L. [Canthaxanthin retinopathy. Follow-up of over 6 years]. Klin Monatsbl Augenheilkd 1992;201:174–177.
36. Stoelting RK, Miller RD. Basics of Anesthesia, 2nd ed. New York: Churchill Livingstone, 1989:64.
37. Bullock JD, Albert DM. Fleck retina. Appearance secondary to oxalate crystals from methoxyflurane anesthesia. Arch Ophthalmol 1975;93:26–31.
38. Novak MA, Roth AS, Levine MR. Calcium oxalate retinopathy associated with methoxyflurane abuse. Retina 1988;8:230–236.
39. Withering W. An Account of the Foxglove, and Some of Its Medical Uses: With Practical Remarks on Dropsy and Other Diseases. London: Robinson, 1785.
40. Weleber RG, Shults WT. Digoxin retinal toxicity. Clinical and electrophysiologic evaluation of a cone dysfunction syndrome. Arch Ophthalmol 1981;99:1568–1572.
41. Ballard SA, Gingell CJ, Tang K, et al. Effects of sildenafil on the relaxation of human corpus cavernosum tissue in vitro and on the activities of cyclic nucleotide phosphodiesterase isozymes. J Urol 1998;159:2164–2171.
42. Goldstein I, Lue TF, Padma-Nathan H, et al. Oral sildenafil in the treatment of erectile dysfunction. N Engl J Med 1998;338: 1397–1404.
43. Gabrieli CB, Regine F, Vingolo EM, Rispoli E, Fabbri A, Isidori A. Subjective visual halos after sildenafil (Viagra) administration: electroretinographic evaluation. Ophthalmology 2001;108:877–881.
44. Tripathi A, O'Donnell NP. Branch retinal artery occlusion: another complication of sildenafil [letter]. Br J Ophthalmol 2000;84:928.
45. Pomeranz HD, Smith KH, Hart WM Jr, Egan RA. Sildenafil-associated nonarteritic anterior ischemic optic neuropathy. Ophthalmology 2002;109(3):584–587.
46. Sildenafil (Viagra) a cause of proliferative diabetic retinopathy? [letter] Eye 2000;14(5):785–786.
47. Allibhai ZA, Gale JS, Sheidow TS. Central serous chorioretinopathy in a patient taking sildenafil citrate. Ophthalmic Surg Lasers Imaging 2004;35:165–167.
48. Luu JK, Chappelow AV, McCulley TJ, Marmor MF. Acute effects of sildenafil on the electroretinogram and multifocal electroretinogram. Am J Ophthalmol 2001;132(3):388–394.
49. Laties AM, Fraunfelder FT. Ocular safety of Viagra (sildenafil citrate). Trans Am Ophthalmol Soc 1999;97:115–125.
50. Marmor MF. Sildenafil (Viagra) and ophthalmology. Arch Ophthalmol 1999;117:518–519.
51. Hayreh MS, Hayreh SS, Baumbach GL, et al. Methyl alcohol poisoning. III. Ocular toxicity. Arch Ophthalmol 1977;95:1851–1858.
52. Ingemansson SO. Clinical observations on ten cases of methanol poisoning. Acta Ophthalmol 1984;62:15–24.
53. McKellar MJ, Hidajat RR, Elder MJ. Acute ocular methanol toxicity: clinical and electrophysiological features. Aust N Z J Ophthalmol 1997;25:225–230.

54. McCuen BW II, Bessler M, Tano Y, Chandler D, Machemer R. The lack of toxicity of intravitreally administered triamcinolone acetonide. Am J Ophthalmol 1981;91:785–788.
55. Hida T, Chandler D, Arena JE, Machemer R. Experimental and clinical observations of the intraocular toxicity of commercial corticosteroid preparations. Am J Ophthalmol 1986;101:190–195.
56. Pendergast SD, Eliott D, Machemer R. Retinal toxic effects following inadvertent intraocular injection of Celestone Soluspan. Arch Ophthalmol 1995;113:1230–1231.
57. McDonald HR, Schatz H, Allen AW, et al. Retinal toxicity secondary to intraocular gentamicin. Ophthalmology 1986;93:871–877.
58. Campochiaro PA, Conway BP. Aminoglycoside toxicity—a survey of retinal specialists: implications for ocular use. Arch Ophthalmol 1991;109:946–950.
59. D'Amico DJ, Caspers-Velu L, Libert J, et al. Comparative toxicity of intravitreal aminoglycoside antibiotics. Am J Ophthalmol 1985;100:264–275.
60. Seawright AA, Bourke RD, Cooling RJ. Macula toxicity after intravitreal amikacin. Aust N Z J Ophthalmol 1996;24:143–146.
61. Tse DT, Ober RR. Talc retinopathy. Am J Ophthalmol 1980;90: 624–640.
62. AtLee WE. Talc and cornstarch emboli in eyes of drug users. JAMA 1972;219:49.
63. Martidis A, Yung CW, Ciulla TA. Talc embolism: a static retinopathy. Am J Ophthalmol 1997;124:841–843.
64. Friberg TR, Gragoudas ES, Regan CDJ. Talc emboli and macular ischemia in intravenous drug abuse. Arch Ophthalmol 1979;97:1089.
65. Kresca LJ, Goldberg MF, Jampol LM. Talc emboli and retinal neovascularization in a drug abuser. Am J Ophthalmol 1979;87:334.
66. Brucker AJ. Disc and peripheral neovascularization secondary to talc and cornstarch emboli. Am J Ophthalmol 1979;88:864.
67. Gombos GM, Moreno DH, Bedrossian PB. Retinal vascular occlusion induced by oral contraceptives. Ann Ophthalmol 1975; 7:215–217.
68. Perry HD, Mallen FJ. Cilioretinal artery occlusion associated with oral contraceptives. Am J Ophthalmol 1977;84:56–58.
69. Stowe GC, Jakov AN, Albert DM. Central retinal vascular occlusion associated with oral contraceptives. Am J Ophthalmol 1978; 86:798–801.
70. Petersson GJ, Fraunfelder FT, Meyer SM. Oral contraceptives. Ophthalmol 1981;88:368–371.
71. Garg SK, Chase P, Marshall G, et al. Oral contraceptives and renal and retinal complications in young women with insulin-dependent diabetes mellitus. JAMA 1994;271:1099–1102.
72. Guyer DR, Tiedeman J, Yannuzzi LA, et al. Interferon-associated retinopathy. Arch Ophthalmol 1993;111:350–356.
73. Nadir A, Amin A, Chalisa N, et al. Retinal vein thrombosis associated with chronic hepatitis C: a case series and review of the literature. J Viral Hepat 2000;7(6):466–470.
74. Tokai R, Ikeda T, Miyaura T, et al. Interferon-associated retinopathy and cystoid macular edema. Arch Ophthalmol 2001;119(7): 1077–1079.
75. Willson RL, Ross RD, Willson LM, et al. Interferon-associated retinopathy in a young, insulin-dependent diabetic patient. Retina 2000;20:413–415.
76. Thomas JV, Gragoudas ES, Blair NP, Lapus JV. Correlation of epinephrine use and macular edema in aphakic glaucomatous eyes. Arch Ophthalmol 1978;96:625–628.
77. Mehelas TJ, Kollarits CR, Martin WG. Cystoid macular edema presumably induced by dipivefrin hydrochloride (Propine). Am J Ophthalmol 1984;94:682.
78. Hoyng PFJ, Rulo AH, Greve EL, Astin M, Gjotterberg M. Fluorescein angiographic evaluation of the effect of latanoprost treatment on blood-retinal barrier integrity: a review of studies conducted on pseudophakic glaucoma patients and on phakic and aphakic monkeys. Surv Ophthalmol 1997;41(suppl 2): S83–S88.
79. Heier JS, Steinert RF, Frederick AR Jr. Cystoid macular edema associated with latanoprost use. Arch Ophthalmol 1998;116: 680–682.
80. Moroi SE, Gottfredsdottir MS, Schteingart MT, et al. Cystoid macular edema associated with latanoprost therapy in a case series of patients with glaucoma and ocular hypertension. Ophthalmology 1999;106:1024–1029.
81. Wand M, Gaudio AR, Shields MB. Latanoprost and cystoid macular edema in high-risk aphakic or pseudophakic eyes. J Cataract Refract Surg 2001;27(9):1397–1401.
82. Gass JDM. Nicotinic acid maculopathy. Am J Ophthalmol 1973;76:500–510.
83. Millay RH, Klein ML, Illingworth DR. Niacin maculopathy. Ophthalmology 1988;95:930–936.
84. Dajani HM, Lauer AK. Optical coherence tomography findings in niacin maculopathy. Can J Ophthalmol 2006;41(2): 197–200.
85. Jampol LM. Niacin maculopathy. Ophthalmology 1988;95: 1704–1705.
86. O'Brien DM, Farmer SG, Kalina RE, Leon JA. Acute macular neuroretinopathy following intravenous sympathomimetics. Retina 1989;9:281–286.
87. Desai UR, Sudhamathi K, Natarajan S. Intravenous epinephrine and acute macular neuroretinopathy. Arch Ophthalmol 1993;111: 1026–1027.
88. Maddalena MA. Transient myopia associated with acute glaucoma and retinal edema: following vaginal administration of sulfanilamide. Arch Ophthalmol 1968;80:186–188.
89. Ryan EH, Jampol LM. Drug-induced acute transient myopia with retinal folds. Retina 1986;6:220–223.
90. Grinbaum A, Ashkenazi I, Avni I, Blumenthal M. Transient myopia following metronidazole treatment for trichomonas vaginalis. JAMA 1992;267:511–512.
91. Soylev MF, Green RL, Feldon SE. Choroidal effusion as a mechanism for transient myopia induced by hydrochlorothiazide and triamterene. Am J Ophthalmol 1995;120:395–397.
92. Banta JT, Hoffman K, Budenz DL, Ceballos E, Greenfield DS. Presumed topiramate-induced bilateral acute angle-closure glaucoma. Am J Ophthalmol 2001;132:112–114.

Part II
Optical Coherence Tomography (OCT)

10
How Does Optical Coherence Tomography Work? Basic Principles

J. Fernando Arevalo, Daniel Krivoy, and Carlos F. Fernandez

Optical coherence tomography (OCT) (Stratus OCT, Carl Zeiss Meditec, Inc., Dublin, CA) (Fig. 10.1) is a commercially available computer-assisted precision optical instrument that generates cross-sectional images (tomograms) of ocular structures with close to 10-μm axial resolution.[1] This technology is evolving, and its axial resolution has been reported to be as high as 3 μm in laboratory settings (ultrahigh-resolution OCT).[2,3] Optical coherence tomography is analogous to B-mode ultrasound, except that it uses light rather than sound. Unlike ultrasound, OCT does not require contact with the tissue examined.

The technology relies on low-coherence interferometry to generate the images.[1] A low coherence near-infrared light beam (820 nm) is directed toward the target tissue. The magnitude and relative location of the backscattered light from the tissue's microstructures are interpreted by the OCT to generate an image. The image generated is based on the optical properties of the microstructures present in the tissue imaged. The use of a near infra-red, low-coherence light source allows for good tissue penetration and to register the reflections from a narrow region of the retina[4] and the anterior segment of the eye. [5] To be able do this, the light beam generated by a superluminescent diode is split and simultaneously directed onto the imaged tissue and onto an internal reference mirror. When the backscattered light from both sources is combined, a phenomenon known as interference occurs. A photodetector receives the combined signal and measures the interference. The relative location of the light backscattered from the imaged tissue is then determined based on the information obtained from the controlled internal reference mirror (Fig. 10.2).

Each imaged point generates information on the longitudinal axis (A-scan). To generate the cross-sectional image, the beam directed toward the tissue is guided in a linear, controlled manner to cover a known distance. With each scan pass, the current OCT captures from 128 to 768 longitudinal (axial) range samples, that is, A-scans. Each A-scan consists of 1024 data points. Thus the OCT integrates from 131,072 to 786,432 data points to construct a cross-sectional image (tomogram). It displays the tomograms in real time using false color scale that represents the amount of light backscattering from microstructures at different depths of the imaged tissue corresponding to different anatomic or histologic structures (Figs. 10.3 and 10.4). In the false color scale, the display of bright colors (red to white) corresponds to high reflectivity and dim colors (blue to black) minimal or no reflectivity (Fig. 10.4).

The system stores the data, which are then available for analysis using different protocols designed for different applications. The OCT offers 19 scan acquisition protocols for macular measurement. We use the macular thickness acquisition protocol and the optic disc acquisition protocol to scan the optic disc. It offers five analysis protocols for the retina: (1) retinal thickness (one eye), (2) retinal map (one eye), (3) retinal thickness/volume (both eyes), (4) retinal thickness/volume tabular (both eyes), and (5) retinal thickness/volume change (both eyes). Cross-sectional images of a normal macula with OCT show a physiologic foveal pit with an intraretinal-layered structure that closely resembles the well-known histology of the tissue. Normative data for retinal nerve fiber layer analysis (Fig. 10.5) as well as macular thickness (Fig. 10.6) are available. The retinal thickness at the central fovea is approximately 133.4 ± 9.3 μm. Hee et al.[4] found a mean plus-or-minus standard deviation (SD) retinal thickness of 174 ± 18 μm for the central 500 μm. Konno et al.[6] found a mean plus-or-minus SD value of 155 ± 15 μm. Massin et al.[7] found a mean plus-or-minus SD value for a central area 1 mm in diameter centered on the fovea of 178 ± 17 μm. Finally, Neubauer et al. [8] found a mean plus-or-minus SD value of 153 ± 16 μm.

Optical coherence tomography offers protocols for nerve fiber layer (Fig. 10.7) and optic nerve head analysis (Fig. 10.8). The peripapillary scan typically is a circular scan with a diameter of 3.4 mm centered on the optic nerve head. Like the macular scan, the optic nerve head scan is composed of six linear scans in a spoke pattern separated by 30-degree intervals.

FIG. 10.1. Third-generation optical coherence tomograph (Stratus OCT Model 3000 Zeiss-Humphrey Inc., Dublin, CA), with software application version 4.0.

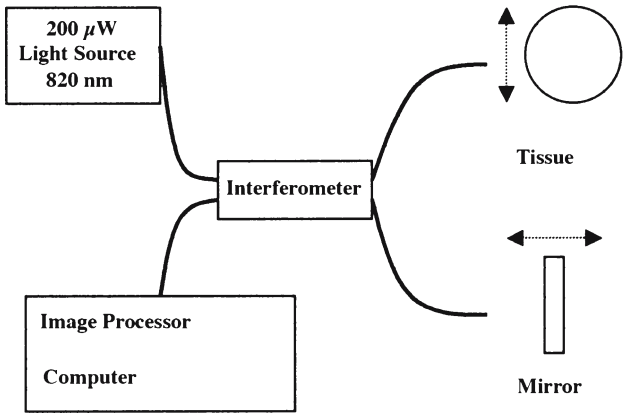

FIG. 10.2. Optical coherence tomography (OCT) contains an interferometer that resolves retinal structures by measuring the echo delay time of light that is reflected and backscattered from different microstructural features in the retina. The OCT projects a broad bandwidth near-infrared light beam (820 nm) onto the retina from a superluminescent diode. It then compares the echo time delays of light reflected from the retina with the echo time delays of the same light beam reflected from a reference mirror at known distances. When the OCT interferometer combines the reflected light pulses from the retina and reference mirror, a phenomenon known as interference occurs. A photodetector detects and measures interference. Although the light reflected from the retina consists of multiple echoes, the distance traveled by various echoes is determined by varying the distance to the reference mirror.

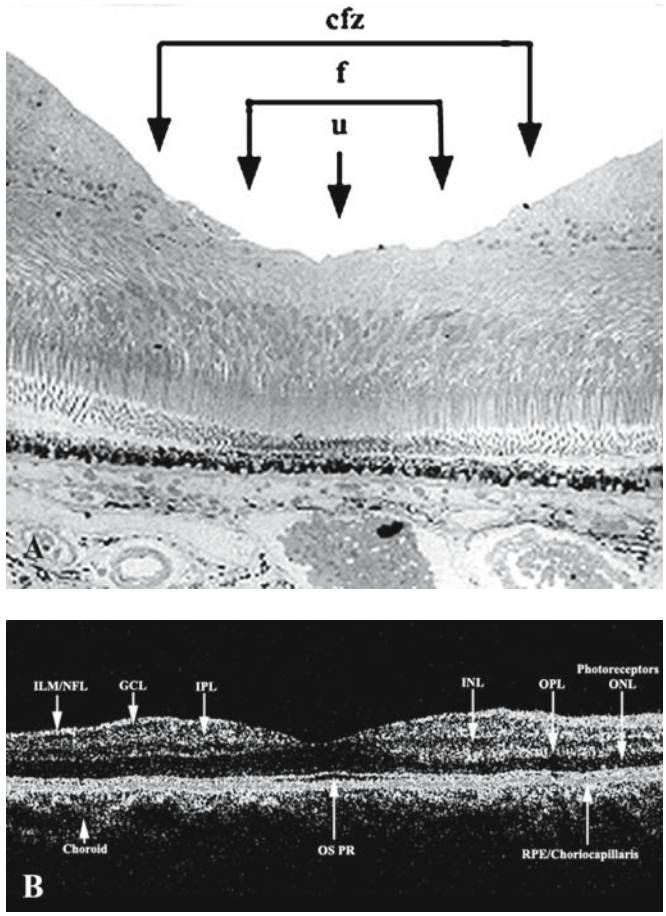

FIG. 10.3. (A) Histology of the normal macula: f, foveola; cfz, capillary-free zone; u, umbo. (B) Optical coherence tomography of normal macula. ILM/NFL, internal limiting membrane/nerve fiber layer; GCL, ganglion cell layer; IPL, inner plexiform layer; INL, inner nuclear layer; OPL, outer plexiform layer of Henle; ONL, outer nuclear layer; OS PR, photoreceptor's outer segments.

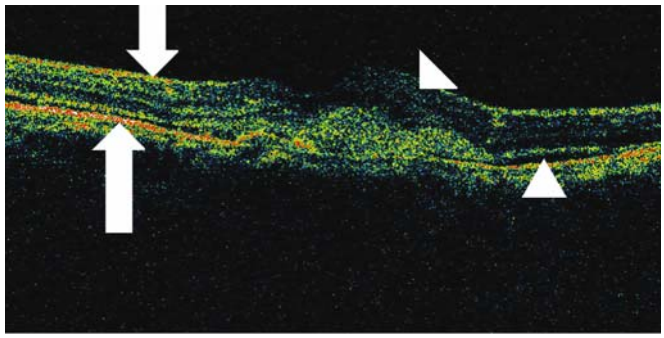

FIG. 10.4. The images are displayed in false color. Bright colors (red to white) correspond to high reflectivity (arrows); dim colors (blue to black) correspond to minimal reflectivity (arrowheads).

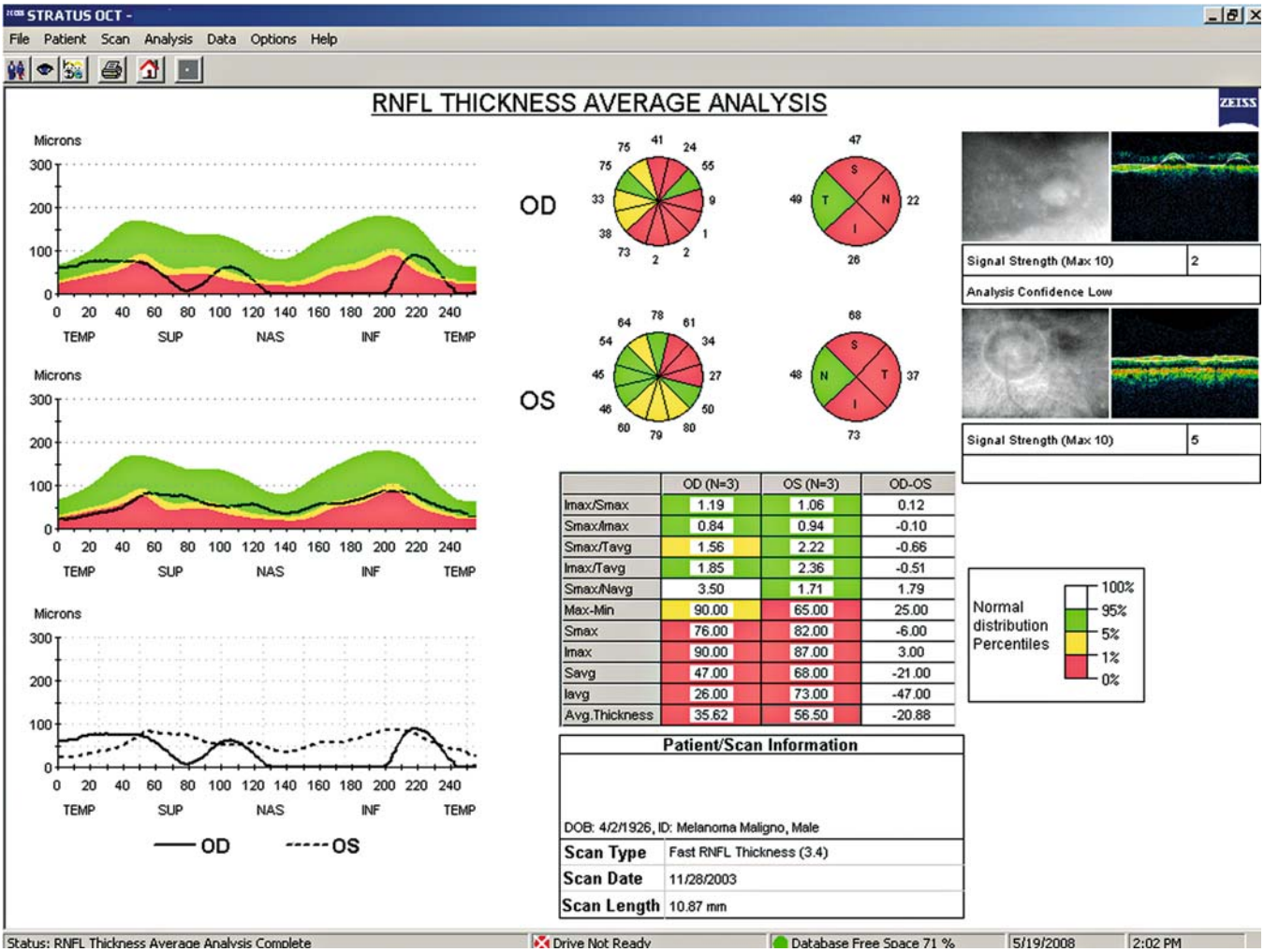

FIG. 10.5. Normative data for retinal nerve fiber layer analysis are available: advanced glaucoma patient.

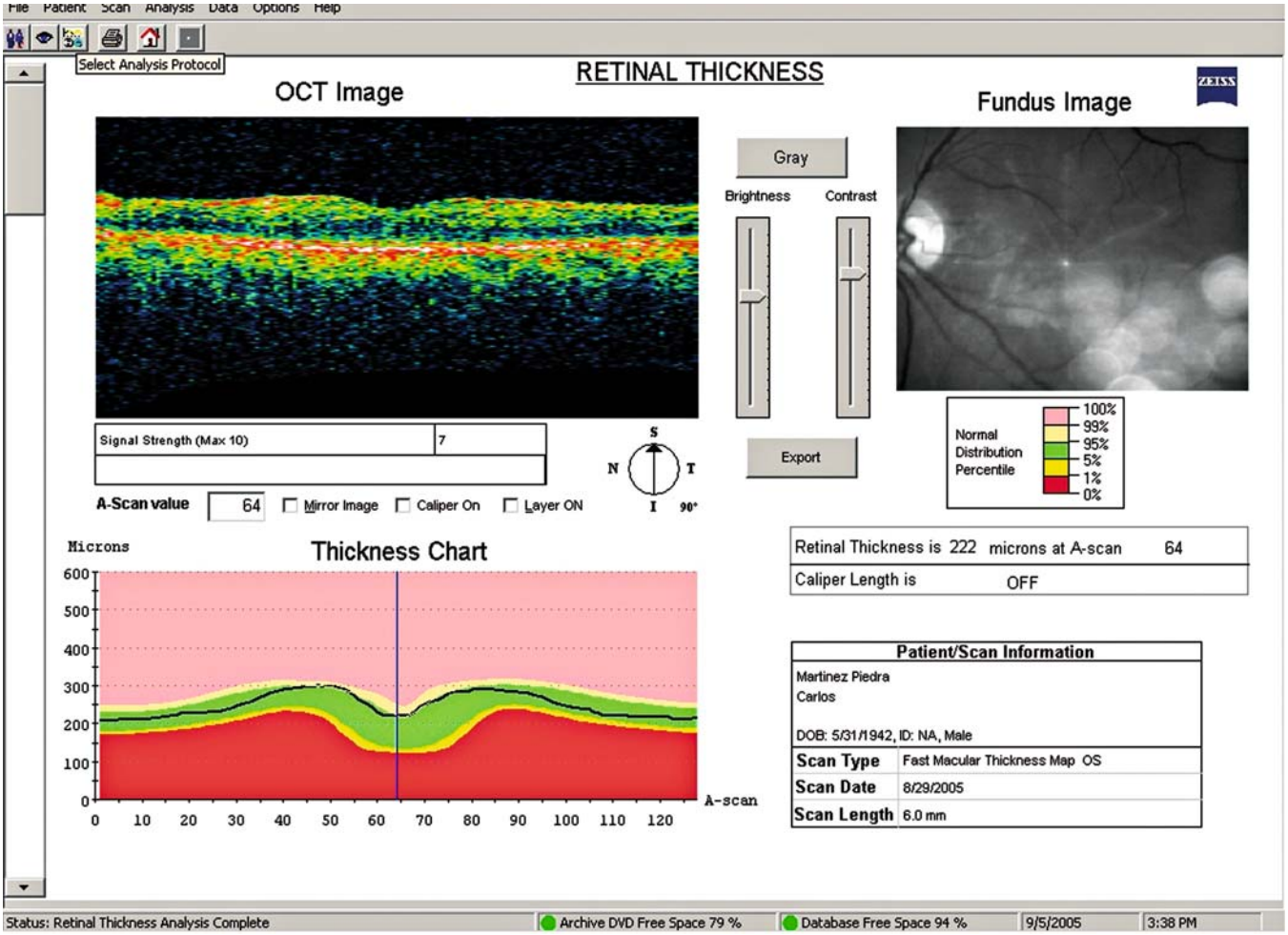

FIG. 10.6. Normative data for macular thickness analysis are available. Normal macular thickness is shown.

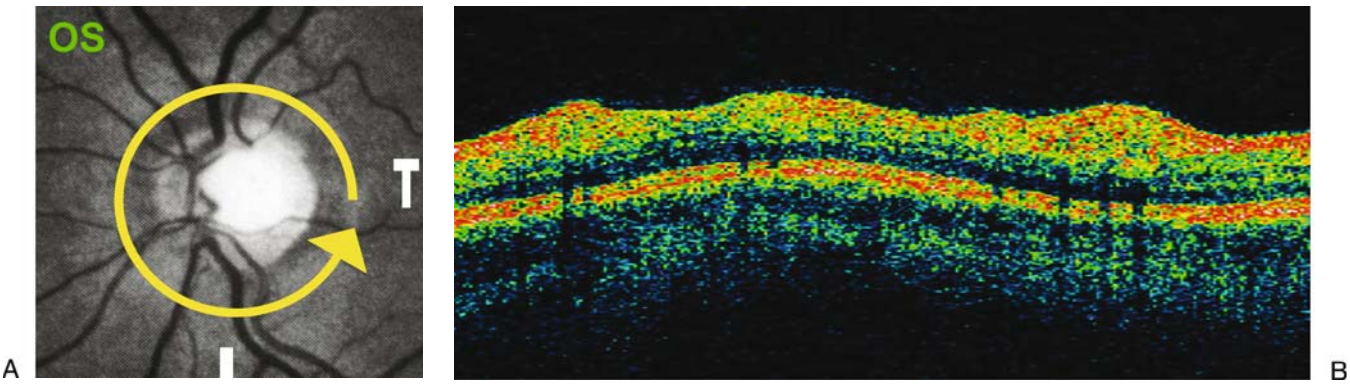

FIG. 10.7. (A) Retinal nerve fiber analysis is performed by circular scans around the optic nerve head at a radius of 1.73 mm. The scan begins temporally. Three scans are acquired and data are averaged. (B) Healthy retinal nerve fiber layer is seen to be thicker at superior and inferior quadrants. (Courtesy of Carl Zeiss Meditec Inc., Dublin, CA.)

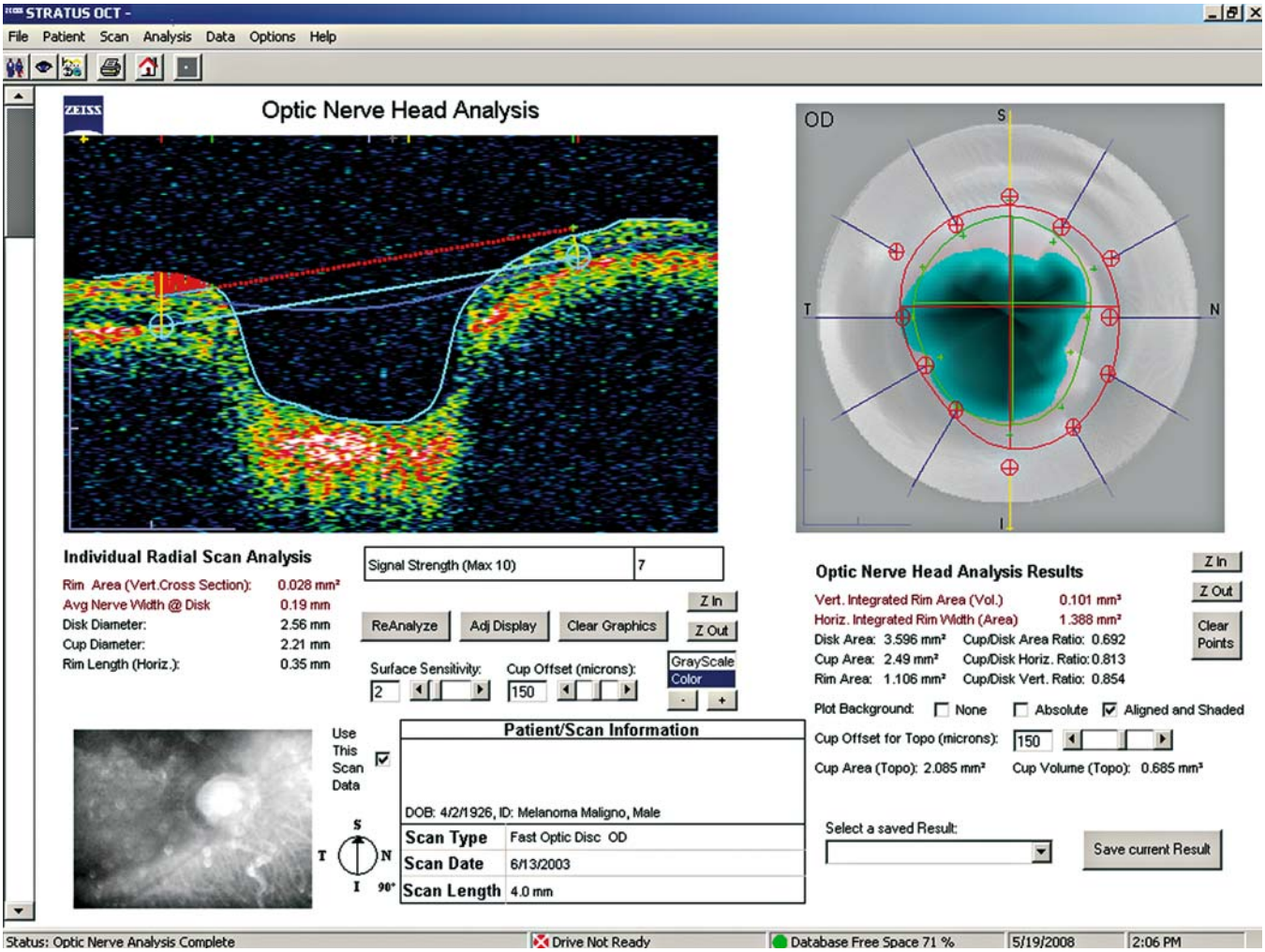

FIG. 10.8. Optic nerve head analysis. Analysis software automatically detects the edge of optic disc based on a signal from the retinal pigment epithelium on an advanced glaucoma patient.

Conclusion

Optical coherence tomography is a noninvasive, patient- and operator-friendly technique that has the advantage of imaging and quantitatively analyzing retinal thickness, nerve fiber layer, and optic nerve structures with good reproducibility. An operator needs only minimal training to perform OCT scans; however, experience will be important to overcome some of the limitations of OCT (see Chapter 21).

Acknowledgments. The authors have no proprietary or financial interest in any products or techniques described in this chapter. This work is supported in part by the Fundacion Arevalo-Coutinho para la Investigacion en Oftalmologia (FACO), Caracas, Venezuela.

References

1. Huang D, Swanson EA, Lin CP, et al. Optical coherence tomography. Science 1991;254:1178–1181.
2. Drexler W, Morgner U, Gantha RK, et al. Ultrahigh-resolution ophthalmic optical coherence tomography. Nat Med 2001;7:502–507.
3. Drexler W, Morgner U, Kartner FX, et al. In vivo ultrahigh-resolution optical coherence tomography. Opt Lett 1999;24:1 221–1223.
4. Hee MR, Izatt JA, Swanson EA, et al. Optical coherence tomography for ophthalmic imaging. IEEE Eng Med Biol 1995;14: 67–76.
5. Muscat S, McKay N, Parks S, Kemp E, Keating D. Repeatability and reproducibility of corneal thickness measurements by optical coherence tomography. Invest Ophthalmol Vis Sci 2002;43(6):1791–1795.
6. Konno S, Akiba J, Yoshida A. Retinal thickness measurements with optical coherence tomography and the scanning retinal thickness analyzer. Retina 2001;21:57–61.
7. Massin P, Vicaut E, Haouchine B, et al. Reproducibility of retinal mapping using optical coherence tomography. Arch Ophthalmol 2001;119:1135–1142.
8. Neubauer A, Priglinger S, Ullrich S, et al. Comparison of foveal thickness measured with the retinal thickness analyzer and optical coherence tomography. Retina 2001;21:596–601.

11
Clinical Applications of Optical Coherence Tomography in Macular Diseases

J. Fernando Arevalo, Aristides J. Mendoza, Carlos F. Fernandez,
Juan G. Sanchez, and Reinaldo A. Garcia

Optical coherence tomography (OCT) is a new type of medical diagnostic imaging modality that performs high-resolution, micron-scale, cross-sectional tomography imaging of ocular structures in vitro and in vivo.[1] Researchers at Harvard, the Massachusetts Institute of Technology, and Tufts University developed this technology. The first commercial device for use in posterior segment structures became available in 1995 (Humphrey Instruments, Dublin, CA). The OCT image has an axial resolution of 10 μm, and this resolution is significantly higher than those achieved by the scanning laser ophthalmoscope, B-scan ultrasound, and ultrasound biomicroscopy (UBM), which have image resolutions of 300, 150, and 20 μm, respectively.[2]

Basic Principles

Optical coherence tomography imaging is analogous to B-scan ultrasound imaging, except that it uses infrared light reflections instead of ultrasound of ocular tissues. Optical coherence tomography is based on an optical measurement technique known as low coherence interferometry, which can be used to measure distances to objects (ocular structures) with high precision by measuring the light reflected from them. The low coherence light used is produced by a superluminescent diode that is directly coupled into an optical fiber of Michelson's interferometer. Two hundred microwatts (μW) of infrared light at 820 nm are emitted on the retina, which are consistent with the American National Standards Institute (ANSI) for intrabeam viewing.[3] The interferometer divides the light source into a measurement light path, and a reference light path. The light beam is launched into the eye, and backscattered or back-reflected light gives information about the distance and thickness of the different retinal microstructures.

The coherence length of the light source determines the axial resolution of the OCT, and systems used in experimental research can achieve resolutions of 14 μm in air and 10 μm in the retina.[4] A high-power objective lens (+78 diopters) is used so that the retina is imaged onto an image plane inside the instrument. Optical coherence tomography generates cross-sectional images of the internal structures by measuring the echo time delay and intensity of backscattered or back-reflected light, this measurement is analogous to A-scan ultrasound, except that light is used rather than sound. Optical coherence tomography bidimensional B-scan images are constructed by performing rapid, successive axial measurements at different transverse points, similar to B-scan ultrasound imaging. The OCT instrument has an axial scan repetition rate of approximately 400 (128 to 768) axial scans per 2.5 seconds (1 second in the commercial unit). Each A-scan consists of 1.024 pixels in the axial direction so that the current OCT integrates from 131,072 to 786,432 pixels to build a cross-sectional image.

Optical coherence tomography is well tolerated because it is a noninvasive procedure, and images can be acquired rapidly without eye contact and low light intensity. The position of each scan is registered by the computer to allow future OCT examinations to be performed on the same exact location. The final OCT image is displayed using a false color map that corresponds to detected backscattered light levels from the incident light. The high reflectivity signals are represented by white and red colors, while the low reflectivity signals are represented by black and blue colors. The scattering from cataracts, vitreous hemorrhage, and corneal edema produces a reduction in image intensity; however, it does not degrade image quality except in cases of severe opacity.

Ophthalmology Applications

Optical coherence tomography is especially convenient in ophthalmology, due to the optic eye properties and easy accessibility of the retina for the exam. The OCT system hardware consists of the patient module and the computer unit (Fig. 11.1). The patient module sends the OCT scan to the retinal area of interest, and the video monitor receives and analyzes the OCT image. Optical coherence tomography has characterized a wide variety of retinal disease, and the OCT

FIG. 11.1. Optical coherent tomographer (OCT 3000).

images correspond with the retinal morphology of these illnesses view by light microscopy.[5,6] Optical coherence tomography provides a powerful adjunct to conventional fundus and fluorescein angiography (FA) that can function not only as a sensitive disease diagnostic test, but also to track disease progression and monitor treatment.

Interpretation

Optical coherence tomography is a new method of high-resolution, cross-sectional visualization of tissue that requires appropriate knowledge of the normal anatomy of the eye fundus. Optical coherence tomography enables carrying out an "optic biopsy" because it delineates the layers of the retina (Fig. 11.2). Foveal thickness has been calculated to be 147 ± 17 μm in normal eyes with OCT.[7] A highly scattering layer (70 μm in thickness), which is visible as red, delineates the posterior boundary of the retina in the tomogram and corresponds to the retinal pigment epithelium (RPE) and choriocapillaris complex.[8] The nerve fiber layer appears as a highly backscattering red layer at the vitreoretinal interface. The RPE and nerve fiber layer define the posterior and anterior boundaries of the sensory retina, respectively; these boundaries are important in quantifying neurosensorial retinal thickness on OCT.[9] Retinal areas of relative low reflection correspond to the location of the nuclear layers, and the photoreceptor inner and outer segments. The vitreoretinal interface can be seen in OCT images as a high-contrast boundary between the vitreous and retina. The normal vitreous gel is optically transparent and therefore not visible in OCT imaging. The choroid and RPE together match to a wide band of retinal high reflection that decreases at greater choroidal depth and sclera.

Optical coherence tomography images demonstrate reproducible patterns of retinal morphology that correspond to the

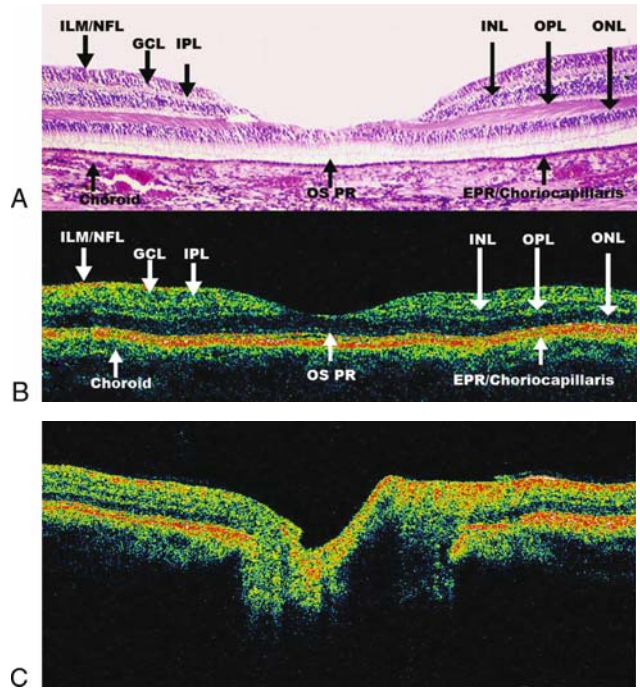

FIG. 11.2. Optical coherence tomography (OCT) of a normal eye. It has been found that OCT enables carrying out an "optic biopsy" because it delineates the layers of the retina. (A) Pathologic anatomy of the fovea. ILM/NFL, internal limiting membrane/nerve fiber layer; GCL, ganglion cell layer; IPL, inner plexiform layer; INL, inner nuclear layer; OPL, outer plexiform layer of Henle; ONL, outer nuclear layer; OS PR, photoreceptor's outer segments; RPE/Choriocapillaris, retinal pigment epithelium and choriocapillaris complex. (B) Optical coherence tomography of normal macula with different layers of the retina labeled. (C) Optical coherence tomography showing the optic nerve head.

location of retinal layers seen on light microscopic.[10] Layers of relative high reflectivity corresponded to horizontally aligned retinal components such as the nerve fiber layer and plexiform layers as well as to RPE and choroid. In contrast, the nuclear layers, and the photoreceptors inner and outer segments demonstrate relative low reflectivity. In the fovea, there is convergence of relative low reflection layers with only a single outer band of relative low reflection present in the center of the fovea (Fig. 11.2A,B).

Vitreomacular Traction and Epiretinal Membranes

Optical coherence tomography can reveal macular traction in the vitreomacular traction syndrome (VMTS) associated with incomplete posterior vitreous detachment (PVD) (Fig. 11.3). Posterior vitreous detachment is visible on the OCT image as a linear reflectivity suspended above the retinal surface. The OCT tomogram can demonstrate increased retinal thickness associated with VMTS. Careful comparative analysis of OCT

images between visits can determine the need for or timing of surgical intervention in VMTS.[11]

Epiretinal membranes are visible as a highly reflective layer on the inner retinal surface (Fig. 11.4) on OCT. Optical coherence tomography provides a means to evaluate the cross-sectional characteristics of an epiretinal membrane, enabling a quantitative measurement of retinal thickness, membrane thickness, and the separation between the membrane and inner retina. The OCT tomogram can help to distinguish between membranes globally adherent to the retina, and epiretinal membranes separated from the inner retina.[12] Quantitative measurements of membrane thickness and reflectivity can be used to establish the degree of membrane opacity.[6] In addition, OCT can reveal retinal distortion caused by epiretinal membrane contraction. Optical coherence tomography information such as membrane location and membrane thickness may be prognostic indicators of operative success after epiretinal membrane surgery. Preoperatively, OCT can help direct the operative approach, and postoperative imaging can be used to document surgical response. Optical coherence tomography measurements of macular thickness have been correlated with visual acuity in patients with epiretinal membranes.[12]

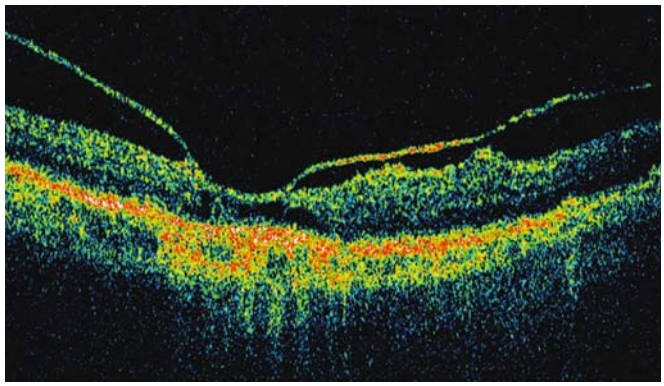

FIG. 11.3. Vitreomacular traction syndrome. Elevation and foveal detachment associated with incomplete posterior vitreous detachment. Notice hyperreflectivity posterior to the retinal pigment epithelium and choriocapillaris complex due to geographic atrophy.

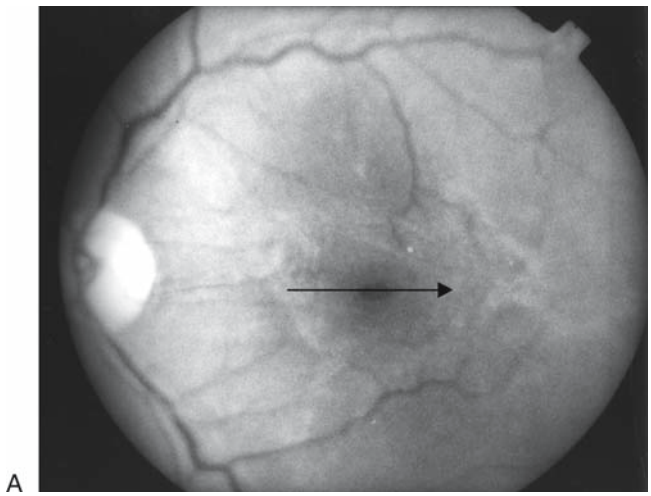

A

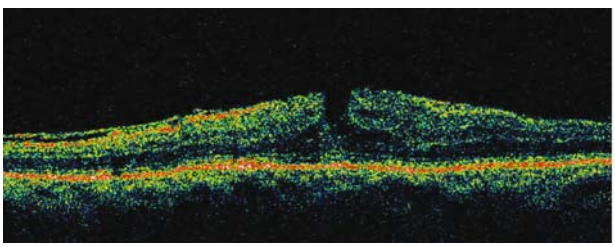

B

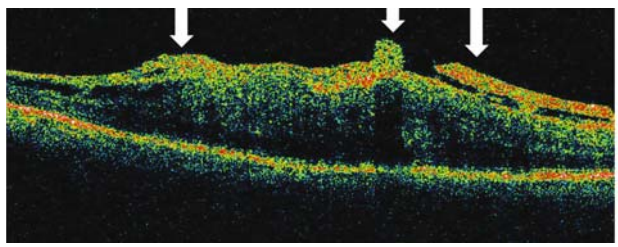

C

FIG. 11.4. Epiretinal membrane with macular pseudohole. (A) Red-free photograph. (B) Aspect with OCT. (C) Another case with an epiretinal membrane, showing an increased retinal thickness (arrows), and modification of the foveal structure.

Macular Hole

Optical coherence tomography is effective in staging macular holes, and quantitative information may be directly extracted from the OCT tomograms, including status of the vitreoretinal interface, the diameter of the hole, and the extent of surrounding subretinal fluid accumulation.[4,13] Stage 1 holes may be distinguished by a reduced or absent foveal pit and the presence of an optically clear space beneath the fovea, suggesting a foveolar detachment. Evidence of traction by the posterior hyaloid on the fovea may be present. Stage 2 holes show a partial break in a surface of the retina with a small full-thickness loss of retinal tissue (Fig. 11.5) <400 μm in size. Stage 3 holes have a full-thickness retinal dehiscence >400 μm in size with a complete break in the outer retinal tissue, and variable amounts of surrounding macular edema that increase retinal thickness and decrease reflectivity in the outer retinal layers (Fig. 11.6). Stage 4 holes can be characterized by the complete loss of tissue >400 μm in size, and a complete detachment of the posterior vitreous. Stage 1 and 2 macular holes are very difficult to differentiate ophthalmoscopically, and high-resolution OCT images can help to classify them. Stage 2 often progresses to stage 3 with some visual loss; therefore, appropriate staging with OCT can help to determine when surgery is indicated.[14]

Vitreoretinal traction is very important in the pathogenesis of macular holes, and it can be identified by OCT.[15] Furthermore, OCT may be a useful method of assessing the risk of hole formation in the fellow eye of patients with a unilateral macular hole. Duker et al.[16] found vitreoretinal interface abnormalities with OCT in 21% in the fellow eye. Posterior vitreous detachment as small as 150-μm elevation over the inner retinal surface can be detected by OCT.[6] In addition, macular hole size and postoperative resolution can be evaluated by OCT. Optical coherence tomography imaging has the ability to differentiate a full-thickness macular hole from a macular pseudohole, partial-thickness hole, or a macular cyst. Lamellar holes show an increased foveal pit contour with an intact outer neurosensory retina. Macular pseudoholes show a steepened foveal pit contour with intact outer neurosensory retina. Macular cysts and retinal detachments show a localized intraretinal and subretinal accumulation of optically clear serous fluid, respectively.

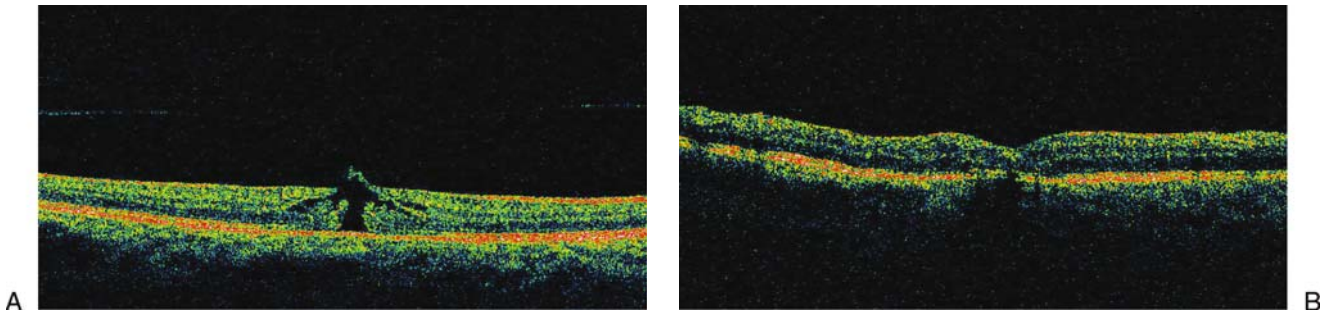

Fig. 11.5. (A) Optical coherence tomography of a stage 2 traumatic macular hole. (B) Optical coherence tomography image of closed macular hole 3 weeks after successfully treated with pars plana vitrectomy, and internal limiting membrane peeling combined with gas.

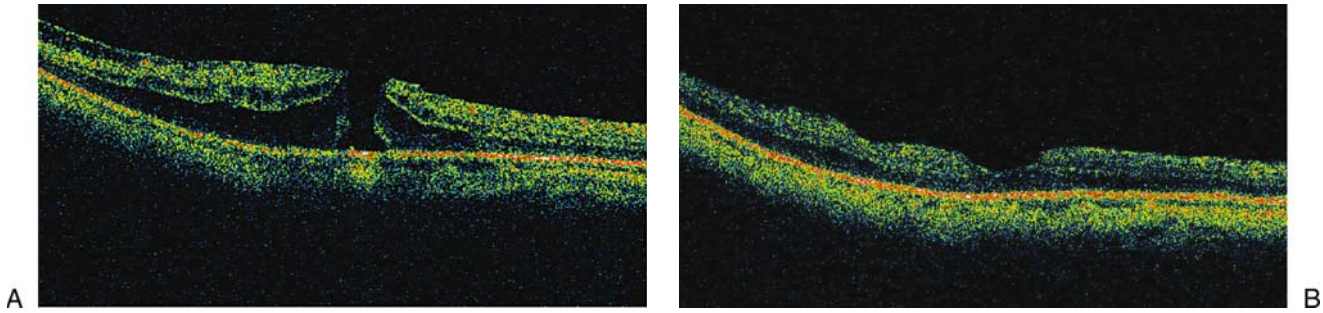

Fig. 11.6. (A) Optical coherence tomography of a stage 3 macular hole. (B) Optical coherence tomography image of macular hole 6 weeks after successfully treated with pars plana vitrectomy, and internal limiting membrane peeling combined with gas.

Retinoschisis and Retinal Detachment

Differentiating the diagnoses retinoschisis and retinal detachment is usually done on the basis of clinical examination, but for those patients in whom the diagnosis cannot be made clinically, OCT appears to be a useful tool. Optical coherence tomography images of retinoschisis show a splitting of the neurosensory retina consistent with classic histopathology findings, and OCT images of patients with retinal detachment show separation of full-thickness neurosensory retina from the underlying RPE.

The principal limitation of OCT in retinoschisis and retinal detachment is the difficulty in obtaining images anterior to the equator. However, most lesions posterior to the equator and lesions with a component posterior to the equator can be effectively imaged with OCT.[17]

Macular Edema

Optical coherent tomography is a retinal imaging technique that has applications in the diagnosis and management of macular edema produced by diabetic retinopathy, retinal vein occlusion, uveitis, epiretinal membrane, and cataract surgery.[6] In addition, OCT is able to quantify the development and resolution of macular edema after treatment (Fig. 11.7).[7]

Optical coherent tomography images of macular edema depict the presence of low intraretinal reflectivity, which corresponds to intraretinal fluid accumulation and is consistent with an increased macular thickness (Fig. 11.7B). Cystoid macular edema has cystic spaces that are visible as rounded low scattering areas, which typically occur in the neurosensorial retina (low reflective intraretinal areas). Retinal thickness is measured easily between the nerve fiber layer, and the highly backscattering red layer that represents the RPE/choriocapillaris complex. Hee et al.[18] designed an OCT protocol for monitoring macular thickness in patients with diabetic macular edema. For each eye, six consecutive OCT scans are obtained in a radial spoke pattern centered on the fovea. Therefore, retinal thickness measurements are performed at a total of 600 points on the macular area. Macular thickness is then represented as a false color topographic map and as numeric averages over nine regions covering the macula (the OCT retinal thickness map) (Fig. 11.7D,E).

The advantages of OCT include high reproducibility and accuracy. Optical coherent tomography may be more sensitive in evaluating small changes on retinal thickness than slit-lamp examination.[7] Although FA shows vascular leakage

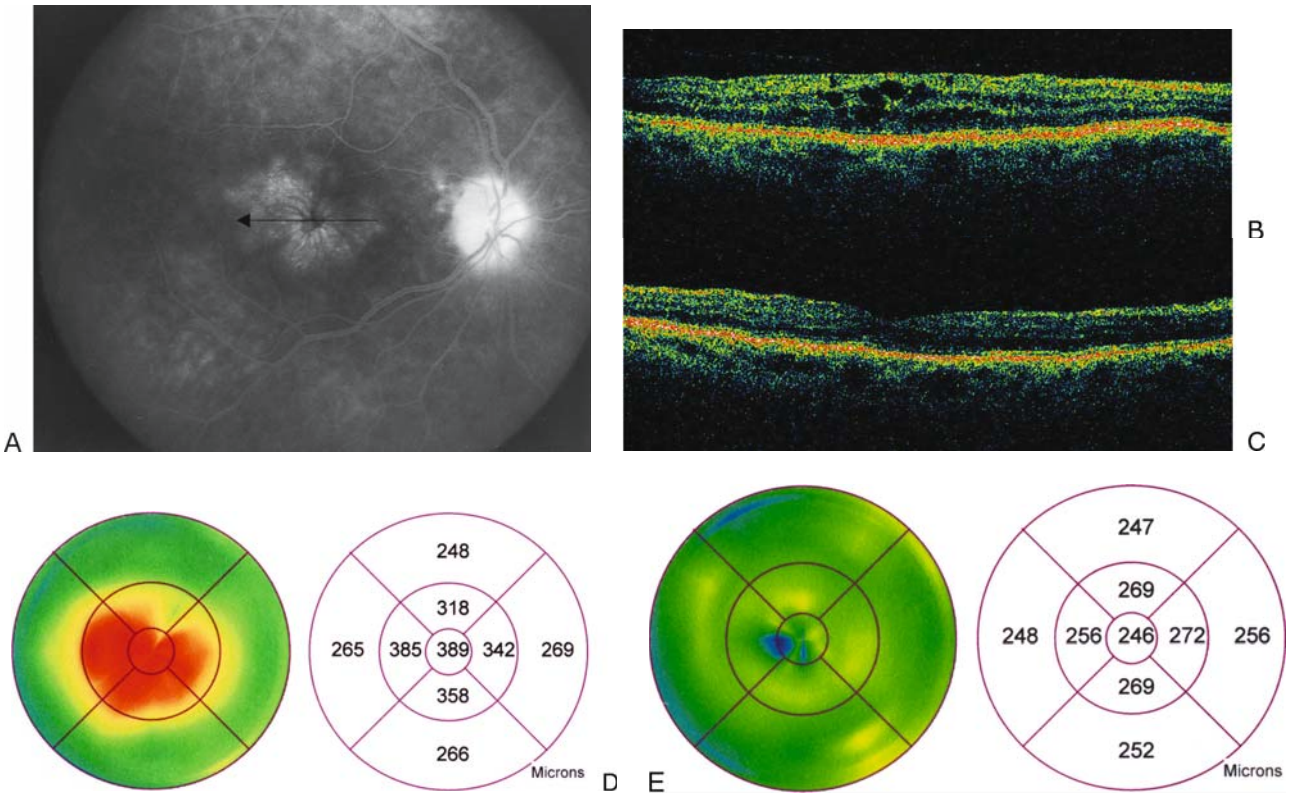

Fig. 11.7. (A) Fluorescein angiography of cystoid macular edema. (B) Optical coherence tomography demonstrates cystic macular changes as low reflective spaces (dark spaces) more prominently at the level of the outer retinal layers. (C) Optical coherence tomography image illustrates the resolution of macular edema after intravitreal triamcinolone. (D,E) Notice the improvement on the macular thickness map from the central macular thickness of 389 μm to 246 μm.

in macular edema, it does not provide a quantitative assessment. Therefore, patients may present with loss of vision with an increment in retinal thickness in the absence of vascular leak detectable by FA. Optical coherent tomography measurements of macular thickness tend to correlate with visual acuity in patients with diabetic macular edema, although that is not always the case depending on the chronicity of macular edema. Similar characteristics have been found in patients with epiretinal membrane (Fig. 11.4).[7,12]

Central Serous Chorioretinopathy

Central serous chorioretinopathy (CSCR) is characterized by serous detachments of the neurosensory retina in the macular region (Fig. 11.8A). The fovea is frequently involved, and small associated RPE detachments are commonly seen. The OCT in a neurosensory detachment appears as a shallow elevation of the retina, with an optically clear space between the retina and the high reflection of RPE/choriocapillaris, and the height of the cavity can be exactly measured (Fig. 11.8B).[6] Examination with OCT is more sensitive to identify small elevations of the neurosensory retina than slit-lamp biomicroscopy.[19] The detached RPE may be distinguished by a focal elevation of the higher reflective layer over a clear cavity (Fig. 11.8B). The detached RPE causes attenuation of the reflected light, resulting in extensive shadowing of the underlying choroidal signal. A neurosensory detachment may be connected with an RPE detachment by the discontinuity on the RPE. Longitudinal examinations with OCT can detect exact changes in height measurements of subretinal fluid, and detect CSCR resolution. Montero and Ruiz-Moreno[20] recently described bulges protruded from the RPE under a neurosensory detachment in acute and chronic CSCR, which probably meant activity of the disease. Optical coherent tomography in CSCR can provide additional information and may help distinguish it from subretinal neovascularization (SRNV) and other macular diseases. Finally, OCT has been shown to be superior to biomicroscopy and FA in identifying CSCR.[21]

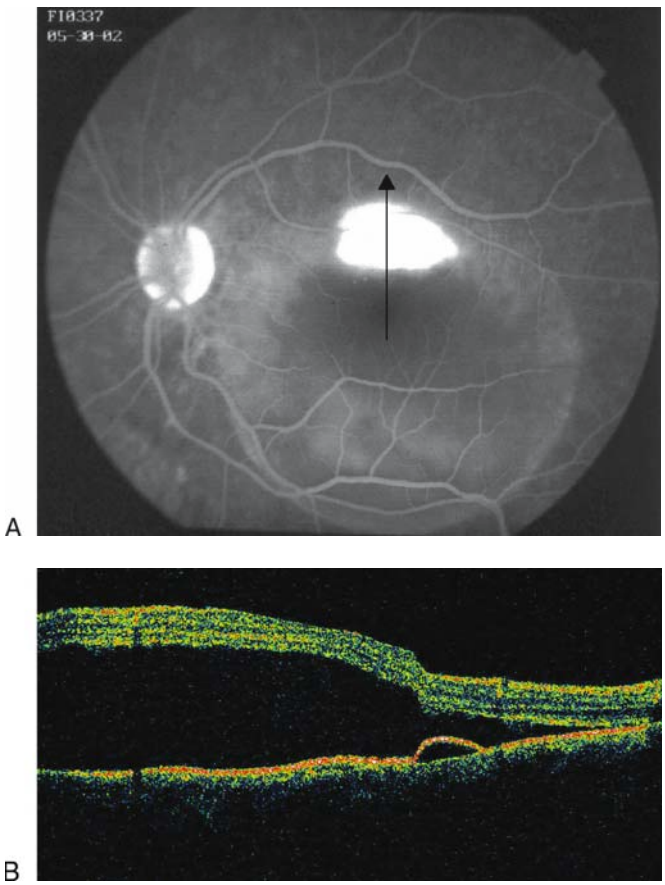

FIG. 11.8. (A) Fluorescein angiography (FA) in central serous chorioretinopathy (CSCR) shows a pinpoint area of dye leakage in the retinal pigment epithelium (RPE) and a large serous detachment under the neurosensory retina. (B) Optical coherence tomography scan through the macula demonstrates the RPE (focal leakage point on FA) and neurosensory detachment.

Choroidal Neovascularization and Age-Related Macular Degeneration

Optical coherent topography has been used to characterize drusen, geography atrophy, choroidal and subretinal neovascularization, neurosensory detachment and RPE detachment associated with age-related macular degeneration (AMD).[6,22] Soft drusen are observed as focal elevations in the external, highly reflective band (RPE/choriocapillaris complex) consistent with the accumulation of amorphous material within or beneath Bruch's membrane. Geographic atrophy is highly distinctive on OCT because the overlying retina is thinned and the hypopigmented RPE causes increased penetration of the optical probe beam into the deeper choroid, significantly enhancing the reflections from this layer. Hyperpigmented RPE areas (hypertrophy or hyperplasia) on OCT show as high reflectivity from the RPE with shadowing of the reflections from the choroid. Intraretinal edema appears as an area of low intraretinal reflectivity, which corresponds to intraretinal fluid accumulation and is consistent with an increased retinal thickness. An RPE detachment demonstrates an elevation of the reflective band corresponding to the RPE/choriocapillaris complex and shadowing of the reflections returning from the deeper choroid. In contrast, neurosensory retinal detachments appear as elevations of the sensory retina above an optically clear space.

Subretinal neovascularization is characterized by increased optical reflectivity of the RPE or disruption of the highly reflective band layer RPE/choriocapillaris. Angiographically well-defined subretinal neovascularization is visualized as a localized disruption and fusiform thickening of the RPE/choriocapillaris reflection with defined boundaries (Fig. 11.9A,B). In contrast, occult subretinal neovascularization tends to show an irregular elevation of the RPE with a

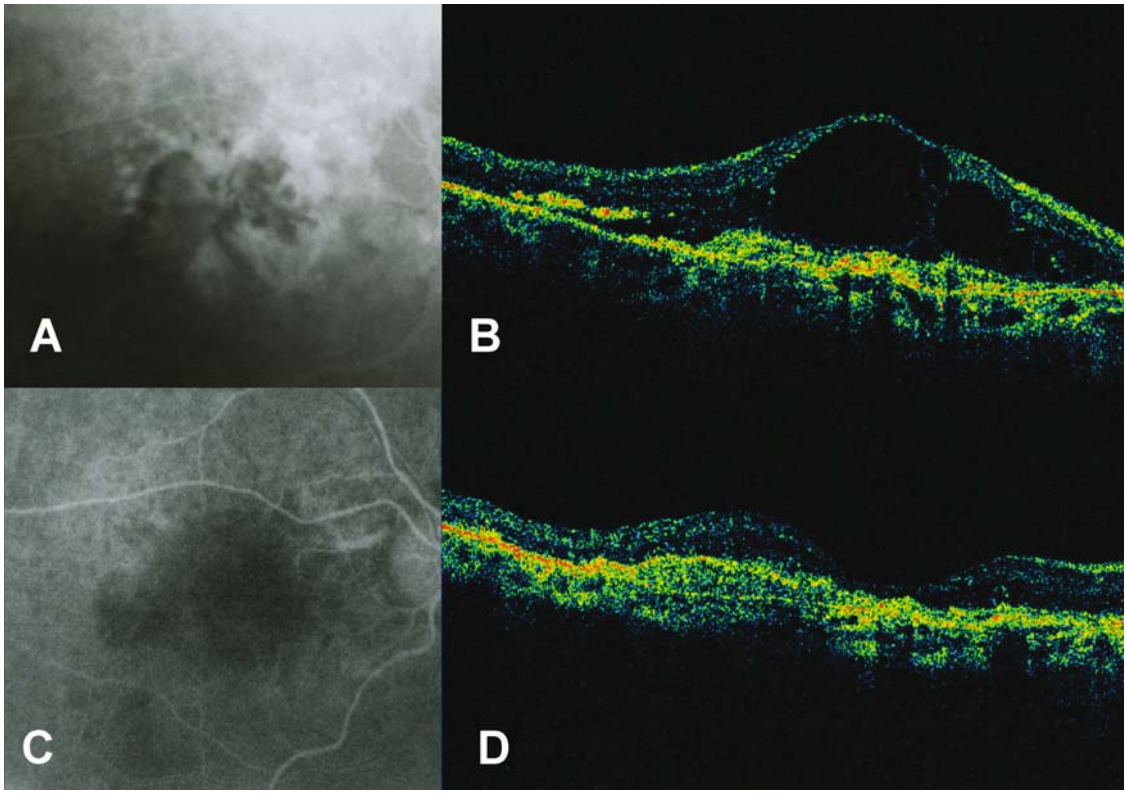

FIG. 11.9. Choroidal neovascularization (CNV) and age-related macular degeneration. (A,B) Choroidal neovascularization located under the retinal pigment epithelium (Gass type I) with cystoid macular edema visualized with fluorescein angiography (FA) and optical coherence tomography (OCT). (C,D) Foveal thickness has been normalized after a photodynamic therapy (PDT) session, OCT shows normalization of the foveal contour, and FA demonstrates hypofluorescence.

deeper area of mild backscattering corresponding to fibrous proliferation. Laser treatment of subretinal neovascularization leads to atrophic scarring, which appear on OCT as highly reflective at the chorioretinal interface. Argon laser retinal lesions evaluated in vivo by OCT demonstrated relative high reflection in the middle of the lesion and relative low reflection around the lesion.[23]

Optical coherence tomography has been used to confirm subretinal neovascularization resolution after photodynamic therapy (PDT) with verteporfin (Visudyne) (Fig. 11.9C,D).[24,25] Optical coherence tomography is effective in AMD because it can detect subretinal neovascularization darkened by a thin layer of fluid or hemorrhage, delineate SRNV boundaries, and quantify changes in response to therapy.

Retinal Vascular Occlusion Disease

Retinal vascular diseases are common etiologies for central visual loss. Optical coherence tomography shows increased retinal thickness with cystic spaces of low reflectivity in patients with branch retinal artery occlusion and central retinal artery occlusion. In addition, the inner retinal layers tend to be more highly reflective in OCT, probably due to ischemia of these layers. Therefore, this high reflection causes shadowing of the optical signal of the RPE/choriocapillaris complex. The increased thickness of the inner retina typically seen in acute artery occlusions corresponds to the intracellular edema (Fig. 11.10). Optical coherence tomography complements the information obtained from FA in retinal vascular diseases.[26]

Occlusion of the retinal venous system is the second most common retinal vascular disease after diabetic retinopathy.[27] Optical coherence tomography findings include cystic macular edema (CME), serous retinal detachment, epiretinal membranes, pseudoholes, lamellar holes, and subhyaloid or preretinal hemorrhages in branch retinal vein occlusion (Fig. 11.11) and central retinal vein occlusion (Fig. 11.12). A significant proportion of patients with occlusion of the retinal venous system have OCT evidence of CME and serous retinal detachment. Optical coherence tomography shows hyporeflective intraretinal cavities in a cross-sectional scan radiating from the center of the macula in CME (Fig. 11.11B,C). Macular edema is associated with serous retinal detachment in retinal venous system occlusion.[27] Optical coherence tomography plays a pivotal role in quantitatively monitoring changes in retinal thickness after treatment such as intravitreal triamcinolone injection or radial optic neurotomy.[28,29]

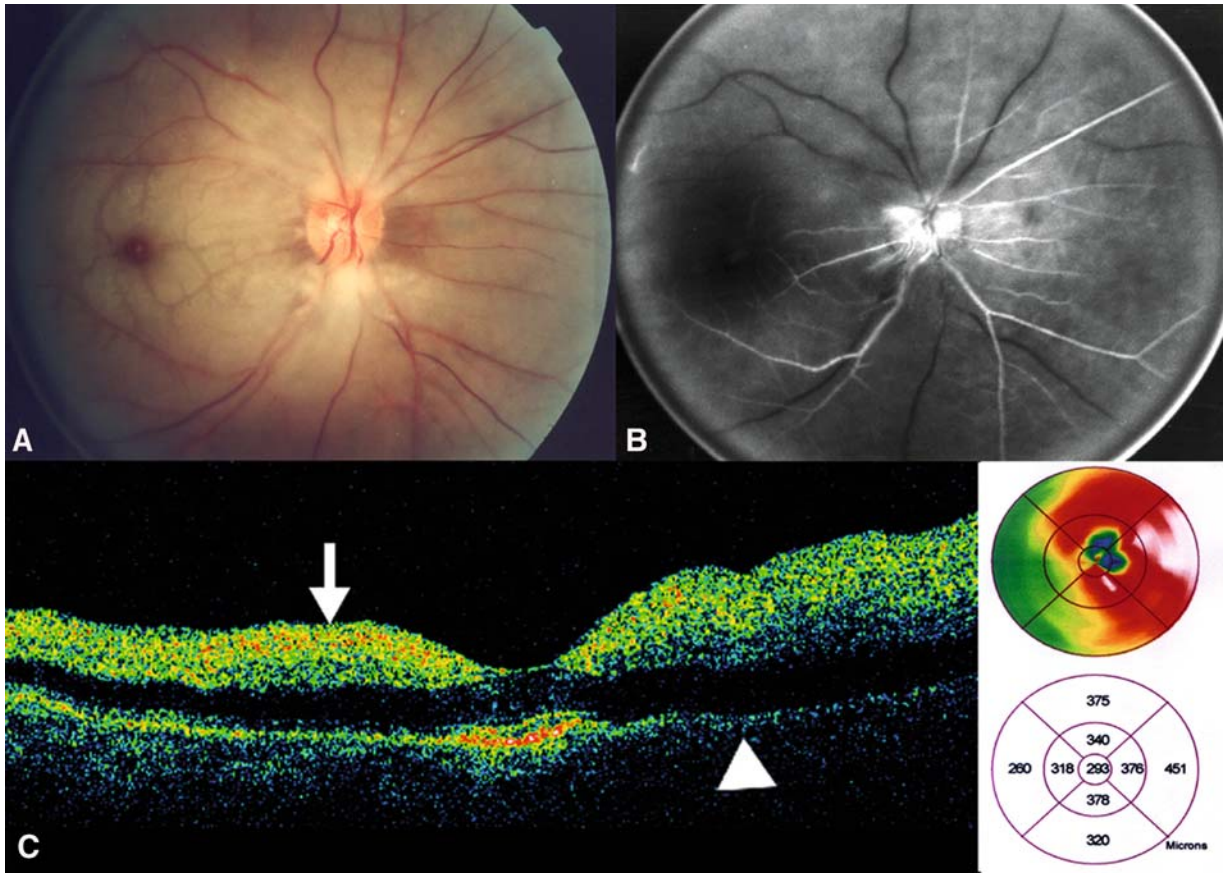

FIG. 11.10. Central retinal artery occlusion. (A) Color fundus photograph demonstrates whitening of the retina and a "cherry-red" spot. (B) Fluorescein angiogram reveals poor retinal vascular filling. The leading edge of dye within the superior arterial system is distinctly abnormal, and indicates hypoperfusion. (C) Horizontal OCT scan shows increased thickness and reflectivity of the inner retinal layers (arrow); this high reflectivity causes shadowing of the optical signals of the outer retinal layers and the retinal pigment epithelium/choriocapillaris complex (arrowhead). The retinal thickness map demonstrates increased central thickness (293 μm), especially nasal to the fovea due to intracellular edema and ischemia of the papillomacular bundle (insert).

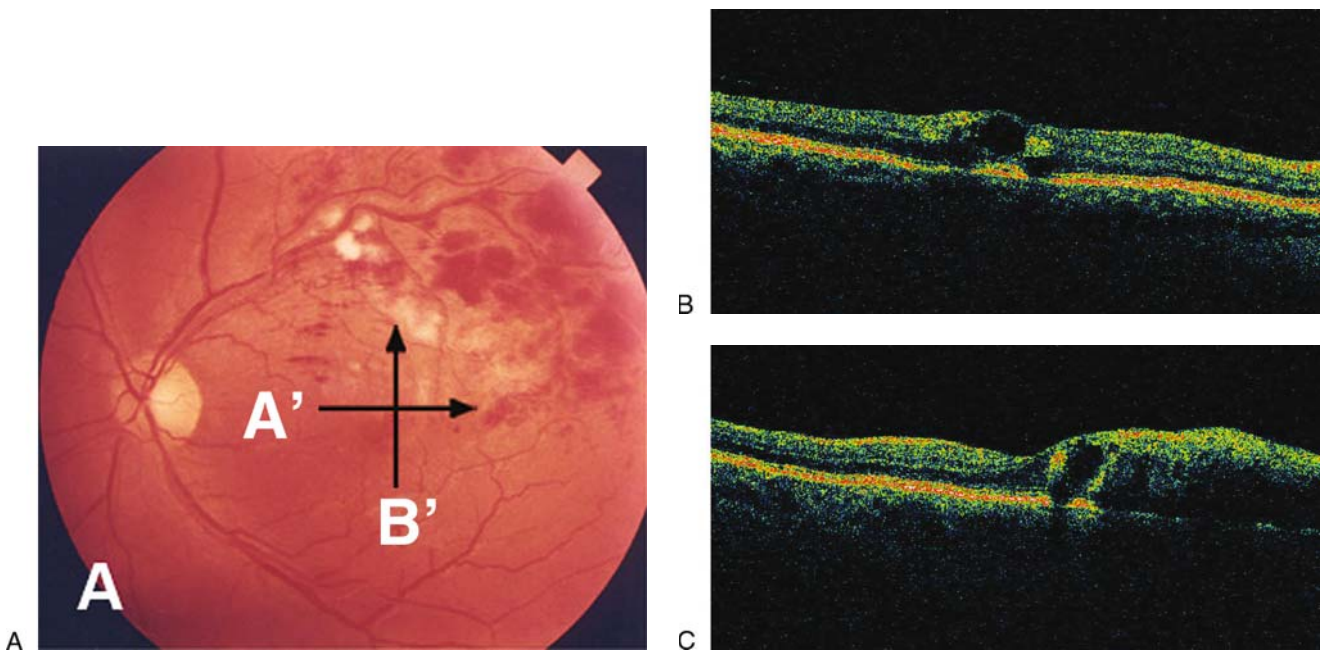

FIG. 11.11. Branch retinal vein occlusion with macular edema. (A) Fundus photograph. (B) Horizontal OCT scan (A' in A) showed diffuse retinal thickening and low reflective spaces consistent with macular cysts. (C) Vertical OCT scan (B' in A) confirms cystoid macular edema.

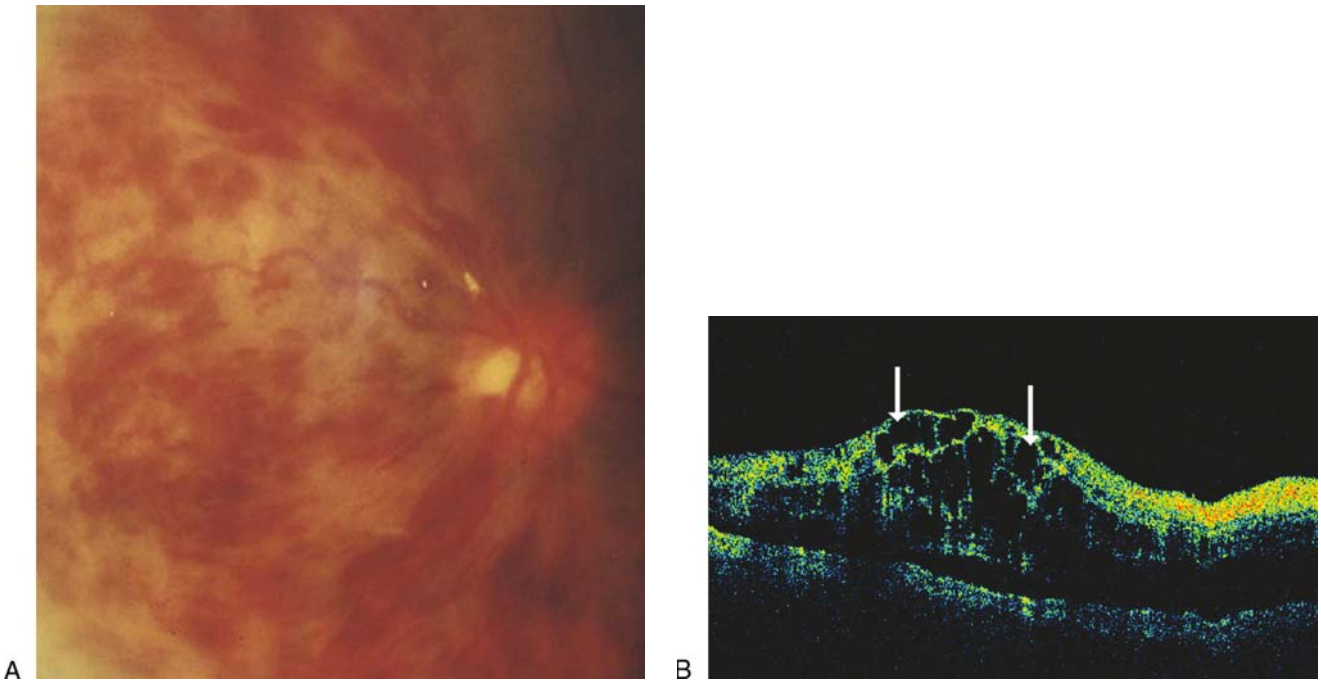

FIG. 11.12. Central retinal vein occlusion with macular edema. (A) Fundus photograph. (B) Optical coherence tomography scan shows a thickened elevated macula with numerous low reflective cystic spaces representing fluid accumulation (arrows). A detachment of the neurosensory retina with subretinal fluid accumulation is observed underneath the fovea.

Parafoveal Telangiectasis

Retinal telangiectasis refers to a developmental retinal vascular disorder characterized by an ectasia of capillaries of the retina, in which irregular capillary dilation and incompetence occur in the retinal periphery of the macula. Gass[30] described a classification of three subgroups.

Optical coherence tomography depicts clearly the involvement of the intraretinal and subretinal spaces in this condition (Fig. 11.13). Parafoveal telangiectasis may show low reflective intraretinal areas of macular edema and highly reflective lipid exudates on OCT. Plaques of RPE hyperplasia appear as intraretinal hyperreflective spots associated with shadowing of the reflections from the tissue below. In addition, OCT may show subretinal neovascularization associated with juxtafoveal telangiectasis.[26]

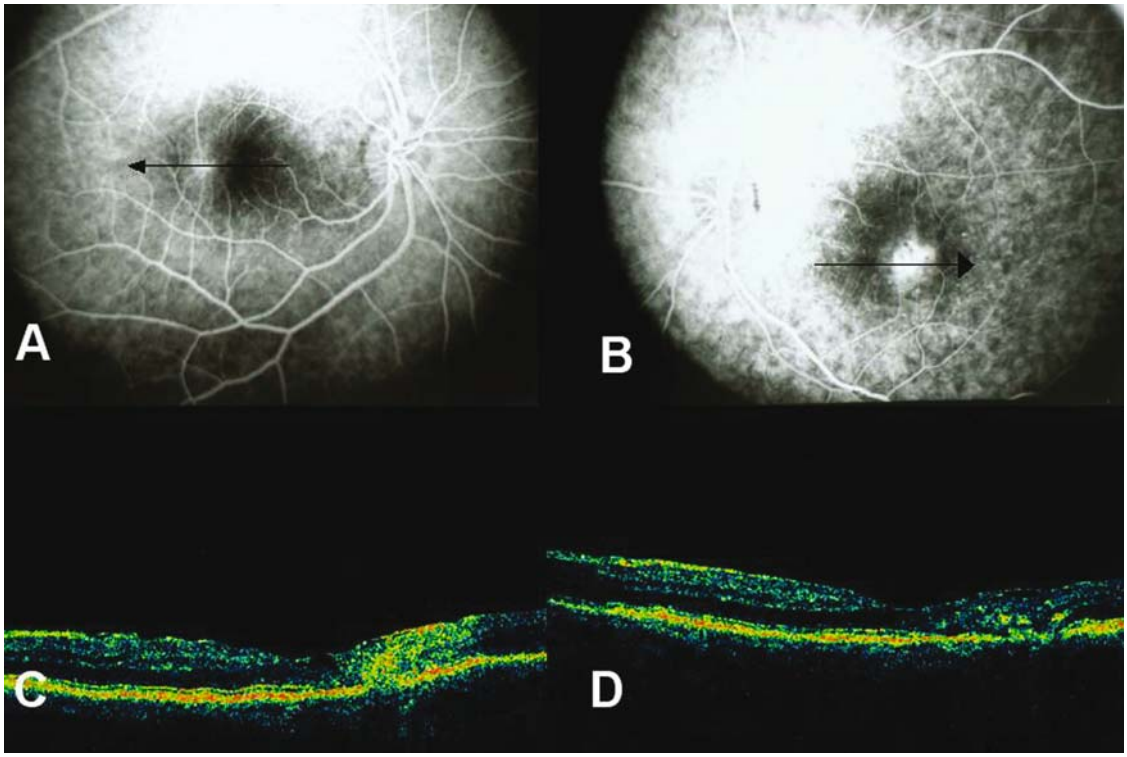

FIG. 11.13. Idiopathic parafoveal telangiectasis. (A,B) Fluorescein angiography of both eyes. (C,D) A horizontal OCT scan of each eye shows vascular area of high intraretinal reflectivity.

Other Retinal Diseases and Response to Therapy

Optical coherence tomography is useful to visualize other retinal diseases such as RPE detachments with or without AMD (Fig. 11.14), subhyaloidal hemorrhages (Fig. 11.15), proliferative diabetic retinopathy with new vessels on disc (NVD) (Fig. 11.16), and cytomegalovirus retinitis with flat retinal detachment in a patient with the acquired immunodeficiency syndrome (Fig. 11.17). Optical coherence tomography enables the differentiation between types I and type II choroidal neovascularization (CNV) (Fig. 11.18). In addition, OCT enables demonstrating subretinal serous fluid accumulation and deposits in choroidal melanoma (Fig. 11.19), the natural course of drusen (Fig. 11.20), diabetic macular edema (Fig. 11.21), and CSCR (Fig. 11.22); these conditions can be followed with OCT as well as the response to therapeutic interventions. Optical coherence tomography provides information in a reproducible way, such as monitoring the course of macular hole in degenerative myopia successfully closed with vitrectomy surgery (Fig. 11.23). Retinoschisis sometimes is very difficult to differentiate ophthalmoscopically in degenerative myopia, and high-resolution OCT images can help to demonstrate its features (Fig. 11.24).

Acknowledgments. The authors have no proprietary or financial interest in any products or techniques mentioned in this chapter. This work is supported in part by the Fundacion Arevalo-Coutinho para la Investigacion en Oftalmologia (FACO), Caracas, Venezuela.

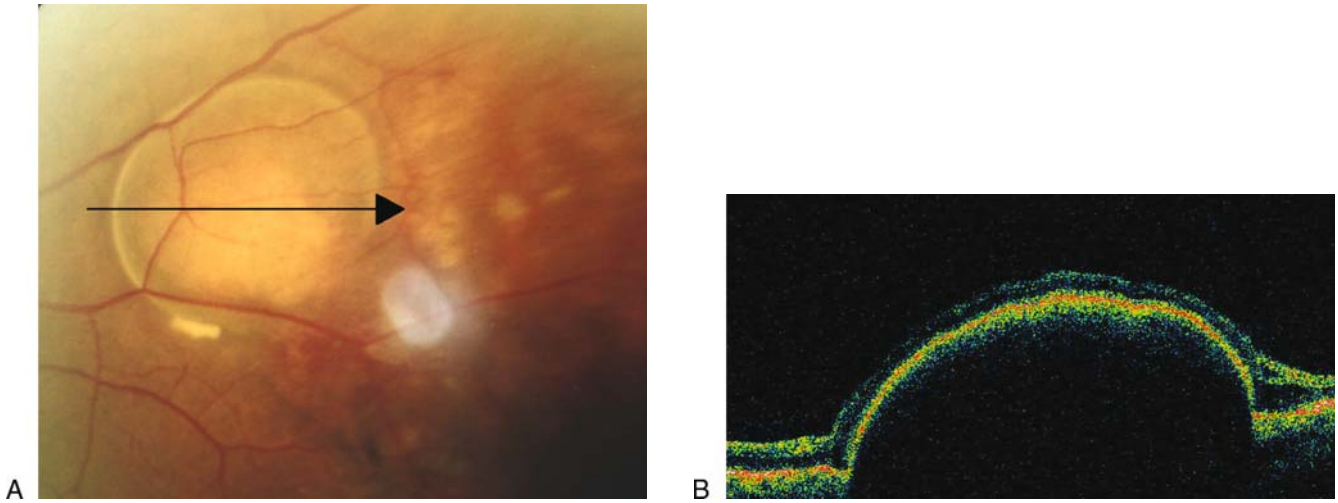

FIG. 11.14. Age-related macular degeneration with eccentric hemorrhagic retinal pigment epithelial detachment. (A) Fundus photograph. (B) Optical coherence tomography shows the retina and hyperreflective band corresponding to the RPE/choriocapillaris elevated over an optically clear cavity.

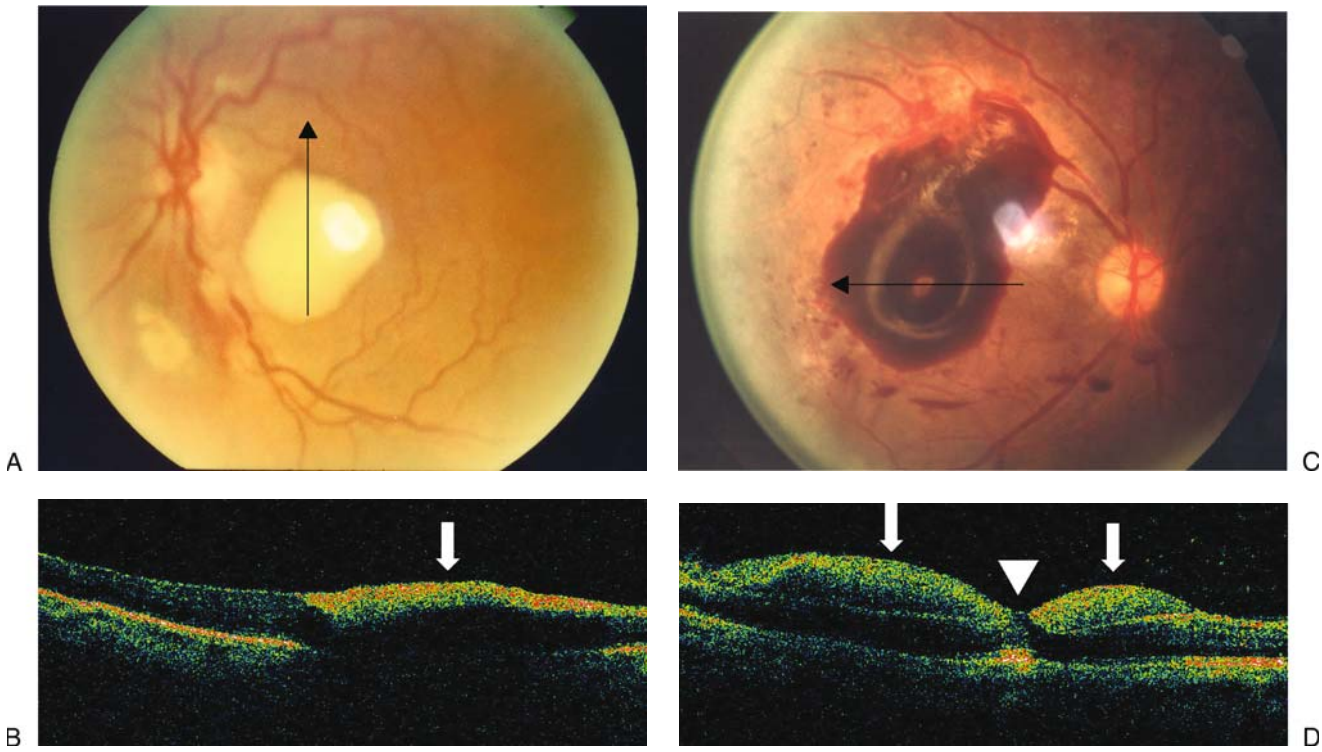

FIG. 11.15. (A) Fundus photograph shows subhyaloidal hemorrhage in reabsorption. (B) Optical coherence tomography. There is a thick and irregular band of high reflectivity that corresponds to subhyaloidal blood (arrow). Attenuation of the signal results in shadowing of the underlying layers, limiting visualization of these structures. (C) Subhyaloidal macular hemorrhage without involving the fovea. (D) Optical coherence tomography image demonstrates a thick band of high reflectivity that corresponds to subhyaloidal blood (arrows) and shows strong attenuation of the incident light shadowing the reflection from the retinal pigment epithelium and choroid. However, the fovea is visualized as highly reflective because there is no hemorrhage in the center (arrowhead).

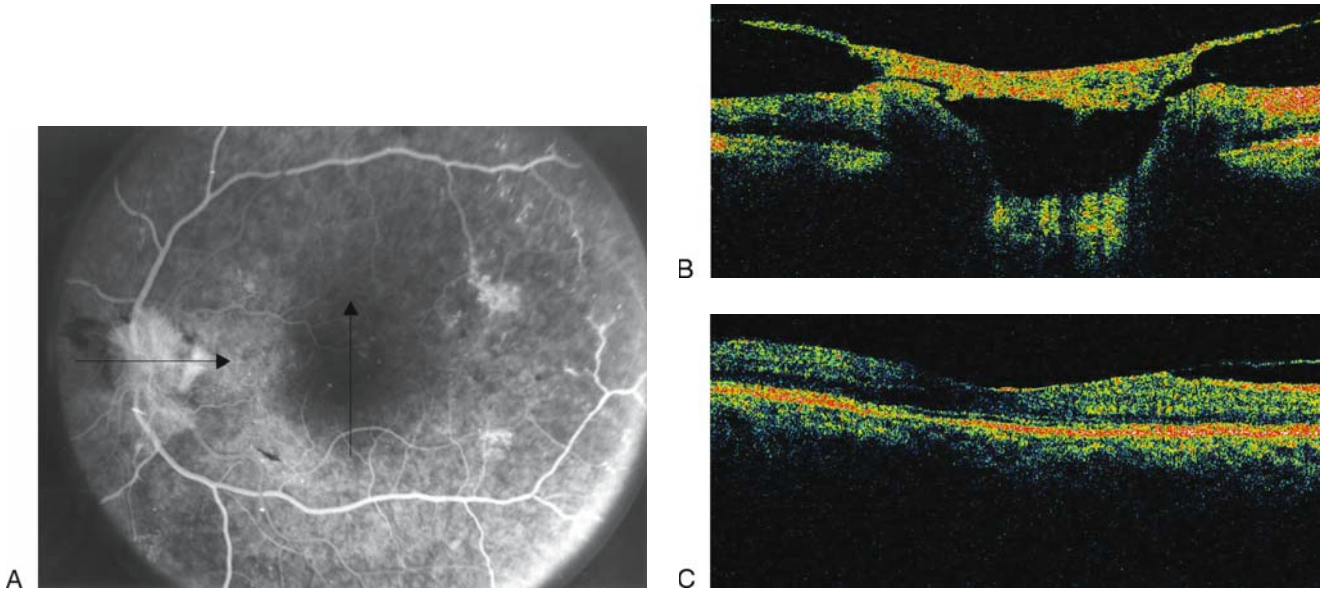

FIG. 11.16. Proliferative diabetic retinopathy with new vessels on disc (NVD). (A) Fluorescein angiography. (B) Horizontal optical coherence tomography scan through the optic disc illustrates NVD. (C) Vertical OCT scan obtained through the macula with retinal traction due to partial posterior vitreous detachment.

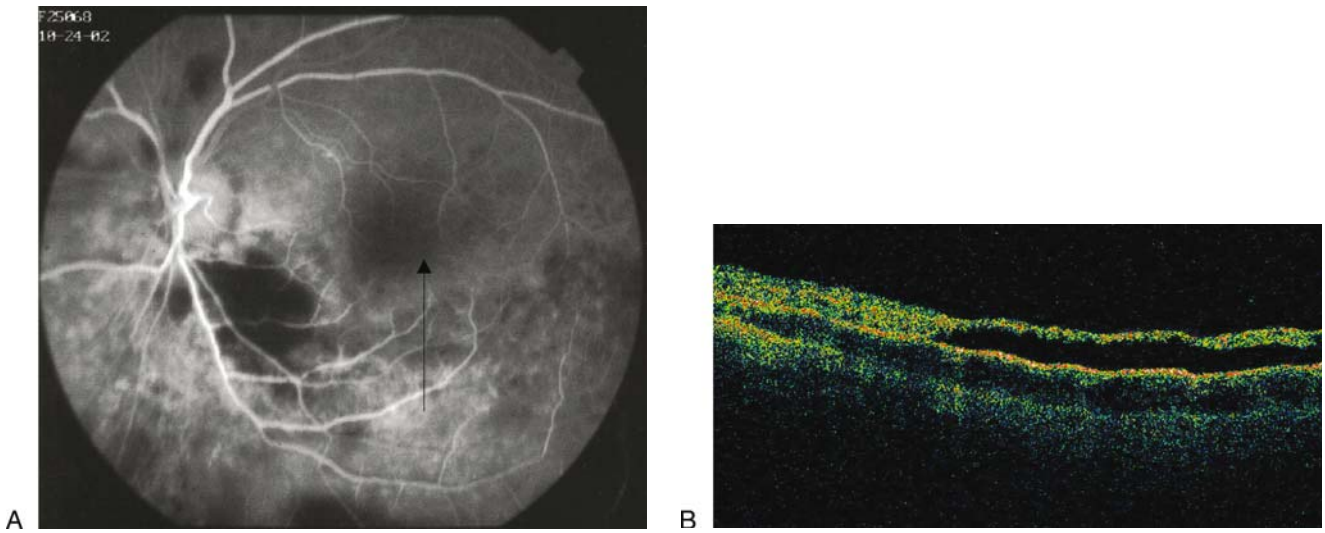

FIG. 11.17. Cytomegalovirus retinitis with flat retinal detachment in a patient with acquired immunodeficiency syndrome. (A) Fluorescein angiography. (B) Optical coherence tomography image shows a flat retinal detachment with retinal atrophy.

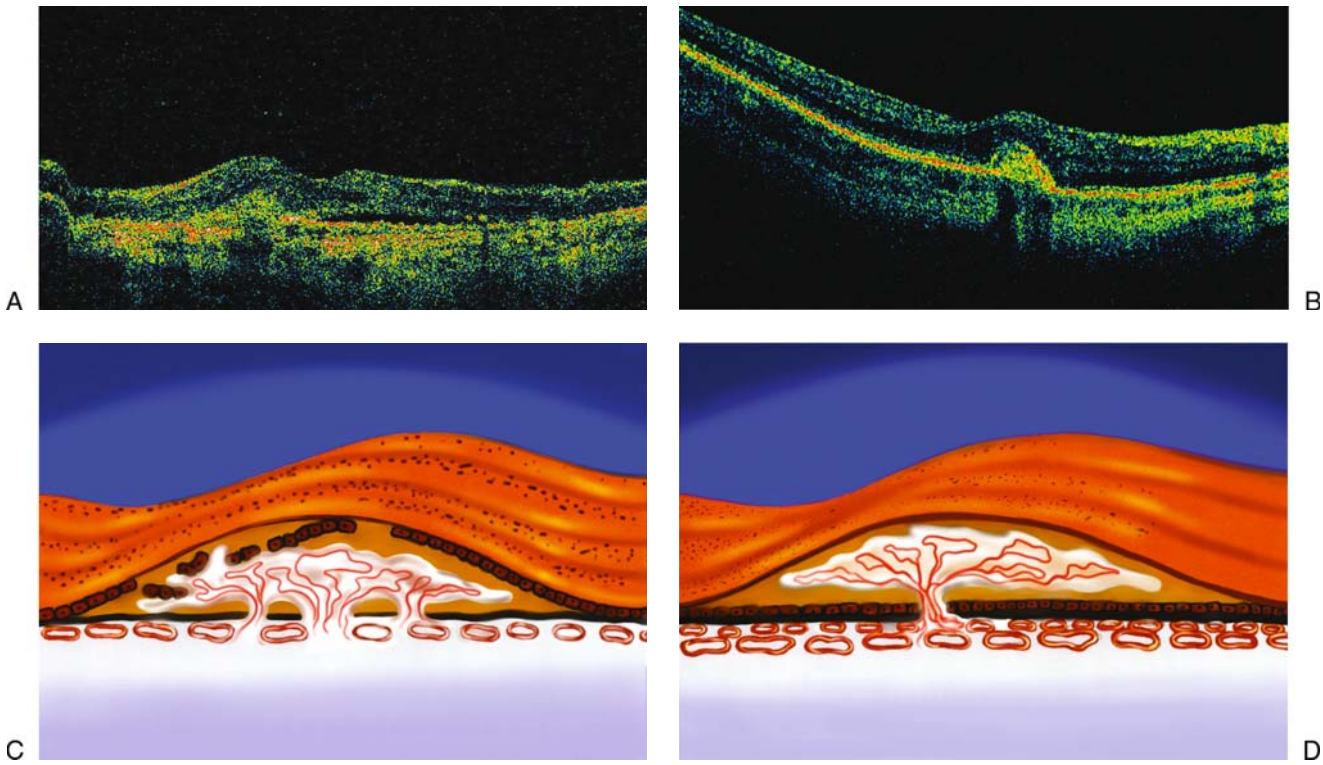

FIG. 11.18. Optical coherence tomography is a reliable technique to differentiate between type I and type II choroidal neovascularization (CNV) membranes. (A) An OCT image shows CNV type I (fibrous-vascular tissue complex is beneath the retinal pigment epithelium [RPE]). (B) An OCT image shows a CNV type II (fibrous tissue complex is between RPE and photoreceptors). (C) Drawing of CNV type I. (D) Drawing of CNV type II.

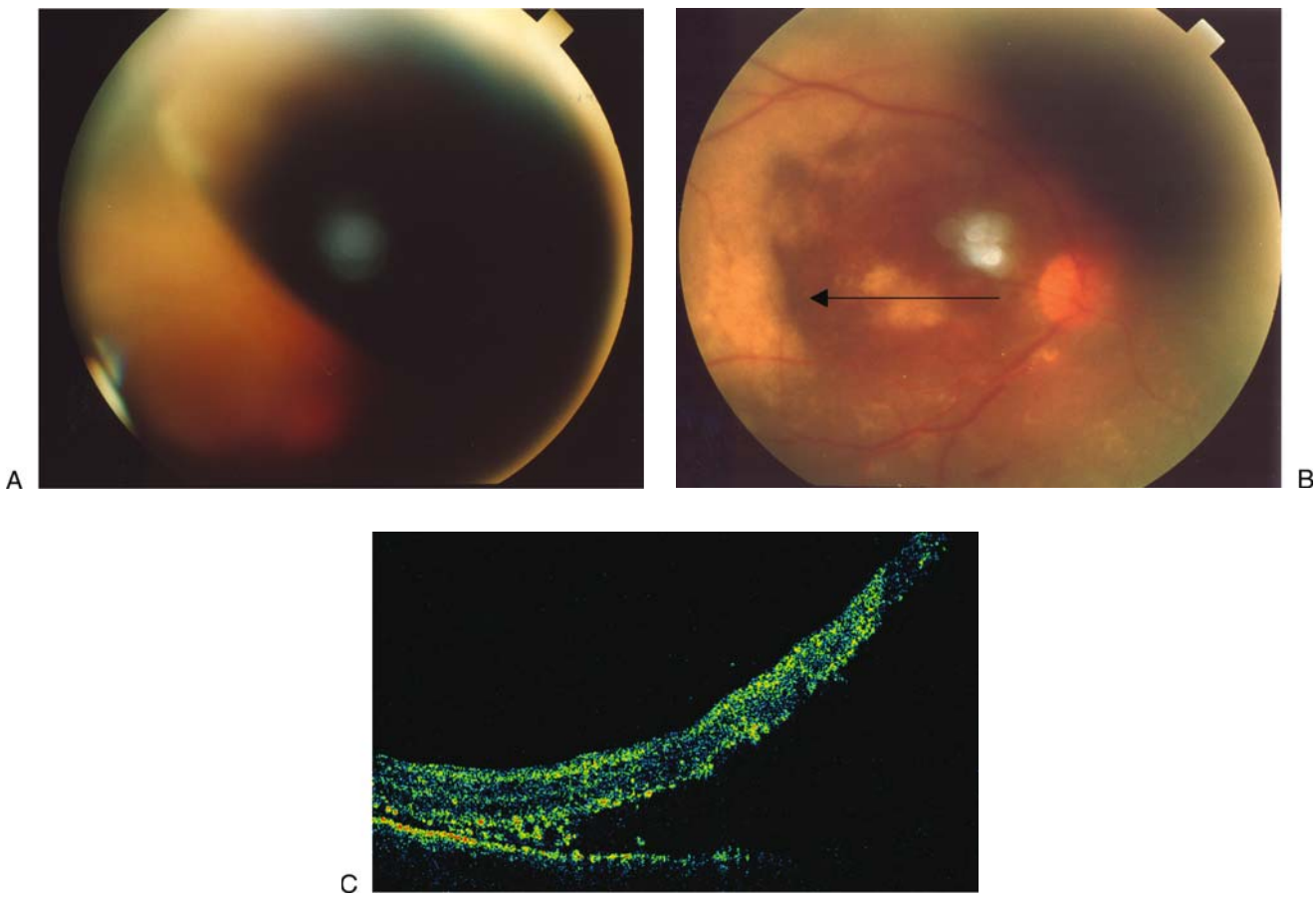

FIG. 11.19. Optical coherence tomography demonstrates subretinal serous fluid accumulation and deposits in choroidal melanoma. (A,B) Fundus photographs. (C) Optical coherence tomography image shows serous retinal detachment and subretinal deposits.

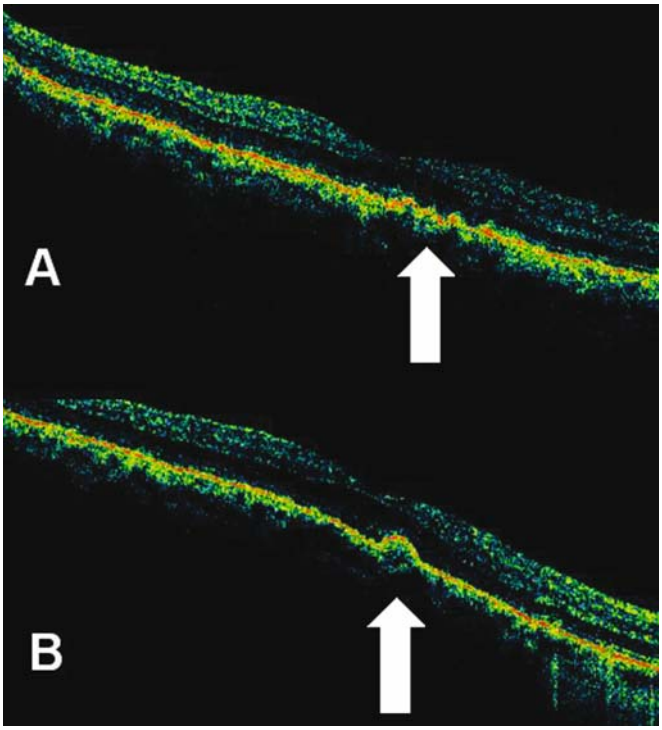

FIG. 11.20. Optical coherence tomography images show multiple nodules along the retinal pigment epithelium/choriocapillaris complex (external band) corresponding to drusen (arrows).

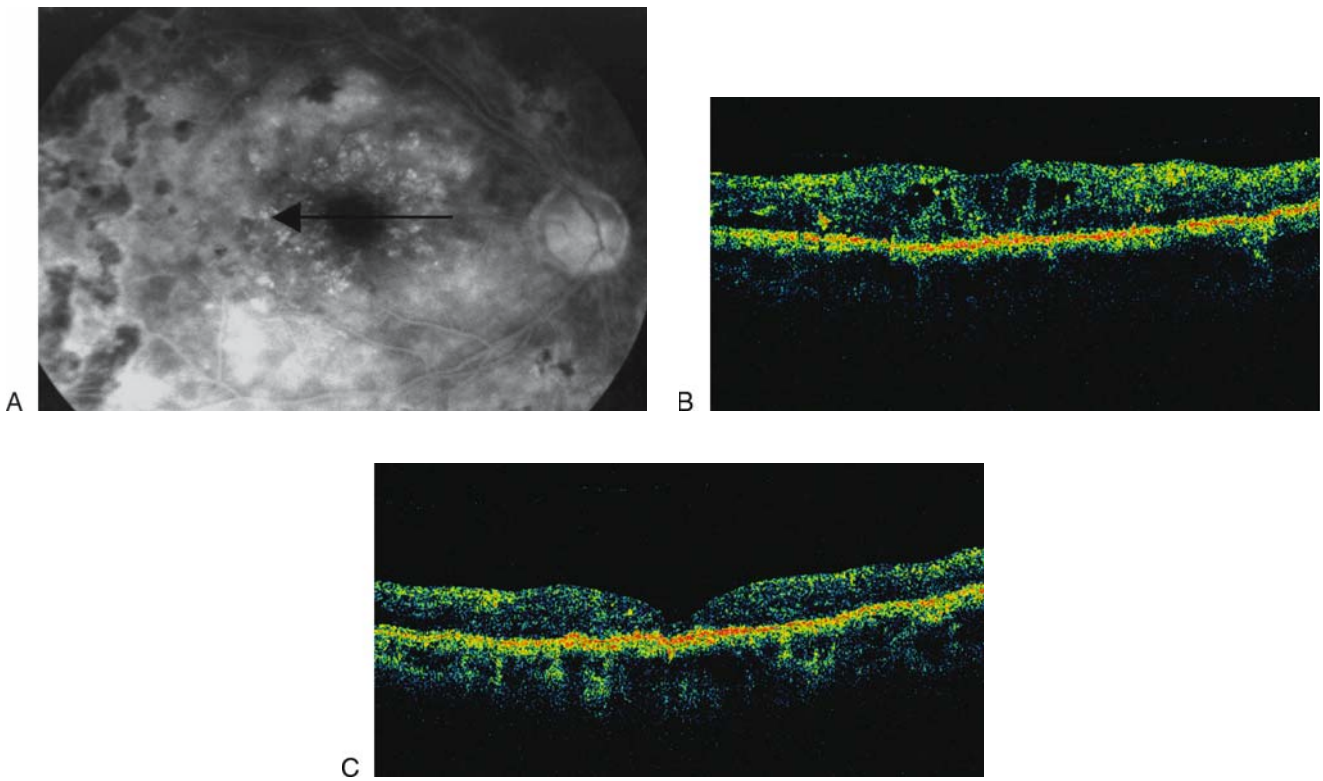

FIG. 11.21. (A) Fluorescein angiography shows diffused diabetic macular edema. (B) Optical coherence tomography illustrates diffuse retinal thickening and cystic spaces consistent with cystoid macular edema (retinal thickness 388 μm). (C) An OCT image illustrates the resolution after intravitreal triamcinolone injection and focal/grid photocoagulation (retinal thickness 197 μm).

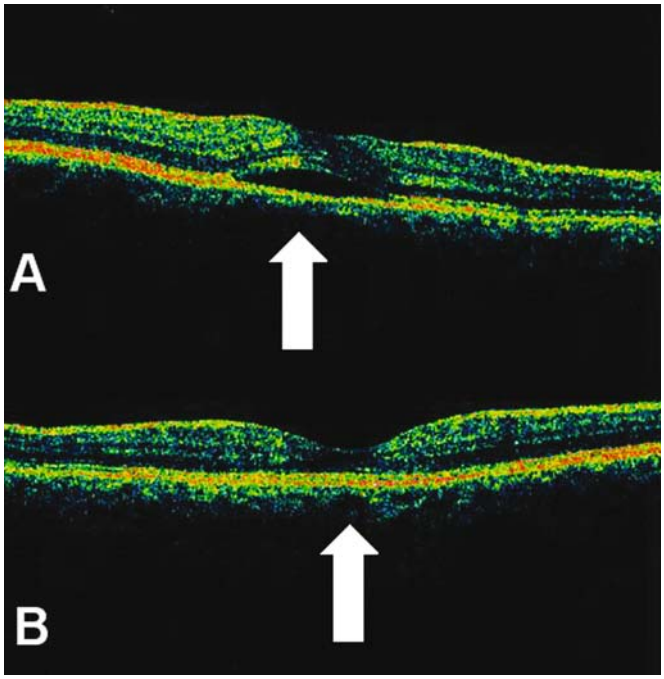

FIG. 11.22. (A) Optical coherence tomography image illustrates shallow neurosensory detachment consistent with central serous chorioretinopathy. (B) Optical coherence tomography confirms the resolution of subretinal fluid after photodynamic therapy.

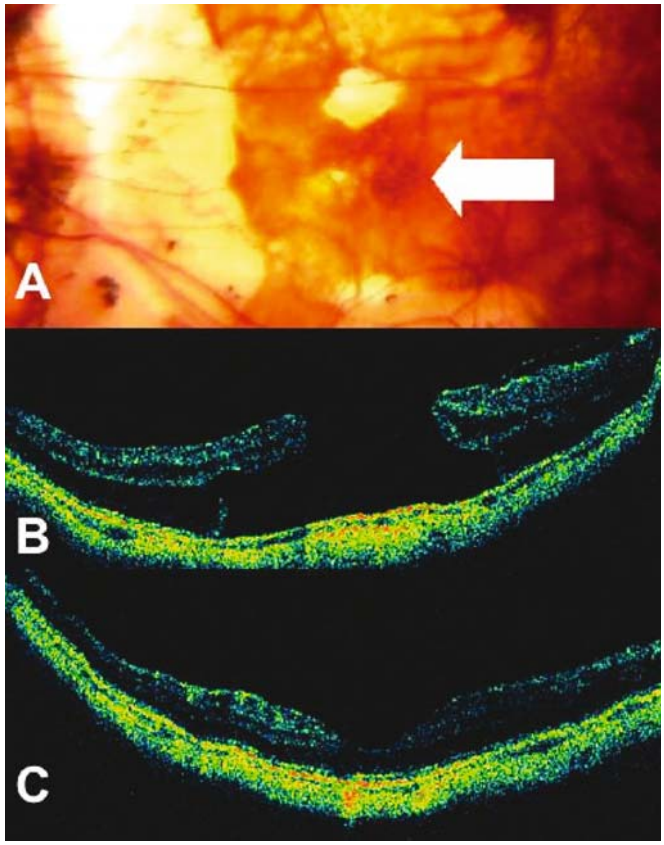

FIG. 11.23. (A) Retinal examination revealed a stage 4 macular hole (arrow) in the left eye associated with a posterior pole retinal detachment, and a best-corrected visual acuity (BCVA) of counting fingers. (B) Optical coherence tomography image shows features of both foveal retinal detachment and retinoschisis. (C) Optical coherence tomography after vitrectomy reveals a closed macular hole with a BCVA of 20/150.

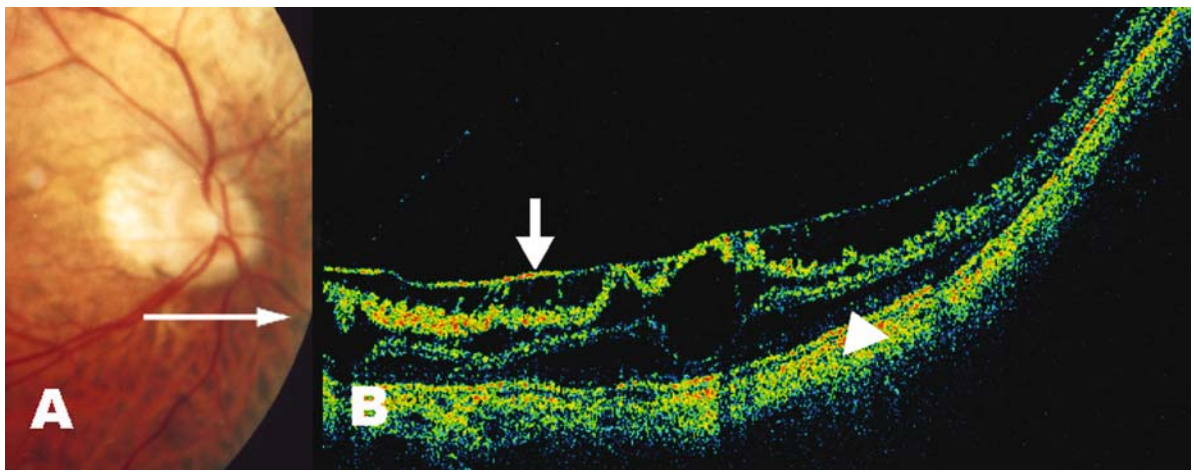

FIG. 11.24. Myopic degeneration with retinoschisis. (A) Color fundus photograph distinctly shows a myopic crescent as a white, sharply defined area where inner surface of the sclera is seen. Retinoschisis inferior to the optic disc was not differentiated ophthalmoscopically. (B) A horizontal OCT scan obtained inferior to the optic disc demonstrates a splitting of the neurosensory retina (arrow) and separation of full-thickness neurosensory retina from the underlying retinal pigment epithelium (arrowhead).

References

1. Huang D, Swanson EA, Lin CP, et al. Optical coherence tomography. Science 1991;254:1178–1181.
2. Pavlin CJ, Harasiewicz K, Sherar MD, Foster FS. Clinical use of ultrasound biomicroscopy. Ophthalmology 1991;98:287–295.
3. Laser Institute of America. American National Standard for the Safe Use of Lasers. Toledo, OH: Laser Institute of America, 1986.
4. Hee MR, Puliafito CA, Wong C, et al. Optical coherence tomography of macular holes. Ophthalmology 1995;102:748–756.
5. Puliafito CA, Hee MR, Lin CP, et al. Imaging of macular diseases with optical coherence tomography. Ophthalmology 1995;102:217–229.
6. Puliafito CA, Hee MR, Schuman JS, Fujimoto JG. Optical Coherence Tomography of Ocular Diseases, 1st ed. Thorofare, NJ: Slack, 1996.
7. Hee MR, Puliafito CA, Wong C, et al. Quantitative assessment of macular edema with optical coherence tomography. Arch Ophthalmol 1995;113:1019–1029.
8. Hee MR, Izatt JA, Swanson EA, et al. Optical coherence tomography of the human retina. Arch Ophthalmol 1995;113:325–332.
9. Baumann M, Gentile RC, Liebmann JM, Ritch R. Reproducibility of retinal thickness measurements in normal eyes using optical coherence tomography. Ophthalmic Surg Lasers 1998;29:280–285.
10. Toth CA, Narayan DG, Boppart SA, et al. A comparison of retinal morphology viewed by optical coherence tomography and by light microscopy. Arch Ophthalmol 1997;115:1425–1428.
11. Munuera JM, Garcia-Layana A, Maldonado MJ, Aliseda D, Moreno-Montanes J. Optical coherence tomography in successful surgery of vitreomacular traction syndrome. Arch Ophthalmol 1998;116:1388–1389.
12. Wilkins JR, Puliafito CA, Hee MR, et al. Characterization of epiretinal membranes using optical coherence tomography. Ophthalmology 1996;103:2142–2151.
13. Gass JD. Reappraisal of biomicroscopic classification of stages of development of a macular hole. Am J Ophthalmol 1995;119:752–759.
14. Gass JD, Joondeph BC. Observations concerning patients with suspected impending macular holes. Am J Ophthalmol 1990;109:638–646.
15. Gass JD. Idiopathic senile macular hole. Its early stages and pathogenesis. Arch Ophthalmol 1988;106:629–639.
16. Duker JS, Puliafito CA, Wilkins JR, et al. Imaging fellow eyes in patients diagnosed with idiopathic macular holes using optical coherence tomography (OCT). Ophthalmology 1995;102(suppl):118.
17. Ip M, Garza-Karren C, Duker JS, et al. Differentiation of degenerative retinoschisis from retinal detachment using optical coherence tomography. Ophthalmology 1999;106:600–605.
18. Hee MR, Puliafito CA, Duker JS, et al. Topography of diabetic macular edema with optical coherence tomography. Ophthalmology 1998;105:360–370.
19. Hee MR, Puliafito CA, Wong C, et al. Optical coherence tomography of central serous chorioretinopathy. Am J Ophthalmol 1995;120:65–74.
20. Montero JM, Ruiz-Moreno JM. Optical coherence tomography characterization of idiopathic central serous chorioretinopathy. Br J Ophthalmol 2005;89:562–564.
21. Wang M, Sander B, Lund Anderson H, Larsen M. Detection of shallow detachments in central serous Chorioretinopathy. Acta Ophthalmol Scand 1999;77:402–405.
22. Hee MR, Baumal CR, Puliafito CA, et al. Optical coherence tomography of age-related macular degeneration and choroidal neovascularization. Ophthalmology 1996;103:1260–1270.
23. Toth CA, Birngruber R, Boppart SA, et al. Argon laser retinal lesions evaluated in vivo by optical coherence tomography. Am J Ophthalmol 1997;123:188–198.
24. Baumal CR, Puliafito CA, Pierrot L, et al. Photodynamic therapy (PDT) of experimental choroidal neovascularization with tin ethyl etiopurpurin (SnET2). Invest Ophthalmol Vis Sci 1996;suppl 37:S122.
25. Rogers AH, Martidis A, Greenberg PB, Puliafito CA. Optical coherence tomography findings following photodynamic therapy of choroidal neovascularization. Am J Ophthalmol 2002;134:566–576.
26. Schuman JS, Puliafito CA, Fujimoto JG. Optical Coherence Tomography of Ocular Diseases, 2nd ed. Thorofare, NJ: Slack, 2004.
27. Spaide RF, Lee JK, Klancnik JM, Gross NE. Optical coherence tomography of branch retinal vein occlusion. Retina 2003;23:343–347.
28. Greenberg PB, Martidis A, Rogers AH, Duker JS, Reichel E. Intravitreal triamcinolone acetonide as treatment of macular edema due to central retinal vein occlusion. Br J Ophthalmol 2002;86(2):247–248.
29. Martinez-Jardon CS, Meza-de Regil A, Dalma-Weiszhausz J, et al. Radial optic neurotomy for ischaemic central vein occlusion. Br J Opthalmol 2005;89:558–561.
30. Gass JDM. Stereoscopic Atlas of Macular Diseases, 4th ed. St. Louis: CV Mosby, 1997:374–376.

12
Clinical Applications of Optical Coherence Tomography in Diabetic Retinopathy

J. Fernando Arevalo, Carlos F. Fernandez, and Aristides J. Mendoza

Optical coherence tomography (OCT) (Stratus OCT Model 3000, Zeiss-Humphrey Inc., Dublin, CA) is a computer-assisted precision optical instrument that generates cross-sectional images (tomograms) of the retina with ≤10 μm axial resolution (Fig. 12.1).[1–8] Diabetic retinopathy is a major cause of visual impairment in the United States and around the world.[9–12] Diabetic macular edema (DME) is one of the main reasons for reduced visual acuity (VA) in patients with diabetic retinopathy. Macular edema affects approximately 29% of diabetic patients with a disease duration of 20 years or more, and is responsible for a significant degree of visual loss in this population.[9] It involves a wide spectrum of pathologic changes, including diffuse or focal edema and cystoid macular edema, which may have hard exudate. Direct clinicopathologic correlation of these pathologic changes is unclear. Macular edema may be the first symptom of diabetic retinopathy and may be associated with proliferative or nonproliferative retinopathy (Fig. 12.2). More than half of these individuals will lose two or more lines of visual acuity within 2 years of follow-up.[13]

Recently, several optical devices, such as the Retina Map,[14] computerized analysis of stereophotography,[15] and the Heidelberg retina tomograph,[16] have been introduced for the objective assessment of DME. These techniques measure retinal thickness but fail to show the intraretinal structures. Optical coherence tomography provides cross-sectional images of the retina, which mimic the histologic sections of light microscopy.[1,3,17–19] Traditional methods of evaluating macular thickening, including slit-lamp biomicroscopy (SLB), indirect funduscopy, and stereo fundus photography (SFP), are qualitative and relatively insensitive to small changes in retinal thickness. Slit-lamp biomicroscopy and SFP may detect increases in thickness only when they show values of more than 60% greater than the reference population, and therefore may be unable to identify mild or localized macular thickening.[20]

Optical coherence tomography is a medical diagnostic imaging technology that can perform micrometer-resolution, cross-sectional or tomographic imaging in biologic tissues. In patients with diabetes and diabetic retinopathy, single measurements of central foveal thickness using OCT tend to correlate with visual acuity (depending on chronicity) and are a successful means of monitoring macular thickening before and after laser therapy[1,19,21] or intravitreous injection of triamcinolone acetonide (TA) (Fig. 12.3).[22,23] The drawback to fundus photographs in stereo pairs is that it takes skilled personnel for both photography and photograph grading. In addition, patients generally find this procedure fairly uncomfortable. Determining the exact thickness of a thickened area in stereo fundus photographs is difficult because it is dependent on the stereopsis of the observer and the quality of the fundus photographs. Sometimes retinal thickening is underestimated in SFP when compared with binocular ophthalmoscopy. Empirically, the fovea is subject to the most thickening in cases of diffuse edema. This can be observed clinically, histologically, and on OCT. Farther from the center of the fovea, the thickened areas tend to be less prominent and much harder to assess for exact thickness. Focal and often rather subtle disease is usually present, which makes an assessment of the exact thickness of the thickened areas even more difficult. One of the advantages of SFP is that it has a large lateral resolution over the whole photographic field. Optical coherence tomography does not have this large lateral resolution unless an immense number of scans are performed.

Optical coherence tomography facilitates quantification of the retinal thickness in patients with diabetes with different degrees of diabetic retinopathy and with clinically significant macular edema (CSME) in an objective way. It enables measurement of retinal thickness from the tomograms by means of computer image-processing techniques. Hee and associates[1,19] reported quantitative assessment of macular edema and visual acuity with best correction with OCT. Objective assessments of the retinal thickness with mapping of the posterior pole has also been demonstrated by Gieser et al.,[24] Baumann et al.,[25] and Koozekanani et al.[4] The latter demonstrated that the OCT algorithm is able to recognize the two high-signal boundaries of the retina with good reproducibility (see Chapter 21 for limitations of OCT) and is therefore a valid tool for retinal thickness measurements (Fig. 12.4).

Very subtle lesions (i.e., above mean retinal thickness, yet below mean retinal thickness +2 standard deviations [SD] in

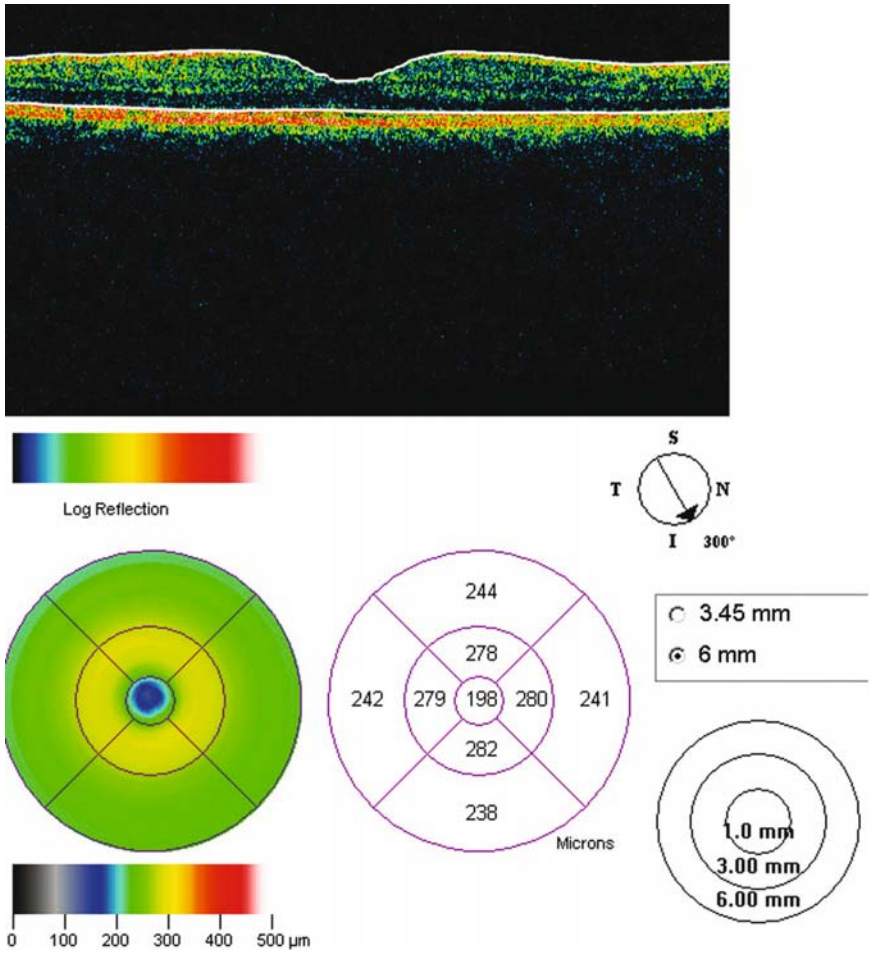

FIG. 12.1. Optical coherence tomograph generates cross-sectional images (tomograms) of the retina with ≤10 µm axial resolution. Normal cross-sectional macular image and normal macular thickness map are shown.

healthy control subjects' eyes) simply would not be detectable on the topographic OCT map. However, these subtle changes can be observed on individual OCT retinal profiles.

Optical coherence tomography has been reported to be more sensitive than SLB for detection of small changes in retinal thickness (i.e., changes of <100 µm greater than the mean retinal thickness in normal subjects).[1] Changes of this magnitude are too subtle for the human eye to detect on SFP or on binocular SLB, the latter presumably being the better way of assessing retinal thickening.[26] Changes in DME can

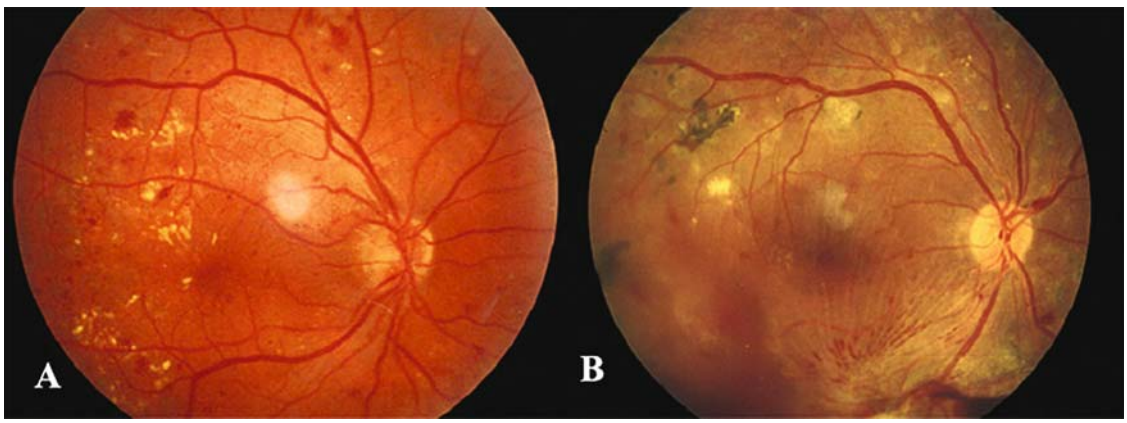

FIG. 12.2. Macular edema may be associated with (A) nonproliferative diabetic retinopathy or (B) proliferative diabetic retinopathy.

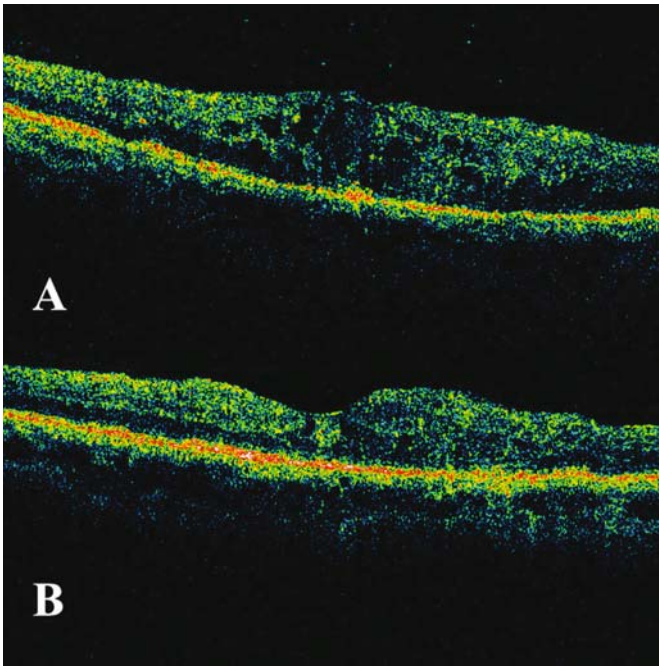

FIG. 12.3. Macular thickening before (A) and after (B) laser therapy plus an intravitreal injection of triamcinolone acetonide.

be accurately and prospectively measured with OCT in both clinical trials and clinical practice.

Optical coherence tomography shows three patterns of diabetic macular edema: retinal swelling, cystoid macular edema, and serous retinal detachment.[21] Retinal swelling shows increased retinal thickness with reduced intraretinal reflectivity and expanded areas of lower reflectivity. Cross-sectional images show a sponge-like swelling of the retina where low reflective areas are expanded, and layered structure becomes irregular. Low reflective areas are mainly located in the outer

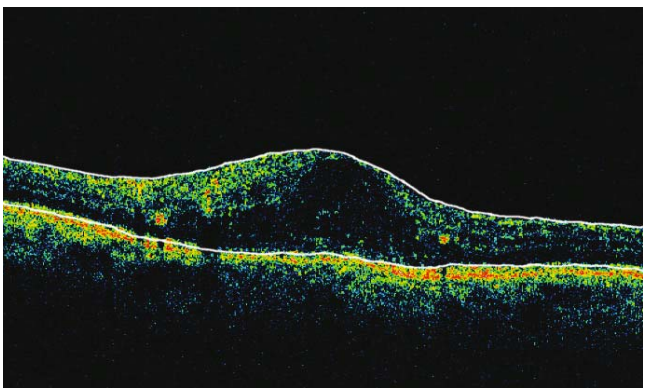

FIG. 12.4. Measurement of retinal thickness from a single scan by means of the optical coherence tomography (OCT). The anterior and posterior borders of the retina (white lines) are identified by the OCT algorithm. Retinal thickness is automatically measured as the distance between the two borders.

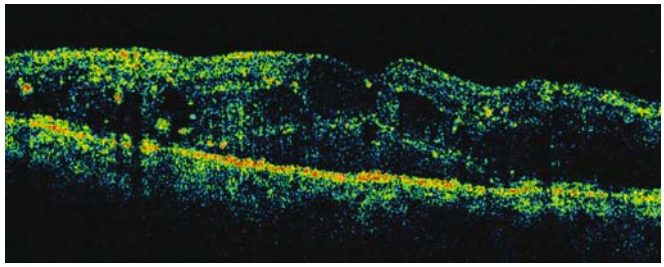

FIG. 12.5. Patterns of diabetic macular edema: retinal swelling.

retinal layers. The inner retinal layers are displaced anteriorly by the swollen outer retinal layers. The layered structure of the inner retinal layers is relatively preserved; however, it is occasionally interspersed with low reflective areas (Fig. 12.5). Cystoid macular edema is characterized by the intraretinal cystoid spaces at the macular area. Cystoid macular edema usually has four or five cystoid spaces located in the macula area within a diameter of 5 mm. In newly (within 3 months) developed cystoid macular edema, cystoid space occupies most of the full-thickness retina, leaving thin inner and outer retinal tissue at the fovea. Perifoveal cystoid spaces are located mainly in the outer retinal layers, and the inner retinal layers are relatively preserved. Each cystoid space is walled with septa. The cystoid spaces expand in a round or oval configuration, resulting in a protruding fovea (Fig. 12.6). In eyes with well-established cystoid macular edema that has persisted for more than 1 year, the cystoid spaces fuse to form a large cystoid cavity (Fig. 12.7). Serous retinal detachment is seen as subretinal fluid accumulation with a distinct outer border of the detached retina, but ophthalmoscopy sometimes fails to detect it. The thickness of the subretinal space is the greatest at the central fovea and it declines peripherally (Fig. 12.8). These basic patterns are frequently combined.

The retina is a compact tissue composed of neural elements and glial cells.[27] Because glial cells occupy all the interneural space, extracellular space is virtually absent. According to the histopathologic report in autopsy eyes with retinal edema, retinal swelling initiates in the intracytoplasmic swelling of Müller cells.[28] Sponge-like swellings in the OCT image may represent intracytoplasmic swelling of Müller cells. According

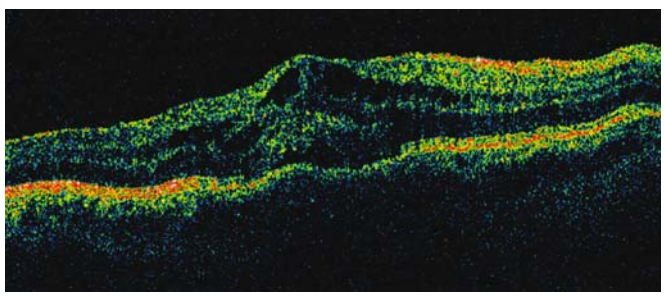

FIG. 12.6. Patterns of diabetic macular edema: cystoid macular edema.

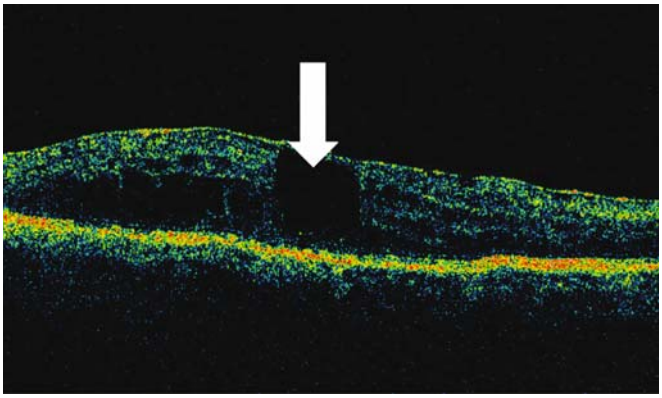

FIG. 12.7. Well-established cystoid macular edema, which has persisted for more than 1 year. The cystoid spaces fuse to form a large cystoid cavity (arrow).

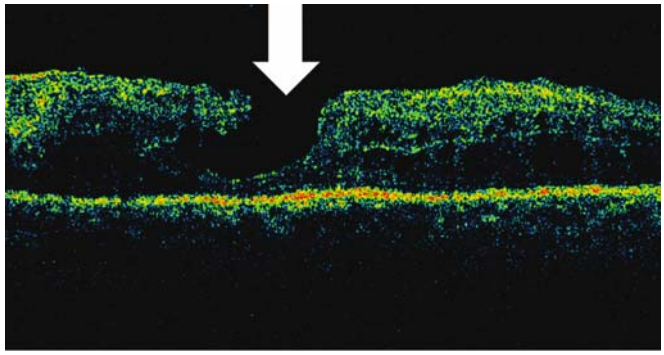

Fig. 12.9. Atrophic chronic cystoid macular edema may lead to the development of a lamellar macular hole (arrow).

to histopathologic studies, the outer plexiform layer or Henle's fiber layer is markedly swollen in macular edema.[28,29] Prominent space with low reflectivity in the outer retinal layers may represent the swollen Müller cells in Henle's fiber layer.

If retinal edema persists, liquefaction necrosis of the Müller cells ensues. Necrosis of the Müller cells and adjacent neural cells leads to cystoid cavity formation in the retina.[29] In the histopathologic study of cystoid macular edema, Tso[30] demonstrated that cystoid spaces were located not only in the outer plexiform layer but also in the inner plexiform and granular layers and even in the ganglion cell layer. Some morphologic differences exist between newly developed and well-established cystoid macular edema: in the former, cystoid spaces primarily were located in the outer retinal layers, and the inner retinal layers were relatively preserved; in the latter, the septa of each cystoid space disappeared, forming confluent large cystoid cavities. Large cystoid spaces may involve the entire retinal layer. The remaining retinal tissue was atrophic. Chronic cystoid macular edema may lead to the development of a lamellar macular hole, which is evident on OCT as a partial-thickness loss of retinal tissue and an abnormal retinal contour suggesting cystic rupture (Fig. 12.9).

Hard exudates, which were located in the outer retinal layers, appeared as spots of high reflectivity with low reflective areas behind them (Fig. 12.10). Histopathologically, hard exudates mainly precipitate in the outer plexiform layer.[31] Hard exudates can be an important factor in relation to the detection of retinal thickening by subjective assessment of edema on fundus photographs. The Early Treatment for Diabetic Retinopathy Study (ETDRS) report five described hard exudates as very likely to be associated with retinal thickening, even if the thickening is not apparent on the fundus photograph.[26] Nevertheless, appreciable macular hard exudates by themselves were not sufficient to qualify the eye as having retinal thickening.

Hard exudates increase retinal thickness in the OCT software algorithm. However, the effect of shadowing caused by exudates on the retinal pigment epithelium (RPE) is modest. Typically, a maximum increase of 5% in retinal thickness is found just beneath the hard exudate. Hemorrhage also blocks the reflections returning from the deeper retinal layers due to the high scattering and associated high attenuation of light propagating though blood. The reflection from the retinal pigment epithelium and choriocapillaris appeared slightly disrupted in areas of previous focal laser photocoagulation treatment (Fig. 12.11).

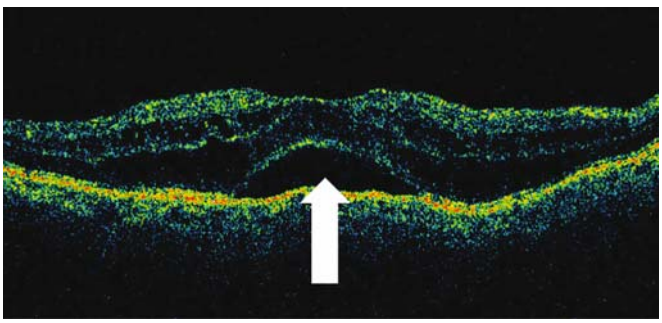

FIG. 12.8. Patterns of diabetic macular edema: serous retinal detachment (arrow).

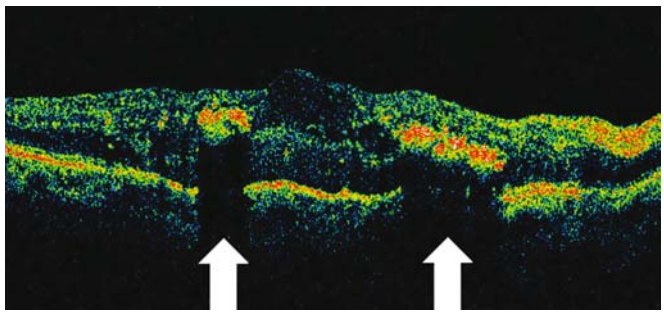

FIG. 12.10. Hard exudates, which are located in the outer retinal layers, appear as spots of high reflectivity with low reflective areas behind them (arrows).

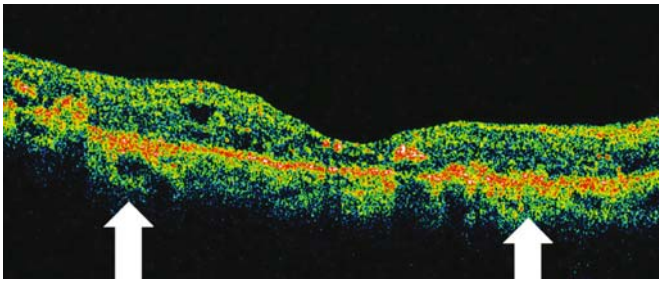

FIG. 12.11. Reflection from the retinal pigment epithelium and choriocapillaris appear slightly disrupted (arrows) in areas of previous focal laser photocoagulation treatment.

The scanning procedure, with the six radiating 6-mm scans, is chosen as the standard procedure for scan acquisition protocol. Retinal thickness can be calculated with the retinal thickness or retinal map. The scans are topographically mapped in a color code, with red indicating a definitely thickened area, blue indicating a definitely nonthickened area, and green indicating a thickness in between. For quantitative evaluation, the macula is divided into nine ETDRS areas, including a central disc with a diameter of 1000 μm and an inner and outer ring, each divided into four quadrants, with diameters of 3000 and 6000 μm, respectively (Fig. 12.12).

The reproducibility of the measurements may alter if the central points of these scans do not coincide because of unstable patient fixation. Internal or external fixation beams may be used with OCT. Internal beam fixation has been shown to provide better reproducibility.[32] The impact of unstable fixation is likely to be greater in the foveal than in the peripheral areas of the posterior pole. Using retinal mapping, intravisit and intervisit reproducibility are good.

We have used OCT to evaluate if primary intravitreal injection of triamcinolone acetonide (TA) plus grid laser photocoagulation (GLP) is effective in treating diffuse diabetic macular edema (Fernandez et al, unpublished data, presented at the American Academy of Ophthalmology annual meeting, Anaheim, CA, November 2003). We studied 30 eyes (18 patients) with clinically significant diffuse diabetic macular edema (CSDME). Fourteen eyes (10 patients) diagnosed with CSDME were treated with GLP according to the ETDRS guidelines plus an intravitreal injection of 4 mg of TA (study group). A control group was included (16 eyes in eight patients), treated with GLP only. The response to treatment was measured by clinical examination, fluorescein angiography (FA), and OCT. The visual and anatomic responses were observed as well as complications related to the injection procedure and corticosteroid administration. Visual acuity and the quantitative change in OCT macular thickness were assessed. Potential complications were monitored, including intraocular pressure (IOP) response, cataract progression, retinal detachment, vitreous hemorrhage, and endophthalmitis. The mean follow-up in our study group was 4.93 months (1 to 11 months). Mean variability in VA in the study group was −0.5 ETDRS lines (range: −6 to +5 lines). In three (21.43%) eyes, VA increased >2 ETDRS lines, in five (35.71%) eyes VA remained the same, and VA decreased >2 ETDRS lines in six (42.86%) eyes. Central macular thickness as measured by OCT decreased a mean of 83.79 μm (22.22%). Four eyes developed

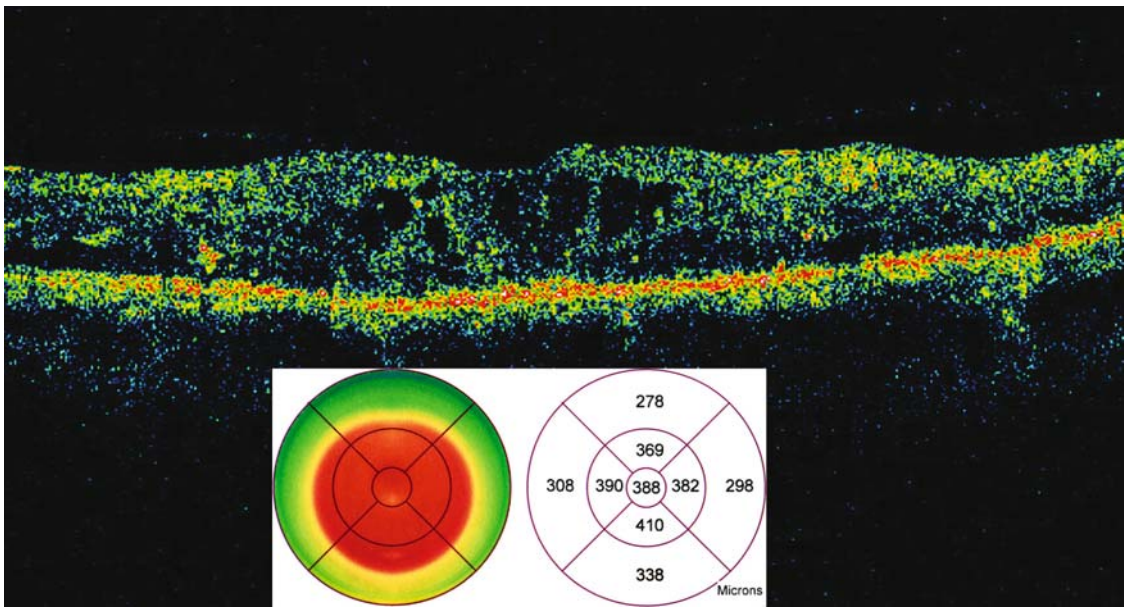

FIG. 12.12. For quantitative evaluation, the macula has been divided into nine Early Treatment for Diabetic Retinopathy Study (ETDRS) areas, including a central disc with a diameter of 1000 μm and an inner and outer ring, each divided into four quadrants, with diameters of 3000 and 6000 μm, respectively.

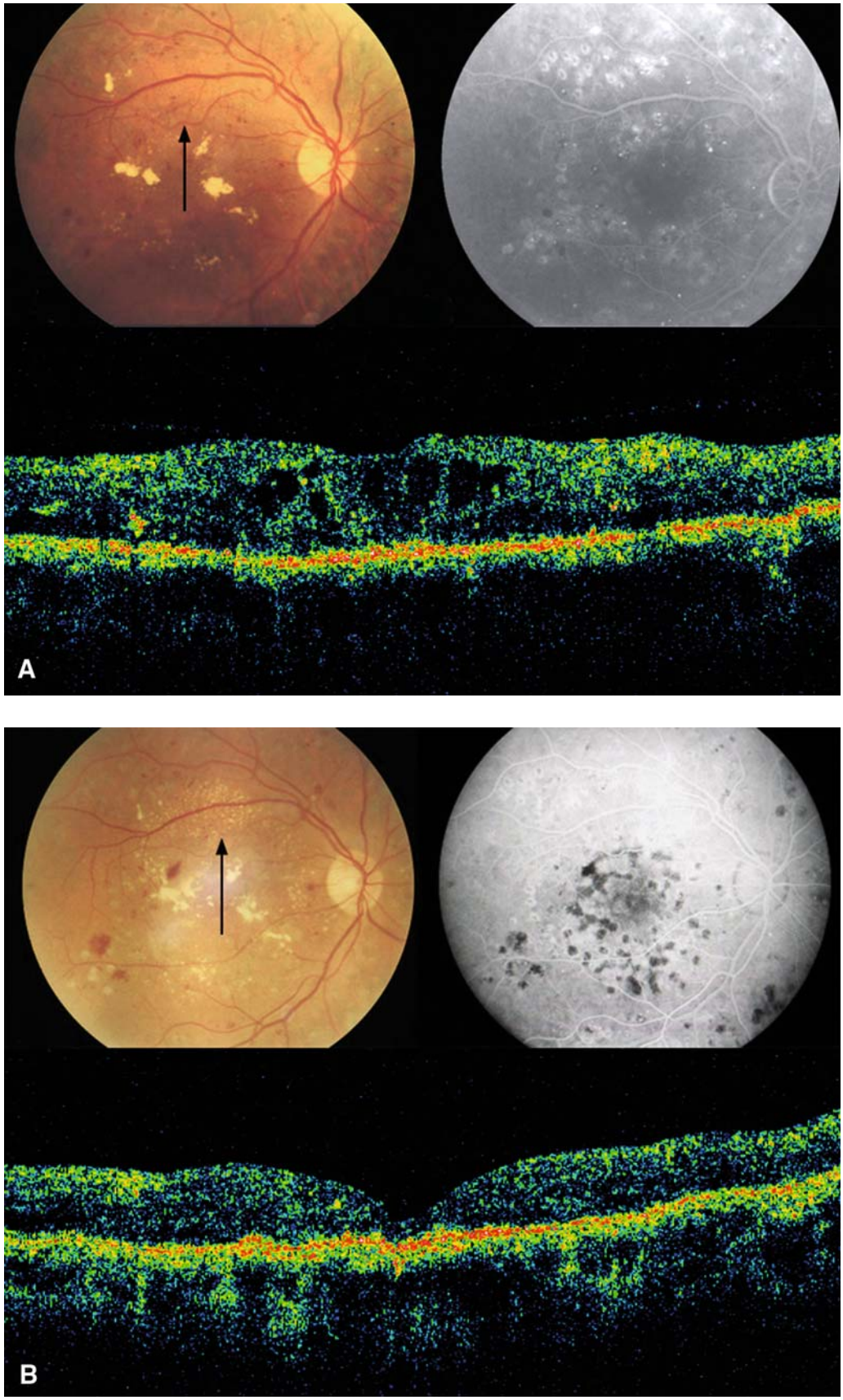

FIG. 12.13. Evaluation of primary intravitreal injection of triamcinolone acetonide plus grid laser photocoagulation in the treatment of diffuse diabetic macular edema. (A) Pretreatment. (B) Posttreatment.

an increased in IOP in our study group. Mean variability in VA in the control group was 0.5 ETDRS lines (range: −8 to +10 lines). In four (25%) eyes VA increased, in 11 (68.7%) eyes VA remained the same, and it decreased in one (6.25%) eye. This difference was not statistically significant ($p = .2$). Although 100% of our patients improved CSDME by means of OCT and FA, 42.86% lost two or more lines in VA with primary intravitreal injection of TA plus GLP.

We believe that other factors might play a roll in VA loss. Primary intravitreal injection of TA plus GLP may not be as efficacious as expected. Optical coherence tomography facilitates quantification of the retinal thickness and follow-up to evaluate the effect of treatment in diabetic patients, with different degrees of diabetic retinopathy with clinically significant macular edema (CSME) in an objective way (Fig. 12.13).

Baumann et al.[25] and Koozekanani et al.[4] showed good reproducibility of macular thickness measurement with OCT in undilated eyes. Changes in axial length or refraction may affect measurements in the transverse direction of the eye but have no effect on measurements in the axial direction.[4] Finally, a nuclear cataract does not seem to affect retinal thickness measurement, [32] although the presence of a dense subcapsular opacity may impair the ability to perform OCT examination.

Proliferative Diabetic Retinopathy and Optical Coherence Tomography

Proliferative diabetic retinopathy often leads to neovascularization and preretinal fibrosis. Preretinal membranes are visible in cross section as thin, reflective bands anterior to the retina (Fig. 12.14). Retinal traction and detachment are often present, and their extent can be directly measured from

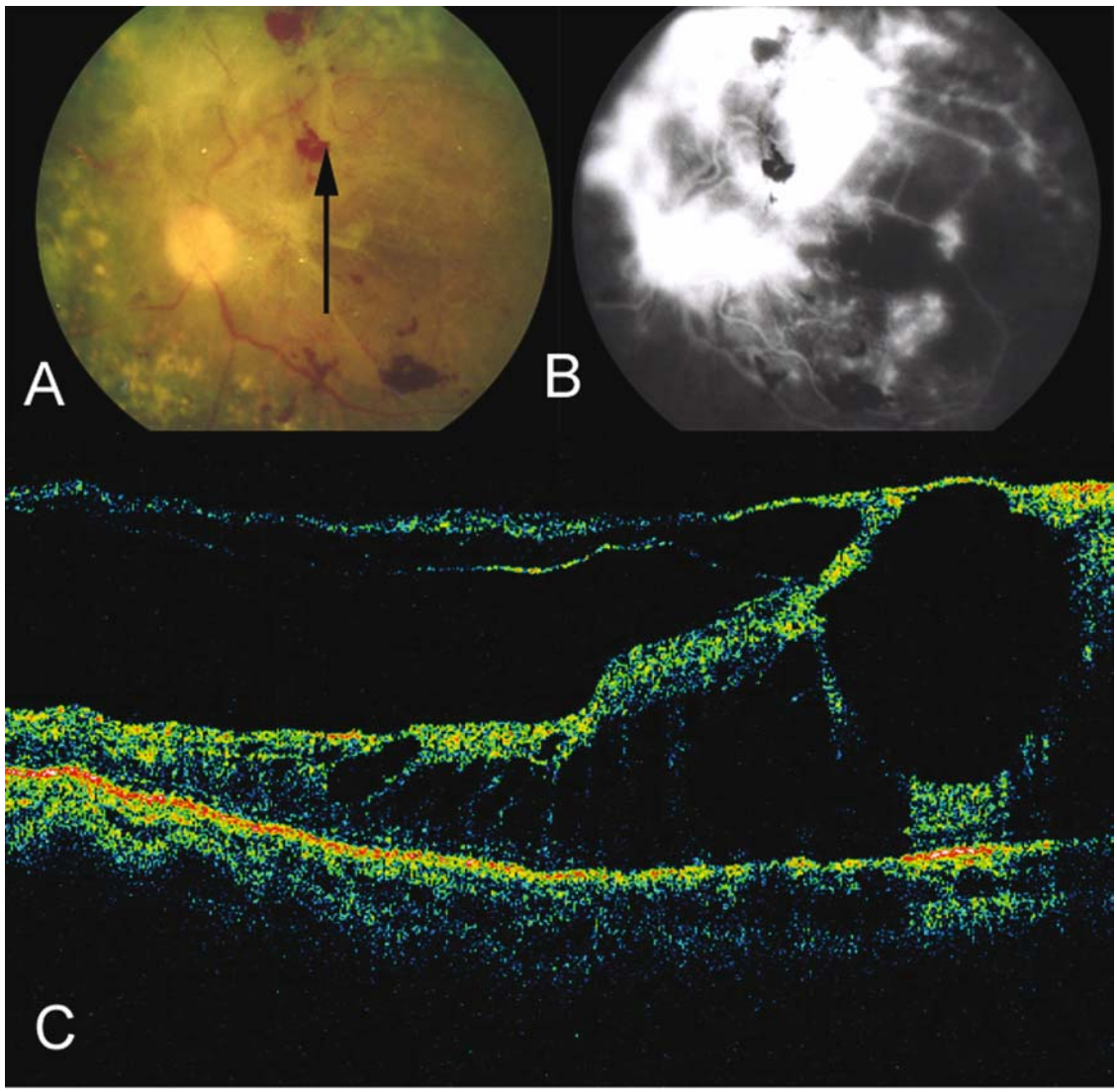

FIG. 12.14. Fundus photography (A), angiofluoresceinography (B), and optical coherence tomography (OCT) (C) of proliferative diabetic retinopathy with preretinal membranes (thin, reflective bands anterior to the retina) and cystoid macular edema.

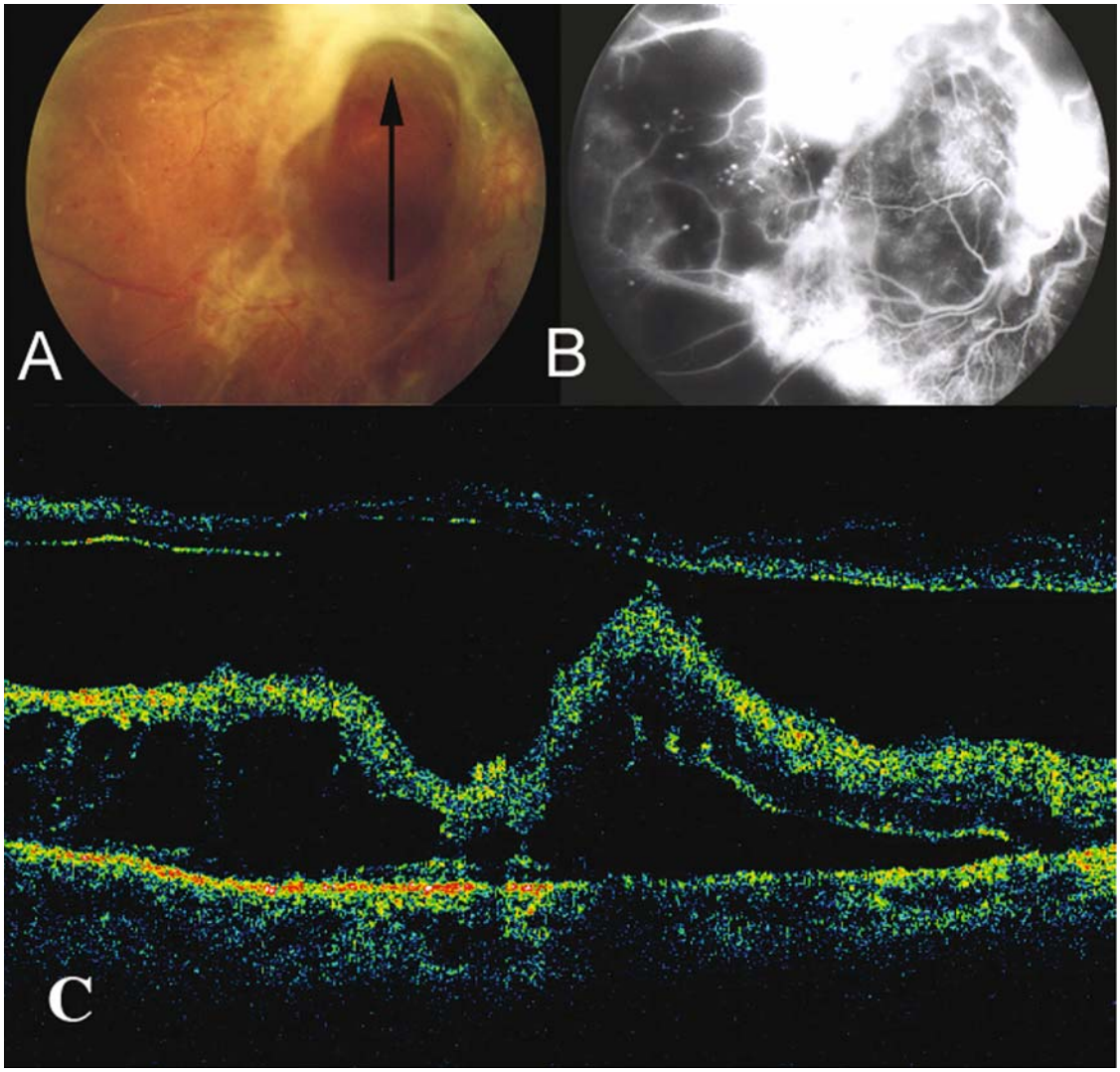

FIG. 12.15. Fundus photography (A), angiofluoresceinography (B), and OCT (C) of proliferative diabetic retinopathy with retinal traction and tractional detachment.

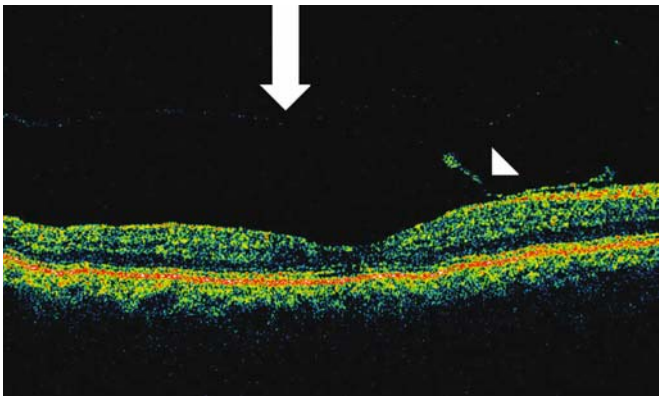

FIG. 12.16. The distinction between preretinal fibrosis and a detached posterior vitreous is made on the basis of reflectivity. The posterior hyaloid typically (arrow) has a lower reflectivity than a preretinal membrane (arrowhead).

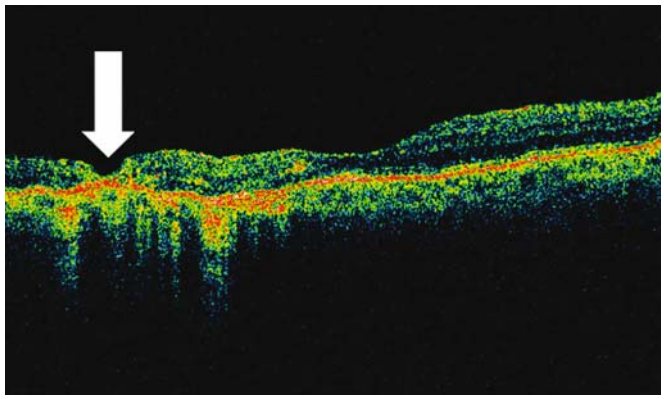

FIG. 12.17. Retinal thinning (arrow) corresponding retinal atrophy can be defined by OCT in the region of photocoagulation treatment.

OCT (Fig. 12.15). The distinction between preretinal fibrosis and a detached posterior vitreous is made on the basis of reflectivity (Fig. 12.16). The posterior hyaloid typically has a lower reflectivity than a preretinal membrane due to the optical transparency of the vitreous. Cotton-wool spots due to retinal ischemia appear in OCT cross section as regions of increased reflectivity of the retinal nerve fiber layer and inner neurosensory retina.[33]

Retinal thinning corresponding to retinal atrophy can be defined by OCT in the region of previous photocoagulation treatment (Fig. 12.17).

Optical Coherence Tomography and Vitreomacular Traction Syndrome

Nasrallah et al.[34] and Hikishi et al.[35] have suggested that the vitreous plays a role in the pathogenesis of DME. In the study by Nasrallah et al., posterior vitreous detachment (PVD) was observed in 42.1% of the eyes of diabetic patients without DME but in no eyes with macular edema. In a prospective study of a cohort of diabetic patients with DME, Hikishi et al. showed that DME resolved in 55% of the eyes with biomicroscopic PVD at study entry compared with only 25% of the eyes with vitreomacular adhesion. These results therefore suggest that complete PVD may prevent or induce spontaneous resolution of DME.

The treatment of DME is mainly based on laser photocoagulation. Several authors have reported that vitrectomy is beneficial for diffuse DME. [36–48] This was especially the case for eyes with diffuse DME and a thickened, taut posterior hyaloid. The favorable results reported in such cases after vitrectomy and mechanical detachment of the posterior hyaloid[36,38,40,42,43] suggest that DME may be exacerbated by tangential vitreomacular traction. In addition, the results of several other studies suggested that vitrectomy may be beneficial for eyes with DME but with a normal-looking posterior hyaloid and no PVD.[39,41,44,45,47] Despite these results, however, the indications for vitrectomy for diffuse DME are still controversial. Vitrectomy must be performed when vitreomacular traction is observed on biomicroscopy or OCT.

Tractional diabetic macular edema (TDME) (Fig. 12.18) on OCT is characterized by macular thickening with loss of the foveal depression in all cases and swelling of the outer retinal layers. The posterior hyaloid on OCT is thick and hyperreflective; it is partially detached from the posterior pole and is taut over it, but remains attached to the disc and to the top of the raised macular surface. The taut thickened posterior hyaloid exerted tangential vitreomacular traction that induced or exacerbated DME.

Biomicroscopy, unlike OCT, is not sufficiently accurate to determine the status of the posterior hyaloid when it is only slightly detached from the macular surface. Optical coherence tomography is indeed more sensitive than biomicroscopy in identifying vitreomacular adhesions[49] (Fig. 12.19) and enables earlier diagnosis of shallow partial PVD.[50,51] In addition, it enables precise assessment of macular thickness, with good reproducibility.[7]

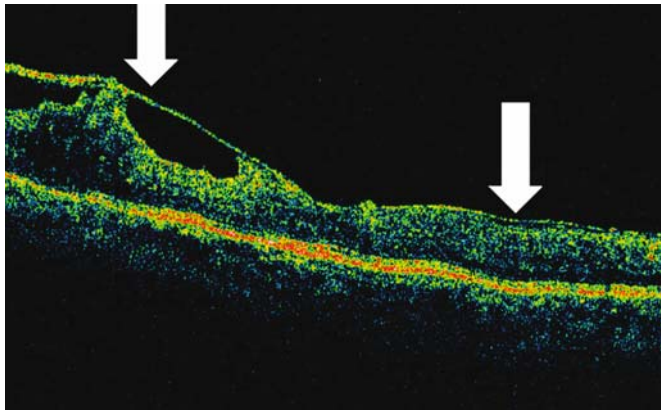

FIG. 12.18. Tractional diabetic macular edema on OCT shows thickening of the posterior hyaloid, which is especially hyperreflective and is taut over the posterior pole (arrows) but remains attached to the top of the elevated macular surface.

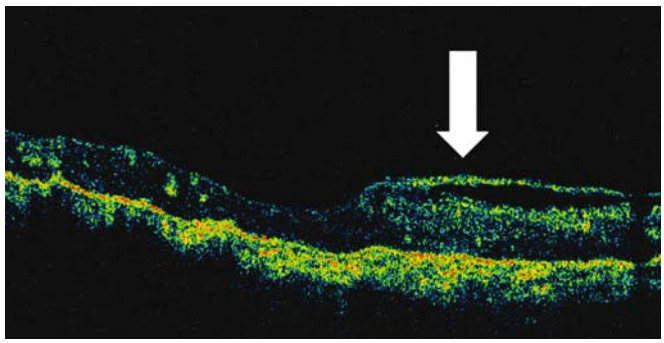

FIG. 12.19. Optical coherence tomography is very sensitive in identifying vitreomacular adhesions (arrow).

Retinal thickness may greatly increase and include large intraretinal hyporeflective cystic-like cavities (Fig. 12.20). Such increased hyporeflectivity may be due to fluid accumulation in the outer layers of the retina or may correspond to tractional schisis cavities. Similar OCT findings were also recently reported by Kaiser.[52] Therefore, OCT could be helpful in diagnosing vitreomacular traction in eyes with TDME that may not have been identified on clinical examination. In addition, OCT enabled very precise and objective quantitative assessment of retinal thickness before and after vitrectomy. However, the persistence of intraretinal cysts on OCT despite the significant decrease in retinal thickness after vitrectomy and the persistence of cystoid changes on fluorescein angiography showed that vitrectomy only removed the tractional component of DME but did not eliminate the effects of diabetic retinal microangiopathy.

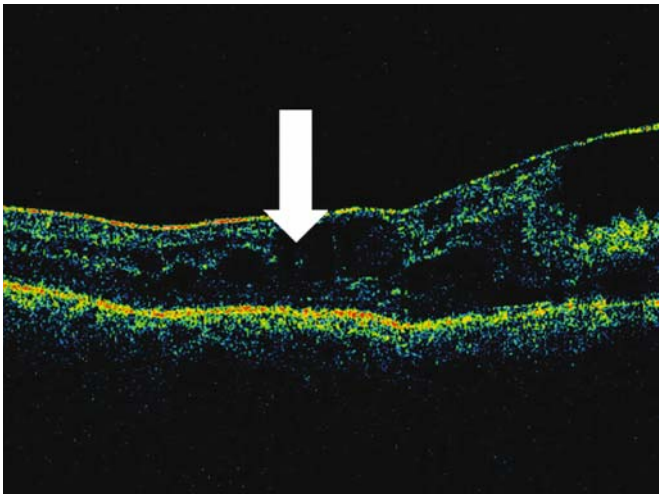

FIG. 12.20. Vitreomacular traction induces or exacerbates diabetic macular edema (DME); retinal thickness increases and includes intraretinal hyporeflective cystic-like cavities (arrow).

The thickening of the posterior hyaloid may be partly due to the structural changes in the vitreous cortex reported in diabetic patients[53,54] and to infiltration of the hyaloid by cells of glial and epithelial origin.[55] Although this rare condition can be suspected on biomicroscopy in most cases, OCT confirms the diagnosis by providing an objective image of vitreomacular traction; in addition, OCT may help detect more subtle traction not visible on biomicroscopy.

Optical coherence tomography can help also in the identification of postoperative complications after vitrectomy. These complications included postoperative retinal detachment, vitreous hemorrhage, hard exudates in the center of the macula (Fig. 12.21), postoperative epiretinal membrane formation, and lamellar macular hole. Optical coherence tomography can show residual posterior vitreous cortex adhesions on the surface of the retina after vitrectomy

Yamamoto et al.[56] reported that the retinal thickness is reduced within 7 days postoperatively with OCT examination after vitrectomy for TDME. The reason why the retinal thickness decreased so quickly after vitrectomy is unknown, but we suggest that the high concentrations of oxygen supplied from the ciliary body cause retinal vasoconstriction, resulting in retinal thickness decreases in the early period after vitrectomy.[57–59] Afterward, the retinal thickness kept on decreasing for at least 4 months. These findings mean that the evaluation of the effectiveness of vitrectomy for diabetic macular edema by retinal thickness changes should be performed no sooner than 4 months after vitrectomy.

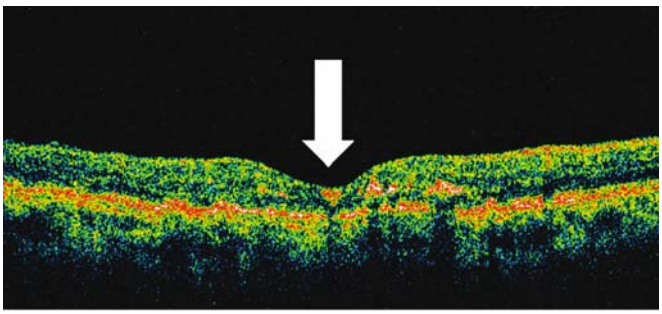

FIG. 12.21. Hard exudates in the center of the macula (arrow).

Diabetic Tractional Papillopathy

Kroll et al.[60] reported partial restoration of vision following vitrectomy in 15 of 17 eyes, ostensibly through removal of diabetic fibrovascular proliferations from the nasal part of the optic disc (Fig. 12.22) and relief of vitreopapillary traction, which, for between 6 months and 6 years, had caused a reversible functional impairment of the papillomacular bundle via stretching and kinking of ganglion cell axons and additional or consecutive effects on their prelaminar blood supply. Eyes with such features (i.e., with traction primarily localized nasally on the disc and unaccountably affecting acuity without any associated disturbance of the central visual field) should be subjected to early vitrectomy in order to prevent irreversible long-term damage to central vision. It merits the careful attention of all ophthalmologists involved in the management of diabetic eye disease.

Optical coherence tomography can be useful to determinate the vitreous state, and can show if the vitreous is attached or detached from the retina and the optic disc (Fig. 12.23). In the vitreopapillary traction, the thickened posterior hyaloid is especially hyperreflective and is attached to the disc. Also, the thickened posterior hyaloid exerts tangential or anteroposterior vitreopapillary traction.

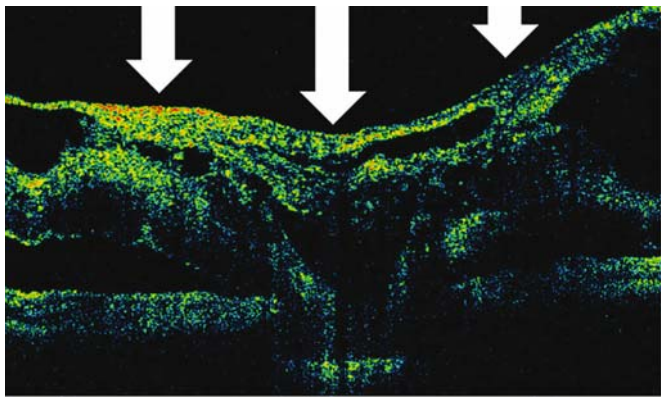

FIG. 12.22. Diabetic fibrovascular proliferations of the optic disc (arrows).

FIG. 12.23. The OCT can determinate the vitreous state. (A) Fibrovascular proliferations of the optic disc. (B) Thickening of the posterior hyaloid, which is especially hyperreflective and is attached to the optic disc. (C) Optic disc without vitreous traction.

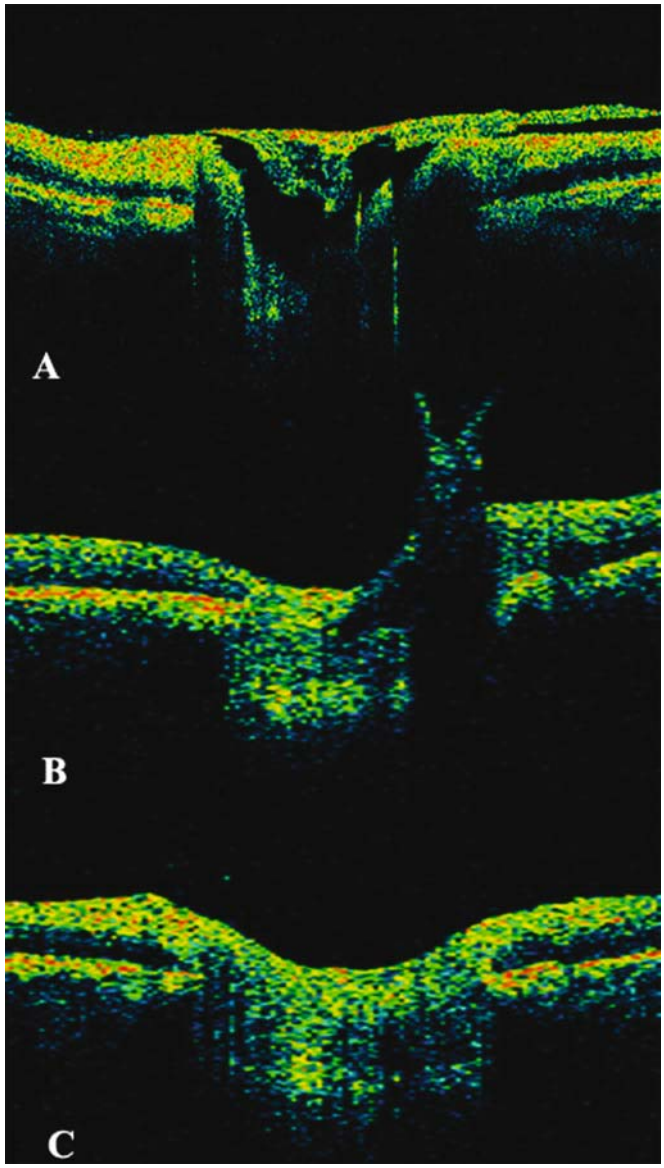

Conclusion

Optical coherence tomography facilitates quantification of the retinal thickness and enables precise follow-up to evaluate the effect of the management of diabetic patients with different degrees of diabetic retinopathy with clinically significant macular edema in an objective way. In addition, OCT may be very useful in the evaluation of the vitreoretinal and vitreopapillary interface.

Acknowledgments. The authors have no proprietary or financial interest in any products or techniques described in this chapter.

References

1. Hee M, Puliafito C, Duker J, et al. Topography of diabetic macular edema with optical coherence tomography. Ophthalmology 1998;105:360–370.
2. Pedut-Kloizman T, Pakter H, Schuman J, et al. Ophthalmic diagnosis using optical coherence tomography. Ophthalmol Clin North Am 1998;11:465–486.
3. Hee M, Izatt J, Swanson E, et al. Optical coherence tomography of the human retina. Arch Ophthalmol 1995;113:325–332.
4. Koozekanani D, Roberts C, Katz S, et al. Intersession repeatability of macular thickness measurements with the Humphrey 2000 OCT. Invest Ophthalmol Vis Sci 2000;41:1486–1491.
5. Hee MR, Izatt JA, Swanson EA, et al. Optical coherence tomography for ophthalmic imaging. IEEE Eng Med Biol 1995;14:67–76.

6. Konno S, Akiba J, Yoshida A. Retinal thickness measurements with optical coherence tomography and the scanning retinal thickness analyzer. Retina 2001;21:57–61.
7. Massin P, Vicaut E, Haouchine B, et al. Reproducibility of retinal mapping using optical coherence tomography. Arch Ophthalmol 2001;119:1135–1142.
8. Neubauer A, Priglinger S, Ullrich S, et al. Comparison of foveal thickness measured with the retinal thickness analyzer and optical coherence tomography. Retina 2001;21:596–601.
9. Klein R, Klein BEK, Moss SE, et al. The Wisconsin Epidemiologic Study of Diabetic Retinopathy. IV. Diabetic macular edema. Ophthalmology 1984;91:1464–1474.
10. Early Treatment Diabetic Retinopathy Study Research Group. Photocoagulation for diabetic macular edema. Early Treatment Diabetic Retinopathy Study report number 1. Arch Ophthalmol 1985;103:1796–1806.
11. Moss SE, Klein R, Klein BEK. Ten-year incidence of visual loss in a diabetic population. Ophthalmology 1994;101:1061–1070.
12. Moss SE, Klein R, Klein BEK. The 14-year incidence of visual loss in a diabetic population. Ophthalmology 1998;105:998–1003.
13. Ferris FL III, Patz A. Macular edema. A complication of diabetic retinopathy. Surv Ophthalmol 1984;28:452–461.
14. Zeimer R, Shahidi M, Mori M, et al. A new method for rapid mapping of the retinal thickness at the posterior pole. Invest Ophthalmol Vis Sci 1996;37:1994–2001.
15. Kiri A, Dyer DS, Bressler NM, et al. Detection of diabetic macular edema: Nidek 3Dx stereophotography compared with fundus biomicroscopy. Am J Ophthalmol 1996;122:654–662.
16. Zambarakji HJ, Amoaku WM, Vernon SA. Volumetric analysis of early macular edema with the Heidelberg Retina Tomograph in diabetic retinopathy. Ophthalmology 1998;105:1051–1059.
17. Huang D, Swanson EA, Lin CP, et al. Optical coherence tomography. Science 1991;254:1178–1181.
18. Puliafito CA, Hee MR, Lin CP, et al. Imaging of macular diseases with optical coherence tomography. Ophthalmology 1995;102:217–229.
19. Hee MR, Puliafito CA, Wong C, et al. Quantitative assessment of macular edema with optical coherence tomography. Arch Ophthalmol 1995;113:1019–1029.
20. Shahidi M, Ogura Y, Blair N, et al. Retinal thickness analysis for quantitative assessment of diabetic macular edema. Arch Ophthalmol 1991;109:1115–1119.
21. Otani, T, Kishi, S, Maruyama, Y. Patterns of diabetic macular edema with optical coherence tomography Am J Ophthalmol 1999;127:688–693.
22. Martidis A, Duker JS, Greenberg PB, et al. Intravitreal triamcinolone for refractory diabetic macular edema. Ophthalmology 2002;109:920–927.
23. Jonas JB, Kreissig I, Sofker A, et al. Intravitreal injection of triamcinolone for diffuse diabetic macular edema. Arch Ophthalmol 2003;121:57–61.
24. Gieser, JP, Rusin, MM, Mori M, et al. Clinical assessment of the macula by retinal topography and thickness mapping Am J Ophthalmol 1997;124:648–660.
25. Baumann M, Gentile RC, Liebmann JM, et al. Reproducibility of retinal thickness measurements in normal eyes using optical coherence tomography. Ophthalmic Surg Lasers 1998;29:280–285.
26. Kinyoun J, Barton F, Fisher M, et al. Detection of diabetic macular edema: ETDRS report number 5. Ophthalmology 1989;96:746–751.
27. Hogan MJ, Alvarado JA, Weddell JE. Histology of the Human Eye. Philadelphia: WB Saunders, 1971.
28. Yanoff M, Fine BS, Brucker AJ, et al. Pathology of human cystoid macular edema. Surv Ophthalmol 1984;28:505–511.
29. Fine BS, Brucker AJ. Macular edema and cystoid macular edema. Am J Ophthalmol 1981;92:466–481.
30. Tso MOM. Pathology of cystoid macular edema. Ophthalmology 1982;89:902–915.
31. Murata T, Ishibashi T, Inomata H. Immunohistochemical detection of extravasated fibrinogen (fibrin) in human diabetic retina. Graefes Arch Clin Exp Ophthalmol 1992;230:428–431.
32. Schuman JS, Pedut-Kloizman T, Hertzmark E, et al. Reproducibility of nerve fiber layer thickness measurements using optical coherence tomography. Ophthalmology 1996;103:1889–1898.
33. Puliafito CA, Hee MR, Schuman JS, et al. Optical Coherence Tomography of Ocular Diseases. Thorofare, NJ: Slack, 1996.
34. Nasrallah FP, Jalkh AE, Van Coppenhole F, et al. The role of the vitreous in diabetic macular edema. Ophthalmology 1988;95:1335–1339.
35. Hikishi T, Fujio N, Akiba J, et al. Association between the short-term natural history of diabetic macular edema and the vitreomacular relationship in type II diabetes mellitus. Ophthalmology 1997;104:473–478.
36. Lewis H, Abrams GH, Blumenkranz MS, et al. Vitrectomy for diabetic macular traction and edema associated with posterior hyaloidal traction. Ophthalmology 1992;99:753–759.
37. Van Effenterre G, Guyot-Argenton C, Guiberteau B, et al. Oedémes maculaires induits par la contraction de la hyaloý de posterieure. J Fr Ophtalmol 1993;16:602–610.
38. Harbour JW, Smiddy WE, Flynn HW, et al. Vitrectomy for diabetic macular edema associated with a thickened and taut posterior hyaloid membrane. Am J Ophthalmol 1996;121:405–413.
39. Tachi N, Ogino N. Vitrectomy for diffuse macular edema in cases of diabetic retinopathy. Am J Ophthalmol 1996;122:258–260.
40. Pendergast SD. Vitrectomy for diabetic macular edema with a taut premacular posterior hyaloid. Curr Opin Ophthalmol 1998;9:71–75.
41. Ikeda T, Sato K, Katano T, et al. Vitrectomy for cystoid macular edema with attached posterior hyaloid membrane in patients with diabetes. Br J Ophthalmol 1999;83:12–14.
42. Pendergast SD, Hassan TS, Williams GA, et al. Vitrectomy for diffuse diabetic macular edema associated with a taut premacular posterior hyaloid. Am J Ophthalmol 2000;130:178–186.
43. Gandorfer A, Messmer M, Ulbig MW, et al. Resolution of diabetic macular edema after surgical removal of the posterior hyaloid and the inner limiting membrane. Retina 2000;20:126–133.
44. Otani T, Kishi S. Tomographic assessment of vitreous surgery for diabetic macular edema. Am J Ophthalmol 2000;129:487–494.
45. Ikeda T, Sato K, Katano T, et al. Improved visual acuity following pars plana vitrectomy for diabetic cystoid macular edema and detached posterior hyaloid. Retina 2000;2:220–222.
46. Giovannini A, Amato G, Mariotti C, et al. Optical coherence tomography findings in diabetic macular edema before and after vitrectomy. Ophthalmic Surg Lasers 2000;31:187–191.
47. La Heij ECs, Hendrikse F, Kessels AG, et al. Vitrectomy results in diabetic macular oedema without evident vitreomacular traction. Graefes Arch Clin Exp Ophthalmol 2001;239:264–270.
48. Yamamoto T, Akabane N, Takeuchi S. Vitrectomy for diabetic macular edema: the role of posterior vitreous detachment and epimacular membrane. Am J Ophthalmol 2001;132:369–377.
49. Gallemore RP, Jumper JM, McCuen BW, et al. Diagnosis of vitreoretinal adhesions in macular disease with optical coherence tomography. Retina 2000;20:115–120.

50. Gaudric A, Haouchine B, Massin P, et al. Macular hole formation, new data provided by optical coherence tomography. Arch Ophthalmol 1999;117:744–751.
51. Haouchine B, Massin P, Gaudric A. The foveal cyst as the first step in macular hole formation. A prospective study by optical coherence tomography. Ophthalmology 2001;108:15–22.
52. Kaiser PK, Riemann CD, Sears JE, et al. Macular traction and diabetic macular edema associated with posterior hyaloidal traction. Am J Ophthalmol 2001;131:44–49.
53. Sebag J, Buckingham B, Charles MA, et al. Biochemical abnormalities in vitreous of humans with proliferative diabetic retinopathy. Arch Ophthalmol 1992;110:1472–1479.
54. Stitt AW, Moore JE, Sharkey JA, et al. Advanced glycation end products in vitreous: structural and functional implications for diabetic vitreopathy. Invest Ophthalmol Vis Sci 1998;39:2517–2523.
55. Jumper JM, Embabi SN, Toth CA, et al. Electron immunocytochemical analysis of posterior hyaloid associated with diabetic macular edema. Retina 2000;20:63–68.
56. Yamamoto T, Hitani K, Tsukahara I, et al. Early postoperative retinal thickness changes and complications after vitrectomy for diabetic macular edema. Am J Ophthalmol 2003;135:14–19.
57. Stefansson E, Novack RL, Hatchell DL. Vitrectomy prevents retinal hypoxia in branch retinal vein occlusion. Invest Ophthalmol Vis Sci 1990;31:284–289.
58. Bill A. Ocular circulation. In: Moses RA, ed. Adler's Physiology of the Eye: Clinical Application, 7th ed. St. Louis: CV Mosby, 1981:193–194.
59. Deutsch TA, Read JS, Ernest JT, et al. Effects of oxygen and carbon dioxide on the retinal vasculature in humans. Arch Ophthalmol 1983;101:1278–1280.
60. Kroll p, Wiegand W, Schmidt J. Vitreopapillary traction in proliferative diabetic vitreoretinopathy. Br J Ophthalmol 1999;83:261–264.
61. Minkler DS, McLean IW, Tso MOM. Distribution of axonal and glial elements in the rhesus optic nerve head studied by electron microscopy. Am J Ophthalmol 1976;82:179–187.

13
Clinical Applications of Optical Coherence Tomography in Age-Related Macular Degeneration

J. Fernando Arevalo and Reinaldo A. Garcia

Optical coherence tomography (OCT) is a noninvasive, dynamic technology ideal for observing the natural course of age-related macular degeneration (AMD). The structural information provided by OCT is becoming a valuable diagnostic adjunct to fluorescein angiography (FA) and indocyanine green videoangiography (ICGV). The goal of using OCT is to correlate these observed structural changes with changes in visual acuity (VA), not only to better understand the mechanism of vision loss associated with AMD, but also to understand the mechanism of VA benefits attributed to various treatments. In particular, OCT is a valuable tool to monitor the treatment effects associated with photodynamic therapy (PDT) as well as periocular and intraocular pharmacologic therapy in neovascular AMD.[1]

In AMD the cross-sectional appearances on OCT can identify several lesions, including geographic atrophy (GA); soft drusen; subretinal and intraretinal fluid accumulation; serous, hemorrhagic, and fibrovascular detachments of the retinal pigment epithelium (RPE); choroidal neovascularization (CNV); and scarring.

Nonexudative Age-Related Macular Degeneration

Soft Drusen

Soft drusen are generally larger, with less sharply defined edges, than hard drusen. They tend to become confluent and therefore show greater variation in size and shape. They evolve and fade more rapidly than do hard drusen, On fluorescein angiography, soft drusen fill more slowly and are not as brightly fluorescent as hard drusen, but remain fluorescent for a longer period.[2] On OCT they show small modulations in the contour of the RPE. They appeared as focal elevations of the reflective layer, which corresponds to the RPE. The localized elevation of the external band associated with drusen is shallow compared to the more pronounced scatter-free elevation observed with a serous pigment epithelial detachment (PED) (Fig. 13.1). The lack of optical shadowing below these contour changes is consistent with the accumulation of soft drusen beneath the neurosensory retina and within Bruch's membrane, or between Bruch's membrane and the RPE. Within the elevation associated with drusen, there is a mild backscatter of the signal, probably resulting from the accumulated material that forms the drusen.[1]

Drusenoid Pigment Epithelial Detachments

Further confluence leads to larger soft drusen that resemble serous PED, often retaining a scalloped outline representing the original drusen. This subset of serous PEDs was characterized as the "drusenoid form" when it was noted to have different ophthalmoscopic and angiographic features, as well as a better prognosis. The term *drusenoid RPE detachment* may be arbitrarily applied to drusen over 500 μm but may be better reserved for those 1000 μm in greatest length involving the foveal center.[3] Roquet et al.[4] have reported that if drusenoid PEDs were greater than two disc diameters (DDs) or were associated with metamorphopsia at initial presentation, progression to atrophy or ingrowth of CNV occurred after 2 years ($p < .01$). They proposed that evaluation of eyes at risk requires the use of all imaging means in order to ascertain the diagnosis of CNV. Optical coherence tomography was helpful in distinguishing coalescent soft drusen from drusenoid PEDs (Fig. 13.2), and disclosed the accumulation of sub- or intraretinal fluid in eyes with CNV (Fig. 13.3). At long term (over 10 years), geographic atrophy and CNV had occurred in 75% and 25% respectively, with a poor visual outcome.

Geographic Atrophy

Geographic atrophy is the end result of the atrophic form of AMD and is currently defined as any sharply delineated round or oval area of hypopigmentation or depigmentation or apparent absence of the RPE, in which choroidal vessels are more visible than in surrounding areas and which must be at least 175 μm in diameter.[3] Optical coherence tomography shows

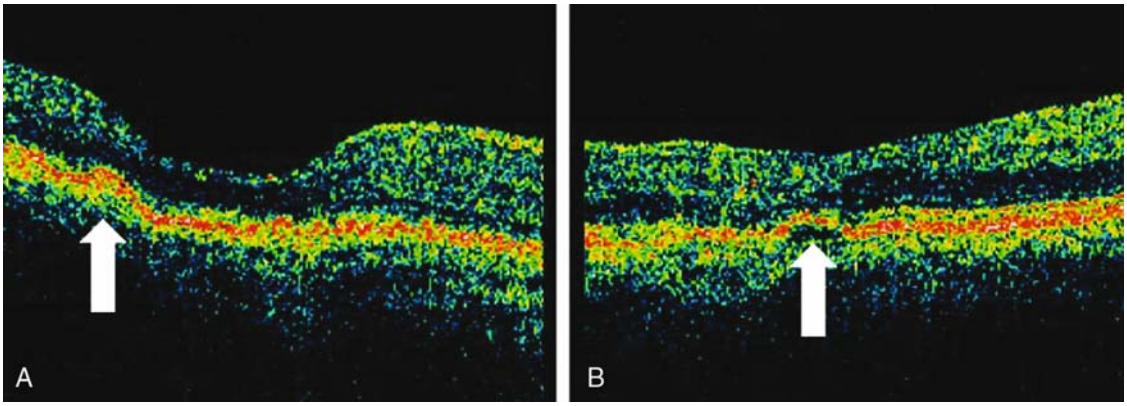

FIG. 13.1. The localized elevation of the external hyperreflective retinal pigment epithelium-choriocapillaris complex band associated with drusen (arrow in A) is shallow compared to the more pronounced scatter-free elevation observed with a serous pigment epithelial detachment (arrow in B).

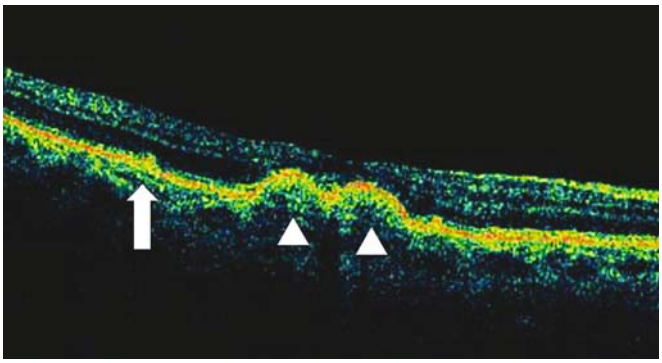

FIG. 13.2. Optical coherent tomography demonstrates a bilobed retinal pigment epithelial detachment (arrowheads). In contrast, observe a shallow localized elevation of external hyperreflective retinal pigment epithelium-choriocapillaris complex band associated with drusen (arrow).

a well-defined region of increased optical reflectivity from the choroid due to increased penetration of both incident and reflected light through the atrophic RPE.[5] In this condition, there is thinning of the overlying retina and the external band, which represents the RPE/Bruch's/choriocapillaris complex (Fig. 13.4). The loss of the choriocapillaris and the resulting scatter caused by the circulating red blood cells permit increased penetration of the light deeper into the choroid, significantly enhancing the reflections from this layer.[1] Hassenstein et al.[5] have shown that atypical macular holes may be found in 5%

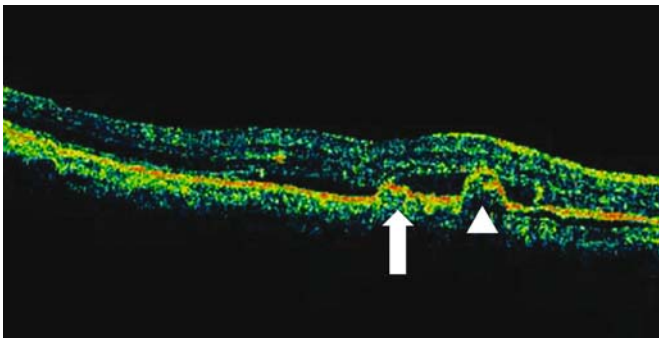

FIG. 13.3. Optical coherence tomography is helpful in distinguishing coalescent soft drusen (arrow) from drusenoid pigment epithelial detachment (arrowhead), and discloses the accumulation of subretinal fluid in eyes with choroidal neovascularization.

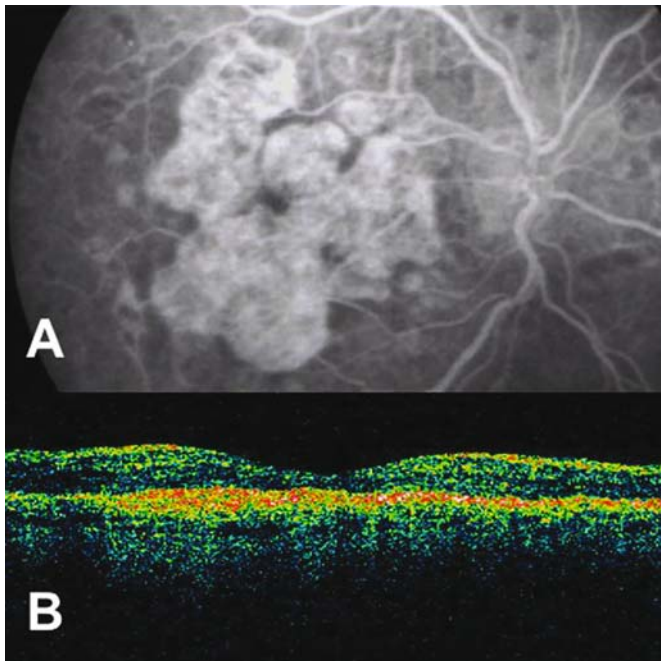

FIG. 13.4. (A) Fluorescein angiography in geographic atrophy shows a round area of hyperfluorescence (window defect). (B) Optical coherence tomography demonstrates thinning of the overlying retina and the external hyperreflective retinal pigment epithelium-choriocapillaris complex band. The loss of choriocapillaris and the resulting scatter caused by the circulating red blood cells permit increased penetration of light deeper into the choroid, significantly enhancing reflections from this layer.

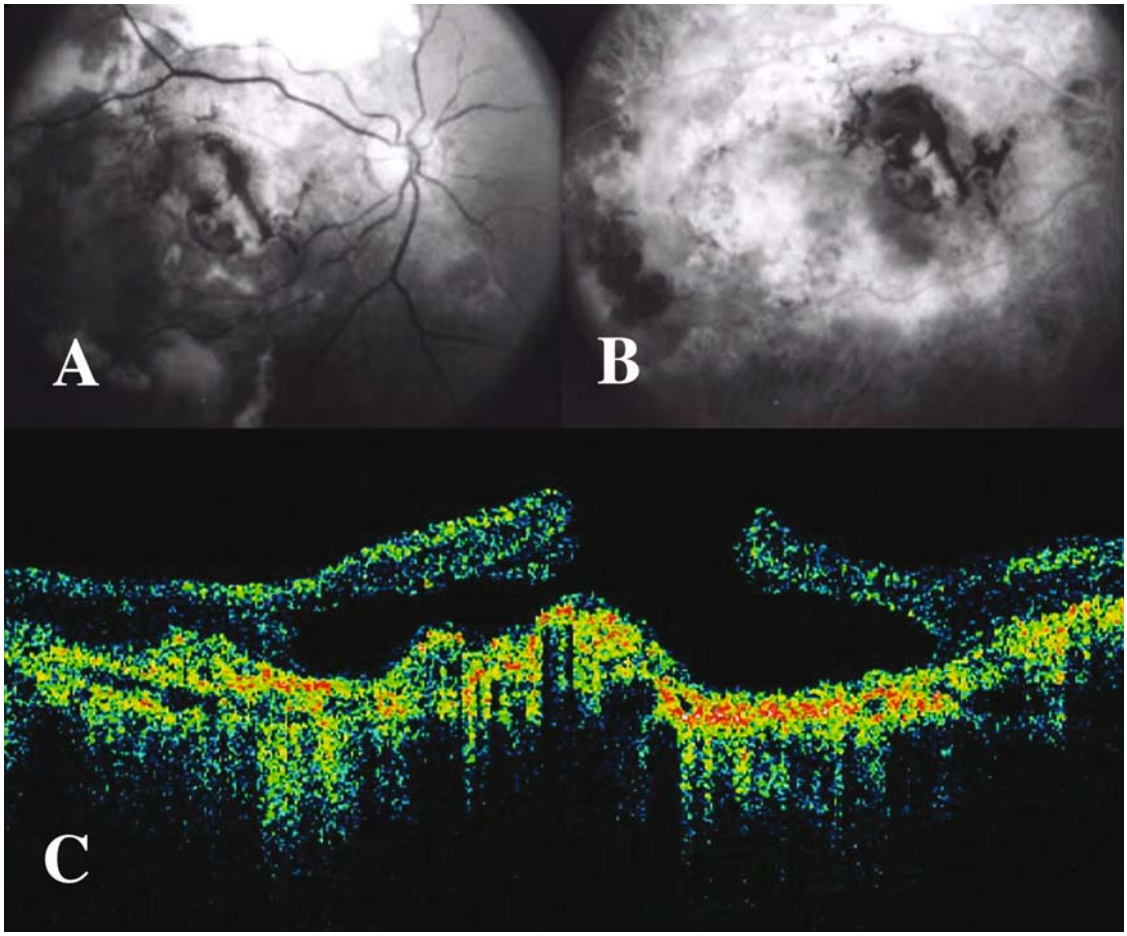

FIG. 13.5. (A,B) Atypical macular hole in geographic atrophy not observed by biomicroscopy nor fluorescein angiography. (C) Optical coherence tomography demonstrates atypical macular hole.

of eyes with GA, appearing neither in biomicroscopy nor in fluorescein angiography. An occult choroidal neovascularization can be differentiated by OCT from geographic atrophy because there is no spindle-like thickening of the RPE and no enhanced choroidal reflectivity (Fig. 13.5).

Neovascular (Exudative) Age-Related Macular Degeneration

Serous Pigment Epithelial Detachments

Retinal PEDs appear clinically as sharply demarcated, dome-shaped elevations of the RPE. They usually transilluminate if they are filled with serous fluid only. The fluorescein angiographic pattern can differentiate a drusenoid PED, which does not have CNV, from a fibrovascular PED, which is a form of occult CNV, as well as from serous PED, which may or may not overlie an area with CNV.[6] Usually it is confirmed by pooling of fluorescein dye beneath the detachment on angiography. Initially OCT shows a focal area of enhanced backscatter and mild elevation of the RPE. A formal serous PED presents as localized, dome-shaped elevations of the external high reflective band that appear optically empty with sharp margins. In the area of PED the posterior margin of the detached retina is defined by a thin, red reflection, which corresponds to the RPE. Usually, the reflection from the detached RPE shadows the reflections returning from the choroid (Fig. 13.6). However, reflections from the deeper choroid can sometimes be appreciated. This ability to visualize the deeper choroid can be attributed to increased penetration of the light probe through the decompensated RPE, a PED containing low-reflective serous fluid, and diminished circulation within the choriocapillaris.[1]

Neurosensory Retinal Detachment

Although an overlying sensory retinal detachment may be a clue to the presence of CNV beneath a PED, sometimes a shallow neurosensory detachment may occur as a result of breakdown

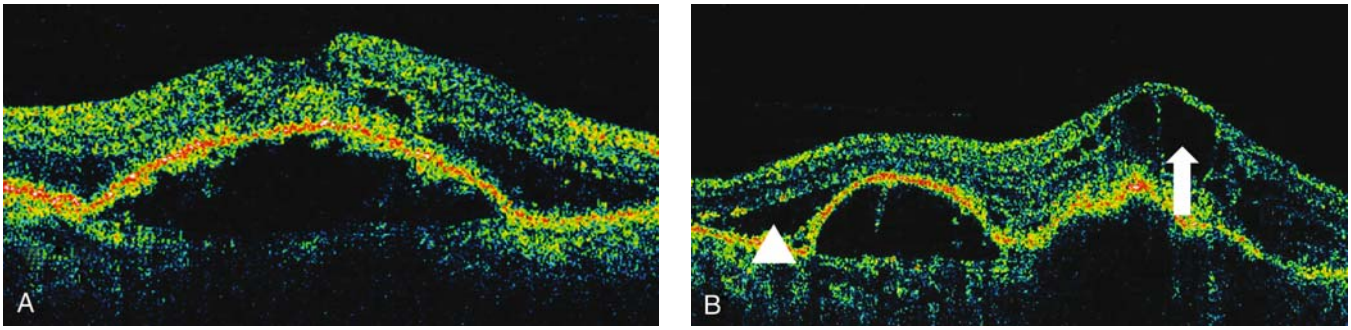

Fig. 13.6. (A) Optical coherence tomography (OCT) demonstrates serous pigment epithelial detachment (PED) as a localized, dome-shaped elevation of the external hyperreflective retinal pigment epithelium-choriocapillaris complex band that appear optically empty with sharp margins. (B) Optical coherence tomography can differentiate a serous PED that may or may not overlie an area with choroidal neovascularization. Optical coherence tomography shows intraretinal hyporeflective spaces that correspond to intraretinal cyst edema (arrow) and subretinal fluid (arrowhead) with an underlying choroidal neovascularization.

of the physiologic RPE pump or from disruption of the tight junctions between adjacent RPE cells in the absence of CNV. Unlike a PED, the borders of a neurosensory detachment are not sharply demarcated. Optical coherence tomography shows an optically clear space beneath the retina, which corresponds to serous fluid accumulation (Fig. 13.7). The reflection from the detached RPE shadows the reflection returning from the choroid, whereas no such shadowing is observed in the region of the neurosensory retinal detachment.[7]

Hemorrhagic Pigment Epithelial Detachments

Several clinical signs suggest the presence of CNV underlying an area of PED identified biomicroscopically, including overlying sensory retinal detachment and lipid, blood, and chorioretinal folds radiating from the PED.[8] Blood within or surrounding a PED implies the presence of CNV.[7] Fluorescein angiography shows a hypofluorescent lesion consistent with hemorrhage. Optical coherence tomography shows an elevation of both the neurosensory retina and a reflective red band, which corresponds to the RPE/choriocapillaris. Moderate reflections can be observed directly beneath the detached RPE, which correspond to the region of hemorrhage (Fig. 13.8). This last point differentiates a hemorrhagic from a serous detachment of the RPE.[7] Hemorrhagic PEDs show absence of reflectance from the choroid with loss of the choroidal image due to the scattering of light from the blood under the RPE (Fig. 13.9). The loss of choroidal detail correlates with the thickness of blood.[1]

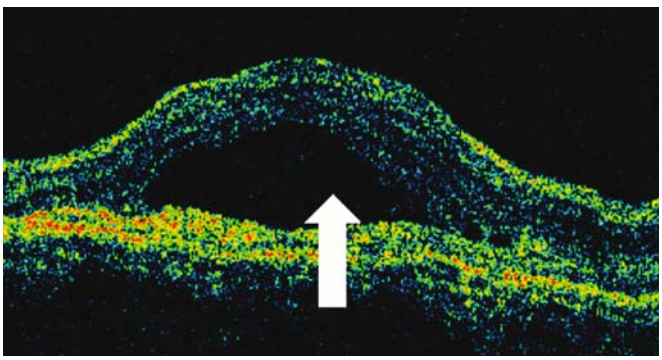

Fig. 13.7. The borders of a neurosensory retinal detachment are not sharply demarcated. Optical coherence tomography demonstrates an optically clear space beneath the retina that corresponds to serous fluid accumulation (arrow), and no shadowing is observed.

Retinal Pigment Epithelial Tear

Retinal pigment epithelial tear has been described as a complication associated with CNV, often in an eye with a serous or fibrovascular PED, and secondary to or unassociated with laser photocoagulation.[6] Tears occur at the junction of attached and detached RPE, perhaps when the PED no longer can resist the stretching forces from the fluid in the sub-RPE space emanating from the underlying occult CNV or from the contractile forces of the underlying fibrovascular tissue. When the RPE tears, the free edge of the RPE retracts and rolls toward the mound of fibrovascular tissue. [6] Fluorescein angiographic images demonstrate RPE-tear formation with blocked filling in the area of the contracted RPE and a well-demarcated hyperfluorescence in the bed of the torn RPE.[8] Optical coherence tomography shows a more elevated, less dome-shaped lesion with a steeper contour of the neurosensory retina and RPE,[1] with a shadow of reflections from the choroid below. Two red reflective layers can be visible below the sensory retina in the area of the detachment consistent with a folded, double layer of RPE. A nonreflective region of subretinal fluid can be evident inferior to the detachment. Enhanced reflectivity and optical penetration of the choroid is noted in this region, consistent with the lack of RPE.[7] No

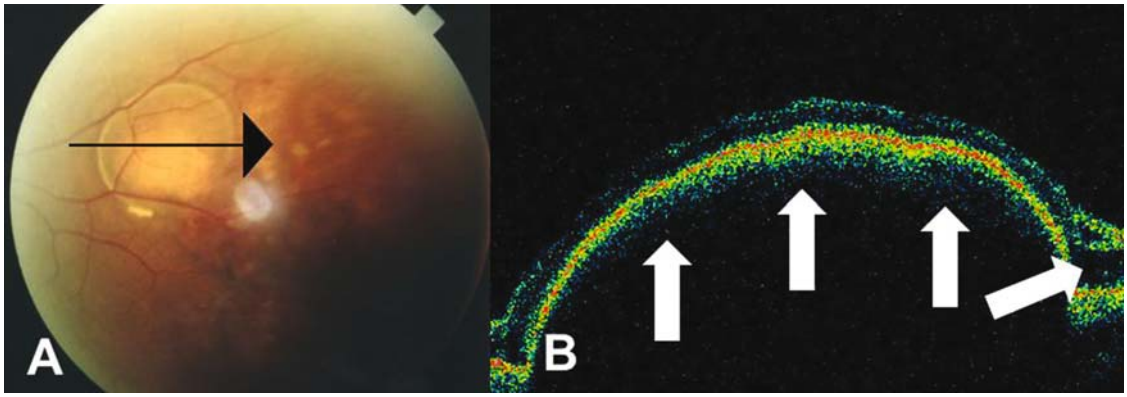

FIG. 13.8. (A) Fundus photograph shows a hemorrhagic pigment epithelial detachment (arrow). (B) Optical coherence tomography shows an elevation of both the neurosensory retina and a reflective red band, which corresponds to the retinal pigment epithelium (RPE). Moderate reflections can be observed directly beneath the detached RPE, which correspond to the region of hemorrhage (arrows).

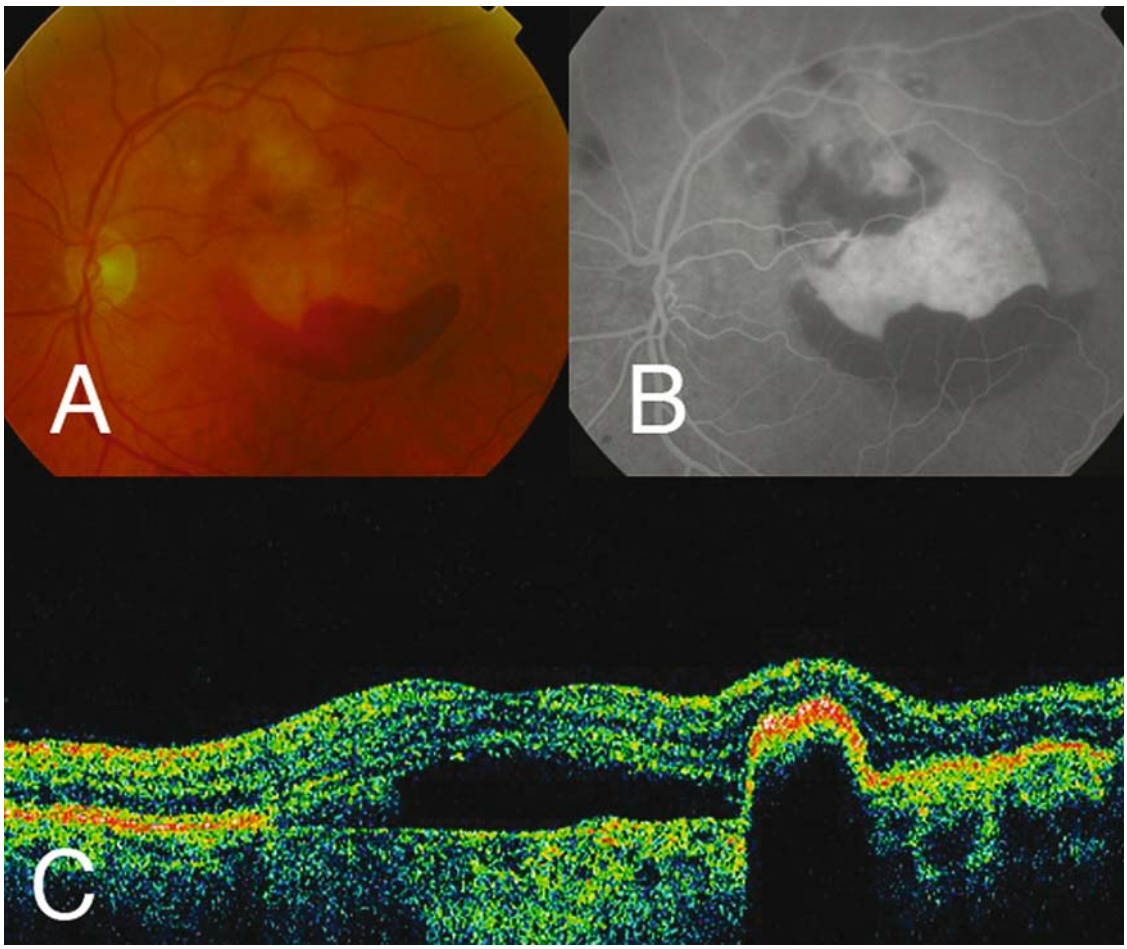

FIG. 13.9. (A,B) Fundus photograph and fluorescein angiography of retinal pigment epithelium (RPE) rip shows the area of RPE loss along the inferotemporal border of the lesion. (C) Optical coherence tomography shows more elevated, less dome-shaped, with a steeper contour elevation of the neurosensory retina and RPE, which shadow reflections from the choroid below. Two red reflective layers can be visible below the sensory retina in the area of the detachment consistent with a folded, double layer of RPE. A nonreflective region of subretinal fluid can be evident inferior to the rip. Enhanced reflectivity and optical penetration of the choroid are noted in this region, consistent with the lack of RPE. (Courtesy of Larry Yannuzzi, MD.)

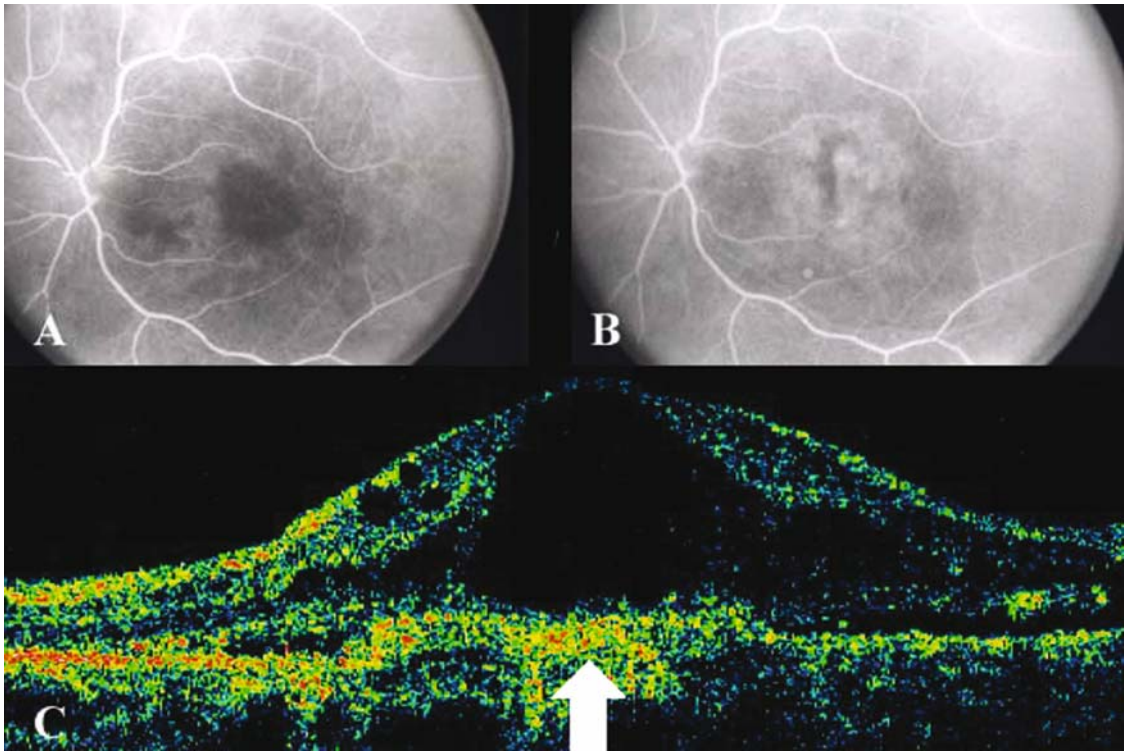

FIG. 13.10. (A,B) Macular edema in neovascular age-related macular degeneration may be difficult to detect angiographically in the presence of exudation from the choroidal neovascularization (CNV) membrane. (C) Optical coherence tomography shows reduced density of optical backscatter sites within the retina with an underlying CNV (arrow).

choroidal neovascularization may be visualized using OCT, either at the acute or at the scarring stages.[9] Meyer and Toth[10] reported three cases with RPE tear with vitreomacular attachment, and they concluded that the magnitude, variation of mechanical forces, and continuous shear stress of the aged vitreous gel transmitted across vitreoretinal attachments may cause a chronic stimulus to retina and RPE. Vitreomacular traction may contribute to the subsequent formation of RPE tears via mechanical or cell mediator pathways.

Macular Edema

Cystoid macular edema (CME) and diffuse macular edema (DME) have been infrequently reported in neovascular AMD since they may difficult to detect angiographically in the presence of exudation from the CNV (Fig. 13.10).[11] Ting et al.[12] found CME in 28 (46%) of 61 eyes. They found that CME is more common with CNV that has a classic component, and discussed the possibility that macular edema may play a role in contributing to worse VA found in eyes with occult CNV. The cause of CME in patients with neovascular AMD is not well elucidated. Gass[13] hypothesized that the extension of a CNV into the capillary free zone in the macula may disrupt the photoreceptor–external limiting membrane complex and lead to CME. Kirber et al.[14] hypothesized that the disruption of RPE metabolism has been implicated to alter the structure and permeability of the retinal capillary circulation. Alternatively, CME formation in neovascular AMD may be mediated by an inflammatory pathway.[13,15] Diffuse retinal edema is manifested as increased retinal thickness and a diffuse decrease in retinal reflectivity due to a reduced density of optical backscatter sites within the retina. Monitoring retinal thickness may also be useful in evaluating efficacy of treatment and in the future may prove to be a valuable tool in assessing patients for re-treatment.

Choroidal Neovascularization

Well-Defined Classic Choroidal Neovascularization

Classic CNV shows a distinct area of choroidal hyperfluorescence with well-demarcated borders that can be seen in the choroidal and early arterial phase of FA. As the angiogram progresses, the intensity and extent of hyperfluorescence increases (Fig. 13.11A). During the later phases of the FA, leakage of fluorescein dye and pooling in the overlying subsensory retinal space typically obscures the boundaries of the CNV and details of the capillary plexuses.[16,17] Optical

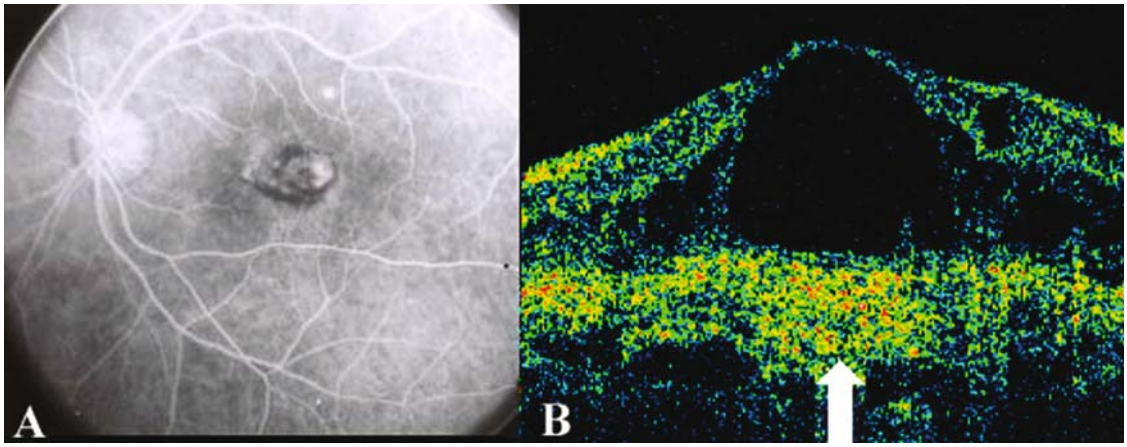

Fig. 13.11. (A) Classic choroidal neovascularization (CNV) shows a distinct area of choroidal hyperfluorescence with well-demarcated borders. As the angiogram progresses, the intensity and extent of hyperfluorescence increases. (B) Optical coherence tomography imaging reveals a fusiform enlargement of the retinal pigment epithelium (RPE)/choriocapillaris reflective band with defined borders (arrow). The highly reflective band appears disrupted, irregular, and duplicated, with high backscattering material between the two bands. Occasionally, it may be possible to image the membrane above the RPE (type 2 CNV).

coherence tomography imaging may reveal a fusiform enlargement of the RPE/Bruch's/choriocapillaris reflective band with defined borders. The highly reflective band may appear disrupted, irregular, and duplicated, with high backscattering material between the two bands. Occasionally, it may be possible to image the membrane above the RPE (type 2 CNV) (Fig. 13.11B).[1]

Occult Choroidal Neovascularization

Hee et al.[7] categorized CNV visible on OCT as well defined, poorly defined, or as a fibrovascular pigment epithelial detachment (FVPED). This classification did not necessarily correspond to similar FA descriptions, in which occult CNV refers to two hyperfluorescent patterns.[7,18] The first pattern, termed a fibrovascular PED, appears as an irregular elevation of the RPE, often stippled with hyperfluorescent dots. The boundaries may or may not show leakage in the late phase frames as fluorescein collects within the fibrous tissue or pools in the subretinal space overlying the FVPED. The exact boundaries of an FVPED usually can be determined most accurately only when fluorescence sharply outlines the elevated RPE. The amount of elevation depends on the quality of the stereoscopic photographs and the thickness of the fibrovascular tissue. [6] Optical coherence tomography imaging of FVPEDs includes a well-defined RPE elevation of the external band with a deeper area of mild backscattering corresponding to fibrous proliferation. A clear distinction is noted between the bright reflection from the RPE (red) and the moderate sub-RPE reflections (green/yellow) (Fig. 13.12). No optical shadowing of the choroid is visible. The optical penetration through this lesion can be significantly greater than that observed through subpigment epithelial hemorrhage.[7]

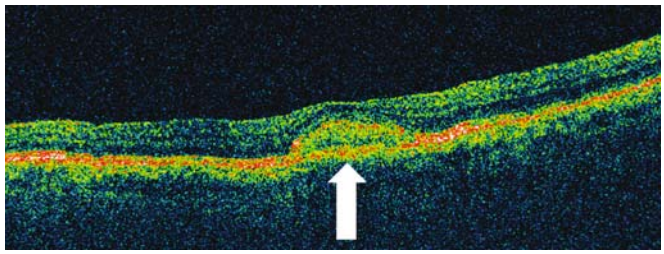

Fig. 13.12. Optical coherence tomography imaging of fibrovascular pigment epithelial detachment shows a well-defined retinal pigment epithelium (RPE) elevation of the external band with a deeper area of mild backscattering corresponding to fibrous proliferation (arrow). A clear distinction is noted between the bright reflection from the RPE (red) and the moderate sub-RPE reflections (green/yellow). No optical shadowing of the choroid is visible.

The second pattern, late leakage of an undetermined source, refers to late choroidal based leakage in which there is no clearly identifiable classic CNV (Fig. 13.10A,B) or FVPED in the early or middle phase of the angiogram to account for the area of leakage in the late phase. Often this pattern of occult CNV can appear as speckled hyperfluorescence with pooling of dye in the subretinal space overlying the speckles without a corresponding source of leakage in the early phase (Fig. 13.10A,B). Usually the boundaries of this type of CNV cannot be determined precisely.[5] Hee et al.[7] proposed two OCT descriptions, the well-defined CNV (Fig. 13.13) and the poorly defined CNV (Fig. 13.10) in occult choroidal CNV. Well-defined CNV shows a fusiform thickening and disruption of the reflective band, which corresponds to the RPE and choriocapillaris with well-defined boundaries. In their cases no significant retinal thickening was noted. Sometimes a thin

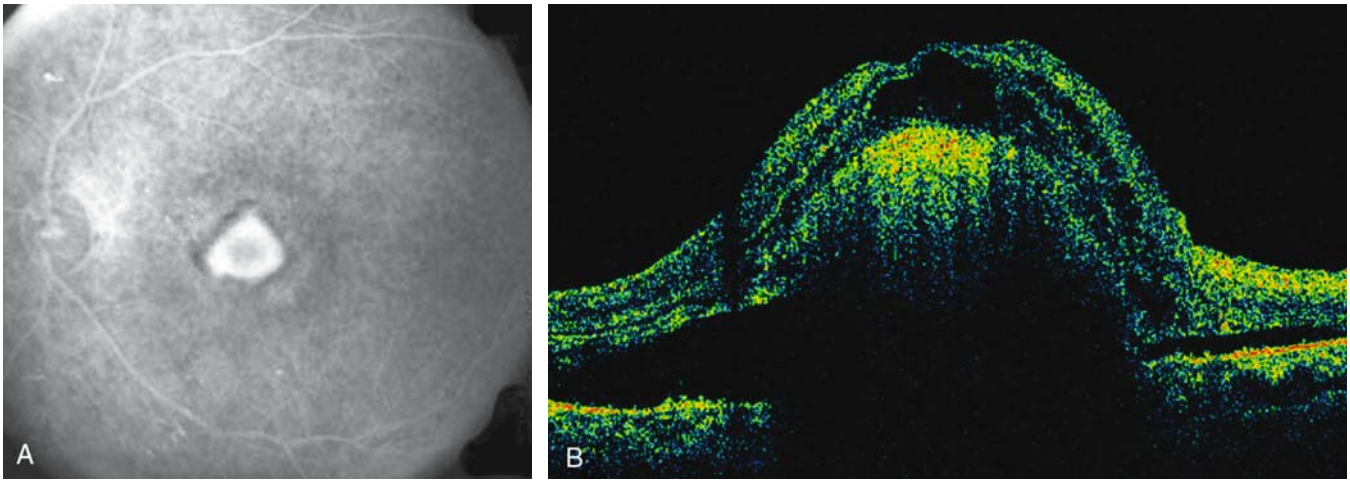

Fig. 13.13. Fluorescence angiography (A) and optical coherence tomogram (B) of a classic well-defined choroidal neovascular membrane.

line of enhanced backscatter from within the neurosensory retina immediately superior to the lesion consistent with intraretinal hemorrhage can be seen. Poorly defined CNV diffusely enhances choroidal backscatter and disrupts reflections from the RPE and choriocapillaris with poorly defined boundaries and is associated with subretinal or intraretinal fluid or cyst formation (Fig. 13.10C). The enhanced reflectivity is confined below and blends into the normal contour of the disrupted RPE, which is unaffected. Subretinal or intraretinal fluid or fragmentation of the RPE/choriocapillaris must be observed to distinguish this enhanced choroidal reflectivity from increased choroidal reflections due to pigmentary atrophy.[7]

Optical Coherence Tomography and Fluorescein Angiography

In general, angiographically classic CNV appeared as well-defined CNV on OCT, whereas angiographically occult CNV was characterized as either fibrovascular PED or poorly defined CNV. However, Hee et al.[7] reported some important exceptions. Classic CNV sometimes presented as fibrovascular PED on OCT. In these cases, OCT may have been sensitive to the difference between predominantly subretinal versus predominantly sub-RPE neovascularization. Thus well-defined CNV on OCT may represent new vessels, which are penetrating through single or multiple focal breaks in Bruch's membrane. In contrast, the reflection from the RPE in a fibrovascular PED on OCT appears intact and suggests that neovascularization is confined below the RPE.[7] In addition, Hee et al. described a subset (12 of 50 eyes) of angiographically occult CNV as well-defined CNV on OCT. Some of these findings were characterized by hemorrhage that obscured FA but not OCT. The near-infrared wavelength and high detection sensitivity of OCT allowed enhanced penetration and imaging capability through blood compared with FA. In other cases of occult CNV they described a well-defined thickening and disruption of the RPE/choriocapillaris complex noted on OCT in the absence of large hemorrhage. Although hyperfluorescence observed by FA and ICGV in patients with CNV indicates the extent of the CNV, it is unclear if it represents the total area of the lesion. Kim et al.[19] found that CNV size on OCT is always smaller than CNV size on FA.

Blood in the Subretinal or Subretinal Pigment Epithelium Space

When confined to the sub-RPE space, blood may appear as a directly elevated, green or dark red mound. Hemorrhage can dissect through the RPE into the subsensory retinal space or into the retina. Rarely, blood may pass through the retina into the vitreous cavity, causing extensive vitreous hemorrhage.[7] Blood in the subretinal space shows an elevated and often edematous retina with a highly reflective underlying layer that is blood. This blood causes shadowing of the underlying RPE/Bruch's/choriocapillaris complex, and this external band is not visualized. Blood in the sub-RPE space shows an elevated an intact external band with an underlying area of high reflectivity and shadowing corresponding to blood. Choroidal details are not observed.[1]

Subretinal Fibrosis

Fibrosis is the end stage of exudative AMD. Scarring consists of white, fibrous tissue under the retina involving the RPE/Bruch's/choriocapillaris complex. In FA, a fibrovascular scar frequently hyperfluoresces from both fluorescein leakage and staining (Fig. 13.14A). One may also notice chorioretinal

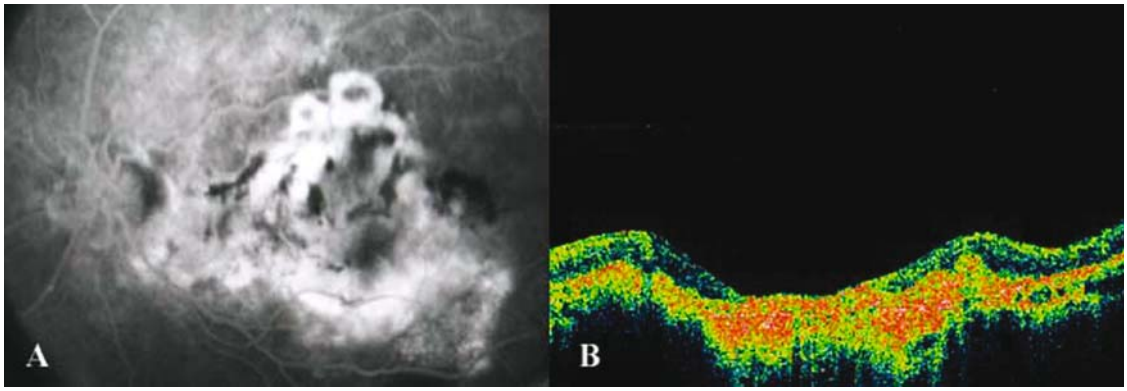

FIG. 13.14. (A) This area of scarring consists of white, fibrous tissue under the retina involving the retinal pigment epithelium (RPE)/choriocapillaris complex. In fluorescein angiography a fibrovascular scar frequently hyperfluoresces from both fluorescein leakage and staining. (B) On optical coherence tomography the tissue under the retina involving the RPE/choriocapillaris complex is highly reflective and is frequently associated with overlying retinal atrophy.

anastomoses or, more precisely, retinal anastomoses into fibrovascular tissue. The area of anastomoses, when noted before development of extensive visible scar tissue, often shows a bright area of fluorescence in the early phase, occasionally accompanied by a small area of intraretinal hemorrhage.[6] With OCT the tissue under the retina involving the RPE/Bruch's/choriocapillaris complex is highly reflective, and is frequently associated with overlying retinal atrophy (Fig. 13.14B).[1]

Retinal Angiomatous Proliferation

Retinal angiomatous proliferation (RAP) has emerged as an increasingly recognized variant of neovascular AMD.[20,21] Retinal angiomatous proliferation lesions are suggested to begin as fronds of intraretinal neovascularization. These fronds may grow into the subretinal space causing serous RPE detachments and may ultimately anastomose with choroidal neovascular complexes.[22] Retinal angiomatous proliferation appears early as small intraretinal hemorrhages, and often has these intraretinal hemorrhages overlying a serous PED. As RAP evolves, macular edema is associated with multiple intraretinal hemorrhages and PED. The small intraretinal hemorrhages often correspond to small interruptions in the layers of neurosensory retina as seen by OCT, often followed by the formation of an intraretinal or subretinal neovascular complex. Later in the course of the disease, the lesion appears to extend into the sub-RPE space.[1] In the early phase of FA, Zacks and Johnson[22] have demonstrated flow through the intraretinal vascular lesion. Late frames show pooling of fluorescein in the serous PED. The intraretinal lesion may show washout of fluorescein. Optical coherence tomography imaging centered on the red lesion may demonstrate an intraretinal focus of hyperreflectivity. In Zacks and Johnson's patient, OCT imaging clearly illustrates the intraretinal location of the RAP lesion. Because none of the imaging studies revealed choroidal neovascularization, they believe that the neovascularization in these case originated within the retina and is the cause of the accumulation of the sub-RPE fluid.[22] In addition, Yannuzzi et al.[21] described OCT findings of RAP and showed detachment of the pigment epithelium with an acoustically clear subpigment epithelial space and irregular reflectance from RAP, which can show associated intraretinal edema or serous neurosensory detachment (Fig. 13.15).

Optical Coherence Tomography Findings Following Choroidal Neovascular Removal in Age-Related Macular Degeneration

Zolf et al.[23] found that in patients with myopic neovascularization, OCT reflectivity might provide a clue about the ease with which CNV might be removed and about the postoperative visual outcome. Eyes for which OCT reveals the triad of hyperreflective tissue with anterior location, a separation zone, and an optically clear zone underneath should be considered for CNV removal. However, several investigators have reported their clinical experience with surgical removal of subfoveal CNV in different conditions. Favorable results were found in young patients with presumed ocular histoplasmosis syndrome and idiopathic CNV but not in patients with myopia, angioid streaks, and AMD. Stanga et al.[24] described the feasibility of a new surgical technique to enhance visual function over translocated RPE cells in patients operated for subfoveal CNV secondary to AMD. They described postoperative single-line OCT scans of the posterior pole showing a well-delimited pattern of increased higher relative reflectivity in the choroidal tissues corresponding to the area devoid of RPE. A single line scan across the translocated RPE showed a well-delimited higher relative reflectivity in the layers assigned to the RPE-choriocapillaris complex similar to that observed

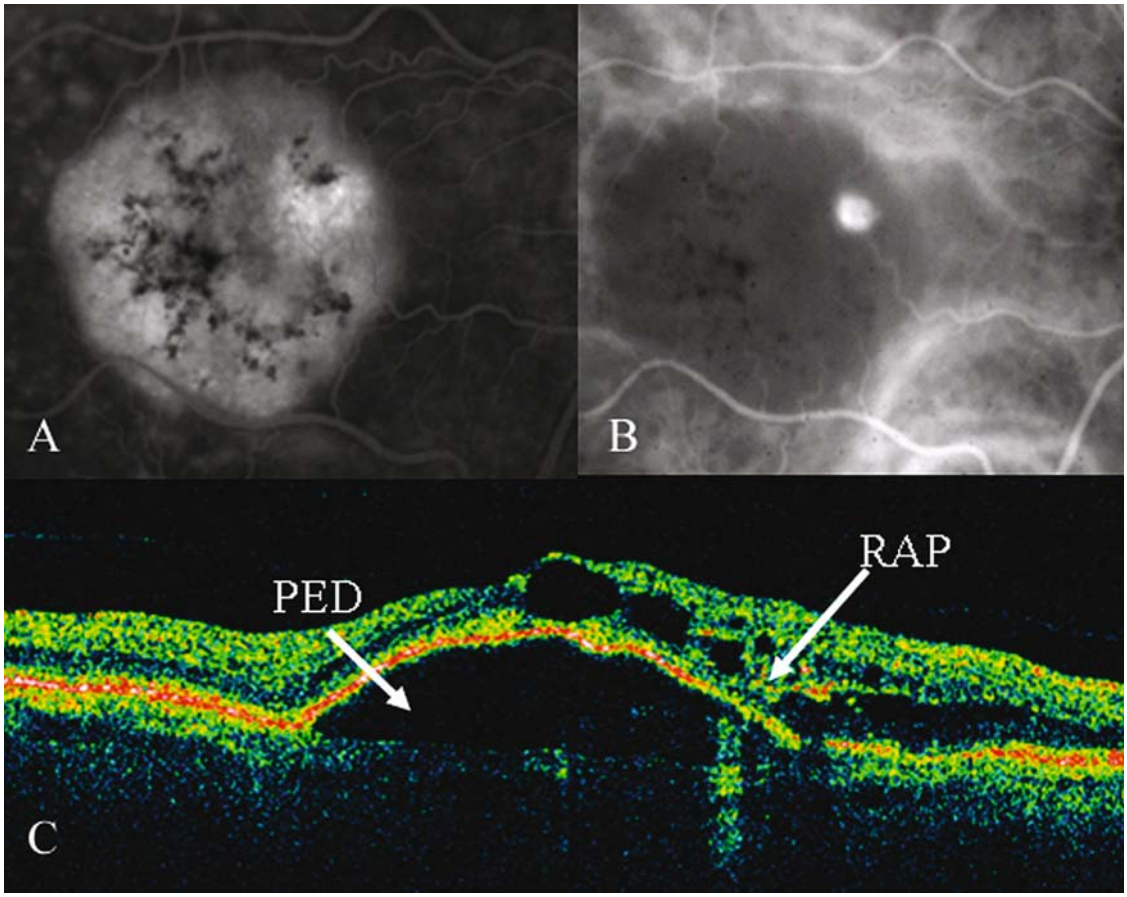

FIG. 13.15. (A) Late-phase fluorescence angiography shows complete staining of the subpigment epithelial space, simulating occult choroidal neovascularization. There is an increase in the intensity of the hyperfluorescence in the area of retinal angiomatous proliferation (RAP) from leakage of these capillaries as well as intraretinal and subretinal leakage. (B) Indocyanine green videoangiography study shows hypofluorescence at the site of the serous pigment epithelial detachment (PED) and a "hot spot " corresponding to RAP. (C) Optical coherence tomography shows PED with an acoustically clear subpigment epithelial space and irregular reflectance from RAP, which may show associated intraretinal edema or serous neurosensory detachment. (Courtesy of Larry Yannuzzi, MD.)

external to the defect. As initially described by Hee et al.[7] in 1996, OCT produces cross-sectional tomographs of the logarithm of reflectivity in the retina, which are displayed in real time as two-dimensional false color images. The well-defined increased optical reflectivity observed in the choroidal tissues in the area devoid of RPE was interpreted as an increase in light transmission toward sclera secondary to the absence of RPE. This contrasted with the area of transplanted RPE in which the normal distribution of reflectance was seen.

Optical Coherence Tomography Findings Following Photodynamic Therapy of Choroidal Neovascularization

Response to therapy is one of the most important clinical uses of OCT. Optical coherence tomography can be used to quantify changes in central retinal thickness and volume as well as in subretinal fluid. Optical coherence tomography currently provides useful information when deciding if patients require additional courses of therapy following their initial treatment with verteporfin therapy. Optical coherence tomography, when used in conjunction with FA, is helpful in characterizing changes following verteporfin therapy and in detecting early accumulation of subretinal fluid associated with recurrence of CNV.[1]

Rogers et al.[25] described five OCT stages in the retina following PDT and correlated with clinical and angiographic findings from predominantly classic subfoveal CNV in 79 eyes:

Stage I

This stage represents an acute transient inflammatory response to the photodynamic process. Costa et al.[26] described increased leakage by ICGV from the neovascular lesion at 20 minutes after PDT. A progressive increase in retinal thickness was seen during the first 80 minutes after treatment. The amount of fluid appeared to remain stable until 5 days. Rogers et al.[25] demonstrated an

increase in intraretinal fluid, with leakage of dye in both the CNV and treatment area on FA. They think that release of inflammatory mediators may explain the induced incompetence of the retinal vasculature and CNV in the treatment zone, acute damage to the endothelial cell layer may also explain this finding. However, Costa et al.[26] proposed that the leakage from CNV is an acute event that lasts for a short period (24 to 48 hours), with persistence of the subretinal and intraretinal fluid resulting from transient dysfunction of the RPE cells. This is consistent with the damage to retinal RPE cells seen in experimental PDT studies.[27] The increase in intraretinal fluid occurring in stage I may cause the transient visual fluctuations that some individuals report in the week following PDT treatment.

Stage II

One to 2 weeks following treatment, resolution of intraretinal fluid with the establishment of a normal foveal contour occurs, creating a stage II OCT lesion. Hypoperfusion of the choroid and CNV are evident as a circular hypofluorescent treatment spot. Choroidal hypoperfusion may diminish the ability of CNV to leak fluid, theoretically enabling the RPE to pump out accumulated intraretinal and subretinal fluid without rapid reaccumulation. As a matter of interest, this is the time interval at which treated individuals report the greatest visual benefit. This visual improvement logically occurs given the restoration of a more normal foveal anatomy on OCT from transient elimination of retinal fluid. Stage II OCT lesions coincide with hypoperfusion of the choriocapillaris and typically persist for 4 weeks following PDT. It is interesting that restoration of the choroidal vessels perfusion led to concurrent CNV reperfusion to some degree, suggesting that transient occlusion of these vessels may play an essential role in CNV.

Stage III

Reperfusion of the choroid and CNV occurring 4 to 12 weeks following initial treatment induces the formation of a stage III OCT lesion. Stage III is usually evident at 3-month follow-up, at which time a decision on re-treatment is made. The degree of fluid and fibrosis determines whether a lesion is classified as stage IIIa or IIIb. Stage IIIa lesions have a relatively low degree of fibrosis with intraretinal and subretinal fluid on OCT. In contrast, stage IIIb lesions exhibit minimal intraretinal and subretinal fluid. Given the predominantly fibrotic nature of stage IIIb lesions, they may not benefit from re-treatment (Fig. 13.16).

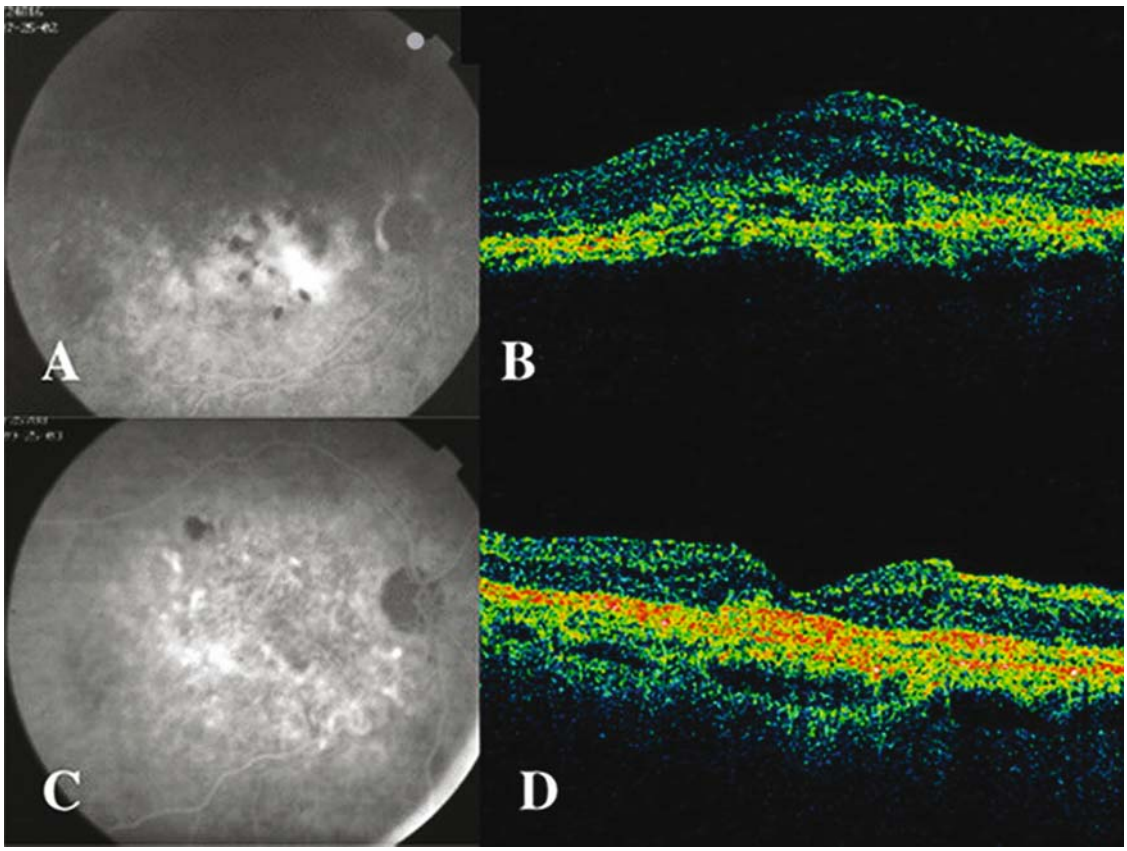

Fig. 13.16. (A,B) Fluorescein angiography (FA) and optical coherence tomography (OCT) of a minimally classic choroidal neovascularization (CNV) membrane before photodynamic therapy (PDT). (C,D) Fluorescein angiography and OCT after PDT for CNV. (D) Choroidal neovascularization stage IIIb shows minimal intraretinal and subretinal fluid. Given the predominantly fibrotic nature of stage IIIb lesions, they may not benefit from re-treatment with PDT.

Stage IV

Optical coherence tomography is particularly valuable in identifying stage IV lesions. The CNV, which exhibits fibrosis, continues to leak FA. This angiographic finding may easily be misinterpreted as active leakage from recurrent CNV, prompting re-treatment with PDT. Optical coherence tomography correctly identifies the leakage of fluorescein as CME. Cystoid macular edema on OCT appears as hyporeflective black circular spaces separated by reflective septa within the retina. The CNV is fibrotic and inactive, and the leakage presumably results from dysfunctional RPE in the area of subretinal fibrosis. Re-treatment at this stage leads to the resolution of macular edema with ultimate progression to a stage V lesion.

Stage V

As CME resolves, a stage V lesion naturally evolves. Retinal fluid reabsorbs and localized retinal atrophy ensues in the area of treatment.[25]

Disadvantages of Optical Coherence Tomography

Because OCT is a cross-sectional imaging modality, one OCT provides information only on CNV boundaries within a thin tissue slice. The current acquisition time of 2.5 seconds per tomogram limits the feasibility of acquiring multiple tomograms through an area of suspected CNV to adequately define the entire CNV boundary.[7] Optical coherence tomography in its current configuration also does not provide much additional information when there are angiographic features that obscure the boundaries of neovascular membranes. In a serous detachment of the RPE, for example, the bright hyperfluorescence from the window defect may obscure the hyperfluorescence from the CNV in the region beneath the detachment on FA. Optical coherence tomography also does not effectively image CNV beneath PEDs because of optical shadowing by the detached RPE. Similarly, blood often obscures the boundaries of CNV on angiography. Although OCT is successfully able to image CNV obscured on FA by thin hemorrhage, the OCT probe light is attenuated by dense subretinal or intraretinal hemorrhage, which prevents adequate imaging of the choroid. Finally, the reflections from particular structures within the retina on OCT are influenced by the absorption and scattering properties of intervening layers. This limitation is most apparent when distinguishing true alterations in choroidal reflectivity from changes in RPE pigmentation, which affects the propagation of the OCT probe beam to and from the choroid.[7]

Optical coherence tomographic images are degraded in the presence of media opacity. For example, it may be difficult to obtain optimal scans in the presence of dense cataract or vitreous opacity. Optical coherence tomography scanning may not be possible in patients who are unable to cooperate with the study. Measurements of foveal thickness may be inaccurate if the operator is not careful to center the scan over the fovea. With retinal thickness scan and analysis maps, if one of the six radial scans is missing, an inaccurate retinal thickness map and calculation of retinal thickness in different regions will be produced. Furthermore, if the computer misidentifies the inner or outer retinal layer from which the retinal thickness measurement is calculated, then the retinal thickness measurement will not be accurate. However, it is often possible to correct the thickness measurement for scanning artifact by rescanning the particular inaccurate radial scan. Finally, the OCT machine is relatively expensive.[28]

Future Development

The further development of OCT for imaging CNV is attractive for a number of reasons. Unlike FA, OCT provides purely structural information concerning abnormal vessels, which may be more informative in localizing CNV than leakage of fluorescein dye, which is both a structural and functional measurement. The eligibility criteria used in the Macular Photocoagulation Study (MPS) clinical trials, which are based solely on angiography, apply only to a small group of patients with AMD.[7,29] Hee et al.[7] characterized CNV as well-defined or fibrovascular PED on OCT, and that could conceivably be used to guide laser treatment. Twelve of their 23 cases with membranes had an occult appearance on FA and therefore would not have been eligible under MPS guidelines. Additionally, OCT is a fiber optic technique; therefore, imaging potentially could be directly integrated with conventional laser photocoagulation treatment, providing online monitoring and visualization of the lesion boundaries. Finally, they think three-dimensional reconstructions of the retina could be obtained from multiple cross-sectional tomograms to provide complete information on the location of CNV. Recently, the integration of the scanning laser ophthalmoscope (SLO) and OCT has produced a dynamic new instrument, the OCT ophthalmoscope, which simultaneously images the fundus in numerous ways with point to point correlation.

Conclusion

Optical coherence tomography is a noninvasive, dynamic technology ideal for observing the natural course of AMD. The structural information provided by OCT is becoming a valuable diagnostic adjunct to FA and ICGV. Optical coherence tomography demonstrates and quantifies macular pathology in AMD. In addition, OCT measures in an objective way macular thickness and foveal changes associated with CNV. The goal of using OCT is to correlate these observed structural changes to changes in VA, not only to better understand the mechanism of vision loss associated with AMD, but also to

understand the mechanism of VA benefits attributed to various treatments. In particular, OCT is a valuable tool to monitor the treatment effects associated with PDT as well as periocular and intraocular pharmacologic therapy in neovascular AMD.[1]

Limitations of OCT can be overcome with an experience OCT technician and attention to anatomic landmarks.

Acknowledgments. This work is supported in part by the Arevalo-Coutinho Foundation for Research in Opthalmology, Caracas, Venezuela.

References

1. Mavrofrides EC, Villate N, Rosenfeld PJ, Puliafito CA. In: Schuman JS, Puliafito CA, Fujimoto JG, eds. Optical Coherence Tomography of Ocular Diseases: Age Related Macular Degeneration, 2nd ed. Thorofare, NJ: Slack, 2004:243–343.
2. Sarks SH, Sarks JP. In: Ryan SJ, ed. Retina: Age-Related Macular Degeneration: Atrophic Form, 2nd ed. St. Louis: Mosby, 1994:1071–1102.
3. Sarks SH, Sarks JP. In: Ryan SJ, ed. Retina: Age-Related Maculopathy: Nonneovascular Age Related Macular Degeneration and the Evolution of Geographic Atrophy, 3rd ed. St. Louis: Mosby, 2001:1064–1099.
4. Roquet W, Roudot-Thoraval F, Coscas G, Soubrane G. Clinical features of drusenoid pigment epithelial detachment in age related macular degeneration. Br J Ophthalmol 2004;88:638–642.
5. Hassenstein A, Ruhl R, Richard G. [Optical coherence tomography in geographic atrophy—a clinicopathologic correlation]. Klin Monatsbl Augenheilkd 2001;218:503–509.
6. Bressler NM, Bressler SB, Fine SL. In: Ryan SJ, ed. Retina: Neovascular (Exudative) Age Related Macular Degeneration, 3rd ed. St. Louis: Mosby, 2001:1100–1135.
7. Hee MR, Baumal CR, Puliafito CA, et al. Optical coherence tomography of age-related macular degeneration and choroidal neovascularization. Ophthalmology 1996;103:1260–1270.
8. Bressler NM, Bressler SB, Fine SL. Age-related macular degeneration. Surv Ophthalmol 1988;32:375–413.
9. Giovannini A, Amato G, Mariotti C, Scassellati-Sforzolini B. Optical coherence tomography in the assessment of retinal pigment epithelial tear. Retina 2000;20:37–40.
10. Meyer CH, Toth CA. Retinal pigment epithelial tear with vitreomacular attachment: a novel pathogenic feature. Graefes Arch Clin Exp Ophthalmol 2001;239:325–333.
11. Bressler NM, Bressler SB, Alexander J, Javornik N, Fine SL, Murphy RP. Loculated fluid. A previously undescribed fluorescein angiographic finding in choroidal neovascularization associated with macular degeneration. Macular Photocoagulation Study Reading Center. Arch Ophthalmol 1991;109:211–215.
12. Ting TD, Oh M, Cox TA, Meyer CH, Toth CA. Decreased visual acuity associated with cystoid macular edema in neovascular age-related macular degeneration. Arch Ophthalmol 2002;120:731–737.
13. Gass JDM. Pathophysiologic and histopathologic bases for interpretation of fluorescein angiography. In: Stereoscopic Atlas of Macular Diseases: Diagnosis and Treatment, 4th ed. St. Louis: Mosby-Year Book, 1997:40–41.
14. Kirber WM, Nichols CW, Grimes PA, Winegrad AI, Laties AM. A permeability defect of the retinal pigment epithelium. Occurrence in early streptozocin diabetes. Arch Ophthalmol 1980;98:725–728.
15. Penfold PL, Killingsworth MC, Sarks SH. Senile macular degeneration: the involvement of immunocompetent cells. Graefes Arch Clin Exp Ophthalmol 1985;223:69–76.
16. Koenig F, Soubrane G, Coscas G. [Angiographic aspects of senile macular degeneration: spontaneous course] J Fr Ophthalmol 1984;7:93–98.
17. Elman MJ, Fine SL. In: Ryan SJ, ed. Retina: Exudative Age-Related Macular Degeneration, 2nd ed. St. Louis: Mosby, 1994:1071–1102.
18. Subfoveal neovascular lesions in age-related macular degeneration. Guidelines for evaluation and treatment in the macular photocoagulation study. Macular photocoagulation study group. Arch Ophthalmol 1991;109:1242–1257.
19. Kim SG, Lee SC, Seong YS, Kim SW, Kwon OW. Choroidal neovascularization characteristics and its size in optical coherence tomography. Yonsei Med J 2003;44:821–827.
20. Fernandes LH, Freund KB, Yannuzzi LA, et al. The nature of focal areas of hyperfluorescence or hot spots imaged with indocyanine green angiography. Retina 2002;22:557–568.
21. Yannuzzi LA, Negrao S, Iida T, et al. Retinal angiomatous proliferation in age-related macular degeneration. Retina 2001;21:416–434.
22. Zacks DN, Johnson MW. Retinal angiomatous proliferation: optical coherence tomographic confirmation of an intraretinal lesion. Arch Ophthalmol 2004;122:932–933.
23. Zolf R, Glacet-Bernard A, Benhamou N, Mimoun G, Coscas G, Soubrane G. Imaging analysis with optical coherence tomography: relevance for submacular surgery in high myopia and in multifocal choroiditis. Retina 2002;22:192–201.
24. Stanga PE, Kychenthal A, Fitzke FW, et al. Retinal pigment epithelium translocation after choroidal neovascular membrane removal in age-related macular degeneration. Ophthalmology 2002;109:1492–1498.
25. Rogers AH, Martidis A, Greenberg PB, Puliafito CA. Optical coherence tomography findings following photodynamic therapy of choroidal neovascularization. Am J Ophthalmol 2002;134:566–576.
26. Costa RA, Farah ME, Cardillo JA, Calucci D, Williams GA. Immediate indocyanine green angiography and optical coherence tomography evaluation after photodynamic therapy for subfoveal choroidal neovascularization. Retina 2003;23:159–165.
27. Husain D, Kramer M, Kenny AG, et al. Effects of photodynamic therapy using verteporfin on experimental choroidal neovascularization and normal retina and choroid up to 7 weeks after treatment. Invest Ophthalmol Vis Sci 1999;40:2322–2331.
28. Jaffe GJ, Caprioli J. Related articles, links abstract optical coherence tomography to detect and manage retinal disease and glaucoma. Am J Ophthalmol 2004;137:156–169.
29. Moisseiev J, Alhalel A, Masuri R, Treister G. The impact of the macular photocoagulation study results on the treatment of exudative age-related macular degeneration. Arch Ophthalmol 1995;113:185–189.

14
The Role of Optical Coherence Tomography in the Evaluation of Ocular Photodynamic Therapy

Caroline R. Baumal and Rubin W. Kim

Assessment of the Therapeutic Response in Retinal Disorders

Clinical studies in vitreoretinal disorders utilize a variety of modalities in order to assess the retina's response to different therapies. The standard methods include visual acuity assessment, clinical examination, angiography, and electrophysiologic testing. Visual acuity is a primary outcome in most ophthalmology studies. It is measured by standardized techniques such as the Early Treatment for Diabetic Retinopathy Study (ETDRS) chart or the modified Bailey-Lovie chart. Clinical examination may involve a certified study examiner or multiple examiners and it may be performed in a masked fashion. Angiography with fluorescein dye is used to assess the posterior segment circulation. It has traditionally been the gold standard test to diagnose and classify choroidal neovascularization (CNV), as well as to evaluate the response of CNV to therapy. Indocyanine green (ICG) dye, which was originally used in cardiovascular imaging, has recently found applications in ophthalmology. The molecular and fluorescent properties of ICG permit improved imaging of the choroidal circulation. In some cases, ICG may permit evaluation of pathology, which is not visualized with fluorescein angiography due to blockage by hemorrhage. Electrophysiologic tests such as the electroretinogram (ERG) and electro-oculogram (EOG) are useful to localize pathology to a specific level or location in the retina and to monitor the effect of therapy.

Within the past decade, a new innovative imaging technique known as optical coherence tomography (OCT) has provided invaluable information about the nature and pathogenesis of retinal diseases and the response to various therapies. This technology was developed by the combined effort of researchers from the Massachusetts Institute of Technology (MIT) and Tufts University in Boston, Massachusetts. The details of the mechanism and technique of OCT imaging are described in Chapter 10. Optical coherence tomography produces high-resolution, cross-sectional retinal images in a manner similar to ultrasound.[1] However, the use of optical rather than acoustic waves in OCT produces an image with resolution up to 10 μm. For comparison, B-scan ultrasonography has a resolution of 150 μm and scanning laser ophthalmoscopy has a longitudinal resolution of approximately 300 μm. The ultrasound biomicroscope has an image resolution of 20 to 40 μm, but it is limited to anteriorly located ocular structures. As OCT technology improves, the micrometer resolution continues to increase. The OCT-2 and the OCT-3 have resolutions between 10 to 15 μm and 8 to 10 μm, respectively. The most recent investigational ultrahigh resolution (UHR) OCT has an image resolution up to 3 μm with 600 × 3000 pixels used for the image.[2] Figure 14.1 compares the images obtained with successive generations of OCT technology, and shows the improvement in visualization of anatomic details.

Cross-sectional imaging with OCT permits precise and reproducible evaluation of the foveal contour, the retinal and choroidal layers, and collections of fluid and fibrosis. Optical coherence tomography has been utilized to characterize and diagnose a variety of findings in posterior segment disorders including age-related macular degeneration (AMD), epiretinal membrane, macular hole, macular edema, central serous chorioretinopathy, and detachments of the neurosensory retina and RPE.[3] Optical coherence tomography is useful in monitoring and quantitatively assessing retinal disorders over time and evaluating the retinal anatomic response to therapy. For example, OCT images provide a means to localize the presence of macular edema and qualitatively measure changes in retinal thickness over time as demonstrated in Figure 14.2. Based on the ability of OCT to produce reproducible high-resolution cross-sectional images of the retina and its noncontact and noninvasive properties, OCT has become an important tool to precisely evaluate the anatomic response to a variety of treatments. It has become a critical imaging technique in multiple multicenter studies for diabetic retinopathy and AMD. The potential benefits of OCT imaging when evaluating a new retinal therapy include its ability to identify the retinal layers that are affected, to uncover small pockets of fluid that may not be clinically apparent, to distinguish intraretinal or subretinal

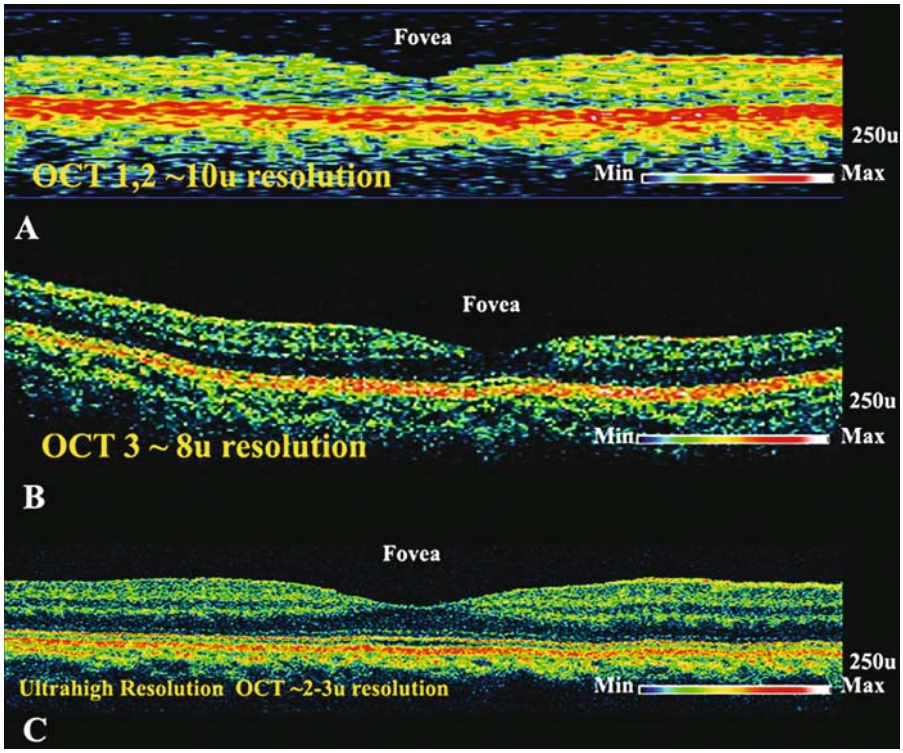

FIG. 14.1. (A–C) The optical coherence tomography (OCT) image resolution has improved with successive generations of OCT imaging technology. This is noted with more precise details visualized with ultrahigh resolution OCT (C) compared to earlier OCT models.

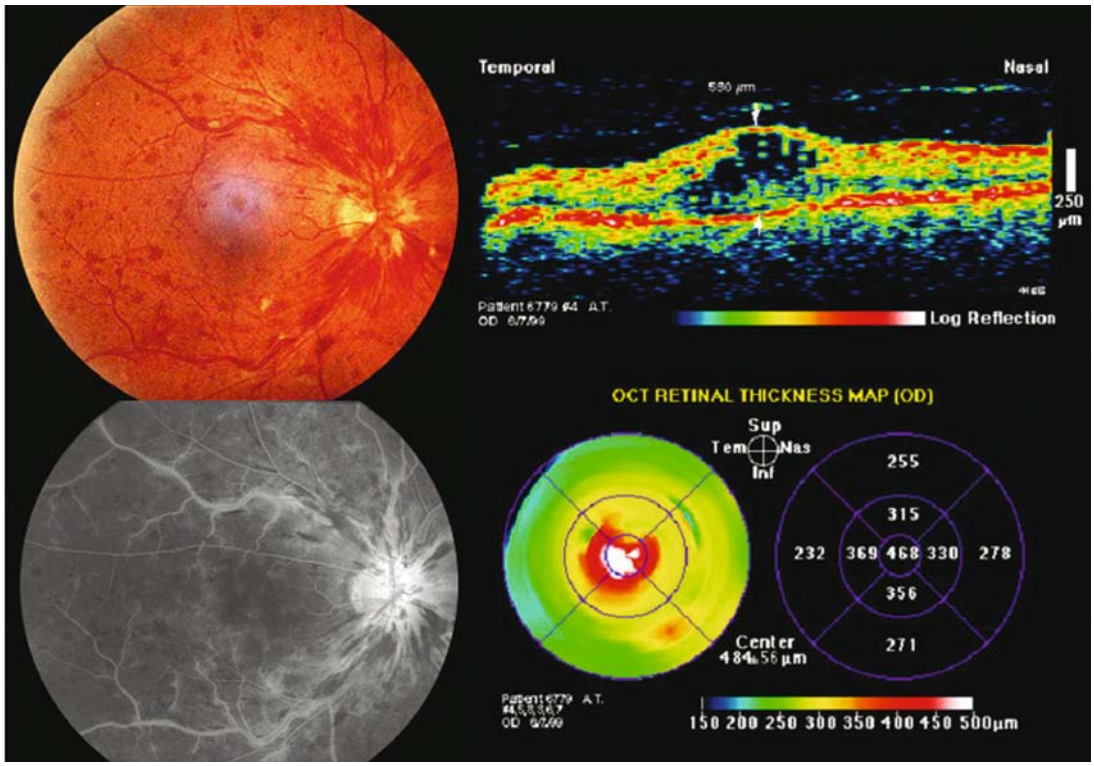

FIG. 14.2. (A) Cystoid macular edema secondary to central retinal vein occlusion is demonstrated by color photograph, fluorescein angiography, and OCT examination. Note the intraretinal cystic spaces demonstrated by OCT. (B) Resolution of the cystoid macular edema is demonstrated by OCT. The corresponding color photograph and fluorescein angiogram are shown.

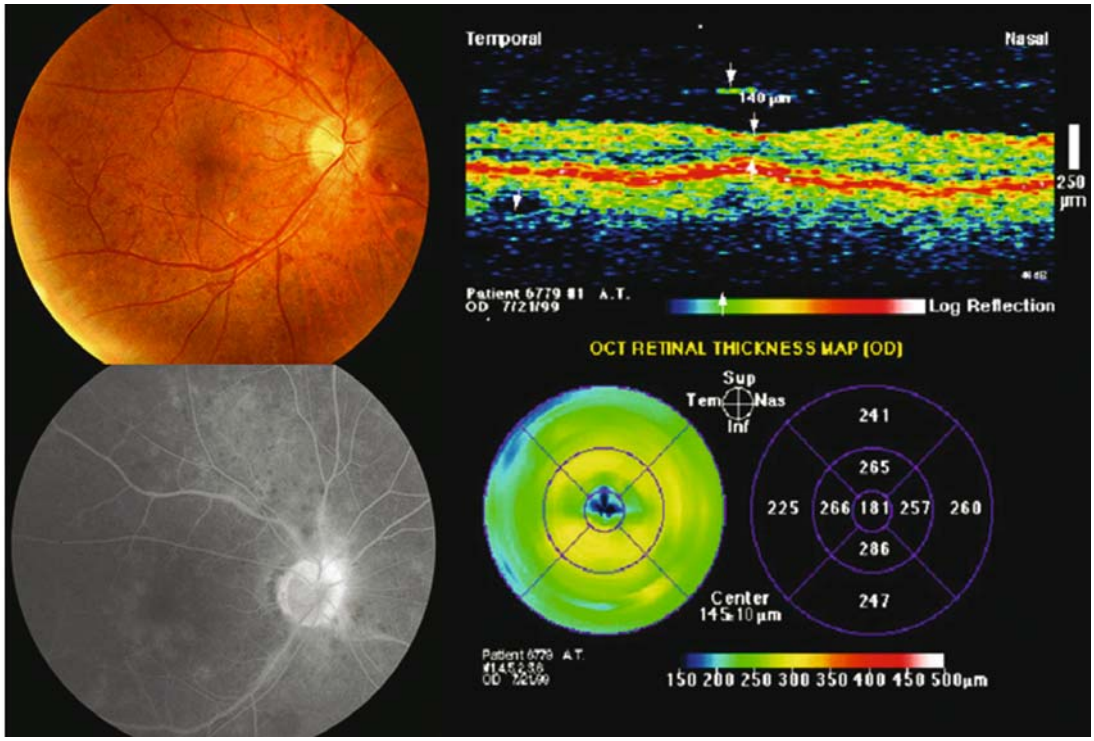

FIG. 14.2. (continued).

fluid from fibrosis (Fig. 14.3), and to provide information about an eye that may already be altered anatomically from a previous treatment. Other benefits include its noninvasive and noncontact method, its ability to be performed through a cataract or smaller pupil, and its brief image acquisition time. It is easy to perform repeat OCT imaging on multiple occasions in order to assess the clinical response. There is no inherent risk of allergy such as with fluorescein angiography (FA) and ICG dyes, intravenous access is not necessary, and there is less discomfort for the patient when compared to angiography or ERG. Thus, OCT has quickly joined the armamentarium of tests used to evaluate retinal disorders primarily and to assess their response to therapy.

Age-Related Macular Degeneration

Age-related macular degeneration (AMD) is the leading cause of vision loss in the elderly in developed countries. It is classified into two general categories: nonexudative (also known as dry) AMD and exudative (or wet) AMD. The exudative form is less common but it is responsible for the majority of severe vision loss. This form includes choroidal or subretinal neovascularization (CNV), pigment epithelial detachment (PED), and subretinal fibrosis.[4] Choroidal neovascularization is composed of abnormal new blood vessels that emanate from the choroid and can grow into the subretinal space. The CNV leaks subretinal fluid, hemorrhage, or exudate. The leakage eventually resolves, but subretinal fibrosis may develop in these areas, leading to loss of vision as demonstrated by the scenario of images in Figure 14.3. There are very few treatments with limited effectiveness for CNV in AMD. Laser photocoagulation is more effective than observation for treatment of specific types of classic CNV in AMD as demonstrated by the Macular Photocoagulation Study (MPS). However, laser is limited by a high rate of recurrent CNV leakage and by the production of a scotoma in the laser treated area, which limits its usefulness for subfoveally located CNV.[5–7] For these reasons, new therapies are continually being investigated in an effort to treat more patients with this disorder and to improve visual results. Photodynamic therapy (PDT) or ocular photodynamic therapy (OPT) has been one treatment investigated and approved for specific subtypes of CNV in AMD.

Photodynamic Therapy

A brief description of the mechanism of PDT is crucial to understand the PDT effect and the induced alterations in retinal anatomy. Photodynamic therapy involves two steps: the

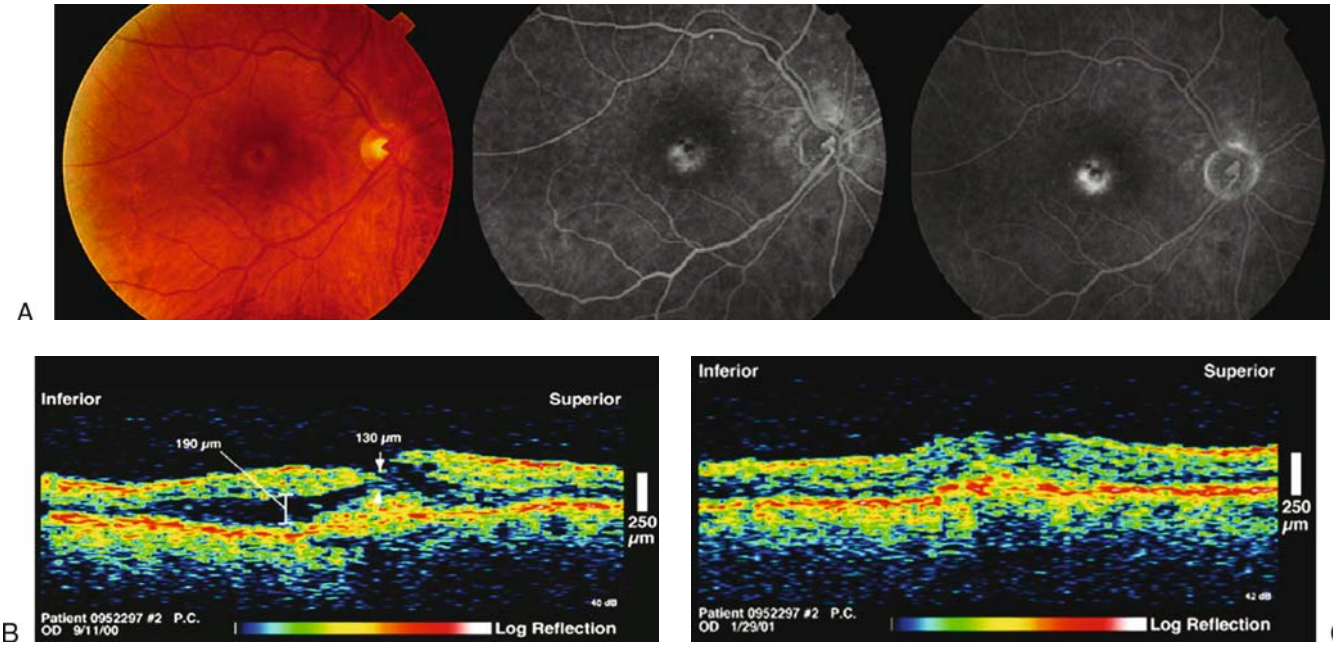

FIG. 14.3. (A) Subfoveal choroidal neovascularization (CNV) secondary to age-related macular degeneration. (B) The OCT demonstrates a discoid elevated area at the level of the retinal pigment epithelium corresponding to choroidal neovascularization. The adjacent hyporeflective areas represent intraretinal and subretinal fluid. (C) After multiple treatments with photodynamic therapy, the OCT demonstrates a resolution of the intraretinal and subretinal fluid with residual subretinal fibrosis noted as thickening of the deep red retinal pigment epithelium (RPE)/choriocapillaris layer.

administration of a photosensitizing agent that localizes within the target tissue, and the precise application of light of a specific wavelength that activates the photosensitizer to commence the PDT effect. The interaction of the photosensitizer with the activating light induces a "photochemical reaction" that liberates by-products that are toxic to the target tissue. This reaction results in the occlusion of the vascular bed secondary to damage to the vascular endothelial cells, platelet adhesion and aggregation, and subsequent thrombus formation. The localization of the photosensitizing agent within the target tissue and the direct application of low-energy focused light to the lesion are the main features that limit damage to the surrounding normal tissue.

Based on the mechanism of action of PDT to produce vascular occlusion, it has been investigated in ophthalmology as a potential therapy for retinal and choroidal vascular disorders as well as for vascular ocular tumors. The retina is an ideal location for PDT due to the ability to directly focus light with a contact lens onto the retina target tissue and the ease of access to the retina through a dilated pupil. As CNV in AMD is composed of an underlying chorioretinal vascular abnormality, PDT has been sought as a new therapy for this poorly treated disorder. In the year 2000, the United States Food and Drug Administration (FDA) approved PDT for treatment of subfoveal CNV with specific features in AMD. Photodynamic therapy was evaluated to treat CNV in myopia and ocular histoplasmosis syndrome and was subsequently approved for these indications.[8] The Treatment of Age-Related Macular Degeneration with Photodynamic Therapy (TAP) Study Group demonstrated the beneficial effect of PDT compared to placebo for treatment of predominantly classic CNV in AMD.[3] Photodynamic therapy as treatment of other vascular disorders and ocular tumors has been evaluated in small reported series.

Optical Coherence Tomography Imaging of the Retinal Response to Photodynamic Therapy

Most major studies of AMD have evaluated the efficacy of PDT with FA. However, OCT contributes additional information to the evaluation of CNV after PDT treatment. Optical coherence tomography is useful to assess intraretinal and subretinal fluid and fibrosis and to distinguish neurosensory detachments and pigment epithelial detachments (Fig. 14.4).[9] These qualities make OCT useful in structurally monitoring exudative AMD before and after PDT treatment.

The OCT findings were correlated with the fluorescein angiographic findings after PDT treatment of 79 total eyes in

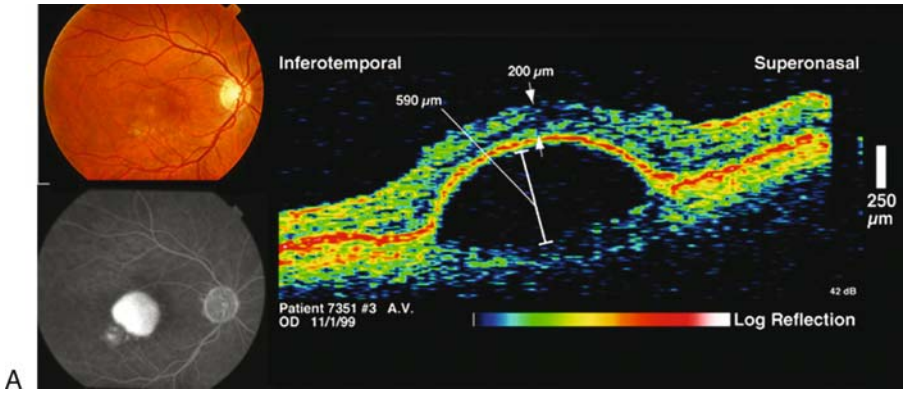

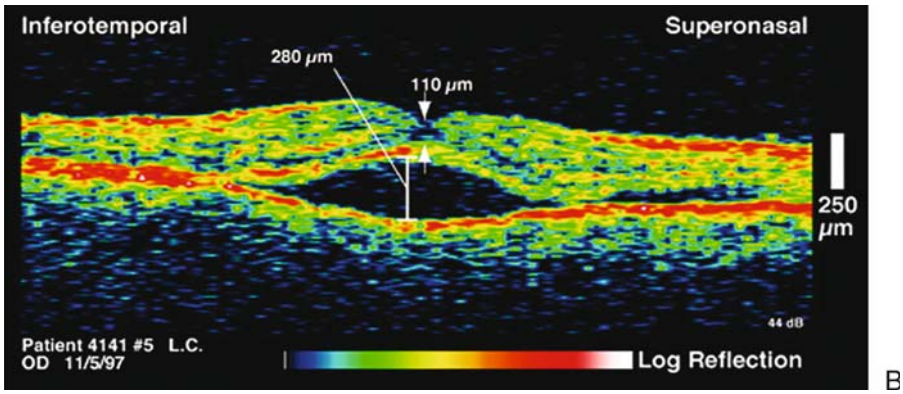

FIG. 14.4. (A) A serous elevation of the RPE in age-related macular degeneration evident on clinical examination and fluorescein angiography. Optical coherence tomography demonstrates a dome-shaped optically empty zone beneath the RPE. (B) Serous elevation of the RPE centrally at the fovea in central serous chorioretinopathy. There is subretinal fluid with a small neurosensory detachment noted with OCT in the superonasal retina.

TABLE 14.1. Optical coherence tomography classification of choroidal neovascularization (CNV) and changes after photodynamic therapy (PDT)[10]

Stage	Features
Stage 1: acute inflammatory response	Acute macular thickening corresponds to PDT treatment spot • Noted as early as 1 hour after PDT • Resolves spontaneously by 1 week
Stage 2: resolution of subretinal fluid with reduced CNV perfusion	Resolution of subretinal fluid at 1 to 2 weeks after PDT • Return of foveal contour toward normal • May correlate with subjective visual improvement
Stage 3: reaccumulation of subretinal fluid with subretinal fibrosis	Stage 3a: fluid component is more prominent than the fibrotic component • May correspond to actively leaking CNV • Often requires PDT re-treatment Stage 3b: fibrotic component is more prominent than the fluid component • May represent less active lesions • Typically occurs after re-treatment or with chronic primary lesions • These lesions may not benefit from re-treatment
Stage 4: increasing subretinal fibrosis with cystoid macular edema	The lesion does not appear active Regressing CNV is replaced by subretinal fibrosis • The "leakage" within the lesion may represent cystoid macular edema overlying dysfunctional RPE
Stage 5: subretinal fibrosis with retinal atrophy	Organization of subretinal fibrosis with resolution of subretinal fluid • Subnormal central macular thickness • Overall visual benefit of PDT may correlate with limitation of the size of this lesion

a study by Rogers and colleagues.[10] Eyes with subfoveal CNV that were predominately classic (equal to or greater than 50% classic CNV of the total CNV lesion) were treated according to the TAP study protocol.[3] These eyes were evaluated with FA and OCT prior to PDT and on subsequent examinations at various time intervals after PDT. The follow-up regimen was not standardized, given the retrospective nature of the study, and this also varied based on the practice of the treating physician. Photodynamic therapy re-treatment was performed if there was evidence of recurrent leakage from CNV on FA as per the TAP protocol. The results of the OCT and FA imaging were correlated with the clinical findings after PDT, and the authors developed a five stage classification to characterize the OCT findings (Table 14.1).

Stage 1: Acute Inflammatory Response (Fig. 14.5)

Stage 1 describes the OCT and clinical findings that may be noted acutely after PDT. These changes can occur as early as 1 hour after PDT and last up to 1 week after treatment. The fluorescein angiogram may show increased hyperfluorescence of CNV with late leakage from the entire PDT treatment area. Optical coherence tomography demonstrates increased intraretinal thickening in the treated CNV area corresponding to intraretinal fluid. These findings appear to correspond to an acute inflammatory response occurring immediately after PDT. Stage 1 changes typically resolve spontaneously by 1 week.[11] The development of this acute inflammatory response may explain the transient visual loss that is experienced shortly after PDT in some patients and resolves spontaneously within 1 week.

Stage 2: Resolution of Subretinal Fluid (Fig. 14.6)

Resolution of subretinal fluid typically occurs 1 to 2 weeks after PDT. Fluorescein and ICG angiography show an area of hypofluorescence corresponding to the PDT treatment spot. With resolution of subretinal fluid, there is reestablishment of a more normal foveal contour that can be seen on OCT. The OCT measurements of central foveal thickness may become more normal than pre-PDT values, and return of the foveal depression may occur. This stage appears to correspond with the time of greatest visual benefit and lasts for approximately 4 weeks.

Stage 3: Reaccumulation of Subretinal Fluid with Fibrosis (Figs. 14.7 and 14.8)

Starting as early as 4 weeks following PDT, although this interval is variable, reperfusion of the CNV may start to appear as the PDT-induced vascular occlusion effect is typically not permanent. Intraretinal or subretinal fluid may slowly reaccumulate, and subretinal fibrosis can start to form. Variable degrees of leakage and staining are present on fluorescein

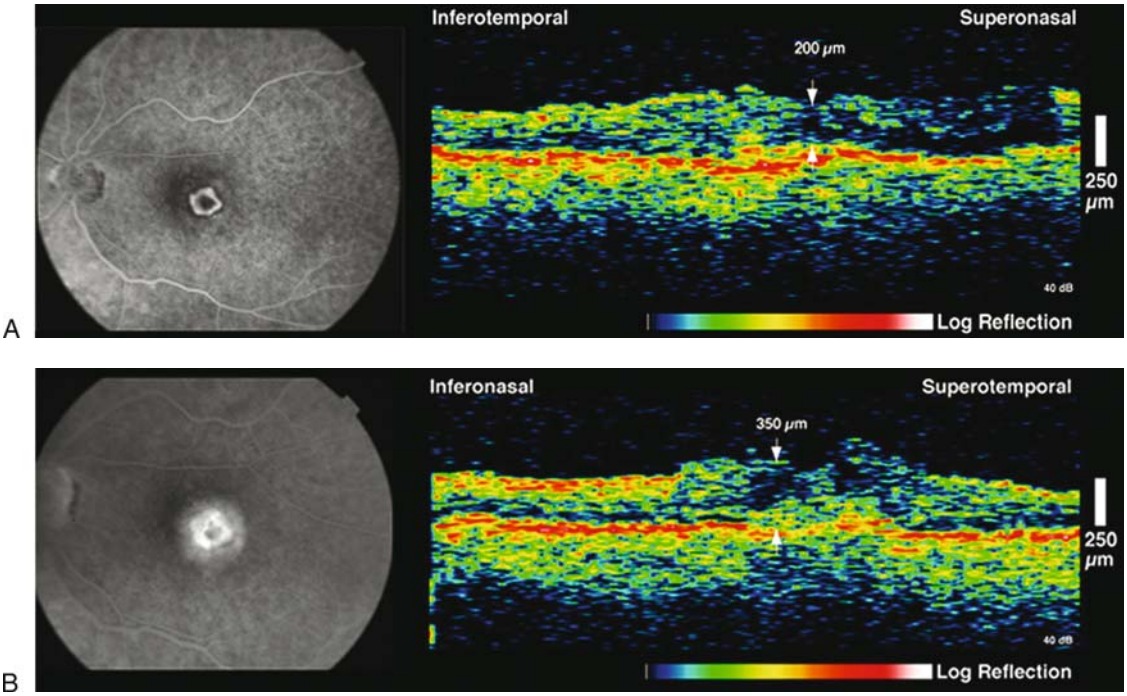

FIG. 14.5. (A) Optical coherence tomography and fluorescein angiography (FA) show classic subfoveal CNV prior to photodynamic therapy (PDT). (B) Stage 1 findings are noted on OCT at 1 hour acutely after PDT. The OCT demonstrates increased intraretinal thickening and intraretinal fluid in the PDT-treated area. The central foveal thickness has increased to 350 μm from 200 μm in pre-PDT (A).

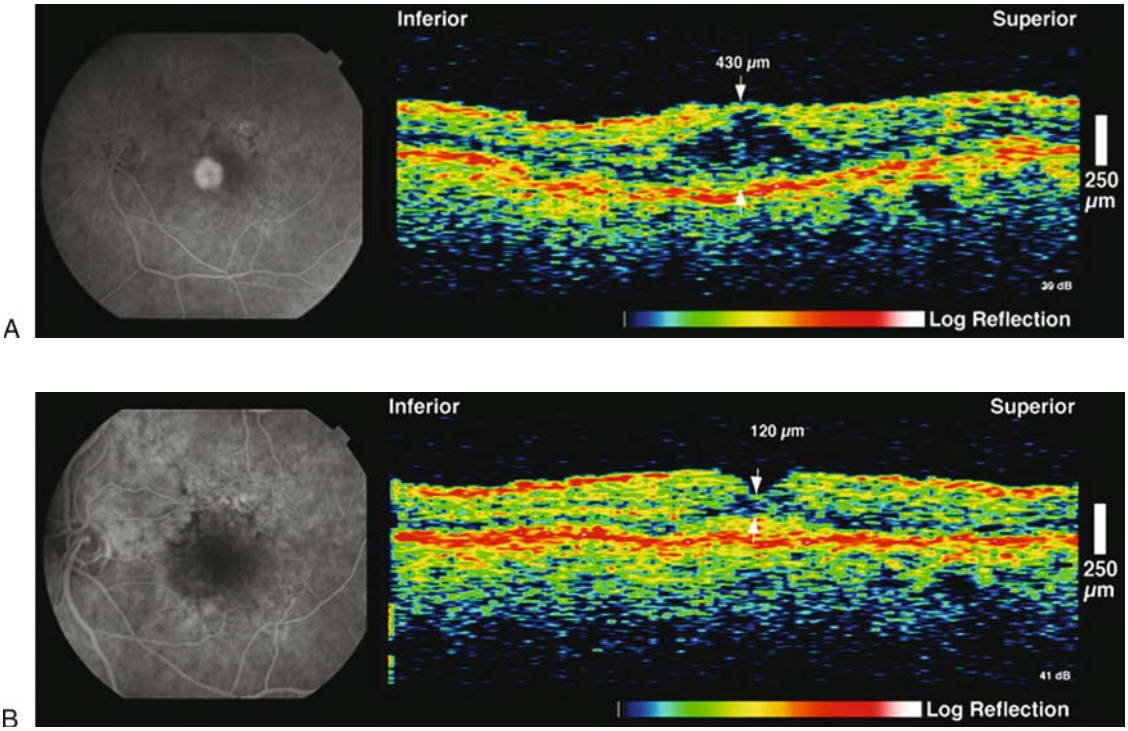

FIG. 14.6. (A) Fluorescein angiogram show 100% classic subfoveal CNV prior to PDT. Optical coherence tomography is consistent with CNV accompanied by intraretinal and subretinal fluid. (B) Stage 2 lesion on OCT is noted at 2 weeks after PDT. There is resolution of the intraretinal fluid and the foveal contour has returned to normal, measuring 120 μm compared to 430 μm before PDT.

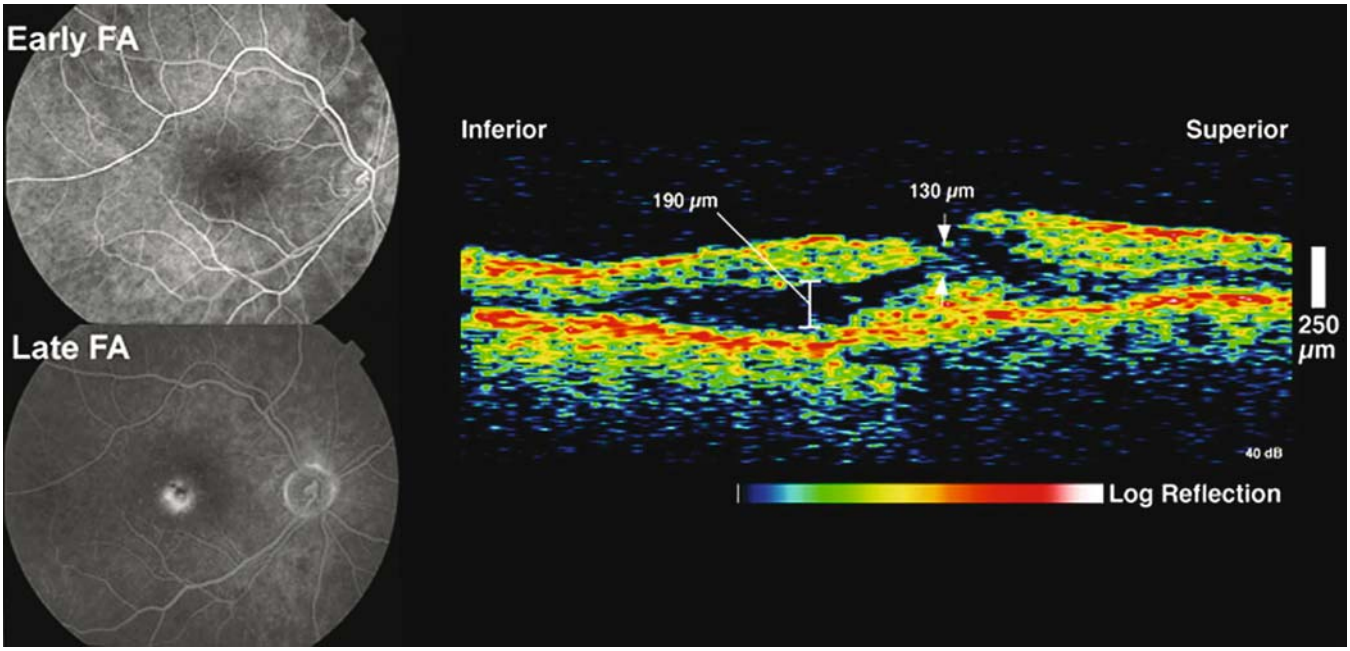

FIG. 14.7. Stage 3a lesion noted on OCT with accumulation of intraretinal and subretinal fluid. The fluid component is more marked than the fibrotic component, and repeat PDT may be indicated in this lesion.

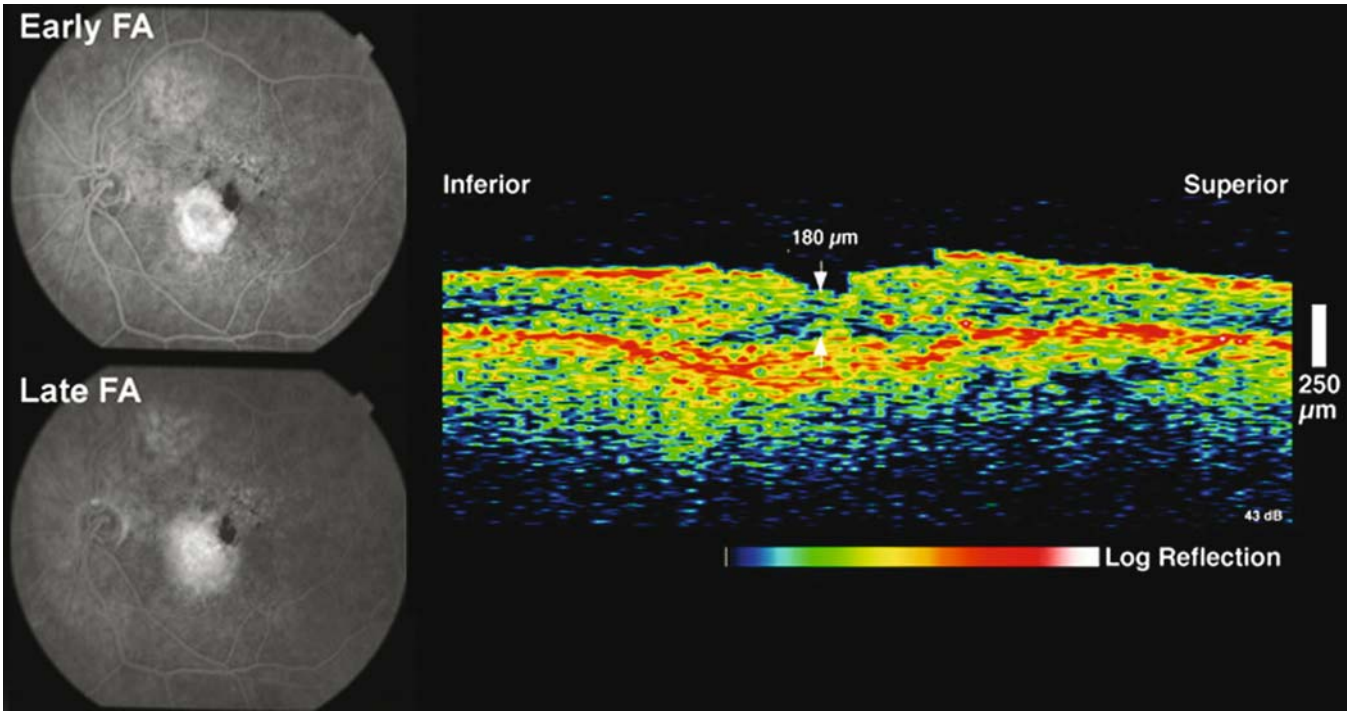

FIG. 14.8. Stage 3b lesion in which the fibrotic component is dominant and well visualized by OCT examination at 2 months after PDT.

angiogram, corresponding to areas of recurrent intraretinal or subretinal fluid leakage and fibrosis respectively. The PDT treatment spot is no longer visible on fluorescein angiography as the choriocapillaris reperfuses. Early subretinal fibrosis is depicted on OCT as a band of increased signal reflectivity between the retina and RPE. On OCT, subretinal fluid accumulation is noted as hyporeflective areas below the neurosensory retina and is apparent as an increase in the measurement of total retinal thickness,

Stage 3 lesions have been identified by OCT on average 2 to 3 months after PDT (range, 1 to 7 months) and are subdivided into two different categories depending on the ratio of fluid to fibrosis noted with OCT. Stage 3a lesions demonstrate a higher proportion of intraretinal or subretinal fluid than the fibrotic component (Fig. 14.7). This is hypothesized to signify recurrent active leakage from CNV. The fluorescein angiogram often shows recurrent CNV leakage and it was noted that these lesions typically require PDT re-treatment at the 3 months assessment. The TAP study showed that an average of three PDT treatments were needed at 1 year and five PDT treatments were typically performed by 2 years after starting therapy.[3] Stage 3b lesions have a more significant fibrotic component compared to the fluid component (Fig. 14.8). This stage occurs more often after PDT re-treatments or with more chronic appearing primary CNV lesions. Stage 3b appears to represent CNV lesions that are less active and starting to develop fibrous tissue. In contrast to stage 3a, the OCT demonstrates minimal intraretinal and subretinal fluid while there is a prominent fibrotic component to the CNV lesion. Fluorescein angiography shows more apparent late staining of the lesion than leakage. Retreatment of stage 3b lesions with PDT appears to promote progression to stage 5; therefore, these stage 3b lesions appear to benefit less from PDT re-treatment compared to stage 3a. Stage 3b lesions tend to progress to stage 4 and stage 5 or remain as stage 3b. They may reactivate to stage 3a lesions and therefore should be examined at regular intervals.

Stage 4: Increasing Fibrosis with Persistent Fluid (Fig. 14.9)

As active CNV regresses, it is replaced by subretinal fibrosis. The lesion is essentially inactive and the borders remain essentially fixed with a large staining component on fluorescein angiography. A component of cystoid macular edema within the lesion may be present overlying the dysfunctional RPE. The cysts are more clearly defined on OCT as hyporeflective black circular spaces within the retina, separated by reflective septa. The involuting CNV appears as a highly reflective band that merges with the RPE/choriocapillaris layer. Stage 4 occurred an average of 5 months following treatment in the study by Rogers and colleagues.[10]

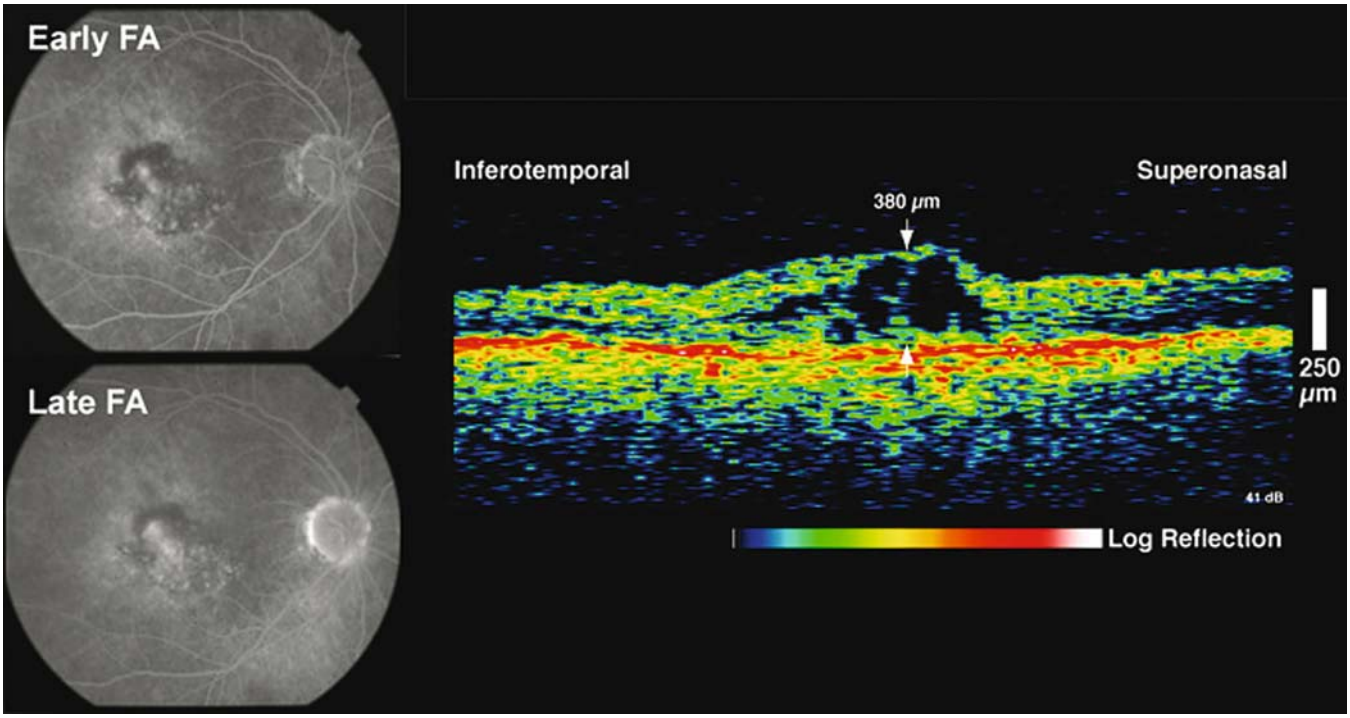

FIG. 14.9. Stage 4 lesion demonstrates cystoid macular edema prominently on OCT. A component of staining of the lesion is noted on fluorescein angiography.

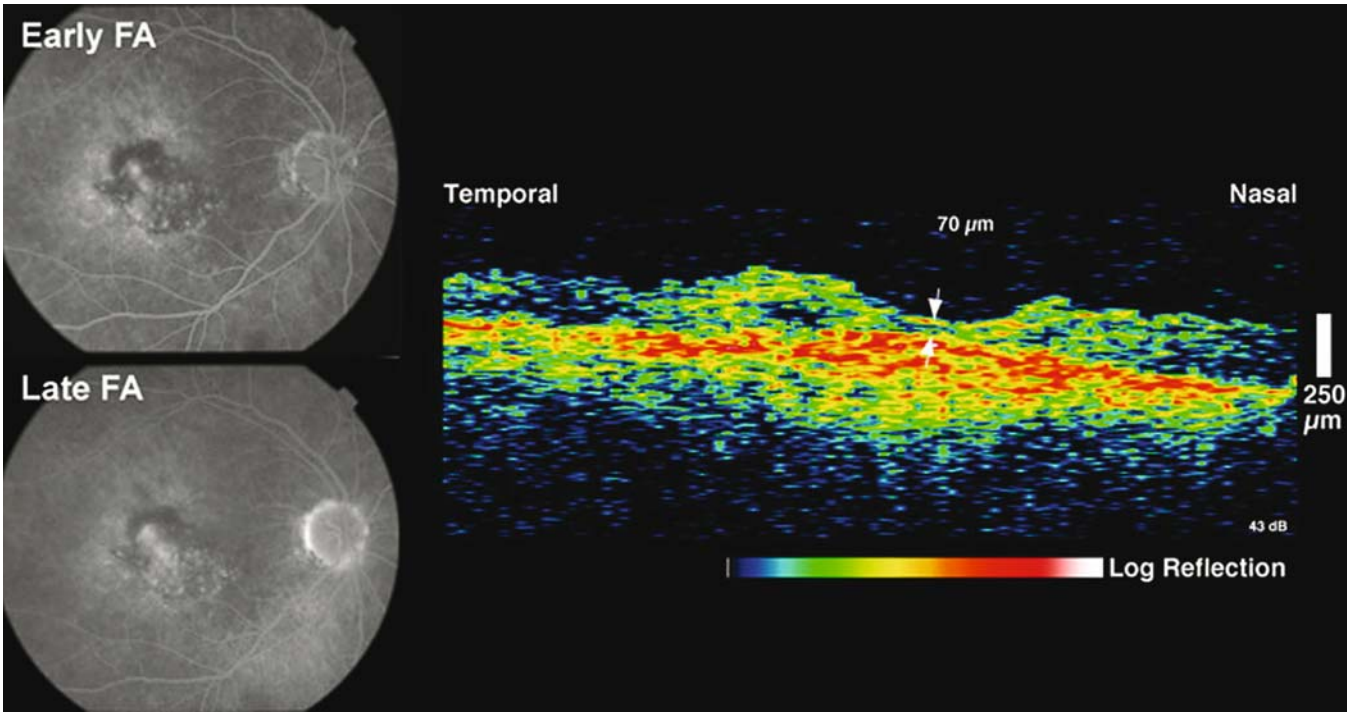

FIG. 14.10. Stage 5 lesion develops 3 months after the stage 4 lesion in Figure 14.9. The predominant finding on OCT as well as fluorescein angiography is subretinal fibrosis. Foveal thickness is subnormal at 70 μm.

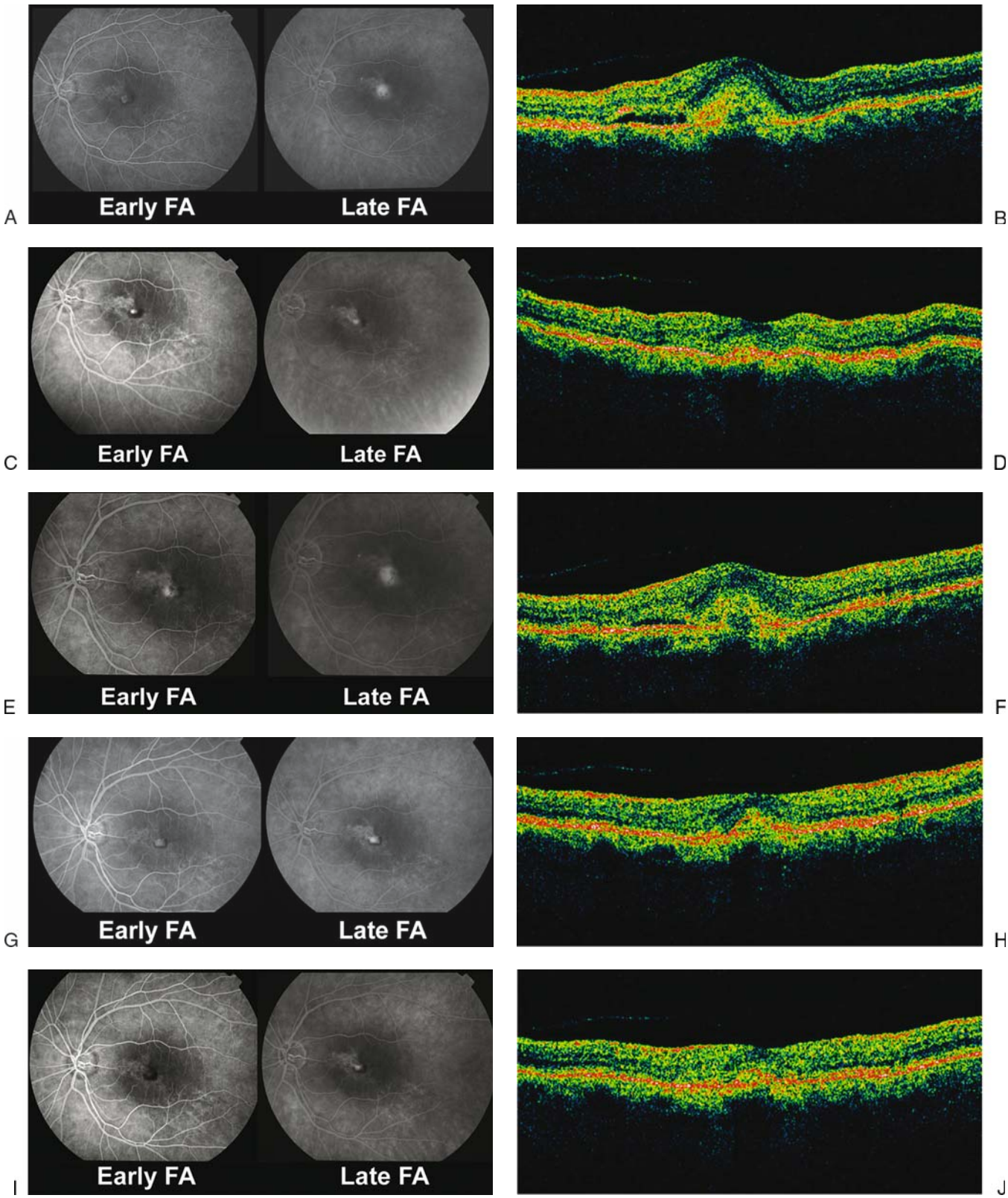

FIG. 14.11. (A) Predominantly classic subfoveal CNV is noted on fluorescein angiography. Vision measures 20/200. (B) Optical coherence tomography shows a discoid-shaped subretinal area consistent with classic subfoveal CNV. Photodynamic therapy was performed with a 1700-μm spot as per the Treatment of Age-Related Macular Degeneration with Photodynamic Therapy (TAP) protocol. (C) Five weeks after PDT, vision improved to 20/70 and symptoms of metamorphopsia had improved. The fluorescein angiogram shows decreased size of the CNV. (D) Five weeks after PDT, the corresponding OCT shows resolution of the subretinal fluid. The vision improved to 20/70. (E) Three months after the initial PDT, fluorescein angiogram shows increased leakage from CNV. Vision was 20/50. (F) Three months after the initial PDT, OCT shows recurrent CNV with intraretinal and subretinal fluid, indicating active CNV leakage. This is consistent with a stage 3a lesion.

Stage 5: Subretinal Fibrosis with Retinal Atrophy (Fig. 14.10)

As the remaining subretinal fluid resolves, there is organization of residual subretinal fibrosis leading to subnormal central foveal thickness. Optical coherence tomography demonstrates an elevated reflective mound at the site of fibrotic CNV. It has been hypothesized that the visual benefit from PDT may correlate with limitation in the size of this subretinal fibrotic lesion compared with the natural history of untreated classic CNV in AMD.

The OCT findings may play a role in predicting the visual and anatomic results after the initial PDT session. These findings may also be useful to determine the optimal candidates for PDT re-treatment and the optimal timing for re-treatment. Lesions with intraretinal or subretinal fluid associated with the initial or recurrent CNV appear to be the best candidates for further PDT re-treatment. Eyes with the predominant finding of subretinal fibrosis or cystic macular edema as imaged by OCT do not appear to show much benefit from repeated PDT. Further evaluation of these early hypotheses by controlled studies would be useful to identify the optimal candidates to benefit visually from PDT treatments. Figure 14.11 shows the ability of OCT to follow a patient chronically during the course of PDT and demonstrates its role in determining the utility of PDT re-treatment.

Optical Coherence Tomography Evaluation of Photodynamic Therapy for Non–Age-Related Macular Degeneration Causes of Choroidal Neovascularization

Since publication of the TAP studies, a variety of retinal disorders other than AMD have been treated by PDT. Optical coherence tomography has been a useful adjunct to further characterize the response of these conditions to PDT and to describe some of the PDT-related complications.

Optical coherence tomography was used to image the newly reported finding of partial detachment and folding of subfoveal CNV in AMD following PDT.[12] This entity developed in 1 of approximately 300 (0.5%) AMD patients treated with PDT and occurred 6 weeks after the second PDT treatment for a classic CNV. The CNV was large and located between the retina and the RPE. The detached nasal portion of the CNV folded over the underlying attached temporal portion of the CNV. Optical coherence tomography helped in distinguishing this folded CNV from an RPE tear. Optical coherence tomography demonstrated differences in the reflectivity and in the thickness of the layers of tissue as being distinct from an RPE tear. The visual acuity of this patient improved after the CNV detachment, suggesting that this is not an adverse outcome. The authors hypothesized that this phenomenon may be explained by the low energy and selectivity of PDT, and they described a similar case occurring in an eye after transpupillary thermotherapy (TTT).

In a report describing retinal hemorrhages after PDT for subfoveal CNV in AMD, OCT was useful in identifying the location of the hemorrhage and in following the clinical course.[13] Optical coherence tomography was able to demonstrate whether the hemorrhage was located intraretinally or subretinally, as well as identify the presence of subretinal fluid.

Recent studies have utilized information from OCT studies to further characterize and quantify outcome measures. For example, a recent study evaluating PDT combined with intravitreal triamcinolone acetonide for treatment of CNV used OCT imaging to further investigate patients who lacked fluorescein leakage on their follow-up.[14] Optical coherence tomography was used to assess for small amounts of subretinal or macular fluid consistent with subtle leakage that may not be detected with FA.

Imaging with OCT has been included in the study protocol of some phase 3 trials, for example the intravitreal fluocinolone implant and the anti—vascular endothelial growth factor (VEGF) intraocular injection studies.[15] The central retinal thickness and retinal volume response to anti-VEGF treatment have been evaluated with OCT (see Chapter 15).[16]

Optical Coherence Tomography Evaluation of Photodynamic Therapy for Non–Choroidal Neovascularization Disorders

Optical coherence tomography was used to evaluate the effect of PDT for treatment of chronic central serous chorioretinopathy.[17] This study found OCT particularly useful in establishing the presence of a macular detachment and to follow the course after PDT treatment. Optical coherence tomography was helpful in identifying the presence of cystoid macular edema and retinal atrophy, which may play a role in determining visual prognosis and anatomic outcome.

FIG. 14.11. (continued) A PDT re-treatment was performed at this time. (G) Two-and-a-half months after the second PDT, fluorescein angiogram shows staining of the CNV area that was treated twice with PDT. Acuity was 20/40. (H) Two-and-a-half months after the second PDT, OCT shows resolution of the intraretinal fluid. Observation was recommended. (I) Four-and-a-half months after the second PDT, there is staining of the lesion. Acuity was 20/30. (J) Four-and-a-half months after the second PDT, OCT shows subretinal fibrosis consistent with a stage 3B lesion. There is no fluid identified by OCT imaging. Continued observation was recommended at this time.

Future Horizons

The diagnostic and treatment modalities for AMD have undergone some advances within the past decade. Diagnostically, OCT has provided micrometer-resolution cross-sectional retinal images. Therapeutically, PDT with verteporfin (Visudyne; Novartis Ophthalmics, Duluth, GA) has been demonstrated as effective to treat certain forms of subfoveal CNV.

Most studies to date have used more conventional imaging techniques such as FA and ICG angiography to evaluate the treatment efficacy of PDT. Optical coherence tomography can offer valuable information in describing the changes occurring in the retina and choroid following the treatment of subfoveal CNV with PDT. New therapies are continually being investigated to uncover more effective therapies for AMD and other retinal diseases. The development of ultrahigh resolution OCT imaging offers unique insight into the pathophysiology of retinal disease and into the evaluation of new therapies on a micrometer imaging level.

Acknowledgments. Figures 14.5 through 14.11 were compiled and graciously provided by Adam Rogers, MD, New England Eye Center, Tufts University School of Medicine, Boston, Massachusetts.

References

1. Puliafito CA, Hee MR, Lin, CP, et al. Imaging of macular diseases with optical coherence tomography. Ophthalmology 1995;102:217–229.
2. Drexler W, Sattmann H, Hermann B, et al. Enhanced visualization of macular pathology with the use of ultrahigh-resolution optical coherence tomography. Arch Ophthalmol 2003;121:695–706.
3. Treatment of Age-related Macular Degeneration with Photodynamic Therapy (TAP) Study Group. Photodynamic therapy of subfoveal choroidal neovascularization in age-related macular degeneration with verteporfin: two-year results of 2 randomized clinical trials—TAP report 2. Arch Ophthalmol 1999;117:1329–1345.
4. Bird AC, Bressler NM, Bressler SB, et al. An international classification and grading system for age-related maculopathy and age-related macular degeneration. The international ARM epidemiological study group. Surv Ophthalmol 1995;39:367–374.
5. Persistent and recurrent neovascularization after laser photocoagulation for subfoveal choroidal neovascularization of age-related macular degeneration. Macular photocoagulation study group. Arch Ophthalmol 1994;112:489–499.
6. Visual outcome after laser photocoagulation for subfoveal choroidal neovascularization secondary to age-related macular degeneration. The influence of initial lesion size and initial visual acuity. Macular photocoagulation study group. Arch Ophthalmol 1994;112:480–488.
7. Laser photocoagulation of subfoveal neovascular lesions of age-related macular degeneration. Updated findings from two clinical trials. Macular photocoagulation study group. Arch Ophthalmol 1993;111:1200–1209.
8. Verteporfin in photodynamic therapy (VIP) study group. Verteporfin therapy of subfoveal choroidal neovascularization in pathologic myopia. Ophthalmology 2003;110:667–673.
9. Hee MR, Baumal CR, Puliafito CA, et al. Optical coherence tomography of age-related macular degeneration and choroidal neovascularization. Ophthalmology 1996;103:1260–1270.
10. Rogers AH, Martidis A, Greenberg PB, Puliafito CA. Optical coherence tomography findings following photodynamic therapy of choroidal neovascularization. Am J Ophthalmol 2002;134:566–576.
11. Costa RA, Farah ME, Cardillo JA, et al. Immediate indocyanine green angiography and optical coherence tomography evaluation after photodynamic therapy for subfoveal choroidal neovascularization. Retina 2003;23:159–165.
12. Rumelt S, Kaiserman I, Rehany U, et al. Detachment of subfoveal choroidal neovascularization in age-related macular degeneration. Am J Ophthalmol 2002;134:822–827.
13. Theodossiadis GP, Panagiotidis D, Georgalas IG, et al. Retinal hemorrhage after photodynamic therapy in patients with subfoveal choroidal neovascularization caused by age-related macular degeneration. Graefes Arch Clin Exp Ophthalmol 2003;241:13–18.
14. Spaide RF, Sorenson J, Maranan L. Combined photodynamic therapy with verteporfin and intravitreal triamcinolone acetonide for choroidal neovascularization. Ophthalmology 2003;110:1517–1525.
15. Rosenfeld PJ, Heier JS, Chung CY, McCluskey ER. RhuFab V2 Dose-escalation trial: safety and tolerability of 3 escalating dosing regimens in subjects with age-related macular degeneration. Abstract. New York: American Society of Retina Specialists, August 2003.
16. Antoszyk AN, Sy JP, McCluskey ER, rhuFabV2 Study Group. RhuFab V2 in wet AMD: changes in OCT measures of the ocular edema. Abstract. New York: American Society of Retina Specialist, August 2003.
17. Yannuzzi LA, Slakter JS, Gross NE, et al. Indocyanine green angiography-guided photodynamic therapy for treatment of chronic serous chorioretinopathy: a pilot study. Retina 2003;23:288–298.

15
The Role of Optical Coherence Tomography in Anti–Vascular Endothelial Growth Factor Therapies

Anne Fung, Nikolas London, and Philip Rosenfeld

Anti–Vascular Endothelial Growth Factor Therapies

Vascular endothelial growth factor (VEGF) has emerged as a key mediator of angiogenesis and macular edema in ocular diseases such as neovascular macular degeneration, vein occlusions, and diabetic retinopathy.[1,2] Therapies to neutralize VEGFs action in ocular diseases have been used to successfully combat VEGFs pathogenic role in the eye.

Ophthalmology entered a new era of treatment for neovascular and exudative retinal diseases in December 2004 with the Food and Drug Administration (FDA) approval of pegaptanib (Macugen OSI/Eyetech Inc., Melville, NY) for neovascular age-related macular degeneration (AMD).[3] Pegaptanib, an RNA aptamer that neutralizes VEGF isoforms of at least 165 amino acids, is administered as an intravitreal injection and shown to slow vision loss in neovascular AMD patients. Preliminary work has also been completed on the efficacy of pegaptanib therapy in diabetic macular edema.[4–6]

Another approach to anti-VEGF therapy is ranibizumab (Lucentis, Genentech Inc., South San Francisco, CA), a recombinant humanized antigen-binding antibody fragment that neutralizes all biologically active forms of VEGF, both the isoforms and the proteolytic products. Preclinical trials of ranibizumab were initiated in 2001, and early impressions of the molecule were favorable. The FDA approved ranibizumab for treatment of neovascular AMD in June 2006, and it became the first FDA-approved AMD therapy to maintain or improve vision in ≥90% patients with the potential to improve vision ≥15 letters in approximately one third of patients over 2 years.[7,8]

During the phase III clinical trials of ranibizumab, the clinical benefit of pan-VEGF blockade for neovascular AMD became increasingly clear. A trial was initiated in early 2004 to evaluate the off-label use of an intravenous systemic therapy for patients with bilateral advanced neovascular AMD using a full-length pan-VEGF antibody known as bevacizumab (Avastin, Genentech, Inc).[9,10] Enthusiasm for intravenous bevacizumab as a treatment for AMD was tempered in August 2004 when a warning letter described an increased risk of thromboembolic events in cancer patients undergoing chronic therapy every 2 weeks. Although no thromboembolic events were observed in 18 patients given two or three infusions of bevacizumab over 6 months, the theoretical safety concern limited the off-label systemic use of Avastin.

In May 2005, the intravitreal off-label use of bevacizumab was initiated. Injections of bevacizumab were administered safely with visual acuity benefits for neovascular AMD and macular edema secondary to central retinal vein occlusion.[11,12] Since the use of intravitreal bevacizumab injections was introduced in mid-2005, many additional papers have been published describing the lack of in vitro and in vivo toxicity with intravitreal bevacizumab,[13–16] as well as the clinical safety and efficacy of intravitreal bevacizumab in several ocular diseases,[17–28] and its safety as assessed by an on-line safety survey using the World Wide Web.[29]

Pegaptanib, ranibizumab, and bevacizumab are the three anti-VEGF therapies now available for the treatment of neovascular and exudative diseases of the retina. Optical coherence tomography (OCT) technology matured in parallel during these anti-VEGF therapies and has proven to be uniquely well suited for determining the response to treatment and the need for re-treatment with anti-VEGF therapy. Optical coherence tomography also permits direct visualization and quantification of retinal edema, as well as visualization of other structural pathologic alterations that may or may not be apparent by other imaging techniques such as fluorescein angiography (FA) or indocyanine green (ICG) angiography.

Optical Coherence Tomography in Antiangiogenic Therapy for Wet Age-Related Macular Degeneration

In 1996, Hee et al.[30] published the first paper describing the use of OCT in AMD, stating that OCT was "useful in quantitatively evaluating subretinal and intraretinal fluid, assessing

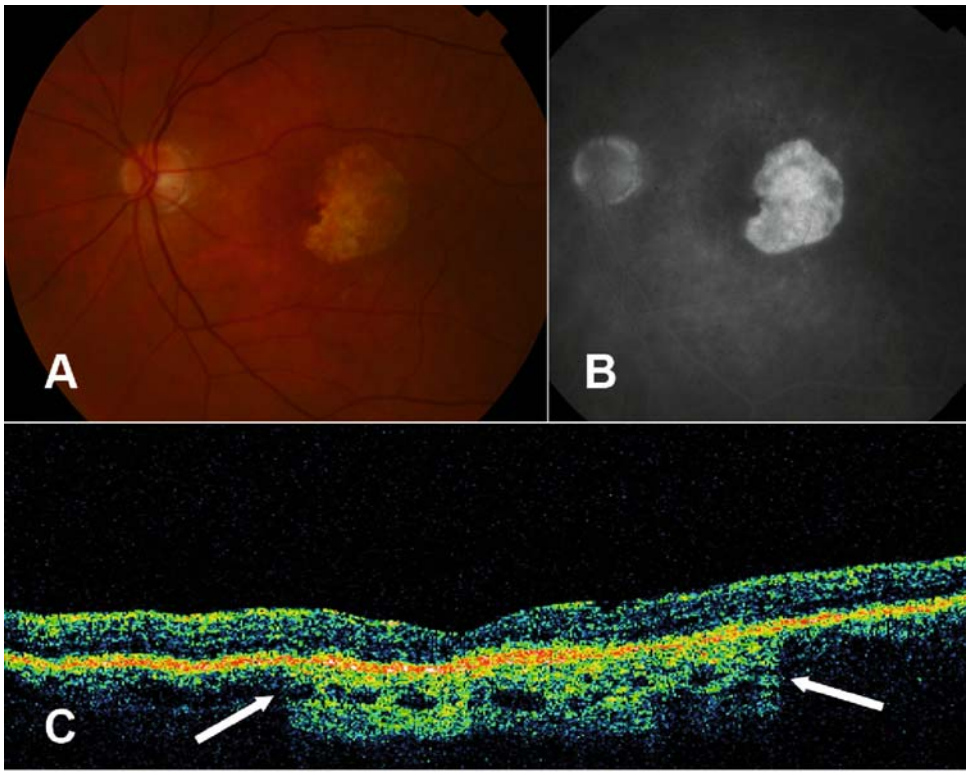

FIG. 15.1. Geographic atrophy on color photograph (A), as a window defect in late-phase fluorescein angiography (B), and on optical coherence tomography (OCT) (C). Central area of OCT shows increased transmission defect (arrows) where OCT scanning beam has penetrated the atrophic retinal pigment epithelium (RPE) to reveal a choroidal shadowing pattern.

possible subfoveal involvement of neovascularization, and in monitoring CNV before and after laser photocoagulation" and that "OCT may have potential in accurately defining the boundaries in a subset of angiographically occult CNV." Since then, OCT imaging for the retina has matured through multiple software versions and has entered the mainstream of AMD management, including photodynamic therapy (PDT) and anti-VEGF treatments.[31–35]

Optical coherence tomography has gained utility in both nonexudative and exudative AMD. In nonexudative AMD, OCT can identify diffuse retinal atrophy, or geographic atrophy of the retinal pigment epithelium (RPE) by a pattern of increased choroidal reflectivity (Fig. 15.1).[36] In neovascular AMD, OCT plays a more important role and includes both diagnosis and management of the disease. A pilot study of macular OCT as a screening tool for exudative AMD concluded that OCT was very sensitive and acceptably specific for this purpose.[37] Optical coherence tomography data are also increasingly used as main outcome measures of clinical results in studies of therapies for exudative AMD.[9,10,17,19,38]

This chapter further discusses the OCT characteristics of neovascular AMD including a quantitatively thickened central retinal thickness (CRT), and qualitative findings including the cystic appearance of intraretinal fluid, subretinal fluid, retinal pigment epithelial detachments (PEDs), and choroidal neovascularization.[10,39–41]

Optical Coherence Tomography Interpretation

Optical coherence tomography evaluation of the macula provides both qualitative and quantitative information.

Fast Macular Maps and Central Retinal Thickness

Central retinal thickness (CRT) measurements are calculated from a fast macular map scan. The OCT scan setting captures six diagonal lines at 30-degree intervals centered on the fovea (like cuts in a pie). To increase the reliability of the thickness data by minimizing patient movement between scans, these six fast lower-resolution (128 A-scans) scans are taken in rapid succession. Ideally, the lines overlap in the fovea to provide an accurate central 1-mm retinal thickness measurement (Fig. 15.2A, black and white image).

The retinal thickness is calculated by measuring the distance between the inner and outer retinal boundaries. The Stratus OCT-3 has an internal algorithm that determines the CRT by tracing the boundaries of the inner retina (vitreous/retinal interface) and the outer retina (the RPE-Bruch's/photoreceptor junction) and calculating the distance in micrometers between these two boundaries (Fig. 15.2A, color image).

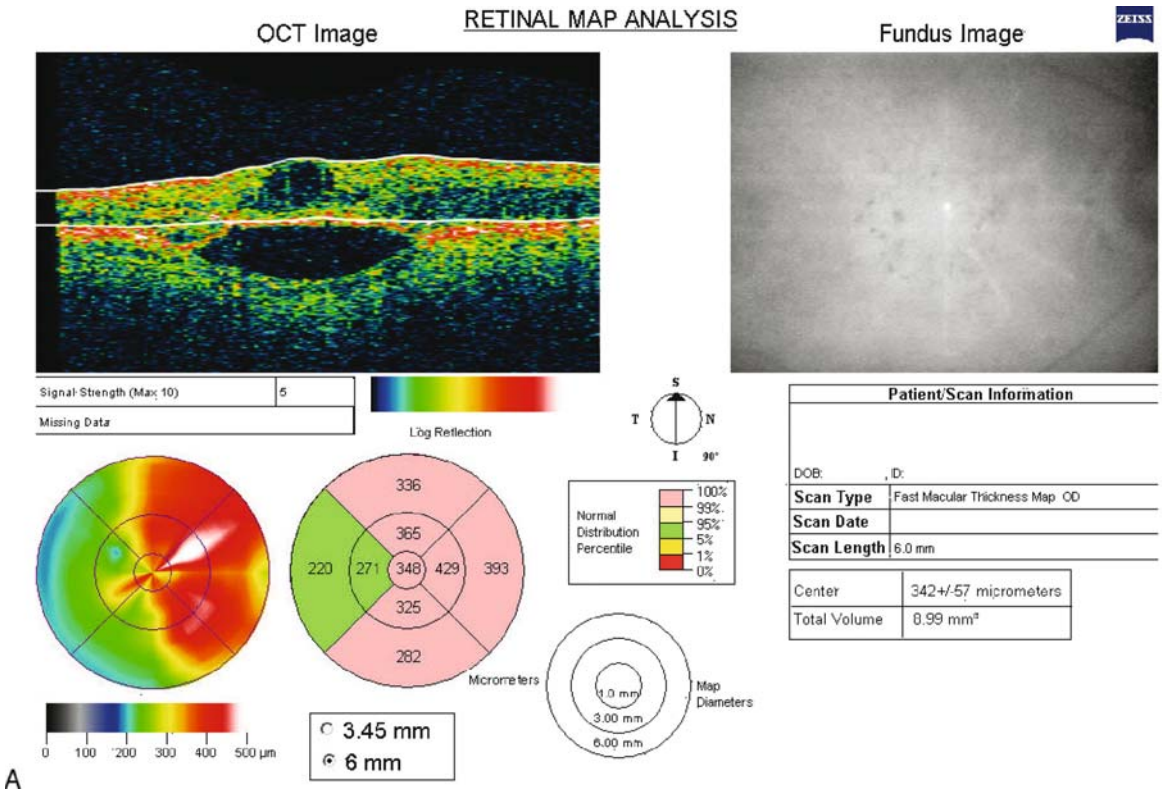

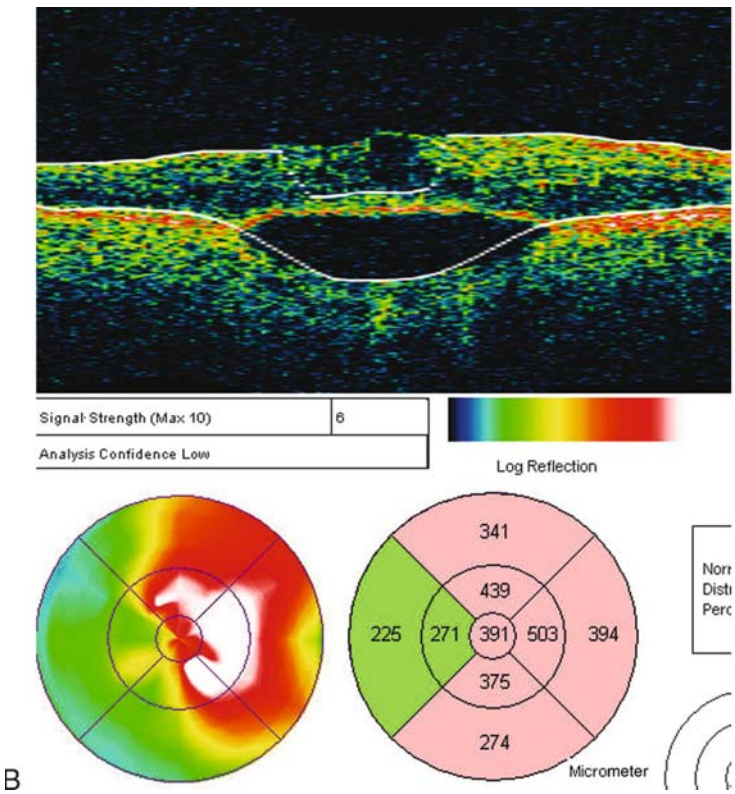

FIG. 15.2. (A) Baseline fast macular thickness map. Top left: The single low-resolution line scan shows the white line tracing the Stratus OCT's algorithm for tracing the internal and external boundaries of the retina. Bottom left: The first circle provides topographic representation of retinal thickening in the central 6-mm macula. The second circle presents macular thickness data: central retinal thickness (CRT) is 348 µm, and the thickness measurements in the outer ring are interpolated from the line scans. Upper right black and white image is the video scan image showing the position of the six line scans used for the fast macular map. (B) White lines not following the retinal boundaries will be inaccurate in CRT measurements. Note that the white line inaccurately traces the inner and outer retinal boundaries: CRT measurement is 391 µm, about 40 µm greater than the accurately traced map.

If the OCT boundary tracings are inaccurate, the algorithm calculation will also be inaccurate (Fig. 15.2B) (see Chapter 21). For this reason, OCT technicians must identify the appropriate demarcation boundaries within the image to ensure that the thickness measurements are accurate. Technicians should repeat the fast macular map until all six scans overlap in the fovea and are correctly traced.

Fast macular scans produce both a quantitative measurement of the CRT and a qualitative colored topographic retinal thickness map. The topographic map is a graphic representation of the numeric data acquired in the six line scans. Centrally, the retinal thickness should be accurate due to the overlapping of the six data points. Points near the perimeter of the map between the line scans are interpolated from available data and not directly measured with the OCT-3. Quantitative data for peripheral macular thickness are also provided from the interpolation, but caution should be used considering the methods. The reliability of the map has been evaluated.[42–44]

Normal 1-mm central retinal thickness is generally between 200 and 240 μm. While most anti-VEGF therapies strive to "dry" the retina and be free of excess thickness as represented by cystic changes and subretinal fluid, the central retinal thickness can be less than 200 μm or thinner than a normal retina. Values of 170 μm or less may represent a pathologically thinned central macula. Analyses of the CRT 1-mm data and the topographic map may explain poor vision following anti-VEGF therapy by revealing retinal atrophy despite apparently "good" macular anatomy with a normal foveal contour free of cystic spaces, subretinal fluid, pigment epithelial detachment (PED), or scarring. Correlations between CRT and visual acuity are variable and are likely influenced by which layers of the retina are atrophic. Future generations of OCT will provide finer detail of the retinal layers, particularly the photoreceptor layer, and allow a better understanding of the relationship among retinal thickness, anatomy, and visual acuity.

Radial Line Scans: Following the Fluid

Optical coherence tomography also provides important qualitative information about the fluid in the macula and its response to anti-VEGF therapy. In radial lines mode, six high-resolution scans are acquired at 30-degree intervals, each diagonal composed of 512 A-scans. The result is a series of six detailed, cross-sectional images of the central 6 mm of the macula, each at a different angle: 90, 60, 30, 0, 330, and 300 degrees. These images provide qualitative anatomic information about the central macula on a nearly histologic level revealing retinal fluid as cystic alterations in the middle and superficial layers of the retina, pockets of subretinal fluid, or fluid under the RPE as an RPE detachment (RPED). These high-resolution slow scans can theoretically be used to calculate retinal thickness within each section, but are generally not used for quantitative data due to the high likelihood of movement artifact between scans.

Injections of ranibizumab and bevacizumab for neovascular AMD produce a pattern of fluid resolution on OCT that has been studied prospectively. During phase I and II trials of ranibizumab for neovascular AMD, qualitative changes on OCT were observed within weeks following initiation of therapy. The Prospective OCT imaging of Neovascular AMD patients Treated with intraOcular ranibizumab (PrONTO) study was subsequently developed and organized to capture the OCTs of neovascular AMD patients treated with ranibizumab on postinjection days 1, 2, 4, 7, 14, and 30 following the first two treatments. Thereafter, OCTs were obtained monthly for 24 months with additional ranibizumab treatments as needed. To obtain the best qualitative information for the PrONTO study, six radial line slow scans were performed at each monthly visit. Quantitative retinal thickness calculations were taken from fast macular maps as mentioned previously. Technical expertise was important to reliably and reproducibly center all six scans on the foveal center so that sequential comparisons between visits were possible.

The PrONTO study found that macular fluid resolved in a predictable pattern following ranibizumab therapy.[45] First, the cystic changes in the retina resolved and made the largest contribution to a dramatic and rapid reduction in CRT. Shrinkage or complete disappearance of cystic fluid spaces was seen usually following one ranibizumab treatment. Pockets of subretinal fluid were the next component to reabsorb, followed by gradual, incremental resolution of the serous PED component (Figs. 15.3 to 15.5). While most PEDs improved over time, they were variable in their response to ranibizumab treatment and some never completely resolved at 1 year with intermittent ranibizumab therapy.

When monitoring patients on ranibizumab and bevacizumab therapies, trends in vision and OCT data from the PrONTO study should prove to be clinically useful. Changes in OCT occurred within the first day following initiation of ranibizumab therapy and steadily improved (decrease in average CRT and sequential qualitative improvements) through the first 3 to 4 months. Average visual acuity also improved within 2 weeks and steadily increased during the first few months. Generally, changes in OCT preceded changes in vision. Similarly, the recurrence of cystic changes on OCT in a previously fluid-free macula was seen before vision deterioration. Monthly observations from the PrONTO study confirmed the suspicion that once fluid appears, more fluid follows and vision eventually worsens (although vision loss may lag a few months). With this information, it makes sense to re-treat with an anti-VEGF agent as soon as fluid first reappears in the macula or just before the fluid is predicted to reappear based on prior observations.

Some patients present clinical challenges when sequential treatments with ranibizumab or bevacizumab do not improve macular anatomy on OCT at monthly intervals. One possibility is that the improvement on OCT is short-lived, and may be obvious 1 week after an injection, but rebounds quickly over the ensuing 3 weeks, so little change is observed if only the monthly scans are compared. If no change is observed even at 1 week after an injection, then the OCT scans should be

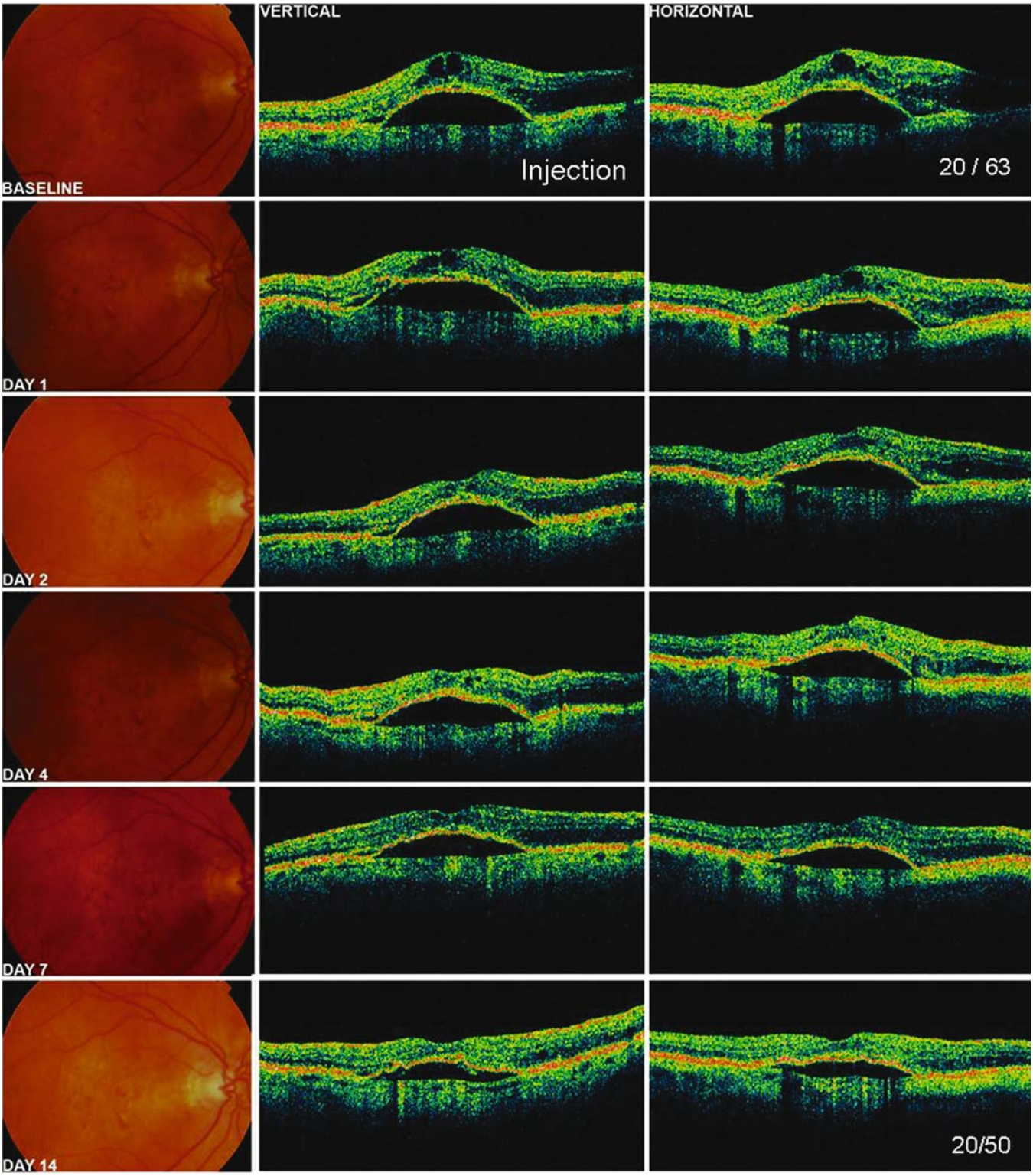

FIG. 15.3. A 90-year-old woman with treatment-naive new diagnosis of neovascular age-related macular degeneration (AMD) involving the fovea of the right eye. Baseline visual acuity is 20/63 (59 letters). Patient receives initial 3-month injections and requires re-treatment according to the PrONTO protocol at months 7 and 12. Optical coherence tomography (OCT) images from baseline through day 14 demonstrate rapid reduction in cystic edema, followed by subretinal fluid and lastly pigment epithelial detachment (PED) after initiation of Lucentis therapy.

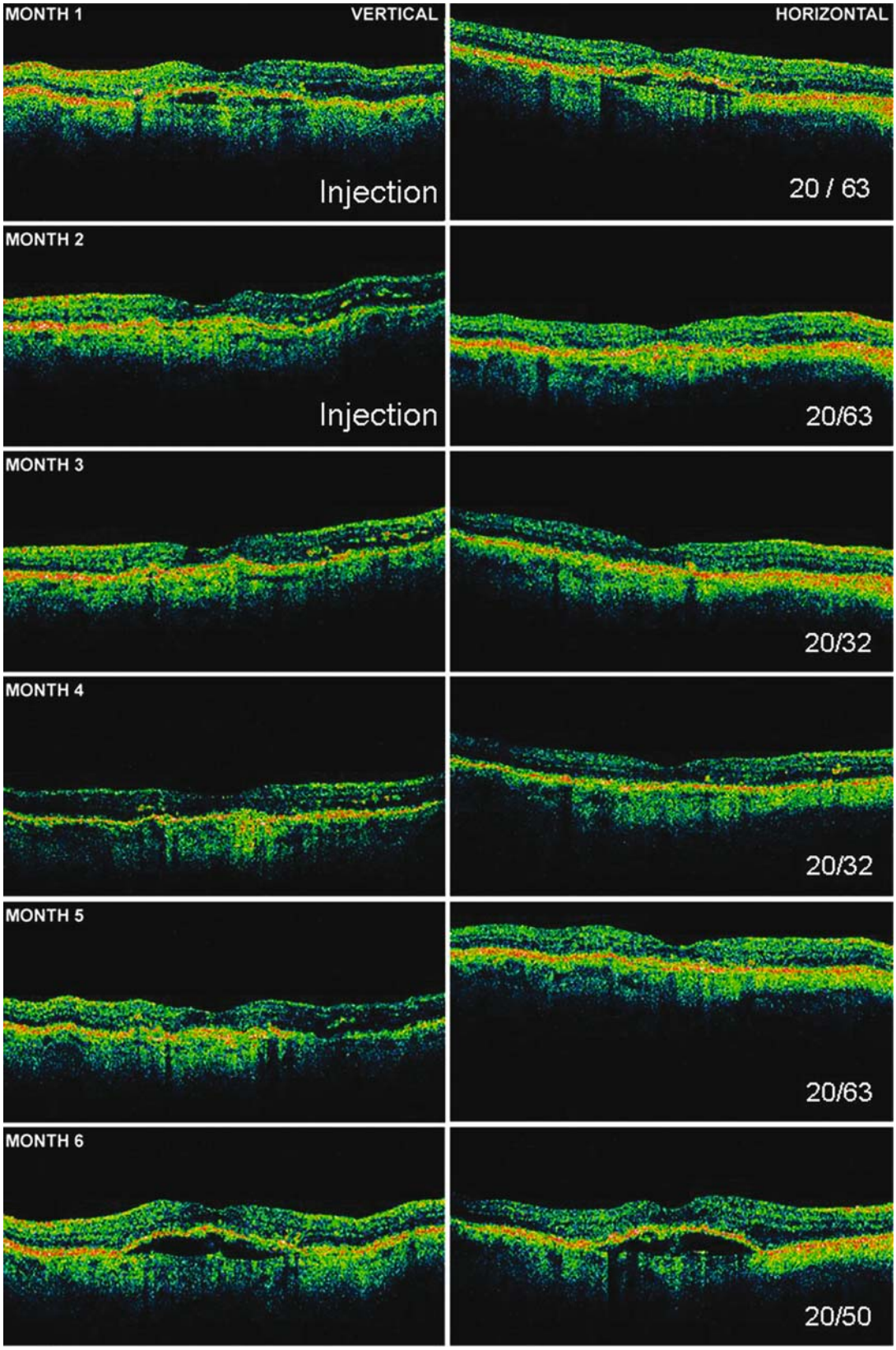

FIG. 15.4. Same patient as in Figure 15.3. Optical coherence tomography composite from months 1 to 6 demonstrates resolution of macular edema through month 3 with consecutive injections and gradual reaccumulation of fluid at month 6.

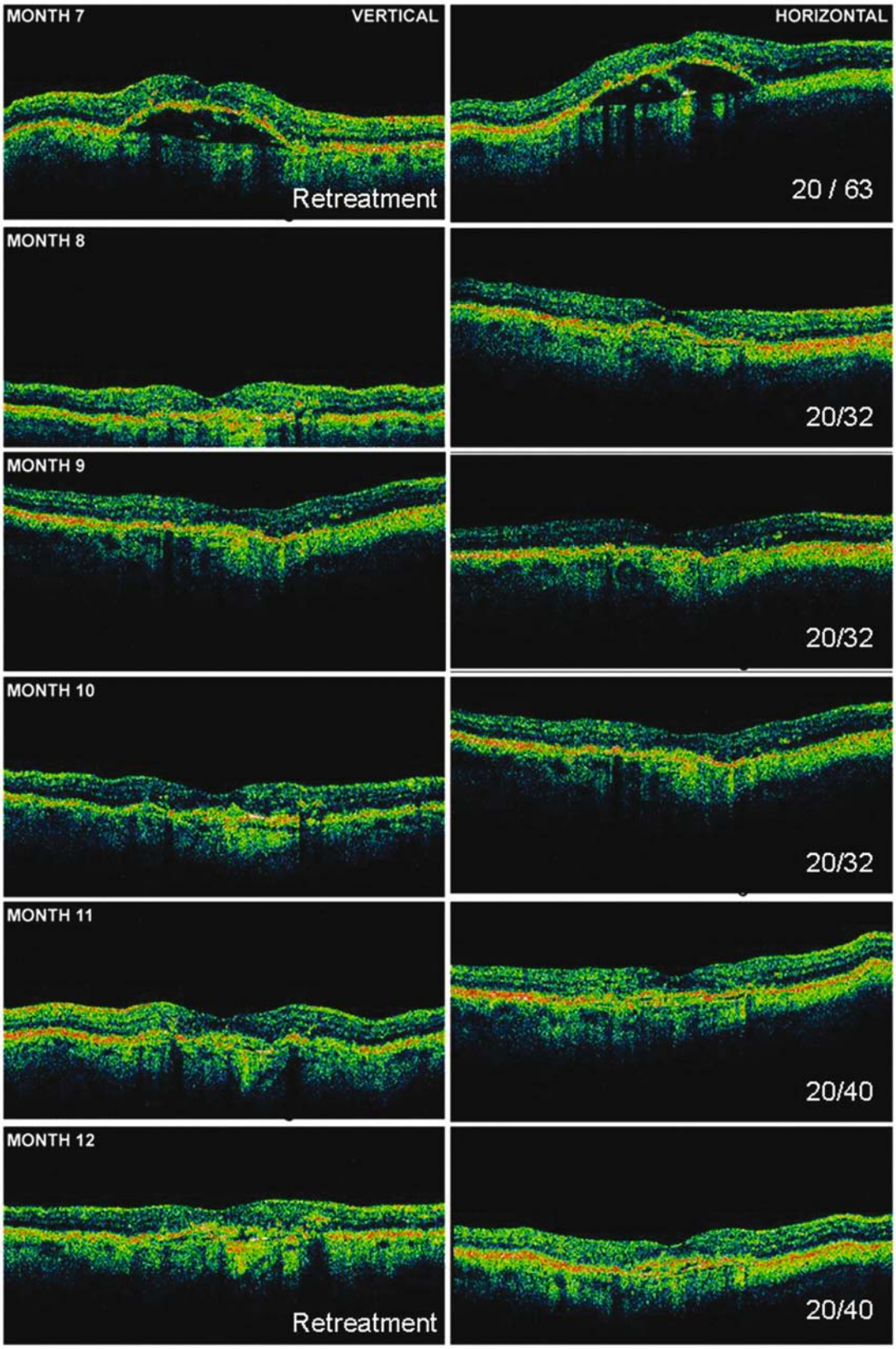

FIG. 15.5. Same patient as in Figures 15.3 and 15.4. Optical coherence tomography composite from months 7 to 12 with further increased macular edema at month 7, and resolution of the macular edema at month 8 following re-treatment. Patient re-treated again at month 12 for >5 letter decrease in vision associated with macular fluid on OCT.

evaluated for confounding causes of increased retinal thickness such as vitreomacular traction or an epiretinal membrane. The OCT characteristics of each are beyond the scope of this chapter (see Chapter 16).

Errors associated with the placement of line scans were potential confounding variables when evaluating PrONTO patients, and caution was needed when using qualitative OCT information in a sequential fashion. Variability in the placement of each diagonal scan may result in an apparent qualitative change between visits where no change actually exists. For example, a radial line scan that is incorrectly centered can miss a pocket of subretinal fluid that was present previously, resulting in the misdiagnosis of a fluid-free macula and therefore can lead to the inappropriate cessation of therapy. To prevent this possibility, OCT technicians must learn to identify the appropriate center of the macula. Unfortunately, using current OCT technology, the technician's job is made even more difficult by having only an indistinct, low-contrast, black-and-white video image of the macula to guide positioning (see Figs. 15.3 to 15.5). This is particularly problematic when the patient's vision is poor and the macula is distorted with fibrosis or fluid. For this reason, landmarks such as the optic nerve, the retinal vessels, or notable scars or pigment play a crucial role in identifying the fovea. Future OCT technology will help resolve these issues, but until then it is essential for the retina specialist to play an active role in training OCT technicians and reviewing the scans prior to accepting any changes in CRT measurements or macular fluid between visits.

Fluorescein Angiography in the Era of Optical Coherence Tomography and Anti–Vascular Endothelial Growth Factor Therapy

The question has been inevitably raised as to how OCT compares to established imaging modalities. Since the 1960s, FA has become the gold standard for the diagnosis and monitoring of AMD, diabetic retinopathy, vascular occlusive disease, and macular edema from a myriad of causes. Several studies have compared FA and OCT, and both advantages and disadvantages of each have been revealed. Fluorescein angiography benefits from decades of use and comprehensive understanding, relative ease of reproducibility, and the dynamic nature of fluorescein leakage or staining over time. However, while FA is relatively safe, it is an invasive procedure with a low but potentially life-threatening risk due to anaphylaxis. Also, in eyes with significant retinal/macular scarring it is challenging to differentiate staining from leakage. On the other hand, OCT is a static imaging modality, but it is a fast, noninvasive procedure that provides structural images of the retina.

The role of FA for AMD treatment is now shifting as the noninvasive, faster technique of OCT becomes an imaging standard. In clinical practice, a wide spectrum exists in current use of FA versus OCT among retinal specialists: some continue to image with FA regularly while others have nearly abandoned the technique. At a minimum, a baseline FA is appropriate to confirm the diagnosis of neovascular AMD. Fluorescein angiography is also appropriate to repeat in cases of unexplained vision loss and poor response during ranibizumab therapy. Fluorescein angiography is thought to be the gold-standard for establishing a particular cause of unexplained vision loss in AMD–the RPE tear. Tears of the RPE, generally following the presence of a PED, are occasional sequelae of neovascular AMD. While impending or early tears of the RPE may be recognized clinically or by using OCT (e.g., attenuation or corrugation of the RPE/Bruch's complex), FA remains the standard for establishing this diagnosis once a tear of the RPE has evolved. However, OCT is generally the most useful tool for following the fluid and for revealing other causes of vision loss such as atrophy of the photoreceptor outer layer, vitreomacular traction, or epiretinal membrane.

Optical Coherence Tomography in Antiangiogenic Therapy for Retinal Vein Occlusion

Vascular endothelial growth factor is believed to play a role in the increased vascular permeability that causes impaired vision from macular edema in retinal vein occlusions. Off-label bevacizumab has also been used for the treatment of branch and central venous occlusions of the retina to achieve short-term gains in visual acuity and improvements in retinal anatomy.[11,22,23,28,46] Trials are also underway to evaluate ranibizumab in retinal edema from venous occlusions. Optical coherence tomography findings in retinal vein occlusions may include an increase in retinal thickness, cystic changes, and pockets of subretinal fluid, but not pigment epithelial detachments. Interpretation of OCTs for antiangiogenic therapy in vascular occlusions may be undertaken in a similar manner to neovascular AMD. Comparisons may be made between visits of reliable central thickness measurements and qualitative changes in the retinal appearance. Gradual reductions in the edema should be observed following ranibizumab or bevacizumab therapy, and this edema may recur at various time points after monthly therapy is discontinued.

Optimizing Optical Coherence Tomography Information: The Importance of Technician Skill

Technical expertise is required to obtain high-quality OCT images that are reliable for interpretation. Rapid improvements can be seen in the macula following anti-VEGF therapy, but true change must be distinguished from artifacts associated with scan placement or unreliable thickness calculations.

Optical coherence tomography retinal thickness scan modes perform differently depending on AMD severity,[47] and incorrect delineation of the outer and inner boundaries may occur with the automated retinal thickness measurement tool.[48] These OCT scan artifacts that can adversely affect retinal thickness measurements and topographic maps are surprisingly common.[49] Therefore, good technical skill is crucial to using OCT as a tool in anti-VEGF therapy.

Fluorescein angiography requires the fine skills of a photographer, but macular OCT demands the reflexes of a video gamer. Optical coherence tomography images are acquired as a laser beam repeatedly scans the retina, and when a quality scan has been taken, the technician has only a moment to "capture" the scan with the click of a button. Slower high-resolution radial line scans require approximately 1 second for each scan. Faster low-resolution scans for macular thickness calculations require about 0.5 seconds apiece.

An optimal OCT technician is both well trained to understand macular anatomy and sufficiently dexterous to capture the image at the correct moment. Slow reflexes or an inability to recognize macular anatomy will produce inferior data. Although the OCT has internal algorithms to correct mild to modest fixation or movement errors, significant deviations cause inaccuracies. Obtaining an image from a patient with a Parkinson's tremor and poor central fixation from AMD requires the ability to diligently chase the fovea while capturing images.

Future Directions

As OCT imaging technology evolves with spectral-domain technology, faster scanning along with higher-resolution images and improved thickness algorithms will result in better, more reliable images and thickness measurements. As this technology improves, the importance of OCT for elucidating and following macular diseases will only be enhanced along with its role in monitoring pharmacologic therapies.

References

1. Ferrara N, Damico L, Shams N, et al. Development of ranibizumab, an anti-vascular endothelial growth factor antigen binding fragment, as therapy for neovascular age-related macular degeneration. Retina 2006;26(8):859–870.
2. Bhisitkul RB. Vascular endothelial growth factor biology: clinical implications for ocular treatments. Br J Ophthalmol 2006;90(12):1542–1547.
3. Gragoudas ES, Adamis AP, Cunningham ET Jr, et al. Pegaptanib for neovascular age-related macular degeneration. N Engl J Med 2004;351(27):2805–2816.
4. Adamis AP, Altaweel M, Bressler NM, et al. Changes in retinal neovascularization after pegaptanib (Macugen) therapy in diabetic individuals. Ophthalmology 2006;113(1):23–28.
5. Cunningham ET Jr, Adamis AP, Altaweel M, et al. A phase II randomized double-masked trial of pegaptanib, an anti-vascular endothelial growth factor aptamer, for diabetic macular edema. Ophthalmology 2005;112(10):1747–1757.
6. Starita C, Patel M, Katz B, Adamis AP. Vascular endothelial growth factor and the potential therapeutic use of pegaptanib (Macugen®) in diabetic retinopathy. Dev Ophthalmol 2007;39:122–148.
7. Rosenfeld PJ, Brown DM, Heier JS, et al. Ranibizumab for neovascular age-related macular degeneration. N Engl J Med 2006;355(14):1419–1431.
8. Brown DM, Kaiser PK, Michels M, et al. Ranibizumab versus verteporfin for neovascular age-related macular degeneration. N Engl J Med 2006;355(14):1432–1444.
9. Moshfeghi AA, Rosenfeld PJ, Puliafito CA, et al. Systemic bevacizumab (Avastin) therapy for neovascular age-related macular degeneration: twenty-four-week results of an uncontrolled open-label clinical study. Ophthalmology 2006;113(11):2002 e1–12.
10. Michels S, Rosenfeld PJ, Puliafito CA, et al. Systemic bevacizumab (Avastin) therapy for neovascular age-related macular degeneration twelve-week results of an uncontrolled open-label clinical study. Ophthalmology 2005;112(6):1035–1047.
11. Rosenfeld PJ, Fung AE, Puliafito CA. Optical coherence tomography findings after an intravitreal injection of bevacizumab (Avastin) for macular edema from central retinal vein occlusion. Ophthalmic Surg Lasers Imaging 2005;36(4):336–339.
12. Rosenfeld PJ, Moshfeghi AA, Puliafito CA. Optical coherence tomography findings after an intravitreal injection of bevacizumab (Avastin) for neovascular age-related macular degeneration. Ophthalmic Surg Lasers Imaging 2005;36(4):331–335.
13. Manzano RP, Peyman GA, Khan P, Kivilcim M. Testing intravitreal toxicity of bevacizumab (Avastin). Retina 2006;26(3):257–261.
14. Maturi RK, Bleau LA, Wilson DL. Electrophysiologic findings after intravitreal bevacizumab (Avastin) treatment. Retina 2006;26(3):270–274.
15. Shahar J, Avery RL, Heilweil G, et al. Electrophysiologic and retinal penetration studies following intravitreal injection of bevacizumab (Avastin). Retina 2006;26(3):262–269.
16. Spitzer MS, Wallenfels-Thilo B, Sierra A, et al. Antiproliferative and cytotoxic properties of bevacizumab (Avastin) on different ocular cells. Br J Ophthalmol 2006;90:1316–1321.
17. Aisenbrey S, Ziemssen F, Volker M, et al. Intravitreal bevacizumab (Avastin) for occult choroidal neovascularization in age-related macular degeneration. Graefes Arch Clin Exp Ophthalmol 2007;245:941–948.
18. Avery RL. Regression of retinal and iris neovascularization after intravitreal bevacizumab (Avastin) treatment. Retina 2006;26(3):352–354.
19. Avery RL, Pieramici DJ, Rabena MD, et al. Intravitreal bevacizumab (Avastin) for neovascular age-related macular degeneration. Ophthalmology 2006;113(3):363–372, e5.
20. Bashshur ZF, Bazarbachi A, Schakal A, et al. Intravitreal bevacizumab for the management of choroidal neovascularization in age-related macular degeneration. Am J Ophthalmol 2006;142(1):1–9.
21. Costa RA, Jorge R, Calucci D, et al. Intravitreal bevacizumab for choroidal neovascularization caused by AMD (IBeNA Study): results of a phase 1 dose-escalation study. Invest Ophthalmol Vis Sci 2006;47(10):4569–4578.
22. Costa RA, Jorge R, Calucci D, et al. Intravitreal bevacizumab (Avastin) for central and hemicentral retinal vein occlusions: IBeVO study. Retina 2007;27(2):141–149.

23. Iturralde D, Spaide RF, Meyerle CB, et al. Intravitreal bevacizumab (Avastin) treatment of macular edema in central retinal vein occlusion: a short-term study. Retina 2006;26(3):279–284.
24. Reichel E. Intravitreal bevacizumab for choroidal neovascularization and cystoid macular edema: a cost-effective treatment? Ophthalmic Surg Lasers Imaging 2005;36(4):270–271.
25. Rich RM, Rosenfeld PJ, Puliafito CA, et al. Short-term safety and efficacy of intravitreal bevacizumab (Avastin) for neovascular age-related macular degeneration. Retina 2006;26(5):495–511.
26. Spaide RF, Fisher YL. Intravitreal bevacizumab (Avastin) treatment of proliferative diabetic retinopathy complicated by vitreous hemorrhage. Retina 2006;26(3):275–278.
27. Spaide RF, Laud K, Fine HF, et al. Intravitreal bevacizumab treatment of choroidal neovascularization secondary to age-related macular degeneration. Retina 2006;26(4):383–390.
28. Spandau UH, Ihloff AK, Jonas JB. Intravitreal bevacizumab treatment of macular oedema due to central retinal vein occlusion. Acta Ophthalmol Scand 2006;84(4):555–556.
29. Fung AE, Rosenfeld PJ, Reichel E. The international intravitreal bevacizumab safety survey: using the internet to assess drug safety worldwide. Br J Ophthalmol 2006;90:1344–1349.
30. Hee MR, Baumal CR, Puliafito CA, et al. Optical coherence tomography of age-related macular degeneration and choroidal neovascularization. Ophthalmology 1996;103(8):1260–1270.
31. Kim SG, Lee SC, Seong YS, et al. Choroidal neovascularization characteristics and its size in optical coherence tomography. Yonsei Med J 2003;44(5):821–827.
32. Brancato R, Introini U, Pierro L, et al. Optical coherence tomography (OCT) angiomatous proliferation (RAP) in retinal. Eur J Ophthalmol 2002;12(6):467–472.
33. Rogers AH, Martidis A, Greenberg PB, Puliafito CA. Optical coherence tomography findings following photodynamic therapy of choroidal neovascularization. Am J Ophthalmol 2002;134(4):566–576.
34. Giovannini A, Amato GP, Mariotti C, Scassellati-Sforzolini B. OCT imaging of choroidal neovascularisation and its role in the determination of patients' eligibility for surgery. Br J Ophthalmol 1999;83(4):438–442.
35. Spraul CW, Lang GE, Lang GK. [Value of optical coherence tomography in diagnosis of age-related macular degeneration. Correlation of fluorescein angiography and OCT findings]. Klin Monatsbl Augenheilkd 1998;212(3):141–148.
36. Hassenstein A, Ruhl R, Richard G. [Optical coherence tomography in geographic atrophy—a clinicopathologic correlation]. Klin Monatsbl Augenheilkd 2001;218(7):503–509.
37. Talks J, Koshy Z, Chatzinikolas K. Use of optical coherence tomography, fluorescein angiography and indocyanine green angiography in a screening clinic for wet age-related macular degeneration. Br J Ophthalmol 2007;91:600–601.
38. Yoganathan P, Deramo VA, Lai JC, et al. Visual improvement following intravitreal bevacizumab (Avastin) in exudative age-related macular degeneration. Retina 2006;26(9):994–998.
39. Ozdemir H, Karacorlu SA, Karacorlu M. Early optical coherence tomography changes after photodynamic therapy in patients with age-related macular degeneration. Am J Ophthalmol 2006;141(3):574–576.
40. Michels S, Aue A, Simader C, et al. Retinal pigment epithelium tears following verteporfin therapy combined with intravitreal triamcinolone. Am J Ophthalmol 2006;141(2):396–398.
41. Sahni J, Stanga P, Wong D, Harding S. Optical coherence tomography in photodynamic therapy for subfoveal choroidal neovascularisation secondary to age related macular degeneration: a cross sectional study. Br J Ophthalmol 2005;89(3):316–320.
42. Gurses-Ozden R, Teng C, Vessani R, et al. Macular and retinal nerve fiber layer thickness measurement reproducibility using optical coherence tomography (OCT-3). J Glaucoma 2004;13(3):238–244.
43. Massin P, Vicaut E, Haouchine B, et al. Reproducibility of retinal mapping using optical coherence tomography. Arch Ophthalmol 2001;119(8):1135–1142.
44. Paunescu LA, Schuman JS, Price LL, et al. Reproducibility of nerve fiber thickness, macular thickness, and optic nerve head measurements using StratusOCT. Invest Ophthalmol Vis Sci 2004;45(6):1716–1724.
45. Fung AE, Lalwani GA, Rosenfeld PJ, et al. An OCT guided, variable dosing regimen with intravitreal ranibizumab (Lucentis) for neovascular age-related macular degeneration. Am J Ophthalmol 2007;143(3):566–583.
46. Pai SA, Shetty R, Vijayan PB, et al. Clinical, anatomic, and electrophysiologic evaluation following intravitreal Bevacizumab for macular edema in retinal vein occlusion. Am J Ophthalmol 2007.
47. Menke MN, Feke GT. Assessment of the effects of morphological changes related to age-related macular degeneration on optical coherence tomography retinal thickness measurements. Ophthalmic Surg Lasers Imaging 2005;36(4):310–314.
48. Costa RA, Calucci D, Skaf M, et al. Optical coherence tomography 3: automatic delineation of the outer neural retinal boundary and its influence on retinal thickness measurements. Invest Ophthalmol Vis Sci 2004;45(7):2399–2406.
49. Ray R, Stinnett SS, Jaffe GJ. Evaluation of image artifact produced by optical coherence tomography of retinal pathology. Am J Ophthalmol 2005;139(1):18–29.

16
Optical Coherence Tomography Findings in Vitreomacular Interface Disorders

Javier Elizalde, Santiago Abengoechea, and María F. de la Paz

Optical coherence tomography (OCT) images of the interface between the macula and vitreous are very well defined because of the difference in reflectivity of the relatively acellular vitreous and the parallel-fiber orientation of the inner retina.[1] Disorders such as epiretinal membranes (ERMs), vitreomacular traction syndrome (VMTS), and macular holes are readily imaged and recognized even by persons inexperienced in biomicroscopy. Optical coherence tomography has also significantly contributed to making an accurate differential diagnosis of all these entities and to better understanding the varying structural anomalies of the retina that can explain visual loss in highly myopic eyes. The information obtained from high-resolution evaluation of retinal anatomy in all these conditions also improves the clinician's ability to make the optimal treatment decision and provides an objective means to monitor disease progression and therapeutic response.

Epiretinal Membrane

The ERM is known by many names in clinical and educational circles, including preretinal membrane, idiopathic preretinal macular gliosis, cellophane maculopathy, macular pucker, and surface wrinkling retinopathy.[2] The ERM represents an abnormal glial or fibrocellular proliferation on the surface of the retina, commonly located over the central fovea that can result in distortion of the macular architecture and the development of macular edema.[1] In early stages, epiretinal membrane may be asymptomatic, or it may create only a mild reduction in visual acuity. Its progression may cause metamorphopsia and lead to severe visual impairment. The ophthalmoscopic picture of this disorder ranges from a fine, glistening membrane overlying the macula (cellophane maculopathy) to a thickened, whitish tissue that obscures the underlying vasculature (Fig. 16.1).

As the epiretinal membrane progresses, traction at the level of the internal limiting membrane (ILM) creates a puckering effect. In this situation retinal folds radiating outward from the macula might be seen (Fig. 16.2). Adjacent retinal vessels that course under the ILM often assume a "corkscrew" pattern, which is quite dramatic with fluorescein angiography. In very severe cases, macular edema and even retinal detachment have been known to occur (Fig. 16.3). Occasionally, ERMs can evolve into macular pseudoholes (Fig. 16.4), and ERMs are often seen in conjunction with either vitreomacular traction syndrome or idiopathic full-thickness macular holes.[1,3] More rarely, fibrocellular tissue growing from the ERM toward the vitreous cavity might also be seen.

Optical coherence tomography images of ERMs may be classified into two broad categories: globally adherent membranes and partially nonadherent membranes.[3] Both types of ERMs are usually visible on OCT images as a taut hyperreflective line contiguous with or anterior to the inner retinal surface.

Partially nonadherent ERMs are clearly visible on OCT images as they have sections of tissue that are separated from the anterior surface of the retina (Figs. 16.1 and 16.2). The ERM appears as a linear, thin, reflective band anterior to the retina with focal areas of attachment to the retinal surface. The appearance of such an ERM might be mimicked by a partially detached posterior vitreous surface. However, ERMs tend to be thicker and more reflective than the posterior vitreous. The reflection from an ERM may measure up to 60 μm in thickness; this is rarely observed with a partially detached posterior vitreous.

Globally adherent ERMs are visible on OCT images as a contrast in reflectivity between the highly reflective ERM and the less reflective anterior surface of the retina. The adherence between the ERM and the anterior retina is uninterrupted in contrast to partially nonadherent ERMs (Fig. 16.5). Approximately 10% of globally adherent membranes detected clinically cannot be detected by OCT.[1,3] This is the result of difficulty, in some cases, in distinguishing the highly reflective ERM from the underlying reflective nerve fiber layer of the anterior retina. In these cases, the secondary effects of the membrane, such as loss of the normal foveal contour, variable

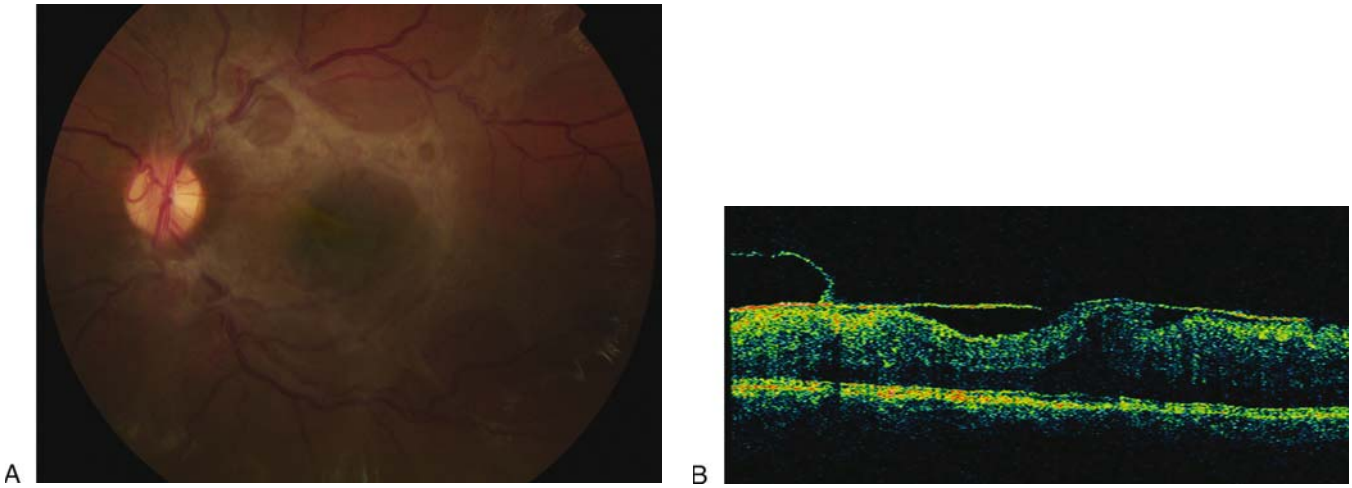

FIG. 16.1. A 37-year-old woman reports metamorphopsia in her left eye. Her visual acuity is 20/40 in this eye. (A) A dense star configuration of the central epiretinal membrane (ERM) was noted with foveal distortion (fold). Some vessels' segments are obscured by the membrane. (B) Optical coherence tomography (OCT) examination shows the ERM as a hyperreflective band with two focal well-defined points of attachment on the inner retinal surface and retinal thickening with folds. Note the correlation between the ophthalmoscopic appearance and the cross-sectional OCT image.

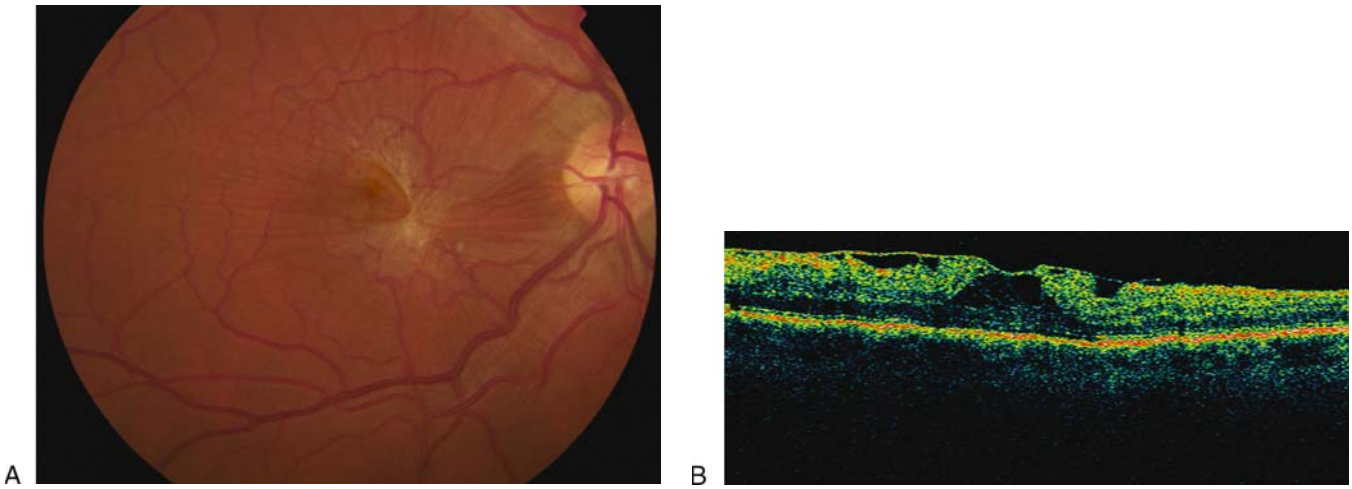

FIG. 16.2. (A) An ERM causing retinal folds radiating outward from the macula. (B) Optical coherence tomography reveals that the membrane is separated from the inner retina with multiple focal points of attachment.

irregularity of the inner retinal layers and macular thickening are used to establish the presence of the membrane.

In addition, characterization of the ERM with OCT may help in preoperative planning for membrane peeling.[4] In cases with separation between the membrane and retina, the surgeon may be directed to these areas to initiate membrane dissection. When the membrane is globally attached to the inner retina, the surgeon may anticipate more difficulty in peeling the membrane. The surgeon may also proceed with particular caution when extensive intraretinal edema leaves a thin, friable inner retinal layer beneath the membrane.

Postoperative OCT imaging can be used to document surgical response (Fig. 16.5). The completeness of ERM removal can often be assessed by comparing preoperative and postoperative images. Usually retinal thickness decreases following successful ERM peeling,[4,5] visual acuity improves, and the distorted vascular pattern comes back to its normal morphology.

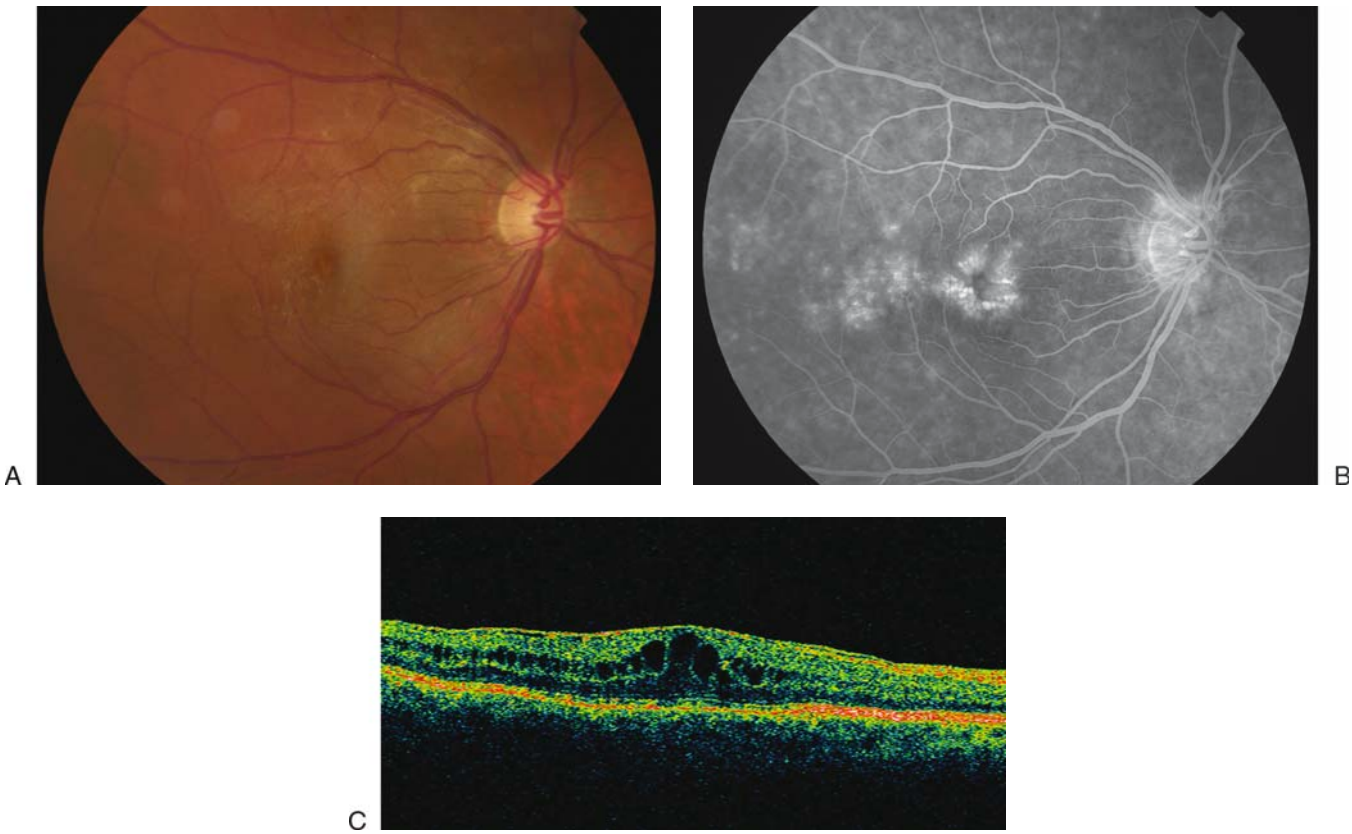

FIG. 16.3. (A) Bright reflex on the macula corresponding to an epiretinal proliferation. (B) Fluorescein angiography reveals late hyperfluorescence consistent with cystoid macular edema complicating this case. (C) Although the proliferation is globally adherent to the inner retina, the ERM can still be seen as a highly reflective band on the retinal surface. The fovea is extensively thickened from intraretinal edema with loss of the foveal depression and multiple intraretinal cysts are seen.

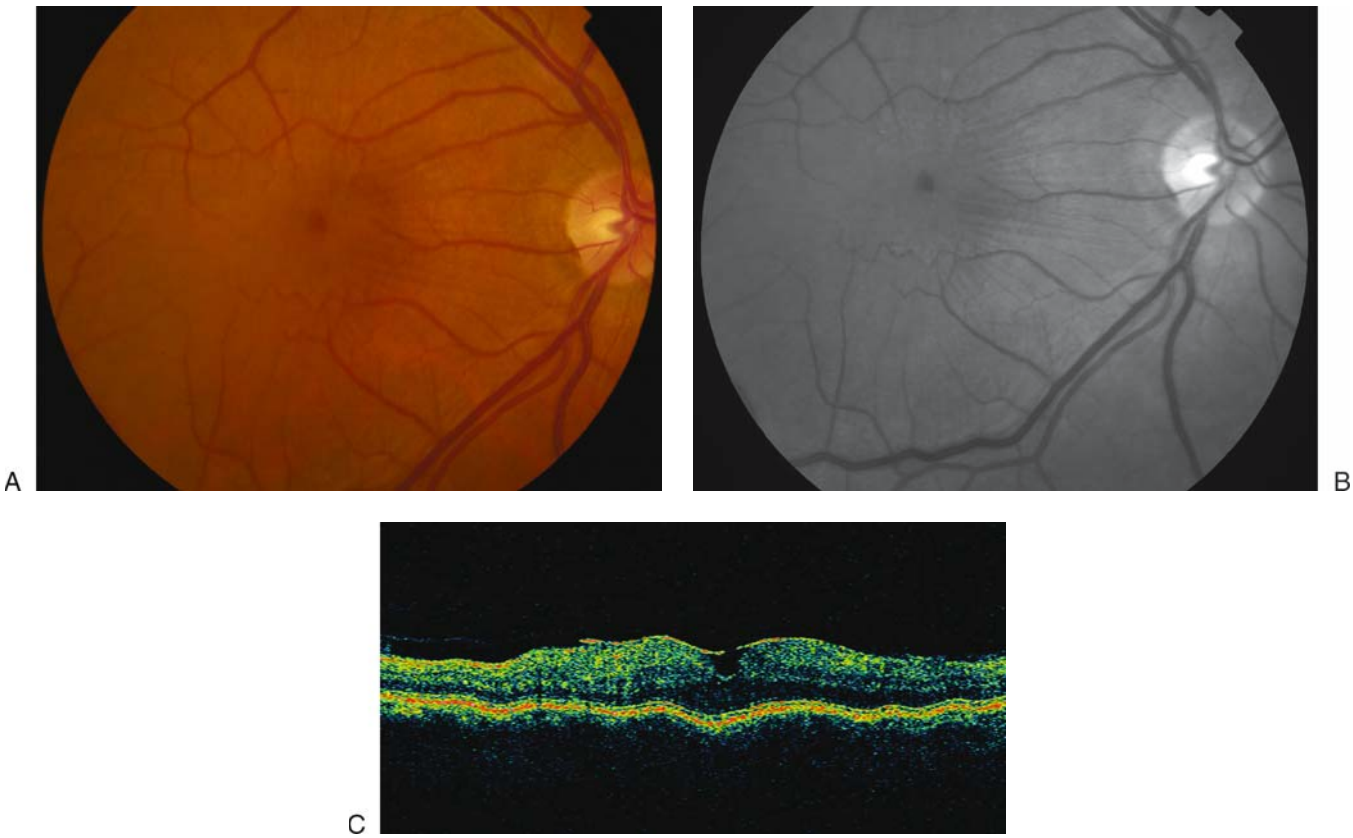

FIG. 16.4. (A-C) Epiretinal membrane and radial folds simulating a macular hole image (pseudomacular hole). (A) Color photograph. (B) Fluorescein angiography. (C) Optical coherence tomography.

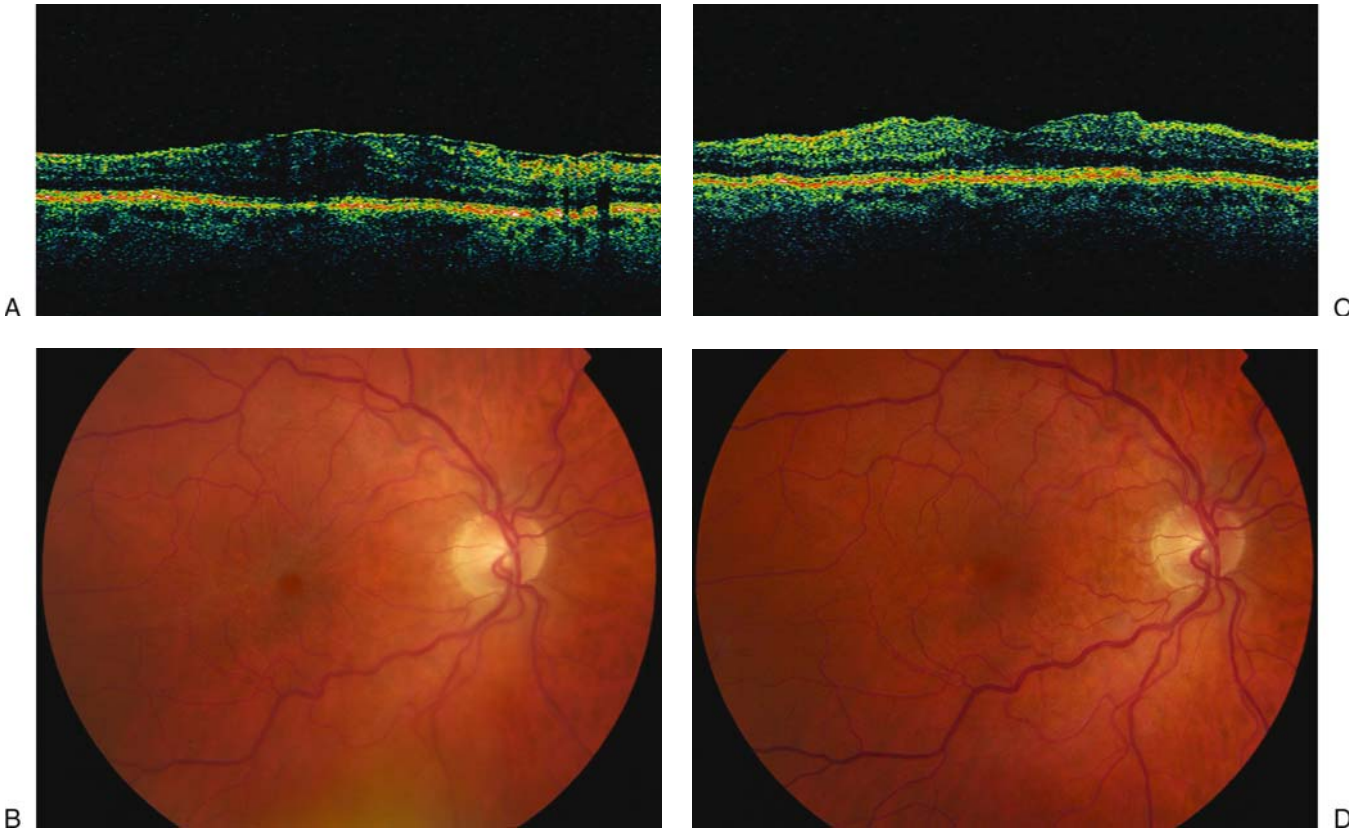

FIG. 16.5. Epiretinal membrane before (A,B) and after (C,D) surgical treatment. Postoperative OCT (C) demonstrates complete removal of the membrane, resulting in a normal foveal contour.

Vitreomacular Traction Syndrome

Vitreomacular traction syndrome (VMTS) refers to conditions in which retinal changes develop from incomplete posterior vitreous detachment (PVD) with persistent vitreous adhesion to the macula. It differs from idiopathic ERM in that the posterior hyaloid, rather than being generally totally detached from the posterior retina surface, remains attached to the perifoveal region. It is also frequently attached at the optic nerve or at multiple other points along or inside the vascular arcades. Sometimes the vitreous adherence can be difficult or impossible to identify directly on clinical exam, yet will be obvious by OCT.[6] The VMTS membranes are frequently less reflective than ERMs and are associated with substantial foveal traction, intraretinal cystoid changes, cystoid macular edema (CME), and frank detachment of the fovea (Fig. 16.6). These changes result in central vision loss and metamorphopsia.

Although the vitreous attachment to the macula usually appears broad on clinical exam, OCT typically shows an incomplete V-shaped PVD temporally and nasally to the fovea but remaining attached to the fovea. This configuration appears identical to the vitreous attachment identified in idiopathic macular hole. Why some patients with these findings progress to CME (VMTS) while others develop macular holes remains unclear. Variations in the location, density, and diameter of the vitreoretinal adhesion may explain these differences. Other VMTS cases can have a PVD temporally to the fovea but no posterior detachment nasally to it. In these cases prominent CME may develop, which may result in a macular hole or macular atrophy.[7]

As with other vitreoretinal interface abnormalities, OCT is extremely useful in monitoring the progression of patients with VMTS. Spontaneous resolution of vitreoretinal traction with normalization of the retinal contour has been documented with OCT.[8,9] On the other hand, persistent traction can lead to progressive retinal edema and thickening. Quantifying such changes with the OCT can be valuable in determining the need and timing of surgical intervention. As with ERMs, OCT can provide useful information in counseling the VMTS patient preoperatively with regard to visual potential. Eyes demonstrating massive traction, distortion of retinal architecture, intraretinal edema, and foveal detachment may be anticipated to have a relatively poor ultimate outcome compared to eyes not exhibiting these features. After surgery, OCT can be used to evaluate the anatomic response. Cases in the literature have documented improved retinal anatomy in association with increased visual acuity following vitrectomy surgery.[10,11]

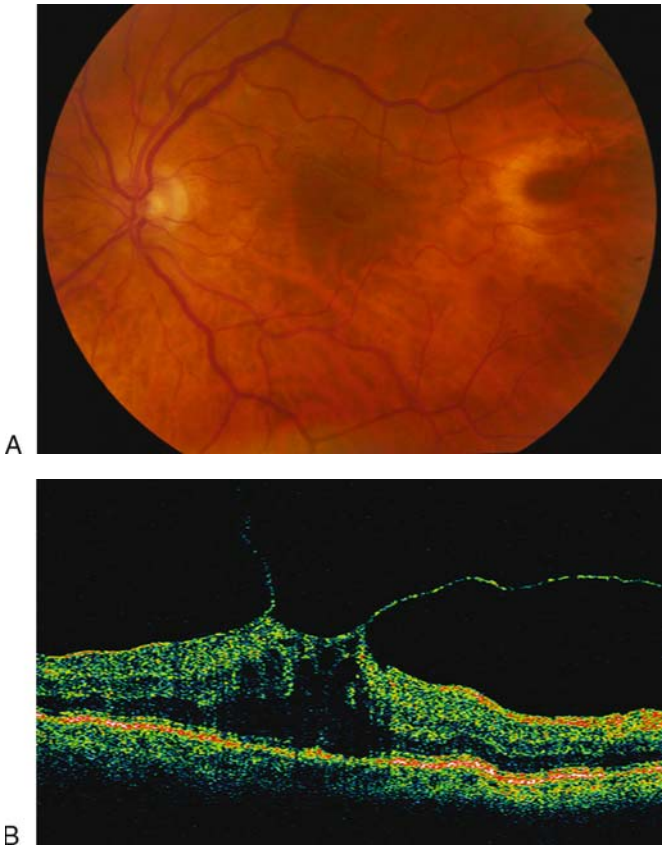

FIG. 16.6. A 58-year-old woman notes a progressive decrease in vision of the left eye over the past 6 months. (A) Fundus examination demonstrates a perifoveal ring-shaped fold with a glistening ERM. (B) Optical coherence tomography defines vitreomacular traction with attachment of the posterior hyaloid directly to the fovea. The tractional forces from the vitreous have resulted in retinal thickening with associated cystic spaces.

Idiopathic Macular Hole

An idiopathic macular hole is a retinal defect in the foveal area. Its incidence is around 3 in 1000, and it is more common in women in the sixth and seventh decades of life. [12,13] The classification of idiopathic macular holes as proposed by Gass[14,15] has always been the standard in staging macular holes until the advent of the OCT. In stage 1, there is vitreomacular traction due to incomplete vitreous detachment, lifting the foveal area and the formation of an impending macular hole. This clinically appears as a yellowish spot on the fovea. As traction increases, the spot enlarges to form a yellowish cyst (stages 1a and 1b). In stage 2, Gass describes a break in the retinal contour while the operculum is still attached to the retina, or separated from the underlying retina but with a hole diameter of less than 400 μm. In stage 3, there is complete separation of the operculum from the underlying retina, with a hole diameter more than 400 μm. In stage 4, there is complete posterior vitreous detachment with release of the anteroposterior tractional forces.

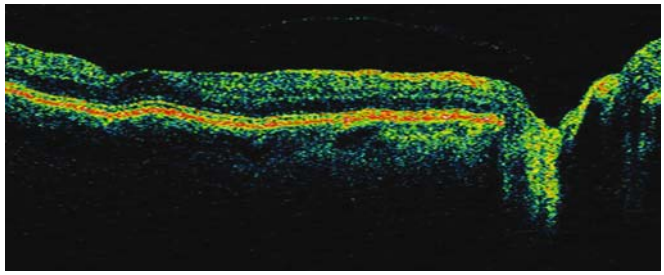

FIG. 16.7. Stage 1A macular hole. Vitreomacular traction with partial-thickness foveal pseudocyst. Papillomacular axis.

Since the introduction of the OCT, staging of macular holes has changed, especially with respect to the early stages. Gaudric et al.[16] described stage 1 as the presence of a cystic retinal space without foveal detachment similar to the clinical description of Gass. The authors proposed that this space was brought about by the anteroposterior traction from the posterior hyaloid, causing damage to central structures of the cellular processes of Müller cells. Optical coherence tomography imaging shows a hyporeflective space in the inner third of the fovea, along with loss of the normal foveal contour and a hyperreflective band adherent to the inner retina (posterior hyaloid). The early detection of stage 1 idiopathic macular holes was made possible by doing OCT imaging of the contralateral eye of those with already diagnosed macular holes. The initial finding is an incomplete detachment of the posterior hyaloid around the fovea with no changes in the underlying retina. This is probably because of the existing vitreofoveal adhesion. The presence of a tight bond of the posterior hyaloid over the fovea and the optic nerve head gives rise to vitreomacular traction. There is no consensus as to how the foveal cyst or pseudocyst evolves into a full-thickness macular hole. However, some authors, such as Gaudric et al., believe that a full-thickness macular hole proceeds from a break in the inner retinal surface caused by the existing tractional forces. Some consider that the foveal cystic space burrows deep until the photoreceptor layer prior to the breaking of the inner retinal wall.[15] Altaweel and Ip[17] published the latest staging of idiopathic macular holes based on OCT findings:

- Stage 1A: Pseudocysts form (hyporeflective image on OCT) without affecting all retinal layers and with an intact outer retina (Figs. 16.7 and 16.8).
- Stage 1B: The foveal pseudocyst affects all retinal layers including photoreceptor layer and with intact roof. There is incomplete posterior vitreous detachment with persistent adhesion onto the fovea in stages 1A and 1B.
- Stage 2A: A break in the roof of the pseudocyst gives rise to a full-thickness macular hole. There is persistent traction of the posterior hyaloid that is firmly attached to the inner retina (Fig. 16.9).
- Stage 2B: Appearance of a retinal operculum is due to complete detachment of the posterior hyaloid from the inner retina. At this point, there is release of the anteroposterior

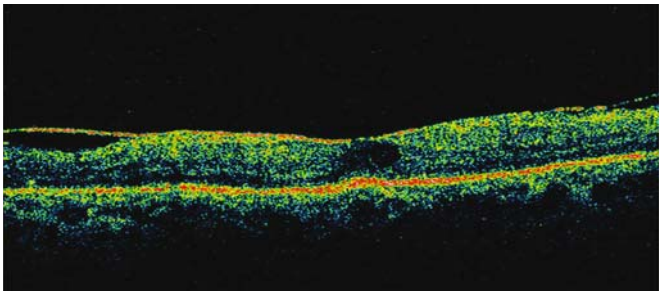

FIG. 16.8. Stage 1A macular hole. Foveal pseudocyst with intact photoreceptor layer and vitreomacular traction.

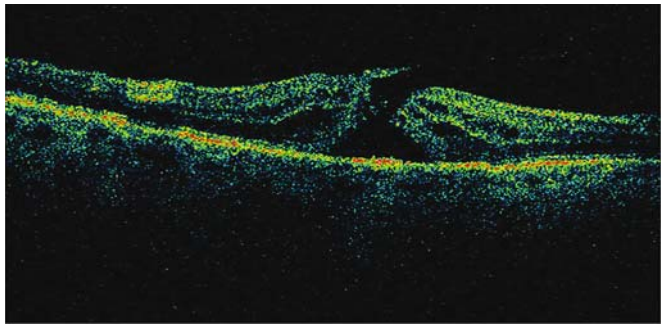

FIG. 16.9. Stage 2A macular hole. Vitreomacular traction (focal vitreous attachment to flap) with break in the roof of the foveal cyst.

tractional forces. The distance between the edges of the hole is less than 400 μm (Fig. 16.10).

- Stage 3: The prefoveal operculum can still be appreciated but the distance between the hole edges is greater than 400 μm. The posterior hyaloid is completely detached from the inner retina as opposed to the description of Gass wherein the former remains attached to the perifoveal area (Fig. 16.11).
- Stage 4: Complete detachment of the vitreous occurs, which cannot be seen tomographically and can only be confirmed by slit-lamp biomicroscopy or ultrasonography (Fig. 16.12).

Therefore, the main differences between the biomicroscopic and the OCT staging of idiopathic macular holes are the presence of a tight focal foveolar adherence of the posterior hyaloid versus a perifoveal vitreomacular detachment, the formation of a foveal pseudocyst versus a detachment in Gass's stage 1 hole, and the subdivision of stage 2 into two distinct anatomical types.

Optical coherence tomography is likewise useful in assessing the prognosis of an idiopathic macular hole. In the study of Gaudric et al.[16] in which 76 contralateral eyes were studied using OCT, the authors found the presence of intraretinal changes or traction in 15 eyes. Considering that the probability of developing a macular hole in the contralateral eye is 13% in 48 months,[18] it is then mandatory to perform bilateral tomographic imaging in patients affected by this pathology for early detection in the other eye. In another study of 66 contralateral asymptomatic eyes, the authors concluded that the presence of a foveal cyst connotes a 55% risk of developing a full-thickness macular hole in asymptomatic eyes, and that vitreofoveal separation signifies good prognosis.[19] Moreover, it has been shown that the smaller the diameter of the macular hole preoperatively, the higher the probability of anatomic closure. In those cases with a base diameter less than 400 μm as measured by OCT, an anatomic closure was achieved in 92%, and in those with a base diameter more than 400 μm, this value decreased to 56%.[20]

Several variables, such as preoperative visual acuity, duration of symptoms, OCT measurement of hole diameter (as a single variable), and stereoscopic funduscopy, may predict the final visual outcome.[21] One study demonstrated that the

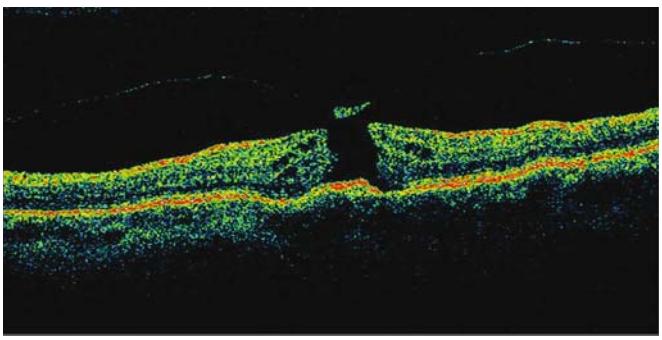

FIG. 16.10. Stage 2B macular hole. Preretinal operculum with distance between hole edges less than 400 μm. Microcystic spaces are seen at the edges of the hole.

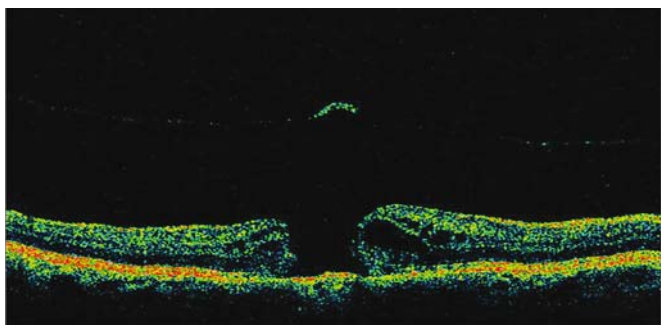

FIG. 16.11. Stage 3 macular hole. Preretinal operculum with distance between hole edges greater than 400 μm. Cystic degeneration of the borders of the hole is more evident.

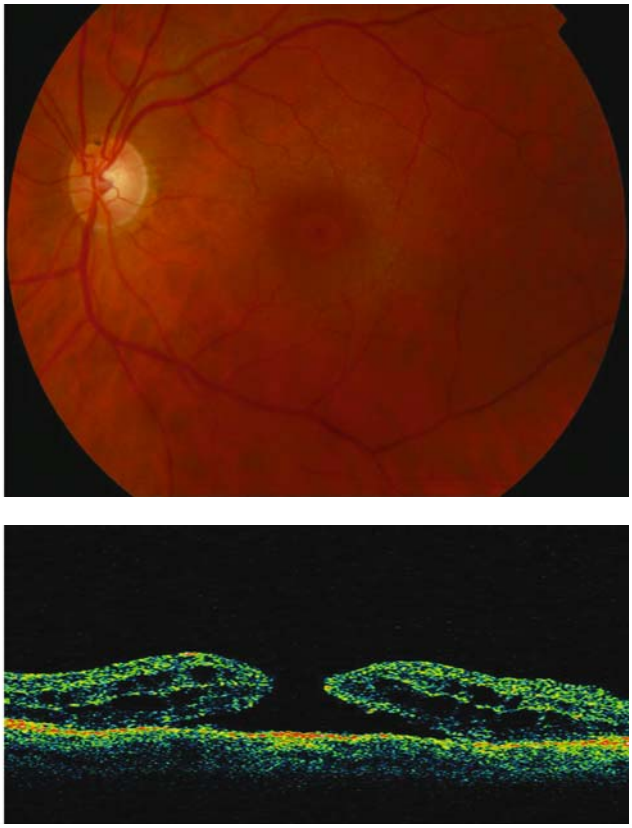

Fig. 16.12. (A) Biomicroscopic image of a full-thickness macular hole. (B) Stage 4 macular hole. Big intraretinal cysts are seen with lifting of the borders. No vitreomacular traction is noted.

OCT measurement is predictive not only of the possibility of anatomic closure but also of postoperative visual acuity. By using the maximum hole diameter, minimum hole diameter and height as reference values, the authors use a formula to infer macular hole prognosis.[22]

Optical coherence tomography is likewise useful in evaluating anatomic closure after macular hole surgery. The flattening of the retina and the disappearance of the retinal cysts may be appreciated postoperatively. The closure of the horizontal component of a hole wherein there is complete detachment usually takes place in the first postoperative month. Absence of closure within the first postoperative month entails a poor prognosis.[23] In the normal course of an idiopathic macular hole, about 2% may close by themselves spontaneously when there is release of vitreomacular traction (Fig. 16.13). In such cases, the photoreceptors may be affected due to the previously existing traction, and, as a consequence, may give rise to an absolute central scotoma. The differential diagnosis of macular pseudoholes and lamellar holes is discussed in the following chapter on myopic tractional maculopathy.

Thus, OCT imaging is a highly important tool in the diagnosis, in the evaluation of the etiopathogenesis, in the postoperative follow-up, and as a predictive factor in the prognosis of idiopathic macular holes.

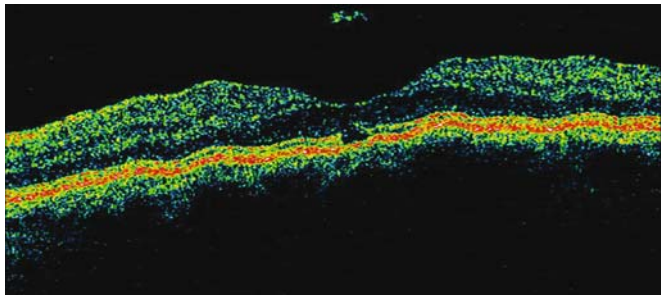

Fig. 16.13. Spontaneous closure of a macular hole with a preretinal operculum and central defect in the photoreceptor layer.

Myopic Tractional Maculopathy

High myopia is defined as an elongation of the anteroposterior axis of the globe associated with an axial length greater ≥26 mm. This pathology causes a progressive weakening of the scleral wall and axial elongation, which in severe cases may give rise to a posterior staphyloma. A posterior staphyloma may cause lesions such as chorioretinal atrophy, focal breaks in Bruch's membrane (lacquer cracks), subretinal hemorrhages, and chorioretinal neovascular membranes entailing very poor visual outcome. High myopia is known to have a prevalence of about 2% in the general population and about 22% to 33% in myopic eyes.[24] This clinical entity is usually bilateral, affecting patients of working age, and may produce an average legal blindness duration of 17 years.[25]

Optical coherence tomography enables us to capture high-resolution images of the posterior pole. This imaging technique is highly useful in examining the vitreomacular interface. Moreover, it enables precise characterization of the lesions that previously could only be appreciated on histologic sections. For example, with OCT, we can now distinguish between a retinoschisis and a flat retinal detachment at the macular area. The imaging protocol that we use for myopic tractional maculopathy consists of six sections, each 6 mm long centered on the fovea, a section along the optic nerve linking with the macula and six parallel sections connecting the temporal vascular arcades. With the said imaging protocol, we can scan the entire macula and visualize the presence or absence of traction, and the possible consequences on the fovea.

Myopic tractional maculopathy encompasses several lesions such as macular thickening, retinoschisis, lamellar holes, and retinal detachment due to tractional phenomena in patients with high myopia. Traction may be tangential or anteroposterior. Takano and Kishi[26] were the first ones to describe this clinical entity using OCT. Slit-lamp examination of these patients using a standard 60, 78, or 90 diopter lens is usually normal and neither traction nor retinal detachment can be appreciated. In some cases, we may find a microcystic appearance in the area of the posterior staphyloma that could make us suspect a possible tractional maculopathy. Rochon-Duvigneaud[27] was

the first one to describe the biomicroscopic findings of this pathology, but it was not until the advent of OCT that its characteristics were described in full detail. Green[28] described the presence of schisis in the peripheral retina in histopathologic studies but was not able to demonstrate where the traction came from. He related that these lesions were brought about by the lack of elasticity of some retinal components, especially the retinal vessels and the internal limiting membrane, in the light of an already weakened scleral wall and progressive elongation of the globe.

The first OCT finding in these patients is a thickening of the macular area along with loss of the normal foveal contour. In these cases, we should perform a scan of the macular area to find out what is causing this retinal thickening. Nonetheless, it may take years for this clinical process to evolve until such time that the patient may note some visual symptoms.

Another characteristic finding of myopic tractional maculopathy is the presence of a hyporeflective space dividing the sensorineural retina into two layers. The first is a fine layer of moderate reflectivity in apposition to the retinal pigment epithelium, and the second is a thicker hyperreflective layer in the inner retina. In this wide hyporeflective space, we may find some strands uniting the inner and the outer retina. The tomographic patterns of myopic retinal schisis may vary. The internal fibers may take on a "V" pattern and delineate the central cyst, or it may demarcate the boundary of a lamellar hole (superior opening of the cyst) or it may be associated with a foveal retinal detachment (Figs. 16.14 to 16.17). Nevertheless, when there is some degree of detachment in the internal retina, it may be called retinoschisis of the inner layers.

Other tomographic findings of myopic tractional maculopathy include retinal detachment. These are hyporeflective areas apposed to the retinal pigment epithelium with well-defined borders. They are usually located in the foveal area and associated with retinoschisis of the outer layers. Benhamou et al.[29] suggested that this finding may be a precursor of the myopic macular hole. Most cases would show that the widest area of detachment coincides with the peak of the vitreomacular traction (Fig. 16.16). Lamellar macular holes may likewise be found in these tractional phenomena (Fig. 16.18). However, the tomographic image is different from an idiopathic macular pseudohole (Fig. 16.19). The latter presents with an epiretinal membrane and is firmly adherent to the inner retinal surface. The edges of a pseudohole form a straight angle, while those of a lamellar hole form a more open angle. In most cases, the lamellar holes are brought about by a break in the roof of a retinal cyst (Fig. 16.20), but in myopic tractional maculopathy we may find some traction in the edges of the retinal hole. There are different anomalies existing in the vitreomacular interface that bring about this clinical entity. There may be anteroposterior forces such as vitreomacular traction wherein there is a perifoveal vitreous detachment with focal adhesion to the macula. Likewise, there may be tangential forces such as in the case of an epiretinal membrane where various points of traction may be found. Sometimes it may be difficult to determine the

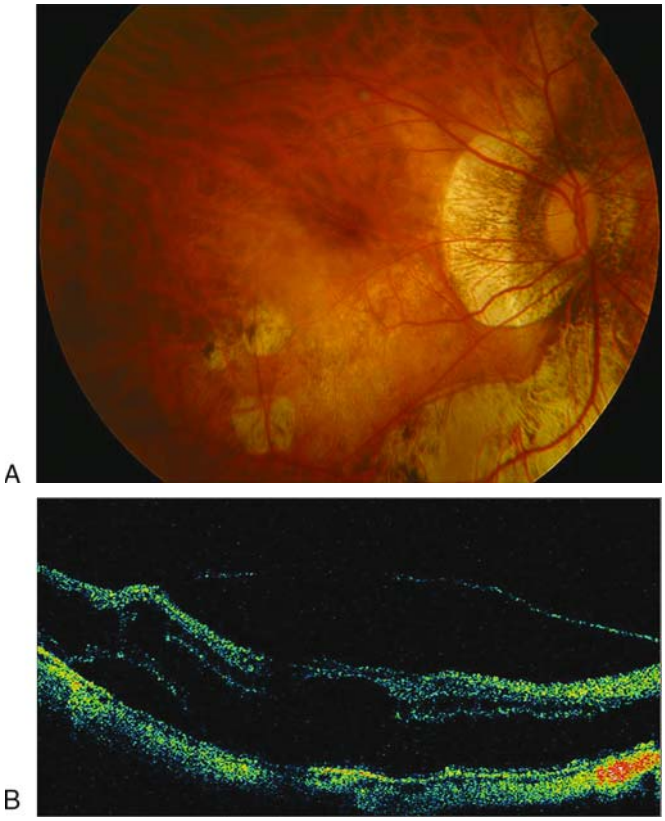

Fig. 16.14. (A) Myopic fundus with posterior staphyloma. (B) Retinoschisis of the outer retinal layers with foveal cyst and tractional retinal detachment.

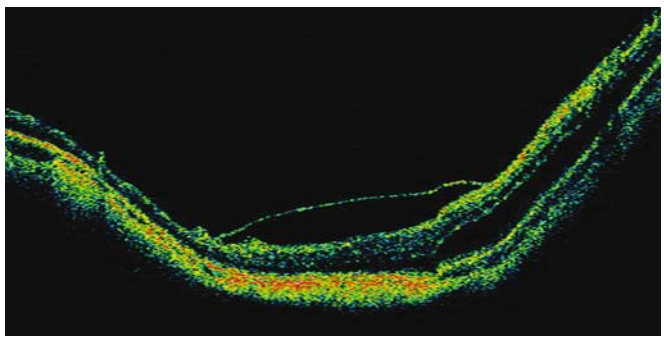

Fig. 16.15. Vitreomacular traction with retinoschisis of outer layers. Note the posterior staphyloma.

principal cause of the traction since the lesions and the tomographic images of the said entities are very similar. Moreover, a combination of both mechanisms may exist. There may be anteroposterior traction, tangential traction, incomplete posterior vitreous detachment, and an epiretinal membrane.

Another mechanism that must not be overlooked is the presence of an external traction brought about by the inherently weakened scleral walls and the posterior staphyloma. The said external tractional forces heightens the internal tractional forces similar to what occurs in non–high myopes who have epiretinal

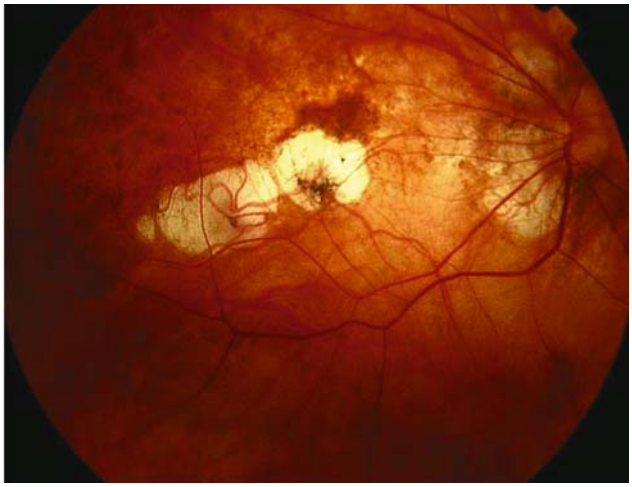

A

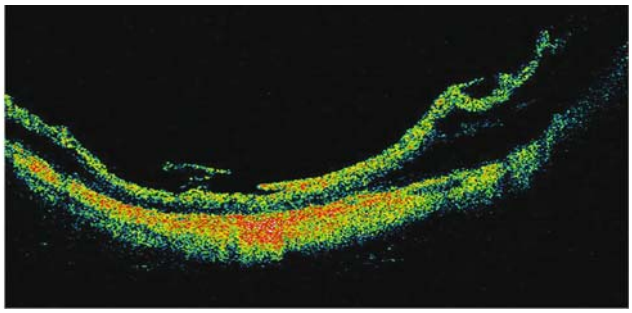

B

FIG. 16.16. (A) Retinography of a high myopic eye without evidence of vitreomacular traction. (B) Retinoschisis of the outer layers with peaking of vitreomacular traction in the form of a tent.

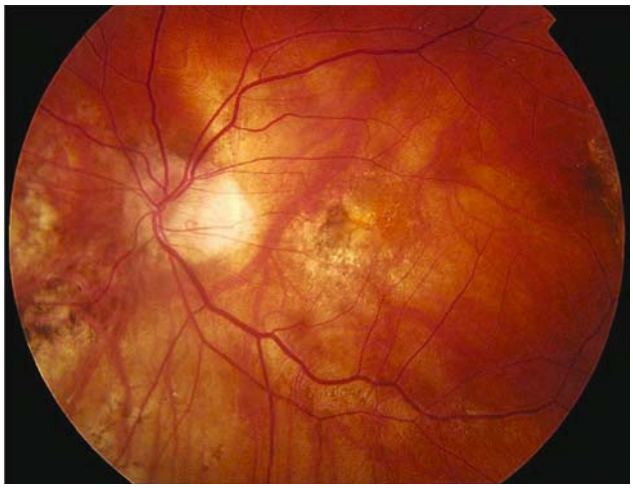

A

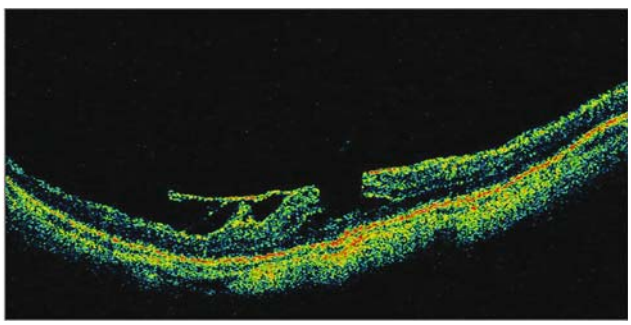

B

FIG. 16.18. (A) Myopic fundus with macular pigmented epithelium atrophy. (B) Lamellar hole with vitreomacular traction. Note the opened angle and the elevation of the hole's border.

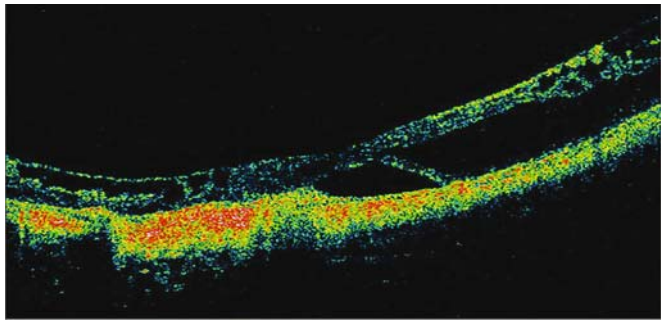

FIG. 16.17. Retinoschisis of the outer layers, inner layers, and dome-shaped retinal detachment.

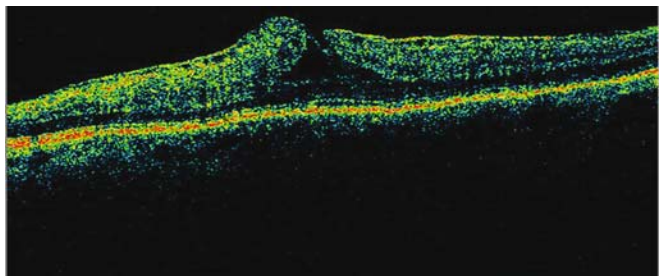

FIG. 16.19. Macular pseudohole with an internal hyperreflective band corresponding to an epiretinal membrane.

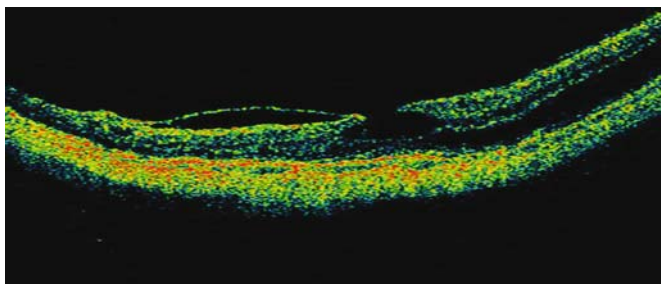

FIG. 16.20. Lamellar hole without vitreomacular traction in a non-myopic patient.

Table 16.1. Summary of results from 125 myopic eyes focusing on traction and retinal damage.

	No. of eyes (%)
Sample size	125
Epiretinal traction	58 (46.4)
•Epiretinal membrane	31 (24.8)
•Vitreomacular traction	11 (8.8)
•Epiretinal membrane + vitreomacular traction	16 (12.8)
Consequent retinal lesions	43 (34.4)
•Macular retinoschisis	25 (20.0)
•Retinal thickening	10 (8.0)
•Lamellar hole	6 (4.8)
•Retinal detachment	2 (1.6)
Staphyloma	53 (42.4)

Source: Adapted from Pannozzo and Mercanti.[30]

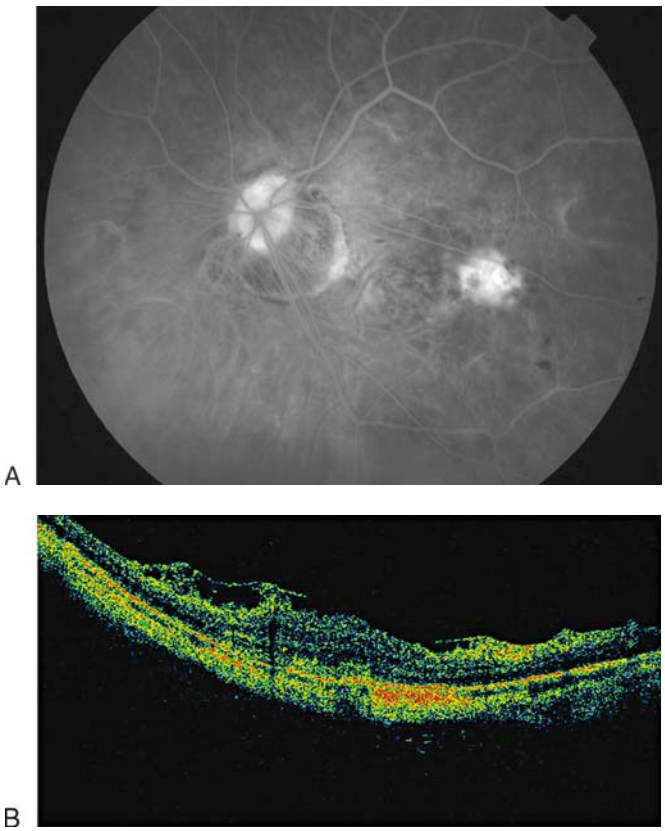

Fig. 16.21. (A) Central hyperfluorescence area corresponding to a subretinal neovascular membrane in high myopia. (B) Neovascular membrane over the retinal pigment epithelium with associated macular edema and preretinal tractional phenomena.

membranes and vitreomacular traction. Panozzo and Mercanti[30] reported the lesions encountered in 125 eyes with high myopia and the corresponding causes of the said lesions (Table 16.1).

The existing tractional forces in the macular area may likewise be associated with other lesions such as subretinal neovascularization. In such cases, imaging with OCT is useful to demonstrate the tractional forces that a simple fluorescein/indocyanine angiography would not reveal (Fig. 16.21).

At present, there is no consensus about the proper term of this clinical entity. Some authors refer to the OCT image of the lesions and label them as myopic macular retinoschisis[28] or myopic macular foveoschisis. [31] We consider it more appropriate to refer to the encompassing origin of these retinal lesions and call this clinical entity "myopic tractional maculopathy" as Panozzo and Mercanti[30] introduced the term recently.

References

1. Voo I, Mavofrides EC, Puliafito C. Clinical applications of optical coherence tomography for the diagnosis and management of macular diseases. Ophthalmol Clin North Am 2004;17:21–31.
2. Gass JDM. Macular dysfunction caused by vitreous and vitreoretinal interface abnormalities. Vitreous traction maculopathies. In: Gass JDM (Ed.). Stereoscopic Atlas of Macular Diseases. St Louis: Mosby, 1987.
3. Wilkins JR, Puliafito CA, Hee MR, et al. Characterization of epiretinal membranes using optical coherence tomography. Ophthalmology 1996;103:2142–2151.
4. Massin P, Allouch C, Haouchine B, et al. Optical coherence tomography of idiopathic epiretinal membranes before and after surgery. Am J Ophthalmol 2000;130:732–739.
5. Gallemore RP, Jumper JM, McCuen BW, et al. Diagnosis of vitreoretinal adhesions in macular disease with optical coherence tomography. Retina 2000;20:115–120.
6. Smiddy WE, Michels RG, Glaser BM, De Bustros S. Vitrectomy for macular traction caused by incomplete vitreous separation. Arch Ophthalmol 1988;106:624–628.
7. Yamada N, Kishi S. Tomographic features and surgical outcomes of vitreomacular traction syndrome. Am J Ophthalmol 2005;139:112–117.
8. Sulkes DJ, Ip MS, Baumal CR, Wu HK, Puliafito CA. Spontaneous resolution of vitreomacular traction documented by optical coherence tomography. Arch Ophthalmol 2000;118:286–287.
9. Kusaka S, Saito Y, Okada AA, et al. Optical coherence tomography in spontaneously resolving vitreomacular traction syndrome. Ophthalmologica 2001;215:139–141.
10. Munuera JM, García-Layana A, Maldonado MJ, et al. Optical coherence tomography of successful surgery of vitreomacular traction syndrome. Arch Ophthalmol 1998;116:1388–1389.
11. Uchino E, Uemura A, Doi N, Ohba N. Postsurgical evaluation of idiopathic vitreomacular traction syndrome by optical coherence tomography. Am J Ophthalmol 2001;132:122–123.
12. Ho AC, Guyer DR, Fine SL. Macular hole. Surv Ophthalmol 1998;42:393–416.
13. Chew EY, Sperduto RD, Hiller R, et al. The eye diseases case-control study. Clinical course of macular holes. Arch Ophthalmol 1999;117:242–246.
14. Gass JDM. Idiopathic senile macular holes: its early stages and pathogenesis. Arch Ophthalmol 1988;106:629–639.
15. Gass JDM. Reappraisal of biomicroscopic classification of stages of development of a macular hole. Am J Ophthalmol 1995;119:752–759.
16. Gaudric A, Haouchine B, Massin P, Paques M, Blain P, Erginay A. Macular hole formation: new data provided by optical coherence tomography. Arch Ophthalmol 1999;117:744–751.

17. Altaweel M, Ip M. Macular hole: improved understanding of pathogenesis, staging, and management based on optical coherence tomography. Semin Ophthalmol 2003;18(2):58–66.
18. Lewis MI, Cohen SM, Smiddy WE, Gass JD. Bilaterality of idiopathic macular holes. Graefes Arch Clin Exp Ophthalmol 1996;234:241–245.
19. Spiritus A, Dralands L, Stalmans P, Stalmans I, Spileers W. OCT study of fellow eyes of macular holes. Bull Soc Belge Ophthalmol 2000;275:81–84.
20. Ip M, Baker BJ, Duker JS, et al. Anatomical outcomes of surgery for idiopathic macular hole as determined by optical coherence tomography. Arch Ophthalmol 2002;120(1):29–35.
21. Tilanus MAD, Cuupyers MHM, Bemelmans NAM, et al. Predictive value of pattern VEP, pattern ERG and hole size in macular hole surgery. Graefes Arch Clin Exp Ophthalmol 1999;237: 629–635.
22. Ullrich S, Haritoglou C, Gass C, Schaumberger M, Ulbig MW, Kampik A. Macular hole size as a prognostic factor in macular hole surgery. Br J Ophthalmol 2002;86(4):390–393.
23. Jumper M, Gallemore R, McCuen BW, Toth CA. Features of macular hole closure in the early postoperative period using optical coherence tomography. Retina 2000;20:232–237.
24. Mondon H. Physiopathologie de la myopie forte. In: Mondon H, Metge P, eds. La Myopie Forte. Paris: Masson, 1994:29–57.
25. Green JS, Bear JC, Johnson GJ. The burden of genetically determined eye disease. Br J Ophthalmol 1986;70:696–699.
26. Takano M, Kishi S. Foveal retinoschisis and retinal detachment in severely myopic eyes with posterior staphyloma. Am J Ophthalmol 1999;128:472–476.
27. Rochon-Duvigneaud M. Déformation et lésions de l' œil myope. In: Mawas J, ed. Introduction à L'étude de la myopie et des chorio-rétinites myopiques. Bull Soc Ophtalmol Paris 1938;1:1–10.
28. Green WR. Retina, myopia. In: Spencer WH ed. Ophthalmic Pathology: An Atlas and Textbook, vol 2, 4th ed. Philadelphia: WB Saunders, 1996:913–924.
29. Benhamou N, Massin P, Haouchine B, Erginay A, Gaudric A. Macular retinoschisis in highly myopic eyes. Am J Ophthalmol 2002;133:794–800.
30. Panozzo G, Mercanti A. Optical coherence tomography findings in myopic traction maculopathy. Arch Ophthalmol 2004;122: 1455–1460.
31. Ikuno Y, Sayanagi K, Ohji M, et al. Vitrectomy and internal limiting membrane peeling for myopic foveoschisis. Am J Ophthalmol 2004;137:719–724.

17
Optical Coherence Tomography Findings in Uveitis

Anil Vedula and Janet L. Davis

The development of optical coherence tomography (OCT) in the early 1990s was one of the most powerful and exciting advances for imaging the internal microstructure of biologic tissues.[1] Optical coherence tomography is a particularly powerful ophthalmic imaging technique, as it provides real-time, noncontact, cross-sectional imaging of the anterior eye and retina, yielding images of tissue pathology without the need for invasive biopsy procedures and histopathologic staining. While OCT has far-reaching applications, it has been used increasingly to evaluate and manage a variety of posterior segment disorders, in particular, retinal pathologies. For example, it has been used to diagnose and guide treatment decisions in eyes with macular holes, vitreomacular traction, choroidal neovascularization, epiretinal membranes, and many more conditions. Moreover, it has been particularly useful for diagnosis and monitoring of retinal nerve head fiber thickness for glaucoma[2] and macular edema associated with diabetic retinopathy or other macular conditions.[3,4] This chapter reviews the basic principles of OCT and presents cases of chorioretinal inflammatory disease in which OCT was helpful in diagnosis or management.

Basic Principles of Optical Coherence Tomography

The Medical Literature Analysis and Retrieval System (MEDLARS) defines OCT as "an imaging method using lasers that is used for mapping subsurface structure. When a reflective site in the sample is at the same optical path length (coherence) as the reference mirror, the detector observes interference fringes." The basic principle of OCT imaging is analogous to conventional ultrasonic pulse echo imaging, except that OCT uses light while ultrasound uses acoustic waveforms. This difference gives OCT the advantage of not requiring direct contact with the tissue that is being investigated. Image resolution, which depends highly on waveform frequency, is another marked difference between ultrasound and OCT technology. Standard ultrasound uses high-frequency sound waves on the order of 10 MHz, and is thus limited to a resolution of approximately 150 μm. Optical coherence tomography, on the other hand, uses low coherence length light (830 nm), resulting in optical resolutions on the order of 10 μm.[5] Moreover, while high-frequency ultrasound technology is available, acoustic waveforms are strongly attenuated in tissue, leading to poor-quality images beyond a tissue thickness of 5 mm.

The physical principles behind OCT are based on Michelson interferometry, which is similar to Sir Isaac Newton's first description of white-light interference. Using fiber optic technology, low coherence light from a superluminescent diode is directed onto a beam splitter, which creates a *measurement* beam and a *reference* beam. The measurement beam of light is directed to the patient's eye and is reflected from optical boundaries of differing indices of refraction. The indices of refraction at these boundaries are an optical property of the tissue being imaged and surrogate markers for histologic structure. The single reference beam is reflected off a reference mirror so that it returns and combines with the complex measurement echo. This combination is termed *interference* in optics. The distance between the beam splitter and the reference mirror is continuously varied and the interference pattern is monitored by a photoelectric detector that processes it into an electric signal. When there is maximal constructive interference between the light from the patient's eyes and the reference paths, then the distance traveled by the light in both paths matches to within the coherence length of the light. Each of the multiple reflections will form a unique interference pattern with the reference beam, and this information will be translated into measurements of distance and thickness of the different ocular tissue structures.[1,6]

Two-dimensional cross-sectional images of ocular tissue microstructure are constructed by performing multiple axial measurements with the light source at different transverse positions. These data are then digitally filtered and analyzed and finally displayed as two-dimensional gray-scale or false-color representations. In the false-color representation, highly reflective structures are shown with bright colors, including red and white, while those with low reflectivity, such as vitreous, are

shown with darker colors, including blue and black. False-color representations have the advantage of improving one's ability to differentiate tissue structures, but they have the disadvantage of producing artifacts in the image. With false-color representations, it is also important to understand that different colors represent different optical back-reflections and are not analogous to histologic staining. The most common OCT machine (OCT-3) that is being used in clinical practice currently consists of approximately 512 individual color-coded axial scans with high-resolution images (<8 μm).[7] In comparison, the older OCT-2 machine created images composed of only 100 axial scans. The OCT-3 machine has the further advantage of being able to capture up to six images in 1 second (Table 17.1).[8]

The image resolution of OCT images is typically broken into two axes, corresponding to axial and transverse resolutions.[5] Axial resolution increases inversely with respect to wavelength and proportionally with respect to the broadness of the spectral bandwidth. Shorter wavelength light has the advantage of not being absorbed by high water content structures such as the vitreous, and broader spectral bandwidth produces shorter coherence light beams. Axial resolution will not vary according to the scanning protocol selected. Transverse resolution is determined by the focused, diffraction-limited spot size on the retina[9] and basically equates to the number of axial (A) scans performed during each sweep of the scanning beam. More A-scans require more time, which creates more difficulty in maintaining fixation for the patient and may therefore result in images with more "noise. " A standard scan consists of 512 A-scans distributed over a 6-mm transverse sweep.

There are several different ways to scan OCT images. Scanning patterns include single lines of differing length and orientation; lines arranged radially, which are useful for mapping the optic disc; circumpapillary images, which are useful to assess the nerve fiber layer; and sequential parallel lines, which are useful to appreciate the three-dimensional structure of specific parts of the retina, particularly the fovea.[10,11] The scans are always read from left to right, but the point at which the scan starts must be known. With older OCT software, the horizontal scan lines began in the temporal macula and passed toward the optic nerve in each eye. The right eye, therefore, would have 90-, 60-, 30-, 0-, 300-, and 330-degree scans performed clockwise, and the left eye 90-, 120-, 150-, 180-, 210-, and 240-degree scans performed counterclockwise. In newer OCT software, the scan lines of both right and left eyes pass from left to right as the patient is viewed by the doctor. Horizontal scans, therefore, now pass toward the optic nerve in the right eye and away from the optic nerve in the left eye. Vertical scans are always oriented from inferiorly to superiorly and are designated as 90-degree scans.

In an OCT image of normal retina, the nerve fiber and plexiform layers are highly reflective images, as illustrated by the bright colors in the false color image. The ganglion cell layer, inner and outer nuclear layers, photoreceptors, and choroid are weakly reflective as evidenced by their green-blue-black appearance. The boundary between the photoreceptor inner segments and outer segments is visible as a thin, highly reflective band due to the visual pigment rhodopsin. Immediately posterior to the photoreceptor band is the melanin-containing retinal pigment epithelium, which is similarly reflective. Finally, the choriocapillaris/choroid complex is similarly bright in color due to the vascular nature of this layer. It is difficult to distinguish the separation of the RPE/choriocapillaris/choroid using current OCT technology.

Because both the nerve fiber layer and the RPE/choriocapillaris layer are brightly reflective, the OCT is able to calculate retinal thickness, a useful parameter in the evaluation of macular disease. Retinal thickness is usually plotted as a central 1.0-mm foveal zone, four wedge-shaped zones between 1 and 3 mm from the center, and four larger wedge-shaped zones between 3 and 6 mm from the center. Thickness maps of the central macula are susceptible to inaccuracy related to poor fixation. Standard deviations of more than 10% in the central, foveal subfield suggests unreliable fixation and mapping. In addition, some maps contain artifact because they are off-center or there is inaccurate identification of the inner or outer retinal surface. This can occur with vitreous membranes, for example, or with large subretinal fluid collections. However, retinal maps can provide very graphic and useful images (Fig. 17.1).

Involuntary eye movement produces artifact that appears as undulations in the raw image. Processing refines the image by realigning the A-scans according to the anterior-posterior distance from the machine. Fixation loss is minimized by rapid scanning and use of a low-intensity fixation target that is visible to the patient, or by use of a fixation target for the fellow eye. The diode OCT beam itself is 830-nm wavelength, in the near infrared, and produces minimal patient discomfort, facilitating fixation.

Table 17.1. Comparison between optical coherence tomography (OCT) and ultrasonography.

OCT	Ultrasonography
• Light	• Sound
• Units: wavelength	• Units: MHz
• Axial resolution 3 μm (research) 10 μm (standard OCT-2) 8 μm (standard OCT-3)	• Axial resolution 150 μm at 10 MHz 20 μm at 50 MHz
• Noncontact	• Contact
• Better penetration and resolution at higher frequencies	• Poorer penetration at higher frequencies—4 to 5 mm only

Highly reflective structures produce shadowing of underlying tissues, which can be mistaken for fluid collections. Cylindrical hyporeflective streaks oriented perpendicular to the retinal surface can arise from vitreous opacities or from large retinal vessels. In the case of retinal blood vessels they are helpful to confirm that the same portion of the retina is being scanned on sequential examinations. Media opacities degrade the resolution of the OCT scan, but usually do not completely obliterate it. Even in scans of very low resolution, important information can be gained by confirming that there is either no or little macular edema, based on a relatively normal-appearing macular thickness. Small pupils have relatively little effect on OCT scanning. In the presence of clear media, OCT imaging through a small pupil will usually provide more usable information than fluorescein angiography.

The recent years have seen a significant advance in OCT technology, with new instruments of higher axial resolution currently only being used in research laboratories. In 2001, Drexler et al.[9] described a new ultrahigh resolution, noninvasive in vivo method of ophthalmologic imaging of the retina and cornea in which short pulse laser light sources are capable of generating broadband light that provide axial image resolutions of 2 to 3 μm, enabling visualization of internal retinal architectural morphology. In fact, several of the 10 distinct layers of the retina can be visualized, and the comparison to a histologic micrograph is remarkable.[7,9] Commercialization of the high-resolution technology will further increase information gained by OCT scanning.

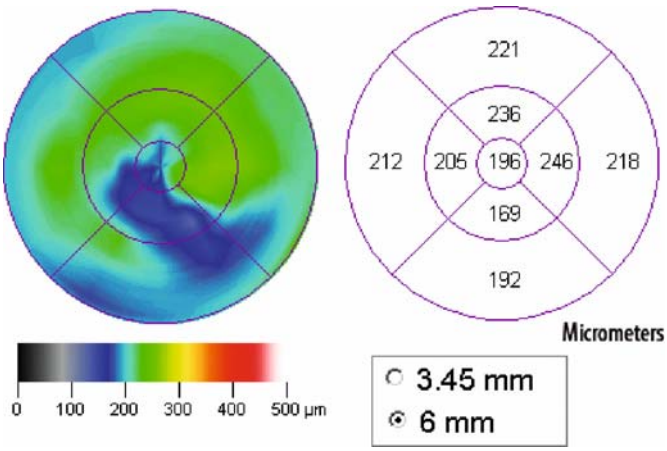

Fig. 17.1. Retinal map of a patient with healed, macular cytomegalovirus (CMV) retinitis. The patient presented with a history of CMV retinitis diagnosed elsewhere and a color photograph of a small white lesion possibly consistent with a cotton-wool spot. There was a question as to whether specific antiviral therapy needed to be continued. An optical coherence tomography (OCT) map clearly demonstrated retinal thinning depicted in blue and gray at the site of the previous white lesion, consistent with a prior necrotizing infection and not with a cotton-wool spot, which is characterized by inner retinal edema. The color scale corresponding to various thicknesses is shown below the map. Severe macular edema would appear yellow, red, or white on a map. The standard nine-ring array next to the map displays the average thicknesses in each of the areas. The central 1 mm thickness is normal. Vision was 20/20.

Applications of Optical Coherence Tomography in Uveitis

Changes in Intraocular Fluid Content

Fluid accumulations, including macular edema, subretinal fluid, pigment epithelial detachments, and retinoschisis, result in lower amounts of backscattering on OCT imaging and appear hypolucent (Fig. 17.2).[8] Hemorrhagic accumulations, or those with a significant exudative component, are usually

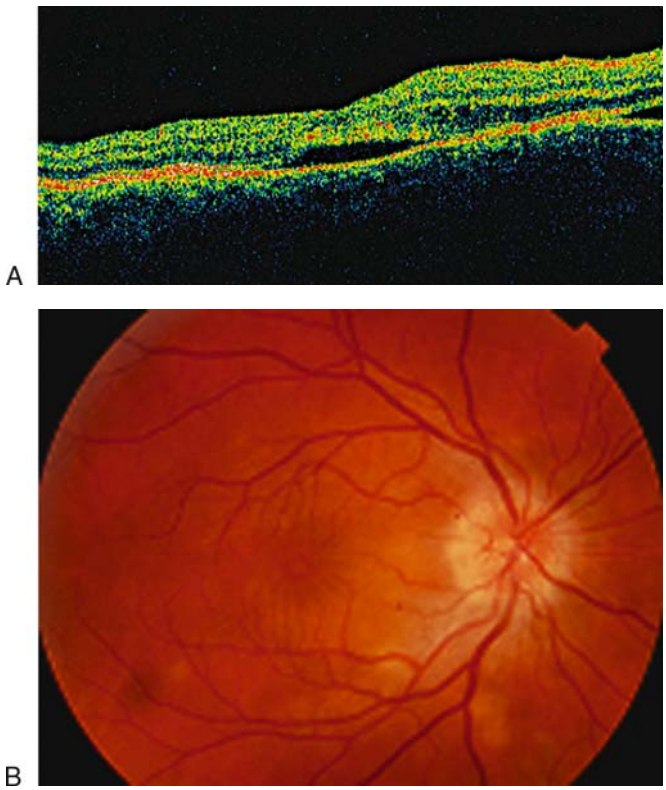

Fig. 17.2. Sudden vision loss in multifocal evanescent white dot syndrome with optic nerve edema. (A) Horizontal radial macular scan in a young woman with a sudden, unilateral reduction in vision and no vitreous inflammation. The hypolucent area under the foveal depression is fluid. The detached photoreceptors above it appear somewhat hyperreflective and may be involved in the inflammatory process. On either side of the foveal depression there is mild diffuse intraretinal edema indicated by the reduced density of the tissue, but the photoreceptors are attached. The aspect of the scan at right, closest to the optic nerve, shows another subretinal fluid collection. The hyperreflectivity of the inner retina on this aspect of the scan identifies this as a right eye. By convention the 0-degree (horizontal) scan in the right eye begins temporally and scans toward the nerve. Earlier versions of software had the horizontal scan of the left eye also directed toward optic nerve. More recently the 0-degree scan has been directed from the patient's right to the patient's left, as for the right eye. (B) Color photograph. There is optic nerve edema. The yellow color under the papillomacular bundle and the subfoveal yellow spot correspond to the fluid seen on the scan, and there is perifoveal edema. Indocyanine green (ICG) angiography showed hypofluorescent spots consistent with an atypical multifocal evanescent white dot syndrome.

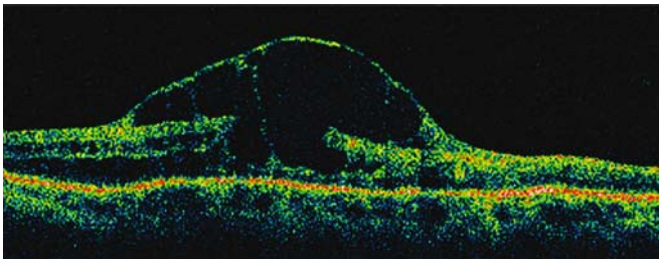

FIG. 17.3. In this patient with long-standing uveitis and 20/60 visual acuity, there is a thin membrane elevated over the retina that probably corresponds to the internal limiting membrane as a thin connection from the membrane to the outer retina and appears to be a Müller cell. The foveal region consists of a lamellar hole and attached photoreceptors. The long-standing edema is evidenced by the overall poor definition of retinal layers. A thin layer of subretinal fluid is visible on the left side of the frame, and the retinal thinning on the right side of the frame has led to hyperreflectivity of the retinal pigment epithelium (RPE)-choriocapillaris layer as more light reaches these layers when the overlying tissue is thin. There might be some benefit to reduction of the fluid seen on the left, but the chances of a significant improvement in vision in this eye are small.

hyperreflective, but in addition block any backscattering from the tissue underlying the fluid. There may be some minimal backscatter from the fluid cavity.

Macular Edema

Detection

Cystoid macular edema in uveitis provides an elegant demonstration of the retinal anatomy that influences the classic petaloid appearance or, when long-standing, produces more complicated patterns (Fig. 17.3). In uveitis, where thin-walled central cysts can be confused with macular holes, OCT can help distinguish between true cystoid edema, which would likely respond to medical treatment, and a macular hole, which would not.

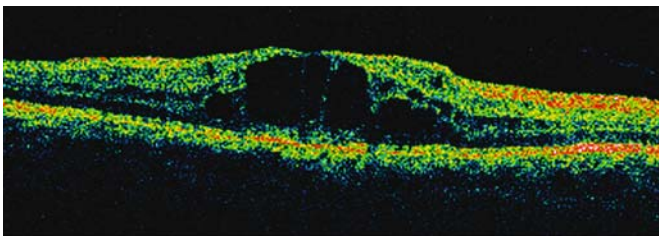

FIG. 17.4. Optical coherence tomography (OCT) scan of a uveitis patient with long-standing cystoid macular edema and the clinical appearance of a large central cyst or macular hole. Vision was 20/50. The scan shows two items of interest. The first is that the inner retina is intact but extremely thin, and there is no macular hole. The second is that the foveal photoreceptors are intact and attached, accounting for the relatively good vision. Given the thin appearance of the retina, treatment with injectable corticosteroids might lead to flattening of the cyst but little visual improvement. Note that the same linear signals are seen connecting the inner and outer retinas as in Figure 17.3. These probably represent Müller cells.

The appearance of macular edema on OCT has been described as three typical patterns: cystic retinal changes manifested as hyporeflective spaces within the retina, diffuse thickening of the macula, and subfoveal fluid detected by loss of normal signal from the subretinal space.[12,13] Optical coherence tomography imaging has also led to the realization that patients with cystoid macular edema and good vision typically show maintained attachment of photoreceptors without subfoveal fluid (Fig. 17.4). Thus, morphologic information gained by OCT aids understanding of the anatomic features affecting vision.

Correlation with Visual Prognosis

Optical coherence tomography technology has recently been used to correlate the morphologic features of macular edema and macular thickness with visual acuity in patients with uveitis. Markomichelakis and colleagues[14] studied 84 eyes of 60 patients with uveitis and macular edema. Optical coherence tomography was used to detect the three patterns of macular edema: diffuse macular edema, cystoid macular edema, and serous retinal detachment. Diffuse macular edema was the most common type, involving 54.8% of eyes, with cystoid edema in 25% of eyes. An additional 14.3% of eyes had both cystoid macular edema and serous retinal detachment, and 5.9% of eyes had both diffuse macular edema and serous retinal detachment. Epiretinal membrane was common. Maculas with cystoid edema were thicker than those with diffuse edema. Visual acuity was inversely related to macular thickness, presence of cystoid edema, and subretinal fluid. For examples of diffuse and cystoid edema, and subretinal fluid see Figures 17.2A, 17.4, and 17.5B.

Reinthal and colleagues[15] also investigated OCT in the management of macular edema in uveitis. They reported no difficulty in obtaining scans in patients with mild to moderate media opacity. A wide range of macular thicknesses was detected in the uveitic group, with foveal heights from 168 to 810 nm. Various patterns of cystic change were detected, the most common being confluent cysts. Other patterns included several discrete cystic spaces, and a single large central cyst.

Monitoring Response to Treatment

Serial examination of macular edema is thought to allow for more accurate follow-up of response to treatment.[16] Optical coherence tomography is now commonly used in long-term monitoring of macular edema, especially in patients undergoing treatment (Fig. 17.5). It is difficult to ensure perfect registration between serial images,[17] but this does not seem to be strictly necessary for macular edema, in which the changes in the retina occur on a fairly gross scale. Macular thickness in the central subfield or total macular volume can be used as single measures that summarize the overall status of the macula.

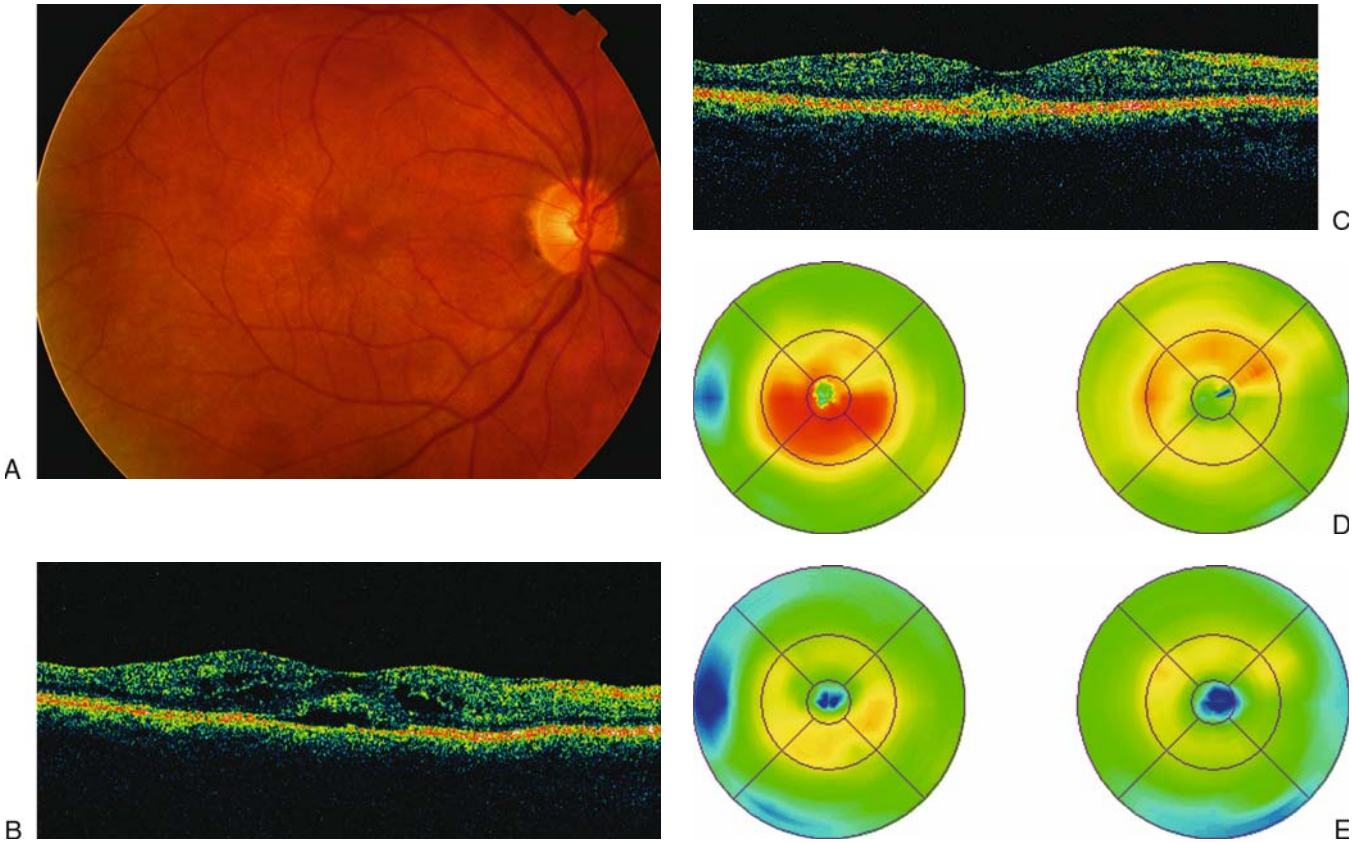

FIG. 17.5. Cystoid macular edema (CME) in a patient with birdshot choroidopathy before and after treatment with posterior subtenon triamcinolone acetonide. (A) Color photo of the right eye showing mild macular thickening but no discernible cysts. There is a yellow spot in the center of the macula and subtle birdshot lesions nasal to the optic nerve. Radial spokes corresponding to edema in Henle's layer are also seen. Visual acuity was 20/30 with complaints of reduced color vision. (B) Optical coherence tomography scan through the fovea prior to treatment. The cystic spaces in the outer retinal layers are nicely demonstrated. There is subretinal fluid with compaction of the photoreceptor layer in the foveal region. (C) One month after injection, the cystic spaces have shrunk. The subfoveal deposit may consist of shed photoreceptors and other debris. Visual acuity improved to 20/20 with subjective improvement in the ability to discriminate between blues and violets. The patient was a jeweler and could now match stones, but was still unable to grade diamonds. (D) Pretreatment retinal maps. Central thickness is 334 and 253 μm in the right and left eye, respectively. The right eye is displayed on the left side of the printout according to convention. (E) Posttreatment retinal maps. Thickness in the central 1-mm ring is still greater than normal at 227 and 192 μm. The dark blue spot in the temporal outer ring of the right eye is a constant feature of both pre- and posttreatment scans and is unlikely to be artifact. Peripheral thinning would be expected in birdshot chorioretinopathy from retinal degeneration.

Correlation with Change in Visual Acuity During Treatment

Reinthal and associates[15] documented changes in visual acuity that correlated with changes in OCT appearance during follow-up. Documentation of an anatomic change with reduction in intraretinal fluid without visual improvement probably indicates outer retinal damage that will not respond to additional treatment with corticosteroids. Small residual collections of subfoveal fluid are an additional cause of the failure of vision to completely recover following treatment. These collections of fluid are probably also the source of the central yellow "spot" recognized as a minimal form of noncystic macular edema in uveitis (Figs. 17.2 and 17.5A,B). A perhaps underappreciated aspect of OCT documentation of CME is the ability of the clinician to use the images to educate the patient as to the cause of reduced, distorted, or minimized vision. With very little teaching, the OCT images become very obvious and interpretable to most patients.

Subretinal and Intraretinal Exudations

Whereas the formation of cystoid or diffuse macular edema is generally a slow process that minimally disrupts tissue planes, preserves the architecture of the Müller cells, and probably results from capillary leakage combined with poor reuptake of fluid, the formation of large collections of subretinal or intraretinal fluid is likelier to be a more rapid process with a higher

grade leak. This hypothesis is supported by fluorescein angiography in which staining of the macular cysts may not be seen until the late stages of the angiogram, but the pinpoint leaks causing serous retinal detachments appear in the earliest stages of the angiogram and are often markedly hyperfluorescent.

Vogt-Koyanagi-Harada Syndrome

Optical coherence tomography has provided insight into patterns of fluid leakage in some disorders. Maruyama and Kishi[18] studied 42 eyes of 21 patients with acute Vogt-Koyanagi-Harada (VKH) syndrome with OCT. Retinal detachment with subretinal fluid was found in 69% of eyes, whereas 17 eyes (40%) had principally fluid accumulation in the outer retina. Four eyes had both patterns. Intraretinal fluid was associated with greater leakage of dye on fluorescein angiography. This pattern appears to be highly characteristic of VKH, but is not a formal aspect of the diagnostic criteria for VKH, which were formulated prior to the widespread use of OCT. The explanation for this distribution of exudative fluid is unclear. Either there is substantial leakage from the intraretinal vessels in the outer plexiform layer in addition to the presumed trans-retinal pigment epithelium (RPE) choroidal leaks, or the phenomenon relates to tissue compliance in the face of a large pressure gradient around the leak point.

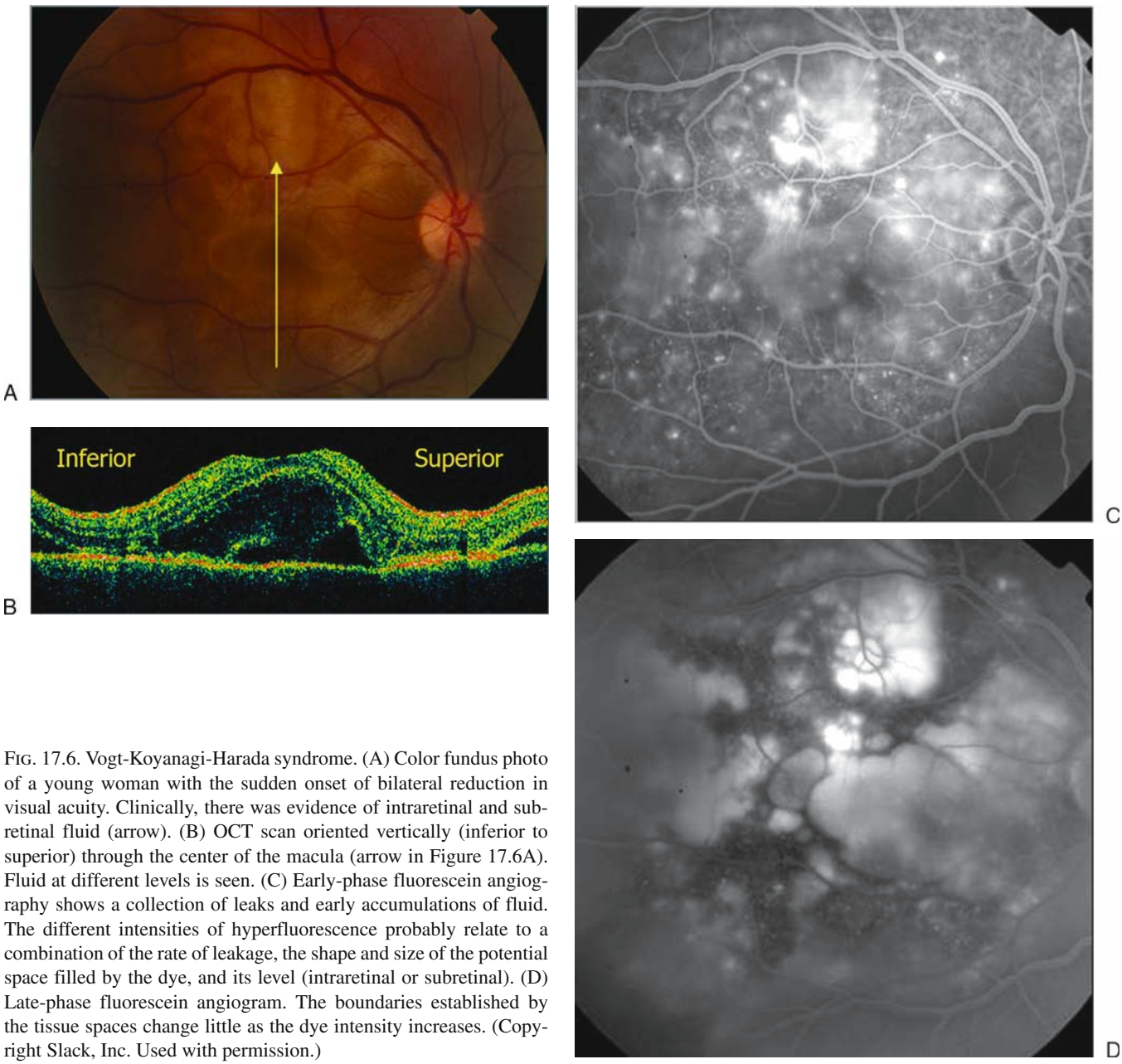

Fig. 17.6. Vogt-Koyanagi-Harada syndrome. (A) Color fundus photo of a young woman with the sudden onset of bilateral reduction in visual acuity. Clinically, there was evidence of intraretinal and subretinal fluid (arrow). (B) OCT scan oriented vertically (inferior to superior) through the center of the macula (arrow in Figure 17.6A). Fluid at different levels is seen. (C) Early-phase fluorescein angiography shows a collection of leaks and early accumulations of fluid. The different intensities of hyperfluorescence probably relate to a combination of the rate of leakage, the shape and size of the potential space filled by the dye, and its level (intraretinal or subretinal). (D) Late-phase fluorescein angiogram. The boundaries established by the tissue spaces change little as the dye intensity increases. (Copyright Slack, Inc. Used with permission.)

Figure 17.6 demonstrates the complex patterns of fluid leakage in VKH that produce overlapping fluid collections at various depths. Unlike central serous choroidopathy in which fluid leakage comes mainly from the choroidal layer, there are no serous retinal pigment epithelial detachments. The OCT findings are therefore somewhat different than predicted for a primarily choroidal inflammation. The discrepancy may arise because the leakage is so diffuse that it does not have time to collect in well-defined RPE detachments, but the OCT suggests that the exudative fluid may also arise from the retinal circulation.

Syphilitic Chorioretinitis and Sympathetic Ophthalmia

Syphilitic chorioretinitis and sympathetic ophthalmia show similar patterns of intraretinal and subretinal fluid accumulation (Figs. 17.7 and 17.8). The pattern therefore seems to be one that indicates a common mechanism rather than a common etiology. None of the three disorders is typically considered to be a retinal vasculitis with obvious hyperfluorescence of large retinal vessels, although this is occasionally seen in some cases. Leakage from smaller caliber retinal vessels is compatible both with the fluorescein angiogram and the OCT appearance.

Changes in Intraocular Tissue Density

Disease-related alterations in tissue can produce changes in reflectivity as well as in thickness. Thickening with hypolucency indicates increased fluid content, but thickening with increased reflectivity probably indicates an infiltration. These hyperreflective infiltrations can be seen in both the retina and the choroid in inflammatory diseases. Scar tissue, inflammatory infiltrates, hard exudates, or hemorrhage also result in higher reflectivity. These are generalizations. Since the degree of reflectance is a property of contrast between the lesion and the surrounding tissue, some infiltrates or scars could result in low backscattering or might produce no change in reflectivity; however, an increase in reflectance is the general rule. Since these lesions are generally clearly visible, the usefulness of OCT compared to fluid accumulations is somewhat less; however, the assignment of the level of involvement is very helpful in inflammatory disease. Because the penetration of light is limited into the choroid, only the innermost lesions can be imaged.

Retinal Hyperreflective Lesions

Toxoplasmic chorioretinitis on OCT produces a distinctive inner retinal hyperreflectivity that can be helpful diagnostically (Fig. 17.9). Presumably this is due to both the proliferation of tachyzoites and the infiltration of inflammatory cells. This can occur at a stage when the lesion itself is not yet white.[19] Cytoid bodies (cotton-wool patches) also display inner retinal hyperreflectivity, but would ordinarily be distinguishable from toxoplasmic chorioretinitis by other features, such as vitreous inflammation and a feathered appearance of the retinal whitening corresponding to the nerve fiber layer.

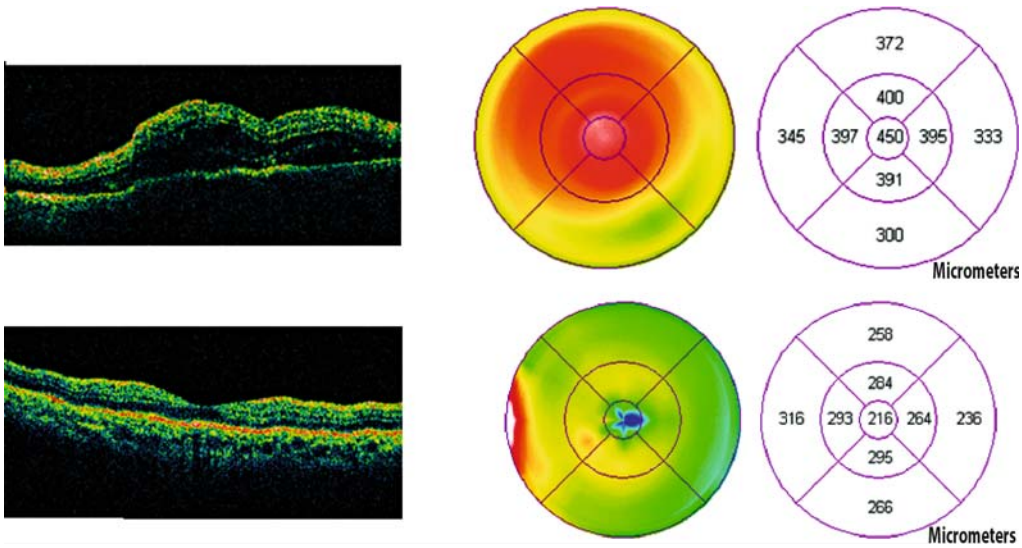

Fig. 17.7. Syphilitic chorioretinitis. The top panel shows an oblique 240-degree OCT scan, retinal map, and retinal thicknesses in the nine concentric zones prior to treatment with penicillin. There is shadowing and hyporeflectivity of the subretinal tissue, which indicates light-blocking exudation in the serous detachment despite its low reflectance. In the bottom panel, after treatment, there is normalization of the retinal thickness and contour, and the subretinal tissues become visible again. Visual acuity had returned to 20/30 at the time that the lower panel scans were taken. This is a left eye. The residual retinal thickening seen on the retinal map in the lower panel relates to residual swelling in the optic nerve. The retinal nerve fiber layer thickening is not apparent in this 240-degree radial scan.

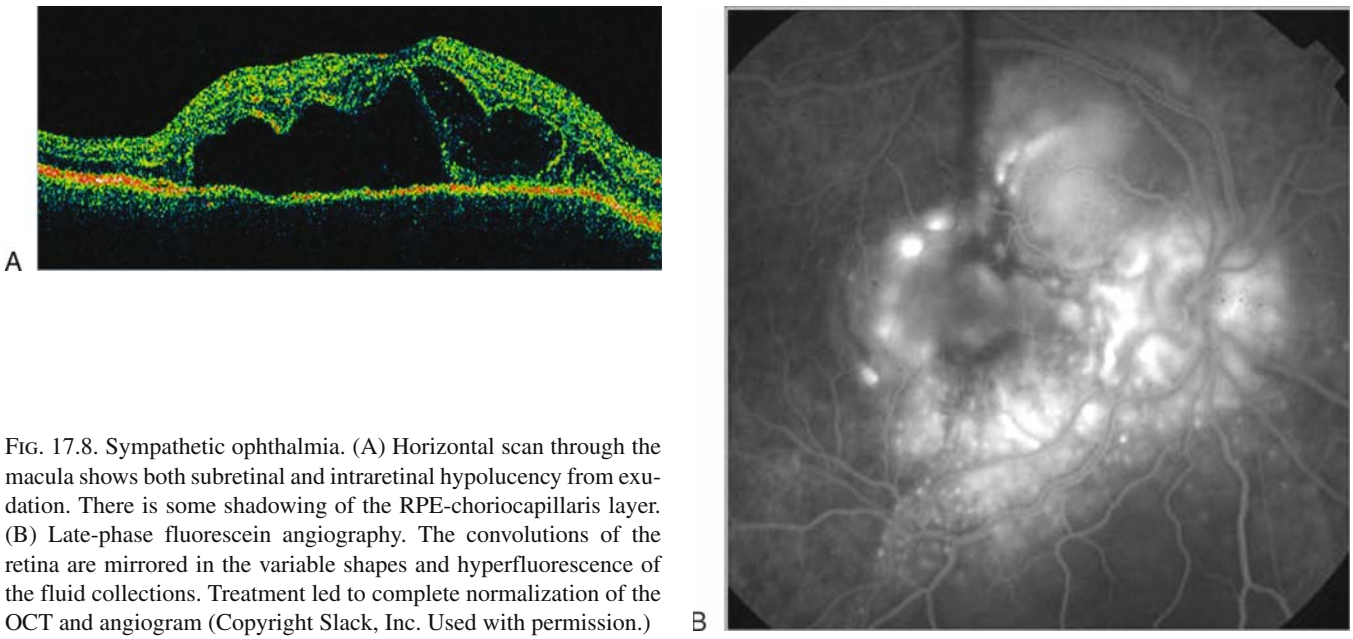

FIG. 17.8. Sympathetic ophthalmia. (A) Horizontal scan through the macula shows both subretinal and intraretinal hypolucency from exudation. There is some shadowing of the RPE-choriocapillaris layer. (B) Late-phase fluorescein angiography. The convolutions of the retina are mirrored in the variable shapes and hyperfluorescence of the fluid collections. Treatment led to complete normalization of the OCT and angiogram (Copyright Slack, Inc. Used with permission.)

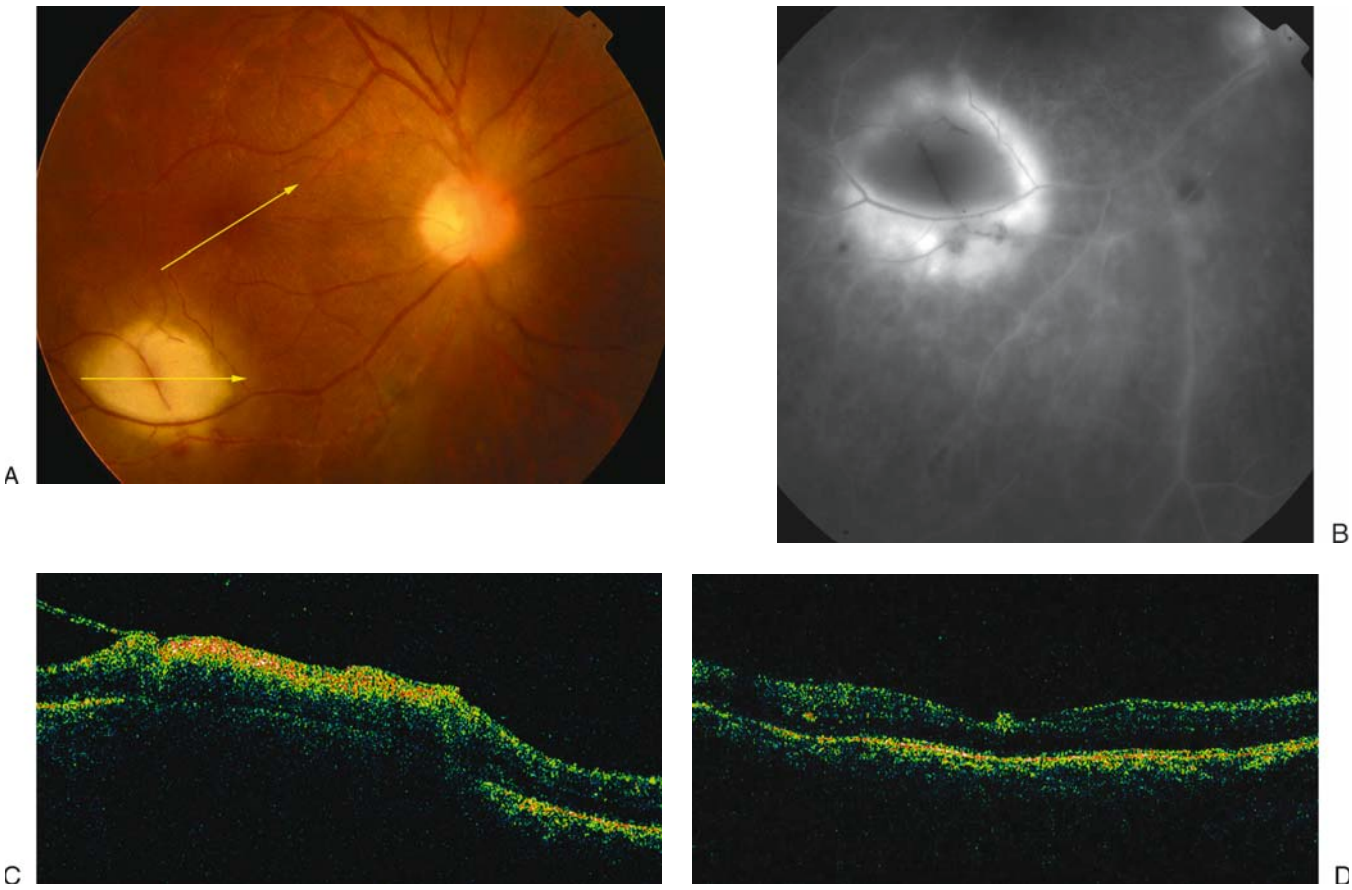

FIG. 17.9. Toxoplasmic chorioretinitis. (A) Fundus photograph of a focal chorioretinitis. There is evidence of retinal vascular inflammation and a few oblique striae are seen in the central macula (arrows). (B) Late-stage angiogram shows the typical hyperfluorescent edge of a toxoplasmic chorioretinitis. There is central hypofluorescence, presumably from cellular and parasitic infiltration. Arterial and venular retinal vascular leakage is prominent. Blockage from a few small hemorrhages is seen. (C) Optical coherence tomography scan through the lesion. There is adherent posterior hyaloid with traction. The inner retina is hyperreflective and there is a secondary hyporeflectance of the underlying RPE choroidal layer. The retina overall is mildly thickening. Adjacent to the lesion itself, retinal thickening is also seen, probably corresponding to the leakage noted on the late-stage angiogram. (D) Optical coherence tomography scan through the center of the macula. The poor quality of the scan and the multiple punctate vitreous reflexes are due to vitreous inflammatory debris. Shadowing of the retina on the left side of the scan indicates blockage of the scanning laser by a denser vitreous opacity. The hyperreflective opacities in the foveal depression and under the retina are of uncertain significance; they probably represent inflammatory deposits.

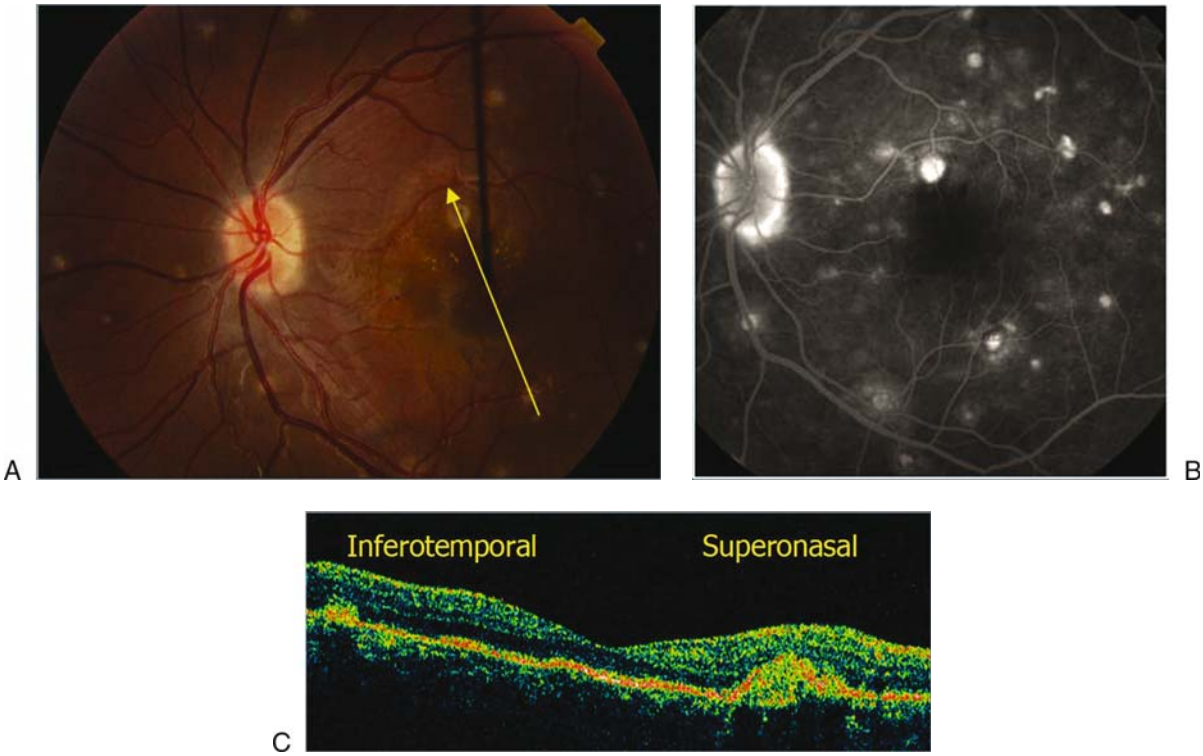

FIG. 17.10. Multifocal choroiditis. (A) Color photograph show multiple subretinal lesions. There is exudate surrounding the large superioring lesion, as well as tiny flecks of blood. (B) Fluorescein angiogram shows multiple window defects. There are two lesions with halos of blocked fluorescence, the larger of which is surrounded by exudates and hemorrhage. Both are suspicious for choroidal neovascularization with increasing staining during the angiogram and questionable leakage. (C) Optical coherence tomography scan corresponding to the directional line in Figure 17.10A (arrow). Both lesions are seen to involve the inner choroid and to cause anterior protrusion of the RPE-choriocapillaris layer. They block underlying reflections. There is no invasion into the subretinal space and no subretinal fluid. Treatment with corticosteroids rather than laser was selected in this 10-year-old girl. The lesions healed and definite neovascularization was not confirmed (Copyright Slack, Inc. Used with permission.)

Choroidal Hyperreflective Lesions

Multifocal choroiditis produces very distinctive inner choroidal lesions that are hyperreflective (Fig. 17.10). A major clinical dilemma is determining whether secondary choroidal neovascularization is present in fresh, elevated lesions. Optical coherence tomography is useful in imaging subretinal extension of the lesions and fluid collections, both of which would be suggestive of neovascularization that might require laser photocoagulation.

Conclusion

Optical coherence tomography imaging of inflammatory lesions provides additional information that can be correlated with clinical examination and angiographic findings to improve diagnosis and treatment. Its exact role in the management of uveitic diseases remains to be defined. It is anticipated that more clinical studies of OCT will be done in specific uveitic entities in the future and that interpretive criteria will be further refined.

References

1. Huang D, Swanson EA, Lin CP, et al. Optical coherence tomography. Science 1991;254:1178–1181.
2. Schuman JS, Hee MR, Arya AV, et al. Optical coherence tomography: a new tool for glaucoma diagnosis. Curr Opin Ophthalmol 1995;6:89–95.
3. Hee MR, Puliafito CA, Wong C, et al. Quantitative assessment of macular edema with optical coherence tomography. Arch Ophthalmol 1995;113:1019–1029.
4. Hee MR, Puliafito CA, Duker JS, et al. Topography of diabetic macular edema with optical coherence tomography. Ophthalmology 1998;105:360–370.
5. Hee MR, Izatt JA, Swanson EA, et al. Optical coherence tomography of the human retina. Arch Ophthalmol 1995;113:325–332.
6. Fujimoto JG. Principles of optical coherent tomography. In: Schuman JS, Puliafito CA, Fujimoto JG, eds. Optical Coherent Tomography in Ocular Diseases. Thorofare, NJ: Slack, 2004.
7. Jaffe GJ, Caprioli J. Optical coherence tomography to detect and manage retinal disease and glaucoma. Am J Ophthalmol 2004;137:156–169.
8. Thomas D, Duguid G. Optical coherence tomography—a review of the principles and contemporary uses in retinal investigation. Eye 2004;18:561–570.

9. Drexler W, Morgner U, Ghanta RK, Kartner FX, Schuman JS, Fujimoto JG. Ultrahigh-resolution ophthalmic optical coherence tomography. Nat Med 2001;7:502–507.
10. Schuman JS, Hee MR, Puliafito CA, et al. Quantification of nerve fiber layer thickness in normal and glaucomatous eyes using optical coherence tomography. Arch Ophthalmol 1995;113: 586–596.
11. Schuman JS, Pedut-Kloizman T, Hertzmark E, et al. Reproducibility of nerve fiber layer thickness measurements using optical coherence tomography. Ophthalmology 1996;103:1889–1898.
12. Yamamoto S, Yamamoto T, Hayashi M, Takeuchi S. Morphological and functional analyses of diabetic macular edema by optical coherence tomography and multifocal electroretinograms. Graefes Arch Clin Exp Ophthalmol 2001;239:96–101.
13. Yang CS, Cheng CY, Lee FL, Hsu WM, Liu JH. Quantitative assessment of retinal thickness in diabetic patients with and without clinically significant macular edema using optical coherence tomography. Acta Ophthalmol Scand 2001;79: 266–270.
14. Markomichelakis NN, Halkiadakis I, Pantelia E, et al. Patterns of macular edema in patients with uveitis: qualitative and quantitative assessment using optical coherence tomography. Ophthalmology 2004;111:946–953.
15. Reinthal EK, Volker M, Freudenthaler N, Grub M, Zierhut M, Schlote T. [Optical coherence tomography in the diagnosis and follow-up of patients with uveitic macular edema]. Ophthalmologe 2004;101:1181–1188.
16. Hee MR, Baumal CR, Puliafito CA, et al. Optical coherence tomography of age-related macular degeneration and choroidal neovascularization. Ophthalmology 1996;103:1260–1270.
17. Puliafito CA, Hee MR, Lin CP, et al. Imaging of macular diseases with optical coherence tomography. Ophthalmology 1995;102:217–229.
18. Maruyama Y, Kishi S. Tomographic features of serous retinal detachment in Vogt-Koyanagi-Harada syndrome. Ophthalmic Surg Lasers Imaging 2004;35:239–242.
19. Lieb DF, Scott, IU, Flynn HW, Davis JL, Demming SM. Acute acquired toxoplasma retinitis may present similarly to unilateral acute idiopathic maculopathy. Am J Ophthalmol 2004;137:940–942.

18
Clinical Applications of Optical Coherence Tomography in Glaucoma

Daniel Krivoy, Noga Harizman, Celso Tello, and Jeffrey Liebmann

Glaucomatous optic neuropathy is characterized by specific structural and functional changes that result from the loss of retinal ganglion cells and their corresponding axons.[1,2] These structural changes are evidenced clinically by thinning of the neuroretinal rim and have traditionally been evaluated by direct clinical observation of the optic disc and surrounding area, aided by stereoscopic photographs of the optic disc and photographs of the nerve fiber layer. It has been reported that structural changes precede the functional abnormalities detectable through standard automated achromatic perimetry.[3,4] Studies have also shown that there is significant variability in the appearance of the optic disc among individuals[5–7] and that important variability exists in its assessment among different observers.[8–10]

Optical coherence tomography (OCT) enhances our ability to diagnose glaucoma and its progression by generating more objective information about the ocular structures involved in the glaucomatous process. It provides imaging of the optic disc, peripapillary, and macular areas, and generates reproducible measurements of the nerve fiber layer,[11,12] retinal thickness,[13,14] as well as topographic measurements of the optic nerve head (ONH). Topographic measurements of the optic nerve head have been shown to be comparable to other imaging technologies.[15] Studies have shown that OCT has the ability to discriminate glaucomatous from healthy eyes.[16–18]

The current OCT, which is characterized by increased scan rate and image resolutions up to 8 to 10 μm, offers different options for image acquisition and analysis used in glaucoma, which include retinal nerve fiber layer (RNFL), macular and ONH scans, and ONH analysis.

Retinal Nerve Fiber Layer Scans

Cross-sectional images of the peripapillary retina are obtained through a circular scan centered on the optic nerve head with a diameter of 3.4 mm using the standard and fast RNFL protocols (Fig. 18.1).

The standard RNFL scans consist of 512 A-scan measurements along the circular scan. Fast RNFL instead obtains 256 A-scan measurements along the same circular scan (Fig. 18.2). The thickness of the RNFL is calculated automatically by the software through an algorithm that determines its inner and outer limits based on the intensity of reflectivity (white lines on the OCT image).

A normative database of age-matched peripapillary retinal nerve fiber layer thickness incorporated into the software[19] enhances the ability of OCT to differentiate between glaucomatous and nonglaucomatous eyes (Fig. 18.3).[20] The software generates a classification using its database to indicate nerve fiber layer values that are within normal limits (within 95% confidence interval for the healthy age-matched population), borderline (between 95% and 99% confidence interval) or abnormal (lower than 99% confidence interval). In addition, the data from the two eyes is superimposed in one graph to enhance our ability to detect asymmetries between them.

The average RNFL thickness is calculated for the four quadrants (temporal, superior, nasal, and inferior) and for the 12 clock hours. The average thickness, the superior maximum (Smax), and inferior maximum (Imax) values are displayed along with parameters based on their relationship.

Optic Nerve Head Scans

Optic nerve head and macular scans are composed of six linear scans in a spoke pattern separated by 30-degree intervals centered on the ONH (Fig. 18.4).

In this protocol, the disc margin is detected automatically by the software through delineating the end of the backscattering signal thought to correspond to the retinal pigment epithelium and choriocapillaris, although it can be manually altered to increase its accuracy. A parallel line 150 μm anterior to it is used to define the cup (area below) and the neuroretinal rim (area above) (Fig. 18.5).

Based on the data obtained from individual radial scans, the vertically integrated rim area reflects the total volume of rim tissue. It is calculated by multiplying the average of individual rim areas by the circumference of the disc. The horizontally integrated rim width reflects the total rim area and is

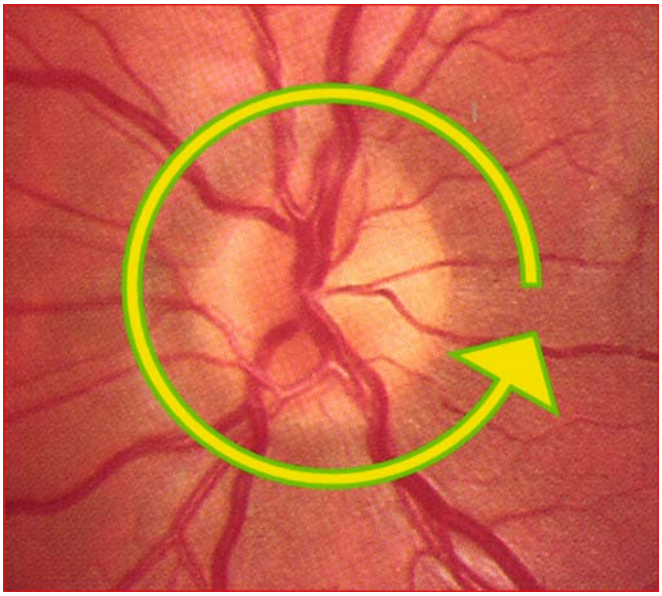

Fig. 18.1. Cross-sectional images of the peripapillary retina are obtained through a circular scan centered on the optic nerve head with a diameter of 3.4 mm. The image illustrates the location and direction of the peripapillary scan.

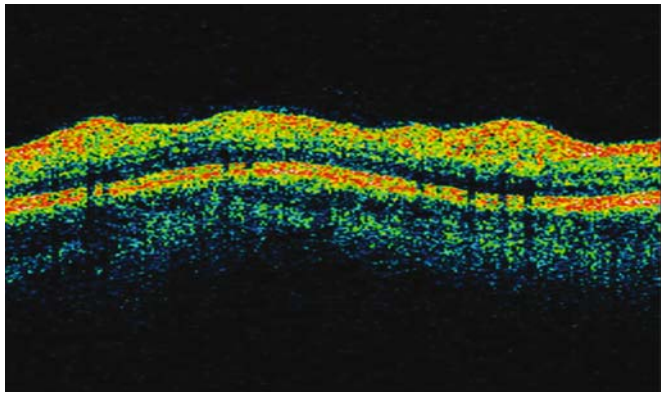

Fig. 18.2. The image of the peripapillary retina obtained by optical coherence tomography (OCT). It is composed of a series of A-scan measurements along the circular scan.

calculated by multiplying the average of the individual rim widths by the circumference of the disc. In addition the disc area, cup area, rim area, cup/disc area ratio, and horizontal and vertical cup/disc ratios are displayed.

Macular Thickness Scans

Macular thickness scans have a complementary role in the diagnosis and management of glaucoma. Ganglion cells are thought to constitute between 30% and 35% of the total retinal thickness at the macular area. The loss of ganglion cells in glaucoma has been demonstrated experimentally.[21,22] Clinically, measuring the changes in macular thickness may prove to be of value in the assessment of glaucoma,[23] and the role of OCT has been investigated.[24]

The macular thickness protocols, explained in detail elsewhere in this book, generate data based on six radial scans in a spoke pattern centered on the fovea, each separated by 30-degree intervals (Fig. 18.6). The data are interpolated to fill the missing areas. The retinal thickness is calculated automatically after delineating the vitreoretinal interface and the change in reflectivity that occurs above the retinal pigment epithelium corresponding to the junction of inner and outer segments of the photoreceptors.

Case 1: Normal

A healthy 69-year-old woman without contributory medical, ocular, or family history presented for routine evaluation. Her corrected visual acuity was 20/20 in each eye, intraocular pressures were 18 mm Hg in each eye, and she had a normal ophthalmologic examination. Examination of her optic nerves (Fig. 18.7A, B) revealed sharp disc margins with healthy, pink neuroretinal rims with a cup-to-disc ratio of 0.2. Humphrey achromatic automated perimetry was reliable and full in both eyes (Fig. 18.7C, D).

Fast RNFL scan displays symmetric RNFL thickness in both eyes that is within normal limits for her age; this is indicated by the green background present on the displayed parameters (Fig. 18.8). The RNFL thickness follows the normal pattern, being thicker superotemporally and inferotemporally with minimal asymmetry between the two eyes.

Optic nerve head analysis (Fig. 18.9) shows the delineation of the disc and cup areas on the right of the display. The cross-sectional scan is seen on the left of the display. A healthy and symmetric neuroretinal rim can be appreciated throughout all clock hours of her optic discs. Normal optic nerve head analysis parameters such as the vertical integrated rim area and horizontal integrated rim width are displayed as well as individual radial scan parameters. Analysis of her macular scans (Fig. 18.10) display normal retinal thickness values and patterns on both eyes. This is illustrated by the green background on the tabular output.

Case 2: Unilateral Exfoliation

A 64-year-old woman was diagnosed with unilateral exfoliative glaucoma in her right eye. She presented with intraocular pressures of 33 mm Hg in her right eye and 18 mm Hg in her left eye. Findings on slit-lamp examination were consistent with her diagnosis. Funduscopic examination revealed marked thinning of the neuroretinal rim in her right eye throughout the superior, temporal, and inferior aspects of the disc. This is in contrast to the healthy-appearing optic disc on her left eye (Fig. 18.11A, B). The Humphrey visual field of her right

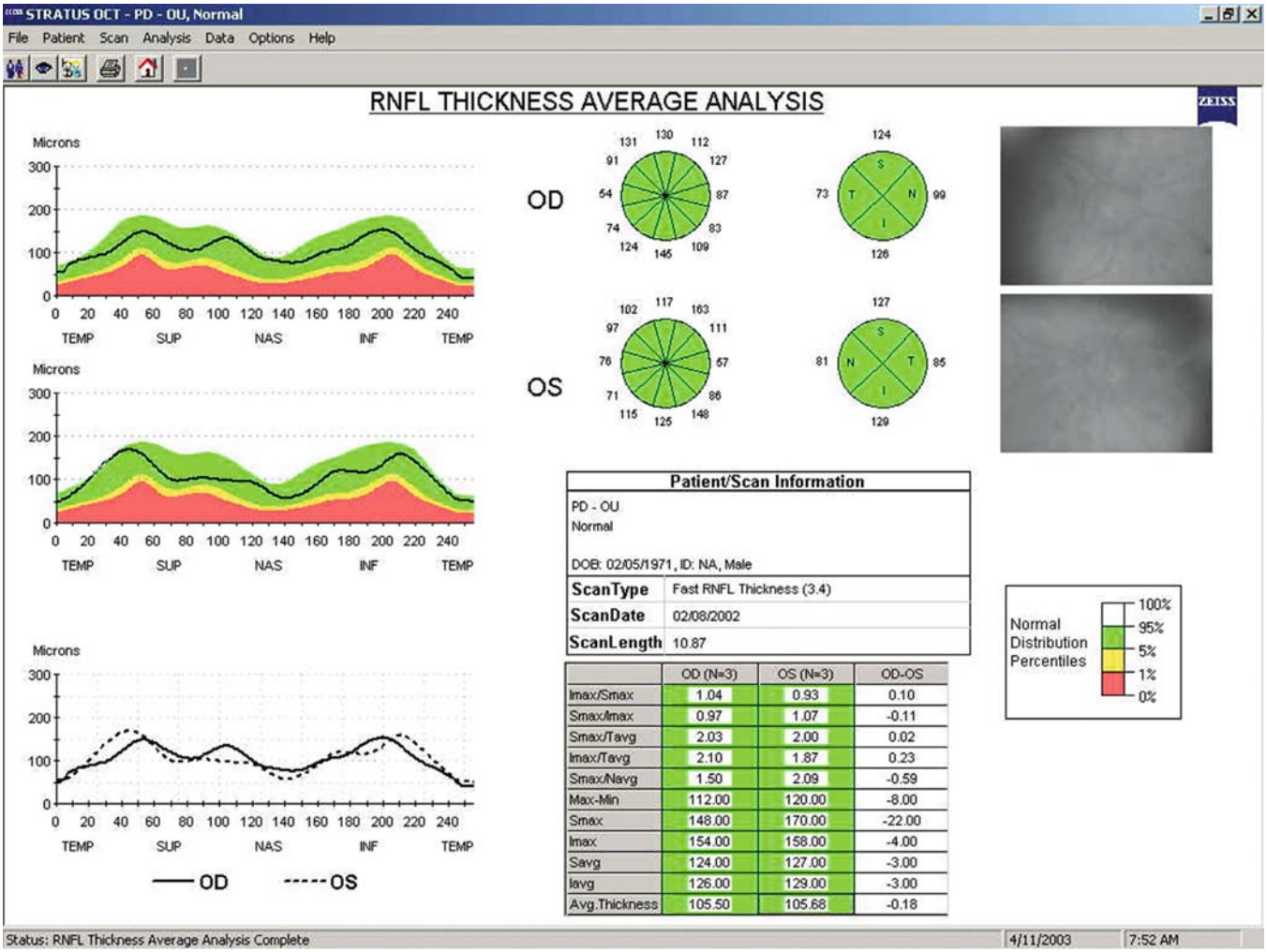

FIG. 18.3. The retinal thickness average analysis displays the data generated by the software using its normative database. It is used to classify the nerve fiber layer thickness values based on their statistical significance as normal, borderline, or abnormal. In addition, the data from the two eyes are superimposed in one graph to enhance our ability to detect asymmetries between them.

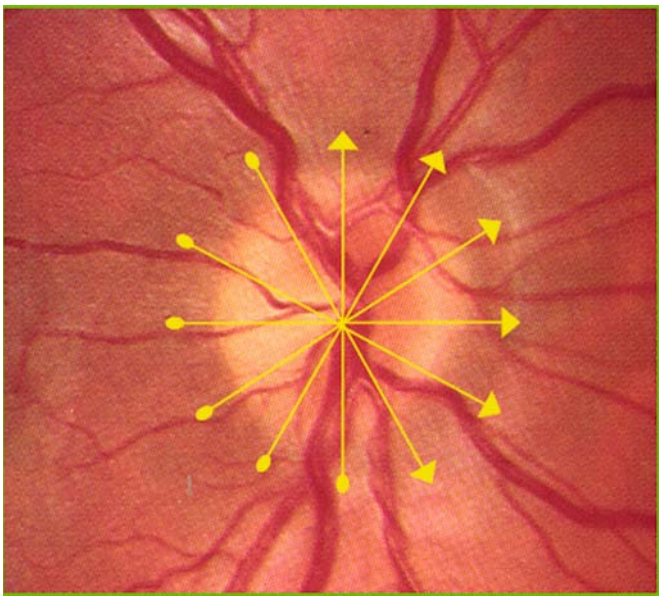

FIG. 18.4. Optic nerve head scans are composed of six linear scans in a spoke pattern separated by 30-degree intervals centered on the optic nerve head (ONH). The data are used for the optic nerve head analysis.

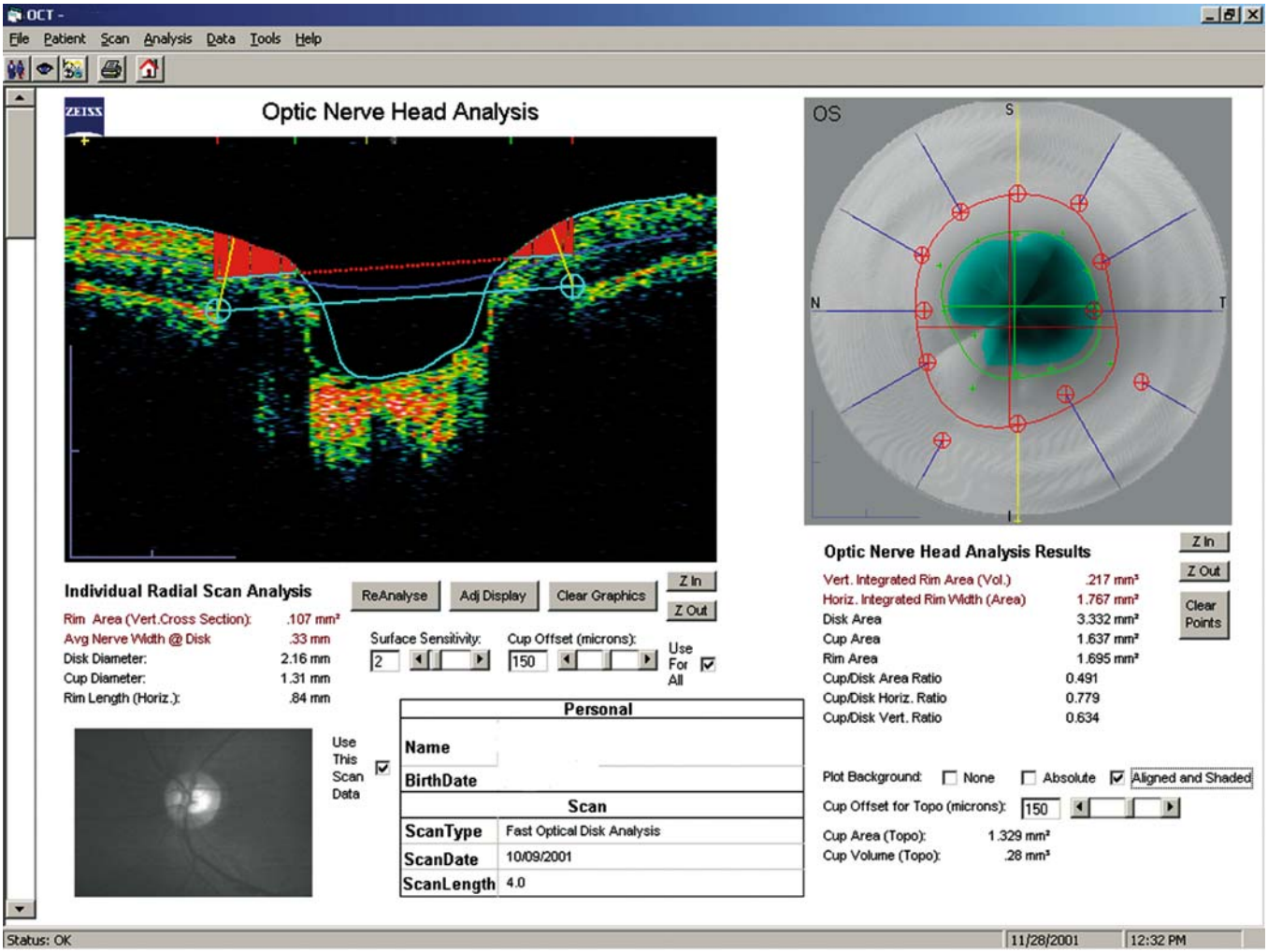

FIG. 18.5. Optic nerve head analysis screen. In this protocol, the disc margin is detected automatically by the software. A parallel line 150 μm anterior to it is used to define the cup (area below) and the neuroretinal rim (area above).

eye shows classic glaucomatous abnormality with a decrease in mean deviation (MD) and an inferior arcuate scotoma (Fig. 18.11C); her left visual field was normal (Fig. 18.11D). On her RNFL thickness average analysis (Fig. 18.12), the plotted RNFL graph of the right eye shows marked statistically significant thinning at the superior and inferior poles of the disc. This finding is highlighted by the clock-hour analysis to the right of the graph. The RNFL of the left optic nerve head falls within the statistically normal values. The superimposed plots at the bottom left of the display enhances our ability to detect asymmetries between the RNFL of the optic nerves. In her case the RNFL thickness is clearly reduced when compared to the left. The absolute values of the maximum superior (S_{max}) and inferior (I_{max}) RNFL thickness as well as their average thickness (S_{avg} and I_{avg}) are abnormally thin and their statistical significance is highlighted by the red background.

Case 3: Suspicious for Glaucoma

A 62-year-old woman was referred as being suspicious for glaucoma based on large cup-to-disc ratio in both eyes and a family history of glaucoma. She had normal intraocular pressures and an otherwise unremarkable ophthalmic examination. Her optic discs showed a large cup-to-disc ratio (Fig. 18.13A), although achromatic Humphrey visual fields and Humphrey frequency doubling technology perimetry (FDT) were normal (Fig. 18.13B, C).

In spite of the glaucomatous appearance of the optic nerve, analysis of the RNFL scan evidences normal thickness values throughout all clock hours (Fig. 18.14). Given the variability of normal optic nerve head sizes and shapes, OCT proves to be a valuable tool in the assessment of the peripapillary

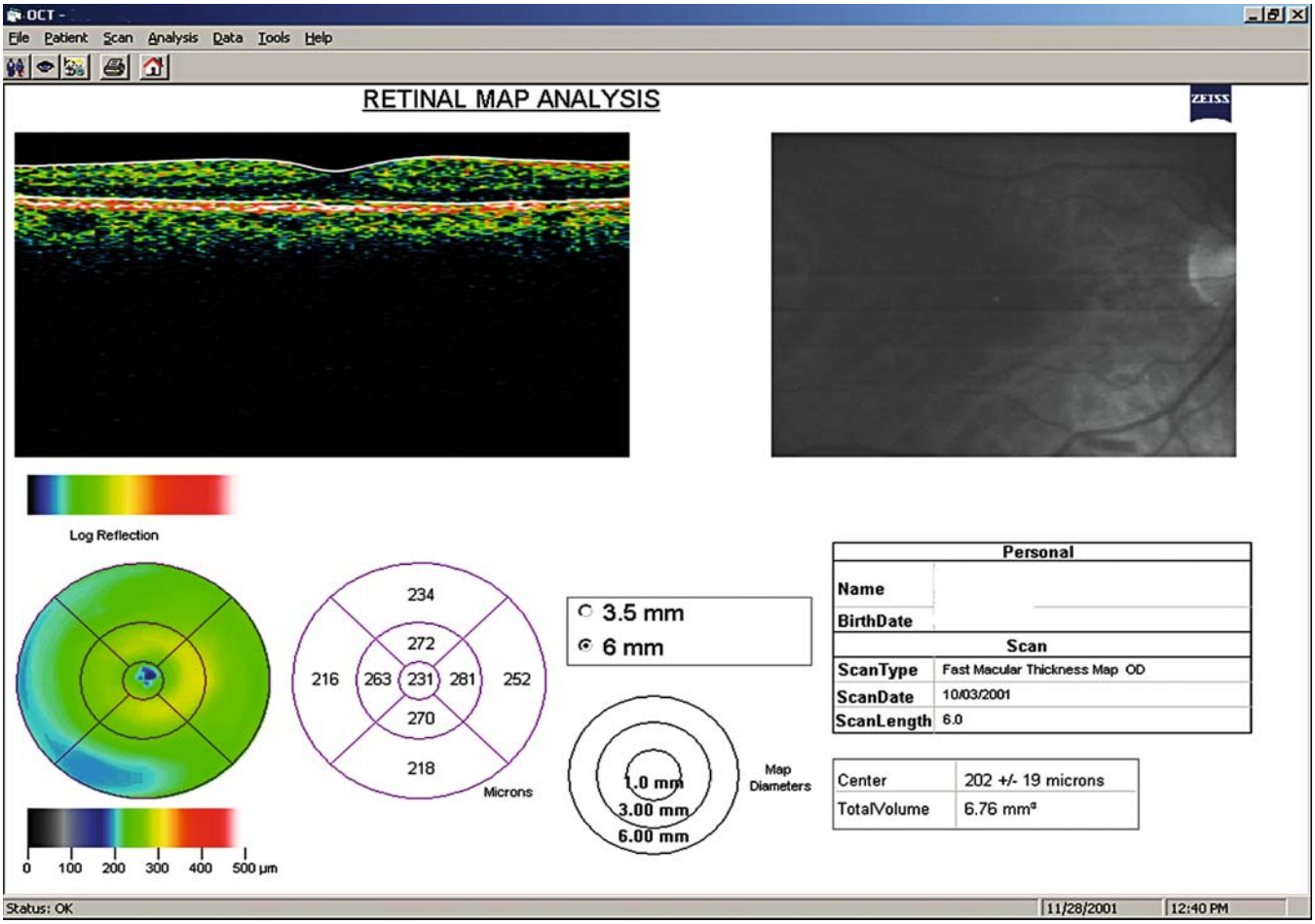

FIG. 18.6. Macular thickness analysis screen. The macular thickness protocols generate data based on six radial scans in a spoke pattern centered on the fovea. The retinal thickness is calculated automatically.

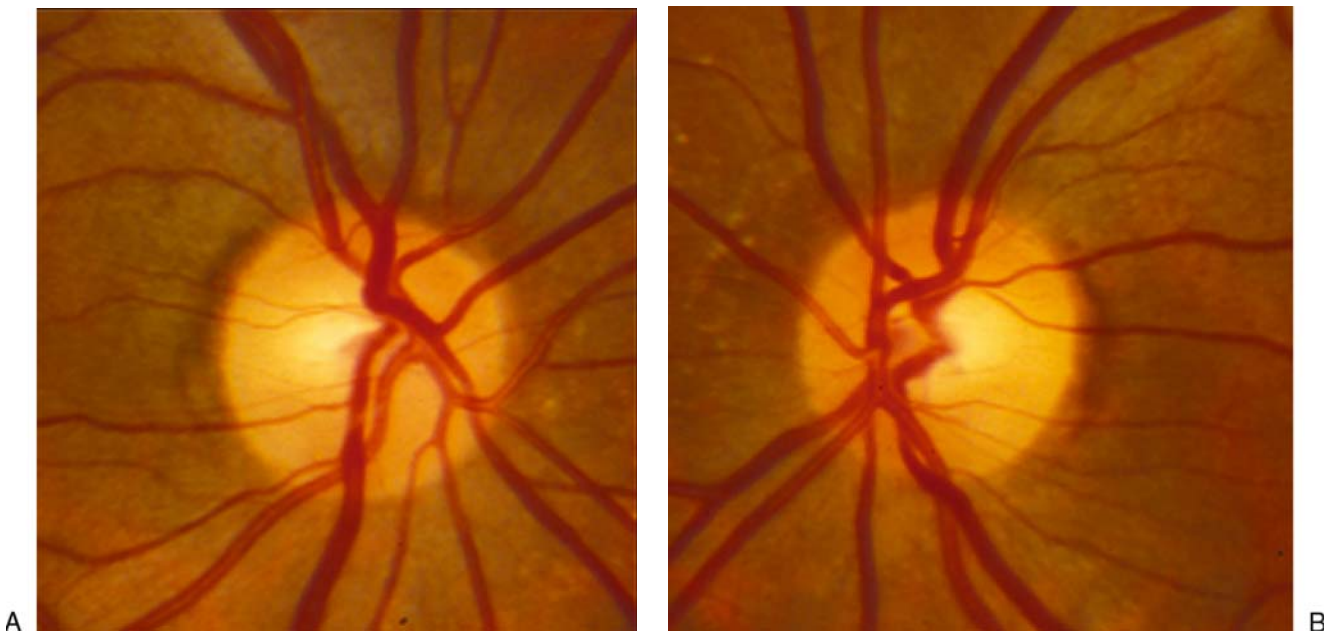

FIG. 18.7. Disc photographs and visual fields of 69-year-old woman without evidence of glaucomatous optic neuropathy.

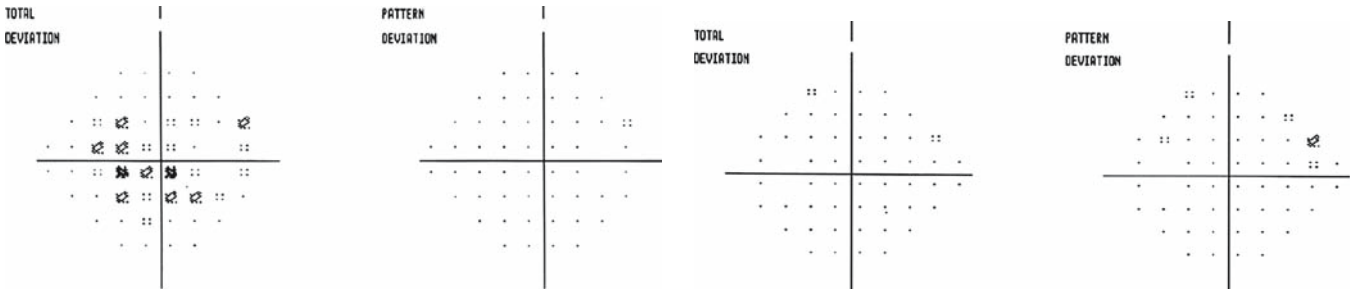

FIG. 18.7. (continued).

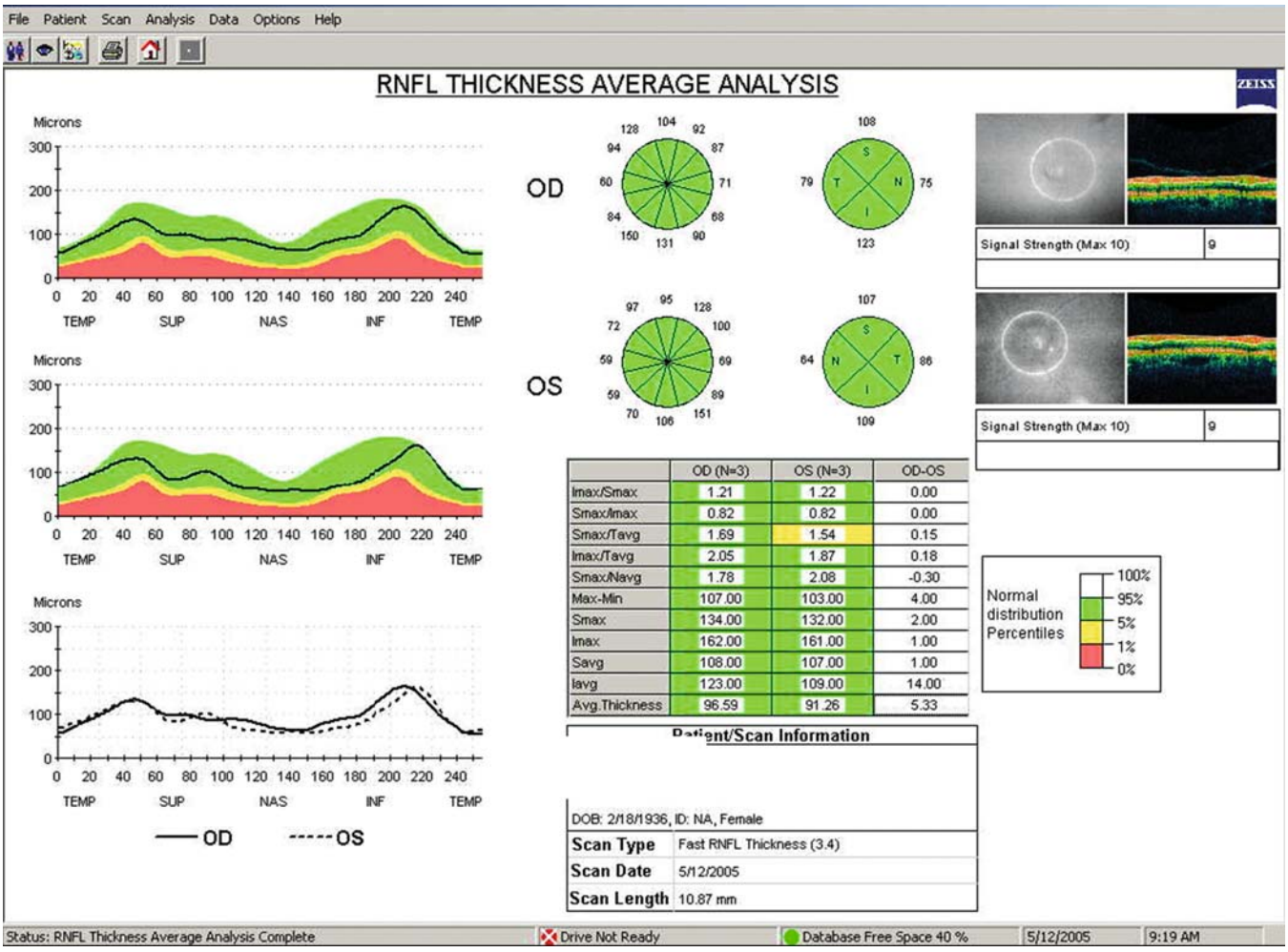

FIG. 18.8. Retinal thickness average analysis screen. The fast retinal nerve fiber layer (RNFL) scan displays symmetric RNFL thickness in both eyes within normal limits for the patient's age. The RNFL thickness follows the normal pattern with minimal asymmetry between the two eyes.

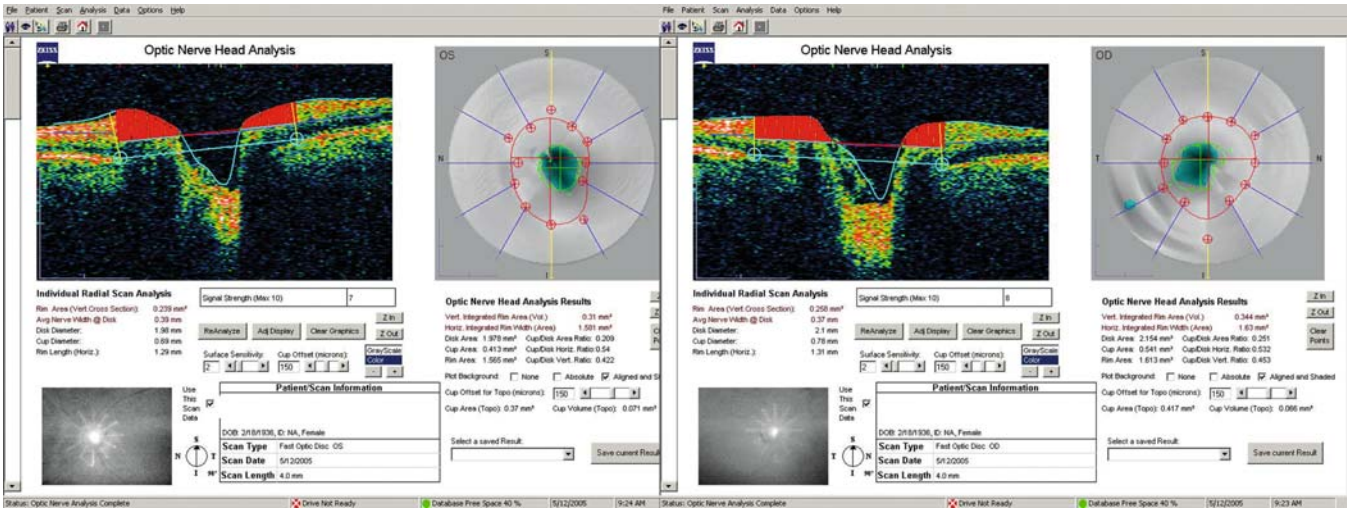

FIG. 18.9. Optic nerve head analysis screen. The delineation of the disc and cup areas is shown on the right of the display. The cross-sectional scan is seen on the left. A healthy and symmetric neuroretinal rim can be appreciated throughout all clock hours of the patient's optic discs.

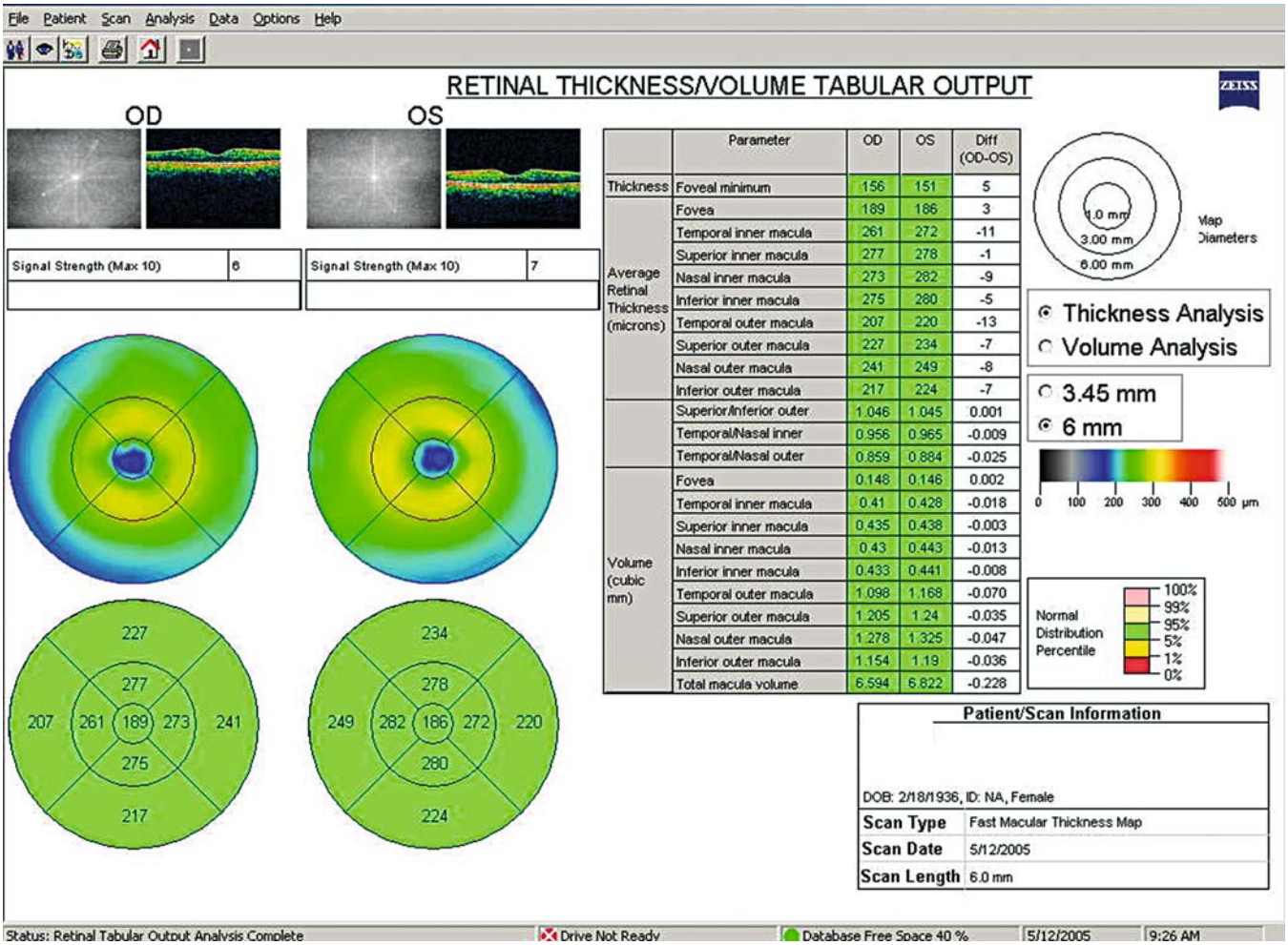

FIG. 18.10. Retinal thickness volume/tabular output. Analysis of the patient's macular scans shows normal retinal thickness values and patterns on both eyes, illustrated by the green background on the tabular output.

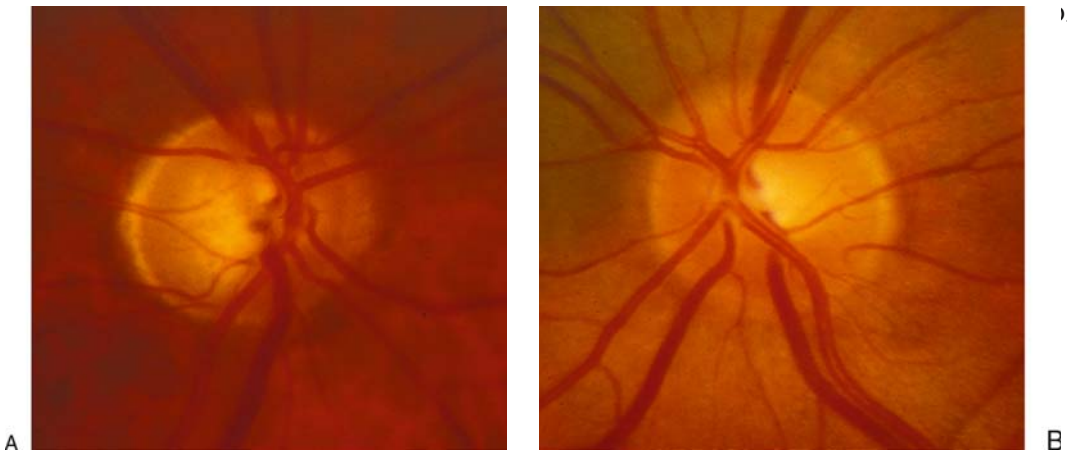

FIG. 18.11. Disc photos and visual field of a patient with unilateral exfoliative glaucoma of her right eye. Loss of neuroretinal rim with marked thinning at the poles and the corresponding visual field display a classic arcuate scotoma on her right eye.

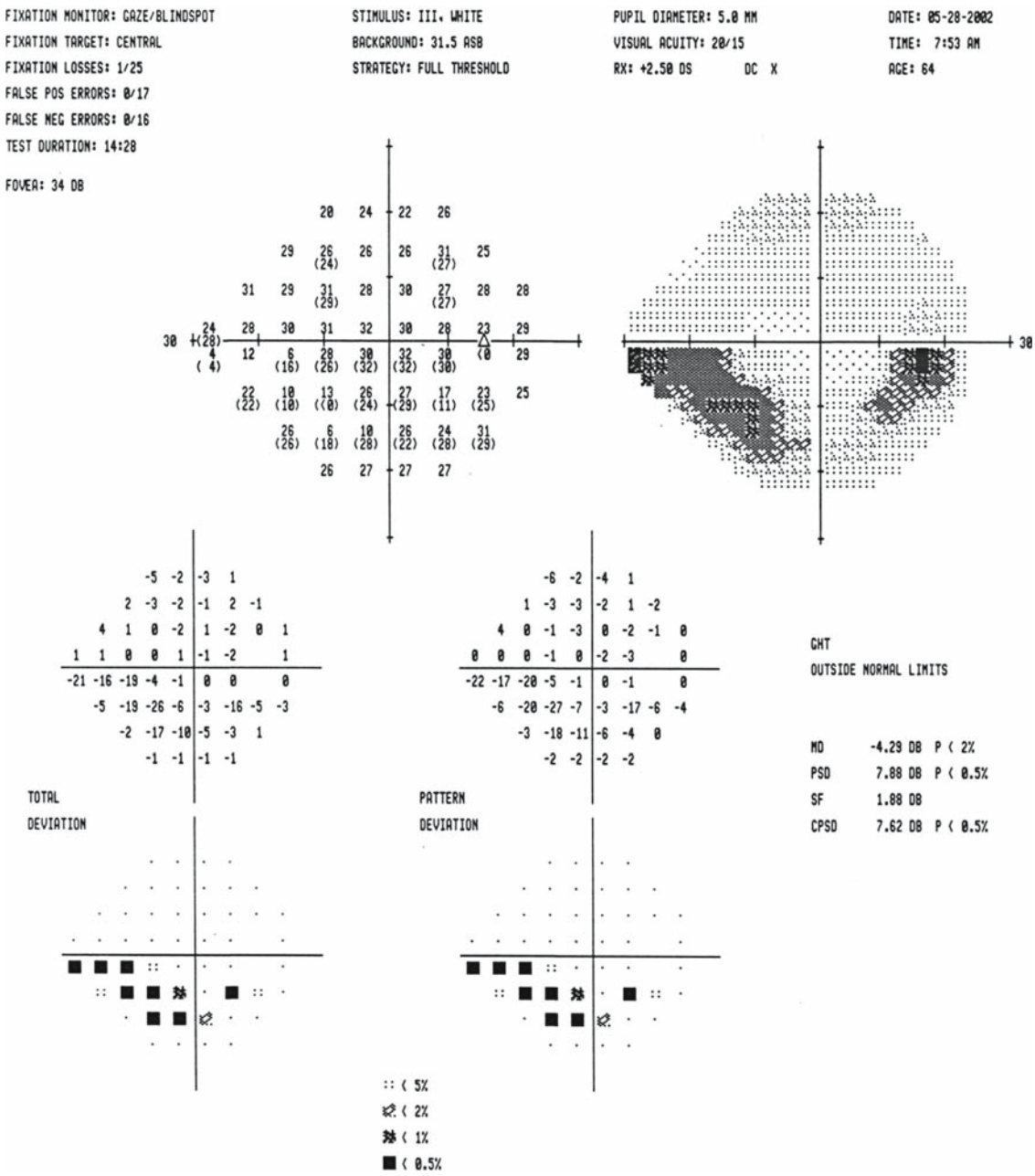

FIG. 18.11. (continued).

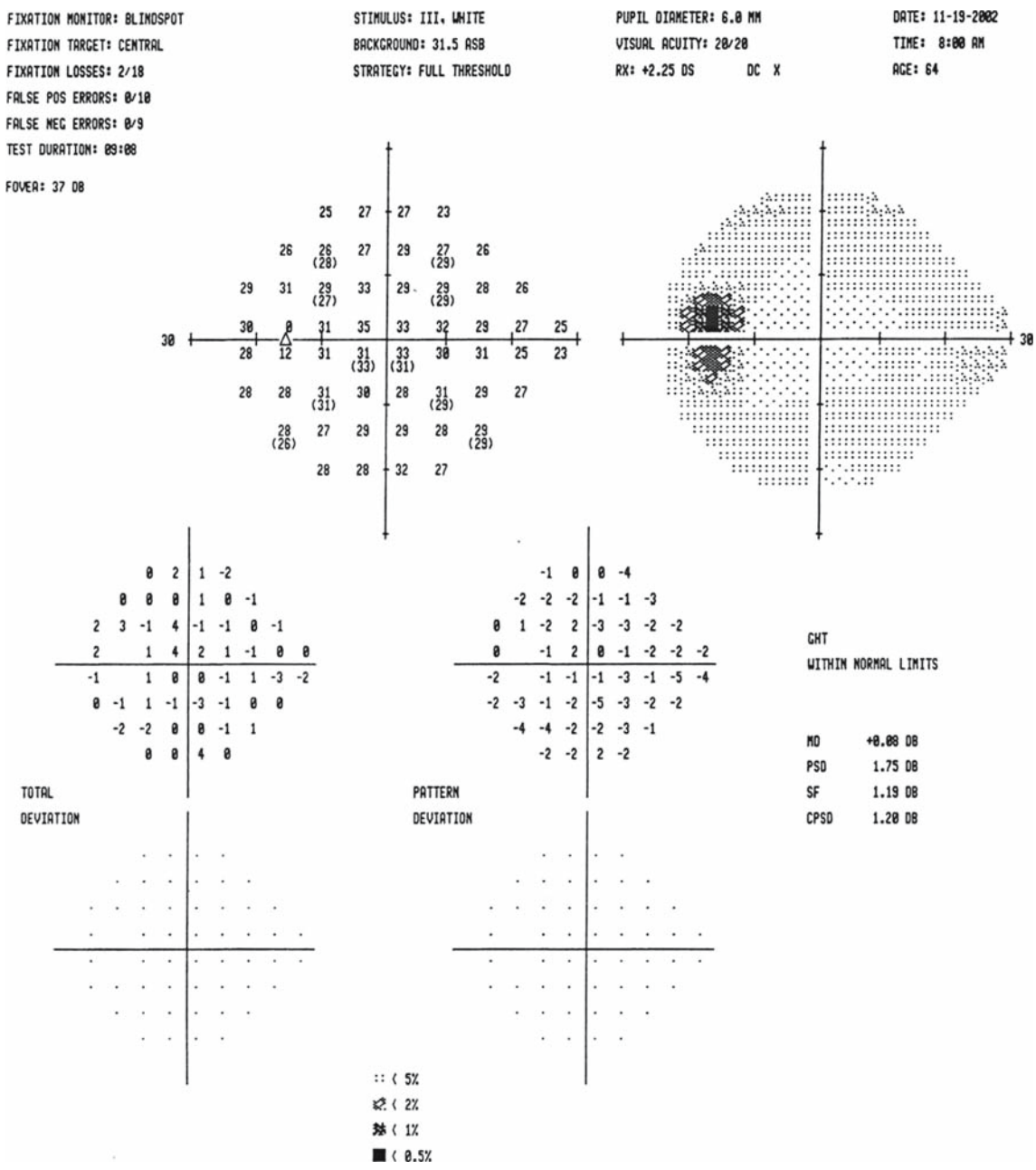

FIG. 18.11. (continued).

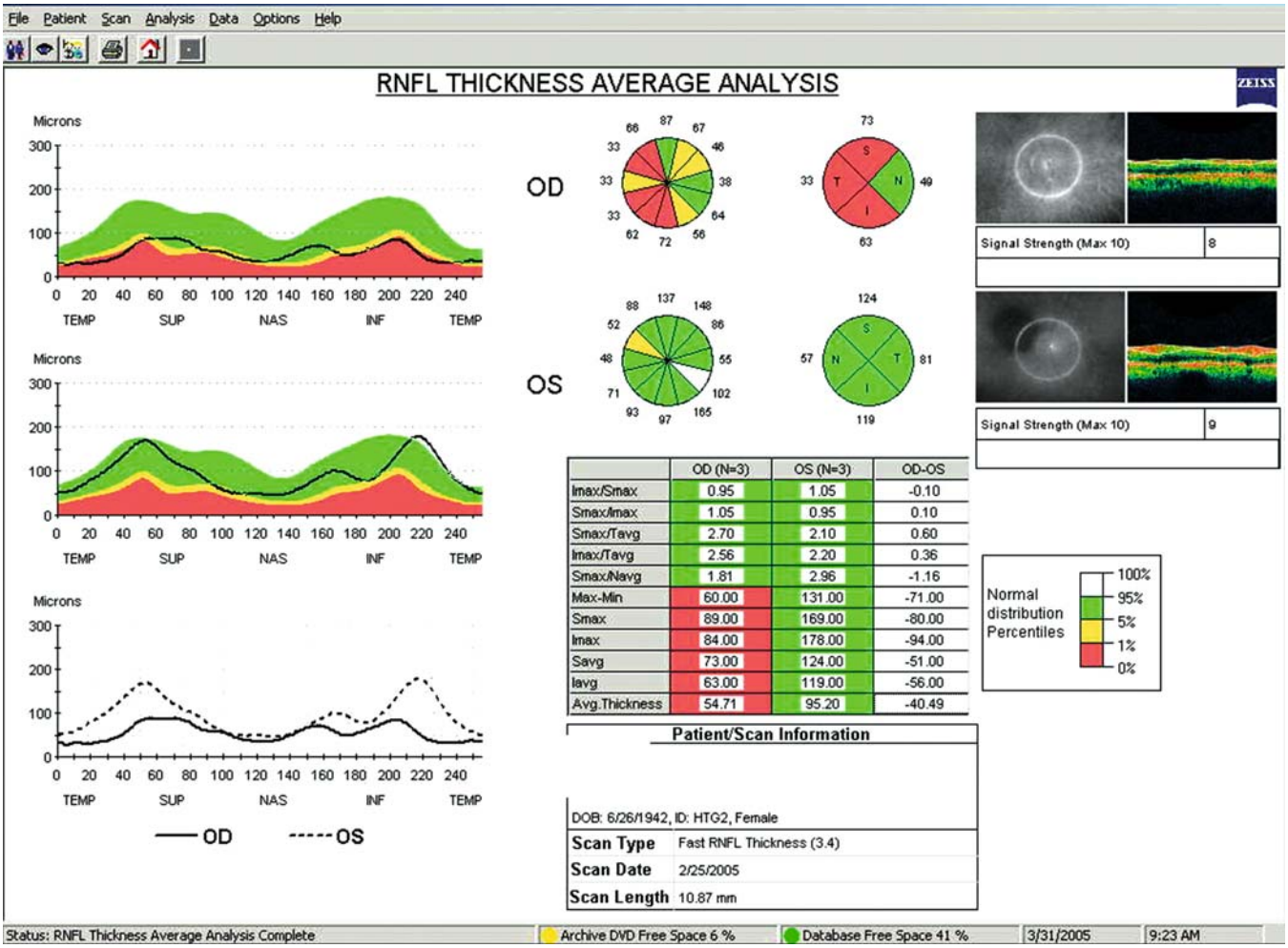

FIG. 18.12. The RNFL thickness average analysis screen. The plotted RNFL graph of the right eye shows marked statistically significant thinning at the superior and inferior poles of the disc. This finding is highlighted by the clock-hour analysis to the right of the graph.

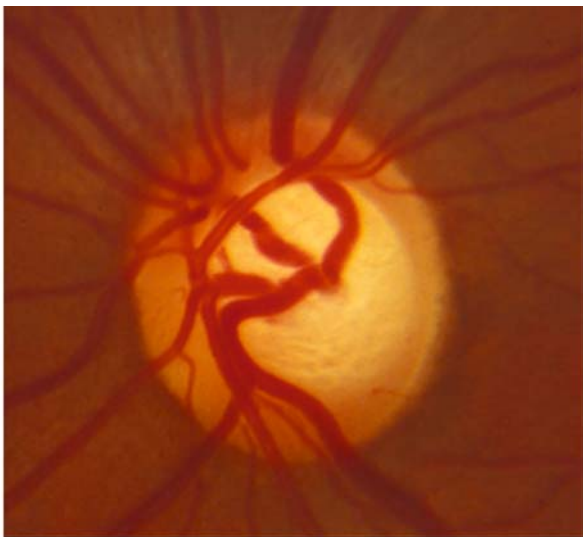

A

FIG. 18.13. A 62 year-old woman was referred as being suspicious for glaucoma based on a large cup-to-disc ratio in both eyes and a family history of glaucoma. Her optic discs showed a large cup-to-disc ratio, although achromatic Humphrey visual fields and the FDT were normal.

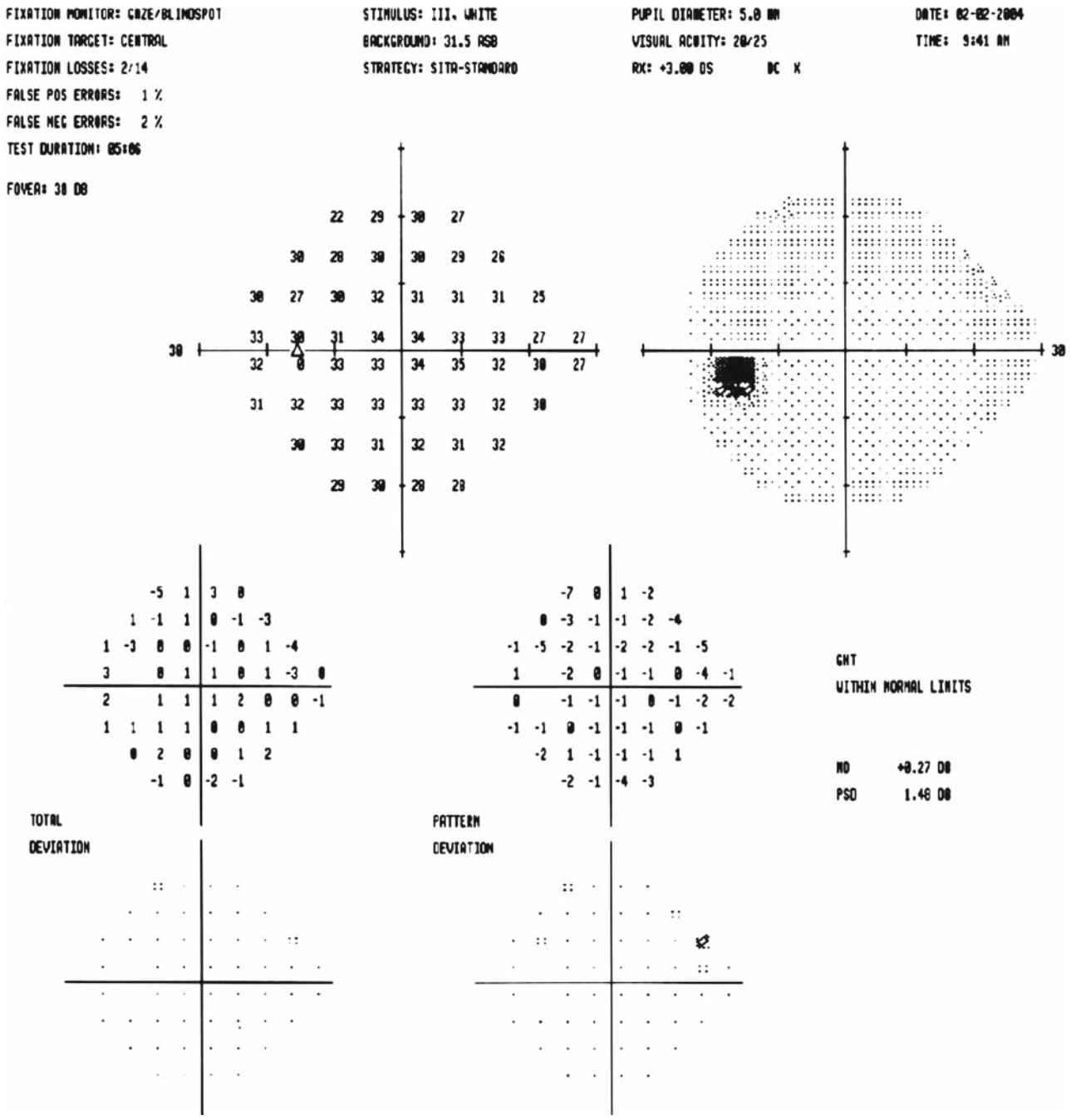

FIG. 18.13. (continued).

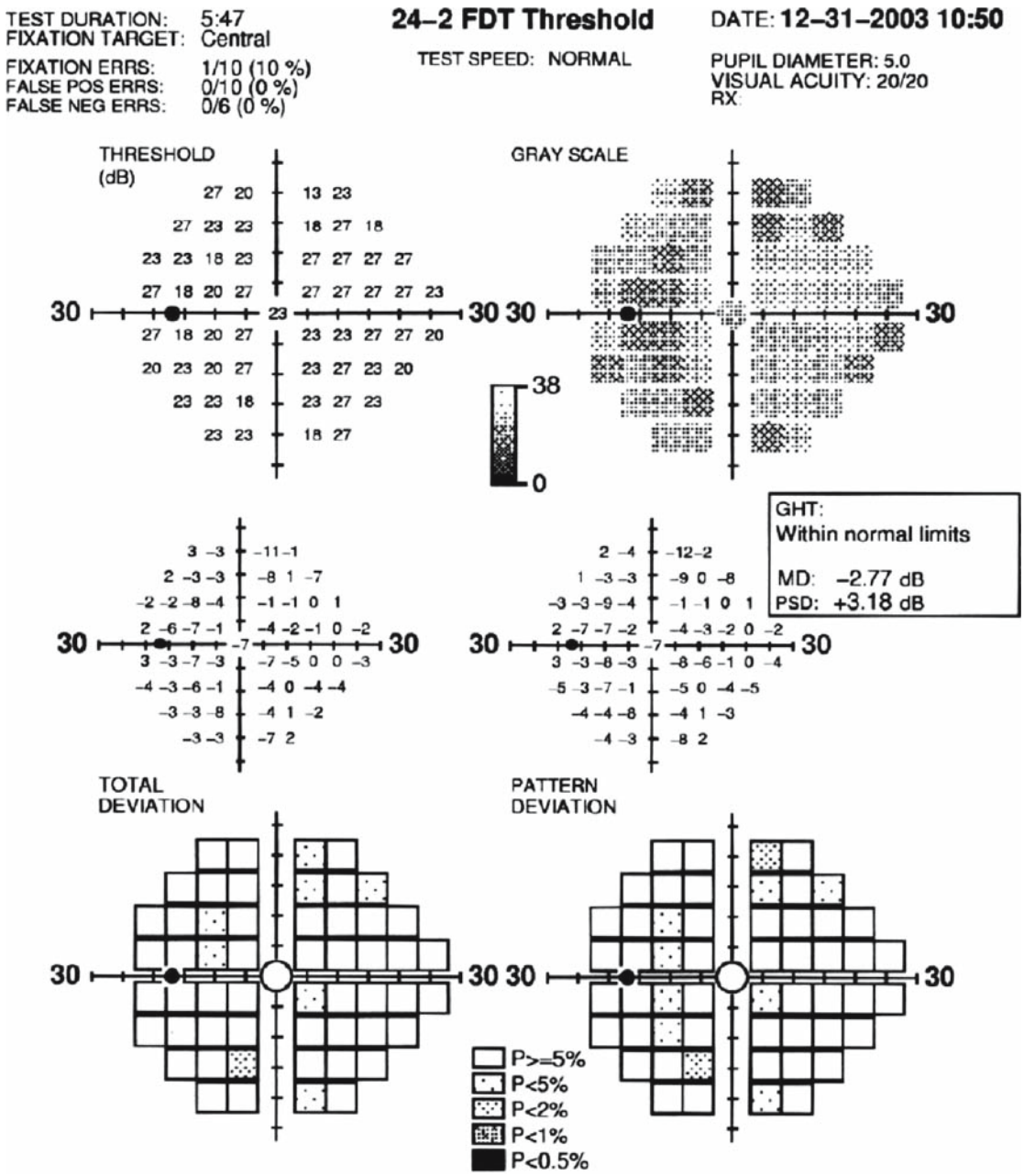

FIG. 18.13. (continued).

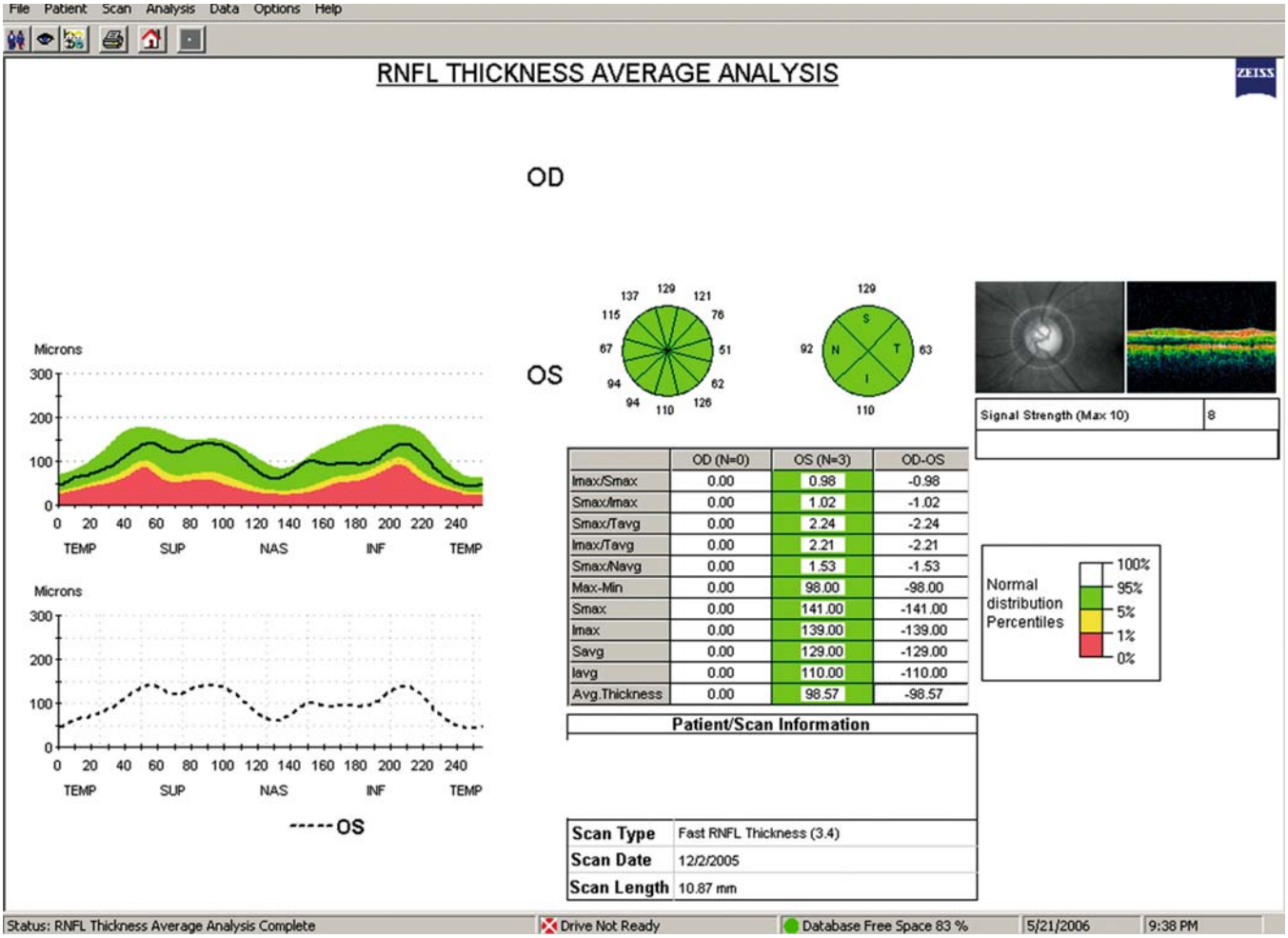

FIG. 18.14. Retinal thickness average analysis screen. In spite of the glaucomatous appearance of the optic nerve, analysis of the RNFL scan evidences normal thickness values throughout all clock hours.

nerve fiber layer. Optic nerve head analysis correlates well with the clinical characteristics of the optic nerve with the benefit of objectively measuring the large cup, disc size, and other parameters. In this patient, a relatively large disc area and increased cup-to-disc ratio are noted (Fig. 18.15).

The optic nerve head analysis may play a valuable role in the long-term follow-up of this patient by establishing objective baseline measurements and enhancing our ability to detect changes over time.

Case 4: Ocular Hypertension, Suspicious for Glaucoma

A patient with ocular hypertension and suspicious optic nerve heads was observed over a period of time (Fig. 18.16). Achromatic Humphrey visual fields do not show evident glaucomatous damage, and FDT results are borderline (Fig. 18.17). An OCT was performed using the RNFL scan, which showed

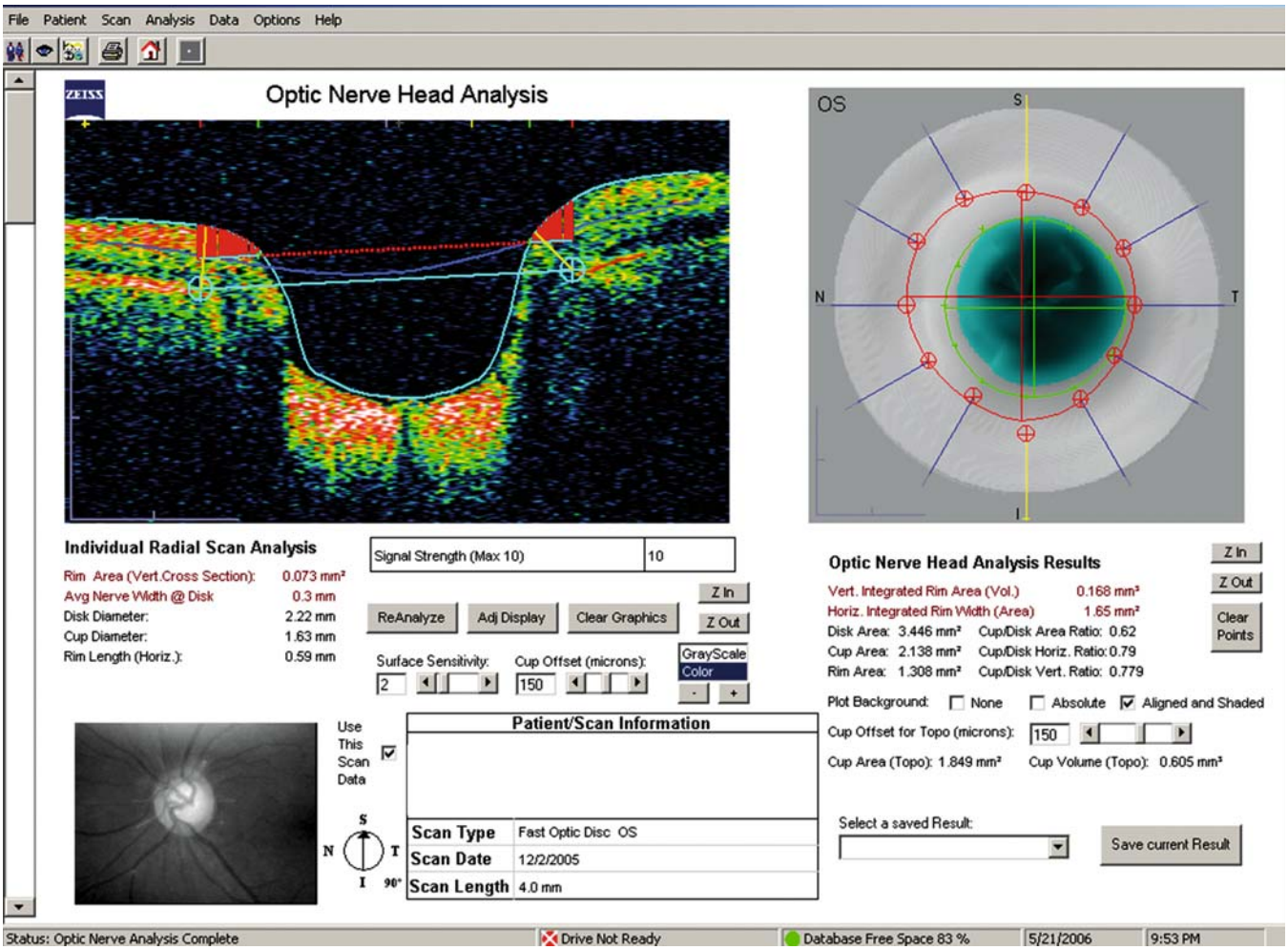

FIG. 18.15. Optic nerve head analysis screen. Optic nerve head analysis correlates well with the clinical characteristics of the optic nerve with the benefit of objectively measuring the cup, disc size, and other parameters. In this patient, a relatively large disc area and increased cup-to-disc ratio are noted.

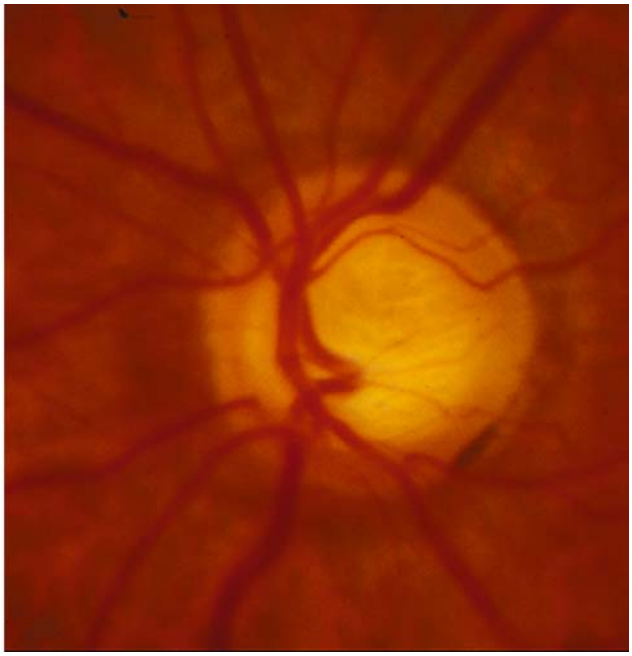

A

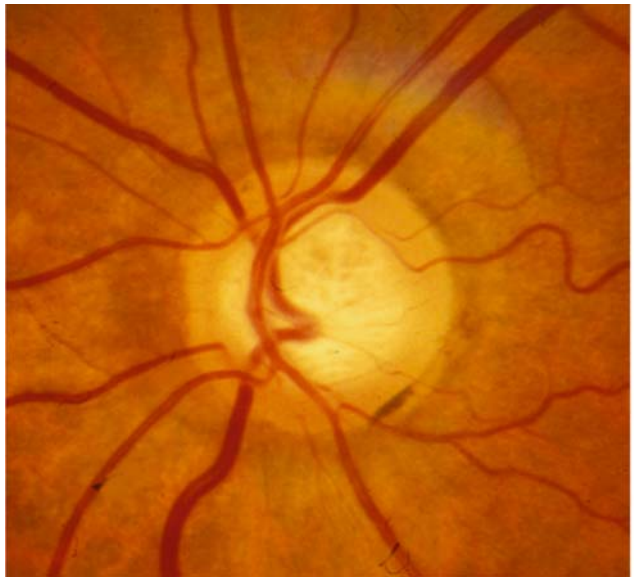

C

B

FIG. 18.16. Disc photographs of a patient with ocular hypertension and suspicious optic nerve heads observed over a period of time.

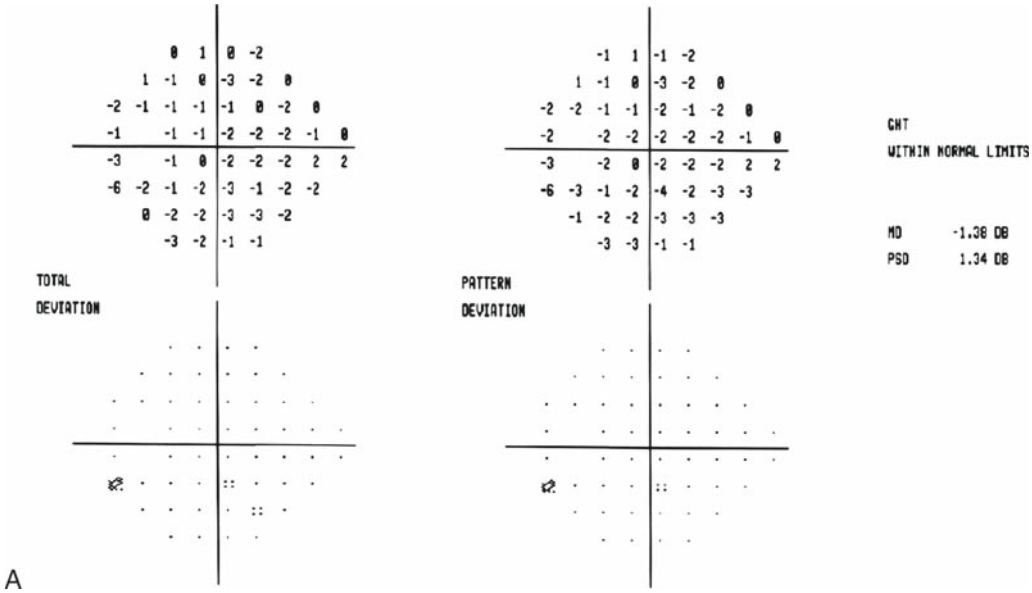

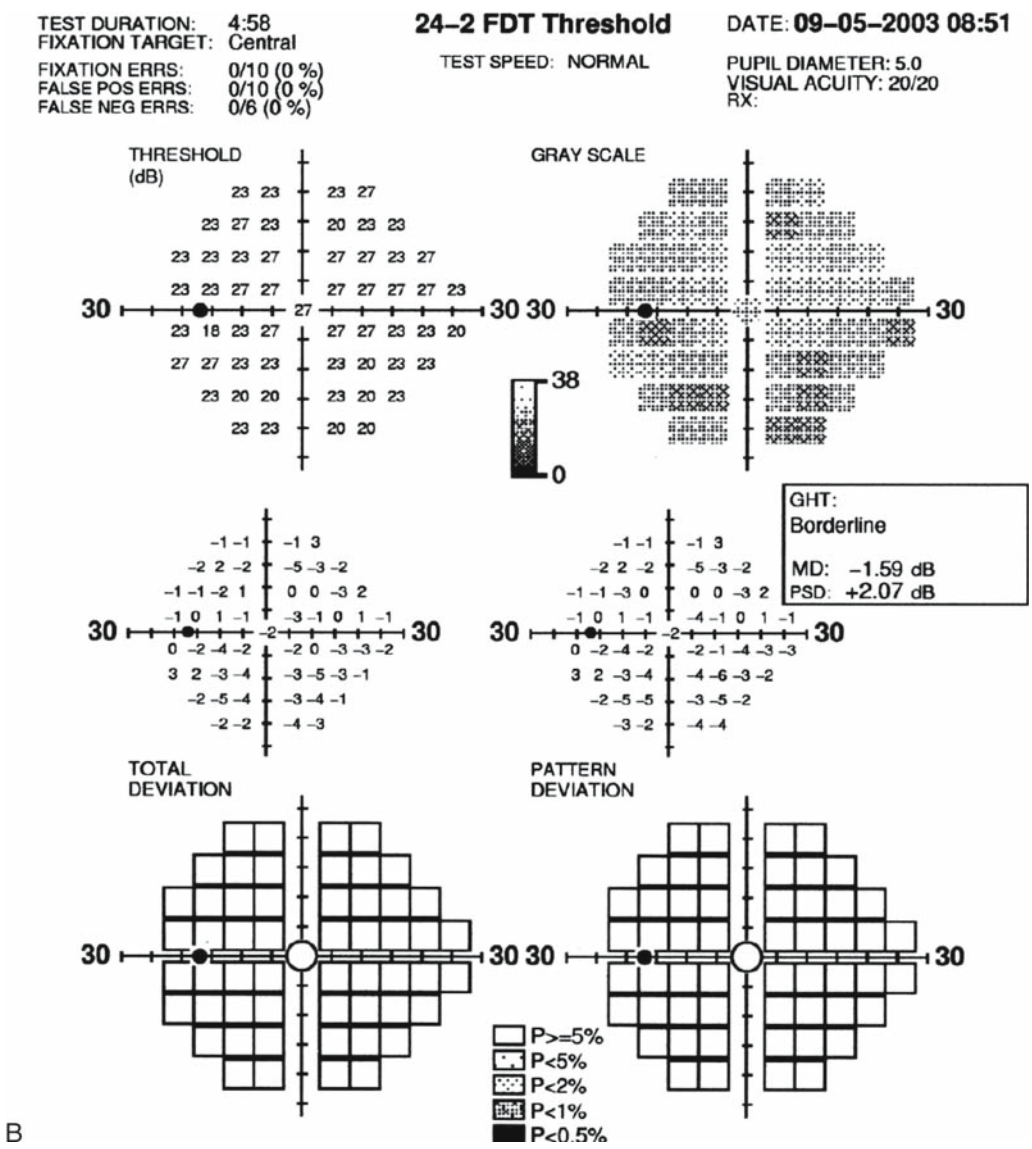

FIG. 18.17. Achromatic Humphrey visual fields do not show evident glaucomatous damage. The FDT results are borderline.

borderline thickness values, alerting us with the yellow background in the display, indicating statistical significance. The thinning is more evident at the RNFL located at the superior and inferior poles of the disc (Fig. 18.18).

In this case, serial RNFL analysis proved to be very useful, indicating that the RNFL thickness remained stable over time as displayed by the superimposed plots on the graph representing the different scans (Fig. 18.19).

Case 5: Structure Function Correlation

A 56-year-old woman with open-angle glaucoma presented with localized nerve fiber layer loss on the inferior pole of her right optic nerve head on clinical examination. Humphrey automated achromatic perimetry (Fig. 18.20) showed a dense superior glaucomatous defect that correlated well with the clinical findings.

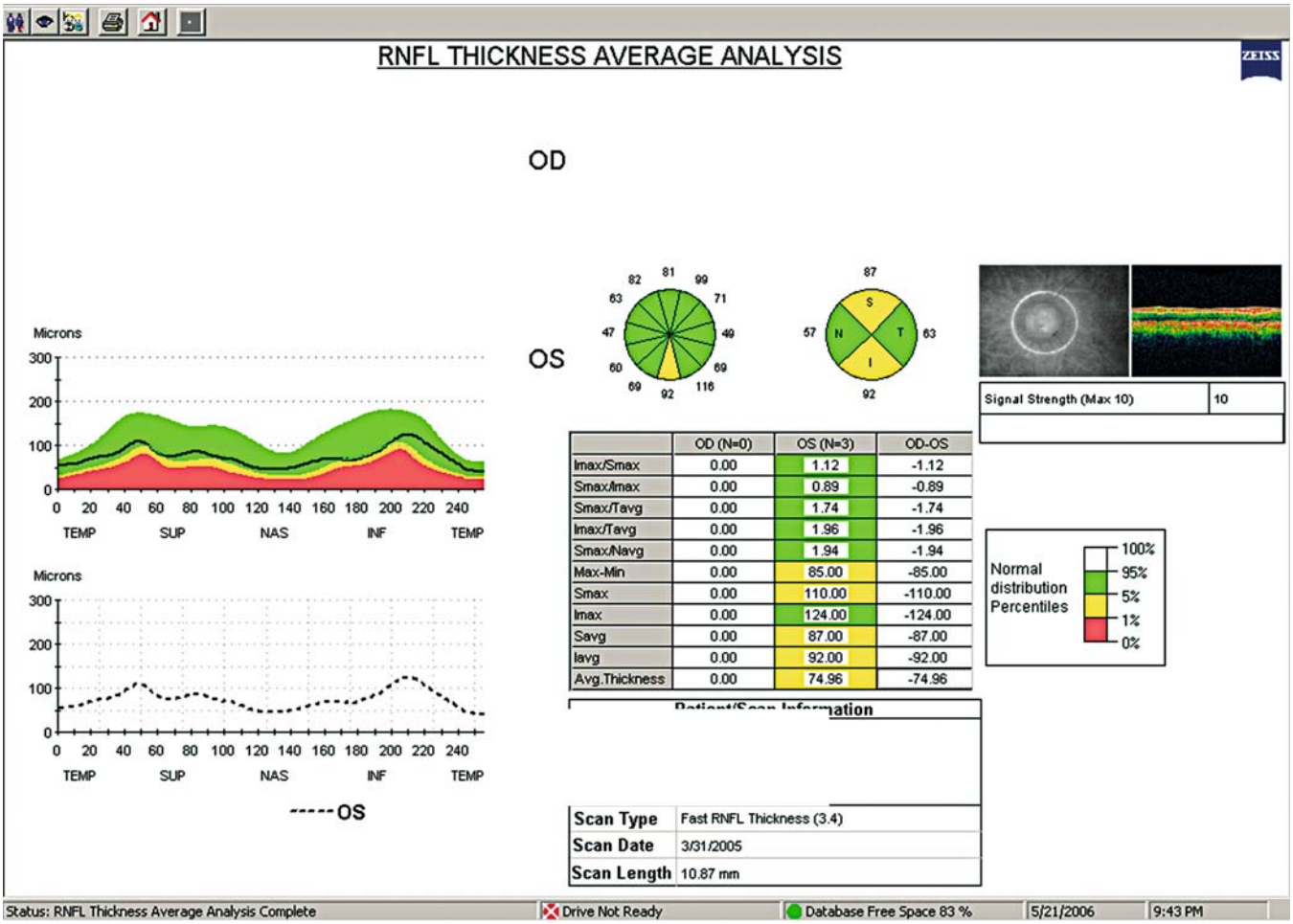

FIG. 18.18. The RNFL thickness average analysis. The RNFL scan shows borderline thickness values, alerting us with the yellow background in the display, indicating statistical significance. The thinning is more evident at the RNFL located at the superior and inferior poles of the disc.

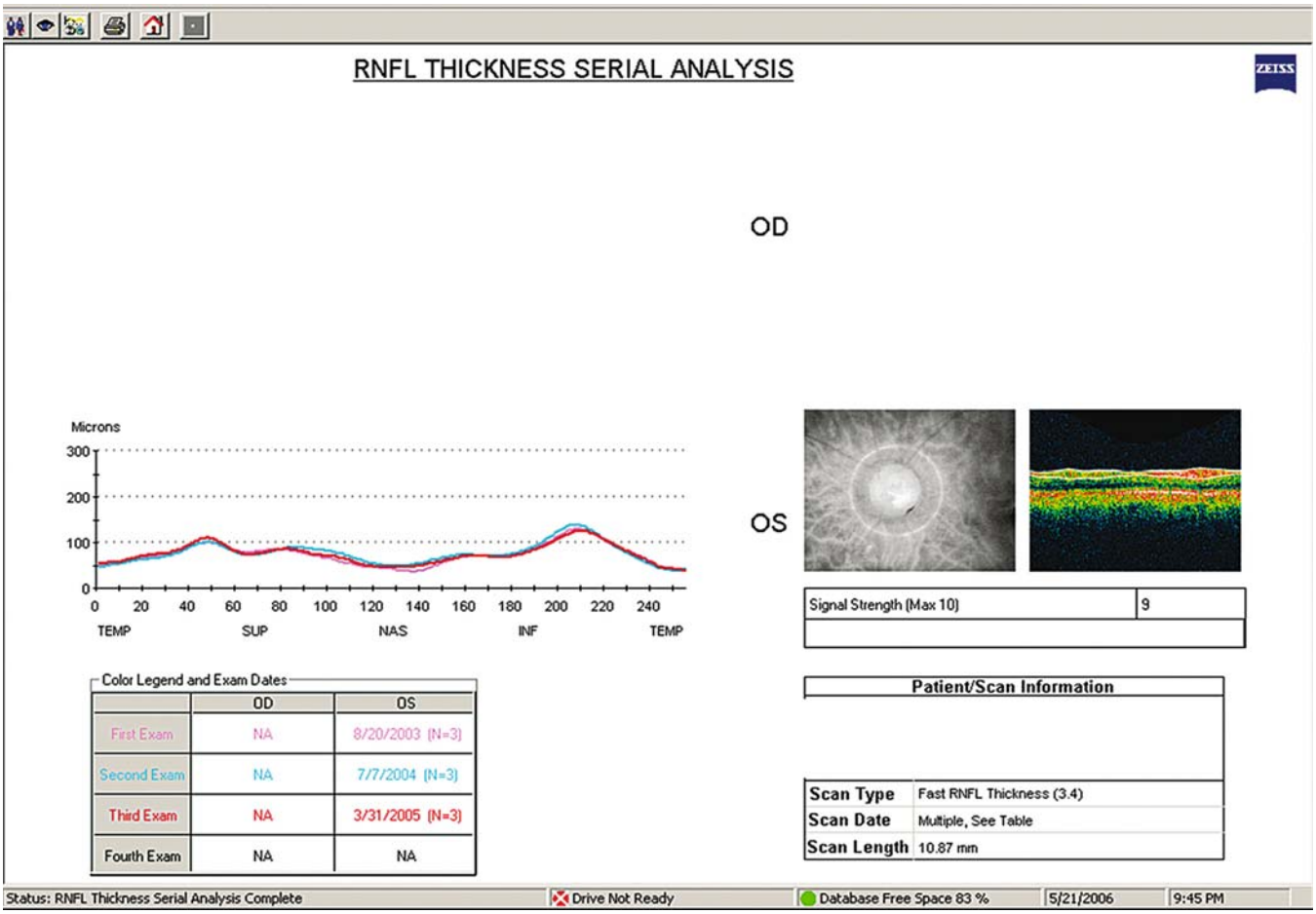

FIG. 18.19. Serial RNFL analysis proved to be very useful indicating that the RNFL thickness remained stable over time as displayed by the superimposed plots on the graph representing the different scans.

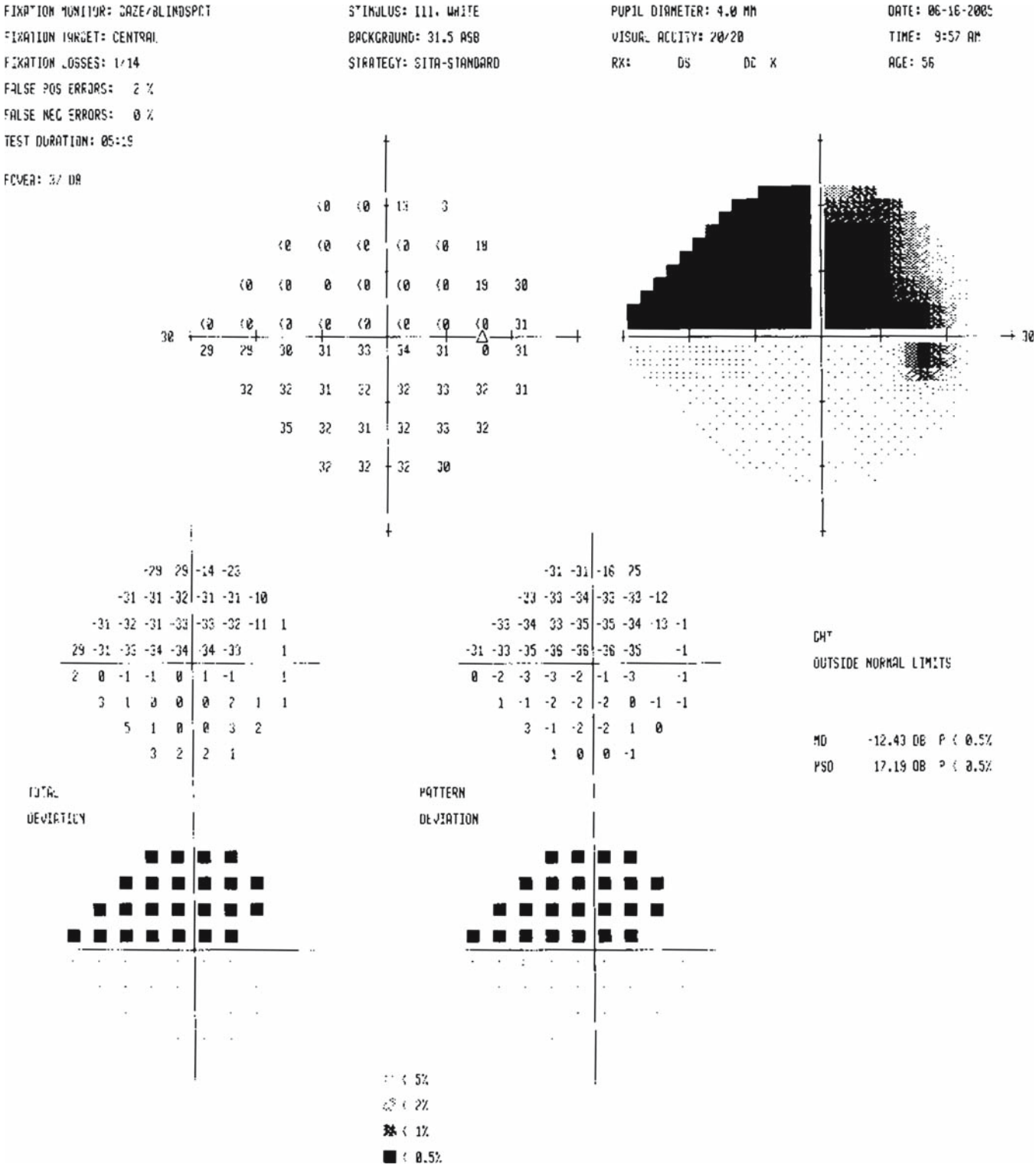

FIG. 18.20. A 56-year-old woman with open-angle glaucoma presented with localized nerve fiber layer loss on the inferior pole of her right optic nerve head on clinical examination. Humphrey automated achromatic perimetry shows a dense superior glaucomatous defect, which correlated well with the clinical findings.

The RNFL scan of her right optic nerve clearly displays statistically significant thinning of the nerve fiber layer limited to the inferior pole (Fig. 18.21).

A macular scan was obtained on the same eye of the same patient, and it demonstrated thinning of the inferior macula, which correlates well with the expected loss of ganglion cells in that location, given the clinical, perimetric, and OCT RNFL findings (Fig. 18.22).

Case 6: Suspicious for Glaucoma: Detection of Early Glaucoma

A 59-year-old man was referred for a second opinion due to large suspicious optic nerves in the presence of a normal achromatic Humphrey visual field using the Swedish interactive test algorithm (SITA™). The patient denied a history of elevated intraocular pressures or family history of glaucoma. Serial diurnal intraocular pressures measured in the office were in the range of 9 to 12 mm Hg in both eyes. Examination of his anterior segment was unremarkable. Funduscopic exam revealed bilateral, fairly symmetric thinning of the neuroretinal rims (Fig. 18.23). This patient underwent short wavelength automated perimetry (SWAP), scanning laser polarimetry, and macular and RNFL OCT scans.

Short wavelength automated perimetry revealed a visual field defect in the form of a nasal step suggestive of glaucoma in his left eye (Fig. 18.24A, B).

An OCT was performed using first a RNFL scan (Fig. 18.25). The analysis evidenced statistically significant thinning of the RNFL in the inferior pole of both eyes, more pronounced in the left eye correlating with the observed visual field defect on SWAP.

An OCT scan of the macula also evidenced thinning of the retinal thickness inferiorly, suggesting that the extent of damage in the left eye is more advanced (Fig. 18.26). This corresponded to the location of RNFL and visual field defect observed on SWAP.

Scanning laser polarimetry was performed and confirmed the OCT findings of thinning of the RNFL in both eyes. This is in spite of a normal achromatic perimetry in the right eye (Fig. 18.27).

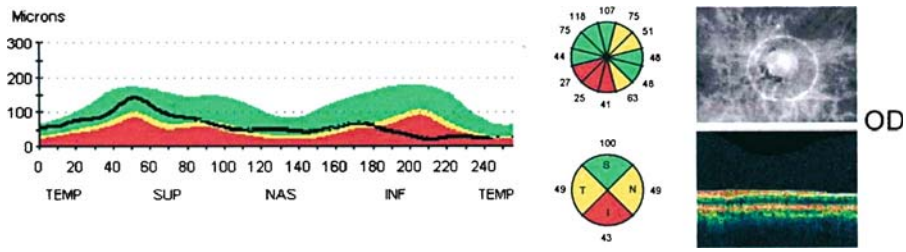

FIG. 18.21. An RNFL scan of the right optic nerve clearly displays statistically significant thinning of the nerve fiber layer limited to the inferior pole.

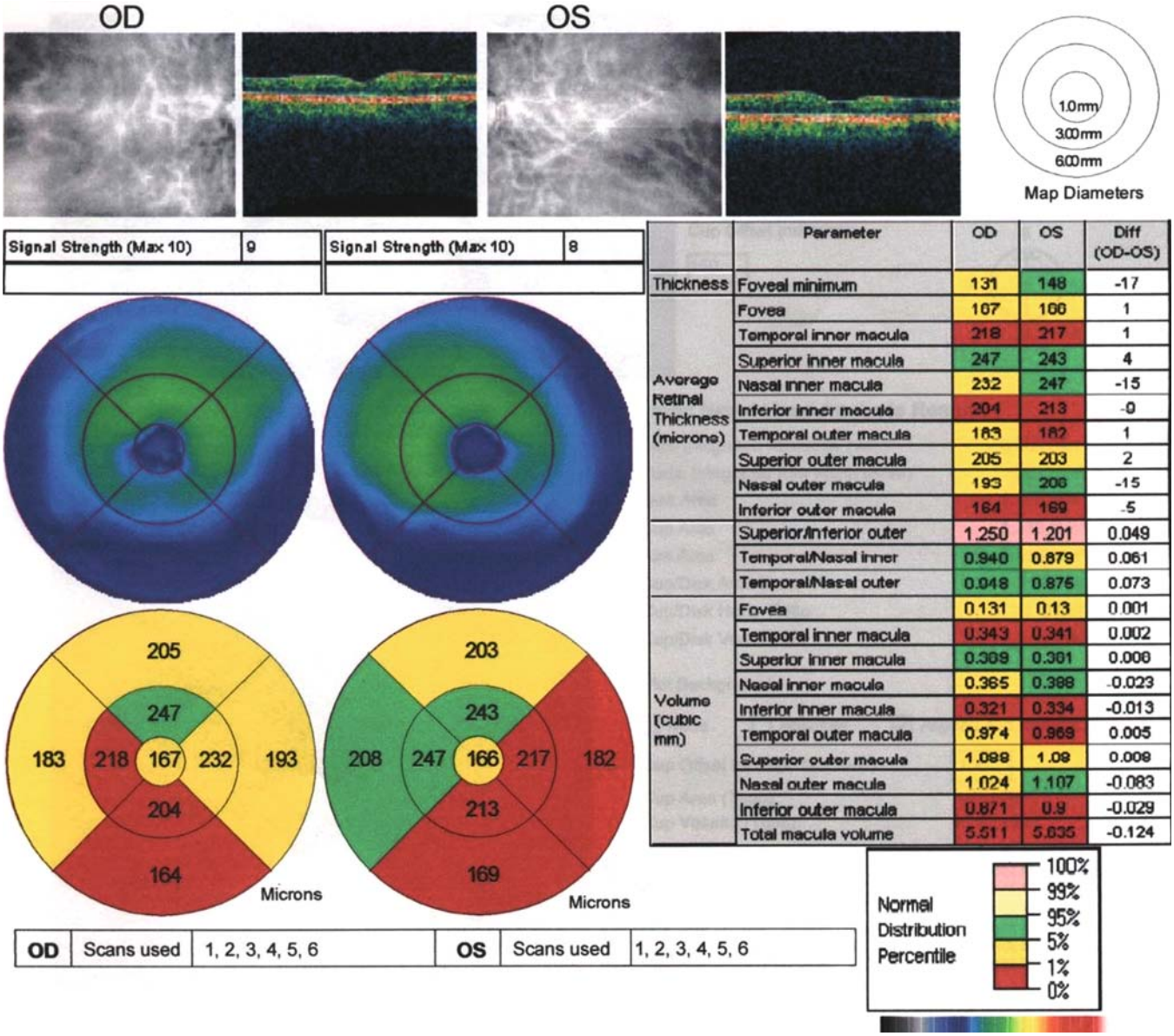

	Parameter	OD	OS	Diff (OD-OS)
Thickness	Foveal minimum	131	148	-17
Average Retinal Thickness (microns)	Fovea	167	166	1
	Temporal inner macula	218	217	1
	Superior inner macula	247	243	4
	Nasal inner macula	232	247	-15
	Inferior inner macula	204	213	-9
	Temporal outer macula	183	182	1
	Superior outer macula	205	203	2
	Nasal outer macula	193	208	-15
	Inferior outer macula	164	169	-5
	Superior/Inferior outer	1.250	1.201	0.049
	Temporal/Nasal inner	0.940	0.879	0.061
	Temporal/Nasal outer	0.048	0.876	0.073
Volume (cubic mm)	Fovea	0.131	0.13	0.001
	Temporal inner macula	0.343	0.341	0.002
	Superior inner macula	0.309	0.301	0.008
	Nasal inner macula	0.365	0.388	-0.023
	Inferior inner macula	0.321	0.334	-0.013
	Temporal outer macula	0.974	0.969	0.005
	Superior outer macula	1.099	1.09	0.009
	Nasal outer macula	1.024	1.107	-0.083
	Inferior outer macula	0.871	0.9	-0.029
	Total macula volume	5.511	5.635	-0.124

FIG. 18.22. Macular scan analysis screen demonstrates thinning of the inferior macula, which correlates well with the expected loss ganglion cells in that location.

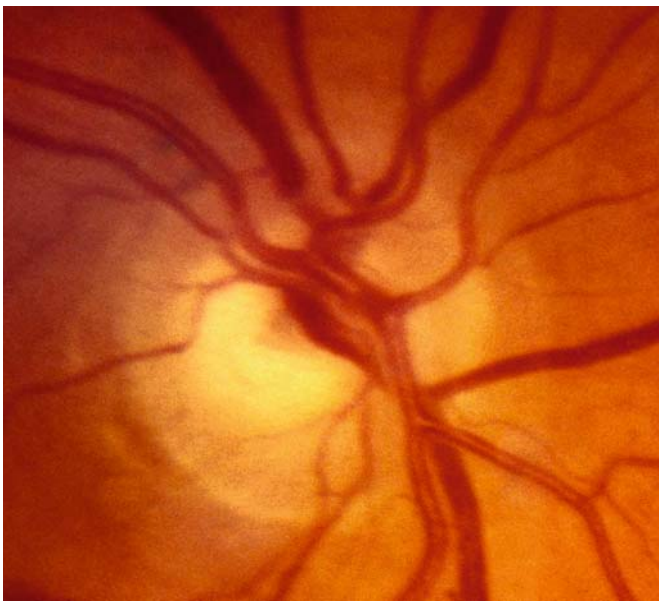

FIG. 18.23. A 59-year-old man was referred for a second opinion due to large suspicious optic nerves in presence of a normal achromatic Humphrey visual field using the Swedish interactive test algorithm (SITA™). Disc photos demonstrated bilateral, fairly symmetric thinning of the neuroretinal rims (only right eye shown).

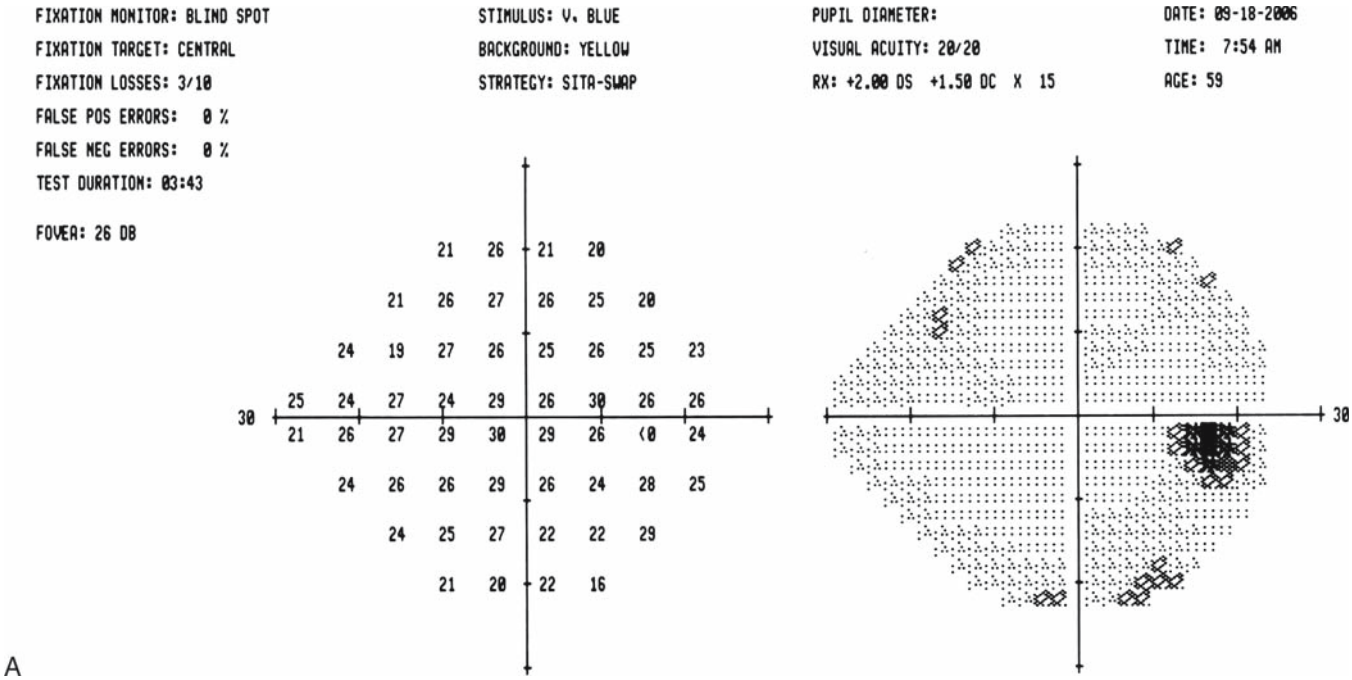

A

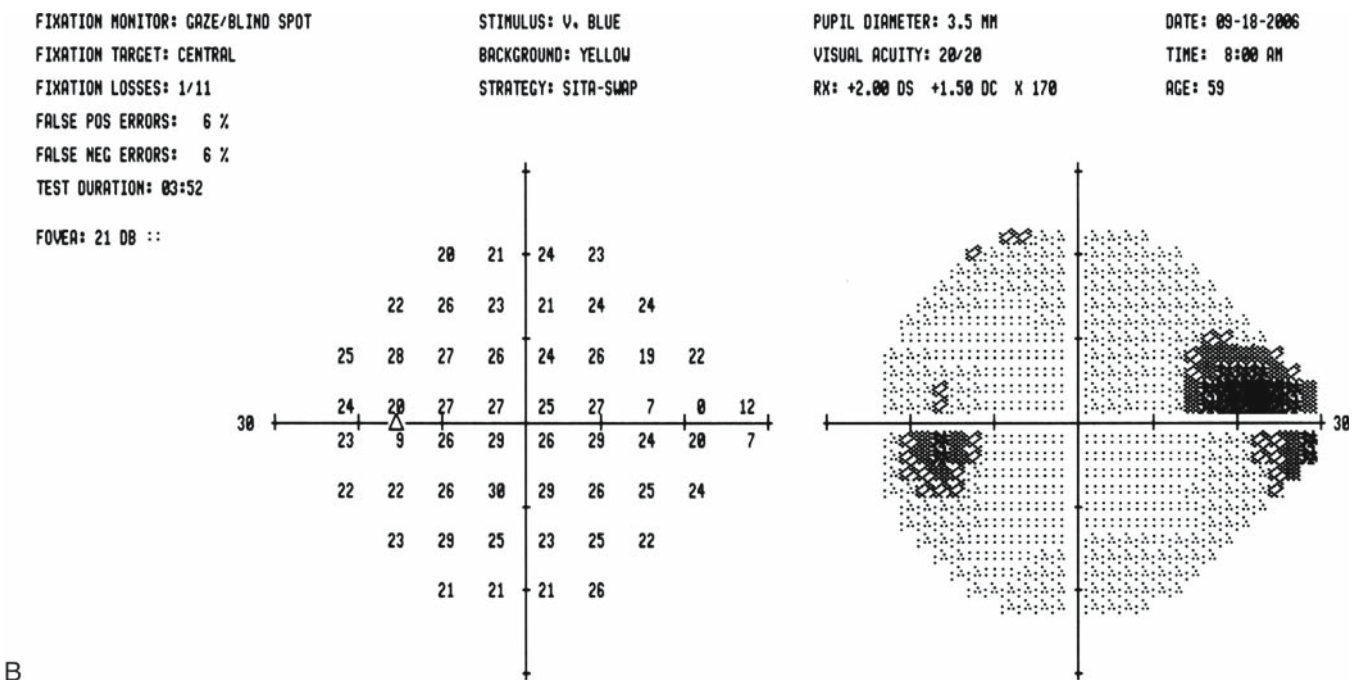

B

FIG. 18.24. Short wavelength automated perimetry (SWAP) reveals a visual field defect in the form of a nasal step suggestive of glaucoma in the patient's left eye.

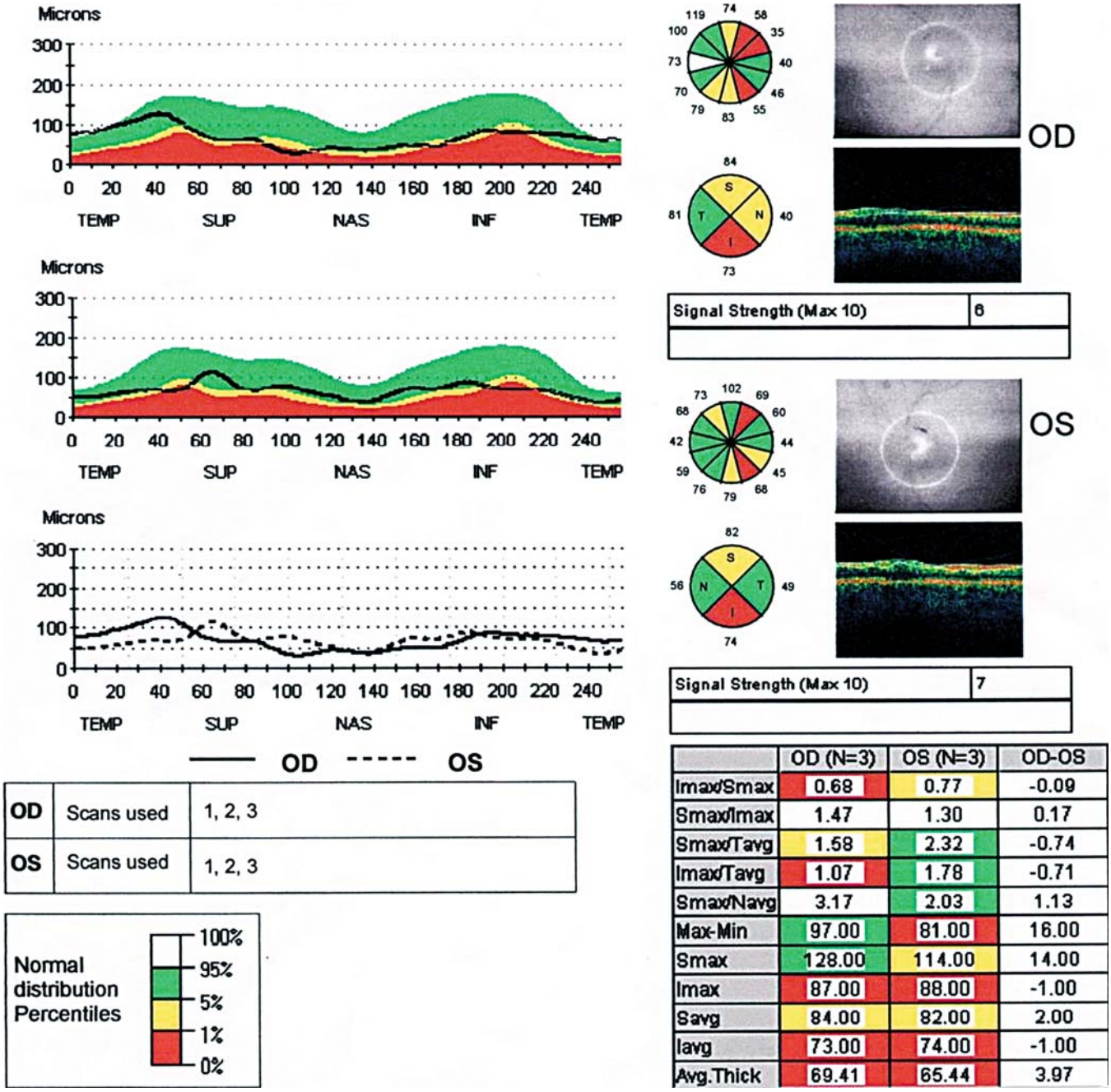

FIG. 18.25. An RNFL scan evidenced statistically significant thinning of the RNFL in the inferior pole of both eyes, more pronounced in the left eye correlating with the observed visual field defect on short wavelength automated perimetry (SWAP).

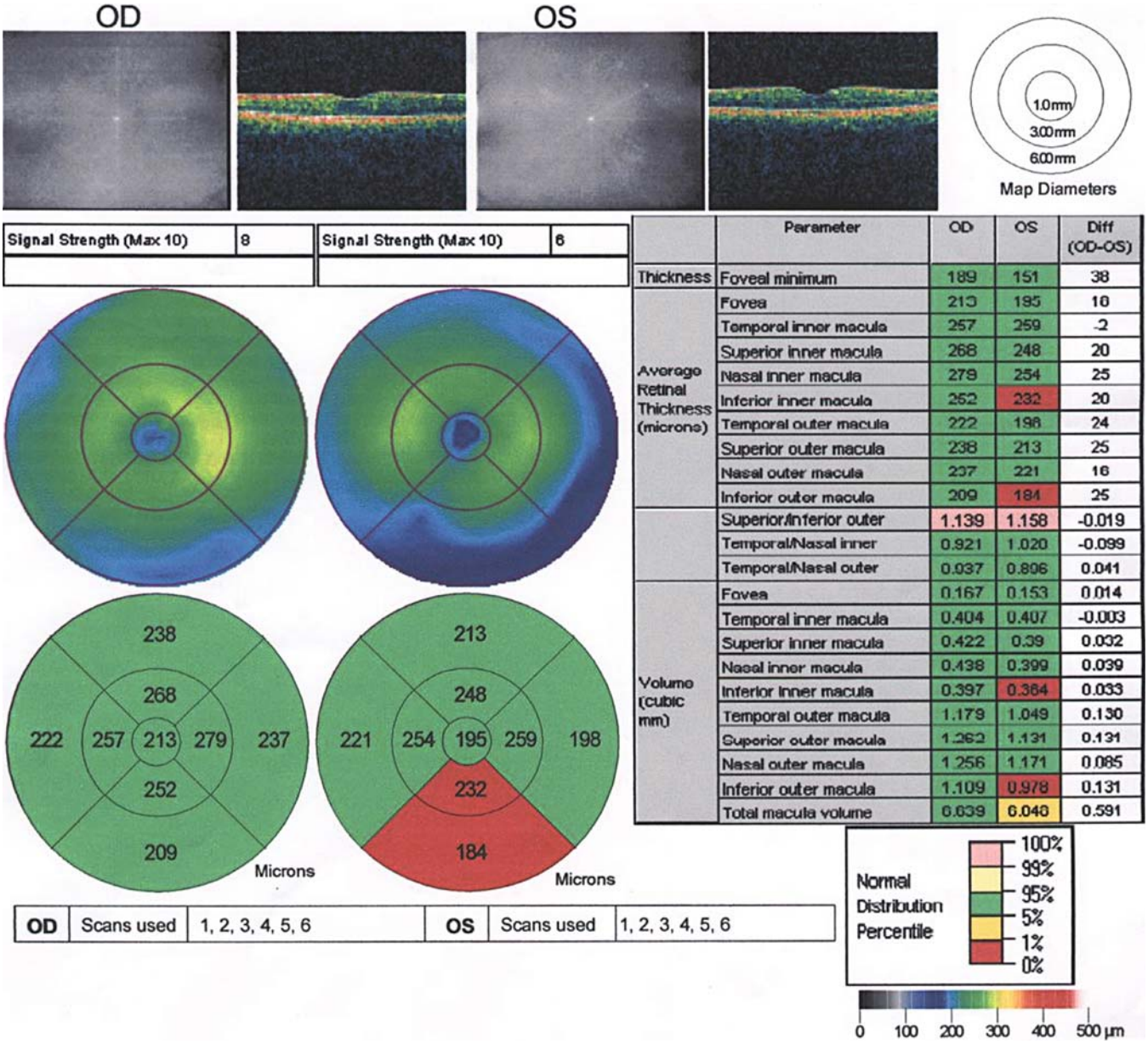

	Parameter	OD	OS	Diff (OD-OS)
Thickness	Foveal minimum	189	151	38
Average Retinal Thickness (microns)	Fovea	213	195	18
	Temporal inner macula	257	259	-2
	Superior inner macula	268	248	20
	Nasal inner macula	279	254	25
	Inferior inner macula	252	232	20
	Temporal outer macula	222	198	24
	Superior outer macula	238	213	25
	Nasal outer macula	237	221	16
	Inferior outer macula	209	184	25
	Superior/Inferior outer	1.139	1.158	-0.019
	Temporal/Nasal inner	0.921	1.020	-0.099
	Temporal/Nasal outer	0.937	0.896	0.041
Volume (cubic mm)	Fovea	0.167	0.153	0.014
	Temporal inner macula	0.404	0.407	-0.003
	Superior inner macula	0.422	0.39	0.032
	Nasal inner macula	0.438	0.399	0.039
	Inferior inner macula	0.397	0.364	0.033
	Temporal outer macula	1.179	1.049	0.130
	Superior outer macula	1.262	1.131	0.131
	Nasal outer macula	1.256	1.171	0.085
	Inferior outer macula	1.109	0.978	0.131
	Total macula volume	6.039	6.048	0.591

FIG. 18.26. Macular scan shows thinning of the retinal thickness inferiorly, suggesting that the extent of damage in the left eye is more advanced. This corresponded to the location of RNFL and visual field defect observed on SWAP.

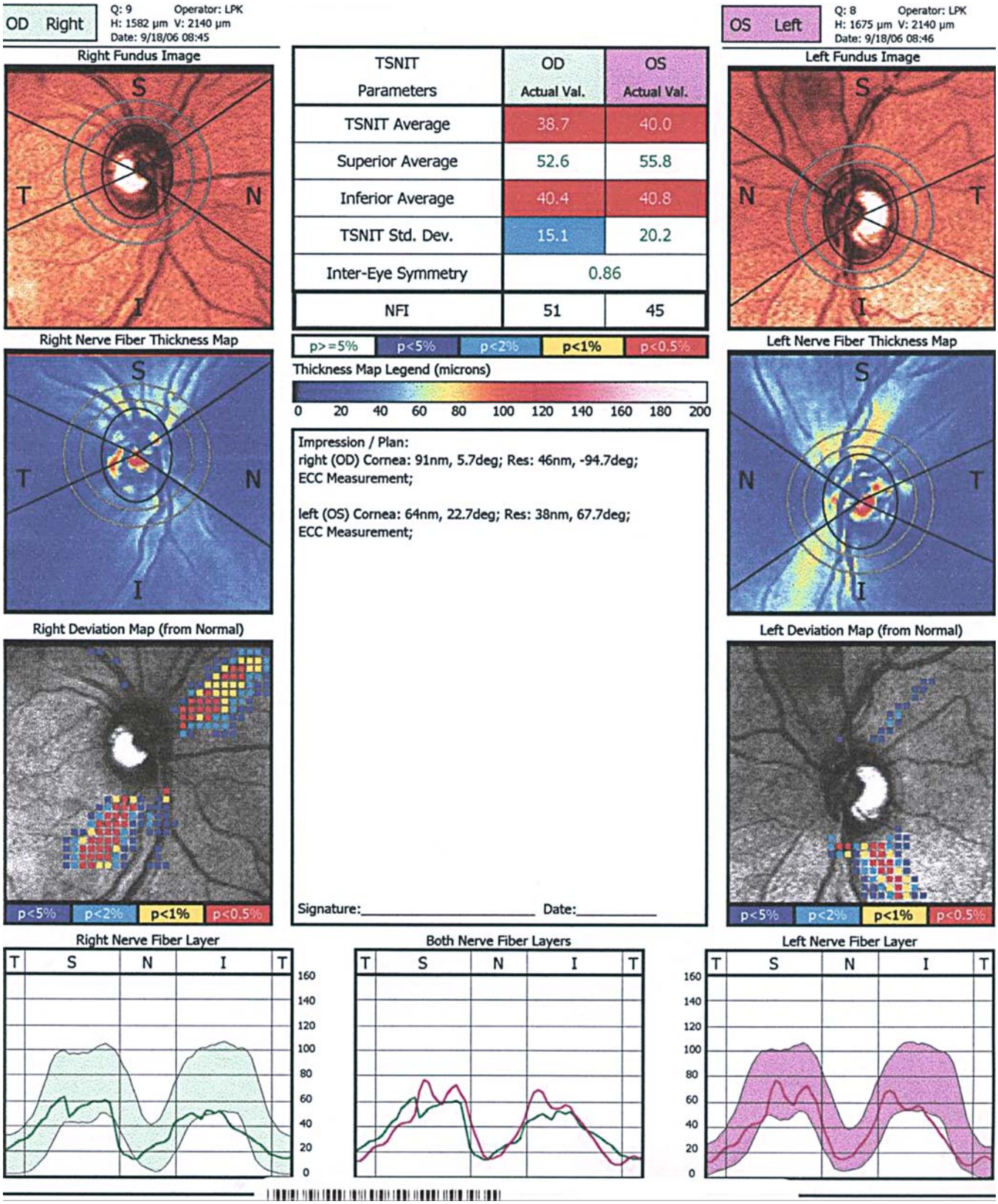

FIG. 18.27. Scanning laser polarimetry confirms the findings of the OCT showing thinning of the RNFL in both eyes.

Acknowledgments. The authors have no proprietary or financial interest in any products or techniques described in this chapter.

References

1. Quigley HA, Addics EM, Green WR. Optic nerve damage in human glaucoma. III. Quantitative correlation of nerve fiber loss and visual field defect in glaucoma, ischemic optic neuropathy, papilledema and toxic neuropathy. Arch Ophthalmol 1982;100:135–146.
2. Harwerth RS, Carter-Dawson L, Shen F, et al. Ganglion cell losses underlying visual field defects from experimental glaucoma. Invest Ophthalmol Vis Sci 1999;40:2242–2250.
3. Sommer A, Miller NR, Pollack I, et al. The nerve fiber layer in the diagnosis of glaucoma. Arch Ophthalmol 1977;95:2149–2156.
4. Sommer A, Katz J, Quigley HA, et al. Clinically detectable nerve fiber atrophy precedes the onset of glaucomatous field loss. Arch Ophthalmol 1991;109:77–83.
5. Jonas JB, Zach FM, Gusek GC, Naumann GO. Pseudoglaucomatous physiologic large cups. Am J Ophthalmol 1989;107:137–144.
6. Varma R, Tielsch J, Quigley H, et al. Race-, age-, gender-, and refractive error-related differences in the normal optic disc. Arch Ophthalmol 1994;112:1068–1076.
7. Quigley HA, Brown AE, Morrison JD, Drance SM. The size and shape of the optic disc in normal human eyes. Arch Ophthalmol 1990;108:51–57.
8. Lichter P. Variability of expert observers in evaluating the optic disc. Trans Am Ophthalmol Soc 1976;74:532–572.
9. Tielsch J, Katz J, Quigley H, Miller N, Sommer A. Intraobserver and interobserver agreement in measurement of optic disc characteristics. Ophthalmology 1988;95:350–356.
10. Varma R, Steinmann W, Scott I. Expert agreement in evaluating the optic disc for glaucoma. Ophthalmology 1992;99:215–221.
11 Schuman JS, Pedut-Kloizman T, Hertzmark E, et al. Reproducibility of nerve fiber layer thickness measurements using optical coherence tomography. Ophthalmology 1996;103:1889–1898.
12. Budenz DL, Chang RT, Huang X, et al. Reproducibility of retinal nerve fiber thickness measurements using the Stratus OCT in normal and glaucomatous eyes. Invest Ophthalmol Vis Sci 2005;46(7):2440–2443.
13. Massin P, Vicaut E, Haouchine B, et al. Reproducibility of retinal mapping using optical coherence tomography. Arch Ophthalmol 2001;119:1135–1142.
14. Baumann M, Gentile RC, Liebmann JM, Ritch R. Reproducibility of retinal thickness measurements in normal eyes using optical coherence tomography. Ophthalmic Surg Lasers 1998;29:280–285.
15. Schuman JS, Wollstein G, Farra T, et al. Comparison of the optic nerve head measurements obtained by optical coherence tomography and confocal scanning laser ophthalmoscopy. Am J Ophthalmol 2003;135:504–512.
16. Schuman JS, Hee MR, Puliafito CA, et al. Quantification of nerve fiber layer thickness in normal and glaucomatous eyes using optical coherence tomography. Arch Ophthalmol 1995;113:586–596.
17. Bowd C, Weinreb RN, Williams JM, Zangwill LM. The retinal nerve fiber layer thickness in ocular hypertensive, normal and glaucomatous eyes with optical coherence tomography. Arch Ophthalmol 2000;118:22–26.
18. Zangwill LM, Bowd C, Berry CC, et al. Discriminating between normal and glaucomatous eyes using the Heidelberg retina tomograph, GDx nerve fiber layer analyzer and optical coherence tomograph. Arch Ophthalmol 2001;119:985–993.
19. Patella VM, Stratus OCT. Establishment of Normative Reference Values for Retinal Nerve Fiber Layer Thickness Measurements. Dublin, CA: Carl Zeiss Meditec, 2003.
20. Jeoung JW, Park KH, Kim TW, et al. Diagnostic ability of optical coherence tomography with a normative database to detect localized retinal nerve fiber layer defects. Ophthalmology 2005;112:2157–2163.
21. Glovinsky Y, Quigley HA, Pease ME. Foveal ganglion cell loss is size dependent in experimental glaucoma. Invest Ophthalmol Vis Sci 1993;34:395–400.
22. Frishman LJ, Shen FF, Du L, et al. The scotopic electroretinogram of macaque after retinal ganglion cell loss from experimental glaucoma. Invest Ophthalmol Vis Sci 1996;37:125–141.
23. Zeimer R, Asrani S, Zou S, et al. Quantitative detection of glaucomatous damage at the posterior pole by retinal thickness mapping. A pilot study. Ophthalmology 1998;105:224–231.
24. Medeiros FA, Zangwill LM, Bowd C, et al. Evaluation of retinal nerve fiber layer, optic nerve head and macular thickness measurements for glaucoma detection using optical coherence tomography. Am J Ophthalmol 2005;139:44–55.

19
Clinical Applications of Optical Coherence Tomography in Optic Nerve Disease

Emely Z. Karam, Thomas R. Hedges III, and Carlos E. Mendoza

Optical coherence tomography (OCT) is a relatively new technology that provides information about the retina, optic nerve, and nerve fiber layer (NFL) differently from other instruments.[1] Newer versions of the OCT allow better resolution, which makes it useful for management of optic nerve disease. For neuro-ophthalmology, OCT methods employed for retinal as well as glaucoma analysis are used, because some optic nerve pathologies have macular complications, but also because many retinal conditions may mimic optic nerve disease.

The tomograms used are radial, linear, and circular. Radial scans are made up of linear sections through the optic nerve in a clockwise manner that may provide information regarding the diameter of the optic disc, physiologic/pathologic excavation and swelling, and the integrity of the neuroretinal rim. In addition to radial scans of the macula, linear scans can be made horizontally through both the disc and the macula, which can supply some information regarding the relationship of optic nerve head pathology to macular pathology. Circular tomograms centered at the optic disc can be made with different diameters. Each of these circular tomograms is displayed in an unwrapped manner and can be interpreted in three different ways: (1) following each clock hour, which produces 12 measurements of the nerve fiber layer; (2) by quadrants, producing four different measurements of the nerve fiber layer; and (3) as an average of the nerve fiber layer thickness of all four quadrants. These values can provide information regarding segmental nerve fiber layer thinning and swelling, as well as overall nerve fiber layer thickness.

Neuro-Ophthalmic Diseases

Optic Disc Pit

Optic disc pit is a congenital anomaly associated with retinal detachment in 25% to 75% of the cases, frequently involving the macular region. The debate about the origin of the subretinal fluid has not been completely settled, and includes speculation that it may arise from the cerebrospinal fluid, the vitreous cavity, or the orbit. Chronic retinal detachment can result in lamellar macular holes, cystic retinal degeneration, or retinal pigment epithelial atrophy. There is also controversy regarding management.[2,3]

Radial tomograms are useful in demonstrating the optic disc pit, which appears as a focal excavation within the nerve head (Fig. 19.1). Circular as well as radial tomograms can show the neurosensory retinal detachment, and can document the relationship of the fluid to the macular region. [4] Optical coherence tomography can also demonstrate resolution of retinal detachment after surgical or laser treatment.[2,3,5]

Segmental Optic Nerve Hypoplasia

Segmental optic nerve hypoplasia, also called “topless disc,” is an anomaly characterized by incomplete development of the upper portion of the optic nerve head, although other regions of the optic nerve may be involved. In most cases the superior part of the optic nerve is absent, and the upper scleral halo is more prominent. The central retinal artery entrance is also more superior than nasal, and the retinal nerve fiber layer of this area is deficient, correlating with an inferior visual field defect. The pathogenesis is presumed to be due to interruption of normal migration of the retinal nerve fibers, or exaggerated dying-back of nerve fibers that do not normally reach the lateral geniculate body. This is more common among patients born of diabetic mothers.[6]

Unoki et al.[7] demonstrated in vertically oriented optical coherence tomograms a disproportion between the normal lower part of the optic disc and the hypoplastic upper portion. There was thinning of the superior retinal nerve fiber layer and, in some cases, overlap or intrusion of the superior peripapillary pigment epithelium and choroid over the edge of the lamina cribrosa. Horizontal OCT sections through the optic disc and fovea showed that the papillomacular nerve fiber layer was intact, correlating with normal visual acuity and color vision seen in patients with segmental optic nerve hypoplasia, although in more severe cases there may be poor acuity and even nystagmus.

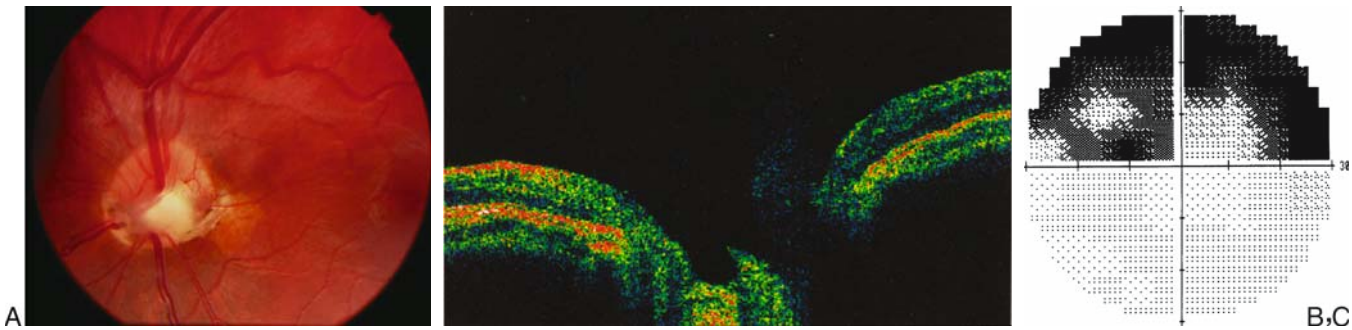

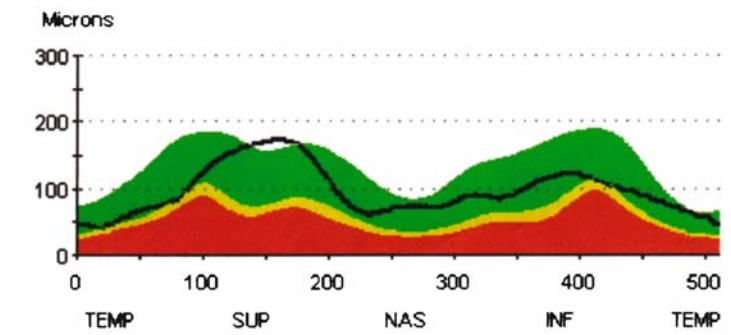

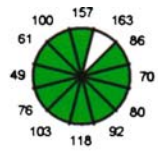

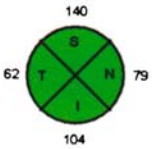

OD

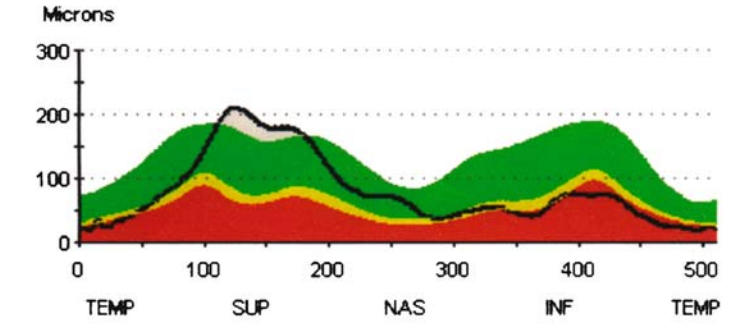

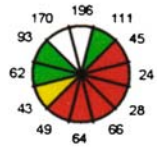

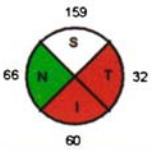

OS

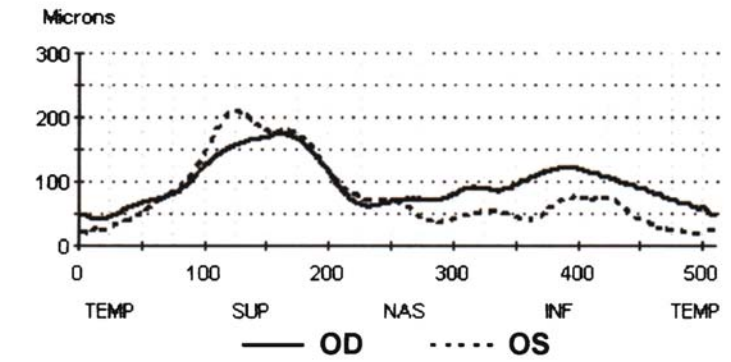

	OD (N=1)	OS (N=1)	OD-OS
Imax/Smax	0.70	0.36	0.35
Smax/Imax	1.42	2.80	-1.38
Smax/Tavg	2.80	6.48	-3.68
Imax/Tavg	1.97	2.31	-0.35
Smax/Navg	2.20	3.18	-0.98
Max-Min	132.00	189.00	-57.00
Smax	173.00	210.00	-37.00
Imax	122.00	75.00	47.00
Savg	140.00	159.00	-19.00
Iavg	104.00	60.00	44.00
Avg.Thick	96.36	79.27	17.09

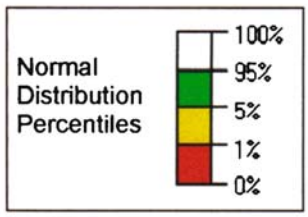

D

FIG. 19.1. A 16-year-old girl was found to have an optic nerve pit. (A) This case demonstrated temporal coloboma and nasal pit of the optic disc; two cilioretinal arteries emerged from the margin of the pit. (B) Radial optical coherence tomography (OCT) demonstrated a full pit with some glial tissue over it. (C,D) The visual field showed superior arcuate defect (C) correlating with the inferior thinning of the nerve fiber layer demonstrated in the circular OCT (D).

Optic Disc Tilt

Optic disc tilt is characterized by an oval optic nerve head that can be observed funduscopically in patients usually with myopic astigmatism. The superotemporal portion of the optic nerve appears elevated, whereas the inferonasal portion appears ectatic, often with associated thinning of the retinal pigment epithelium and choroid. It is also associated with situs inversus of the retinal arteries and veins. In some cases there may be degenerative findings including breaks in Bruch's membrane, subretinal neovascularization, subretinal hemorrhage, or polypoidal subretinal pseudocysts. Optical coherence tomography demonstrates a normal appearance of the retinal layers, but it may be useful in documenting some of the rare complications of optic disc tilting.[8]

Dominant Optic Atrophy

Dominant optic atrophy (DOA) or Kjer optic atrophy is an autosomal dominantly inherited optic neuropathy linked to the *OPA-1* gene. The initial visual manifestations occur at 4 to 6 years of age, with symmetric reduction of visual acuity, blue-yellow axis dyschromatopsia or tritanopia, central/centrocecal scotomas, and temporal or diffuse pallor of the optic disc. Because patients with DOA tend to have large, triangular optic cups, they may be misdiagnosed as having low-tension glaucoma.[9] Association with sensorineural hearing loss and mental abnormalities can be observed. Optical coherence tomography shows excavation of the optic nerve head, and decreased optic nerve fiber layer thickness in the maculopapillary area, which correlates with what can be seen ophthalmoscopically (Fig. 19.2).

Leber's Hereditary Optic Neuropathy

Leber's hereditary optic neuropathy is initially associated with swelling of the retinal nerve fiber layer in the acute phase and with gradual loss of the maculopapillary nerve fiber layer in the chronic phase. Optical coherence tomography may demonstrate nerve fiber layer thickening before visual loss as well. Ultimately the appearance of the retinal nerve fiber layer both ophthalmoscopically as well as by OCT is similar to that seen in patients with nutritional and toxic optic neuropathy.

Optic Nerve Head Drusen

Optic nerve head drusen are hyaline bodies that result from stasis of axoplasmic transport associated with crowding of the axons in a smaller than normal scleral opening. The blood vessels also are crowded into the center of the optic disc and may show anomalous patterns. Optic nerve head drusen may be difficult to identify when they are buried within the optic nerve head. In this situation there may be some confusion with papilledema. As optic nerve head drusen become more prominent, visual field defects may occur. Most often these are arcuate visual field defects, but there may also be generalized constriction of the visual field as well as enlargement of the blind spot. Rare complications include peripapillary hemorrhages and anterior ischemic optic neuropathy. Optical coherence tomography may show optic disc drusen within the nerve head in the form of shadows similar to those caused by the central retinal artery and vein. It demonstrates thinning of the nerve fiber layer, and, as in glaucoma, OCT may be more sensitive than visual field testing in detecting the degrees and patterns of NFL loss (Fig. 19.3).[10,11] Optical coherence tomography may be valuable in following the status of the nerve fiber layer in patients with optic nerve head drusen, [12] although no treatment is available for this condition.

Papilledema

Papilledema refers to optic nerve head swelling due to increased intracranial pressure. In the initial stages, the visual acuity is relatively preserved, but with time there may be progressive loss of the nerve fiber layer, especially superiorly. Papilledema is also associated with macular complications in some cases. Visual field testing demonstrates an increase in the size of the blind spot, and progressive constriction of the visual field, especially inferonasally. Clinically, the distinction between mild papilledema and pseudopapilledema, or congenital crowding of the optic nerve, may be difficult. Unfortunately, this distinction cannot be made with OCT. In a review of patients with mild papilledema and those with crowded optic nerves, without optic disc drusen, OCT demonstrated that the nerve fiber layer is thicker in patients with mild papilledema, as expected, but also in patients with pseudopapilledema when compared to normal controlled subjects.[13] However, OCT can be useful in following the retinal nerve fiber layer in patients with congenital crowding of the optic nerve in whom no changes occur over time, and in patients with papilledema in whom the optic nerve will change as the papilledema resolves or progresses. In monitoring patients with confirmed papilledema due to increased intracranial pressure, OCT changes need to be interpreted with caution. As the swollen retinal nerve fiber layer becomes thinner over time, one has to be aware that this could represent either improvement in the papilledema or damage to the nerve fiber layer from chronic papilledema. Therefore, correlation with visual field changes is critical. Optical coherence tomography can also demonstrate macular pathology in the presence of papilledema.

In some patients, subretinal fluid may develop with associated loss of visual acuity. In papilledema the subretinal fluid cannot be identified with fundus fluorescein angiography, but it is readily visible with OCT. The degree of thickening in the macular region is associated with the degree of visual acuity loss. This is a reversible phenomenon (Figs. 19.4 to 19.6).[14]

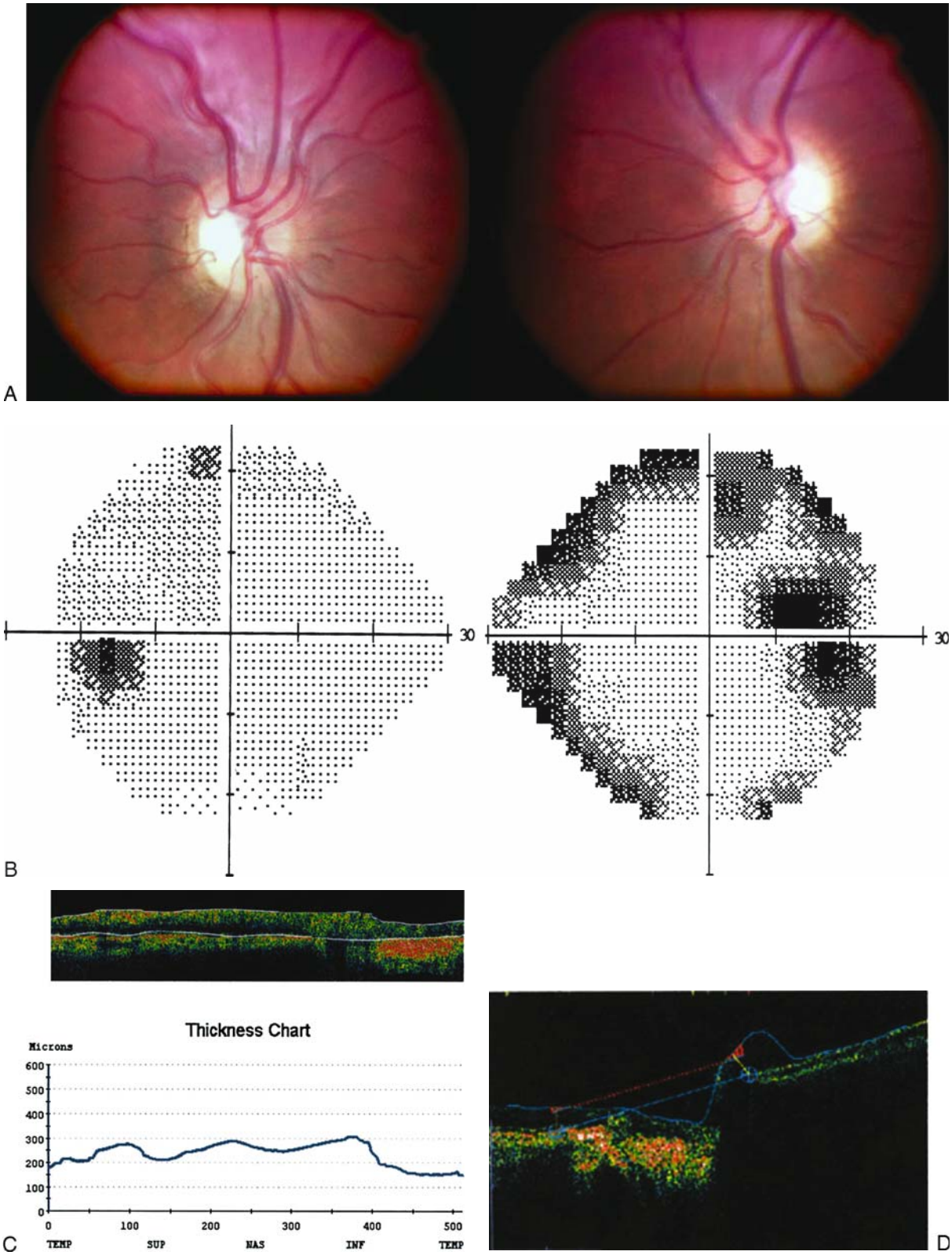

FIG. 19.2. A 9-year-old boy was noted to have visual difficulties in school. His father also has visual difficulties. (A) The fundus of the eye showed triangular optics cups, with temporal pallor. (B) The visual field demonstrated a big blind spot with a superior arcuate defect. (C) Radial OCT in the right eye showed some optic disc excavation. (D) Circumferential OCT showed thinning of the retinal nerve fiber layers, especially temporally.

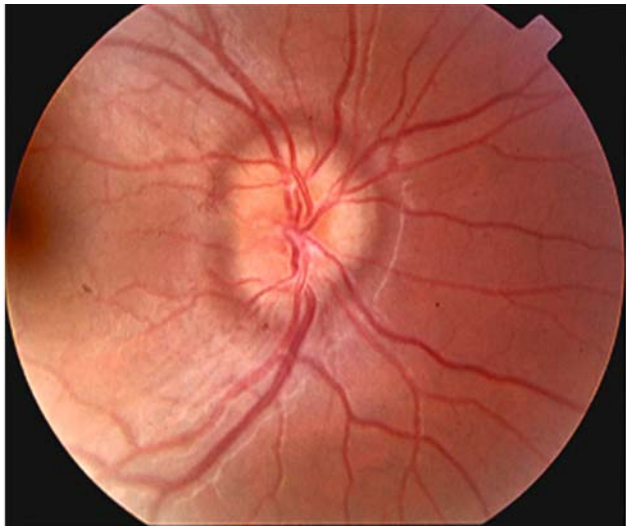
A

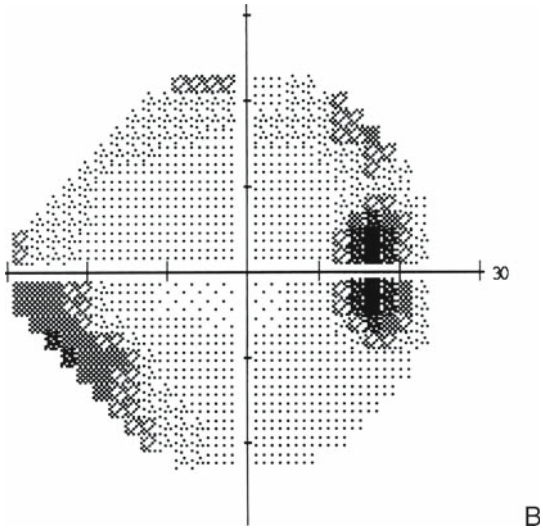

B

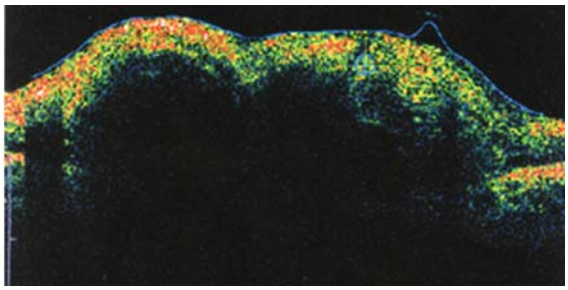
C

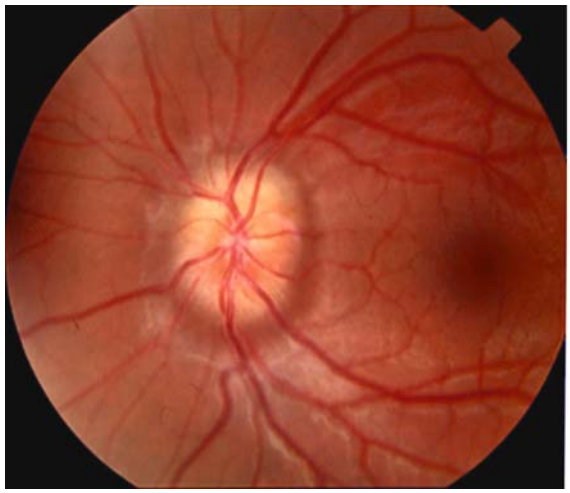
D

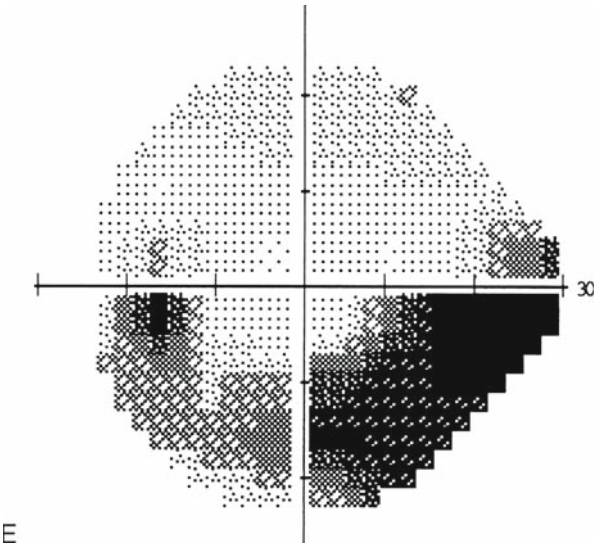

E

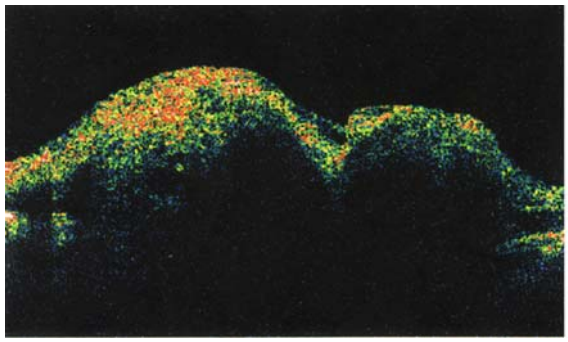
F

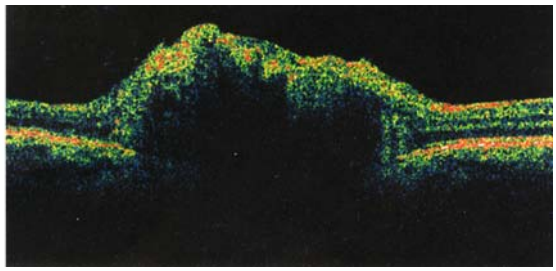
G

FIG. 19.3. A 22-year-old man was followed over several years because of optic nerve drusen. (A,B) The right eye showed occult optic nerve drusen with a big blind spot and mild nasal defect. (C) In the radial OCT, the 90-degree tomogram showed elevation of the optic disc with shadows. (D,E) In the left eye, drusen were exposed and the visual field demonstrated an inferior arcuate defect. (F,G) The 90-degree section of the radial OCT showed elevation of the optic disc, shadows (F), and thinning of nerve fiber layer in the 180-degree section as well (G).

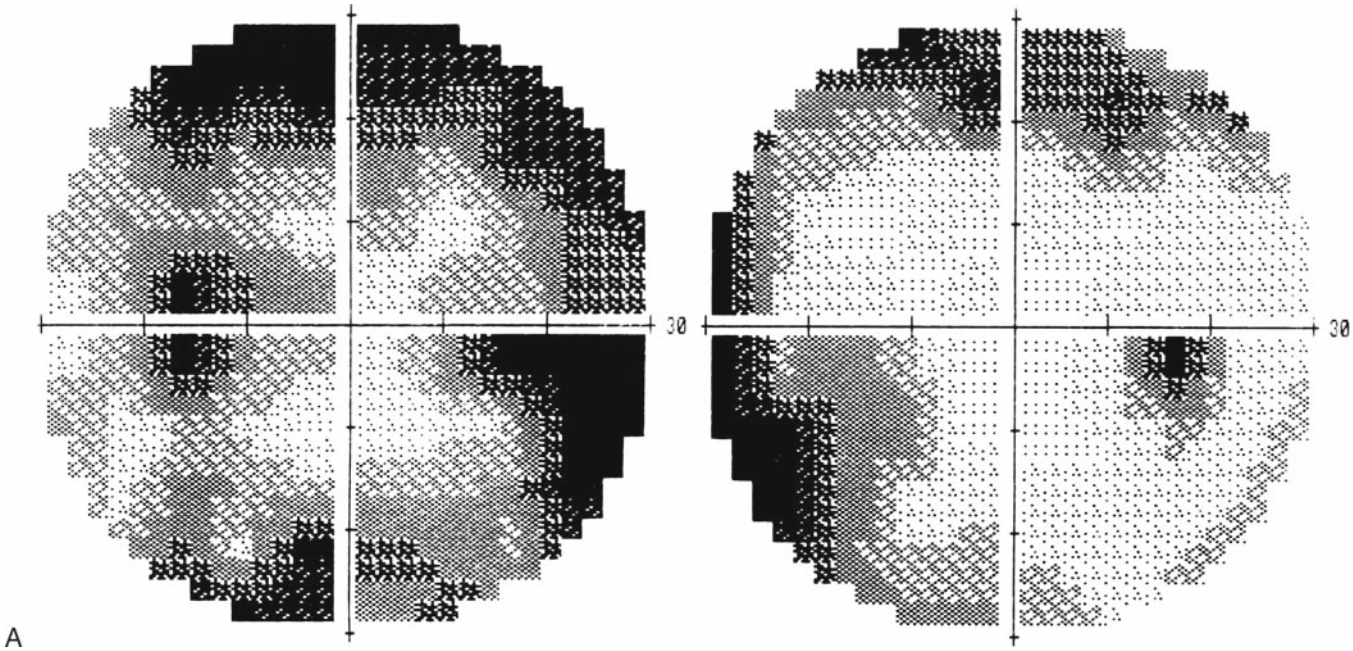

A

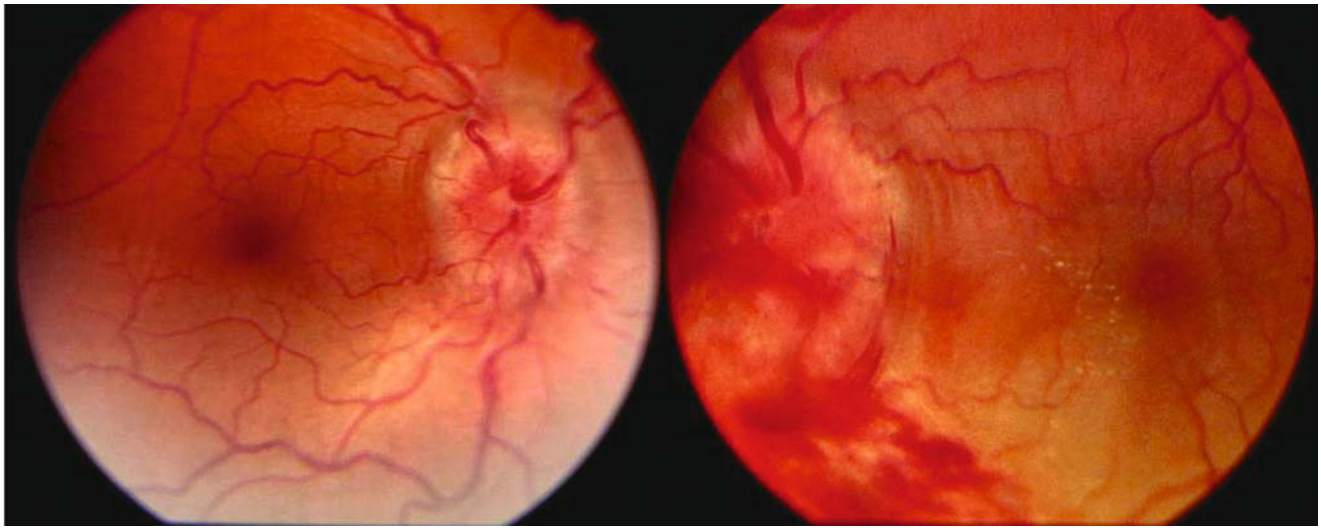

B

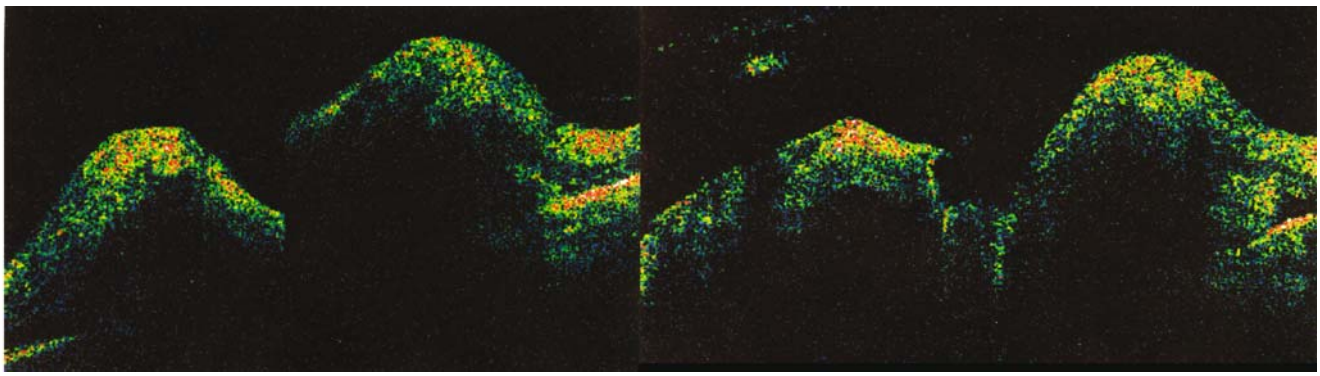

C

FIG. 19.4. A 41-year-old man developed transient visual obscurations and diplopia. He is obese, weighing 130 kg. A cerebral magnetic resonance imaging (MRI) was normal and the intracranial pressure by lumbar puncture was 480 mm H_2O. The visual acuities were 20/20 OD and 20/40 OS. (A) There was visual field constriction of the visual fields, more marked in the left eye. (B) The optic discs showed marked swelling with adjacent hemorrhages, exudates, macular edema, and retinal folds. (C,D) Optical coherence tomography showed elevation of the both optic discs, especially in the inferotemporal area. (E) Macular scans of the left eye demonstrated subretinal fluid.

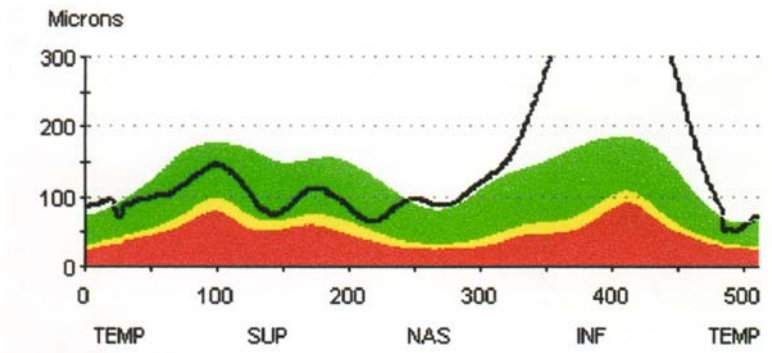

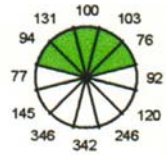

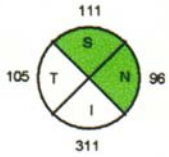

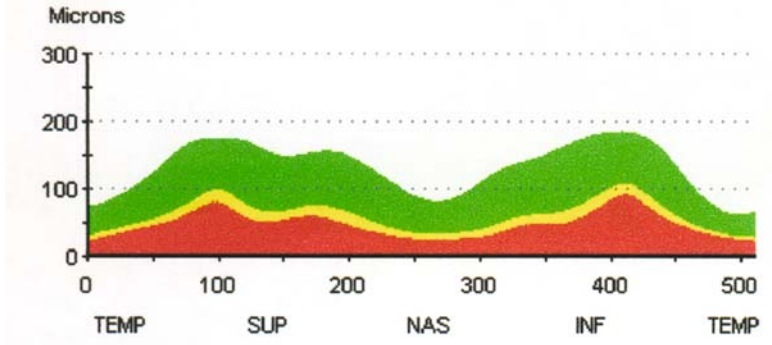

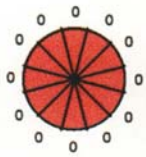

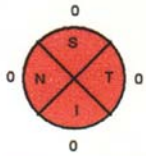

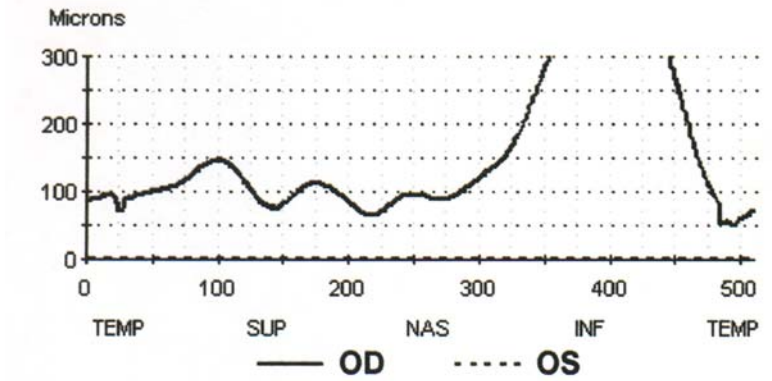

	OD (N=1)	OS (N=1)	OD-OS
Imax/Smax	2.55	NaN	2.55
Smax/Imax	0.39	NaN	0.39
Smax/Tavg	1.38	NaN	1.38
Imax/Tavg	3.51	NaN	3.51
Smax/Navg	1.51	NaN	1.51
Max-Min	319.00	0.00	319.00
Smax	145.00	0.00	145.00
Imax	370.00	0.00	370.00
Savg	111.00	0.00	111.00
Iavg	311.00	0.00	311.00
Avg.Thick	156.06	0.00	156.06

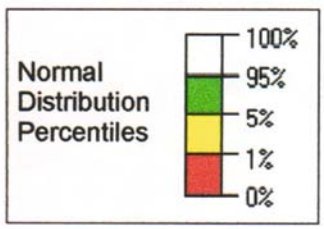

D

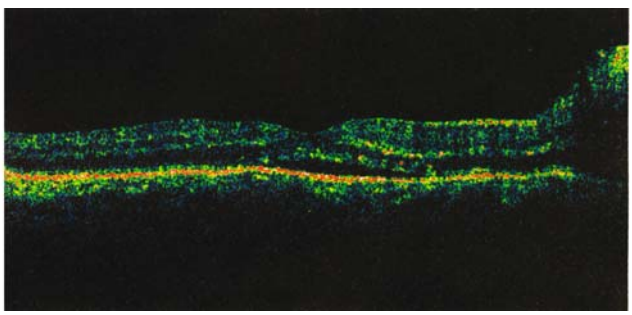

E

FIG. 19.4. (continued).

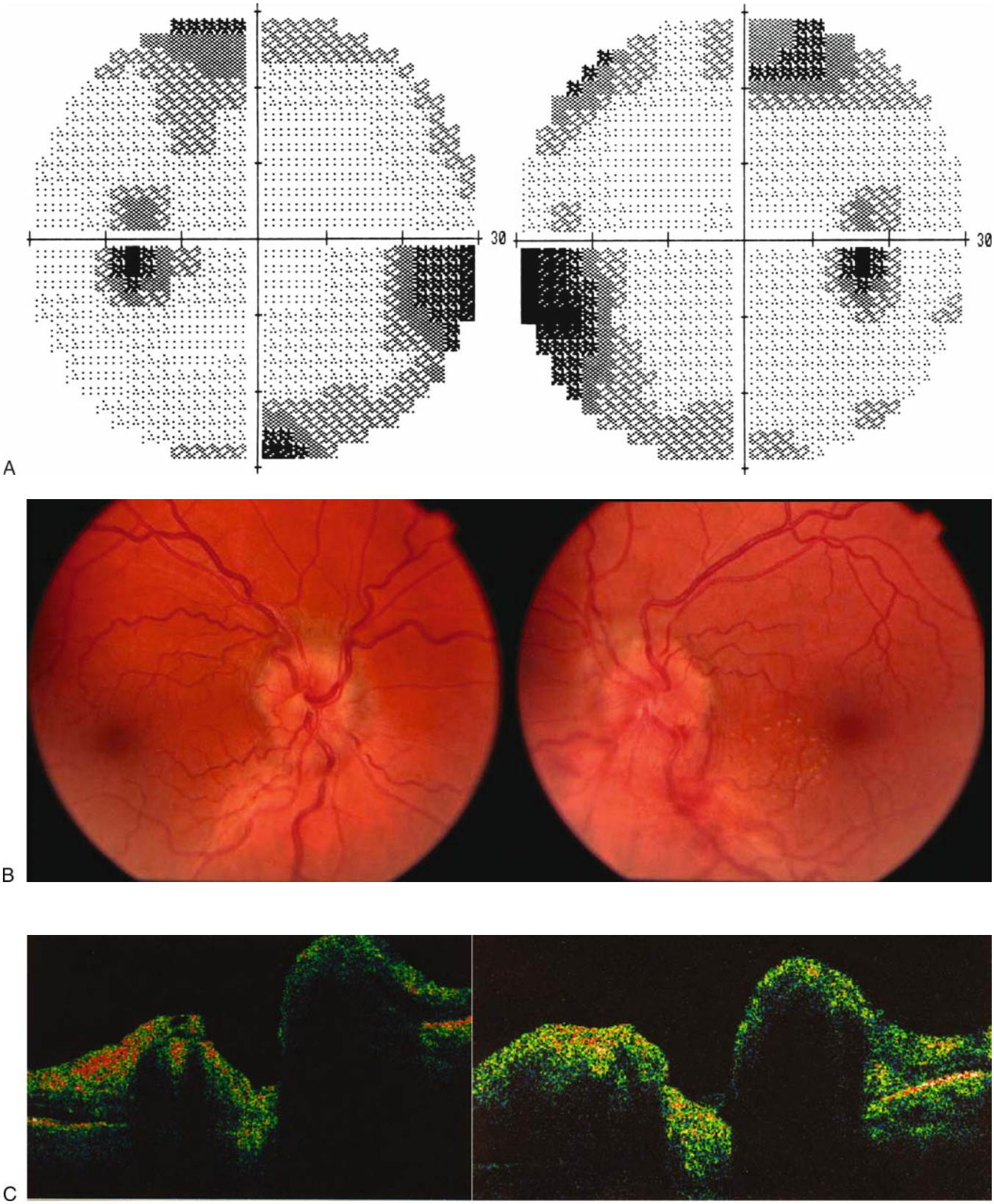

Fig. 19.5. After 1 month of treatment, the patient in Fig 19.4 showed improvement. The visual acuities were 20/20 in both eyes; the visual field showed reduction of the visual defect (A) and the optic discs were less swollen (B). The OCT demonstrated decreased edema (C,D) with absorption of the subretinal fluid in the macula area (E).

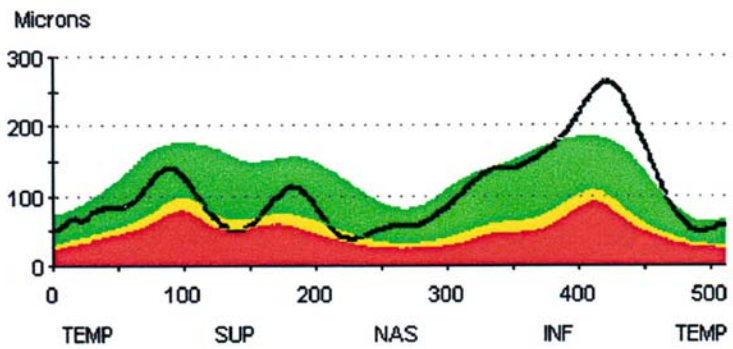

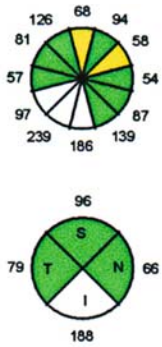

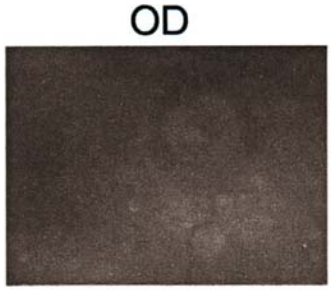

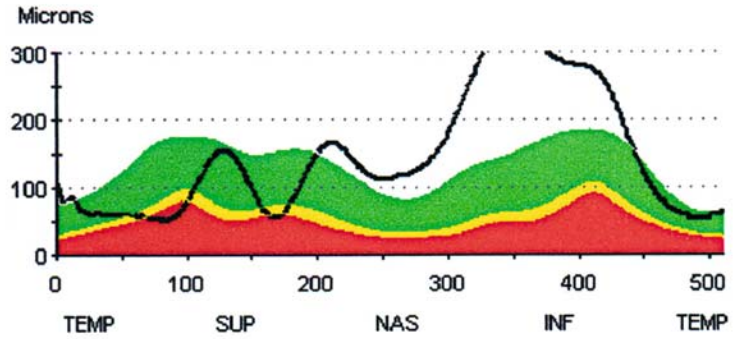

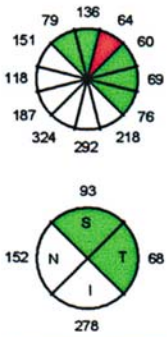

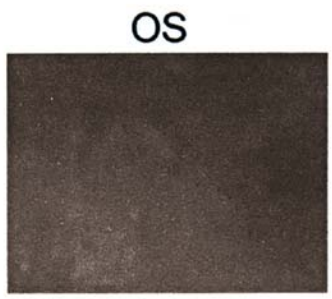

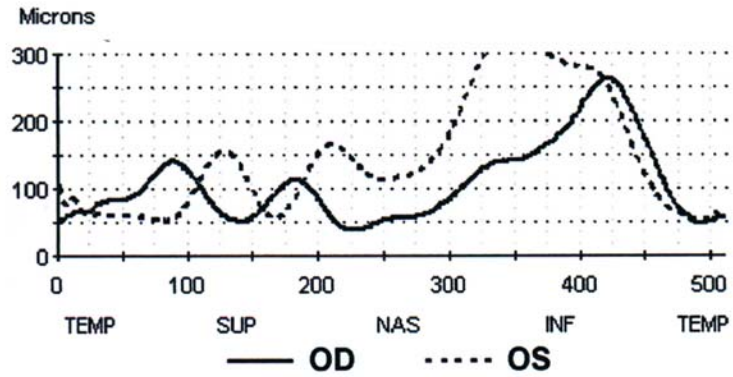

	OD (N=1)	OS (N=1)	OD-OS
Imax/Smax	1.88	2.22	-0.34
Smax/Imax	0.53	0.45	0.08
Smax/Tavg	1.78	2.24	-0.46
Imax/Tavg	3.35	4.98	-1.64
Smax/Navg	2.12	1.01	1.11
Max-Min	225.00	289.00	-64.00
Smax	140.00	154.00	-14.00
Imax	263.00	341.00	-78.00
Savg	96.00	93.00	3.00
Iavg	188.00	278.00	-90.00
Avg.Thick	107.12	147.87	-40.74

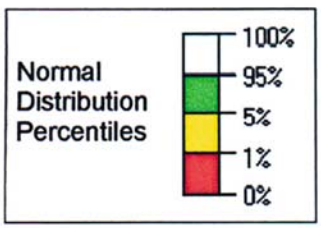

D

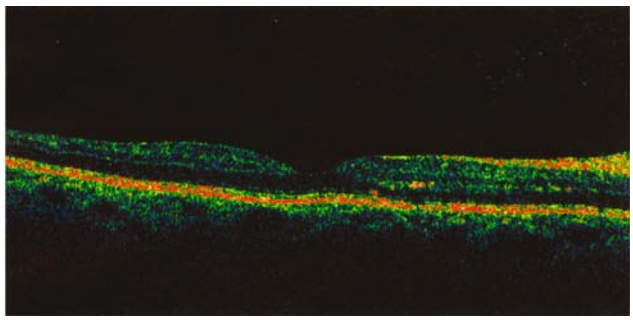

E

FIG. 19.5. (continued).

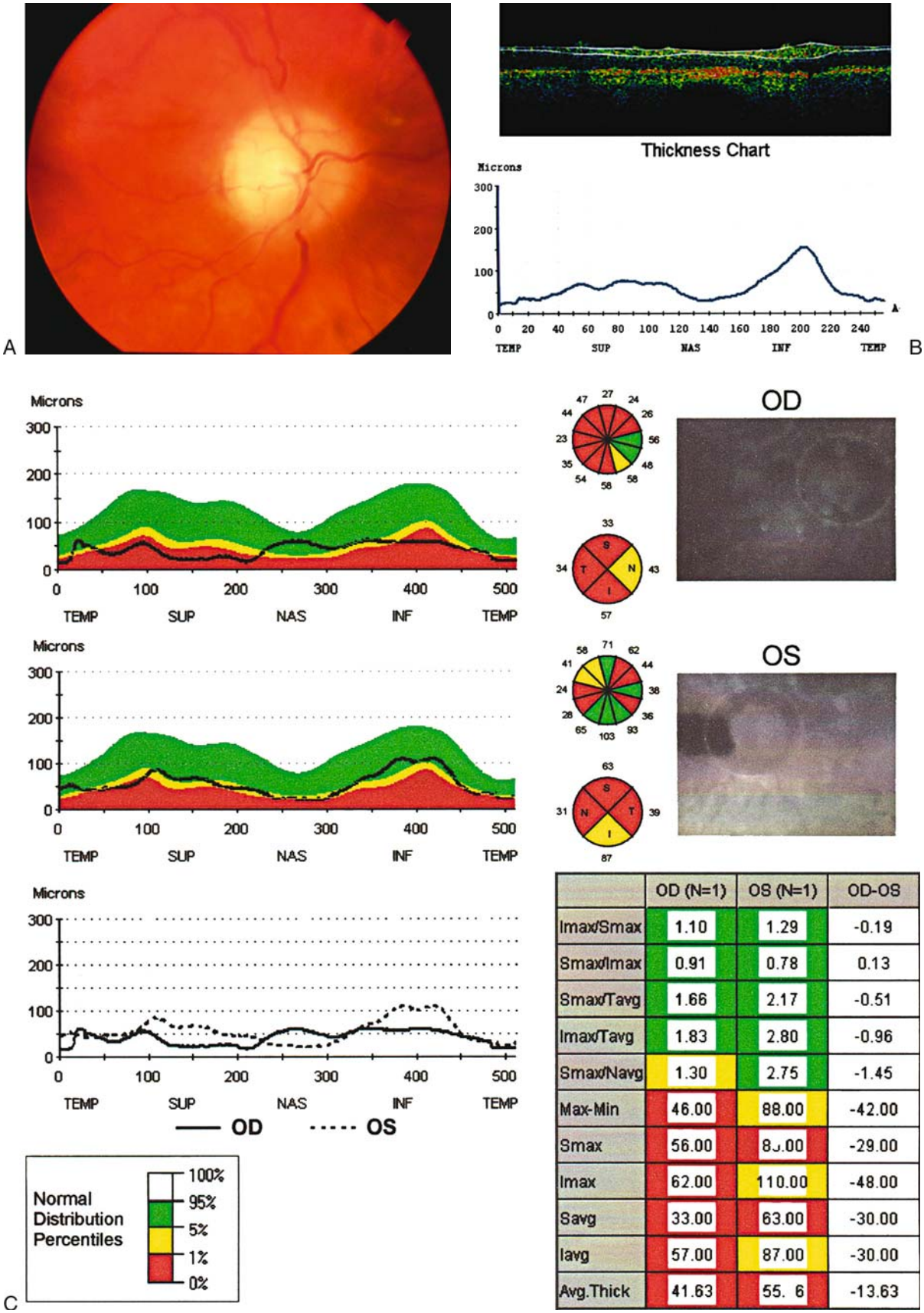

	OD (N=1)	OS (N=1)	OD-OS
Imax/Smax	1.10	1.29	-0.19
Smax/Imax	0.91	0.78	0.13
Smax/Tavg	1.66	2.17	-0.51
Imax/Tavg	1.83	2.80	-0.96
Smax/Navg	1.30	2.75	-1.45
Max-Min	46.00	88.00	-42.00
Smax	56.00	85.00	-29.00
Imax	62.00	110.00	-48.00
Savg	33.00	63.00	-30.00
Iavg	57.00	87.00	-30.00
Avg.Thick	41.63	55. 6	-13.63

FIG. 19.6. (A) Papilledema in atrophic period. (B,C) Optical coherence tomography thinning of the nerve fiber layer.

Optic Neuritis

When it is retrobulbar, optic neuritis is associated with NFL thinning, which may be observed with OCT. This can be correlated with electrophysiologic responses including pattern electroretinograms.[15,16] When optic neuritis affects the optic nerve head as papillitis, OCT can document the degree of optic nerve head and nerve fiber layer swelling (Fig. 19.7).

Anterior Ischemic Optic Neuropathy

Anterior ischemic optic neuropathy is associated with acute loss of vision or visual field, which occasionally may be progressive. Optical coherence tomography can demonstrate the degree of nerve fiber layer thickening during the acute phase and demonstrates nerve fiber layer loss in affected quadrants, which ultimately occurs over time. Optical coherence tomography may be useful in detecting incipient ischemic optic neuropathy in the opposite eye, which may be difficult to detect ophthalmoscopically. As in patients with papilledema, subretinal fluid may also develop in rare cases (Figs. 19.8 and 19.9).

Big Blind Spot Syndrome

Big blind spot syndrome is a peripapillary chorioretinal disturbance of unknown etiology, which can occur in isolation or in association with different forms of chorioretinitis including multiple evanescent white dot syndrome (MEWDS), multifocal choroiditis with panuveitis (MCP), acute macular neuroretinitis (AMN), diffuse subretinal fibrosis (DSF), punctate inner choroidopathy (PIC), and pseudo–presumed ocular histoplasmosis syndrome (P-POHS).[17] Abnormal findings have been demonstrated in visual fields, multifocal electroretinogram, and fluorescein and indocyanine green angiography. In the acute phase, when the peripapillary swelling is present, the OCT showed thickness of all the retinal layers and choroid around the optic nerve head that is correlated with the optic disc staining observed in the angiography fluorescein study (Fig. 19.10). After edema resolution, pigmentary findings can be found around the optic disc, and the OCT demonstrated fragmentation of the retinal pigment epithelium, which is related with the angiographic findings (Fig. 19.11).[18]

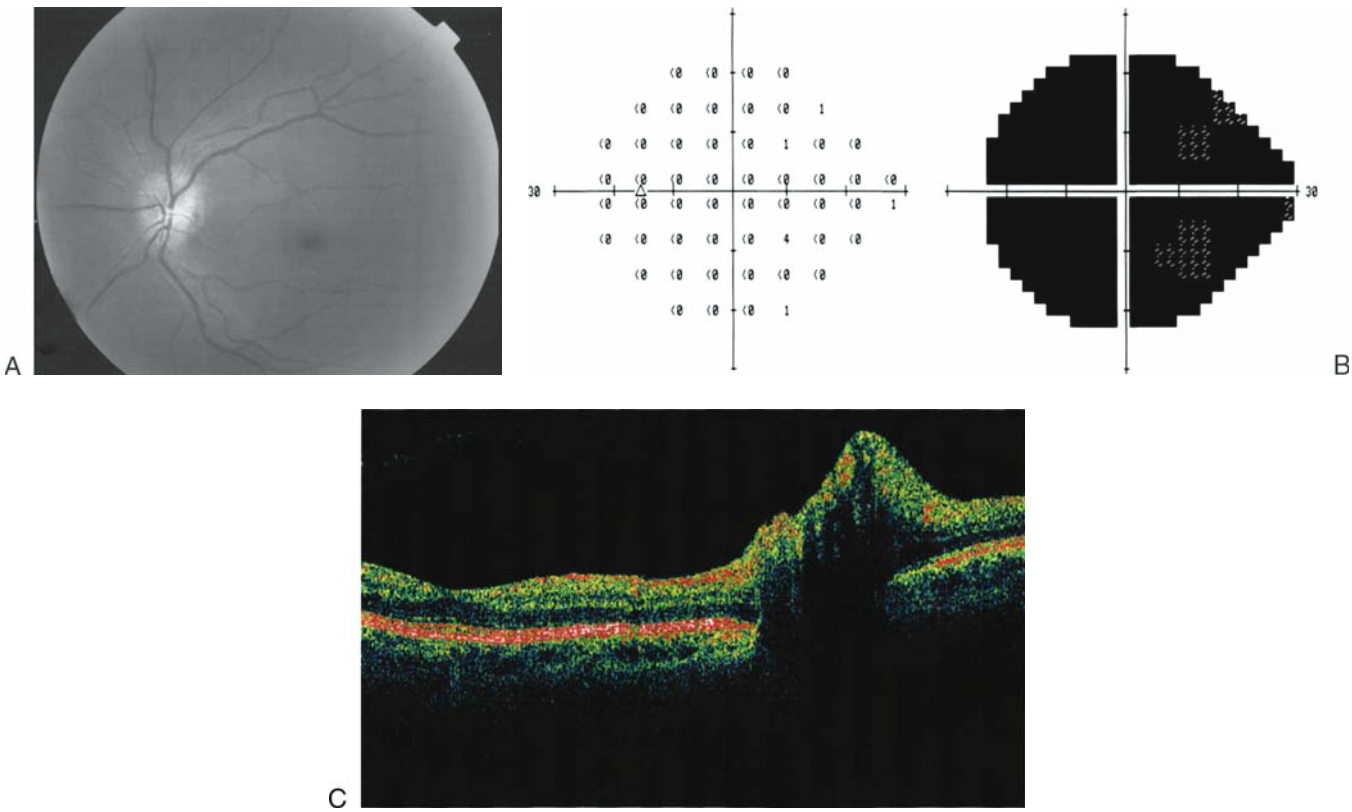

FIG. 19.7. A 48-year-old woman lost vision in the left eye. She had an afferent pupillary defect, optic disc swelling (A), and a central scotoma (B). Several demyelinating plaques were seen on MRI. (C,D) Initial OCT showed retinal nerve fiber layer (RNFL) swelling. (E) She was treated with high-dose steroids and recovered much of her vision and visual field. (F) After 1 year, the fundus of the eye demonstrated loss of superior and papillomacular nerve fiber layer. (G,H) Follow-up OCT showed RFNL dropout in the same area.

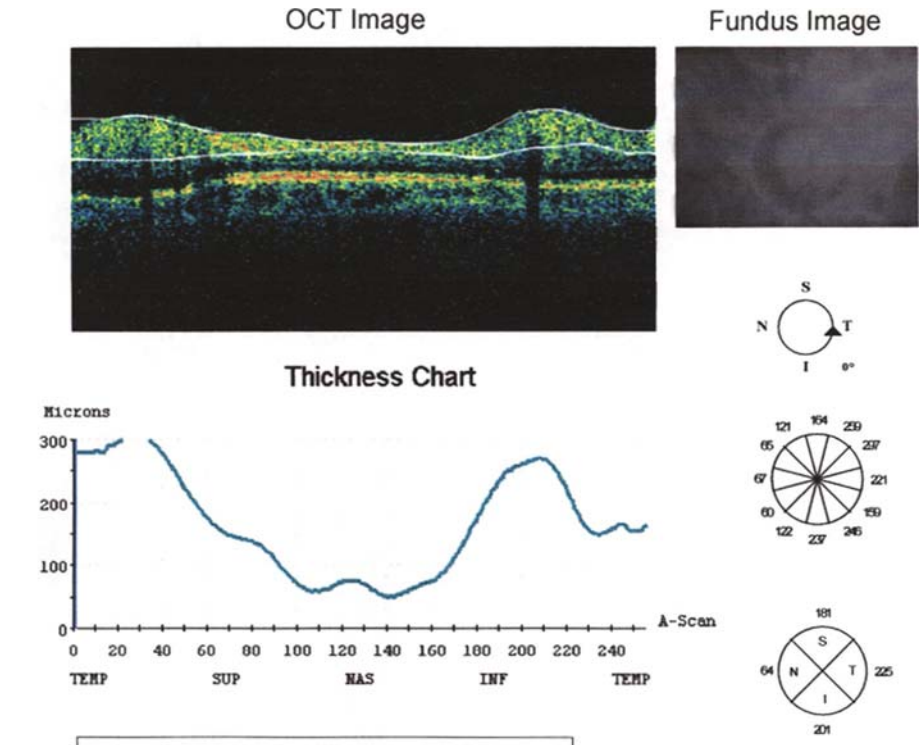

RNFL Average is	169
RNFL Thickness is	281 microns at A-scan 1
Caliper Length is	OFF
SNR	33.0
Accepted A-scans %	100.0

D

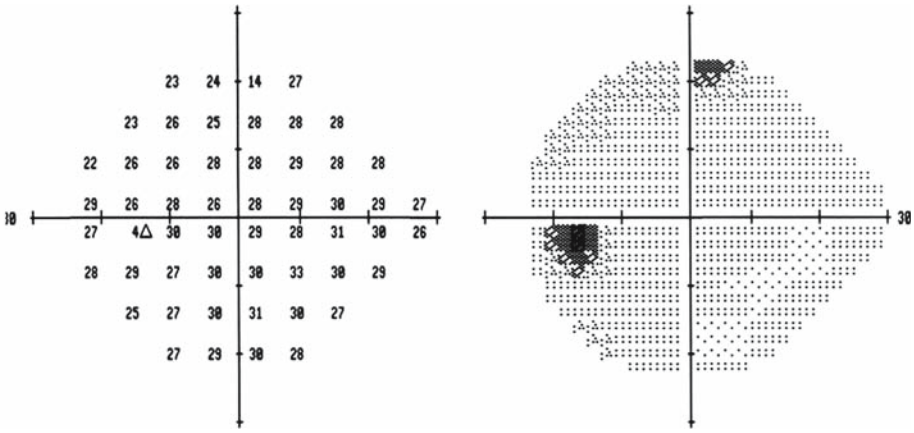

E

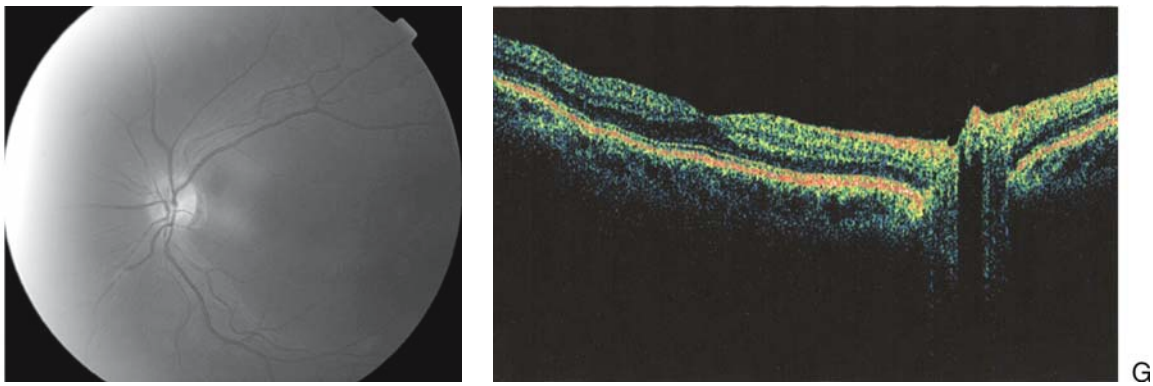

F G

FIG. 19.7. (continued).

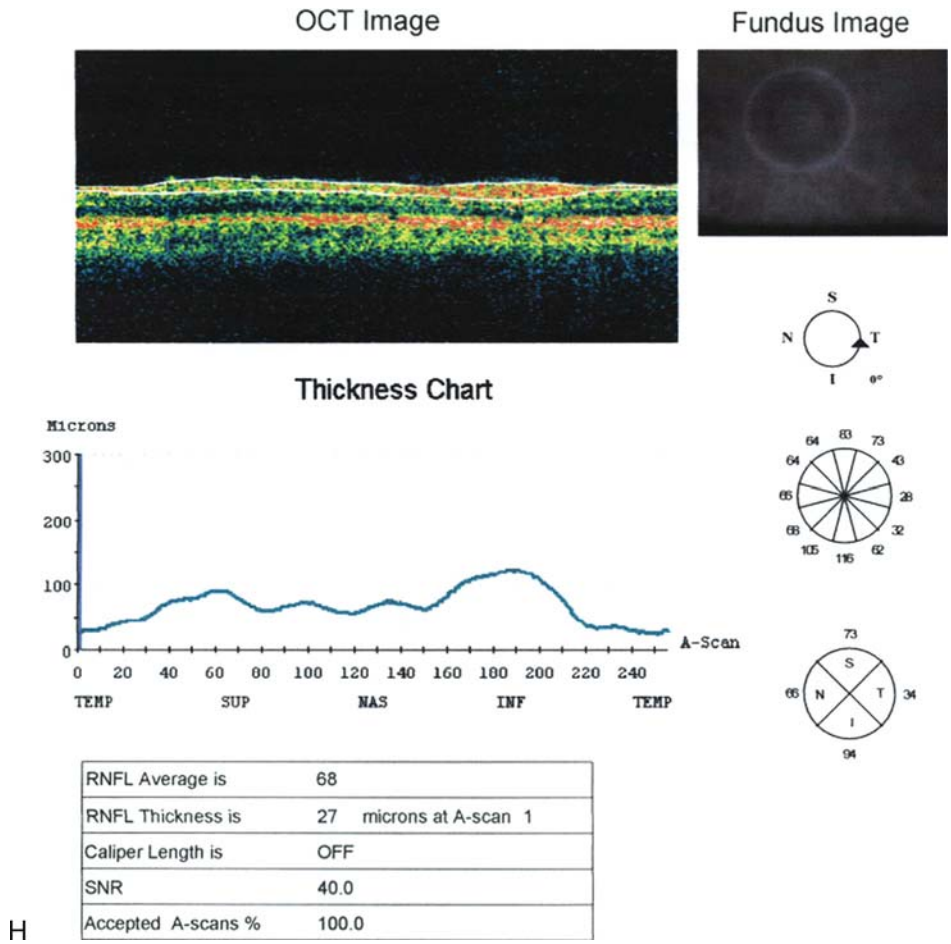

FIG. 19.7. (continued).

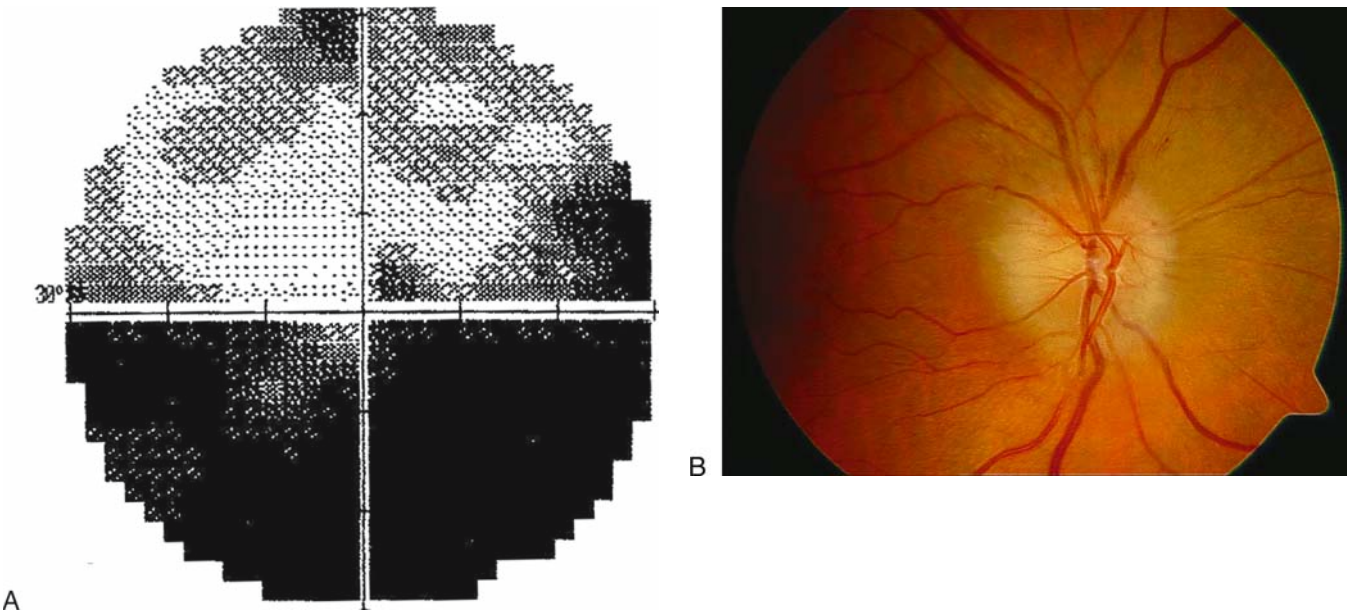

FIG. 19.8. A 57-year-old man with hypertension woke up one morning with acute visual loss. (A) The visual field demonstrated an altitudinal defect. (B) There was optic disc swelling with peripapillary, flame-shape hemorrhages. (C) The OCT showed retinal nerve fiber layer thickening.

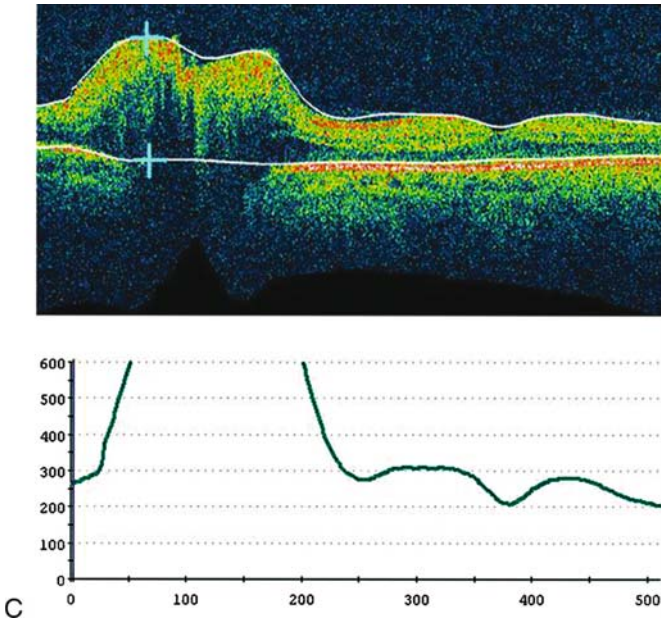

Fig. 19.8. (continued).

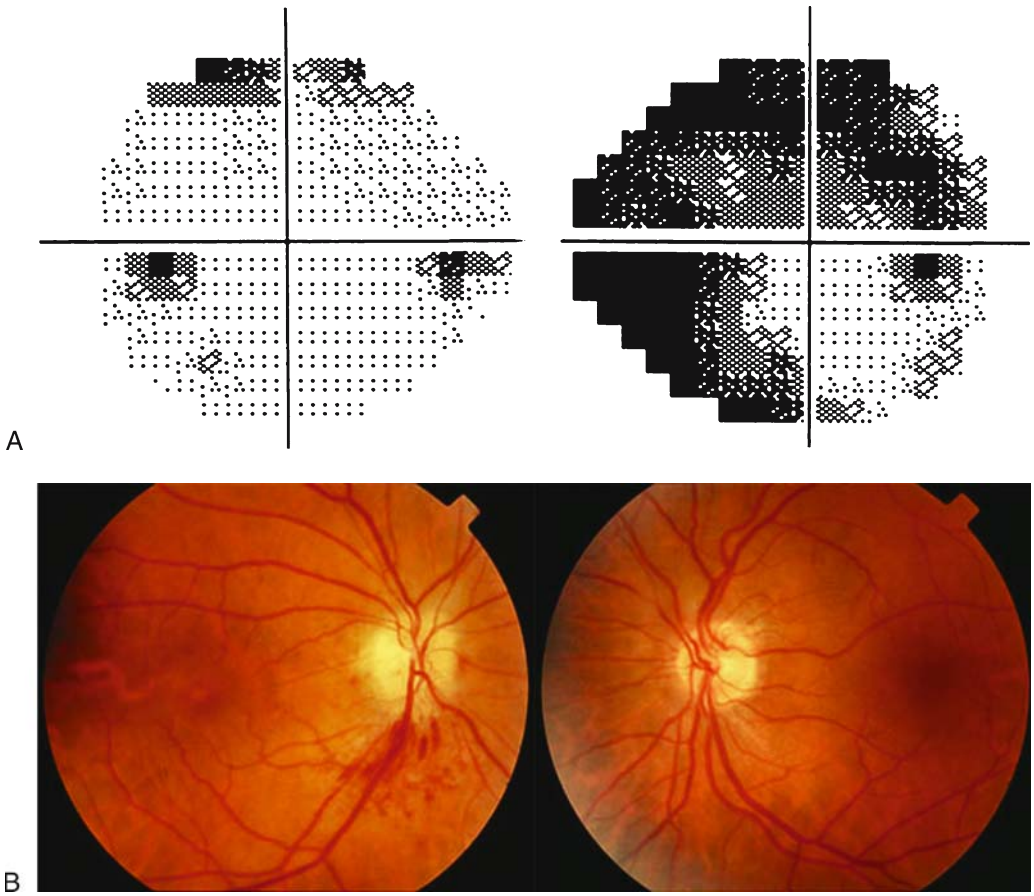

Fig. 19.9. A 71-year-old man with hypertension, hypercholesterolemia, and mitral valve prolapse developed blurred vision in the right eye. The visual acuities were 20/60 OD and 20/20 OS. (A) The right visual field demonstrated an altitudinal visual field defect. (B) The optic disc was swollen with flame hemorrhages in OD and crowding (optic disc at risk) OS. (C) Optical coherence tomography showed thickness of the nerve fiber layer with subretinal fluid in OD, and a small disc without excavation OS. (D) After 1 month, the visual field improved. (E) The optic disc edema decreased and appeared pale in the superior area. (F) The OCT demonstrated thinning of the retinal nerve fiber layer without subretinal fluid.

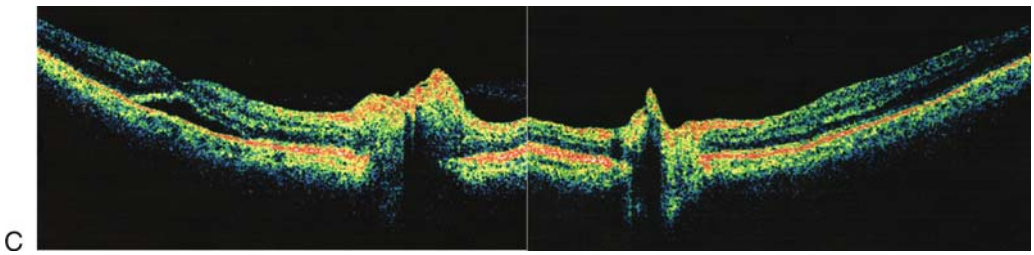

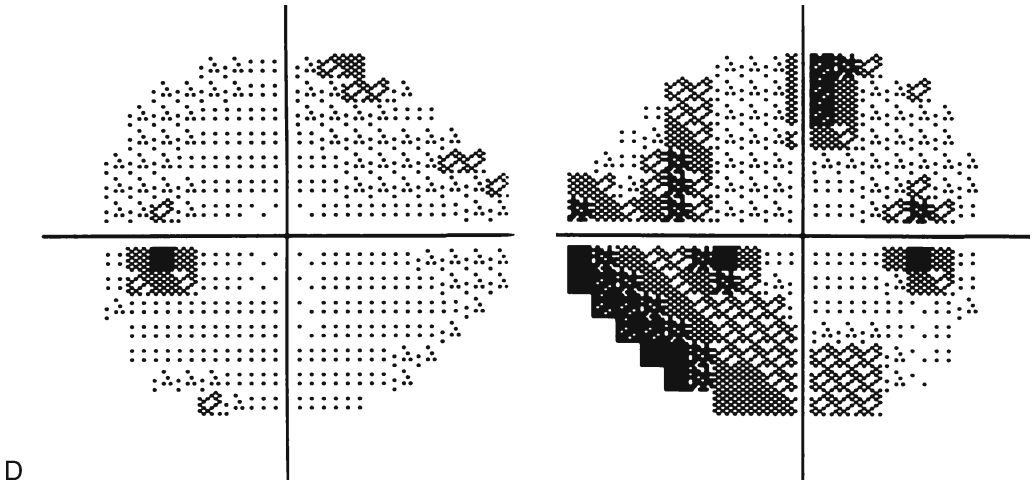

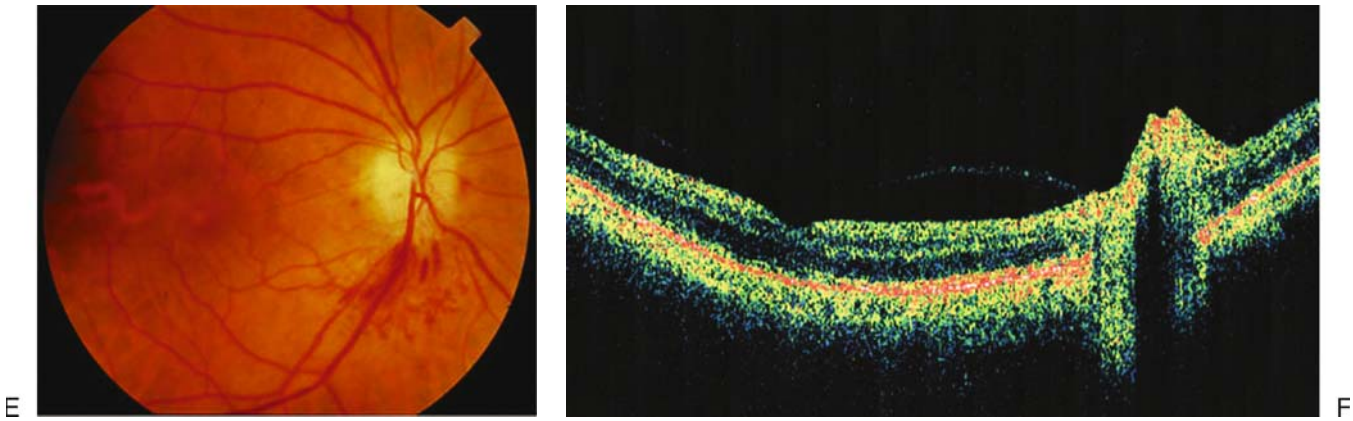

FIG. 19.9. (continued).

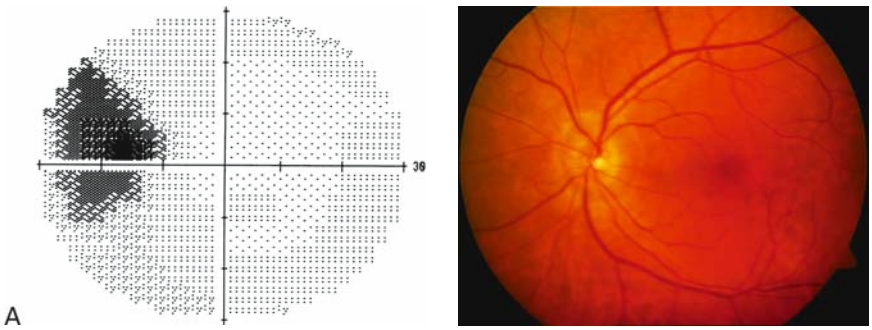

FIG. 19.10. A 51-year-old man developed unilateral blindness in the temporal field of his left eye. Flickering lights appeared intermittently within the blind area. The visual acuities were 20/20 in both eyes. (A) The visual field revealed an enlarged blind spot in the left eye. (B) The left optic disc was slightly elevated with a halo surrounding it. (C) Fluorescein angiography demonstrated peripapillary hyperfluorescence in the venous phase and multiple hyperfluorescent spots scattered throughout the retina. (D) Optical coherence tomography showed, in the radial section, thickening of the nerve fiber and retinal layers in the peripapillary area, and some backscattering in the choroid with disruption in the retinal pigment epithelium. (E) The circular tomograms showed slight thickening of the nerve fiber layer.

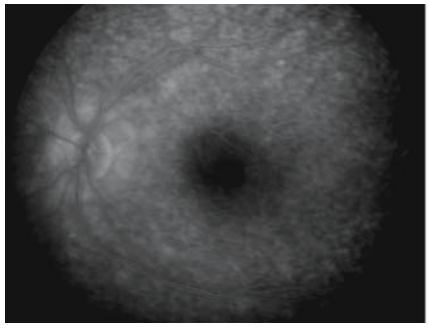

B.C

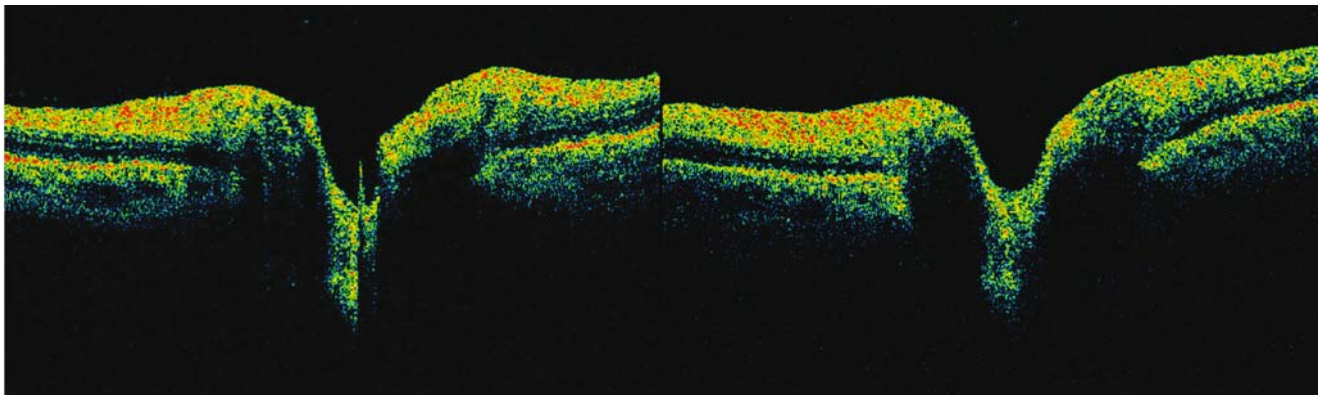

D

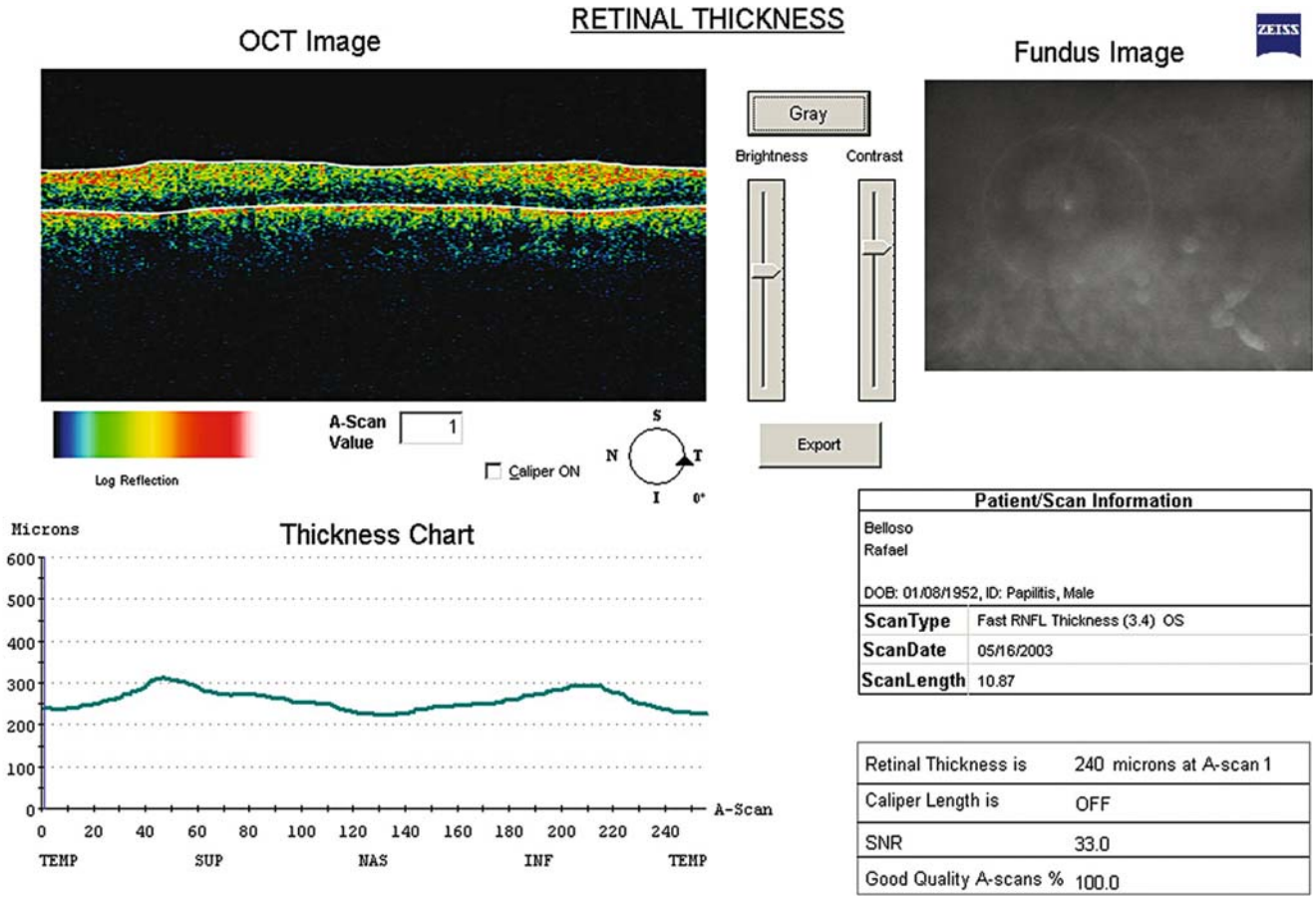

E

FIG. 19.10.(continued).

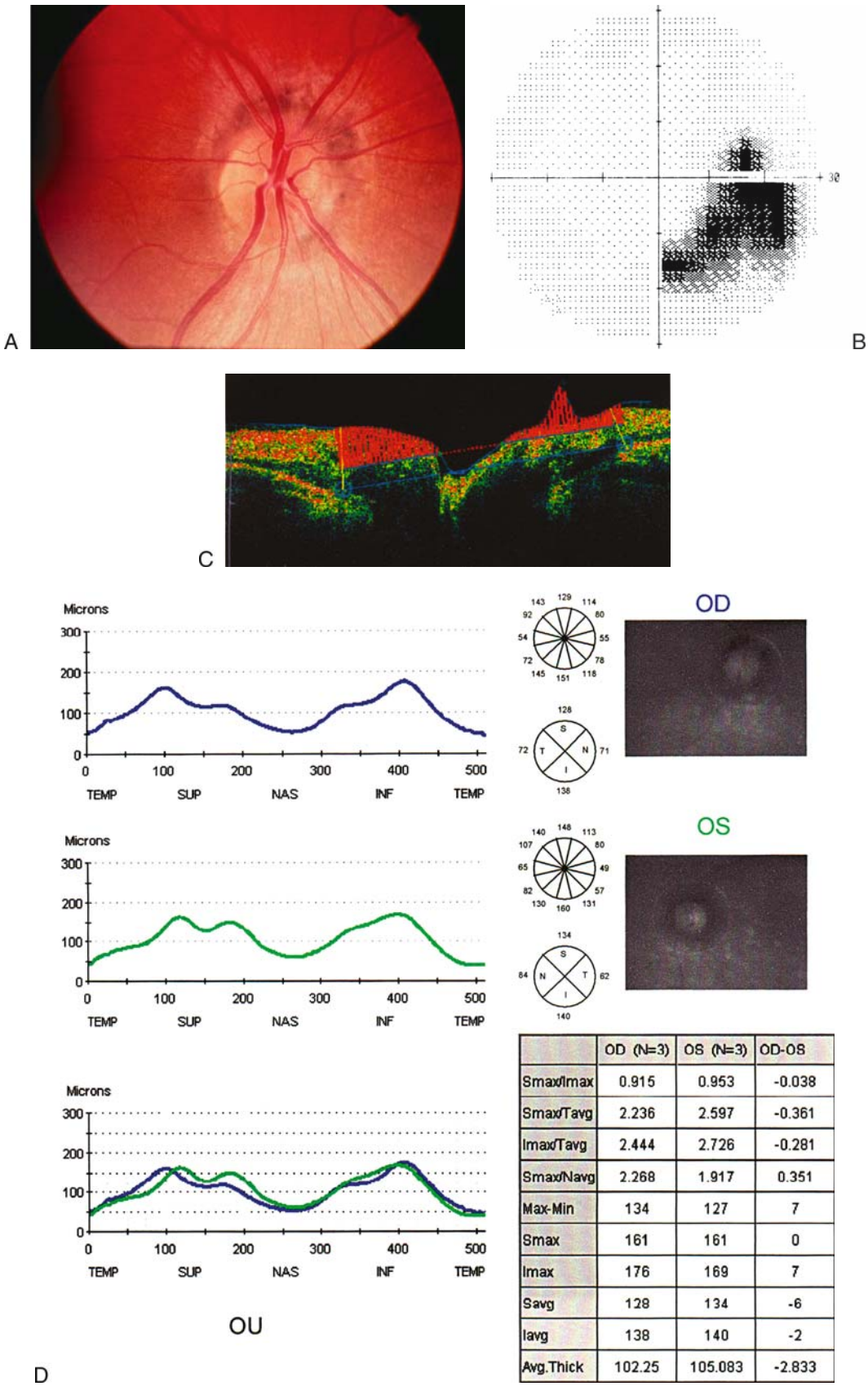

	OD (N=3)	OS (N=3)	OD-OS
Smax/Imax	0.915	0.953	-0.038
Smax/Tavg	2.236	2.597	-0.361
Imax/Tavg	2.444	2.726	-0.281
Smax/Navg	2.268	1.917	0.351
Max-Min	134	127	7
Smax	161	161	0
Imax	176	169	7
Savg	128	134	-6
Iavg	138	140	-2
Avg.Thick	102.25	105.083	-2.833

FIG. 19.11. A 34-year-old woman was followed because of several episodes blind enlargement. (A) During the last one, optic disc swelling and extensive pigmentary findings were observed in the superior area. (B) The visual field showed enlargement of the blind spot. (C) Optical coherence tomographic radial sections (90-degree) showed fragmentation of the retinal pigment epithelium in the peripapillary area. (D) The nerve fiber layer demonstrated slight diminution of the nerve fiber layer in the superior area.

Optic Nerve Melanocytoma

Optic nerve melanocytoma is an optic nerve head pigmented tumor that can extend to the adjacent retina or lamina cribrosa. Local infiltration can cause obstruction of the axoplasmic fluid with consequent optic disc edema, central vein occlusion, or sporadic malignant melanoma transformation.[19–22] In OCT, the melanocytoma shows a high reflectivity layer that continues to the high reflectance signal produced by nerve fiber layer, with optical shadowing behind it (Fig. 19.12). Optical coherence tomography is useful in following the tumor's growth, local infiltration, and occasional neurosensorial retinal detachment.[23]

Optic Nerve Meningioma

Optic nerve meningioma and other compressive optic neuropathies lead to optic atrophy, which can be demonstrated by OCT (Fig. 19.13). However, in these cases, visual field loss precedes the nerve fiber layer loss and, ideally, treatment should be provided before permanent nerve fiber layer degeneration appears. In some cases, optic nerve sheath meningioma may lead to swelling of the optic nerve head, which in many ways resembles papilledema. This also could be documented with OCT.

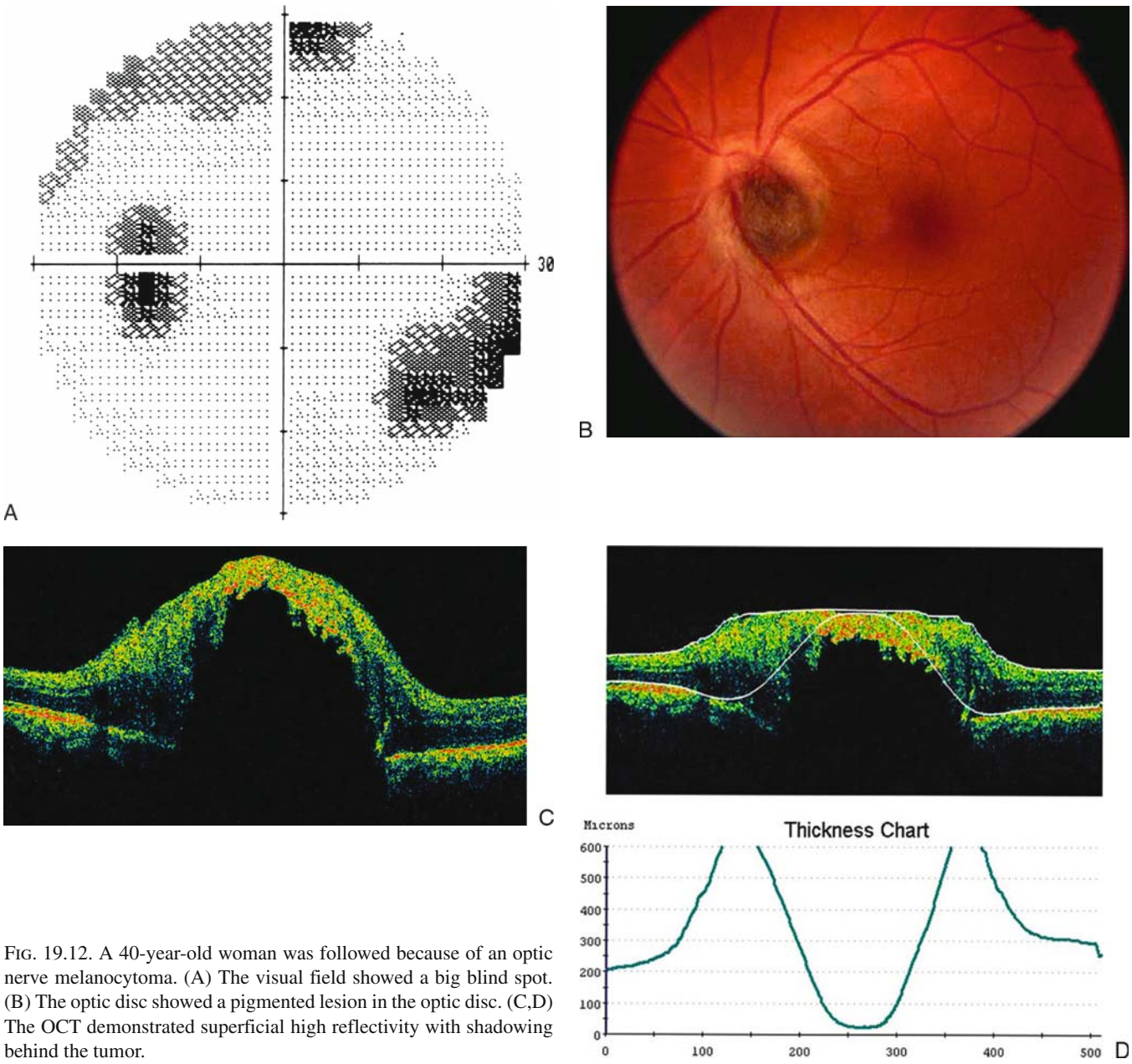

Fig. 19.12. A 40-year-old woman was followed because of an optic nerve melanocytoma. (A) The visual field showed a big blind spot. (B) The optic disc showed a pigmented lesion in the optic disc. (C,D) The OCT demonstrated superficial high reflectivity with shadowing behind the tumor.

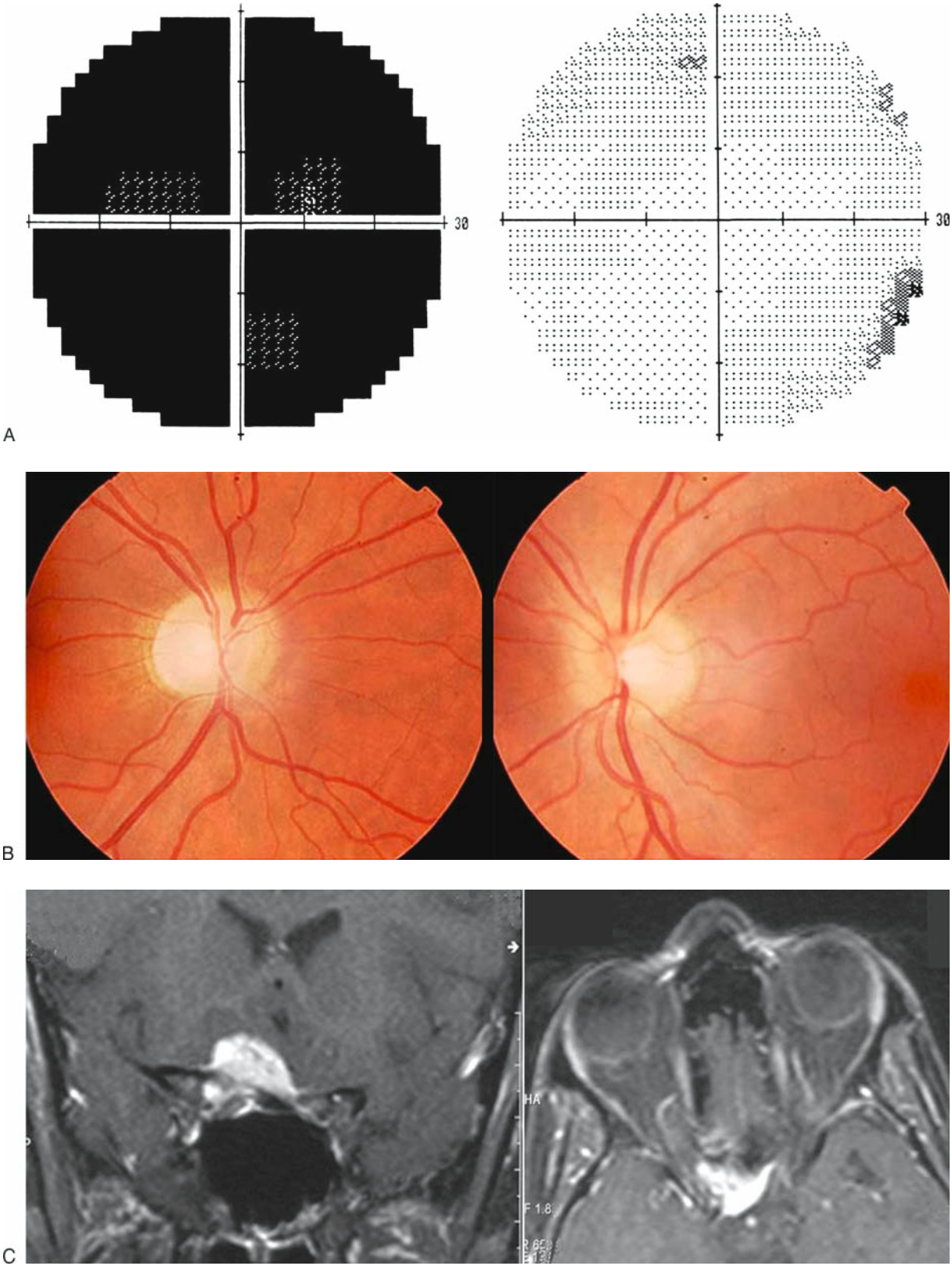

FIG. 19.13. (A) A chiasmal meningioma was associated with a visual deficit in both eyes, more marked in the right eye, in this patient. (B) The optic disc was pale. (C) The MRI demonstrated chiasmal tumor with the "tail" sign. (D,E) Optical coherence tomography showed depletion of the nerve fiber layer especially in the right eye.

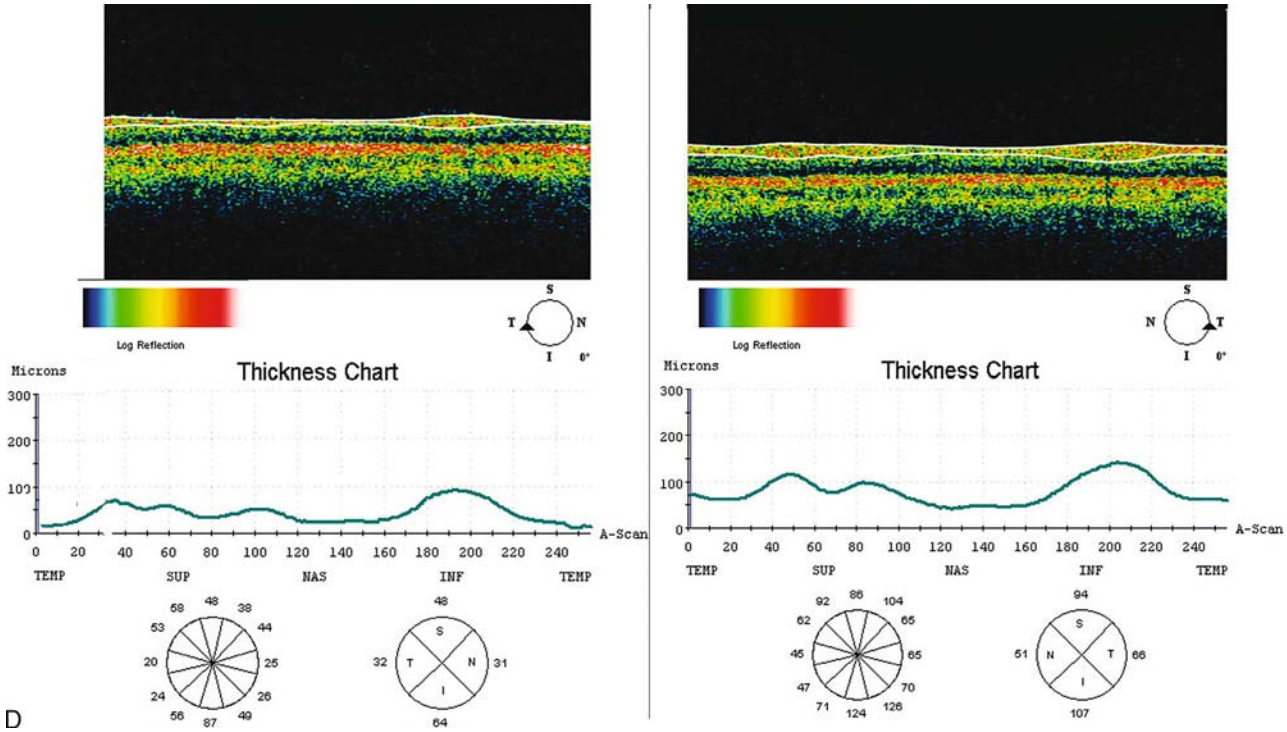

D

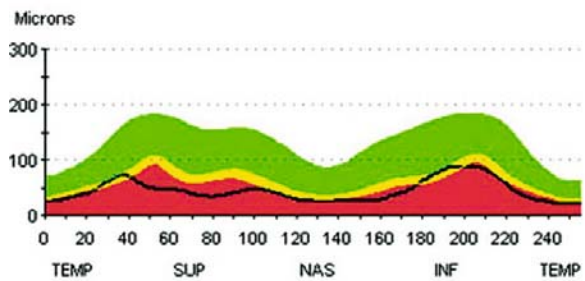

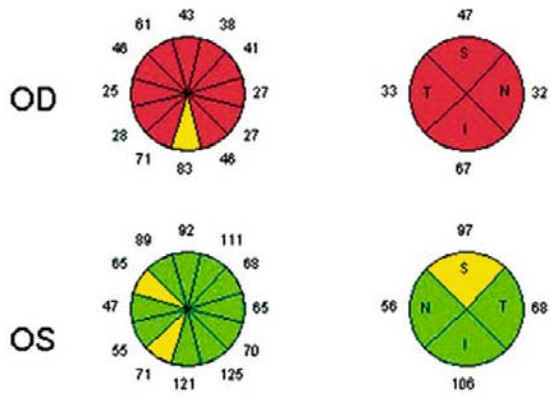

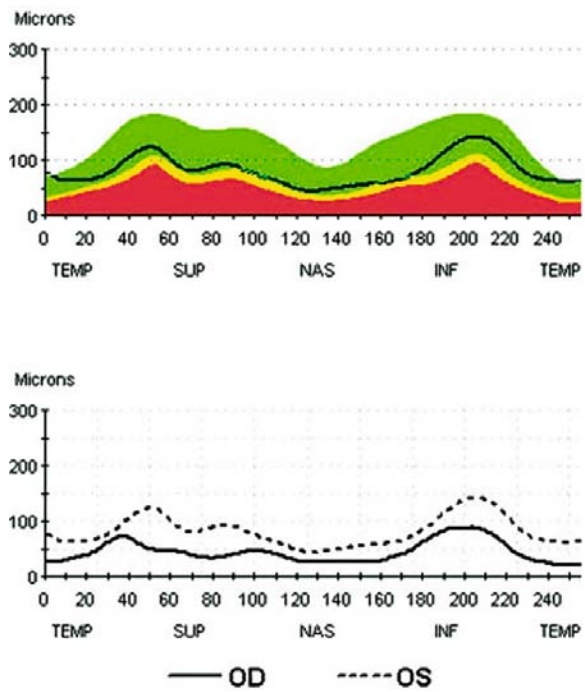

E

Patient/Scan Information	
	Female
ScanType	Fast RNFL Thickness (3.4)
ScanDate	01/05/2004
ScanLength	10.87

	OD (N=3)	OS (N=3)	OD-OS
Imax/Smax	1.24	1.14	0.10
Smax/Imax	0.81	0.88	-0.07
Smax/Tavg	2.16	1.83	0.33
Imax/Tavg	2.68	2.08	0.60
Smax/Navg	2.24	2.23	0.01
Max-Min	68.00	96.00	-28.00
Smax	72.00	124.00	-52.00
Imax	89.00	141.00	-52.00
Savg	47.00	97.00	-50.00
Iavg	67.00	106.00	-39.00
Avg.Thickness	44.71	81.61	-36.90

FIG. 19.13. (continued).

Traumatic Optic Neuropathy

The retinal nerve fiber layer loss begins between 4 and 8 weeks after the onset of the injury. Over time, the nerve fiber layer becomes thinner, but some nerve fiber layer preservation is evident even when the optic nerve head becomes atrophic. Optical coherence tomography is useful in demonstrating the nerve fiber layer loss over time.[24]

References

1. Jaffe GJ, Caprioli J. Optical coherence tomography to detect and manage retinal disease and glaucoma. Am J Ophthalmol 2004;137(1):156–169.
2. Krivoy D, Gentile R, Liebmann JM, et al. Imaging congenital optic disc pits and associated maculopathy using optical coherence tomography. Arch Ophthalmol 1996;114(2):165–170; erratum in Arch Ophthalmol 1996;114(7):840.
3. Theodossiadis GP, Theodossiadis PG. Optical coherence tomography in optic disc pit maculopathy treated by the macular buckling procedure. Am J Ophthalmol 2001;132(2):184–190.
4. Rutledge BK, Puliafito CA, Duker JS, Hee MR, Cox MS. Optical coherence tomography of macular lesions associated with optic nerve head pits. Ophthalmology 1996;103(7):1047–1053.
5. Konno S, Akiba J, Sato E, Kuriyama S, Yoshida A. OCT in successful surgery of retinal detachment associated with optic nerve head pit. Ophthalmic Surg Lasers 2000;31(3):236–239.
6. Landau K, Djahanshahi-Bajka J, Kirchschläger BM. Topless optic discs in children of mothers with type I diabetes mellitus. Am J Ophthalmol 1998;125(5):605–611.
7. Unoki K, Ohba N, Hoyt WF. Optical coherence tomography of superior segmental optic hypoplasia. Br J Ophthalmol 2002;86: 910–914.
8. Becquet F, Ducournau D, Ducournau Y, Goffart Y, Spencer WH. Juxtapapillary subretinal pigment epithelial polypoid pseudocysts associated with unilateral tilted optic disc. Ophthalmology 2001;108:1657–1662.
9. Fournier AV, Damji KF, Epstein DL, Pollock SC. Disc excavation in dominant optic atrophy. Differentiation from normal tension glaucoma. Ophthalmology 2001;108:1595–1602.
10. Roh S, Noecker RJ, Schumman J, Hedges TR III, Weiter JJ, Mattox C. Effect of optic nerve head drusen on nerve fiber layer thickness. Ophthalmology 1998;105(5):878–885.
11. Roh S, Noecker RJ, Schumman J. Evaluation of coexisting optic nerve head drusen and glaucoma with optical coherence tomography. Ophthalmology 1997;104(7):1138–1144.
12. Ocakoglu O, Ustundag C, Koyluoglu N, Oguz V, Kendiroglu G, Ozkan S. Long term follow-up of retinal nerve fiber layer thickness in eyes with optic nerve head drusen. Curr Eye Res 2003;26(5):277–280.
13. Karam EZ, Hedges TR, Szwarts. Optical coherence tomography shows increased nerve fiber layer thickness in pseudo- and mild papilledema. Association for Research in Vision and Opthalmology (ARVO) Meeting Abstracts 1998;704(B627):S150.
14. Hoye VJ, Berroca AM, Hedges TR III, Amaro ML. Optical coherence tomography demonstrates subretinal macular edema from papilledema. Arch Ophthalmol 2001;119:1287–1290.
15. Parisi V. Correlation between morphological and functional retinal impairment in patients affected by ocular hypertension, glaucoma, demyelinating optic neuritis and Alzheimer's disease. Semin Ophthalmol 2003;18(2):50–57.
16. Parisi V, Manni G, Spadaro M, et al. Correlation between morphological and functional retinal impairment in multiple sclerosis patients. Invest Ophthalmol Vis Sci 1999;40(11):2520–2527.
17. Gray RH. Unilateral enlargement of the blind spot: a diagnostic dilemma. Br J Ophthalmol 2002;86(8):936–938.
18. Karam EZ, Morales SJ, Belloso M, Perret K. Optical coherence tomography: a new tool in the diagnosis of big blind syndrome. Poster presented at North American Neuro-ophthalmology Society Meeting, March 27 to April 1, 2004, Orlando, FL.
19. Apple DJ, Craythorn JM, Reidy JJ, Steinmetz RL, Brady SE, Bohart WA. Malignant transformation of an optic nerve melanocytoma. Can J Ophthalmol 1984;19(7):320–325.
20. Shields JA, Shields CL, Eagle RC Jr, Lieb WE, Stern S. Malignant melanoma associated with melanocytoma of the optic disc. Ophthalmology 1990;97(2):225–230.
21. Meyer D, Ge J, Blinder KJ, Sinard J, Xu S. Malignant transformation of an optic disc melanocytoma. Am J Ophthalmol 1999;127(6):710–714.
22. Shields JA, Shields CL, Eagle RC Jr, Singh AD, Berrocal MH, Berrocal JA. Central retinal vascular obstruction secondary to melanocytoma of the optic disc. Arch Ophthalmol 2001;119(1):129–133.
23. Antcliff RJ, Ffytche TJ, Shilling JS, Marshall J. Optical coherence tomography of melanocytoma. Am J Ophthalmol 2000;130(6):845–847.
24. Medeiros FA, Moura FC, Vessani RM, Susanna R. Axonal loss after traumatic optic neuropathy documented by optical coherence tomography. Am J Ophthalmol 2003;135(3):406–408.

20
Clinical Applications of Optical Coherence Tomography in Intraocular Tumors

Carol L. Shields, Miguel A. Materin, and Jerry A. Shields

There are several tumors that can occur in the posterior segment of the eye.[1,2] They are generally classified based on the main tissue involved such as the choroid, retinal pigment epithelium (RPE), or retina. The spectrum of tumors in each tissue varies. For example, tumors in the choroid include the melanocytic nevus, melanoma, metastasis, cavernous hemangioma, and other less common tumors such as lymphoma, neurilemoma, leiomyoma, and osteoma.[1,2] Lesions of the RPE include congenital hypertrophy, congenital simple hamartoma, combined hamartoma, reactive hyperplasia, adenoma, and adenocarcinoma. Those affecting the retina include capillary hemangioma, cavernous hemangioma, racemose hemangioma, vasoproliferative tumor, astrocytic hamartoma, and retinoblastoma. The differentiation of these tumors by experienced clinicians is made primarily by indirect ophthalmoscopy. Ancillary testing with intravenous fluorescein angiography, indocyanine green angiography, ultrasonography, optical coherence tomography (OCT), color Doppler testing, magnetic resonance imaging, computed tomography, and fine-needle aspiration biopsy can assist in confirming the diagnosis.[1,2] This chapter presents the OCT findings of selected intraocular tumors.

Optical coherence tomography provides cross-sectional imaging of the retina and RPE primarily, and deeper tissues, including the choroid and sclera, show poorer resolution. With this in mind, OCT of retinal and RPE tumors shows good resolution, whereas OCT of choroidal tumors shows only superficial information of the choroidal tumor, but more extensive information of the overlying retina and RPE.

Choroidal Tumors

Choroidal Nevus

Choroidal melanocytic nevus is a benign tumor that is seen with increasing frequency in the latter decades of life. It is estimated that between 4% and 6% of Caucasians manifest a uveal nevus.[3] It can occur in the iris, ciliary body, or choroid, and is most frequent in the posterior choroid. Choroidal nevus varies in size from a fraction of a millimeter to several millimeters in the base. The degree of pigmentation can extend from dark brown to slate gray to completely yellow, or it can be amelanotic. The shape of a choroidal nevus is generally round to oval, and it usually manifests smooth regular margins, but slightly irregular margins can be found. Overlying degenerative changes of the retina and RPE can occur, with the most common being drusen, retinal pigment epithelial atrophy and hyperplasia, and clumped orange pigment. Less commonly, subretinal neovascularization and serous and hemorrhagic detachments of the retina and RPE can occur.

Most choroidal nevi are less than 2 mm in thickness. It is often difficult to differentiate those nevi that are near 2 mm in thickness from small choroidal melanoma. The following risk factors predictive of small melanoma have been identified: (1) tumor thickness greater than 2 mm; (2) overlying orange pigment; (3) associated subretinal fluid; (4) symptoms of flashes, floaters, or blurred vision; and (5) location of the mass at the optic disc.[4–6] The presence of three or more of these five risk factors imparts greater than 50% risk that the tumor will grow, a sign of malignant melanoma.

In general, a choroidal nevus is poorly imaged on OCT due to its location deep in the choroid; however, the overlying retina can show several alterations. In an assessment of 120 eyes with choroidal nevus using OCT, Shields and coworkers[7] found related retinal findings that included overlying retina edema (15%), subretinal fluid (26%), retinal thinning (22%), drusen (41%), and RPE detachment (12%) (Figs. 20.1 to 20.3). Furthermore, OCT permitted classification of the overlying retinal edema as focal cystoid (3%), diffuse cystoid (8%), coalescent cystoid (3%), and noncystoid edema (1%). On OCT, the overlying retina was normal thickness (32%), thinned (22%), or thickened (45%), and photoreceptor loss or attenuation was noted in 51% of cases. Specific OCT findings of the choroidal nevus were limited to its anterior surface with minimal information deeper within the mass. These findings included increased thickness of the RPE/choriocapillaris layer (68%) and optical qualities within the anterior portion of the nevus of hyporeflectivity (62%), isoreflectivity (29%),

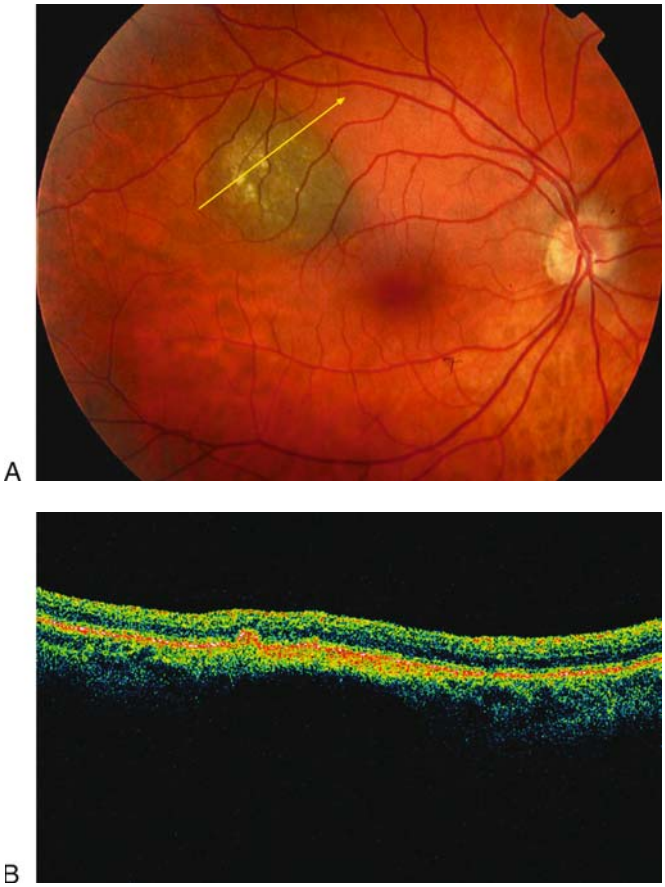

FIG. 20.1. Choroidal nevus. (A) Pigmented choroidal nevus displays overlying drusen. (B) Optical coherence tomography (OCT) shows thickening and hyperreflectivity of the retinal pigment epithelium (RPE)/choriocapillaris layer and hyporeflectivity (optical shadowing) of the choroid at the site of the nevus. Note the subtle multifocal elevations at the level of the RPE/choriocapillaris suggestive of drusen.

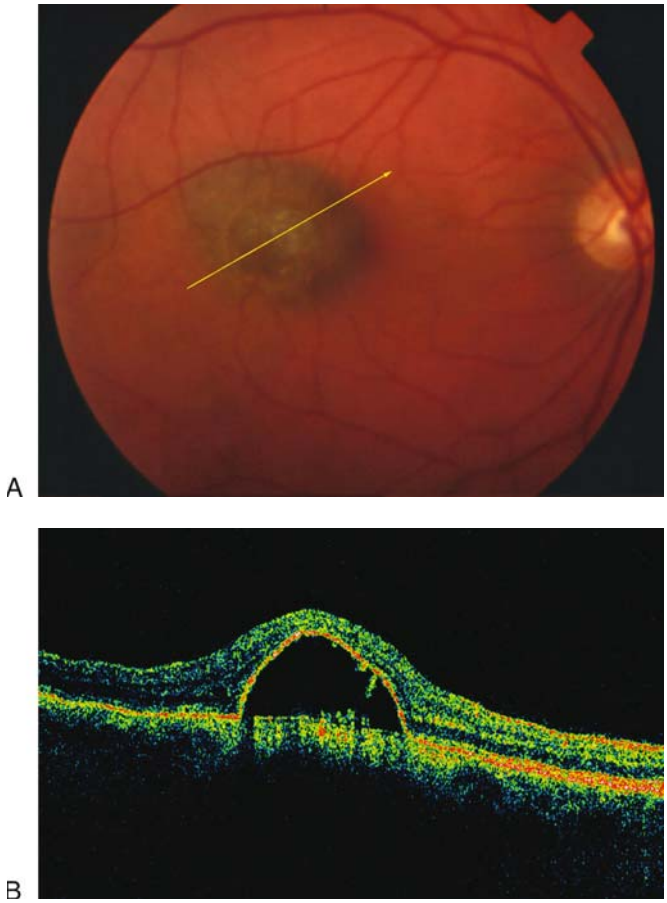

FIG. 20.2. Choroidal nevus. (A) Pigmented choroidal nevus shows overlying RPE detachment outlined with subtle orange pigment. (B) Optical coherence tomography shows obvious overlying RPE detachment with debris in the subpigment epithelial space.

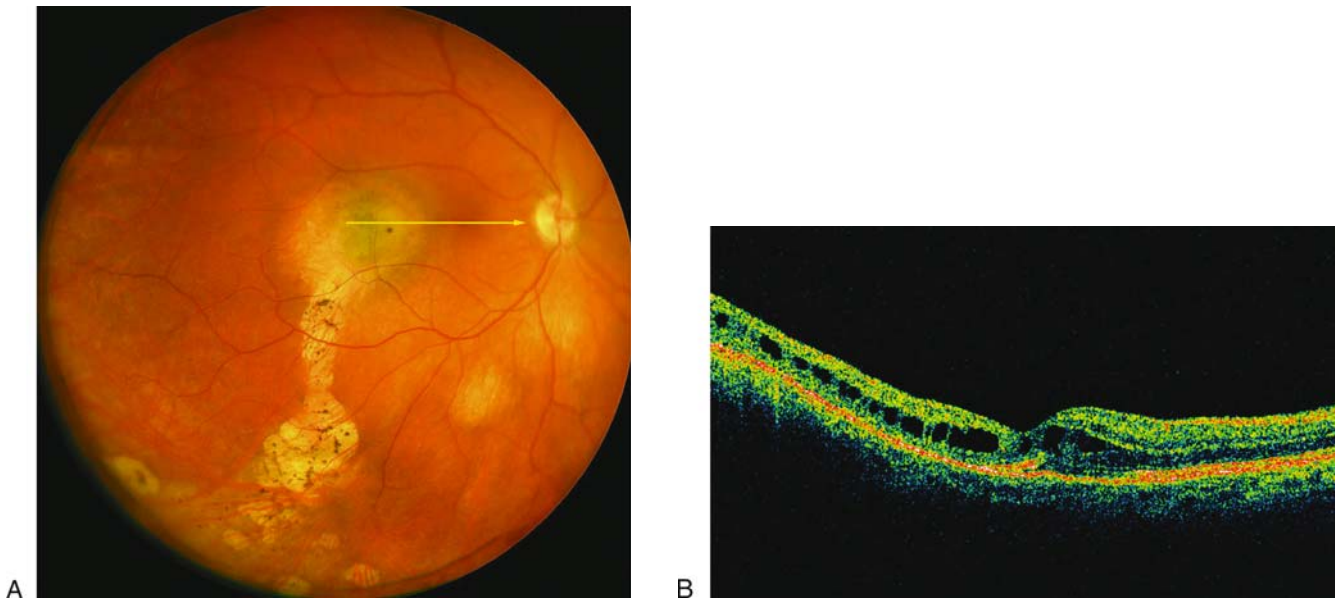

FIG. 20.3. Choroidal nevus. (A) Lightly pigmented choroidal nevus displays chronic RPE alterations inferiorly suggestive of resolved subretinal fluid. (B) Optical coherence tomography reveals diffuse cystoid retinal edema over the elevated portion of the nevus and extending into the fovea.

Table 20.1. Optical coherence tomography (OCT) in 120 eyes of 120 patients with choroidal nevus: correlation between nevus pigmentation and OCT findings.[7]

Findings	Pigmented choroidal nevus (*n* = 109)	Nonpigmented choroidal nevus (n = 11)
Retinal findings		
Retinal edema	16 (15%)	2 (18%)
Retinal thinning	22 (22%)	4 (40%)
Photoreceptor layer loss or thinning	55 (50%)	5 (45%)
Retinal pigment epithelium (RPE)/ choriocapillaris findings		
RPE/choriocapillaris thickening	76 (70%)	6 (55%)
RPE/choriocapillaris hyperreflectivity	58 (53%)	4 (36%)
RPE/choriocapillaris fragmentation	16 (15%)	7 (64%)
RPE/choriocapillaris surface irregularity	48 (44%)	7 (64%)
Choroidal findings		
Anterior choroid reflectivity[a]		
Hyporeflective	61 (68%)	2 (18%)
Isoreflective	23 (26%)	6 (55%)
Hyperreflective	6 (7%)	3 (27%)

[a]Information on anterior choroid reflectivity was available only for 101 nevi. There were 19 pigmented and 0 nonpigmented nevi where the data was unavailable.

and hyperreflectivity (9%). Hyporeflectivity was observed in 68% of pigmented nevi and 18% of nonpigmented nevi (Table 20.1). When comparing OCT to clinical examination, these authors concluded that OCT was more sensitive in the detection of related retinal edema, subretinal fluid, retinal thinning, photoreceptor attenuation, and RPE detachment.[7]

The findings on OCT of retinal edema, RPE alterations, photoreceptor loss, and RPE detachment are related to chronic retinal degeneration and suggest a stable, chronic choroidal nevus.[7] On the other hand, the presence of subretinal fluid and photoreceptor preservation suggests a more acute situation and potentially a more active lesion with risk for growth into melanoma.[8]

Choroidal Melanoma

Malignant melanoma of the choroid is uncommon, found in six persons per million population.[1,2,9,10] Melanoma usually grows as a localized elevated mass protruding toward the vitreous cavity on its inner aspect and limited by the sclera on its outer aspect. Occasionally, it grows into a mushroom configuration or grows horizontally as a diffuse, flat lesion.[11] As the tumor grows, it may become associated with widespread changes in the overlying RPE including atrophy and degeneration, clumped orange pigment, serous RPE detachment, sensory retinal detachment, sensory retinal infiltration or erosion, cystoid retinal edema, and occasionally hemorrhage.

Choroidal melanoma, in general, is poorly imaged on OCT. However, detection of overlying subretinal fluid by OCT could be important in confirming the suspicion of melanoma in eyes with borderline small or intermediate-size tumors.[8] This confirms the previous clinical observations that the presence of subretinal fluid is a risk factor for eventual growth of the tumor.[4–6] Espinoza and coworkers[8] showed that OCT findings of subretinal fluid might have a predictive value in identifying choroidal melanocytic tumors that are likely to grow. In an assessment using OCT on 30 eyes with suspicious choroidal melanocytic lesions, tumor growth was found in only 8% of those with no subretinal fluid, 50% of those with active subretinal fluid, and 11% of those with retinal atrophy or edema.

Optical coherence tomography is particularly useful for determining the presence and degree of radiation-related maculopathy or papillopathy following radiotherapy of choroidal melanoma. Radiation retinopathy is the most common cause of irreversible visual loss in patients treated with plaque or charged particle radiotherapy for choroidal melanoma. The clinical manifestations of radiation retinopathy appear as slow-onset occlusive retinal vasculopathy leading to intraretinal edema, exudation, hemorrhage, and eventual retinal atrophy. Optical coherence tomography can detect intraretinal edema before it is visually symptomatic or clinically appreciable. It is also useful in monitoring resolution of radiation-induced macular edema following therapy with laser photocoagulation or intravitreal triamcinolone acetonide (Fig. 20.4). In an assessment of 31 patients with plaque-irradiated choroidal melanoma and radiation maculopathy, foveal thickness by OCT at the time of clinical detection of maculopathy was a mean of 417 μm, and following intravitreal triamcinolone acetonide, the thickness decreased to 207 μm at 1 month, 305 μm at 6 months, and 273 μm at 12 months.[12] The long-term effects of intravitreal triamcinolone for radiation maculopathy is not known, but monitoring of the macular edema with OCT is informative and provides an objective guideline for documentation of treatment results.

Choroidal Metastasis

Cancer metastatic to the choroid is probably more common than generally realized.[1,2,13] It typically originates from breast carcinoma or lung carcinoma. Choroidal metastases can be unilateral and unifocal or bilateral and multifocal. The bilateral lesions are related to breast carcinoma in nearly 70% of cases.[13] Lung carcinoma metastasis is usually unifocal. Most choroidal metastases occur posterior to the equator of the fundus in the macular or paramacular regions. It generally appears as a flat or slightly elevated amelanotic lesion with poorly discernible margins. Scattered clumps of brown pigment can be seen over the lesion, which correlates histopathologically with lipofuscin pigment within macrophages at the level of the RPE. Overlying RPE changes and sensory retinal detachment can accompany these lesions.

Like other choroidal tumors, choroidal metastasis is not well imaged by OCT, but the overlying retinal and RPE changes can be illustrated. Optical coherence tomography can depict overlying subretinal fluid, RPE hyperplasia, RPE detachment, and clumps of orange pigment. Resolution of subretinal fluid on OCT can be documented following therapy of the metastasis (Fig. 20.5).[14]

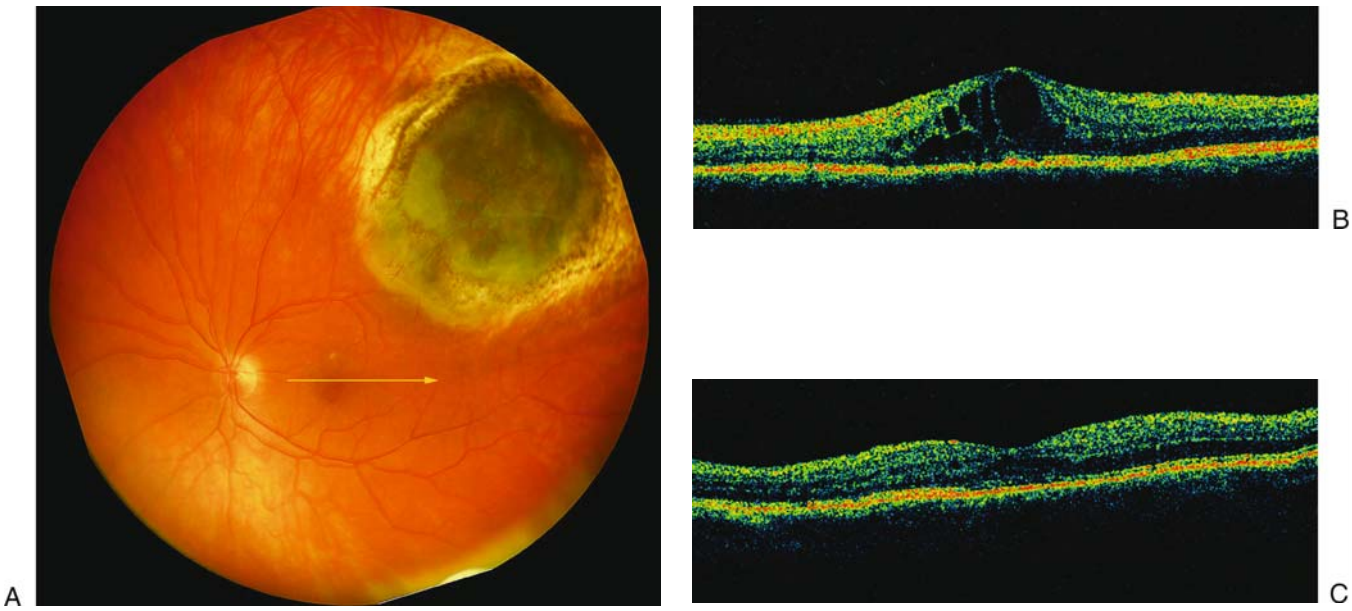

FIG. 20.4. Choroidal melanoma. (A) Twelve months following plaque radiotherapy for a choroidal melanoma, tumor regression was achieved but radiation maculopathy was noted. (B) At that time, OCT revealed cystoid macular edema of 446 μm and intravitreal triamcinolone acetonide was injected. (C) Four months after injection, the foveal anatomy was restored with foveal thickness of 207 μm.

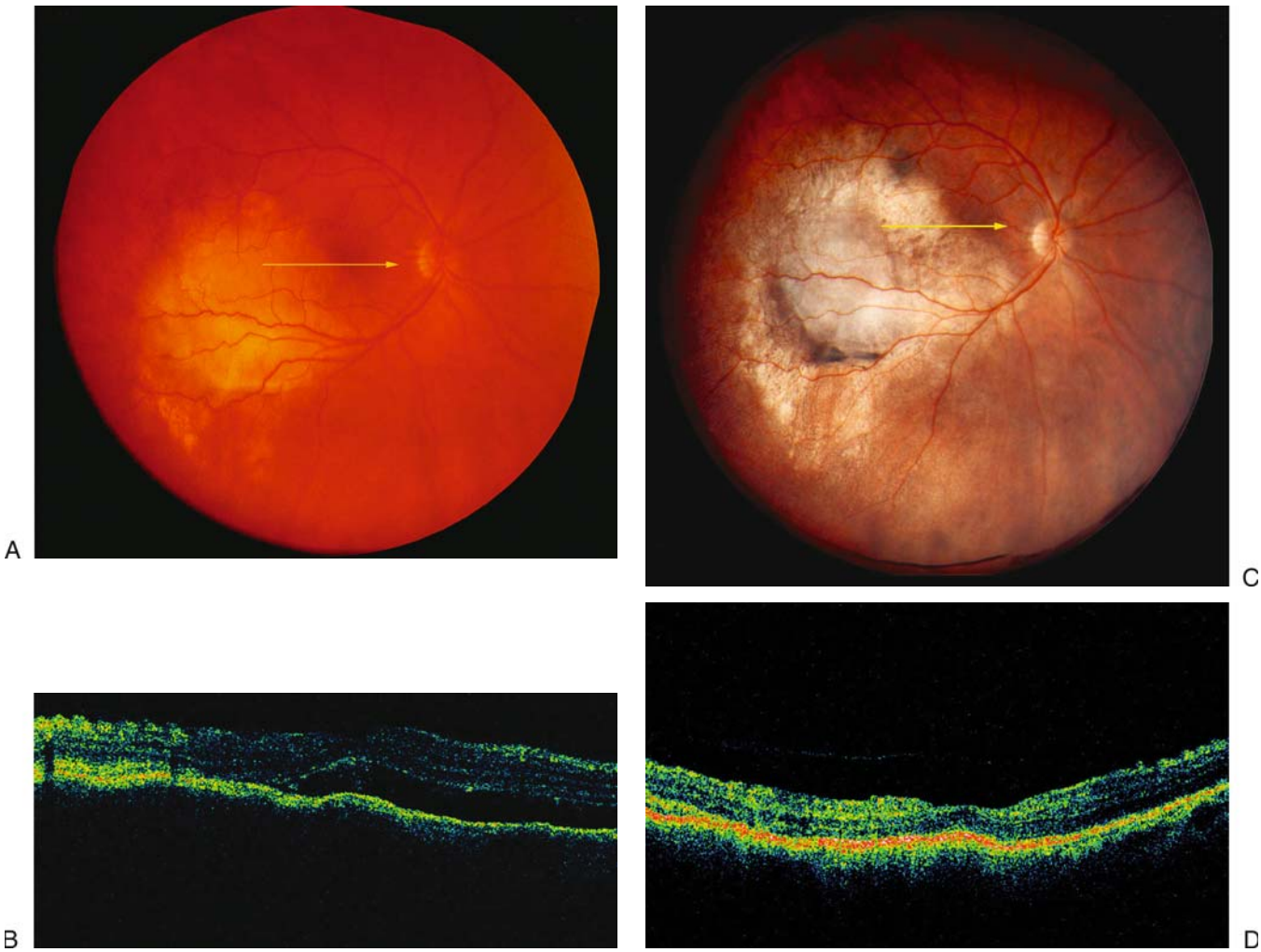

FIG. 20.5. Choroidal metastasis. (A) Amelanotic choroidal metastasis (arrow) in the foveal region produced subretinal fluid. (B) Optical coherence tomography before therapy demonstrates subfoveal fluid. (C) Following 9 months of hormonal therapy, the choroidal metastasis regressed (arrow). (D) Following 9 months of hormonal therapy, the subretinal fluid regressed.

Choroidal Hemangioma

Choroidal hemangioma is considered a hamartomatous vascular tumor and is usually not clinically detectable until the second or third decade of life.[1,2,15–17] This lesion appears typically as a round or oval, slightly elevated, orange-colored tumor. It can vary in size from 2 to 10 mm in diameter, with a mean of 6 mm diameter, and 3 mm in thickness at the time of discovery.[15] Classically, choroidal hemangioma occurs in the posterior pole.[15] It usually exhibits slow enlargement in early life and by young adulthood it can develop overlying atrophic changes in the RPE, cystoid degeneration of the sensory retina, and sensory retinal detachment. The diffuse choroidal hemangioma that permeates throughout the entire choroid is frequently associated with facial hemangioma (Sturge-Weber disease).

On OCT, choroidal hemangioma is imaged with poor resolution of the mass itself. The mass appears to be optically reflective at its anterior surface with little detail deeper into the choroidal mass. On the other hand, OCT is quite beneficial for imaging the overlying retina and ascertaining the reason for visual loss. Visual loss occurs due to subretinal fluid, intraretinal edema, chronic photoreceptor loss, induced hyperopia, tilt of the fovea on the elevated mass, as well as long-standing related amblyopia. Newly active choroidal hemangioma shows subretinal fluid and a preserved photoreceptor layer with minimal intraretinal edema.[18] Chronically leaking choroidal hemangioma displays additional photoreceptor attenuation and overlying intraretinal edema and even bullous retinoschisis.[19] When a tumor is discovered with newly active or chronic features causing visual loss, treatment is advised. Options for treatment include laser photocoagulation, transpupillary thermotherapy, application of a radiation plaque, and, most recently, photodynamic therapy. Optical coherence tomography is an important tool in depicting resolution of subretinal fluid and foveal edema following therapy. It is especially helpful for those eyes that receive photodynamic therapy for management of choroidal hemangioma, as the subretinal or intraretinal fluid generally resolves rapidly and parallels return of visual acuity (Figs. 20.6 and 20.7).[18,19]

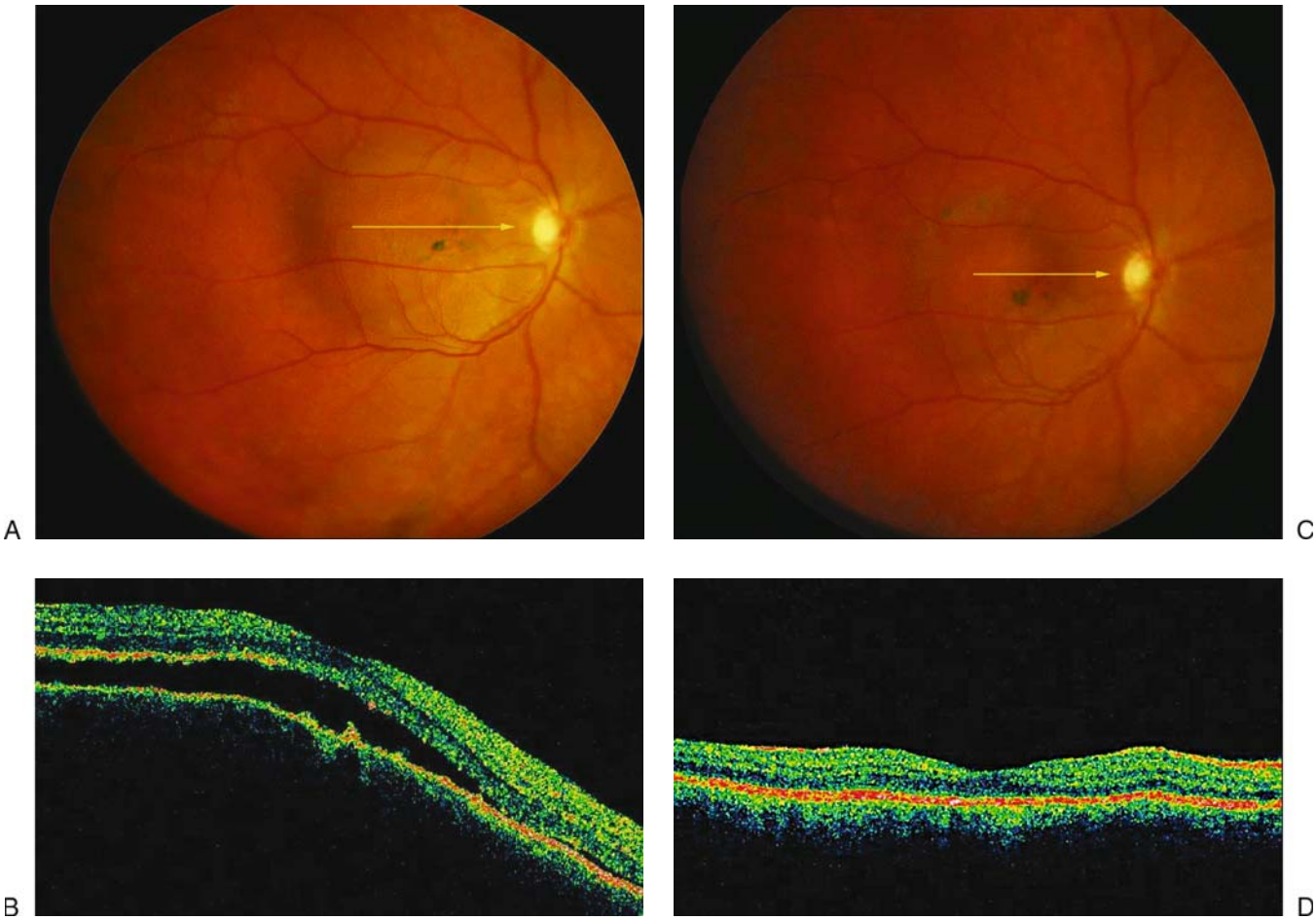

Fig. 20.6. Choroidal hemangioma. (A) Subfoveal choroidal hemangioma (arrow) with overlying subretinal fluid and visual acuity of 20/50 is noted. (B) Subretinal fluid and focal RPE hyperplasia is documented on OCT. (C) Following photodynamic therapy, the tumor regressed (arrow) and visual acuity returned to 20/20. (D) Following photodynamic therapy, the subretinal fluid resolved on OCT.

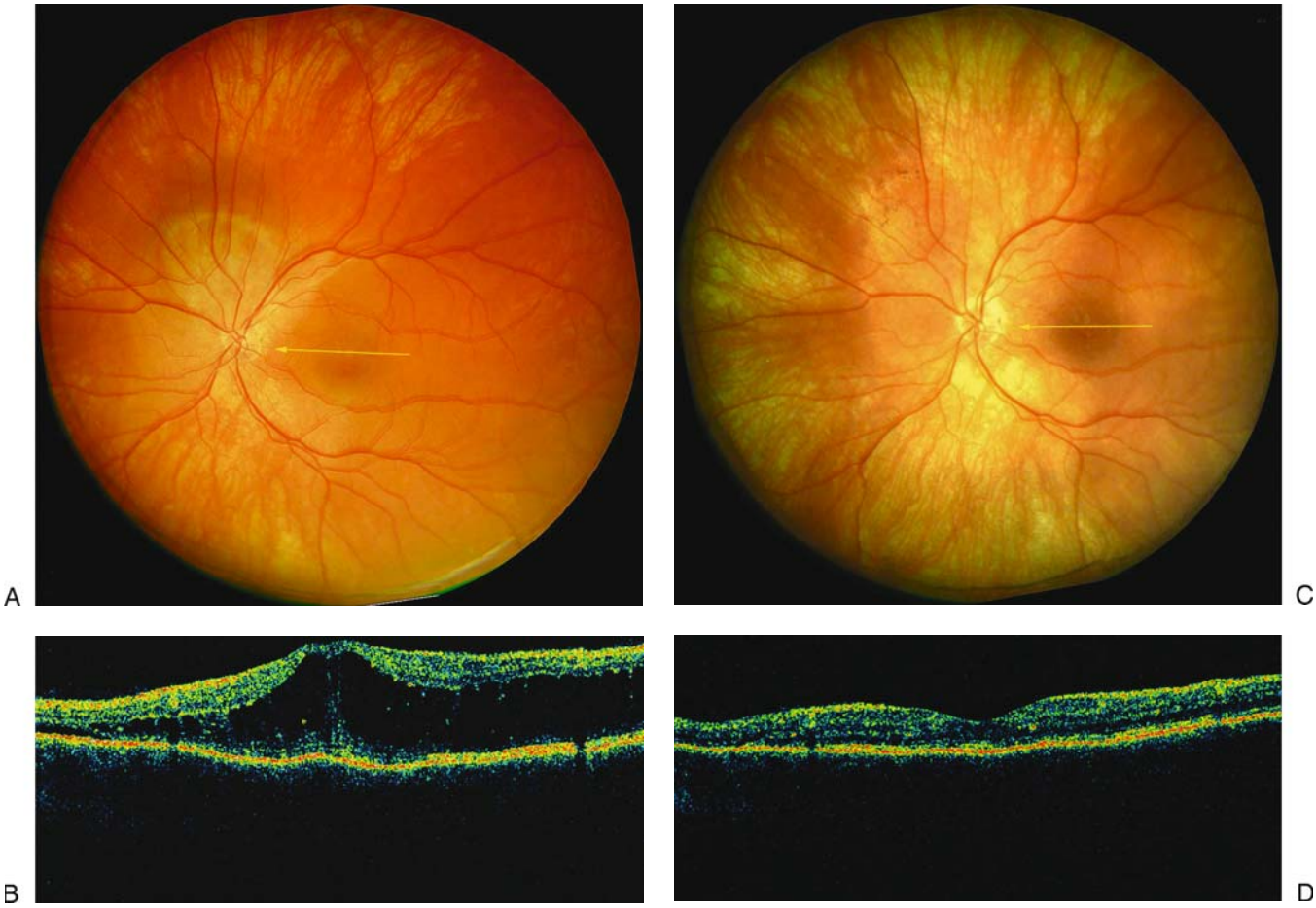

Fig. 20.7. Choroidal hemangioma. (A) Juxtapapillary choroidal hemangioma (arrow) with cystoid macular edema accounted for visual acuity of 20/200. (B) Optical coherence tomography shows extensive cystoid macular edema. (C) Following photodynamic therapy, the tumor (arrow) appears atrophic and visual acuity improved to 20/25. (D) Following photodynamic therapy, the cystoid edema resolved on OCT.

Choroidal Osteoma

Choroidal osteoma is a benign intraocular tumor composed of mature bone that typically replaces the full-thickness choroid. This tumor classically manifests as an orange-yellow plaque deep to the retina in the juxtapapillary or macular region.[20–23] It most often occurs as a unilateral condition in teenaged girls or young women. Unfortunately, the etiology and pathogenesis of this tumor is poorly understood. Despite its benign histopathology, it can compromise visual acuity. Aylward and associates[22] analyzed 36 affected patients and found the 10-year probability for tumor growth was 41%, related choroidal neovascularization was 47%, and poor visual acuity was 58%. Shields and associates[23] later reported on a group of 74 affected eyes; the 10-year probability of tumor growth was 51%, tumor decalcification was 46%, related choroidal neovascularization was 31%, visual acuity loss was 45%, and poor visual acuity was 56%. Since this condition typically occurs in otherwise healthy young patients, most can anticipate experiencing one or many of these outcomes.[23]

The OCT features of choroidal osteoma include preservation of the inner retinal layers with atrophy of the outer layers, especially the photoreceptor layer of the retina. Often subretinal fluid or separation of the neurosensory retina from the excavation underlying choroidal tumor is noted. The RPE layer is indistinct, as both the calcified tumor and RPE layer appear as one layer of bright signal.[24,25] Abrupt elevation of the choroidal tumor at its margin, dense optical reflectivity, and complete shadowing are characteristic of the choroidal osteoma. Areas of elevation and excavation can be found (Fig. 20.8). In the areas of osteoma decalcification, where the lesion clinically appears atrophic and white, there is mild transmission of light through the tumor, whereas in areas where the osteoma is calcified and appears orange, light transmission is blocked and more complete shadowing is noted.[25]

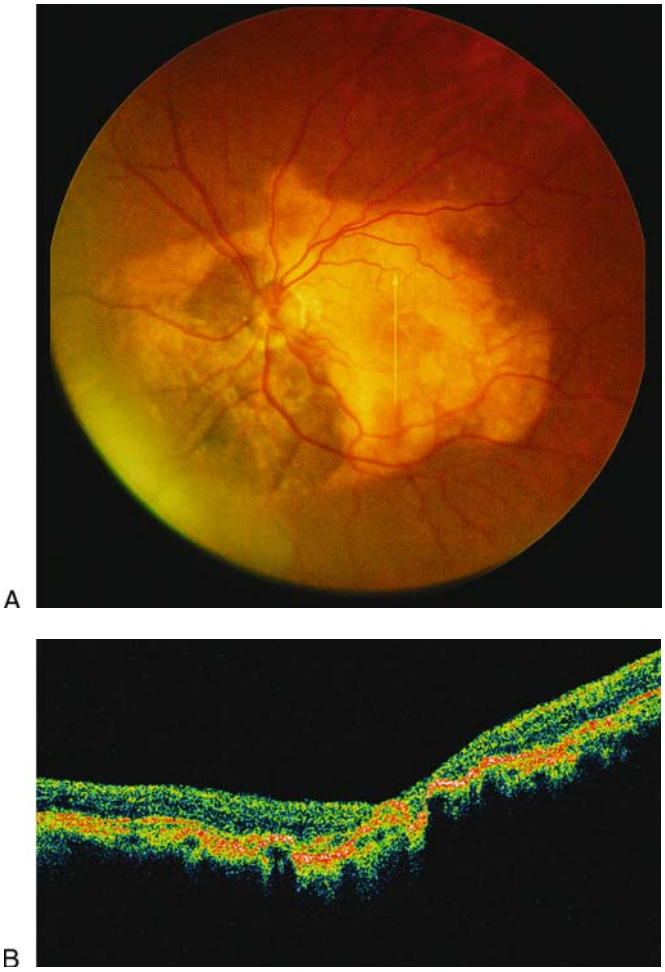

FIG. 20.8. Choroidal osteoma. (A) Panoret image shows calcified circumpapillary choroidal osteoma (arrow). (B) Optical coherence tomography demonstrates preservation of the inner retinal layers but loss of photoreceptor layer of the retina overlying the irregular choroidal mass. The slightly nodular appearance to the RPE layer could represent RPE hyperplasia or irregular surface of the choroidal osteoma.

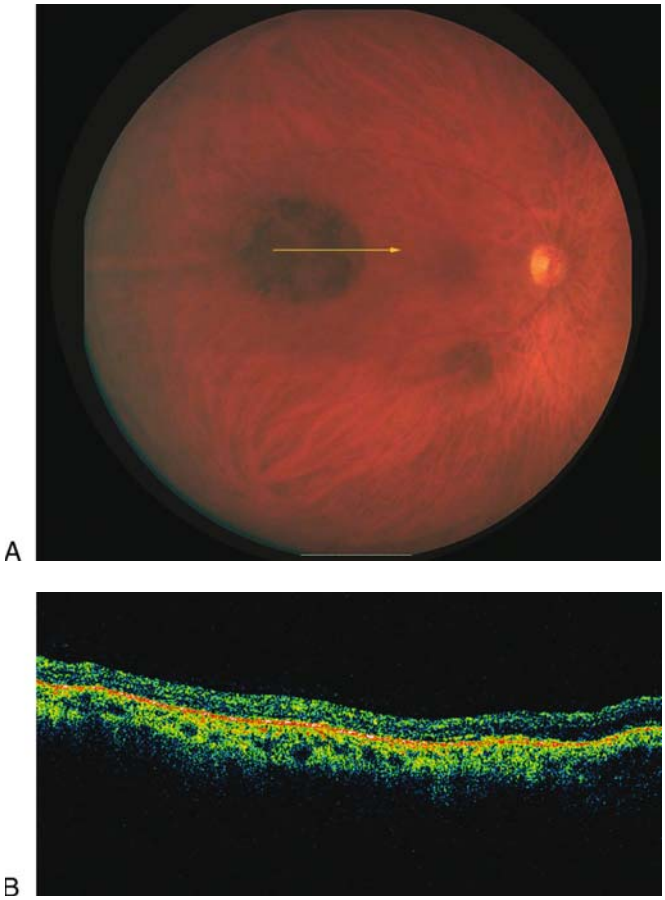

FIG. 20.9. Congenital hypertrophy of the RPE (CHRPE). (A) Panoret image shows CHRPE temporal to the fovea (arrow). (B) Optical coherence tomography shows slight thickening and increased reflectivity of the RPE layer with thinned overlying retina and loss of photoreceptors in the region of the flat CHRPE. Note the normal adjacent retina with lucent photoreceptor layer.

Lesions of the Retinal Pigment Epithelium

The lesions affecting the RPE that will be discussed in this section are congenital hypertrophy of the RPE, congenital simple hamartoma of the RPE, and combined hamartoma of the RPE and retina. Other lesions of the RPE are well documented in the literature.[26]

Congenital Hypertrophy

Congenital hypertrophy of the RPE (CHRPE) is a flat, heavily pigmented benign lesion that varies in diameter from 1 mm to several millimeters and may be found anywhere in the fundus (Fig. 20.9).[27] This lesion displays sharp margins that may be associated with a surrounding clear halo, which, in turn, is surrounded by a halo of pigmentation. Patchy round areas of hypopigmentation within the central portion of the lesion are termed lacunae. Occasionally, more than one CHRPE can be seen in the eye and these congenital lesions can rarely occur bilaterally. Slight growth of CHRPE over many years has been documented.[1,2,27] Histopathologically, these lesions represent hypertrophy of the RPE with the enlarged RPE cells containing large round melanosomes. Rarely, adenoma or adenocarcinoma can develop within CHRPE.[28]

On OCT, CHRPE shows slight increased thickness of the RPE layer with slight shadowing deep to the lesion. The overlying retina is thinned and there is loss of the photoreceptor layer (Fig. 20.9). This tumor is typically difficult to image by OCT as it is usually located in the peripheral fundus.

Congenital Simple Hamartoma

Simple hamartoma of the RPE is an uncommon, presumed congenital lesion that has been recognized to have characteristic ophthalmoscopic, angiographic, and OCT features.[29,30] On clinical examination, this circumscribed benign tumor appears as a small black mass in the macular region measuring a mean of 0.8 mm in basal dimension and 1.6 mm in thickness, involving the full-thickness retina and protruding into the vitreous. Minimally dilated retinal vessels feeding the mass and mild retinal traction can be noted. The lesion blocks fluorescence on angiography and often manifests a ring of staining around the small tumor. There is only one report in the literature on the OCT of this tumor, and the features included an abruptly elevated, dome-shaped, optically dense mass protruding from the retina into the vitreous cavity, with complete shadowing of the deeper levels (Fig. 20.10).[30]

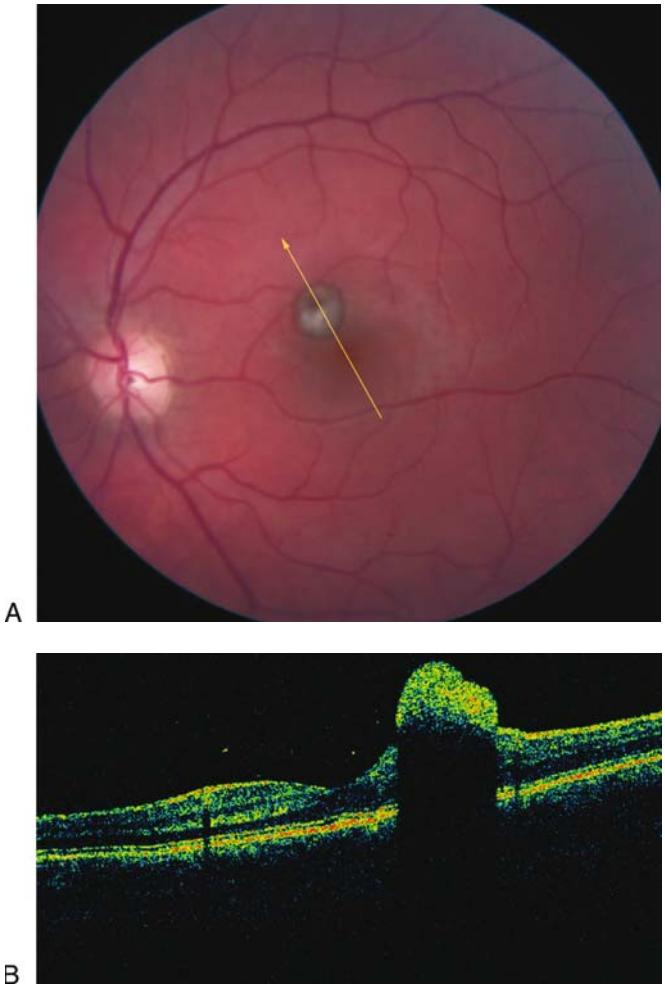

Fig. 20.10. Congenital simple hamartoma of the RPE. (A) The hamartoma (arrow) appears as a small black mass in the foveal retina. (B) On OCT, the mass shows a domed, reflective appearance protruding into the vitreous cavity with abrupt shadowing of deeper tissues and barely sparing the foveola.

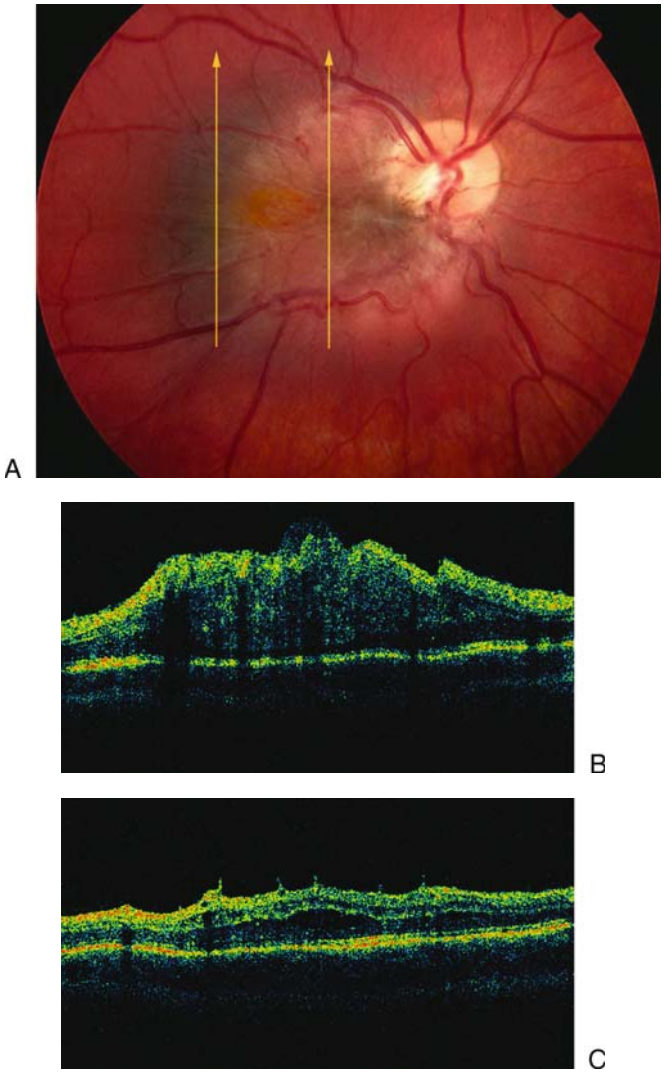

Fig. 20.11. Combined hamartoma of the retina and RPE. (A) The hamartoma (arrows) is located in the papillomacular bundle with visual acuity of 20/100. (B) Vertical OCT through the center of the mass shows retinal disorganization and thickening of 990 μm. Peaks of retinal traction toward the vitreous is noted. (C) Vertical OCT through the temporal margin of the mass shows fine retinal traction peaks and relative preservation of the retinal microarchitecture with outer retinal tenting.

Combined Hamartoma of the Retina and Retinal Pigment Epithelium

The combined hamartoma of the retina and RPE represents a disorganized proliferation of glial and vascular elements of the retina along with RPE cells.[31] It is generally associated with vitreoretinal interface disturbance and retinal folds or striae. While most commonly found adjacent to the disc, it can also occur in the macula or midperiphery.

The combined hamartoma of the RPE and retina shows many interesting findings on OCT. In 2002, Ting and

associates[32] reported the first OCT observations in two adult patients with this tumor. They noted important findings such as a thickened retinal mass with a hyperreflective (high backscatter) surface and deep shadowing, and they commented that the adjacent retina appeared normal and separate from the mass. Cystoid edema was found in one case. Shields and associates[33,34] reported a series of 11 patients, eight of whom were teenagers or children. They found a distinct epiretinal membrane with secondary retinal folds and striae in nearly all 11 cases.[34] The membrane showed horizontal traction in all cases, and in two cases the membrane was configured in multiple peaks, suggesting vertical traction into the vitreous cavity (Fig. 20.11). The membrane, suspected to be glial tissue, was preretinal with no evidence of intertwining into the tumor. It was associated with soft, undulating retinal folds on OCT consistent with the clinical features of retinal traction. Additional findings on OCT included full-thickness retinal disorganization in all cases. Interestingly, the adjacent retina was normal in architecture and seemed to gradually thicken into the disorganized tissue. One might speculate that the tractional component from the epiretinal membrane was the sole source of the distorted retinal findings.[34] On the other hand, others have speculated that the epiretinal component could be secondary to the retinal tumor.[35]

Tumors of the Retina and Optic Disc

There are six different entities mentioned in this discussion of tumors of the sensory retina and disc: (1) capillary hemangioma, (2) cavernous hemangioma, (3) racemose hemangioma, (4) astrocytic hamartoma, (5) retinoblastoma, and (6) melanocytoma.

Capillary Hemangioma

Retinal capillary hemangioma is a vascular hamartoma that may involve the optic disc or retina.[1,2,36–38] It can be sporadic or can have a dominant hereditary pattern. When associated with similar lesions of the central nervous system, it is called von Hippel–Lindau syndrome.[1,2,36–38] Retinal capillary hemangioma located away from the disc is usually associated with one or more feeding arteries and draining veins. Lipid exudation in the macula and retinal detachment are common accompanying manifestations. At the disc the tumor may occur as an inner retinal (endophytic) or deep retinal (exophytic) juxtapapillary lesion. It appears as reddish-orange tumor of variable size, ranging from less than 1 mm to several millimeters in diameter. Intraretinal and subretinal lipid exudation may extend into the macula, even if the tumor rests in the far periphery. Histopathologically, it is characterized by dilated and hyperplastic capillaries and typical clear cells called foam cells.

With OCT, retinal capillary hemangioma displays thickening and disorganization of the retinal layers. The lesion is optically dense due to multiple interfaces of the diffuse capillary channels within the vascular mass. Slight shadowing of deeper tissues is often seen. Optical coherence tomography is most beneficial in detecting subretinal fluid, intraretinal edema, and preretinal fibrosis in the macular region that can accompany retinal capillary hemangioma (Fig. 20.12). Chronic cases with intraretinal edema can manifest with a cystoid appearance and even the appearance of retinoschisis. Chronic subretinal fluid shows thinning of the photoreceptor layer. Optical coherence tomography is used to monitor the response to therapy with resolution of the macular subretinal fluid and edema.

Cavernous Hemangiomas

Cavernous hemangioma of the retina or optic nerve is an uncommon tumor that appears as dark grape-like lesion in the sensory the retina.[1,2,36,37] It can vary in size from a few vascular clusters to larger lesions 10 to 15 mm in diameter. Intraretinal and subretinal exudations are not generally associated with this lesion, although occasionally vitreous hemorrhage can occur. There is occasionally a familial tendency, with an autosomal dominant pattern of inheritance in which case intracranial and cutaneous hemangiomas can be present. The tumor is relatively stable and rarely shows true growth. Histopathologically, it is characterized by a cluster of thin-walled dilated veins that replace the normal architecture of the retina or optic nerve head.

Optical coherence tomography of retinal cavernous hemangioma shows an optically dense mass with a lobulated surface. Preretinal fibrosis from chronic vitreous hemorrhage can be seen. If the aneurysms are large, a cystic appearance might be suggested on OCT; however, the anterior reflectivity might cause shadowing and blunt the visibility of deeper levels.

Racemose Hemangioma

The retinal racemose hemangioma is actually a congenital–arteriovenous malformation that can be a simple communication or a complex array of intertwining vessels.[1,2,36,37,39] The involved vessels are dilated, tortuous, and often more numerous than in the normal eye. Visual function can be normal, and spontaneous hemorrhage rarely occurs. Branch retinal vascular obstruction is a concern at the site of crossing of the large angiomatous vessels.[40] When this arteriovenous malformation is associated with similar midbrain, mandibular, maxillary or pterygoid fossa lesions, it is called the Wyburn-Mason syndrome. With OCT, the racemose hemangioma appears as a relatively large intraretinal cystic mass due to the dilated vessels.[39] Rarely, surrounding retinal changes of retinal atrophy, edema, and hemorrhage can be found (Fig. 20.13).

Astrocytic Hamartoma of the Retina

Astrocytic hamartoma is a retinal lesion typically seen in patients who have tuberous sclerosis.[1,2,36,37] It occurs in the

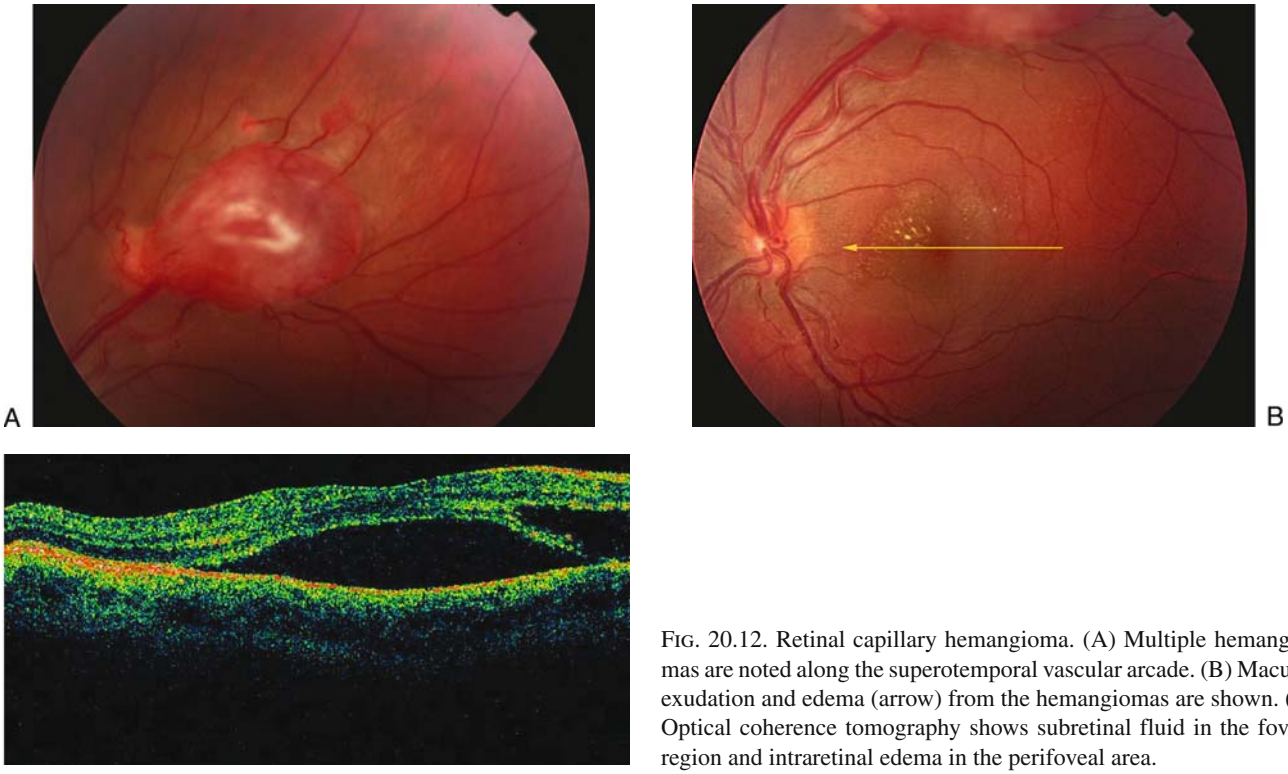

FIG. 20.12. Retinal capillary hemangioma. (A) Multiple hemangiomas are noted along the superotemporal vascular arcade. (B) Macular exudation and edema (arrow) from the hemangiomas are shown. (C) Optical coherence tomography shows subretinal fluid in the foveal region and intraretinal edema in the perifoveal area.

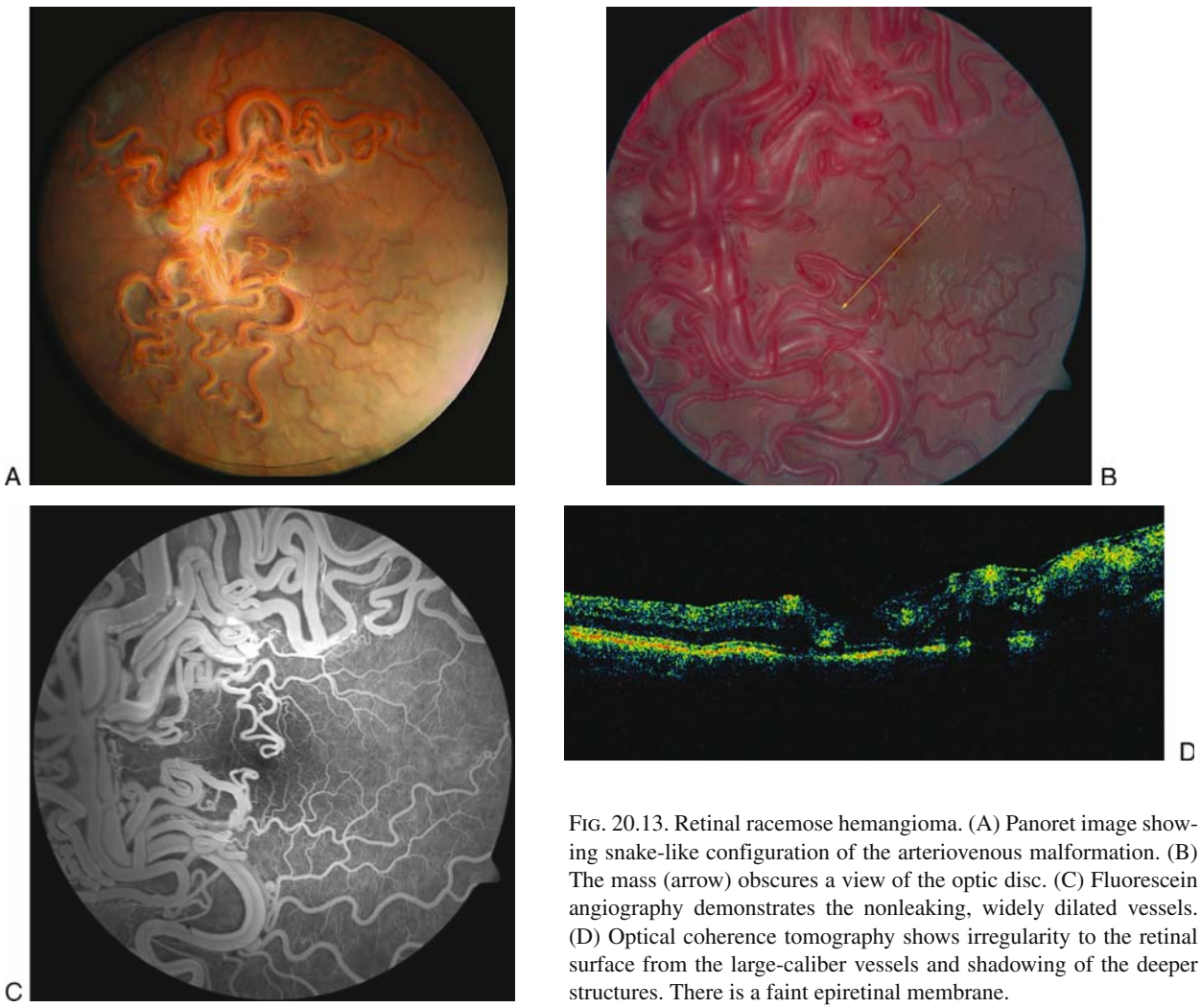

FIG. 20.13. Retinal racemose hemangioma. (A) Panoret image showing snake-like configuration of the arteriovenous malformation. (B) The mass (arrow) obscures a view of the optic disc. (C) Fluorescein angiography demonstrates the nonleaking, widely dilated vessels. (D) Optical coherence tomography shows irregularity to the retinal surface from the large-caliber vessels and shadowing of the deeper structures. There is a faint epiretinal membrane.

superficial retina or optic disc as a white, round or oval, elevated mass with occasional intralesional calcification imposing a mulberry-like appearance. Mild associated retinal traction can be found. The astrocytic hamartoma is frequently multiple and, despite its white color, is usually highly vascularized. It carries minimal growth potential. Histopathologically, it is usually composed of fibrillary astrocytes, although a giant cell variant is occasionally seen.

With OCT, retinal astrocytic hamartoma shows gently sloping irregular surface overlying an optically dense, disorganized mass replacing the retinal architecture. If there is calcification within the astrocytic hamartoma, then the reflectivity of the mass is high and deep shadowing is noted (Fig. 20.14).

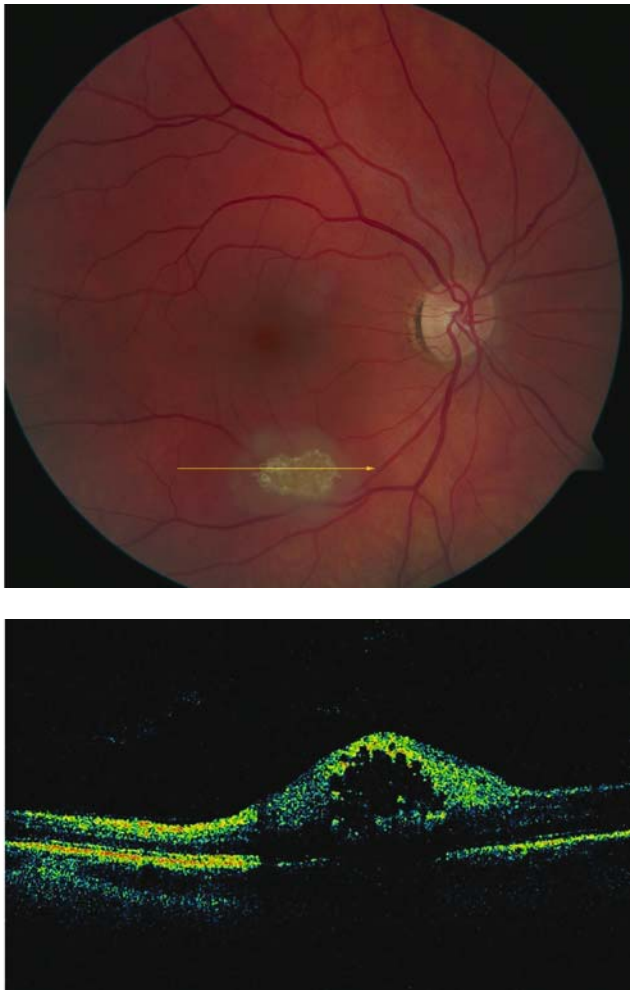

FIG. 20.14. Retinal astrocytic hamartoma. (A) A calcified retinal astrocytic hamartoma (arrow) is noted inferior to the macula. (B) Optical coherence tomography shows an intraretinal mass with anterior homogeneous appearance but with deeper "moth-eaten" appearance and abrupt reflectivity and shadowing consistent with nodules of calcification.

Retinoblastoma

Retinoblastoma is the most common intraocular malignancy of childhood.[1,2,41,42] This tumor grows in either an endophytic or exophytic pattern. The endophytic retinal mass usually has a vascular, cauliflower appearance with scattered tumor nodules along the inner retinal surface and in the vitreous cavity. In the exophytic form there is marked prominence of the vasculature of the tumor and the overlying retina. Histopathologically, retinoblastoma is composed of well differentiated to undifferentiated neuroblastic cells, with scanty cytoplasm, and sometimes characteristic rosettes.

During the very early phases of the fluorescein angiogram, vascular hyperfluorescence is evident from the large vessels that course throughout this cellular tumor. As the study continues, there is leakage from the tumor vasculature, causing an increasing hyperfluorescence diffusely within the mass. On OCT, retinoblastoma shows an optically dense appearance with shadowing of the deep tissues. Intralesional calcification can cause higher internal reflectivity (backscattering) and denser shadowing posterior to the tumor. There is abrupt transition of the normal retinal architecture to the retinal mass. If the mass is intraretinal, the full-thickness retina is involved (Fig. 20.15). An endophytic retinoblastoma may be difficult to image due to overlying vitreous seeds. An exophytic tumor shows retinal detachment overlying the neoplasm. In rare cases, intraretinal empty cavities can be visualized, and they are usually found in well-differentiated portions of the tumor (Fig. 20.15).[43] Optical coherence tomography is a useful test in monitoring reasons for visual loss following treatment of retinoblastoma. Causes of visual loss include retinal atrophy, retinal edema, persistent retinal detachment, optic disc edema or atrophy, macular tumor scar, cataract, corneal dryness and scarring, and amblyopia. In some instances, eyes with total retinal detachment from retinoblastoma have recovered complete function of the retina both clinically and anatomically, confirmed on OCT (Fig. 20.16).[44]

Melanocytoma of the Optic Nerve

Melanocytoma is a heavily pigmented benign tumor that is usually located on the optic disc.[1,2,45] It can vary in size from less than one disc diameter to a much larger liaison extending into the overlying vitreous and adjacent retina and choroid. Histopathologically, it is composed of large pigmented melanocytes found near the region of the lamina cribrosa.

Because of the heavily pigmented cells, this lesion shows hypofluorescence throughout fluorescein angiogram. On OCT, melanocytoma is found to occupy the anterior portion of the optic nerve in a sessile or dome-shaped fashion (Fig. 20.17). There is disorganization of the normal optic nerve features. Shadowing of deeper tissues is present. The mass often spills over, into and under the adjacent retina. By OCT, the retinal involvement appears as optically dense material in the nerve fiber layer and the choroidal involvement appears as slight elevation of the choroid, sometimes with subretinal fluid.

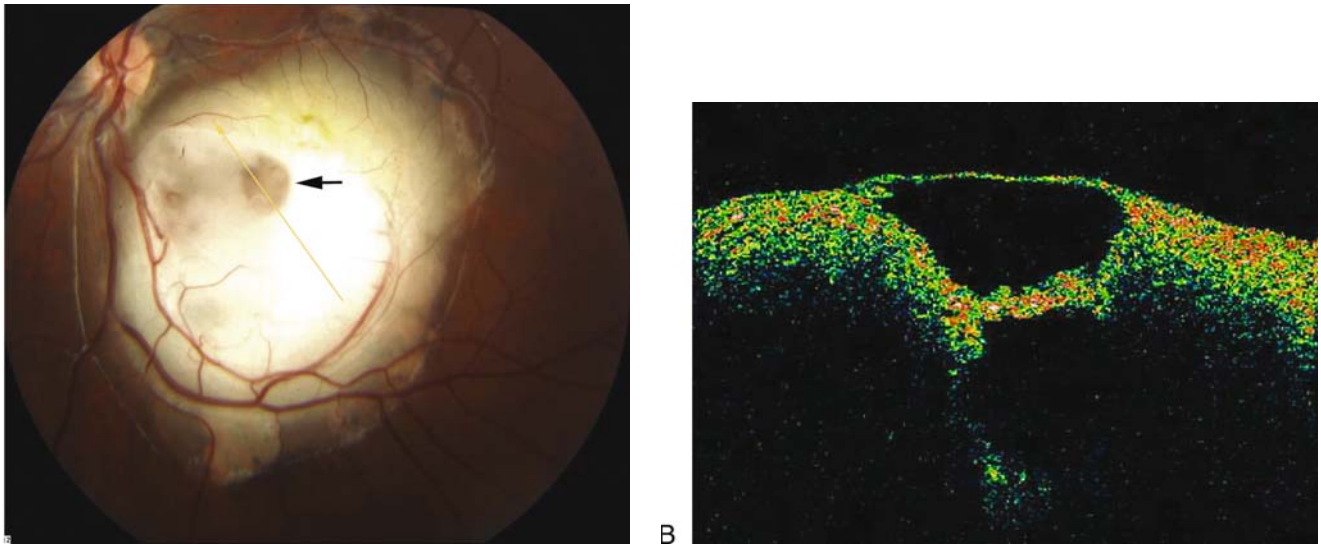

FIG. 20.15. Retinoblastoma. (A) Retinoblastoma with cavities (arrow) was found in a 4-year-old girl. (B) Optical coherence tomography shows a dense homogeneous retinal mass with cavities anteriorly.

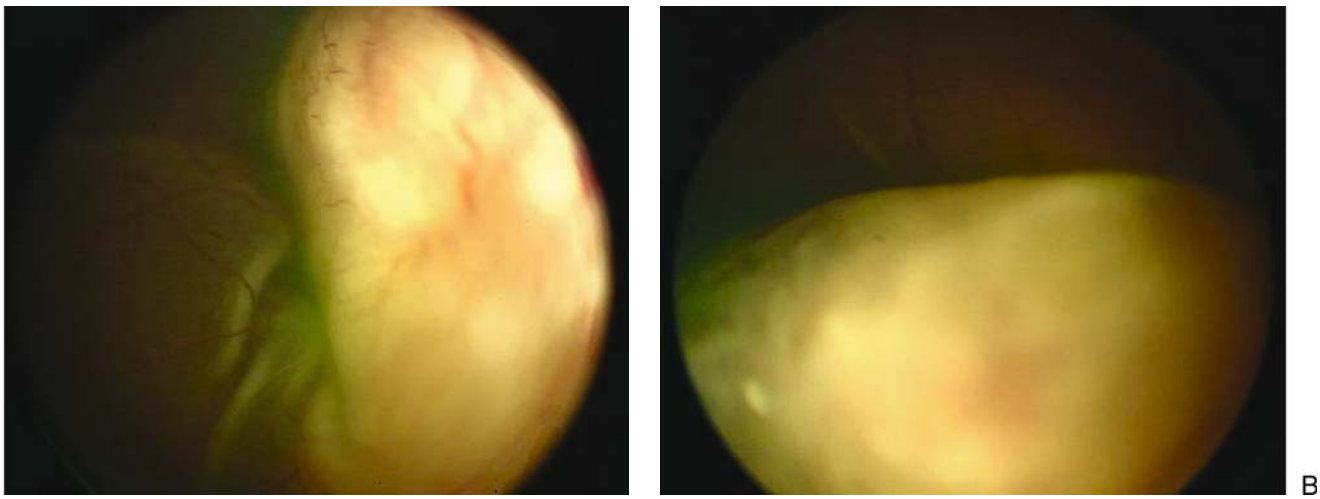

FIG. 20.16. Retinoblastoma. (A) Advanced retinoblastoma with total retinal detachment in the right eye. (B) Advanced retinoblastoma with total retinal detachment in the left eye. (C) Following chemoreduction and thermotherapy, the tumors (arrow) regressed and the retina flattened in the right eye. (D) Following chemoreduction and thermotherapy, the tumors (arrow) regressed and the retina flattened in the left eye. (E) Six years following stable regression, OCT of the right eye shows normal macular architecture without edema or subretinal fluid but with blunted foveal depression. (F) Six years following stable regression, OCT of the left eye shows normal superotemporal macular architecture without edema or subretinal fluid and with normal foveal depression, but with retinal pigment epithelial thickening.

Conclusion

Optical coherence tomography is a useful technique for imaging the primary and secondary effects of intraocular tumors. It is most suited for information regarding tumors of the retina and RPE. Information regarding details of choroidal tumors is currently limited due to lack of penetration of the light into the choroid. Optical coherence tomography is especially helpful in imaging the retina following treatment of intraocular tumors and provides important information on the reasons for visual acuity change.

Acknowledgments This work is supported by the Eye Tumor Research Foundation, Philadelphia (for author C.L.S.), the Macula Foundation, New York (C.L.S.), the Rosenthal Award

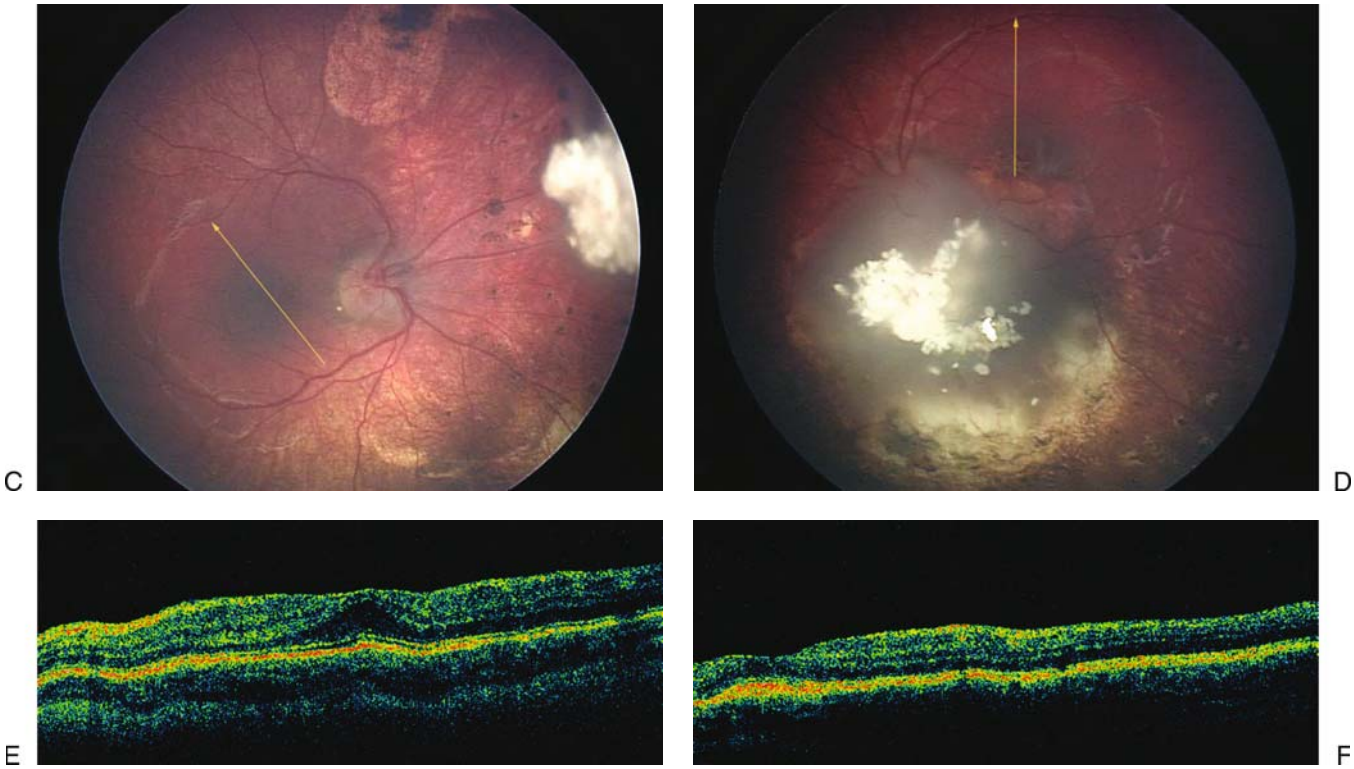

FIG. 20.16. (continued).

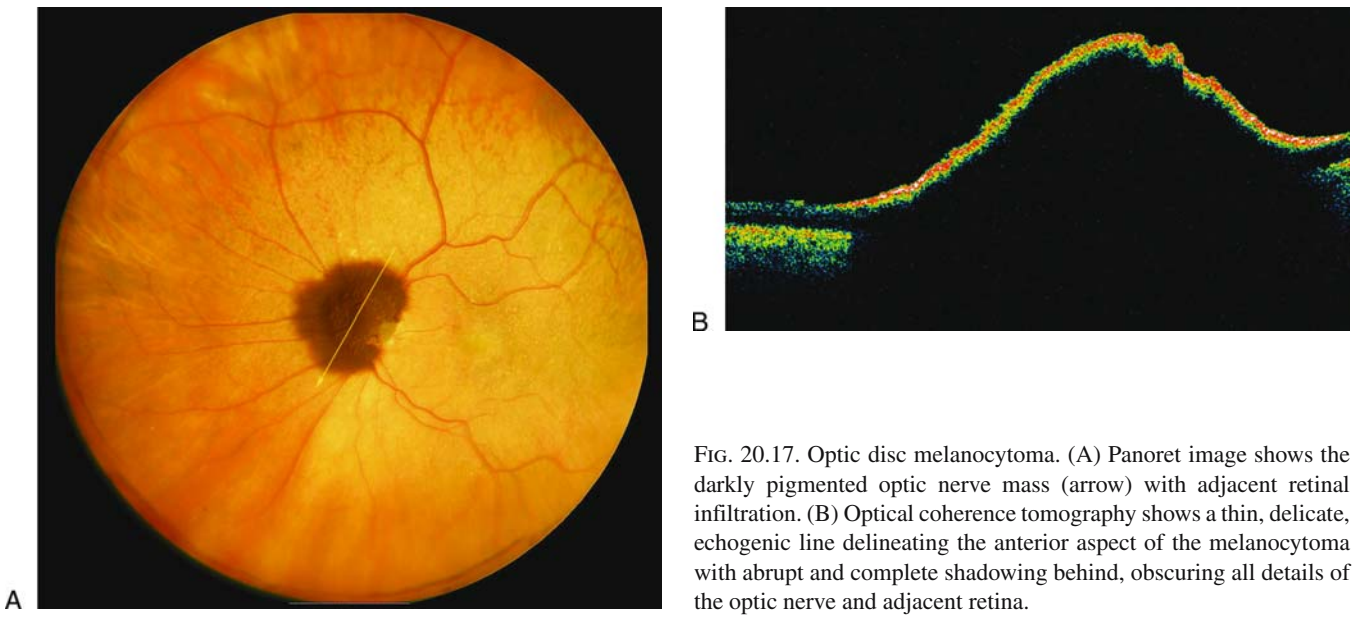

FIG. 20.17. Optic disc melanocytoma. (A) Panoret image shows the darkly pigmented optic nerve mass (arrow) with adjacent retinal infiltration. (B) Optical coherence tomography shows a thin, delicate, echogenic line delineating the anterior aspect of the melanocytoma with abrupt and complete shadowing behind, obscuring all details of the optic nerve and adjacent retina.

of the Macula Society, Barcelona, Spain (C.L.S.), and the Paul Kayser International Award of Merit in Retina Research, Houston, TX (J.A.S.).

References

1. Shields JA, Shields CL. Intraocular Tumors: A Text and Atlas. Philadelphia: WB Saunders, 1992.
2. Shields JA, Shields CL. Atlas of Intraocular Tumors. Philadelphia: Lippincott Williams & Wilkins, 1999.
3. Sumich P, Mitchell P, Wang JJ. Choroidal nevi in a white population: the Blue Mountains Study. Arch Ophthalmol 1998;116:645–650.
4. Shields CL, Shields JA, Kiratli H, Cater JR, De Potter P. Risk factors for growth and metastasis of small choroidal melanocytic lesions. Ophthalmology 1995;102:1351–1361.
5. Shields CL, Cater JC, Shields JA, Singh AD, Santos MCM, Carvalho C. Combination of clinical factors predictive of growth of small choroidal melanocytic tumors. Arch Ophthalmol 2000;118:360–364.
6. Shields CL, Demirci H, Materin MA, Marr BP, Mashayekhi A, Shields JA. Clinical factors in the identification of small choroidal melanoma. Can J Ophthalmol 2004;39:351–357.
7. Shields CL, Mashayekhi A, Materin MA, Luo CK, Marr BP, Demirci H, Shields JA. Optical coherence tomography of choroidal nevus in 120 patients. Retina 2005;25:243–252.
8. Espinoza G, Rosenblatt B, Harbour JW. Optical coherence tomography in the evaluation of retinal changes associated with suspicious choroidal melanocytic tumors. Am J Ophthalmol 2004;137:90–95.
9. Shields JA, Shields CL, Donoso LA. Management of posterior uveal melanomas. Surv Ophthalmol 1991;36:161–195.
10. Shields CL, Shields JA. Recent developments in the management of choroidal melanoma. Curr Opin Ophthalmol 2004;15: 244–251.
11. Shields CL, Shields JA, DePotter P, Cater J, Tardio D, Barrett J. Diffuse choroidal melanoma: clinical features predictive of metastasis. Arch Ophthalmol 1996;114:956–963.
12. Shields CL, Demirci H, Dai V, Marr BP, Mashayekhi A, Materin MA, Manquez ME, Shields JA. Intravitreal triamcinolone acetonide for radiation maculopathy after plaque radiotherapy for choroidal melanoma. Retina 2005;25:868–874.
13. Shields CL, Shields JA, Gross N, Schwartz G, Lally S. Survey of 520 uveal metastases. Ophthalmology 1997;104: 1265–1276.
14. Manquez ME, Shields CL, Karatza EC, Shields JA. Regression of choroidal metastases from breast carcinoma using aromatase inhibitors. Br J Ophthalmol 2005;89:776–777.
15. Shields CL, Honavar SG, Shields JA, Cater J, Demirci H. Circumscribed choroidal hemangioma. Clinical manifestations and factors predictive of visual outcome in 200 consecutive cases. Ophthalmology 2001;108:2237–2248.
16. Mashayekhi A, Shields CL. Circumscribed choroidal hemangioma. Curr Opin Ophthalmol 2003;14:142–149.
17. Shields JA, Shields CL, Materin MA, Marr BP, Demirci H, Mashayekhi A. Changing concepts in management of circumscribed choroidal hemangioma. The 2003 J. Howard Stokes Lecture, part 1. Ophthalmic Surg Lasers Imaging 2004;35:383–393.
18. Materin MA, Shields CL, Marr BP, Shields JA. Restoration of anatomic fovea following photodynamic therapy (PDT) for circumscribed choroidal hemangioma. Submitted for publication.
19. Shields CL, Materin MA, Marr BP, Mashayekhi A, Shields JA. Resolution of advanced cystoid macular edema following photodynamic therapy of choroidal hemangioma. Ophthalmic Surg Lasers Imaging 2005;36:237–239.
20. Gass JD, Guerry RK, Jack RL, Harris G. Choroidal osteoma. Arch Ophthalmol 1978;96:428–435.
21. Shields CL, Shields JA, Augsburger JJ. Choroidal osteoma. Surv Ophthalmol 1988;33:17–27.
22. Aylward GW, Chang TS, Pautler SE, Gass JD. A long-term follow-up of choroidal osteoma. Arch Ophthalmol 1998;116: 1337–1341.
23. Shields CL, Sun H, Demirci H, Shields JA. Factors predictive of tumor growth, tumor decalcification, choroidal neovascularization, and visual outcome in 74 eyes with choroidal osteoma. Arch Ophthalmol 2005;123:1658–1666.
24. Ide T, Ohguro N, Hayashi A, et al. Optical coherence tomography patterns of choroidal osteoma. Am J Ophthalmol 2000;130: 131–134.
25. Fukasawa A, Iijima H. Optical coherence tomography of choroidal osteoma. Am J Ophthalmol 2002;133:419–421.
26. Shields JA, Shields CL, Gunduz K, Eagle RC Jr. Neoplasms of the retinal pigment epithelium. The 1998 Albert Ruedemann Sr. Memorial Lecture. Part 2. Arch Ophthalmol 1999;117:601–608.
27. Shields CL, Mashayekhi A, Ho T, Cater J, Shields JA. Solitary congenital hypertrophy of the retinal pigment epithelium: clinical features and frequency of enlargement in 330 patients. Ophthalmology 2003;110:1968–1976.
28. Shields JA, Shields CL, Singh AD. Acquired tumors arising from congenital hypertrophy of the retinal pigment epithelium. Arch Ophthalmol 2000;118:637–641.
29. Shields CL, Shields JA, Marr BP, Sperber DE, Gass JDM. Congenital simple hamartoma of the retinal pigment epithelium. A study of five cases. Ophthalmology 2003;110: 1005–1011.
30. Shields CL, Materin MA, Karatza E, Shields JA. Optical coherence tomography (OCT) of congenital simple hamartoma of the retinal pigment epithelium. Retina 2004;24: 327–328.
31. Schachat AP, Shields JA, Fine SL, et al. The Macula Society Research Committee. Combined hamartomas of the retina and retinal pigment epithelium. Ophthalmology 1984;91: 1609–1614.
32. Ting TD, McCuen BW II, Fekrat S. Combined hamartoma of the retina and retinal pigment epithelium: optical coherence tomography. Retina 2002;22:98–101.
33. Shields CL, Mashayekhi A, Dai VV, Materin MA, Shields JA. Optical coherence tomography findings of combined hamartoma of the retina and retinal pigment epithelium in 11 patients. Arch Ophthalmol 2005;123:1746–1750.
34. Shields CL, Mashayekhi A, Luo CK, Materin MA, Shields JA. Optical coherence tomography in children: analysis of 44 eyes with intraocular tumors and simulating conditions. J Pediatr Ophthalmol Strabismus 2004;41:338–344.
35. Stallman JB. Visual improvement after pars plana vitrectomy and membrane peeling for vitreoretinal traction associated with com-

bined hamartoma of the retina and retinal pigment epithelium. Retina 2002;22:101–104.
36. Shields JA, Shields CL. Tumors of the retina and optic disc. In: Regillo CD, Brown GC, Flynn HW Jr eds. Vitreoretinal Disease. The Essentials. New York: Thieme, 1999: 439–454.
37. Shields CL, Shields JA. Phakomatoses. In: Regillo CD, Brown GC, Flynn HW Jr, eds. Vitreoretinal Disease. The Essentials. New York: Thieme, 1999:377–390.
38. Singh AD, Shields CL, Shields JA. Major review: Von Hippel-Lindau disease. Surv Ophthalmol 2001;46:117–142.
39. Materin MA, Shields CL, Marr BP, Demirci H, Shields JA. Retinal racemose hemangioma. Retina 2005;25:936–937.
40. Shah GK, Shields JA, Lanning R. Branch retinal vein obstruction secondary to retinal arteriovenous communication. Am J Ophthalmol 1998;126:446–448.
41. Shields CL, Shields JA. Recent developments in the management of retinoblastoma. J Pediatr Ophthalmol Strabism 1999;36:8–18.
42. Shields CL, Meadows AT, Leahey AM, Shields JA. Continuing challenges in the management of retinoblastoma with chemotherapy. Retina 2004;24:849–862.
43. Mashayekhi A, Shields CL, Eagle RC Jr, Shields JA. Cavitary changes in retinoblastoma: relationship to chemoresistance. Ophthalmology 2005;112:1145–1150.
44. Shields CL, Materin MA, Shields JA. Restoration of foveal anatomy and function following chemoreduction for bilateral advanced retinoblastoma with total retinal detachment. Arch Ophthalmol 2005;123:1610–1612.
45. Shields JA, Demirci H, Mashayekhi A, Shields CL. Melanocytoma of the optic disc in 115 cases. The 2004 Samuel Johnson Memorial Lecture. Ophthalmology 2004;111: 1739–1746.

21
Artifacts and Limitations in Time-Domain Optical Coherence Tomography Images

J. Fernando Arevalo, Juan G. Sanchez, and Reinaldo A. Garcia

The clinician uses a variety of imaging techniques to evaluate pathology and to make therapeutic decisions in ophthalmology. Optical coherence tomography (OCT) is a new technology that has been used increasingly to evaluate and manage a variety of retinal diseases. It is used to obtain a cross section of the retina based on the reflectivity of different layers within the retina, allowing detection of morphologic and micrometric changes in retinal tissue.

Macular lesions associated with optic nerve head pits, epiretinal membranes, central serous chorioretinopathy, age-related macular degeneration, choroidal neovascularization, and diabetic macular edema are just some of the diseases that have been studied using OCT. There are several advantages of OCT as a diagnostic imaging technique: images can be acquired rapidly without contacting the eye, no dye is used for these studies, and it provides quantitative information regarding macular thickness changes over time. However, there also are some limitations and potential pitfalls to its use.

Optical coherence tomography imaging is powerful because a wide range of image-processing algorithms can be used to obtain quantitative information from OCT images. One of the most useful applications of OCT is its ability to sensitively and reproducibly monitor retinal thickness. Special care is required to ensure that initial image data are of sufficient quality before these image-processing and measurement algorithms are applied. As with all forms of imaging, perfection is rarely achieved and all imaging systems are subject to artifacts. Fundus photography and fluorescein angiography depend on a well-trained photographer, media quality, pupil dilatation, and patient collaboration.

This chapter describes limitations, artifacts, and errors in OCT imaging. In addition, it provides the basic principles for correction of those pitfalls.

Basic Principles of Optical Coherence Tomography

Optical coherence tomography generates cross-sectional images of tissue, which depend on the back-reflection or backscattering of light from structures at different depths. Before discussing the detailed artifacts and errors in OCT, it is helpful to consider the general concepts and limitations of light propagation through tissue as a basis for interpreting OCT images.

Quality

Special care is required to ensure that OCT images have sufficient quality. The signal-to-noise ratio, or the brightness of retinal features when compared to background noise, is an important indicator of OCT image quality.[1] Optical coherence tomography images of good quality have not artifacts. Optical coherence tomography with a low signal has a washed-out and dim appearance, with loss of signal and reduced dynamic range and may be cause by opaque media. Structures with low backscattering, such as the internal nuclear layer, the ganglion cell layer, and the outer nuclear layer of the retina, have a blue-black appearance in false color images, indicating that their signal level is close to the background noise level. Additionally, sufficient lost of signal can decrease the higher scattering layers such as the retinal pigment epithelium (RPE) and nerve fiber layer (Fig. 21.1).

Image Resolution

Spatial resolution is also an important parameter of OCT. There are two important kinds of spatial resolution for standard OCT systems: axial and transversal resolution. Axial resolution is determined by the resolution of the optical distance measurements. It depends on two features of laser: pulse duration and coherence length of the light source. Transverse resolution is determined by the focused spot size of the optical beam. The spot size is a function of the optics used to project the beam into the eye. Therefore, the minimum spot size is limited by the aberrations in the optics of the eye. Axial resolution with the third-generation OCT (Stratus OCT, Carl Zeiss Meditec, Dublin, CA) is approximately 10 μm, and transversal resolution is 20 to 25 μm in retinal tissue.[2] The focus adjustment knob retracts and extends the ocular lens and adjusts the

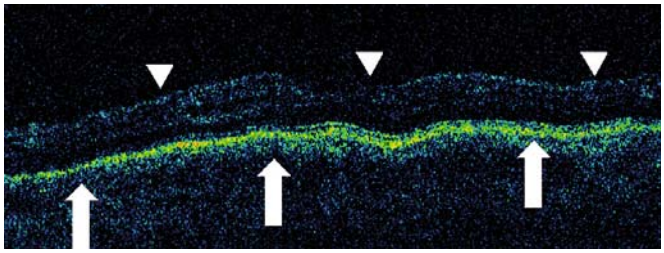

FIG. 21.1. Optical coherence tomography (OCT) must be of good quality to minimize artifacts and misdiagnosis. The OCT image shown here is washed-out and dim in appearance with loss of signal and reduced dynamic range in a patient with severe ocular opacity. Sufficient lost of signal may decrease the higher scattering layers of retinal pigment epithelium (arrows) and nerve fiber layer (arrowheads).

focus of the video camera. We have had difficulties obtaining images in high myopic and hypermetropic eyes because the focus adjustment knob is limited to between +12.00 and −12.00 diopters.

Image resolution refers to the number of pixels in an image. Resolution is sometimes identified by the width and height of the image as well as the total number of pixels in the image. Even if the instrument has high resolution, images will still be grainy if there are an insufficient number of pixels. The pixel number is important for the transverse dimension of an OCT image; larger images with finer features require more pixels. Additionally, the image acquisition time increases in proportion to the number of axial scans, so higher transverse pixel density images require longer acquisition times. Therefore, the number of pixels in the axial direction is limited by the speed of detection of the electronics and computer.

Eye Motion

Optical coherence tomography uses a simple imaging processing technique, and it is essential to compensate eye motion during image acquisition. Small changes in axial eye motion have a severe effect in blurring OCT images.[3] However, transverse changes in position do not produce significant degradation of image. This difference is due to the fact that axial resolution of OCT is finer than transverse resolution.

The best OCT images are captured when a cooperative patient with good fixation is properly aligned with the examining beam. The available headrest is helpful in controlling gross movement. Unfortunately, head movement, ocular oscillations, and even the pulsatile effects of blood flow can radically degrade high-resolution image quality. Many of the problems of movement image degradation relate to the basic method of OCT image formation. This device creates a cross section of tissue by combining a family of individual A-scans (up to 512 per line scan). The software interpolates information between scans. Movements of any type degrade alignment and image quality. For example, large movements are not compensated and the OCT image shows discontinuities that are generated when the patient's fixation point change during the scan (Fig. 21.2).

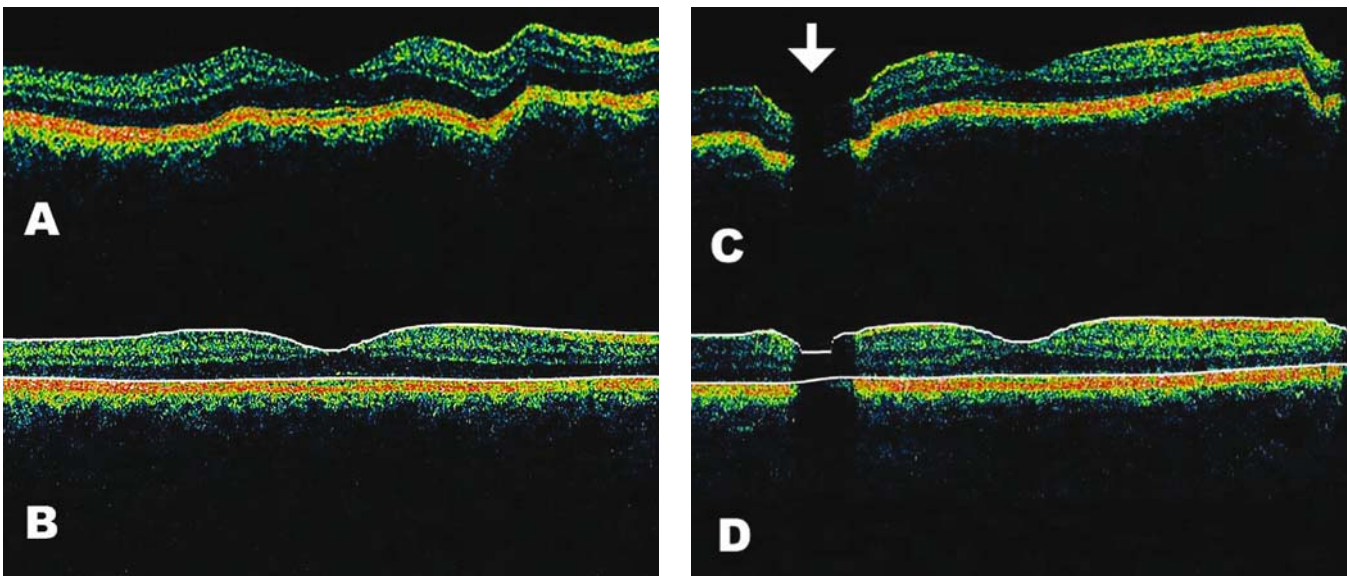

FIG. 21.2. Large drifts in patient fixation are not compensated by computer image processing. (A) Optical coherence tomography scan before processing image demonstrating eye motion. (B) Optical coherence tomography scan though the macula after compensating for eye motion during image acquisition. (C) Optical coherence tomography scan showing discontinuities that are generated when the patient's fixation point change during the scan (arrow). (D) Optical coherence tomography scan cannot sufficiently compensate these discontinuities.

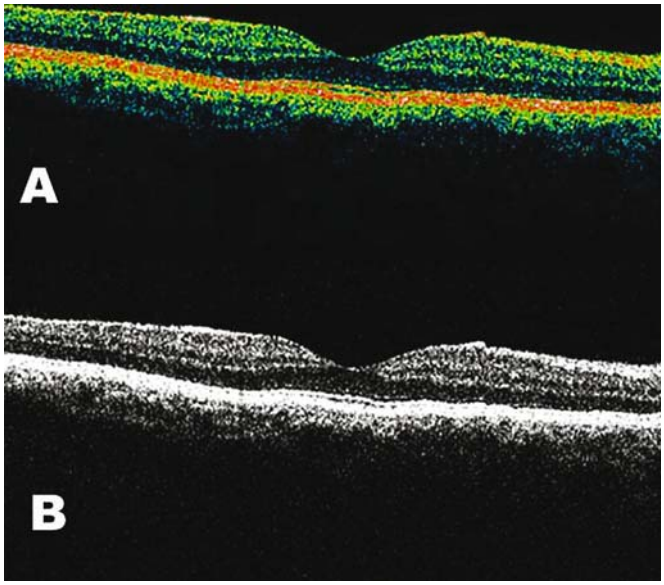

FIG. 21.3. (A) False-color OCT retinal image. The colors enhance the ability to detect small differences in the signal level. (B) Gray scale OCT image. It is difficult to visualize differences between retinal layers.

Sensitivity

The backscattered signal level typically ranges from −50 dB maximum signals to −95 dB, which corresponds to the detection sensitivity limit. The final OCT image is displayed using a false color map that corresponds to detected backscattered light levels from the incident light. The high reflectivity signals are represented by white and red colors, while the low reflectivity signals are represented by white and blue colors. The color is computer-assigned on the basis of the strength of the returning signal. Therefore, the interpreter must remember that the colors only relate to the strength of the returning light (tissue reflectivity), not to the histology. However, one disadvantage of false color display is that it can produce artifacts in image. In addition, images can be displayed in gray scale but its main disadvantage is the low ability to differentiate variations in intensities (Fig. 21.3).[4]

Retinal Scanning Protocols

Several OCT scan modes are available to evaluate retinal pathology. These can be applied to identify and measure layers of the retina automatically. Retinal scanning protocols are registered by the computer to allow presentation and future comparison between visits. Some retinal scanning protocols are complementary because each protocol has limitations. One good example is the fast scan protocols that are designed to simplify the process and shorten the time to acquire the scan series used most frequently to detect retinal pathologies. Its resolution is lower but the chance of error from patient movement is less.

Retinal Thickness Measurements

Retinal morphology and morphometry may be disrupted in many diseases. In addition, retinal thickness is an important consideration in the assessment of many macular diseases. A good example is macular edema as a consequence of diabetic retinopathy, intraocular inflammation, or cataract extraction. In these instances, measurement of retinal thickness is important in quantifying abnormal fluid accumulation within neurosensory retina. The high axial image resolution of OCT, combined with its ability to clearly identify the anterior and posterior boundaries of the retina, makes OCT well suited for the quantitative measurement of retinal thickness. Therefore, a good segmentation (boundary detection) is necessary for accurate measurements.

Anatomic retina thickness measurement is critical for boundary detection algorithms. Based on differences in the image reflectance patters, OCT locates the inner retina at the vitreoretinal interface and the outer retina at the RPE-photoreceptor outer segment interface. The software then places a line on the inner retina–vitreous interface and another on the RPE–outer retina interface and determines retinal thickness as the distance between these lines at each measurement point along the scan's x-axis.

Signal-to-noise conditions can vary with instrument alignment and media opacity. In low signal-to-noise conditions, retinal reflections are minimally visible, particularly in the fovea. In high signal-to-noise conditions and in ocular inflammation, intravitreal reflections might be confused with retinal reflections. If the OCT image quality is sufficiently degraded, it is possible to have incorrect measurements or artifacts. It is important because only one of the six cross-sectional scans of the topography map is needed to have a boundary detection abnormality and to create an artifact in the retinal map.

Retinal Thickness/Volume Analysis

In these protocols, multiple OCT cross-sectional images are acquired in a variety of scan patterns on the retina in order to create a three-dimensional data set. These scan patterns concentrate measurements in the central fovea, where accurate information is most important. Hee et al.[5] developed a protocol for scanning and topographically displaying macular thickness with OCT. This protocol is used commonly to evaluate and follow retinal disorders that involve the macular area.

The Stratus OCT software has the macular thickness map (MTM) scan mode and analysis function, and the fast macular thickness map (FMTM) scan mode and analysis function. In MTM mode, each of the six sequential scans is acquired manually by the operator, while in the FMTM mode each of the sequential scan is obtained automatically by the OCT software. Six optical coherence tomograms are obtained in a radial spoke pattern centered on the fovea. Retinal thickness is computed automatically from each tomogram at a total of 600 locations throughout the macula. The surface map is displayed

as a false color image in which retinal thickness at each point is represented by a different color.

Morphologic topographic information and quantitative retinal thickness data produced by the MTM and FMTM scanning modes are crucial to identify OCT scan artifacts. The calculated central retinal thickness measurement may be inaccurate when there are artifacts in these OCT scan modes. Several different types of surface scan artifacts can influence retinal thickness measurements and have an adverse effect of therapeutic decisions.[6,7]

Artifacts Types

Misidentification Artifacts

The artifacts caused by limitations in the computer software entail misidentification of the inner and outer retina by the OCT software (Figs. 21.4 and 21.5). The release of the third generation OCT offered the theoretical possibility of high-resolution measurements of the neural retina. Recent reports have demonstrated two well-defined, parallel, red/white, highly reflective layers (HRLs) separated from each other by one thin layer of low to moderate reflectivity (green/yellow) at the outer aspect of the neural retina in presumably unaffected or normal macular regions (Fig. 21.6).[8–10] It has been suggested that the inner HRL may correspond to the junction between the inner and outer segments of the photoreceptors and that the outer HRL quite possibly corresponds to the RPE-choriocapillaris hyperreflective complex commonly seen in first-generation OCT scans.[9,10]

When automated measurements of retinal thickness are performed, the analysis protocol of the Stratus OCT software automatically delineates the boundaries of the neural retinal. Apparently, the automatic software delineation has considered the inner HRL to be the outer boundary of the neural retina in some patients, which may lead to erroneous retinal thickness estimates. Costa et al.[8] demonstrated that the outer boundary of the neural retina has been inaccurately delineated with the automated measurement tool in subjects with no clinically evident macular conditions, as well as in patients with well-established macular diseases, because it considers the inner HRL, whenever present, as the outer boundary of the neural retina. Moreover, the automated measurements of retinal thickness may be underestimated, particularly in the fovea, by the scanner software, because the inner HRL has a forward bowl-shaped configuration in this region.[8]

These inconsistencies in the alignment of the outer retinal boundaries of the macular region using the automated software measurement tool are more easily perceptible in patients with macular holes (Fig. 21.7), age-related macular degeneration (Fig. 21.8), photodynamic therapy, and central serous chorioretinopathy,[7,8] because delineation of the outer HRL as the outer boundary occurs automatically whenever loss of the inner HRL in affected outer retinal areas occur.

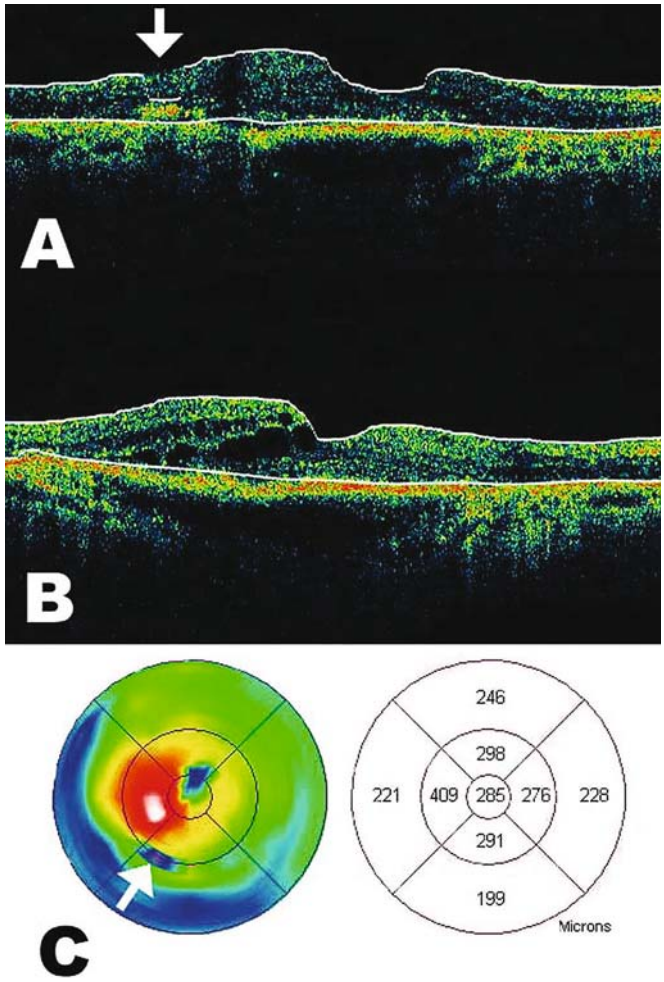

FIG. 21.4. The macular thickness map (MTM) scan mode of a retina with age-related macular degeneration. (A) Cross-sectional retinal scan obtained from 7:00 to 1:00 meridian with inner retina misidentification (arrow). (B) Cross-sectional retinal scan without artifacts obtained from 10:00 to 4:00 meridian. (C) The blue area of the retinal surface map corresponds to a falsely thin area (arrow).

Acquisition Artifacts

The following artifacts are derived from poor scan acquisition:

1. Out-of-register artifact, defined as a scan that is shifted superiorly such that the inner retina is truncated (Fig. 21.9)
2. Artifact caused by a degraded scan image (Fig. 21.10)
3. Cut-edge artifact, defined as an artifact that occurs when the edge of the scan is truncated inappropriately (Fig. 21.11)

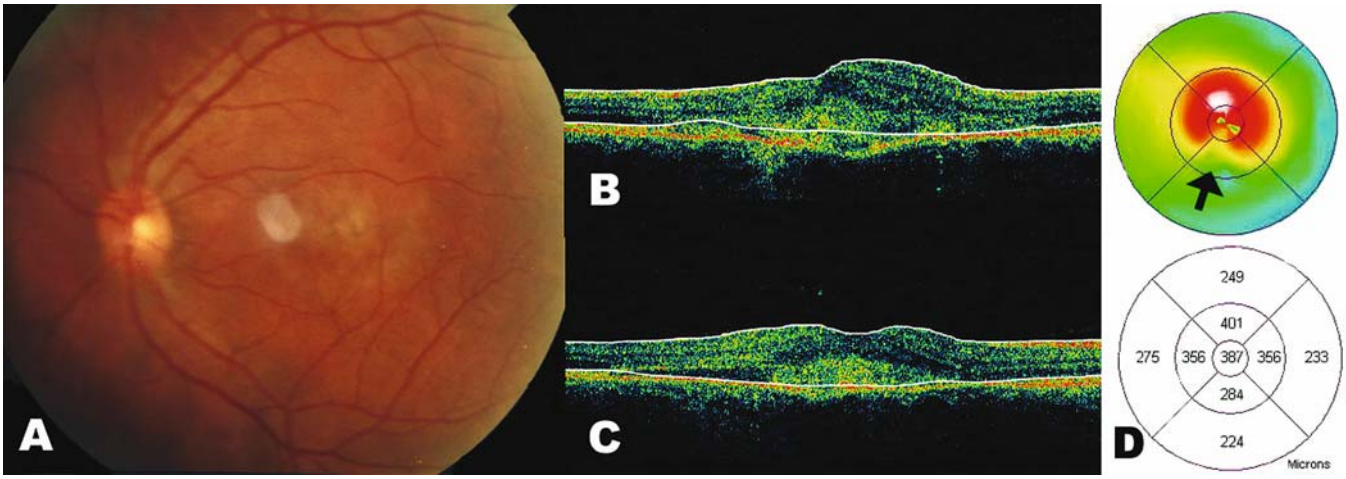

FIG. 21.5. The macular thickness map (MTM) scan mode of a retina with age-related macular degeneration. (A) Fundus photograph. (B) Cross-sectional retinal scan obtained from 6:00 to 12:00 meridian with outer retina misidentification. Notice that the automatic retinal thickness measurement tool uses the external retina and part of choroidal neovascular membrane as the high reflective retinal layer (outer white line). (C) Cross-sectional retinal scan without artifacts obtained from 3:00 to 9:00 meridian. (D) The green inferior area of the retinal surface map corresponds to a falsely normal area (arrow). Therefore, the inferior retinal thickness (284 μm) is an unreal measurement.

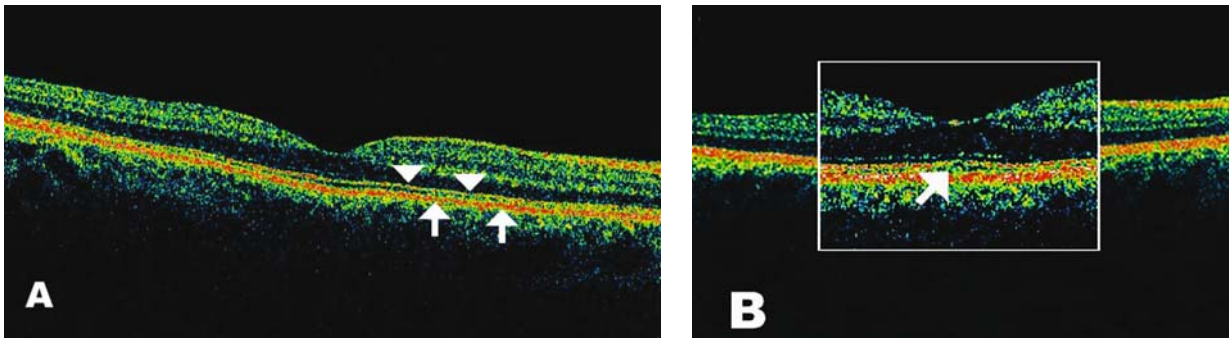

FIG. 21.6. Optical coherence tomography scan of the central 3.00-mm macular region of a normal eye. (A) Two well-defined, linear high retinal layers (HRLs) are visible at the outer aspect of the neural retina. The inner HRL is thinner than the outer and is characterized by a mild, forward, bowl-shaped configuration at the foveal center (arrowheads). The outer HRL may correspond to the retinal pigment epithelium-choriocapillaris complex (arrows). (B) Notice the increase in the distance between the inner and outer HRLs on the fovea of a healthy subject (arrow), which is consistent with the well-known increase in length of the external segments of the cones in such region.

4. Off-center artifact, which occurs when the foveal center is misidentified (Fig. 21.12)

In these cases, the patient may not be able to fixate well on the target during the OCT scan. It is especially important for the OCT operator to monitor through an infrared camera the patient's fixation and the position of the scan lines relative to the foveal center during the scanning procedure. Often, if the scanning procedure is repeated, an artifact free scan is obtained.

Optical coherence tomography scan artifacts cause a false representation of the retinal surface map but do not affect the cross-sectional image. In many cases, scan artifacts are avoidable with particular attention to scan technique. Finally, particular types OCT scan artifacts can be anticipated with the retinal clinical diagnosis.[7] These artifacts can be eliminated if the six cross-sectional images used to create a topographic map are obtained individually by the examiner, such as in the standard map protocol.[11]

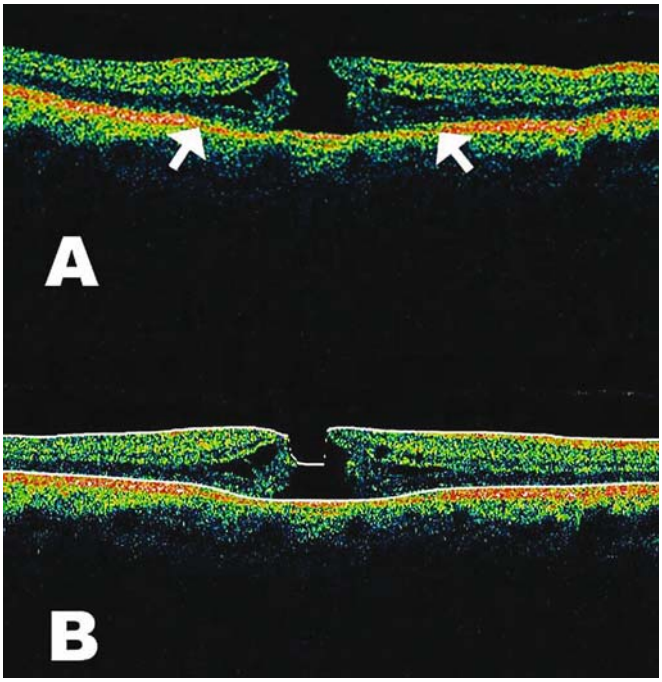

FIG. 21.7. Optical coherence tomography scans of patients with idiopathic macular hole. (A) The scan shows loss of optical reflectivity and complete disappearance of the inner HRL in the affected area (between arrows). In the unaffected macular region, a similar outer retinal tomographic appearance as that in normal eyes is present. (B) Notice that the automatic retinal thickness measurement tool uses the inner HRL in the unaffected macular area and the outer HRL in the affected area to delineate the outer neural retina border (outer white line). These inconsistencies in the alignment of the outer retinal boundaries of the macular region using the automated software measurement tool lead to erroneous retinal thickness estimates.

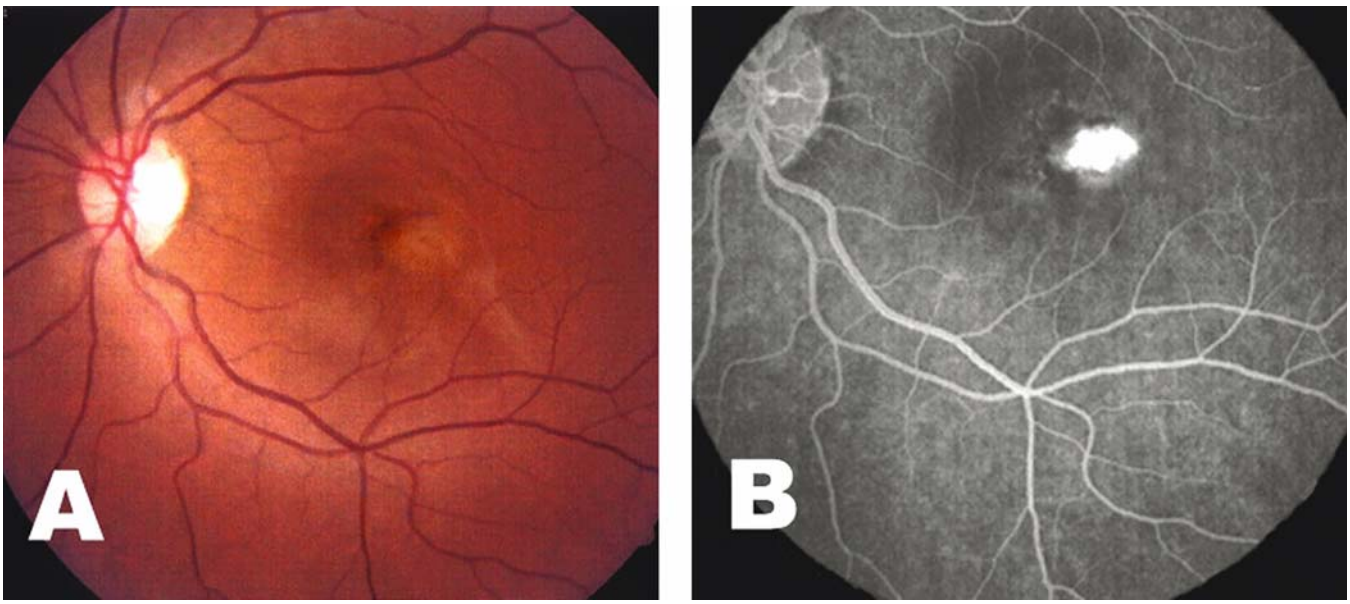

FIG. 21.8. A 28-year-old woman presented with a history of decreased vision in her left eye. (A) Fundus photograph shows a pigmented lesion extending on the foveal center with surrounding subretinal fluid. (B) Fluorescein angiography shows a juxtafoveal idiopathic classic choroidal neovascularization. (C) Cross-sectional retinal scan obtained from 3:00 to 9:00 meridian shows retinal elevation and an increase in retinal thickness at the macula, due to subretinal fluid accumulation and intraretinal edema. The inner HRL detaches from the outer HRL jointly with the rest of the retina at the edges of the neurosensory retinal detachment. (D) Notice that the

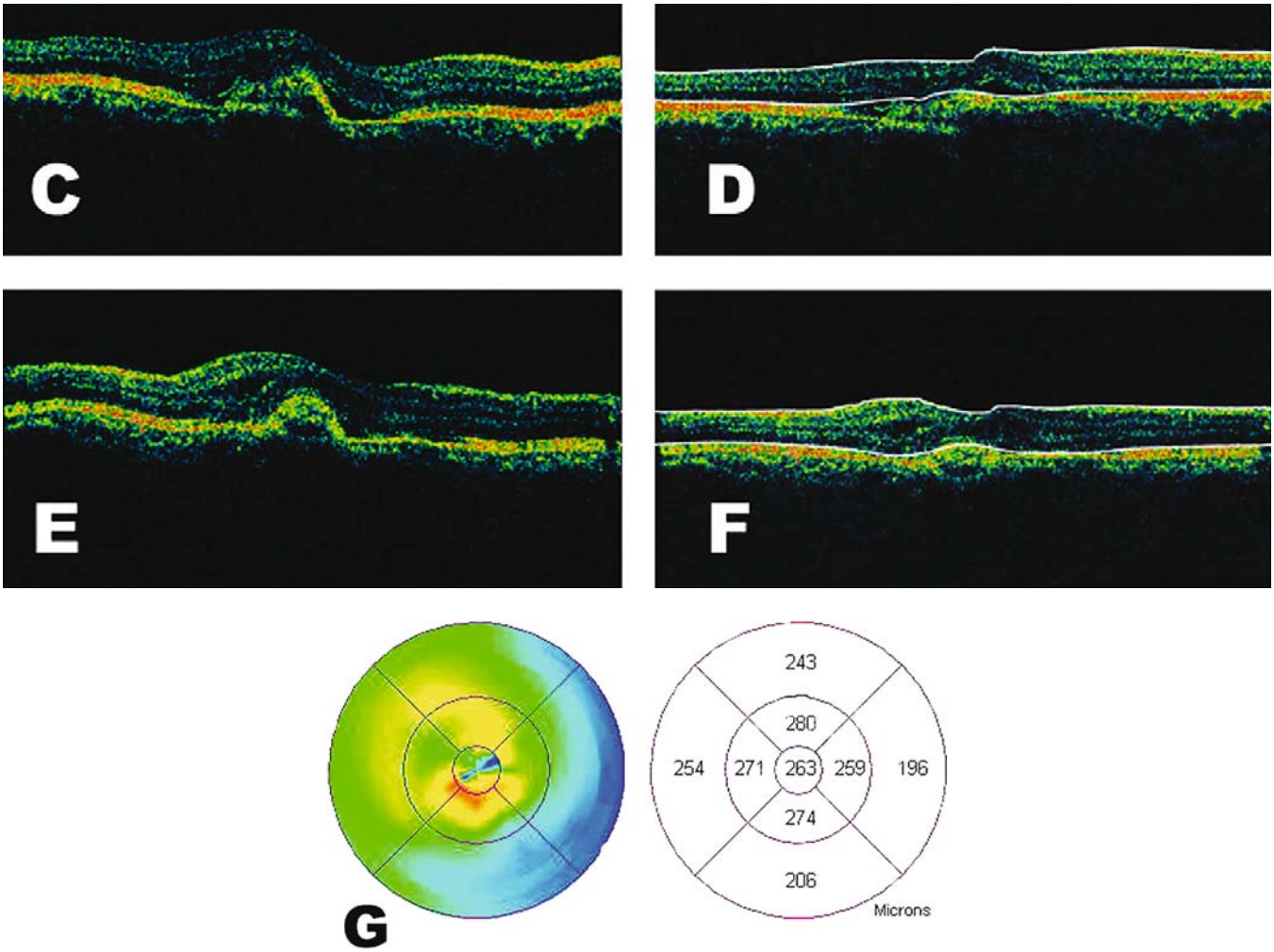

FIG. 21.8. (continued) automatic retinal thickness measurement tool uses the inner HRL to draw the outer limits in less affected regions and the outer HRL in the area of the neurosensory retinal detachment. However, automatic delineation of the neural retina boundaries used a low retinal layer that is reflective above the interrupted retinal pigment epithelium to complete the drawing of the line at the choroidal neovascularization site. (E) Cross-sectional retinal scan obtained from 6:00 to 12:00 meridian shows loss of optical reflectivity and complete disappearance of the inner HRL in the affected area. (F) Automatic delineation of the neural retina boundaries used the inner HRL to draw the outer limits in less affected regions and the outer HRL in the area of the neurosensory retinal detachment. (G) Macular thickness map.

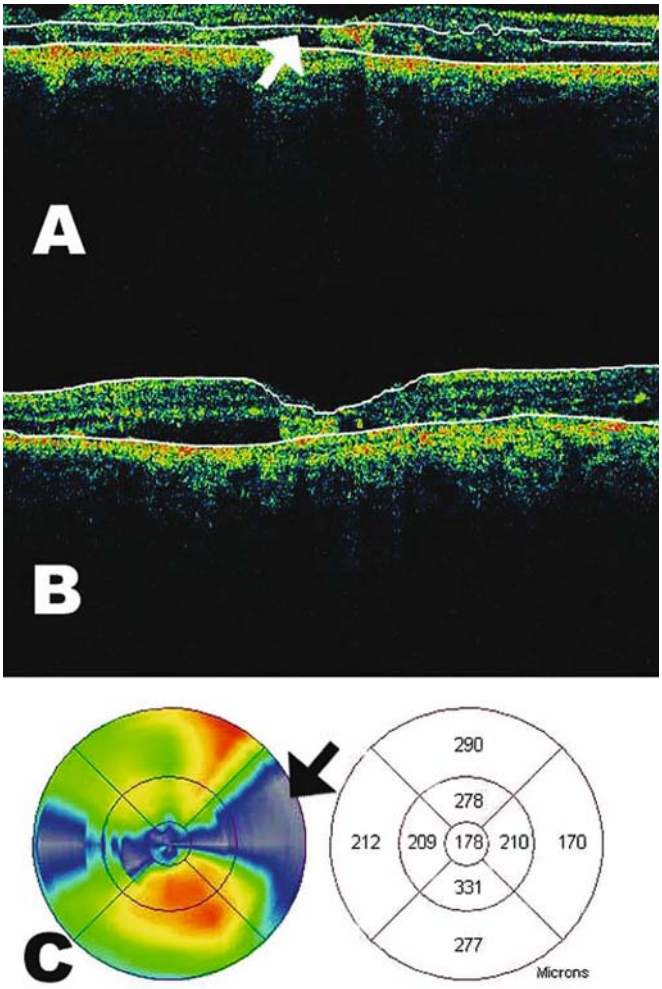

FIG. 21.9. The macular thickness map (MTM) scan of a retina with age-related macular degeneration. (A) The cross-sectional retinal scan obtained from 3:00 to 9:00 meridian shows that the image is out of register and the inner retina is misidentified (arrow). (B) Cross-sectional retinal scan without artifacts obtained from 6:00 to 12:00 meridian. (C) Retinal surface map shows out-of-register artifact. The blue area corresponds to a falsely thin area (arrow).

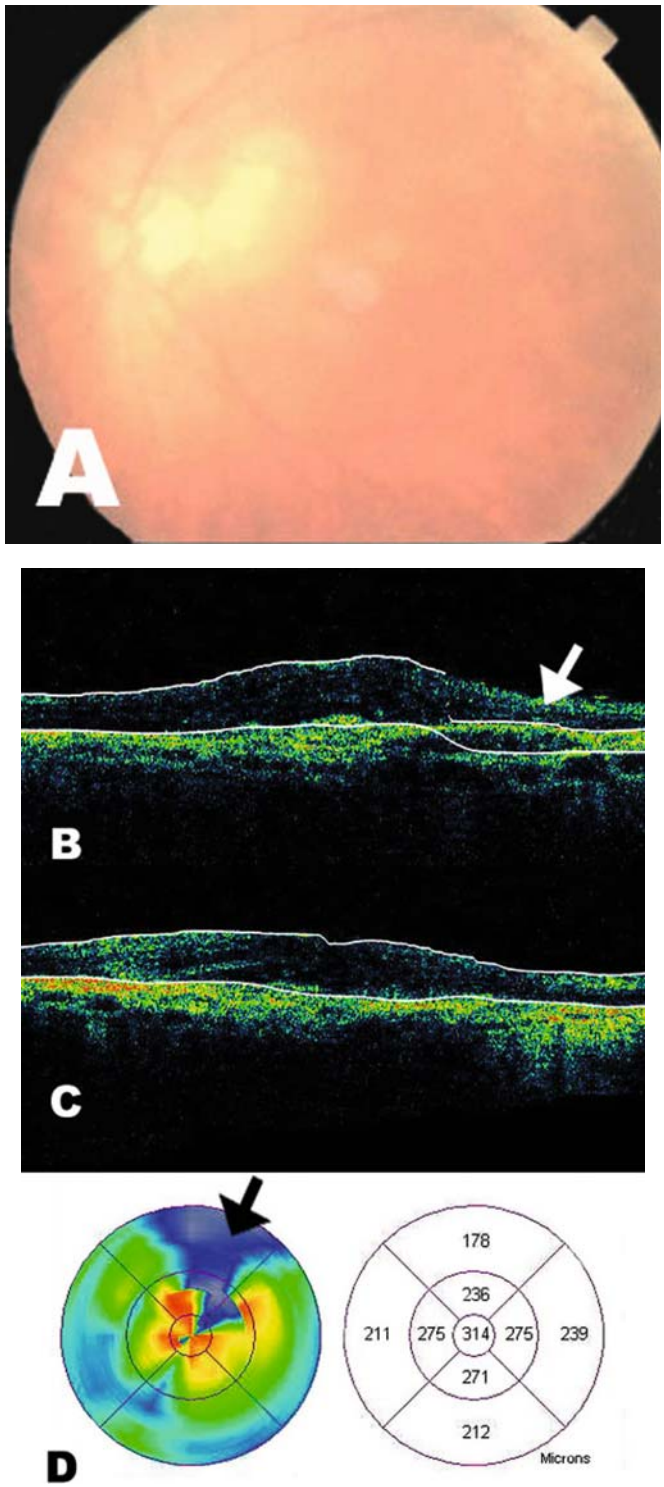

FIG. 21.10. The macular thickness map (MTM) scan mode of an eye with age-related macular degeneration and subcapsular posterior cataract. (A) Fundus photograph. (B) Cross-sectional retinal scan obtained from 6:00 to 12:00 meridian with inner and outer retina misidentification (arrow). (C) Cross-sectional retinal scan obtained from 3:00 to 9:00 shows the degraded image of the inner retinal surface. Obtaining useful data of central foveal thickness or retinal morphology is not possible. (D) Retinal surface map shows artifact produced by the inner and outer retina misidentification (arrow).

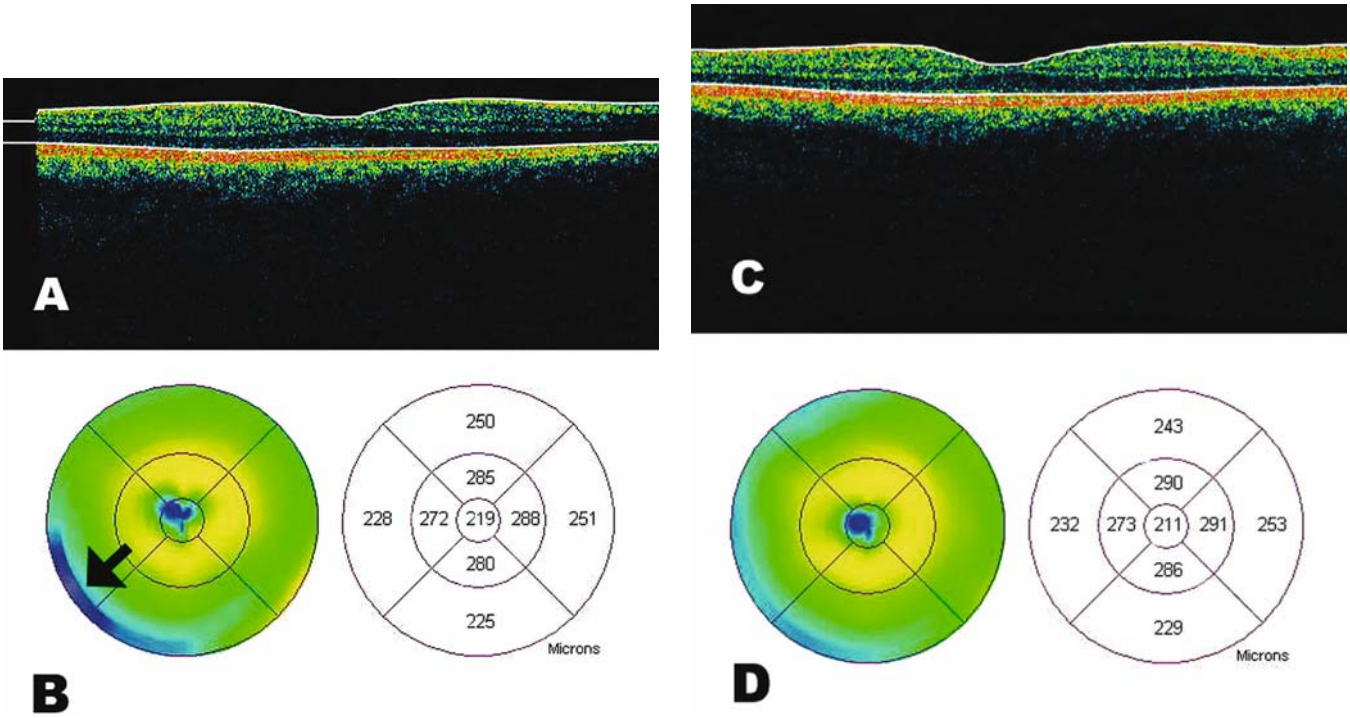

FIG. 21.11. (A) Cross-sectional retinal scan obtain from 8:00 to 2:00 meridian with a cut-edge artifact causing inner and outer retina misidentification. (B) Retinal surface map shows the blue area corresponding to a cut-edge artifact (arrow). (C) Cross-sectional retinal scan obtained from 8:00 to 2:00 meridian without artifacts in the same patient. (D) Surface map of a retina without artifacts in the same patient.

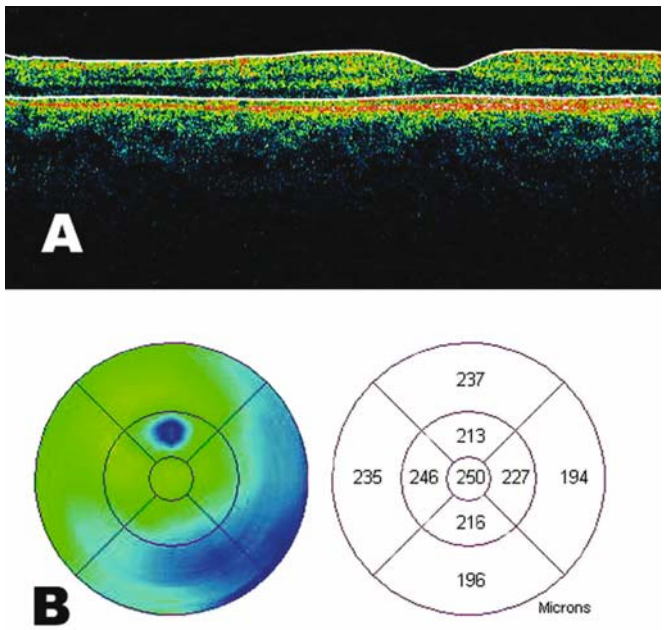

FIG. 21.12. In some cases the foveal center could not be clearly identified on the surface map because of underlying pathology. (A) Cross-sectional retinal scan shows off-center artifact that occurs when the foveal center is misidentified. (B) Surface map with off-center artifact. Retinal thickness measurement is inaccurate.

Pathologies that Limit Optical Coherence Tomography Interpretation

Computer algorithms may fail to identify the boundaries of the retina if the retinal architecture is distorted due to severe pathology. The intensity of the OCT image is determined by both the feature being imaged and the scattering and absorption characteristics of the overlying tissue. Thus, care is required in interpreting OCT images because the brightness of various features may be affected by abnormalities in the cornea, lens, and vitreous.

Optical Aberrations

A higher incidence of vitreoretinal disorders is found in highly myopic eyes; however, in the same eyes, several factors contribute to make visualization of the macular area more difficult. The absolute minimum spot size is limited by the aberrations in the optics of the eye. In these instances, much finer transverse resolutions can be achieved by the use of high numerical aperture focusing. A degraded image is possibly secondary to poor scan acquisition, for example, maladjustment of the OCT focus in highly myopic or hypermetropic eyes. Additionally, perpendicularity of the examining beam to the target tissue is also important for good image quality. Deformities of the posterior globe, such as staphylomatous changes in highly myopic patients, make perpendicularity very difficult if not impossible. Furthermore, axial length issues further distort the image, making interpretation more tenuous. Coppe and Ripandelli[12] studied 124 eyes with myopia over −18.00 diopters, and found that in 85% of these eyes there was a vitreoretinal disorder.

Corneal Opacity

Since OCT is basically a distance-measuring device and the time between send and receive is critical, anything that interferes with this premise will affect imaging. Media clarity from the cornea may absorb, deflect, or refract examining signals. Therefore, any pathology that alters the corneal clarity severely produces images of low quality, and these can affect retinal measurements.

Small Pupil

Pupil size is also important if the opening is very small, but usually an experienced operator can obtain reasonable images if the rest of the ocular media are clear. Vignetting occurs when the OCT imaging beam is blocked by the iris during a portion of the beam scan and is characterized by loss of signal over a specific portion of the OCT image (Fig. 21.13).[1] This problem is the result of improper alignment of the OCT imaging beam. Optical coherence tomography is designed so that the OCT imaging beam pivots about the pupil when the beam is scanned on the retina. Although the pupil limits the available aperture for focusing on the retina, the absolute minimum spot size is limited by the aberrations in the optics of the eye.

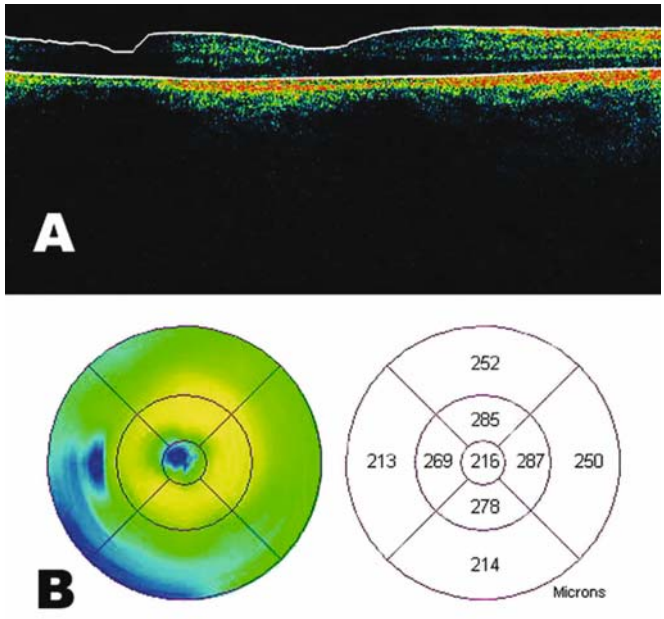

Fig. 21.13. Small pupil. (A) Cross-sectional retinal scan obtained from 9:00 to 3:00 meridian. Notice that a portion of the image has a low signal-to-noise ratio and appears dim because the iris blocks the OCT beam during part of the scan. (B) Retinal surface map shows the blue area that corresponds to the dim area in A.

The older versions of the OCT required dilation with at least a 5-mm pupil. The newer third-generation OCT (Stratus) can be used in the absence of dilatation in many individuals, and usually requires a 3-mm pupil for adequate visualization. To ensure that the OCT pivots about the pupil of the eye, the patient's eye must be located at a given distance (1 cm) from the ocular objective lens.[6] If the patient's eye is too far from or too close to this position, the OCT beam will change position instead of pivoting about the pupil, and a vignette will occur. In summary, spot size is a function of the optics used to project the beam into the eye, and a good resolution of the image in the transverse direction needs a minimum of 3-mm pupil size.

Lens Opacity

Optical scattering is a property of a heterogeneous medium and occurs because of microscopic spatial variations in the refractive within tissue. Although scattering from cataracts produces a reduction in image intensity, it usually does not degrade image quality, except in cases of severe opacity. The high sensitivity of OCT allows these weak optical signals to be detected, and the retinal tissues can be imaged, although they are virtually transparent. However, care must be taken with these patients, and careful imaging technique must be used to ensure that images have sufficient signal levels. In patients with posterior subcapsular cataract, a technician can erroneously place a radial scan over lens opacities, producing artifactual lack of retinal thickness.

When scan placement is shifted away from lens opacities, artifacts disappear.

Degraded image artifacts can be observed frequently but they are not associated significantly with cataracts.[7] Because OCT is based on near-infrared interferometry, it is not affected by changes in nuclear sclerotic cataract density or similar media opacity; however, posterior subcapsular and cortical cataracts do impart the ability to perform OCT. The ability to produce artifact-free OCT images in these cases points to the usefulness of OCT, even in eyes with moderately opacified ocular media.[13,14] In addition, the results indicate that uncomplicated cataract surgery does not influence retinal thickness measurements in eyes without ocular pathologies.[15]

Vitreous Opacity

Pathologies where the vitreous has inflammatory infiltrate, vitreous condensations, or hemorrhage result in increased optical scattering and are visible in the OCT images. Therefore, OCT images are degraded. In the presence of vitreous opacity, it may be difficult to obtain optimal scans because there is reduction in image intensity. The macular status can be assessed by OCT examination in the presence of a moderate vitreous opacity (vitreous hemorrhage). In this instance, scan acquisition depends on the skill of the OCT examiner. However, preretinal hemorrhage produces strong attenuation of the incident light shadowing the reflection from the retina, retinal pigment epithelium, and choroid below the hemorrhage. In these cases, the attenuation of the incident light depends on the thickness of the scattering medium. Thin hemorrhages appear as thin, highly reflective bands that have little effect on the underlying tissue. Thick hemorrhages completely attenuate the incident light and produce strong shadowing of underlying structures (Fig. 21.14).

Eccentric Fixation

The central fovea often is slightly displaced laterally from the center of the OCT image in patients with eccentric or varying fixation. In these cases, the computer provides an estimate of the lateral displacement by identifying the position of minimum total retinal reflectivity, which usually is characteristic of the relative absence of plexiform layers in the central fovea. The examiner should then choose to offset the center of the OCT to this position. We prefer to acquire sequential scans manually by the operator than sequential scans obtained automatically by the OCT software in patients with eccentric fixation. When patients have poor vision in one eye, the contralateral eye provides fixation. However, if eccentric fixation is present, identification of the center of the fovea from video funduscopic images can be difficult, especially when foveal pathology is present and scan acquisition depends on the skill of the examiner. Future development in the feature recognition algorithm should lead to a completely automated identification technique.

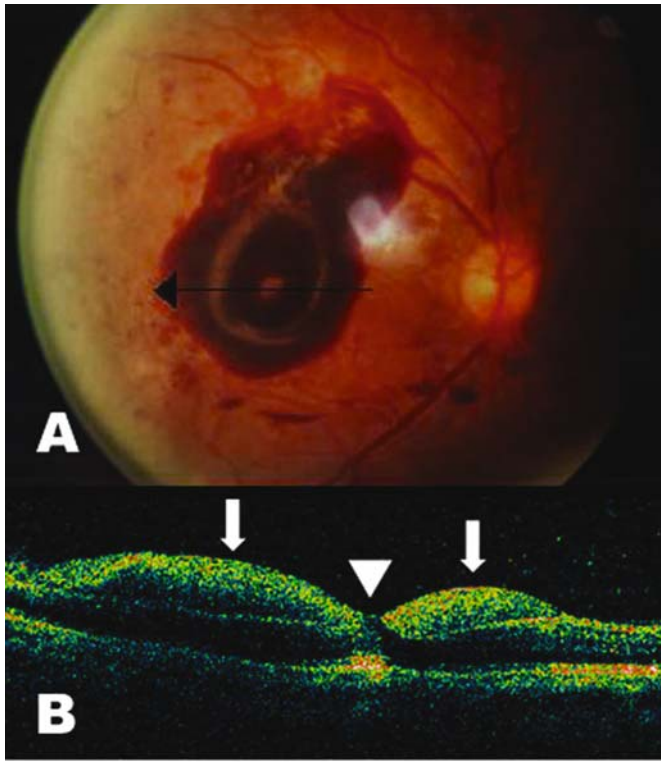

Fig. 21.14. (A) Fundus photograph shows a subhyaloidal premacular hemorrhage without foveal involvement. (B) A horizontal tomogram demonstrates a large area of subhyaloidal hyperreflectivity corresponding to hemorrhage (arrows). Strong attenuation of the incident light shadowed the reflection from the retina, retinal pigment epithelium, and choroid below the hemorrhage. However, the fovea is visualized as highly reflective because there is no hemorrhage in the center (arrowhead).

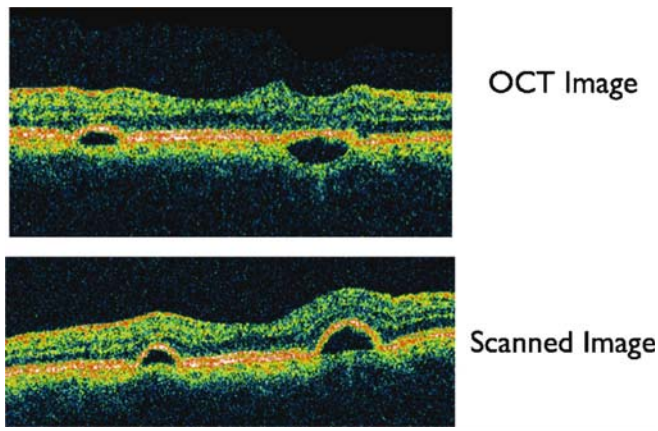

Fig. 21.15. The scanned image correctly shows the pigment epithelial detachment (bottom), whereas the processed OCT image (top) incorrectly tries to flatten the pigment epithelial detachment. (Courtesy of Lihteh Wu, MD.)

Pigment Epithelial Detachment

The scanned image correctly shows the pigment epithelial detachment, whereas the processed OCT image incorrectly tries to flatten the pigment epithelial detachment (Fig. 21.15).

The Future

The OCT device and examination technique continue to evolve. Hardware and software have been modified and improved. Recognition and upgrading of these changes are critical to the interpreting clinician since image quality is often affected. Problems of acquisition and interpretation will be addressed with constant development of future generations of the OCT and with new technology. Nevertheless, as with any imaging modality, some artifacts will always remain.

The Stratus OCT software version 4.0 automatically identifies scans in the fast macular thickness map that are likely to have artifacts because of poor scan acquisition or problematic pathology and provides a framework for the examiner to easily reacquire those images. Therefore, it improves image segmentation.[11]

Spectral domain OCT is a new technology that effectively acquires an entire A-scan simultaneously and promises image acquisition at 50 to 100 times the current speed with equal or improved spatial resolution. Ultrahigh-resolution OCT leads to the possibility that OCT will be applied to the quantitative assessment of cellular morphology (see Chapters 25, 26, and 27).[16,17]

Acknowledgments. The authors have no financial or proprietary interest in any of the products or techniques mentioned in this chapter. This work is supported in part by the Fundacion Arevalo-Coutinho para la Investigacion en Oftalmologia (FACO), Caracas, Venezuela.

References

1. Hee MR, Fujimoto JG, Ko T, et al. Interpretation of the optical coherence tomography image. In: Shuman JS, Puliafito CA, Fujimoto JG, eds. Optical Coherence Tomography of Ocular Diseases, 2nd ed. Thorofare, NJ: Slack, 2004:21–53.
2. Hee MR, Izatt JA, Huang D, et al. Optical coherence tomography of the human retina. Arch Ophthalmol 1995;113:325–332.
3. Swanson EA, Izatt JA, Hee MR, et al. In vivo retinal imaging by retinal coherence tomography. Opt Lett 1993;18:1864–1866.
4. Fujimoto JG, Hee MR, Huang D, Shuman JS, Puliafito CA, Swanson EA. Principles of optical coherence tomography. In: Shuman JS, Puliafito CA, Fujimoto JG, eds. Optical Coherence Tomography of Ocular Diseases, 2nd ed. Thorofare, NJ: Slack, 2004:3–19.
5. Hee MR, Puliafito CA, Duker JS, et al. Topography of diabetic macular edema with optical coherence tomography. Ophthalmology 1998;105:360–370.
6. Jaffe GJ, Caprioli J. Optical coherence tomography to detect and manage retinal disease and glaucoma. Am J Ophthalmol 2004;137:156–169.
7. Ray R, Stinnett SS, Jaffe GJ. Evaluation of image artifact produced by optical coherence tomography of retinal pathology. Am J Ophthalmol 2005;139:18–29.
8. Costa RA, Calucci D, Skaf M, et al. Optical coherence tomography. 3. Automatic delineation of the outer neural retinal boundary and its influence on retinal thickness measurements. Invest Ophthalmol Vis Sci 2004;45:2399–2406.
9. Jorge R, Costa RA, Quirino LS, et al. Optical coherence tomography findings in patients with late solar retinopathy. Am J Ophthalmol 2004;137:1139–1143.
10. Drexler W, Sattmann H, Hermann B, et al. Enhanced visualization of macular pathology with the use of ultrahigh-resolution optical coherence tomography. Arch Ophthalmol 2003;121:695–706.
11. Hee MR. Artifacts in optical coherence tomography topographic maps. Am J Ophthalmol 2005;139:154–155.
12. Coppe AM, Ripandelli G. Optical coherence tomography in the evaluation of vitreoretinal disorders of the macula in highly myopic eyes. Sem Ophthalmol 2003;18:85–88.
13. Sanchez-Tocino H, Alvarez-Vidal A, Maldonado MJ, Moreno-Montanes J, Garcia-Layana A. Retinal thickness study with optical coherence tomography in patients with diabetes. Invest Ophthalmol Vis Sci 2002;43:1588–1594.
14. Polito A, Shah SM, Haller JA, et al. Comparison between retinal thickness analyzer and optical coherence tomography for assessment of foveal thickness in eyes with macular disease. Am J Ophthalmol 2002;134:240–251.
15. Grewing R, Becker H. Retinal thickness immediately after cataract surgery measured by optical coherence tomography. Ophthalmic Surg Lasers 2000;31:215–217.
16. Nassif N, Cense B, Park BH, et al. In vivo human retinal imaging by ultrahigh-speed spectral domain optical coherence tomography. Opt Lett 2004;29:480–482.
17. Wojtkowski M, Srinivasan V, Fujimoto JG, et al. Three-dimensional retinal imaging with high-speed ultrahigh-resolution optical coherence tomography. Ophthalmology 2005;112:1734–1746.

Part III
Ophthalmic Imaging, Spectral Domain, and New Technologies

22
Ophthalmic Fundus Imaging

Michael D. Ober, Lawrence A. Yannuzzi, Jason S. Slakter, Richard F. Spaide, Yale L. Fisher, Robert W. Flower, Richard Rosen, Christina M. Klais, and Nicole E. Gross

The medical-retina specialty finds its origins in the classic 1967 study, "The Pathogenesis of Disciform Detachment of the Neuro-epithelium" by Dr. J. Donald Gass, which was published initially as a supplemental issue of the *American Journal of Ophthalmology*. Prior to this milestone in the field, specialists in "retina" were essentially "bucklers," that is, individuals trained to excel in indirect ophthalmoscopy in order to find "breaks" and to reattach the retina.

Armed with a new diagnostic adjunct (fluorescein angiography), inspired by Gass's brilliant and original work along a broad, chorioretinal front, and catalyzed by the potential for new forms of treatment (most notably laser photocoagulation), a new breed of retinal specialists began to emerge in the beginning of the 1970s. Coincidental with and consequential to evolutionary changes in ophthalmologic subspecialization was the appearance of a number of superb medical-retina texts and atlases by a score of academicians from Japan, England, Italy, Germany, United States, and most recently India. Distinguished international retinal figures published the first texts, which expanded our clinical knowledge of medical-retina diseases, enhanced by enlightening illustrations utilizing fluorescein angiography.[1–5] However, it was Gass[6] and his *Stereoscopic Atlas of Macular Diseases* in 1970 that set new standards in fundus diagnosis, and, with the advent of medical lasers, treatment of a variety of chorioretinal disorders. This classic textbook, its subsequent revisions, and contributions by an elite corps of medical-retina pioneers produced a series of texts, slides, and atlases on retinal vascular disease and chorioretinal disorders. In the early publications they described new diseases and new manifestations of previously known abnormalities to expand the spectrum of the medical-retina specialist and to establish this ophthalmic discipline as a distinct subspecialty. All of their work was supported and embellished by stereo film-based images for analysis of fundus disorders from the vitreoretinal interface through the retinal vasculature and into the retinal pigment epithelial-choroidal layers. Standard technology for acquisition of these images was designed and developed to enhance resolution, stereopsis, and field of view, in that order.

A generation of newly created and defined medical-retinal specialists were dedicated to acquiring, interpreting, and archiving these images as a guide for treatment, first with a new driving technologic concept—ophthalmic lasers—and later with advances in vitreoretinal surgery and pharmacotherapeutics. The initial standards of care were based on impressions such as regression of retinal neovascularization in diabetic retinopathy from xenon photocoagulation and scatter ruby laser treatment. Assumptions shared by leaders in the field were eventually replaced by evidence-based decisions drawn from well-designed clinical trials, beginning with diabetic retinopathy, branch vein occlusion, age-related macular degeneration (AMD) of the neovascularized type, and sickle cell retinopathy. All of these applications were dependent on fundus imaging to demonstrate patient eligibility for treatment. In short, fundus imaging was the fundamental basis for clinical research, teaching, and patient care in this subspecialty.

These founding-father medical-retinal specialists were collectively referred to by some as "stereo film-based fanatics" because of their unbending commitment to this form of imaging, which served to segregate the retinal from the choroidal circulations and to isolate anatomic compartments in the fundus, such as detachment at the retinal pigment epithelium and neurosensory retina and the cystic spaces in the retina itself. However, for the current generation of retinal specialists, these standards have changed in response to evolving technology, framed within one cardinal principle: digital imaging. Medical-retinal specialists today are now obliged to master the art of digital imaging for fluorescein and indocyanine green (ICG) angiography, three-dimensional ultrasound, and ophthalmic coherence tomography (OCT). In addition, there is an array of other digital imaging concepts currently under development to improve tissue differentiation, even on a cellular level, to determine the physiologic state of the dual chorioretinal circulations, and to assist in eye care for the general population by facilitating ophthalmic screening, physician interactive communication, and clinical research.

This conversion from stereo film-based photographs to digital images has evolved slowly but progressively over the

past decade. One of us (L.A.Y.) recalls an attempt to meet the demands of a voluminous mail consultation correspondence in the late 1980s utilizing the fax machine to transmit clinical information and photographs. Unfortunately, at that time the existing technology and the prevailing regulatory agencies could not and would not accommodate this concept, which required highly resolved photography and interstate medical consultations. Several years later, motivated by the obligatory nature of digital imaging for ICG angiography, there was a more compelling need to utilize digital rather than film-based imaging. Enter the world of the Internet, and the development and availability of digital technology to acquire and transmit high-resolution images for accurate diagnosis. Commercial interests promptly responded with advances in imaging quality and transmission and derivative systems for specialized studies. High-resolution cameras heavily weighted to provide required wave lengths for fluorescence, corresponding video display terminals, and high-speed computers with expanded memory and sophisticated software for image manipulation led the parade of new digital technology.

With this perspective on fundus imaging, this chapter discusses pertinent issues related to advances in the medical-retinal subspecialty, which are very much dependent on imaging of the posterior segment of the eye. To begin, we review the gains and losses associated with a film to digital conversion and applications of digital imaging in a clinical and research setting. Next, we offer an example of how a scientific concept can be applied to modify a digital fundus camera in order to obtain valuable clinical information on macular diseases. Then we review B-scan ophthalmic ultrasonography and recent advances that promise to establish new standards in real-time three-dimensional imaging. Next, we discuss the use of high-speed angiography to identify subtle perfusion abnormalities in the choroidal circulation and its potential applications for improvement in patient care. And finally, we provide an update on the collaborative work between retina specialists and several basic scientists to develop a method for the next generation of OCT imaging combined with simultaneous confocal laser ophthalmoscopy for pixel to pixel or so-called point to point correlation, reconstructive topographic area representation, and three-dimensional volumetric analysis—termed OCT-ophthalmoscopy.

Fundus Digital Imaging

The first fluorescein angiograms in the late 1960s were made with the classic black body Zeiss fundus camera. It was equipped with a Contax camera, which advanced the film with a circular turning knob and recycled the photographic flash every 1 to 3 seconds, depending on its intensity. Several technologic innovations promptly emerged to update fundus cameras, including bayonet camera mounts with triggers and eventually motors for film advance, electronic flash rapid recycling systems, stereo devices, and interference filters for dye excitation and fluorescence transmission. For over 20 years, many research centers utilized hand-drawn tracings of the fluorescein angiographic studies using table-mounted stereo viewers, taken from negative or positive black-and-white photos for the evaluation and diagnosis of chorioretinal diseases.

Since their introduction in the mid-1980s, however, digital angiographic systems have gained widespread use in the ophthalmic community and have undergone technical improvements that have advanced their ability to provide high-resolution images. Advances in digital camera technology, improvements in computer storage, and enhanced photographic evaluation techniques have also resulted in the creation of an imaging system equal to, or in many respects superior to, the traditional film-based techniques of the past (Fig. 22.1).

Comparative Analysis: Clinical Setting

In the clinical setting, film-based photography has two theoretical advances over digital imaging, image resolution, and stereoscopic viewing. A film-based angiographic image contains 10,000 lines of resolution. In contrast, most digital images contain approximately 1000 lines of resolution (Table 22.1). In a practical setting, however, these differences are not as apparent as they might seem. The film edges are approximately one square inch in size and must be magnified to view, thus reducing the effective image resolution. The digital image, on the other hand, is displayed on a large computer screen that allows for viewing at full resolution. The theoretical film advantage exists only in the setting of clear media with perfect image acquisition, an uncommon occurrence even for the most gifted photographers. Furthermore, film camera settings are usually based on the midphase of the angiogram, leading to overexposure of the early photos and underexposure of the late photos. Dodging and burning techniques are of limited value in compensating for this phenomenon. While digital imaging may surrender to film-based imaging with regard to resolution, this is not an unconditional surrender. Good-quality stereo images are now obtainable with low-cost digital systems as well. New digital camera and fundus imaging systems will continue to close the gap on film-based techniques.

An alternate point of view reveals certain advantages that digital imaging has over film-based imaging that outweigh the potential superiority of film in resolution and stereoscopic viewing. For instance, digital imaging may provide equal or sometimes superior images because of the capabilities of the technique itself. With film imaging, the photographer is unaware of the quality of the image until the film is developed. In contrast, photographers using digital cameras can view the images as they are obtained. Adjustments in gain, focus, and flash intensity can be made on a real-time basis to provide for maximum quality of the angiographic images. Moreover, there is a minimal cost associated with obtaining additional images by digital photography. In contrast, film-based

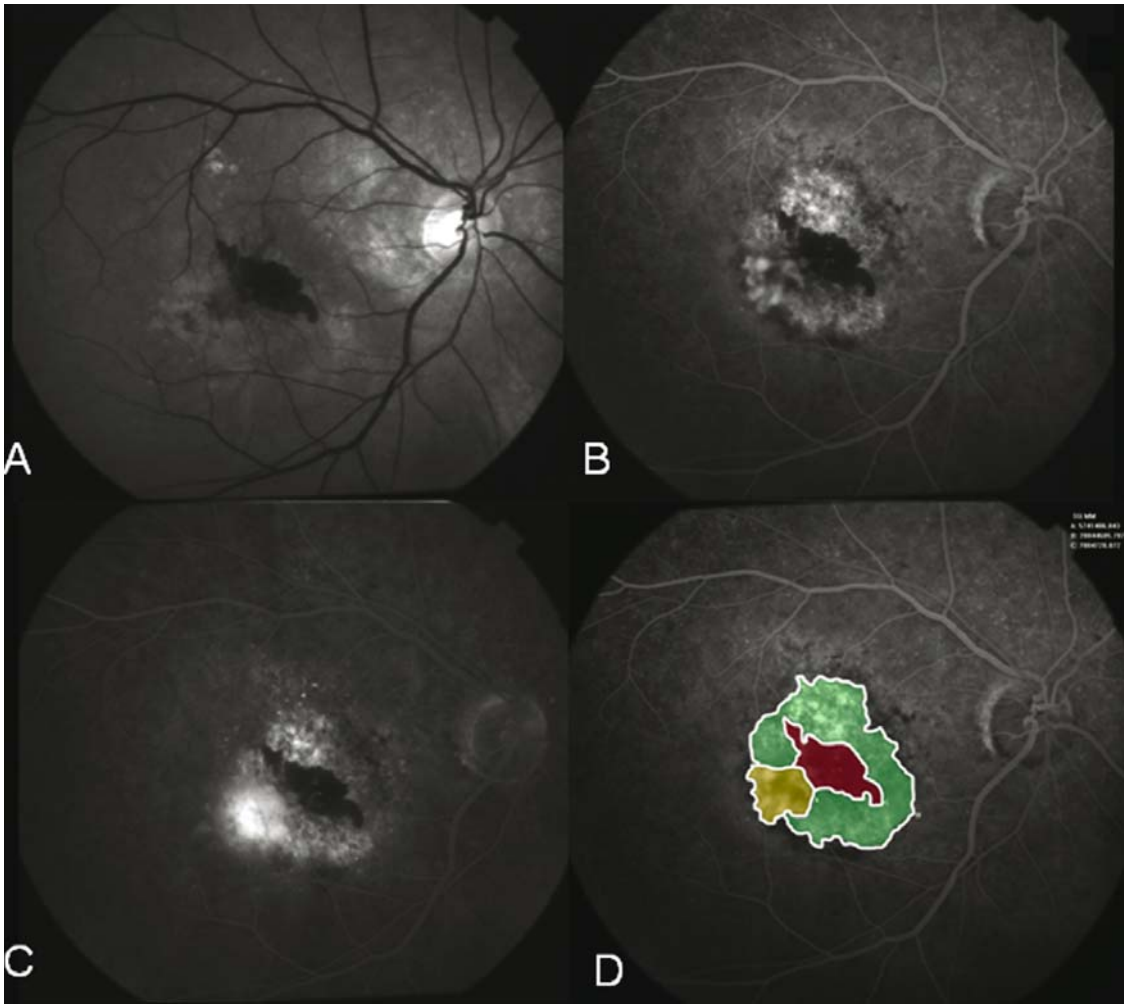

FIG. 22.1. Demonstration of area measurements taken from fluorescein angiography. The images represent early (A), middle (B), and late (C) angiographic images, respectively, of choroidal neovascularization containing classic and occult components as wells as blood. The final image (D) shows individual area measurements for the classic, occult, and hemorrhage components superimposed over the angiogram.

TABLE 22.1. Comparison of digital fundus imaging with film-based fundus imaging.

	Digital	Film-based
Resolution	1000 lines (improving)	10,000 lines
Stereoscopic viewing	Available	Available (easier)
Image manipulation	Easy	Difficult
Equipment cost	$$$$	$$
Processing time	Seconds	Hours
Duplication time	Seconds	Hours
Lesion measurement	Irregular tracing made easy	Best fit circles
Transmission	Available world wide with Internet	Mail/manual delivery of copies only

photography requires additional rolls of film, even for a single supplementary image. In addition, with film-based angiography, the highest resolution of the angiogram is the negative, for which only one copy exists. Reproductions of this image are available only in a form of low-resolution contact sheets. With digital imaging, however, multiple exact duplicates of the original angiographic study can be produced with no loss of resolution.

Another major advantage of the digital technique is the ability of the treating physician to evaluate a study and deter-

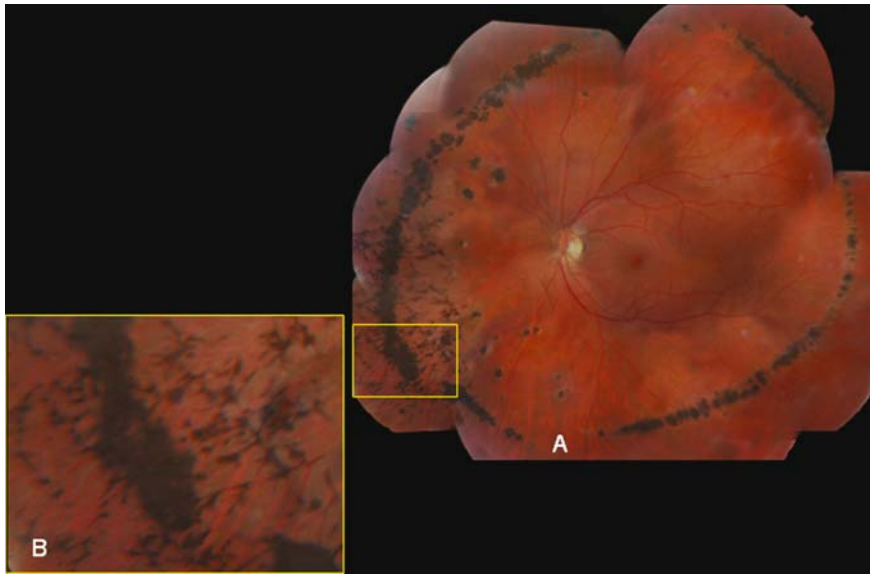

FIG. 22.2. Manipulation of digital images. The larger images represent a montage of several individual digital photos arranged using widely available software to simulate a pan-fundus image. The smaller image shows that even with 8× magnification, resolution remains sufficient for detailed viewing.

FIG. 22.3. Panaret 1000A by Medibell Medical Vision Technologies.

mine an appropriate patient diagnosis and treatment options immediately. Comparison of previous imaging studies can be easily performed using digital overlay techniques that allow for precise evaluation of changes in fundus abnormalities detected on the angiographic studies. Magnifying and mapping an image for laser guidance is simulated and enhanced with digital images, which can be displayed on a computer screen next to a therapeutic laser. Another key advantage to digital imaging is in the area of patient education. The ability to manipulate and display an angiographic study to facilitate an explanation of diagnostic and treatment options to the patients on a real-time basis cannot be overemphasized (Fig. 22.2). Finally, the use of digital imaging and telecommunication technology permits the rapid transmission of images between one clinician and another for examination and consultation.[7]

Indocyanine green angiography has clearly been shown to be useful in the diagnosis and evaluation of exudative age-related macular degeneration, inflammatory diseases, and other chorioretinal abnormalities. This imaging technique can only be obtained using a digital imaging system.[8] New computer software allows physicians to display as well as archive digital images from various techniques (such as ophthalmic coherence tomography and ultrasonography) on the same computer.

Recent advances in digital imaging include high-resolution wide-angle as well as nonmydriatic cameras. The Panaret 1000A (Medibell Medical Vision Technologies, Valley Stream, NY) is a wide-angle contact digital imaging system utilizing capable of 1024 × 1024 pixel still images and 30 image per second live video (Fig. 22.3). It utilizes trans-scleral illumination for even lighting and elimination of flash artifacts. The Panaret Non-Mydriatic 60 system (Medibell) is a nonmydriatic camera capable of 30- or 60-degree fundus images taken through an undilated 2-mm pupil. The Panoramic 200 Optomap (Optos, Malborough, MA) is a scanning laser ophthalmoscope (SLO) that records a digital image of the retina that includes up to 200 degrees taken through an undilated pupil (Fig. 22.4). Another camera capable of wide-angle photos is the Topcon TRC-NW6S (Topcon, Paramus, NJ), which uses nine digital images that are assembled into a single montage via semiautomated software (Fig. 22.5). An alternative automated montage software is AutoMontage, from Ophthalmic Imaging Systems, Sacramento, CA. This software has the ability to piece together multiple fundus images into a single wide-field view and has recently been shown to be highly effective when compared with a manual method of montage construction.[9]

By combining digital fundus imaging with computerized perimetry, the MP1 Microperimeter (NIDEK Technologies, Fremont, CA) provides automated assessment of macular function. It takes a red-free fundus photo and locks onto identifiable features such as vessel crossings, which allows for accurate tracking during visual field testing. The end result is a fundus photo with overlying notations for fixation and measurements of visual sensory responses on their exact locations (Fig. 22.6).

Comparative Analysis: Research Setting

In the past, clinical trials have historically utilized film-based angiographic studies for interpretation by a centralized reading center. With few exceptions, this has resulted in eligibility determination and stratification of patients after they have already been enrolled and entered in the trial. In some cases, patients received study therapy including medications before they were found to be angiographically ineligible for participation in a trial. In part, this is due to the fact that angiographic images were transmitted via conventional mail delivery systems, which slowed up the evaluation process. In addition, film-based angiography necessitates manual image evaluation and comparison. This process, which has been performed with an exceptionally high level of quality and reproducibility in the past, is a tedious and time-consuming process. It is also restricted by the need for all readers to be present in a single physical location where the film studies are available for evaluation and comparison.

With the advent of digital imaging, an opportunity arose to apply this new technology in the setting of a clinical trial. Our facility, the first of its kind, is the Digital Angiography Reading Center (DARC). There are now several others in the United States and abroad. The real-time image quality assessment provided with digital angiography enables photographers to obtain precise images necessary for study protocol examination. A treating physician is able to evaluate these images immediately in order to determine patient eligibility, and to provide patient education directly on a video monitor. Additional advantages include the ability to archive and store angiographic studies digitally, thus making them available for future evaluation by both the study centers and reading centers involved in a clinical trial.

Computer-assisted programs also provide for more rapid and potentially more accurate comparisons between imaging studies performed over time. When compared with the film-based technique of attempting to fit lesions into predetermined circles, the ability to trace the irregular borders of fundus lesions enables not only more precise measurements but also a far greater ability to discern variations in size over time (L.A. Campeas, Association for Research and Vision in Ophthalmology [ARVO] meeting, 1998, abstract). These changes can easily and accurately be determined by computer overlay techniques.

The use of high-speed data transfer and communication technology enables reading centers using digital imaging to receive images from study sites around the world on the same day. This permits prescreening or pre-entry determination of patients prior to enrollment in a clinical trial. This process of screening patients prior to randomization has ensured 100% angiographic eligibility in clinical trials, which reduces the number of patients needed to be enrolled. The result is a trial that can be completed in a shorter period of time and at less cost.

A final practical advantage of a digital reading center in the context of a clinical trial is its ability to have readers at

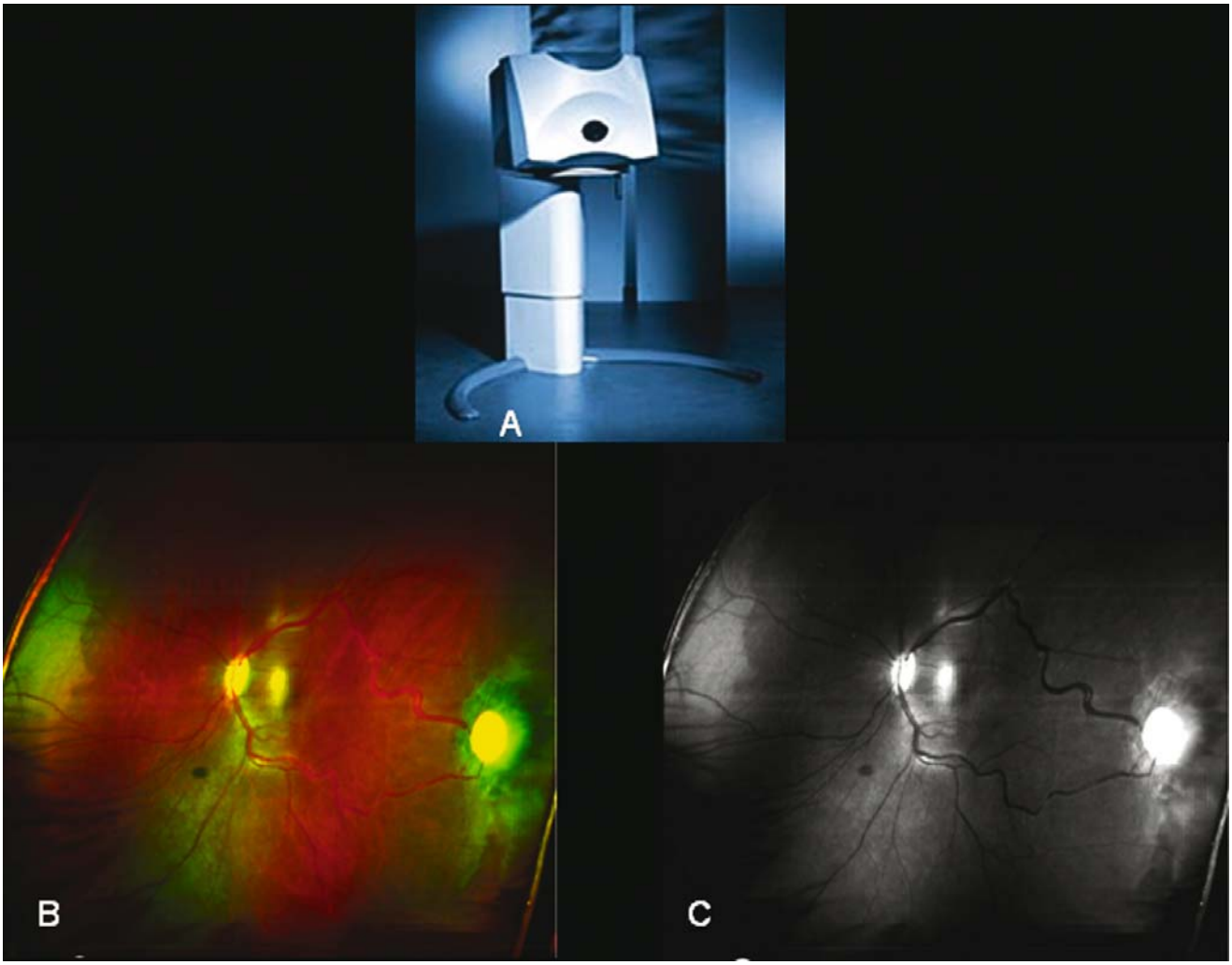

FIG. 22.4. The Panoramic 200 Optomap by Optos.

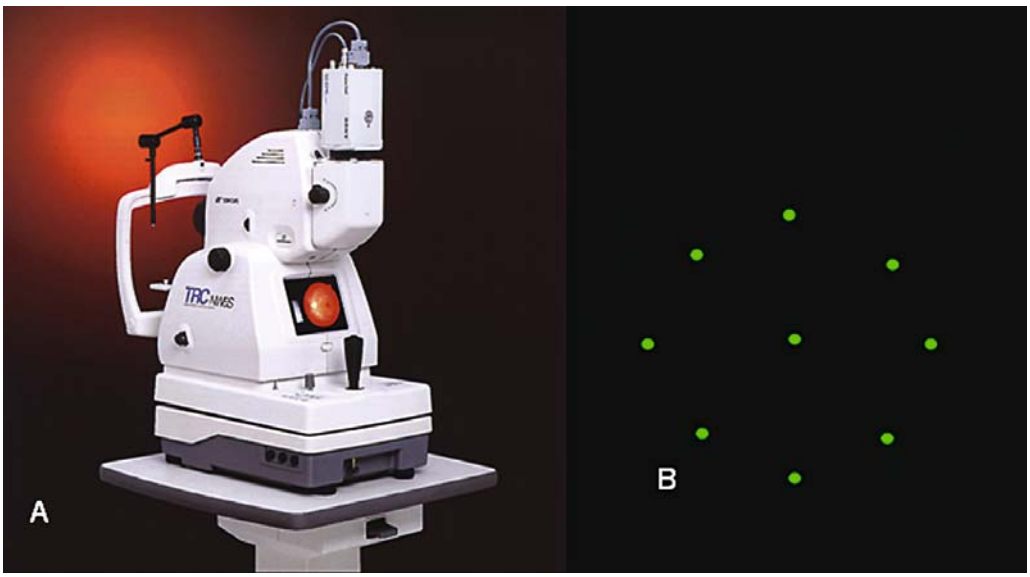

FIG. 22.5. (A) Topcon TRC-NW6S camera by Topcon America Corp. (B) The single central and eight peripheral fixation targets shown to patients allowing automated fundus mapping. (C) Individual photos of external as well as central and peripheral retina. (D) Photomontage assembled from images in C.

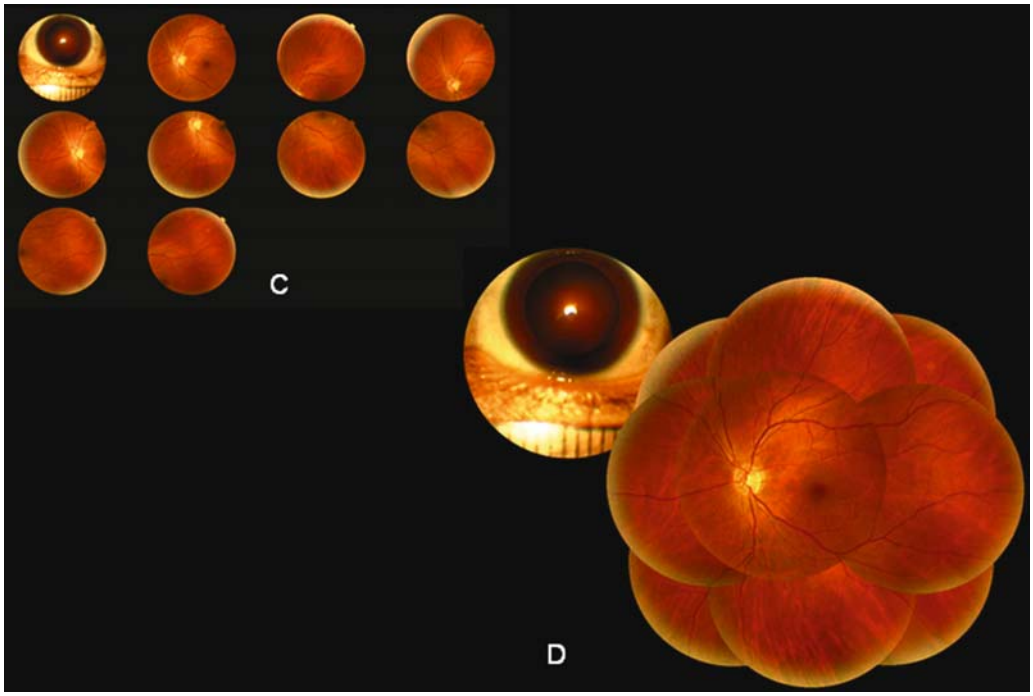

FIG. 22.5. (continued).

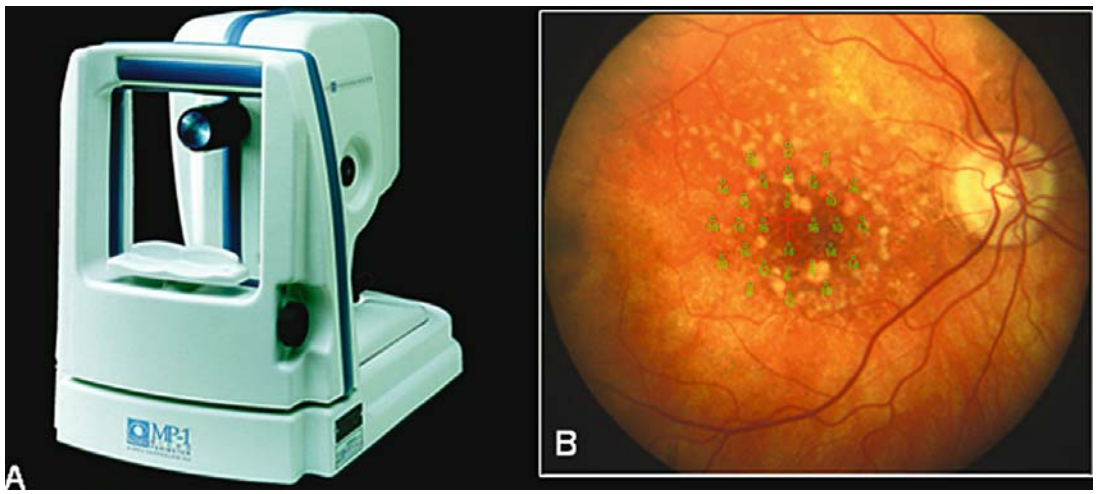

FIG. 22.6. (A) MP1 Microperimeter by NIDEK Technologies, Inc. (B) Sample image from MP1 Microperimeter showing localized visual response results overlying the fundus image.

multiple locations. With conventional film-based angiography, readers evaluating images must be physically present in the same location. With digital technology, readers evaluating these images can be located anywhere around the world as long as they have access to a computer, an Internet connection line, and the software program required for the evaluation of the digital angiographic studies. Our digital angiography reading center uses readers in five states in the U.S. and in four countries in Europe and South America.

In addition to research coordination, digital imaging and the Internet allow the long-distance screening of patients in underserved areas. The Digiscope (EyeTel Imaging Corp., Centreville, VA) is an automated fundus camera designed to be operated by the office staff of primary care physicians rather than by

specialized ophthalmic photographers. It enables high-resolution, wide-angle images to be recorded and sent via the Internet to trained screening physicians at a third location who then decide if the patient needs referral to an ophthalmologist (Fig. 22.7). This type of technology may become a major tool in the early treatment of widespread diseases such as diabetic retinopathy.

There are some practical issues to consider with the use of digital angiography. These include higher equipment costs related to the initial start-up and purchase of the camera and image acquisition system as well as system maintenance and upgrade requirements. A dependence on telecommunication and software technology also exists, a factor that can be problematic in some clinical settings, depending on the location of the physician. Finally, there is an adjustment period for both the physician and the photographer as they each adapt to a new method of image acquisition and evaluation. Otherwise, the advances in digital imaging systems and telecommunication technology have made digital angiography the new standard in the ophthalmic community. Whereas just 10 years ago, retinal practices with digital angiography systems were in the minority, the vast majority of retinal specialists, particularly those who have recently completed their training, now use these digital systems. Film-based teaching slides are now being scanned for digital presentation at local institutions, for regional and national meetings, and for scientific presentations, including textbooks that now routinely include a CD-ROM for viewing clinical illustrations. It is likely that film imaging will vanish from the profession within the next decade.

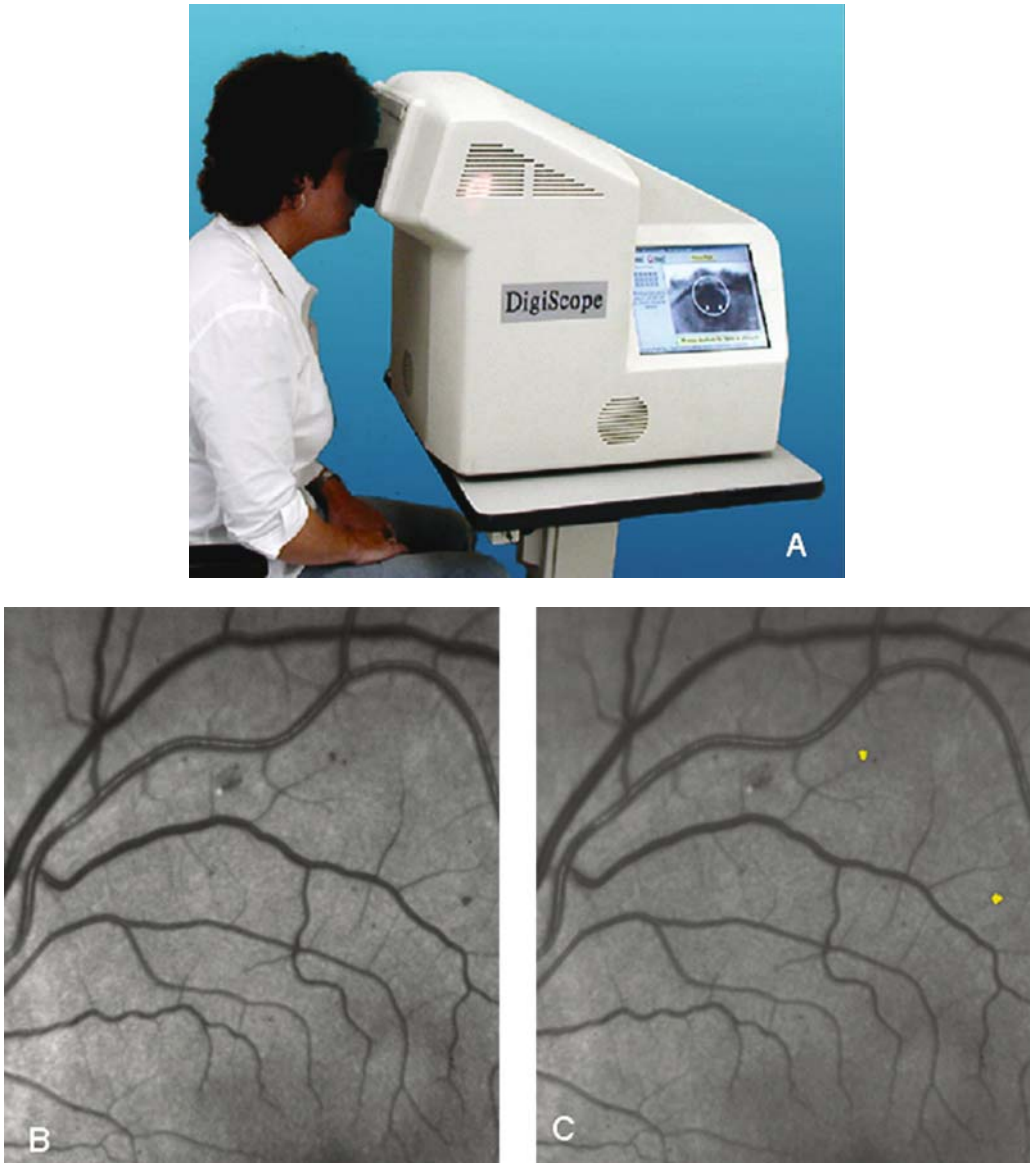

FIG. 22.7. (A) Digiscope by EyeTel Imaging Corporation. (B) Fundus image taken with the Digiscope. (C) Fundus image with highlighted microaneurysms.

Fundus Autofluorescence

Autofluorescent imaging of the ocular fundus relies on the stimulated emission of light from molecules, chiefly lipofuscin, in the retinal pigment epithelium (RPE).[10] Lipofuscin is a diverse group of molecular species, yellow to brown in color, that accumulates in all postmitotic cells, especially in the RPE. Lipofuscin is a complex mixture that results from the oxidative breakdown and rearrangement of a number of different molecules including polyunsaturated fatty acids, retinoids, and proteins. Components of lipofuscin inhibit lysosomal protein degradation, are photoreactive, and are capable of producing a variety of reactive oxygen species and other radicals, and lipofuscin may induce apoptosis of the RPE.[11] The intensity of fundus autofluorescence parallels the amount and distribution of lipofuscin. The amount of autofluorescence, then, is a sign of previous and possible future, oxidative injury.[12]

A fundus camera–based system for autofluorescence photographs was developed, and the wavelengths for the excitation (580 nm) and barrier (695 nm) filters were based on known transmission and autofluorescent characteristics of the ocular media. Fellow eyes of patients with AMD and typical choroidal neovascularization (CNV) had larger amounts of autofluorescence than the eyes of patients without a history of exudative AMD. Patients with retinal vascular anastomosis to the vascular proliferation of exudative AMD (those with retinal angiomatous proliferation or retinal choroidal anastomosis), a less typical form of exudative AMD, were much more likely to have focal areas of intense autofluorescence in their fellow eye that corresponded, for the most part, with focal areas of hyperpigmentation best seen by infrared monochromatic fundus photography (Fig. 22.8). The histopathologic correlate to focal hyperpigmentation is detached cells with pigment in the subretinal and outer retinal space. In rabbits, injection

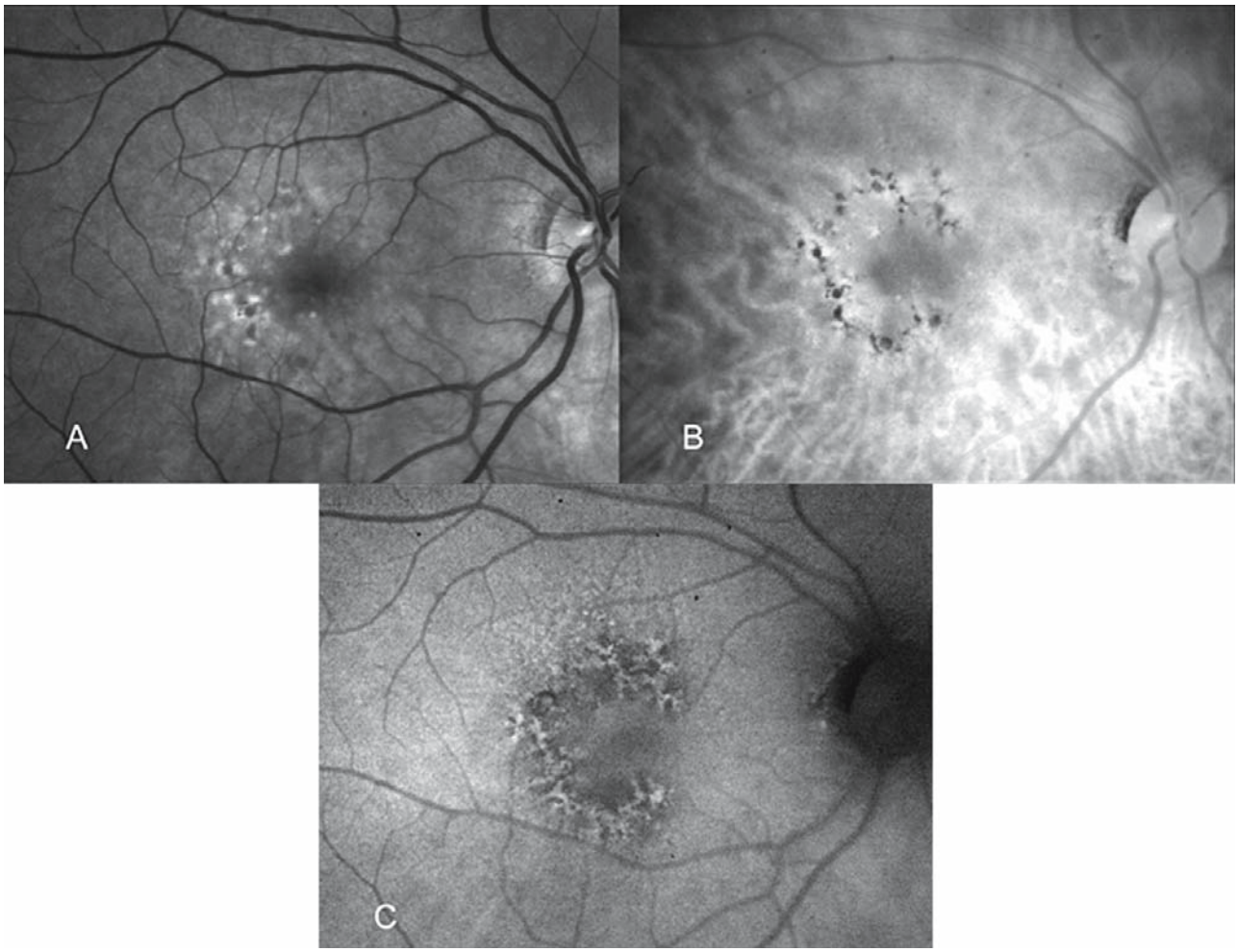

Fig. 22.8. (A) The red-free photograph demonstrates drusen, and the suggestion of focal hyperpigmentation in the perifoveal macula of this patient with frank retinal-choroidal anastomosis in the fellow eye. (B) When imaged with near infra-red light the focal hyperpigmentation is evident. At these wavelengths melanin is relatively transparent. (C) Autofluorescence photography demonstrates that this pigment is highly autofluorescent, suggesting the pigment seen is composed of lipofuscin.

of lipid peroxide in the subretinal space caused migration of RPE cells and macrophages into the subretinal space and outer retina, and these RPE cells had phagocytosed droplets of lipid peroxide.[13] These findings suggest RPE cells may detach and migrate into the subretinal space or outer retina when exposed to oxidative stress. Because the amount of fluorescence is directly related to the amount of lipofuscin, which in turn is related to the cumulative amount of oxidative damage, these findings suggest possible explanations for certain patterns of vessel growth seen in exudative AMD. Oxidative stress and damage have been linked to secretion of vascular endothelial growth factor (VEGF) and a number of other vasogenic cytokines. Fellow eyes of patients with exudative AMD have higher levels of lipofuscin, a sign of increased oxidative damage, and this suggests there is consequentially more VEGF produced. Increased production of VEGF by the RPE has been linked to the development of CNV. Focal areas of RPE cell accumulation containing lipofuscin in the subretinal and outer retinal space would lead to VEGF production in that location, with the recruitment of the overlying retinal vessels stimulated to proliferate along the VEGF gradient within the thickness of the retina.[10]

Ultrasonography of the Posterior Segment

For over 50 years diagnostic ocular ultrasonography has been a critical adjunct to the evaluation of eyes with opaque media, intraocular tumors, and orbital disease. Developed by a host of pioneer physicians and gifted engineers, ocular ultrasonography progressed from a novel curiosity to a reliable diagnostic modality within a 20-year period.[14–16] By 1970, contact scanners were introduced and became widely accepted throughout the ophthalmic community. Over time, improved sensitivity and image quality permitted expanded use of diagnostic ultrasonography to include clear media evaluation for imaging the status of the posterior hyaloid, critical to the understanding and treatment of vitreoretinal interface disease.[17] Over the last 13 years, digital format technology revolutionized ultrasonography yet again, with major changes in examination technique, information storage, recall, and transmission of original data. New software programs improved image quality still further. In contrast to bulky, traditional ultrasound devices, current multifunctional units weigh less than 2 pounds, are cigar-box in size, easily portable, and compatible with standard desktop or laptop computers. The digital format and constant advances in computer speed permit sufficient information capture and processing to create static, virtual three-dimensional reconstructions of wide areas of the posterior globe in short periods of time (2 to 4 seconds) along with two-dimensional, real-time movies (up to 1-minute segments) of two-dimensional B and A scans (Fig. 22.9).[18] By repeating the scan process in a standardized format, entire examinations of the posterior globe can be captured and stored. In addition, interchangeable parts allow the same unit to record ultrasound images from the anterior segment. For the first time, contact ultrasound examination can be saved and reviewed from original data. All of these innovations have made current contact devices truly multifunctional.

In the clinical setting each examination can be managed according to its complexity. In eyes free of pathology the ultrasonographic examination might include only a traditional B-scan and A-scan technique with representative images and a summary report. For more complicated eyes, the traditional technique could be expanded to include more involved static, three-dimensional images and two-dimension movie segments with simultaneous voice-over. These supplements to traditional contact ultrasound devices have transformed the examination and reporting technique from one requiring a highly skilled, experienced operator who would produce a written report from selected images without the possibility of alternate analysis, to an examination that is relatively easy to perform, capture, store, and transmit in its entirety, including a voice-over audio narrative, to colleagues around the world for review. Interpretation and reports are generated with appropriate images from saved and stored original information. Optical disc storage and direct Internet transmission make reviews and reports simple. Furthermore, interactive viewing software is available for any computer operating system, allowing direct access to original ultrasonic data and permitting review of examinations with any available computer operating system.

These advanced imaging techniques have also altered the methods for teaching ultrasonography. Traditionally, instructional courses in ultrasonography relied heavily on sample images taken from slide libraries. Current programs utilize entire examinations from a wide variety of pathologic clinical cases relying on interactive capabilities to teach and test ultrasonographic knowledge and proficiency. This technology can document and establish detailed depictions of various pathologies including vitreoretinal traction, schisis, detachments, myopia, staphyloma, and various combinations of these abnormalities. Such evaluations enable morphologic, topographic, and volumetric qualification of normal and pathologic conditions.

Future developments already in the pipeline include faster acquisition capability with higher frequency transducers coupled to signal enhancing software that will increase resolution without increasing potential tissue damage from higher gain. Ultimately, real-time three-dimensional reconstruction will be possible. Anterior segment ultrahigh-resolution ultrasonography (50 megacycle plus transducers) has been available since the late 1980s. Commercially available units have proved useful, but they are not portable. Recent adaptation of posterior segment ultrasonography described in this chapter has been applied to anterior imaging. For the posterior segment surgeon, examination of this region is critical to the evaluation of hypotony, trauma, and anterior segment disease. A small, reusable water bath device permits anterior segment imaging from the cornea to the region of the rectus muscle insertions, utilizing a 35-megacycle transducer, separate software, and the portable ultrasound unit.

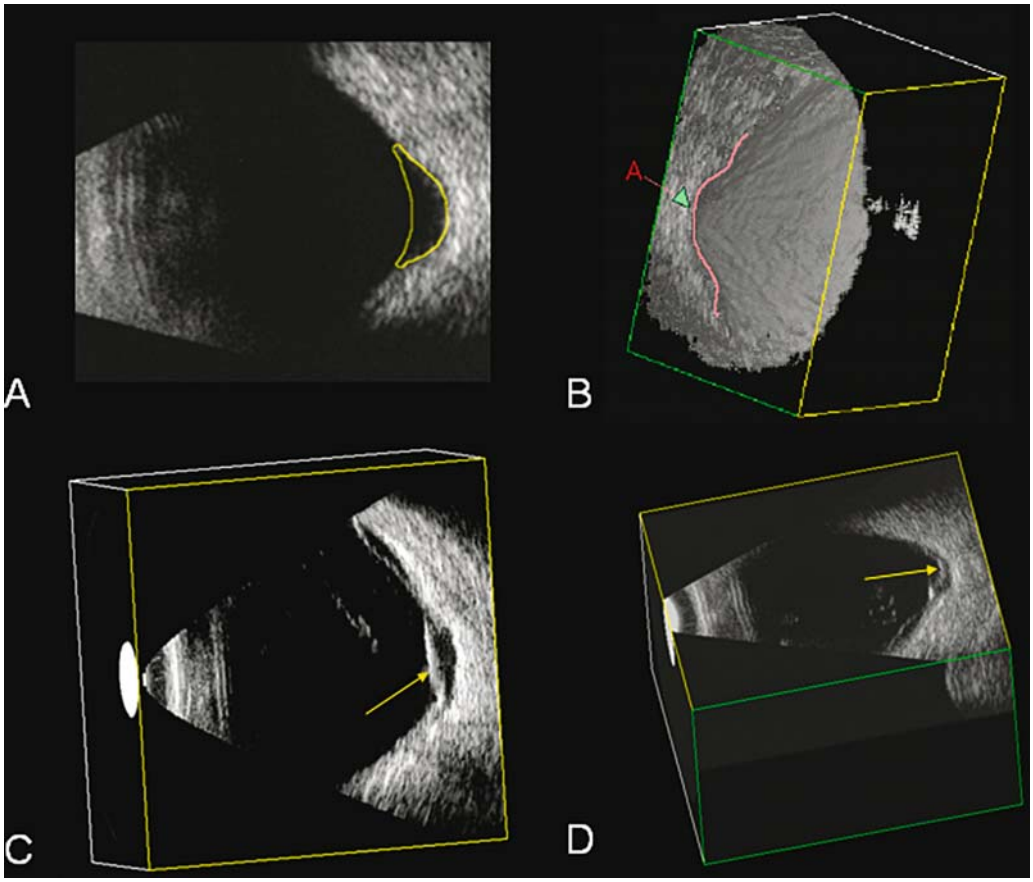

FIG. 22.9. (A) B-scan image of a myopic staphyloma showing how the cross-sectional area can be calculated. (B) Three-diopter ultrasonographic image of the same myopic staphyloma where manipulation of the image as well as area measurements are possible. (C,D) Three-ultrasonographic images of pathologic myopic eyes demonstrating retinal detachment (yellow arrow) overlying a staphyloma, as well as vitreous detachment (red arrow) elsewhere.

Diagnostic ultrasonography continues to be a major adjunct to ocular evaluation. Technologic changes have made this technique easy to use, portable, and reliable.

High-Speed Angiography

During the past several years, interest in high-speed ocular angiography has increased markedly, most likely as a result of the higher level of attention being focused on new treatments for AMD and associated CNV. In particular, high-speed ICG angiography has been employed as a diagnostic aid for locating the so-called feeder vessels that carry blood to CNV membranes with the aim of facilitating focal laser photocoagulation. This allows treatment at a distance from the lesion, thereby minimizing additional damage to already compromised retinal tissue. As a by-product of the requisite pre- and posttreatment high-speed angiograms made during most CNV feeder vessel treatments, data related to choroidal vascular hemodynamics are being collected. Although more sophisticated analytic techniques are needed for interpreting high-speed ICG angiogram image sequences than with fluorescein angiograms, high-speed angiography clearly is expanding our understanding of the relationship between ocular blood flow and chorioretinal disease. It is expected that data from such images are and will continue to be a vital adjunct to examination of the choroidal circulation, rather than relying solely on fluorescein angiography.

High-speed angiography generally entails an acquisition rate of less than 1 image per second (IPS), traditionally associated with fluorescein angiography. That 1-IPS rate was a consequence of the maximum rate at which the xenon flash lamp light sources in most early fundus cameras could be fired, and for decades it has remained the accepted rate for producing image sequences capturing all the so-called retinal vascular filling phases. Although the technology for performing high-speed fluorescein angiography is commercially available today, the majority of high-speed angiograms performed are ICG angiograms of the choroid, and that probably will continue to be the case. The high resistance to flow of the end-arteriolar

retinal vasculature causes blood flow to be slow enough that acquisition at a rate of 1 IPS is adequate for recording retinal vascular dye transit. In contrast, the choroidal vasculature has the highest per-unit-tissue-weight blood flow found anywhere in the body, roughly 20 to 30 times greater than that of the retinal circulation.[19] It therefore stands to reason that choroidal angiogram image acquisition rates should be significantly greater than those employed in retinal angiography.

It has long been recognized that the near-infrared wavelength absorption and fluorescence spectra of the ICG dye facilitate better documentation of the choroidal circulation than the visible wavelength spectra of fluorescein dye. Moreover, since a significantly greater portion of injected ICG dye molecules remain in circulating blood than with fluorescein dye, sequential images of ICG dye transmission correlate better with blood movement through the ocular vasculature. Fluorescein images, on the other hand, tend to be more useful in demonstrating fluid leakage from blood vessels. Therefore, high-speed angiography will likely remain primarily within the province of ICG angiography.

Today, there are two basic optical systems for acquisition of ocular angiogram images: the fundus camera and the scanning laser ophthalmoscope (SLO). Of these, only the SLO currently is commercially available in a configuration that permits ICG angiography image acquisition at rates up to 16 IPS. Fundus camera optical systems have been used to acquire ICG angiogram images at 30 IPS (images have a spatial resolution of 9 μm/pixel for a 30-degree field of view, about twice the SLO resolution), but these devices are not yet commercially available. There are fundamental differences between the methods of image acquisition for the two optical systems, which results in images with inherently different characteristics. The SLOs create images one pixel at a time by scanning a small spot of 810-nm wavelength laser light over the fundus in a raster pattern. Fundus cameras, by comparison, create all the pixels of an image at the same instant by projecting the entire fundus image onto the entire pixel array of a charge-coupled device (CCD) camera. Acquisition time for individual SLO images, therefore, is determined by the raster scan time (current minimum is about 32 msec), whereas for fundus images it is determined by the duration of fundus illuminations (current minimum is 1 msec). By virtue of the very small fundus area illuminated at any instant during image acquisition by the SLO, intraocular light scatter is less, and hence contrast is greater than in fundus camera images.[20] In general, high-speed angiogram images acquired with fundus camera optics are of higher temporal and spatial resolution than SLO images, while the SLO images are of higher contrast (Fig. 22.10).

The main clinical application of high-speed angiography to date has been in identification of CNV feeder vessels (Fig. 22.11), which relies on the ability to determine the direction of blood flow in order to discriminate between afferent and efferent vessels. Also, real-time ICG videoangiography is being used to facilitate precision aiming of laser photocoagulation once the feeder vessels have been identified. High-speed angiograms inherently contain hemodynamics data, and

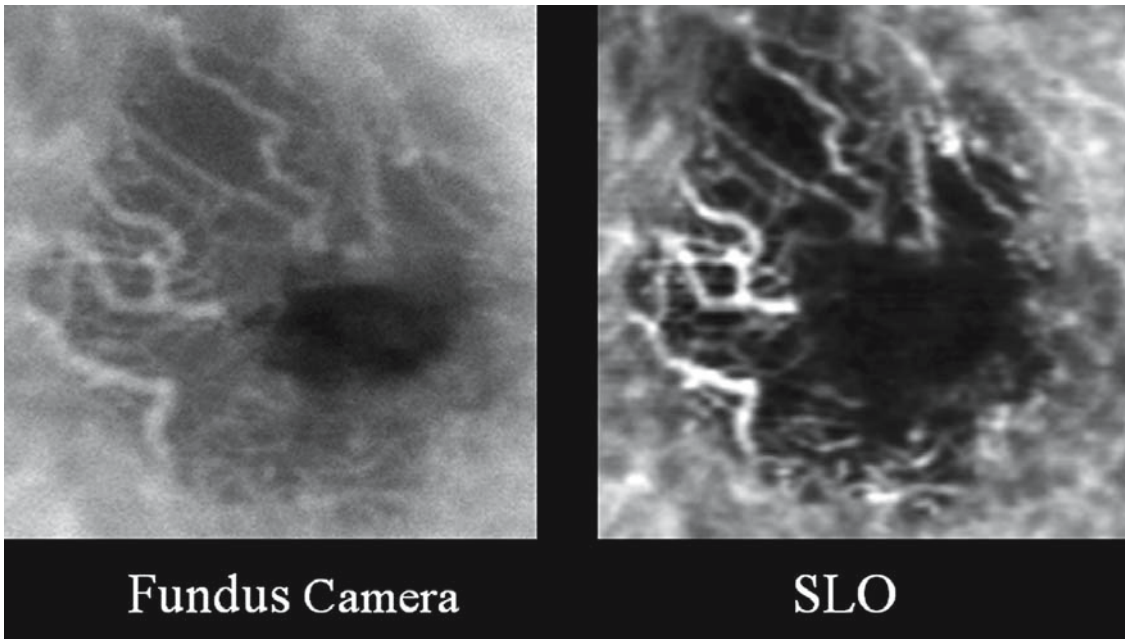

FIG. 22.10. These two images are from indocyanine green (ICG) angiogram sequences of the same eye acquired within minutes of each other, using a 30-IPS fundus camera and a 12-IPS scanning laser ophthalmoscope (SLO). Both images were magnified identically to the extent that image pixilation became apparent in the lower resolution SLO image.

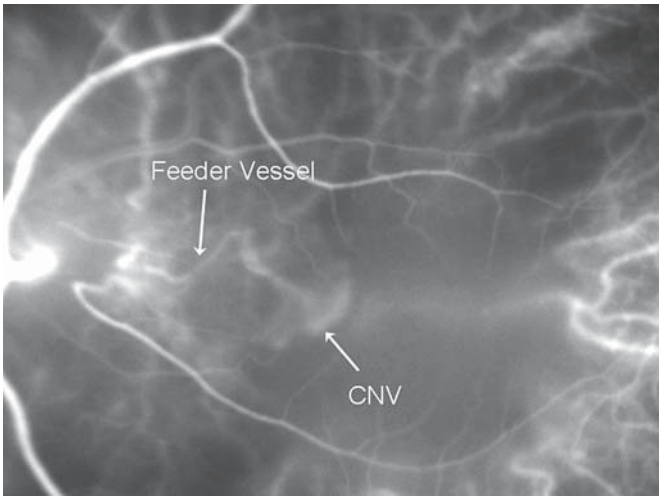

FIG. 22.11. An ICG angiogram demonstrates a feeder vessel supplying a classic choroidal neovascularization (CNV) membrane.

routine examination of these data may prove to be the most important future clinical application of high-speed angiography. Various computer-based algorithms have been developed for extraction of hemodynamic information from sequences of ICG choroidal angiogram images, including sequential image subtraction, which has been demonstrated to enhance visualization of dye wavefront transit through the vasculature. Sequential image subtraction has been used to enhance visualization of blood flow through CNV feeder vessels,[21] and it has been used to enhance visualization of choriocapillaris blood flow.[22] Sequential subtraction is based on the fact that pixel-by-pixel subtraction of two images acquired in close temporal proximity produces a resultant image in which the brightness of each pixel is proportional to the magnitude of brightness change between the corresponding pixels in the subtracted images. That is, a dim or black pixel in a resultant image indicates an area in which little or no change in brightness (i.e., little or no change in the amount of ICG dye present) occurred between acquisition of the two subtracted images, whereas a bright pixel indicates a proportionally large change (Fig. 22.12).

Note that the resultant subtracted images display progression of the dye wavefront through the choroidal arteriolar vessels and into the choriocapillaris. In addition to the formation of the lobular filling pattern, this demonstrates that the lobular filling pattern of the choriocapillaris is a functional one, resulting from a complex network of local perfusion pressure gradients, rather than a consequence of choriocapillaris angioarchitecture itself.[23] It also confirms that choriocapillaris blood flow is pulsatile at a very rapid frequency, suggesting that subtle changes in choriocapillaris perfusion, visible only at sub–cardiac-cycle temporal resolution, may significantly affect its ability to meet the metabolic requirements of the overlying sensory retina. The capacity to observe choriocapillaris perfusion at appropriately high spatial and temporal resolutions may be of particular value in understanding the pathogenesis of ischemic chorioretinal abnormalities such as AMD or other abnormalities such as anterior ischemic optic neuropathy, diabetes, radiation toxicity, and even glaucoma. Since devices for performing high-speed angiography are now readily available, it is likely that high-speed choroidal angiography will increasingly prove to be a vital diagnostic aid for retinal specialists.

Optical Coherence Tomography Ophthalmoscopy

In the early 1980s retinal imaging moved beyond classical optics with the introduction of the SLO by Webb and colleagues.[24] This technology produced high-resolution nonmydriatic images of the retinal surface from reflected linear streams of sequentially illuminated points. It was also capable of projecting complex stimuli onto a live fundus image, permitting psychophysical studies such as micro-perimetry and potential acuity. Optical aberrations of the eye, however, constrain its resolving power to almost 300 μm, which is considerably thicker than the tissue under study, limiting its usefulness for revealing details below the retinal surface.

Optical coherence tomography appeared in the early 1990s through the efforts of Fujimoto and Puliafito as a technique for acquiring optical B-scan images of the macula and optic nerve with near-histologic detail.[25] Based on the principle of partial coherence interferometry, the resolving power of OCT for details was limited only by the illuminating source employed and approached 10 to 15 μm. Advances in this technology promise resolution promise axial resolution of approximately 3 μm for the ultrahigh-resolution OCT currently in development and testing.[26] This tool in effect provided a microscope available in a clinical setting that was capable of revealing certain histopathologic aspects of macular disease in the living eye. The limitation of this technology has been the difficulty in obtaining

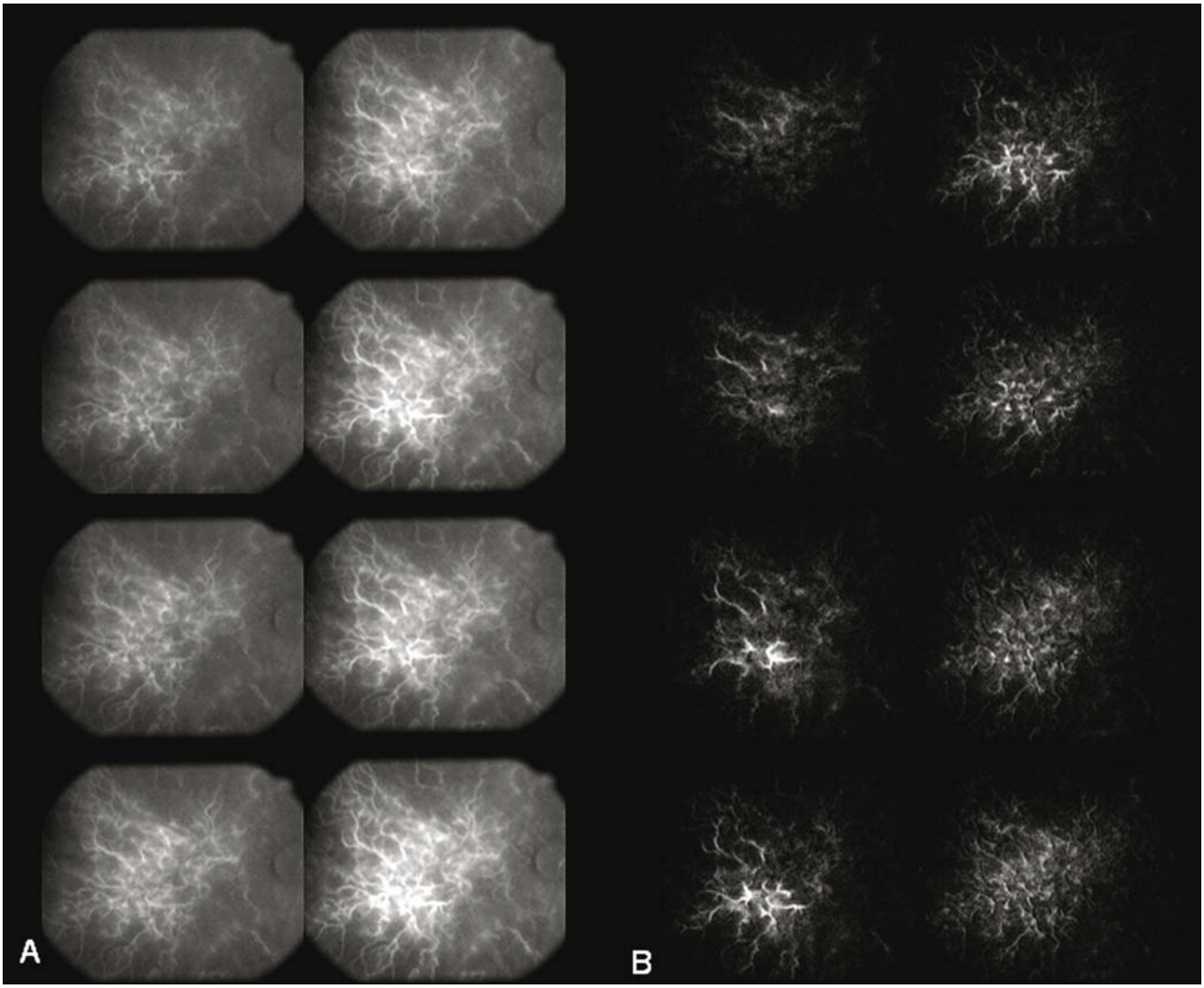

FIG. 22.12. Sequential subtraction of ICG angiogram images from the eye of a normal young male eye, acquired at 30 IPS using fundus camera optics. The left two columns of images (read from top to bottom) are the original angiogram images. The right two columns are the resultant subtracted images; the first image resulted from subtracting the first original image from the second, the second image resulted from subtracting the second image from the third, and so on.

accurate localization of the cross-sectional slices and correlating them with our conventional *en face* view of the fundus.

A novel integration of SLO and OCT technologies, the OCT ophthalmoscope, was developed by Podoleanu and colleagues[27] in the late 1990s. Employing the transverse scanning strategy of the SLO (C-scan) and the interferometric signal processing of the OCT, this device produces simultaneous, paired images that document retinal surface detail and progressively deeper slides of subsurface anatomy. Utilizing a single illumination source provides point-to-point correspondence between pairs of C-scan images, permitting accurate overlays and B-scans originating from precisely designated locations on the SLO image.[28]

C-scan imaging, while new in its application to OCT, is quite familiar as the perspective ophthalmologists appreciate in conventional ophthalmoscopy. As a scanning approach it offers the flexibility of a variable-angle viewing with consistent transverse resolution and the potential for acquisition of three-dimensional images from stacks of slices. It also holds the promise of accurate topographic mapping and volume determination. C-scan OCT images are challenging at first glance since they reveal details of inner retinal structure that until now has only been looked at in cross section or B-scan perspective. Saccadic movements and shifts in fixation are captured along with details of more than one retinal layer within a slice. Interpretation is often facilitated by correlation with matching SLO

images of the overlying retinal surface. A variably transparent overlay feature of the viewing software allows the observer to compare the simultaneous images in depth along with corresponding B-scan OCTs (Figs. 22.13 and 22.14).[29]

Prototype versions of the OCT ophthalmoscope (OTI, Toronto, Canada) are currently in beta-testing under institutional review board (IRB) approval in several clinical sites in North America, Europe, and Japan (Advanced Retinal Imaging Center of the New York Eye and Ear Infirmary, New York, NY; LuEsther T. Mertz Retinal Research Center of the Manhattan Eye, Ear, and Throat Hospital, New York, NY; Academic Medical Center, Amsterdam, the Netherlands; and Asahikawa Medical College, Asahikawa, Japan). The system is built around a superluminescent diode source, with a central wavelength of 850 nm and bandwidth of 20 nm producing a calculated axial resolution of 10 nm. Field of view can vary from 5 to 35 degrees, and scan rate can be adjusted between one and eight frames per second. The light travels through a modified Michelson interferometer to the patient's eye, and upon return is joined with its twin reference beam to form an OCT signal. Portions of the returning rays are diverted to a confocal detector to generate the corresponding SLO image. Independent x and y scanners generate planar C-scan or linear B-scan raster patterns according to software directions.

The multiplanar imaging capability of the OCT ophthalmoscope offers exciting new perspectives for the full range of macular abnormalities. Its scanning strategy of coronal planar acquisition enables precise and easy comparison of

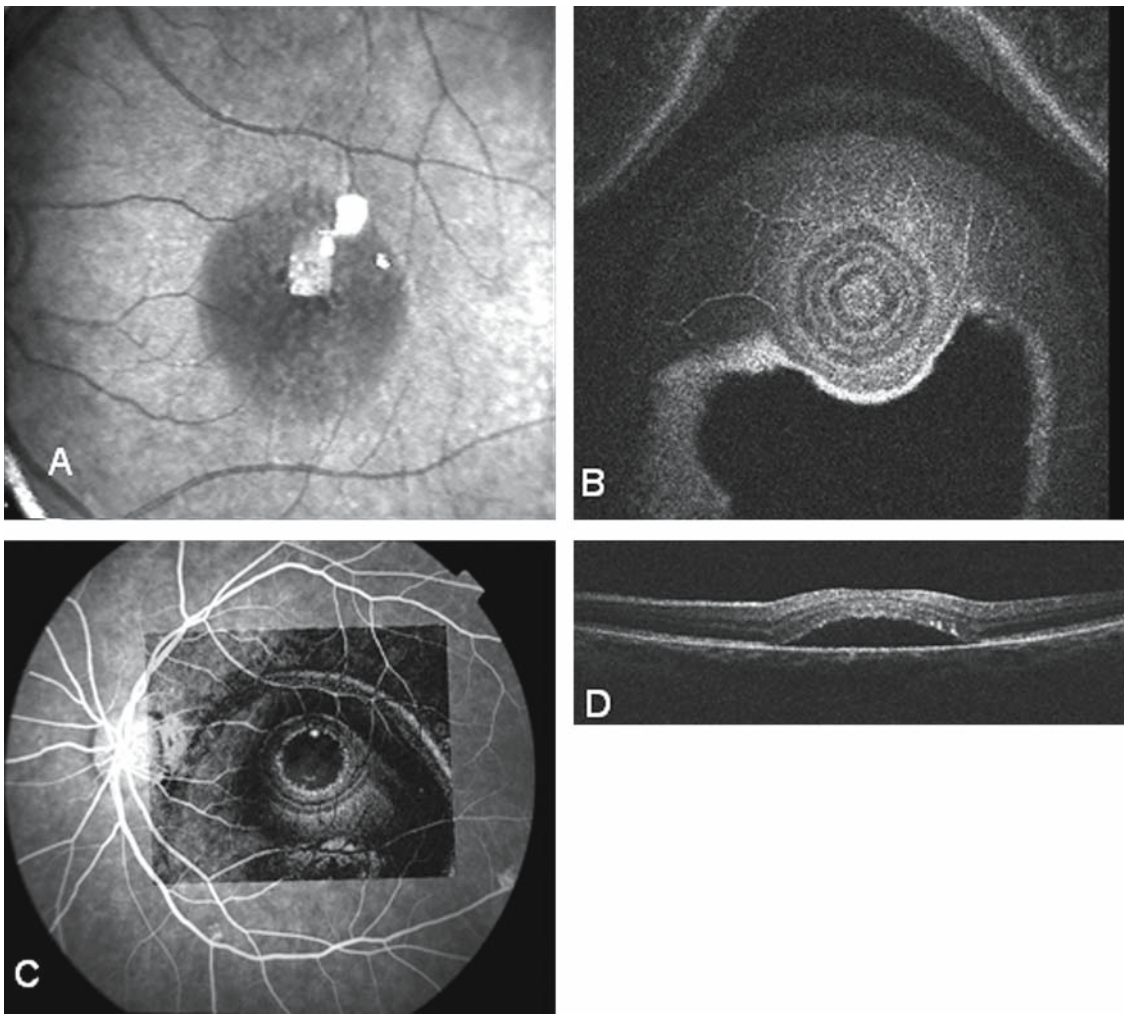

FIG. 22.13. Central serous chorioretinopathy. The confocal image shows normal vasculature with loss of normal foveal reflex. (A) The tilted white bow-tie–shaped reflex is a lens artifact. (B) The C-scan optical coherence tomography (OCT) reveals a bull's-eye pattern produced by the convex serous elevation of the fovea. The rings correspond to alternating light and dark internal retinal layers seen on the B-scan OCT below. (C) Confocal images can be precisely matched to the vessel pattern in fluorescein images enabling creation of an accurate montage, which reveals the relationship between vascular leakage and surface elevation. (D) The B-scan OCT is also given for comparison.

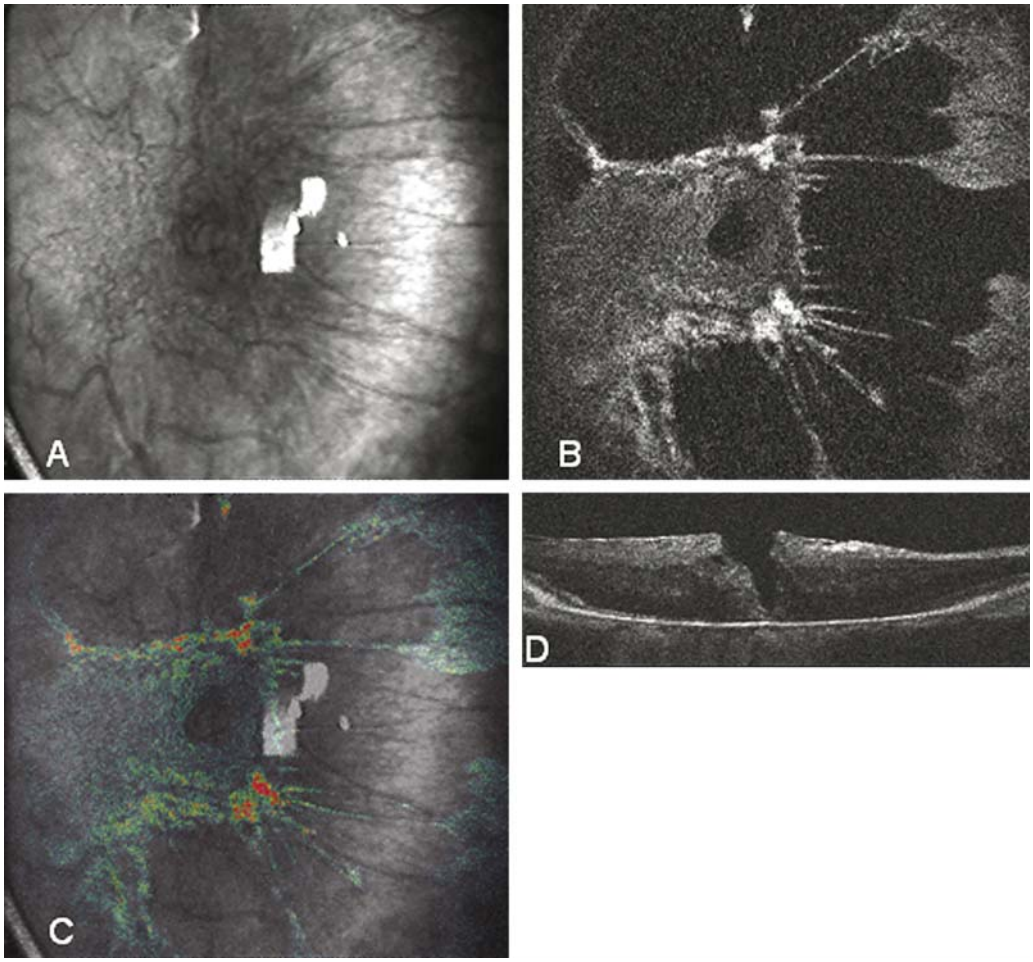

FIG. 22.14. Macula pucker. The confocal image (A) is shown with the corresponding C-scan OCT (B). The C-scan image shows a characteristic stellate pattern of epiretinal membrane proliferation, which is difficult to appreciate in the confocal fundus image despite the notable vascular pattern distortion. (C) The adjustable transparency feature of the software reveals the contours of the membrane in pseudocolor in relation to vessels, which may be valuable in planning a surgical approach. (D) The B-scan OCT slice emphasizes the constriction of the foveal cone and the tractional flattening of the inner retinal surface induced by the membrane, creating the illusion of a full-thickness macular hole on clinical examination.

surface and subsurface anatomy. In addition, it opens the door to fusion with other imaging technologies that employ a similar perspective such as fluorescein and ICG angiography and multifocal electroretinogram (ERG) and visual evoked response (VER). The unique technical design of the system also holds promise for accurate three-dimensional reconstruction and quantitative topographic mapping, which are still in development. With the continued advances in high-speed scanner technologies and high-resolution sources, the system in the future may provide a real-time diagnostic and therapeutic capability with feedback-controlled laser therapy for the spectrum of chorioretinal disease.

Optical coherence tomography development continues to advance in different directions. Improvements in laser technology along with adaptive optics to correct for higher order aberrations have led to an ultrahigh-resolution OCT with axial resolution of up to 3 μm. This allows identification of individual retinal layers nearly on a cellular basis.[30,31] Meanwhile, spectral OCT has reduced the acquisition time to 64 μs, allowing for up to 19,000 A-scans per second. At this level, it is possible to obtain real-time physiologic data such as functional information on retinal blood flow as well as three-dimensional images.[32]

The retinal thickness analyzer (RTA, Talia Technology, Mevaseret Zion, Israel) is a similar noncontact imaging technique that allows for quantification of retinal thickness. It produces a topographical map of the retina by analyzing reflected light from an obliquely directed beam (Fig. 22.15). A comparison study between the OCT and RTA showed qualitatively similar

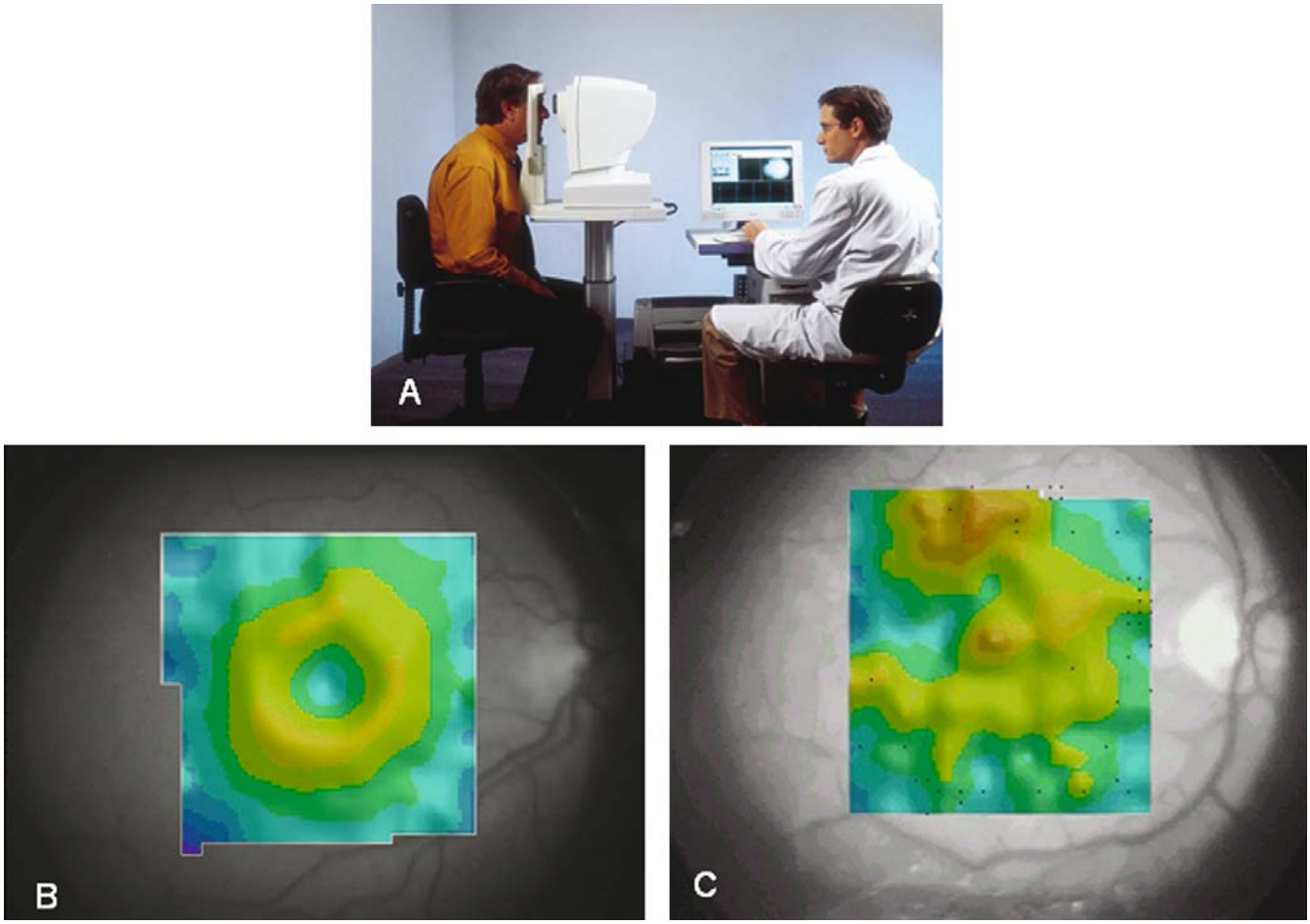

FIG. 22.15. (A) The retinal thickness analyzer by Talia Technology. (B,C) Examples of thickness maps of patients with macular edema.

information, with each device showing excellent reproducibility of retinal thickness and dimensions.[33]

Conclusion

Ophthalmic imaging technology has undergone explosive growth in the past decade. Current techniques for fundus imaging have contributed significantly to our understanding of the pathophysiology and treatment of posterior segment disorders, and this is just the beginning. Digital technology has now given us the capability to acquire, edit, archive, retrieve, compare, and transmit fundus images with several diagnostic systems for patient management, remote constellation, teaching, and collaborative research.

It is conceivable that future advances would in time be used to substitute for histopathologic analysis of intraocular fluids and tissue, and even determine the etiology of inflammatory and infectious diseases as well as the cellular nature of mass lesions. For sure, future generations of ophthalmologists will rely exclusively on digital fundus imaging and other digital diagnostic systems. They also will communicate among themselves digitally, collaborate within multicentered trials with digital reading centers, and make all of their teaching presentations with digital photographs. In fact, it is conceivable that imaging for retinal specialists could originate in the offices of comprehensive ophthalmologists institutional medical settings or even at neighborhood pharmacies and shopping malls.

Acknowledgments. This chapter was published, and is reprinted in part here with permission from Yannuzzi LA, Ober MD, Slakter JS, Spaide RF, Fisher YL, Flower RW, Rosen R. Ophthalmic fundus imaging: today and beyond. Am J Ophthalmol 2004;137:511–24.

References

1. Shikano S, Koichi S. Atlas of Fluorescence Fundus Angiography. Philadelphia: WB Saunders, 1968.
2. Wessing A, von Noorden GK. Fluorescein Angiography of the Retina: Textbook and Atlas. St. Louis: CV Mosby, 1969.
3. Rosen ES, Ashworth B, Järpe S. Fluorescence Photography of the Eye: A Manual of Dynamic Clinical Ocular Fundus Pathology. New York: Appleton-Century-Croft, 1969.

4. Schatz H, Burton TC, Yannuzzi LA, Raab ML. Interpretation of Fundus Fluorescein Angiography. St. Louis: CV Mosby, 1978.
5. Yanuzzi LA, Gitter KA, Schatz H, eds. The Macula: A Comprehensive Text and Atlas. Baltimore: Williams & Wilkins, 1979.
6. Gass JDM. Stereoscopic Atlas of Macular Diseases: Diagnosis and Treatment. St. Louis: CV Mosby, 1970.
7. Slakter JS. ARVO meeting 1998, abstract.
8. Yannuzzi LA, Slakter JS, Sorenson JA, et al. Digital indocyanine green angiography and choroidal neovascularization. Retina 1992;12:191–223.
9. Ober MD, Del Priore LV, Freund KB, et al. Comparison between automated software and manual construction of photo montage: a quality and time-efficiency analysis. The 22nd annual meeting of the American Society of Retinal Specialists, August 20, 2004, San Diego, CA.
10. Delori FC, Dorey CK, Staurenghi G, et al. In vivo fluorescence of the ocular fundus exhibits retinal pigment epithelium lipofuscin characteristics. Invest Ophthalmol Vis Sci 1995;36:718–729.
11. Gaillard ER, Atherton SJ, Eldred G, Dillon J. Photophysical studies on human retinal lipofuscin. Photochem Photobiol 1995;61:448–453.
12. Spaide RF. Fundus autofluorescence and age-related macular degeneration. Ophthalmology 2003;110:392–399.
13. Tamai K, Spaide RF, Ellis EA, et al. Lipid hydroperoxide stimulates subretinal choroidal neovascularization in the rabbit. Exp Eye Res 2002;74:301–308.
14. Coleman DJ. Reliability of ocular and orbital diagnosis with G-scan ultrasound. 1. Ocular diagnosis. Am J Ophthalmol 1972;73:501–516.
15. Coleman DJ. Reliability of ocular and orbital diagnosis with B-Scan ultrasound. 2. Orbital diagnosis. Am J Ophthalmol 1972;74:704–718.
16. Bronson NR, Fisher YL, Pickering NC, Trayner EM. Ophthalmic Contact B-Scan Ultrasonography for the Clinician. Westport, CT: Intercontinental Publications, 1976.
17. Pavlin CJ, Harasiewicz K, Sherar MD, Foster FS. Clinical use of ultrasound biomicroscopy. Ophthalmology 1991;98:287–295.
18. Shammas HJ, Dunne S, Fisher YL. Three-Dimensional Ultrasound Tomography of the Eye. Toronto: Nova Coast Publishing; 1999.
19. Alm A. Physiology of the choroidal circulation. In: Yannuzzi LA, Flower RW, Slakter JS, eds. ICG Angiography. New York: CV Mosby, 1987.
20. Flower RW, Csaky KG, Murphy RP. Disparity between fundus camera and scanning laser ophthalmoscope indocyanine green imaging of retinal pigment epithelium detachments. Retina 1998;18:260.
21. Shiraga F, Ojima Y, Matsuo T, et al. Feeder vessel photocoagulation of subfoveal choroidal neovascularization secondary to age-related macular degeneration. Ophthalmology 1998;105:662.
22. Flower RW. Extraction of choriocapillaris hemodynamic data from ICG fluorescence angiograms. Invest Ophthalmol Vis Sci 1993;34:2720.
23. Flower RW, Fryczhowski AW, McLeod DS. Variability in choriocapillaris blood flow distribution. Invest Ophthalmol Vis Sci 1995;36:1247.
24. Webb RH, Hughes GW, Delori FC. Confocal scanning laser ophthalmoscope. Appl Opt 1987;26:1492–1499.
25. Huang D, Swanson EA, Lin CP, et al. Optical coherence tomography. Science 1991; 254:1178–1181.
26. Drexler W, Sattmann H, Hermann B, et al. Enhanced visualization of macular pathology with the use of ultrahigh-resolution optical coherence tomography. Arch Ophthalmol 2003;121:695–706.
27. Podoleanu AG, Seeger M, Dobre GM, et al. Transversal and longitudinal images from the retina of the living eye using low coherence reflectometry. J Biomed Opt 1998;3:12–20.
28. Rosen RB, Podoleanu AG, Dunne S, Garcia P. Optical coherence tomography ophthalmoscopy. In: Ciulla TA, Regillo CD, Harris A, eds. Retina and Optic Nerve Imaging. Philadelphia: Lippincott Williams & Wilkins, 2003.
29. Podoleanu AG, Dobre GM, Cucu RG, et al. Combined multiplanar optical coherence tomography and confocal scanning ophthalmoscopy. J Biomed Opt 2004;9(1):86–93.
30. Drexler W. Ultrahigh-resolution optical coherence tomography [review]. J Biomed Opt 2004;9(1):47–74.
31. Drexler W, Sattmann H, Hermann B, et al. Enhanced visualization of macular pathology with the use of ultrahigh-resolution optical coherence tomography. Arch Ophthalmol 2003;121(5):695–706.
32. Wojtkowski M, Bajraszewski T, Gorczynska I, et al. Ophthalmic imaging by spectral optical coherence tomography. Am J Ophthalmol 2004;138(3):412–419.
33. Polito A, Shah SM, Haller JA, et al. Comparison between retinal thickness analyzer and optical coherence tomography for assessment of foveal thickness in eyes with macular disease. Am J Ophthalmol 2002;134:240–251.

23
Ultra-Widefield Fluorescein Angiography

Scott C.N. Oliver and Steven D. Schwartz

For the last 50 years, fluorescein angiography (FA) has played a pivotal role in the evaluation and management of retinal diseases. Patterns of hyper- and hypofluorescence provide insights into the pathophysiologic processes involved in vascular, degenerative, dystrophic, traumatic, infectious, inflammatory, and neoplastic diseases of the choroid and retina. Despite recent advances in other imaging techniques, including indocyanine green (ICG) angiography and optical coherence tomography (OCT), FA still plays a primary role in the diagnosis of common retinal diseases, including diabetic retinopathy, macular degeneration, retinal vascular occlusion, and posterior uveitis. Fluorescein angiography remains a vital method to assess success of treatment methods including laser photocoagulation, intraocular pharmacologic therapy such as steroid and antivascular endothelial growth factor (anti-VEGF) agents, and surgical membrane peeling.

The ability to capture a single image of the entire ocular fundus has been limited until recently. Standard FA using film or digital cameras captures an image 30 degrees across. This chapter discusses a new fluorescein imaging technique that captures fundus images up to 200 degrees in breadth. Optomap *fa* dynamic ultra-widefield angiography is a digital panoramic technique performed with the Optos P200MA scanning laser ophthalmoscope (SLO) (Optos plc, Dunfermline, UK). The ability to image the peripheral retina using Optomap *fa* provides a more comprehensive assessment of the extent of a retinal disease process, and may detect abnormalities that alter a treatment plan based initially on clinical examination and traditional angiography. This chapter presents selected examples of images obtained with the first commercially available unit.

History

The desire of the retinal specialist to capture widefield images of the fundus is long-standing. Some macular disease processes including age-related macular degeneration, selected macular dystrophies, and cystoid edema may be fully evaluated using high magnification, narrow-field techniques. However, evaluation of many retinal diseases depends partly, if not entirely, on imaging the peripheral fundus.

Traditional FA technique involves obtaining multiple 30-degree photographic images. A protocol consisting of seven standard 30-degree images was developed for the Diabetic Retinopathy Study.[1] The width of this composite set of images is approximately 75 degrees. Photographs anterior to the equator may be obtained, but such photography is limited by patient alignment problems, focus irregularities, marginal corneal astigmatism, poor fixation, and light reflex artifacts. Newer noncontact camera systems may capture images up to 50 degrees across; however, peripheral images still must be mentally "stitched" together by the practitioner to formulate a composite.

Early attempts to obtain widefield images began with a moving fixation lamp and rotatable mirrors that created a composite fundus image of 96 degrees.[2] Contact lenses coupled with traditional systems achieved single panoramic images of 90 degrees.[3,4] Contact lenses with antireflective coatings and infrared angiography have been used to obtain 160-degree ICG angiograms.[5] A specialized contact lens-based camera was developed by Pomerantzeff[6] that used limbal fiber optic illumination to minimize lens reflections and obtain a 148-degree field. The RetCam 120, a contact-based, limbal illumination system, obtains 120-degree-wide photographs requires excellent patient cooperation or sedation.[7]

A major cause of artifact with any fundus imaging arises from reflection of light from interfaces in the ocular media. Elimination of these reflections is achieved using confocal scanning laser ophthalmoscopy (cSLO), which separates the illuminating and imaging beam within the eye. Staurenghi et al.[8] developed a combined contact and noncontact handheld lens system coupled with a cSLO that obtained high-resolution images with a 150-degree field. However, this technique is cumbersome for the photographer.

The painstaking process of manually creating photomontages was simplified partially with the advent of digital photography. Distortions in the periphery of each image due to astigmatism nevertheless made exact landmark matching

difficult. A software package was developed for automated photomontage creation using images from the Heidelberg retinal angiograph (HRA) system.[9] Montages up to 140 degrees across could be obtained rapidly.

The ability to obtain images wider than 150 degrees required modification of the optical properties of the camera system. Optos plc, incorporated in 1992, developed a novel ellipsoidal mirror with dual focal points, one of which lies posterior to the iris plane. Combination of this mirror with a noncontact SLO imaging platform now allows rapid acquisition of 200-degree panoramic fundus images. In 1999 the Panoramic 200 scanning laser ophthalmoscope received Food and Drug Administration (FDA) clearance as a fundus photography device. Early study using these panoramic images for the detection of diabetic retinopathy yielded a sensitivity and specificity both equal to 76%.[10] Subsequent platforms added fluorescein angiographic capability, and a commercially available FA instrument, the Optomap *fa*, became commercially available in 2007.

Technical Specifications

Confocal Optics

Standard camera systems have a defined focal plane. Depending on aperture size, there is a limited depth of field and focus that can be captured within the focal plane. The concave nature of the fundus renders portions of an image out of focus if the focal plane is exceeded. Confocal imaging, patented by Marvin Minsky in 1957, uses point illumination and a pinhole in an optically conjugate plane to eliminate out-of-focus information. As only one point is illuminated at a time in confocal microscopy, two-dimensional imaging requires scanning each pixel point in a raster over the area to be imaged. All points within the computer-generated panoramic image are in focus, as each was obtained separately.

Scanning Laser Ophthalmoscope

Traditional photography uses white light to illuminate a target, and then record an image of the reflected light. Limitations of broad-field white light illumination include scatter from media opacities, induced mydriasis, and subtle pigment epithelial bleaching. The Optos P200MA utilizes a green (532 nm) laser to image the retina and inner retinal pigment epithelium (RPE) and a red (633 nm) laser to image the outer RPE and choroid. The images may be digitally combined to create a simulated color picture, or each red-free and green-free image may be reviewed individually. A blue (488 nm) laser matches the absorption peak for fluorescein excitation.[11]

Ellipsoidal Mirror

Ultra-widefield imaging is enabled by the optical properties of a large ellipsoidal mirror. Instead of using standard scanning geometry, the ellipsoidal mirror provides two conjugate focal points. This first real focal point, located high on the ellipsoidal mirror, translates the scanning laser beams to a virtual focal point located posterior to the patient's iris plane.

Resolution

The charge-coupled device (CCD) detector for the camera system has a 3000 by 3000 pixel resolution capacity, with each pixel subtending about 6 to 10 μm on the retinal surface. Picture detail is obtained up to the fifth vessel bifurcation.

Imaging Technique

Patients are positioned in front of the machine with a chin rest and forehead support. Space is available for manual lid lifting, if required. Red, green, and simulated color images are obtained initially using the P200 SLO, requiring 0.25 seconds per scan. Five milliliters of 10% sodium fluorescein is injected in a standard fashion, and FA images are captured sequentially. Images are stored using a digital, searchable database that may be reviewed or printed in thumbnail or composite formats.

Limitations

Proper patient positioning with the medial and lateral canthi parallel to the machine is essential. Improvements in image processing and detector noise reduction have greatly enhanced early-phase photos, which were grayed-out in early prototypes due to fluorescence from the anterior segment. Image artifacts have been reduced with improved manufacturing techniques for the ellipsoidal mirror. Image processing has greatly improved contrast resolution in the FA images.

Potential Applications

It has long been established that ischemia and capillary nonperfusion occur commonly in the midperiphery in diabetic retinopathy.[12–14] Neovascularization often occurs at the watershed zone between perfused and nonperfused retina. Furthermore, nonperfused retina may serve as a source of upregulated VEGF. Ultra-widefield fluorescein angiography readily demonstrates abnormal perfusion or vascular incompetance in retinal vascular disease.[15]

Visualization of peripheral RPE abnormalities or vasculitis may enhance diagnostic sensitivity and specificity for non-retinal vasular disease. Visual complaints in patients with peripheral retinal pathology, such as dystrophies, retinal detachment, or uveitis, may correspond with anatomic abnormalities depicted using Optomap *fa* images.

Clinical Examples

Optomap *fa* images may be reviewed at a digital workstation or in printout format. Fundus photos views may be reviewed

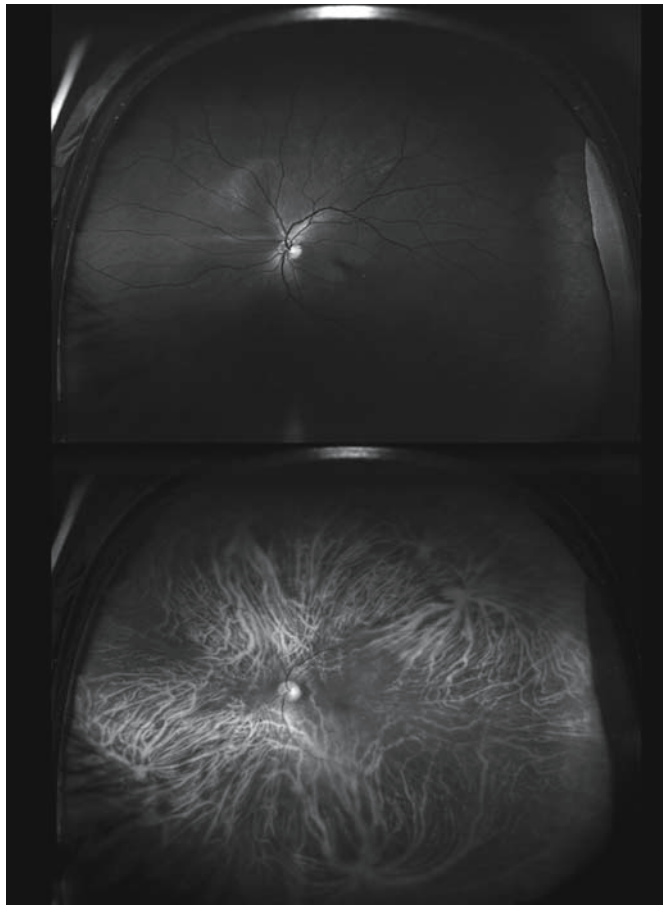

Fig. 23.1. Scanning laser ophthalmoscopic ultra-widefield photographs may be obtained using both wavelengths of the Optomap scanning laser ophthalmoscope (SLO). Images obtained with a 532-nm green laser ("red-free") primarily display the inner retinal layers (top), while images obtained with the 633 nm red laser ("green-free") image the retinal pigment epithelium (RPE) and choroid.

in simulated color, red-free, or green-free formats. A normal example is shown in Figure 23.1.

Retinal Vascular Disease

The ability to image retinal vascular disease serves a primary utility for FA. Hyperfluorescence due to leakage, transmission defects, or staining, and hypofluorescence from hypoperfusion or blockage are all easily delineated with FA. Optomap *fa* images simultaneously provide high-resolution posterior pole images similar to those obtained with traditional techniques, as well as identification of peripheral pathology that may not have been detected with clinical examination or standard fundus photography.

Diabetic Retinopathy

Fluorescein angiography may be used to diagnose protean manifestations of diabetic retinopathy. High magnification images of the macula may detect clinically significant macular edema (CSME) (Fig. 23.2) or macular ischemia (Fig. 23.3). A 3000 by 3000 pixel image capture resolves retinal details within 6 μm.

Neovascularization from proliferative diabetic retinopathy (PDR) may be detected on clinical exam or revealed by leakage on FA. Neovascularization elsewhere (NVE), particularly that present in the peripheral fundus, may be missed by clinical exam; it is readily detected on ultra-widefield FA (Fig. 23.4).[15] Optomap *fa* may also detect NVE in the setting of dense asteroid hyalosis. [16] Peripheral capillary nonperfusion from diabetic retinopathy may be localized, associated with NVE, or diffuse (Fig. 23.5). Diffuse capillary nonperfusion may contribute to retinal ischemia and upregulation of vascular endothelial growth factor (VEGF), and may signal a high risk of progression to severe PDR. Targeted retinal photocoagulation (TRP) to ischemic sectors of the retina may diminish vasogenic drive and preclude the need for more extensive panretinal photocoagulation (PRP). [17]

Tractional retinal detachment (TRD) results from the most advanced stages of PDR, and may demonstrate arteriolar and capillary nonperfusion, leakage from traction, and pooling within the detachment (Fig. 23.6).

Retinal Vascular Occlusion

Retinal vein occlusion results in nonperfusion of the involved vein or veins, as well as possible capillary nonperfusion in the involved areas (Fig. 23.7). Retinal neovascularization may occur, typically at the margin of an area of nonperfusion (Fig. 23.8).

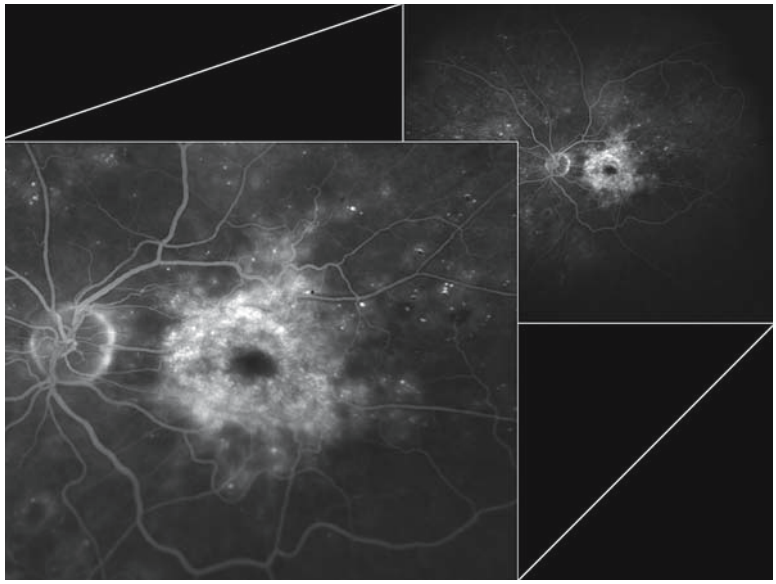

FIG. 23.2. Clinically significant macular edema is readily visualized in high resolution using magnification of the Optomap *fa* image.

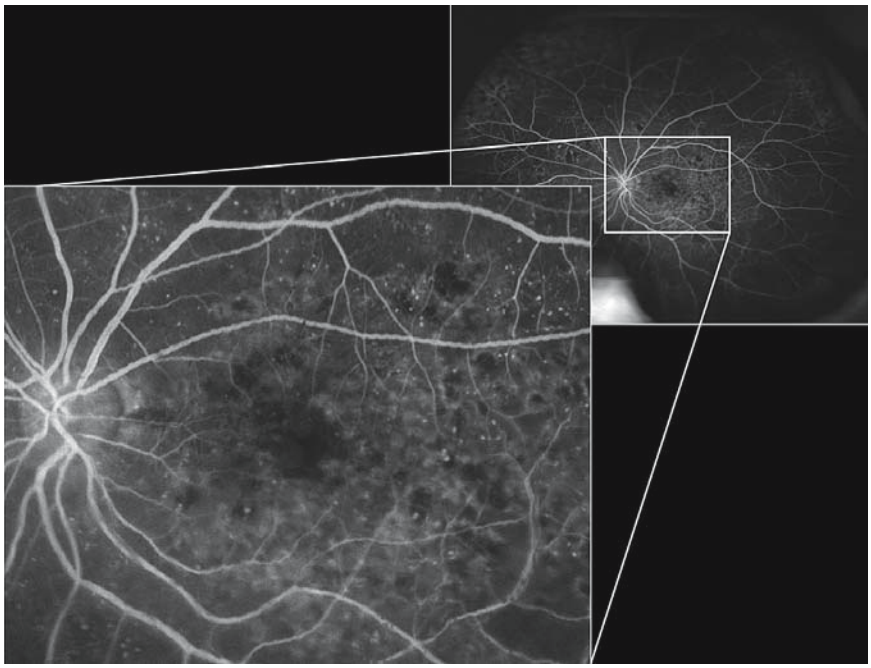

FIG. 23.3. Macular capillary nonperfusion, inferotemporal capillary nonperfusion, and microaneurysms are clear in this magnified Optomap *fa* image of nonproliferative diabetic retinopathy.

Both branch and central retinal vein occlusions (BRVO and CRVO, respectively) may lead to cystoid macular edema (CME), which is detectable with a magnified view of the posterior pole (Fig. 23.9).

Ophthalmic artery occlusion results in greatly delayed arterial filling of the choroidal or retinal circulation (Fig. 23.10). Panoramic imaging reveals areas of retina and choroid perfused by long posterior ciliary branch arteries.

Coats' Disease

Peripheral microaneurysms, macroaneurysms, vessel telangiectasiae, and exudation may be present in Coats' disease or the adult form of Coats' disease, known also as Leber's miliary aneurysms. Subtle macular edema may herald more extensive peripheral pathology (Fig. 23.11). Identification of peripheral pathology may enable curative treatment for this vascular hyperpermeability disorder.

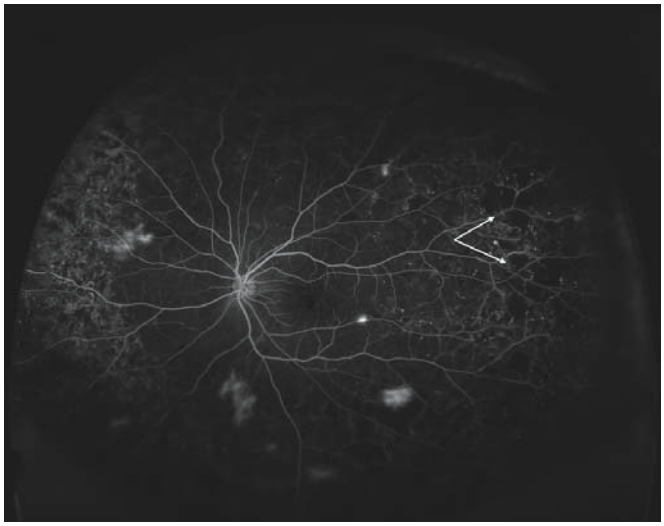

FIG. 23.4. Proliferative diabetic retinopathy (PDR) is evidenced by multiple areas of leakage corresponding to neovascularization elsewhere (NVE). Note also patchy areas of capillary nonperfusion (arrows).

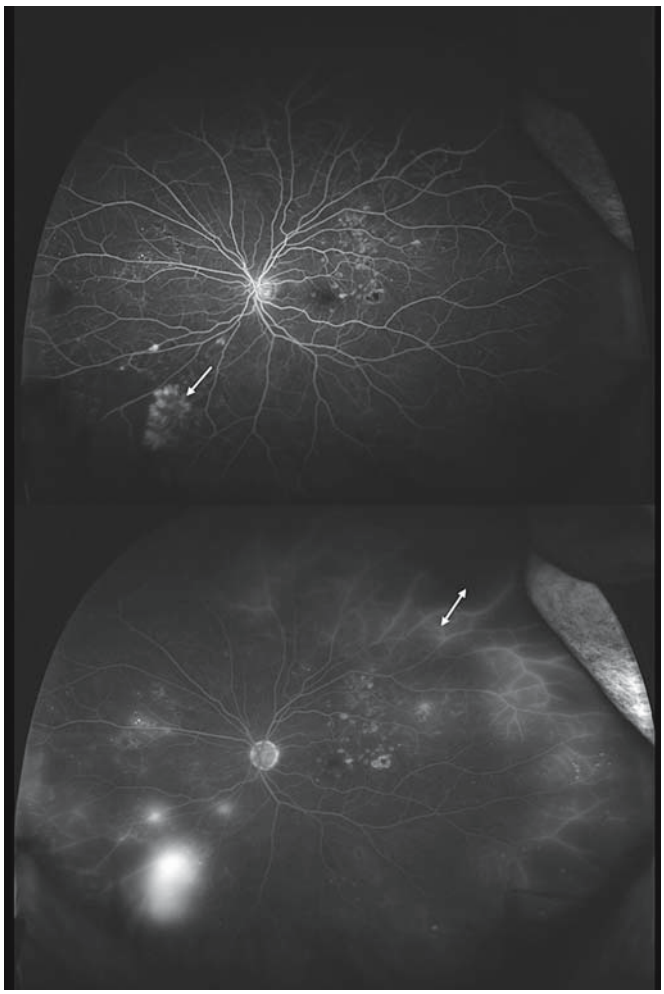

FIG. 23.5. Midphase fluorescein angiography (FA) (top) demonstrates peripheral NVE at the margin of a zone of capillary nonperfusion (arrow). Late-phase FA (bottom) also reveals broad areas of peripheral nonperfusion next to perivascular staining (double arrow). A reflection of the patient's nose is noted in the upper right side of both images.

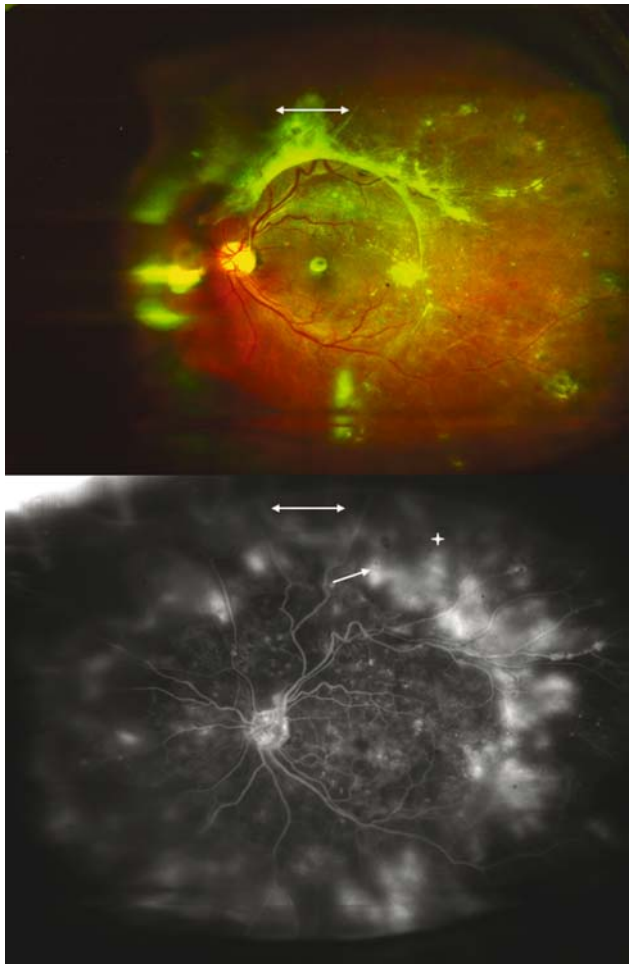

FIG. 23.6. Simulated color photograph and midphase angiogram of a diabetic tractional retinal detachment (TRD) demonstrates leakage at traction sites (arrow) and pooling in areas of neurosensory retinal elevation (star). Hypoperfusion is present along sclerotic retinal vessels (double-headed arrow, both images).

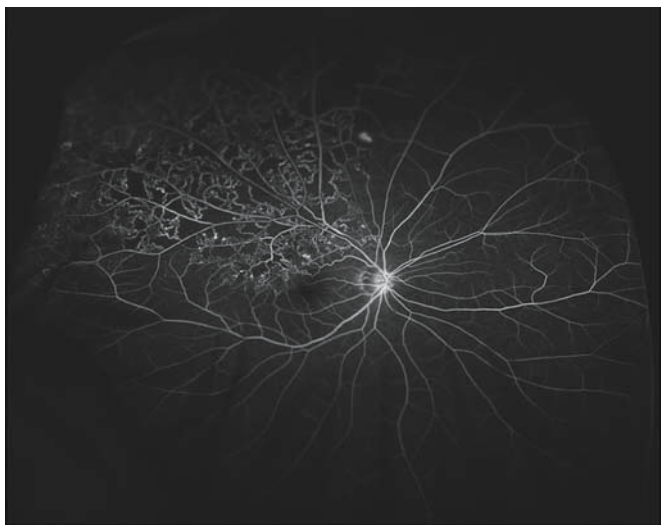

FIG. 23.7. Ultra-widefield midphase angiogram of a branch retinal vein occlusion (BRVO). Patchy ischemia extends into the far periphery, but cystoid macular edema (CME) is absent.

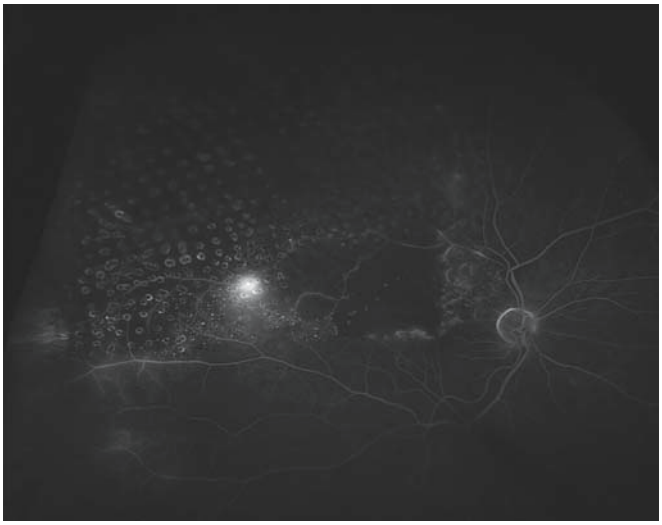

FIG. 23.8. Following sectoral retinal photocoagulation for BRVO, NVE is present at the margin of lasered and ischemic retina, and capillary nonperfusion extends into the macula.

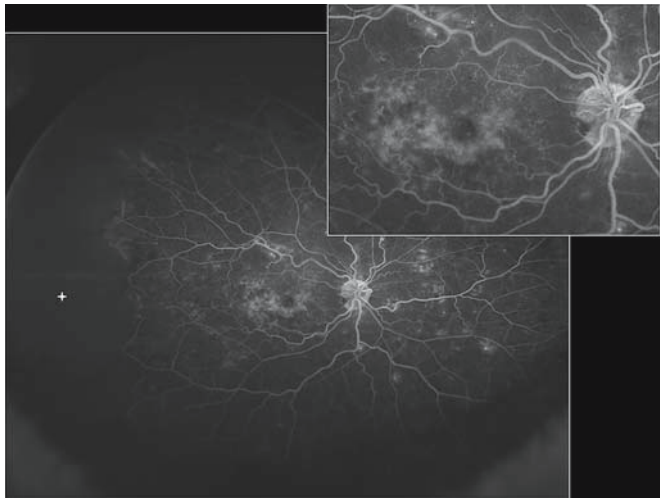

FIG. 23.9. Cystoid macular edema from central retinal vein occlusion is evident on high magnification (top) and widefield (bottom) images. Extensive peripheral capillary nonperfusion is present in the widefield image (star).

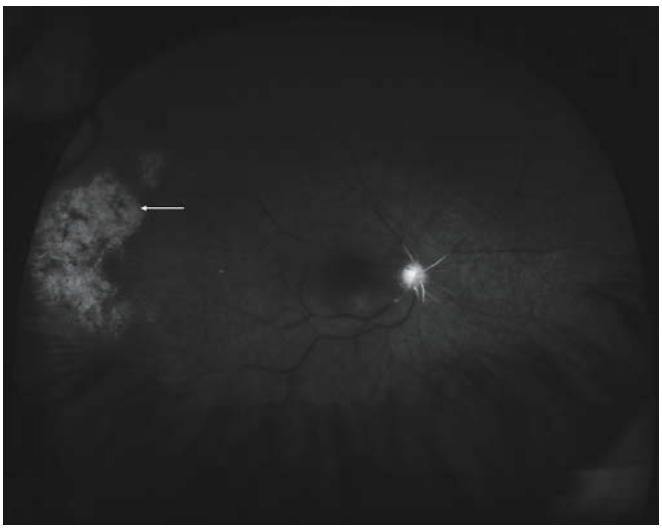

Figure 23.10. Ophthalmic artery occlusion following chemoembolization for epistaxis results in severe choroidal and retinal arterial filling defects in this late-phase angiogram. Choroidal perfusion in the temporal periphery is due to late perfusion of some long posterior ciliary arteries (arrow).

Sickle Cell Retinopathy

Peripheral vascular occlusion, ischemia, and neovascularization in sickle cell retinopathy may be readily identified with ultra-widefield FA.[18,19] Targeted photocoagulation to areas of ischemia may result in regression of the neovascularization without the need for extensive PRP.

Degenerative Disease

Age-Related Macular Degeneration

High-resolution, magnified imaging of the posterior pole is essential to the evaluation and treatment of AMD. The magnified image of an Optomap *fa* provides excellent macular detail, while still allowing the option to view other peripheral pathology (Fig. 23.12).

Dystrophic Chorioretinal Disease

Retinitis Pigmentosa

Peripheral RPE atrophy and bone spicule formation may be imaged with panoramic angiography (Fig. 23.13).

Choroideremia

The widespread, scallop-shaped RPE dropout present in choroideremia is readily captured using ultra-widefield FA (Fig. 23.14).

Rhegmatogenous Retinal Detachment

Rhegmatogenous retinal detachment may be diagnosed with panoramic imaging.[20] Rhegmatogenous or exudative retinal detachment results in hyperfluorescence from subneurosensory fluorescein pooling. Chronic retinal detachment may be associated with pigmentary blocking defects, RPE loss, and vascular hypoperfusion (Fig. 23.15). Despite successful anatomic reattachment after retinal detachment repair, RPE and retinal dysfunction may resolve slowly (Fig. 23.16). If sufficient RPE

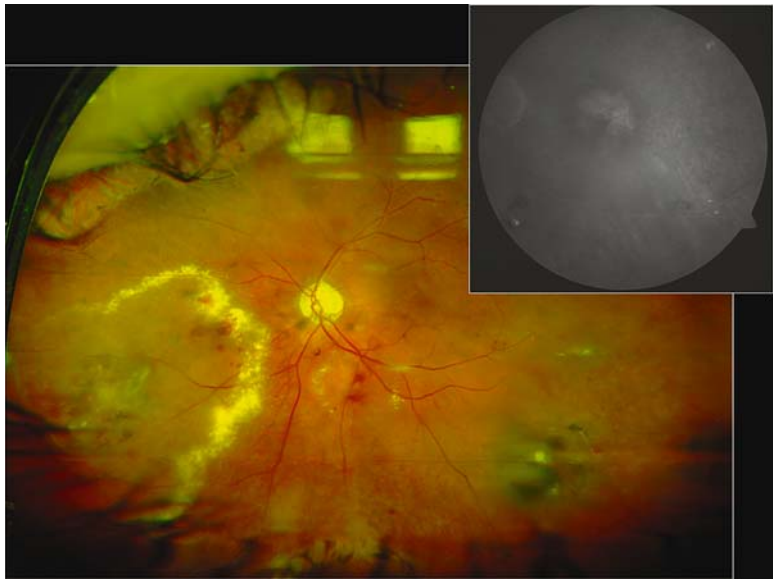

FIG. 23.11. Cytoid macular edema (top) seen with standard angiography had been treated repeatedly using intravitreal triamcinolone acetonide. Examination of the retinal periphery (bottom) revealed vessel telangiectasiae, exudation, and macroaneurysms, consistent with a diagnosis of adult Coats' disease.

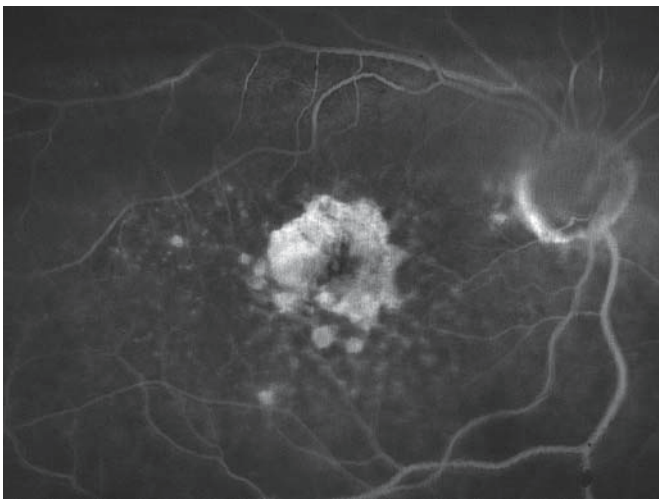

FIG. 23.12. Magnified macular view of midphase angiogram shows transmission defects from pigment epithelial abnormalities and early staining of a disciform scar in age-related macular degeneration (AMD).

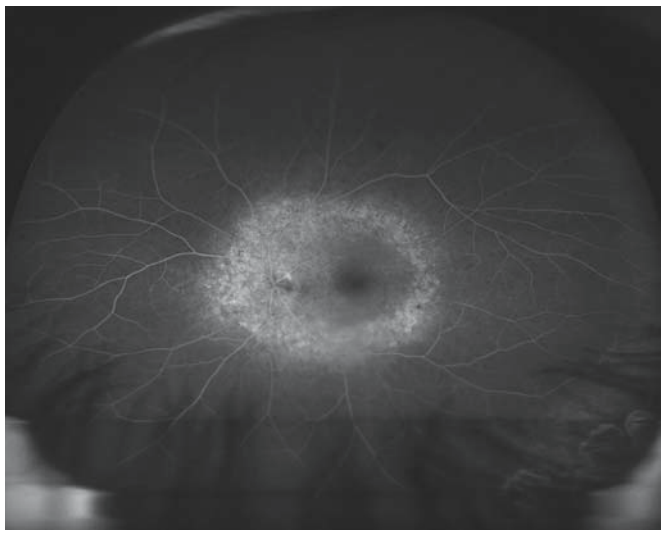

FIG. 23.13. Hyperfluorescence from RPE window defects are present peripheral to the vascular arcades in this patient with retinitis pigmentosa. Cystoid macular edema is absent.

injury occurs due to the detachment, RPE loss may be detectable on panoramic FA (Fig. 23.17).

Infectious and Inflammatory Chorioretinal Disease

Vasculitis may result from a variety of inflammatory etiologies, including systemic lupus erythematosus (SLE), Behçet disease, Wegener granulomatosis, toxoplasmosis, sarcoidosis, and syphilis.

Lupus-Associated Retinopathy

Increased vascular hyperpermeability from SLE vasculitis results in vascular staining. Severe inflammation may lead to

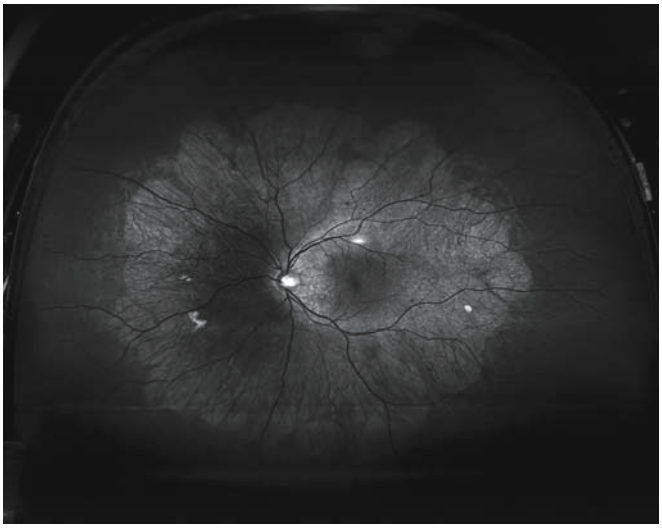

FIG. 23.14. Red-free panoramic photograph of choroideremia demonstrates broad, scalloped atrophy of the retinal pigment epithelium.

vascular occlusion, with subsequent development of CME, capillary nonperfusion, and proliferative retinopathy (Fig. 23.18).

Sarcoidosis

Manifestations of sarcoid range from anterior and posterior uveitis to occlusive phlebitis, capillary dropout, and proliferative retinopathy. [21] Laser photocoagulation to the nonperfused regions may be required.

Acute Posterior Multifocal Placoid Pigment Epitheliopathy (APMPPE) and Serpiginous Choroiditis

Idiopathic inflammation of the retinal pigment epithelium occurs most commonly in young adults following a viral prodrome. The classic angiographic findings of early blockage with late staining may be seen on FA. Serpiginous choroidopathy, also called geographic helicoid peripapillary choroidopathy, is a rare disorder characterized by hypoperfusion from progressive geographic choroidal and RPE atrophy rimmed by hyperfluorescent margins from RPE transmission defects. Overlap syndromes between APMPPE and serpiginous exist (Fig. 23.19).

Diffuse Unilateral Subacute Neuroretinitis

Chronic subretinal infection by a nematode, most commonly *Baylisascaris procyonis* or *Ancylostoma caninum*, may lead to insidious, severe vision loss. Progressive RPE atrophy, sometimes linear along the migration path of the worm, may be seen on panoramic FA (Fig. 23.20).

Presumed Ocular Histoplasmosis Syndrome (POHS)

Atrophic chorioretinal lesions from POHS may extend into the periphery (Fig. 23.21). Care must be taken to exclude choroidal neovascularization.

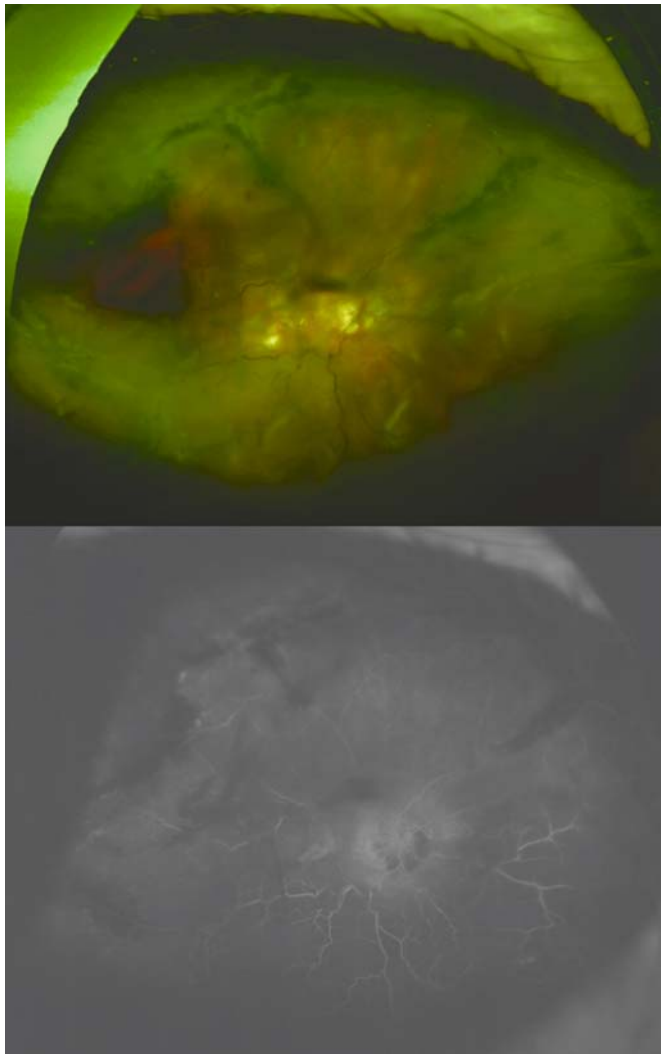

FIG. 23.15. Chronic rhegmatogenous retinal detachment is demonstrated in color (top) and angiographic (bottom) images. Vessel nonperfusion, blocking from pigment clumping, and pooling in the subneurosensory space is present.

Cystoid Macular Edema

Cystoid macular edema (CME) occurring from a variety of inflammatory causes, including uncomplicated cataract surgery, may be readily identified with a magnified Optomap image of the posterior pole (Fig. 23.22). A petaloid hyperfluorescence pattern is evident.

Neoplastic

Melanoma

The delineation of the margins of a pigmented choroidal tumor is greatly enhanced using a green-free image, as the red laser penetrates the deep retina, RPE, and choroid (Fig. 23.23). Angiography may also be useful to identify intrinsic circulation in a melanoma.

FIG. 23.16. Bilateral scleral buckles were placed for inferior retinal detachments in this young myopic woman. Hyperfluorescent transmission defects in the former bed of the detachments are evident due to RPE derangement (stars).

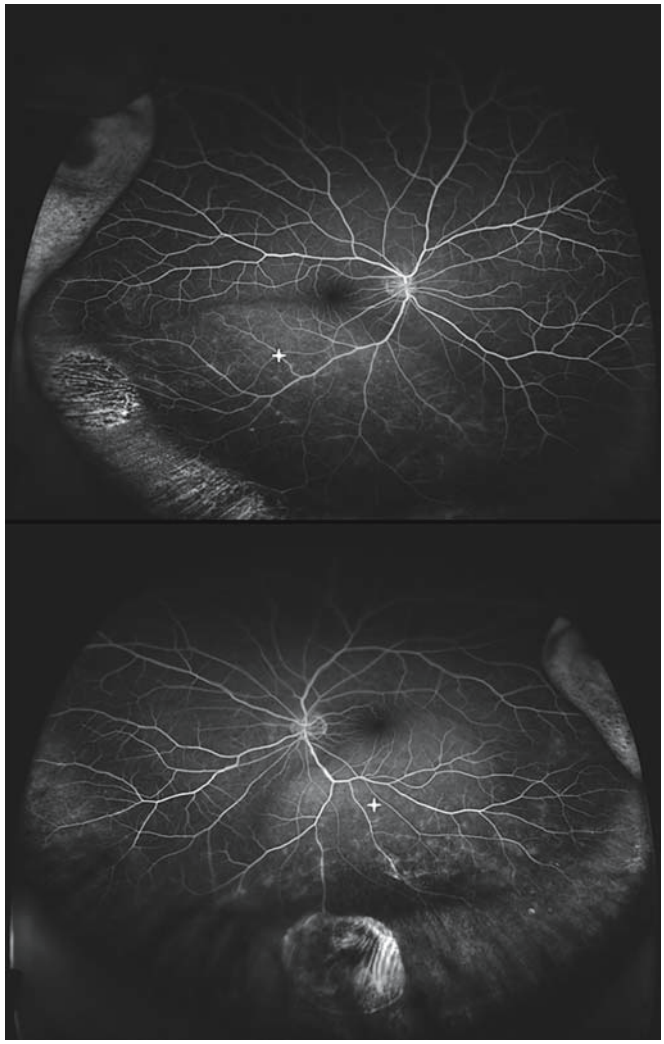

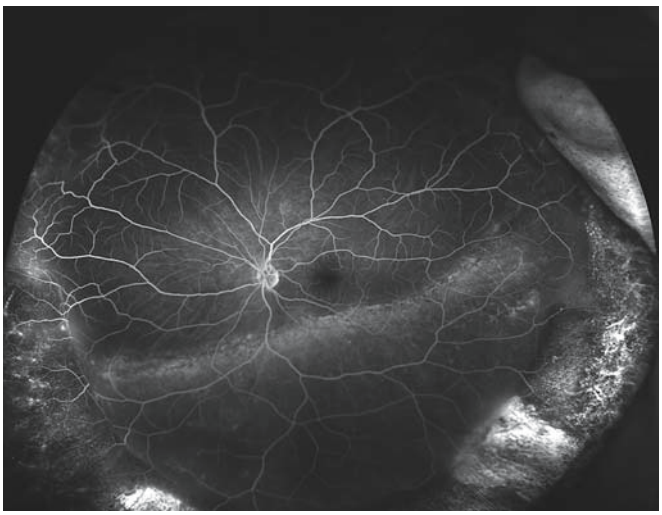

FIG. 23.17. Transmission and blocking defects are present along a prior demarcation line in this patient with a history of chronic inferior retinal detachment treated with scleral buckling.

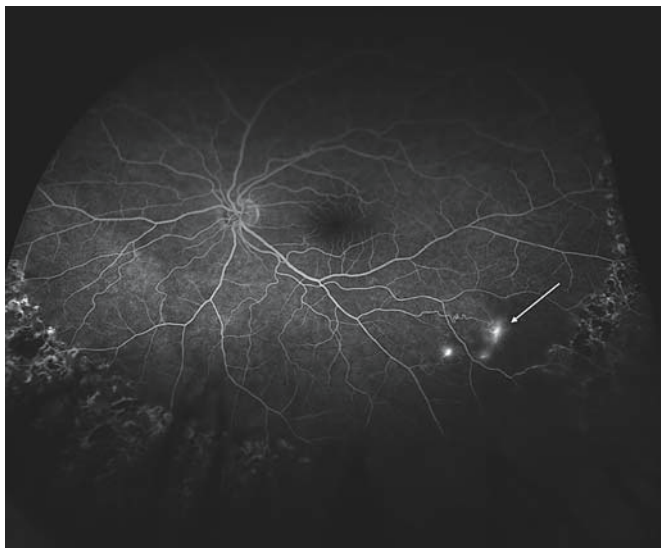

FIG. 23.18. Lupus-associated proliferative retinopathy has been previously treated with peripheral panretinal photocoagulation (PRP); however, progression of vascular obliteration resulted in a patch of capillary nonperfusion with associated neovascularization (arrow).

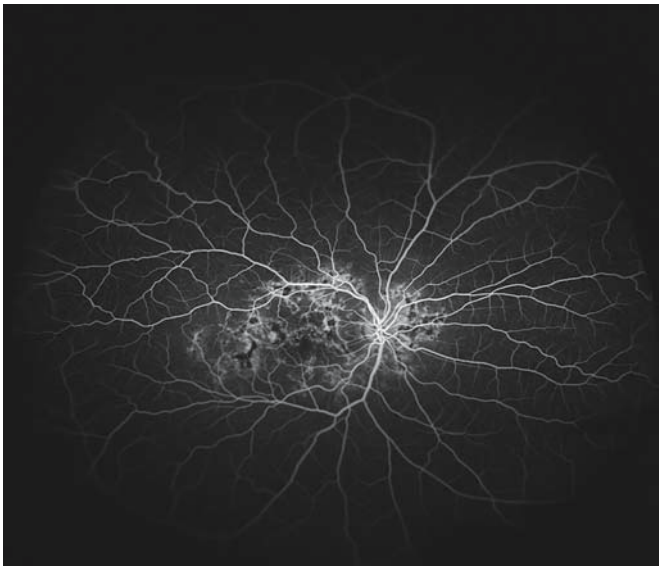

FIG. 23.19. Midphase fluorescein angiogram demonstrates hypofluorescent lesions rimmed by hyperfluorescent transmission defects in this patient with an overlap syndrome of acute posterior multifocal placoid pigment epitheliopathy (APMPPE) and serpiginous choroiditis.

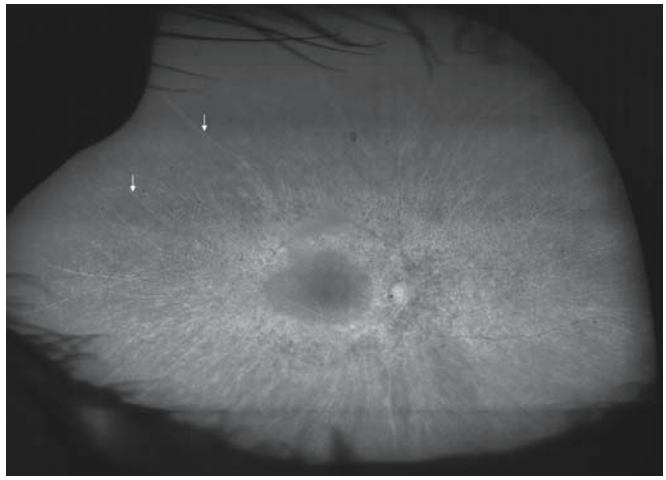

FIG. 23.20. Early-phase angiogram reveals diffuse RPE transmission defects, in addition to linear transmission defects (arrows), corresponding to the presumed track of a nematode in diffuse unilateral subacute neuroretinitis.

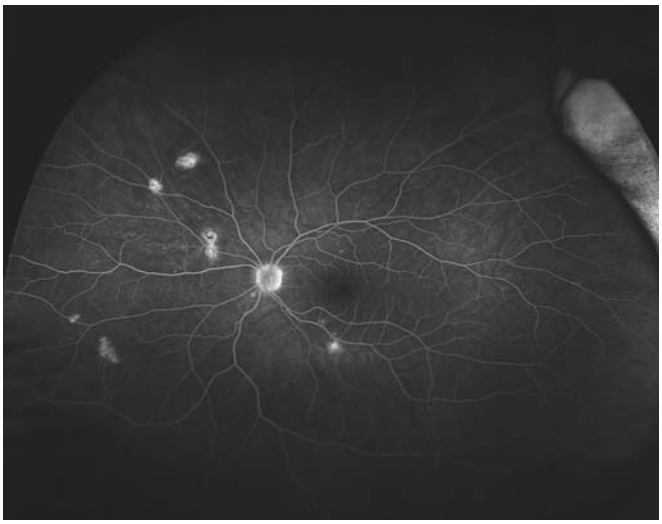

FIG. 23.21. Midphase angiogram demonstrates punched out areas of chorioretinal atrophy consistent with presumed ocular histoplasmosis syndrome (POHS).

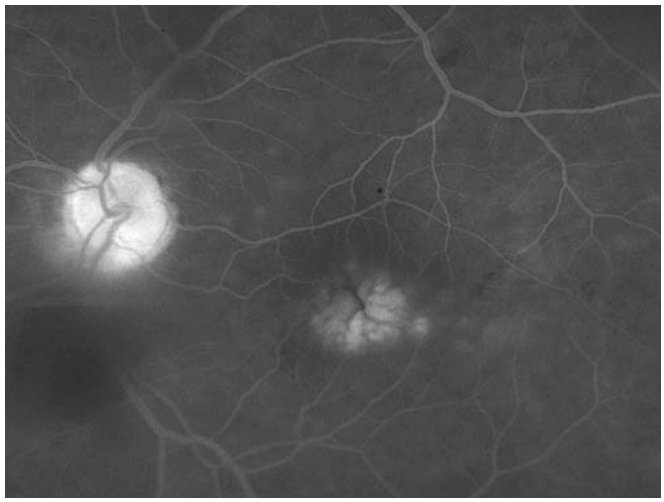

FIG. 23.22. Irvine-Gass syndrome, with cystoid macular edema and mild optic nerve leakage, is present following scleral buckling for retinal detachment.

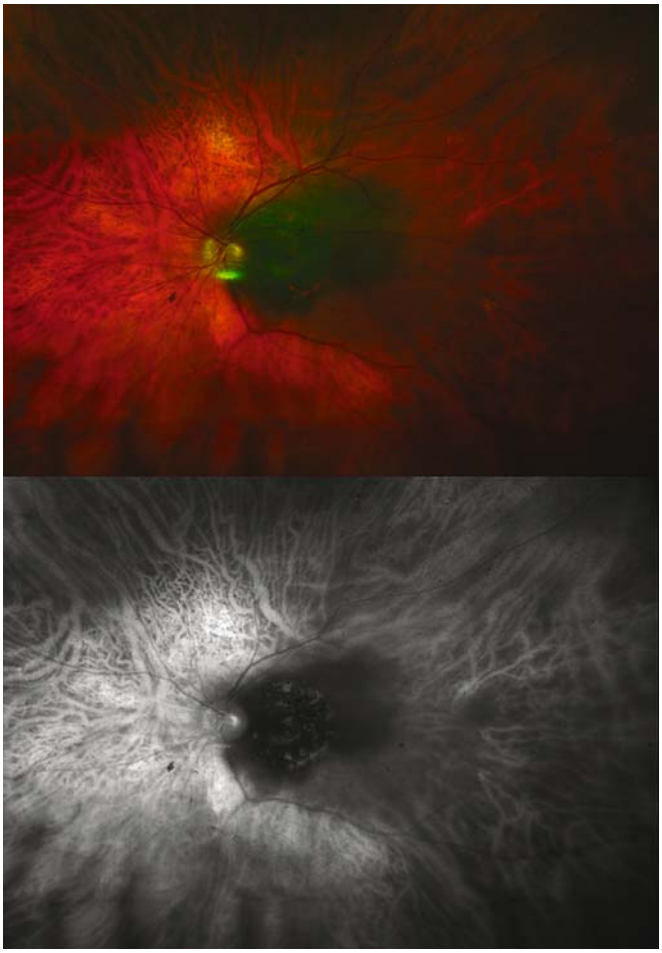

FIG. 23.23. Simulated color photograph (top) of choroidal malignant melanoma exhibits high-risk characteristics, including orange lipofuscin pigmentation and close proximity to the optic nerve. Red wavelength laser penetrates RPE and choroid, providing delineation of the peripheral margins of the tumor (bottom).

Conclusion

Dynamic ultra-widefield angiography using the Optos P200MA scanning laser ophthalmoscope offers a powerful advance in the ability of the retinal specialist to image the ocular fundus. Advantages of the Optomap *fa* include 200 degrees of wide-field imaging, scanning laser ophthalmoscope platform, rapid acquisition time, and digital image review. Future research will entail quantification of previously unidentified peripheral retinal pathology, determination of change in treatment patterns based on the result of ultra-widefield angiography, and assessment of the effectiveness of targeted laser photocoagulation to regions of retinal ischemia.

References

1. Diabetic retinopathy study. Report Number 6. Design, methods, and baseline results. Report Number 7. A modification of the Airlie House classification of diabetic retinopathy. Prepared by the Diabetic Retinopathy. Invest Ophthalmol Vis Sci 1981;21 (1 pt 2):1–226.
2. Lotmar W. [A fixation lamp for panoramic fundus pictures (author's transl)]. Klin Monatsbl Augenheilkd 1977;170(5): 767–774.
3. Noyori KS, Chino K, Deguchi T. Wide field fluorescein angiography by use of contact lens. Retina 1983;3(2):131–134.
4. Ozerdem U, Freeman WR, Bartsch DU, Clark TM. A simple noncontact wide-angle fundus photography procedure for clinical and research use. Retina 2001;21(2):189–190.
5. Spaide RF, Orlock DA, Herrmann-Delemazure B, et al. Wide-angle indocyanine green angiography. Retina 1998;18(1):44–49.
6. Pomerantzeff O. Equator-plus camera. Invest Ophthalmol 1975;14(5):401–406.
7. Roth DB, Morales D, Feuer WJ, Hess D, Johnson RA, Flynn JT. Screening for retinopathy of prematurity employing the Retcam 120: Sensitivity and specificity. Arch Ophthalmol 2001;119(2):268–272.
8. Staurenghi G, Viola F, Mainster MA, Graham RD, Harrington PG. Scanning laser ophthalmoscopy and angiography with a wide-field contact lens system. Arch Ophthalmol 2005;123(2):244–252.
9. Rivero ME, Bartsch DU, Otto T, Freeman WR. Automated scanning laser ophthalmoscope image montages of retinal diseases. Ophthalmology 1999;106(12):2296–2300.
10. Friberg TR, Pandya A, Eller AW. Non-mydriatic panoramic fundus imaging using a non-contact scanning laser-based system. Ophthalmic Surg Lasers Imaging 2003;34(6):488–497.
11. Webb RH, Hughes GW, Delori FC. Confocal scanning laser ophthalmoscope. Appl Opt 1987;26:1492–1499.
12. Niki T, Muraoka K, Shimizu K. Distribution of capillary nonperfusion in early-stage diabetic retinopathy. Ophthalmology 1984;91(12):1431–1439.
13. Shimizu K, Kobayashi Y, Muraoka K. Midperipheral fundus involvement in diabetic retinopathy. Ophthalmology 1981;88(7): 601–612.
14. Kimble JA, Brandt BM, McGwin G Jr. Clinical examination accurately locates capillary nonperfusion in diabetic retinopathy. Am J Ophthalmol 2005;139(3):555–557.
15. Manivannan A, Plskova J, Farrow A, McKay S, Sharp PF, Forrester JV. Ultra-wide-field fluorescein angiography of the ocular fundus. Am J Ophthalmol 2005;140(3):525–527.
16. Win PH, Young TA. Optos Panoramic200A fluorescein angiography for proliferative diabetic retinopathy with asteroid hyalosis. Semin Ophthalmol 2007;22(2):67–69.
17. Theodossiadis G, Micha M. [Peripheral neovascularization of the retina in diabetic retinopathy: fluorescein angiography classification and results of panretinal laser treatment]. Klin Monatsbl Augenheilkd 1990;196(3):143–149.
18. Cruess AF, Stephens RF, Magargal LE, Brown GC. Peripheral circumferential retinal scatter photocoagulation for treatment of proliferative sickle retinopathy. Ophthalmology 1983;90(3): 272–278.
19. Kimmel AS, Magargal LE, Stephens RF, Cruess AF. Peripheral circumferential retinal scatter photocoagulation for the treatment of proliferative sickle retinopathy. An update. Ophthalmology 1986;93(11):1429–1434.
20. Anderson L, Friberg TR, Singh J. Ultrawide-angle retinal imaging and retinal detachment. Semin Ophthalmol 2007;22(1):43–47.
21. Duker JS, Brown GC, McNamara JA. Proliferative sarcoid retinopathy. Ophthalmology 1988;95(12):1680–1686.

24
Fundus Autofluorescence

Antonio P. Ciardella and Chiara M. Eandi

Fundus spectrophotometric studies by Delori et al.[1,2] have shown that fundus autofluorescence (FAF) in vivo is mainly derived from retinal pigment epithelium (RPE) lipofuscin. In the past, lipofuscin accumulation has been largely studied in vitro using fluorescence microscopic techniques.[3–5] Excessive accumulation of lipofuscin represents a common pathogenetic pathway in various complex retinal diseases and is believed to precede photoreceptor degeneration.[6–8]

With the advent of confocal scanning laser ophthalmoscopy (cSLO) it is possible to visualize FAF and its spatial distribution in vivo.[9–12] It represents a tool to evaluate the RPE during aging and in ocular disease.[13]

The RPE is a single layer of cells between the neurosensory retina and the choroid; the choroid is separated from the RPE by Bruch's membrane. The RPE is an important structure for the maintenance of the outer blood–retina barrier. It takes part in different functions such as vitamin A circulation, synthesis of extracellular matrix, transport of molecules, and most importantly phagocytosis of the outer discs of the photoreceptors,[1,14] which happens in special intracellular compartments, the lysosomes. The end-products usually are excreted though the basal side of the RPE cells and transported by choroidal circulation. Age or different diseases may alter RPE function, which might be incomplete, and accumulation of the intralysosomal molecules, lipofuscin, takes place.[3,7,14,15] The accumulation of lipofuscin contains at least 10 different fluorophores.[16] Thus it is believed that metabolic activity of RPE correlates with the content of lipofuscin in RPE cells.[17] Excessive accumulation of lipofuscin within the RPE may play a major role in the pathogenesis of age-related macular degeneration (AMD)[11,18,19] or other hereditary macular diseases such as Best's disease or Stargardt's disease,[20–24] all leading to significant loss of vision due to degeneration of RPE and consecutively degeneration of the photoreceptor layer. The intrinsic FAF of the RPE was shown to be derived from the lipofuscin within the RPE.[1,19,21,25] However, there are other fluorophores both anterior and posterior to the RPE cell monolayer with autofluorescent properties, even in the excitation and emission wavelength range applied here. Their intensity, however, is far below that of the lipofuscin-derived autofluorescent signal.[25]

Correlating with specific diseases or with distinct levels of metabolic activity, different intracellular concentrations of lipofuscin seem to be present, and therefore autofluorescent activity of the RPE layer might offer specific patterns. With the introduction of highly sensitive confocal scanning laser ophthalmoscopes in the 1990s, imaging of autofluorescence (AF) as an index of lipofuscin and its spatial distribution over large retinal areas in vivo became possible. Fundus autofluorescence imaging was shown to provide very detailed information about the levels and distribution of lipofuscin of the RPE in the living eye.[11,19,25]

Lipofuscin

Lipofuscin is a generic term that is given to an autofluorescent, brown to yellow, electron dense, heterogeneous, polymorphous, nondegradable group of waste materials. Lipofuscins are also called "age pigments" not only because the amount of lipofuscins increases with age, but also because the rate of lipofuscins accumulation correlates negatively with longevity, which makes lipofuscins biomarkers of aging.

Lipofuscin accumulates in the cytoplasmic space of the RPE as clusters of granules and can occupy between 20% and 30% of this space by the age of 70 years. Under the spectrophotometric microscope these granules appear as dense and roughly spherical, with a diameter of 1 μm and height ranging from 500 to 800 nm. Lipofuscin contains at least 10 different fluorophores. Despite the fact that the entire composition of the lipofuscin pigments is still unclear, *N*-retinylidin-*N*-retinylethanolamin (A2-E) was recently identified as one of the major fluorophores of the lipofuscin.[26–28] A2-E seems to play a major role in the degradation of the RPE cell due to a toxic effect secondary to the alteration of intracellular pH and phototoxic effects mediated by blue light that causes disintegration of lysosomal membranes.[25,29]

Studies on experimentally induced lipofuscin-like pigments have contributed to the understanding of the mechanisms involved in RPE lipofuscin formation. It appears that visual cycle retinoids, in particular all-trans-retinaldehyde, are precursors of the RPE lipofuscin fluorophores and that oxidative stress promotes the generation of these retinaldehyde-derived compounds.[25]

Emission Spectrum and Distribution of Lipofuscin

Fundus fluorescence reveals a broad band of emission between 500 and 750 nm, a maximum of approximately 630 nm, and optimal excitation of approximately 510 nm.[1] Maximum absorption is for blue light, while the highest fluorescence is for red light. Emission spectra from a single granule are not uniform, which might be due to the presence of different fluorophores with different emissions that contribute to the fluorescence signal. In vivo fluorescence spectra are consistent with those obtained ex vivo on human RPE. Measurements with short wavelength excitation are strongly influenced by ocular media absorption and reveal an additional minor fluorophore in the fovea. Exhibiting a significant increase with age, this fluorescence is highest at 7 to 15 degrees from the fovea, shows a well-defined foveal minimum, and decreases toward the periphery.[1]

Fundus Autofluorescence Imaging

Autofluorescent imaging of the ocular fundus consists of the stimulated emission of light from molecules, mainly lipofuscin, in the RPE, in the photoreceptor outer segments, and in the space between the photoreceptor outer segments and the RPE. Nowadays, there are two ways to acquire fundus autofluorescent images: by cSLO,[11] and by using a fundus camera-based system.[30]

Confocal Scanning Laser Ophthalmoscopy

Fundus autofluorescent images were first recorded with cSLO (Heidelberg retina angiograph [HRA] classic and HRA 2, Heidelberg Engineering, Dossenheim, Germany).[1,11,31] A small pinhole aperture suppresses light originating from outside the focal plane to enhance image contrast compared with nonconfocal images. For excitation at 488 nm, an argon blue laser is used, and emission is recorded above 500 nm (HRA) with a barrier filter. The illumination beam is 3 mm in diameter and the full aperture of a dilated or undilated pupil is used to collect the emitted fluorescence light from the posterior pole. For acquisition of FAF images, standard operation procedures were developed including focusing of the retinal image in reflection and red-free mode, sensitivity adjustment, and acquisition of 30- × 30-degree FAF images. The images encompassed the entire macular area. The frame grabber of the HRA can digitize image frames at a programmable rate of up to 5 frames per second. Each frame contains 1536 pixels vertically and 1536 pixels horizontally in the high-resolution mode (digital resolution 5 μm/pixel). The best nine single images were aligned, and a mean image was generated to amplify the FAF signal using image analysis software (Heidelberg eye explorer [HEE]; Heidelberg Engineering). With the cSLO a series of images of each eye was recorded at standard video scanning rates on VHS videotape. Later, images were digitized at a 768 × 576 resolution with a frame grabber (Millennium; Matrox Imaging Products Group, Dorval, Quebec, Canada). Media opacities, mostly cataract, influence the quality of the image during the acquisition process.

Fundus Camera-Based System

Usually, fundus cameras can image FAF using the same wavelengths, but autofluorescence of the crystalline lens would also be imaged, particularly in the presence of nuclear sclerosis, creating fogging of the image. To avoid this problem Spaide[30] introduced a new filter set. A barrier filter of 695 nm (bandwidth 675 to 715 nm) was selected (Spectrotech, Saugus, MA) to avoid imaging the autofluorescence of the lens, which lies mainly from 510 to 670 nm. The excitation light of 580 nm (bandwidth 500 to 610 nm) was selected to help reduce any variation in stimulating light reaching the fundus caused by absorptive changes in the crystalline lens. The gain of the digital camera was set at the maximum level through the Topcon IMAGEnet software. The selected wavelengths are different from those used for both fluorescein and indocyanine angiography. The light exposure to the fundus was calculated to be orders of magnitude less than that used for typical angiography with fluorescein.[30]

Interpretation of Fundus Autofluorescence

Distribution of AF was evaluated in healthy subjects and in several macular diseases including AMD, hereditary diseases, macular hole formation, and other RPE-related diseases, such as central serous chorioretinopathy (CSCR).[25,32] Fundus autofluorescence images usually are evaluated for the presence of areas of decreased (hypoautofluorescence) or increased (hyperautofluorescence) fundus autofluorescence.

Normal Fundus Autofluorescence

A normal pattern of FAF is characterized by decreased intensity at the fovea, under the retinal blood vessels, in the peripapillary region, and over the optic disc, which appears dark (Fig. 24.1). The autofluorescence in the fovea is decreased because there is less accumulation of lipofuscin and it is affected by the presence of the macular pigments. A topographic distribution of RPE lipofuscin content throughout the fundus has been described, being higher at the posterior pole and lower toward the peripheral retina. This is consistent with histologic

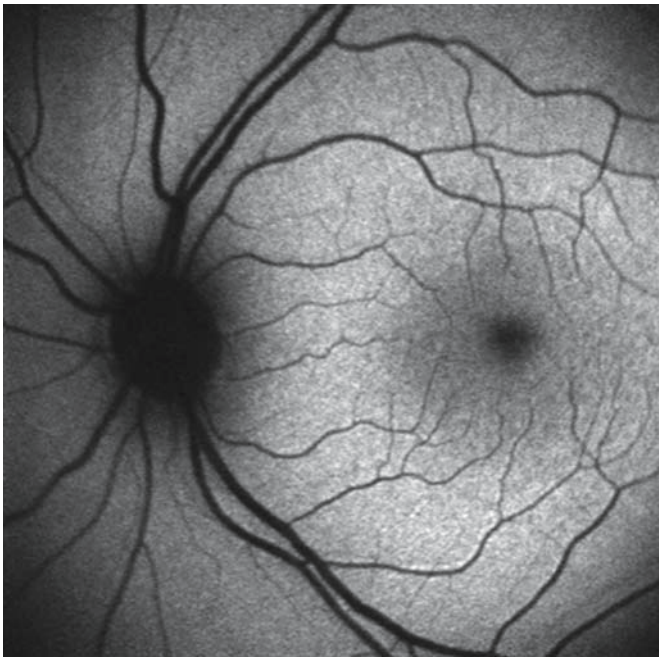

FIG. 24.1. Normal fundus autofluorescence is characterized by decreased intensity at the fovea and in the peripapillary region.

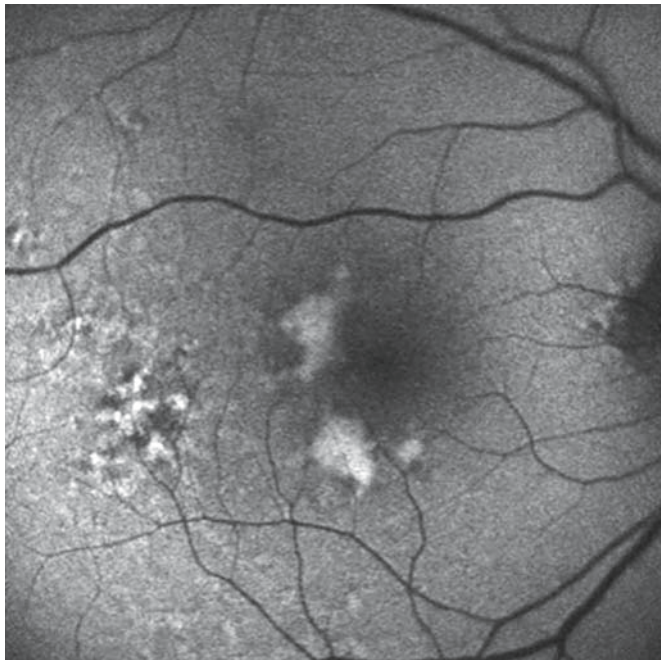

FIG. 24.2. Fundus autofluorescence of early-stage dry age-related macular degeneration (AMD) shows focal hyperautofluorescent areas corresponding to the soft drusen.

findings that correlate a decay of lipofuscin and the density of photoreceptors.

Fundus Autofluorescence in Dry Age-Related Macular Degeneration

Age-related macular degeneration has become the most common cause of legal blindness in industrialized countries. The RPE plays an important role in the pathogenesis of both early and late manifestations. The early stage of dry AMD is characterized by the presence of hard and soft drusen, focal pigmentation, and RPE changes. These are usually localized in the parafoveal region and differ for extension. Fundus autofluorescence alterations on the corresponding areas are described according to the International Fundus Autofluorescence Classification Group (IFAG).[33] A minimal change pattern with mild hyper- or hypofluorescence is observed in the presence of hard or soft drusen (Fig. 24.2). Areas of hypopigmentation at the level of the RPE, focal well-defined or larger and linear areas, determine a focal increased, patchy, linear pattern of autofluorescence. When these alterations of the RPE involve the macular region, the corresponding hyperfluorescent pattern is defined as linear, lace-like, reticular, and speckled when a larger portion of the macula is involved.

Advanced stages of dry AMD are characterized by the atrophy of the RPE, neurosensory retina, and choriocapillaris (Fig. 24.3A–C). Eyes with geographic atrophy present different patterns of abnormal FAF at the posterior pole outside the actual atrophic patches. These are classified into banded, patchy, focal and diffuse patterns.[33,34] However, many alterations are only seen on FAF images without corresponding funduscopically visible alterations. Sometimes the patient with geographic atrophy has preservation of small foveal islands, which provide residual central vision. However, as the foveal island progressively decreases in size, the central visual field gets progressively smaller, so that fewer words or facets of the visual images fit into the functional region, even though relatively good acuity with letters may be preserved. Finally, when the foveal region is completely affected, significant visual loss occurs.

Enhanced perifoveal FAF might lead to an earlier and faster progression to geographic atrophy. In geographic atrophy, smaller patches or large areas of complete RPE atrophy are present. As described by Keilhauer et al.[34] using FAF imaging, the area of RPE atrophy is dark with very sharp borders revealing complete loss of fluorophores (Fig. 24.3B–D). It can be correlated with histologic findings of a sharp margin between the relatively normal retina and choroid and a zone of absence of the outer retinal layers and RPE are seen. A possible explanation of the absence of fluorophores in the area of the atrophy could be the phagocytosis of free lipofuscin derived from the apoptotic cells by macrophages or by RPE cells in the border of the atrophic area. Interestingly, usually a smaller or broader band of significantly increased FAF in the junctional zone is found, indicating a higher level of intracellular lipofuscin and thus a higher risk

for consecutive cell death (Fig. 24.3D). Actually, over time a progression of geographic atrophy is present within the area of previously increased FAF. Such an area may therefore be regarded as incipient atrophy and may therefore serve as novel prognostic determinants for the enlargement of geographic atrophy over time and progressive visual loss.

Fundus Autofluorescence in Neovascular Age-Related Macular Degeneration

Most of the studies using FAF imaging in AMD address the dry form of the disease, and only a few address the wet form.[25,30] Fundus autofluorescence imaging shows decreased

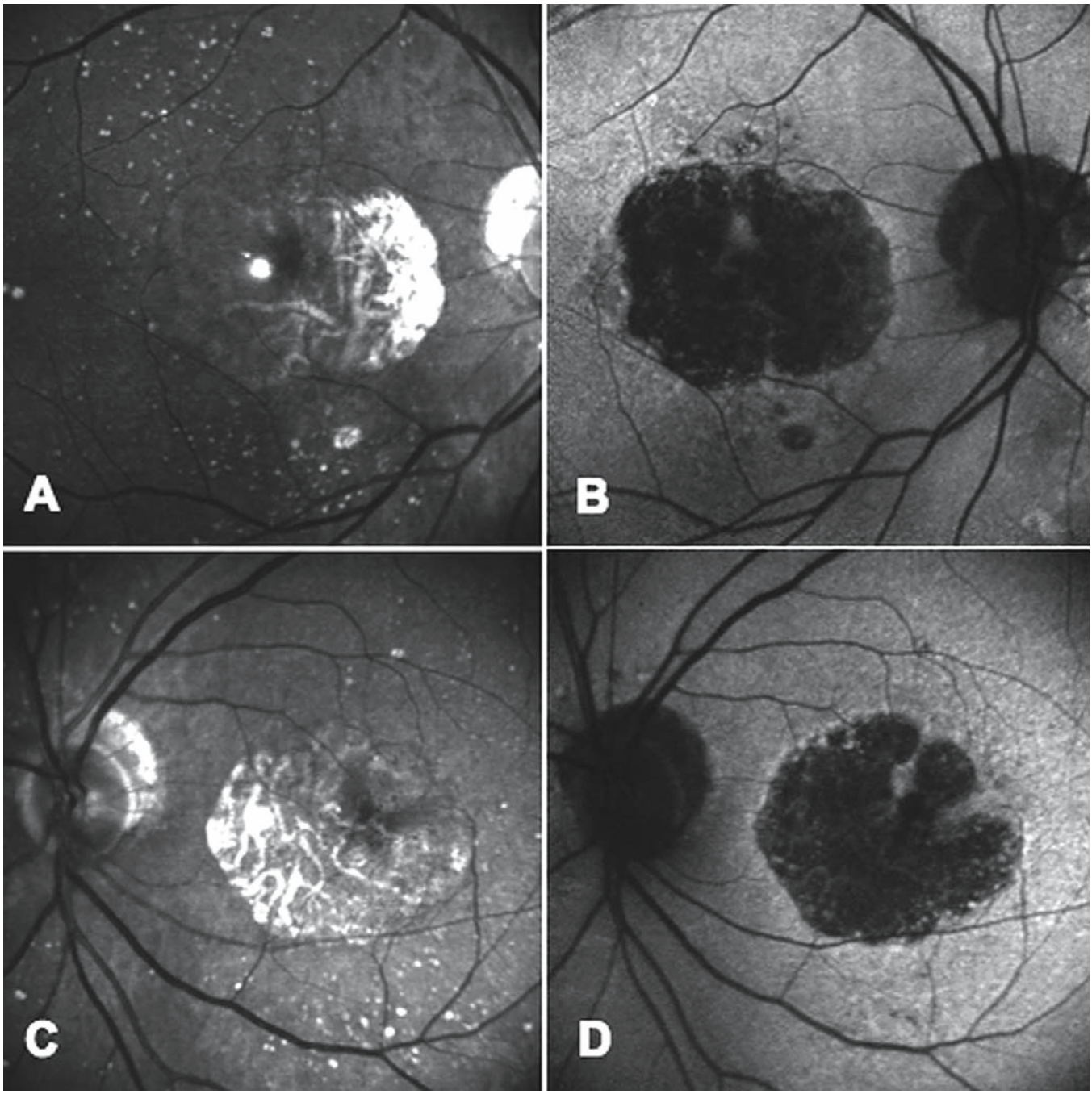

FIG. 24.3. (A,C) The red-free photographs show a central area of geographic atrophy with diffuse hard and soft drusen. (B,D) The corresponding fundus autofluorescence images evidence a central area of hypoautofluorescence with sharp borders revealing complete loss of fluorophores secondary to the absence of RPE cells. (D) A smaller band of significantly increased fundus autofluorescence in the junctional zone is evident, indicating a higher level of intracellular lipofuscin and thus a higher risk for consecutive cell death.

FAF in the majority of eyes with classic choroidal neovascularization (CNV) over the area of the neovascular membrane surrounded by enhanced FAF (Fig. 24.4A–C). Whereas only slightly irregular and decreased FAF is found in occult CNV, these features in autofluorescence imaging correlate with the fluorescein angiogram features. Classic CNVs proliferate in the subsensorial retina over the RPE producing blockage of the FAF also because of the alterations of the photoreceptor RPE complex. The areas of enhanced autofluorescence correspond to the reactive proliferation of the RPE cells around the margin of the subretinal new blood vessels. Occult neovascularization growing under the RPE can produce some alterations in the metabolism of the RPE/photoreceptor complex with decrease production of fluorophores.

Choroidal neovascularization can be associated with bleeding. Hemorrhages in the subsensorial retinal space produce significant decrease in the autofluorescence by blockage. The area corresponding to the hemorrhage becomes hyperautofluorescent in relation with the degradation of blood. This hyperautofluorescence decreases with time in relation to the reabsorption of the bleeding, leaving an hypofluorescent area after complete resolution of the hemorrhage. The final hypofluorescent area can be related to the damage of the photoreceptors and the RPE cells for the toxic effects of the blood.

The end phase of the CNV is the production of a fibrotic scar (Fig. 24.4D,E). It can have different shapes and may contain brown or black pigment. Overlying the fibrotic scar the photoreceptor/RPE complex suffers degeneration with the decreased distribution of lipofuscin in the compromised area. Therefore, FAF imaging shows areas of decreased autofluorescence that correspond to the area of the fibrotic scar. The borders of the fibrotic tissue can be surrounded by enhanced autofluorescence, which corresponds to increased production of lipofuscin and other fluorophores by the pathologic photoreceptor/RPE complex (Fig. 24.4F).

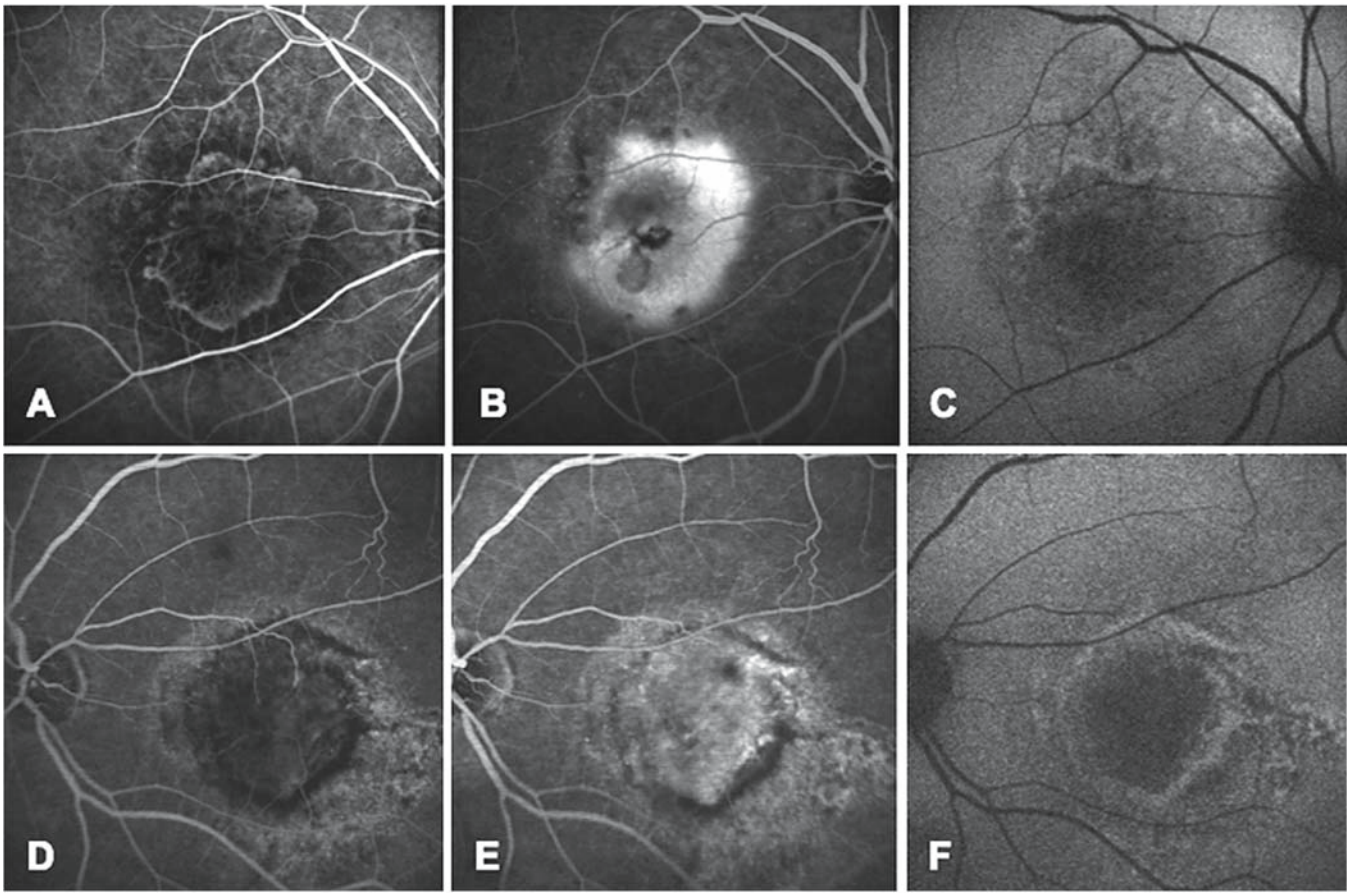

Fig. 24.4. (A) The early-phase fluorescein angiography (FA) shows the presence of a classic subfoveal choroidal neovascularization (CNV). (B) The late-phase FA demonstrates the leakage of the lesion. (C) The corresponding fundus autofluorescence shows decreased fundus autofluorescence over the area of the neovascular membrane surrounded by enhanced fundus autofluorescence. The early- (D) and late- (E) phase FA images demonstrate a disciform lesion. (F) The fundus autofluorescence shows an area of decreased autofluorescence that corresponds to the area of the fibrotic scar. The borders of the fibrotic tissue are surrounded by enhanced autofluorescence, which corresponds to increased production of lipofuscin and other fluorophores by the pathologic photoreceptor/retinal pigment epithelium (RPE) complex.

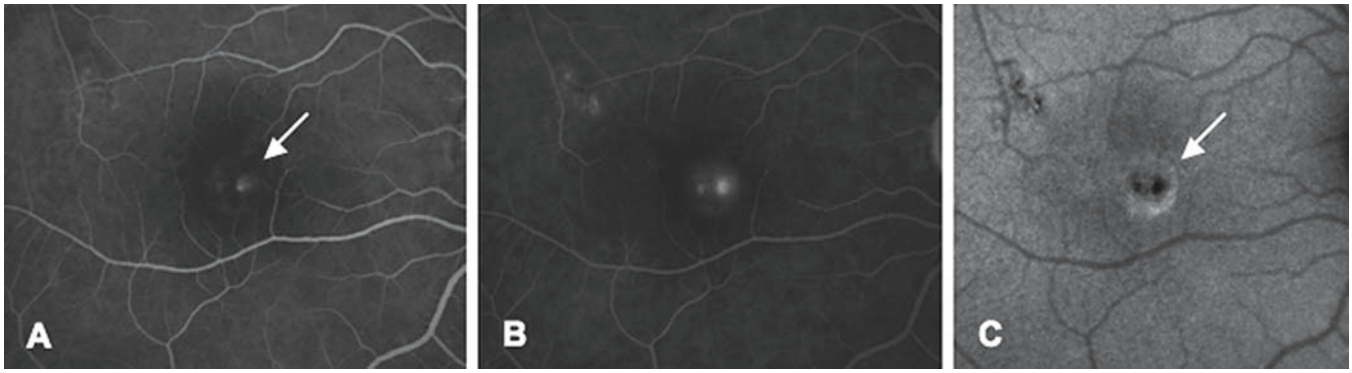

FIG. 24.5. (A) The early-phase FA shows a focal RPE leak (arrow) along the superior temporal vascular arcade. (B) The late-phase FA reveals the area of the RPE detachment. (C) The corresponding fundus autofluorescence image, with fundus camera-based system, shows hypoautofluorescence at the site of the acute RPE leak (arrow).

Fundus Autofluorescence in Central Serous Chorioretinopathy

Central serous chorioretinopathy is another interesting disease with FAF changes. The disease is characterized by idiopathic leaks from the level of the RPE leading to serous detachment of the neurosensory retina; however, small detachments of the RPE may also occur. In the early phases of the disease the visual acuity may be quite good despite the presence of macular detachment, and after resolution the acuity often shows improvement. More chronic forms of CSCR are associated with atrophic and degenerative changes of the retina and RPE and consequently with visual acuity decline. In addition, subretinal deposits are seen, some being ascribed to lipid or proteins like fibrin, while many patients with CSCR have fine dot-like subretinal precipitates that have not been characterized.

Recently, FAF imaging has been used to study the posterior pole alterations in the course of acute and chronic CSCR. The analysis of autofluorescence might be used to study the metabolism of RPE cells leading to a better understanding of the pathophysiology of this condition. In eyes with acute CSCR a hyperautofluorescent spot corresponding to the focal leak at the level of the RPE has been described.[32] However, other studies showed an hypoautofluorescence associated with the focal leak (Fig. 24.5).[35] Adjacent hypo- and hyperautofluorescent areas were also described on the progressed neuroepithelium detachment. These findings seem to confirm the etiopathologic hypothesis proposed of an RPE defect (blow-out), which corresponds to the focal leak evident on fluorescein angiography. The hypofluorescent spot was described both with the scanning laser ophthalmoscope and the fundus camera-based system. In the acute phase, over a period of 1 to 2 months, the area of the detachment was seen to be increasingly hyperautofluorescent.[36] This autofluorescence was diffuse, but also contained discrete granular structures (Fig. 24.6). These granules correspond to the accumulation of material on the outer surface of the retina, visible as yellow flecks on biomicroscopy and on optical coherence tomography (OCT). This material

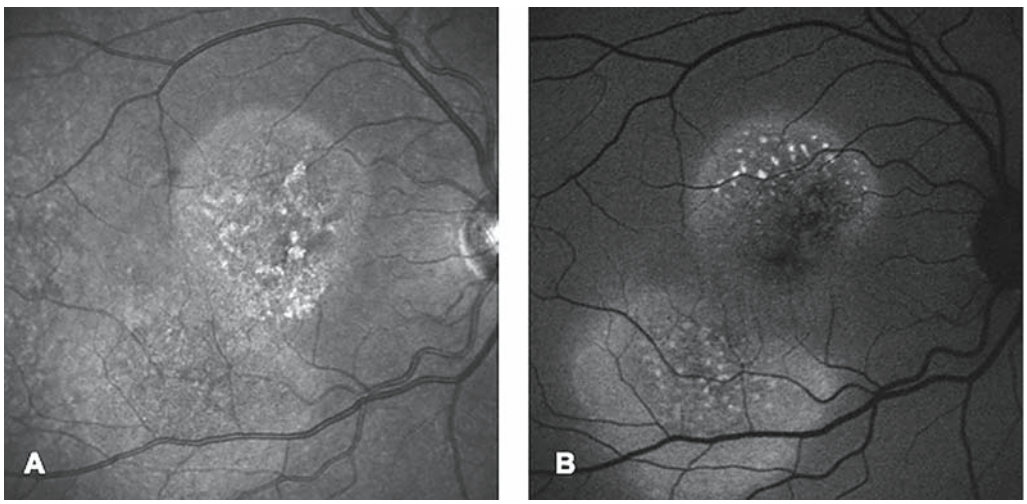

FIG. 24.6. (A) The red-free photograph and (B) the fundus autofluorescence in the acute phase of a chronic central serous chorioretinopathy (CSCR) shows an increased a diffuse hyperautofluorescence in the area of the central and descending detachment with discrete granular structures corresponding to the accumulation of material on the outer surface of the retina.

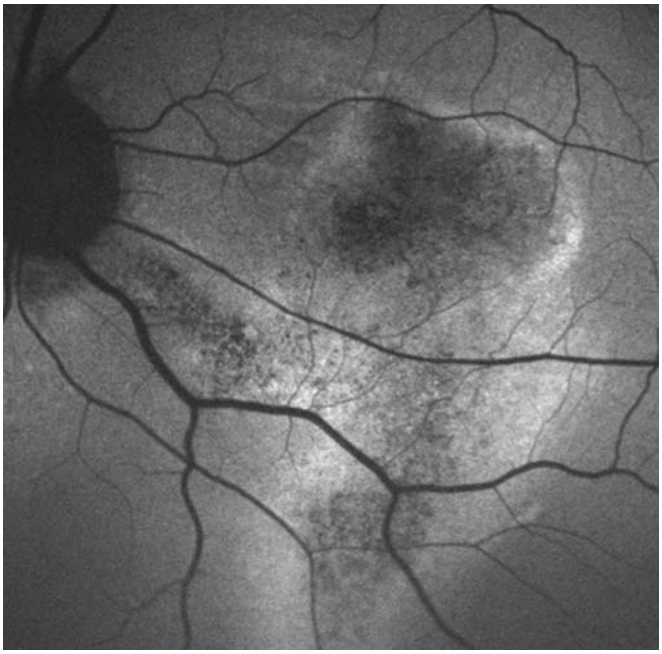

Fig. 24.7. The scanning laser ophthalmoscope autofluorescence imaging in a chronic CSCR demonstrates a central hypofluorescent area corresponding to the progressed retinal detachment and descending tract with hyperautofluorescent borders.

may represent accumulation of photoreceptor outer segments secondary to the lack of direct apposition and phagocytosis by the RPE.[36]

Patients with chronic CSC have varying degrees of atrophy, including broader areas of geographic atrophy in the macula and within fluid tracts descending inferiorly. Descending tracts of more recent origin and the outer borders of more chronic descending tracts were hyperautofluorescent (Fig. 24.7). Patients who were known to have a history of chronic CSCR that had been inactive for several years were left with hypoautofluorescent areas and no hyperautofluorescent regions. The OCT scans on the hypoautofluorescent areas in the central macula confirm the presence of the RPE atrophy and correlate with a decreased visual function.

Fundus Autofluorescence in Angioid Streaks

Angioid streaks are caused by linear crack-like dehiscence in the collagenous and elastic portion of Bruch's membrane, with thinned or atrophic RPE overlying the linear defects in Bruch's membrane. These angioid streaks can be narrow or wide, radial or circumferentially parallel to the nerve. Angioid streaks are visualized in FAF imaging (Fig. 24.8). Recent angioid streaks do not produce alteration in the autofluorescence

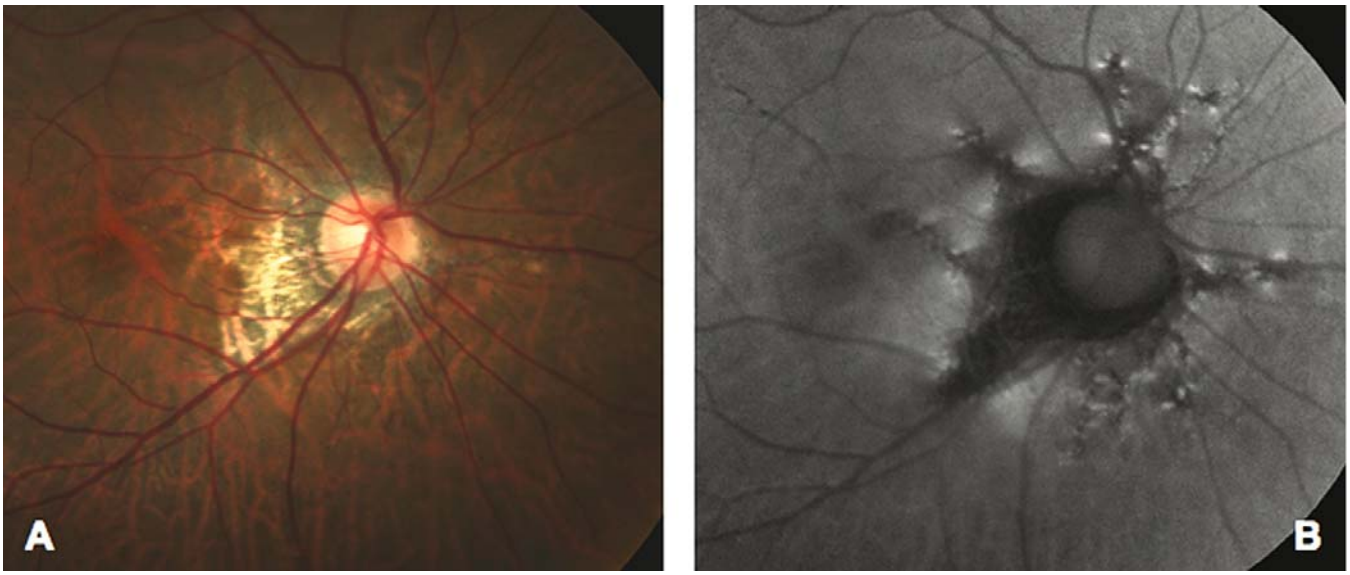

Fig. 24.8. (A) Color photograph shows peripapillary atrophy and angioid streaks. (B) Fundus autofluorescence clearly demonstrates the presence of angioid streaks, as irregular hypofluorescent lines with an enhanced autofluorescence border.

imaging, but as the RPE/photoreceptor complex starts to be atrophic, irregular hypofluorescent lines with an enhanced autofluorescence border appear. Later, these hypofluorescent lines become wider, in response to a larger RPE/photoreceptor complex atrophy. Areas of peripapillary chorioretinal atrophy and disciform scar showed decreased autofluorescence. Solitary or multiple drusen-like spots showed increased autofluorescence. We can also see hyperautofluorescence in the area of neovascularization if there is growing of vessels through the break in the Bruch's membrane. Sometimes the presence of optic nerve drusen can be found associated with the angioid streaks. Optic nerve drusen can be seen as a hyperautofluorescent spot in the head of the optic nerve.

Fundus Autofluorescence in Macular Holes

Macular holes are full-thickness defects in the neurosensory retina. They are discovered after a patient notices blurred vision, metamorphopsia, or often incidentally. The incidence is estimated at 33 per 100,000, with the typical patient being a woman in the seventh decade of life.[37] Reports estimate a female preponderance of 67% to 91%.[38] Macular holes are usually

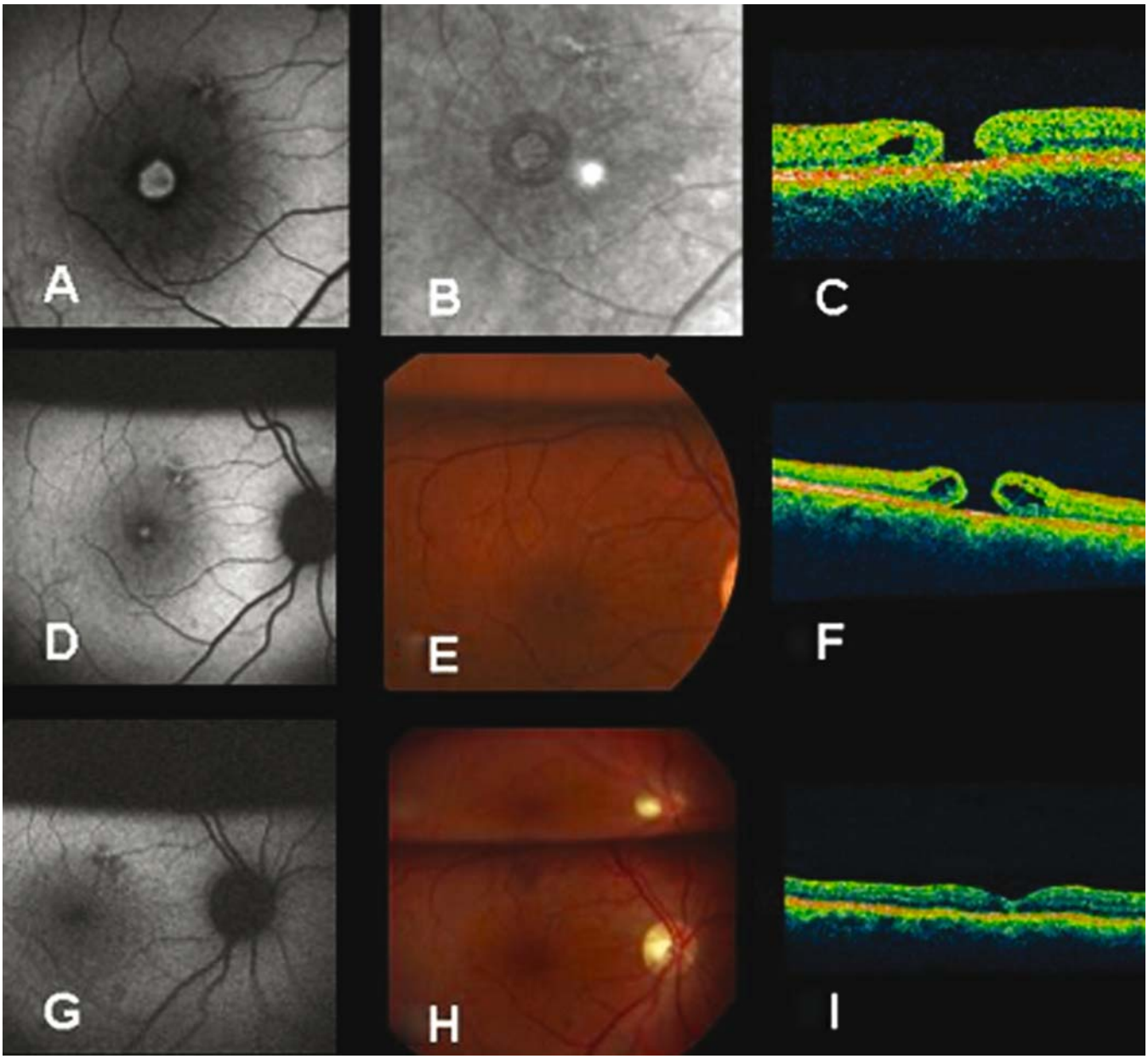

Fig. 24.9. (A) Fundus autofluorescence image of a stage 3 macular hole (note the cuff of subretinal fluid). (B) Red-free photograph (hyperintensity is artifactual). (C) Full-thickness defect on optical coherence tomography (OCT). (D–F) The same eye after vitrectomy with gas bubble with persistent macular hole. (G–I) Closure of hole after second surgery.

unilateral but can be bilateral in 0% to 29% of patients.[37] They can occur secondary to trauma, laser treatment, or macular pucker; however, the majority are idiopathic. The pathogenesis of idiopathic macular holes is controversial, but may be due to tangential or anteroposterior traction. The tight adherence of the vitreous to the macula and specifically the fovea is thought to contribute to the anteroposterior traction.

The current staging system for macular holes was first described by Johnson and Gass[39] in 1988 and later revised by Gass[40] in 1995. Stage IA is an impending macular hole with loss of foveal depression. Biomicroscopic examination characteristically shows a yellow foveal spot between 100 and 200 μm in size. Patients report metamorphopsia or mild visual acuity loss. Stage IB macular hole is defined as expansion of the lipofuscin-colored spot to a ring 200 to 350 μm in diameter.

Forty percent of stage 1 macular holes progress to stage 2.[38] Progression from stage 1 to 2 takes an average of 4.1 months. Stage 2 macular holes are full-thickness defects measuring less than 400 μm seen either centrally or eccentrically within the yellow ring. With time, the yellow ring can become gray or disappear altogether. This is thought to occur secondary to a neurosensory detachment surrounding the hole. Patients typically complain of increased metamorphopsia or further decreased central vision. However, there may be a paradoxical improvement in visual acuity from partial release of vitreofoveal traction.

As the size of the full-thickness hole grows to greater than 400 μm and a posterior hyaloid separation from the macula develops, it is classified as a stage 3 macular hole. An overlying operculum may or may not be present. On biomicroscopy, the stage 3 macular hole has drusen-like deposits on the retinal pigment epithelium and a cuff of subretinal fluid. A stage 4 macular hole is similar to a stage 3 except a complete posterior vitreous detachment is present as evidenced by a Weiss ring.

The diagnosis of macular holes has traditionally been based on clinical exam with or without ancillary tests. Some clinical tests include the Watzke-Allen test, laser-aiming beam test, and Amsler grid test. However, the diagnosis of macular hole and more specifically differentiation from pseudohole and lamellar macular hole is often difficult without additional tests. Fluorescein angiography has been used for years to aid in diagnosis. More recently OCT has become the standard of care in diagnosing and staging macular holes. Other tests useful in the management of macular holes include high-resolution ultrasound, reflective imaging using scanning laser ophthalmoscope, and recently FAF.

Stage 1 macular holes may show normal or slightly increased autofluorescence. von Ruckmann et al.[41] described autofluorescence in six patients with stage 1 macular holes. Three eyes showed normal FAF, while the other three had increased intensity equal to that of the parafoveal area.

Stage 2, 3, and 4 macular holes have hyperintense autofluorescence at the full-thickness defect.[42] Stage 2 is distinguished by its smaller size from stages 3 and 4. The cuff of subretinal fluid is seen as a ring of hypofluorescence surrounding the hyperintensity (Fig. 24.9). The presence of an operculum overlying the full-thickness macular hole causes a focal hypointensity in the macular hole due to the blockage of excitation (Fig. 24.10). Fundus autofluorescence is a useful adjunct postoperatively to confirm closure of the macular hole (Fig. 24.9D–I).[43]

It is often difficult to distinguish between a pseudo macular hole and an actual macular hole on clinical exam.

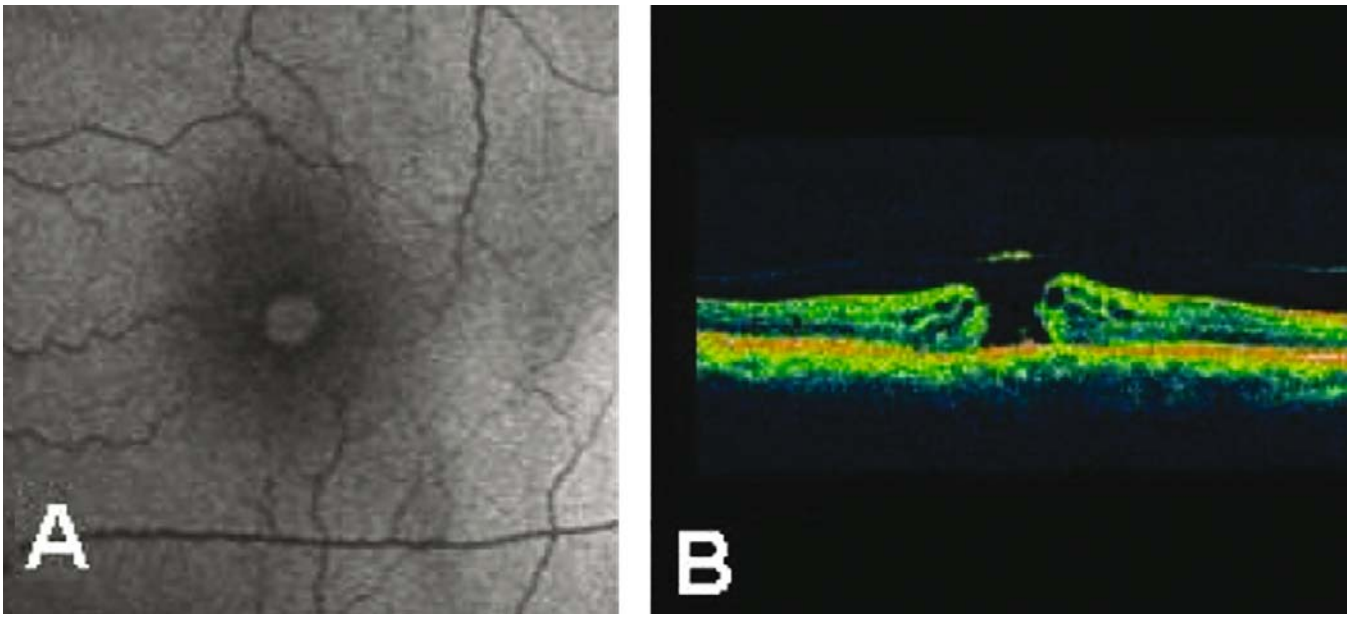

FIG. 24.10. (A) Fundus autofluorescence image of a stage 4 macular hole with an overlying operculum. (B) Optical coherence tomography demonstrates the full-thickness defect with an operculum.

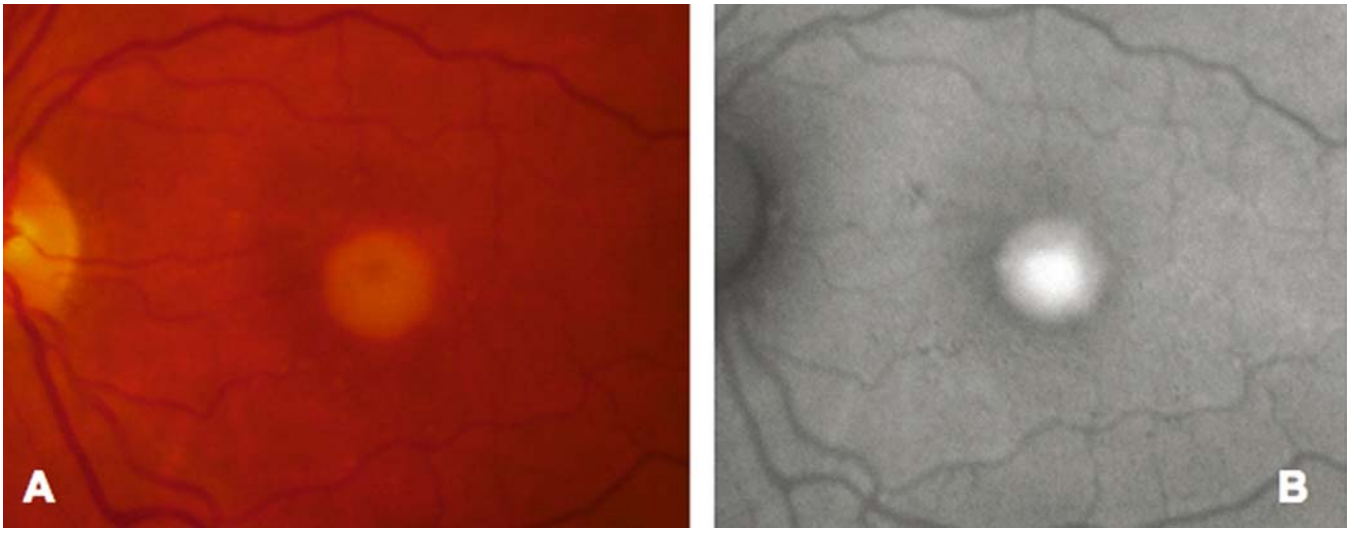

FIG. 24.11. (A) The color photograph shows yellowish deposits in the central macula in young patients (egg yolk–like lesion) characterizing the vitelliform macular dystrophy or Best's dystrophy. (B) The corresponding fundus autofluorescence demonstrates a high level of autofluorescence secondary to accumulation of fluorophores in the subretinal space.

Fundus autofluorescence is a useful modality for distinguishing between the two. Patients who on fundus exam appear to have a full-thickness macular hole (pseudo macular hole) at the autofluorescent imaging show a normal FAF. The lack of autofluorescence indicates the absence of a full-thickness neurosensory retinal defect or the presence of a coexistent RPE defect. The lack of RPE abnormality on biomicroscopy is very suggestive of a pseudohole, and this may be confirmed by OCT. The intact neurosensory retina in the pseudohole yields a normal macular autofluorescence pattern.

Multiple studies have shown success of vitrectomy with tamponade with or without internal limiting membrane peel for treatment of subacute macular holes. On average, chronic macular holes of two or more years of duration do not fair as well.[44–46] However, some chronic macular hole repairs do have significant improvement in vision. The worse overall response is possibly due to RPE atrophy that develops under the neurosensory detachment surrounding the hole.

Autofluorescence has been shown to be a useful modality to distinguish and demarcate RPE loss in geographic atrophy from dry AMD. In the future, autofluorescence may be able to help quantitate RPE atrophy in eyes with chronic macular holes. Although not reported to date, the test potentially could be used to differentiate between eyes that are likely to benefit from surgery and those with a worse surgical prognosis.

Macular holes are a common retinal pathology that often require adjunctive tests to confirm the diagnosis. Optical coherence tomography has recently become widely used for staging and diagnosing macular holes. Another useful modality with a unique and reproducible pattern that can help distinguish this entity from other vitreoretinal pathologies is FAF, a noninvasive test with minimal risk. In the future, this may help to select eyes most likely to benefit from surgical treatment of macular holes.

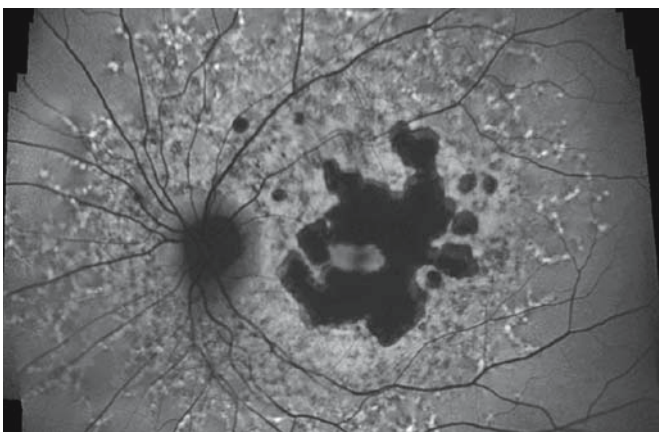

FIG. 24.12. Fundus autofluorescence of Stargardt's disease with central geographic atrophy surrounded by focal hyperfluorescent flecks.

Fundus Autofluorescence in Macular and Retinal Dystrophies

Mutations in several genes produce increased accumulation of lipofuscin and are related to the etiology of different macular and retinal dystrophies. Because of the excessive accumulation of lipofuscin present in diseases such as Stargardt's or Best's disease, we can use FAF imaging to confirm the diagnosis in some macular and retinal dystrophies.[20–25]

Vitelliform Macular Dystrophy

Vitelliform macular dystrophy or Best's dystrophy is a rare condition with autosomal dominant transmission. It is characterized by yellowish deposits in the central macula in young patients (egg yolk–like lesion). Later in the disease it is common to see a partial or almost complete resorption of the yellowish material. The electro-oculogram shows generalized abnormalities, secondary to mutation of the chloride channel protein, bestrophin. Histopathologic analysis of vitelliform macular dystrophy demonstrates widespread accumulation of lipofuscin in RPE cells across the fundus. High levels of FAF detected at the center of the macula in Best's disease corresponded well with the intense signal from the pseudohypopyon (Fig. 24.11).

The impaired phagocytosis of the outer segments by the RPE has the end result of a deposit of A2-E fluorescent precursors or other unidentified fluorophores in the subretinal space. There are three patterns of autofluorescence in the posterior pole in the late stages of the disease[23,25]: a spokelike pattern, a diffuse pattern, and a combination of these two patterns. Vitelliform macular dystrophy is not limited to the macula. The autofluorescence photographs show that lipofuscin accumulation also occurs later in the disease, often in a fractal pattern, extending toward the periphery.[23,25]

Stargardt's Disease

Mutations in the gene encoding *ABCR* are responsible for a variety of autosomal recessive retinal degenerative diseases, including Stargardt's macular dystrophy, fundus flavimaculatus, cone-rod dystrophy, and retinitis pigmentosa.[20–22]

In Stargardt's disease focal flecks typically show bright, increased FAF and may fade as atrophy develops (Fig. 24.12). This reflects abnormal regions of RPE engorged with abnormal lipofuscin-like material. In addition to high FAF, Lois et al.[47] also described normal and low autofluorescence. A low level of FAF in such eyes was associated with peripheral cone and rod dysfunction, whereas eyes with normal or high levels of FAF have normal peripheral cone and rod function. There was no relationship between levels of FAF and macular dysfunction. This imaging technique is able to confirm the diagnosis of Stargardt's disease due to the specific pattern.

Conclusion

Fundus autofluorescence imaging is a noninvasive diagnostic tool that visualizes age- and disease-related metabolic changes of the RPE. The autofluorescence signal mainly derives from dominant fluorophores in lipofuscin granules of the RPE. Lipofuscin accumulation represents a common downstream pathogenetic pathway in many retinal and macular disease entities. This recently introduced adjunct imaging technique represents one of various diagnostic tools together with fundus photography, angiography with fluorescein and indocyanine green, and OCT. In particular, FAF contributes significantly to our understanding of the pathophysiology and treatment of various retinal diseases.

References

1. Delori FC, Dorey CK, Staurenghi G, Arend O, Goger DG, Weiter JJ. In vivo fluorescence of the ocular fundus exhibits retinal pigment epithelium lipofuscin characteristics. Invest Ophthalmol Vis Sci 1995;36:718–729.
2. Delori FC, Staurenghi G, Arend O, Dorey CK, Goger DG, Weiter JJ. In vivo measurement of lipofuscin in Stargardt's disease-fundus flavimaculatus. Invest Ophthalmol Vis Sci 1995;36:2327–2331.
3. Feeney-Burns L, Berman ER, Rothman H. Lipofuscin of human retinal pigment epithelium. Am J Ophthalmol 1980;90:783–791.
4. Weiter JJ, Delori FC, Wing GL, Fitch KA. Retinal pigment epithelial lipofuscin and melanin and choroidal melanin in human eyes. Invest Ophthalmol Vis Sci 1986;27:145–152.
5. Dorey KC, Wu G, Ebenstein D, Garsd A, Weiter JJ. Cell loss in aging retina: relationship to lipofuscin accumulation and macular degeneration. Invest Ophthalmol Vis Sci 1989;30:1691–1699.
6. Wing GL, Blanchard GC, Weiter JJ. The topography and age relationship of lipofuscin concentration in the retinal pigment epithelium. Invest Ophthalmol Vis Sci 1978;17:601–607.
7. Weiter JJ, Delori FC, Wing GL, Fitch KA. Retinal pigment epithelial lipofuscin and melanin and choroidal melanin in human eyes. Invest Ophthalmol Vis Sci 1986;27:145–152.
8. Dorey CK, Wu G, Ebenstein D, Garsd A, Weiter JJ. Cell loss in the aging retina: relationship to lipofuscin accumulation and macular degeneration. Invest Ophthalmol Vis Sci 1989;30:1691–1699.
9. von Rückmann A, Fitzke FW, Bird AC. Distribution of fundus autofluorescence with a scanning laser ophthalmoscope. Br J Ophthalmol 1995;79:407–412.
10. Bellmann C, Holz FG, Schapp O, Volcker HE, Otto TP. Topography of fundus autofluorescence with a new confocal scanning laser ophthalmoscope [in German]. Ophthalmologe 1997;94:385–391.
11. Holz FG, Bellmann C, Margaritidis M, Schutt F, Otto TP, Volcker HE. Patterns of increased in vivo fundus autofluorescence in the junctional zone of geographic atrophy of the retinal pigment epithelium associated with age-related macular degeneration. Graefes Arch Clin Exp Ophthalmol 1999;237:145–152.

12. Bindewald A, Jorzik JJ, Loesch A, Schutt F, Holz FG. Visualization of retinal pigment epithelial cells in vivo using digital high-resolution confocal scanning laser ophthalmoscopy. Am J Ophthalmol 2004;137:556–558.
13. Delori FC, Fleckner MR, Goger DG, Weiter JJ, Dorey CK. Autofluorescence distribution associated with drusen in age-related macular degeneration. Invest Ophthalmol Vis Sci 2000;41:496–504.
14. Kennedy CJ, Rakozcy PE, Constable IJ. Lipofuscin in the retinal pigment epithelium: a review. Eye 1995;9:763–771.
15. Katz ML. Incomplete proteolysis may contribute to lipofuscin accumulation in the retinal pigment epithelium. Adv Exp Med Biol 1989;266:109–116.
16. Eldred GE, Katz ML. Fluorophores of human retinal pigment epithelium: separation and spectral characterization. Exp Eye Res 1988;47:71–86.
17. Kitagawa K, Nishida S, Ogura Y. In vivo quantitation of autofluorescence in human RPE. Ophthalmologica 1989;199:116–121.
18. Green WR, Enger C. Age-related macular degeneration histopathologic studies. Ophthalmology 1993;100:1519–1535.
19. von Rückmann A, Fizke FW, Bird AC. Fundus autofluorescence in age related macular disease imaged with a laser scanning ophthalmoscope. Invest Ophthalmol Vis Sci 1997;38:478–486.
20. Allikmets R, Shroyer NF, Singh N, et al. Mutation of the Stargardt disease gene (ABCR) in age-related macular degeneration. Science 1997;277:1805–1807.
21. Delori FC, Staurenghi G, Arend O, et al. In vivo measurement of Stargardt's disease—fundus flavimaculatus. Invest Ophthalmol Vis Sci 1995;36:2327–2331.
22. Eagle RC, Lucier AC, Bernadino VB, Janoff M. Retinal pigment epithelial abnormalities in fundus flavimaculatus; a light and electron microscopical study. Ophthalmology 1980;87: 1189–2000.
23. Frangieh GT, Green WR, Fine SL. A histopathologic study of Best's macular dystrophy. Arch Ophthalmol 1982;100:1115–1121.
24. Lopez PF, Maumenee IH, de la Cruz Z, Green WR. Autosomal dominant fundus flavimaculatus: clinicopathologic correlation. Ophthalmology 1990;97:798–809.
25. Framme C, Roider J, Sachs HG, Brinkmann R, Gabel VP. Noninvasive Imaging and Monitoring of retinal pigment epithelium patterns using fundus autofluorescence—review. Curr Med Imag Rev 2005;1:89–103.
26. Eldred GE, Lasky MR. Retinal age-pigments generated by self-assembling lysosomotropic detergents. Nature 1993;361:145–152.
27. Eldred GE. Age pigment structure. Nature 1993;364(6436):396.
28. Parish CA, Hashimoto M, Nakanishi K, et al. Isolation and one-step preparation of A2E and iso-A2E, fluorophores from human retinal pigment epithelium. Proc Natl Acad Sci USA 1998;95:14609–14613.
29. Holz FG, Schutt F, Kopitz J, et al. Inhibition of lysosomal degradative functions in RPE cells by a retinoid component of lipofuscin. Invest Ophthalmol Vis Sci 1999;40:737–743.
30. Spaide RF. Fundus autofluorescence and age-related macular degeneration. Ophthalmology 2003;110:392–399.
31. Holz FG, Bellmann C, Rohrschneider K, Burk ROW, Volcker HE. Simultaneous confocal scanning laser fluorescein- and indocyanine green angiography. Am J Ophthalmol 1998;125:227–236.
32. von RRückmann A, Fitzke FW, Fan J, Halfyard A, Bird AC. Abnormalities of fundus autofluorescence in central serous retinopathy. Am J Ophthalmol 2002;133:780–786.
33. Bindewald A, Bird AC, Dandekar SS, et al. Classification of fundus autofluorescence patterns in early age-related macular disease. Invest Ophthalmol Vis Sci 2005;46:3309–3314.
34. Keilhauer CN, Delori FC. Near-infrared autofluorescence imaging of the fundus: visualization of ocular melanin. Invest Ophthalmol Vis Sci 2006;47(8):3556–3564.
35. Staurenghi G, Wolf S, Holz FG, Bellman C, Staudt S, Schutt F, Volcker HE. Fundus autofluorescence and development of geographic atrophy in age-related macular degeneration. Invest Ophthalmol Vis Sci 2001;42:1051–1056.
36. Eandi CM, Ober M, Iranmanesh R, et al. Acute central serous chorioretinopathy and fundus autofluorescence. Retina 2005;25:989–993.
37. Spaide RF, Klancnik JM Jr. Fundus autofluorescence and central serous chorioretinopathy. Ophthalmology 2005;112:825–833.
38. Sjaarda RN, Thompson JT. Macular hole. In: Ryan SJ, ed. Retina. Philadelphia: Elsevier, 2006.
39. Johnson RN, Gass JDM. Idiopathic macular holes. Observations, stages of formation, and implications for surgical intervention. Ophthalmology 1988;95:917–924.
40. Gass JDM. Reappraisal of biomicroscopic classification of stages of development of a macular hole. Am J Ophthalmol 1995;119:752–759.
41. von Ruckmann A, Fitzke FW, Gregor ZJ. Fundus autofluorescence in patients with macular holes imaged with a laser scanning ophthalmoscope. Br J Ophthalmol 1998;82:346–351.
42. Ciardella AP, Lee GC, Langton K. Autofluorescence as a novel approach to diagnosing macular holes. Am J Ophthalmol 2004;137:956–959.
43. Framme C, Roider J. Fundus autofluorescence in macular hole surgery. Ophthalmic Surg Lasers 2001;32:383–390.
44. Roth DB, Smiddy WE, Feuer W. Vitreous surgery for chronic macular holes. Ophthalmology 1997;104:2047–2052.
45. Thompson JT, Sjaarda RN, Lansing MB. The results of vitreous surgery for chronic macular holes. Retina 1997;17:493–501.
46. Lois N, Halfyard AS, Bird AC, Holder GE, Fitzke FW. Fundus autofluorescence in Stargardt macular dystrophy—fundus flavimaculatus. Am J Ophthalmol 2004;138:55–63.

25
Future of Optical Coherence Tomography: Ultrahigh-Resolution Versus Standard-Resolution OCT

Jay S. Duker, Lelia Adelina Paunescu, and James G. Fujimoto

Optical coherence tomography (OCT) is a noninvasive technology that enables high-resolution cross-sectional imaging of tissue by measuring backscattered light.[1] Optical coherence tomography imaging is analogous to ultrasound B-mode imaging but uses light instead of sound. By performing multiple longitudinal scans at different transverse locations, a two-dimensional (2D) scanned image is obtained. Noncontact, noninvasive human eye imaging using OCT proved to advance ophthalmic diagnostics by enabling direct cross-sectional retinal layer visualization and quantification.[2]

A third-generation commercial OCT (Stratus OCT, Carl Zeiss Meditec, Dublin, CA) provides high-resolution images with 8-μm resolution and 512 A-scans per image, acquired in about 1 second. The image produced by Stratus OCT system is generated using ~10-μm axial and 20-μm transverse resolution in the eye and consists of 1024 axial and 512 transverse A-scans per image, as indicated in the user manual for Stratus OCT.

Recent improvements to the OCT technology allowed ultrahigh-resolution (UHR) images of the eye. The first demonstration of UHR OCT imaging in ophthalmology was published by Drexler et al.[3] The UHR OCT provides images with outstanding resolution, with 2 to 3 μm axial and 15 to 20 μm transverse resolution and 3000 axial and 600 transverse A-scans per image in vivo in the human eye. The UHR OCT can provide significantly higher resolutions as fine as ~1 μm for laboratory imaging in animal models. A review by Fujimoto[4] presents the technical improvements and clinical applications, especially in ophthalmology, of the UHR OCT.

The retinal morphology of the intraretinal layers was previously well correlated with the histologic morphology of the retina in the macula region.[5] In the OCT images, the most optically backscattering layers are the nerve fiber layer (NFL) and the retinal pigment epithelium (RPE) represented as red or white false color in the OCT images.[6] The inner (IPL) and outer plexiform (OPL) layers are more backscattered than the inner (INL) and outer nuclear (ONL) layers. The low backscattering layers are the ganglion cell layer (GCL), INL, and ONL, which are seen as blue or black false color in the OCT images. The external limiting membrane (ELM) is the thin backscattering layer below the ONL. The junction between the photoreceptor inner segment (PRIS) and outer segment (PROS) is a thin highly backscattering layer below the ELM. The reflection between the inner segment and outer segment of this junction is considered to be the result of the abrupt boundary between the inner segments and the highly organized structure of the outer segments containing stacks of membranous disc that are rich in the visual pigment rhodopsin.[7] This layer was thought previously to be the RPE layer.[3] The choriocapillaris and choroid layers are highly vascular and are visualized as a strongly optically backscattering layer. Due to these vascular structures, the imaging for deeper structures is limited.

Ultrahigh resolution OCT enhances the ability to detect subtle structural abnormalities associated with early disease as well as improve the potential to image progressive changes in pathologies affecting the retina. The UHR OCT images make possible detection of the intermediate layers of the retina, such as the ganglion cell, inner plexiform, inner nuclear, outer plexiform, and outer nuclear layers as well as enabling differentiation of the choriocapillaris and choroid from the RPE, which is not possible with any previous device. The UHR OCT image of the macula area in a normal eye shows a significant improvement over the images obtained with the most recent commercial OCT, Stratus OCT. Figure 25.1 shows a comparison of a macula image of a 22-year-old woman with normal vision obtained with the Stratus OCT and UHR OCT at the same visit.

Comparison of the high-resolution Stratus OCT image (Fig. 25.1A) to the UHR OCT image (Fig. 25.1B) of the normal human macula shows that the GCL and ELM are not clearly visualized in the Stratus OCT image.

A long-standing record of studies using previous generations of OCT shows that this technology is able to detect various retinal diseases such as macular holes, diabetic retinopathy, macular degeneration, retinal pigment epithelial detachment, chorioretinal inflammatory disease, retinal dystrophies, retinal trauma, and diseases of the optic nerve such as glaucoma, optic disc pitting, and optic disc swelling.[8]

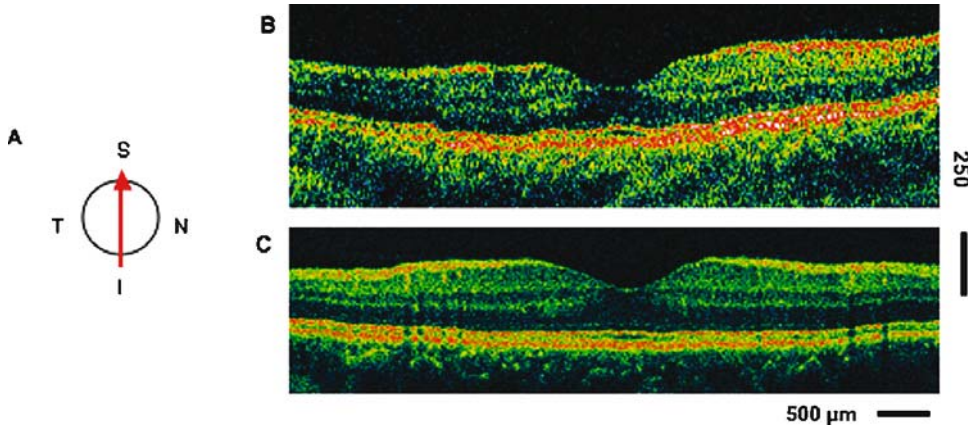

FIG. 25.1. Stratus OCT and ultrahigh-resolution (UHR) OCT of a normal eye scanned at the same visit. Graphical representation (A) of the OCT scanning orientation. S, superior; N, nasal; I, inferior; T, temporal. (B) Stratus OCT image. (C) UHR OCT image.

Retinal Clinical Imaging

In the retina, previous generations of OCT proved to be useful in the diagnosis and monitoring of different disease such as macular holes, macular edema, and retinal detachment,[9] and OCT can provide structural assessment of the macula pre- and postoperatively.[10] Optical coherence tomography may be useful in screening and monitoring patients with diabetic retinopathy.[10] It can also assess retinal thickness, which is automatically calculated between the anterior and posterior boundaries of the retina. The retinal thickness can be used as a measure of retinal pathologies such as edemas and retinopathies where the retinal thickness increases, or of atrophy where the retinal thickness decreases.

Stratus OCT, with its enhanced image quality, made possible clear differentiation of the affected retinal layers. As an example of the improvements achieved by both Stratus OCT as well as UHR OCT, a macular cyst from a patient suffering from branch retinal vein occlusion (BRVO) is well defined in both Stratus OCT and UHR OCT images due to high-resolution scans (Fig. 25.2).

However, due to higher resolution, the UHR OCT image shows much more detail in the affected area. An example of such improvements due to resolution is detection of cyst-like spaces in a 59-year-old white woman diagnosed with cystoid macular edema/blunting of foveal reflex in the left eye (Fig. 25.3).

Figure 25.4 shows images taken from a 72-year-old woman diagnosed with age-related macular degeneration (AMD) in

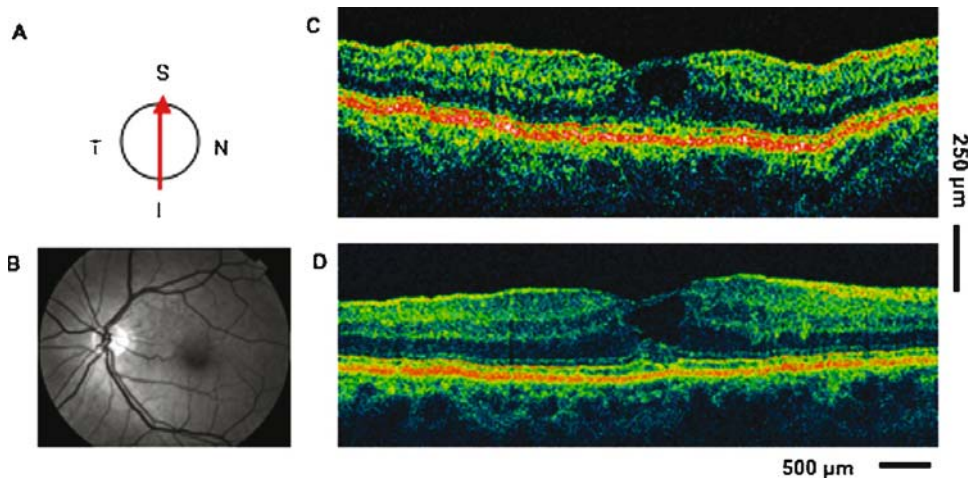

FIG. 25.2. Stratus OCT and UHR OCT of macular cyst and branch retinal vein occlusion (BRVO) in the left eye. Graphical representation (A) of the OCT scanning orientation (C,D). S, superior; N, nasal; I, inferior; T, temporal. (B) Red-free photograph. (C) Stratus OCT image. (D) UHR OCT image.

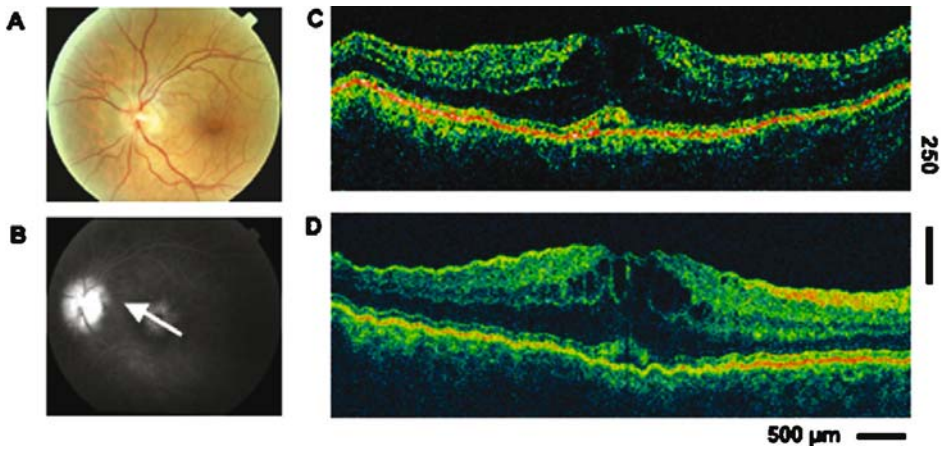

FIG. 25.3. Stratus OCT and UHR OCT of cystoid macular edema. Both image were acquired at the same visit and location in the eye. (A) Color fundus. (B) Fluorescein angiogram showing the orientation of the OCT scanning (210 degrees). (C) Stratus OCT image. (D) UHR OCT image.

the left eye. Both Stratus OCT and UHR OCT images reveal clearly the disruptions of the RPE layer as well as the photoreceptor inner and outer segments characteristic to this disease. The boundary between the photoreceptor inner and outer segments is not observable in the fovea.

Optical coherence tomography technology has been previously proven clinically important for tracking disease changes and progression over time.[11,12] Both Stratus OCT and UHR OCT are capable of following patients over time and tracking disease progression.

Figures 25.5 and 25.6 show images obtained from a 50-year-old Hispanic man suffering from central serous chorioretinopathy (CSCR) in his left eye. The OCT scanning orientation was the same for both systems and on both office visits. Stratus OCT and UHR OCT images show serous fluid accumulation under the sensory retina producing retinal detachment. All the retinal layers appear to be normal.

Figure 25.6 shows CSCR resolving spontaneously after 5 weeks apparent in Stratus OCT as well as UHR OCT images by the decrease in the retinal thickness due to decrease in the fluid under the retina. The recovery showed in the OCT images correlates with the recovery of the visual function.

In both Figures 25.5 and 25.6, the higher resolution of the UHR OCT image allows the ELM and inner segment/outer segment (IS/OS) photoreceptor layers to be seen showing them intact. This is not easily apparent in the Stratus OCT images.

Although Stratus OCT made significant improvements in the OCT technology, UHR proved to give enhanced visualization of the fine internal retinal structures characteristic

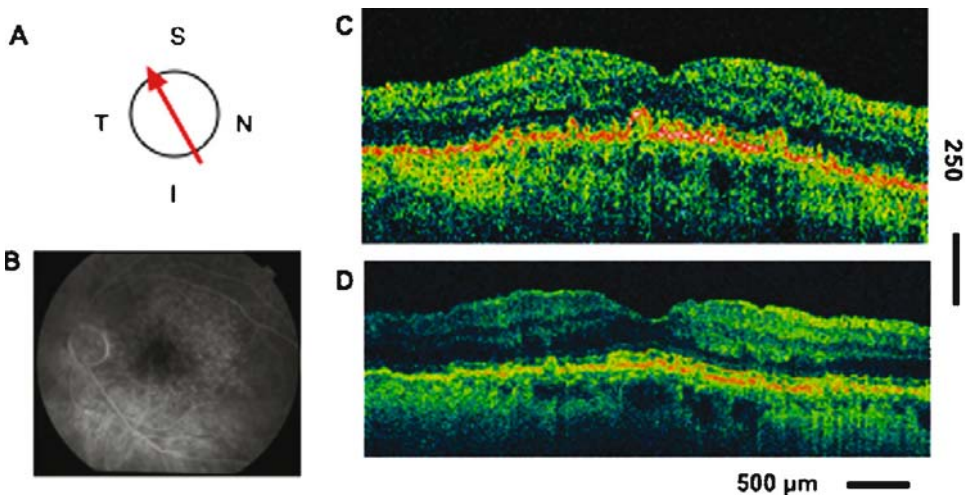

FIG. 25.4. Stratus OCT and UHR OCT dry of age-related macular degeneration. Graphical representation (A) of the OCT scanning orientation (C,D). S, superior; N, nasal; I, inferior; T, temporal. (B) Fluorescein angiogram. (C) Stratus OCT image. (D) UHR OCT image.

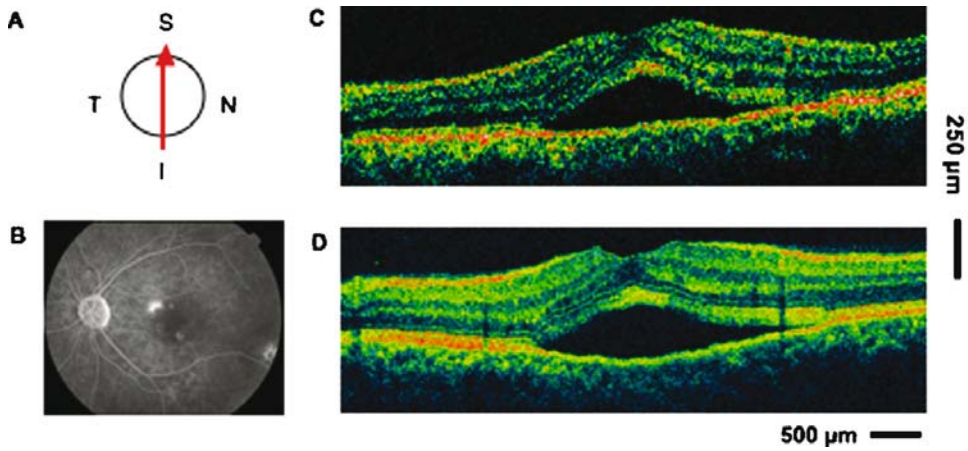

FIG. 25.5. Stratus OCT and UHR OCT of central serous chorioretinopathy. Graphical representation (A) of the OCT scanning orientation (C,D). S, superior; N, nasal; I, inferior; T, temporal. (B) Fluorescein angiogram. (C) Stratus OCT image. (D) UHR OCT image.

of different pathologies.[13] Moreover, the UHR OCT images reveal retinal structures that are not easily detected on the Stratus OCT images.[7,13]

Retinal or RPE detachments and macular lesions such as holes and fibrosis are detected on an OCT image. Recent improvements in resolution facilitate distinguishing RPE and choriocapillaris, providing useful information in AMD and choroidal neovascularization.

An example of macular edema due to retinal vein occlusion in a 79-year-old white man is shown in Figure 25.7. Both Stratus OCT and UHR OCT images exhibit resolution allowing small irregularities in the inner nuclear layer to be visualized on the left side of the OCT images. These irregularities correspond to the occlusion as shown in the fluorescein angiogram.

Another example of a 72-year-old white woman with history of BRVO in the right eye who is suffering from dry AMD, posterior vitreous detachment, punctate drusen in both eyes, and epiretinal membrane in the right eye is presented in Figure 25.8. Stratus OCT and UHR OCT images illustrate the appearance of a hole in the fovea region that is due to posterior vitreous detachment. Disruptions in the RPE layer and atrophy of the inner and outer segments, noted in both Stratus OCT and UHR OCT images, cause the highly backscattering IS/OS junction not to be clearly differentiated. Small irregularities in the retinal NFL with evidence of epiretinal membrane formation can also be observed in the UHR OCT image as well as in the Stratus OCT.

Both Stratus OCT as well as UHR OCT images show the location and structure of the vasculature characteristic of the choroidal neovascularization (CNV) that produces a focal increase in retinal thickness and alters the normal contour of the foveal pit in this region (Fig. 25.9). However, the UHR OCT image (Fig. 25.9D) with its ultrahigh resolution can provide clearer details of the contour of the vasculature and the

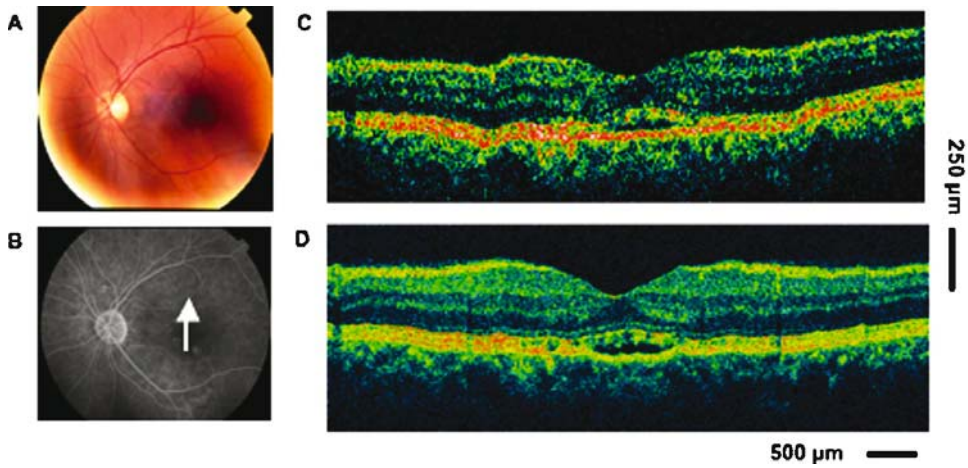

FIG. 25.6. Stratus OCT and UHR OCT of central serous chorioretinopathy resolving after 5 weeks. (A) Color fundus. (B) Fluorescein angiogram showing the orientation of the OCT scanning. (C) Stratus OCT image. (D) UHR OCT image.

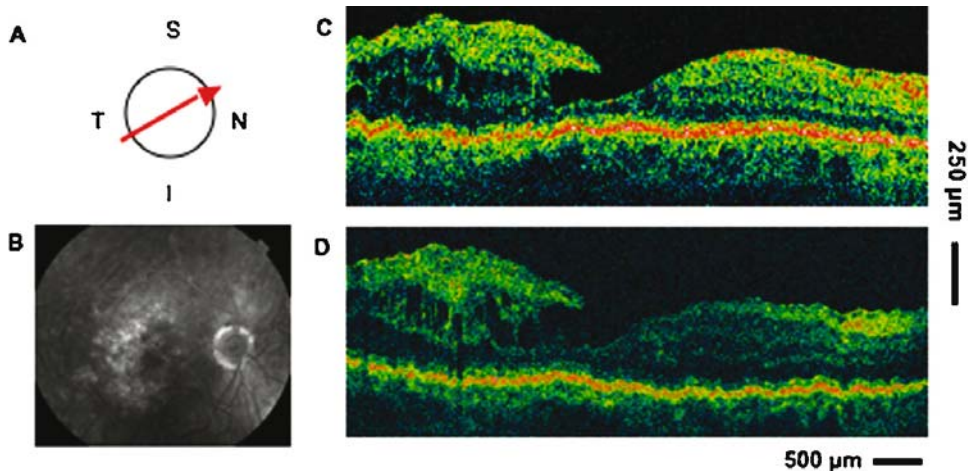

FIG. 25.7. Stratus OCT and UHR OCT of retinal vein occlusion in the right eye with persistent macular edema. Graphical representation (A) of the OCT scanning orientation (C,D). S, superior; N, nasal; I, inferior; T, temporal. (B) Fluorescein angiogram. (C) Stratus OCT image. (D) UHR OCT image.

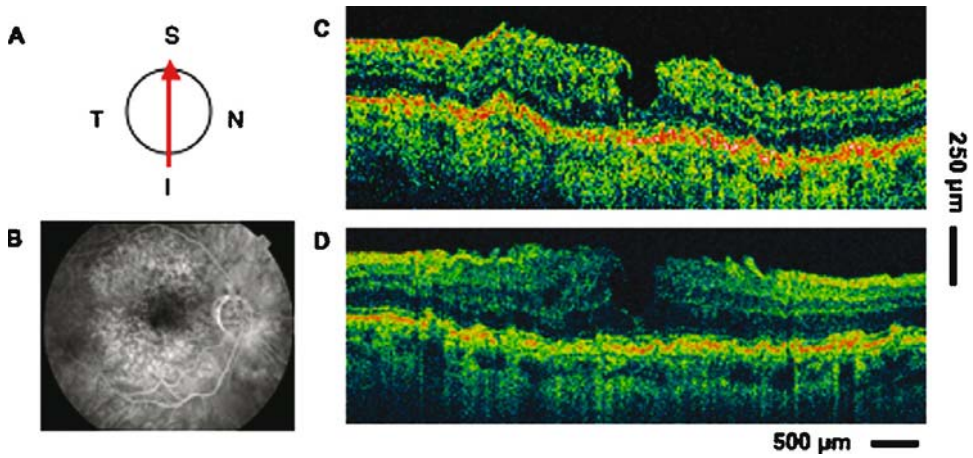

FIG. 25.8. Stratus OCT and UHR OCT of dry age-related macular degeneration (AMD), posterior vitreous detachment, punctate drusen, and epiretinal membrane in the right eye. Graphical representation (A) of the OCT scanning orientation (C,D). S, superior; N, nasal; I, inferior; T, temporal. (B) Fluorescein angiogram. (C) Stratus OCT image. (D) UHR OCT image.

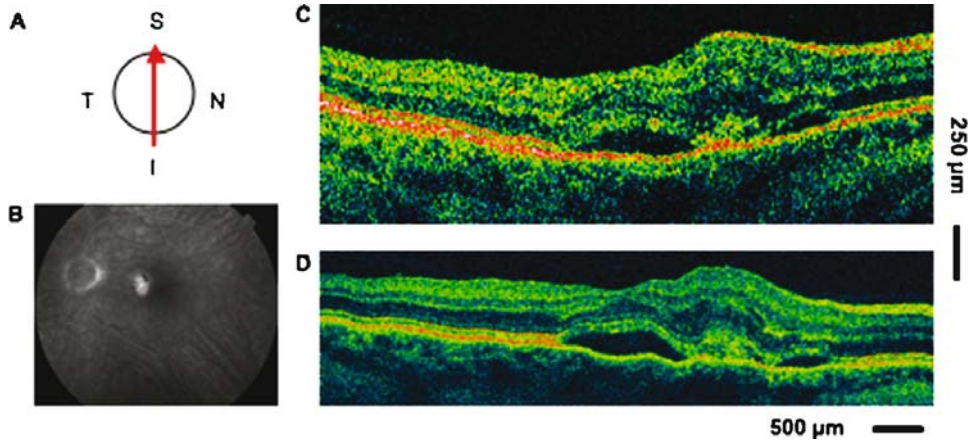

FIG. 25.9. Stratus OCT and UHR OCT of idiopathic choroidal neovascularization (CNV) in the left eye. Graphical representation (A) of the OCT scanning orientation (C,D). S, superior; N, nasal; I, inferior; T, temporal. (B) Fluorescein angiogram. (C) Stratus OCT image. (D) UHR OCT image.

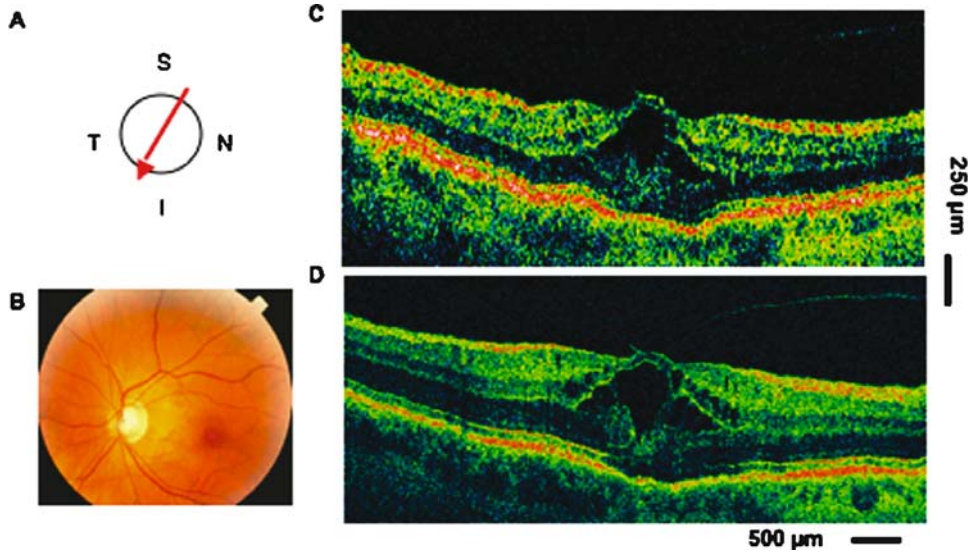

FIG. 25.10. Stratus OCT and UHR OCT of stage 1B macular hole in the left eye. Graphical representation (A) of the OCT scanning orientation (C,D). S, superior; N, nasal; I, inferior; T, temporal. (B) Color fundus photograph. (C) Stratus OCT image. (D) UHR OCT image.

retinal layers involved in this pathology, showing the de novo blood vessels located between the photoreceptor outer segment layer and RPE layer. This is not easily apparent from the Stratus OCT (Fig. 25.9C).

Stratus OCT and UHR OCT scans of a stage 1B macular hole can be clearly visualized in both images (Fig. 25.10). Cystic structures associated with the macular hole are present and appear localized in the ONL and INL of the parafoveal region; however, only UHR OCT allows visualization of the cystic structures in the INL. The hole in both OCT images looks closed, which is characteristic of a macular hole stage 1. The UHR OCT enables enhanced visualization of the smaller cystic structures in the GCL. The improved resolution in the UHR OCT image enables improved visualization and identification of the posterior hyaloid pulling the retina. The posterior hyaloid is difficult to see in the Stratus OCT image because of the lower image resolution. The UHR OCT image shows that the photoreceptor inner and outer segments are preserved even in the region of the macular hole, explaining the successful outcome of the macular hole surgeries. An extensive study of the OCT imaging of macular hole pathology and repair was done to present the advantages of UHR OCT imaging.[13]

Figure 25.11 shows Stratus OCT and UHR OCT scans of a retinitis pigmentosa patient. Both images show that there is

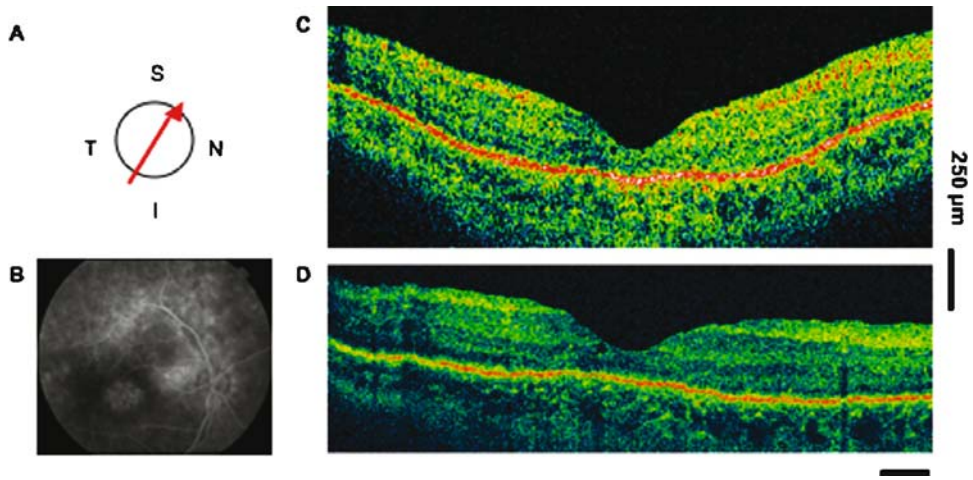

FIG. 25.11. Stratus OCT and UHR OCT of retinitis pigmentosa in the right eye. Graphical representation (A) of the OCT scanning orientation (C,D). S, superior; N, nasal; I, inferior; T, temporal. (B) Fluorescein angiogram. (C) Stratus OCT image. (D) UHR OCT image.

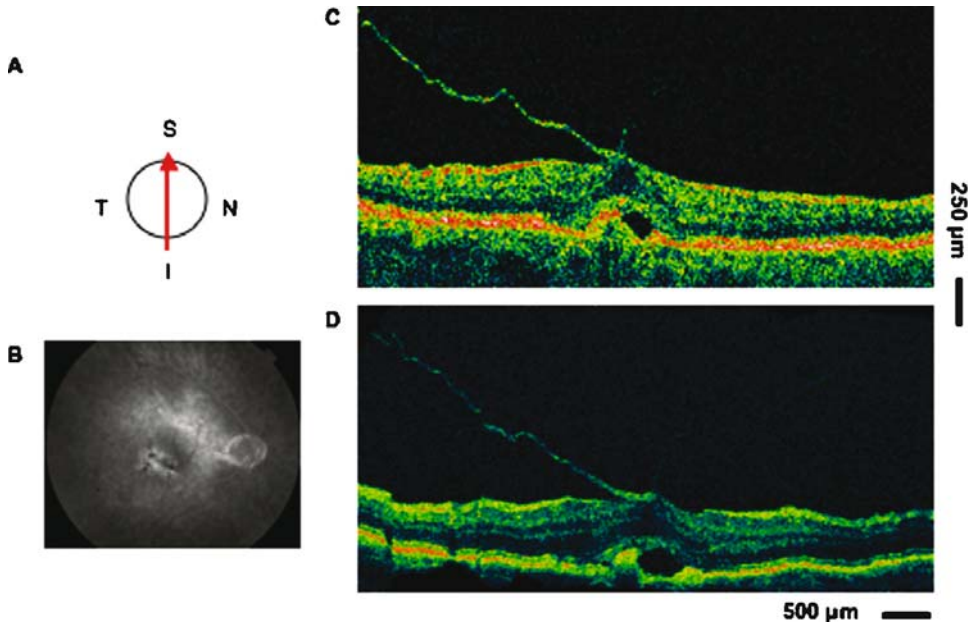

FIG. 25.12. Stratus OCT and UHR OCT of vitreomacular traction in the right eye. Graphical representation (A) of the OCT scanning orientation (C,D). S, superior; N, nasal; I, inferior; T, temporal. (B) Fluorescein angiogram. (C) Stratus OCT image. (D) UHR OCT image.

marked decrease in the retinal thickness due to atrophy. However, in the Stratus OCT image the location of the atrophy is not very well defined, but in the UHR OCT image it is clear that the atrophy is in the photoreceptor cells layer as well as in the ONL, compared with the OCT images of a normal subject (Fig. 25.1). Other intraretinal layers such as the NFL, IPL, INL, and OPL appear relatively normal in the OCT scans.

Stratus OCT and UHR OCT scans show the vitreomacular traction syndrome, with insertion of the vitreous into the retina and the pulling of the retina, which causes a separation of the sensory retinal layers (Fig. 25.12). The UHR OCT image shows that the separation occurs between the photoreceptor layer and RPE. The UHR OCT image shows clearly that the NFL, IPL, INL, OPL, ONL, and ELM are intact in spite of the vitreomacular traction. These areas are also visible in the Stratus OCT image, although the ELM is less well demarcated.

References

1. Huang D, Swanson EA, Lin CP, et al. Optical coherence tomography. Science 1991;254(5035):1178–1181.
2. Swanson E, Izatt, Hee M, et al. In vivo retinal imaging by optical coherence tomography. Opt Lett 1993;18:1864–1866.
3. Drexler W, Morgner U, Ghanta RK, Kartner FX, Schuman, JS, Fujimoto JG. Ultrahigh-resolution ophthalmic optical coherence tomography. Nat Med 2001;7(4):502–507.
4. Fujimoto JG. Optical coherence tomography for ultrahigh resolution in vivo imaging. Nat Biotechnol 2003;21(11):1361–1367.
5. Gass JDM. Stereoscopic Atlas of Macular Diseases: Diagnosis and Treatment. St. Louis: CV Mosby, 1987:46–65.
6. Toth CA, Narayan DG, Boppart SA, et al. A comparison of retinal morphology viewed by optical coherence tomography and by light microscopy. Arch Ophthalmol 1997;115(11):1425–1428.
7. Ko TH, Fujimoto JG, Duker JS, Paunescu LA, Drexler W, Baumal CR, Puliafito CA, Reichel E, Rogers AH, Schuman JS. Comparison of ultrahigh- and standard-resolution optical coherence tomography for imaging macular hole pathology and repair. Ophthalmology 2004;(111):2033–2043.
8. Puliafito CA, Hee MR, Lin CP, et al. Imaging of macular diseases with optical coherence tomography. Ophthalmology 1995;102(2):218–229.
9. Wilkins JR, Puliafito CA, Hee MR, et al. Characterization of epiretinal membranes using optical coherence tomography. Ophthalmology 1996;103(12):2142–2151.
10. Hee MR, Puliafito CA, Duker JS, et al. Topography of diabetic macular edema with optical coherence tomography. Ophthalmology 1998;105(2):360–369.
11. Schuman JS, Pedut-Kloizman T, Hertzmark E, et al. Reproducibility of nerve fiber layer thickness measurements using optical coherence tomography. Ophthalmology 1996;103(11):1889–1898.
12. Guedes V, Schuman JS, Hertzmark E, et al. Optical coherence tomography measurement of macular and nerve fiber layer thickness in normal and glaucomatous human eye. Ophthalmology 2003;110(1):177–189.
13. Drexler W, Sattmann H, Hermann B, et al. Enhanced visualization of macular pathology with the use of ultrahigh-resolution optical coherence tomography. Arch Ophthalmol 2003;121(5):695–706.

26
Spectral/Fourier Domain Optical Coherence Tomography

Royce W.S. Chen, James G. Fujimoto, and Jay S. Duker

Principles of Optical Coherence Tomography

Optical coherence tomography (OCT) is a powerful diagnostic imaging tool with which multiple quantitative and qualitative studies on diseases of the eye have been performed.[1–7] Optical coherence tomography imaging is analogous to ultrasonic imaging, except that it measures echo time delays of light instead of sound.[1,8] Because light travels extremely quickly, echo time delays cannot be directly measured, and correlation techniques are required. Using a technique called low-coherence interferometry, a beam of light from a low-coherence light source, such as a superluminescent diode (SLD), is directed through a beam splitter and is divided into a sample and a reference beam. Light from the sample beam is reflected back from retinal structures with different echo time delays, depending on internal properties of ocular structures. Light from the reference beam is reflected from a reference mirror whose distance is known. The echoes from the two arms are combined by an interferometer and detected.

Standard OCT systems use time-domain detection, where the position of the reference mirror is mechanically scanned, or adjusted, to produce different time delays for the reference beam echoes. In this way, axial scans (measurements of sample beam light echoes versus depth) may be acquired (Fig. 26.1). By scanning the beam of light in the transverse direction, a cross-sectional OCT image, or OCT B-scan, may be obtained. With standard time-domain detection, OCT systems typically acquire 400 axial scans per second.

In OCT, image resolution can be considered both axially (along the incident light beam) and transversally (perpendicular to the incident light beam). The axial resolution of the OCT system is governed by the coherence length of the light source, which is inversely proportional to the bandwidth. Commercial OCT systems use low-coherence SLD light sources at near-infrared wavelengths of ~820 nm. The Stratus OCT (Carl Zeiss Meditec, Dublin, CA) uses a bandwidth of ~25 nm and achieves 8- to 10-μm axial resolution in tissue. Research prototype ultrahigh resolution OCT systems using broadband light sources can achieve axial resolution of 2 to 3 μm.[9–11] Recent commercially available OCT systems using spectral/Fourier domain detection can achieve 5- to 8-μm axial resolution.

Transverse resolution is determined by the size of the focused light beam incident on the retina and is independent of bandwidth. Because there is a trade-off between depth of focus and spot size, most commercial OCT systems use a 20-μm transverse resolution in order to have adequate depth of focus. Aberrations in the human eye have limited transverse resolution to 10 to 15 μm; recently, however, adaptive optics that compensate for ocular aberrations can achieve transverse resolutions of ~4 μm. At this resolution, individual rods and cones may be visualized.[12–14]

Limitations of Time-Domain Optical Coherence Tomography

Although OCT achieves high-resolution images of the eye, image quality in time-domain OCT systems is limited by the speed of image acquisition. With each successive axial scan, patient axial eye motion becomes an increasingly important factor in image quality and accuracy. Following image acquisition, digital processing may remove axial motion artifacts; however, it can also introduce errors in retinal topography.[15]

Image acquisition speed also limits the total number of cross-sectional images that can be acquired in succession. Eye motion, drying tear film, and blinks may all contribute to poor-quality images with increased image acquisition time. As a result, time-domain OCT coverage of the retina is limited. Focal pathologies may not be detected on a given OCT B-scan, resulting in sampling errors. Additionally, because the number of OCT B-scans is limited, it is difficult to register OCT findings to fundus features.

Principles of Spectral/Fourier Domain Optical Coherence Tomography

Spectral/Fourier domain detection represents a recent advance in OCT technology that enables imaging speeds of >25,000 axial scans per second, or ~50 times faster than time-domain detection.[16–22] Spectral or Fourier domain OCT is so named because the interference spectrum of echo time delays of light is measured by a spectrometer and high-speed charge-coupled device (CCD) camera. Because the interference spectrum is composed of oscillations whose frequencies are proportional to the echo time delay, axial scan measurements can be obtained by calculating the Fourier transform. (A Fourier transform is a mathematical operation that extracts the frequency content of a signal.) In contrast to time-domain detection, spectral/Fourier domain detection measures all echoes of light simultaneously, and the position of the reference arm does not need to be adjusted (Fig. 26.2). The result is a significant improvement over time-domain OCT in sensitivity and image acquisition speed.

The primary disadvantage of spectral/Fourier domain detection is that detection sensitivity and image resolution depend on imaging depth because of limitations in spectrometer resolution. This could impact morphometric imaging, and studies investigating these effects are currently in progress.

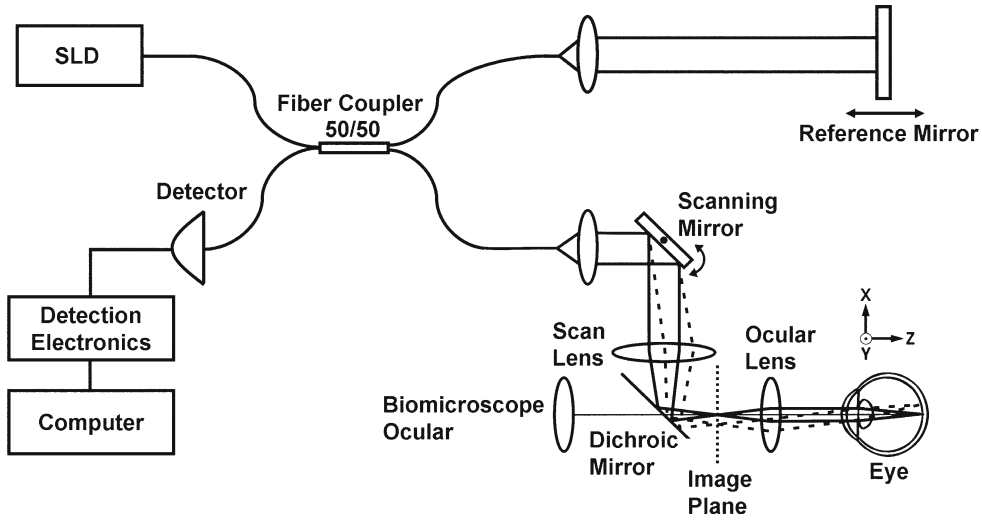

FIG. 26.1. Schematic of time-domain optical coherence tomography (OCT) imaging system. The light source in most time-domain OCT systems is a low-coherence, superluminescent diode (SLD) that is coupled to an optical fiber. The reference mirror is mechanically scanned to produce different time delays.

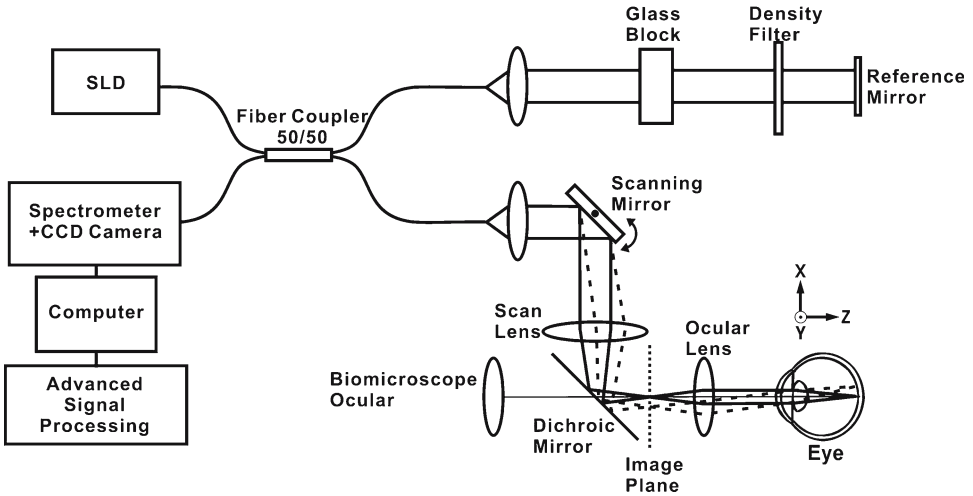

FIG. 26.2. Schematic of spectral/Fourier domain OCT imaging system. In contrast to time-domain OCT systems, a spectrometer coupled to a charge-coupled device (CCD) camera detects the entire interference spectrum, from which the Fourier transform is calculated. The position of the reference arm does not need to be adjusted.

Advantages of Spectral Optical Coherence Tomography

Improved Image Quality

Because of the increased speed of image acquisition, motion artifacts are minimized, resulting in higher quality images and finer discrimination of intraretinal layers. Individual images are acquired within a fraction of a second, and digital processing to correct for axial eye motion is not required. Therefore, spectral/Fourier domain OCT images more accurately represent true retinal topography than do time-domain OCT images.[15] Optical coherence tomography B-scans with a high density of axial scans may also be acquired to create high-definition cross-sectional images. Figure 26.3 shows a comparison of a standard time-domain OCT scan acquired in 1.3 seconds (512 axial scans, ~8- to 10-μm axial resolution at 400 axial scans per second) and a spectral/Fourier domain OCT scan acquired in 0.039 seconds (4096 axial scans, 5-μm axial resolution at 26,000 axial scans per second).

Improved Coverage of the Retina

The ability to acquire a large number of cross-sectional images quickly allows for improved coverage of the retina. One of the most useful features of standard time-domain OCT systems is the ability to map macular thickness and volume in patients. These measurements may be acquired and data from different visits compared to determine patient response to medical or surgical therapies. However, because of slower image acquisition times, only a limited number of cross-sectional scans may be acquired, and maps on time-domain systems rely on data interpolation to generate thickness and volume estimates in the areas between cross-sectional scans. While this is useful for studying trends in an individual patient, focal changes in areas between scans can be missed, and data from these areas can be inaccurate (Fig. 26.4).

Spectral/Fourier domain OCT allows for multiple cross-sectional OCT scans to be taken successively in a dense raster pattern to cover a large area of the retina. Specialized imaging protocols have been developed to take advantage of the high speed of spectral/Fourier domain OCT. These protocols have the potential to detect focal changes that might be missed on time-domain OCT.

In one protocol on a commercial spectral/Fourier domain OCT instrument, a 5 mm × 5 mm square region centered around the fovea is scanned with eleven 5-mm horizontal images (668 axial scans per image) spaced 0.5 mm apart, and eleven 5-mm vertical images (668 axial scans per image) spaced 0.5 mm apart. In the center of this square, 12 additional scans provide more dense coverage: six 3-mm horizontal images (400 axial scans per image) spaced 0.5 mm apart intersect six 3-mm vertical images (400 axial scans per image) spaced 0.5 mm apart. Thickness and volume measurements are automatically calculated, and data from specific retinal layers may be isolated (Fig. 26.5). Because more

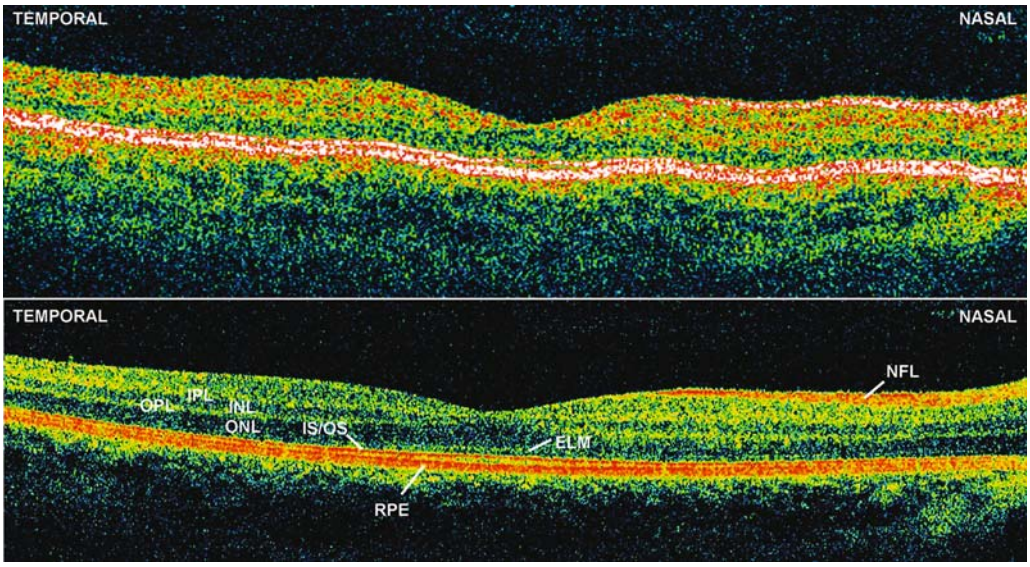

FIG. 26.3. Normal retina comparison of time-domain OCT image with 8- to 10-μm axial resolution and 512 axial scans (taken in 1.3 seconds, above) and spectral/Fourier domain OCT image with 5-μm axial resolution and 4096 axial scans (taken in 0.039 seconds, below). Motion artifact manifests in the time-domain OCT image as a wavy retinal contour. The spectral/Fourier domain OCT image does not have motion artifact and shows better discrimination of retinal layers. ELM, external limiting membrane; INL, inner nuclear layer; IPL, inner plexiform layer; IS/OS, photoreceptor inner segment/outer segment junction; NFL, nerve fiber layer; ONL, outer nuclear layer; OPL, outer plexiform layer; RPE, retinal pigment epithelium.

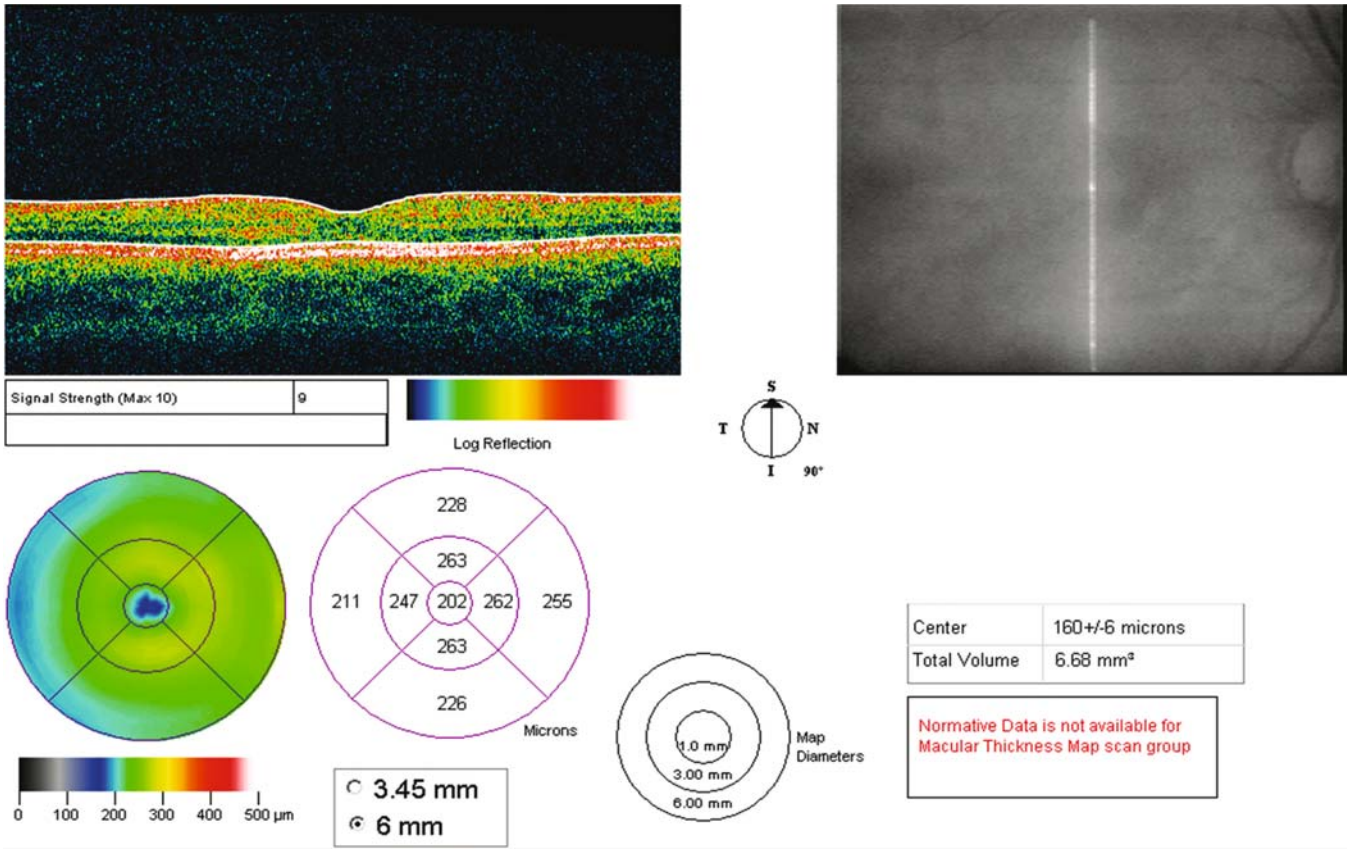

FIG. 26.4. Example of a time-domain OCT macular map of a normal eye created from six radial OCT images. Thickness measurements in the areas between radial scans are interpolated from data in the radial OCT scans.

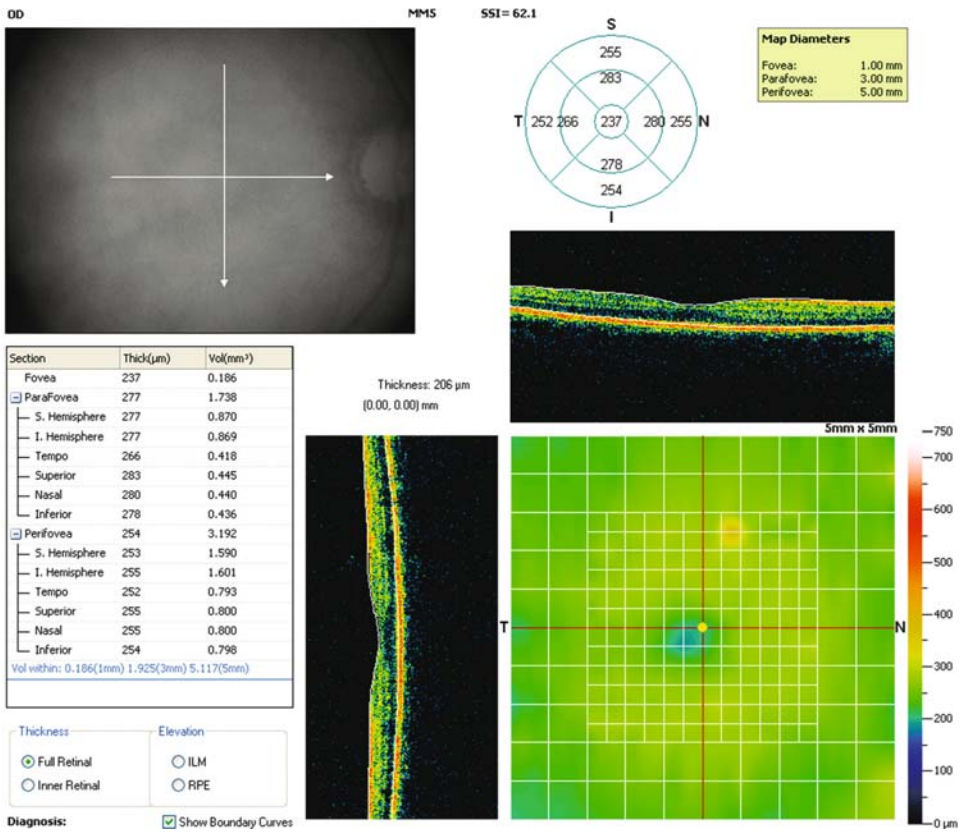

FIG. 26.5. Example of a spectral/Fourier domain OCT macular map of a normal eye. Thirty-four cross-sectional scans (17 horizontal and 17 vertical) are used to create the map. ILM, inner limiting membrane; RPE, retinal pigment epithelium.

scans are used to create the data, this protocol can produce more accurate measurements of volume and thickness than maps from time-domain OCT systems.

For comprehensive coverage, three-dimensional (3D) OCT data sets may be acquired. Protocols differ among commercial instruments, but all take advantage of the increased speed of spectral/Fourier domain detection to acquire many cross-sectional scans in succession. These data sets are useful for tracking pathology in three dimensions or for detecting focal pathologies.

Registration of Optical Coherence Tomography Findings to Fundus Features

Three-dimensional OCT data sets can be used to create an OCT fundus image that shows fundus features, such as blood vessels, the macula, and the optic disc. Because the OCT fundus image is created directly from the cross-sectional scans, each OCT B-scan is precisely registered to the fundus image. The OCT fundus image allows direct comparison to other diagnostic modalities, such as fundus photography, fluorescein angiography (FA), and indocyanine green angiography (ICGA). Some commercial spectral/Fourier domain OCT systems allow images from these other diagnostic instruments to be imported and superimposed upon the OCT fundus image. Following alignment of vessels and other fundus landmarks, cross-sectional OCT scans may be precisely registered to fundus photography, FA, or ICGA findings.

In Figure 26.6, a patient with nonneovascular age-related macular degeneration (AMD) has multiple drusen in her right eye. Figure 26.6A shows the fundus photograph with a yellow box indicating the location of the OCT raster scan. Figure 26.6B demonstrates the OCT fundus image, and a selected cross-sectional OCT scan is shown in Figure 26.6C. The white arrows in Figure 26.6A–C point to one particular druse identified in the fundus photograph, OCT fundus image, and cross-sectional OCT image, respectively.

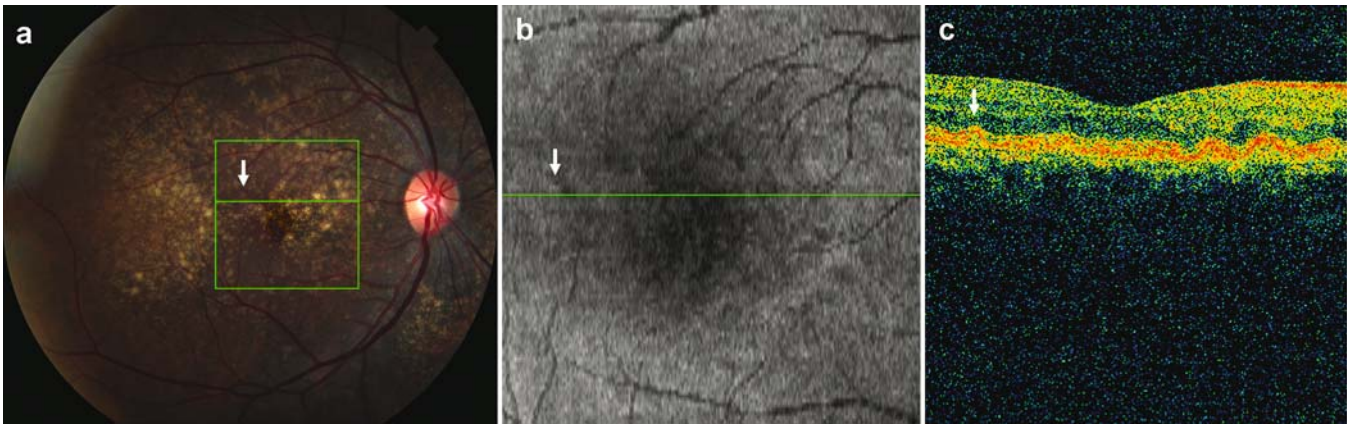

FIG. 26.6. Fundus photograph (A), OCT fundus image (B), and three-dimensional (3D) OCT image (C) of a patient with nonneovascular age-related macular degeneration (AMD). Precise registration of OCT findings to fundus features is possible with 3D imaging. The appearance of an individual druse (white arrow) is shown in all three images.

Longitudinal Tracking of Pathology

With 3D data sets and OCT fundus images, data taken from different points in time may also be compared. Fundus landmarks, such as blood vessels, can be used to align two OCT fundus images from the same patient taken at different times, and then focal pathology on cross-sectional scans may be compared longitudinally. Although differences in alignment between imaging sessions may result in slight differences in tilt in the OCT images, the effects can be minimized by a skilled operator. Some commercial systems may also use different software algorithms to correct for these slight differences in curvature.

Figure 26.7 shows the previous patient with nonneovascular AMD imaged at two different points in time. With progressive scan comparisons of 3D data sets, the same cross-sectional scans from different visits may be selected, and changes in focal pathologies can be studied.

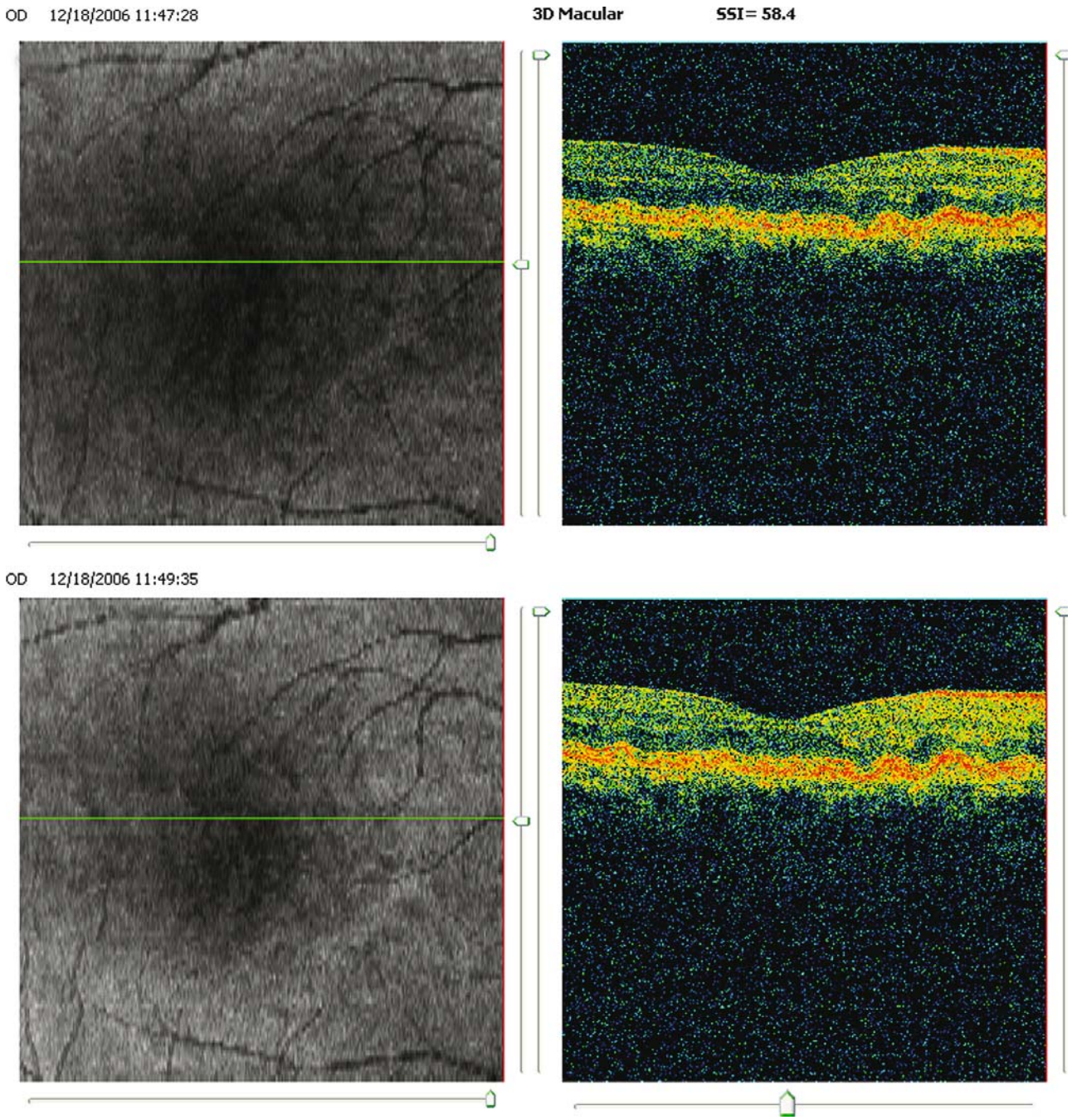

FIG. 26.7. Optical coherence tomography fundus image and selected 3D OCT image of a patient with nonneovascular AMD at two different points in time. The same focal pathology can be isolated during different visits and compared for changes in morphology.

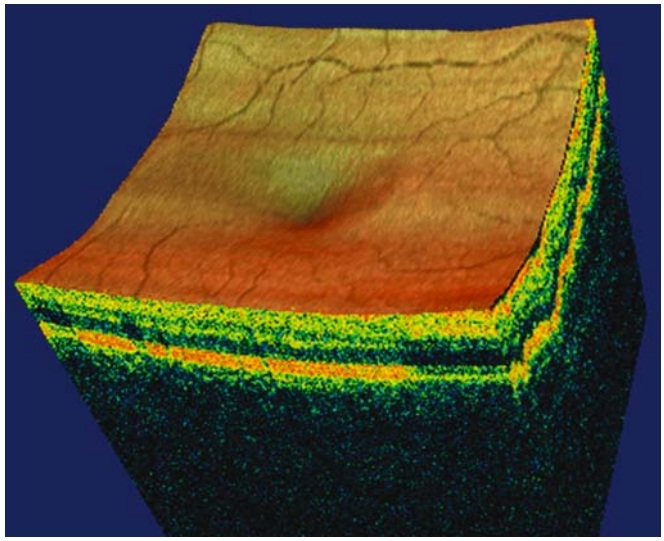

FIG. 26.8. Three-dimensional OCT image of a normal retina shows fundus features on the surface and stacked cross-sectional OCT scans below.

Three-Dimensional Imaging

Another advantage of 3D OCT data sets is the ability to perform three-dimensional imaging of the retina. Three-dimensional OCT images may be generated by any imaging protocol that generates a high sampling density in all three dimensions. On one commercial 3D OCT protocol, 101 cross-sectional images with 512 axial scans (transverse pixels) each cover a 4 mm × 4 mm area and are acquired in 2.0 seconds. These 101 scans are stacked on top of each other to form a 3D image of the retina or optic nerve that can be rotated along any axis and zoomed in and out (Fig. 26.8). Individual OCT B-scans can be isolated and immediately registered to the surface fundus features. Three-dimensional protocols in other systems may cover a larger area with lower transverse pixel density, or a smaller area with greater transverse pixel density. Three-dimensional OCT data sets can also be used for segmentation of intraretinal layers and mapping of thickness and volume.

Selected Cases

Case 1: Nonneovascular Age-Related Macular Degeneration

Optical coherence tomography is useful in the imaging of neovascular AMD. Because it measures retinal thickness accurately and reproducibly, OCT is effective in assessing the response to treatment for choroidal neovascularization and is increasingly being used to guide treatment decisions.

With the improved image quality and faster image acquisition speeds of spectral/Fourier domain OCT, more attention is being turned to patients with nonneovascular AMD. Different types of drusen are being identified, and studies are in progress to detect early markers for progression to late stage nonneovascular or neovascular AMD.

In Figure 26.9, a 54-year-old man with nonexudative AMD in the left eye had a visual acuity of 20/20. Funduscopic

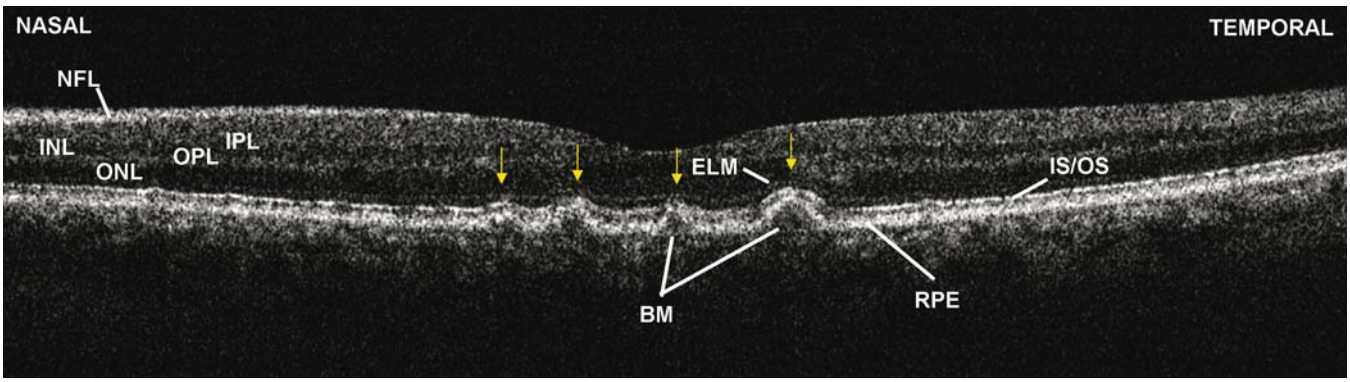

FIG. 26.9. Spectral/Fourier domain cross-sectional scan of a patient with nonneovascular AMD and multiple drusen (yellow arrows). The ELM follows the contour of the raised RPE overlying drusen. Bruch's membrane (BM) is visible as a fine, backscattering line underneath drusen. INL, inner nuclear layer; IPL, inner plexiform layer; IS/OS, photoreceptor inner segment/outer segment junction; NFL, nerve fiber layer; ONL, outer nuclear layer; OPL, outer plexiform layer.

examination revealed multiple macular drusen. In the spectral/Fourier domain OCT image, it is possible to identify all major layers of the retina. Underneath the drusen (yellow arrows), Bruch's membrane (BM) may be identified as a fine, backscattering line. The external limiting membrane (ELM) can be traced over the length of the image and follows the contour of the raised RPE overlying drusen.

Case 2: Full-Thickness Macular Hole

A 70-year-old woman had a full-thickness macular hole in her left eye and visual acuity of 20/200. Figure 26.10 shows the OCT fundus image and the scan locations of four OCT B-scans. With time-domain OCT, sampling errors sometimes occur when a cross-sectional scan just misses the region of pathology. In Figure 26.10B, the topography of the 4 mm × 4 mm macular area of the retina is shown, and there is an elevated region in the center (asterisk). Figure 26.10C and E show horizontal scans taken at the bottom and top edge of the macular lesion, respectively. If these scans were viewed in isolation, they could lead the clinician to suspect cystoid macular edema (CME). But in the next image, exactly through the center of the lesion, the cross-sectional scan reveals a full-thickness macular hole, with cystoid intraretinal edema on either side of the hole.

Case 3: Cystoid Macular Edema

In Figure 26.11, a 93-year old woman developed CME in her left eye following cataract extraction. Visual acuity was 20/40. The high pixel density and axial resolution enable visualization of several pockets of intraretinal fluid in the fovea and parafovea, as well as subtle changes in the outer retina. Red arrows demonstrate two focal areas of disruption of the inner segment/outer segment (IS/OS) photoreceptor junction that may result in permanent visual defects following resolution of CME.

Case 4: Central Serous Chorioretinopathy

Figure 26.12 shows 3D images of a 35-year-old man diagnosed with acute central serous chorioretinopathy (CSCR) after experiencing metamorphopsia for 2 weeks. Best corrected visual acuity (BCVA) was 20/50. Fluorescein angiography (Fig. 26.12A) revealed a hyperfluorescent spot just superior

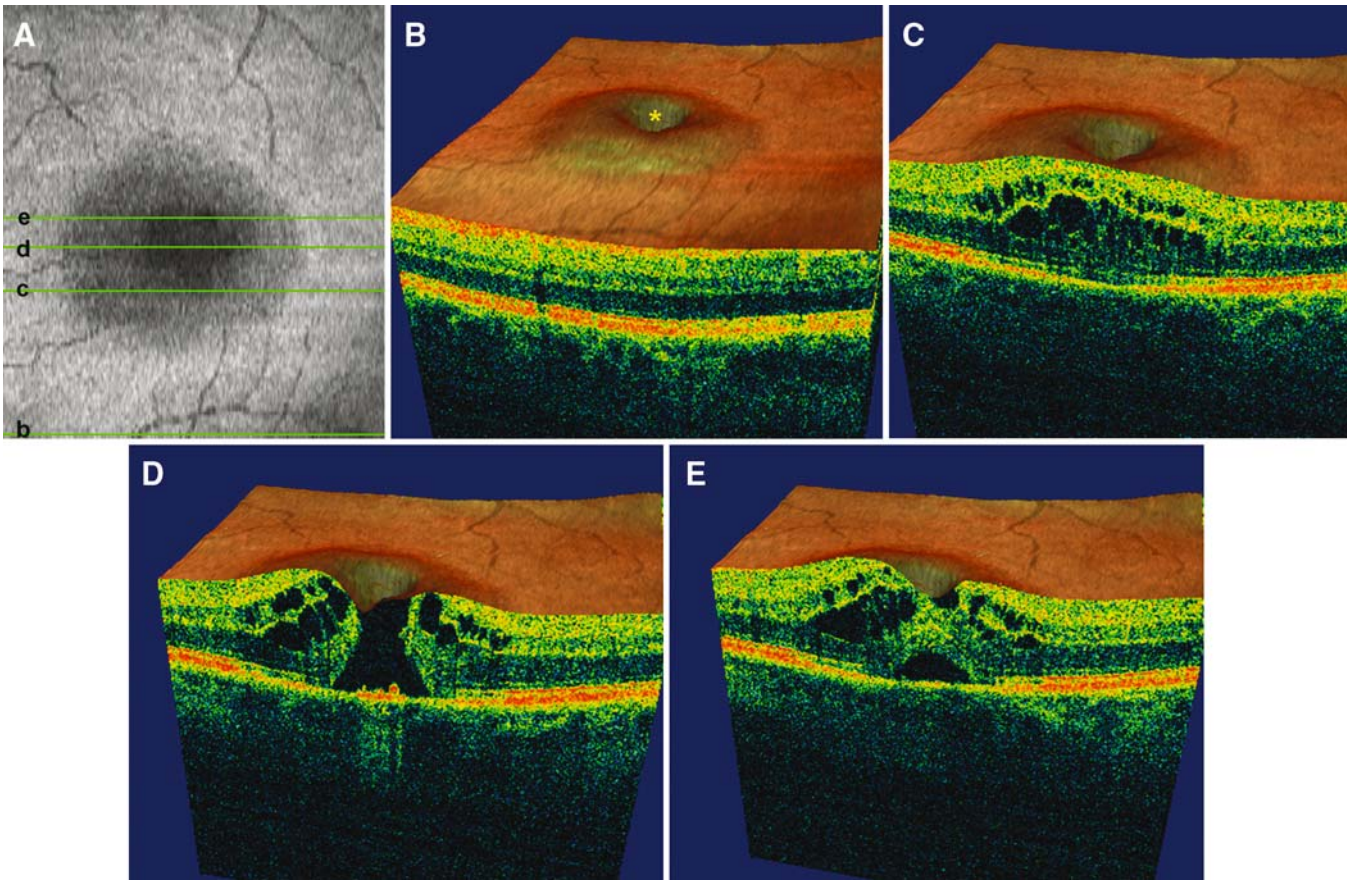

Fig. 26.10. Optical coherence tomography fundus image and selected 3D cross-sectional images of a patient with full-thickness macular hole. (B) The asterisk is shown in the center of the hole. (C,E) Scans are immediately adjacent to the hole. In C, the patient appears to have cystoid macular edema (CME) and in E, subretinal fluid. (D) The full-thickness hole is readily apparent.

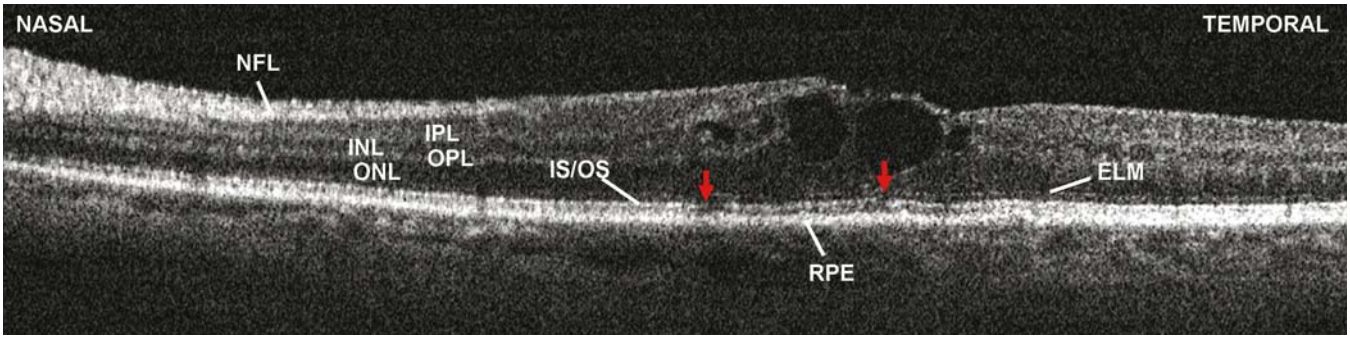

FIG. 26.11. Spectral/Fourier domain cross-sectional scan of a patient with CME following cataract extraction. Intraretinal fluid is visible in the fovea and parafovea, and focal defects of the IS/OS can be visualized. ELM, external limiting membrane; INL, inner nuclear layer; IPL, inner plexiform layer; NFL, nerve fiber layer; ONL, outer nuclear layer; OPL, outer plexiform layer; RPE, retinal pigment epithelium.

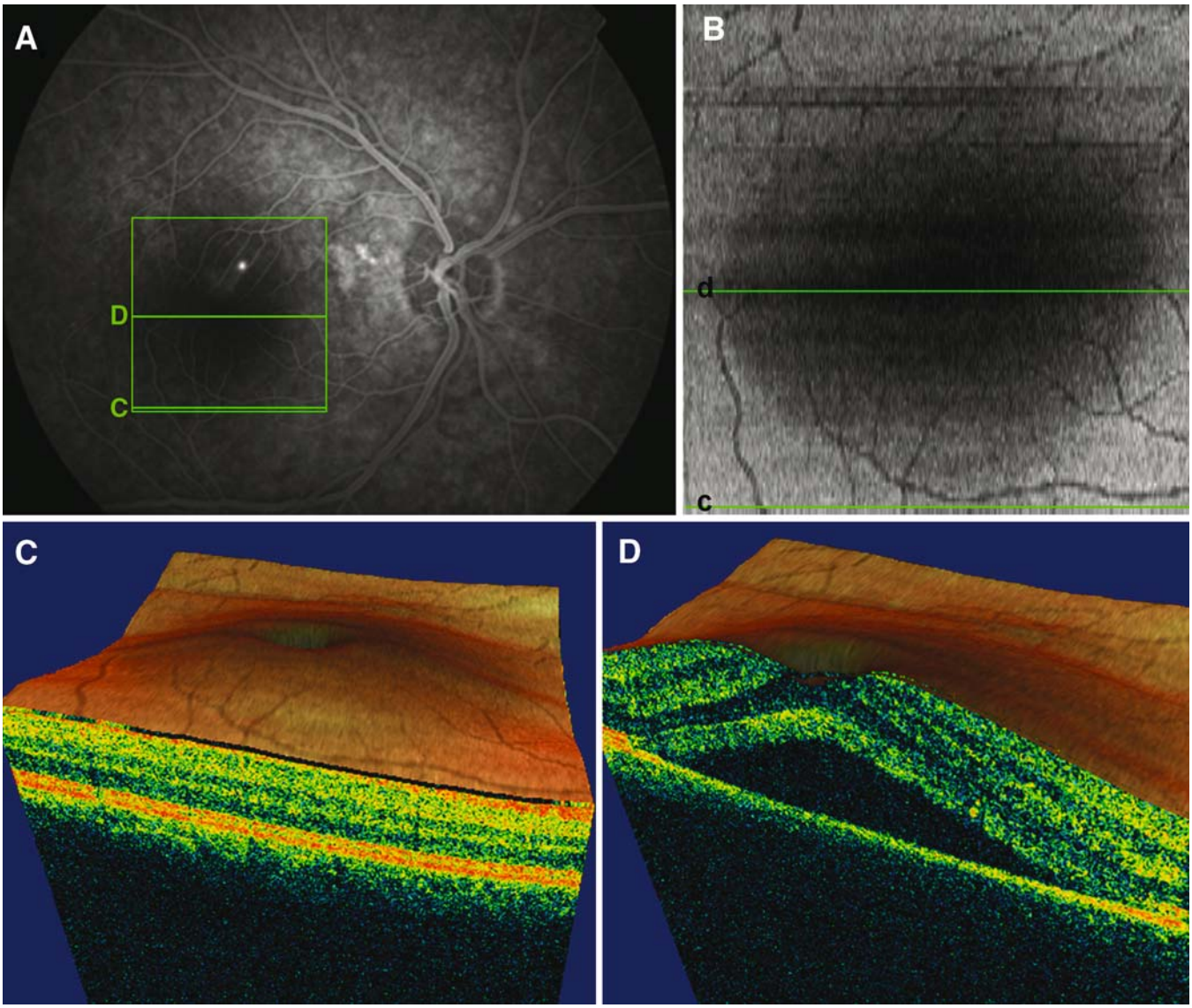

FIG. 26.12. Fluorescein angiography (A), OCT fundus image (B), and 3D OCT images (C,D) of a patient with acute central serous chorioretinopathy. (C) The swollen retinal contour is visualized. (D) The neurosensory detachment of the retina can be seen. The photoreceptor layer above the detachment is well preserved.

to the fovea. Figure 26.12B shows the OCT fundus image and the scan locations of Figure 26.12C and D. The full retinal topography can be seen in Figure 26.12C. There is a bulge in the macula that represents the serous neurosensory retinal detachment. Figure 26.12D, a cross-sectional scan through the center of the detachment, shows the neurosensory detachment of the retina with preservation of the foveal contour. The photoreceptor architecture is intact over the length of the detachment.

Glaucoma

Optical coherence tomography is useful in glaucoma because of its ability to detect changes in retinal nerve fiber layer (RNFL) thickness prior to the onset of visual loss.[6] The RNFL is thickest in the superior and inferior quadrants, and RNFL thinning has been shown to correspond with areas of visual field loss.

As in time-domain OCT systems, glaucoma-specific protocols have been developed for spectral/Fourier domain OCT to calculate RNFL thickness measurements and optic nerve head topography. The RNFL scan protocol on one commercial system (imaging protocol from the commercially available RTVue-100, Optovue, Inc., Fremont, CA; Figures 26.3 [lower image], 26.5 through 26.14, and 26.16 [lower image] were acquired with the RTVue-100) is designed to acquire four circle scans of 3.45-mm diameter around the optic disc. Following image acquisition, the RNFL thickness can be assessed at individual points on either a cylindrical or linear tomogram in the peripapillary region (Fig. 26.13). Normative databases will become available for the commercial systems to compare patient nerve fiber layer thickness values to a normal population.

In addition to RNFL thickness measurements, OCT analysis of the optic nerve head has been shown to be effective in the assessment of glaucomatous damage and comparable to other

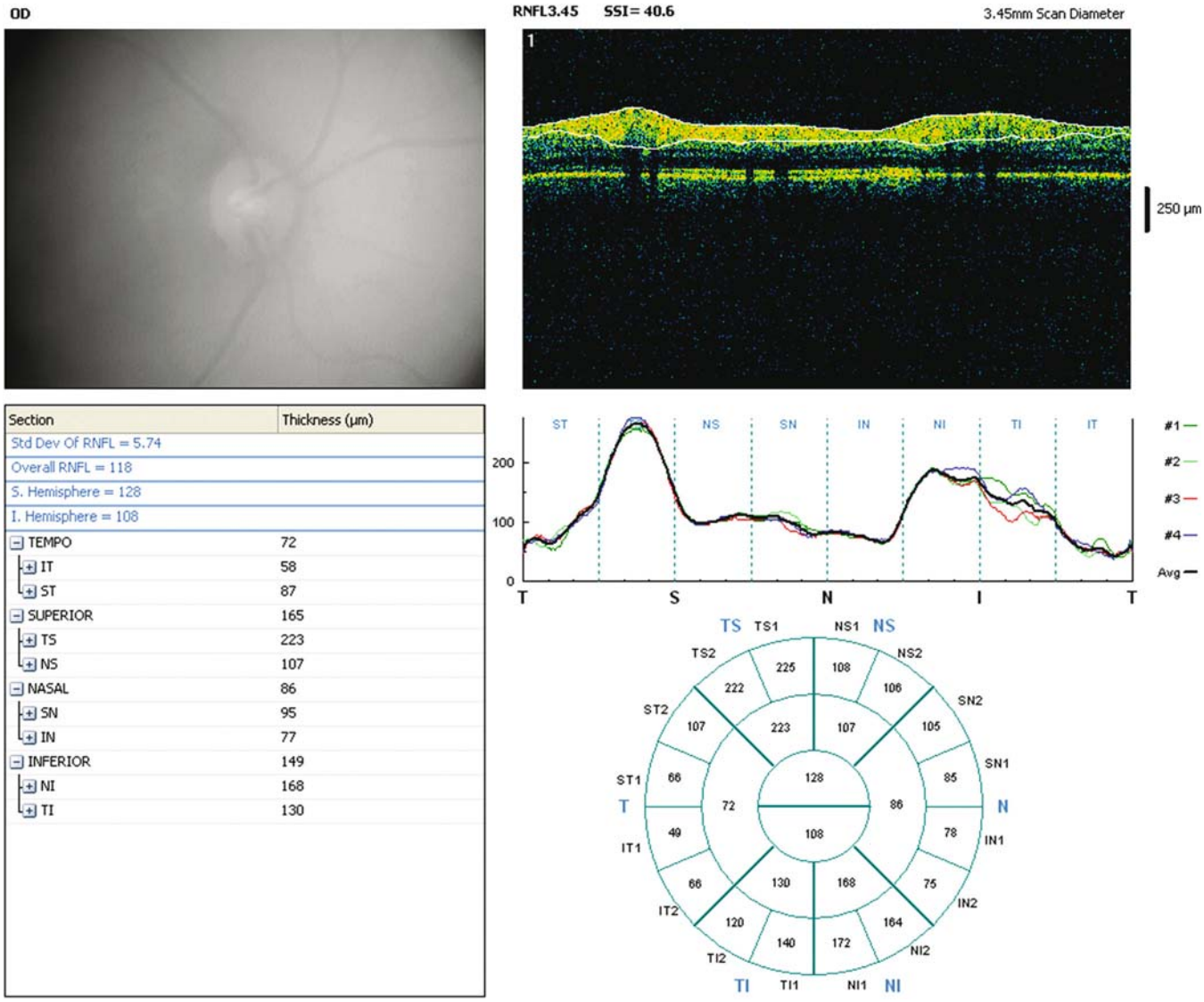

FIG. 26.13. Example of retinal nerve fiber layer analysis protocol from a spectral/Fourier domain OCT instrument.

diagnostic modalities such as the Heidelberg retinal tomograph (Heidelberg Engineering, Heidelberg, Germany).[23] The nerve head measurement protocol on one commercial spectral/Fourier domain OCT system acquires 12 radial line scans 3.4 mm in length (452 axial scans per line) and six concentric rings, 2.5 to 4.0 mm in diameter around the optic disc in 0.39 seconds. Following the scan, the operator draws the boundary for the optic nerve head, and computer software then provides information such as disc area, cup area, and the cup/disc ratio (Fig. 26.14). Because more information is acquired than in time-domain OCT, it is possible that the data from spectral/Fourier domain systems will be more accurate.

Cornea

Recently, there has been greater interest in using OCT for corneal applications. Corneal pachymetry mapping with OCT has been shown to be equivalent to ultrasound for central corneal thickness measurements.[24] This could be useful in planning for keratorefractive surgical procedures. Spectral/Fourier domain OCT has also been studied for identifying pathologies in specific layers of the cornea.[25] As more studies are conducted, it is likely that spectral/Fourier domain OCT will be more widely used for corneal applications in the future.

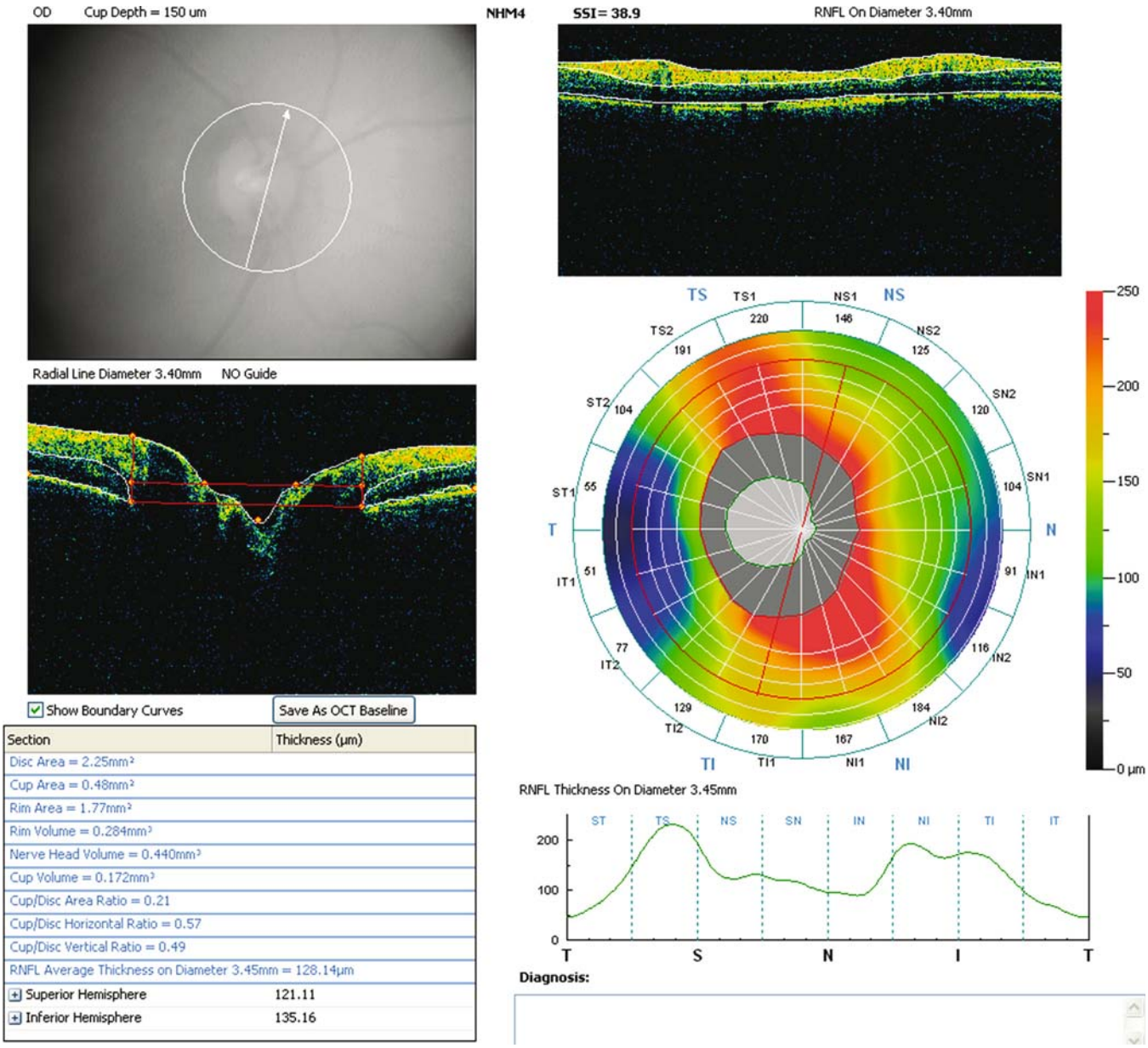

FIG. 26.14. Example of nerve head measurement protocol from a spectral/Fourier domain OCT instrument.

Spectral/Fourier Domain Ultrahigh-Resolution Optical Coherence Tomography

High-speed ultrahigh-resolution OCT (UHR OCT) prototype systems based on spectral/Fourier domain detection have been demonstrated to be capable of 3.5-mm axial image resolution in tissue and have image acquisition times of approximately 25,000 axial scans per second.[21,22] Compared to commercial spectral OCT systems, high-speed UHR OCT prototypes have higher axial image resolution, and greater detail of retinal features can be seen (Fig. 26.15). Though currently not commercially feasible, prototypes are being used extensively for clinical and research purposes, with projects ranging from imaging animal models of disease to the development of new image acquisition and analysis algorithms for better detection and understanding of retinal disease.

Limitations

Despite many improvements over time-domain OCT, spectral/Fourier domain OCT still has some limitations. Because OCT measures the changes in tissue refractive indices, cross-sectional images may not correlate directly with histologic anatomy.

Media opacities, such as dense cataracts or corneal edema, decrease image quality; in some cases, time-domain OCT images have better quality than spectral/Fourier domain OCT images of the same patient. Figure 26.16 shows a comparison of a standard time-domain OCT image (above) and spectral/Fourier domain OCT image (below) of a patient with CME. Because of a dense cataract, there is shadowing of intraretinal details, and it is difficult to discriminate intraretinal layers and the CME in the spectral/Fourier domain OCT image. Conversely, the discrete pockets of intraretinal fluid are easily identified in the time-domain OCT image.

Some problems that occur with time-domain OCT systems have less of an impact on spectral/Fourier domain OCT. Because of improved coverage, eccentric fixation may not result in a sampling error. If a line scan is not placed directly through the fovea or area of pathology, it is likely that protocols with denser raster patterns will cover the regions of interest.

Computer algorithms used to calculate thickness and volume of the retina or nerve fiber layer may be a source of errors in both time-domain and spectral/Fourier domain OCT. This is especially true when there is a greater degree of pathology. For example, in some cases of patients with choroidal neovascularization, the outer retinal boundary may be obscured or discontinuous, and automated software segmentation algorithms may fail. In patients with vitreomacular traction, the posterior hyaloid may be mistakenly identified as the inner retinal boundary. As in time-domain OCT, thickness and volume maps must be checked carefully for segmentation errors that could affect the accuracy of data.

The amount of data collected in information-rich protocols, such as 3D or dense macular mapping protocols, is a double-edged sword. While a vast amount of information is available to the clinician, these data translate into significantly greater storage space requirements. Additionally, as opposed to a single OCT line scan, the advantages of 3D imaging cannot be

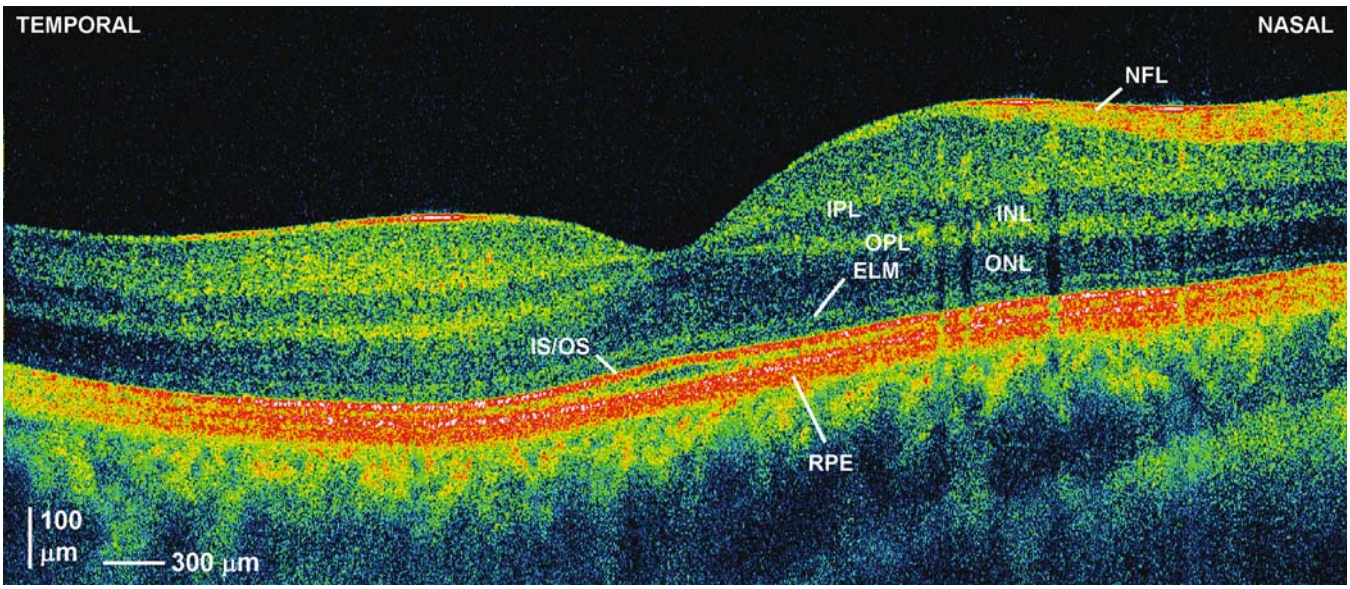

FIG. 26.15. Spectral/Fourier domain ultrahigh-resolution OCT (UHR OCT) of a normal retina. Prototype ultrahigh-resolution OCT systems provide greater detail than time-domain or current commercial spectral/Fourier domain OCT systems. ELM, external limiting membrane; INL, inner nuclear layer; IPL, inner plexiform layer; NFL, nerve fiber layer; ONL, outer nuclear layer; OPL, outer plexiform layer; RPE, retinal pigment epithelium.

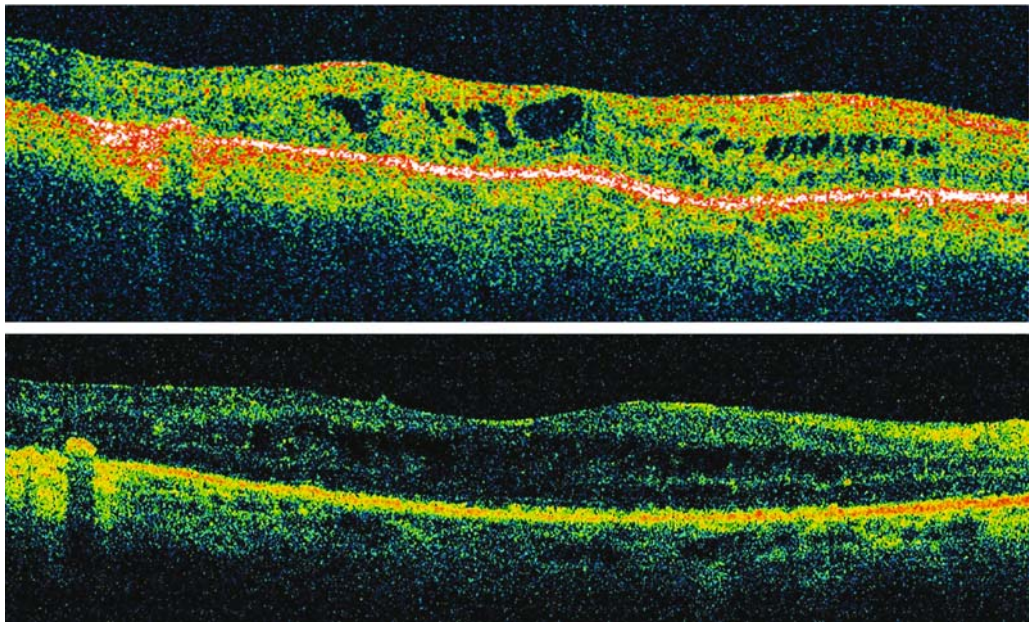

FIG. 26.16. Comparison of time-domain OCT image (above) and spectral/Fourier domain OCT image (below) of a patient with cystoid macular edema (CME). Because of a dense cataract, there is impaired visualization of CME and intraretinal structures in the spectral/Fourier domain OCT image, but the CME is easily identified in the time-domain OCT image.

easily captured on a single sheet of paper. As clinicians begin to take advantage of spectral/Fourier domain OCT imaging, it is likely that more computer viewing stations will need to be set up in order to maximize 3D analysis capabilities.

Conclusion

In recent years, OCT has been established as a useful tool in the diagnosis and clinical evaluation of macular disease and glaucoma. With spectral/Fourier domain OCT, advantages such as improved retinal coverage, registration of OCT findings to fundus features, longitudinal tracking of pathology, and 3D imaging promise to improve sensitivity and specificity in diagnosis, as well as enhance our understanding of disease pathogenesis. Earlier markers of disease may be detected, possibly identifying different candidates for medical or surgical therapies.

Over the next few years, many studies will be performed to determine the relative advantages and disadvantages of spectral/Fourier domain OCT over time-domain OCT and other widely used imaging modalities such as fluorescein angiography or Heidelberg retina tomograph (HRT). Spectral/Fourier domain OCT will likely expand into other areas as well, with applications for corneal imaging, real-time morphometric imaging, and studies on animal models of disease. Taken together, these advances should further enhance the role of OCT as an important instrument in both the clinical and research setting.

References

1. Hee MR, Izatt JA, Swanson EA, et al. Optical coherence tomography of the human retina. Arch Ophthalmol 1995;113:325–332.
2. Puliafito CA, Hee MR, Lin CP, et al. Imaging of macular diseases with optical coherence tomography. Ophthalmology 1995;102:217–229.
3. Hee MR, Puliafito CA, Wong C, et al. Quantitative assessment of macular edema with optical coherence tomography. Arch Ophthalmol 1995;113:1019–1029.
4. Hee MR, Puliafito CA, Wong C, et al. Optical coherence tomography of macular holes. Ophthalmology 1995;102:748–756.
5. Schuman JS, Hee MR, Arya AV, et al. Optical coherence tomography: a new tool for glaucoma diagnosis. Curr Opin Ophthalmol 1995;6:89–95.
6. Schuman JS, Hee MR, Puliafito CA, et al. Quantification of nerve fiber layer thickness in normal and glaucomatous eyes using optical coherence tomography. Arch Ophthalmol 1995;113:586–596.
7. Hee MR, Puliafito CA, Duker JS, et al. Topography of diabetic macular edema with optical coherence tomography. Ophthalmology 1998;105:360–370.
8. Huang D, Swanson EA, Lin CP, et al. Optical coherence tomography. Science 1991;254:1178–1181.
9. Drexler W, Morgner U, Ghanta RK, et al. Ultrahigh-resolution ophthalmic optical coherence tomography. Nat Med 2001;7:502–507.
10. Drexler W, Sattmann H, Hermann B, et al. Enhanced visualization of macular pathology with the use of ultrahigh-resolution optical coherence tomography. Arch Ophthalmol 2003;121:695–706.

11. Ko TH, Fujimoto JG, Schuman JS, et al. Comparison of ultrahigh- and standard-resolution optical coherence tomography for imaging macular pathology. Ophthalmology 2005;112:1922.
12. Fernandez EJ, Povazav B, Hermann B, et al. Three-dimensional adaptive optics ultrahigh resolution optical coherence tomography using a liquid crystal spatial light modulator. Vision Res 2005;45:3432–3444.
13. Zawadzki R, Jones S, Olivier S, et al. Adaptive-optics optical coherence tomography for high-resolution and high-speed 3D retinal in vivo imaging. Opt Express 2005;13:8532–8546.
14. Zhang Y, Cense B, Rha J, et al. High-speed volumetric imaging of cone photoreceptors with adaptive optics spectral-domain optical coherence tomography. Opt Express 2006;14:4380–4394.
15. Swanson EA, Izatt JA, Hee MR, et al. In-vivo retinal imaging by optical coherence tomography. Opt Lett 1993;18:1864–1866.
16. Fercher AF, Hitzenberger CK, Kamp G, Elzaiat SY. Measurement of intraocular distances by backscattering spectral interferometry. Opt Commun 1995;117:43–48.
17. Wojtkowski M, Leitgeb R, Kowalczyk A, et al. In vivo human retinal imaging by Fourier domain optical coherence tomography. J Biomed Opt 2002;7:457–463.
18. Nassif NA, Cense B, Park BH, et al. In vivo high-resolution video-rate spectral-domain optical coherence tomography of the human retina and optic nerve. Opt Express 2004;12:367–376.
19. Leitgeb RA, Drexler W, Unterhuber A, et al. Ultrahigh resolution Fourier domain optical coherence tomography. Opt Express 2004;12:2156–2165.
20. Wojtkowski M, Bajraszewski T, Gorczynska I, et al. Ophthalmic imaging by spectral optical coherence tomography. Am J Ophthalmol 2004;138:412–419.
21. Wojtkowski M, Srinivasan V, Fujimoto JG, et al. Three-dimensional retinal imaging with high-speed ultrahigh-resolution optical coherence tomography. Ophthalmology 2005;112:1734–1746.
22. Srinivasan VJ, Wojtkowski M, Witkin AJ, et al. High-definition and 3-dimensional imaging of macular pathologies with high-speed ultrahigh-resolution optical coherence tomography. Ophthalmology 2006;113:2054e1–14.
23. Schuman JS, Wollstein G, Farra T, et al. Comparison of optic nerve head measurements obtained by optical coherence tomography and confocal scanning laser ophthalmoscopy. Am J Ophthalmol 2003;135:504–512.
24. Li Y, Shekhar R, Huang D. Corneal pachymetry mapping with high-speed optical coherence tomography. Ophthalmology 2006;113:799e1–2.
25. Kaluzy BJ, Kaluzny JJ, Szkulmowska A, et al. Spectral optical coherence tomography: a novel technique for cornea imaging. Cornea 2006;25:960–965.

27
Spectral Optical Coherence Tomography/Scanning Laser Ophthalmoscope: The Next Generation

Richard B. Rosen and Patricia M. T. Garcia

Optical coherence tomography (OCT) was introduced by Fujimoto and associates in the mid-1990s, and for the first time offered physicians a view similar to histologic cross-sections of the retina in a living patient.[1,2] Over the ensuing decade it has become a standard tool for diagnosing and monitoring retinal diseases.[3]

The OCT scanning laser ophthalmoscope (OCT/SLO) developed by Podoleanu and colleagues in 2000 advanced the utility of OCT technology by combining it with the SLO in an integrated package.[4–9] It added precise localization of the OCT slices with point-to-point correspondence to retinal surface landmarks, and for the first time made accurate serial OCT imaging a possibility.[10,11]

Both OCT systems were based on a modified Michaelson interferometer operating in a time-domain mode. Zeiss's OCT produced images from optical A-scans that were assembled into B-scan cross sections, while the Ophthalmic Technologies Inc. (OTI, Toronto, CA) OCT/SLO employed transverse scanning (T-scans) to generate coronal (C-scans) OCTs plus paired SLO as well as conventional B-scan OCTs with associated SLO.[12–14] The C-scan approach facilitated creation of volumetric stacks for topographic mapping.[15] Both systems utilized superluminescent diode light sources that produced resolutions of 10 μm at speeds of 1 to 2 frames per second. Even when ultrahigh resolution systems (~3-μm resolution) were demonstrated, their quality was limited by the speed of image acquisition.[16,17] The limitations in image quality were in large part due to the relatively slow speed of the technology.[18–20]

As early as 2004 prototype spectral domain (also called Fourier transform) OCT systems were reported by several groups.[21–25] These new devices are higher-resolution, higher-speed systems able to capture images with resolutions of up to 3 μm at speeds of up to 64 frames per second.

The OTI spectral OCT/SLO combines cross-sectional imaging of retinal layers with live surface imaging of the retina using the SLO. Because these two images are taken simultaneously, it facilitates direct correlation of the information obtained from these two sources. This machine is capable of several different testing modalities, which are enumerated below.

Longitudinal (B-Scans)

A longitudinal scan or B-scan provides a cross-sectional view of the retina through a line projected onto the retinal surface. The scan line may be rotated around the central axis, or moved up or down (horizontal scan) or side to side (vertical scan) to target the specific pathology or area of interest. The best views are obtained of the posterior pole. More peripheral scans may be attempted, but in the periphery scans tend to become distorted due to the nonlinear optics of the eye and are more difficult to interpret.

A raster scan sequence is used to rapidly sweep vertically across the posterior pole (central 30 degrees) with 64 longitudinal scans in 2 seconds. This provides a quick overview of the macular area, and may be useful for detecting areas of interest not originally targeted at the initiation of the study. The set of raster scan images can be reconstructed to create a variety of informative and novel views. Figure 27.1 is an example of a normal longitudinal scan, and an interpretation of the various landmarks seen. Appreciation of the normal longitudinal scan enables us to identify pathologic changes, some of which are shown in Figures 27.2 to 27.4.

Retinal Thickness Map

The spectral OCT/SLO is able to capture up to 128 longitudinal scans in 2 seconds over a 5-mm area, and generate a retinal thickness map from the data obtained. This is useful for following retinal thickness over time and for evaluating the effects of treatment on retinal edema. This map can be presented in various ways, some of which are shown below. The 8 × 8 grid shown in Figure 27.5 is the format most often presented. It divides the central 5 mm into 64 squares and gives the average retinal thickness in each square. Virtual horizontal and vertical longitudinal scans (extracted from the retinal thickness map) is shown below and to the right of the thickness map. These virtual longitudinal scans are taken from slices through the retinal thickness map as indicated by

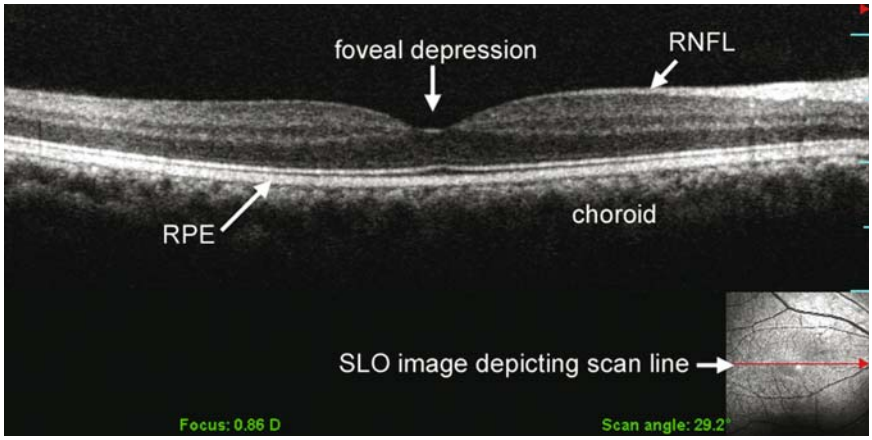

FIG. 27.1. Normal longitudinal optical coherence tomography/scanning laser ophthalmoscope (OCT/SLO) image (B-scan). RNFL, retinal nerve fiber layer; RPE, retinal pigment epithelium.

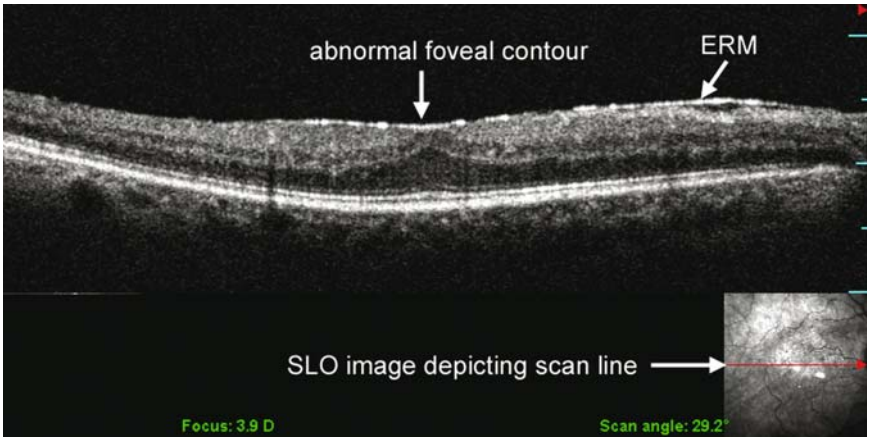

FIG. 27.2. Epiretinal membrane (ERM) (B-scan).

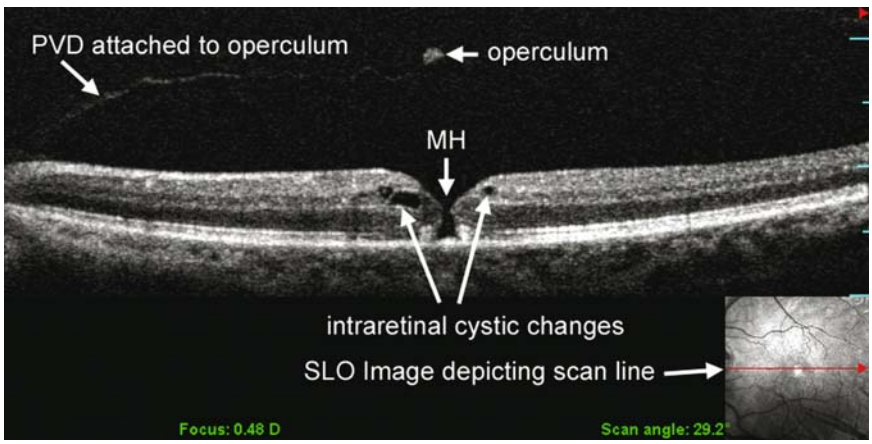

FIG. 27.3. Small macular hole (MH) with operculum, showing attachment to posterior vitreous detachment (PVD) (B-scan).

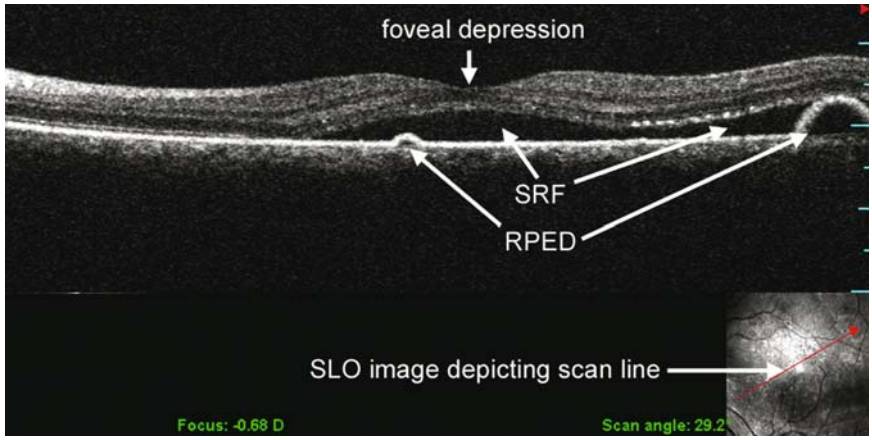

FIG. 27.4. Central serous retinopathy (CSR) with subretinal fluid (SRF) and retinal pigment epithelial detachments (RPED) (B-scan).

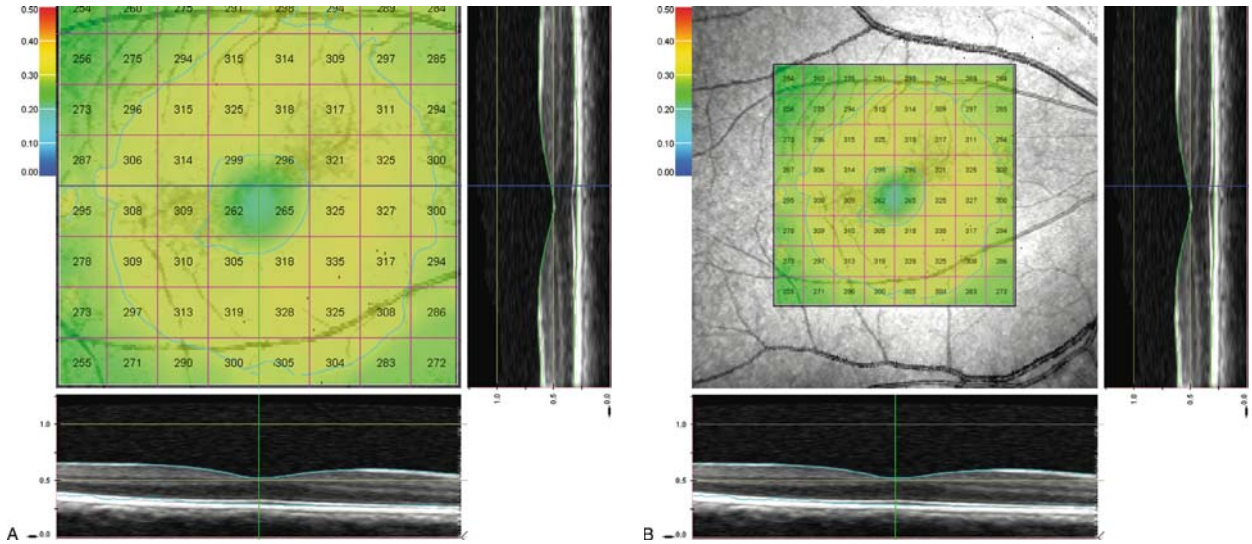

FIG. 27.5. (A) An 8 × 8 macular topography thickness grid with vascular pattern. Green and blue lines depict areas where vertical and horizontal B-scans are extracted from. (B) An 8 × 8 grid zoomed out to show retinal landmarks on SLO.

the blue (horizontal) and green (vertical) lines on the 8 × 8 grid. As the blue and green lines are moved on the screen, the corresponding OCT images change to indicate the underlying retinal condition. Note the blue (and green) outlines that mark the retinal nerve fiber layer (RNFL) and retinal pigment epithelium (RPE) layer on the OCT scans. Thickness measurements are based on these outlines, so when these lines do not accurately trace the RNFL and RPE, the thickness measurements at those areas should be disregarded. Occasionally, the computer algorithm fails to accurately identify the correct landmarks. This can occur due to artifacts produced by movement or opacities in the optical media. Examples of such errors are demonstrated in Figure 27.6.

In the first image (Fig. 27.6A), the RNFL and RPE are accurately represented in the horizontal scan (below), but not in the vertical scan (to the right). When the horizontal (blue) scan line is moved inferiorly on the thickness map (Fig. 27.6B), it is evident that the algorithm failed to detect the RNFL properly in the inferior part of the scan, and therefore thickness measurements seen in this area should be ignored. If the errors are limited to a small portion of an image, the system provides a correction tool that can be used to manually redraw the outlines. While this technique is more time-consuming than the automated feature, it is particularly useful if the errors are discovered after the patient is no longer present or available to be rescanned.

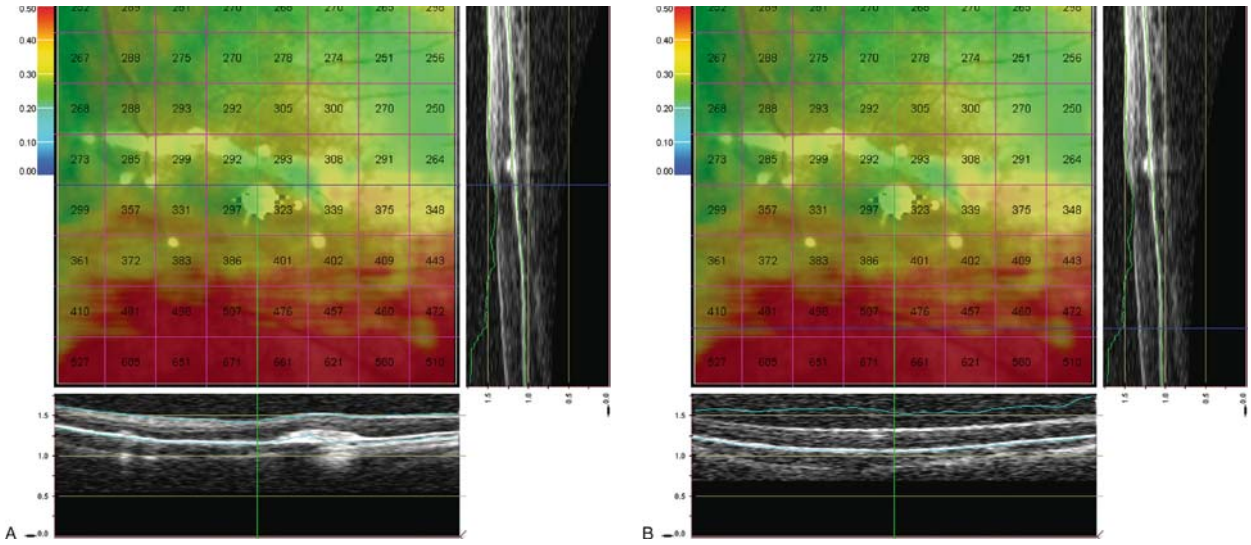

FIG. 27.6. (A) Inaccurate RNFL and RPE outlines in vertical scan window. (B) Inaccurate RNFL and RPE outline in both horizontal and vertical scan windows when the horizontal scan is moved inferiorly on thickness map.

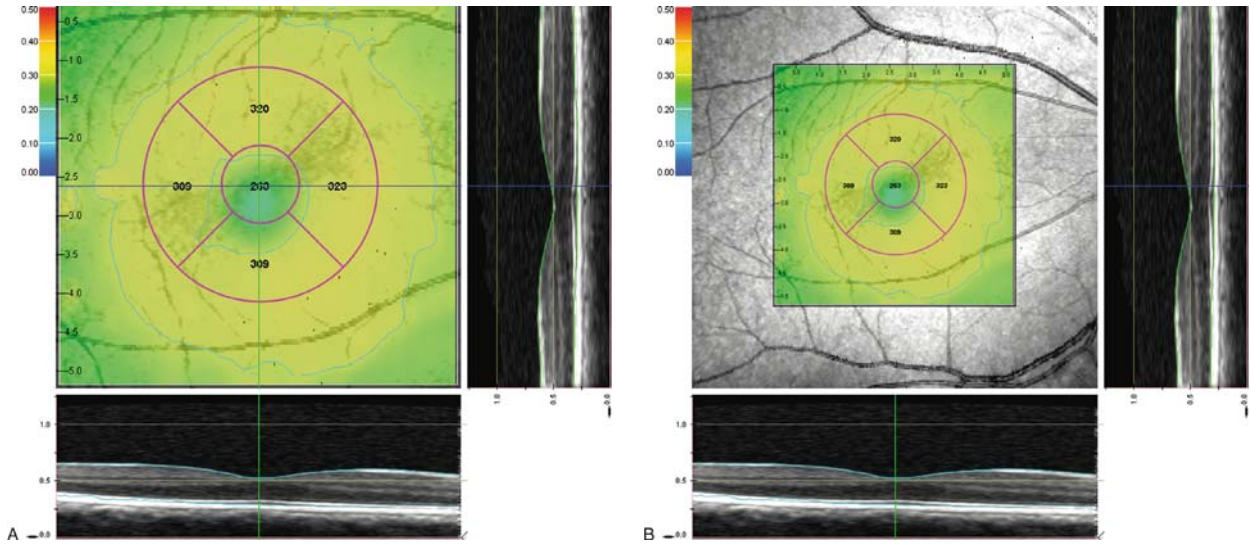

FIG. 27.7. (A) Five-zone macular thickness map corresponding to Early Treatment for Diabetic Retinopathy Study (ETDRS) grid. (B) Five-zone map zoomed out to show retinal landmarks on SLO.

Retinal thickness measurements can also be delineated into five zones that correspond to those defined in the Early Treatment for Diabetic Retinopathy Study (ETDRS). These are shown in Figure 27.7. The retinal thickness map presented this way gives a quick overview of the retinal thickness in the central 1 mm, as well as the four areas (superior, inferior, temporal, and nasal) in the surrounding 3 mm. A virtual horizontal and vertical longitudinal scan (extracted from the retinal thickness map) is also shown below and to the right of the thickness map.

Clinical Example: Diabetic Maculopathy

A patient presents with diabetic maculopathy. Figures 27.8 and 27.9 show B-scan cross sections at 180, 135, 90, and 45 degrees and the corresponding thickness map in detail and against the SLO fundus image.

The system software is also designed to compare thickness maps over time. By aligning the retinal vessel patterns recorded in the SLO image, thickness measurements taken on different days can be compared. This is useful for following a

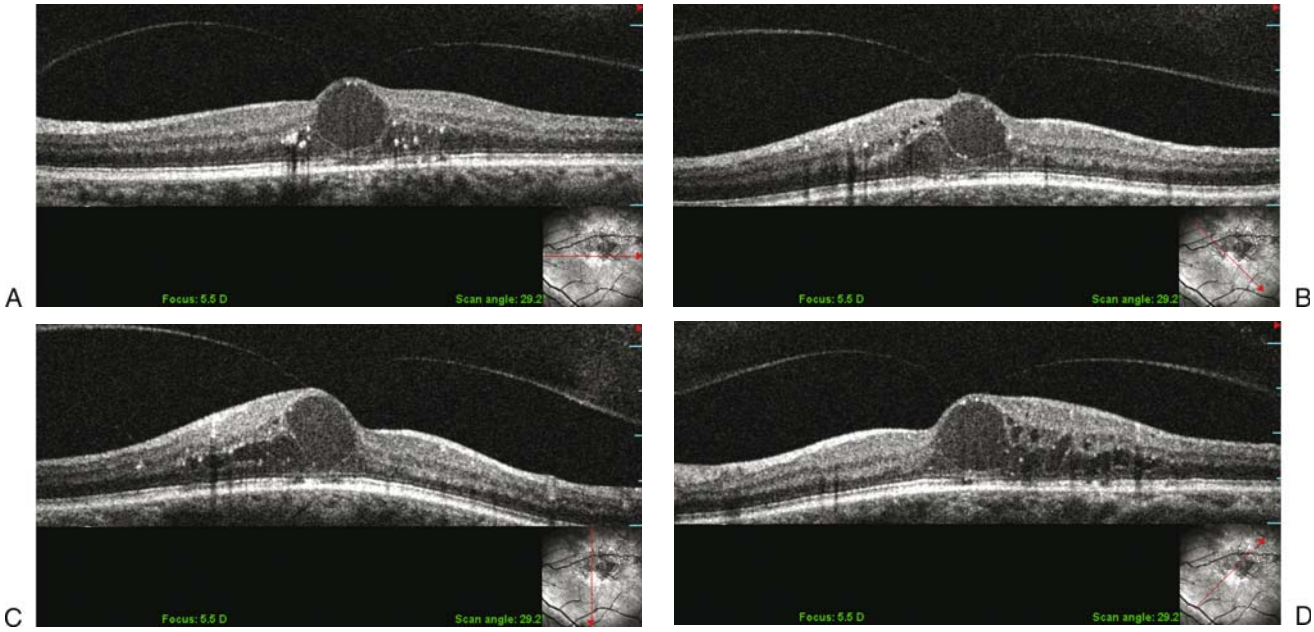

FIG. 27.8. Diabetic maculopathy (radial scans). (A) 180 degrees (horizontal scan). (B) 135 degrees. (C) 90 degrees (vertical scan). (D) 45 degrees.

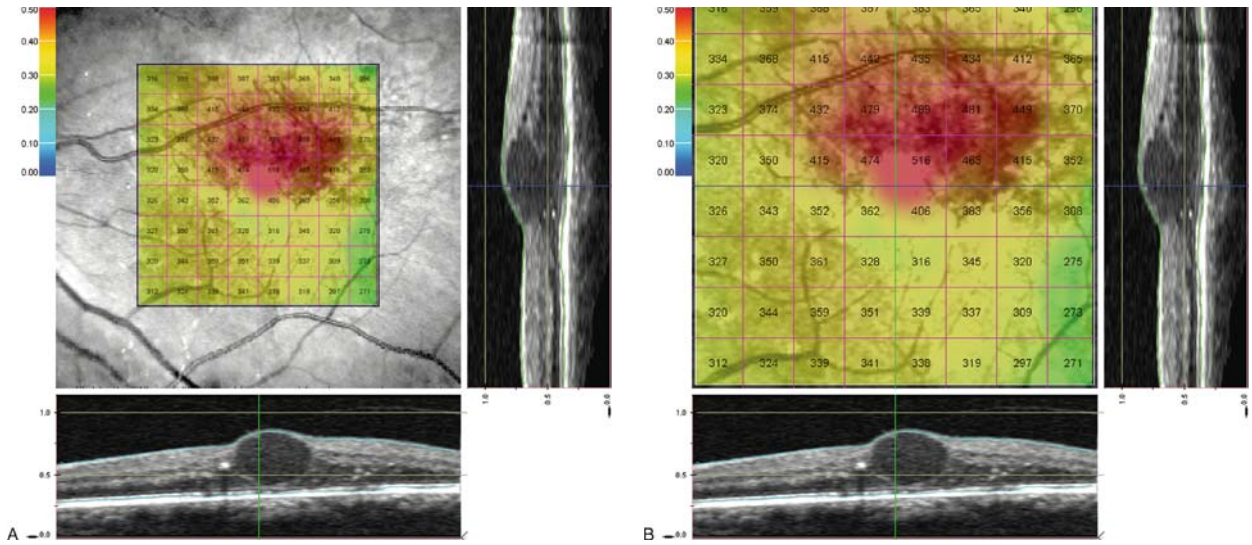

FIG. 27.9. (A) Diabetic macular edema thickness map over SLO image. (B) Diabetic macular edema thickness map close-up.

progression of a disease process over time, or for monitoring treatment effects.

Clinical Example: Central Serous Retinopathy

Retinal thickness maps obtained 3 months apart show a decrease in retinal thickness (Fig. 27.10 A,B). A subtraction of these thickness maps after automated vessel alignment shows the average decrease in retinal thickness to be 63.26 μm (Fig. 27.11). A three-dimensional rendering of any thickness map is also available (Fig. 27.12). These 3D images may be rotated and sliced to enable the examiner to explore direct relationship between the retinal thickness measurement and the associated underlying OCT anatomy. Errors in the computer's detection on boundaries may also be picked up using this facility.

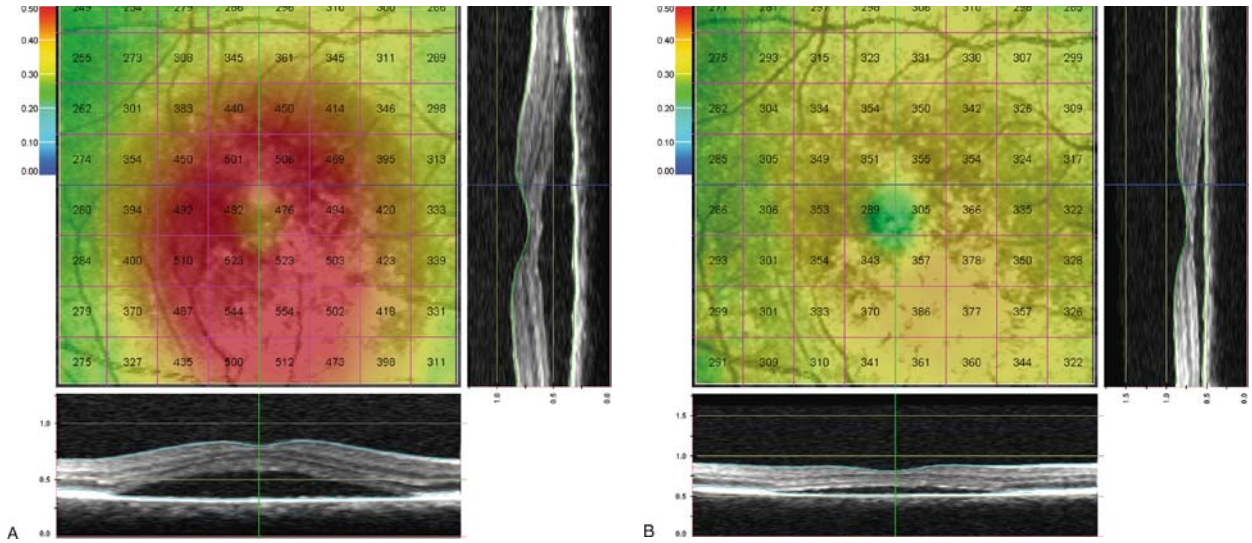

FIG. 27.10. (A) Central serous retinopathy map. (B) Same case of central serous retinopathy map 3 months later showing decrease in subretinal fluid.

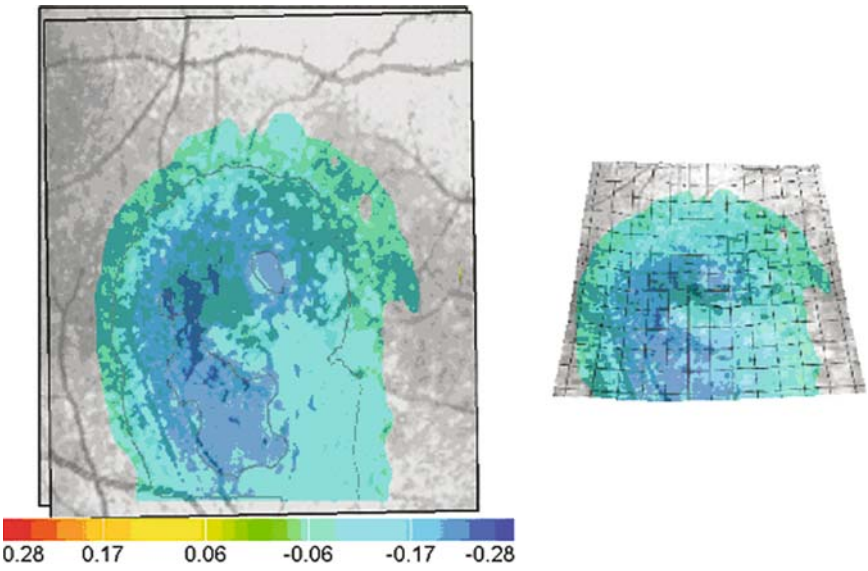

FIG. 27.11. Subtraction map of serial OCT/SLO topography maps of central serous retinopathy. (A) Flat overlay showing reconciliation of tilt between studies. (B) Three-dimensional rendering of subtraction map.

The OTI time-domain OCT/SLO employed transverse scanning, which provided native coronal scans (C-scans). These were particularly useful for localizing OCT features in relation to SLO fundus landmarks. The faster axial scanning of the spectral OCT/SLO is able to achieve the same localization by rapid raster scanning to generate a 3D set from which virtual C-scans may be extracted. While the quality of the virtual C-scans is less than that of the native C-scans of the time domain OCT/SLO, they have several advantages. The virtual C-scans may be corrected for tilt, which is helpful in facilitating their interpretation. There is the capacity to see the corresponding horizontal and vertical longitudinal scans simultaneously when the C-scans are viewed in topography viewer. Testing time is significantly shortened as separate C-scans, and B-scan sequences are not required. Figure 27.13 is an example of a virtual C-scan from the topography map.

Virtual C- and B-scan slices can also be produced from the 3D volumetric reconstructions. Below are images of the diabetic patient shown above taken from the 3D stack. Here the C-scan's value can be seen as it shows the relationship of the edema to the foveal depression (Fig. 27.14).

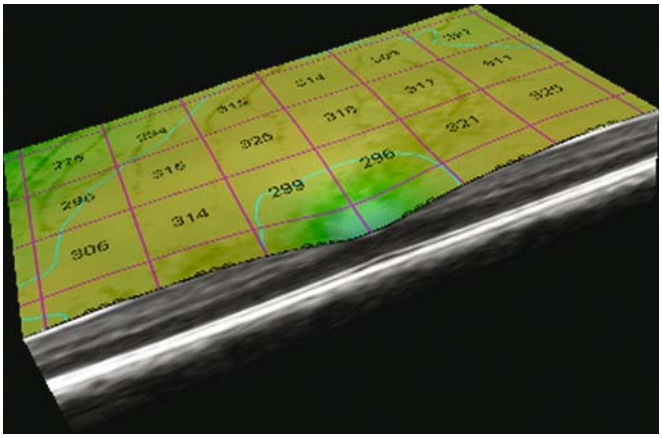

FIG. 27.12. Three-dimensional topography thickness map sliced to reveal underlying OCT image.

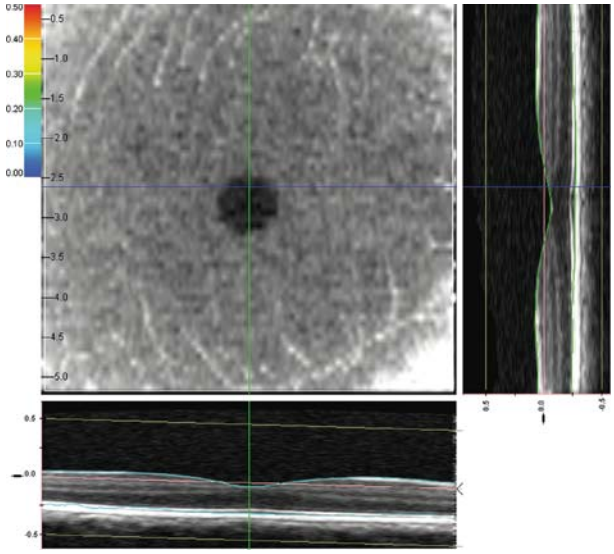

FIG. 27.13. Virtual C-scan slice obtained from a thickness map. This cut is taken through the foveal depression at the depth of the macular arcade vessels.

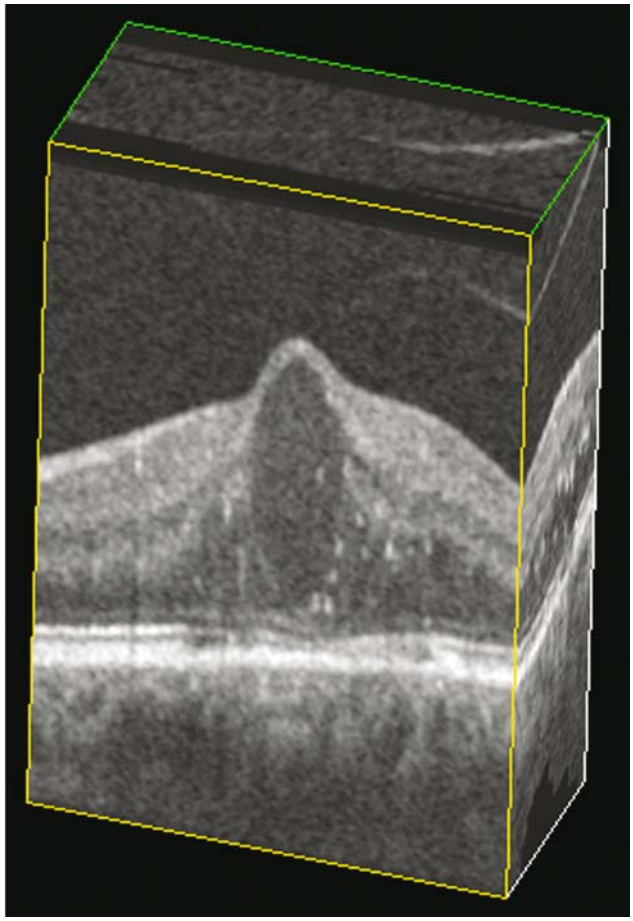

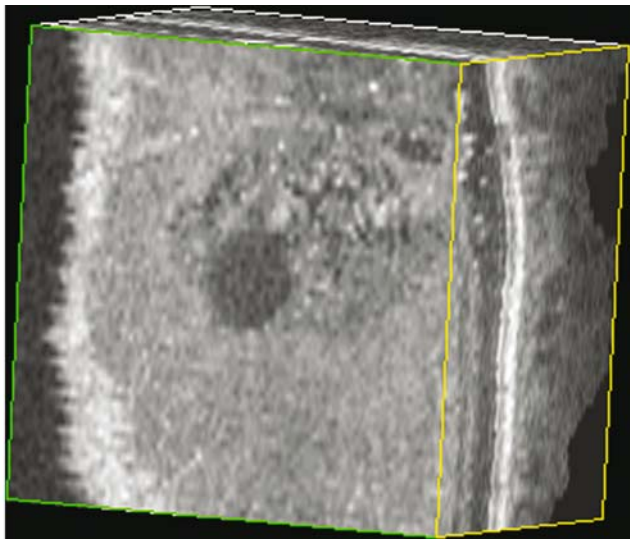

FIG. 27.14. (A) Virtual B-scan from three-dimensional OCT stack. (B) Virtual C-scan from three-dimensional OCT stack.

The 3D volumetric reconstruction is entirely interactive in real time, allowing rotation and sectioning of the image to the examiner's desire. A series of autosegmentation algorithms have been developed to permit sequential examination of the images at different depths. The vitreous, RNFL, retina, and RPE may be viewed separately by peeling off the vitreous, RNFL, and retinal layers one at a time. This can provide unobstructed views of the different layers as well as discrete volumetric calculations of drusen and subretinal fluid (Fig. 27.15).

Retinal Nerve Fiber Layer Scans

The spectral OCT/SLO can also generate a thickness map over the optic nerve area in the same way that it obtains a thickness map in the macula (128 scans in 2 seconds over a 5-mm area). With this information the machine can extract a 3.4-mm RNFL scan at a precise (user defined) location around the optic nerve. If the clinician is not satisfied with the way the optic nerve was centered, the extraction of the RNFL scan can be repeated at a different location without rescanning the patient (Fig. 27.16). Figure 27.16A shows an RNFL thickness scan with the 3.4 mm circular RNFL scan placed eccentrically around the optic nerve, leading to an erroneous RNFL calculation. In Figure 27.16B, the same RNFL thickness scan is shown with the 3.4 mm circular scan correctly centered on the optic nerve. The ability to extract RNFL thickness measurements from optic nerve scans is also important in ensuring that the same area is compared in follow-up studies.

Microperimetry

Microperimetry testing can also be performed using the live SLO image of the spectral OCT/SLO. The high speed of scanning that the spectral system affords allows accurate tracking of the patient's fixation to ensure the continuous realignment of the images. The only requirement of the study is reasonably stable fixation and clear media. Similar to visual field testing, the machine evaluates the patient's ability to perceive different light intensities (ranging from 0 to 20 dB) at different locations on the macula. A variety of patterns including square, polar, and diamond-shaped grids can be chosen with different densities of points. Like in visual field testing, the patient's fixation is monitored. Unlike visual field testing, the area being tested is clearly seen by the examiner, as the threshold intensities are overlaid on the SLO image. This is useful in determining the patient's visual function at clinically apparent lesions.

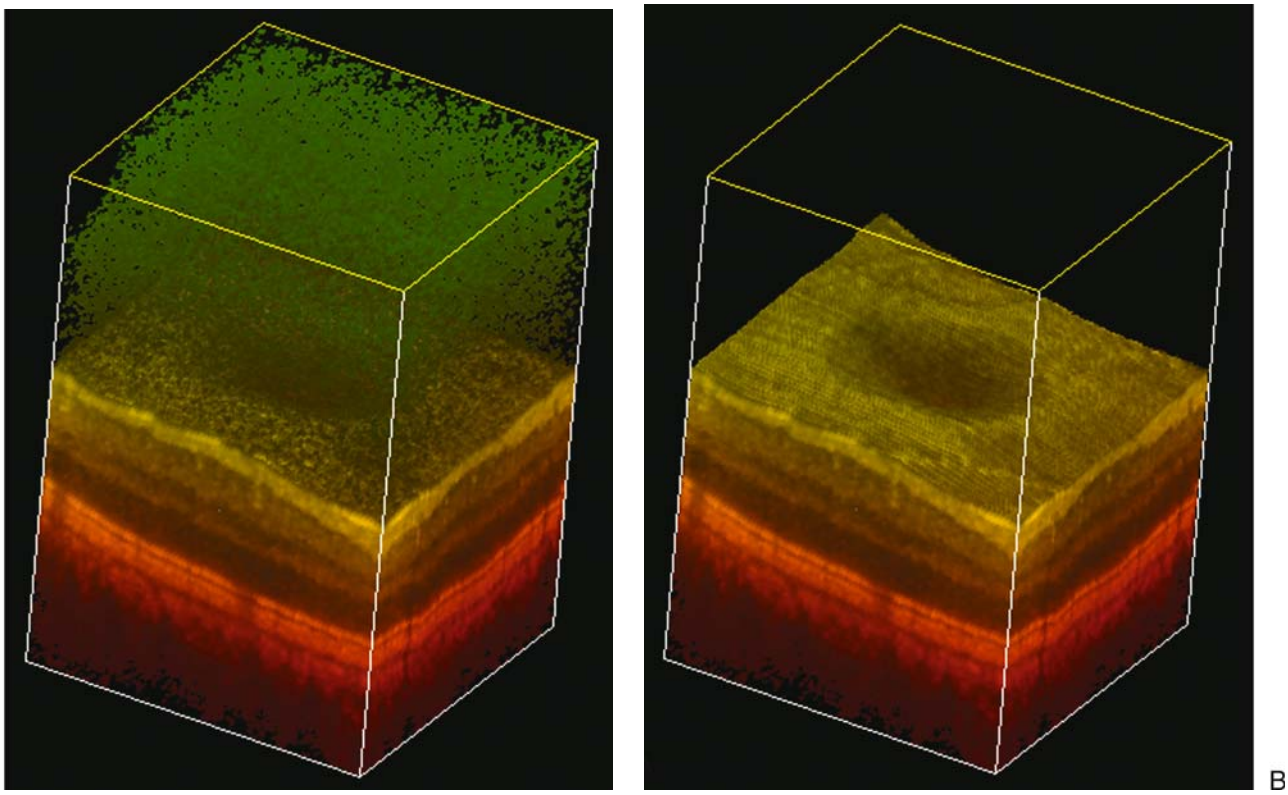

FIG. 27.15. (A) Three-dimensional OCT of normal retinal with overlying vitreous in place. (A) Three-dimensional OCT of normal retinal with vitreous stripped off.

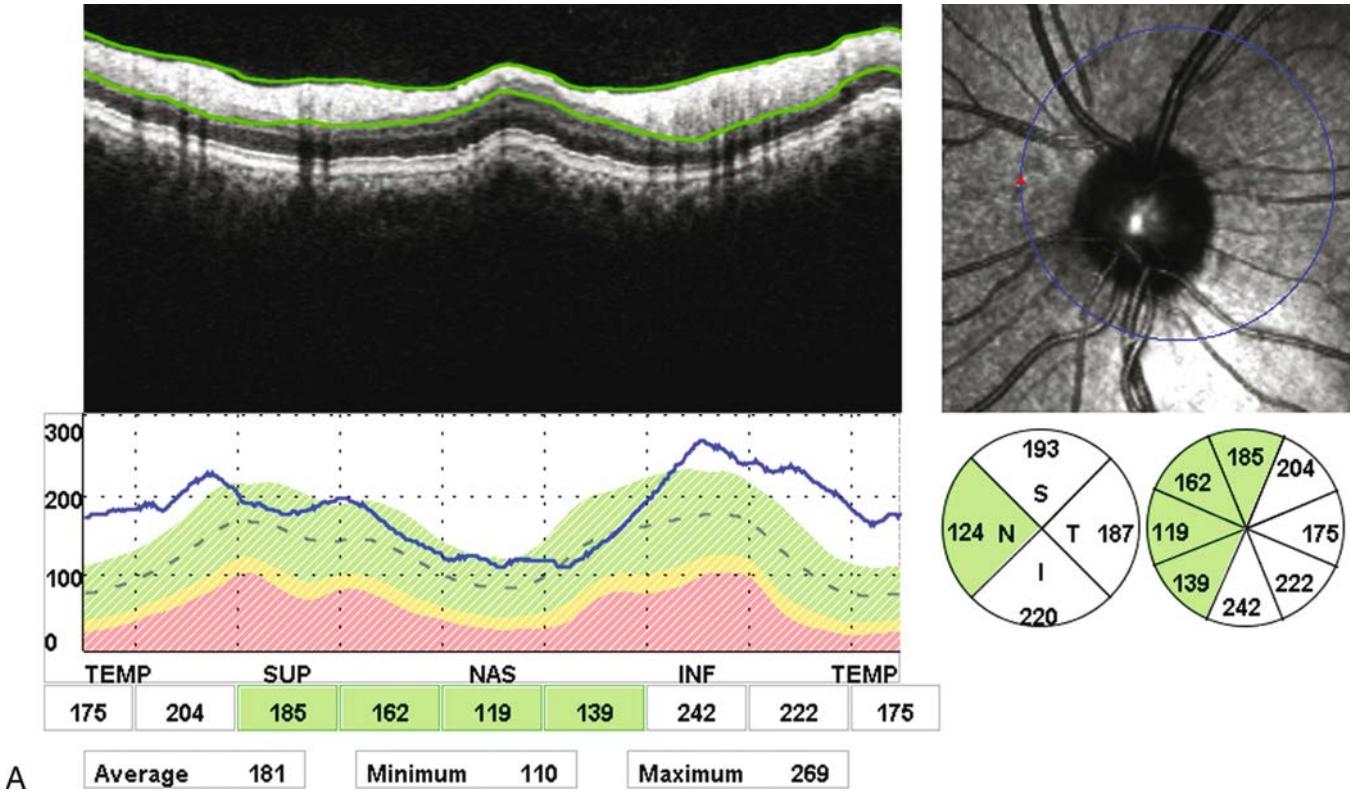

A

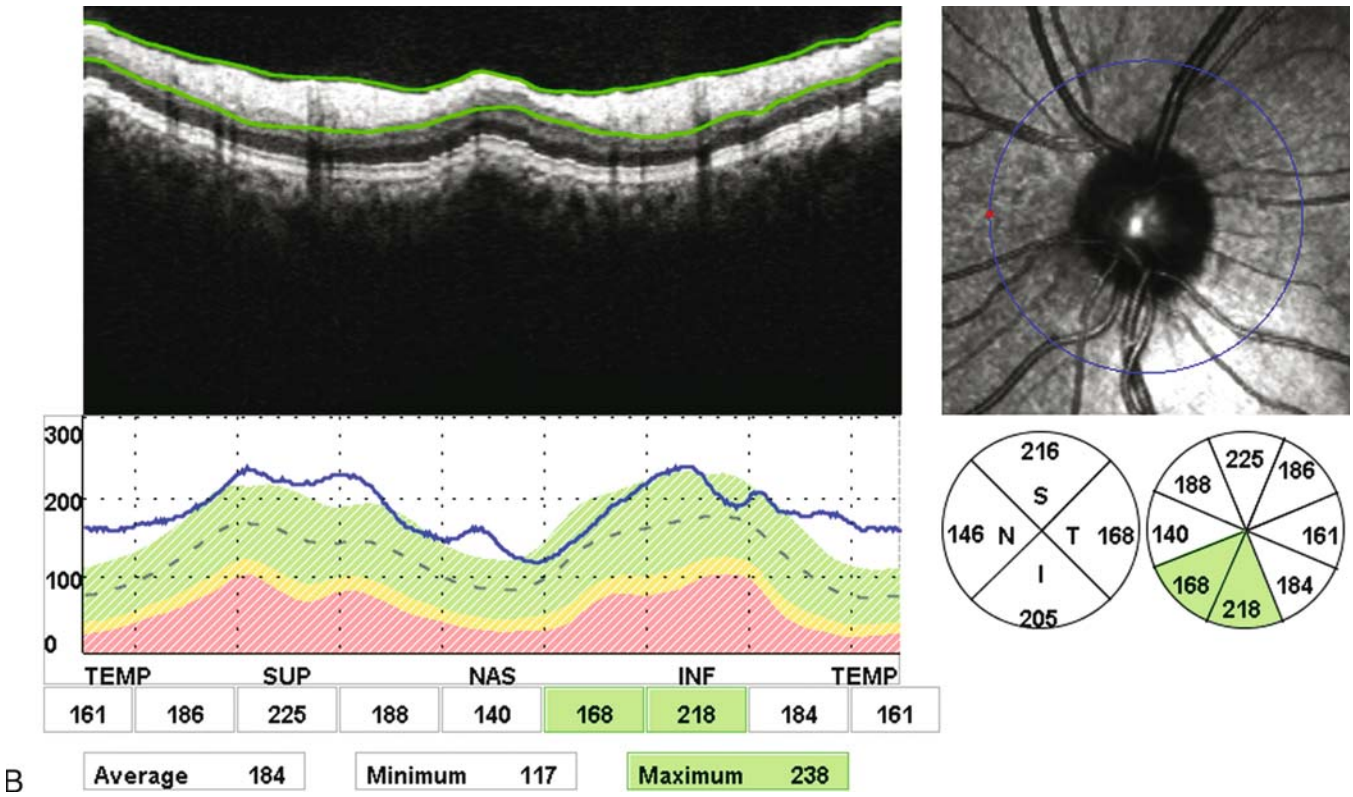

B

FIG. 27.16. (A) Eccentric RNFL scan. (B) Correctly centered RNFL scan.

Clinical Example: Age-Related Macular Degeneration

A patient presents with macular degeneration. The topographic thickness map of the patient's macula is shown on (Fig. 27.17A), against the backdrop of the fundus image. Fig. 27.17B is the close-up of the map, which shows the grid labeled with the average thickness measurements. Fig. 27.18 depicts an OCT/SLO slice diagonally through the fovea to catch the lesion, which is in the superonasal quadrant of the macula. The microperimetry image, shown on Fig. 27.19, maps the visual function grid of the macula revealing the depression associated with the lesion.

Functional Optical Coherence Tomography/Scanning Laser Ophthalmoscope Integrated Microperimetry and Three-Dimensional Topography

The ability to precisely register the different modalities of the OCT/SLO using the vascular patterns enables superimposition of functional microperimetry data onto the 3D data set of the topography maps. Using the 3D rendering feature of the topography maps, it then becomes possible to view the underlying

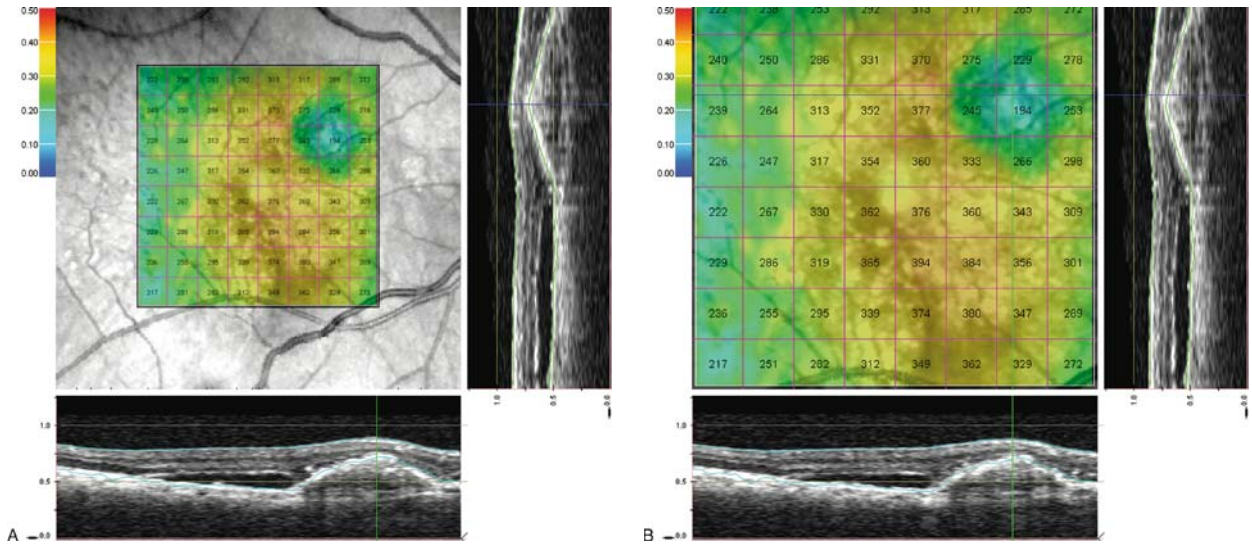

FIG. 27.17. (A) Age-related macular degeneration with choroidal neovascularization (CNV) topography on SLO. (B) Age-related macular degeneration with CNV topography close-up.

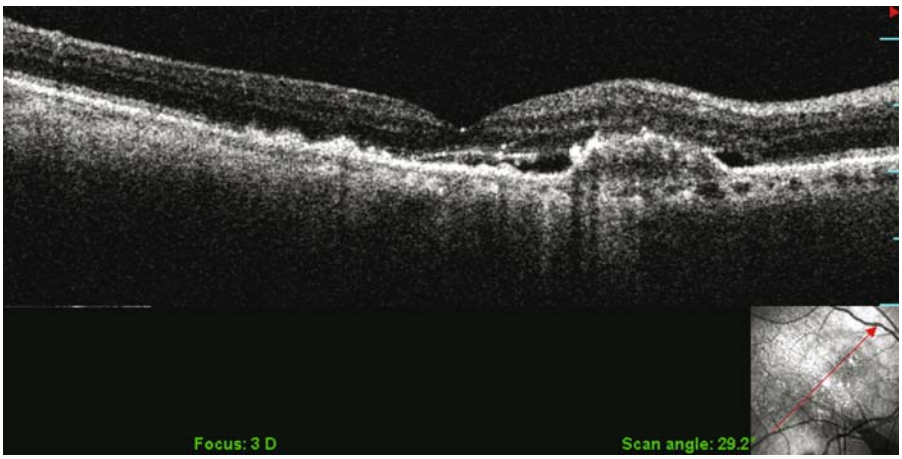

FIG. 27.18. Age-related macular degeneration with CNV B-scan OCT/SLO.

OCT details beneath the combined perimetry/thickness maps. For the first time we are able to look at specific retinal surface features and precisely correlate associated thickness, OCT internal anatomy, and threshold visual sensitivity. An example of this kind of analysis is displayed in Figures 27.20 to 27.23 in a case of myopic choroidal neovascularization.

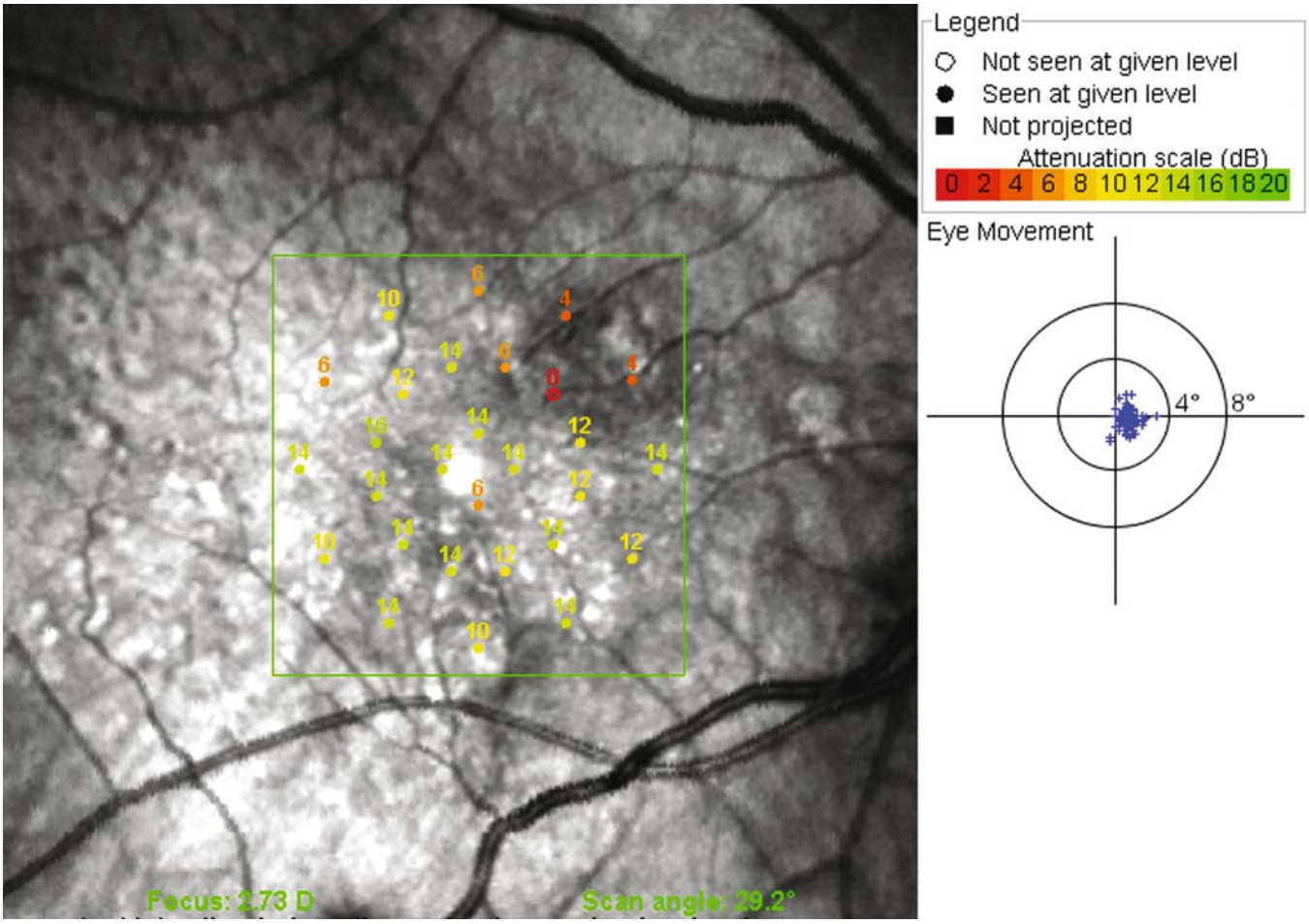

FIG. 27.19. Age-related macular degeneration with CNV OCT/SLO microperimetry.

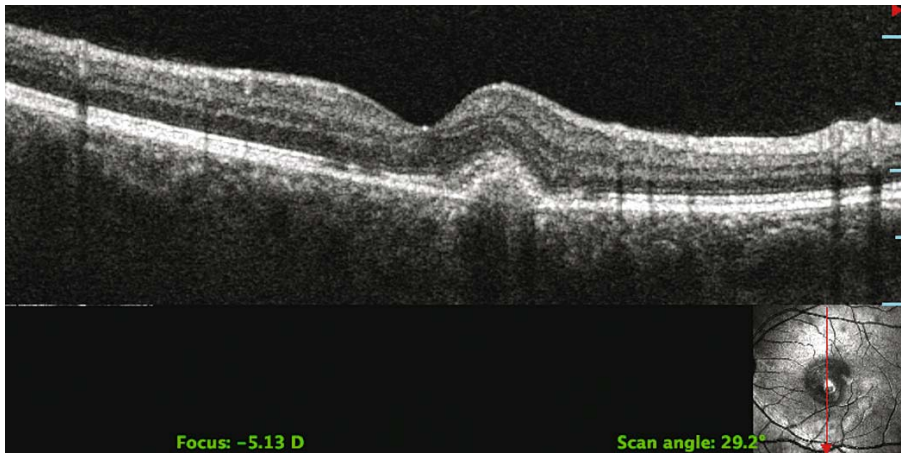

FIG. 27.20. Myopic CNV B-scan OCT/SLO.

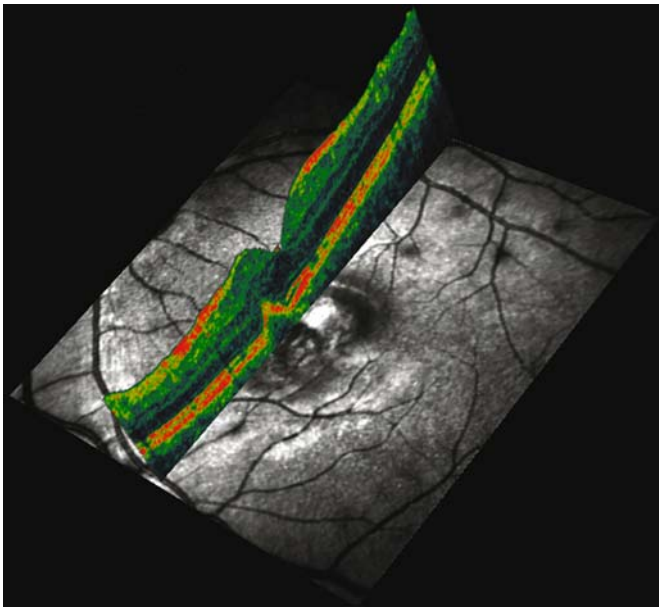

FIG. 27.21. Myopic CNV intersecting OCT and SLO planes view.

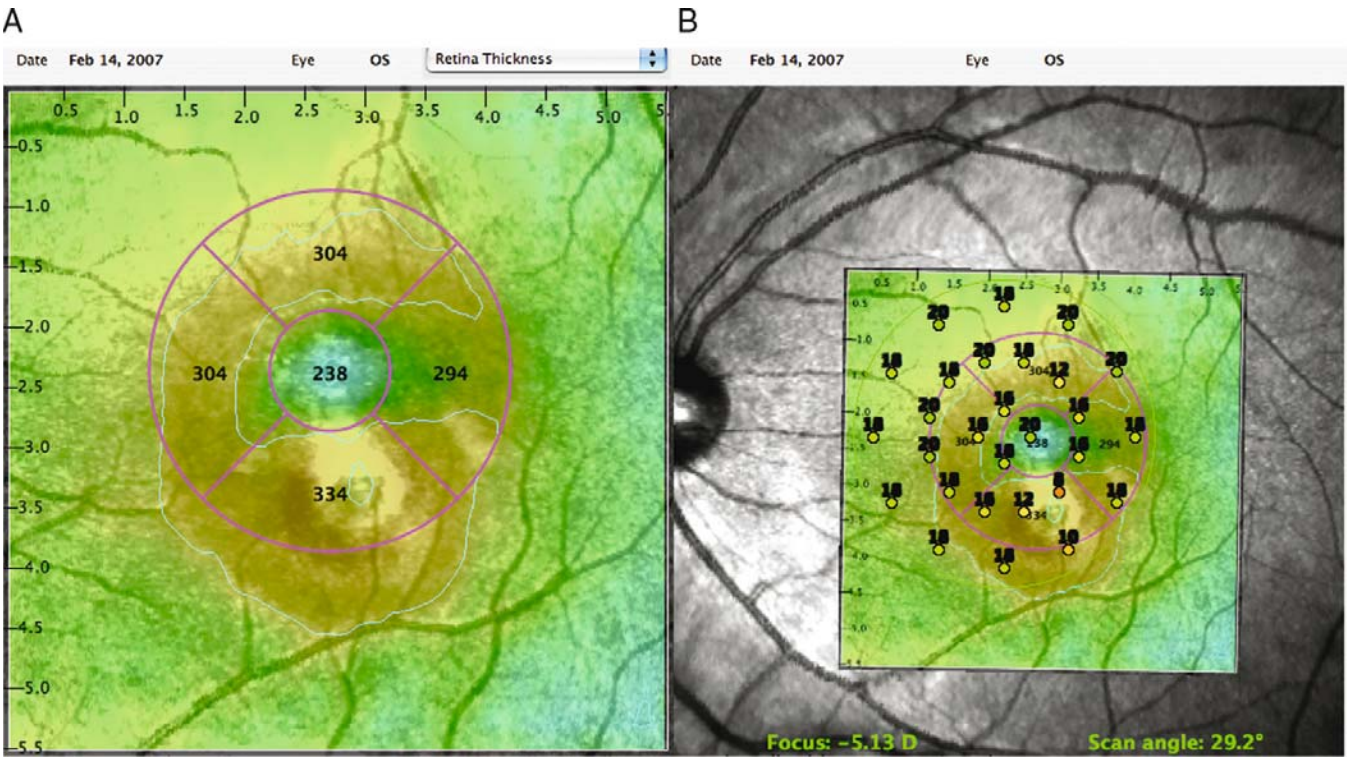

FIG. 27.22. Perimetry topography overlays of myopic CNV. (A) Retinal thickness map. (B) Microperimetry/retinal thickness on SLO.

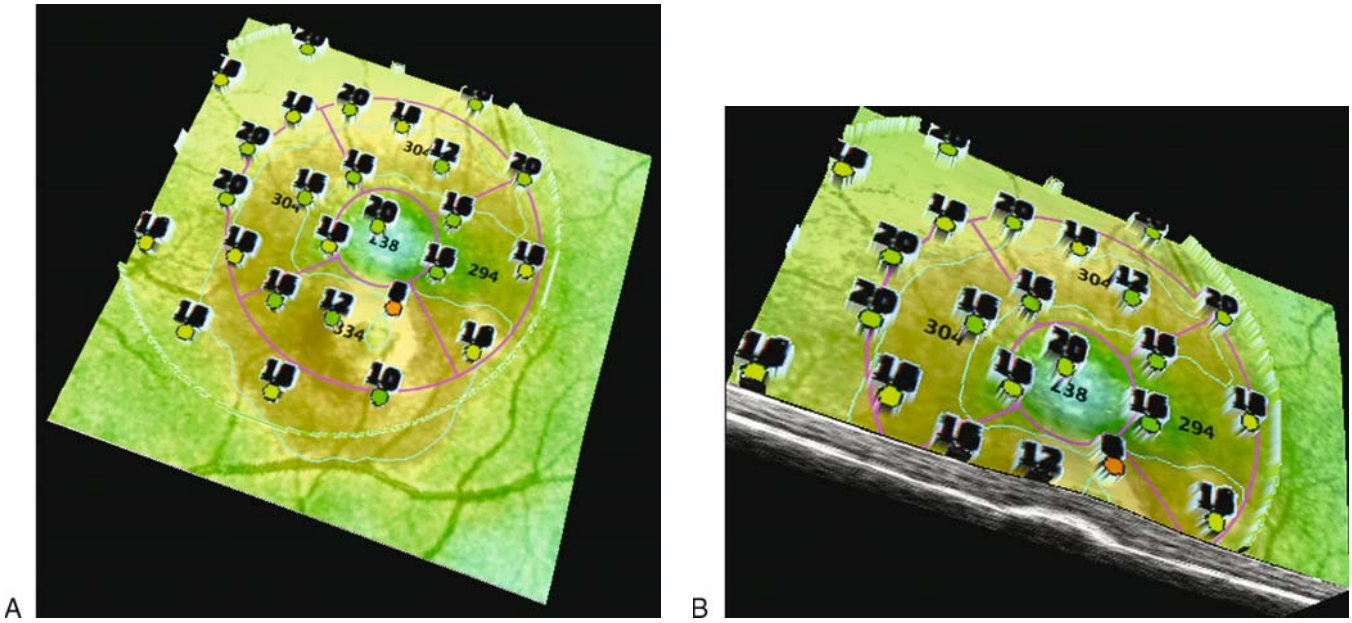

FIG. 27.23. Perimetry topography three-dimensional renderings of myopic CNV. (A) Three-dimensional OCT/SLO retinal thickness map with microperimetry overlay. (B) Four-dimensional OCT/SLO—microperimetry and three-dimensional OCT retinal thickness.

Conclusion

The OTI spectral OCT/SLO has the potential to provide the ophthalmologist with a wealth of information useful in the diagnosis and care of patients. As with any diagnostic modality, the maximization of this potential is dependent on an understanding of the machine's capabilities and the accurate interpretation of its results. The expanding variety of views and integrated features should help further our understanding of many of the retinal conditions that we now struggle to manage.

References

1. Huang D, Swanson EA, Lin CP, et al. Optical coherence tomography. Science 1991;254:1178–1181.
2. Hee MR, Izatt JA, Swanson EA, et al. Optical coherence tomography of the human retina. Arch Ophthalmol 1995;113:325–332.
3. Schuman JS, Puliafito CA, Fujimoto JG. Optical Coherence Tomography of Ocular Diseases, 2nd ed. Thorofare, NJ: Slack, 2004.
4. Podoleanu AG, Dobre GM, Seeger M, et al. Low coherence interferometry for *en-face* imaging of the retina. Lasers and Light 1998;8:187–192.
5. Podoleanu A Gh, Dobre GM, Cucu RG, et al. Combined multiplanar optical coherence tomography and confocal scanning ophthalmoscopy. J Biomed Opt 9(1):86–93.
6. Yannuzzi LA, Ober MA, Slakter JS, et al. Ophthalmic fundus imaging: today and beyond. Am J Ophthalmol 2004;137:511–524.
7. Dobre GM, Podoleanu AG, Rosen RB. Simultaneous optical coherence tomography—indocyanine green dye fluorescence imaging system for investigations of the eye's fundus. Opt Lett 2005;30(1):58–60.
8. Podoleanu A, Charalambous I, Plesea L, Dogariu A, Rosen R. Correction of distortions in optical coherence tomography imaging of the eye. Phys Med Biol 2004;49(7):1277–1294.
9. Podoleanu AG, Dobre GM, Cucu RG, Rosen RB. Sequential optical coherence tomography and confocal imaging. Opt Lett 2004;29(4):364–366.
10. van Velthoven ME, Verbraak FD, Garcia PM, Schlingemann RO, Rosen RB, de Smet MD. Evaluation of central serous retinopathy with en face optical coherence tomography. Br J Ophthalmol 2005;89:1483–1488.
11. van Velthoven ME, Verbraak FD, Yannuzzi LA, et al. Imaging the retina by *en-face* optical coherence tomography. Retina 2006;26:129–136.
12. Rosen RB, Dunne S, Podoleanu A, Gh Garcia PM. Multiplanar OCT/confocal ophthalmoscopy. In: Ciulla T, Regillo C, Harris A, eds. Ocular Posterior Segment Imaging. Philadelphia: Lippincott Williams & Wilkins, 2003.
13. Rosen RB, Will D, Garcia PM, Dunne S, Fisher, Y, Podoleanu AGH. OCT ophthalmoscope. In: Age-Related Macular Degeneration: A Comprehensive Textbook. Philadelphia: Lippincott Williams & Wilkins, 2005.
14. Rosen RB, Dunne S, Podoleanu A Gh, Garcia PM. OCT ophthalmoscopy. In: Huang D, ed. Posterior Segment Imaging of the Eye. Elsevier, 2006.
15. Rosen RB, Muldoon TO, Garcia PM. Evaluating retinal thickness during pegaptanib sodium therapy. Ret Phys 2006;35–38.

16. Drexler W, Morgner U, Ghanta RK, et al. Ultrahigh-resolution ophthalmic optical coherence tomography. Nat Med 2001;7:502–507.
17. Drexler W, Sattmann H, Hermann B, et al. Enhanced visualization of macular pathology with the use of ultrahigh-resolution optical coherence tomography. Arch Ophthalmol 2003;121:695–706.
18. Ko TH, Fujimoto JG, Schuman JS, et al. Comparison of ultrahigh- and standard-resolution optical coherence tomography for imaging macular pathology. Ophthalmology 2005;112:1922.
19. Cucu RG, Podoleanu AG, Rogers JA, Pedro J, Rosen RB. Combined confocal/en face T-scan-based ultrahigh-resolution optical coherence tomography in vivo retinal imaging. Opt Lett 2006;31(11):1684–1686.
20. Rosen RB, van Velthoven MEJ, Garcia PMT, et al. Ultrahigh-resolution combined coronal optical coherence tomography confocal scanning ophthalmoscope (OCT/SLO): A pilot study. Spektrum Augenheilkd 2007;21(1):17–28.
21. Wojtkowski M, Leitgeb R, Kowalczyk A, Bajraszewski T, Fercher AF. In-vivo human retinal imaging by Fourier domain optical coherence tomography. J Biomed Opt 2002;7:457–463.
22. Wojtkowski M, Srinivasan VJ, Ko TH, Fujimoto JG, Kowalczyk A, Duker JS. Ultrahigh-resolution, high-speed, Fourier domain optical coherence tomography and methods for dispersion compensation Opt Exp 2004;12(11):2404–2422.
23. Cense B, Nassif NA, Chen TC, et al. Ultrahigh-resolution high-speed retinal imaging using spectral-domain optical coherence tomography. Opt Exp 2004;12(11):2435–2447.
24. Nassif N, Cense B, Park BH, et al. In vivo human retinal imaging by ultrahigh-speed spectral domain optical coherence tomography. Opt Lett 2004;29:480–482.
25. Leitgeb RA, Drexler W, Unterhuber A, et al. Ultrahigh resolution Fourier domain optical coherence tomography. Opt Exp 2004;12:2156–2165.

Index